



ULUSLARARASI
KAYNAK
TEKNOLOJİLERİ
KONFERANSI VE
SERGİSİ



INTERNATIONAL
CONFERENCE ON
WELDING
TECHNOLOGIES
AND EXHIBITION

BOOK OF PROCEEDINGS

ISBN 978-605-245-232

Edited by:

Prof. Dr. Adem KURT
Prof. Dr. Ahmed YILDIRIM
Assoc. Prof. Dr. Ayhan EROL
Assist. Prof. Dr. Ahmet YONETKEN

Published Afyon Kocatepe University, 2018
icwet18@gmail.com

5. INTERNATIONAL CONFERENCE ON WELDING TECHNOLOGIES AND EXHIBITION



ICWET'18

Sarajevo/Bosnia Herzegovina

26-28 September 2018

<https://icwet.ius.edu.ba>

Book of Proceedins

ISBN: 978-605-245-232

Book of Proceedings of the 5th International Conference on Welding Technologies and Exhibition (ICWET'18)

Edited by

Prof. Dr. Adem Kurt

Prof Dr. Ahmet YILDIRIM

Assoc. Prof. Dr. Ayhan EROL

Assist. Prof. Dr. Ahmet YÖNETKEN

Published Afyon Kocatepe University, September 2018,

icwet18@gmail.com

This work is subject to copyright. All rights are reserved, whether the whole or part of the material is concerned. Nothing from this publication may be translated, reproduced, stored in a computerized system or published in any form or in any manner, including, but not limited to electronic, mechanical, reprographic or photographic, without prior written permission from the publisher <https://icwet.ius.edu.ba> icwet18@gmail.com The individual contributions in this publication and any liabilities arising from them remain the responsibility of the authors. The publisher is not responsible for possible damages, which could be a result of content derived from this publication.

Welcome to ICWET'18

On behalf of the organizing committee, we are pleased to welcome you to the 5th International Conference on Welding Technologies and Exhibition (ICWET'18) which is to be held between 26 - 28 September, 2018 in Sarajevo, Bosnia and Herzegovina. ICWET'18 provides an ideal academic platform for researchers to present the latest research findings, and directions in Welding Technology issues. The conference seeks to contribute to the advancement of novel research in all aspects of Welding Technologies and Exhibition. The conference aims to bring the leading academic scientists, experts and research scholars together to share their experiences and up-to-date research outcomes about Welding and its Technology. It also provides a leading interdisciplinary forum for scientists, engineers, and practitioners to present their latest research results, ideas, developments, and applications in all areas of related to academic and industrial aspects of welding. The conference will bring together leading academic scientists, researchers and scholars in the domain of interest from around the world. ICWET'18 is the oncoming event of the successful conference series focusing on Welding Technologies and Exhibition. The scientific program focuses on current advances in the research, the production and the use of Welding Technologies with particular focus on their role in maintaining academic level in Welding Technologies and elevating its scientific level.

Best regards,

Chairman of Conference

Prof. Dr. Adem KURT

INTERNATIONAL SCIENTIFIC COMMITTEE

CONFERENCE CHAIRS

- Prof. Dr. Adem KURT Welding Technology Society
Prof. Dr. Ahmet YILDIRIM International University of Sarajevo
Assoc. Prof. Dr. Ayhan EROL Afyon Kocatepe University

INTERNATIONAL SCIENTIFIC COMMITTEE

- Dr. Abdulkadir EK – Çukurova Üniversitesi
- Dr. Abdul MATEEN – Institute of Space Technology
- Dr. Adnan ÇALIK – Süleyman Demirel Üniversitesi
- Dr. Ahmad Azmin MOHAMAD - Universiti Sains Malaysia
- Dr. Ahmet KARAASLAN – Yıldız Teknik Üniversitesi
- Dr. Ahmet TÜRK – Celal Bayar Üniversitesi
- Dr. Ahmet Durgutlu – Gazi University
- Ahmet SEVÜK – Askaynak-Lincoln Elektrik
- Dr. Aleksandar SEDMAK – University of Belgrade
- Dr. Ali GÜRSEL – Düzce Üniversitesi
- Dr. Ali Hussein – University of Malakand
- Dr. Americo SCOTTI – University West
- Dr. Anas M. ATIEH - German Jordanian University
- Dr. Aydın ŞIK – Gazi Üniversitesi
- Dr. Behçet GÜLENC – Gazi Üniversitesi
- Dr. Boumerzoug ZAKARIA – University of Biskra
- Dr. Bülent KURT – Nevşehir Hacı Bektaş Veli Üniversitesi
- Dr. Cemal ÇARBOĞA – Nevşehir Üniversitesi
- Dr. Cemal MERAN – Pamukkale Üniversitesi

- Dr. Cemil Cetinkaya– Gazi Üniversitesi
- Dr. Dattaguru Ananthapadmanaban - SSN College of Engineering -India
- Dr. Dheerendra K. DWIVEDI - Indian Institute of Technology Roorkee
- Dr. Dorin DEHELEAN – Romanian Welding Society
- Dr. Eyüp GERÇEKÇİOĞLU – Erciyes Üniversitesi
- Dr. Gürel ÇAM – İskenderun Teknik Üniversitesi
- Dr. Halil ARIK- Gazi üniversitesi
- Dr. Hanefi ÇİNİCİ – Gazi Üniversitesi
- Dr. Hazman SELİ – University of Sains Malaysia
- Dr.İbrahim QAZİ – University of Sheffield
- Dr. İlyas UYGUR – Düzce Üniversitesi
- Dr. Livius MİLOŞ – Universitatea Politehnica Timișoara
- Dr. Mehmet Burak BİLGİN – Amasya Üniversitesi
- Dr. Mehmet ŞİMŞİR – Sivas Cumhuriyet Üniversitesi
- Dr. Michael Rethmeier – TU Delft
- Dr. Mustafa ACARER – Selçuk Üniversitesi
- Dr. Mustafa BOZ – Karabük Üniversitesi
- Dr. Mustafa Erer – Karabük University
- Dr. M. Kemal KÜLEKÇİ – Mersin Üniversitesi
- Dr. Nizamettin KAHRAMAN – Karabük Üniversitesi
- Dr. Nurullah KIRATLI – Dumlupınar Üniversitesi
- Dr. Oğuzhan YILMAZ – Gazi Üniversitesi
- Dr. Ramazan ÇITAK – Gazi Üniversitesi
- Dr. Salim ASLANLAR – Sakarya Üniversitesi
- Dr. Sead PASİC – University Dzamal Bijedic- Bosnia and Herzegovina
- Dr. Serdar SALMAN – Marmara Üniversitesi

- Dr. Serkan ÖZEL – Bitlis Eren Üniversitesi
- Dr. Shabana P.S. SHAIKH – Pune Üniversitesi
- Dr. Süleyman GÜNDÜZ – Karabük Üniversitesi
- Dr. Şükrü TALAS – Afyon Kocatepe Üniversitesi
- Dr. Tahir KHAN – University of Bradford
- Dr. Tanju TEKER – Adıyaman Üniversitesi
- Dr. Tayfun FINDIK- Gazi Üniversitesi
- Dr. Uğur ARABACI - Gazi Üniversitesi
- Dr. Uğur ÇALIGÜLÜ – Fırat Üniversitesi
- Dr. Uğur ÖZSARAÇ – Sakarya Üniversitesi
- Dr. Yusuf ÖZÇATALBAŞ – Gazi Üniversitesi
- Yücel UYGUR – Magmaweld- Oerlikon Holding

ORGANISING COMMITTEE

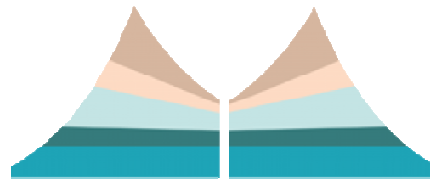
- Prof. Dr. Adem KURT
- Prof. Dr. Ahmet YILDIRIM
- Assoc. Prof. Dr. Ayhan EROL
- Assoc. Prof. Dr. Necip Fazıl YILMAZ
- Assoc. Prof. Dr. Ersin BAHÇECİ
- Prof. Dr. Hakan ATEŞ
- Prof. Dr. Ramazan KAÇAR
- Prof. Dr. Ramazan YILMAZ
- Prof. Dr. Mustafa TAŞKIN
- Prof. Dr. Mustafa AYDIN
- Prof. Dr. Niyazi ÖZDEMİR
- Prof. Dr. Livu Brandusan
- Assist. Prof. Dr. Ahmet YÖNETKEN

- İrem Burcu ALGAN
- Özgür Akçam-GSI SLV- TR
- Hayri YILMAZ - MEKSAN A.

Organized by



Supported by



SEDEF
BOSNIA

CONTENTS

	Page
Effect Of Welding Time And Current Parameters On Tensile-Shear Strength Of Spot Welded Twip1000/Martensitic1500 Steel Joints <i>Fatih Özen, Volkan Onar, Yusuf Sadi Aslanlar, Zafer Barlas, Uğur Öz Saraç, Salim Aslanlar</i>	1-9
Tensile Peel Strength Of Resistance Spot Welded Twip1000/Ms1500 Joints <i>Fatih Özen, Volkan Onar, Yusuf Sadi Aslanlar, Zafer Barlas, Uğur Öz Saraç, Salim Aslanlar</i>	10-17
Microstructural Evolution, Phase Transition And Mechanical Properties Of Fe-Ti-B Hardfacing Alloys <i>Eray Abakay, Engin Kocaman, Mustafa Durmaz, Bülent Kılınç, Şaduman Şen, Uğur Şen</i>	18-27
The Effect Of Molybdenum Addition On The Microstructure And Wear Behaviours Of Fe-Mo-B Based Alloyed Steel <i>Bülent Kılınç, Engin KOCAMAN, Mustafa Durmaz, Eray Abakay, Uğur Şen, Şaduman Şen</i>	28-38
Microstructural Characterisation Of Fe-Ti-B-Cr Hardfacing Alloy Coated By Tıg Welding <i>Engin Kocaman, Bülent Kılınç, Mustafa Durmaz, Eray Abakay, Şaduman Şen, Uğur Şen,</i>	39-48
Çok Pasolu Kaynaklarda; Isı Girdisinin Kaynak Metaline Etkisi <i>Nisanur Sarıcaoğlu, Tuğçe Çam, Selay Aydın, Adem Kurt</i>	49-56
Mıg-Mag Kaynak Ünitesi Kullanılarak 3 Boyutlu Metal Yazıcıyla Kremayer Dişli Parçasına Diş Ekleme İşlemi <i>Yusuf Ayan, Nizamettin Kahraman</i>	57-66
Su Altı Örtülü Elektrod Ark Kaynak Yönteminde Derinliğin Kaynak Kalitesine Etkisi <i>Zahit Çolak, Kadir İmdat, Yusuf Ayan, Behçet Gülenç, Nizamettin Kahraman</i>	67-78
Effect Of Processing On Galvanized Dp 600 Steel Plates In Cold Metal Transfer Technology <i>Faruk Varol</i>	79-90

Investigation Of Mechanical Properties Of Overlap Joint Form In Cmt-Brazed Joints Of Dp800 Steel Plates Using Different Current Intensity

Faruk Varol, İbrahim Acar, Veli ŞıkŞık, Erman Ferik, Salim Aslanlar, Yusuf Sadi Aslanlar
.....91-99

The Investigation Of Effect On Shear Strength Of Nickel Interlayer In Inserted Powder Injection Moulding

Mehmet SUBAŞI, Harun KOÇAK, Çetin KARATAŞ100-106

The Effect Of Molybdenum Addition On The Microstructure And Wear Behaviours Of Fe-Mo-B Based Alloyed Steel

Bülent Kılınç, Engin KOCAMAN, Mustafa Durmaz, Eray Abakay, Uğur Şen, Şaduman Şen
.....107-117

Microstructural Evolution, Phase Transition And Mechanical Properties Of Fe-Ti-B Hardfacing Alloys

Eray Abakay, Engin Kocaman, Mustafa Durmaz, Bülent Kılınç, Şaduman Şen, Uğur Şen,
.....118-127

Investigation Of Effect Of Nickel Interlayer On Diffusion In WC-Co Part Produced By Inserted Powder Injection Molding

Mehmet SUBAŞI, Harun KOÇAK, Çetin KARATAŞ128-134

A Titanyum Levhaların TIG Kaynağı İle Birleştirilmesinde Kaynak Parametrelerinin Mekanik Özellik Ve Mikroyapıya Etkisi

Sefa Enes Kılıç, Murathan Kalender, Yahya Bozkurt, Serdar Salman135-145

Farklı Malzemelerin Sürtünme Karıştırma Kaynağında Takim Geometrisinin Mekanik Özelliklere Etkisi

Murathan Kalender, Sefa Enes Kılıç, Yahya Bozkurt, Serdar Salman.....146-156

A MIG Welding Automation Equipped Double Torch For Fillet Welding Of Transformer Sidewall Strengthening Part's Fillet Weldings With Linearity Correction Ability

Nihat ÇELİK, İlker EREN, Ersin AKYÜZ, Sercan SÜZEN.....157-164

Microstructural Properties Of High Chromium White Cast Iron / Aisi 1030 Steel With Nickel Interlayer Welded By Friction Welding

Tanju TEKER, Eyyüp Murat KARAKURT..... 165-171

The Investigation Of Microstructure Of Binary Iron Niobium Alloy Coating By Pack Boronizing Method

Tanju TEKER, Eyyüp Murat KARAKURT..... 172-177

Surface properties of FeCrC alloy coating produced by powder feeding GTA cladding on AISI1040 steel

S. Osman YILMAZ, Tanju TEKER, Savaş DALMIŞ 178-186

Influence Of Dynamic Strain Ageing On Microstructural And Mechanical Properties Of Aisi 316l Austenitic Stainless Steel Weld Metal

Guma Alnaji Muhamed, Süleyman Gündüz..... 187-201

The Effects Of Cu And Ni Coating On Friction Stir Spot Welded For 2024 Al Alloys

Adnan Türker, Gamze Soytemiz, Yahya Bozkurt, Serdar Salman 202-209

Investigation Of Mechanical Properties Of Friction Stir Spot Welded Light Metal Alloys

Ahmet ATAĞ, Aydın ŞİK..... 210-219

The Effect Of The Occupational Health And Safety Education On Student Awareness Level In Vocational And Technical Secondary Education Institutions

Arslan Kıvanç YILDIRIM, Ömer ASAL 220-226

Effect Of PWHT Temperature And Time On Hardness And Microstructure Of 410NiMo Weld Metal

Uğur Özdemir, Selçuk Keskinılıç, Filiz K. Acar, Fikret Kabakci, Mustafa Acarer..... 227-232

Effect Of Cobalt On Themicrostructure And Toughness-Hardness Properties On P91 Weld Metal

Fikret KABAKCI, Mustafa ACARER, Selçuk KESKINKILIC, Filiz KUMDALI ACAR, Uğur ÖZDEMİR 233-240

Numerical Modelling Of Dynamics Of Crash Box Collision Geometry

Oktay Çetinel, Hakan Ateş..... 241-254

Farklı İlave Metaller Kullanılarak Tig Kaynak Yöntemi İle Birleştirilen 316 L Paslanmaz Çelik Ve L-605 Kobalt Esaslı Süperalaşım Levhaların Metalurjik Özelliklerinin Değerlendirilmesi

Tolga Yılmaz, Ahmet Durgutlu..... 255-262

Patlamalı Kaynak Yöntemi Kullanılarak S235jr Levha Yüzeylerinin Östenitik Paslanmaz Çelik (Aisi 316l) Ve Ferritik Paslanmaz Çelik (Aisi 430) Levhalar İle Kaplanabilirliğinin Araştırılması

Özer Pamuk, Ahmet Durgutlu..... 263-272

Investigation Of Microstructure And Corrosion Properties Of The Inconel 625 Weld

Mustafa Tümer, Alptekin Kısasöz, Ahmet Karaaslan, Mithat Kerimak..... 273-277

Trip Çeliklerinin Plazma Ark Kaynak Kabiliyeti

*Büşra Karaoğlu, Ramazan KAÇAR, Hayriye Ertek EMRE, Batuhan BOZKURT
..... 278-287*

Kaynak İlerleme Hızının Lazer Kaynaklı Titanyum (Grade 5) Alaşımının Mikroyapı Ve Mekanik Özelliklerine Etkisi

Şennur ARSLAN, Hayriye ERTEK EMRE, Ramazan KAÇAR..... 288-302

A Research On The Difference Between Automated And Hand Made Esd Coatings Produced On Steel Plates

Ş. Talaş, B. Gökçe, Y. Kayalı..... 303-308

Otomatik Esd Kaplama İçin Mekatronik Bir Sistem Tasarımı

B. Gökçe, Ş. Talaş 309-316

The Influence Of Thickness Of Interlayer Materials: Bonding Time And Bonding Pressure On Bonding Strength In Diffusion Welding

Ömer Faruk Özbilen, Ali Gürsel, Enes Akca 317-323

3D Surface Morphology And Roughness On Treated Surface Of Ti-6al-4v Alloy By Nd:Yag Laser: Effect Of Spot Size

Ali GURSEL 324-335

The Effect Of Pulse Duration On Nd:Yag Laser Surface Treatment For Ti-6al-4v Alloy

Ali GÜRSEL..... 336-353

Joinability Of Brass Alloy By Furnace And Microwave Brazing

Yasemin Aksu, İrem Burcu Algan, Ramazan Çıtak, Adem Kurt 354-359

Sandwich Composite Production By Forming And Joining Sic Ceramic Foams Between Al Foam Plates

*Ersin BAHÇECİ, Yusuf ÖZÇATALBAŞ, Volkan AYLIKCI, Mehmet Hakan DEMİR, Tolga DEPCI
..... 360-368*

Effect Of Filler Wire Chemical Composition On Joint Properties Of 1050aluminum Alloy	
<i>Oktay Cetinel, Volkan Kilicli, Hakan Ates,.....</i>	<i>369-374</i>
Residual Stress Changes After Heat Treatment On Smaw Welded Plates	
<i>Galip BÜYÜKYILDIRIM, Georgy BATOV.....</i>	<i>375-384</i>
Electroplating Of Passive Metal Hydroxide Coating On Steel For Corrosion Prevention	
<i>Metin Bedir, Abdulcabbar Yavuz.....</i>	<i>385-394</i>
Arc Stud Welding Of Hollow Parts With Different Cross Sections	
<i>Necip Fazıl YILMAZ, M. Veysel ÇAKIR, H. Ahmet EROL.....</i>	<i>395-405</i>
Investigation Of Carbide Precipitation Of Tig Welded Aisi 304 Pipes	
<i>Necip Fazıl Yılmaz, Musa Yılmaz, Mahmut Furkan Kalkan.....</i>	<i>406-414</i>
Joinability Of Different Powder Metal Materials With Microwave And Induction Heating	
<i>İrem Burcu Algan, Yasemin Aksu, Yusuf Çiftçi, Nurcan Ünlü Ramazan Çıtak, Yusuf Özçatalbaş, Adem Kurt</i>	<i>415-420</i>
Automated Ultrasonic Testing For Spirally Saw Welded Pipes	
<i>Hakan ATEŞ, Galip BÜYÜKYILDIRIM.....</i>	<i>421-429</i>
Nokta Direnç Kaynaklı İleri Yüksek Mukavemetli Çelik Saclarin Taguchi Metodu İle Dayanım Optimizasyonu	
<i>Ramazan KAÇAR, Khaled Omer Marwan, Hayriye ERTEK EMRE.....</i>	<i>430-438</i>
Gas Metal Arc Weldability Of Aa5083-A Grade Couple By Using Transition Plate	
<i>Alparslan Parlak,Ramazan Kaçar.....</i>	<i>439-452</i>
Nokta Direnç Kaynağı İle Çelik Hasir Örgü İmalatında Kaynak Akiminin Birleşmeye Etkisi	
<i>Adem KURT, Aytaç TALAŞ, Emre ALPKAYA, Yusuf ÖZÇATALBAŞ.....</i>	<i>453-461</i>
Investigation Of Diffusion Area Of WC-Co Part Produced By Inserted Powder Injection Molding Method	
<i>Harun KOÇAK, Mehmet SUBAŞI , Çetin KARATAŞ</i>	<i>462-470</i>
Farkli Toz Metal Malzemelerin Mikrodalga Ve İndüksiyon Isıtma İle Birleştirilebilirliği	
<i>İrem Burcu Algan, Yasemin Aksu, Yusuf Çiftçi, Nurcan Ünlü, Ramazan Çıtak, Yusuf Özçatalbaş,Adem Kurt.....</i>	<i>471-476</i>

Invar36 Çeliğinin Mig Kaynak Yöntemi İle Kaynaklanabilirliğinin Araştırılması	
<i>Selçuk Tombul, Mehmet AKKAŞ, Mustafa BOZ.....</i>	<i>477-483</i>
Solid State Diffusion Welding Of Copper With Aluminum Alloy	
<i>Walid Bedjaoui, Zakaria Boumerzoug, Lamia Baghdadi.....</i>	<i>484-489</i>
Api Borularinin Kaynakli Birleştirmelerinde Akma Mukavemeti Değerlerinin Taguchi Metodu İle Optimizasyonu	
<i>Hakan ADA, Cemil ÇETİNKAYA, Tayfun FINDIK, Ahmet DURGUTLU.....</i>	<i>490-502</i>
Ray Birleştirmede Alüminotermite Ve Yakma Alın Kaynak Yöntemleri; Teknik Ve Maliyet Yönünden Karşılaştırılması	
<i>M. Emin AKAY, Fikri DEMİR.....</i>	<i>503-514</i>
Metal-Metal Kompozit Üretiminde Döküm Birleştirme Tekniği Ve Normalizasyonun Etkilerinin İncelenmesi	
<i>Hasan HASIRCI.....</i>	<i>515-525</i>
EN 10346:2015 Çeliği Nokta Direnc Kaynağının Sonlu Elemanlar İle Analizi	
<i>Ahmet Çetkin, Mehmet Çakmakkaya, Halil AYTEKİN.....</i>	<i>526-536</i>
The Effects Of Welding Parameters On Penetration In Duplex Stainless Steels Weldments	
<i>Ramazan Yılmaz, Merve Koruç.....</i>	<i>537-544</i>
Dissimilar Welding Of Aisi 316l And Aisi 2205 Stainless Steels By Gtaw	
<i>Ramazan Yılmaz, Büşra Nur Yıldırım, Esra Tokmak.....</i>	<i>545-554</i>
Soğuk Basınç Kaynağında Basınç Periyotunun Birleşebilirliğe Ve Elektriksel İletkenliğine Etkisi	
<i>Hüseyin KÜÇÜKÖNER, Adem KURT.....</i>	<i>555-565</i>
Çelik Yapılarda Kullanılan T Profilin Kaynakli İmalatında Oluşan Açısız Distorsiyonların Optimizasyonu	
<i>İlhan YİĞİT, Serkan APAY.....</i>	<i>566-574</i>
Electrical And Optical Properties Of Cadmium Oxide Carbon Nanotube Nanocomposite	
<i>Ömer Güler, Öyküm Başgöz, M. Gökhan Albayrak, Seval Hale Güler, Mehmet Takgün, Kazım Buğra Gürbüz, Mustafa Taşkın.....</i>	<i>575-592</i>

The Effect On Tensile-Shear Strength Of Electrode Plunge Depth Depending On Welding Time In Resistance Spot Welding Of Trip 800 And Micro Alloyed Steel Sheets

Volkan Onar, Fatih Özen, Uğur Özserağ, Melih Kekik, Yusuf Sadi Aslanlar, Salim Aslanlar.....593-599

Effect Of Nugget Sizes On Tensile-Shear Strength In Resistance Spot Welding Of Trip 800 And Micro Alloyed Steel Sheets Used In Automotive Industry

Volkan Onar, Uğur Özserağ, Fatih Özen, Melih Kekik, Yusuf Sadi, Aslanlar, Salim Aslanlar600-608

İstihdam Odakli Yeni Bir Mesleki Ve Teknik Eğitim Modeli Tasarimi

Mehmet YAZAR, Mustafa KÖROĞLU.....609-619

An Investigation On The Diffusion Bonding Ability Of B4c-Fe-Ni Ceramic-Metal Composites

Ahmet.YONETKEN, Ayhan. EROL.....620-628

The Effect Of Thermal Cycle On Mechanical Properties Of Trip Steels In Gas Metal Arc Welding(Gmaw)

Gökhan ERİAN, Adem KURT.....629-643

Overview of Recent Progress in Soldering Materials

Muhamad Zamri Yahaya, Ahmad Azmin Mohamad.....644-650

Investigation On Wear Behaviors Of WCAnd Ti6al4V Coated AISI 316l Stainless Steel By Esd Coating Method

Yusuf KAYALI, Şükrü TALAŞ.....651-659

Toz Metalurjisi İle Üretilen Malzemelerin Lazer Kesme Üzerine Bir Araştırma

Ş. Talaş, Y. Kayalı, A. Çetkin.....660-666

EFFECT OF WELDING TIME AND CURRENT PARAMETERS ON TENSILE-SHEAR STRENGTH OF SPOT WELDED TWIP1000/MARTENSITIC1500 STEEL JOINTS

Fatih Özen^{1,a}, Volkan Onar^{2,b}, Yusuf Sadi Aslanlar^{3,c}, Zafer Barlas^{1,d}, Uğur
Özsaraç^{1,e}, Salim Aslanlar^{1,f}

¹Sakarya University of Applied Sciences, Faculty of Technology, Sakarya, Turkey
²Pamukkale University, Faculty of Technology, Denizli, Turkey
³Yıldız Kalp A.Ş., R&D Center, Arnavutköy, Istanbul, Turkey
^afatihozen@sakarya.edu.tr, ^bvonar@pau.edu.tr, ^cyusuf.aslanlar@yildizkalip.com,
^dyusuf.aslanlar@yildizkalip.com, ^eozsarac@sakarya.edu.tr, ^faslanlar@sakarya.edu.tr

Abstract

Recently, material technologies in automotive industries have been advanced with an unprecedented pace. Various materials needs in different sections of automobiles give rise to special material designs. For example; twinning induced plasticity (TWIP) steels have been designed for crash parts. Since, TWIP steels absorb more energy at crash moment than any conventional steels. High energy absorption made the crash elements on automobile more safe. Another significant material among Advanced High Strength Steels is Martensitic Steels. These steels have high strength values with low elongations and it allow reducing fuel costs by lighten the automobile chassis. Although these materials have upmost properties, its properties are bound to its welding quality. Due to this reason welding quality of advanced materials should be investigated in detailed. In this work, tensile shear strengths of spot welded TWIP1000/MS1500 steels have been investigated in terms of current intensities and welding times. The results shows that high Mn content in high heat inputs heavily affect tensile-shear strengths of TWIP/Mart joints.

Key Words: Martensitic Steels, TWIP steels, Resistance Spot Welding, AHSS.

1. Introduction

Advanced High Strength Steels have been widely utilized because of sensibility greenhouse gas emissions in automotive industries [1]. Among Advanced High Strength Steels (AHSS), TWIP steels have gained high importance because of excellent mechanical properties such as high tensile strength with high elongation [2]. These austenitic steels have high Mn content which reduces stacking fault energy (SFE). Deformation twins which causes also deformation hardening are formed because of low SFE that controls dislocation gliding [3-4]. As twins come into being, the grain sizes gradually decreases. The refined grains increase strength of steel. This situation have been called as “Dynamic Hall-Petch effect”[5]. This effect also increases elongation at break. However, these steels have some troubles such as expensive, poor weldability [6].

Another brilliant steel in AHSS family is Martensitic (Mart) steels. Mart steels have high strength with limited elongation due to high martensite content in ferrite matrix with low carbon

content [7]. Mart steels have been used for raising safety and lightening purposes such as load transferring barriers, B-pillars, anti-intrusion and high stiffness parts.

Basically, joining of dissimilar metals allows the designer to versatility for different working conditions. Welding is a common joining method for metal joints. Especially, Resistance Spot Welding (RSW) is the most utilized technique in automotive industry[8-9]. Because it is cheap, quick and reliable. However, During design of the body-in-white especially joined with RSW, as well as material properties, mechanical properties of welded structures also should be taken into account. Because local heat input generated during welding may distort the microstructure of joints which causes unexpected failures [9]. The welded dissimilar metals can be said successful when strength and ductility of the metals are at least equal to the weaker of the joint metal [10].

However, TWIP steels are hard to weld compared to low carbon steels because of high Mn content [11]. Mart steels are also of high importance on Body-in-white. However, As well as their own mechanical properties, mechanical performance of joints should be considered.

In this work, effects of welding parameters on tensile-shear performance of Mart1500/TWIP1000 have been investigated. Also, some failures and microstructural problems have been inspected.

2. Experimental Procedure

The TWIP1000 used in this study were obtained from Posco via Tiberina Automotive, a local sheet part manufacturer. Mart steel were supplied from SSAB through Çelikform Gestamp. Their chemical compositions and tensile properties are shown in Table 1. The thickness of TWIP and Mart steel were 1.5 and 2 mm respectively.

Table 1. Chemical compositions and tensile properties of investigated materials

	% wt						Tensile Properties		
	C	Mn	Si	Al	S	Cu	YS (Mpa)	US (Mpa)	EL. (%)
Mart1500	0.28	1.3	0.4	0.015	0.01	0.2	1220	1510	3,1
TWIP1000	0.503	16.77	0.201	2.808	0.255	-	410	963	44

The experiment materials were sliced to 100x30 mm. Then, the specimens overlapped and positioned with a fixture and welded. The dimensional details are shown in Figure 1.

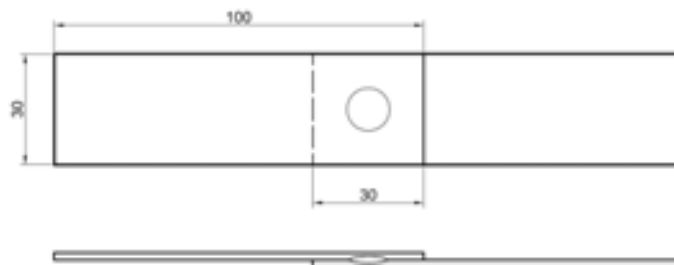


Figure 1. Dimensional details of Tensile-shear specimens

Figure 2 illustrates welding parameters used in experiments. Welding currents have been adjusted between 4-16,5 kA with 1.5 kA current increments. These values have been determined by nugget formability in 5 period welding time (1 period=0.02 sec). Below 4 kA currents nugget diameter was too low. Above 16,5 kA currents, the nugget was too thin to bear any useful loads. Squeezing times before welding and holding time after welding were adjusted to 25 period. The welding times were selected between 5-30 periods with 5 period increments. The electrode force was kept constant as 5 kN. A current and timer controlled 120 kVA capacity RSW machine with single pneumatic lever mechanism was used.

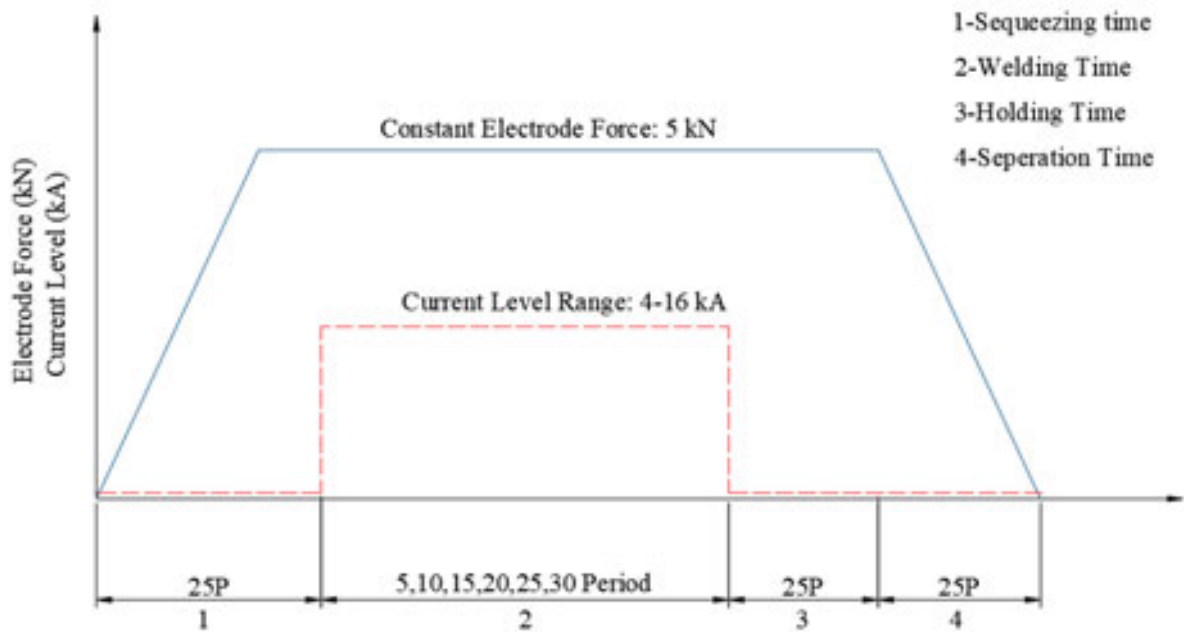


Figure 2. Adjusted welding cycles of RSW machine.

Nikon Nikon Eclipse L150A stereo microscope was used for observations. Also, the welded specimens have investigated by JEOL JSM-5600 Scanning Electron Microscope (SEM). Tensile-Shear tests executed with Shimadzu universal tensile machine having 50 kN capacity.

3. Result and Discussions

3.1. Effect of Current Intensity on Tensile-Shear Strengths

Figure 3 shows effect of welding currents on tensile shear load capacity of Mart1500 and TWIP1000 RSW joints. As seen from the figure, in lower currents in 5 period have the lowest tensile- shear strength and also interfacial fracture was occurred in 6.3 kA. The highest tensile shear load have been obtained in 30 period in 6.3 kA currents. However, above 6.3 kA in 30 period, there have been a sharp decrease in tensile-shear loads. The similar decrease can be seen in the whole periods. It is attributed to low undercut due to high softening of weld section, expulsions and Mn evaporation which will be discussed on next subsections[12] .

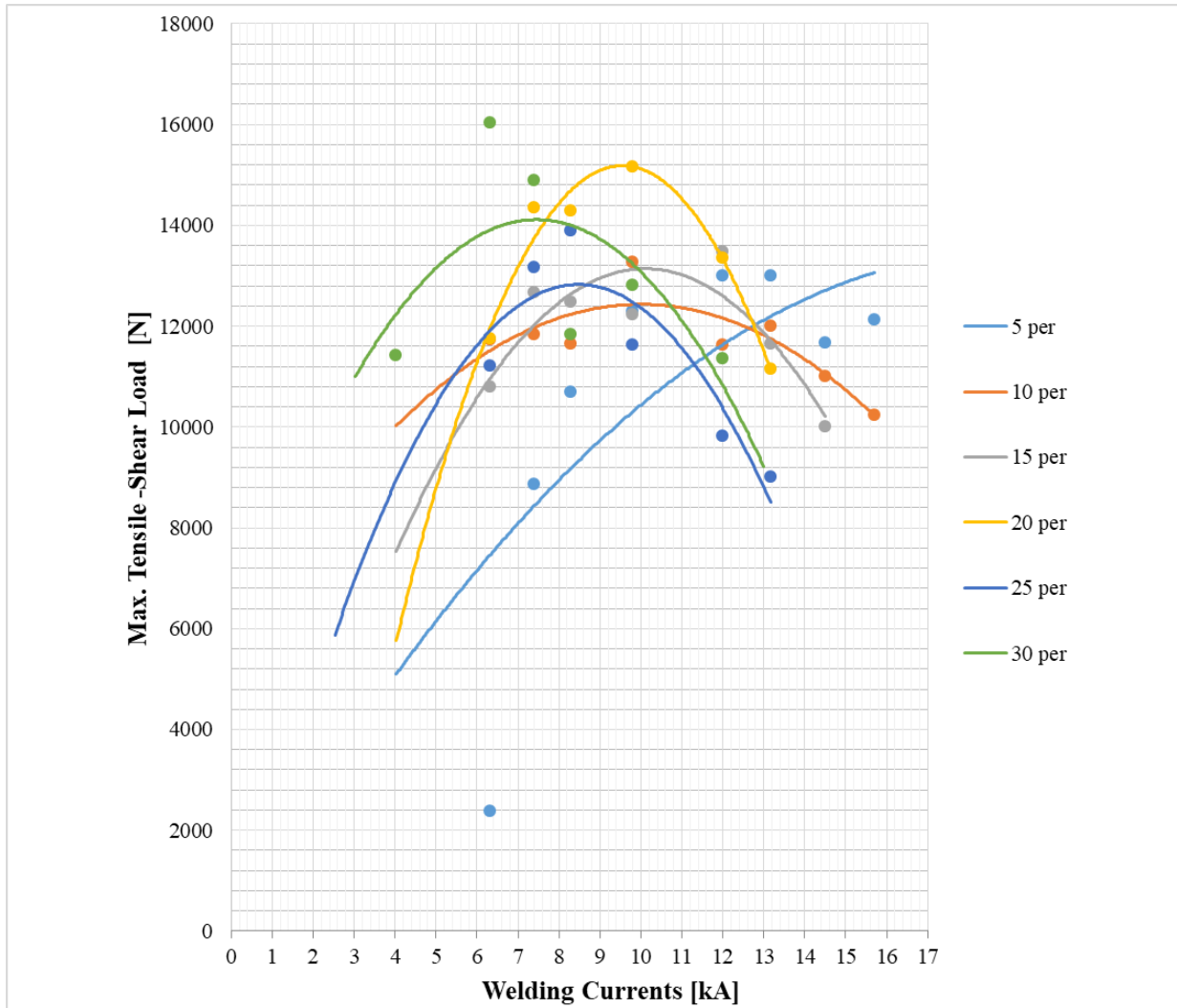


Figure 3. Effect of current levels on Tensile-Shear Strengths

3.2. Effect of Welding Times on Tensile-Shear Strengths

Effect of welding currents on tensile-shear bearing capacity of joints is illustrated in Figure 4. In highest current intensities, applicable current ranges decreased. Up to 14.5 kA currents, the tensile-shear strengths have been increased. However, above 14.5 kA current levels, the applicable welding ranges have been limited because of expulsions and too high undercuts [13]. Above these limits, there have been even drilling on the joint due to high undercut. Additionally, except for 13.6 and 14.5 kA welding currents, there have been an increase and a decrease in tensile-shear strengths. This increase and decrease are caused by heat inputs. Heat input can be described with (1). Here, Q is heat input, I is welding current, R is total resistance of joints including surface resistances, and t is welding time[14]. On climax points, heat input (Q) reaches optimum value. The high heat input in high welding times causes shrinkage voids, evaporation voids and secondary phases. These factors highly affect tensile-shear strengths of joints[15].

$$Q=I^2Rt \quad (1)$$

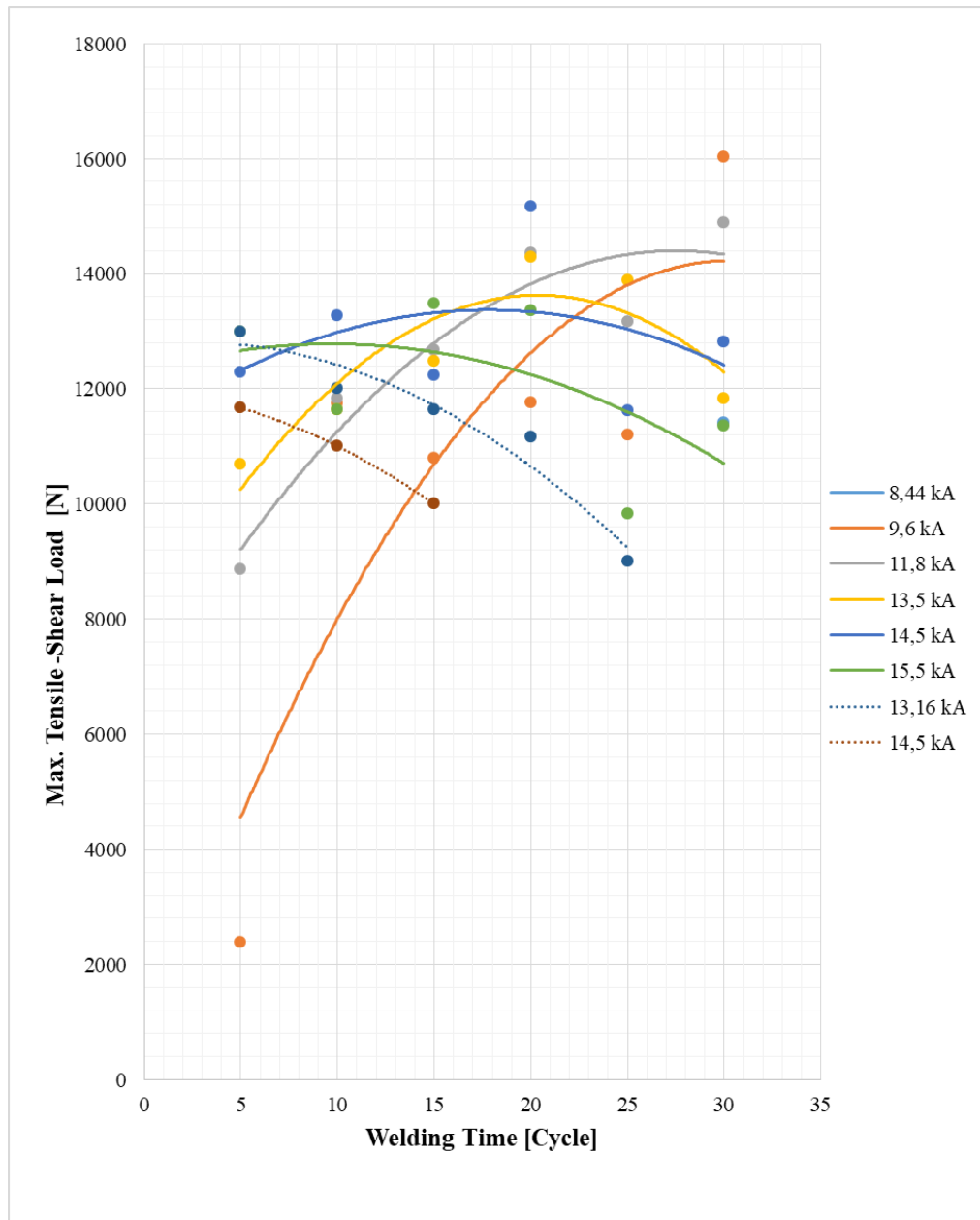


Figure 4. Effect of current levels on Tensile-Shear Strengths

3.3. Optical and SEM Observations

Figure 5 shows a interfacial separation in consequence of tensile-shear test. The image have been captioned with multi-layer grab technique, collecting best displaying pixels and combining in an image. The full round voids originating from evaporation of Mn can easily be seen. This situation also described in literature. Ma [16] reported that there have been violent Mn evaporation in laser beam welded TWIP joints in the light of EDS results. These round voids reduce the bearing capacity of tensile-shear load.

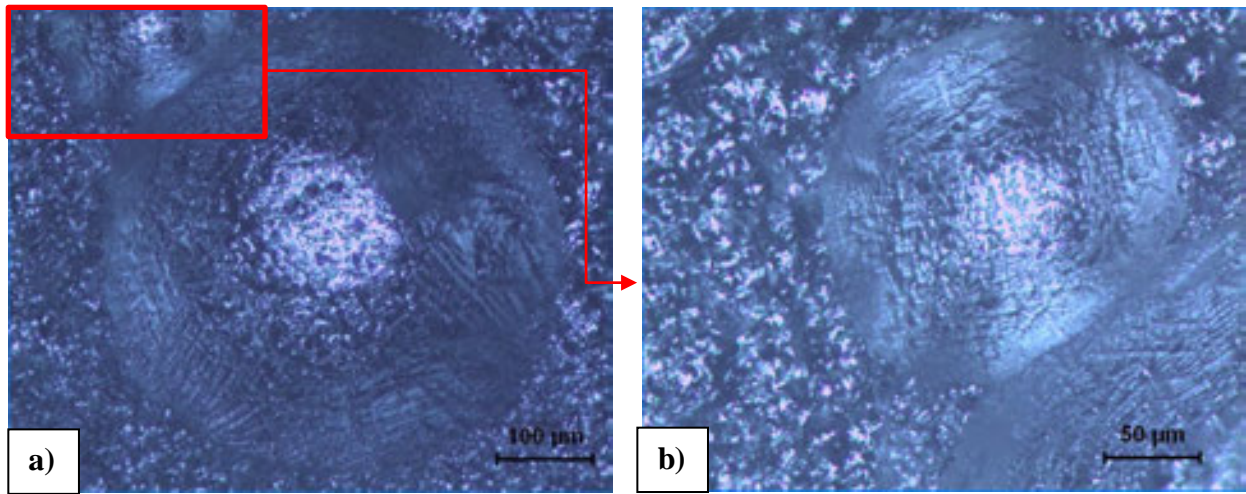


Figure 5. Separation interface of TWIP/Mart specimen a)100x b)50x

Figure 6. shows the cross section of weld nugget. As seen from the figure, although some of the voids are round which indicates evaporation of Mn, the others also indicates evaporation and shrinkages[17]. This situation also attributed to inhomogeneity of Mn in fusion zone. The Mn concentrated regions induces larger Mn evaporation voids. The Heat Affected Zones (HAZ) also exhibited Mn induced voids. These porosities highly reduces tensile-shear strength.

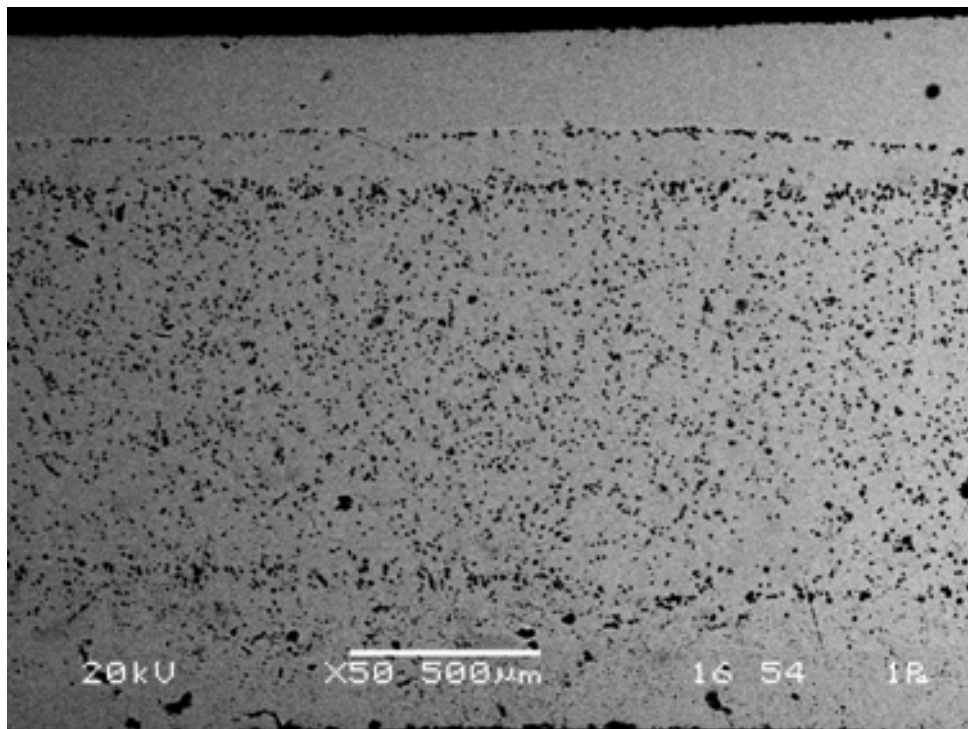


Figure 6. SEM⁶ image of weld nugget

4. Conclusion

Among the most promising AHSSs, TWIP and Mart steel joined with RSW technique. Based on this study following conclusions can be drawn;

- 1- As welding current levels and welding time increased, the applicable welding ranges decreased.
- 2- As welding current levels and welding time increased, the tensile-shear strengths increased to a value, then decreased.
- 3- The high Mn content vaporizes in high heat inputs causes rounded voids which reduces tensile-shear strengths of joints.
- 4- The heat input should be strictly controlled to obtain sound joints. Because high Mn content is heavily affected by heat input.
- 5- The maximum tensile-shear load achieved in 30 period welding time and 9,6 kA welding currents as 16056 N.
- 6- Preheating and slow cooling can be recommended for TWIP/Mart joints.

5. Acknowledgement

The authors would like to thank for material support of Tiberina and Çelikform Gestamp companies.

6. References

- [1]Y. Liu, D. Dong, L. Wang, X. Chu, P. Wang, and M. Jin: Strain rate dependent deformation and failure behavior of laser welded DP780 steel joint under dynamic tensile loading, *Materials Science and Engineering A*, 627 (2015), pp. 296–305.
- [2]J. Kovac, J. Epp, A. Mehner, B. Köhler, B. Clausen, and H. W. Zoch: On the potential of magnetron sputtering for manufacturing of thin high Mn TWIP steel foils, *Surface and Coatings Technology*, 308 (2016), pp. 136–146.
- [3]K. T. Park: Tensile deformation of low-density Fe-Mn-Al-C austenitic steels at ambient temperature, *Scripta Materialia*, 68 (2013), pp. 375–379.
- [4]K. Jeong, J. E. Jin, Y. S. Jung, S. Kang, and Y. K. Lee: The effects of Si on the mechanical twinning and strain hardening of Fe-18Mn-0.6C twinning-induced plasticity steel, *Acta Materialia*, 61 (2013), pp. 3399–3410.
- [5]T. Niendorf and F. Brenne: Steel showing twinning-induced plasticity processed by selective laser melting - An additively manufactured high performance material, *Materials Characterization*, 85 (2013), pp. 57–63.
- [6]S. J. Lee, Y. Sun, and H. Fujii: Stacking-fault energy, mechanical twinning and strain hardening of Fe-18Mn-0.6C-(0, 1.5)Al twinning-induced plasticity steels during friction stir welding, *Acta Materialia*, 148 (2018), pp. 235–248.
- [7]D. M. Fabijanic and T. B. Hilditch: Effect of carburising on geometrical control during quenching of martensitic sheet steel channels, *Journal of Materials Processing Technology*, 212 (2012), pp. 1802–1809.
- [8]J. P. Kong, T. K. Han, K. G. Chin, B. G. Park, and C. Y. Kang: Effect of boron content and

welding current on the mechanical properties of electrical resistance spot welds in complex-phase steels, *Materials and Design*, 54 (2014), pp. 598–609.

[9]A. Ramazani, K. Mukherjee, A. Abdurakhmanov, M. Abbasi, and U. Prahl: Characterization of Microstructure and Mechanical Properties of Resistance Spot Welded DP600 Steel, *Metals*, 5 (2015), pp. 1704–1716.

[10]A. Angelastro, G. Casalino, P. Perulli, and P. R. Spena: Weldability of TWIP and DP steel dissimilar joint by laser arc hybrid welding with austenitic filler, *Procedia CIRP*, 67 (2018), pp. 607–611.

[11]B. C. De Cooman, O. Kwon, and K.-G. Chin: State-of-the-knowledge on TWIP steel, *Materials Science and Technology*, 28 (2012), pp. 513–527.

[12]M. H. H. Razmpoosh, M. Shamanian, and M. Esmailzadeh: The microstructural evolution and mechanical properties of resistance spot welded Fe – 31Mn – 3Al – 3Si TWIP steel, *Materials and Design*, 67 (2015), pp. 571–576.

[13]J. P. Kong, T. K. Han, K. G. Chin, B. G. Park, and C. Y. Kang: Effect of boron content and welding current on the mechanical properties of electrical resistance spot welds in complex-phase steels, *Materials and Design*, 54 (2014), pp. 598–609.

[14]J. F. Lancaster: *Metallurgy of welding*, Sixth Edit., (1999). Cambridge, England: Abington Publishing, 1999.

[15]J. Lorthios, M. Mazière, X. Lemoine, P. Cugy, J. Besson, and A. F. Gourgues-Lorenzon: Fracture behaviour of a Fe-22Mn-0.6C-0.2V austenitic TWIP steel, *International Journal of Mechanical Sciences*, 101–102 (2015), pp. 99–113.

[16]L. li Ma, Y. hui Wei, L. feng Hou, and B. Yan: Microstructure and mechanical properties of TWIP steel joints, *Journal of Iron and Steel Research International*, 21 (2014), pp. 749–756.

[17]K. Han, J. Yoo, B. Lee, I. Han, and C. Lee: Effect of Ni on the hot ductility and hot cracking susceptibility of high Mn austenitic cast steel, *Materials Science and Engineering A*, 618 (2014), pp. 295–304.

CORRESPONDENCE ADDRESS: Fatih ÖZEN, Sakarya University of Applied Science, Faculty of Technology, Sakarya,

Telephone: +90 264 295 64 82

E-mail address: fatihozen@sakarya.edu.tr

SHORT BIOGRAPHIES

Fatih ÖZEN –He was born in Trabzon, Turkey in 1989. He graduated from Sakarya University, Faculty of Engineering, Mechanical Engineering department. He is PhD student in Manufacturing engineering. He is research assistant since 2014 in Sakarya University. His main interest area are welding and manufacturing processes.

Volkan ONAR – He was born in İstanbul in 1984. He completed his primary and secondary education in Kocaeli. He got B.Sc. degree from Gazi University, Department of Technical Education in 2007. Besides, He graduated M. Sc. Degrees from Gazi University, Department of Metal Education in 2010. He graduated Ph. D. at Sakarya University, Department of Metarial and Metalurgy Engineering in 2017. He worked as a Research Assistant in the Department of Manufacturing Engineering at Pamukkale University 2012 to 2017. He has been working as a Assistant Professor in the Department of Mechanical and Manufacturing Engineering at Pamukkale University since 2017.

Uğur ÖZSARAÇ – He was born in Çorum, Turkey in 1971. He graduated from METU, Department of Metallurgical Engineering as an engineer in 1995. He started to Sakarya University as Research Assistant. He has been working in same University as an Associate Professor since 1995. His research areas are Welding metallurgy, Brazing and cold metal transfer (CMT)

Yusuf Sadi ASLANLAR–He was born in Sakarya in 1993. He completed my primary, secondary and high school education in Sakarya. He got B.Sc. degree from Sakarya University, Department of Industry Engineering in 2016. He has been continuing M. Sc. Degrees at Sakarya University, Department of Metarial and Metalurgy Engineering since 2016.

Zafer BARLAS– He was born in İstanbul, Turkey, in 1976. He received the Ph.D. degree from Sakarya University, Turkey, in 2009. He is an associate professor from Sakarya University since 2016 and works welding techniques especially frictional methods.

Salim ASLANLAR– He was born in Adapazarı, Turkey, in 1963. He completed primary, secondary and high school in Adapazarı. he graduated from fachhochschule niederrhein university in krefeld, Germany as a high engineer in 1987 after completing mechanical engineering construction and manufacturing department successfully. He received the Ph.D. degree from Sakarya University, Turkey, in 2009. He has been working in same University as an Professor. His research areas are Welding metallurgy, Brazing, cold metal transfer (CMT), AHSS and bonding techniques.

TENSILE PEEL STRENGTH OF RESISTANCE SPOT WELDED TWIP1000/MS1500 JOINTS

Fatih Özen^{1,a}, Volkan Onar^{2,b}, Yusuf Sadi Aslanlar^{3,c}, Zafer Barlas^{1,d}, Uğur
Özsaraç^{1,e}, Salim Aslanlar^{1,f}

¹Sakarya University of applied sciences, Faculty of Technology, Sakarya, Turkey

²Pamukkale University, Faculty of Technology, Denizli, Turkey

³Yıldız Kalıp A.Ş., R&D Center, Arnavutköy, Istanbul, Turkey

^afatihozen@sakarya.edu.tr, ^bvonar@pau.edu.tr, ^cyusuf.aslanlar@yildizkalip.com,
^eyusuf.aslanlar@yildizkalip.com, ^dbarlas@sakarya.edu.tr, ^eozsarac@sakarya.edu.tr,
^faslanlar@sakarya.edu.tr

Abstract

Reducing carbon emissions are of high importance in these days. Moreover, fossil fuels are have been significantly decreased. These compelling situations caused applying strict measures for increasing efficient fuel utilization and fuel saving policies for automotive manufacturers. One of the most important measures is reducing car weight without reducing the safety of automobiles. These reasons bring about new material designs. TWIP steels and Martensitic Steels can be given as example. TWIP steels combine high elongation and high strength. On the other hand, MS have high strength with low elongation compared to conventional metals which allows lighter part designs on automobile. However, the mechanical properties of these materials not always mean this design works. Since, mechanical properties of joints have to be considered. In this study, tensile-peel strengths of TWIP1000/MS1500 steel have been investigated under different welding time and current levels. Maximum tensile-peel strength of TWIP/Martensitic steels was obtained in 7.4 kA welding currents and 20 period welding times as 2050 N.

Key Words: AHSS, Resistance Spot Welding, Martensitic Steels, TWIP steels.

1. Introduction

As automotive industry manufactured more comfortable and high quality vehicles, weights of cars have been gradually elevated. The increase in weights resulted in higher standards for safety. Then, the vehicles regained weight[1]. This situation raised a question “Is it possible to reduce the weight without reducing the safety?”. Today, the right answer to this question is Advanced High Strength Steels (AHSS).

AHSS offer exceptional enhancements compared to traditional steels such as high safety, high stiffness and reduced car weight that highly affect fuel consumptions which also means reduced emissions to air with different mechanical property combinations [1-2].

Among AHSSs, TWIP steels are of high importance due to high elongation with high tensile strength attained by strain induced twinning effect [3-5]. High Mn content of TWIP steels lowers Stacking Fault Energy (SFE) that give rise to twinning [6]. Deformation twinning results in increase in strain hardening rate, because it limits dislocation gliding which act as obstacle [7]. This situation also means that higher energy absorption can be achieved by dissipating kinetic

energy by plastic deformation[8-9]. Therefore, TWIP steels have found extensive usage area on automotive body such as crash boxes [9].

However, processing and welding of high Mn steels are too difficult [10]. Considering joining on automotive chassis, the most utilized method is Resistance Spot Welding (RSW) [11]. It is reported that a vehicle can contain more than 3000 spot welds [12]. Considering the problems about welding of TWIP steels, it can be drawn that weldability of these steels with new generation AHSSs should be studied in detail.

Martensitic steels with exceptional ultimate tensile strength have been newly utilized in automotive bodies. These steels contains high amount of martensite in a ferrite matrix [13]. Some of the grades of martensitic steels can achieve up to 1700 Mpa tensile strength.

In this study, effect of welding parameters on tensile-peel strength of Mart1500/TWIP1000 has been investigated. Also, some failures and microstructural problems have been inspected.

2. Experimental Procedure

The TWIP steels with 1.5 mm thickness were acquired from Posco by a local dealer. Martensitic Steels having 2 mm thickness were supplied from SSAB through Çelikform Gestamp. Tensile strengths and chemical compositions are illustrated in Table 1.

Table 1. Chemical compositions and tensile strengths of experiment materials

	% wt						Tensile Properties		
	C	Mn	Si	Al	S	Cu	YS (Mpa)	US (Mpa)	EL. (%)
Mart1500	0.28	1.3	0.4	0.015	0.01	0.2	1120	1510	3,1
TWIP1000	0.503	16.77	0.201	2.808	0.255	-	410	963	44

The specimens were sliced to 30x100 mm, positioned with a fixture and welded through 6mm diameter Cu electrodes under 5 kN electrode force. Then, the welded specimen bended 30mm from ends. The dimensional details are shown in Figure 1.

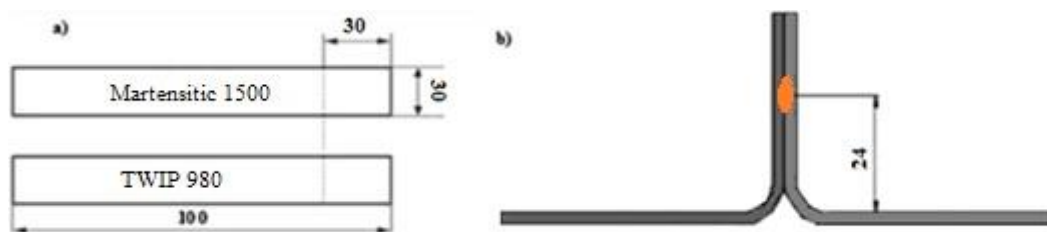


Figure 1. a)Dimensions b) Welding position of Tensile-peel specimens

A timer and current controlled 120 kVA capacity RSW machine with single pneumatic lever mechanism was used. Welding current ranges have been selected between 4-16,5 kA with 1.5 kA current increments. These values have been determined by nugget evolution in 5 period welding time (1 period=0.02 sec). Squeezing times before welding and holding time after welding were adjusted to 25 period. The welding times were selected between 5-30 periods with 5 period increments.

3. Result and Discussions

3.1. Tensile-Peel Strengths in Terms of Current Levels

Effect of current levels on tensile-peel strength of TWIP100/Mart1500 is presented in Figure 2. Except for 20, 25 and 30 period, as current levels increased, there have been a rise in tensile-peel values up to a climax, then, tensile-peel strengths of joins have been decreased. In 20 and upper periods, the climax point have already been reached in lower current levels, tensile-peel bearing capacity have been decreased. This climax points also represents the lower limit values for evaporation voids, shrinkage voids, expulsions and secondary phases[14]. The evaporation of Mn due to high heat input have been mentioned in literature [15]. The lowest tensile peel strengths have been attained in high current levels.

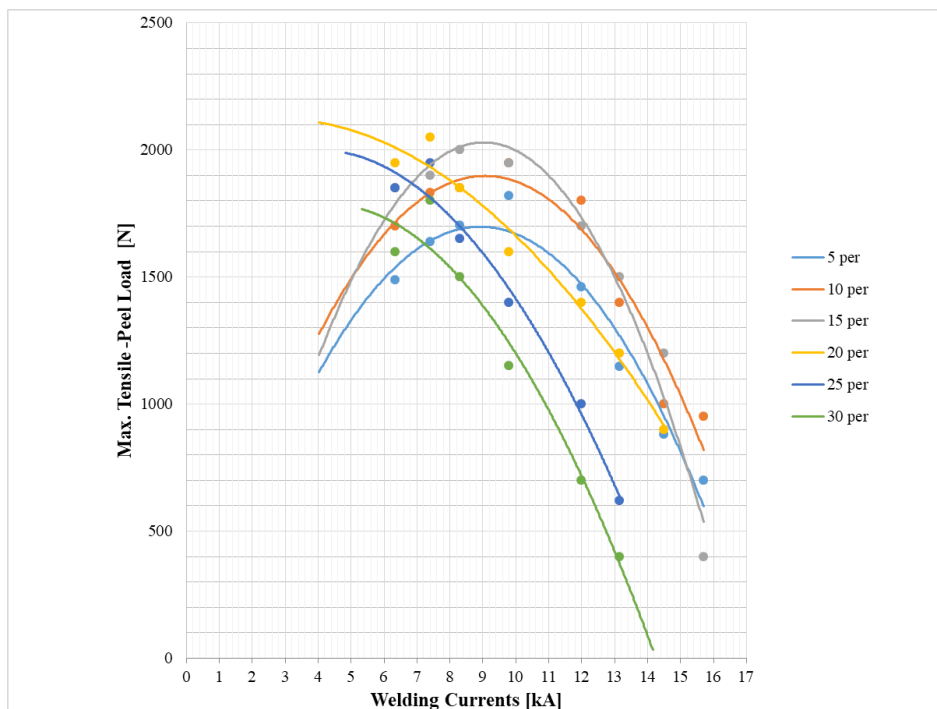


Figure 2. Effect of current levels on Tensile-Peel Strengths

3.2. Tensile-Peel Strengths in Terms of Welding Duration

Effect of welding duration on tensile-peel strength of TWIP1000/Mart 1500 joins are shown in Figure 3. As welding time increases, the tensile-peel strength have been increased and slowly decreased. In each welding currents, the maximum tensile-peel have been obtained between 10-25 period welding times. The maximum tensile-peel strength has been acquired in 20 period welding time and 11.8 kA welding currents. The Mn evaporation and expulsions are main the reason for decreasing in tensile-peel values [15-16].

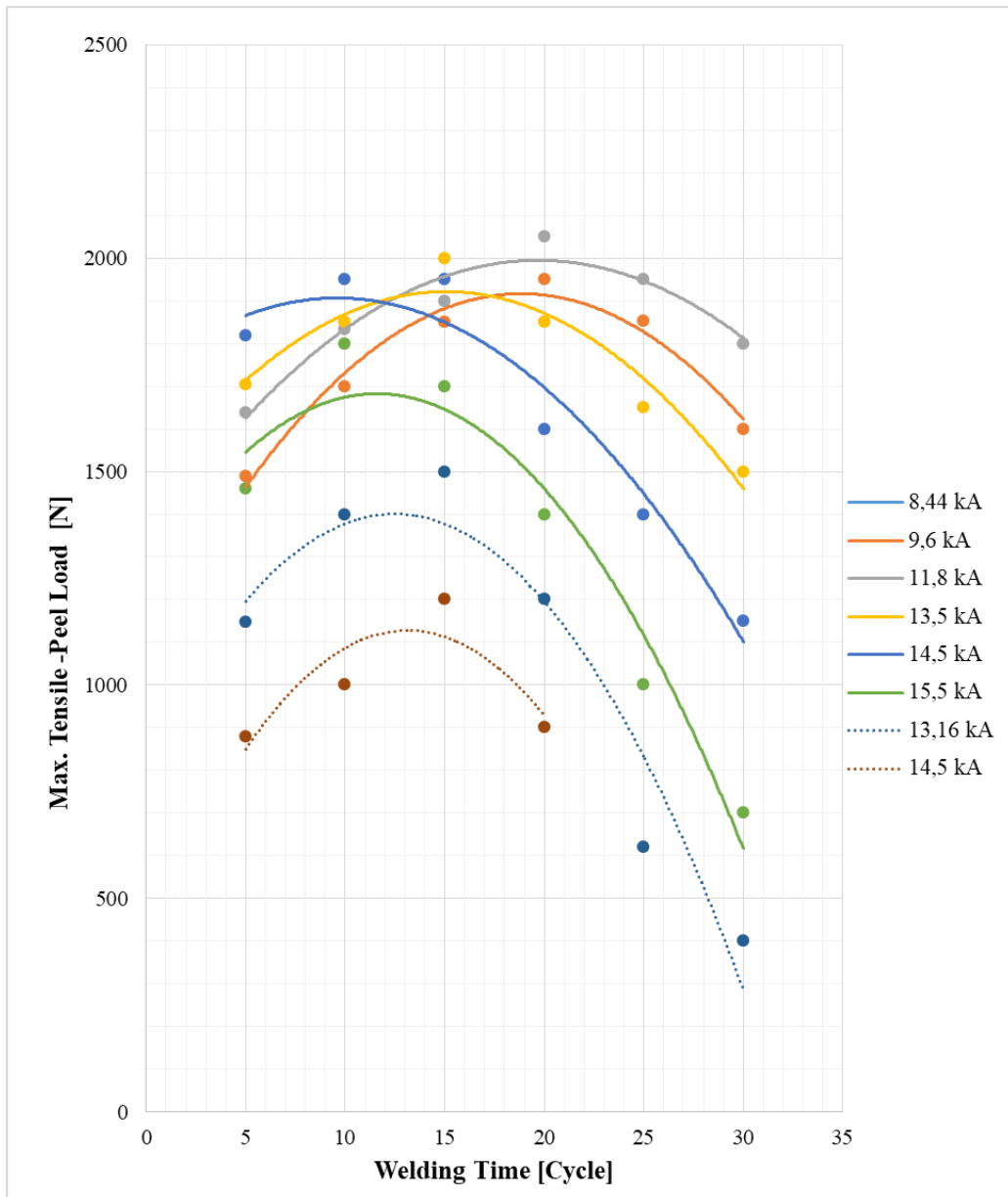


Figure 3. Effect of current levels on Tensile-Peel Strengths

3.3. The observation of separation faces

Some of separation faces of tensile-peel specimens are presented in Figure 4. In Figure 4.a, separation faces of a specimen which has 20 period welding time and 13,5 kA welding current is shown. In these moderate welding conditions, expulsions from weld nugget can be seen. If welding duration and current slightly increases (to 25 period with 2 kA increment), the elevated expulsion rates from weld zone can easily be seen (Figure 4.b). This situation also decreases tensile-peel loads of joints. The main reason behind expulsions is, still, high Mn content which reduces melting point and results in expulsions in low heat inputs compared to martensitic structure[15-16]. The separation modes were pull-out mode above 8,5 kA and 15 period welding times. Below these welding conditions the separation modes were interfacial mode, which also means early stage fracture with low load values.

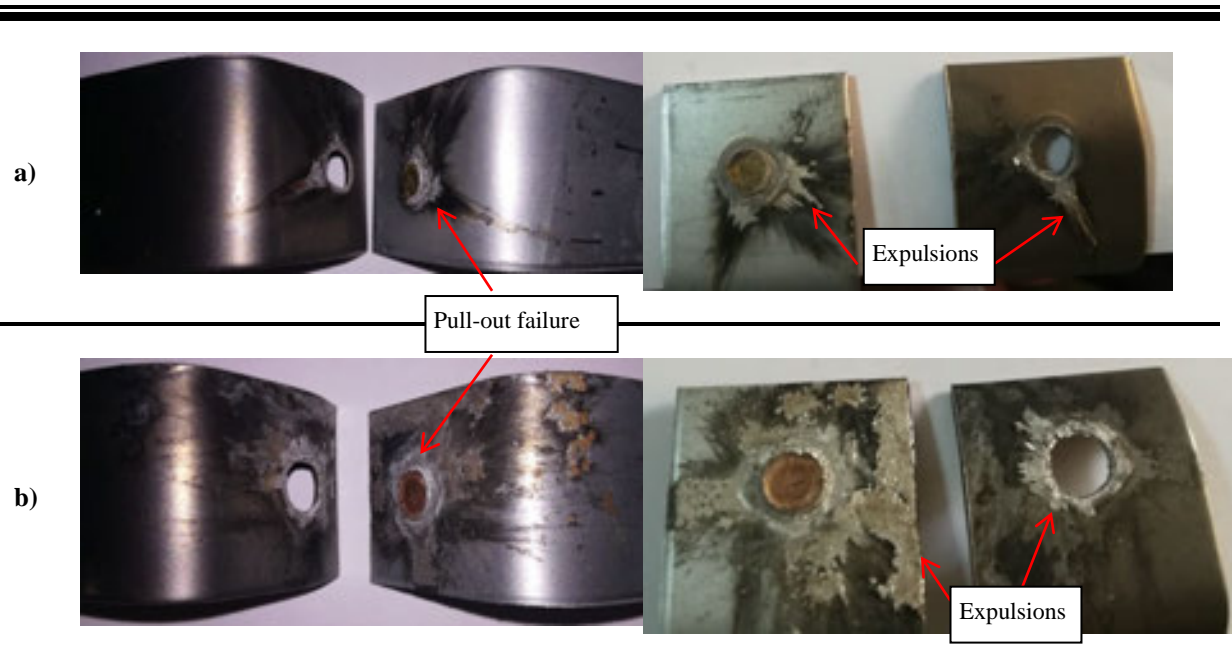


Figure 4. Separation faces of specimens; a) 20 period 13,5 kA, b) 25 period 15,5 kA

4. Conclusion

TWIP steels and Martensitic steels from AHSS family, which are newly utilized in automotive chassis, are of high importance. Especially, weldability of these materials should be investigated in detail due to micro structural differences. Based on this study, following conclusions can be drawn;

- 1- The maximum tensile-peel strength obtained in 20 period, 11.8 kA as 2050 N.
- 2- Mn content adversely affected tensile-peel loads.
- 3- Tensile-peel loads were nominal in low and high currents and welding times.
- 4- Up to 4 kA currents, unacceptable weld nuggets have been developed.
- 5- The sheets can be heated before welding to obtain higher tensile-peel loads by reducing defects.
- 6- The expulsions in moderate welding conditions have been occurred and heavily affected tensile-peel loads.
- 7- Pull-out failures are commonly seen except for low heat inputs.

5. References

- [1] B. C. De Cooman, O. Kwon, and K.-G. Chin: State-of-the-knowledge on TWIP steel, *Materials Science and Technology*, 28 (2012), pp. 513–527.
- [2] B. Mohammed, T. Park, H. Kim, and F. Pourboghrat: Materials Science & Engineering A The forming limit curve for multiphase advanced high strength steels based on crystal plasticity finite element modeling, *Materials Science & Engineering A*, 725 (2018), pp. 250–266.
- [3] S. Brauser, L. A. Pepke, G. Weber, and M. Rethmeier: Deformation behaviour of spot-welded high strength steels for automotive applications, *Materials Science and Engineering A*, 527 (2010), pp. 7099–7108.

- [4] D. Li *et al.*: Influences of Nb-microalloying on microstructure and mechanical properties of Fe-25Mn-3Si-3Al TWIP steel, *Materials and Design*, 84 (2015), pp. 238–244.
- [5] G. Park, S. Jeong, H. Kang, and C. Lee: Improvement of circumferential ductility by reducing discontinuities in a high-Mn TWIP steel weldment, *Materials Characterization*, 139 (2018), pp. 293–302.
- [6] A. Hamada *et al.*: Effect of silicon on the hot deformation behavior of microalloyed TWIP-type stainless steels, *Materials and Design*, 154 (2018), pp. 117–129.
- [7] J. K. Kim and B. C. De Cooman: Stacking fault energy and deformation mechanisms in Fe-xMn-0.6C-yAl TWIP steel, *Materials Science and Engineering A*, 676 (2016), pp. 216–231.
- [8] J. Chen, F. tao Dong, H. long Jiang, Z. yu Liu, and G. dong Wang: Influence of final rolling temperature on microstructure and mechanical properties in a hot-rolled TWIP steel for cryogenic application, *Materials Science and Engineering A*, 724 (2018), pp. 330–334.
- [9] M. Bambach, L. Conrads, M. Daamen, O. Güvenç, and G. Hirt: Enhancing the crashworthiness of high-manganese steel by strain-hardening engineering, and tailored folding by local heat-treatment, *Materials and Design*, 110 (2016), pp. 157–168.
- [10] G. K. Bansal, D. A. Madhukar, A. K. Chandan, K. Ashok, G. K. Mandal, and V. C. Srivastava: On the Intercritical Annealing Parameters and Ensuing Mechanical Properties of Low-Carbon Medium-Mn Steel, *Materials Science and Engineering: A*, 733 (2018), pp. 246–256.
- [11] V. Onar, S. Aslanlar, and N. Akkaş: Effect of Welding Current on Tensile-Peel Loading of Welding Joints in TRIP 800 and Micro-Alloyed Steels in Resistance Spot Welding, *Acta Physica Polonica A*, 132 (2017), pp. 822–824.
- [12] B. Wang *et al.*: Investigation on fatigue fracture behaviors of spot welded Q&P980 steel, *International Journal of Fatigue*, 66 (2014), pp. 20–28.
- [13] V. H. L. Cortéz, F. A. R. Valdés, and L. T. Treviño: Weldability of martensitic steel by resistance spot welding a neural network optimization in the automotive industry, *Materials and Manufacturing Processes*, 24 (2009), pp. 1412–1417.
- [14] J. P. Kong, T. K. Han, K. G. Chin, B. G. Park, and C. Y. Kang: Effect of boron content and welding current on the mechanical properties of electrical resistance spot welds in complex-phase steels, *Materials and Design*, 54 (2014), pp. 598–609.
- [15] L. li Ma, Y. hui Wei, L. feng Hou, and B. Yan: Microstructure and mechanical properties of TWIP steel joints, *Journal of Iron and Steel Research International*, 21 (2014), pp. 749–756.
- [16] M. H. H. Razmpoosh, M. Shamanian, and M. Esmailzadeh: The microstructural evolution and mechanical properties of resistance spot welded Fe – 31Mn – 3Al – 3Si TWIP steel, *Materials and Design*, 67 (2015), pp. 571–576.
- [17] C. W. Shao, P. Zhang, Y. K. Zhu, Z. J. Zhang, Y. Z. Tian, and Z. F. Zhang: Simultaneous

improvement of strength and plasticity: Additional work-hardening from gradient microstructure, *Acta Materialia*, 145 (2018), pp. 413–428.

CORRESPONDENCE ADDRESS: Fatih ÖZEN, Sakarya University of Applied Science, Faculty of Technology, Sakarya,

Telephone: +90 264 295 64 82

E-mail address: fatihozen@sakarya.edu.tr

SHORT BIOGRAPHIES

Fatih ÖZEN – He was born in Trabzon, Turkey in 1989. He graduated from Sakarya University, Faculty of Engineering, Mechanical Engineering department. He is PhD student in Manufacturing engineering. He is research assistant since 2014 in Sakarya University. His main interest area are welding and manufacturing processes.

Volkan ONAR – He was born in İstanbul in 1984. He completed his primary and secondary education in Kocaeli. He got B.Sc. degree from Gazi University, Department of Technical Education in 2007. Besides, He graduated M. Sc. Degrees from Gazi University, Department of Metal Education in 2010. He graduated Ph. D. at Sakarya University, Department of Material and Metallurgy Engineering in 2017. He worked as a Research Assistant in the Department of Manufacturing Engineering at Pamukkale University 2012 to 2017. He has been working as a Assistant Professor in the Department of Mechanical and Manufacturing Engineering at Pamukkale University since 2017.

Uğur ÖZSARAÇ – He was born in Çorum, Turkey in 1971. He graduated from METU, Department of Metallurgical Engineering as an engineer in 1995. He started to Sakarya University as Research Assistant. He has been working in same University as an Associate Professor since 1995. His research areas are Welding metallurgy, Brazing and cold metal transfer (CMT)

Yusuf Sadi ASLANLAR–He was born in Sakarya in 1993. He completed my primary, secondary and high school education in Sakarya. He got B.Sc. degree from Sakarya University, Department of Industry Engineering in 2016. He has been continuing M. Sc. Degrees at Sakarya University, Department of Material and Metallurgy Engineering since 2016.

Zafer BARLAS– He was born in İstanbul, Turkey, in 1976. He received the Ph.D. degree from Sakarya University, Turkey, in 2009. He is an associate professor from Sakarya University since 2016 and works welding techniques especially frictional methods.

Salim ASLANLAR– He was born in Adapazarı, Turkey, in 1963. He completed primary, secondary and high school in Adapazarı. he graduated from fachhochschule niederrhein university in krefeld, Germany as a high engineer in 1987 after completing mechanical engineering construction and manufacturing₁ department successfully. He received the Ph.D. degree from Sakarya University, Turkey, in 2009. He has been working in same University as an

Professor. His research areas are Welding metallurgy, Brazing, cold metal transfer (CMT), AHSS and bonding techniques.

MICROSTRUCTURAL EVOLUTION, PHASE TRANSITION AND MECHANICAL PROPERTIES OF Fe-Ti-B HARDFACING ALLOYS

Eray Abakay^{1,a}, Engin Kocaman^{2,b}, Mustafa Durmaz^{1,c}, Bülent Kılınç^{3,d},
Şaduman Şen^{1,e} and Uğur Şen^{1,f}

¹Sakarya University, Department of Metallurgical and Materials Engineering, Sakarya, Turkey

²Bulent Ecevit University, Department of Metallurgical and Materials Engineering, Zonguldak, Turkey

³Sakarya University, Arifiye Vocational School, Sakarya, Turkey

^aeabakay@sakarya.edu.tr, ^benginkocaman@gmail.com, ^cmdurmaz@sakarya.edu.tr,

^dbkilinc@sakarya.edu.tr, ^esdmnsen@sakarya.edu.tr and ^fugursen@sakarya.edu.tr

Abstract

The use of the steels with high hardness and abrasion resistance is very important for industrial applications. In many cases, instead of having a high hardness of an entire part, only the hardness of the surface is sufficient and the cost is lower. In the hardfacing method, the coatings of the metal matrix composite structure containing non-oxide hard reinforcement structure can be realized by the organizing the chemical composition of the starting powders. In this study, three alloys containing Fe, Ti and B elements were prepared and microstructural investigations, phase transformations and hardness values were investigated depending on the increasing ratio of titanium. Alloy powders consisting of ferrous-titanium, ferrous-boron and Armco iron on the surface of SAE 1320 plates with the dimensions of 50 x 100 x 10 mm³ were melted with tungsten inert gas (TIG) welding technique. Microstructural investigations were carried out using by scanning electron microscopy (SEM) and optical microscope (OM) from the cross-section of metallographically prepared samples. It has been determined that TiB₂ phase content and microstructure of the alloyed layer are observed depending on the amount of increase in titanium content. The chemical analysis of the resulting structures was carried out using by energy dispersive spectroscopy (EDS). The phases formed in the coated layer by varying amounts of titanium were determined by x-ray diffraction (XRD). According to the XRD analysis, α -Fe, TiB₂ and Fe₂B phases were determined.

Key Words: Hardfacing, TIG Welding, Titanium diboride, phase analysis.

1. Introduction

Many machine parts are subjected to severe wear and impact during their use in harsh environments. In such cases, faults can occur in a short time on the devices and can cause great damage to the plants. In many cases, the use of parts made entirely of materials with high wear and impact resistance creates high costs. With the hardfacing method it is possible to obtain a coating layer with high wear and impact resistance on the surface of many materials. A metal matrix composite coating layer with a ductile matrix and carbide, nitride and boron based reinforcing phases can be obtained by melting various ferrous alloy powders on the surface of low cost and low cost materials using different welding methods[1-5].

TiB₂-Fe composites have been an important research topic for researchers for the last 10 years. The TiB₂ phase is characterized by high hardness (3400 HV), high melting temperature (3225 °

C), low density (4.451 g/cm³), high chemical stability, high wear resistance, high corrosion resistance, good wettability and thermodynamic stability properties in liquid steel. The use of titanium diboride as a reinforcing phase in iron matrix composites has been a subject of interest with these properties. There are several studies in the literature that use different methods such as powder metallurgy (PM), conventional melting and casting, carbothermic reduction, self-propagating high-temperature synthesis (SHS), aluminothermic reduction and hard-facing for obtaining TiB₂-Fe metal matrix composites. There are studies using laser and plasma-transferred-arc (PTA) methods in the production of TiB₂-Fe composites by the hardfacing method [1], [6-7], [8-9]. An alternative to the mentioned welding methods is tungsten-inert-gas (TIG) or also known as gas-tungsten-arc welding (GTAW) welding method. This method, which is performed with an arc formed between the tungsten electrode and the base metal, combines parts made of materials such as steel, aluminum, titanium etc. The welding obtained after the process has good appearance and high quality compared to other welding methods [10-12].

In this study, the coating layers obtained by melting the alloy powders containing Armco iron, ferrous titanium and ferrous boron by TIG welding method were investigated at various ratios on the surface of SAE1320 low carbon steel. The changes in the microstructure, phase and mechanical properties were investigated depending on the varying powder mixture ratios and comparisons were made with the coating layers obtained by different methods.

2. Experimental

SAE1320, a low carbon steel, was selected as the base material. The chemical composition of the steel supplied as sheet of 5 mm thickness is given in Table 1. After sectioned in 20x10x5 mm³ dimensions, the surfaces of the samples were sanded and cleaned with acetone. Ferrous titanium and ferrous boron are crushed and milled to be under the 45 µm sieve. After grinding, mixing with Armco iron was carried out at the ratios given in Table 2. The iron, titanium and boron ratios in the prepared compositions are given in Table 3 as at. %. In order to obtain a homogeneous mixture, the mixing process was carried out for 2 hours at the ball mill. Subsequently, the mixture was weighed at a certain ratio and pressed with a die to obtain a homogeneous layer on the surface of the substrate. The hardfacing process was performed by using the parameters given in Table 4 with the TIG welding method after the specified pre-treatment.

Table 1. The chemical composition of SAE1320 used as the substrate (wt. %).

C	Cr	Mn	Si	P	S	Ni	Mo	Fe
0.183	0.021	1.370	0.204	0.018	0.002	0.062	0.006	98.000

Metallographic analyzes of the prepared samples were carried out using an optical microscope (Nikon Epiphot 200, Japan) and a scanning electron microscope (JEOL JSM 6060, Japan). After sectioned, the samples were gradually sanded to 1200 mesh sanding step and then polished with 0.3 µm alumina paste. Polished samples were chemically cleaned with 3% Nital solution after their surfaces were cleaned with acetone. Energy dispersive X-ray spectroscopy (EDS) was used in chemical analysis of the various regions of the samples. X-ray diffraction (XRD) was used to investigate the phase shifts and the changes in the phases depending on the changing Fe, Ti and B ratios.

Table 2. % Atomic percentages of boron, titanium and iron in the prepared compositions

Compound	Code	% B	% Ti	% Fe
1	C1	40	15	45
2	C2	40	10	50
3	C3	40	5	55

Table 3. Chemical composition of ferrous alloys and Armco iron used (wt. %).

	Ti	B	C	Al	Si	P	S	Fe
Ferro-titanium	70.950		0.129	3.690	-	0.008	0.004	25.200
Ferro-boron		18.58	0.310	0.084	0.390	0.029	0.003	80.6
Armco iron	-	-	0.010	-	-	-	-	99.990

Hardness measurements of the coatings obtained on the surface were made by Vickers micro hardness measurement. The hardness of all the phases in all the samples was taken under the loads of 10 gf.

Table 4. The main parameters of TIG hardfacing

Parameter	Value
Electrode	Type W-2 pctThO
Diameter	2.4 mm
Angle	70 °
Voltage	20 V
Current	110 A
Heat input	2.2 MJ/m
Protective gas	Type Ar (%99.9 Ar)
Flow	12 L/min
Welding speed	Travel speed 60 mm/min
Heat input $Q = 60 \times I \times V/S$, I: current, V: voltage, and S: travel speed	

3. Results and Discussion

In Fig. 1, samples with hardfacing of 3 different compositions containing Fe, Ti and B elements were given optical microscope images. Due to the decreasing amount of titanium and increasing amount of iron relative to the image, changes in the microstructure have occurred. Generally cracks and porosities are observed on the surfaces obtained by hardfacing method [13-15]. In the obtained samples, no crack or porosity were formed. For C1 and C2 compounds, the structure consists of ferrite-based matrix, needle-like, spherical and blocky phases. However, there are no needle-like phases for the C3 composition. For this reason, it can be said that there is a decrease needle-like phases due to the decreasing amount of titanium and the amount of iron being increased.

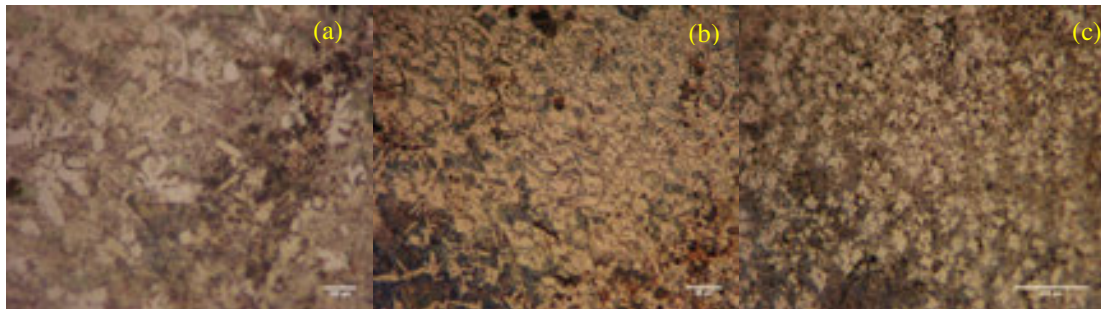


Figure 1. Optical microscope images of hardfacing sample surfaces for C1, C2 and C3 compounds, respectively.

In Figure 2, SEM image and EDS analyzes of sample C1 are given. According to these images and analyzes, it is seen that one of the phases based on iron (figure 2 b) and the one based on titanium (figure 2 c) are formed on the steel based matrix (Figure 2 d). Fe, Fe₂B and TiB₂ phases should be present in the structure according to the B-Fe-Ti ternary phase diagram, and the EDS analyzes taken from different regions are consistent with the EDS analyzes of said phases [16-18]. Considering also the optical microscope images in Figure 1, it can be said that the black-colored TiB₂ phase in the spherical form decreases with the decreasing amount of titanium.

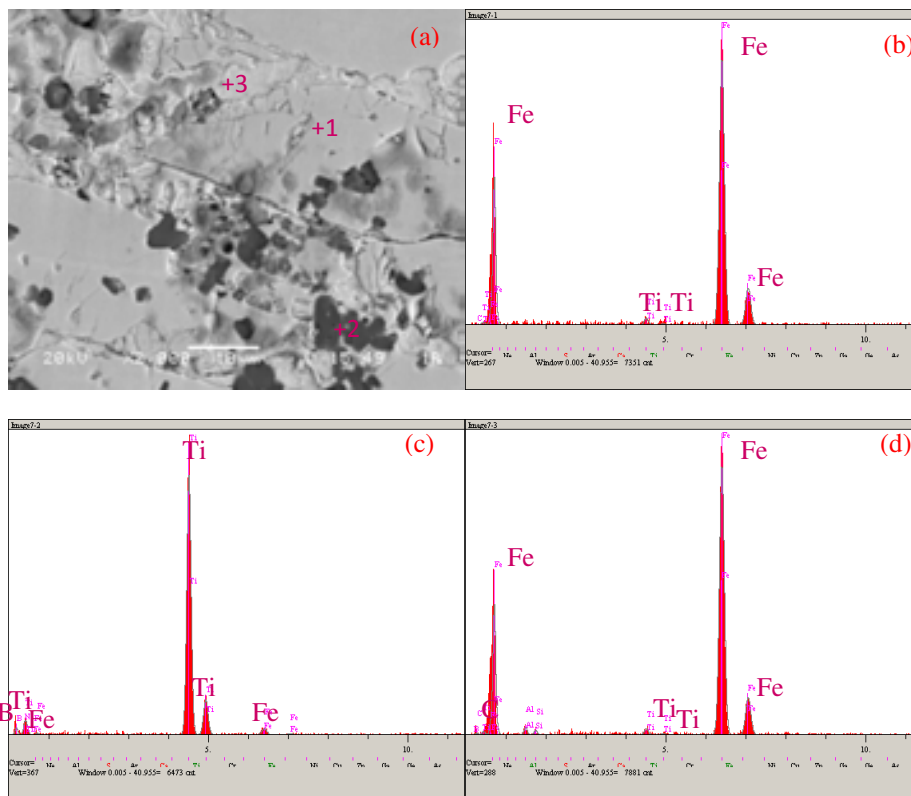


Figure 2. (a) Cross-sectional SEM image, (b), (c) and (d) EDS analyzes from different regions of C1-coded sample.

The structure according to the SEM image taken from the cross-section of the C2-coded sample differs from C1, although the EDS analyzes are similar (Fig. 3). TiB_2 phase is larger than C1 and Fe_2B is formed in lamellar structure. Depending on the increased cooling rate, the Fe_2B phase has a lamellar structure instead of a blocky and needle-like structure [19].

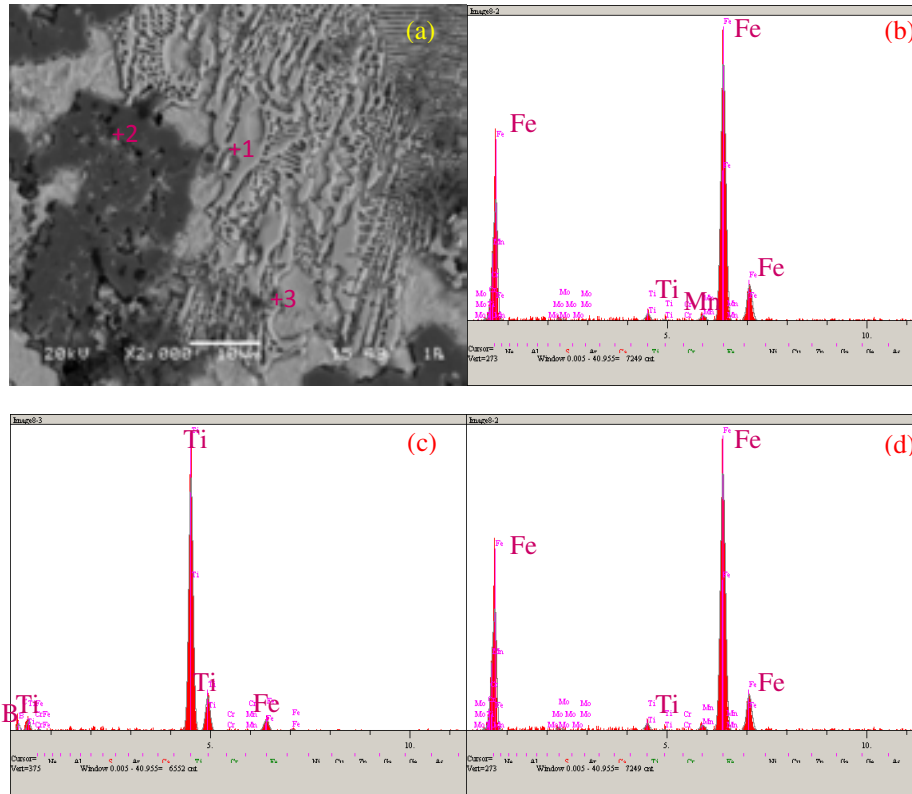


Figure 3. (a) Cross-sectional SEM image, (b), (c) and (d) EDS analyzes from different regions of C2-coded sample.

In Fig. 4 a, when the SEM image is viewed, it can be said that the image of the Fe_2B phase in the C3 code sample resembles C1. EDS analyzes from points 1 and 3 are similar to those of C1 and C2 samples. As seen in Figure 1.c, the TiB_2 phase is present in this structure as very small particles. However, in the analysis taken from point 2 in figure 4c, oxide is seen in the structure. According to similar studies, oxidation occurs in compositions containing Fe-Ti-B at high temperatures [20].

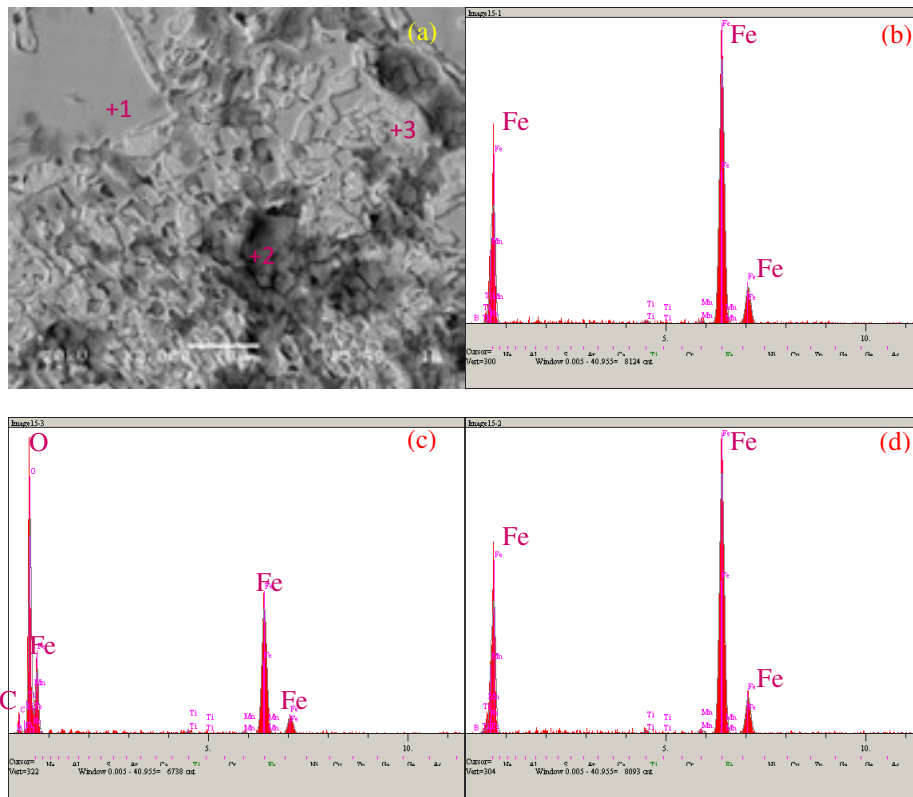
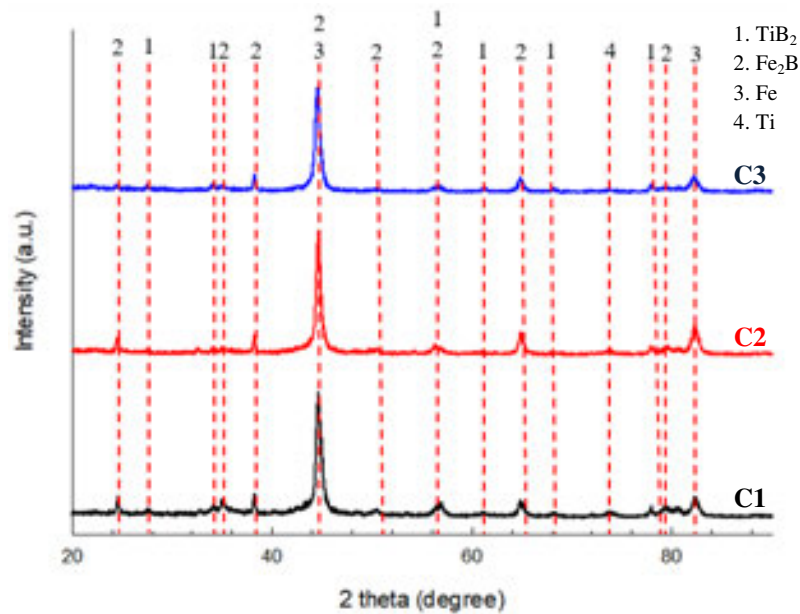


Figure 4. (a) Cross-sectional SEM image, (b), (c) and (d) EDS analyzes from different regions of C3-coded sample.

Fig. 5 shows X-ray diffractions of the samples. As mentioned in previous chapters, the structure consists of TiB_2 , Fe_2B , Fe phases. In addition to these phases, the Ti phase was also determined. The Ti phase is not seen in C3 due to increased iron and decreased titanium content. Contrary to expectations, the Fe_2B phase at 24° is not visible in the C3 composition. Except for the two changes mentioned above, the three compounds have similar patterns.



According to the result of Vickers micro hardness measurement, 324 HV hardness value is determined for steel based matrix. The measured values are about 1480 HV Fe₂B and 3727 HV TiB₂ for the reinforcing phases. The hardness measurement results are similar to the literature and it can be said that C1 compound is the most preferable composition because of TiB₂ content [21-22].

4. Conclusion

On the surface of SAE 1320 steel, a hardfacing process with TIG welding of different compositions prepared with ferro titanium, ferroboron and armco iron powders resulted in a structure consisting of steel matrix, TiB₂ and Fe₂B reinforcing phases. In addition, the TiB₂ phase in the structure has also increased due to the increased amount of ferro titanium. Considering the hardness measurements made, it is thought that it would be more appropriate to use the compositions containing high amounts of ferro titanium for applications requiring high hardness and wear resistance.

5. References

- [1] Q. Ming, L. C. Lim, Z. D. Chen: Laser cladding of nickel-based hardfacing alloys, *Surface and Coatings Technology*, 106 (1998), pp. 174-182.
- [2] Y. Bayhan: Reduction of wear via hardfacing of chisel ploughshare, *Tribology International*, 39 (2006), pp. 570-574.
- [3] M. F. Buchely, J. C. Gutierrez, L. M. León, A. Toro: The effect of microstructure on abrasive wear of hardfacing alloys, *Wear*, 259(2005) 52-61.
- [4] J. J. Coronado, H. F. Caicedo, A. L. Gómez: The effects of welding processes on abrasive wear resistance for hardfacing deposits, *Tribology International*, 42(2009) 745-749.
- [5] S. Chatterjee, T. K. Pal: Wear behaviour of hardfacing deposits on cast iron, *Wear* 255 (2003), pp.417-425.
- [6] D. Wu, X. Wang, P. Zhang, L. Cai, H. Sun: Defects in the in situ synthesized TiB₂/Fe composite coatings during PTA process, *Applied Surface Science*, 257 (2011) ,pp. 10119-10125.

- [7] Y. Wang, Z. Q. Zhang, H. Y. Wang, B. X. Ma, Q. C. Jiang: Effect of Fe content in Fe–Ti–B system on fabricating TiB₂ particulate locally reinforced steel matrix composites, *Materials Science and Engineering: A*, 422 (2006) 339-345.
- [8] B. Li, Y. Liu, J. Li, S. Gao, H. Cao, L. He: Effect of tungsten addition on the microstructure and tensile properties of in situ TiB₂/Fe composite produced by vacuum induction melting, *Materials & Design*, 31 (2010), pp. 877-883.
- [9] B. Du, Z. Zou, X. Wang, S. Qu: In situ synthesis of TiB₂/Fe composite coating by laser cladding, *Materials Letters*, 62 (2008), pp. 689-691.
- [10] S. C. Juang, Y. S. Tarn, H. R. Lii: A comparison between the back-propagation and counter-propagation networks in the modeling of the TIG welding process, *Journal of Materials Processing Technology*, 75(1998), pp. 54-62.
- [11] P. J. Modenesi, E. R. Apolinário, I. M. Pereira: TIG welding with single-component fluxes, *Journal of Materials Processing Technology*, 99 (2000), pp. 260-265.
- [12] C.-M. Chang, C.-M. Lin, C.-C. Hsieh, J.-H. Chen, W. Wu: Micro-structural characteristics of Fe–40wt%Cr–xC hardfacing alloys with [1.0–4.0wt%] carbon content, *Journal of Alloys and Compounds*, 487 (2009), pp. 83-89.
- [13] V. E. Buchanan, D. G. McCartney, P. H. Shipway: A comparison of the abrasive wear behaviour of iron-chromium based hardfaced coatings deposited by SMAW and electric arc spraying, *Wear*, 264 (2008), pp. 542-549.
- [14] A. S. C. M. D'Oliveira, R. S. C. Paredes, R. L. C. Santos: Pulsed current plasma transferred arc hardfacing, *Journal of Materials Processing Technology*, 171 (2006), pp. 167-174.
- [15] L. Sexton, S. Lavin, G. Byrne, A. Kennedy: Laser cladding of aerospace materials, *Journal of Materials Processing Technology*, 122 (2002), pp. 63-68.
- [16] V. Raghavan, B-Fe-Ti (Boron-Iron-Titanium), 24 (2003), pp. 2-3.
- [17] O. Ozdemir, M. A. Omar, M. Usta, S. Zeytin, C. Bindal, A. H. Ucisik: An investigation on boriding kinetics of AISI 316 stainless steel, *Vacuum* 83 (2008), pp. 175-179.
- [18] J. P. Tu: Preparation and properties of TiB₂ nanoparticle reinforced copper matrix composites by in situ processing, *Materials Letters*, 52 (2002), pp. 448-452.
- [19] L. C. Lim, Q. Ming, Z. D. Chen: Microstructures of laser-clad nickel-based hardfacing alloys, *Surface and Coatings Technology*, 106 (1998), pp. 183-192.
- [20] X. Wang, H. Shun, C. Li, X. Wang, D. Sun: The performances of TiB₂-contained iron-based coatings at high temperature, *Surface and Coatings Technology*, 201 (2006), 2500-2504.
- [21] T. S. Srivatsan, G. Guruprasad, D. Black, R. Radhakrishnan, T. S. Sudarshan: Influence of TiB₂ content on microstructure and hardness of TiB₂–B₄C composite, *Powder Technology*, 159 (2005) 161-167.
- [22] Z. Huang, J. Xing, C. Guo: Improving fracture toughness and hardness of Fe₂B in high boron white cast iron by chromium addition, *Materials & Design*, 31 (2010) 3084-3089.

CORRESPONDENCE ADDRESS:

Eray Abakay, Sakarya University, Esentepe Campus, Department of Metallurgical and Materials Engineering 54187 Serdivan Sakarya Turkey, +902642957076, eabakay@sakarya.edu.tr

SHORT BIOGRAPHIES

Eray Abakay (32)

Eray Abakay has been working as a research assistant at Sakarya University since 2012. He graduated from Yıldız Technical University Metallurgical and Materials Engineering department in 2010 and Sakarya University in 2013 with his master's degree in "Nb-Al-N Coating of Steel Surfaces by Thermo Reactive Deposition Method". There are many articles available in hardfacing and thermo reactive deposition. He is currently working on PH.D. thesis titled "Electrodeposition of nickel boron coating of magnesium and its alloys".

Engin KOCAMAN (29)

Engin Kocaman was born on April 17 1989 - Akşehir. He graduated from his bachelor degree at Sakarya University Metallurgical and Materials Engineering department in 2013 and his master's degree at same university in 2017. He is currently working on PH.D. thesis titled "Development of Fe-M-Cr-B (M=Ti, Mo) based In-Situ Composite Hard Surface Alloying Coated Electrodes". He has been working as a research assistant at Bulent Ecevit University since 2016. His research interests are casting of aluminum, hard-facing coatings, solidification and nickel based single crystal super-alloys.

Mustafa Durmaz (29)

The author was born in 1989 in Samsun. He completed BSc in 2011, MSc in 2015 and he started to study PhD in 2016 in the department of Metallurgy and Materials Engineering at the University of Sakarya. Mustafa Durmaz is research assistant at the Sakarya University since 2013. His research interests lie in the area of mechanical alloying, thermochemical coating process and tribology, and he published several papers on these topics.

Bülent Kılınç (39)

Bülent KILINÇ, He completed BSc in 2003, MSc in 2010 in the Department of Technical Education at the University of Sakarya. Bülent KILINÇ has completed his PhD in Metallurgy and Materials Science Department of the Science Institute of Sakarya University In 2018. Bülent Kılınç is a lecturer in Department of Welding Technology at Vocational School at the University of Sakarya since 2012. His research interests Thermo-chemical coating, melting Based Coatings, Corrosion and tribology, and he published several papers on these topics.

Şaduman Şen (49)

Şaduman Şen has entered in 1987 to the Metallurgical Engineering Department of Sakarya Engineering Faculty of Istanbul Technical University. She graduated at the Institute of Materials Science department of Science Institute at 1994 and completed her master's degree. Şaduman Sen has completed his PhD in Metallurgy and Materials Science Department of the Science Institute of Sakarya University In 1998. She has worked as an Assistant Professor and Associate Professor in the Department of Metal Education Department of Faculty of Technical Education

of Sakarya University. She has been working as a professor at the Department of Metallurgy and Materials Engineering of Engineering Faculty of Sakarya University. The Author has been studied on hard coatings, especially nitride, carbide and boride base coatings, thermochemical coatings, corrosion, Tribology and powder metallurgy subjects. She has been managing masters and doctoral theses and scientific projects. There are also a number of international and national articles and papers on these issues of the Author.

Uğur Şen (52)

Uğur ŞEN, has entered in 1984 to the Metallurgical Engineering Department of Sakarya Engineering Faculty of İstanbul Technical University. He graduated at the Institute of Materials Science department of Science Institute at 1993 and completed his master's degree. Uğur ŞEN has completed his PhD in Materials Science Department of the Science Institute of İstanbul Technical University at 1998. He has worked as an Assistant Professor in the Department of Metal Education Department of Faculty of Technical Education of Sakarya University. He has worked as an Associate Professor at the Department of Metallurgy and Materials Engineering of Engineering Faculty of Sakarya University. Uğur ŞEN has been working as a professor at the Department of Metallurgy and Materials Engineering of Engineering Faculty of Sakarya University. The Author has been studied on hard coatings, thermo-chemical coatings, corrosion, tribology, powder metallurgy and electronic ceramics subjects. He has been managing masters and doctoral theses and scientific projects. There are also a number of international and national articles and papers on these issues of the Author.

THE EFFECT OF MOLYBDENUM ADDITION ON THE MICROSTRUCTURE AND WEAR BEHAVIOURS OF Fe-Mo-B BASED ALLOYED STEEL

Bülent Kılınç^{1,a}, Engin KOCAMAN^{2,b}, Mustafa Durmaz^{3,c}, Eray Abakay^{3,d},
Uğur Şen^{3,e}, Şaduman Şen^{3,f}

¹Sakarya University / Arifiye Vocational High School / Department of Welding Technologies / Arifiye /
Sakarya / Turkey

²Bulent Ecevit University / Engineering Faculty / Department of Metallurgy and Materials Engineering /
Farabi Campus / Zonguldak / Turkey

³Sakarya University / Engineering Faculty / Department of Metallurgy and Materials Engineering / Esentepe
Campus / Sakarya / Turkey

^abkilinc@sakarya.edu.tr, ^benginkocaman@beun.edu.tr, ^cmdurmaz@sakarya.edu.tr, ^deabakay@sakarya.edu.tr,
^eugursen@sakarya.edu.tr, ^fsdmnsen@sakarya.edu.tr

Abstract

In this study, Fe-Mo-B based hard surface alloy samples with three different compositions were produced by Tungsten inert gas (TIG) welding method and the effects of molybdenum addition on the microstructure and wear behaviors of hard surface alloy layer were investigated. For this purpose, powder mixtures of different proportions prepared from ferrous boron, ferrous molybdenum and iron powder were melted on steel substrate by TIG welding method to form a hard surface alloy layer. Coated layers were characterized by optical (OM) and scanning electron microscopy (SEM), X-ray diffraction analysis (XRD), micro-hardness and ball on disk wear tests. The surface alloying results indicate good quality thick coating and porosity free of the hard-facing. As a result of X-ray diffraction analyses, the presence of α -Fe, Fe₂B, MoB₂, Fe_{9,7}Mo_{0,3} and FeMo₂B₂ phases was determined. Wear tests of the surface alloyed AISI 1010 steels were carried out at atmospheric test conditions under 2.5N, 5N and 10N loads at 0.1 m/s sliding speed against alumina ball.

Key Words: TIG welding, Surface Alloying, Hard-facing, Phase analysis, Wear

1.Introduction

Especially abrasive wear is highly important for the mine, agriculture and metal shaping industry etc. [1–3] Several technologies are used nowadays to fighting with wear, corrosion and worn surface. Hard-facing is one of the most economically method to improve of the surface properties. This method can be applied by an appropriate welding techniques such as tungsten inert gas (TIG), shield manual arc (SMAW), plasma arc welding (PAW) and submerged arc welding (SAW) etc. [4–6]. The welding method is applied a substrate material which is usually Fe, Co and Ni based [7–9]. Coated layer usually requires higher hardness than substrate material to enhance of protection against wear. In order to obtain required hardness with surface alloying has to be hard phases onto the substrate metal. As typical phases, carbides, borides and nitrides of some metal such as chromium, titanium, tungsten can be used. After surface alloying these

hard phases show a dense and uniform distribution onto the substrate metal. Efficiency of the coating layer is mostly dependent on coating composition. Researchers were mostly investigated Fe-Cr-X alloys (X: different carbide and boride forming elements such as vanadium, niobium, boron, tungsten and titanium)[10–12]. However, there is a just limited accomplishment by mentioned above. Fe-Mo-B based hard-facing alloys are newly-developed iron-based wear resistant materials.

Molybdenum and iron are a strong boride-forming element, which forms stable borides like FeB, Fe₂B, Mo₂B, MoB, Mo₂B₅, Fe₁₃Mo₂B₅, Fe₁₄MoB₅, FeMo₂B₂, FeMo₈B₁₁ etc. These compounds have high melting temperature, hardness and wear resistance like Zr, Ti and Cr borides[13]. In this paper, Fe-Mo-B based hard surface alloy samples with three different compositions were produced. Effect of the Molybdenum addition on microstructure and wear resistant of the Fe-Mo-B alloy was investigated.

2. Experimental

In this study, an AISI 1010 steel samples with the dimensions 30mm x70mm x5mm were used as substrate material. The substrate material was cleaned by using acetone and dried. Ferromolybdenum, ferrous boron and iron powder received from AVEKS Co was prepared according to nominal composition which is given Table 1. The powders with specified atomic ratios were mixed by a ball milling for 60 min at a speed of 600 rpm. The powders prepared were ratios determined and mixed to form Fe₁₆MoB₃, Fe₁₄Mo₃B₃ and Fe₁₂Mo₅B₃ compounds. Finally, the powders were pressed on 100 MPa by using hydraulic press. Then the pressed powders were melted together with the substrate using a TIG welding technique.

Table 1. Compositions of powders used in hard surface alloying (by weight)

Powders	%Fe	%B	%Mo	%Cu	%C	%Al	%Si
Ferrous-boron	78,9	19,63	-	-	0,44	0,05	0,98
Ferrous-molybdenum	33,39	-	63,62	0,5	0,98	-	1,51
Pure iron	100	-	-	-	-	-	-

Tungsten inert gas (TIG) welding method was used to obtain surface alloying. Main welding process parameters such as welding current, voltage, arc length, electrode properties and shielding gas are given Table 2.

Table 2. Experimental Parameters of TIG Surface alloying

Parameter	Value
Electrode	Type W-2 pctThO
Electrode Diameter	2.4 mm
Angle	70 degrees
Voltage	20 V
Current	110 A
Heat input	2.2 MJ/m
Protective gas	Type Ar (%99.9 Ar)
Flow	12 L/min
Welding speed	Travel speed 60 mm/min
Heat input $Q = 60 \times I \times V/S$, I: current, V: voltage, and S: travel speed [14]	

The samples were prepared according to standard metallographic procedure by grinding, polishing and etching with (3%) Nital reagent respectively. For microstructural characterization of samples were carried out by using a Nikon Epiphot 200 optical microscope (OM) and JEOL JSM – 6060 scanning electron microscopy (SEM). An X-ray diffraction (XRD) was detected with RigakuXRD/D/MAX/2200/PC model X-ray diffractometer using Cu-Ka radiation. To measure Vickers hardness, tests were performed with a load of 10g using Future Tech FM 700Vickers-hardness tester.

Wear and friction tests of the surface alloyed steels were carried out in a tribometer device conforming to ASTM G-99 standard. The experiments were carried out using Ball-On-Disk method using 10 mm diameter Alumina (Al_2O_3) balls. Alumina ball has mirror like surface finish with a hardness value of 2720 $HV_{0,05}$ [15]. Most of the materials are encountered with ambient temperature and humidity in the industrial applications. Therefore, the friction and wear tests were carried out at room temperature (21 ± 3 °C), relative humidity being 64±5 conditions. The wear tests were carried out under loads of 2,5N, 5N and 10N at a speed of 0.1 m / s at a distance of 200 m. Wear rate was measured primarily by volumetric (volume loss) means. To evaluate wear resistance, the wear volume was calculated from the worn cross-sectional area of the surface alloyed plate which was measured by KMA P6 optical profilometer.

3.Results and Discussion

The optical and SEM microstructure images obtained from the Fe-Mo-B based hard surface alloy layers coated on the AISI 1010 steel substrate surface are shown in Figure 1. In the microstructure studies, the thickness of the layer seen as molten zone on the substrate is about 2-3 mm and a good bonding with the substrate is observed. It has been determined that this rather thick coating layer has a smooth surface topography with no porosity. In the microstructure studies, it is seen a structure consisting of three different layers on the surface; the substrate, the transition zone and the layer considered to be the boron phases dispersed in the eutectic matrix. It has been observed that the general structure of the Fe-Mo-B-based layer is dendritic. It is also seen that as the molybdenum ratio increases in the hard surface alloy layer, the primer α -Fe grain size decreases.

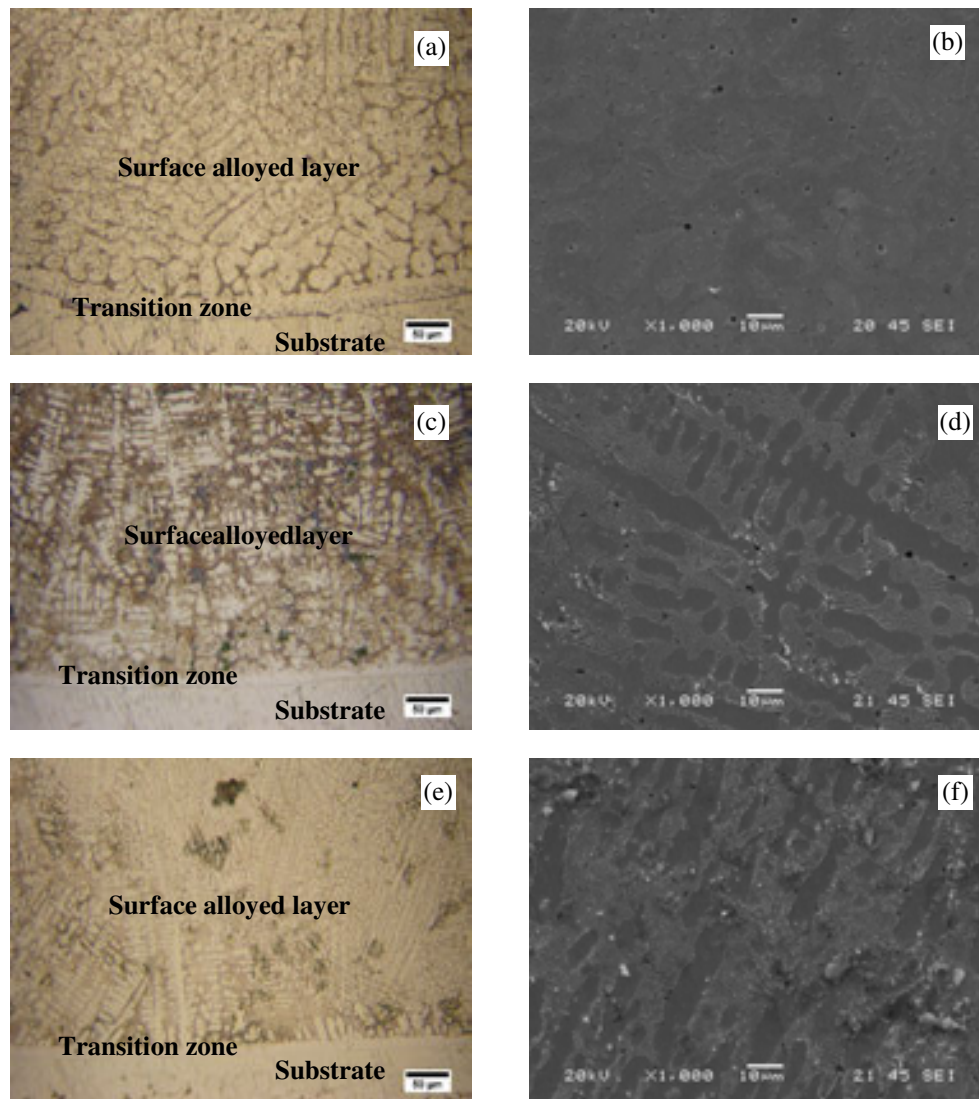


Figure 1. Optical and SEM microstructure images of Fe-Mo-B based hard surface coating layers;
(a-b) $\text{Fe}_{16}\text{MoB}_3$; (c-d) $\text{Fe}_{14}\text{Mo}_3\text{B}_3$; (e-f) $\text{Fe}_{12}\text{Mo}_5\text{B}_3$.

As shown from Figure 1 boride phases are well-distributed in the steel matrix as in situ composite structure. Some parts of the alloyed layer have much more dense boride phase in the alloyed layer as seen in Figure 1. It is possible that the boride phases of the alloyed layer consist of Fe_2B , FeMo_2B_2 , MoB_2 and iron phases which were detected by X-ray diffraction (XRD) analysis. The results are supported by phase diagram of Fe-Mo-B [16]. As known, the hardness of transition metals ranged from 2000 HV to 4000 HV [17].

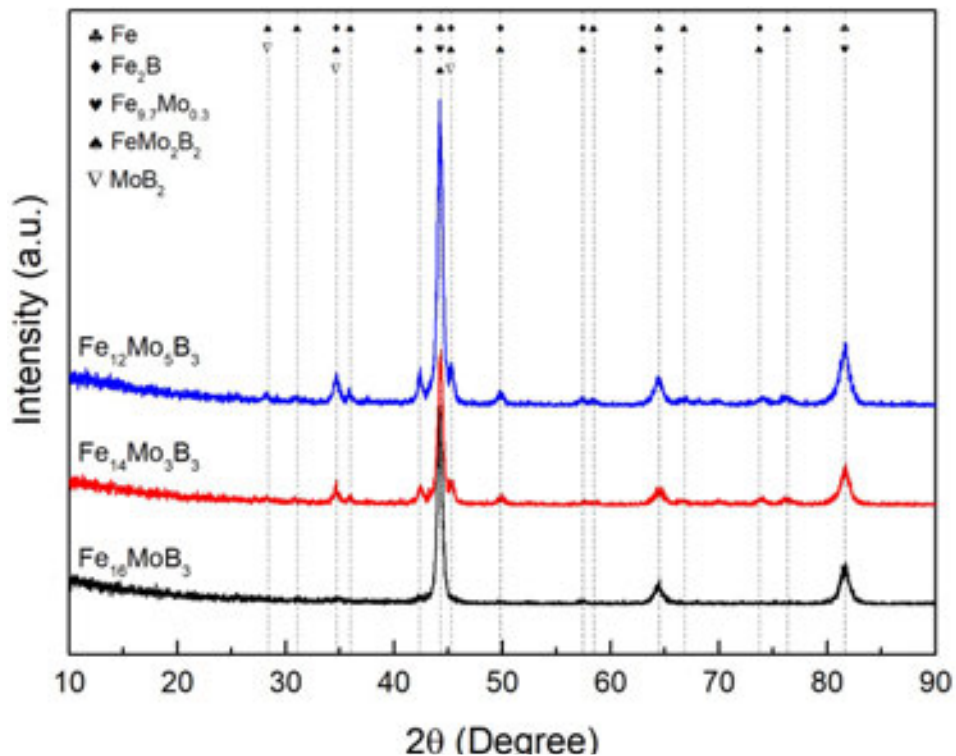


Figure 2. X-ray diffraction pattern of Fe-Mo-B based hard surface alloyed steels

According to the XRD analysis of the Fe-Mo-B based coatings formed on the steel substrate with the TIG source given in Figure 4 the presence of Fe, Fe₂B, FeMo₂B₂, Fe_{9,7}Mo_{0,3} and B₁₅MoB₂ phases were detected.

The hardness values of the boron phases, eutectic columns, transition zone and substrate material in the Fe-Mo-B based coating layer formed on the steel surfaces by TIG welding in three different compositions were 2093±228 HV_{0,01}, 1178±83 HV_{0,01}, 381±59 HV_{0,01} and 191±10 HV_{0,01}, respectively. The hardness of the boron phases varies from 1600 to 2000 HV[18,19]. As a result, the boron phases and the hardness of the eutectic structure are higher than the stiffness of the substrate metal.

As can be seen from the Figure 3(a) in abrasion tests carried out against alumina (Al₂O₃) ball, It has been observed that the friction coefficient values of Fe-Mo-B-based surface alloying materials decrease with increasing Mo content. It is also seen that the friction coefficient values are decreased for the Fe₁₆MoB₃, Fe₁₄Mo₃B₃ compounds depending on the increase of the wear load, but it increases for the Fe₁₂Mo₅B₃ composition. It was determined that the friction coefficient values measured depending on the wear load ranged from 0,387 to 0,788.

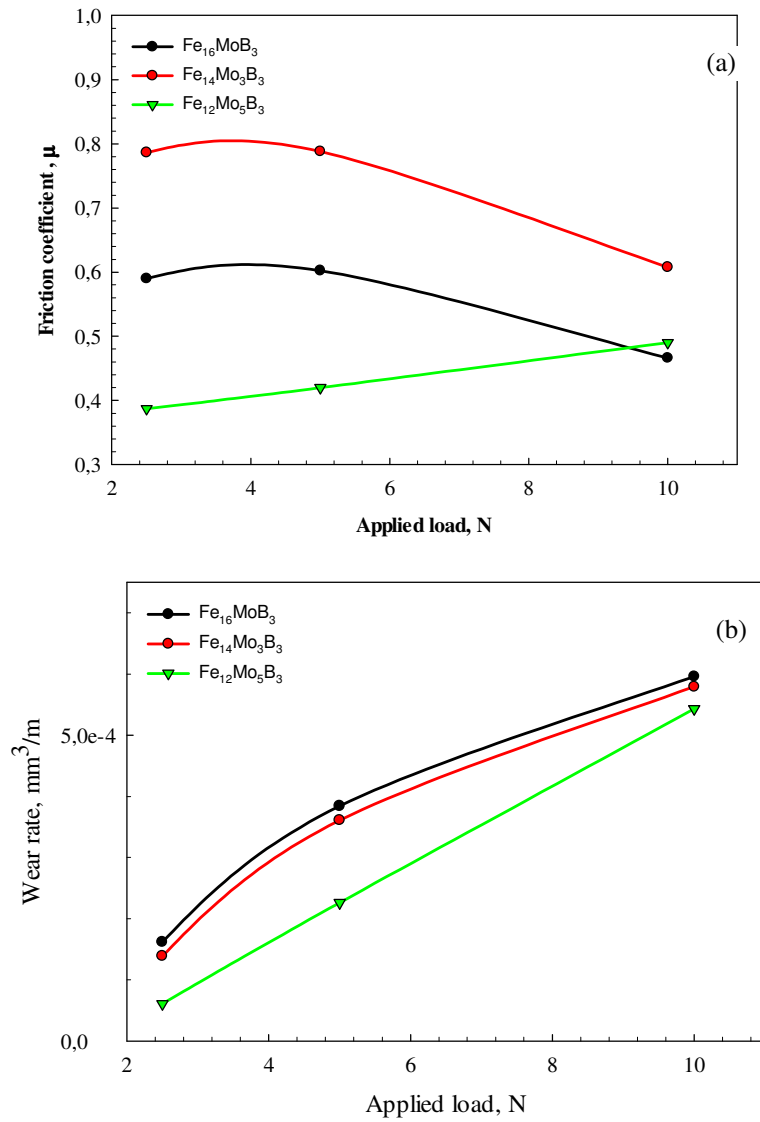


Figure 3.(a)Friction coefficient and (b) wear rate of Fe-Mo-B based hard surface alloyed steels

When the changes in wear rates calculated from the wear tests are examined, it is seen that the abrasion rates of hard coated steels against alumina balls are increased with depending on applied load (Figure 3(b)). In addition, it is seen that the wear rate is decreased for all loads with increasing Mo content in Fe-Mo-B based hard surface alloy layer.

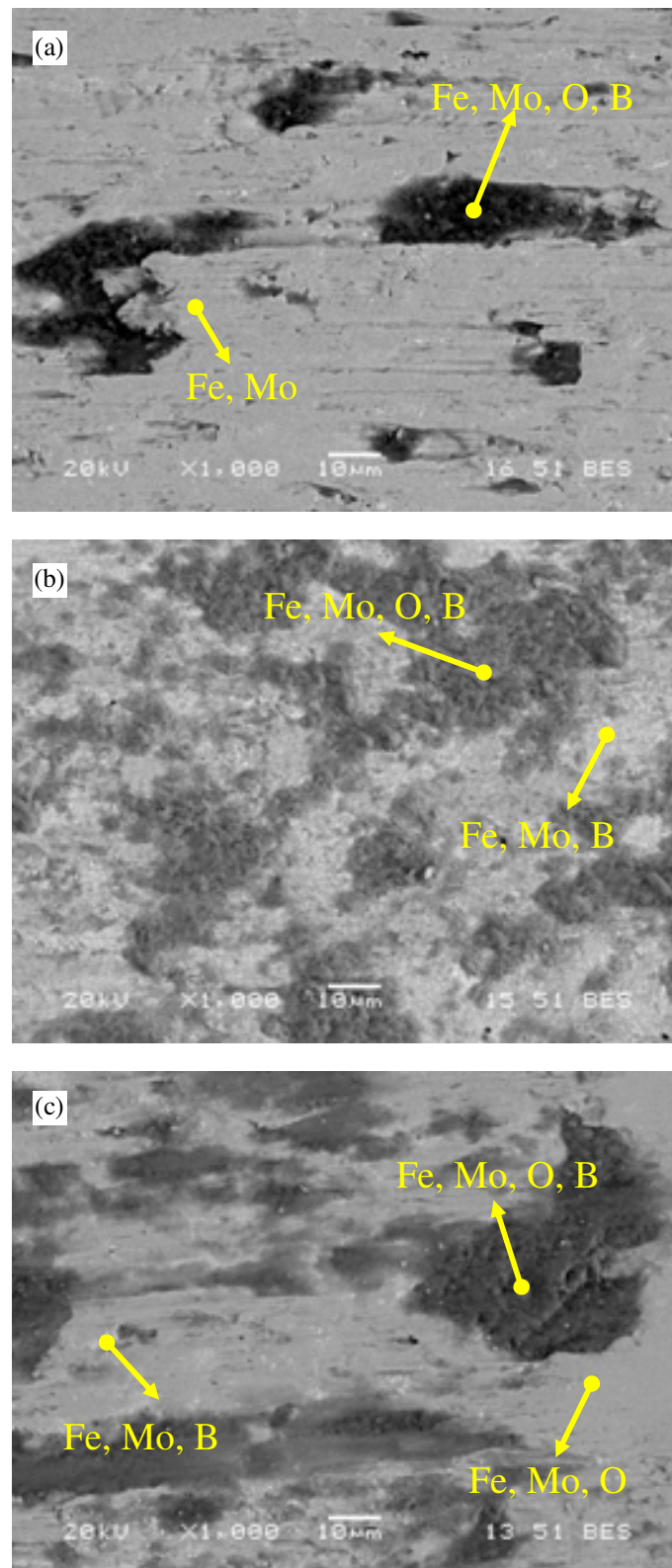


Figure 4. SEM micrographs of the worn surfaces of Fe-Mo-B based hard surface alloyed steels for 5N load (a) $\text{Fe}_{16}\text{MoB}_3$; (b) $\text{Fe}_{14}\text{Mo}_3\text{B}_3$; (c) $\text{Fe}_{12}\text{Mo}_5\text{B}_3$.

SEM microstructure and EDS analysis of the wear traces of Fe-Mo-B based hard surface alloys under 0,1 m/s and 5N load are shown in Figure 4. As a result of EDS analysis taken from the trace of abrasion, the presence of boron, molybdenum and iron as well as oxygen was determined. The wear mechanism of the surface alloyed layers showed that micro abrasive scratches and oxidative wear took place on the worn surface. Wear mechanism was changing with molybdenum content increment from the severe abrasive wear to mild abrasive wear. It is considered that the mechanism of wear is abrasive-oxidative.

4. Conclusion

1. The Fe-Mo-B based hard surface alloy layer has been successfully produced by TIG welding on the AISI 1010 steel surface.
2. The alloyed layers of Fe-Mo-B gave a good quality thick coating, porosity free and moderately smooth rippled surface topography.
3. Increase of the molybdenum content in the alloy composition caused the increase of boride phases formed in the alloyed layers.
4. The possible phases in the surface alloyed layer consist of Fe_2B , FeMo_2B_2 , $\text{Fe}_{9,7}\text{Mo}_{0,3}$, and MoB_2 phases beside the iron boride phases.
5. The hardness of the boride phases, eutectic colonies took place in the alloyed layer, transition zone and base metal are 2093 ± 228 HV0.01, 1178 ± 83 HV0.01, 381 ± 76 HV0.01, and 191 ± 10 HV0.1, respectively.
6. The friction coefficient is changing between 0.387 and 0.788 according to alloy composition and applied load. It has been observed that the friction coefficient values of Fe-Mo-B-based surface alloying materials decrease with increasing Mo content.
7. Increase in applied load caused the increase of wear rate for all alloy compositions. But increase of molybdenum content in the alloy composition caused the decrease of wear rate for all applied loads.
8. Wear mechanism of the surface alloyed layer was changing with molybdenum content increment from the severe abrasive wear to mild abrasive wear.

5. References

- [1] V. E. Buchanan, P. H. Shipway, en D. G. McCartney; Microstructure and abrasive wear behaviour of shielded metal arc welding hardfacings used in the sugarcane industry, vol 263 (2007) pp 99–110.
- [2] A. Singh, G. Singh, en G. Singh: Improving wear resistance via hardfacing of cultivator shovel, Mater. Today Proc., vol 4 (2017), pp 7991–7999.
- [3] S. Singla: Wear behavior of weld overlays on excavator bucket teeth, vol 5 (2014), pp 256–266.
- [4] D. Leroy, T. A. Siewert, S. Liu, en G. R. Edwards, Welding Brazing and Soldering. ASM International, USA (1990).
- [5] X. Wang, F. Han, X. Liu, S. Qu, en Z. Zou: Microstructure and wear properties of the Fe – Ti – V – Mo – C hardfacing alloy, vol 265 (2008), pp 583–589.
- [6] V. Jankauskas, M. Antonov, V. Varnauskas, en R. Skirkus: Effect of WC grain size and

- content on low stress abrasive wear of manual arc welded hardfacings with low-carbon or stainless steel matrix, *Wear*, vol 328–329 (2015) pp 378–390.
- [7] D. G. Ahn: Hardfacing technologies for improvement of wear characteristics of hot working tools: A review, *Int. J. Precis. Eng. Manuf.*, vol 14(2013), pp 1271–1283.
- [8] J. Gou, Y. Wang, Z. Sun, en X. Li: Study of work function and dry sliding wear behavior of Fe-based hardfacing alloys with and without nano rare earth oxides, *J. Alloys Compd.*, vol 713 (2017), pp 255–265.
- [9] C. Katsich en E. Badisch: Effect of carbide degradation in a Ni-based hardfacing under abrasive and combined impact/abrasive conditions, *Surf. Coatings Technol.*, vol 206 (2011), pp 1062–1068.
- [10] Y. F. Zhou, Y. L. Yang, Y. W. Jiang, J. Yang, X. J. Ren, en Q. X. Yang: Fe-24 wt.%Cr-4.1 wt.%C hardfacing alloy: Microstructure and carbide refinement mechanisms with ceria additive, *Mater. Charact.*, vol 72 (2012), pp 77–86.
- [11] J. Gou, P. Lu, Y. Wang, S. Liu, en Z. Zou: Effect of nano-additives on microstructure, mechanical properties and wear behaviour of Fe–Cr–B hardfacing alloy, *Appl. Surf. Sci.*, vol 360 (2016) pp 849–857.
- [12] D. Liu, R. Liu, Y. Wei, Y. Ma, en K. Zhu: Microstructure and wear properties of Fe – 15Cr – 2 . 5Ti – 2C – x B wt .% hardfacing alloys, *Appl. Surf. Sci.*, vol 271 (2013), pp 253–259.
- [13] E. Abakay, B. Kilinc, S. Sen, en U. Sen: Wear properties of TIG surface alloyed steel with 50%Fe-10%W-40%B alloy, *Acta Phys. Pol. A*, vol 127 (2015), pp 957–960.
- [14] S. Buytoz: Microstructural properties of SiC based hardfacing on low alloy steel, *Surf. Coatings Technol.*, vol 200 (2006), pp 3734–3742.
- [15] J. F. Shackelford en W. Alexander, *Mechanical Properties of Materials*. WasCRC Press, Washington (2001).
- [16] V. Raghavan, *Phase Diagrams of Ternary Iron Alloys*. ASM International; Indian Institute of Technology, Delhi (1992).
- [17] B. Aronsson en T. Lundström, *Borides, Silicides and Phosphides: A Critical Review of Their Preparation, Properties and Crystal Chemistry*, London (1965).
- [18] S. O. Yilmaz, M. Ozenbas, en M. Yaz: Synthesis of TiB₂-reinforced iron-based composite coating”, *Tribol. Int.*, vol 42 (2009), pp 1220–1229.
- [19] Z. Pala et al., “Study of residual stresses, microstructure, and hardness in FeB and Fe₂B ultra-hard layers”, *Powder Diffr.*, vol 30 (2015), pp S83–S89.

CORRESPONDENCE ADDRESS: Bülent Kılınç, **Arifiye Vocational School** Department of Welding Technologies, Arifiye/Sakarya TURKEY, bkilinc@sakarya.edu.tr

SHORT BIOGRAPHIES

Bülent Kılınç (39)

Bülent KILINÇ, He completed BSc in 2003, MSc in 2010 in the Department of Technical Education at the University of Sakarya. Bülent KILINÇ has completed his PhD in Metallurgy and Materials Science Department of the Science Institute of Sakarya University In 2018. Bülent Kılınç is a lecturer in Department of Welding Technology at Vocational School at the University of Sakarya since 2012. His research interests Thermo-chemical coating, melting Based Coatings, Corrosion and tribology, and he published several papers on these topics.

Engin KOCAMAN(29)

EnginKocaman was born on April 17 1989 - Akşehir. He graduated from his bachelor degree at Sakarya University Metallurgical and Materials Engineering department in 2013 and his master's degree at same univesity in 2017. He is currently working on PH.D. thesis titled "Development of Fe-M-Cr-B (M=Ti, Mo) based In-Situ Composite Hard Surface Alloying Coated Electrodes". He has been working as a research assistant at Bulent Ecevit University since 2016. His research interests are casting of aluminum, hard-facing coatings, solidification and nickel based single crystal super-alloys.

Mustafa Durmaz (29)

The author was born in 1989 in Samsun. He completed BSc in 2011, MSc in 2015 and he started to study PhD in 2016 in the department of Metallurgy and Materials Engineering at the University of Sakarya. Mustafa Durmaz is research assistant at the Sakarya University since 2013. His research interests lie in the area of mechanical alloying, thermochemical coating process and tribology, and he published several papers on these topics.

ErayAbakay(32)

ErayAbakay has been working as a research assistant at Sakarya University since 2012. He graduated from Yıldız Technical University Metallurgical and Materials Engineering department in 2010 andSakarya University in 2013 with his master's degree in "Nb-Al-N Coating of Steel Surfaces by Thermo Reactive Deposition Method". There are many articles available in hard-facing and thermo reactive deposition. He is currently working on PH.D. thesis titled "Electrodeposition of nickel boron coating of magnesium and its alloys".

ŞadumanŞen(49)

ŞadumanŞen has entered in 1987 to the Metallurgical Engineering Department of Sakarya Engineering Faculty of Istanbul Technical University. She graduated at the Institute of Materials Science department of Science Institute at 1994 and completed her master's degree. Şaduman Sen has completed his PhD in Metallurgy and Materials Science Department of the Science Institute of Sakarya University In 1998. She has worked as an Assistant Professor and Associate Professor in the Department of Metal Education Department of Faculty of Technical Education of Sakarya University. She has been working as a professor at the Department of Metallurgy and Materials Engineering of Engineering Faculty of Sakarya University.The Author has been studied on hard coatings, especially nitride, carbide and boride base coatings, thermochemical coatings, corrosion, Tribology and powder metallurgy subjects. She has been managing masters and doctoral theses and scientific projects. There are also a number of international and national articles and papers on these issues of the Author.

UğurŞen (52)

Uğur ŞEN, has entered in 1984 to the Metallurgical Engineering Department of Sakarya Engineering Faculty of İstanbul Technical University. He graduated at the Institute of Materials Science department of Science Institute at 1993 and completed his master's degree. Uğur ŞEN has completed his PhD in Materials Science Department of the Science Institute of Istanbul Technical University at 1998. He has worked as an Assistant Professor in the Department of Metal Education Department of Faculty of Technical Education of Sakarya University. He has worked as an Associate Professor at the Department of Metallurgy and Materials Engineering of

Engineering Faculty of Sakarya University. Uğur ŞEN has been working as a professor at the Department of Metallurgy and Materials Engineering of Engineering Faculty of Sakarya University. The Author has been studied on hard coatings, thermo-chemical coatings, corrosion, tribology, powder metallurgy and electronic ceramics subjects. He has been managing masters and doctoral theses and scientific projects. There are also a number of international and national articles and papers on these issues of the Author.

MICROSTRUCTURAL CHARACTERISATION of Fe-Ti-B-Cr HARDFACING ALLOY COATED by TIG WELDING

Engin Kocaman^{1,a}, Bülent Kılınç^{2,b}, Mustafa Durmaz^{3,c}, Eray Abakay^{3,d},
Şaduman Şen^{3,e}, Uğur Şen^{3,f}

¹Bulent Ecevit University/ Engineering Faculty / Department of Metallurgy and Materials Engineering /
Farabi Campus / Zonguldak / Turkey

²Sakarya University/ Arifiye Vocational High School / Department of Welding Technologies / Arifiye /
Sakarya / Turkey

³Sakarya University/ Engineering Faculty / Department of Metallurgy and Materials Engineering / Esentepe
Campus / Sakarya / Turkey

^a enginkocaman@beun.edu.tr, ^b bkilinc@sakarya.edu.tr, ^c mdurmaz@sakarya.edu.tr, ^d eabakay@sakarya.edu.tr,
^e sdmnsen@sakarya.edu.tr, ^f ugursen@sakarya.edu.tr

Abstract

Hardfacing is one of the most useful method to improve surface properties against to wear, corrosion and impact. This method can be applied by using various welding method such as SMAW, GTAW and SMA. The properties of coated layer can be changed with changing of chemical composition of hardfacing alloy. In this study, microstructural investigation and phase transformation was investigated of Fe-Cr-Ti-B hardfacing alloy which have different chromium ratio coated by TIG welding on a DIN St 37 steel plate with dimensions 100x50x8 mm³. Surface topography of the layer was analyzed by using scanning electron microscopy (SEM) and optical microscope (OM). Chemical analysis of the structures were determined with energy dispersive X-ray spectroscopy (EDS). Hardness of the surface layer was measured according to Vickers method. Results show that TiB₂, FeB and Fe₂B phases existed in the structure and these phases have about 1500 - 3000 HV hardness.

Key Words: Surface Alloying, Hard-facing, Phase analysis, TIG welding

1.Introduction

Hard-facing is one of the most useful method to improve surface properties against to wear resistance, impact resistance, and corrosion resistance[1]. This method is applied in various industry such as agriculture, chemical engineering, petroleum, automotive, cement production and mining to mostly struggled with wear[2–4]. In this technique, hard and wear resistant surface layer are homogeneously coated by appropriate method onto surface of a metallic substrate[5,6]. To obtain hard faced layer lot of method can be used such as physical vapor deposition, chemical vapor deposition, boronizing, carburizing, carbo-nitriding, nitriding, plasma and welding methods [7,8]. Welding coating processes contain tungsten inert gas (TIG), plasma transferred arc welding (PTA), submerged arc welding (SAW) and oxyacetylene gas welding (OAW). These techniques form an excellent metallurgical bond between coating layer and substrate material[9], [10]. Among of welding methods TIG welding has some advantage like easier, faster and more economical than others. Welding arc melts ductile substrate and hard facing powders on the substrate metal then rapidly solidified to obtain a coating layer metallurgically bonded, in TIG method[11]. In the layer various metal carbide and boride phases such as M₃C, M₇C₃, M₂₃C₆, MB and M₂B layer occurs depending on alloying composition[12], [13]. Properties of the hard-faced layer such as corrosion behavior, fracture toughness and wear resistance is related with morphology of phases, orientation, volume fraction, hardness and

matrix type[14]. Surface alloying with TIG welding, allows with rapid heating and cooling rate provided unique opportunity for the non-equilibrium synthesis of materials and produces rapidly solidified fine microstructures with extended solid solution of alloying elements[15]. It is possible to change morphology by adjusting welding parameter and alloying composition. The researchers mentioned investigated various composition but, not enough work especially Fe-Ti-B-Cr alloys has been studied yet. The present research aims characterization of an AISI 1020 substrate metal was coated with three different ferro hard-facing alloys by applied TIG welding. Morphology of coating layer was investigated assorted characterization method.

2. Experimental

In this study, an AISI 1020 steel with dimensions 100 mm X 50 mm X 8 mm was used as substrate material. Before coating, the substrate material was cleaned with acetone to remove any oil and oxide then dried ferrous powders were grounded by ring grinder and sieved to be under 75 μm grain size. Then, powders of ferrous titanium, ferrous boron, ferrous chromium and iron were mixed by different ratio. The chemical composition of substrate material and ferrous alloys were given in Table 1.

Table 1. Chemical composition of SAE 1020 steel, ferrochrome, ferrous-boron and ferrous-titanium (%wt)

	Fe	C	Si	P	S	Al	Cr	B	Ti
Substrate (AISI 1020)	Bal.	0.348	0.274	0.0047	0.0023	0,000	0.163	0,000	0,000
Ferro-chrome	26,683	0,038	0,190	0,023	0,005	0,000	73,060	0,000	0,000
Ferro-boron	80,602	0,312	0,390	0,029	0,003	0,084	0,000	18,58	0,000
Ferro-titanium	25,222	0,126	0,000	0,008	0,004	3,690	0,000	0,000	70,95
Iron powder	100,000	0,000	0,000	0,000	0,000	0,000	0,000	0,000	0,000

To produce hard-facing layer on the substrate, TIG welding was employed with using three different ferrous alloy powder mixture ($\text{Fe}_{11}\text{Ti}_4\text{B}_5$, $\text{Fe}_8\text{Ti}_4\text{B}_5\text{Cr}_3$ and $\text{Fe}_7\text{Ti}_4\text{B}_5\text{Cr}_4$). Welding was carried out electrode negative polarity (DCEP) at 140 Amperes with 2% thoriated tungsten electrode. flowing argon at 12 L/min was used to avoid the oxidation of molten pool. Other parameters which were used on TIG welding processes are seen at Table 2.

Table 2. Experimental parameters of TIG surface alloying

Parameter	Value
Electrode	Type W-2 pctThO
Diameter	2.4 mm
Angle	70 °
Voltage	20 V
Current	140 A
Heat input	2.2 MJ/m
Protective gas	Type Ar (%99.9 Ar)
Flow	12 L/min
Welding speed	Travel speed 60 mm/min
Heat input $Q = 60 \times I \times V/S$, I: current, V: voltage, and S: travel speed[16]	

Samples were prepared for microstructural characterization by cutting cross-sectional, grinding 400, 600, 1000, 1200 and 2000 mesh SiC paper respectively and finally polished. The microstructure of the sample was revealed with Nital reagent (%3 HNO_3). Surface topography of the layer was analyzed by using JEOL JSM – 6060 scanning electron microscopy (SEM) and Nikon Epiphot 200 optical microscope (OM). Chemical analysis of the structures was determined with energy dispersive X-ray spectroscopy (EDS). Rigaku XRD/D/MAX/2200/PC X-ray diffractometer (XRD) which was generated with Cu-K α radiation at 40 KV and 35 mA

was used to examine present phases in the specimens. Hardness of the surface layer was measured according to Vickers method by using Future-Tech FM 700 micro-hardness tester.

3. Results and Discussion

Microstructure and SEM images according to varying chromium ratios in the coating on AISI 1020 steel surface are given in Fig 1. It is observed that layer of the as seen molten zone onto the substrate has thickness of about 2-3 mm and shows a metallurgical bonding with the substrate. It has been determined that this rather thick coating layer has a non-porous and smooth surface structure. In the micro structures examined, the matrix, transition zone and coating layers are clearly visible.

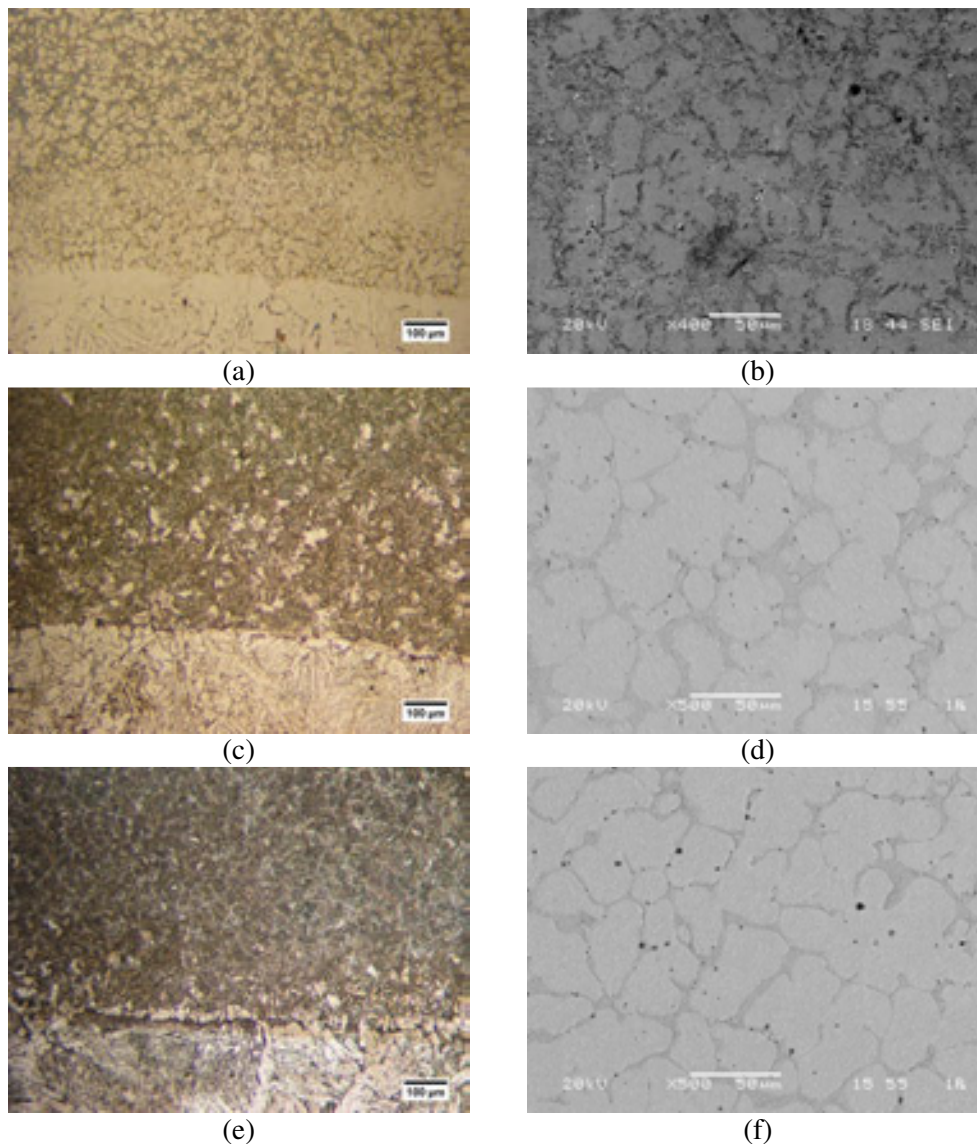


Figure 1. Optical and SEM microstructure images of Fe-Ti-B-Cr based hard surface coating layers; (a-b) $\text{Fe}_{11}\text{Ti}_4\text{B}_5$; (c-d) $\text{Fe}_8\text{Ti}_4\text{B}_5\text{Cr}_3$; (e-f) $\text{Fe}_7\text{Ti}_4\text{B}_5\text{Cr}_4$

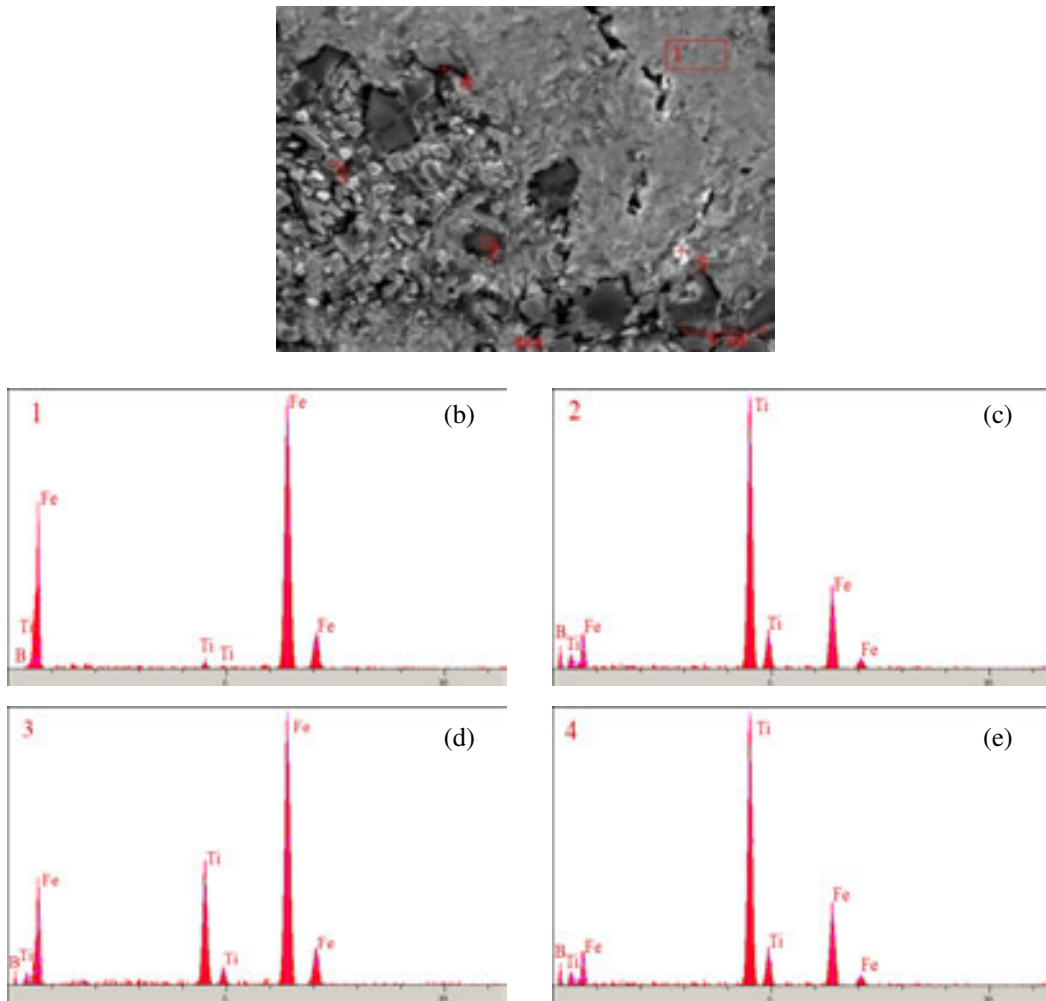


Figure 2. (a) SEM microstructure images analysis of the $Fe_{11}Ti_4B_5$ sample and (b-f) results of

Figure 1 and 2 show that Optical microstructure images, SEM microstructure images and EDS analyses taken from various regions of the $Fe_{11}Ti_4B_5$ sample. It is seen that limited block phases and eutectic structures in the SEM microstructures. The Fe-Ti-B ternary equilibrium diagram [17] shows that possible phases of the layer obtained as a result of surface alloying may be $\alpha + TiB_2 + Fe_2Ti$ at room temperature. However, it is possible that some deviation from the starting powder composition because of mixing a portion of the substrate metal with surface alloys during the TIG melting process. In this case, it is estimated that the possible phases of the layer obtained as a result of surface alloying may be $\alpha + TiB_2$ at room temperature. The EDS results in Figure 2 give an information on the phases in the structure. Considering EDS analysis and equilibrium diagram, it is probable that number 1 can be Fe, 2 is TiB_2 , 3 and 4 is Fe_2Ti . It is believed that the $(Fe,Cr)_{23}B_6$ precipitates formed in the α -Fe matrix and they grow with time occurring $\alpha + Fe_2B$ eutectic on grain boundaries.

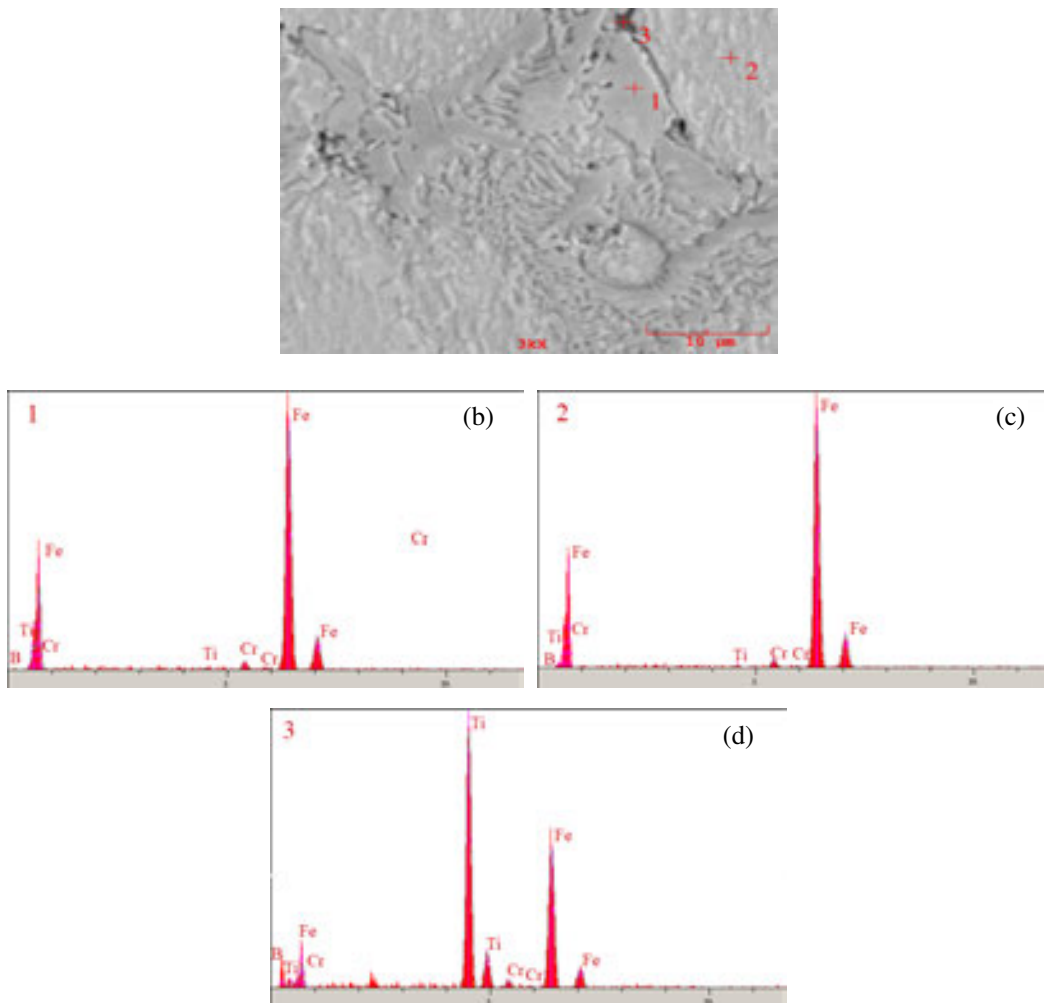
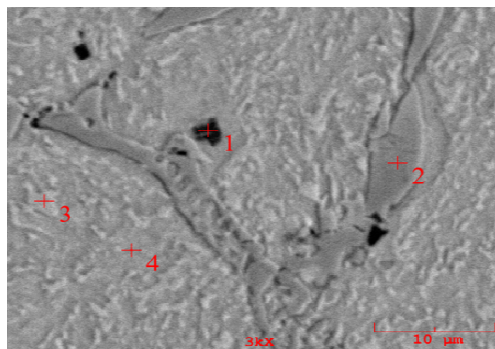


Figure 3. (a) SEM microstructure images analysis of the $\text{Fe}_8\text{Ti}_4\text{B}_5\text{Cr}_3$ sample and (b-d) results of EDS taken from various regions



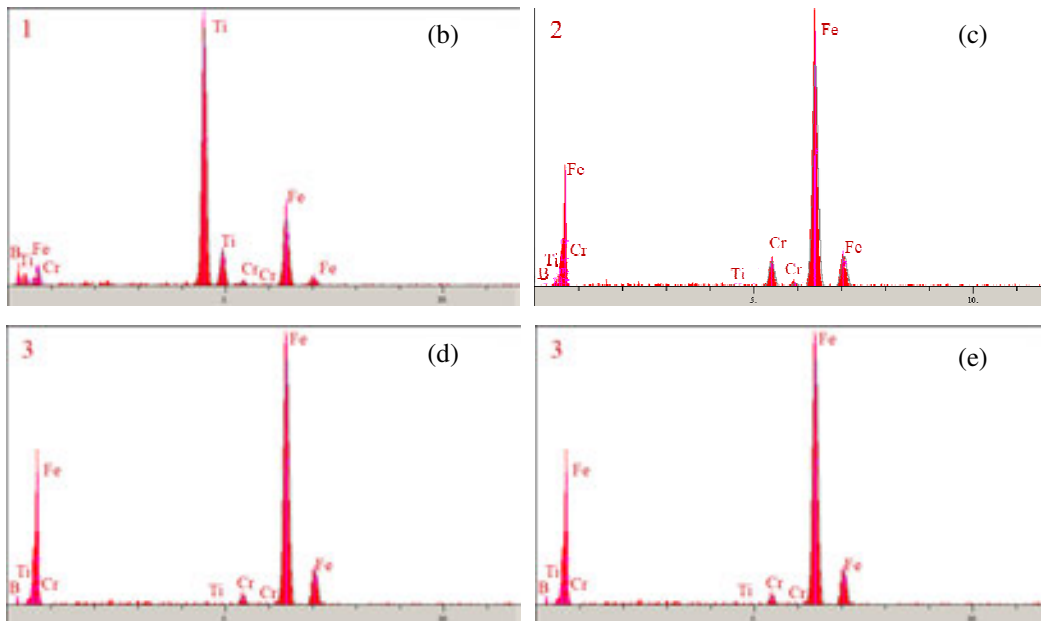


Figure 4. (a) SEM microstructure images analysis of the $Fe_7Ti_4B_5Cr_4$ sample and (b-e) results of EDS taken from various regions

The optical microstructure images, SEM microstructure images and EDS analyzes taken from various regions of $Fe_8Ti_4B_5Cr_3$ and $Fe_7Ti_4B_5Cr_4$ hard surface alloys with similar microstructures are shown in Figure 1, Figure 3 and Figure 4. However, a quantity of dilution can be occurred between surface alloying and substrate material due to high fusion temperature of TIG welding. As a result of microstructure images and EDS analyzes of these alloys; SEM microstructure images show black spots, white block-structured phases, and the existence of a eutectic phase among these phases.

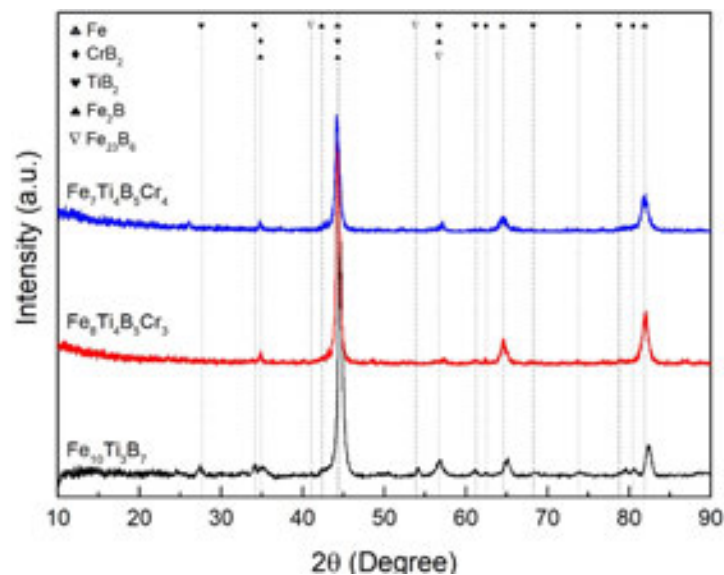


Figure 5. X-ray diffraction pattern of Fe-Ti-B-Cr based hard surface alloyed steels

According to EDS analyzes; black spots are (Fe,Ti)B₂ phase due to containing Ti and B elements, light colored block structures are (Fe,Cr)B₂ and small amount of FeB₂ phase because of containing Fe, Cr, B elements. (Fe,Cr)₂₃B₆ precipitates occur in the α -Fe matrix and α +Fe₂B alloy is formed on the grain boundaries with the precipitates growing over time. As a result of the examinations, in the surface alloy with the increase of chromium addition, (Fe,Cr)₂₃B₆ precipitates formed, contribute to form in the grain boundaries α +Fe₂B eutectic alloy. In addition, while block structure of the plane TiB₂ phase decreasing, coaxial TiB₂ phase structure increased.

Figure 5 shows the XRD analysis of Fe₁₁Ti₄B₅, Fe₈Ti₄B₅Cr₃ and Fe₇Ti₄B₅Cr₄ hard surface alloys formed on a steel substrate with a TIG source. As a result of analysis, in the non-chromium Fe₁₁Ti₄B₅ alloy, with α -Fe phase, Fe₂B, TiB₂ and Fe₂Ti phases; in the Fe₈Ti₄B₅Cr₃ and Fe₇Ti₄B₅Cr₄ alloys which is containing of chrome, the presence of CrB₂, TiB₂, Fe₂₃B₆, Fe₂B and α -Fe phases was detected. The hardness values of the boron phases in the Fe-Ti-B and Fe-Ti-B-Cr hard surface alloy plates formed on the steel surfaces by TIG welding were measured as 3050±85 HV_{0.01} for titanium-boron, for chromium-boron and 1689±85 HV_{0.01} for iron-boron. The hardness values of the eutectic columns, transition zones and substrate materials in the coating layers were 1425±76 HV_{0.01}, 650±42 HV_{0.01} and 181±7 HV_{0.01}, respectively. According to literature studies, the hardness values of the titanium boron, chrome-boron and iron-boron phases are 2300-3300 HV, 1600-2000 HV and 1500-2000 HV [18–21] respectively. The measured hardness values of samples were found to be consistent with literature. As a result, the boron phases and the hardness of the eutectic structure are considerably higher than the hardness of the base metal.

4. Conclusion

1. It is an economical method to obtain Fe-Ti-B-Cr based hard surfaces on AISI 1020 steel by TIG welding method.
2. It was determined that the hard surface alloy layer, which was found to be between 2-3 mm, had a non-porous and smooth surface structure.
3. As a result of the examinations, in the surface alloy with the increase of chromium addition, (Fe,Cr)₂₃B₆ precipitates formed, contribute to form in the grain boundaries α +Fe₂B eutectic alloy.
4. As a result of analysis, in the non-chromium Fe₁₁Ti₄B₅ alloy, with α -Fe phase, Fe₂B, TiB₂ and Fe₂Ti phases; in the Fe₈Ti₄B₅Cr₃ and Fe₇Ti₄B₅Cr₄ alloys which is containing of chrome, the presence of CrB₂, TiB₂, Fe₂₃B₆, Fe₂B and α -Fe phases was detected.
5. The hardness of boride phases and eutectic structure is very high according to the base steel.

5. References

- [1] J. Gou, Y. Wang, J. Sun, en X. Li: Surface & Coatings Technology Bending strength and wear behavior of Fe-Cr-C-B hardfacing alloys with and without rare earth oxide nanoparticles, 311 (2017), pp. 113–126.
- [2] J. Gou, P. Lu, Y. Wang, S. Liu, en Z. Zou: Effect of nano-additives on microstructure, mechanical properties and wear behaviour of Fe–Cr–B hardfacing alloy, Appl. Surf. Sci., 360(2016) pp 849–857.
- [3] Y. Bayhan: Reduction of wear via hardfacing of chisel ploughshare, vol 39 (2006), pp

- 570–574.
- [4] S. Singla: Wear behavior of weld overlays on excavator bucket teeth, vol 5 (2014), pp 256–266.
 - [5] E. O. Correa, N. G. Alcântara, L. C. Valeriano, N. D. Barbedo, en R. R. Chaves: The effect of microstructure on abrasive wear of a Fe–Cr–C–Nb hardfacing alloy deposited by the open arc welding process, *Surf. Coat. Technol.*, vol 276 (2015), pp 479–484.
 - [6] D. Leroy, T. A. Siewert, S. Liu, en G. R. Edwards: *Welding Brazing and Soldering*, 1st edition, ASM International, USA (1990).
 - [7] S. Buytoz, M. Ulutan, en M. M. Yildirim: Dry sliding wear behavior of TIG welding clad WC composite coatings, *Appl. Surf. Sci.*, vol 252 (2005), pp 1313–1323.
 - [8] F. Bülbül: Sert ve Yumuşak Kaplamalar, *Ordu Univ. J. Sci. Tech.*, no:2 vol 4 (2014), pp 32–41.
 - [9] S. Islak, S. Buytoz, en M. Karagöz: Microstructural development on AISI 1060 steel by FeW/B4C composite coating produced by using tungsten inert gas (TIG) process, *Indian J. Eng. Mater. Sci.*, vol 19 (2012), pp 253–259.
 - [10] D. G. Ahn: Hardfacing technologies for improvement of wear characteristics of hot working tools: A review, *Int. J. Precis. Eng. Manuf.*, vol 14, (2013), pp 1271–1283.
 - [11] M. H. Korkut, O. Yilmaz, en S. Buytoz: Effect of aging on the microstructure and toughness of the interface zone of a gas tungsten arc (GTA) synthesized Fe-Cr-Si-Mo-C coated low carbon steel, *Surf. Coatings Technol.*, vol 157 (2002), pp 5–13.
 - [12] C. M. Chang, C. M. Lin, C. C. Hsieh, J. H. Chen, C. M. Fan, en W. Wu: Effect of carbon content on microstructural characteristics of the hypereutectic Fe-Cr-C cladding, *Mater. Chem. Phys.*, vol 117 (2009), bll 257–261.
 - [13] M. Eroglu: Surface & Coatings Technology Boride coatings on steel using shielded metal arc welding electrode : Microstructure and hardness, *Surf. Coat. Technol.*, vol 203 (2009), pp 2229–2235.
 - [14] J. Wang et al.: Effect of nitrogen alloying on the microstructure and abrasive impact wear resistance of Fe-Cr-C-Ti-Nb hardfacing alloy, vol 309 (2017), pp 1072–1080.
 - [15] B. Kilinc, O. Cegil, E. Abakay, U. Sen, en S. Sen: Characterization of Fe-Nb-B base hardfacing of steel, *Acta Phys. Pol. A*, vol 125 (2014), bll 656–658.
 - [16] S. Buytoz en M. Ulutan: In situ synthesis of SiC reinforced MMC surface on AISI 304 stainless steel by TIG surface alloying, *Surf. Coatings Technol.*, vol 200 (2006), pp 3698–3704.
 - [17] V. Raghavan, *Phase Diagrams of Ternary Iron Alloys*. ASM International: Indian Institute of Technology, Delhi (1992).
 - [18] S. O. Yilmaz, M. Ozenbas, en M. Yaz: Synthesis of TiB₂-reinforced iron-based composite coating, *Tribol. Int.*, vol 42 (2009), pp 1220–1229.
 - [19] Z. Pala et al.: Study of residual stresses, microstructure, and hardness in FeB and Fe₂B ultra-hard layers, *Powder Diffr.*, vol 30 (2015), pp 83–89.
 - [20] L. Han et al.: Hardness, elastic, and electronic properties of chromium monoboride, *Appl. Phys. Lett.*, vol 106 (2015), pp 5–9.
 - [21] M. Audronis, A. Leyland, P. J. Kelly, en A. Matthews: The effect of pulsed magnetron sputtering on the structure and mechanical properties of CrB₂ coatings, *Surf. Coatings Technol.*, vol 201 (2006), pp 3970–3976.

CORRESPONDENCE ADDRESS: Engin Kocaman, Department of Metallurgy and Materials Engineering, 67100, İncivez Zonguldak TURKEY, +90 372 291 1970, enginkocaman@beun.edu.tr

SHORT BIOGRAPHIES

Engin KOCAMAN(29)

Engin Kocaman was born on April 17 1989 - Akşehir. He graduated from his bachelor degree at Sakarya University Metallurgical and Materials Engineering department in 2013 and his master's degree at same university in 2017. He is currently working on PH.D. thesis titled "Development of Fe-M-Cr-B (M=Ti, Mo) based In-Situ Composite Hard Surface Alloying Coated Electrodes". He has been working as a research assistant at Bulent Ecevit University since 2016. His research interests are casting of aluminum, hard-facing coatings, solidification and nickel based single crystal super-alloys.

Bülent Kılınç (39)

Bülent KILINÇ, He completed BSc in 2003, MSc in 2010 in the Department of Technical Education at the University of Sakarya. Bülent KILINÇ has completed his PhD in Metallurgy and Materials Science Department of the Science Institute of Sakarya University In 2018. Bülent Kılınç is a lecturer in Department of Welding Technology at Vocational School at the University of Sakarya since 2012. His research interests Thermo-chemical coating, melting Based Coatings, Corrosion and tribology, and he published several papers on these topics.

Mustafa Durmaz(29)

The author was born in 1989 in Samsun. He completed BSc in 2011, MSc in 2015 and he started to study PhD in 2016 in the department of Metallurgy and Materials Engineering at the University of Sakarya. Mustafa Durmaz is research assistant at the Sakarya University since 2013. His research interests lie in the area of mechanical alloying, thermochemical coating process and tribology, and he published several papers on these topics.

Eray Abakay(32)

Eray Abakay has been working as a research assistant at Sakarya University since 2012. He graduated from Yıldız Technical University Metallurgical and Materials Engineering department in 2010 and Sakarya University in 2013 with his master's degree in "Nb-Al-N Coating of Steel Surfaces by Thermo Reactive Deposition Method". There are many articles available in hard-facing and thermo reactive deposition. He is currently working on PH.D. thesis titled "Electrodeposition of nickel boron coating of magnesium and its alloys".

Şaduman Şen(49)

Şaduman Şen has entered in 1987 to the Metallurgical Engineering Department of Sakarya Engineering Faculty of Istanbul Technical University. She graduated at the Institute of Materials Science department of Science Institute at 1994 and completed her master's degree. Şaduman Şen has completed his PhD in Metallurgy and Materials Science Department of the Science Institute of Sakarya University In 1998. She has worked as an Assistant Professor and Associate Professor in the Department of Metal Education Department of Faculty of Technical Education of Sakarya University. She has been working as a professor at the Department of Metallurgy and

Materials Engineering of Engineering Faculty of Sakarya University. The Author has been studied on hard coatings, especially nitride, carbide and boride base coatings, thermochemical coatings, corrosion, Tribology and powder metallurgy subjects. She has been managing masters and doctoral theses and scientific projects. There are also a number of international and national articles and papers on these issues of the Author.

UğurŞen (52)

Uğur ŞEN, has entered in 1984 to the Metallurgical Engineering Department of Sakarya Engineering Faculty of İstanbul Technical University. He graduated at the Institute of Materials Science department of Science Institute at 1993 and completed his master's degree. Uğur ŞEN has completed his PhD in Materials Science Department of the Science Institute of İstanbul Technical University at 1998. He has worked as an Assistant Professor in the Department of Metal Education Department of Faculty of Technical Education of Sakarya University. He has worked as an Associate Professor at the Department of Metallurgy and Materials Engineering of Engineering Faculty of Sakarya University. Uğur ŞEN has been working as a professor at the Department of Metallurgy and Materials Engineering of Engineering Faculty of Sakarya University. The Author has been studied on hard coatings, thermo-chemical coatings, corrosion, tribology, powder metallurgy and electronic ceramics subjects. He has been managing masters and doctoral theses and scientific projects. There are also a number of international and national articles and papers on these issues of the Author.

ÇOK PASOLU KAYNAKLARDA; ISI GİRDİSİNİN KAYNAK METALİNE ETKİSİ

Nisanur Sarıcaoğlu ^{1,a}, Tuğçe Çam ^{1,b}, Selay Aydın ^{1,c}, Adem Kurt ^{1,d}
¹Gazi Üniversitesi, Teknoloji Fak., Metalurji ve Malzeme Mühendisliği Bölümü,
Merkez Kampüsü,
Yenimahalle- Ankara, Turkey

^a nisaricaoglu@gmail.com, ^b tugcecam95@outlook.com, ^c selay528@gmail.com, ^d ademkurt@gazi.edu.tr

Özet: Bu çalışmada tek ve çok pasolu kaynaklarda ısı girdisinin kaynak metali mikro yapı ve sertlik özelliklerine etkisi araştırıldı. Bu amaçla 10x50x150 mm ebatlarında düşük karbonlu çelik üzerine tek ve çok pasolu kaynak dikişleri çekildi. Artan ısı girdisinin ısıdan etkilenen bölgenin genişliğini artırdığı ve çok pasoların temper etkisi yaparak kaynak metali sertliğini azalttığı gözlemlendi.

Anahtar kelimeler : Kaynak, Mikro yapı, Mikro Sertlik, Isı Girdisi, ITAB

THE EFFECT OF HEAT INPUT TO WELD METAL ON THE MULTI PASS WELDING

Abstract: In this study, the influence of heat input on the weld metal microstructure and hardness properties was investigated in single and multi pass welding. For this purpose, single and multi pass welding seams were made on 10x50x150 mm low carbon steel. It was observed when increased heat input, increased the width of heat affected zone and make the tempering effect of multiple passes reduced the hardness of the weld metal.

Keywords: Welding, Microstructure, Micro hardness, Heat Input, ITAB

1. GİRİŞ (INTRODUCTION)

Son elli yıldır kaynak tekniğinde meydana gelen gelişmeler, kaynakla birleştirmenin imalat sektöründe giderek artan oranda yaygınlaşmasına ve kaynağa uygun yeni çelik türlerinin imalat sektörünün kullanımına sunulmasına neden olmuştur. Özellikle örtülü elektrotlarla ark kaynağında, kaynak makinalarının göreceli olarak ucuz ve basit olması, kaynakçının önemli ölçüde hareket serbestisine sahip ve aynı kaynak makinasıyla sadece elektrot tipini değiştirerek farklı metallerin kaynağının yapılabilmesi bu yöntemin imalatta yaygın biçimde kullanılmasına neden olmuştur. Elektrot seçimi; malzemenin kimyasal bileşimi, kaynaklı birleştirmenin dinamik veya statik yüklere maruz kalması gibi daha bir çok faktör dikkate

alınarak yapılır. Doğal olarak, elektrot imalatçıları, kaynaklı imalat sektöründe kullanılan çeşitli türden çelikleri ve yukarıda değinilen faktörleri göz önüne alarak çeşitli türden çok sayıda örtülü elektrotu piyasaya sürmüşlerdir. ^{1,2} Kaynak parçasının kalınlığı arttıkça yapılan işlemleri sağlamlaştırmak için uygulanan paso sayısı artmalıdır. Artan parça kalınlığına bağlı olarak farklı kaynak ağız açıları ve şekilleri belirlenir. Artan paso sayısı malzemeye ısı girdisini artıracağından malzemede çarpılmalara, kalıntı gerilmelere kaynak bölgesinde metalürjik iç yapı farklılıklarına yol açar. Bu sebeple en az paso ile kaynak yapmak yukarıda bahsedilen çarpılmaların ve kalıntı gerilmelerin miktarının azalmasına sebep olur.

Farklı kaynak tasarımları ve farklı malzemelerin kaynağı için geliştirilmiş elektrod türleri üretilmektedir. Bu nedenle örtülü elektrotu seçimi çok önemlidir. Kullanılacak olan dolgu metalinin; ergimiş olan metali atmosferden korumalı, iyonize yapıda olarak kaynak arkını kararlı yapmalı, absorbe ettiği gazları emebilmeli, uygun kaynak şekline izin sağlayabilmeli, kolay cüruf kaldırma, ekonomik ve sağlığa zararsız gibi özelliklere sahip olabilmelidir.

Bugün endüstriyel uygulamalarda asit, bazik, selülozik, oksit ve rutil tip olmak üzere beş tür elektrod yaygın olarak kullanılmaktadır. Bunlardan rutil örtülü elektrotlar; %40-60 TiO₂, %15-20 SiO₂, %10-14 FeMn, %15'e kadar CaCO₃ ve %15'e kadar organik maddeler içerir. Kaynak metalinde yüksek H₂ (15-30 ppm) difüzyonuna ve yüksek inklüzyona neden olur. ³ Bu elektrodların cürufu kolay kalkar ve seçilecek elektrot çapı büyük ölçüde kaynak edilecek metalin kalınlığına, kaynak pozisyonuna ve bağlantı tipine de (alın, içköşe, dışköşe, bindirme) bağlıdır.

Kaynak bölgesinde ergime çizgisinin esas metal etrafında, kaynak sırasında uygulanmış olan ısının oluşturduğu çeşitli ısıl çevrimlerden etkilenmiş ve dolayısıyla iç yapı değişimine uğramış bir bölge vardır. Bu bölgeye ısının tesiri altında kalan bölge (ITAB) adı verilmektedir. Isının tesiri altında kalan bölge esas metalin birleştiği sınırdan başlayarak, kaynak işlemi anında sıcaklığın iç yapı dolayısıyla ana metalin özelliklerini etkilediği bölgedir. Bu bölgenin sıcaklığı 1450 – 700 °C arasında değişmektedir. ⁴

Sıcaklığa bağlı olarak 1450°C ile 700°C arasında çeliğin bileşimine bağlı olarak beş farklı bölge meydana gelmektedir. Bunlar; iri taneli bölge, ince taneli bölge, kısmen dönüşmüş bölge, kaynak bölgesi ve iç yapı değişimine uğramamış (esas metal) bölgedir.

Kaynak metalinin yapısı, malzemenin kimyasal bileşimi ve soğuma esnasındaki dönüşümünün bir sonucudur. Az alaşımlı, düşük karbonlu çelik malzemelerin kaynak metali ana yapısı ferrittir ve östenit - ferrit faz dönüşüm sıcaklığına bağlı olarak bir çok ferrit morfolojisi oluşabilir. ⁵ Asiküler ferrit (α_n) düşük alaşımlı çeliklerin kaynak metalinde soğuma süresince oluşan bir mikroyapıdır. Bu mikroyapı 650 °C' nin altındaki soğumalarda meydana gelmektedir. Düşük karbonlu alaşımsız çelikler inşaat ve imalat sektöründe geniş kullanım alanlarına sahiptirler.

Yapısında yaklaşık olarak % 0,2 - 0,3 oranda C bulundurlar.

2. DENEYSEL ÇALIŞMALAR (EXPERIMENTAL STUDIES)

Bu çalışmada manuel ark kaynağı yöntemiyle dikiş kaynağı yapılan çok deney numuneleri (Ç1020) 3 tane 10 x 50 x 150 mm ebatlarında kesildikten sonra; jeneratör tipi kaynak makinesi ile tek, üç ve dört pasoda kaynak yapılmıştır. Kaynak esnasında AS R – 143 elektrot kullanılmıştır. 130 Amper akım şiddeti kullanılmıştır. Bütün kaynaklar Ø 3.25 elektrot ile yapılmıştır. Kaynak işlemi biten malzeme açık havada soğutulmaya bırakılmıştır.

Kaynak işleminde ilk parçaya tek pasolu kaynak dikişi atılmıştır. İkinci parçaya üç paso atılmıştır. Üçüncü parçaya bir dikiş yanlarına birer dikiş ve kapak dikişi atılmıştır. Toplam 4 paso atılmıştır. Kaynak işlemi tamamlanan ve açık havada soğutulan 3 numunedeki cüruf, sıçrantı vb. temizlendikten sonra şerit testere tezgâhında soğutma sıvısı ile soğutularak kesme işlemi yapılmıştır. Kesme işleminde kaynaklı numunelerin başlangıç, orta ve bitiş kısımlarına yakın olan kısımlarından 20 mm'lik kısımlar kesilerek atılmıştır. Kesme işleminde her numuneden 3 parça alınmıştır. Kaba ölçülerde kesilmiş olan mikro yapı numuneleri 120, 400, 800, 1200 numaraları SiC su zımparasıyla, her seferinde 90° döndürülerek her yönde eşit miktarda zımparalanmıştır. Zımparalanmış numuneler 3 µm'lik elmas parlaticı kullanılarak keçe üzerinde parlatılmış ve parlatılan numuneler % 2 lik Nital çözeltisi ile dağlanmış. Parlatılmış numunelerin mikro yapısının incelenmesi, PRIOR marka optik mikroskop ile esas metalden, kısmen dönüşmüş bölgeden, ince taneli bölgeden, geçiş bölgesinden ve kaynak metalinden 250x büyütmede gerçekleştirilmiştir. Daha sonra numunelerin sertlik ölçümlerini 136° ve kare tabanlı Vickers uca sahip HMW (micro hardness tester) Shimadzu sertlik cihazıyla (HV 0.2 kg) yük uygulanmıştır. Ölçümler her bir numune için ana malzemeden 2 değer, geçiş bölgesinden 2 değer, kaynak bölgesinden 2 değer, ince taneli bölgeden 2 değer, kısmen dönüşmüş bölgeden 2 değer olacak şekilde alınmıştır ve değerlerin ortalamaları alınmıştır.

Tablo 2.1 Kullanılan Çeliğin Kimyasal Kompozisyonu

ESAS METAL	C %	Mn %	Si %	P %	S %
Ç 1020	0,21	0,45	0,22	0,035	0,035

Tablo 2.2 Kullanılan Elektrotun Kimyasal Bileşenleri

TS 563EN EU20RR	C %	Si %	Mn %
AS R-143	0,08	0,35	0,65

3. SONUÇLAR VE TARTIŞMA

Paso sayısına bağlı olarak; numunelere uygulanan mikrosertlik, mikroyapı, ITAB genişliği incelemeleri sonucu ve her bir numunenin ısı girdileri aşağıda hesaplanmıştır.

3.1 ISI GİRDİSİ HESABI

$$Q = n \times \frac{U \times I \times 60}{1000 \times V}$$

Burada;			
n:	Kaynak		verimi
U: Kaynak voltajı			(V)
I: Kaynak akımı (A)			
V:	Kaynak	hızı	(cm.dak ⁻¹)
U.I:	Ark tarafından oluşturulan ısıdır. (Js ⁻¹)		

1 PASOLU:

$$Q = 0.8 \times \frac{130 \times 28 \times 60}{1000 \times 0,916} = 1,06 \text{ kJ/mm}$$

3.2 MİKRO SERTLİK DENEY SONUÇLARI

TABLO 3.2.1 Mikro Sertlik Sonuç Tablosu

Bölgeler	PASO SAYISI		
	1	3	4
ESAS METAL	206	206	206
İNCE TANE	288	285	275
İRİ TANE	333,5	331,5	186,5
GEÇİŞ	272	222	219
KAYNAK	296	203	168

Bir, üç ve dört paso halinde yapılan kaynak dikişlerinin esas metalden kaynak metaline doğru yapılan mikro sertlik değerlerinde paso sayısı arttıkça sertlik değerinin belirgin bir şekilde geçiş bölgesine kadar arttığı, geçiş bölgesinden kaynak metali merkezine doğru azaldığı gözlemlenmiştir.

Tek pasolu kaynakta esas metal sertliği 206 Vickers'dan ince taneli bölgede 288'e iri taneli bölgede 333,5 Vickers'a, geçiş bölgesinde 272 ve kaynak metalinde 296 Vickers olduğu gözlemlenmiştir.

Üç pasolu kaynakta ince taneli bölge sertliği tek pasoluya göre 288 Vickers'dan 285 Vickers'a, dört pasoluda ise 275 Vickers'a düştüğü gözlemlenmiştir. Paso sayısı arttıkça sertlik değerinin azalması ısı girdisindeki artışın bir sonucu olduğu şeklinde değerlendirilmektedir.

3.3 ITAB GENİŞLİĞİ

$$\frac{1}{T_p - T_0} = \frac{5,44 \times p_c \times t \times y}{Q} + \frac{1}{T_m - T_0}$$

Burada;

T_p	:	Fe- C	denge	diyagramında	A_1	sıcaklığı	(730 °C)
T_0	:				Oda	sıcaklığı	
T_m	:				1510	°C	
t	:				Parça	kalınlığı	
Q	:				Isı	girdisi	
y	:			ITAB		genişliği	
p_c	:						0,0044

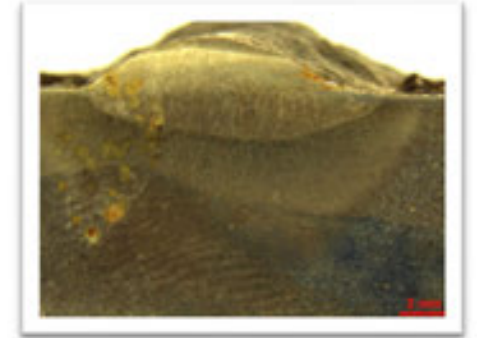
1 PASO İÇİN;

$$\frac{1}{730-25} = \frac{5,44 \times 0,0044 \times 10 \times y}{1,06} + \frac{1}{1510-25} = 0,003 \text{ mm}$$



3 PASO İÇİN;

$$\frac{1}{730-25} = \frac{5,44 \times 0,0044 \times 10 \times y}{1,33} + \frac{1}{1510-25} = 0,04 \text{ mm}$$



4 PASO İÇİN;

$$\frac{1}{730-25} = \frac{5,44 \times 0,0044 \times 10 \times y}{1,60} + \frac{1}{1535-25} = 0,05 \text{ mm}$$



ITAB genişliği ergime sınırından metal tarafına doğru yüksek ısı çevrimler sonucu mesafesi değişen bir bölgedir. ITAB genişliğini etkileyen birçok faktör (parça kalınlığı, esas metalin başlangıç sıcaklığı, esas metalin ısı iletkenliği) etkili olmaktadır. Bu çalışmada 10 mm kalınlığındaki parça üzerine tek ve çok pasolar çekildiğinden ısının iş parçasında üç boyutlu dağıldığı düşünülerek aşağıdaki üç boyutlu dağıldığı düşünülerek aşağıdaki üç boyutlu ısı dağılım formülü ITAB genişliğinin belirlenmesinde kullanılmıştır. ⁶

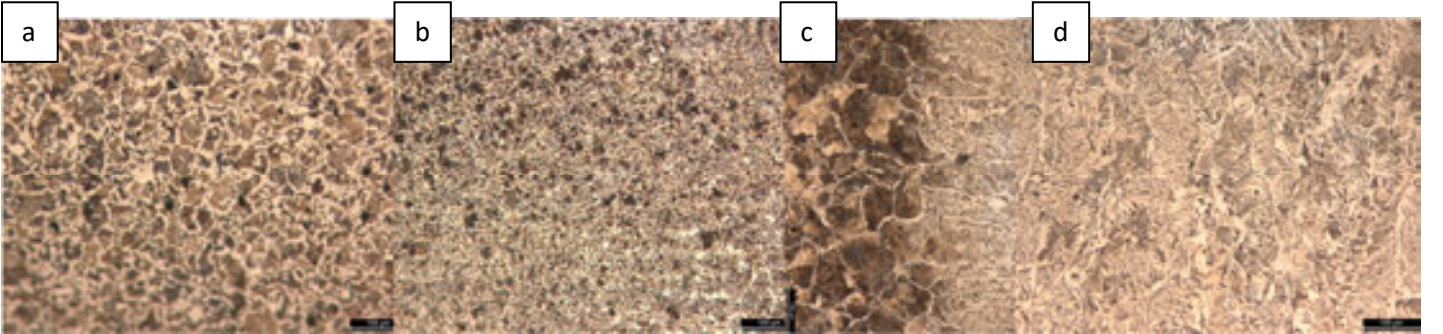
$$\frac{1}{T_p - T_o} = \frac{5,44 \times p_c \times t \times y}{Q} + \frac{1}{T_m - T_o}$$

Buna göre tek pasolu kaynakta 0.03 mm ITAB genişliği hesaplanırken üç pasolu kaynakta 0.01 mm ITAB genişliği çıkmıştır ve dört pasolu kaynakta bu değer 0.155 mm kadar çıkmıştır.

3.4 MİKROYAPI GÖRÜNTÜLERİ VE YORUM

TEK PASO

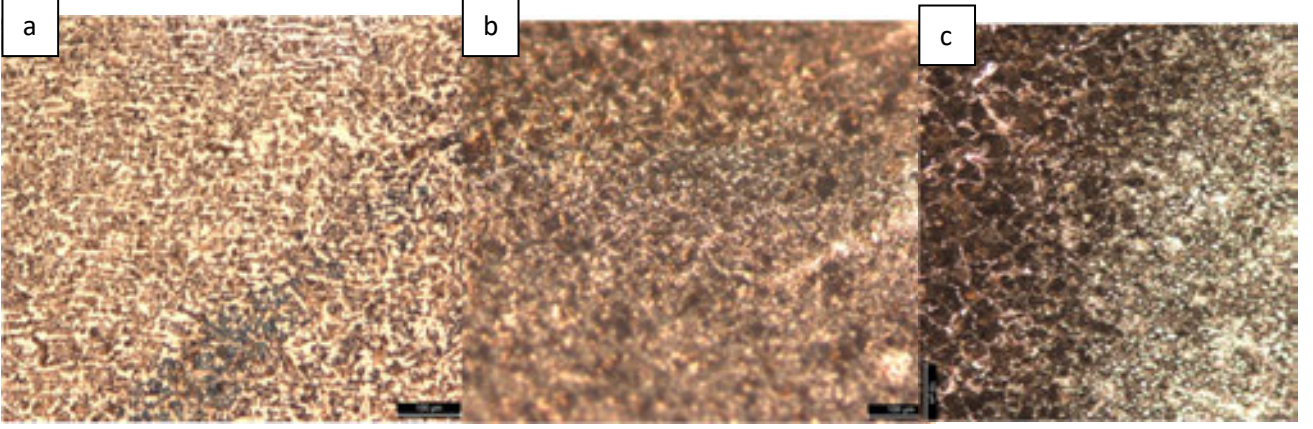
Şekil 1. Tek pasolu kaynak dikişinde esas metal ve kaynak bölgesi mikro yapıları, a- Esas metal, b- Kısmen dönüşmüş ve ince taneli bölge, c- İri taneli ve geçiş bölgesi, d- Kaynak metali mikro yapısı



Şekil 1-a da ısıdan etkilenmeyen esas metale ait mikro yapı görülmektedir. Mikro yapının eş tane boyutu ferrit ve perlitik yapılardan oluştuğu; perlit etrafında beyaz ferrit ağlarının dağıldığı görülmektedir. Esas metalden kaynak bölgesine doğru şekil 1-b de görüleceği gibi ısının esas metalin tanelerinde yeniden kristallenme sıcaklığına çıktığı ve buna bağlı olarak tane yapısının bozularak kısmen dönüşmelerin gerçekleşmesi ve soğuma hızının yükseldiğinden dolayı dönüşüm tamamlanmaya zaman bulamadığında kısmi dönüşmüş yapılar olduğu görülmektedir. Kısmi dönüşmüş bölgeyle şekil 1-c de iri taneli bölge arasında net olmamakla birlikte ince taneli bir tane yapısının oluştuğu kaynak metaline doğru şekil 1-c de görüleceği gibi tanelerin irileşerek erime çizgisine kadar yaklaşık 100µ boyutunda tanenin irileştiği görülmektedir. Erime çizgisinden kaynak metaline doğru kaynak havuzu içerisinde ergiyerek katışan yarım tanelerin epitaksiyel olarak katılarak kaynak merkezine doğru yönlendiği görülmektedir. Kaynak metali mikro yapısı östenitten tane sınırı ferrit ve widmanstatten ferritler şeklinde tane sınırlarını tane içlerine doğru büyüdükleri ve östenit taneler içerisinde asiküler ferritlerin çekirdeklenerek büyümesiyle tanelerin dönüştükleri yapısal dönüşümler gözlemlenmiştir.

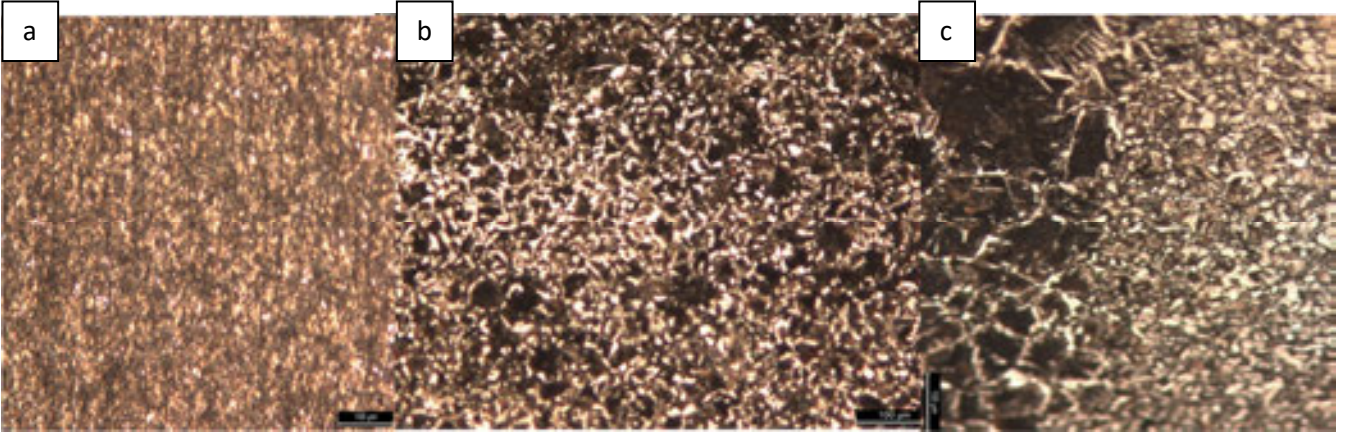
3 PASO

Şekil 2. Üç pasolu kaynak dikişinde esas metal ve kaynak bölgesi mikro yapıları, a- Esas metal, b- Kısmen dönüşmüş ve ince taneli bölge, c- İri taneli ve geçiş bölgesi



4 PASO

Şekil 3. Dört pasolu kaynak dikişinde esas metal ve kaynak bölgesi mikro yapıları, a- Esas metal, b- Kısmen dönüşmüş ve ince taneli bölge, c- İri taneli ve geçiş bölgesi



Pasolar arası sıcaklığın etkisiyle dönüşümün ısının tesiri altında kalan bölgede daha karmaşık yapı içerdiği görülmektedir. İri taneli bölge ve geçiş bölgesinde şekil 2-c de tane boyutu özellikle iri tanede belirgin olmakla birlikte iki ve üçüncü pasolar iri taneli bölgede birinci pasodaki kadar belirgin şekil göstermemektedir. Bunun nedeni muhtemelen iki ve üçüncü pasolar iri taneli bölgede ve kaynak metalinde tekrarlanan dönüşümler meydana getirmiştir. Paso sayısı arttıkça ısı girdisinin artması formül 3 de görüleceği gibi yüksek olduğundan iri taneli bölgede tane sınırı ferrit α tabaka kalınlıkları artması ve iri tane içerisinde widmanstatten ferrit büyümelerine yol açmıştır. Ancak kaynak metalinden son iki pasolar dönüşümlere sebep olarak kaynak merkezine yönelen tanelerinde yeniden kristallenmesine ve ince taneli bir yapı şeklinde olmasına yol açmıştır.

4. SONUÇLAR

Çok pasolu kaynaklarda ısı girdisinin kaynak metali mikro yapısı ve ITAB genişliğine olan etkisinin belirlenmesi amacıyla yapılan bu çalışmada aşağıdaki sonuçlar elde edilmiştir.

1. Tek ve çok pasolu kaynaklarda kaynak dikişlerinin gözle yapılan muayenesinde gözle görülür cüruf kalıntısı, makro çatlak gibi hatalara rastlanmamıştır.
2. Tek pasolu kaynaklarda esas metalden kaynak metaline doğru metalografik dönüşümler net bir şekilde gözlenirken, çok pasolu kaynaklarda ısıl çevrimlerin sonucu daha karmaşık mikro yapısal dönüşümler gözlemlenmiştir.
3. Paso sayısı arttıkça ısı girdisindeki artışa bağlı olarak ITAB genişliklerinin arttığı gözlemlenmiştir.
4. Paso sayısı arttıkça kaynak bölgesinin mikro sertlik değerlerinde azalmaların olduğu son pasoların temper etkisi yaparak sertlik azalmasına neden olduğu anlaşılmıştır.

5. TEŞEKKÜRLER

Bu çalışma Gazi Üniversitesi Kaynak ve Birleştirme Teknolojileri Araştırma ve Uygulama Merkezinde gerçekleştirildiğinden merkez çalışanlarına teşekkür ederiz.

Ayrıca her zaman destekleriyle yanımızda olan ailelerimize teşekkürü bir borç biliriz.

6. KAYNAKÇA

- [1] İ. Barlas ERYÜREK, Kaynak Teknolojisi Gazaltı Ark Kaynağı. sy-55 Baskı 2 İ.T.Ü (2007)
- [2] KAYNAK TEKNOLOJİSİ Gazaltı Ark Kaynağı Prof. Dr. İ. Barlas ERYÜREK İ.T.Ü. Makina Fakültesi Makine Malzemesi ve İmalat Teknolojisi Anabilim Dalı Başkanı sy-55 Baskı 2 (2007)
- [3] KURT Adem, Kaynak Metalurjisi Ders Notları, Ankara 2013
- [4] KURT Adem, Kaynak Metalurjisi Ders Notları, Ankara 2013
- [5] KURT Adem, Kaynak Metalurjisi Ders Notları, Ankara 2013
- [6] Sindo Kou, Welding Metallurgy, USA,1987

MIG-MAG KAYNAK ÜNİTESİ KULLANILARAK 3 BOYUTLU METAL YAZICIYLA KREMAYER DİŞLİ PARÇASINA DİŞ EKLEME İŞLEMİ

Yusuf Ayan^{1,a}, Nizamettin Kahraman^{1,b}

¹İmalat Mühendisliği, Teknoloji Fakültesi, Karabük Üniversitesi
^ayusufayan@karabuk.edu.tr, ^bnkahraman@karabuk.edu.tr

Özet

3 boyutlu yazıcılarla polimer, metal ve seramik esaslı malzemeler kullanılarak bir ürünün genellikle sıfırdan başlanılarak tam haliyle üretilmesi sağlanır. Bu yazıcılar üretilecek bir parçanın sadece tam haline getirilmesi amacıyla değil, aynı zamanda üretilen bir parçaya ek yapmak veya hasarlanan bir parçaya tamir-onarım gibi işlemler uygulamak amacıyla da kullanılabilir. Daha önceden üretimi yapılan 3 boyutlu yazıcıyla bir kremayer dişli parçasına diş ekleme işlemi bu çalışmanın konusunu oluşturmuştur. Diş ekleme işlemleri üzerine MIG-MAG kaynak ekipmanının uyarlandığı tasarlanıp üretimi yapılan 3 boyutlu metal yazıcıyla yapılmıştır. Diş doldurma işlemlerinde MAG kaynak yöntemi kullanılmış olup 4 katmanda gerçekleştirilmiştir. Çalışma sonucunda dolgu işlemleri başarılı bir şekilde tamamlanmış ancak tam diş geometrisinin sağlanması açısından dolgu sonrası yapılabilecek son imalat işlemleri uygulanmamıştır. Bu çalışma 3 boyutlu imalat yöntemiyle bir parçanın sadece tam haline getirilmesi amacıyla değil bir parçaya tamir-onarım ve ekleme işlemi yapmak için kullanılabileceğini göstermiştir.

Anahtar Kelimeler: MIG-MAG kaynağı, 3 boyutluyazıcı, tamir-onarım kaynağı.

PROCESS OF ADDING TOOTH ON THE RACK PART BY USING MIG-MAG WELDING UNIT WITH THE 3 DIMENSIONAL METAL PRINTER

Abstract

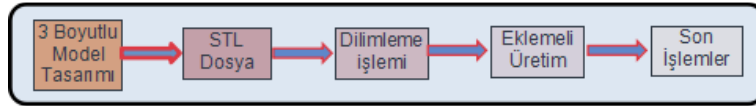
With 3 dimensional printer polymers, metals and ceramic based materials are generally manufactured from their first form to their last shape. These printers not only can be used for getting last shape of any part but also can be used for adding a new piece on a part or to apply repair-maintenance process on a part. In this study, the tooth was added on the rack part by the 3-dimensional metal printer manufactured previous study. Processing of adding teeth performed by the 3-dimensional metal printer which combined with MIG-MAG welding unit. MAG method was used for depositing teeth and depositing process were carried out as four layers. Teeth were filled successfully but smoothing treatments were not be applied for providing exact form of the teeth in this study. This study indicates that 3 dimensional printers cannot be used only for manufacturing a new part and these can be used also for repair-maintenance and adding processes.

Key Words: MIG-MAG welding, 3-dimensional printer, repair-maintenance welding.

1.Giriş

Eklemeli imalat son zamanlarda büyük ilgi gören bir üretim yöntemi olmuştur [1-3]. Bu imalat yöntemi, sanayiye esas olarak değiştirmede büyük potansiyele sahip olmakla birlikte umut veren bir teknolojidir [4]. Bu üretim yöntemi son zamanlarda geleneksel yaklaşımlar kullanılarak ekonomik olarak üretilmeyen karmaşık şekilli parçaların üretimine odaklanmıştır [5]. Bu yöntem geleneksel eksiltmeli imalat yöntemlerinden büyük ölçüde yüksek malzeme kullanımı ve ürün verimliliği sağlaması açısından farklılık göstermektedir [2]. Hafif yapılar, karmaşık parçaların üretimi, üretilen parçaların kısa zaman içinde piyasaya sunulması ve kaynakların büyük ölçüde korunması eklemeli imalat yönteminin bazı avantajlarıdır [4]. Eklemeli imalat yöntemi aynı zamanda; katmanlı imalat, hızlı prototipleme veya 3 boyutlu imalat (baskı) olarak da tanımlanabilir [6].

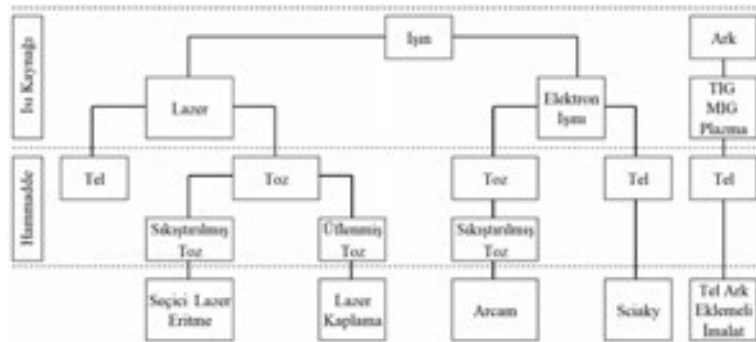
Eklemeli imalat yönteminde 3 boyutlu nesnelerin katman üstüne katman eklenerek üretimi gerçekleşir [1, 2]. Bu işlemde bir nesnenin 3 boyutlu tasarım bilgisi kullanılır [4, 7, 8]. Eklemeli imalat teknikleri esnek, kolay kontrol edilebilirdir ve bu yöntemlerle polimerler en yaygın olmak üzere farklı malzemelerden karmaşık nesnelere üretilir [1]. Şekil 1'de eklemeli imalat işleminin şematik olarak aşamaları gösterilmiştir.



Şekil 1. Eklemeli imalat işleminin aşamaları [9].

Eklemeli imalat yönteminde polimer malzemeler yaygın olarak kullanılmaktadır [1, 10]. Polimer alanında eklemeli imalat işlemi kayda değer gelişim göstermiş, çeşitli türlerde polimerler geliştirilmiş ve karmaşık özelleştirilmiş parçaların 3 boyutlu imalatı gerçekleştirilmiştir [11]. Metal ve seramik malzemelerin de eklemeli imalat yöntemiyle üretimi mümkündür [12]. Mühendislik amaçları için çoğu zaman metalik bileşenler gereklidir ve yeni çalışmalar metal eklemeli imalat yöntemini hedeflemiştir [11]. Son 20 yılda plastik parçaların prototipinden fonksiyonel metalik parçalara dönüşüm konusunda ise eklemeli imalat yöntemi alanında önemli çalışmalar yapılmaktadır [6].

Metal yapıların eklemeli imalat yöntemiyle üretiminde birçok teknik geliştirilmiştir. Bunlar; seçici lazer sinterleme, direk metal biriktirme, elektron ışını ile ergitme, şekil biriktirme ile üretim ve tel ark eklemeli imalattır [13]. Şekil 2' de metal eklemeli imalat yöntemlerinin ısı kaynağına ve kullandığı hammaddeye göre şematik sıralanması gösterilmiştir.



Şekil 2. Metal eklemeli imalat işlemleri [14].

Tel ark eklemeli imalat işlemi ısı kaynağı olarak ark, besleme teli olarak ise metalik teli kullanan direk besleme şeklinde yapılan bir işlemdir [5]. Tel ark eklemeli imalat işleminde tel elektrik arkında oransal kontrol edilerek ana malzeme üzerinde veya daha önceden biriktirilen katman üzerinde ergir [15, 16]. Elektrik arkı koruyucu gaz içerisinde alt katman ve elektrod arasında kurulur. Metal biriktirme işlemi, gaz altı metal ark kaynağı, gaz tungsten ark kaynağı veya plazma ark kaynağı torçları tarafından sağlanır [1]. Ark esaslı eklemeli imalat işlemi standart robotik MIG-MAG, TIG veya plazma kaynak sistemleri gibi metal işi sanayinde yaygın olarak bulunan ekipmanlar olmasından dolayı avantaj sağlar [17].

Eklemeli imalat işlemlerinde hammadde olarak tel veya toz kullanılır [5, 11]. Tel ark eklemeli imalat işlemlerinde ise tel kullanılır. Toz kullanılarak yapılan eklemeli imalat yöntemleriyle karşılaştırıldığında tel kullanılarak yapılan işlemler düşük maliyet, yüksek malzeme kullanımı, yüksek malzeme biriktirme verimliliği ve çevre dostu üretime sahip olması açısından büyük karmaşık parçaların otomobil, medikal ve çeşitli sektörler için üretiminde avantajlara sahiptir [18]. Kanatlar, türbin plakaları ve valfleri gibi büyük 3 boyutlu şekillendirilen parçalar için ekonomik hususlar daha önemli olması durumunda ve eklemeli imalat yöntemiyle üretilen parçaların maliyetlerinin düşük tutulması gerektiğinde; daha ucuz tel ve ucuz ısı kaynağı kullanımı daha pahalı olan tel ile değiştirilmesi üretim ekipman maliyetlerini azaltır. Bu yüzden tel ark eklemeli imalat yöntemi yüksek ekonomik öneme sahiptir [11].

Metal biriktirme işlemi için; farklı enerji kaynağı kullanımına göre tel beslemeli eklemeli imalat işlemleri üç gruba ayrılabilir: lazer, kaynak arkı, elektron ışını [13]. Tel ark eklemeli imalat işlemiyle üretilen belirli büyüklükte bir parçanın maliyeti lazer-toz esaslı üretim yöntemiyle üretilene göre daha düşüktür [15]. Düşük enerji verimliliğine sahip lazer ve elektron ışını kullanılan tel ile beslenen eklemeli imalat işlemleriyle kıyaslandığında tel ark eklemeli imalat işlemi %90 kadar enerji verimliliği sağlar [5]. Malzeme kullanılma verimliliği parça üzerinde biriktirilen tel malzemesi açısından %100'e dayanır [5, 15]. Aynı zamanda bu yöntem yüksek biriktirme oranının yanı sıra daha düşük çözünürlüğe rağmen az hata bakımından da avantajlara sahiptir. Bu yüzden orta dereceden az dereceye karmaşık yapıya büyük ölçekli yapısal parçaların üretiminde tercih edilir [16].

Şimdiye kadar eklemeli imalat yöntemlerinin ve özellikle tel ark eklemeli imalat işleminin geniş olarak anlatılmasının sebebi bu çalışmanın sadece kaynaklı birleştirme işlemi olmadığı, aslında bu çalışmanın tel ark eklemeli imalat işleminin bir örnek uygulaması olduğu içindir. Bu çalışmada daha önceden tasarlanıp üretilen 3 boyutlu yazıcıya MIG-MAG kaynak ekipmanı eklenerek, kremayer dişli parçasına diş ekleme işlemi yapılmıştır. Bu işlemi gerçekleştirmek için MAG kaynak işlemi uygulanmıştır. Şekil 3'de uygulanan işlem şematik olarak gösterilmiştir. MAG kaynak işlemi, gazaltı metal ark kaynağı uygulamalarından birisidir.



Şekil 3. Çalışmada uygulanan eklemeli imalat işlemi.

Gaz altı metal ark kaynağı metallerin birleştirilmesinde dünyada en yaygın olarak kullanılan işlemdir [11]. Bu yöntemle yapılan eklemeli imalat işleminde aynı zamanda tükenir elektrod olarak kullanılan metalik tel ile malzeme ekleme yapılır [1]. Malzeme birikim süresince tel şekillenen malzemeye dik konumdadır [3]. Gaz altı metal ark kaynağı; yüksek biriktirme

verimliliđi, düşük maliyet, otomatik yonetme, mukemmel mekanik ozelliklerden dolayi malzeme birlestirme ve tamir islemlerinde yaygin olarak kullanilir. Bu yontem aynı zamanda buyuk yapıların eklemeli imalatı için de uygulanabilir [2]. Eklemeli imalat yonteminin yukarıda sayılan birçok ustun ozellige sahip olması ve ozellikle de ulkemizde bu konuda yeterli calışmanın bulunmaması bu calışmanın baslatılma sebebinin başka bir amacı olarak gosterilebilir.

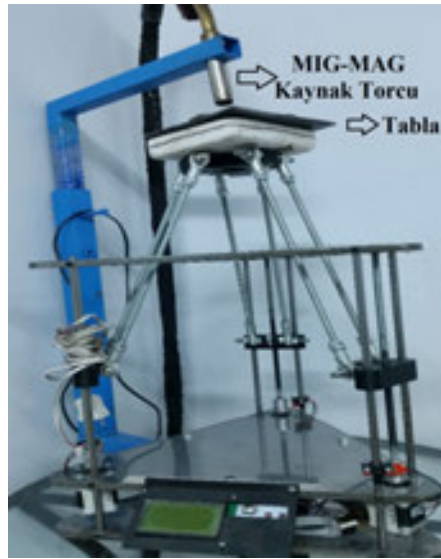
2.Deneysel Calışmalar

Bu calışmada belirlenen boyutlarda lazer kesim ile uretilen kremayer dişli parçasına diş ekleme işlemleri yapılmıştır. Uretilen kremayer dişlinin tum dişleri tam olarak uretilmeyip kasıtlı olarak bazı dişli kısımları boş olarak uretilmiştir. Uzerinde 5 adet diş hazır halde bulunmakta ve daha sonradan ise belirli bölgelerine hazır bulunan dişlerin haricinde 2 diş daha eklenmiştir. Şekil 4’de uzerine diş eklenecek kremayer dişli parçası gosterilmektedir.



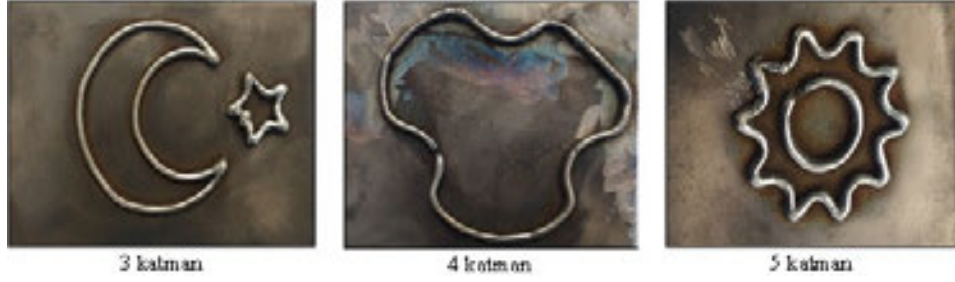
Şekil 4. Kremayer dişli.

Diş ekleme işlemleri uzerine MIG-MAG kaynak ekipmanının uyarlandığı daha önceden tasarlanıp uretimi yapılan Şekil 5’de gosterilen 3 boyutlu yazıcı kullanılarak yapılmıştır.



Şekil 5. 3 boyutlu yazıcı ve kaynak torcu.

Şekil 5’de gösterildiği gibi üretilen yazıcı polimer malzemelerinde üretiminde kullanılan 3 boyutlu delta yazıcıya büyük ölçüde benzemektedir. Yazıcıda metal ergime işleminin sağlıklı yapılabilmesi için bazı değişik tasarımlar ve önlemler uygulanmıştır. Çalışma prensibi tablanın 3 ekseninde hareket etmesi, kaynak torcununda sabit kalarak hareket eden tabla üzerine tel birikimi yapması şeklindedir. Malzeme biriktirme işlemi MIG-MAG torcundan gelen tel ile sağlanmaktadır. Bu yazıcı kullanılarak daha önceden yapılan bazı işlemler Şekil 6 ve Şekil 7’de gösterilmektedir.



Şekil 6. 3 boyutlu yazıcıyla daha önceden yapılan işlemler: Karışık yazdırma işlemleri.



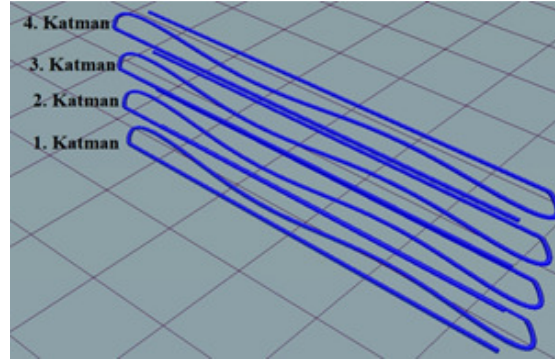
Şekil 7. 3 boyutlu yazıcıyla daha önceden yapılan işlemler: Dişli birleştirme işlemi [19].

Bu çalışmada ise Şekil 4’de gösterilen kremayer dişli parçasına diş ekleme işlemi yapılmıştır. Diş ekleme işleminde Şekil 5’de gösterilen yazıcıyla beraber MIG-MAG kaynak ünitesi kullanılmıştır. Kremayer dişli malzemesi S235JR, MAG kaynak yönteminde kullanılan dolgu teli SG2, koruyucu gaz ise HB212 karışım gazıdır. Kaynak işlemi sırasında kaynak akımı 90 A, kaynak gerilimi 26 V, kaynak hızı ise 10 mm/sn olarak seçilmiştir.

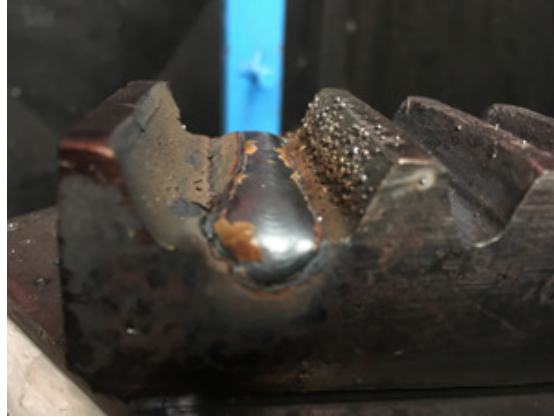
Kremayer dişli Şekil 8’de gösterildiği gibi yazıcı tablasına sabitlenmiştir. Daha sonra kremayer dişli üzerinde bulunan eksik 2 diş 4 katman halinde doldurulmuştur. Kremayer dişli parçasının bilgisayar destekli tasarım verileri kullanılarak Şekil 9’da doldurma yolu belirlenmiştir. Birinci dişin ilk katman doldurulmuş hali ise şekil 10’da gösterilmiştir.



Şekil 8. Kremayer dişli ve sabitlenmesi.



Şekil 9. Kremayer dişli diş doldurma yolu.



Şekil 10. İlk katman.

Belirlenen kaynak parametreleri ve yukarıda anlatılan işlemler uygulanarak kremayer dişli parçasına diş ekleme işlemi yapılmıştır. Bu işlemin sonucu şekil 11'de gösterilmektedir.



Şekil 11. Kremayer dişli parçasının diş eklenmiş durumu.

3.Sonuçlar ve Tartışma

Kremayer dişli parçasına diş ekleme işlemi Şekil 11’de görüldüğü gibi tamamlanmıştır. Eklenen dişler üzerinde gözle görülür herhangi bir hata bulunmamaktadır. Kremayer dişli parçası üzerinde bazı testler uygulanarak doluluk oranı ve kaynak hataları gibi durumlar incelenebilir.

Diş ekleme işlemi tamamlandıktan sonra düzgün diş formunun ve boyutlarının sağlanabilmesi için bazı ek imalat işlemlerine gereksinim duyulduğu Şekil 11’de açıkça görülmektedir. Ancak bu işlemler bu çalışmada uygulanmamıştır.

Eklenen dişlerin uygun konumunu bulabilmek ve istenilen dolgu boyutlarını sağlayabilmek için birkaç ön denemeler yapılmıştır. Eklenecek dişler kremayer dişli parçası üzerinde hali hazırda bulunan iki diş arasına yerleştirilmiştir. Kaynak torcu genişliğinin iki diş arasına girebilecek ve sağlıklı dolgu işlemini yapabilecek boyutlarda olması gereklidir. Bu durumun önceden düşünülmesi nozulun girebileceği ve çalışma esnasında herhangi bir yere çarpmadan hareket edebileceği boşluğun olması gereklidir.

Tel ark eklemeli imalat yöntemleri hakkında daha önceden yapılan çalışmalar genel olarak bu yöntemle çeşitli numuneler üretimine ve üretilen numunelere uygulanan mikro yapı ve mekanik özellikleri inceleme üzerine olmuştur. Örneğin Ti-6Al-4V [8, 15, 20], paslanmaz çelik-nikel esaslı alaşım [21], nikel alüminyum bronz alaşımı [22], alüminyum alaşımı [23, 24], bakır-alüminyum alaşımı [25], paslanmaz çelik [26, 27] gibi malzemeler üretilmiş bu malzemelerden elde edilen numunelerle çeşitli deneyler yapılarak sonuçlar değerlendirilmiştir. Bir başka çalışmada eklemeli imalat yöntemiyle 3 boyutlu bir polimer nesnenin başlangıcından son haline üretimi gerçekleştirilmiştir [28]. Bu çalışmada ise yeni bir parça üretilmemiş, daha önceden üretilmiş metal bir parça üzerine yeni bir metal parça ekleme işlemi yapılmıştır. Çalışma eklemeli imalat yönteminin sadece yeni bir parça üretmek için değil aynı zamanda daha önceden üretilmiş bir parça üzerine ekleme yapmak amacıyla da kullanılabileceğini göstermiştir. Ayrıca bu yöntemle hasarlı olan bir parçaya tamir, onarım gibi işlemler yapmak içinde kullanılabilir [19].

4.Sonuçlar

3 boyutlu yazıcının MIG-MAG kaynağına adapte edilerek tel ark eklemeli imalat yöntemiyle örnek bir kremayer dişlinin dolgusu yapıldığı bu çalışmada;

- ✓ Sanayide sıklıkla kullanılan MIG-MAG kaynak ünitesi kullanılarak tel ark eklemeli imalat işleminin uygulanabileceği,
- ✓ Yöntem kullanılarak sıfırdan yeni bir parçanın üretilebileceği gibi daha önceden üretilen bir parçaya ekleme yapılabileceği,
- ✓ Bu yöntemle tamir onarım işlemi yapılabileceği,
- ✓ Doldurma işlemi esnasında kullanılan değişkenlerin (Kaynak parametreleri, 3 boyutlu yazıcı tabla hareket hızı) iyi ayarlanmasının gerektiği,
- ✓ Düzgün diş formu ve boyutlarının sağlanması için ek imalat işlemlerine gereksinim duyulduğu

sonuçlarına varılmıştır.

5. Referanslar

- [1] J. Y. Hascoët, J. Parrot, P. Mognol, E. Willmann: Induction Heating in a Wire Additive Manufacturing Approach, *Welding in the World*, 62 (2018), pp.249-257
- [2] Z. Hu, X. Qin, T. Shao, H. Liu: Understanding and Overcoming of Abnormity at Start and End of the Weld Bead in Additive Manufacturing with GMAW, *The International Journal of Advanced Manufacturing Technology*, 95 (2018), pp.2357-2368
- [3] X. Fang, L. Zhang, H. Li, C. Li, K. Huang, B. Lu: Microstructure Evolution and Mechanical Behavior of 2219 Aluminum Alloys Additively Fabricated by the Cold Metal Transfer Process, *Materials*, (2018)
- [4] J. Fuchs, C. Schneider, N. Enzinger: Wire-Based Additive Manufacturing Using An Electron Beam As Heat Source, *Welding in the World*, 62 (2018), pp.267-275
- [5] C. Zhang, Y. Li, M. Gao, X. Zeng: Wire Arc Additive Manufacturing Of Al-6Mg Alloy Using Variable Polarity Cold Metal Transfer Arc As Power Source, *Materials Science & Engineering A*, 711 (2018), pp.415-423
- [6] M. A. Somashekara, S. Suryakumar: Studies on Dissimilar Twin-Wire Weld-Deposition for Additive Manufacturing Applications, *The Indian Institute of Metals*, 70:8 (2017), pp.2123-2135
- [7] H. Lockett, J. Ding, S. Williams, F. Martina: Design For Wire + Arc Additive Manufacture: Design Rules And Build Orientation Selection, *Journal of Engineering Design*, 28:7-9 (2017), pp.568-598
- [8] X. Shi, S. Ma, C. Liu, Q. Wu, J. Lu, Y. Liu, W. Shi: Selective Laser Melting-Wire Arc Additive Manufacturing Hybrid Fabrication of Ti-6Al-4V Alloy, *Materials Science & Engineering A*, 684 (2017), pp.196-204
- [9] S. Turhan, A. Özsoy: DMLS Yöntemiyle İmal Edilen Ti6Al4V Alaşım Özelliklerine İşlem Parametrelerinin Etkisi, *SDU International Journal of Technological Science*, 8:2 (2016), pp.15-27

- [10] D. Çelik, K. Çetinkaya: Üç Boyutlu Yazıcı Tasarımları, Prototipler ve Ürün Yazdırma Karşılaştırmaları, İleri Teknoloji Bilimleri Dergisi, 5:2 (2016), pp.151-163
- [11] G. Posch, K. Chladil, H. Chladil: Material Properties of CMT—Metal Additive Manufactured Duplex Stainless Steel Blade-Like Geometries, Weld World, 61 (2017), pp.873-882
- [12] A. Lopez, R. Bacelar, I. Pires, T. Santos, L. Quintino: Mapping of Non-Destructive Techniques for Inspection of Wire and Arc Additive Manufacturing: Proceedings of the 7th International Conference on Mechanics and Materials in Design, 11-15 June Albufeira/Portugal, (2017), pp.1829-1844
- [13] M. Liberini, A. Astarita, G. Campatelli, A. Scippa, F. Montevicchi, G. Venturini, M. Durante, L. Boccarusso, F. Memola, C. Minutolo, A. Squillace: Selection of Optimal Process Parameters for Wire Arc Additive Manufacturing, 10th CIRP Conference on Intelligent Computation in Manufacturing Engineering - CIRP ICME '16, 62 (2017), pp.470-474
- [14] Wire + Arc Additive Manufacturing: properties, cost, parts. https://www.researchgate.net/profile/Filomeno_Martina/publication/278017889_Wire_Arc_Additive_Manufacturing_properties_cost_parts/links/557866a308aeacff200282e0/Wire-Arc-Additive-Manufacturing-properties-cost-parts. Accessed February 25, 2018
- [15] F. Wang, S. Williams, P. Colegrove, A. A. Antonysamy: Microstructure and Mechanical Properties of Wire and Arc Additive Manufactured Ti-6Al-4V, Metallurgical And Materials Transactions A, 44A (2013), pp.968-977
- [16] J. Yang, H. Yang, H. Yu, Z. Wang, X. Zeng: Corrosion Behavior of Additive Manufactured Ti-6Al-4V Alloy in NaCl Solution, Metallurgical And Materials Transactions A, 48A (2017), pp.3583-3593
- [17] C. M. A. Silva, I. M. F. Bragança, A. Cabrita, L. Quintino, P. A. F. Martins: Formability of a Wire Arc Deposited Aluminium Alloy, J Braz. Soc. Mech. Sci. Eng., 39 (2017), pp.4059-4068
- [18] Q. Wu, J. Lu, C. Liu, X. Shi, Q. Ma, S. Tang, H. Fan, S. Ma: Obtaining Uniform Deposition with Variable Wire Feeding Direction During Wire-Feed Additive Manufacturing, Materials and Manufacturing Processes, 32:16 (2017), pp.1881-1886
- [19] Y. Ayan, E. Sarı, N. Kahraman: 3B Metal Yazıcı Kullanılarak MIG-MAG Kaynak Yöntemi İle Tamir-Onarım Kaynak Uygulamasına Bir Örnek, Düzce Üniversitesi Bilim ve Teknoloji Dergisi, 6:4 (2018), pp.1190-1199
- [20] M. Neikter, P. Åkerfeldt, R. Pederson, M. L. Antti: Microstructure Characterisation of Ti-6Al-4V from Different Additive Manufacturing Processes, IOP Conf. Series: Materials Science and Engineering 258 (2017) 012007
- [21] T. Abe, H. Sasahara: Dissimilar Metal Deposition with a Stainless Steel and Nickel-Based Alloy Using Wire and Arc-Based Additive Manufacturing, Precision Engineering, 45 (2016), pp.387-395
- [22] D. Ding, Z. Pan, S. van Duin, H. Li, C. Shen: Fabricating Superior NiAl Bronze Components through Wire Arc Additive Manufacturing, Materials, 9 (2016), 652

- [23] J. Bai, H. L. Ding, J. L. Gu, X. S. Wang, H. Qiu: Porosity Evolution in Additively Manufactured Aluminium Alloy During High Temperature Exposure, IOP Conference Series: Materials Science and Engineering, 167 (2017) 0120145
- [24] A. Horgar, H. Fostervoll, B. Nyhus, X. Ren, M. Eriksson, O. M. Akselsen: Additive Manufacturing Using WAAM with AA5183 Wire, Journal of Materials Processing Tech., 259 (2018), pp.68-74
- [25] B. Dong, Z. Pan, C. Shen, Y. Ma, H. Li: Fabrication of Copper-Rich Cu-Al Alloy Using the Wire-Arc Additive Manufacturing Process, Metallurgical And Materials Transactions B, 48B (2017), pp.3143-3151
- [26] L. Ji, J. Lu, C. Liu, C. Jing, H. Fan, S. Ma: Microstructure and Mechanical Properties of 304L Ateel Fabricated by Arc Additive Manufacturing, MATEC Web of Conferences, 128 (2017) 03006
- [27] X. Chen, J. Li, X. Cheng, B. He, H. Wang, Z. Huang: Microstructure and Mechanical Properties of the Austenitic Stainless Steel 316L Fabricated by Gas Metal Arc Additive Manufacturing, Materials Science & Engineering A, 703 (2017), pp.567-577
- [28] A. Çelebi, H. Tosun, A. C. Önçağ: Hasarlı Bir Kafatasının Üç Boyutlu Yazıcı ile İmalatı ve İmplant Tasarımı, International Journal of 3D Printing Technologies and Digital Industry, 1:1 (2017), ss. :27-35

SU ALTI ÖRTÜLÜ ELEKTROD ARK KAYNAK YÖNTEMİNDE DERİNLİĞİN KAYNAK KALİTESİNE ETKİSİ

ZahitÇolak^{1,a}, Kadir İmdat^{1,b}, Yusuf Ayan^{1,c}, Behçet Güleç^{2,d}, Nizamettin
Kahraman^{1,e}

¹İmalat Mühendisliği, Teknoloji Fakültesi, Karabük Üniversitesi

²Metalurji ve Malzeme Mühendisliği, Teknoloji Fakültesi, Gazi Üniversitesi

^azahitcolak@hotmail.com, ^bkadirimdat@gmail.com, ^cyusufayan@karabuk.edu.tr, ^dbehcetg@gazi.edu.tr, ^e
nkahraman@karabuk.edu.tr

Özet

Bu çalışmada, Grade AH36 gemi sacı örtülü elektrod ark kaynak yöntemiyle, izole edilmiş (bant kaplı) E6013 standardına sahip rutil elektrot kullanılarak, atmosferik şartlarda ve sualtında farklı derinliklerde (4, 8 ve 16 m) birleştirilmiştir. Kaynaklı numunelere gözle muayene, ultrasonik ve sıvı penetrant muayenesi uygulanmış, mekanik özelliklerini belirlemek için çekme testi ve sertlik deneyleri yapılarak değerlendirilmiştir. Ayrıca kaynak bölgesinde meydana gelen yapısal dönüşümleri incelemek amacıyla makro/mikroyapı çalışmaları gerçekleştirilmiştir. Tahribatsız muayeneler sonucunda sualtında birleştirilen kaynaklı numunelerin kaynak metalllerinde cüruf kalıntıları ve gaz boşluklarına rastlanmıştır. Çekme testleri sonucunda kopmalar; sualtında birleştirilmiş numunelerde kaynak metalinden, atmosferik şartlarda birleştirilen numunelerde ise ana malzemeden gerçekleşmiştir. Dolayısıyla, 16 m derinlikte sualtında gerçekleştirilen ve çekme değeri en düşük kaynaklı numunedeki mukavemet düşüşü (atmosferik şartlarda birleştirilene göre) yaklaşık % 15 olarak belirlenmiştir.

Anahtar Kelimeler: Sualtı kaynak yöntemi, gemi sacı, mikroyapı, tahribatsız muayene, mekanik özellikler.

THE EFFECT OF WATER DEPTH ON WELD QUALITY IN UNDERWATER SHIELDED METAL ARC WELDING

Abstract

In this study, Grade AH36 steel ship plates were joined at both the atmospheric conditions and underwater at different depths (4, 8 and 16 m) through shielded metal arc welding process using isolated rutil electrodes conforming to E6013 standard. The welded specimens were subjected to visual inspection, ultrasonic and liquid penetration tests. Tensile and hardness tests were also carried out in order to determine the mechanical properties of the welded joints. In addition, macro and microstructural examines were performed to examine the structural transformation. Non-destructive test results showed that the specimens joined underwater had slag remains and gas porosities. It was seen from the tensile test results that the specimens joined underwater fractured within the weld metal while the specimens joined at atmospheric conditions fractured within the base metal. Therefore, the specimen joined underwater at 16 m depth had the lowest tensile strength and it exhibited a 15 % reduction in tensile strength when compared to the one joined at atmospheric conditions.

Key Words: Underwater welding, ship plate, microstructure, nondestructive testing, mechanical properties.

1.Giriş

Demir esaslı alaşımlar kimyasal bileşiminde demir elementinin ana bileşen olarak yer aldığı ana bileşenler olarak tanımlanır. Çelikleri çeşitli bakımlardan sınıflandırmak mümkündür. Ancak genellikle çelikler alaşımsız (sade karbonlu) ve alaşımlı olmak üzere iki büyük guruba ayrılabilir [1]. Düşük karbonlu çelikler genellikle ağırlıkça %0,25'den daha az oranlarda karbon içerir ve martenzitik dönüşümü hedefleyen ısı işlemlere karşı duyarsızdırlar [2,3]. Gemi inşaatında çoğunlukla kullanılan çelik; fiyat, özellikler ve bulunabilirlik yönünden uygun olan yumuşak çelik (mildsteel) malzemedir. Soğuk ve sıcak şekil vermeye ve kaynağa uygun olan bu malzemenin işleme sıcaklıklarındaki mekanik özelliklerinde önemli bir değişim gözlenmez [4]. Bir çelik malzemenin gemi inşaatında kullanılabilmesi için, öncelikle gemiyi belgeyecek olan klas kuruluşu tarafından denetlenmiş, test edilmiş ve damgalanmış olması gerekir. Klas kuruluşları gemi inşaatında kullanılan çelikleri belirli bir gruptandırmaya tabi tutmuş ve bunlara A, B, C, D ve E harf sembolleri vermiştir. A ve B yumuşak çelik malzeme türleridir. Klas kuralları, hangi çelik malzemelerin hangi şartlar altında kullanılacağını ve mekanik özelliklerinin neler olması gerektiğini net ve açık bir şekilde belirtmektedir [1,5,6].

Gemi inşaatı tekniği günümüze kadar oldukça hızlı ve başarılı bir şekilde gelişmiştir. Günümüzde gemi inşasında elektrik ark kaynağı geniş ölçüde kullanılmaktadır [7]. Elektrik ark kaynağında kaynak için gerekli ısı, elektrik arki tarafından sağlanmaktadır. Günümüzde bir çok ark kaynak yöntemi olmasına rağmen en yaygın kullanılan ergitme kaynağı yöntemi elektrik ark kaynak yöntemidir [8]. Örtülü elektrodla ark kaynağında ark, kaynak banyosunu oluşturmak üzere esas metali ve elektrodu ergitir. Kaynak banyosu elektrodteki örtü nedeniyle oluşan ergimiş curuf tabakası ve gaz tarafından korunur [9,10].

Gemilerde onarım amaçlı sualtı kaynak işlemleri normalde sadece yarı kalıcı bir özelliğe sahiptir [11]. Dalgalı suda gemiler esner ve çok hızlı soğuma sebebi ile sualtı kaynakları mukavemetlerinin %50'sini kaybederler [5,12] Bu nedenle bu tür kaynaklar sadece geçici onarımlar olarak kabul edilmeli ve gemi karaya çıkarıldığında değiştirilmelidir [13]. Bununla birlikte uygun kaynak yapıldığında çelik yapılara ve levhalara yapılan parça yamalar pek çok uygulama için kalıcı bir onarım olarak kabul edilebilir [5,11]. Bu yöntemde aynı zamanda dalgıç olan kaynakçı, sualtında arki tutmaz. Bunun yerine kaynakçı, bağlantı kısmına elektrodu yerleştirir, akım verir bu esnada elektrod uygun basınç ve açıda tutulur ve böylelikle elektrod kendi kendine tükenir [5,14]. Kaynakçı için hazırlanmış bir oluk olmaksızın düz bir paso kaynak yapmak neredeyse imkansızdır. Bu yöntemde de çok paso yapmak gereği duyulabilir. Pasolar arası cüruf kalıntıları temizlenmek suretiyle yöntem çok pasolu kaynak uygulamasına elverişlidir [11,12].

Islak ortam kaynağı için kullanılan elektrodlar atmosferik şartlarda kullanılan elektrodlarla aynı özellikleri taşımakla birlikte suyla temasını önlemek için bir takım kaplama uygulamasına tabi tutulur [5,11,14]. Normal örtülü elektrotlar sualtında kullanıldıkları zaman, kısa sürede örtüsü çözülmekte ve elektrot çıplak duruma geçmektedir. Bu nedenle örtünün suya karşı dayanıklı olması gerekmektedir [13,15]. Bu amaçla, izole bant, lak veya plastik malzemeler ile parafin kullanılmaktadır. İzole bant, doğrudan elektrotun üzerine sarılmaktadır. Gemi lakı veya parafin ile yalıtıldığında en iyi sonuç alınmaktadır [5,11,12,15]. Yaş ortamda yapılan elektrik ark kaynağının kullanım alanları ise; sızdırma çatlakları, sualtındaki gemi gövdelerinde meydana gelen aralıklar, liman ile köprü ayağı ve platform tesislerinde, sahil tesislerinde, çelik levha kazıklarının tamiri gibi alanlarda uygulama yapılır [15,16]. Yukarıda sayılan gerekçelerden yola çıkarak; bu çalışmada gemi inşa sanayiinde sıklıkla kullanılan Grade AH36 gemi sacı, örtülü elektrod ark kaynak yöntemi ile farklı derinliklerde birleştirilmiş ve kaynaklı bağlantıların bazı mekanik/mikroyapı özellikleri araştırılmıştır.

2.Deneysel Çalışmalar

Deneylerde 12 mm kalınlığında 355 MPa minimum akma dayanımı olan Grade AH36 çelik levhalar (Çizelge 1) kullanılmıştır. Kaynaktan önce malzemeler sulu kesim şerit testere aracılığı ile 400x100x12 mm ebatlarına düşürülmüş ve uzun kenarlarına kesit boyunca 22,5°'lik kaynak ağızı açılmıştır. Şekil 1'de görüldüğü gibi malzemeler atölye ortamında bir fikstür aracılığı ile sabitlenmiştir. Kaynak ağız açısında oynama olamaması amacıyla her iki ucundan yine aynı malzeme ile puntalanmak suretiyle sabitlenmiştir.

Çizelge 1. Grade A gemi sacının kimyasal bileşimi (ağırlıkça %).

Malzeme	C	Si	Mn	P	S	Al	Ti	Cu	Cr	Ni	Mo	Fe
Grade A	0.18	0,50	0,90	0,035	0,035	0,015	0,02	0,35	0,20	0,40	0,08	Kalan



Şekil 1. Kaynak ağızı açılmış parçaların kaynak öncesi fikstürle sabitlenmesi.

Atmosferik şartlarda ve su altında elektrik ark kaynak yöntemi uygulaması için Çizelge 2'de mekanik özellikleri verilen E 6013 (C=0.06, Si=0.40, Mn=0.55, Fe=kalan) rutil örtü tipli elektrod kullanılmıştır. Suyun örtüye olan bozunma etkisini önlemek amacıyla elektrodla bant yardımıyla sızdırmazlık özelliği kazandırılmıştır.

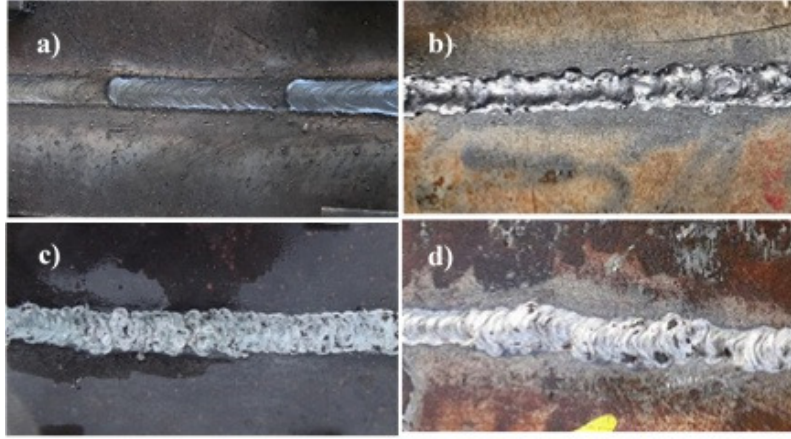
Çizelge 2. E6013 rutil örtülü elektrotun mekanik özellikleri.

Test Şekli	Akma Dayanımı (N/mm ²)	Çekme Dayanımı (N/mm ²)	Uzama (%)	Çentik Darbe Dayanımı (N/mm ²)
Kaynak Sonrası	500	560	28	55

Kaynak işlemi endüstriyel bir dalgıç tarafından tekne ile yeterli derinliği oluşturacak şekilde açılarak çelik bir kafes aracılığı ile gerçekleştirilmiştir. Atmosferik şartlarda bir numune ve su altında 4 m, 8 m ve 16 m olmak üzere üç farklı derinlik ölçülerek kaynak işlemi yapılmıştır. Kaynak uygulaması kök ve kep dahil ortalama altı paso dolgu yapılarak gerçekleştirilmiştir.

Kaynak işlemleri uygulaması endüstriyel dalgiç tarafından bir tekne ile gerek duyulan derinlik miktarı kadar iskeleden açılarak gerçekleştirilmiştir. Uygulama, seçilen üç farklı derinlik parametresinin uygulaması için 4 m, 8 m ve 16 m derinlikler ölçülerek çelik bir kafes içerisinde yapılmıştır.

Bant kaplı elektrotla malzemenin ilk etapta tek pasoda kök birleştirilmesi gerçekleştirilmiş, ardından üç paso dolgu işlemi gerçekleştirilmiştir. Son olarak iki paso dolgu işlemi ve son kapak paso atılarak kaynak işlemi tamamlanmıştır.



Şekil 2. Kaynaklı numunelerin genel görünüşü.

Şekil 2’de verilen görsellerde a) deniz seviyesinde atmosferik şartlarda birleştirilen numune, b) 4 m derinlik, c) 8 m derinlik ve d) 16 m derinlikte birleştirilen numuneleri ifade etmektedir.

Kaynak işlemi tamamlanan numuneler direkt tahribatsız muayene (gözle muayene, sıvı penetran ve ultrasonic muayene) testlerine tabi tutulmuştur. Bu muayeneler akredite firmalara yaptırılarak her bir muayene raporu uzamanı (Level II) tarafından yorumlanmıştır.

Kaynak işlemi sonucu 400x200x12 mm ebatlarında olan kaynaklı parçaların, kaynak başlangıç ve bitiş kısımlarından en az 20 mm’lik kısımları ıskarta olarak ayrılmıştır. Kaynak yönü takip edilerek her parçadan 4 adet çekme ve 1 adet de metalografi/sertlik işlemleri için hesaplanarak kesim işlemi gerçekleştirilmiştir. Çekme deney numuneleri hazırlanırken TS EN ISO 4136 (2012) nolu “Metalik malzemelerin kaynakları üzerinde tahribatlı deneyler – Enine çekme deneyi” isimli standardı uygulanmıştır. Kaynaklı numuneler AG-50 kN SHIMADZU Autograph çekme/basma cihazında çekme testine tabi tutulmuştur. Test esnasında çekme hızı 0.5 mm/dk olarak seçilmiştir. Kaynaklı numunelere uygulanan çekme testi, her bir parametreden 3 adet yapılmış ve ortalamaları değerlendirilmiştir.

Sertlik testi için hazırlanan numunelerde TS EN ISO 9015 (2011) nolu “Metalik malzeme kaynaklarında tahribatlı deneyler-sertlik deneyi-Kısım 2: Kaynaklı birleştirmelerde mikro sertlik deneyi” standardına uyulmuştur. Sertlik testi için ayrılan kaynaklı numuneler, klasik metalografik numune hazırlama işlemine (zımparalama ve parlatma) tabi tutulmuşlardır. Sertlik ölçümleri Shimadzu HMV cihazda yapılmıştır. Sertlik ölçme işlemlerinde 500 g yük ($HV_{0,5}$) uygulanmış ve sonuçlar için her bölgeden gerçekleştirilen 3 ölçümün sonucunun ortalaması ifade edilmiştir.

Mikroyapı numuneleri standart gömme, zımparalama, parlatma ve dağlama işlemlerine tabi tutulmuşlardır. Dağlama, 2 ml HNO₃ (Nitrik Asit) ve 98 ml metanolden oluşan kimyasal solüsyonda 5 s süre ile yapılmıştır. Mikroyapı için hazırlanan numuneler bilgisayara görüntü aktarabilen 1000 büyütme kapasiteli NIKON Epiphot 200 marka optik mikroskop ile görüntülenmiştir.

3.Sonuçlar ve Tartışma

Kayaklı numunelere uygulanan tahribatsız testlerden görsel muayene, gözle muayene sertifikasına sahip bir inspektöre, sıvı penetran ve ultrasonik muayene ise seviye II derecesine sahip bir inspektöre yaptırılmıştır. Seviye II olarak belgelendirilmiş olan kişi, tahribatsız muayene prosedürlerine göre tahribatsız muayene yapacak şekilde uzmanlığını kanıtlamıştır. Bu personel muayeneyi bizzat kendisi yaparak, sonuçları, uygulanabilir standard, kural veya şartnamelere göre yorumlar/değerlendirir ve muayene sonuçlarını raporlandırır. Bu çalışmada kapsamında testler de yukarıda verilen testlerde uzmanlığını kanıtlamış inspektörlere yaptırılmıştır. Bilindiği gibi gözle muayene inspektörleri kaynak yüzeyinin profili ve kökteki sarkma ve kapaktaki taşma miktarlarını inceleyerek, kabul standardına uygun olup/olmadığına bakarlar. Sıvı penetran ve ultrasonikmuayeneciler ise ilgili standarttaki Muayene-Kabul Seviyeleri'ne bakarak karar verirler. TS EN ISO 23277 (2014); Kaynakların Tahribatsız Muayenesi-Kaynakların Penetrant Muayenesi-Kabul Seviyeleri'ni, TS EN ISO 11666 (2010), Kaynakların tahribatsız muayenesi-Ultrasonik muayene- Kabul seviyelerini içerir. Ancak bu kriterler atmosferik şartlarda yapılmış kaynaklar için geçerlidir. Literatürde su altında yapılan kaynaklar için özel bir kabul seviye standardına rastlanılmamıştır. Bu yüzden inspektörler sadece var olan kusurları raporlarında kayıt altına almışlar, kaynağın kabul ve/veya reddine dair bir sonuç beyan etmemişlerdir.

3.1. Gözle Muayene

Gözle muayene işleminde kaynak fazlalığı, yanma olukları, eksen kaçıklığı, dikişin konumu, yüzeydeki ark izleri ve oyukların olup olmadığı standartta belirtilen fiziksel ortam kullanılarak bir uzman tarafından gerçekleştirilmiştir.

Muayene sonucunda, atmosferik kaynakta herhangi bir kaynak hatasının (yetersiz nüfuziyet, yenme oyukları yüzeye açık çatlak gibi) bulunmadığı saptanmıştır. Ancak su altında uygulanan kaynaklarda, cüruf kalıntılarının varlığının yanında, yanma oluklarının ve kökte kısmi çökme hatasının oluştuğu belirlenmiştir.

3.2. Sıvı Penetran Muayenesi

Bu işlem için ilk etapta yüzey temizliği hassas bir şekilde gerçekleştirilmiştir. Kaynak bölgesi penetran sıvısıyla iyice kaplanmış ve daha sonra fazla olan sıvı temizlenmiştir. İkinci aşama olarak emici gücü oldukça yüksek olan beyaz renkli geliştirici uygulanmıştır. Ardından muayene işlemi gerçekleştirilmiş ve sonuçlandırılmıştır. Muayene işlemi sonucunda atmosferik şartlarda yapılan kaynaklı numunede herhangi bir yüzey hatası görülmezken, su altında gerçekleştirilen kaynakların tamamında bazı yüzey hatalarının (cüruf kalıntıları, yenme oyukları) varlığı gözlemlenmiştir.

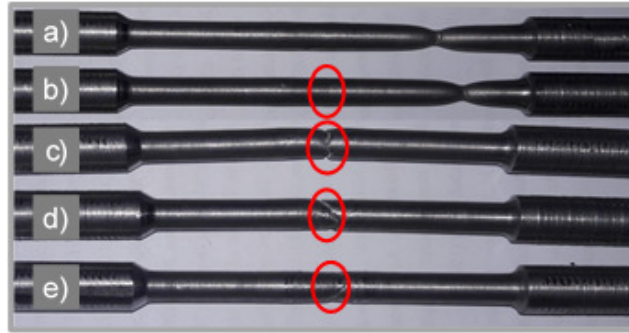
3.3. Ultrasonik Muayene

Sualtı ark kaynak yöntemi ile atmosferik şartlarda ve farklı derinliklerde yapılan birleştirmeler, yüzey altı kusurların tespiti için ultrasonik muayene işlemine tabi tutulmuşlardır. Genellikle

yüzey altı kusurlar için yapılan bu testte, atmosferik şartlarda birleştirilmiş numunelerde kaynak hatasına rastlanılmamıştır. Su altı kaynaklı numunelerin ultrasonik muayene sonucunda, sualtı ark kaynağında oluşabilecek cüruf kalıntıları ve gaz boşlukları hatası dışında herhangi bir iç kaynak hatasına (özellikle de çatlak) rastlanılmamıştır.

3.4. Çekme Deneyi

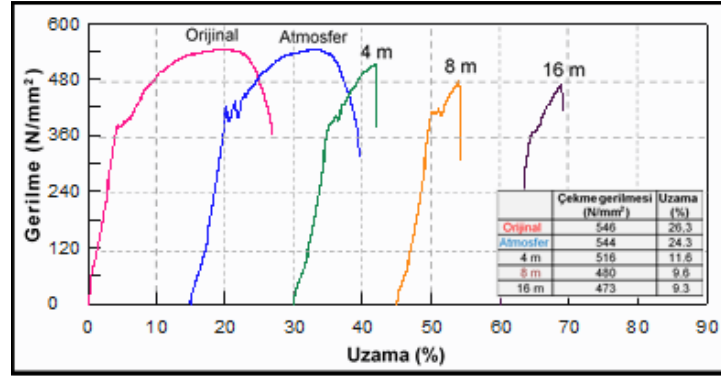
Tahribatsız muayeneler sonucunda tespit edilen iç ve dış hataların kaynaklı bağlantıların mekanik özelliklerine (çekme mukavemeti) etkilerini belirlemek için tüm kaynaklı numuneler ile ana malzemeye çekme testi uygulanmış ve bu vesile ile kaynaklı bağlantıların dayanımlarını ana malzeme ile kıyaslama imkanı bulunmuştur. Şekil 3'te orijinal ana malzeme (Şekil 3-a), atmosferik şartlarda ve farklı derinliklerde birleştirilen numunelerden yapılan çekme testi sonrasında kopma bölgeleri görülmektedir. Şekil 3 incelendiğinde atmosferik şartlarda birleştirilen numunelerde kopma ana malzeme olurken (Şekil 3-b), sualtında farklı derinliklerde birleştirilen numunelerin tamamında (Şekil 3-c-d-e) kopma kaynak metalinden gerçekleşmiştir. Sualtında birleştirilen kaynaklı numunelerdeki kopmaların kaynak metalinden meydana gelmesinin sebebi tahribatsız muayenelerde görülen iç kaynak hatalarının (cüruf kalıntısı ve boşluk) varlığından kaynaklanmaktadır.



Şekil 3. Çekme testi sonrası numunelerin kopma bölgeleri; a) AH36 ana malzeme, b) atmosferik şartlarda, c) 4 m derinlikte, d) 8 m derinlikte ve e) 16 m derinlikte birleştirilen numuneler.

Şekil 4'te orijinal malzeme ile hem atmosferik şartlarda hem de sualtında birleştirilmiş kaynaklı numunelerden elde edilen ortalama grafikler (her bir test için 3 ortalama) verilmiştir. Deneysel çalışmalarda kullanılan Grade AH36 gemi sacı için uygulanan çekme deneyi sonucunda elde edilen veriler ortalama çekme dayanımının $546,541 \text{ N/mm}^2$ olduğu ve yüzde uzamasının da %26,375 olduğu görülmektedir.

Şekil 4 incelendiğinde atmosferik şartlarda birleştirilen numunenin ortalamada 544 N/mm^2 çekme gerilmesi değeri bulunduğu görülmektedir. Bu değer neredeyse ana malzemenin çekme deneyi sonucu verdiği değerlerle benzer değerdir. Buna nazaran sualtı farklı derinliklerde birleştirilen numunelerde derinlik farkı arttıkça çekme-% uzama değerlerinde bir miktar düşüş olduğu anlaşılmaktadır. Bu durumun, kopma yüzeyleri incelendiğinde cüruf kalıntıları ve gaz boşlukları nedeniyle oluştuğu tespit edilmiştir.



Şekil 4. Orjinal ana malzeme, atmosferik şartlarda ve farklı derinliklerde birleştirilen kaynaklı numunelerin çekme sonuçları.

Sayısal olarak çekme-%uzama değerleri ifade edilmek istenilirse, atmosferik şartlarda birleştirilen numune 544 N/mm² çekme mukavemeti %24,3 uzama oranı sunmuştur. Su altında birleştirilen numunelerde ise en yüksek değeri 4 m derinlikte birleştirilen numune 516N/mm² ve %11,6 uzama değeri sunmuştur. 8 m derinlikte birleştirilen numune 480 N/mm² ve %9,6 uzama değeri ve 16 m derinlikte birleştirilen numune 473 N/mm² ve %9,3 uzama değeri elde edilmiştir. Burada derinlik arttıkça porozite ve cüruf kalıntı ihtimalinin arttığı bir gerçektir. Bu kusurlar ise mekaniksel özelliklerin düşmesine neden olan faktörlerdendir. Liu vd. [21] kaynak metalindeki porozitenin çelikler için; tokluk, süneklik, verim ve nihai mukavemet sınırlarında azalma görüldüğünü belirtmiştir.

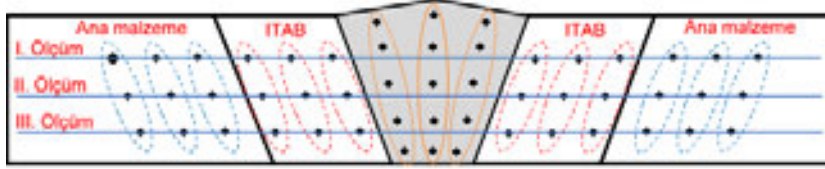
Çekme değerlerinin sonuçlarından da anlaşıldığı üzere atmosferik şartlarda birleştirilen numunelerle farklı derinliklerde birleştirilen numuneler karşılaştırıldığında, derinlik farkı arttıkça su sıcaklığı ve basıncın etkisi ile gerilim değerlerinde ve % uzama miktarlarında azalmalar olmuştur. Malzemenin suyla temas halinde olması katılaşma esnasında meydana gelen tane sınırlarındaki karbür kalıntıları ve kaynak bölgesinin (ITAB ve kaynak metali) sert olması, % uzamanın azalmasına ve gerilim değerlerinin de düşmesine neden olmuştur. Ibarra vd. [22] sualtı kaynağının yüzey kaynağına göre düşük mekanik özellikler gösterdiğini yani kaynak banyosundaki önemli alaşım elementlerinin oksijen, hidrojen ve karbon ile reaksiyona girmesinden dolayı oluştuğunu birbirine kıyas ederek açıklamıştır.

İmdat vd. [17], su altında farklı derinliklerde birleştirdiği kaynaklı numunelere çekme deneyi uygulamış ve uygulama sonucunda atmosferik şartlarda birleştirilen numunelerde kopmanın ana malzemeden, sualtı farklı derinliklerde birleştirilen tüm numunelerde ise kaynak metalinden gerçekleştiğini rapor etmiştir. Literatürde [3] demir karbon alaşımlarının kimyasal bileşimine karbon ve diğer alaşım elementlerinin ilave edilmesi, perlit ve beynit bölgelerine ait burun bölgeleri ile diğer kısımlarının sağa doğru kaymasına neden olduğu belirtilmiştir. Su altında birleştirilen numunelerde kaynak metalinin katılaşması esnasında hızlı soğumadan kaynaklı olarak curuf yapıcı elementlerin kaynak metalinde kalıntı oluşumu ve/veya gaz boşluklarının görüldüğünü ve bu nedenle sualtında birleştirilen numunelerin çekme deneyi sonucunda kopma bölgelerinin kaynak metalinden gerçekleştiğini literatür de [5,11] desteklemektedir.

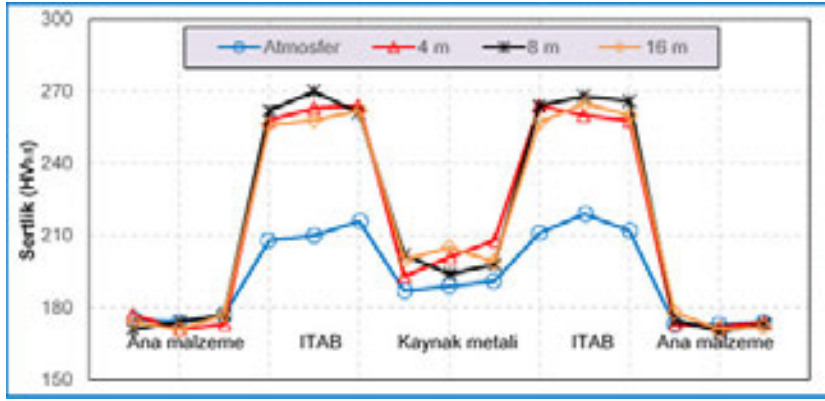
3.5. Sertlik Testi

Özellikle düşük alaşımlı çeliklerde çatlama riski en fazla olan ITAB'da sertliğin 350 HV değerini aşmaması istenmektedir. Yapılan sertlik testlerinde bu değeri geçen herhangi bir değere rastlanmamıştır.

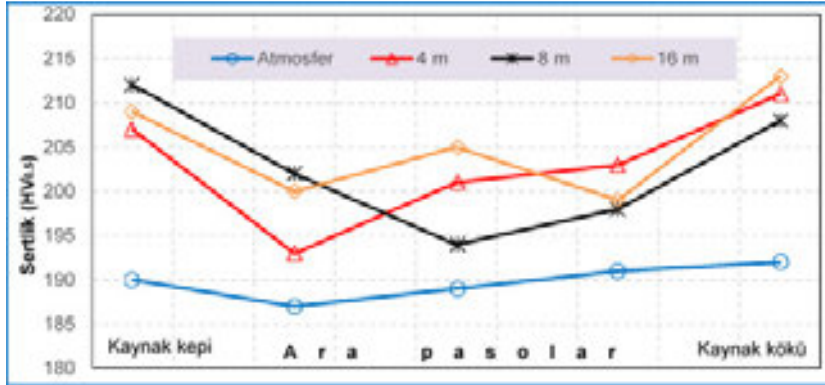
Vickers sertlik ölçme yöntemi kullanılarak 500 g yük altında ($HV_{0,5}$) Şekil 5’de görüldüğü gibi her numuneden yatay ve dikey ekseninde üçer defa olmak üzere sertlik ölçümleri gerçekleştirilmiştir. Yapılan çalışmanın sonucunda elde edilen ortalama sonuç değerleri Şekil 6’da, kaynak metalinde dikey olarak ölçülen sertlik değerleri ise Şekil 7’de verilmiştir.



Şekil 5. Sertlik ölçme yönteminin şematik olarak gösterimi.



Şekil 6. Kaynaklı numunelere ait sertlik deneyi sonuçları.



Şekil 7. Kaynak metalinden ölçülen dikey (kepten köke) sertlik sonuçları.

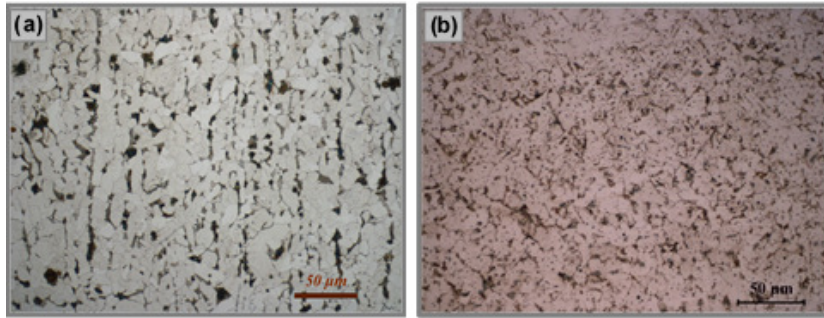
Kaynaklı bağlantılar için kullanılan Grade AH36 gemi sacının ortalama sertlik değeri 173 ± 5 $HV_{0,5}$ olarak ölçülmüştür. Şekil 6’da verilen kaynak bölgesine (kaynak metal ve ITAB) ait sonuçlar değerlendirildiğinde, atmosferik şartlarda birleştirilen numuneden ölçülen sertlik değerlerinin su altında birleştirilen numunelerden ölçülen sertlik değerlerinden daha düşük olduğu bir gerçektir. Ayrıca su altında farklı derinliklerde birleştirilen numunelerde gerek kaynak metalinde gerekse ITAB’da sertlik değerleri birbirlerine çok yakın değerde bulunmuştur. Şekil 6 incelendiğinde, hem atmosferik şartlarda hem de su altında birleştirilen numunelerde en

yüksek sertlik değeri ITAB'dan ölçülürken en düşük sertlik değeri ise ana malzemeden ölçülmüştür. Bir başka ifade ile tüm numunelerin kaynak metali sertli değerleri ITAB'dan düşük ana malzemeden daha yüksek bulunmuştur. Su altında farklı derinliklerde birleştirilen numuneler kendi aralarında kıyaslandığında, derinliğin artmasına veya azalmasına bağlı olarak kaynak bölgesindeki (kaynak metali ve ITAB) sertliğin arttığı ve/veya azaldığına ait bir bulguya rastlanılmamıştır. Çalışmada kaynak işlemlerinin çok pasolu olarak yapıldığı düşünüldüğünde bulunan bu sonuç normal olarak değerlendirilebilir. Çünkü çok pasolu kaynak uygulamalarında bir önceki paso bir sonraki paso esnasındaki ısı girdisiyle kısmen normalizasyon tavlama etkisine girmektedir. Bu durum sertlik ölçüm esnasında kaynak metali ve ITAB'ın normalize etkisi altında kalma durumuna göre değişiklik göstermekte dolayısıyla sertlik ölçümlerinde farklılıklar görülmektedir. Şekil 7'de verilen grafik incelendiğinde ise kaynak kök ve kep pasolarının sertliklerinin diğerlerine göre (ara pasolar) daha yüksek olduğu bir gerçektir. Çünkü bu pasolarda ısıl işlemin etkisinin olmadığı bir gerçektir. Literatürde [19] düşük karbonlu bir çelik malzemeye çok pasolu kaynak uygulaması ile elde edilen sonuca göre kökte bulunan ilk pasoların ince taneli izotrop, dış kapakları oluşturan son pasoların ise iri ve sütunsal taneli yönelmiş yapıları oluşturduğu gözlemlenmiştir. Bu açıklamalar ışığında kaynak metalinde kepen köke doğru yapılan sertlik çalışmalarında elde edilen ortalama sonuçlardaki farklılıkları açıklamak mümkün olmaktadır.

3.6. Mikroyapı İncelemeleri

Literatürde [4], Grade AH36 malzemenin mikroyapısının (Şekil 8-a) ferrit ve perlit tanelerinden oluşan bir yapıya sahip olduğu bildirilmiştir. Ayrıca, AH36 gemi sacı yapısının ferritik-perlitik mikroyapıya sahip olduğu ve hadde yönünde uzama gösteren oksit ve sülfür kalıntıları içeren bir yapı olduğu bildirilmiş, ek olarak mikroyapısında ise beyaz bölgelerin ferritleri, siyah bölgelerin de perlitleri gösterdiğini ve perlit kolonilerinin eş eksenli ferritlerin arasında yer aldığı rapor edilmiştir [20].

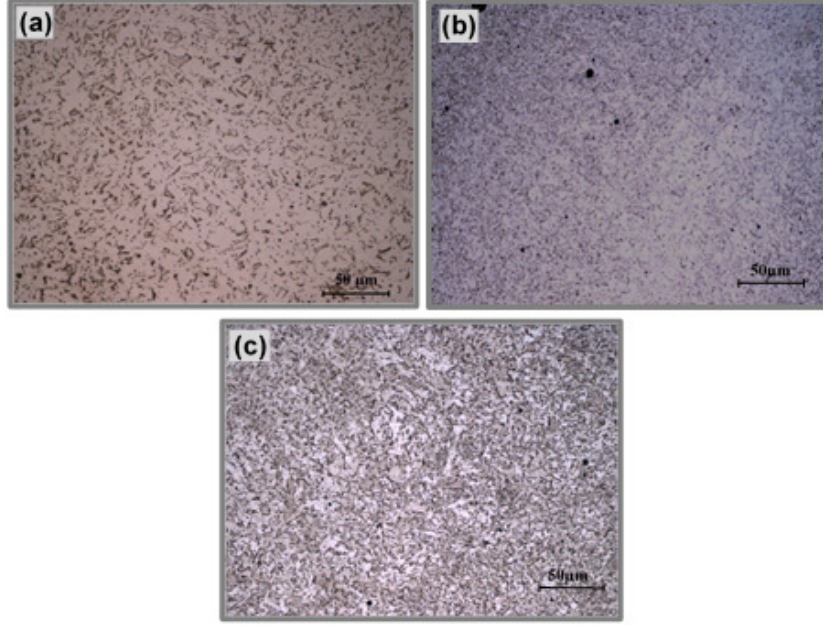
Kaynak bölgesinde (Şekil 8-b); kaynak esnasında çeliğin kaynak metalinde katılma sırasında östenit sıcaklığının altına düşürüldüğünde kolon tipi östenit ile tane sınırlarında ilk olarak tane sınırı ferritlerin (allotriomorfik ferrit) oluştuğu görülmektedir. Çünkü tane sınırı ferrit A₃ sıcaklığının hemen altında oluşan bir fazdır. Ferrit-östenit tane sınırlarında widmanstätten kenar levhaları veya ferrit tane levhalarının çekirdeklendiği ve büyüdüğü görülmektedir. Fotoğraflar incelendiğinde kaynak metali merkezine yönelmiş ferritik ve perlitik yapılar görülmektedir.



Şekil 8. a) Grade AH36 gemi sacının, b) Atmosferik şartlarda birleştirilen numunenin mikroyapı görüntüleri.

Sualtında farklı derinliklerde birleştirilen numunelerin mikroyapılarına bakıldığında, hızlı soğumadan kaynaklanan ve tane sınırlarında oluşan karbür kalıntılarının varlığına rastlanılmıştır.

Yapısal olarak kaynak metali, pasolar arası geçiş sıcaklığından etkilendiği ve bir önceki pasonun da kısmen normalizasyona dönüş sergilediği gözlemlenmiştir. Ayrıca ısının tesiri altında kalan bölge de (ITAB) tane yapısı olarak ince taneli ve kaba taneli bölgenin, atmosferik şartlarda birleştirilen numuneye göre oldukça dar olduğu saptanmıştır.



Şekil 9. a) 4 m, b) 8 m ve c) 16 m derinlikte kaynatılan numune.

Kaynak bölgelerinde (Şekil 9); kaynak esnasında çeliğin kaynak metalinde katılma sırasında östenit sıcaklığının altına düşürüldüğünde kolon tipi östenit ile tane sınırlarında ilk olarak tane sınırı ferritlerin (alotriomorfikferrit) oluştuğu görülmektedir. Ayrıca işlem suyla temas halinde gerçekleştiği için tane sınırlarında yoğunlukla karbür kalıntıları içermektedir. Çünkü kaynak metalini oluşturan sıvı eriyik, suyla temas halinde bulunduğu anda ani soğumaya maruz kalmış ve bu nedenle yapısal olarak karbon atomları katılma sırasında yer bulamayıp tane sınırlarında kalıntı haline dönüşmüştür.

4.Sonuçlar

Grade AH36 gemi sacının rutil örtü tipli E6013 standardına sahip elektrod ve örtülü elektrodla ark kaynak yöntemi kullanılarak atmosferik şartlarda ve su altında farklı derinliklerde birleştirildiği bu çalışmada;

- ✓ Kaynaklı numunelere gözle yapılan muayene sonucunda, atmosferik şartlarda birleştirilen numunelerde kaynak yüzey hatalarına (eksik veya fazla kaynak kepi, kökte çökme vb) rastlanılmazken su altında birleştirilmiş numunelerde yanma oluklarına, cüruf kalıntılara ve kökte kısmi çökme hatasına rastlanılmıştır.
- ✓ Sıvı penetrant ve ultrasonik muayene işlemleri sonucunda, sualtı ark kaynağında oluşabilecek cüruf kalıntıları, gaz boşlukları ve yanma olukları hatalarına rastlanılmıştır. Bu muayenelerde yüzey ve yüzey altı kusurlardan çatlaklara rastlanmamıştır.
- ✓ Çekme test sonuçlarına göre atmosferik şartlarda birleştirilen numunede kopma ana malzemeden olurken, sualtında birleştirilmiş numunelerin tümünde kopma kaynak metalinden olmuştur.

- ✓ Sualtında kaynak yapılan derinliğin artışına bağlı olarak çekme mukavemetlerinde bir miktar düşüş olduğu görülmüştür. Bu da kaynak metalindeki hataların daha fazla olmasından kaynaklanmaktadır.
- ✓ Çekme deneyi sonuçlarına göre, 16 m derinlikte sualtında gerçekleştirilen ve çekme değeri en düşük kaynaklı numunedeki mukavemet düşüşü (atmosferik şartlarda birleştirilene göre) yaklaşık %15 olarak belirlenmiştir.
- ✓ Sertlik ölçümleri sonucunda, tüm numunelerin kaynak metali sertlik değerlerinin ITAB'dan düşük, ana malzemedenden daha yüksek olduğu belirlenmiştir.
- ✓ Kaynak kep ve kök pasodan ölçülen sertlik değerlerinin orta pasolardan ölçülen sertlik değerlerinden daha yüksek olduğu tespit edilmiştir.

5. Teşekkür

Bu çalışmayı KBÜ-BAP-17-YL-432 numaralı proje ile destekleyen, KBÜ Rektörlüğüne ve BAP komisyonuna teşekkür ederiz.

6. Referanslar

- [1] Y. Kaya: Patlamalı Kaynak Yöntemi İle Üretilen Grade A Gemi Sacı-Paslanmaz Çelik Kompozitlerin Mikroyapı, Mekanik ve Korozyon Özelliklerinin İncelenmesi, Doktora Tezi, Karabük Üniversitesi Fen Bilimleri Enstitüsü, Karabük, (2014), pp.7-19
- [2] M. Gavas, M. Yaşar, M. Aydın, Y. Altunpak: Üretim Yöntemleri ve İmalat Teknolojileri, 4. Baskı, Sözkese Matbaacılık Tic. Ltd. Şti., Ankara, (2015), pp.52-65
- [3] W. D. Callister, D. G. Rethwish: Materials Science and Engineering, Çeviri Editörü Kenan Genel, 8. Baskıdan Çeviri, Malzeme Bilimi ve Mühendisliği, Nobel Akademik Yayıncılık, Ankara, (2015) pp.150-155, 360-370
- [4] F. Hayat: Masif ve Özlü Kaynak Telleri İle Birleştirilen Çift-Fazlı Çeliklerin Mekanik ve Mikroyapı Özellikleri, Doktora Tezi, Sakarya Üniversitesi Fen Bilimleri Enstitüsü, Sakarya, (2009), pp.1-58
- [5] K. İmdat: Grade A Gemi Sacının Örtülü Elektrod Ark Kaynak Yöntemi İle Su Altı Ve Atmosferik Şartlarda Birleştirilmesi ve Kaynaklı Birleştirmelerin Mekanik/Mikroyapı Özelliklerinin Karşılaştırılması, Yüksek Lisans Tezi, Karabük Üniversitesi Fen Bilimleri Enstitüsü, Karabük, (2017), pp.2-45
- [6] T. Özalp: Gemi Yapısı ve Elemanları, Özarkadaş Matbaası, İstanbul, (1977), pp. 44-45
- [7] Milli Eğitim Bakanlığı, Gemi Yapımı, MGEP, Ankara, (2012), pp.4-5
- [8] S. Anık, K. Tülbentçi, E. Kaluç: Örtülü Elektrod İle Elektrik Ark Kaynağı, Gedik Holding Yayını, İstanbul, (1991), pp.35-113
- [9] L. M. Gour: Fundamentals of Welding Technology, Çeviri Editörü Dikicioğlu, A., Bodur, O., Eryürek, B., Kaynak Teknolojisinin Esasları, Birsan Yayınevi, İstanbul, (1996), pp.80-92
- [10] A. Durgutlu, N. Kahraman, B. Gülenç: Bakır ve Çelik Levhaların Örtülü Elektrod ve TIG Kaynak Yöntemleri İle Birleştirilmesi ve Arayüzey Özelliklerinin İncelenmesi, Gazi Üniversitesi Mühendislik Mimarlık Fakültesi Dergisi, 20:2 (2005), pp.183-189

- [11] N. Kahraman, B. Gülenç: Modern Kaynak Teknolojisi, 3. Baskı, Epa-Mat Basım Yayın Ltd. Şti., Ankara, (2016)
- [12] B. Oğuz: Ark Kaynağı, Oerlikon Yayını, İstanbul, (1989)
- [13]K. İmdat, Y. Kaya, M. S. Yıldırım, N. Kahraman: Sualtı ve Atmosferik Şartlarda Birleştirilen Grade A Gemi Sacının Mekanik/Mikroyapı Özelliklerinin İncelenmesi, II. Uluslararası Multidisipliner Çalışmaları Sempozyumu (ISMS), Roma,(2017), pp.69-81
- [14] H. Kasapoğlu: Sualtı Kaynak Tekniğinin İncelenmesi, Yüksek Lisans Tezi, Yıldız Teknik Üniversitesi Fen Bilimleri Enstitüsü, İstanbul, (1988), 1-23
- [15] Underwater Cutting & Welding Manual, Published By Direction of Commander, Naval Sea Systems Command, Chapter 3/1-25, Chapter 4/1-20 (2002)
- [16] R. Kalyoncu: Su altı kaynak-kesme yöntemleri ve parametrelerinin incelenmesi, Yüksek Lisans Tezi, Yıldız Teknik Üniversitesi Fen Bilimleri Enstitüsü, İstanbul,(1997), pp.3-18
- [17] K. İmdat, Y. Kaya, N. Kahraman: Grade A Gemi Sacının Örtülü Elektrod Ark Kaynak Yöntemi ile Sualtı ve Atmosferik Şartlarda Birleştirilebilirliğinin Araştırılması, Politeknik Dergisi, 21:3 (2018), pp.543-552
- [18] N. Özden: Kaynağın ısı işlemleri, Nurettin Uycan Cilt Ve Basım Sanayii A.S., İstanbul, (1985), pp.14-23, 90-93
- [19] A. İ. Yükler: Kaynak metali, MÜTEF Matbaası, İstanbul,(1994)pp. 2-60
- [20] N. Özakin: AH ve DH Kalite Gemi Saclarının Değişik Kaynak Yöntemleri ve Kaynak Pozisyonlarındaki Mekanik Özelliklerinin ve Mikroyapılarının İrdelenmesi, Yüksek Lisans Tezi, Zonguldak Karaelmas Üniversitesi Fen Bilimleri Enstitüsü, Zonguldak,(2010) pp.1-4
- [21] H. Li, D. Liu, Y. Song, Y. Yan, N. Guo, J. Feng: Microstructure and mechanical properties of underwater wet welded high-carbon-equivalent steel Q460 using austenitic consumables, Journal of Materials Processing Technology, 249(2017), pp.149-157
- [22] S. Ibarra, C. E. Grupps, S. Liu: State-of-the-art and practice of underwater wet welding of steel, Proceedings: International Workshop On Under- Water Welding Of Marine Structures, New Orleans, USA,(1994), pp 49-67

EFFECT OF PROCESSING ON GALVANIZED DP 600 STEEL PLATES IN COLD METAL TRANSFER TECHNOLOGY

Faruk Varol^{1,a}

¹ Vocational School of Karasu, Sakarya University, Karasu, Sakarya, Turkey
^a fvarol@sakarya.edu.tr

Abstract

In this study, advanced high strength, zinc coated DP 600 (Dual-Phase) steel plates were joined with cold metal transfer technology (CMT) method. Copper-based CuAl8 wire was used as an additive wire in the form of overlap joint. CMT-brazing processes were done in currents as 35, 40, 45, 50, 55, 60, 65 and 70 A. In joint zones, properties of tensile strength, microhardness, macro and microstructure were examined by scanning electron microscope (SEM), stereo optical microscope. These examinations aimed to research the effects of heat treatment and different CMT-brazing current intensities on the joint zones.

Key Words: CMT-brazing, Dual-phase, Interface

1.Introduction

In recent years, manufacturers of automotive industry have been trying to reduce weight of the vehicles for fuel economy and better performance [1]. They have been studying on high strength, thin automotive steel sheets, good plastic strain and mass reduction to achieve reduction of passenger car weight, fuel consumption, reduced emissions and safety of vehicles[2,3,6]. Advanced high strength steels (AHSS) are preferred due to their high strength, good plasticity and high initial workhardening rates by automotive industries. AHSSs can be categorized into DP, TRIP, CP (Complex Phase). DP steels are remarkable because they have high strength and high fracture strain although they have low weight [7]. While producing DP steels by quenching in a temperature between AC1 and AC3, austenite phase in low carbon alloys whose carbon content is less than 0.2% changes into martensite phase and produces a ferrite –martensite structure unlike a ferrite-pearlite structure [8]. Morphology of hard martensite structure among soft ferrite matrix effects of the strength and ductility of DP steels.

Zinc coated carbon steel sheets have been preferred due to their good corrosion resistance, good mechanical properties and low cost by car manufacturers [9]. Galvanized DP 600 steels are used because of their good corrosion resistance, as well[10].

In welding processes such as gas metal arc welding and resistance spot welding, the zinc coating is subjected to evaporation and oxidation and the base metal becomes unprotected against oxidation [11]. However, in CMT technique (Cold Metal Transverse), invented by Fronius Company, heat input and oxidation are less than those in conventional processes [12,13].

The motion of the wire is the most important point in the process control of this technique [14,15,16]. The wire motion is given item by item and shown in Fig. 1.

I. During the arcing period, the filler metal is moved towards the weld-pool. II. When the filler metal dips into the weld-pool the arc is extinguished [17,18,19]. The welding current is lowered. III. The rearward movement of the wire assist droplet detachment during the short circuit. The short-circuit current is kept small. IV. The wire motion is reversed and the process begins all over again [20,21,22].

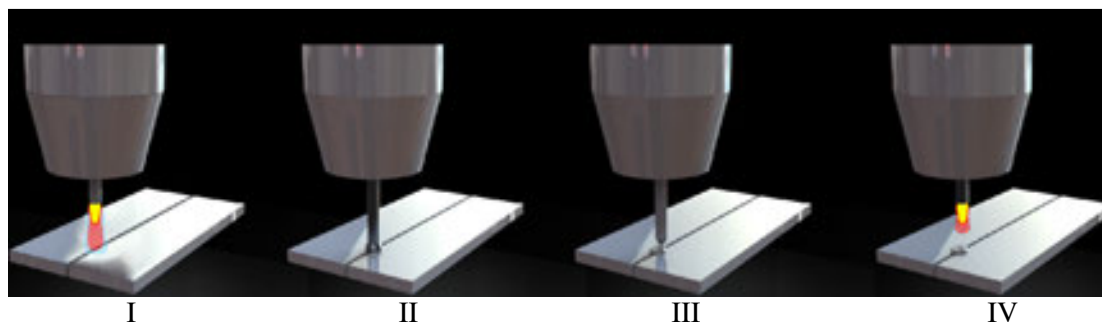


Fig. 1. CMT wire retraction process [23].

The galvanized automotive sheets were also joined by different welding methods. Ozsarac[24] and Aslanlar[25] studied the resistance spot welding of galvanized in automotive applications. Karadeniz et al. determined the penetration depth of butt welded automotive steels in GMAW method [26]. Chovet[27] had studies about MIG and TIG brazing for galvanized automotive steels. Varol et al. and Sushovan et al. studied the MIG-brazing of galvanized in automotive applications [28,29,30].

In this research, advanced high strength, zinc coated DP 600 (Dual-Phase) steel plates were joined by using copper-based filler with CMT-brazing method. CMT process of galvanized steels emphasizes on the microstructure and strengthening behavior and mechanisms of the joint. The rate of zinc evaporation in joint zone was determined in CMT process of galvanized steels.

2. Experimental

In the study, zinc coated DP 600 dual phase automotive steels which were mainly ferritic with a fraction of hard phases martensite were used and shown in Fig. 1. These steel plates had 1.2 mm thickness and 7,5 μm zinc coating. Chemical composition of galvanized DP600 steel was given in Table 1. The filler metal was a solid wire which had 1 mm diameter, classified as AWS ERCuAl8. Table 2 provides the chemical composition of CuAl8.

Table 1 Chemical composition of DP 600 dual phase galvanized steel.

%C	%Si	%Mn	%P	%S	%Cr	%Mo	%Ni	%Al
0,091	0,239	1,858	0,011	0,001	0,573	0,004	0,024	0,039
%Cu	%Nb	%V	%N	%B	%Sn	%Ti	%Al-ZO	%Fe
0,012	0,001	0,004	0,0035	0,0001	0,001	0,002	0,038	96,282

Table 2 Chemical composition of filler metal.

Cu	Al	Mn	Fe	Sn	Melting temperature range (°C)
Remainder	8	<0,5	<0,5	<0,5	1030-1035

DP 600 steel plates were cut 200x200x1.2 mm. They were positioned overlap and had 0.8 mm gap between them and were brazed by the CMT process. The brazing torch angle was 45° as shown on Fig. 4. The shielding gas used in the tests was argon whose flow rate of 12 L/min.

CMT-brazing process is implemented by using Fronius CMT 2700 machine. The current values for CMT operation were determined as 35, 40, 45, 50, 55, 60, 65 and 70A in overlap joint. The surface of the DP 600 steel sheets were cleaned by acetone before CMT-brazing operation. Eight different brazing parameters of heat inputs are as shown in Table 3. The heat input, HI is calculated by using the equation:

$$HI_{linear} = \frac{(60 \times UI)\eta}{v} \quad (1)$$

$$HI_{normalized} = \frac{HI_{linear}}{e} \quad (2)$$

η_{MIG} : 0.7 the arc efficiency factor, e : thickness (mm) U : the arc voltage, I : the current intensity and V (cm/min): the CMT-brazing speed [29]. CMT process parameters such as brazing current intensity, wire feed speed, voltage, shielding gas at a flow rate of 12 L/min, brazing travel speed and brazing gap were presented in Table 3.

Table 3 CMT process parameters.

CMT Parameters					
Current Intensity [A]	Wire Feed Speed [m/min]	Voltage [V]	Shielding gas [L/min]	Travel Speed [cm/min]	Brazing Gap [mm]
35	2.5	13.7	12	24	0.8
40	2.8	14.2	12	24	0.8
45	3.1	14.7	12	24	0.8
50	3.4	15.1	12	24	0.8
55	3.8	15.4	12	24	0.8
60	4.1	15.5	12	24	0.8
65	4.3	15.7	12	24	0.8
70	4.6	15.8	12	24	0.8

The CMT-brazed DP 600 steel was transversally cut with a fine diamond tipped disc, and grinded from 200 to 1200 mesh. Then, it was polished by aluminasolution with a particle size of 0.3µm. A solution consisting of ethyl alcohol, nitric acid (Nital 3 wt. %) was used as etchant. In microstructure and macrostructure examinations, a stereo optical microscope, energy dispersive spectroscopy, scanning electron microscope, techniques were used. The rate of zinc evaporation in joint zone was determined by SEM in DP 600 galvanized steels.

In this study, the uniaxial tensile tests were applied according to ASTM E8 standard test methods. Tensile-shear test was implemented to CMT-brazed DP 600 steel sheets. Shape of

tensile-shear test specimens were shown in Fig. 2 respectively. The micro-hardness of the brazed joints was measured by micro-hardness testing machine Wolpert-Wilson. Hardness values were measured using a microindentation hardness tester with a load of 100 g for 5 s.

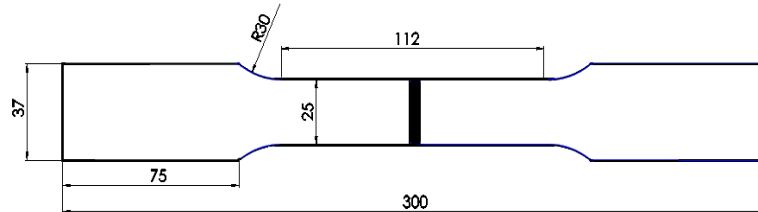


Fig. 2. Tensile test specimen prepared according to EN 895 standard

3. Results and Discussion

Firstly, the tensile testing was performed to measure the strength. 60, 65 and 70 A currents showed that the joint zone's strength was higher than the base metal and CuAl8 filler zone's strength. It was clear that the joint zone was high strength. In 35, 40, 45, 50 A, insufficient wetting occurred as a result of low heat input. 55 A current intensity came about a critical point in increasing maximum tensile strength. Sushovan et al. [30] had studies about MIG-brazing for DP 600 galvanized automotive steels and determined ultimate tensile strength 615 MPa in 108 A current intensity, 18 V ark voltage, 40 cm/min welding speed. In this study, we determined ultimate tensile strength as 650 MPa in 60 A current intensity, 15.5 V ark voltage, 24 cm/min welding speed. Finally, in this study, the value of current intensity was lower than the value in the study of Sushovan but welding speed was slower and so, heat input and wetting in the joint zone increased and as a result of that strength increased.

Table 4 Experimental results for different CMT-brazing currents.

Experimental results			
Current intensity [A]	Tensile strength [MPa]	Heat input (HI _{linear}) [J/cm]	Heat input (HI _{normalized}) [J/cm/mm]
35	81	839	699
40	223	994	828
45	376	1157	964
50	463	1321	1101
55	614	1482	1235
60	650	1627	1356
65	641	1785	1488
70	638	1935	1612

Having examined the strength values in Table 4, it was observed that strength increased with the increase of current intensity, which were parallel with heat input and wetting.

Fig. 3 shows the measured microhardness value of the joints for different CMT-brazing currents. It was seen that microhardness value was highest at HAZ and the HAZ hardness was higher than that of the copper filler and base material. Microhardness value of the joint zone increased with the increase of current intensity.

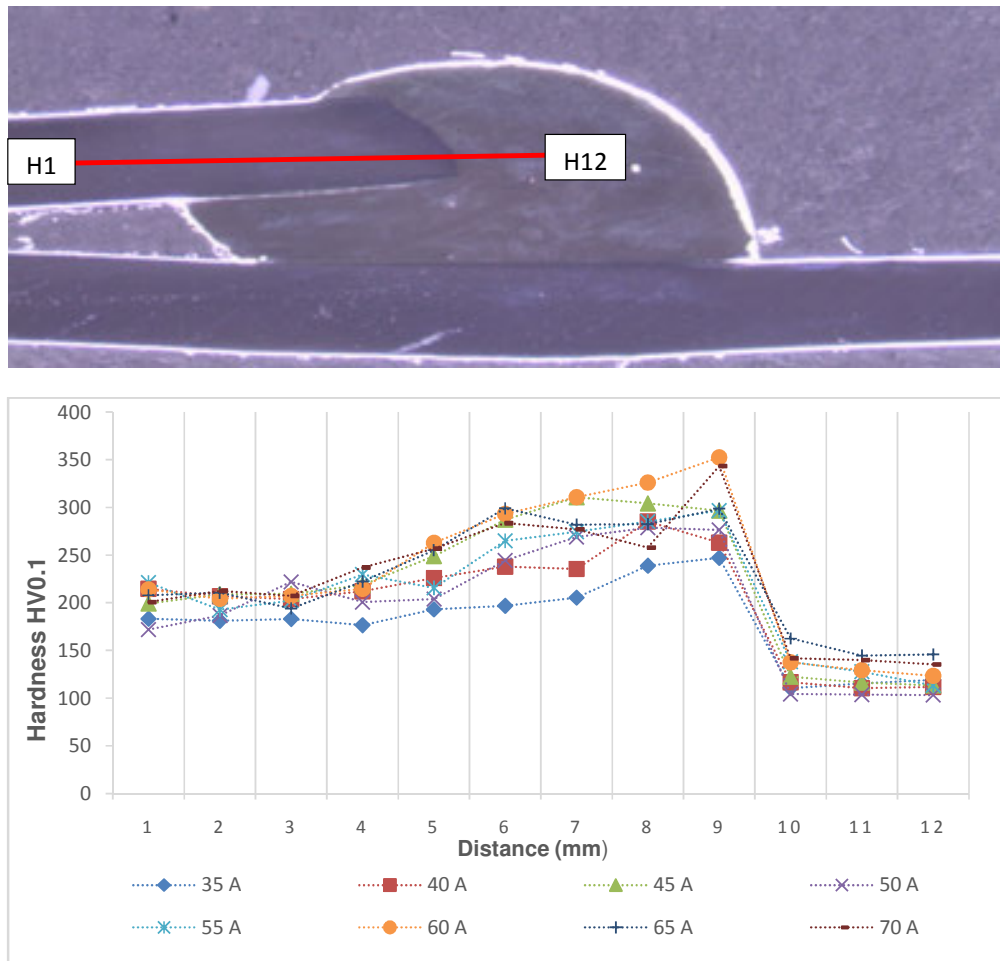


Fig. 3. Micro-hardness along the line H1–H12.

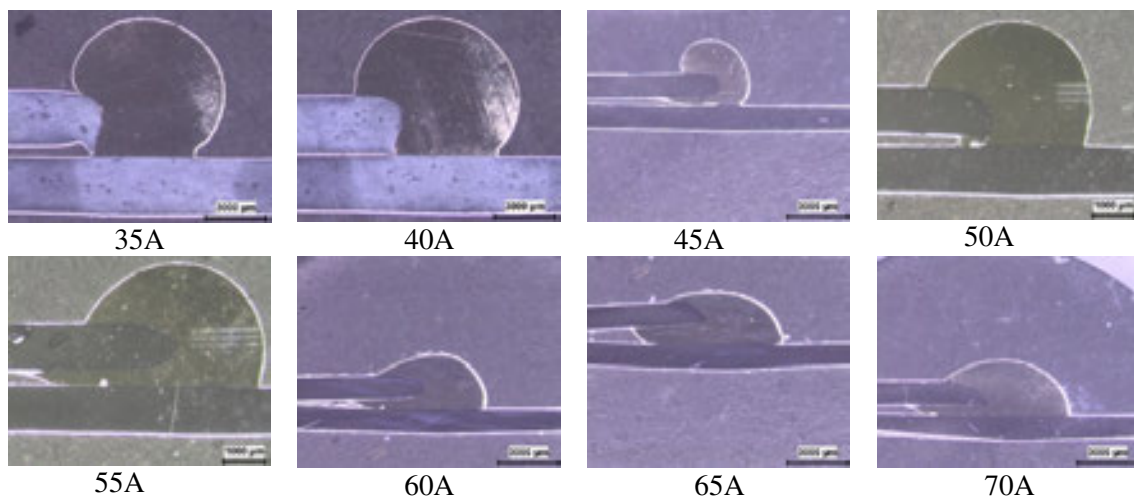


Fig. 4. Macro appearance of brazing seams

Macro appearance of the brazing seams for different CMT-brazing currents are shown in Fig. 4. The molten metal wetted the steel better when using 60, 65, 70 A current intensity, compare Samples 60, 65, 70 A at lower heat input to Samples 35, 40, 45, 50, 55 A.

The braze seams' microstructure appearance for different CMT-brazing currents is shown in Fig. 5. Dendrites' number increased on the surface of the joint zone with the increase of current intensity and thus micro iron particles melt, migrated and distributed towards the filler metal zone. The dendritic structure of the CMT-brazed metal in this study and the one of Varol's and Sushovan's study showed similarity [29,30].

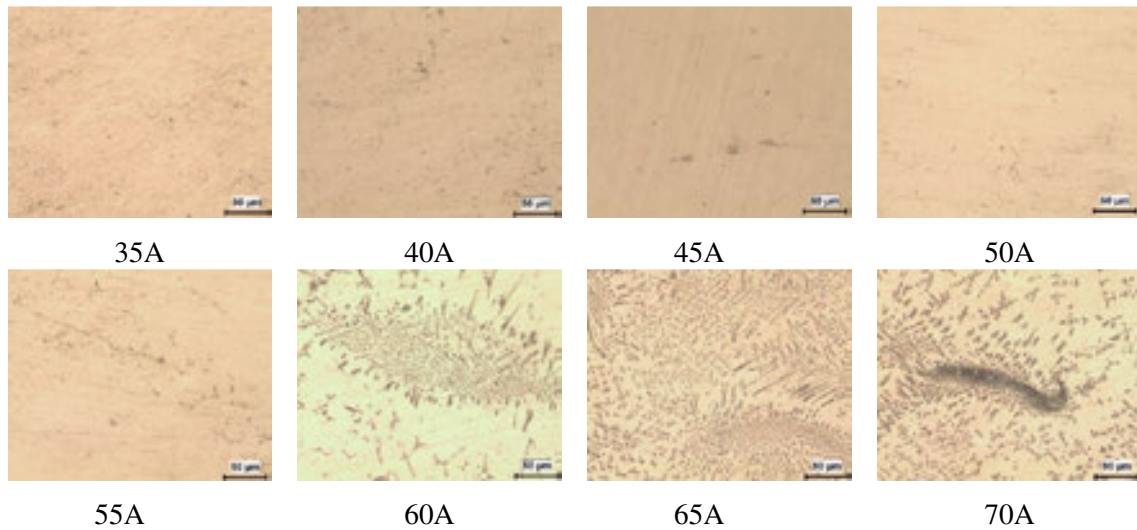


Fig. 5. Micrographs of CMT-brazing joints obtained on DP600 with different currents

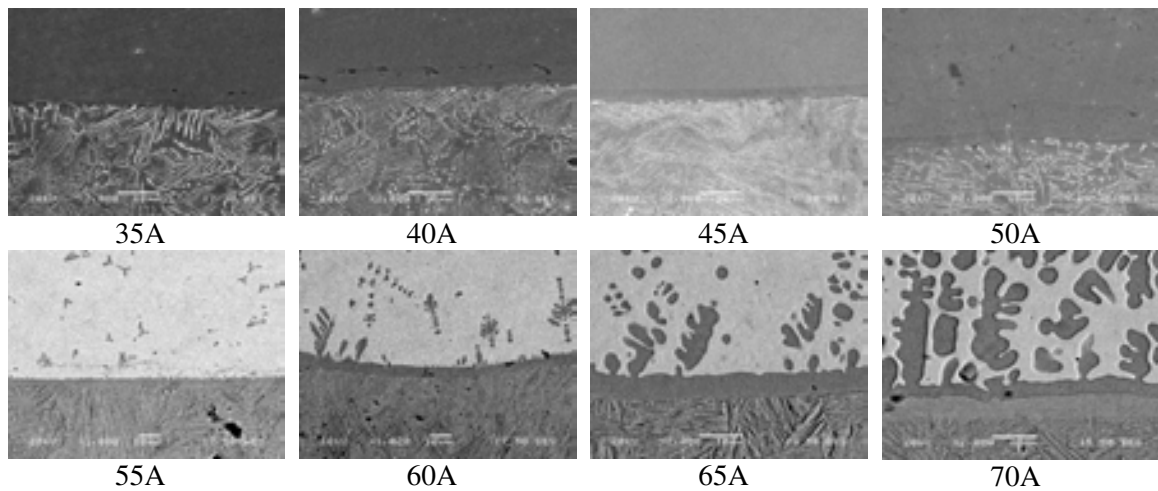
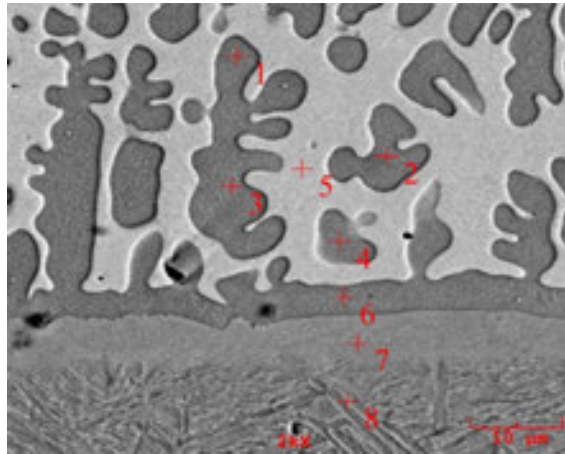


Fig. 6. SEM images for CMT-brazing of DP600 with CuAl8

Having examined the SEM images in Fig. 6, dendrites' forms occurred in the brazed steel were beholden.



Point	Element (wt %)				
	Al	Mn	Fe	Cu	Zn
1	6.281	-	81.066	12.521	0.132
2	7.508	-	76.144	16.224	0.124
3	7.234	-	82.379	10.266	0.121
4	7.466	-	70.016	22.363	0.155
5	7.590	-	6.490	85.731	0.189
6	7.282	0.688	77.568	14.295	0.168
7	-	1.075	89.633	9.137	0.367
8	-	1.169	98.831	-	-

Fig. 7.EDS chemical analysis of areas in base metal(8), interface(6,7), dendrite(1,2,3,4), copper matrix(5) for CMT-brazing of DP600 with CuAl8.

A very fine layer which is about 10 μm was observed at the interface between DP 600 steel plate and brazing bead. SEM and EDX analysis shows the layer's chemical composition in Fig. 7. The interface layer consists of Fe, Cu, Mn, Al and Zn. Fig. 7 also shows that dendrites grow in the copper matrix starting on this interface layer.

It was determined that zinc evaporated beginning from the joint zone towards HAZ and the length of this area was measured. The change in the rate of zinc evaporation because of increasing heat input with increasing current intensity is seen in Fig. 8.

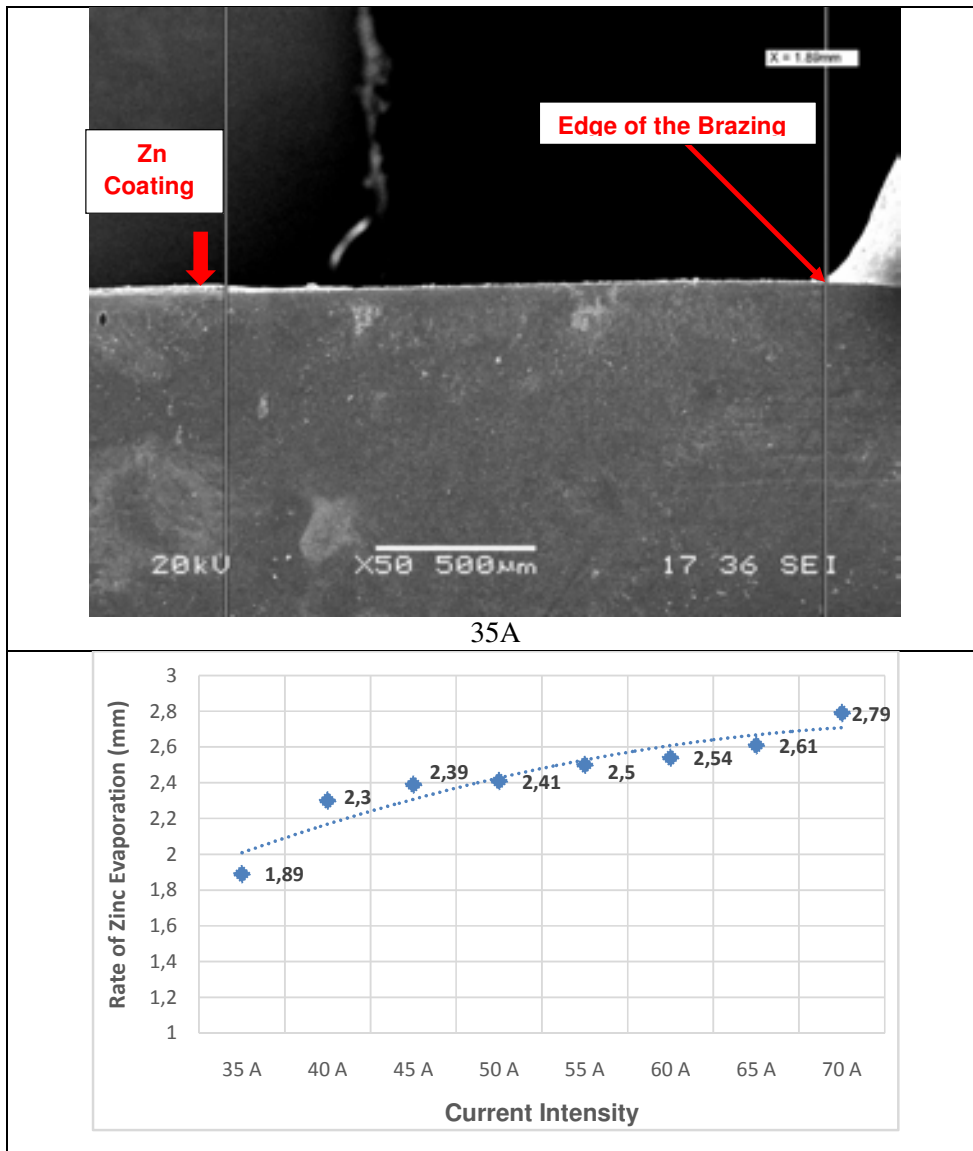
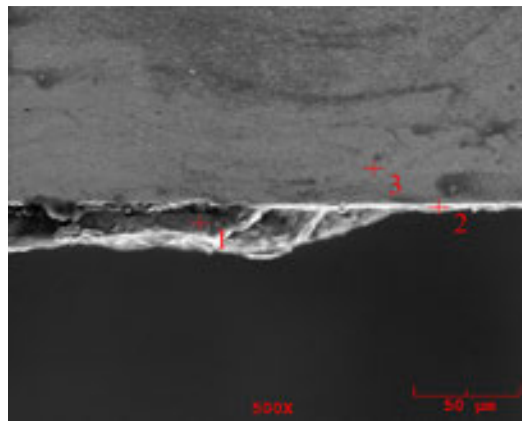
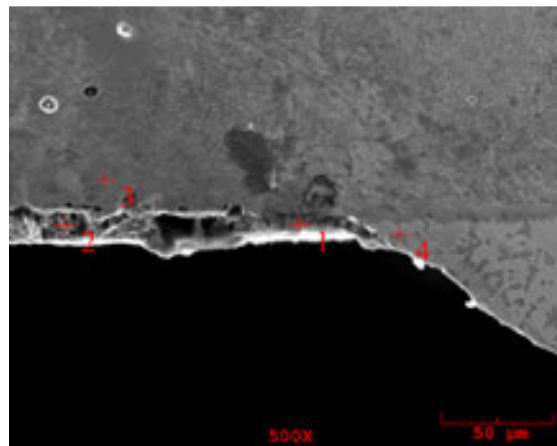


Fig.8. The measurement of quantity of Zinc evaporating from joining zone to HAZ



Point	Element (wt %)						
	Al	Si	O	Mn	Fe	Cu	Zn
1	-	-	6.288	-	9.711	-	84.001
2	17.551	-	-	1.742	80.707	-	-
3	-	-	-	1.426	98.574	-	-

Fig. 9. EDS analysis of the area in which galvanneal layer is seen in 70A current intensity



Point	Element (wt %)						
	Al	Si	O	Mn	Fe	Cu	Zn
1	0.747	0.667	3.672	-	61.914	-	-
2	0.900	-	29.206	1.108	68.787	-	-
3	-	-	10.319	1.624	88.057	-	-
4	6.879	-	-	-	3.687	89.434	-

Fig. 10. EDS analysis of the area in which galvanneal layer was evaporated in 70A current intensity

The joint at the interface between copper matrix and steel was disjoined. X-ray diffraction was used to determine the phase composition in CMT-brazed location 60A, 65A, 70 A current intensity. The results are shown in Fig. 11, Fig. 12 and Fig.13. The compound layer at the interface between steel and weld metal main consists of $AlFe_3$, Cu_3Fe_{17} , $FeCu_4$ and $CuZn_3$ phases.

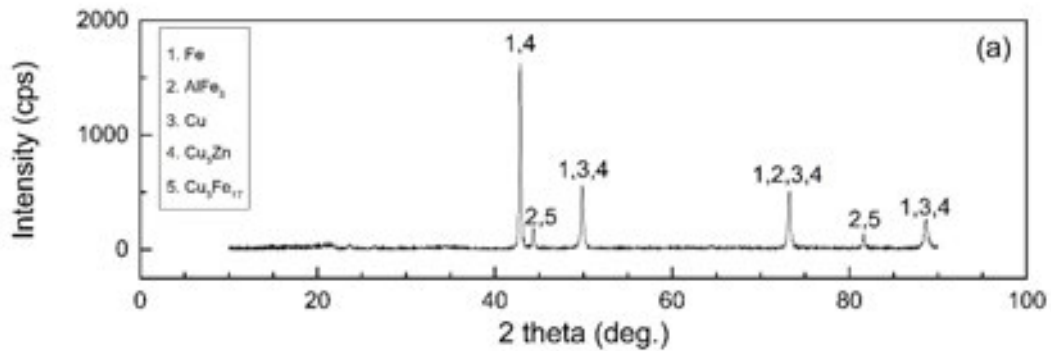


Fig. 11. X-ray diffraction in brazing location 60A current intensity

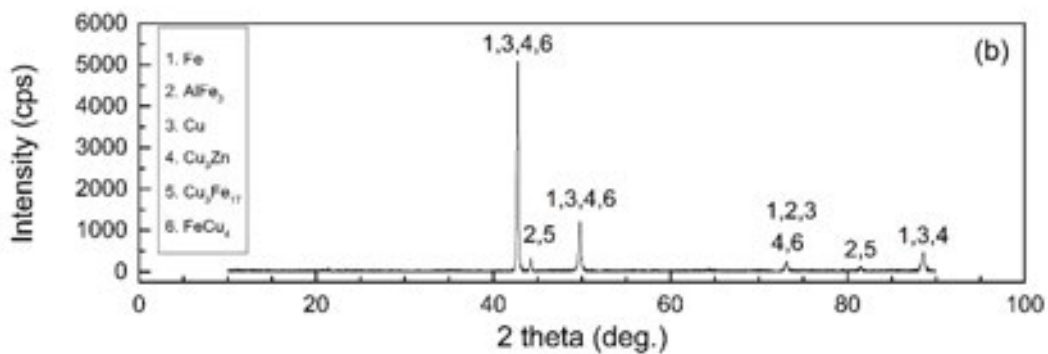


Fig. 12. X-ray diffraction in brazing location 65A current intensity

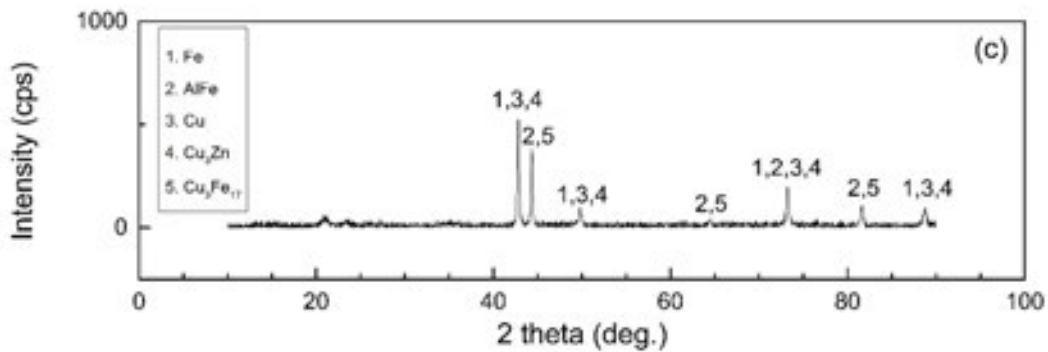


Fig. 13. X-ray diffraction in brazing location 70A current intensity

4. Conclusion

Effect of tensile properties was investigated in joining of DP 600 steel plates by CMT-brazing method and conclusions were drawn:

The joinability of steel DP 600 sheet with CuAl8 filler metal was analyzed with CMT-brazing method and it was demonstrated that joint was gained in the base metal by melting in very little quantities or no. The tensile test results showed that the strength of the joint brazed in high current intensity had the adjacent value with the base metal. The change in the rate of zinc evaporation because of increasing heat input with increasing current intensity was observed.

Low heat input was provided in joining of DP 600 steel plates by CMT brazing method. Therefore, low heat input resulted in lower zinc evaporation from DP 600 galvanized steel sheet. 55 A current intensity in CMT-brazing operation was a critical point in increase of maximum tensile strength.

SEM images confirmed that diffusion of iron atoms increased as a result of high heat input with the rise of current intensity. The increase of iron diffusion brought about stretching of dendrite like branches. Additionally, increase of dendrites resulted in the increase in hardness and strength. The intermetallic layer at the interface between DP 600 and the brazed metal consists of AlFe₃, Cu₃Fe₁₇, FeCu₄ and CuZn₃ phases.

Acknowledgement

The authors wish to thank Sakarya University Scientific Research Foundation (Project No: 2012-05-06-016) for their support.

References

- [1] Ling, Z.; Li, Y.; Luo, Z.; Feng, Y.; Wang, Z. Resistance Element Welding of 6061 Aluminum Alloy to Uncoated 22MnMoB Boron Steel. *Materials and Manufacturing Processes* 2016, 31(16) 2174-2180.
- [2] Halder, C.; Madej, L.; Pietrzyk, M.; Chakraborti, N. Optimization of Cellular Automata Model for the Heating of Dual-Phase Steel by Genetic Algorithm and Genetic Programming. *Materials and Manufacturing Processes* 2015, 30(4) 552-562.
- [3] Savaş, Ö. Effect of some welding parameters on nugget size in electrical resistance spot welding. *Steel and Composite Structures*, 2015, 18(2), 345-355.
- [4] Shah, L.H.; Ishak, M. Review of Research Progress on Aluminum–Steel Dissimilar Welding. *Materials and Manufacturing Processes* 2014, 29(8), 928-933.
- [5] Ashrafi, H.; Shamanian, M.; Emadi, R.; Saeidi, N. A novel and simple technique for development of dual phase steels with excellent ductility. *Materials Science Engineering A* 2017, 680, 197-202.
- [6] Chakraborty, A.; Adhikary, M.; Venugopalan, T.; Singh, V.; Nanda, T.; Ravi Kumar, B. Effect of ferrite-martensite interface morphology on bake hardening response of DP590 steel. *Materials Science Engineering A* 2016, 676, 463-473.
- [7] Alaie, A.; Ziaei-Rad, S.; Kadkhodapour, J.; AsadiAsadabad, M.; Schmauder, S. Effect of microstructure pattern on the strain localization in DP600 steels analyzed using combined in-situ experimental test and numerical simulation. *Materials Science Engineering A* 2015, 638, 251-261.
- [8] Ramazani, A.; Abbasi, M.; Kazemiabnavi, S.; Schmauder, S.; Larson, R.; Prael, U. Development and application of a microstructure-based approach to characterize and model failure initiation in DP steels using XFEM. *Materials Science and Engineering A* 2016, 660, 181-194.
- [9] Bian, J.; Zhu, Y.; Liu, XH. Development of hot dip galvanized steel strip and its application in automobile industry. *Journal of Iron Steel Research International* 2006, 13(3), 47-50.
- [10] AWS. *Welding processes, welding handbook*. 8th ed., vol. 2. Miami: AWS; 1991.
- [11] Gungor, B.; Kaluc, E.; Taban, E.; SIK, A. Mechanical and microstructural properties of robotic Cold Metal Transfer (CMT) welded 5083-H111 and 6082-T651 aluminum alloys. *Materials and Design* 2014, 54, 207–211.
- [12] Feng, J.; Zhang, H.; He, P.W. The CMT short-circuiting metal transfer process and its use in thin aluminum sheets welding. *Materials and Design* 2009, 30, 1850–1852.
- [13] Pavan Kumar, N.; ArungalaiVendan, S.; Siva Shanmugam, N.; Investigations on the parametric effects of cold metal transfer process on the microstructural aspects in AA6061. 2016, *Journal of Alloys and Compounds* 2016, 658, 255-264.
- [14] Cao, R.; Huang, Q.; Chen, J.H.; Pei-Chung Wang. Cold metal transfer spot plug welding of AA6061-T6-to-galvanized steel for automotive applications. *Journal of Alloys and Compounds* 2014, 585, 622–632.

- [15] Yanlin Zhou; Qiaoli Lin. Wetting of galvanized steel by Al 4043 alloys in the first cycle of CMT process. *Journal of Alloys and Compounds* 2014, 589, 307–313.
- [16] Cao, R.; Gang Yu; Chen, J.H.; Pei-Chung Wang. Cold metal transfer joining aluminum alloys-to-galvanized mild steel. *Journal of Materials Processing Technology* 2013, 213, 1753–1763.
- [17] Stelzer, S.; Ucsnik, S.; Pinter, G. Fatigue behavior of composite–composite joints reinforced with cold metal transfer welded pins. *International Journal of Fatigue*, 2015, 81, 37-47.
- [18] Cao, R.; Feng, Z.; Chen, J.H. Microstructures and properties of titanium–copper lap welded joints by cold metal transfer technology. *Materials Design* 2014, 53, 192–201.
- [19] Pickin, C.G.; Williams, S.W.; Lunt, M. Characterisation of the cold metal transfer (CMT) process and its application for low dilution cladding. *Journal of Materials Processing Technology* 2011, 211, 496–502.
- [20] Yang, S.; Zhang, J.; Lian, J.; Lei, Y. Welding of aluminum alloy to zinc coated steel by cold metal transfer. *Materials Design* 2013, 49, 602–612.
- [21] Cao, R.; Wen, B.F.; Chen, J.H.; Pei-Chung Wang. Cold Metal Transfer joining of magnesium AZ31B-to-aluminum A6061-T6. *Materials Science and Engineering A* 2013, 560, 256–266.
- [22] Zhanga, H.T.; Feng, J.C.; He, P.; Zhang, B.B.; Chen, J.M.; Wang, L. The arc characteristics and metal transfer behaviour of cold metal transfer and its use in joining aluminum to zinc-coated steel. *Materials Science and Engineering A* 2009, 499, 111–113.
- [23] Hasselberg, T. P. “Cold Metal Transfer” – Gas Metal Arc Welding CMT-GMAW Material Joining Characterization of Nickel Base Superalloy Inconel 718™. Rensselaer Polytechnic Institute Hartford, Troy, New York, Connecticut April 2009.
- [24] Ozsarac U. Investigation of mechanical properties of galvanized automotive sheets joined by resistance spot welding. *Journal of Materials Engineering Performance* 2012, 21(5), 748–55.
- [25] Aslanlar S. The effect of nucleus size on mechanical properties in electrical resistance spot welding of sheets used in automotive industry. *Materials Design* 2006, 27, 125–31.
- [26] Karadeniz, E.; Ozsarac, U.; Yildiz, C. The effect of process parameters on penetration in gas metal arc welding processes. *Materials Design* 2007, 28, 649–56.
- [27] Chovet, C.; Guiheux, S. Possibilities offered by MIG and TIG brazing of galvanized ultra-high strength steels for automotive applications. *International Conference Super High Strength Steels*. Roma: organized by AIM, 2–4; November 2005.
- [28] Varol, F.; Colak, M.; Akkaş, N.; Ozsarac, U.; Aslanlar S. Investigation of mechanical properties of MIG brazed DP 600 steel joints using different working angles. *Materials Testing* 2014, 56, 858-862.
- [29] Varol, F.; Ferik, E.; Ozsarac, U.; Aslanlar, S. Influence of current intensity and heat input in Metal Inert Gas-brazed joints of TRIP 800 thin zinc coated steel plates. *Materials Design* 2013, 52, 1099–1105.
- [30] Sushovan, B.; Tapan, K.; Mahadev, S. High-cycle fatigue behavior of MIG brazed galvanized DP600 steel sheet joint—effect of process parameters. *International Journal Adv Manufacturing Technology* 2016 82:1197–1211.

CORRESPONDENCE ADDRESS:

Name, FarukVAROL

Postal address, Vocational School of Karasu, Sakarya University, Karasu,Sakarya/ TURKEY

Telephone and E-mail address. 05353338940, fvarol@sakarya.edu.tr

SHORT BIOGRAPHIES

Faruk VAROL - He was born in Balıkesir/Gönen in 1978. He studied in primary and high school in Gönen. He started to study in Technical Training Faculty in SAU in 1998 and graduated in 2002. He had Master of Education in the department of education in Institute of Metal Science. He completed his education in 2006. He started the education of Ph.D. in 2007 in the Institute of Metal Science and Education department in Sakarya University and completed his Ph.D. in 2014. He works in Machine and Metal Technology Department in Karasu Vocational High School in SAU.

INVESTIGATION OF MECHANICAL PROPERTIES OF OVERLAP JOINT FORM IN CMT-BRAZED JOINTS OF DP800 STEEL PLATES USING DIFFERENT CURRENT INTENSITY

Faruk Varol^{1,a}, İbrahim Acar^{1,b}, Veli ŞıkŞık^{1,c}, Erman Ferik^{2d}, Salim Aslanlar^{2e}, Yusuf Sadi Aslanlar^{3f}

¹ Vocational School of Karasu, Sakarya University, Karasu, Sakarya, Turkey

² Department of Metallurgical and Materials Engineering, Sakarya University, Sakarya, Turkey

³ Yıldız Kalıp A.Ş., R&D Center, Arnavutköy / Istanbul

^a fvarol@sakarya.edu.tr, ^b ibrahimacar@sakarya.edu.tr, ^c velis@sakarya.edu.tr, ^d ermanferik@gmail.com, ^e aslanlar@sakarya.edu.tr, ^f yusuf.aslanlar@yildizkalip.com

Abstract

In this study, DP800 (Dual Phase) steel plates having 1 mm thickness were joined by copper-based (CuAl8) wire in CMT-brazing (Cold Metal Transfer) technique. Specimens were prepared in joining forms as overlap joint. CMT-Brazing operations were done with nine different CMT-Brazing current intensity of 60, 65, 70, 75, 80, 85, 90, 95 and 100 A. CuAl8 wire composed largely of copper serves as the filler metal were used. Having accomplished the CMT-brazing operations; tensile properties of joints were detected, and micro and macro-structures of joints were investigated in order to see the joinability of DP800 steel by CMT-brazing technique.

Key Words: DP800 Steel, CMT-Brazing, Cold Metal Transfer

1. Introduction

Factors such as lightness, fuel consumption, safety and environmental pollution are taken into consideration in the selection of the materials to be used in the automotive sector. In recent years there has been increased interest in AHSS (Advanced High Strength Steel) steels due to strength, fuel economy, low yield strength, high fatigue strength and corrosion resistance. In this way, it is possible to achieve lightness and fuel savings without sacrificing safety by using thinner material instead of thicker materials [1,2,10].

DP (Dual Phase) steels from AHSS steels are composed of hard martensite phase in the soft ferrite matrix and shown schematically in Figure1. Such steels have both high strength and excellent ductility due to the coexistence of ferrite and martensite phases. The martensite phase increases the strength and hardness value while the ferrite phase provides high ductility [3]. DP steels are cooled at the appropriate rate after annealing in intercritical zone to obtain martensite and ferrite phases. DP steels have wide used in the automotive industry due to their large elongation, high work hardening rate, good ductility and high tensile strength [4,5,9].

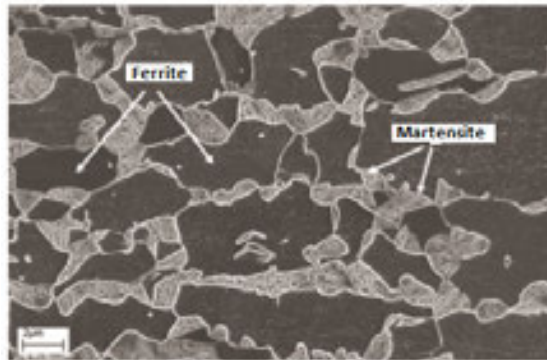


Figure 1. The microstructure of DP steels.

CMT process was invented by Fronius as a relatively new welding technology based on short-circuiting transfer. During the combustion phase the filler metal moves towards the welding pool. When the filler metal is immersed in the welding pool, the arc extinguishes and the current decreases. The filler metal moves backwards and helps to form droplets during short circuit. Short circuit current is kept low. The direction of movement of the filler metal is reversed and the process is restarted. Thus, the joining operation is carried out without splashing by providing a low heat input [6,7]. CMT brazing process steps are given in the Figure 2.



Fig. 2. CMT-Brazing process [7].

Galvanized steel sheets can be joined with different methods. Farabi et al. and Ma et al. joined galvanized steel sheets with laser welding [3,8]. Akkas [11] and Aslanlar [12] studied the resistance spot welding of galvanized steels.

In this research, CMT process of galvanized DP800 steel sheets was studied using copper based filler and it is found that the joint strength is higher than that of the base materials. In present paper, CMT process of galvanized DP800 steels emphasis on the microstructure and strengthening behavior and mechanisms of the joint.

2. Experimental

In this study, galvanized 1 mm thickness DP800 steel sheets were used. The chemical composition of the galvanized DP800 steel is given in Table 1. In addition, CuAl8 copper wire with a diameter of 1 mm and chemical composition given in Table 2 is used as filler metal.

Table 1. Chemical composition of DP800 steel.

Fe	C	Si	Mn	P	S
%Remaining	%0,1028	%0,502	%2,32	%0,0156	%0,0023

Table 2. Chemical composition of CuAl8 filler metal.

Cu	Al	Mn	Fe	Sn
Remaining	8	<0,5	<0,5	<0,5

DP800 steel plates were cut 200x200x1 mm. Steel plates were positioned overlap joint and had 0,5 mm gap between them and applied CMT-brazing process. The brazing torch angel was 45⁰ and argon gas was used as the shielding gas at a flow rate of 12 L/min.

Before brazing, the surfaces of the plates were cleaned with acetone and then CMT brazing was performed. The current values for brazing operation were determined as 60, 65, 70, 75, 80, 85, 90, 95 and 100A in overlap joint. Brazing process parameters such as current intensity, wire feed speed, voltage, shielding gas flow rate, brazing travel speed and brazing gap were presented Table 3.

Table 3. CMT-Brazing process parameters

Current Intensity [A]	Wire Feed Speed [m/min]	Voltage [V]	Gas Flow Rate [L/min]	Travel Speed [cm/min]	Brazing Gap [mm]
60	2.9	10.4	12	24	0.5
65	3.3	10.5	12	24	0.5
70	3.6	10.8	12	24	0.5
75	3.9	11.1	12	24	0.5
80	4.3	11.5	12	24	0.5
85	4.6	11.6	12	24	0.5
90	4.9	11.8	12	24	0.5
95	5.3	12.1	12	24	0.5
100	5.6	12.5	12	24	0.5

Nine sets of welding parameters of heat inputs were selected, as shown in Table 4. The heat input (HI) is calculated by using the Eq.(1) and (2) below.

$$HI_{linear} = \frac{(60 \times UI)\eta}{v} \quad (1)$$

$$HI_{normalized} = \frac{HI_{linear}}{\epsilon} \quad (2)$$

Where U: arc voltage, I: current intensity, η_{CMT} : 0.7 arc efficiency factor, V: travel speed (cm/min) [13] and e: thickness (mm).

After CMT-brazing according to the parameters given in the prepared plates, the samples were cut by laser cutting in accordance with the standards for the tensile test. Figure 3 shows the measurements of the test specimens prepared.

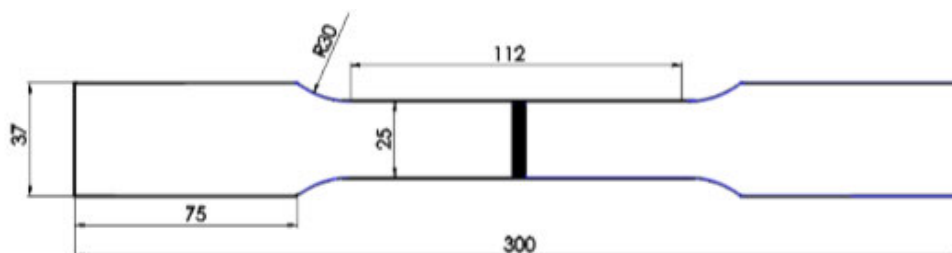


Figure 3. Tensile test specimen dimensions according to EN 895 standard

Micro and macro structure images were taken. After that brazing zone and HAZ zone hardness values were measured. In these measurements used micro-hardness testing machine Wolpert-Wilson. 100 gr load and pyramid sinking tip were used in the measurement. The micro hardness measurements were made at 0.5 mm intervals starting from the brazing zone until reaching the hardness value of the main material.

3. Results and Discussion

According to the tensile test results, as the current value increased to start from 60A, the heat increased and the tensile strength increased. After the current value of 75A, it is seen that the jointing is desired. At the current values of 60, 65, 70 A, no jointing occurred. At a current of 75 A, the strength value is 740 MPa, but it is separated from the brazed zone. The highest tensile strength value was measured as 748 MPa at 80 A current. The maximum tensile strength value of 80A and other specimens are separated from the HAZ zone by an increase in heat input. After the current value of 100 A, it started to be drilled in the main material with the increase of heat input.

Table 4. Experimental results for different current intensity

Current Intensity [A]	Voltage [V]	Tensile Strength [MPa]	Heat Input ($HI_{\text{normalized}}$) [J/cm/mm]
60	10.4	245	1092
65	10.5	307	1194
70	10.8	588	1323
75	11.1	740	1456
80	11.5	748	1610
85	11.6	719	1725
90	11.8	717	1858
95	12.1	718	2011
100	12.5	721	2187

Varol et al. [13] had studies about MIG-Brazing for TRIP 800 zinc coated steel plates and determined maximum tensile strength 754 MPa in 70 A current intensity, 12.4 V arc voltage, 24 cm/min travel speed and 0.8 mm gap. In this study, we determined maximum tensile strength as 748 MPa in 80 A current, 11.5 V arc voltage, 0.5 mm gap and same braze speed.

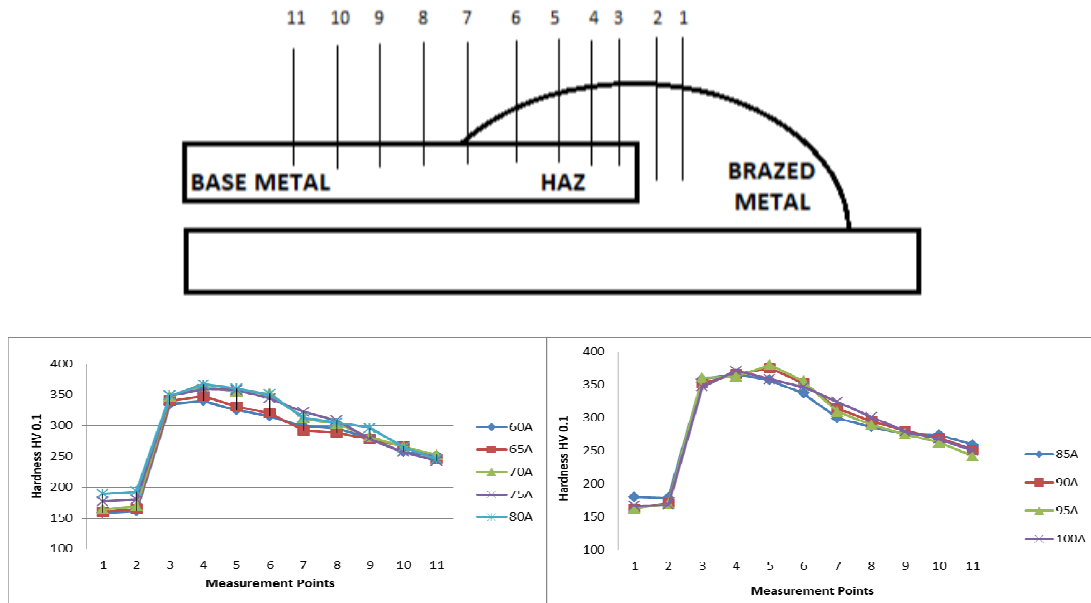


Figure 4. The micro hardness values

The microhardness values of the samples brazed at different current intensities are given in Figure 4. The lowest hardness value appears to be in the brazed zone. The highest hardness value was obtained in the HAZ zone. And this value seems to decrease as towards the main material. The highest hardness values were obtained at current values at 80 A and higher current intensity. Because, as the current value increases, the heat input increases.

Macro structure images of brazed samples at different current intensities are given in Figure 5. Due to the low heat input it appears that there is not enough wetting at 60, 65 and 70 A current intensities. As the current value increases, the heat input increases. Thus, the filler metal is spread over the base material and the wettability is increased. But the high heat input affects the strength result and the jointing.

The microstructure images taken from the brazed regions are given in Figure 6. Due to the heat input during brazing, the micro-iron particles from the joining zone melted and dispersed towards the braze zone. These micro-iron particles formed dendrites. As the current value increases, the dendrite density increases. At the same time, the density of dendrites in the brazing zone affected the micro hardness value.

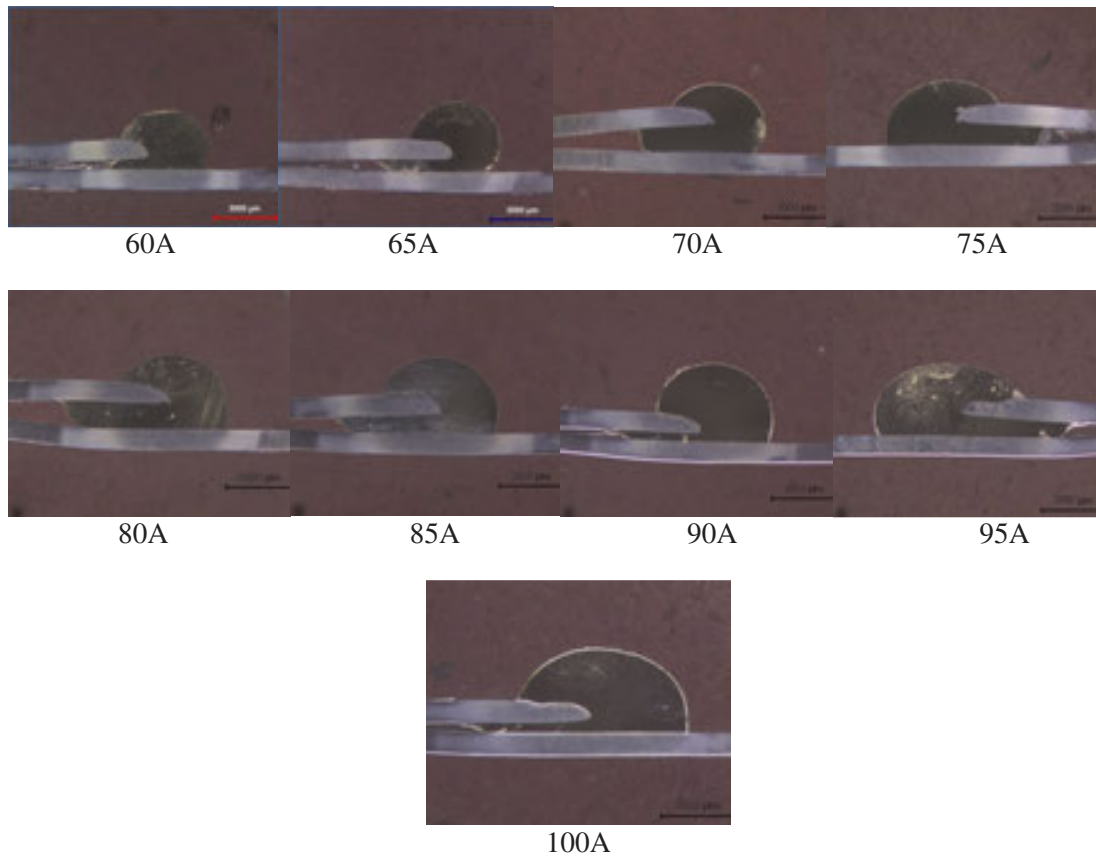
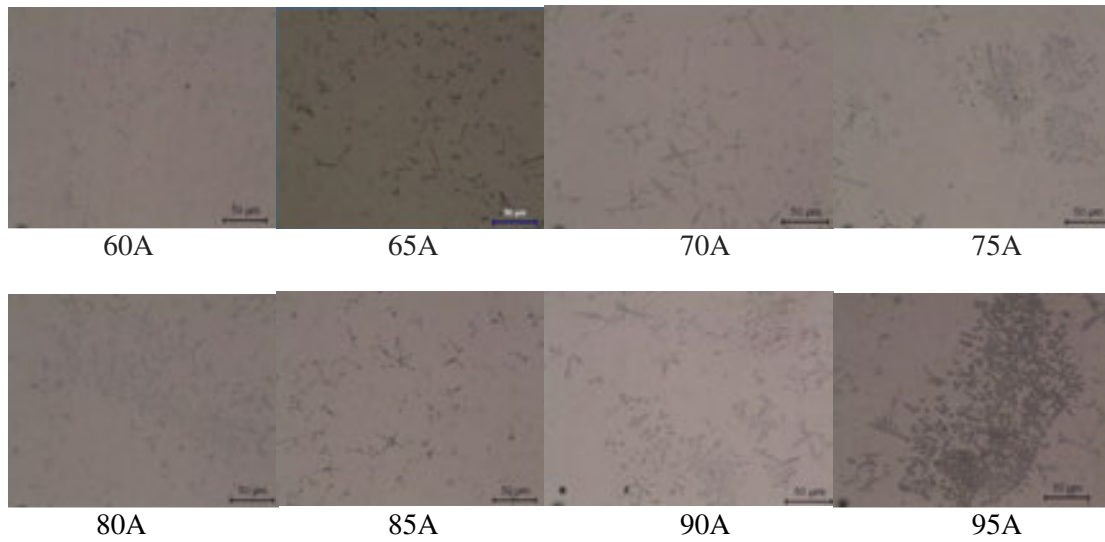
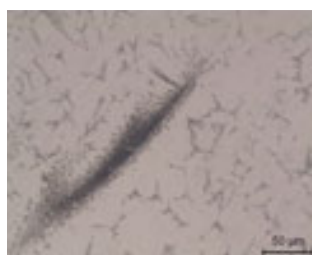


Figure 5. Macrostructure images of different current intensities





100A

Figure 6. Microstructure images of brazed zone at different current intensities.

4. Conclusions

The microstructure and properties of galvanized DP 800 steel overlap joints from CMT-Brazing process for different current intensities were studied in this paper and the following conclusions were drawn:

The joinability of galvanized DP800 steel sheet with CMT-Brazing method has been investigated. And it has been observed that there is very little melting at the main material during the joining process. The increase in current value was found to have a positive impact on tensile strength.

Until the current value of 70A, no jointing occurred. Jointing occurred at samples after current intensity of 75A. It is seen that the 75A current intensity is the critical current value. The highest strength value was obtained at 80A. At later current intensities, the increase in heat input began to reduce the tensile strength of the jointing.

Macro and microstructure images showed that the increase of the current value increased the wettability. And diffusion of iron atoms increased as a result of high heat input with the increase of current intensity and formed dendrites in brazed zone. As a result of the increase of the dendrites, the hardness and strength of the brazed zone increased.

5. Acknowledgement

The authors wish to thank Sakarya University Scientific Research Foundation (Project No: 2017-50-01-010) for their support.

6. References

- [1] S. Kilic, F. Ozturk: Comparison of performances of commercial TWIP900 and DP600 advanced high strength steels in automotive industry, *Journal of the Faculty of Engineering and Architecture of Gazi University*, 31:3 (2016) 567-578.
- [2] F. Hayat: The Investigation of The Use of TRIP Steels in Automotive Industry, *J. Fac. Eng. Arch. Gazi Univ.*, 25:4 (2010) 701-712.
- [3] N. Farabi, D.L. Chen, Y. Zhou: Microstructure and mechanical properties of laser welded dissimilar DP600/DP980 dual-phase steel joints, *Journal of Alloys and Compounds*, 509 (2011) 982-989

- [4] X. N. Wang, Q. Sun, Z. Zheng, H. S. Di: Microstructure and fracture behavior of laser welded joints of DP steels with different heat inputs, *Materials Science & Engineering A*, 699 (2017) 18-25.
- [5] İ. Acar, V. Şıkşık, F. Varol, S. Aslanlar: Investigation of Mechanical Properties of Butt Joint Form in CMT-Brazed Joints of DP1000 Steel Plates Using Different Current Intensity, *European Journal of Science and Technology, Special Issue* (2018) 48-51.
- [6] P. Wang, S. Hu, J. Shen, Y. Liang: Characterization the contribution and limitation of the characteristic processing parameters in cold metal transfer deposition of an Al alloy, *Journal of Materials Processing Technology*, 245 (2017) 122-133.
- [7] www.digitalweldingsolutions.com/CMT.pdf
- [8] J. Ma, F. Kong, W. Liu, B. Carlson, R. Kovacevic: Study on the strength and failure modes of laser welded galvanized DP980 steel lap joints, *Journal of Materials Processing Technology*, 214 (2014) 1696-1709.
- [9] J. Wang, L. Yang, M. Sun, T. Liu, H. Li: Effect of energy input on the microstructure and properties of butt joints in DP 1000 steel laser welding, *Materials and Design*, 90 (2016) 642-649.
- [10] W. Xu, D. Westerbaan, S.S. Nayak, D.L. Chen, F. Goodwin, E. Biro, Y. Zhou: Microstructure and fatigue performance of single and multiple linear fiber laser welded DP980 dual-phase steel, *Materials Science and Engineering A*, 553 (2012) 51-58.
- [11] N. Akkaş, E. Ferik, E. İlhan, S. Aslanlar: The Effect of Nugget Sizes on Mechanical Properties in Resistance Spot Welding of S235JR(Cu) Steel Sheets Used in Railway Vehicles, *Acta Physica Polonica A*, 130 (2016) 60-63.
- [12] S. Aslanlar: The effect of nucleus size on mechanical properties in electrical resistance spot welding of sheets used in automotive industry, *Materials Design*, 28 (2007) 125-131.
- [13] F. Varol, E. Ferik, U. Ozsarac, S. Aslanlar: Influence of current intensity and heat input in Metal Inert Gas-brazed joints of TRIP 800 thin zinc coated steel plates, *Materials Design*, 52 (2013) 1099-1105

CORRESPONDENCE ADDRESS:

Name, FarukVAROL

Postal address, Vocational School of Karasu, Sakarya University, Karasu, Sakarya/ TURKEY

Telephone and E-mail address. 05353338940, fvarol@sakarya.edu.tr

SHORT BIOGRAPHIES

Faruk VAROL -He was born in Balıkesir/Gönen in 1978. He studied in primary and high school in Gönen. He started to study in Technical Training Faculty in SAU in 1998 and graduated in 2002. He had Master of Education in the department of education in Institute of Metal Science. He completed his education in 2006. He started the education of Ph.D. in 2007 in the Institute of Metal Science and Education department in Sakarya University and completed his Ph.D. in 2014. He works in Machine and Metal Technology Department in Karasu Vocational High School in SAU.

İbrahim ACAR -He was born in Erzurum in 1985. He studied primary and high school in Bursa. He started to study in Technical Training Faculty in Sakarya University in 2003 and graduated in 2008. He graduated master degree in Machine Engineering in 2018. He started Ph. D. in 2018 in Manufacturing Engineering in Sakarya Applied Sciences University. He works in Machine and Metal Technology Department in Karasu Vocational High School in SAU.

VeliŞIKŞIK - He was born in Karaman in 1977. He studied primary and high school in Karaman. He started to study Technical Training Faculty in Gazi University in 1998 and graduated in 2002. He started master degree in Machine Engineering in 2015. He works in Machine and Metal Technology Department in Karasu Vocational High School in SAU.

ErmanFERİK - He was born in Bursa in 1987.He studied in primary and high school in Bursa. He started to study in Technical Training Faculty in SAU in 2003 and graduated in 2007. He continues Master of Education in the Metallurgical and Materials Engineering.

Salim Aslanlar- He was born in Sakarya in 1963. He has graduated from Fachhochschule Niederrhein, Germany in Department of Mechanical Engineering. He has graduated from Sakarya University Department of Mechanical Engineering as Ph.D. degree in 1999. He works as a Professor in Sakarya University.

Yusuf Sadi ASLANLAR - He was born inSakarya in 1993 .He studied in primary and high school in Sakarya. He started to study in Faculty of Engineering Department of Industrial Engineering in SAU in 2012 and graduated in 2016. He works as a Project Engineer in YILDIZ KALIP INDUSTRY.

THE INVESTIGATION OF EFFECT ON SHEAR STRENGTH OF NICKEL INTERLAYER IN INSERTED POWDER INJECTION MOULDING

Mehmet SUBAŞI ^{1,a}, Harun KOÇAK ^{2,b}, Çetin KARATAŞ ^{3,c}

¹ Gazi University / Technical Sciences Vocational School

² Selcuk University / Cihanbeyli Vocational School

³ Gazi University / Faculty of Technology / Department of Manufacturing Engineering
^amsubasi@gazi.edu.tr, ^bharunkocak@selcuk.edu.tr, ^ccetink@gazi.edu.tr

Abstract

Inserted Powder Injection Molding (IPIM) is a method which developed to produce thicker parts than 10 mm. Feedstock is injected firstly onto prepared insert in the parts production process by this method. Afterwards, debinding and sintering processes are applied on parts. In this study, firstly inserts were prepared from HSS material. The prepared inserts were divided into two groups with interlayer and without interlayer. Nickel (Ni) layer was formed on inserts in interlayer group with a thickness of 40 µm (± 3 µm). Then WC-Co (9%) feedstock was injected onto all the inserts. After injection process, the samples were subjected to debinding processing. In the study, sintering experiments were performed at 1200 ° C and 1250 ° C and 240 minutes. After the sintering processing, shear test was performed on the intermediate zone of the samples, and the influence of the Ni intermediate layer on the intermediate zone strength was examined. Joining could not be obtained between materials in specimens that directly produced from WC-Co / HSS materials without Ni interlayer. In the samples sintered at 1250 ° C, the WC-Co and Ni interlayer were separated from each other. There was complete joining in the samples with interlayer sintered at 1200 °C. A shear strength of 56.8 N / mm² was achieved in the shear test for these samples.

Key Words: Inserted Powder Injection Molding, WC-Co, Nickel, Sintering

1. Introduction

Tungsten carbide (WC), is known as an expensive hard metal and very hard to be machined due to its high hardness. For this reason, most of the WC parts are produced by powder metallurgy (PM) processes such as powder compaction or powder injection moulding [1]. However the restrictions in the process ability of powder metallurgy cause handicaps to the production of WC parts. Because of these restrictions in PM, an inserted powder injection moulding method has been developed for the production of parts thicker than 10mm [2].

By employing this powder injection moulding method both the production of parts thicker than 10mm and parts having different interior and exterior mechanical characteristics can be made. In this method, first of all inserts are prepared then feeding stock is injected upon them. Afterwards binder removal and sintering processes are applied to the parts.

In the Inserted Powder Injection moulding, obtaining of the desired mechanical characteristics depends on the diffusion between the insert and the part body. All of the materials having suitable chemical and metallurgical properties can be joined by diffusion. So, a number of studies were made on joining by diffusion welding [3-5]. Especially the studies for joining solid

phase diffusion welding of tungsten (W) materials show that nickel decreases the thermal stress level causing to be used as interlayer, [6].

In this study first of all, inserts from HSS (M2) material were prepared by turning. On these inserts 40 µm Ni interlayer was formed. On the HSS inserts with Nickel interlayer and without interlayer ,WC-Co (%9) feeding stock was injected. The parts removed from the mould were subjected to chemical binding removal and sintering processes. Sintering tests were carried out at 1200 °C and 1250 °C for 240 min. After sintering, all of the parts were subjected to cutting strength test and the effect of sintering temperature and interlayer on qthe cutting strength was determined.

2. Material and Method

M2 type HSS (1.3343) insert, WC-Co (9%) feeding stock and Ni interlayer were used in the interior part of the samples, in the outer part and for joining respectively. Feeding stock was purchased from Ryer company. Chemical composition of HSS material is given in Table 1, thermal characteristics in Table 2 and chemical composition of WC feeding stock is in Table 3.

Table 1. Chemical composition of M2 HSS material (%)

C	Si	Mn	Cr	Mo	Ni	V	W	Co
0.9	0.25	0.3	4.10	5.0	0	1.8	6.40	0

Table 2. Thermal characteristics of M2 HSS material

Thermal conductivity (20 °C)	Specific heat (20 °C)	Austenite temperature	Thermal expansion (100-700 °C)
19 W/(m.K)	460 J/(kg.K)	1210 °C	11.5-12.9 10 ⁻⁶ m/(m.K)

Table 3. Chemical composition of WC-Co(9%) feeding stock (%)

Elements	C	Cr	Fe	Mo	Ni	Co	O	W
Mass	5.54	0.01	0.01	0.01	0.01	8.94	0.05	bal.

2.1. Preparation of inserts and application of interlayers

In the study first of all, inserts of 6.40 mm diameter were prepared from HSS material. On these inserts a 40 µm Ni interlayer with (\pm 0,3 µm) tolerance was formed by electrolytic coating method. At the stage of obtaining interlayer the nickel coating bath supplied from Technical Casting company was used. The conditions of obtaining interlayers are given in Table4. The thickness of the obtained interlayer was determined by measuring from the diameter surface with X-Ray measuring device.

Table.4. Electrolytic Ni coating conditions

Anode	Bath temperature	Voltage	Current density	Waiting time
Electrolytic Nickel	50-60 °C	2.5-3 V	4A/dm ²	1 µm for 2 min.

2.2. Inserted powder injection moulding

Injection process was made at the ARBURG Allrounder 220S injection moulding board. The inserts prepared from M2 HSS steel were placed into the mould and WC-Co feedstock was injected on it (Fig. 1). Considering the values advised by the feeding stock company, optimum injection parameters were determined. Parameters used in the injection process are given in Table.5.

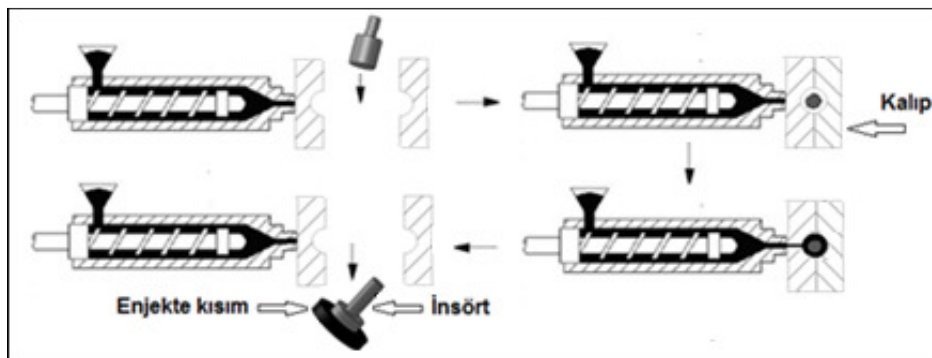


Figure 1. Inserted powder injection moulding process

Table 5. Injection parameters

Injection temperature	Injection pressure	Holding pressure	Injection speed	Mold temperature
200 °C	280 bar	80 bar	10 cm ³ s ⁻¹	60 °C

2.3. Binding removal and sintering processes

Following the injection process test samples were subjected to chemical binding removal treatment in ethanol at 60 °C for 48 hours. After the chemical binding removal treatment, test samples were sintered under control atmosphere (95% N₂ and 5% H₂) at 1200 °C and 1250 °C for 240 min by considering the thermal characteristics of WC-Co (9%) and HSS materials.

2.4. Mechanical Tests

Cutting test is a widely used method to evaluate the strengths and powers between parts consisted of different material [7, 8]. In this study cutting mould method was used for the analysis of joining of the insert and the main material. Three specimens from each sample were prepared and subjected to cutting test.

3. Results and Discussion

In the study, firstly samples from HSS insert and WC-Co feedstock with no interlayer were sintered at 1200 °C and 1250 °C for 240 min. When the samples were examined after sintering it was seen that there was no joining between HSS insert and injected area and there was a gap in the intermediate zone (Fig 2). Furthermore, after sintering the insert moved into the injected part easily and could be taken out. Test was repeated by sintering three sample under the same conditions but again the same results were obtained.

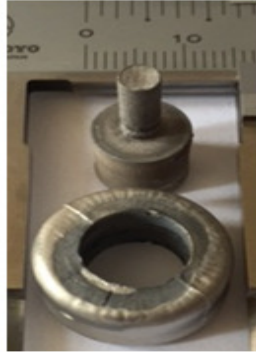


Figure2. Sintered sample (with no interlayer) at 1200 °C for 240 min

In the second stage of the study a 40 µm Ni interlayer was formed on the inserts. Then the inserted samples were sintered at 1200 °C and 1250 °C for 240 min. On the 40 µm Nickel interlayered samples sintered at 1250 °C, WC-Co and Ni interlayers separated from each other (Fig 3).

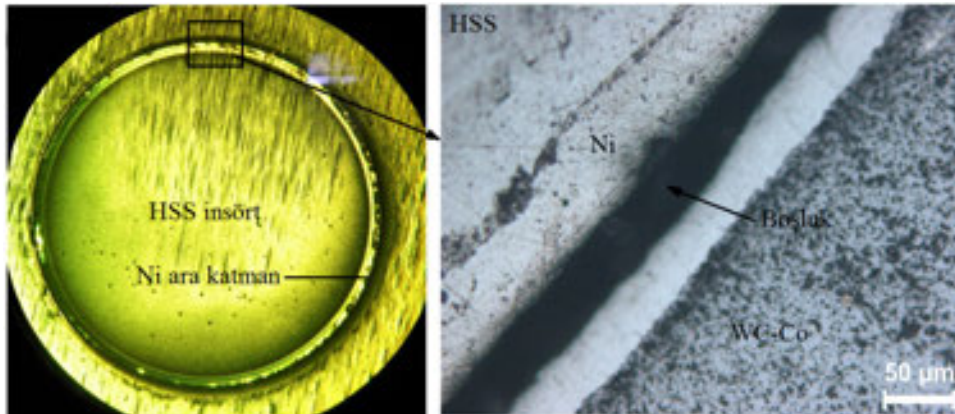


Figure3. Intermediate zone of the sample produced by using 40 µm Ni interlayer (1250 °C 240 min.)

As a result of sintering in the 40 µm Nickel interlayered test specimens at 1200 °C a voidless structure was obtained. In order to have a better examination of the area between the feeding stock and insert, SEM images of the joining area were taken (Fig 4). From the SEM images it was observed that an ideal joining was constituted between the 40 µm thick Ni interlayer with HSS insert and WC-Co.

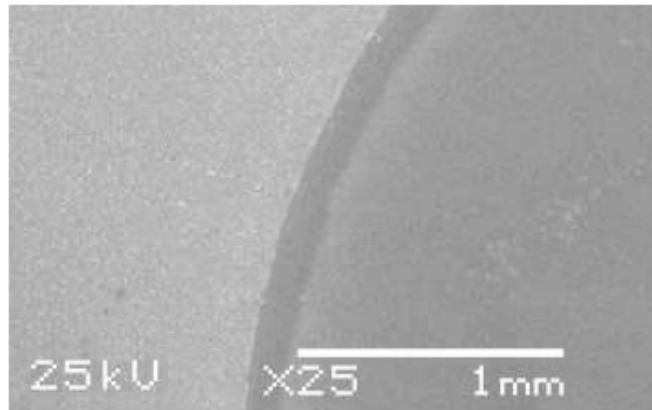


Figure4. Intermediate zone of the sample produced by using 40µm Ni interlayer (1200 °C 240 min.)

On the 40 µm Nickel interlayered samples, cutting tests were made after obtaining a voidless joining. As a result of the cutting tests made for measuring the strength at the intermediate zone produced by using HSS insert and Ni interlayer, a 2.9kN compression force was determined in the samples Sintered at 1200 °C (Fig 5). By using the equations given below a cutting strength of 56.8 N/mm² was obtained in the samples sintered at 1200 C. In the calculation of the area in equation 1 insert diameter and injection thickness were taken as 6.5 mm and 2.5 mm respectively.

$$A = \pi \times D \times t \quad (1)$$

$$\tau = P/A \quad (2)$$

A = Cutting area (mm²), D = Insert diameter (mm), t = Injection thickness (mm), P = Force obtained from compression test (N), τ = Shear strength of intermediate zone (MPa)

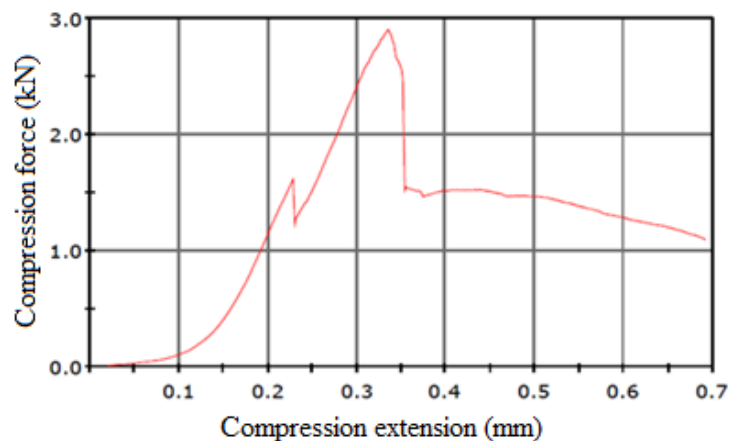


Figure 5. Compression force graph of the 50 µm Nickel interlayered sample

In the studies carried out in literature, it was deduced that nickel interlayer affected the power of diffusion bond positively [3, 9, 10]. Chen and colleagues in one of their studies determined that nickel interlayer strengthened the bond formation in joining the WC-Co cementite carbide and

3Cr13 stainless steel materials with diffusion welding [5]. In this study the target joining in the samples with no nickel interlayer could not be obtained either. It was specified that sintering temperature in the interlayered samples was effective in the joining between the insert and body (feedstock). It was determined that at the specified optimum sintering temperature, parts with sufficient strength can be produced in the intermediate zone.

4. Conclusion

Part production was made from the WC-Co feedstock by Inserted Powder Injection Moulding method. In the parts without Nickel interlayer the target joining could not be obtained. At the end of the tests, while a 56,8 N/mm cutting strength was obtained on the 40mm Nickel interlayered samples, not a complete joining was observed on the sintered samples at 1250 C. As a result of the tests it was observed that nickel interlayer in the insert was effective on joining. However, it was also determined that there has to be an ideal sintering temperature for the joining between the HSS insert and WC-Co material.

6. Acknowledgement

This research was sponsored by the Scientific and Technological Research Council of Turkey (TÜBİTAK), Project No: 115M437. The authors would like to express their sincere appreciation to TÜBİTAK organization and Gazi University for their financial supports.

7. References

1. S.Y.Heng, M. Norhamidi, S. Abu Bakar, F. Abdolali, M. Amin, S.Yulis:Effect of sintering temperature on the mechanical and physical properties of WC–10%Co through micro-powder injection molding (μ PIM), *Ceramics International*, 39(4),(2013), pp. 4457-4464.
2. A.Safarian, M. Subaşı, Ç. Karataş:The effect of sintering parameters on diffusion bonding of 316L stainless steel in inserted metal injection molding, *The International Journal of Advanced Manufacturing Technology*, 89(5),(2017), pp. 2165-2173.
3. J. Zhang, L. Guoqiang, W. Yiyu, S. Qiang, Z. Lianmeng: An investigation on diffusion bonding of aluminum and magnesium using a Ni interlayer, *Materials Letters*, 83,(2012), pp. 189-191.
4. S.Zakipour, M.Samavatian, A.Halvae, A.Amadeh,A. Khodabandeh: The effect of interlayer thickness on liquid state diffusion bonding behavior of dissimilar stainless steel 316/Ti-6Al-4V system, *Materials Letters*, 142,(2015), pp. 168-171.
5. H.Chen,F. Keqin, W. Shifeng, X. Ji, G. Zhixing, W. Hui: Microstructure and properties of WC–Co/3Cr13 joints brazed using Ni electroplated interlayer,*International Journal of Refractory Metals and Hard Materials*, 33,(2012), pp. 70-74.
6. Q.Cai, L. Wensheng, M. Yunzhu, W. Zixuan: Diffusion brazing of tungsten and steel using Ti–Ni liquid phase forming interlayer, *Fusion Engineering and Design*, 91,(2015), pp. 67-72.
7. A.Safarian, Ç. Karataş:Diffusion Welding of Thick Components Fabricated by Inserted Powder Injection Molding, *Materials Testing*, 56(10),(2014), pp. 842-846.
8. A.Safarian, M. Subaşı, Ç. Karataş:Reducing debinding time in thick components fabricated by powder injection molding,*International Journal of Materials Research*, 106(5),(2015), pp. 527-531.

9. H. Chen, L. Chongsheng, W. Tianguo, G. Wen, X. Hongxing, C. Le: Effect of Ni interlayer on partial transient liquid phase bonding of Zr–Sn–Nb alloy and 304 stainless steel. *Materials & Design*, 60,(2014), pp. 358-362.
10. H.Sabetghadam,A.Z. Hanzaki, A. Araee:Diffusion bonding of 410 stainless steel to copper using a nickel interlayer, *Materials Characterization*, 61(6),(2010), pp. 626-634.

Correspondence address

Dr. Mehmet SUBAŞI

Technical Sciences Vocational School Gazi University Ankara TURKEY

Tel: +90 312 354 84 01

E-mail: msubasi@gazi.edu.tr

Dr. Mehmet SUBAŞI, was born in 1979. He completed his undergraduate studies in 2001, his master's degree in 2006 and his doctorate in Gazi University in 2015. He is still working as a lecturer at Gazi University Technical Sciences Vocational School. Academic studies have focused on plastic injection molding, powder injection molding and sheet metal molding techniques.

Dr. Harun KOÇAK, was born in 1985. He completed his undergraduate studies in 2007, his master's degree in 2011 and his doctorate in 2018 at Gazi University. Selçuk University is working as an Instructor at Cihanbeyli Vocational School. Academic studies are focused on machining techniques, powder injection molding and coating techniques.

Assoc. Dr. Çetin KARATAŞ was born in 1958. He completed his master's degree in 1992 and his doctorate in Gazi University in 1998. Despite the fact that manufacturing engineering works in different areas, concentrates on powder injection molding. He is a board member of Turkish Powder Metallurgy Association.

THE EFFECT OF MOLYBDENUM ADDITION ON THE MICROSTRUCTURE AND WEAR BEHAVIOURS OF Fe-Mo-B BASED ALLOYED STEEL

Bülent Kılınç^{1,a}, Engin KOCAMAN^{2,b}, Mustafa Durmaz^{3,c}, Eray Abakay^{3,d},
Uğur Şen^{3,e}, Şaduman Şen^{3,f}

¹Sakarya University / Arifiye Vocational High School / Department of Welding Technologies / Arifiye /
Sakarya / Turkey

²Bulent Ecevit University / Engineering Faculty / Department of Metallurgy and Materials Engineering /
Farabi Campus / Zonguldak / Turkey

³Sakarya University / Engineering Faculty / Department of Metallurgy and Materials Engineering / Esentepe
Campus / Sakarya / Turkey

^abkilinc@sakarya.edu.tr, ^benginkocaman@beun.edu.tr, ^cmdurmaz@sakarya.edu.tr, ^deabakay@sakarya.edu.tr,
^eugursen@sakarya.edu.tr, ^fsdmnsen@sakarya.edu.tr

Abstract

In this study, Fe-Mo-B based hard surface alloy samples with three different compositions were produced by Tungsten inert gas (TIG) welding method and the effects of molybdenum addition on the microstructure and wear behaviors of hard surface alloy layer were investigated. For this purpose, powder mixtures of different proportions prepared from ferrous boron, ferrous molybdenum and iron powder were melted on steel substrate by TIG welding method to form a hard surface alloy layer. Coated layers were characterized by optical (OM) and scanning electron microscopy (SEM), X-ray diffraction analysis (XRD), micro-hardness and ball on disk wear tests. The surface alloying results indicate good quality thick coating and porosity free of the hard-facing. As a result of X-ray diffraction analyses, the presence of α -Fe, Fe₂B, MoB₂, Fe_{9,7}Mo_{0,3} and FeMo₂B₂ phases was determined. Wear tests of the surface alloyed AISI 1010 steels were carried out at atmospheric test conditions under 2.5N, 5N and 10N loads at 0.1 m/s sliding speed against alumina ball.

Key Words: TIG welding, Surface Alloying, Hard-facing, Phase analysis, Wear

1.Introduction

Especially abrasive wear is highly important for the mine, agriculture and metal shaping industry etc. [1–3] Several technologies are used nowadays to fighting with wear, corrosion and worn surface. Hard-facing is one of the most economically method to improve of the surface properties. This method can be applied by an appropriate welding techniques such as tungsten inert gas (TIG), shield manual arc (SMAW), plasma arc welding (PAW) and submerged arc welding (SAW) etc. [4–6]. The welding method is applied a substrate material which is usually Fe, Co and Ni based [7–9]. Coated layer usually requires higher hardness than substrate material to enhance of protection against wear. In order to obtain required hardness with surface alloying has to be hard phases onto the substrate metal. As typical phases, carbides, borides and nitrides of some metal such as chromium, titanium, tungsten can be used. After surface alloying these

hard phases show a dense and uniform distribution onto the substrate metal. Efficiency of the coating layer is mostly dependent on coating composition. Researchers were mostly investigated Fe-Cr-X alloys (X: different carbide and boride forming elements such as vanadium, niobium, boron, tungsten and titanium)[10–12]. However, there is a just limited accomplishment by mentioned above. Fe-Mo-B based hard-facing alloys are newly-developed iron-based wear resistant materials.

Molybdenum and iron are a strong boride-forming element, which forms stable borides like FeB, Fe₂B, Mo₂B, MoB, Mo₂B₅, Fe₁₃Mo₂B₅, Fe₁₄MoB₅, FeMo₂B₂, FeMo₈B₁₁ etc. These compounds have high melting temperature, hardness and wear resistance like Zr, Ti and Cr borides[13]. In this paper, Fe-Mo-B based hard surface alloy samples with three different compositions were produced. Effect of the Molybdenum addition on microstructure and wear resistant of the Fe-Mo-B alloy was investigated.

2. Experimental

In this study, an AISI 1010 steel samples with the dimensions 30mm x70mm x5mm were used as substrate material. The substrate material was cleaned by using acetone and dried. Ferromolybdenum, ferrous boron and iron powder received from AVEKS Co was prepared according to nominal composition which is given Table 1. The powders with specified atomic ratios were mixed by a ball milling for 60 min at a speed of 600 rpm. The powders prepared were ratios determined and mixed to form Fe₁₆MoB₃, Fe₁₄Mo₃B₃ and Fe₁₂Mo₅B₃ compounds. Finally, the powders were pressed on 100 MPa by using hydraulic press. Then the pressed powders were melted together with the substrate using a TIG welding technique.

Table 1. Compositions of powders used in hard surface alloying (by weight)

Powders	%Fe	%B	%Mo	%Cu	%C	%Al	%Si
Ferrous-boron	78,9	19,63	-	-	0,44	0,05	0,98
Ferrous-molybdenum	33,39	-	63,62	0,5	0,98	-	1,51
Pure iron	100	-	-	-	-	-	-

Tungsten inert gas (TIG) welding method was used to obtain surface alloying. Main welding process parameters such as welding current, voltage, arc length, electrode properties and shielding gas are given Table 2.

Table 2. Experimental Parameters of TIG Surface alloying

Parameter	Value
Electrode	Type W-2 pctThO
Electrode Diameter	2.4 mm
Angle	70 degrees
Voltage	20 V
Current	110 A
Heat input	2.2 MJ/m
Protective gas	Type Ar (%99.9 Ar)
Flow	12 L/min
Welding speed	Travel speed 60 mm/min
Heat input $Q = 60 \times I \times V/S$, I: current, V: voltage, and S: travel speed [14]	

The samples were prepared according to standard metallographic procedure by grinding, polishing and etching with (3%) Nital reagent respectively. For microstructural characterization of samples were carried out by using a Nikon Epiphot 200 optical microscope (OM) and JEOL JSM – 6060 scanning electron microscopy (SEM). An X-ray diffraction (XRD) was detected with RigakuXRD/D/MAX/2200/PC model X-ray diffractometer using Cu-K α radiation. To measure Vickers hardness, tests were performed with a load of 10g using Future Tech FM 700Vickers-hardness tester.

Wear and friction tests of the surface alloyed steels were carried out in a tribometer device conforming to ASTM G-99 standard. The experiments were carried out using Ball-On-Disk method using 10 mm diameter Alumina (Al₂O₃) balls. Alumina ball has mirror like surface finish with a hardness value of 2720 HV_{0,05} [15]. Most of the materials are encountered with ambient temperature and humidity in the industrial applications. Therefore, the friction and wear tests were carried out at room temperature (21 \pm 3 °C), relative humidity being 64 \pm 5 conditions. The wear tests were carried out under loads of 2,5N, 5N and 10N at a speed of 0.1 m / s at a distance of 200 m. Wear rate was measured primarily by volumetric (volume loss) means. To evaluate wear resistance, the wear volume was calculated from the worn cross-sectional area of the surface alloyed plate which was measured by KMA P6 optical profilometer.

3. Results and Discussion

The optical and SEM microstructure images obtained from the Fe-Mo-B based hard surface alloy layers coated on the AISI 1010 steel substrate surface are shown in Figure 1. In the microstructure studies, the thickness of the layer seen as molten zone on the substrate is about 2-3 mm and a good bonding with the substrate is observed. It has been determined that this rather thick coating layer has a smooth surface topography with no porosity. In the microstructure studies, it is seen a structure consisting of three different layers on the surface; the substrate, the transition zone and the layer considered to be the boron phases dispersed in the eutectic matrix. It has been observed that the general structure of the Fe-Mo-B-based layer is dendritic. It is also seen that as the molybdenum ratio increases in the hard surface alloy layer, the primer α -Fe grain size decreases.

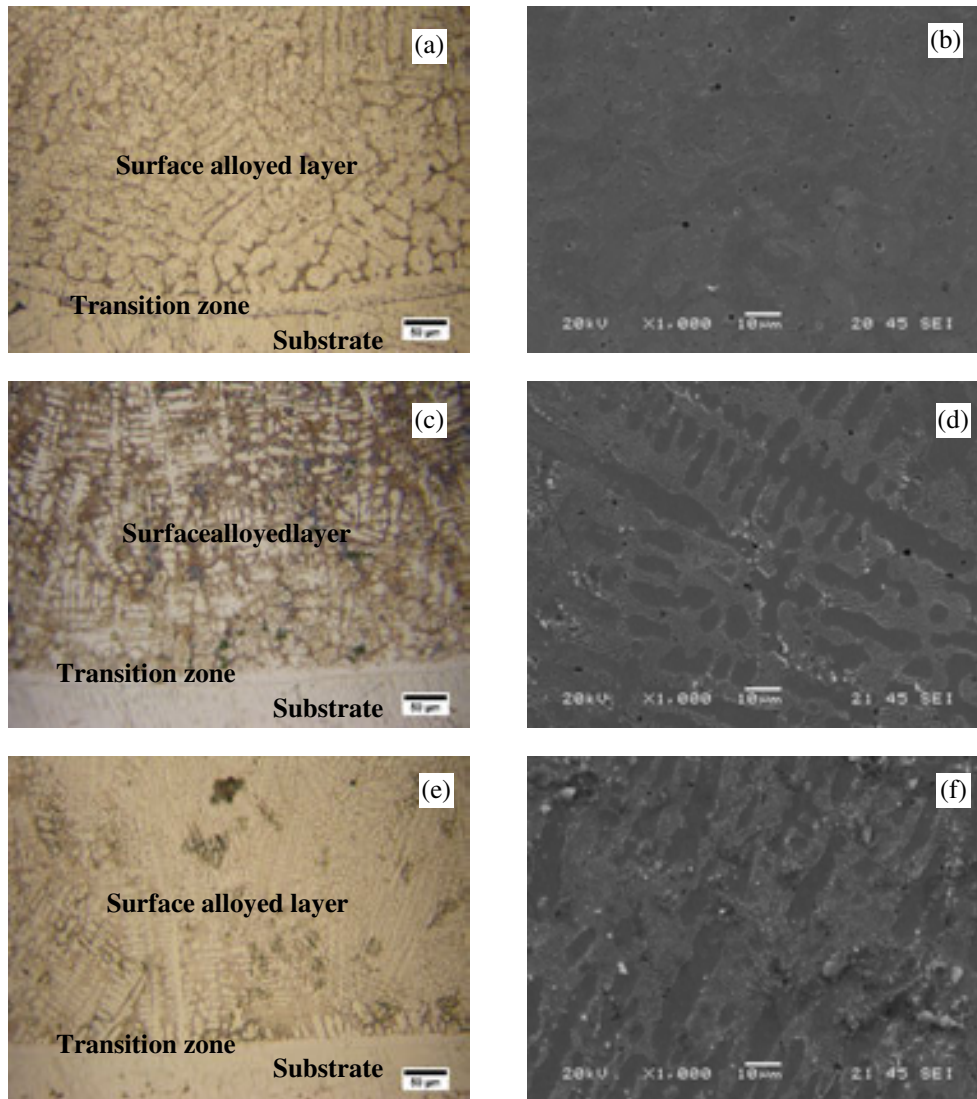


Figure 1. Optical and SEM microstructure images of Fe-Mo-B based hard surface coating layers;
(a-b) $\text{Fe}_{16}\text{MoB}_3$; (c-d) $\text{Fe}_{14}\text{Mo}_3\text{B}_3$; (e-f) $\text{Fe}_{12}\text{Mo}_5\text{B}_3$.

As shown from Figure 1 boride phases are well-distributed in the steel matrix as in situ composite structure. Some parts of the alloyed layer have much more dense boride phase in the alloyed layer as seen in Figure 1. It is possible that the boride phases of the alloyed layer consist of Fe_2B , FeMo_2B_2 , MoB_2 and iron phases which were detected by X-ray diffraction (XRD) analysis. The results are supported by phase diagram of Fe-Mo-B [16]. As known, the hardness of transition metals ranged from 2000 HV to 4000 HV [17].

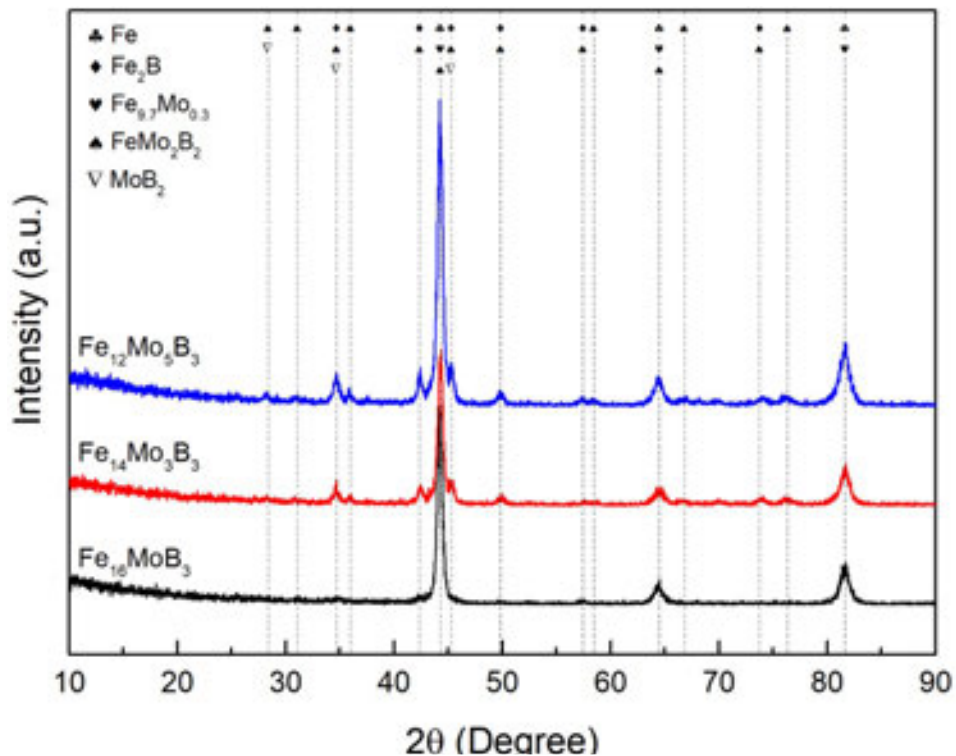


Figure 2. X-ray diffraction pattern of Fe-Mo-B based hard surface alloyed steels

According to the XRD analysis of the Fe-Mo-B based coatings formed on the steel substrate with the TIG source given in Figure 4 the presence of Fe, Fe₂B, FeMo₂B₂, Fe_{9,7}Mo_{0,3} and B₁₅MoB₂ phases were detected.

The hardness values of the boron phases, eutectic columns, transition zone and substrate material in the Fe-Mo-B based coating layer formed on the steel surfaces by TIG welding in three different compositions were 2093±228 HV_{0,01}, 1178±83 HV_{0,01}, 381±59 HV_{0,01} and 191±10 HV_{0,01}, respectively. The hardness of the boron phases varies from 1600 to 2000 HV[18,19]. As a result, the boron phases and the hardness of the eutectic structure are higher than the stiffness of the substrate metal.

As can be seen from the Figure 3(a) in abrasion tests carried out against alumina (Al₂O₃) ball, It has been observed that the friction coefficient values of Fe-Mo-B-based surface alloying materials decrease with increasing Mo content. It is also seen that the friction coefficient values are decreased for the Fe₁₆MoB₃, Fe₁₄Mo₃B₃ compounds depending on the increase of the wear load, but it increases for the Fe₁₂Mo₅B₃ composition. It was determined that the friction coefficient values measured depending on the wear load ranged from 0,387 to 0,788.

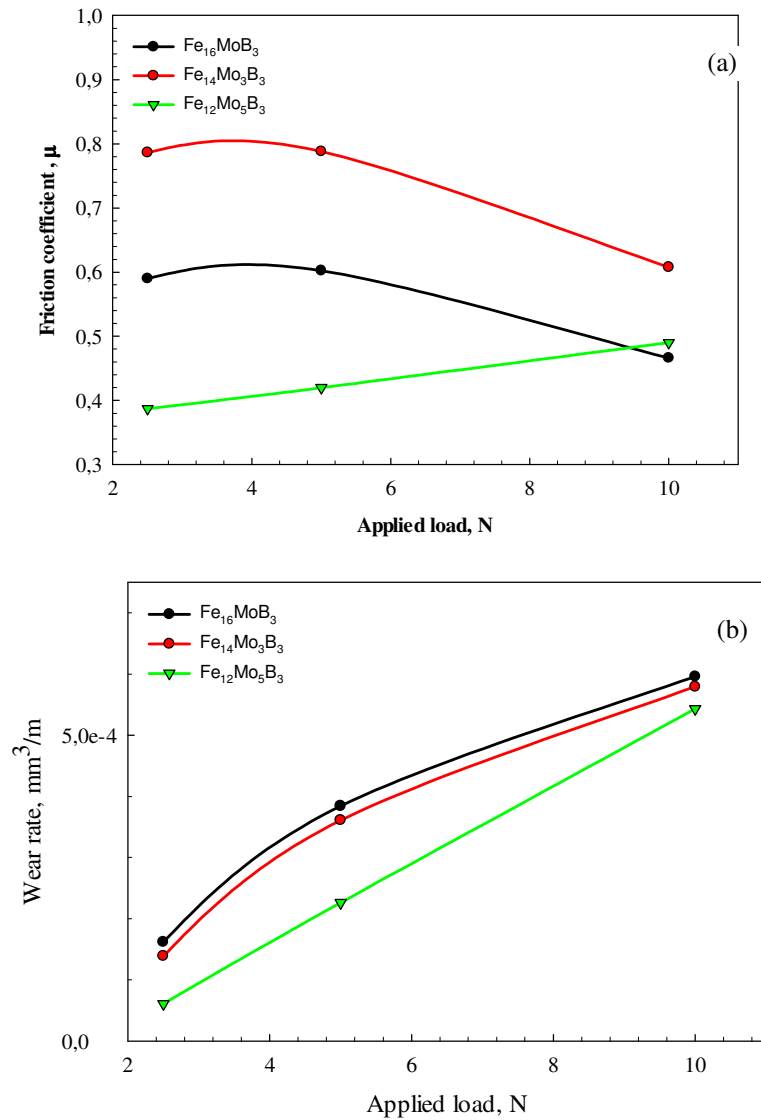


Figure 3.(a)Friction coefficient and (b) wear rate of Fe-Mo-B based hard surface alloyed steels

When the changes in wear rates calculated from the wear tests are examined, it is seen that the abrasion rates of hard coated steels against alumina balls are increased with depending on applied load (Figure 3(b)). In addition, it is seen that the wear rate is decreased for all loads with increasing Mo content in Fe-Mo-B based hard surface alloy layer.

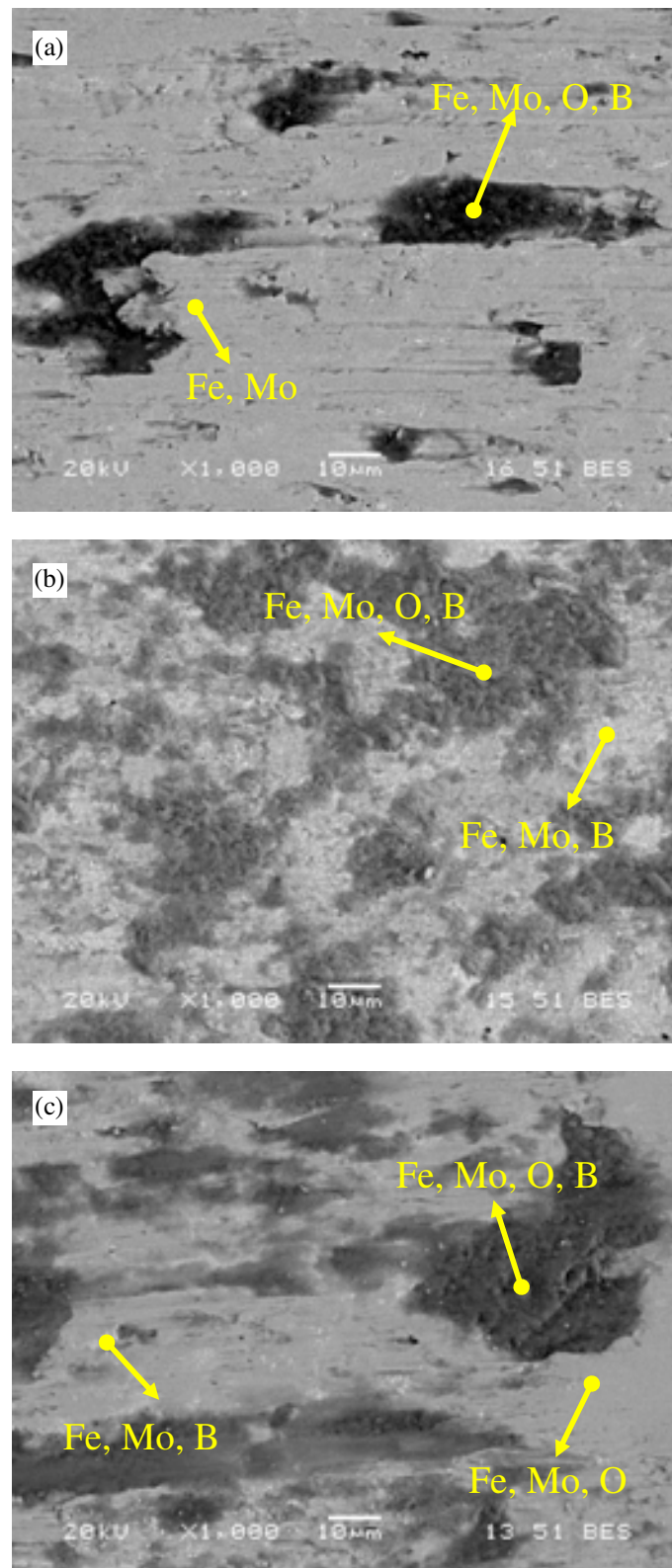


Figure 4. SEM micrographs of the worn surfaces of Fe-Mo-B based hard surface alloyed steels for 5N load (a) $\text{Fe}_{16}\text{MoB}_3$; (b) $\text{Fe}_{14}\text{Mo}_3\text{B}_3$; (c) $\text{Fe}_{12}\text{Mo}_5\text{B}_3$.

SEM microstructure and EDS analysis of the wear traces of Fe-Mo-B based hard surface alloys under 0,1 m/s and 5N load are shown in Figure 4. As a result of EDS analysis taken from the trace of abrasion, the presence of boron, molybdenum and iron as well as oxygen was determined. The wear mechanism of the surface alloyed layers showed that micro abrasive scratches and oxidative wear took place on the worn surface. Wear mechanism was changing with molybdenum content increment from the severe abrasive wear to mild abrasive wear. It is considered that the mechanism of wear is abrasive-oxidative.

4. Conclusion

1. The Fe-Mo-B based hard surface alloy layer has been successfully produced by TIG welding on the AISI 1010 steel surface.
2. The alloyed layers of Fe-Mo-B gave a good quality thick coating, porosity free and moderately smooth rippled surface topography.
3. Increase of the molybdenum content in the alloy composition caused the increase of boride phases formed in the alloyed layers.
4. The possible phases in the surface alloyed layer consist of Fe_2B , FeMo_2B_2 , $\text{Fe}_{9,7}\text{Mo}_{0,3}$, and MoB_2 phases beside the iron boride phases.
5. The hardness of the boride phases, eutectic colonies took place in the alloyed layer, transition zone and base metal are 2093 ± 228 HV0.01, 1178 ± 83 HV0.01, 381 ± 76 HV0.01, and 191 ± 10 HV0.1, respectively.
6. The friction coefficient is changing between 0.387 and 0.788 according to alloy composition and applied load. It has been observed that the friction coefficient values of Fe-Mo-B-based surface alloying materials decrease with increasing Mo content.
7. Increase in applied load caused the increase of wear rate for all alloy compositions. But increase of molybdenum content in the alloy composition caused the decrease of wear rate for all applied loads.
8. Wear mechanism of the surface alloyed layer was changing with molybdenum content increment from the severe abrasive wear to mild abrasive wear.

5. References

- [1] V. E. Buchanan, P. H. Shipway, en D. G. McCartney; Microstructure and abrasive wear behaviour of shielded metal arc welding hardfacings used in the sugarcane industry, vol 263 (2007) pp 99–110.
- [2] A. Singh, G. Singh, en G. Singh: Improving wear resistance via hardfacing of cultivator shovel, Mater. Today Proc., vol 4 (2017), pp 7991–7999.
- [3] S. Singla: Wear behavior of weld overlays on excavator bucket teeth, vol 5 (2014), pp 256–266.
- [4] D. Leroy, T. A. Siewert, S. Liu, en G. R. Edwards, Welding Brazing and Soldering. ASM International, USA (1990).
- [5] X. Wang, F. Han, X. Liu, S. Qu, en Z. Zou: Microstructure and wear properties of the Fe – Ti – V – Mo – C hardfacing alloy, vol 265 (2008), pp 583–589.
- [6] V. Jankauskas, M. Antonov, V. Varnauskas, en R. Skirkus: Effect of WC grain size and

- content on low stress abrasive wear of manual arc welded hardfacings with low-carbon or stainless steel matrix, *Wear*, vol 328–329 (2015) pp 378–390.
- [7] D. G. Ahn: Hardfacing technologies for improvement of wear characteristics of hot working tools: A review, *Int. J. Precis. Eng. Manuf.*, vol 14(2013), pp 1271–1283.
- [8] J. Gou, Y. Wang, Z. Sun, en X. Li: Study of work function and dry sliding wear behavior of Fe-based hardfacing alloys with and without nano rare earth oxides, *J. Alloys Compd.*, vol 713 (2017), pp 255–265.
- [9] C. Katsich en E. Badisch: Effect of carbide degradation in a Ni-based hardfacing under abrasive and combined impact/abrasive conditions, *Surf. Coatings Technol.*, vol 206 (2011), pp 1062–1068.
- [10] Y. F. Zhou, Y. L. Yang, Y. W. Jiang, J. Yang, X. J. Ren, en Q. X. Yang: Fe-24 wt.%Cr-4.1 wt.%C hardfacing alloy: Microstructure and carbide refinement mechanisms with ceria additive, *Mater. Charact.*, vol 72 (2012), pp 77–86.
- [11] J. Gou, P. Lu, Y. Wang, S. Liu, en Z. Zou: Effect of nano-additives on microstructure, mechanical properties and wear behaviour of Fe–Cr–B hardfacing alloy, *Appl. Surf. Sci.*, vol 360 (2016) pp 849–857.
- [12] D. Liu, R. Liu, Y. Wei, Y. Ma, en K. Zhu: Microstructure and wear properties of Fe – 15Cr – 2 . 5Ti – 2C – x B wt .% hardfacing alloys, *Appl. Surf. Sci.*, vol 271 (2013), pp 253–259.
- [13] E. Abakay, B. Kilinc, S. Sen, en U. Sen: Wear properties of TIG surface alloyed steel with 50%Fe-10%W-40%B alloy, *Acta Phys. Pol. A*, vol 127 (2015), pp 957–960.
- [14] S. Buytoz: Microstructural properties of SiC based hardfacing on low alloy steel, *Surf. Coatings Technol.*, vol 200 (2006), pp 3734–3742.
- [15] J. F. Shackelford en W. Alexander, *Mechanical Properties of Materials*. WasCRC Press, Washington (2001).
- [16] V. Raghavan, *Phase Diagrams of Ternary Iron Alloys*. ASM International; Indian Institute of Technology, Delhi (1992).
- [17] B. Aronsson en T. Lundström, *Borides, Silicides and Phosphides: A Critical Review of Their Preparation, Properties and Crystal Chemistry*, London (1965).
- [18] S. O. Yilmaz, M. Ozenbas, en M. Yaz: Synthesis of TiB₂-reinforced iron-based composite coating”, *Tribol. Int.*, vol 42 (2009), pp 1220–1229.
- [19] Z. Pala et al., “Study of residual stresses, microstructure, and hardness in FeB and Fe₂B ultra-hard layers”, *Powder Diffr.*, vol 30 (2015), pp S83–S89.

CORRESPONDENCE ADDRESS: Bülent Kılınç, **Arifiye Vocational School** Department of Welding Technologies, Arifiye/Sakarya TURKEY, bkilinc@sakarya.edu.tr

SHORT BIOGRAPHIES

Bülent Kılınç (39)

Bülent KILINÇ, He completed BSc in 2003, MSc in 2010 in the Department of Technical Education at the University of Sakarya. Bülent KILINÇ has completed his PhD in Metallurgy and Materials Science Department of the Science Institute of Sakarya University In 2018. Bülent Kılınç is a lecturer in Department of Welding Technology at Vocational School at the University of Sakarya since 2012. His research interests Thermo-chemical coating, melting Based Coatings, Corrosion and tribology, and he published several papers on these topics.

Engin KOCAMAN(29)

EnginKocaman was born on April 17 1989 - Akşehir. He graduated from his bachelor degree at Sakarya University Metallurgical and Materials Engineering department in 2013 and his master's degree at same univesity in 2017. He is currently working on PH.D. thesis titled "Development of Fe-M-Cr-B (M=Ti, Mo) based In-Situ Composite Hard Surface Alloying Coated Electrodes". He has been working as a research assistant at Bulent Ecevit University since 2016. His research interests are casting of aluminum, hard-facing coatings, solidification and nickel based single crystal super-alloys.

Mustafa Durmaz (29)

The author was born in 1989 in Samsun. He completed BSc in 2011, MSc in 2015 and he started to study PhD in 2016 in the department of Metallurgy and Materials Engineering at the University of Sakarya. Mustafa Durmaz is research assistant at the Sakarya University since 2013. His research interests lie in the area of mechanical alloying, thermochemical coating process and tribology, and he published several papers on these topics.

ErayAbakay(32)

ErayAbakay has been working as a research assistant at Sakarya University since 2012. He graduated from Yıldız Technical University Metallurgical and Materials Engineering department in 2010 andSakarya University in 2013 with his master's degree in "Nb-Al-N Coating of Steel Surfaces by Thermo Reactive Deposition Method". There are many articles available in hard-facing and thermo reactive deposition. He is currently working on PH.D. thesis titled "Electrodeposition of nickel boron coating of magnesium and its alloys".

ŞadumanŞen(49)

ŞadumanŞen has entered in 1987 to the Metallurgical Engineering Department of Sakarya Engineering Faculty of Istanbul Technical University. She graduated at the Institute of Materials Science department of Science Institute at 1994 and completed her master's degree. Şaduman Sen has completed his PhD in Metallurgy and Materials Science Department of the Science Institute of Sakarya University In 1998. She has worked as an Assistant Professor and Associate Professor in the Department of Metal Education Department of Faculty of Technical Education of Sakarya University. She has been working as a professor at the Department of Metallurgy and Materials Engineering of Engineering Faculty of Sakarya University.The Author has been studied on hard coatings, especially nitride, carbide and boride base coatings, thermochemical coatings, corrosion, Tribology and powder metallurgy subjects. She has been managing masters and doctoral theses and scientific projects. There are also a number of international and national articles and papers on these issues of the Author.

UğurŞen (52)

Uğur ŞEN, has entered in 1984 to the Metallurgical Engineering Department of Sakarya Engineering Faculty of İstanbul Technical University. He graduated at the Institute of Materials Science department of Science Institute at 1993 and completed his master's degree. Uğur ŞEN has completed his PhD in Materials Science Department of the Science Institute of Istanbul Technical University at 1998. He has worked as an Assistant Professor in the Department of Metal Education Department of Faculty of Technical Education of Sakarya University. He has worked as an Associate Professor at the Department of Metallurgy and Materials Engineering of

Engineering Faculty of Sakarya University. Uğur ŞEN has been working as a professor at the Department of Metallurgy and Materials Engineering of Engineering Faculty of Sakarya University. The Author has been studied on hard coatings, thermo-chemical coatings, corrosion, tribology, powder metallurgy and electronic ceramics subjects. He has been managing masters and doctoral theses and scientific projects. There are also a number of international and national articles and papers on these issues of the Author.

MICROSTRUCTURAL EVOLUTION, PHASE TRANSITION AND MECHANICAL PROPERTIES OF Fe-Ti-B HARDFACING ALLOYS

Eray Abakay^{1,a}, Engin Kocaman^{2,b}, Mustafa Durmaz^{1,c}, Bülent Kılınç^{3,d},
Şaduman Şen^{1,e} and Uğur Şen^{1,f}

¹Sakarya University, Department of Metallurgical and Materials Engineering, Sakarya, Turkey

²Bulent Ecevit University, Department of Metallurgical and Materials Engineering, Zonguldak, Turkey

³Sakarya University, Arifiye Vocational School, Sakarya, Turkey

^aeabakay@sakarya.edu.tr, ^benginkocaman@gmail.com, ^cmdurmaz@sakarya.edu.tr,

^dbkilinc@sakarya.edu.tr, ^esdmnsen@sakarya.edu.tr and ^fugursen@sakarya.edu.tr

Abstract

The use of the steels with high hardness and abrasion resistance is very important for industrial applications. In many cases, instead of having a high hardness of an entire part, only the hardness of the surface is sufficient and the cost is lower. In the hardfacing method, the coatings of the metal matrix composite structure containing non-oxide hard reinforcement structure can be realized by the organizing the chemical composition of the starting powders. In this study, three alloys containing Fe, Ti and B elements were prepared and microstructural investigations, phase transformations and hardness values were investigated depending on the increasing ratio of titanium. Alloy powders consisting of ferrous-titanium, ferrous-boron and Armco iron on the surface of SAE 1320 plates with the dimensions of 50 x 100 x 10 mm³ were melted with tungsten inert gas (TIG) welding technique. Microstructural investigations were carried out using by scanning electron microscopy (SEM) and optical microscope (OM) from the cross-section of metallographically prepared samples. It has been determined that TiB₂ phase content and microstructure of the alloyed layer are observed depending on the amount of increase in titanium content. The chemical analysis of the resulting structures was carried out using by energy dispersive spectroscopy (EDS). The phases formed in the coated layer by varying amounts of titanium were determined by x-ray diffraction (XRD). According to the XRD analysis, α -Fe, TiB₂ and Fe₂B phases were determined.

Key Words: Hardfacing, TIG Welding, Titanium diboride, phase analysis.

1. Introduction

Many machine parts are subjected to severe wear and impact during their use in harsh environments. In such cases, faults can occur in a short time on the devices and can cause great damage to the plants. In many cases, the use of parts made entirely of materials with high wear and impact resistance creates high costs. With the hardfacing method it is possible to obtain a coating layer with high wear and impact resistance on the surface of many materials. A metal matrix composite coating layer with a ductile matrix and carbide, nitride and boron based reinforcing phases can be obtained by melting various ferrous alloy powders on the surface of low cost and low cost materials using different welding methods[1-5].

TiB₂-Fe composites have been an important research topic for researchers for the last 10 years. The TiB₂ phase is characterized by high hardness (3400 HV), high melting temperature (3225 °

C), low density (4.451 g/cm^3), high chemical stability, high wear resistance, high corrosion resistance, good wettability and thermodynamic stability properties in liquid steel. The use of titanium diboride as a reinforcing phase in iron matrix composites has been a subject of interest with these properties. There are several studies in the literature that use different methods such as powder metallurgy (PM), conventional melting and casting, carbothermic reduction, self-propagating high-temperature synthesis (SHS), aluminothermic reduction and hard-facing for obtaining $\text{TiB}_2\text{-Fe}$ metal matrix composites. There are studies using laser and plasma-transferred-arc (PTA) methods in the production of $\text{TiB}_2\text{-Fe}$ composites by the hardfacing method [1], [6-7], [8-9]. An alternative to the mentioned welding methods is tungsten-inert-gas (TIG) or also known as gas-tungsten-arc welding (GTAW) welding method. This method, which is performed with an arc formed between the tungsten electrode and the base metal, combines parts made of materials such as steel, aluminum, titanium etc. The welding obtained after the process has good appearance and high quality compared to other welding methods [10-12].

In this study, the coating layers obtained by melting the alloy powders containing Armco iron, ferrous titanium and ferrous boron by TIG welding method were investigated at various ratios on the surface of SAE1320 low carbon steel. The changes in the microstructure, phase and mechanical properties were investigated depending on the varying powder mixture ratios and comparisons were made with the coating layers obtained by different methods.

2. Experimental

SAE1320, a low carbon steel, was selected as the base material. The chemical composition of the steel supplied as sheet of 5 mm thickness is given in Table 1. After sectioned in $20 \times 10 \times 5 \text{ mm}^3$ dimensions, the surfaces of the samples were sanded and cleaned with acetone. Ferrous titanium and ferrous boron are crushed and milled to be under the $45 \mu\text{m}$ sieve. After grinding, mixing with Armco iron was carried out at the ratios given in Table 2. The iron, titanium and boron ratios in the prepared compositions are given in Table 3 as at. %. In order to obtain a homogeneous mixture, the mixing process was carried out for 2 hours at the ball mill. Subsequently, the mixture was weighed at a certain ratio and pressed with a die to obtain a homogeneous layer on the surface of the substrate. The hardfacing process was performed by using the parameters given in Table 4 with the TIG welding method after the specified pre-treatment.

Table 1. The chemical composition of SAE1320 used as the substrate (wt. %).

C	Cr	Mn	Si	P	S	Ni	Mo	Fe
0.183	0.021	1.370	0.204	0.018	0.002	0.062	0.006	98.000

Metallographic analyzes of the prepared samples were carried out using an optical microscope (Nikon Epiphot 200, Japan) and a scanning electron microscope (JEOL JSM 6060, Japan). After sectioned, the samples were gradually sanded to 1200 mesh sanding step and then polished with $0.3 \mu\text{m}$ alumina paste. Polished samples were chemically cleaned with 3% Nital solution after their surfaces were cleaned with acetone. Energy dispersive X-ray spectroscopy (EDS) was used in chemical analysis of the various regions of the samples. X-ray diffraction (XRD) was used to investigate the phase shifts and the changes in the phases depending on the changing Fe, Ti and B ratios.

Table 2. % Atomic percentages of boron, titanium and iron in the prepared compositions

Compound	Code	% B	% Ti	% Fe
1	C1	40	15	45
2	C2	40	10	50
3	C3	40	5	55

Table 3. Chemical composition of ferrous alloys and Armco iron used (wt. %).

	Ti	B	C	Al	Si	P	S	Fe
Ferro-titanium	70.950		0.129	3.690	-	0.008	0.004	25.200
Ferro-boron		18.58	0.310	0.084	0.390	0.029	0.003	80.6
Armco iron	-	-	0.010	-	-	-	-	99.990

Hardness measurements of the coatings obtained on the surface were made by Vickers micro hardness measurement. The hardness of all the phases in all the samples was taken under the loads of 10 gf.

Table 4. The main parameters of TIG hardfacing

Parameter	Value
Electrode	Type W-2 pctThO
Diameter	2.4 mm
Angle	70 °
Voltage	20 V
Current	110 A
Heat input	2.2 MJ/m
Protective gas	Type Ar (%99.9 Ar)
Flow	12 L/min
Welding speed	Travel speed 60 mm/min
Heat input $Q = 60 \times I \times V/S$, I: current, V: voltage, and S: travel speed	

3. Results and Discussion

In Fig. 1, samples with hardfacing of 3 different compositions containing Fe, Ti and B elements were given optical microscope images. Due to the decreasing amount of titanium and increasing amount of iron relative to the image, changes in the microstructure have occurred. Generally cracks and porosities are observed on the surfaces obtained by hardfacing method [13-15]. In the obtained samples, no crack or porosity were formed. For C1 and C2 compounds, the structure consists of ferrite-based matrix, needle-like, spherical and blocky phases. However, there are no needle-like phases for the C3 composition. For this reason, it can be said that there is a decrease needle-like phases due to the decreasing amount of titanium and the amount of iron being increased.

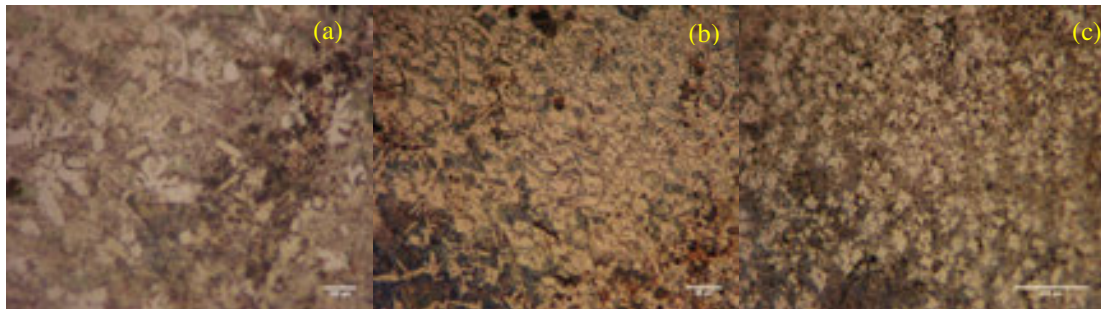


Figure 1. Optical microscope images of hardfacing sample surfaces for C1, C2 and C3 compounds, respectively.

In Figure 2, SEM image and EDS analyzes of sample C1 are given. According to these images and analyzes, it is seen that one of the phases based on iron (figure 2 b) and the one based on titanium (figure 2 c) are formed on the steel based matrix (Figure 2 d). Fe, Fe₂B and TiB₂ phases should be present in the structure according to the B-Fe-Ti ternary phase diagram, and the EDS analyzes taken from different regions are consistent with the EDS analyzes of said phases [16-18]. Considering also the optical microscope images in Figure 1, it can be said that the black-colored TiB₂ phase in the spherical form decreases with the decreasing amount of titanium.

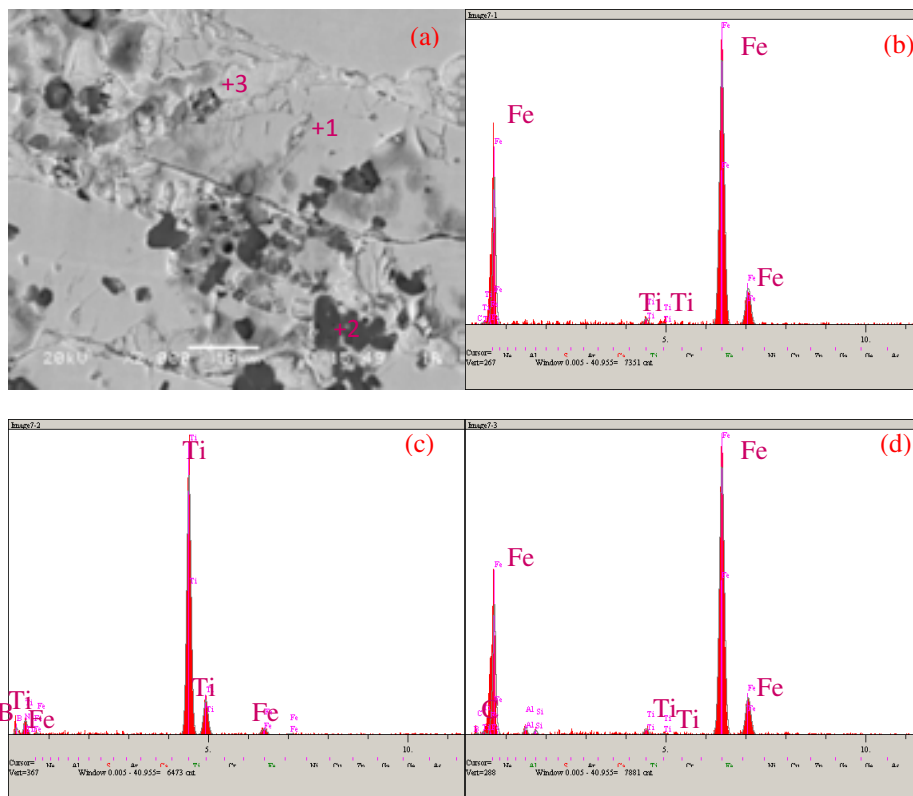


Figure 2. (a) Cross-sectional SEM image, (b), (c) and (d) EDS analyzes from different regions of C1-coded sample.

The structure according to the SEM image taken from the cross-section of the C2-coded sample differs from C1, although the EDS analyzes are similar (Fig. 3). TiB_2 phase is larger than C1 and Fe_2B is formed in lamellar structure. Depending on the increased cooling rate, the Fe_2B phase has a lamellar structure instead of a blocky and needle-like structure [19].

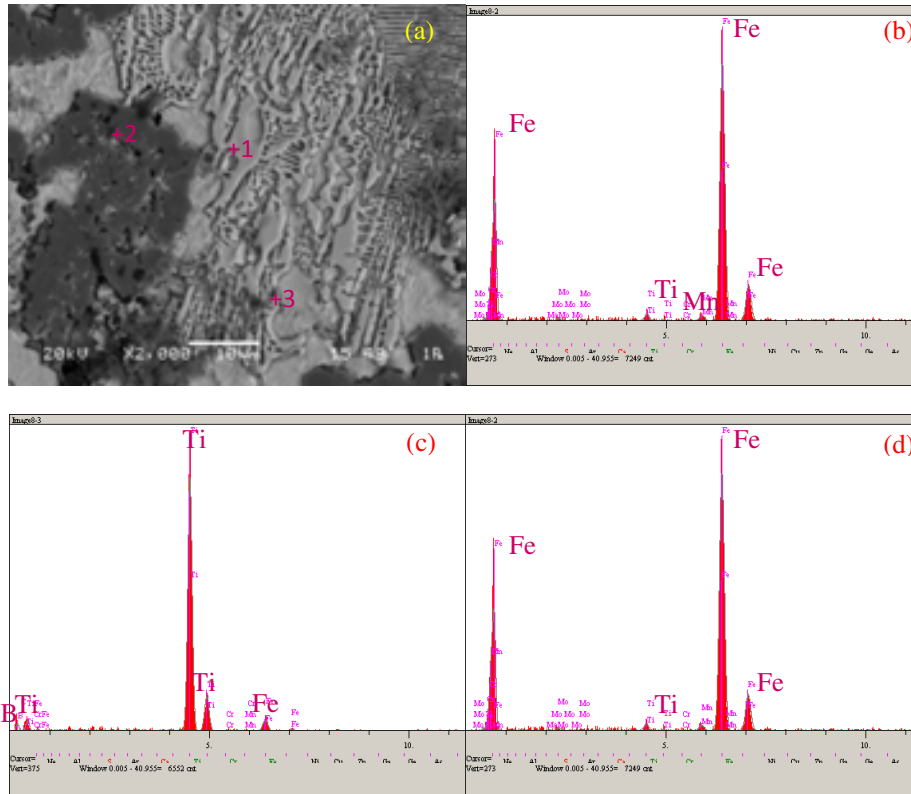


Figure 3. (a) Cross-sectional SEM image, (b), (c) and (d) EDS analyzes from different regions of C2-coded sample.

In Fig. 4 a, when the SEM image is viewed, it can be said that the image of the Fe_2B phase in the C3 code sample resembles C1. EDS analyzes from points 1 and 3 are similar to those of C1 and C2 samples. As seen in Figure 1.c, the TiB_2 phase is present in this structure as very small particles. However, in the analysis taken from point 2 in figure 4c, oxide is seen in the structure. According to similar studies, oxidation occurs in compositions containing Fe-Ti-B at high temperatures [20].

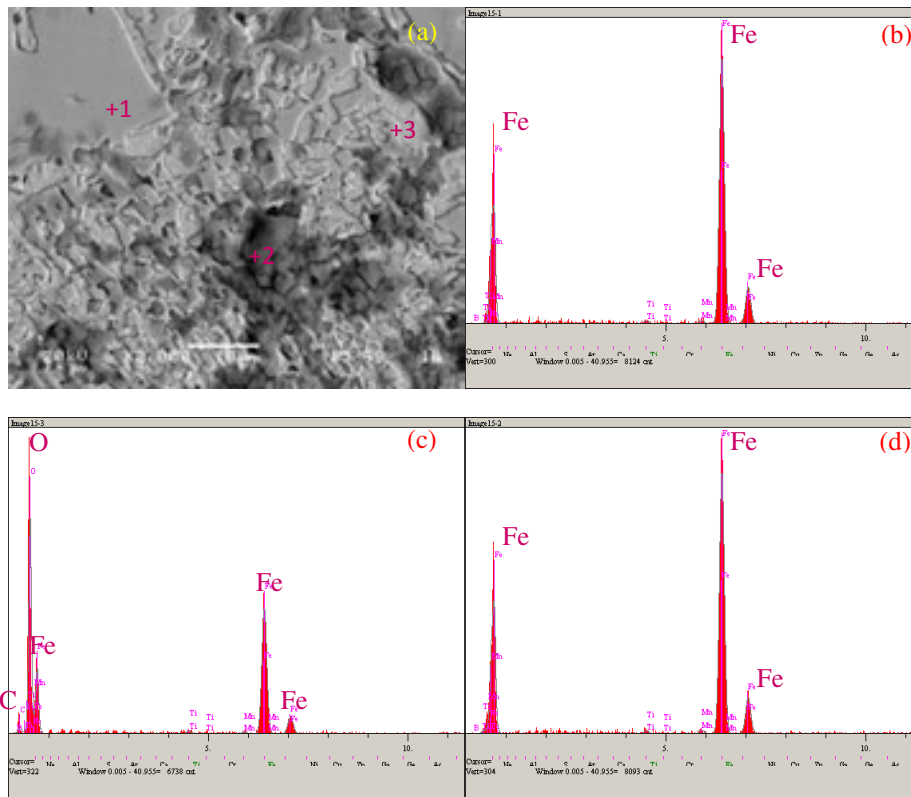
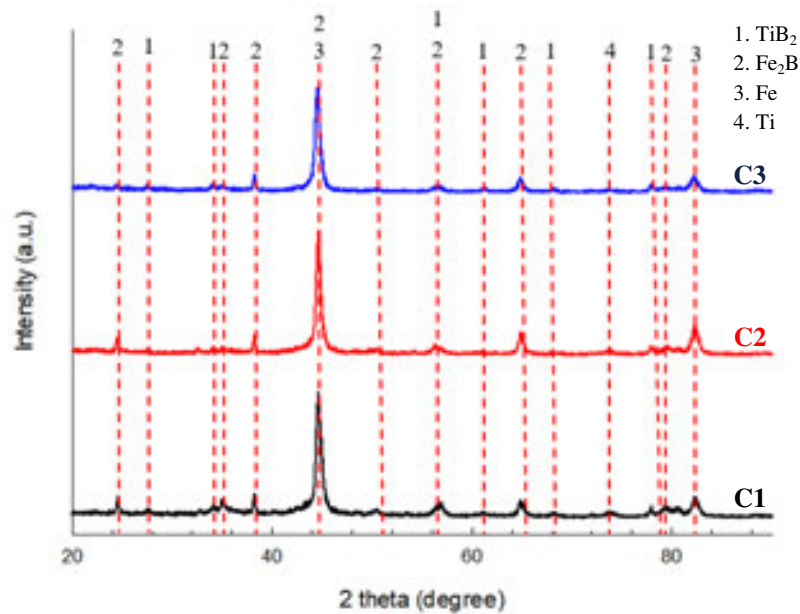


Figure 4. (a) Cross-sectional SEM image, (b), (c) and (d) EDS analyzes from different regions of C3-coded sample.

Fig. 5 shows X-ray diffractions of the samples. As mentioned in previous chapters, the structure consists of TiB_2 , Fe_2B , Fe phases. In addition to these phases, the Ti phase was also determined. The Ti phase is not seen in C3 due to increased iron and decreased titanium content. Contrary to expectations, the Fe_2B phase at 24° is not visible in the C3 composition. Except for the two changes mentioned above, the three compounds have similar patterns.



According to the result of Vickers micro hardness measurement, 324 HV hardness value is determined for steel based matrix. The measured values are about 1480 HV Fe_2B and 3727 HV TiB_2 for the reinforcing phases. The hardness measurement results are similar to the literature and it can be said that C1 compound is the most preferable composition because of TiB_2 content [21-22].

4. Conclusion

On the surface of SAE 1320 steel, a hardfacing process with TIG welding of different compositions prepared with ferro titanium, ferroboron and armco iron powders resulted in a structure consisting of steel matrix, TiB_2 and Fe_2B reinforcing phases. In addition, the TiB_2 phase in the structure has also increased due to the increased amount of ferro titanium. Considering the hardness measurements made, it is thought that it would be more appropriate to use the compositions containing high amounts of ferro titanium for applications requiring high hardness and wear resistance.

5. References

- [1] Q. Ming, L. C. Lim, Z. D. Chen: Laser cladding of nickel-based hardfacing alloys, *Surface and Coatings Technology*, 106 (1998), pp. 174-182.
- [2] Y. Bayhan: Reduction of wear via hardfacing of chisel ploughshare, *Tribology International*, 39 (2006), pp. 570-574.
- [3] M. F. Buchely, J. C. Gutierrez, L. M. León, A. Toro: The effect of microstructure on abrasive wear of hardfacing alloys, *Wear*, 259(2005) 52-61.
- [4] J. J. Coronado, H. F. Caicedo, A. L. Gómez: The effects of welding processes on abrasive wear resistance for hardfacing deposits, *Tribology International*, 42(2009) 745-749.
- [5] S. Chatterjee, T. K. Pal: Wear behaviour of hardfacing deposits on cast iron, *Wear* 255 (2003), pp.417-425.
- [6] D. Wu, X. Wang, P. Zhang, L. Cai, H. Sun: Defects in the in situ synthesized TiB_2/Fe composite coatings during PTA process, *Applied Surface Science*, 257 (2011) ,pp. 10119-10125.

- [7] Y. Wang, Z. Q. Zhang, H. Y. Wang, B. X. Ma, Q. C. Jiang: Effect of Fe content in Fe–Ti–B system on fabricating TiB₂ particulate locally reinforced steel matrix composites, *Materials Science and Engineering: A*, 422 (2006) 339-345.
- [8] B. Li, Y. Liu, J. Li, S. Gao, H. Cao, L. He: Effect of tungsten addition on the microstructure and tensile properties of in situ TiB₂/Fe composite produced by vacuum induction melting, *Materials & Design*, 31 (2010), pp. 877-883.
- [9] B. Du, Z. Zou, X. Wang, S. Qu: In situ synthesis of TiB₂/Fe composite coating by laser cladding, *Materials Letters*, 62 (2008), pp. 689-691.
- [10] S. C. Juang, Y. S. Tarn, H. R. Lii: A comparison between the back-propagation and counter-propagation networks in the modeling of the TIG welding process, *Journal of Materials Processing Technology*, 75(1998), pp. 54-62.
- [11] P. J. Modenesi, E. R. Apolinário, I. M. Pereira: TIG welding with single-component fluxes, *Journal of Materials Processing Technology*, 99 (2000), pp. 260-265.
- [12] C.-M. Chang, C.-M. Lin, C.-C. Hsieh, J.-H. Chen, W. Wu: Micro-structural characteristics of Fe–40wt%Cr–xC hardfacing alloys with [1.0–4.0wt%] carbon content, *Journal of Alloys and Compounds*, 487 (2009), pp. 83-89.
- [13] V. E. Buchanan, D. G. McCartney, P. H. Shipway: A comparison of the abrasive wear behaviour of iron-chromium based hardfaced coatings deposited by SMAW and electric arc spraying, *Wear*, 264 (2008), pp. 542-549.
- [14] A. S. C. M. D'Oliveira, R. S. C. Paredes, R. L. C. Santos: Pulsed current plasma transferred arc hardfacing, *Journal of Materials Processing Technology*, 171 (2006), pp. 167-174.
- [15] L. Sexton, S. Lavin, G. Byrne, A. Kennedy: Laser cladding of aerospace materials, *Journal of Materials Processing Technology*, 122 (2002), pp. 63-68.
- [16] V. Raghavan, B-Fe-Ti (Boron-Iron-Titanium), 24 (2003), pp. 2-3.
- [17] O. Ozdemir, M. A. Omar, M. Usta, S. Zeytin, C. Bindal, A. H. Ucisik: An investigation on boriding kinetics of AISI 316 stainless steel, *Vacuum* 83 (2008), pp. 175-179.
- [18] J. P. Tu: Preparation and properties of TiB₂ nanoparticle reinforced copper matrix composites by in situ processing, *Materials Letters*, 52 (2002), pp. 448-452.
- [19] L. C. Lim, Q. Ming, Z. D. Chen: Microstructures of laser-clad nickel-based hardfacing alloys, *Surface and Coatings Technology*, 106 (1998), pp. 183-192.
- [20] X. Wang, H. Shun, C. Li, X. Wang, D. Sun: The performances of TiB₂-contained iron-based coatings at high temperature, *Surface and Coatings Technology*, 201 (2006), 2500-2504.
- [21] T. S. Srivatsan, G. Guruprasad, D. Black, R. Radhakrishnan, T. S. Sudarshan: Influence of TiB₂ content on microstructure and hardness of TiB₂–B₄C composite, *Powder Technology*, 159 (2005) 161-167.
- [22] Z. Huang, J. Xing, C. Guo: Improving fracture toughness and hardness of Fe₂B in high boron white cast iron by chromium addition, *Materials & Design*, 31 (2010) 3084-3089.

CORRESPONDENCE ADDRESS:

Eray Abakay, Sakarya University, Esentepe Campus, Department of Metallurgical and Materials Engineering 54187 Serdivan Sakarya Turkey, +902642957076, eabakay@sakarya.edu.tr

SHORT BIOGRAPHIES

Eray Abakay (32)

Eray Abakay has been working as a research assistant at Sakarya University since 2012. He graduated from Yıldız Technical University Metallurgical and Materials Engineering department in 2010 and Sakarya University in 2013 with his master's degree in "Nb-Al-N Coating of Steel Surfaces by Thermo Reactive Deposition Method". There are many articles available in hardfacing and thermo reactive deposition. He is currently working on PH.D. thesis titled "Electrodeposition of nickel boron coating of magnesium and its alloys".

Engin KOCAMAN (29)

Engin Kocaman was born on April 17 1989 - Akşehir. He graduated from his bachelor degree at Sakarya University Metallurgical and Materials Engineering department in 2013 and his master's degree at same university in 2017. He is currently working on PH.D. thesis titled "Development of Fe-M-Cr-B (M=Ti, Mo) based In-Situ Composite Hard Surface Alloying Coated Electrodes". He has been working as a research assistant at Bulent Ecevit University since 2016. His research interests are casting of aluminum, hard-facing coatings, solidification and nickel based single crystal super-alloys.

Mustafa Durmaz (29)

The author was born in 1989 in Samsun. He completed BSc in 2011, MSc in 2015 and he started to study PhD in 2016 in the department of Metallurgy and Materials Engineering at the University of Sakarya. Mustafa Durmaz is research assistant at the Sakarya University since 2013. His research interests lie in the area of mechanical alloying, thermochemical coating process and tribology, and he published several papers on these topics.

Bülent Kılınç (39)

Bülent KILINÇ, He completed BSc in 2003, MSc in 2010 in the Department of Technical Education at the University of Sakarya. Bülent KILINÇ has completed his PhD in Metallurgy and Materials Science Department of the Science Institute of Sakarya University In 2018. Bülent Kılınç is a lecturer in Department of Welding Technology at Vocational School at the University of Sakarya since 2012. His research interests Thermo-chemical coating, melting Based Coatings, Corrosion and tribology, and he published several papers on these topics.

Şaduman Şen (49)

Şaduman Şen has entered in 1987 to the Metallurgical Engineering Department of Sakarya Engineering Faculty of Istanbul Technical University. She graduated at the Institute of Materials Science department of Science Institute at 1994 and completed her master's degree. Şaduman Şen has completed his PhD in Metallurgy and Materials Science Department of the Science Institute of Sakarya University In 1998. She has worked as an Assistant Professor and Associate Professor in the Department of Metal Education Department of Faculty of Technical Education

of Sakarya University. She has been working as a professor at the Department of Metallurgy and Materials Engineering of Engineering Faculty of Sakarya University. The Author has been studied on hard coatings, especially nitride, carbide and boride base coatings, thermochemical coatings, corrosion, Tribology and powder metallurgy subjects. She has been managing masters and doctoral theses and scientific projects. There are also a number of international and national articles and papers on these issues of the Author.

UğurŞen (52)

Uğur ŞEN, has entered in 1984 to the Metallurgical Engineering Department of Sakarya Engineering Faculty of İstanbul Technical University. He graduated at the Institute of Materials Science department of Science Institute at 1993 and completed his master's degree. Uğur ŞEN has completed his PhD in Materials Science Department of the Science Institute of İstanbul Technical University at 1998. He has worked as an Assistant Professor in the Department of Metal Education Department of Faculty of Technical Education of Sakarya University. He has worked as an Associate Professor at the Department of Metallurgy and Materials Engineering of Engineering Faculty of Sakarya University. Uğur ŞEN has been working as a professor at the Department of Metallurgy and Materials Engineering of Engineering Faculty of Sakarya University. The Author has been studied on hard coatings, thermo-chemical coatings, corrosion, tribology, powder metallurgy and electronic ceramics subjects. He has been managing masters and doctoral theses and scientific projects. There are also a number of international and national articles and papers on these issues of the Author.

INVESTIGATION OF EFFECT OF NICKEL INTERLAYER ON DIFFUSION IN WC-Co PART PRODUCED BY INSERTED POWDER INJECTION MOLDING

Mehmet SUBAŞI ^{1,a}, Harun KOÇAK ^{2,b}, Çetin KARATAŞ ^{3,c}

¹ Gazi University / Technical Sciences Vocational School

² Selcuk University / Cihanbeyli Vocational School

³ Gazi University / Faculty of Technology / Department of Manufacturing Engineering

^amsubasi@gazi.edu.tr, ^bharunkocak@selcuk.edu.tr, ^ccetink@gazi.edu.tr

Abstract

Inserted Powder Injection Molding (IPIM) is a method which developed to produce thicker parts than 10 mm. Feedstock is injected firstly onto prepared insert in the parts production process by this method. Afterwards, debinding and sintering processes are applied on parts. In this study, firstly inserts were prepared from HSS material. The prepared inserts were divided into two groups with interlayer and without interlayer. Nickel (Ni) layer was formed on inserts in interlayer group with a thickness of 40 µm (± 3 µm). Then WC-Co (9%) feedstock was injected onto all the inserts. After injection process, the samples were subjected to debinding processing. In the study, sintering experiments were performed at 1200 °C and 1250 °C and 240 minutes. After the sintering processing, shear test was performed on the intermediate zone of the samples, and the influence of the Ni intermediate layer on the intermediate zone strength was examined. Joining could not be obtained between materials in specimens that directly produced from WC-Co / HSS materials without Ni interlayer. In the samples sintered at 1250 °C, the WC-Co and Ni interlayer were separated from each other. There was complete joining in the samples with interlayer sintered at 1200 °C. A shear strength of 56.8 N / mm² was achieved in the shear test for these samples.

Key Words: Inserted Powder Injection Molding, WC-Co, Nickel, Sintering

1. Introduction

Tungsten carbide (WC), is known as an expensive hard metal and very hard to be machined due to its high hardness. For this reason, most of the WC parts are produced by powder metallurgy (PM) processes such as powder compaction or powder injection moulding [1]. However the restrictions in the process ability of powder metallurgy cause handicaps to the production of WC parts. Because of these restrictions in PM, an inserted powder injection moulding method has been developed for the production of parts thicker than 10mm [2].

By employing this powder injection moulding method both the production of parts thicker than 10mm and parts having different interior and exterior mechanical characteristics can be made. In this method, first of all inserts are prepared then feeding stock is injected upon them. Afterwards binder removal and sintering processes are applied to the parts.

In the Inserted Powder Injection moulding, obtaining of the desired mechanical characteristics depends on the diffusion between the insert and the part body. All of the materials having suitable chemical and metallurgical properties can be joined by diffusion. So, a number of studies were made on joining by diffusion welding [3-5]. Especially the studies for joining solid phase diffusion welding of tungsten (W) materials show that nickel decreases the thermal stress level causing to be used as interlayer, [6].

In this study first of all, inserts from HSS (M2) material were prepared by turning. On these inserts 40 μm Ni interlayer was formed. On the HSS inserts with Nickel interlayer and without interlayer, WC-Co (9%) feeding stock was injected. The parts removed from the mould were subjected to chemical binding removal and sintering processes. Sintering tests were carried out at 1200 °C and 1250 °C for 240 min. After sintering, all of the parts were subjected to cutting strength test and the effect of sintering temperature and interlayer on the cutting strength was determined.

2. Material and Method

M2 type HSS (1.3343) insert, WC-Co (9%) feeding stock and Ni interlayer were used in the interior part of the samples, in the outer part and for joining respectively. Feeding stock was purchased from Ryer company. Chemical composition of HSS material is given in Table 1, thermal characteristics in Table 2 and chemical composition of WC feeding stock is in Table 3.

Table 1. Chemical composition of M2 HSS material (%)

C	Si	Mn	Cr	Mo	Ni	V	W	Co
0.9	0.25	0.3	4.10	5.0	0	1.8	6.40	0

Table 2. Thermal characteristics of M2 HSS material

Thermal conductivity (20 °C)	Specific heat (20 °C)	Austenite temperature	Thermal expansion (100-700 °C)
19 W/(m.K)	460 J/(kg.K)	1210 °C	11.5-12.9 $10^{-6}\text{m}/(\text{m.K})$

Table 3. Chemical composition of WC-Co (9%) feeding stock (%)

Elements	C	Cr	Fe	Mo	Ni	Co	O	W
Mass	5.54	0.01	0.01	0.01	0.01	8.94	0.05	bal.

2.1. Preparation of inserts and application of interlayers

In the study first of all, inserts of 6.40 mm diameter were prepared from HSS material. On these inserts a 40 μm Ni interlayer with ($\pm 0,3 \mu\text{m}$) tolerance was formed by electrolytic coating method. At the stage of obtaining interlayer the nickel coating bath supplied from Technical Casting company was used. The conditions of obtaining interlayers are given in Table 4. The thickness of the obtained interlayer was determined by measuring from the diameter surface with X-Ray measuring device.

Table 4. Electrolytic Ni coating conditions

Anode	Bath temperature	Voltage	Current density	Waiting time
Electrolytic Nickel	50-60 °C	2.5-3 V 129	4A/dm ²	1 μm for 2 min.

2.2. Inserted powder injection moulding

Injection process was made at the ARBURG Allrounder 220S injection moulding board. The inserts prepared from M2 HSS steel were placed into the mould and WC-Co feedstock was injected on it (Fig. 1). Considering the values advised by the feeding stock company, optimum injection parameters were determined. Parameters used in the injection process are given in Table.5.

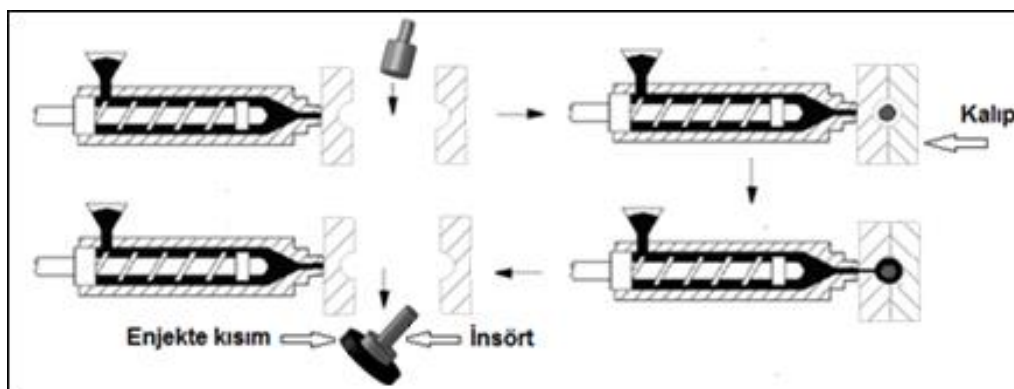


Figure 1. Inserted powder injection moulding process

Table 5. Injection parameters

Injection temperature	Injection pressure	Holding pressure	Injection speed	Mold temperature
200 °C	280 bar	80 bar	10 cm ³ s ⁻¹	60 °C

2.3. Binding removal and sintering processes

Following the injection process test samples were subjected to chemical binding removal treatment in ethanol at 60 °C for 48 hours. After the chemical binding removal treatment, test samples were sintered under control atmosphere (95% N₂ and 5% H₂) at 1200 °C and 1250 °C for 240 min by considering the thermal characteristics of WC-Co (9%) and HSS materials.

2.4. Mechanical Tests

Cutting test is a widely used method to evaluate the strengths and powers between parts consisted of different material [7, 8]. In this study cutting mould method was used for the analysis of joining of the insert and the main material. Three specimens from each sample were prepared and subjected to cutting test.

3. Results and Discussion

In the study, firstly samples from HSS insert and WC-Co feedstock with no interlayer were sintered at 1200 °C and 1250 °C for 240 min. When the samples were examined after sintering it was seen that there was no joining between HSS insert and injected area and there was a gap in the intermediate zone (Fig 2). Furthermore, after sintering the insert moved into the injected part

easily and could be taken out. Test was repeated by sintering three sample under the same conditions but again the same results were obtained.



Figure 2. Sintered sample (with no interlayer) at 1200 °C for 240 min

In the second stage of the study a 40 µm Ni interlayer was formed on the inserts. Then the inserted samples were sintered at 1200 °C and 1250 °C for 240 min. On the 40 µm Nickel interlayered samples sintered at 1250 °C, WC-Co and Ni interlayers separated from each other (Fig 3).

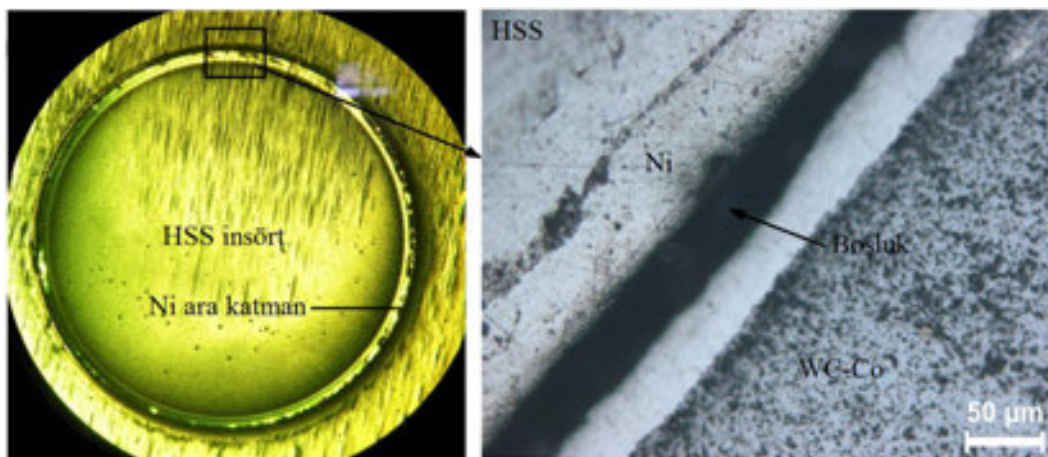


Figure 3. Intermediate zone of the sample produced by using 40 µm Ni interlayer (1250 °C 240 min.)

As a result of sintering in the 40 µm Nickel interlayered test specimens at 1200 °C a voidless structure was obtained. In order to have a better examination of the area between the feeding stock and insert, SEM images of the joining area were taken (Fig 4). From the SEM images it was observed that an ideal joining was constituted between the 40 µm thick Ni interlayer with HSS insert and WC-Co.

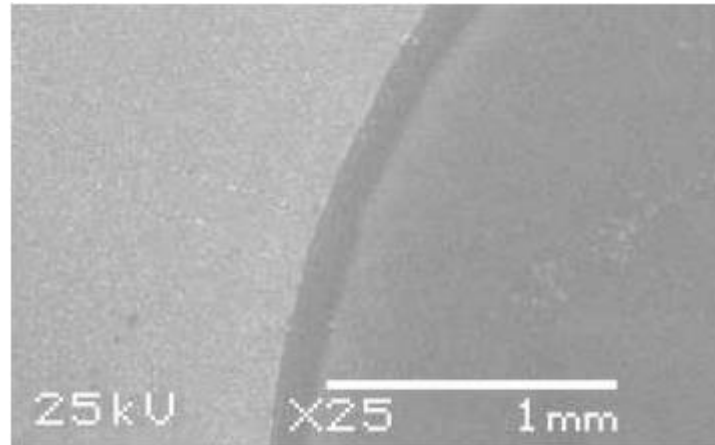


Figure 4. Intermediate zone of the sample produced by using 40µm Ni interlayer (1200 °C 240 min.)

On the 40 µm Nickel interlayered samples, cutting tests were made after obtaining a voidless joining. As a result of the cutting tests made for measuring the strength at the intermediate zone produced by using HSS insert and Ni interlayer, a 2.9kN compression force was determined in the samples Sintered at 1200 °C (Fig 5). By using the equations given below a cutting strength of 56.8 N/mm² was obtained in the samples sintered at 1200 C. In the calculation of the area in equation 1 insert diameter and injection thickness were taken as 6.5 mm and 2.5 mm respectively.

$$A = \pi \times D \times t \quad (1)$$

$$\tau = P/A \quad (2)$$

A = Cutting area (mm²), D = Insert diameter (mm), t = Injection thickness (mm), P = Force obtained from compression test (N), τ = Shear strength of intermediate zone (MPa)

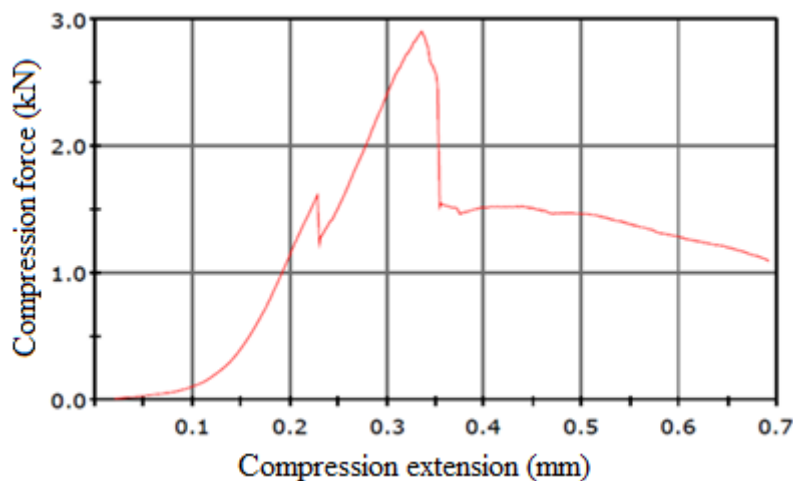


Figure 5. Compression force graph of the 50 µm Nickel interlayered sample

In the studies carried out in literature, it was deduced that nickel interlayer affected the power of diffusion bond positively [3, 9, 10]. Chen and colleagues in one of their studies determined that nickel interlayer strengthened the bond formation in joining the WC-Co cementite carbide and 3Cr13 stainless steel materials with diffusion¹³² welding [5]. In this study the target joining in the

samples with no nickel interlayer could not be obtained either. It was specified that sintering temperature in the interlayered samples was effective in the joining between the insert and body (feedstock). It was determined that at the specified optimum sintering temperature, parts with sufficient strength can be produced in the intermediate zone.

4. Conclusion

Part production was made from the WC-Co feedstock by Inserted Powder Injection Moulding method. In the parts without Nickel interlayer the target joining could not be obtained. At the end of the tests, while a 56,8 N/mm cutting strength was obtained on the 40mm Nickel interlayered samples, not a complete joining was observed on the sintered samples at 1250 C. As a result of the tests it was observed that nickel interlayer in the insert was effective on joining. However, it was also determined that there has to be an ideal sintering temperature for the joining between the HSS insert and WC-Co material.

6. Acknowledgement

This research was sponsored by the Scientific and Technological Research Council of Turkey (TÜBİTAK), Project No: 115M437. The authors would like to express their sincere appreciation to TÜBİTAK organization and Gazi University for their financial supports.

7. References

1. S.Y. Heng, M. Norhamidi, S. Abu Bakar, F. Abdolali, M. Amin, S.Yulis: Effect of sintering temperature on the mechanical and physical properties of WC–10%Co through micro-powder injection molding (μ PIM), *Ceramics International*, 39(4), (2013), pp. 4457-4464.
2. A. Safarian, M. Subaşı, Ç. Karataş: The effect of sintering parameters on diffusion bonding of 316L stainless steel in inserted metal injection molding, *The International Journal of Advanced Manufacturing Technology*, 89(5), (2017), pp. 2165-2173.
3. J. Zhang, L. Guoqiang, W. Yiyu, S. Qiang, Z. Lianmeng: An investigation on diffusion bonding of aluminum and magnesium using a Ni interlayer, *Materials Letters*, 83, (2012), pp. 189-191.
4. S. Zakipour, M. Samavatian, A. Halvae, A. Amadeh, A. Khodabandeh: The effect of interlayer thickness on liquid state diffusion bonding behavior of dissimilar stainless steel 316/Ti-6Al-4V system, *Materials Letters*, 142, (2015), pp. 168-171.
5. H. Chen, F. Keqin, W. Shifeng, X. Ji, G. Zhixing, W. Hui: Microstructure and properties of WC–Co/3Cr13 joints brazed using Ni electroplated interlayer, *International Journal of Refractory Metals and Hard Materials*, 33, (2012), pp. 70-74.
6. Q. Cai, L. Wensheng, M. Yunzhu, W. Zixuan: Diffusion brazing of tungsten and steel using Ti–Ni liquid phase forming interlayer, *Fusion Engineering and Design*, 91, (2015), pp. 67-72.
7. A. Safarian, Ç. Karataş: Diffusion Welding of Thick Components Fabricated by Inserted Powder Injection Molding, *Materials Testing*, 56(10), (2014), pp. 842-846.
8. A. Safarian, M. Subaşı, Ç. Karataş: Reducing debinding time in thick components fabricated by powder injection molding, *International Journal of Materials Research*, 106(5), (2015), pp. 527-531.

9. H. Chen, L. Chongsheng, W. Tianguo, G. Wen, X. Hongxing, C. Le: Effect of Ni interlayer on partial transient liquid phase bonding of Zr–Sn–Nb alloy and 304 stainless steel. *Materials & Design*, 60, (2014), pp. 358-362.
10. H. Sabetghadam, A. Z. Hanzaki, A. Araee: Diffusion bonding of 410 stainless steel to copper using a nickel interlayer, *Materials Characterization*, 61(6), (2010), pp. 626-634.

Correspondence address

Dr. Mehmet SUBAŞI

Technical Sciences Vocational School Gazi University Ankara TURKEY

Tel: +90 312 354 84 01

E-mail: msubasi@gazi.edu.tr

Dr. Mehmet SUBAŞI, was born in 1979. He completed his undergraduate studies in 2001, his master's degree in 2006 and his doctorate in Gazi University in 2015. He is still working as a lecturer at Gazi University Technical Sciences Vocational School. Academic studies have focused on plastic injection molding, powder injection molding and sheet metal molding techniques.

Dr. Harun KOÇAK, was born in 1985. He completed his undergraduate studies in 2007, his master's degree in 2011 and his doctorate in 2018 at Gazi University. Selçuk University is working as an Instructor at Cihanbeyli Vocational School. Academic studies are focused on machining techniques, powder injection molding and coating techniques.

Assoc. Dr. Çetin KARATAŞ was born in 1958. He completed his master's degree in 1992 and his doctorate in Gazi University in 1998. Despite the fact that manufacturing engineering works in different areas, concentrates on powder injection molding. He is a board member of Turkish Powder Metallurgy Association.

TİTANYUM LEVHALARINTİG KAYNAĞI İLE BİRLEŞTİRİLMESİNDE KAYNAK PARAMETRELERİNİN MEKANİK ÖZELLİK VE MİKROYAPIYA ETKİSİ

Sefa Enes Kılıç^{1a}, Murathan Kalender^{1b}, Yahya Bozkurt^{1c}, Serdar Salman^{2d}

¹Marmara Üniversitesi, Teknoloji Fakültesi, Metalurji ve Malzeme Mühendisliği Bölümü, Göztepe
Kampüsü, Kadıköy-İstanbul, Turkey

²Milli Savunma Üniversitesi Rektörlüğü, Milli Savunma Üniversitesi, Maslak-İstanbul, Türkiye

^asefaeneskili@outlook.com, ^bmurathankalender@hotmail.com, ^cybozkurt@marmara.edu.tr,
^dssalman@marmara.edu.tr

Özet

Titanyum ve alaşımlarının birçok alanda ileri teknoloji ürünü olarak kullanımı yaygındır. Metallerle göre kıyaslandığında; yüksek korozyon dayanımı, kolay işlenebilirlik sağlama ve mekanik özelliklerinin yüksek olması titanyumun başlıca tercih edilme sebeplerindedir. Malzemeyi korozyona karşı koruyan titanyum oksit tabakası kaynak işlemi sırasında yüksek ısı girdisinden dolayı kırılır. Titanyum levha atmosfere karşı korumasız hale gelir ve birleştirmenin mekanik özelliklerini düşürür. Ayrıca, yüksek sıcaklıkta çalışma dayanımı da titanyum levhalar için kaynak edilebilirliği kısıtlayan parametrelerdendir.

Bu çalışmada, titanyum ve alaşımlarının TIG kaynağı ile birleştirilmesinde koruyucu gaz, elektrot çeşidi, akım türü ve kaynak öncesi hazırlığın mekanik özellik ve mikroyapıya etkileri literatür kapsamında incelenmiştir.

Anahtar Kelimeler: Titanyum, TIG kaynağı, kaynak, mekanik özellik, mikroyapı, ileri teknoloji.

THE EFFECT OF WELDING PARAMETERS ON MECHANICAL PROPERTIES AND MICROSTRUCTURE OF TITANIUM SHEETS IN JOINING BY TIG WELDING

Abstract

Titanium and its alloys are widely used in many fields as high-tech products. When compared to metal; high corrosion resistance, easy workability and high mechanical properties are the main preferences of titanium. The titanium oxide layer, which protects the material against corrosion, is broken due to the high heat input during the welding process, rendering the material unprotective to the atmosphere, thereby reducing the mechanical properties of the assembly. In addition, working temperature at high temperature is also a parameter limiting weldability of titanium sheets.

In this study, the mechanical properties and microstructural effects of shielding gas, electrode type, current type and pre-welding preparation of titanium and its alloys with TIG welding were investigated within the scope of literature.

Key Words: Titanium, TIG welding, welding, mechanical properties, microstructure, advanced technology.

1.Giriş

Titanyum ve alaşımları endüstride yaygın olarak kullanılan en iyi mühendislik malzemelerinden birisidir [1-3]. Titanyum metalininmükemmel korozyon direnci, biyoyumluluk, iyi kaynaklanabilirlik ve yüksek dayanım sağlaması sayesinde uygulamada başlıca korozyon direnci ve özel dayanım istenilen yapılar için idealdir [1,3-8].Uçakmotor parçaları, deniz araçları, kondenser boruları, kimyasal işlem için reaktör gemileri ve güç üretim tesisinde kullanılır [1,5,8]. Titanyum, reaktif metaller olarak adlandırılan bir metal ailesine girer. Bu özelliğinden dolayı oksijen için güçlü bir çekim gücüne sahiptir. Titanyum ısıtıldığında ise oldukça reaktif hale gelerek oksitler oluşturmak için oksijen, azot, hidrojen ve karbon ile hızlıca tepkimeye girer. Oksit oluştuktan sonra titanyum sert ve kırılğan hale gelerek yüksek mekanik özelliklerini kaybeder. Titanyum levhanın oksit oluşturmaması için kaynak işlemi ve soğuma esnasında kaynak bölgesinin atmosferik gazlardan korunması gerekir. Literatür kapsamında titanyum ve alaşımları, genellikle lazer ışın kaynağı [9,10], elektron ışın kaynağı [11] ve TIG kaynağı ile birleştirildikleri görülmektedir [12]. Gazaltı kaynak yöntemleri kullanılarak yapılan kaynak işlemlerinde kaynak bölgesinin koruyucu gaz tarafından korunmasıyla titanyum malzemenin üzerinde oksit oluşması engellenir.

TIG kaynağı, ergimeyen tunsten bir elektrod ile iş parçası arasında meydana gelen ark ve kaynak bölgesinin de asal bir gaz (argon, helyum, argon-helyum karışımı) tarafından korunduğu bir gazaltı kaynak yöntemidir [13]. Bu kaynak yönteminde yüksek kalitede birleştirmeler elde etmek mümkündür [14]. TIG kaynağı en çok, titanyum, alüminyum, magnezyum, bakır, paslanmaz çelik gibi diğer ergitmeli kaynak yöntemleri ile kaynağı güç olan metallerin birleştirilmesinde kullanılır [15-17].

Son zamanlarda yapılan çalışmalarda, Durgutlu ve arkadaşları[18], Shi ve arkadaşları [19], Karpagaraj ve arkadaşları [20], Wang ve arkadaşları [21],kaynak parametrelerinin değiştirilerek kaynak yapılan titanyum levhanın mekanik özelliklerinin arttığına veya azaldığına, mikroyapının değişim gösterdiğine dair sonuçlarıbelirtmişlerdir.

Bu çalışmada, titanyum ve alaşımlarının TIG kaynağı ile birleştirilmesinde koruyucu gaz, elektrot çeşidi, akım türü, kaynak hızı ve kaynak öncesi hazırlığın mekanik özellik ve mikroyapıya etkileri literatür kapsamında değerlendirilmiştir.

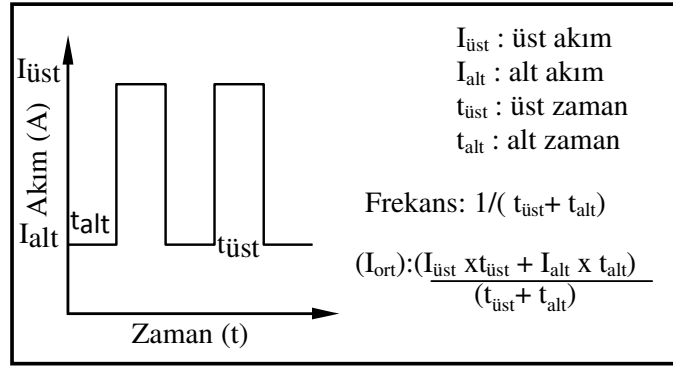
2. Kaynak Parametreleri

Anık, [22] kaynak işleminde ilk aranan şartın birleştirmenin mukavemetinin esas malzemeyle aynı veya ona yakın olması gerektiğini, farklı metallerin kaynağında ise kaynak metali mukavemetinin, mukavemeti düşük olan malzemedenden daha dayanıklı olması gerektiğini belirtmiştir.

Titanyum levhanın üzerinde bulunan koruyucu titanyum oksit tabakası, 535°C'nin altındaki sıcaklıklarda korozyona karşı mükemmel bir direnç sağlar. Ancak, 535°C'nin üzerindeki sıcaklıklarda bu tabaka kırılır ve malzemeyi atmosfere açık hale getirir [23]. Titanyum oksit tabakasının kırılması çeşitli kaynak yöntemlerinin kullanılmasını sınırlamakta ve mekanik özelliklerin düşmemesi için kaynak parametreleri önlemlerinin alınmasını gerektirmektedir[24,25].

2.1. Akım Türü

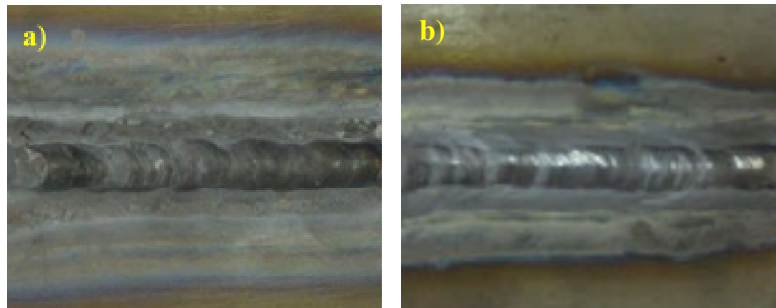
TIG kaynak yönteminde alternatif akım kullanılarak düşük ısı girdisiyle iyi kaynak dikişleri elde edilebilir. Son zamanlarda alternatif akım üreten makinaların geliştirilmesiyle beraber farklı malzemeler üzerinde alternatif akımın kaynak metali mikroyapısına olan etkileri de bir çok araştırmacı tarafından incelenmeye başlanmıştır [26-30]. Durgutlu ve arkadaşları tarafından yapılan çalışmada 1.5 mm kalınlığa sahip ticari saf (Grade 2) titanyum levhalar, TIG kaynak yöntemi ile farklı akım türleri kullanılarak (doğru akım ve alternatif akım) birleştirilmiştir. Alternatif akım formu Şekil 1'de, kaynak parametreleri ise Tablo 1'de gösterilmiştir [18]. Şekil 2' de Doğru ve alternatif akım ile yapılan birleştirmelerde ısı tesiri altında kalan bölgenin genişliği gösterilmektedir.



Şekil 1. Alternatif akım formu [18].

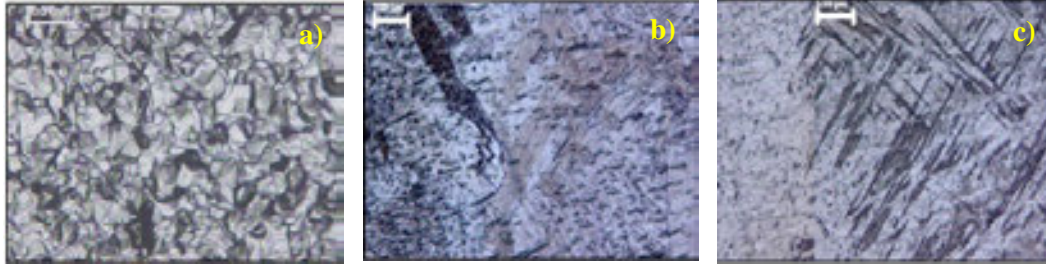
Tablo 1. Ticari saf (Grade 2) titanyum levhalar, TIG kaynak yöntemi ile farklı akım türlerine göre kaynak edilmelerinde kaynak parametreleri [18].

Kaynak Yöntemi	Doğru Akım	Alternatif Akım
Kaynak akımı (A)	70	Alt akım 40 Üst akım 80
Kaynak voltajı (V)	25	25
Kaynak hızı (mm/dk)	150	150
Gaz basıncı (lt/dk)	16	16
Darbe zamanı (%)	-	50
Darbe frekansı (Hz)	-	5
Isı girdisi (kJ/mm)	0,7	0,6



Şekil 2. Farklı akım türlerinde birleştirme işlemlerinde ısı tesiri altında kalan bölgenin genişliği; a) Doğru Akım, b) Alternatif Akım [18].

Kaynak numuneleri üzerinde yapılan gözle muayenesonucundaergiyik metal profillerinde ve krater oluşumlarında farklılıklar meydana geldiğini bildirmişlerdir. Doğru akımla birleştirilen numunede kaynak kraterinin daha geniş bir alanda oluşması ve yığılan kaynak metali yüksekliğinin azalması kaynakta istenmeyen bir durumdur. Kaynak esnasında alternatif akım kullanılarak elde edilen kaynak havuzu kontrolünün, doğru akıma göre daha rahat sağlandığını gözlemlenmiştir. Alternatif akımın kaynak numuneleri üzerinde etkisi oldukça önemlidir. Alternatif akım kullanılarak gerçekleştirilen birleştirmelerin kaynak metallere, yüksek akım (80 A) esnasında eriyen metal, düşük akım (40 A) esnasında katılaşmakta ve bu yüzden tane irileşmesi için yeterince süre bulunmamaktadır. Ayrıca düşük ısı girdisi sebebiyle, kaynak havuzu daha dar bir alanda oluşup kaynak metalinin katılaşma hızı artmaktadır. Bu nedenle, kaynak metalinde oluşan taneler doğru akıma göre daha ince yapılı bir şekilde oluşmaktadır (Şekil 3). TIG kaynağı ile birleştirilmiş numunelerin kaynak bölgesinin esas metalden daha sert olduğunu, farklı akım türleriyle yapılan kaynak işlemlerinin çekme deneyi sonucunda kopma ve kesit daralmasının ana metalde olduğunu, kaynaklı numunelerin esas metale göre tokluğunun az olduğunu ve mikroyapı incelemelerinde ısı girdisine bağlı olarak kaynak bölgesinde ikizlenme ve tane irileşmesi



olduğunu belirtmişlerdir [18].

Şekil 3. Farklı akım türlerinde yapılan kaynak işlemlerinde mikroyapı incelemesi; a) Titanyum levhanın ince eş eksenli α (alfa) tanelerinden oluşan mikroyapı görüntüsü, b) Doğru akım ile yapılan birleştirme işleminde esas metalden kaynak metaline geçişe ait mikroyapı görüntüsü, c) Alternatif akım ile yapılan birleştirme işleminde esas metalden kaynak metaline geçişe ait mikroyapı görüntüsü [18].

Doğru ve alternatif akım kullanılarak yapılmış TIG kaynaklı birleştirme numunelerine ait mikroyapı resimleri incelendiğinde kaynak metalinin mikroyapısının iğnemsiz α yapıya sahip olduğu görülmektedir. Durgutlu ve arkadaşları bu yapının kaynak işlemi sırasında α fazının β bölgesindeki yüksek sıcaklıktan hızlı soğuması sonucu oluştuğunu bildirmişlerdir. Doğru akım kullanılarak elde edilen numunelere ait mikroyapı resimlerini incelediklerinde tane boyutunun alternatif akımla birleştirilmiş numuneye göre daha büyük olduğunu bildirmişlerdir. Kaynak metalindeki iğnemsiz α tanelerinin esas malzemeye doğru yönlendiğini görmüşler ve bunun sebebinin soğuma yönü olduğunu bildirmişlerdir. Kaynak metalinden ısı tesiri altında kalan bölge (ITAB)'a geçişin keskin bir hat boyunca olmadığı, geçişin hemen hemen homojen bir yapıya sahip olduğu ayrıca yapıda siyah olarak görülen oksit tabakalarının yapı içerisinde kaldığı görülmektedir [18].

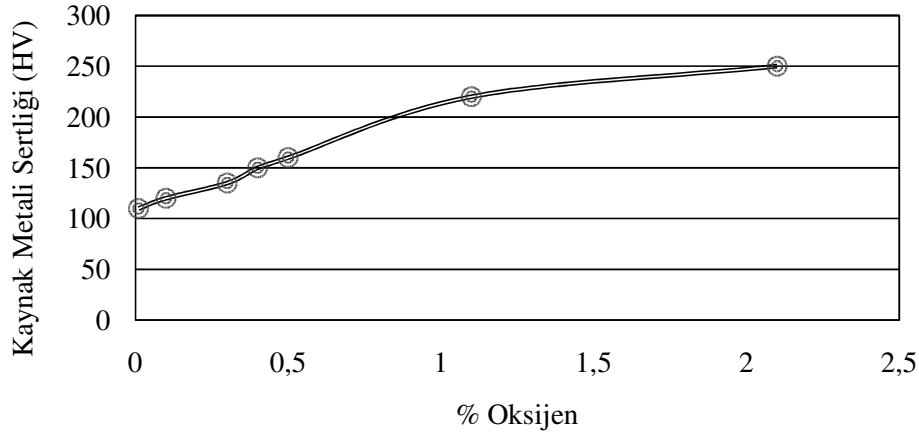
N. Kahraman, [31] saf titanyum metalin 600 ile 700 °C sıcaklıkta tavlınması ile mikroyapının ince eş eksenel α (alfa) taneciklerden oluşacağını bildirmiştir. Babu ve arkadaşları [32], Ti6Al4V levhaları TIG kaynak yöntemi ile alternatif ve doğru akım kullanarak birleştirmiş ve sonuçta normal akımda alternatif akıma göre daha büyük taneli yapı oluştuğunu belirtmişlerdir. Literatür kapsamında [30-34], farklı malzemeler üzerinde yapılan kaynak

işlemlerinde alternatif akım kullanılmasının kaynak metali tane yapısında incelmeye neden olduğu ve alternatif akım ile gerçekleştirilen kaynak dikişlerinde iri ve sütunsal tanelerin olduğu değerlendirilmiştir. Bunun sebebi, alternatif akım ile yapılan kaynak işlemlerinde ısı girdisinin yüksek oluşu, kaynak metali havuzunun geniş olması ve sonuç olarak katılaşmanın yavaş olmasındandır.

Doğan, [35] 3 mm kalınlığa sahip titanyum levha üzerinde TIG kaynağı ile birleştirme yaparak mikroyapı ve mekanik özellikleri incelemiştir. Düşük ısı girdisi ve soğutma hızı nedeniyle kaynak bölgesinin en sert olduğu değerleri düşük arka elde edilebileceğini ve yüksek mekanik özellikler elde etmek için ark aralığının orta seviyelerde olması gerektiğini belirtmiştir.

2.2. Koruyucu Gaz

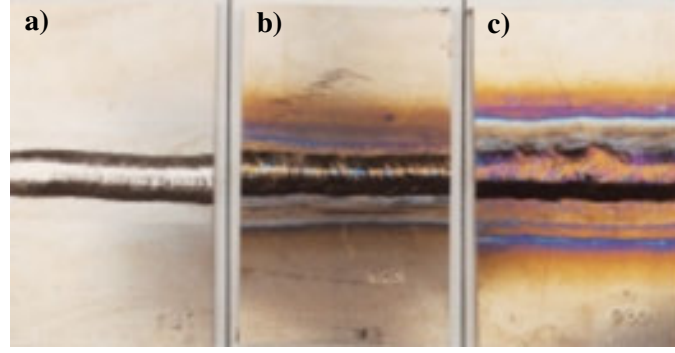
Titanyum ve alaşımlarının kaynağında genellikle koruyucu gaz olarak argon, helyum yada bu iki gazın birleşimi kullanılır. Argon ucuz, kolay bulunabilme, yaygınlığı ve özellikle daha az ısının gerektiği ve ısı girdisinde hissedilir değişme olmadan ark uzunluğunun değiştirilebileceği ince kesitlerde kullanılır. Helyum ise otomatik çalışmalarda kullanılır; helyum gazı ile yapılan çalışmalarda ark kontrolü kolaydır [36]. Titanyum, yüksek ısıya maruz kaldığında reaktif hale gelir ve oksitler oluşturmak için oksijen, azot, hidrojen ve karbon ile kolayca birleşir. Titanyum levha üzerinde oksitlerin meydana gelmesi kaynak işleminden sonra levhanın ve kaynak bölgesinin mekanik özelliklerini olumsuz yönde etkilemektedir. Kaynak işlemi sırasında oksijenin metale girerek oksit oluşturmasıyla kaynak metalinin sertliğini arttırdığı Şekil 4'de gösterilmiştir. Bu nedenle, birleştirme işlemi gerçekleştirildikten sonra ITAB'ın tamamının 343°C'nin altına düşene kadar dış atmosferden korunması gerekmektedir.



Şekil 4. TIG Kaynak işlemi sırasında oksijenin kaynak metaline girmesi sonucu kaynak bölgesinin sertliğini gösteren diyagram [24].

Shi ve arkadaşları titanyum levhaların TIG kaynağında kullanılan argon gazının içerisine belirli oranlarda karbondioksit karıştırarak mekanik özellik ve mikroyapıya etkisini incelemiştir. Uygun (%0 ile %3) oranlarda karbondioksit ilavesinin mikroyapı ve mekanik özelliği etkilemediğini ancak ITAB'ın genişlediğini belirtmişlerdir [19].

Literatür kapsamında yapılan çalışmalar incelendiğinde koruyucu gazın kaynak bölgesine etkisi kaynak işleminden sonra doğrudan gözle muayene işleminde tespit edilebilmektedir. Kaynak işleminden sonra kaynak dikişindeki ve levhadaki renkler incelenerek kaynak işleminin mekanik özellikleri hakkında yorumlar yapılabileceği görülmüştür. Şekil 5'de koruyucu gazın kaynak bölgesine etkileri, kaynak işleminden sonra levhayı nasıl etkilediği ve koruyucu gazdan kaynaklanan renk değişimi görülmektedir. Şekil 5. a)'da koruyucu gazın kaynak bölgesini, kaynak işlemi sırasında ve kaynak işleminden sonra atmosferik gazlardan koruduğu görülmekte ve kaynak bölgesinin rengi gümüş olduğundan dolayı kaynak işleminin gözle muayene işleminde başarılı olduğu söylenebilmektedir. Şekil 5. b)'de koruyucu gazın hem kaynak bölgesini hem de kaynak metalini yeterli seviyede koruyamadığı ve kaynak işleminin kısmen başarısız olduğunu göstermektedir. Şekil 5. c)'de kaynak işleminin koruyucu gaz ulaşmadan veya koruyucu gazın yetersiz olduğu durumda kaynak işlemi yapıldığı görülmektedir [37].



Şekil 5. Koruyucu gazın kaynak bölgesine etkisi a) Koruyucu gaz ile korunan kaynak bölgesi ve kaynak metalini b) Kısmi korunan kaynak bölgesi ve kaynak metalini, c) Koruyucu gazın yetersiz veya hiç olmadığı kaynak işlemi[37].

2.3 İlave Metal ve Elektrot

TIG kaynak işlemi ile birleştirme gerçekleştirilirken levha ve kaynak bölgesinin mekanik özelliklerinin olumsuz etkilenmemesi için kaynak yapılan titanyum levhaya kimyasal bileşim olarak en yakın olan ilave metal seçilmelidir [21]. Tablo 2'de titanyum ve alaşımlarının TIG kaynağı ile birleştirilmesinde kullanılması gereken ilave metaller gösterilmiştir.

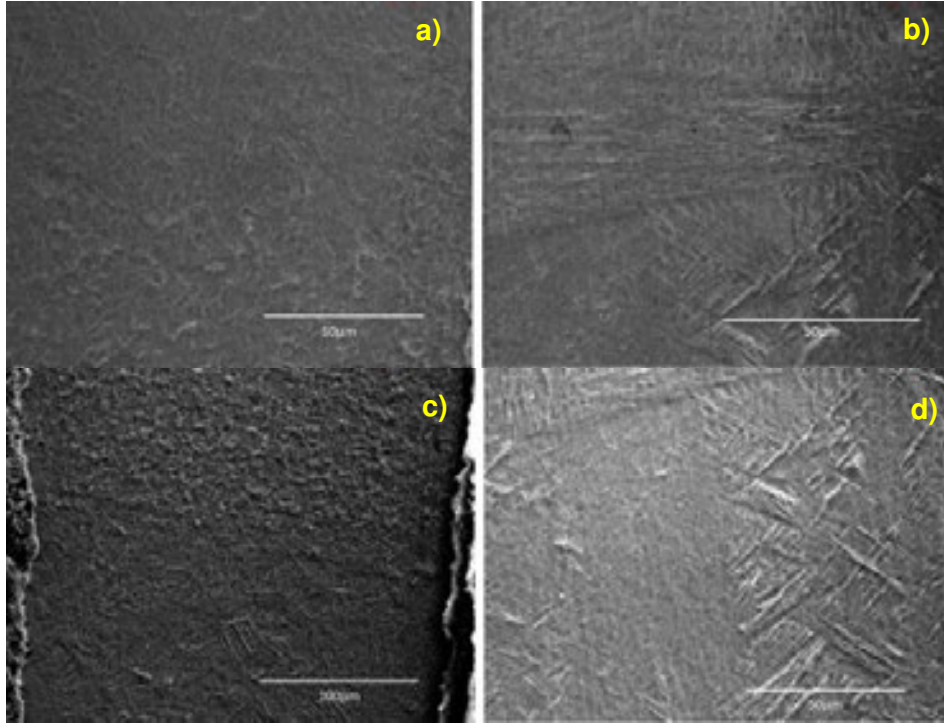
Tablo 2. Titanyum malzeme türüne göre önerilen ilave metal [21].

Titanyum Çeşitleri	AWS A5.16 ERTi-2	AWS A5.16 ERTi-2	AWS A5.18 ERTi-3	AWS A5.16 ERTi-5	AWS A5.16 ERTi-9 ve ERTi-9ELI	AWS A5.18 ERTi-23
Grade 1 (CP-1, ticari açıdan saf)	X					
Grade 2 (CP-2)	X	X				
Grade 3 (CP-3)			X		X	
Grade 9 (Ti-3Al-2.5V)						
Grade 5 (Ti-6Al-4V)				X		X
Grade 23 (Ti-6Al-4V ELI (ekstra düşük						X

yoğunluk)						
-----------	--	--	--	--	--	--

Wang ve arkadaşları, TIG kaynağı ile birleştirilen çeşitli metallerin kaynağı sırasında kullanılan ilave metallere çeşitli kaplamalar yaparak mikroyapı özelliklerinin değiştirildiğini incelemişlerdir. İlave metale kaplanan alaşımların kaynak bölgesinde farklı fazlar oluşturduğunu bildirmişlerdir [38].

Can'ın [39] yaptığı çalışma sonucunda kaynak bölgesine ait Şekil 6'da görülen mikroyapı resimleri incelendiğinde esas metalin ince eş eksenli α (alfa) tanelerinden oluştuğu ve ayrıca dönüşmüş β fazından (iğnemsiz α) oluştuğu görülmektedir. Şekil 6 c ve d mikroyapı görüntüleri incelendiğinde kaynak bölgesinin iğnemsiz α yapıya sahip olduğu görülmektedir. Bu yapının kaynak işlemi sırasında α fazının β bölgesindeki yüksek sıcaklıktan hızlı soğuması sonucu oluştuğu bilinmektedir. Kaynak metalinden ITAB'a geçişin keskin bir hat boyunca olmadığı, geçişin hemen hemen homojen bir yapıya sahip olduğu görülmektedir.



Şekil 6. Titanyum levhaya ait mikroyapı görüntüleri a) Ana metal, b) Kaynak geçiş bölgesi, c ve d) Kaynak bölgesi

3. Sonuçlar

Literatür kapsamında yapılan çalışmalar incelendiğinde kaynak parametrelerinin hem esas metali hem de kaynak bölgesini doğrudan etkilediği araştırmacılar tarafından belirtilmiştir. Farklı akım çeşitleri kullanılarak yapılan TIG kaynak işlemlerinde ise girdisine bağlı olarak farklı mikroyapılar oluşmuş ve mekanik özelliklerin akım türü ile değiştiği değerlendirilmiştir. Alternatif akım kullanılarak yapılan titanyum levhaların TIG kaynak işlemlerinde mekanik özelliklerin iyileştiği görülmüştür. TIG kaynak işleminde kullanılacak olan inert gazın safsızlığı kaynak havuzunu ve esas metali doğrudan etkilemiştir. Kaynak işlemi sırasında ve kaynak işleminden sonra esas metal ve kaynak bölgesinin soğuyana kadar

koruyucu gaz ile korunması mekanik özellikleri ve mikroyapıyı olumlu yönde etkilemiştir. Esas metalin kimyasal bileşimine yakın olan ilave metal ve esas metale uygun olarak kullanılan elektrodun kaynak bölgesinin mekanik özelliklerini ve mikroyapısını doğrudan etkilemiştir. İlave metalin kimyasal bileşimi esas metalin kimyasal bileşimine ne kadar yakın olursa mekanik özellikler de o kadar arttığı belirtilmiştir.

KAYNAKLAR

- [1] N. Kahraman: The influence of welding parameters on the joint strength of resistance spot-welded titanium sheets, *Mater. Design.* (2007) 28, 2, 420-427.
- [2] E. Atasoy, N. Kahraman: Diffusion bonding of commercially pure titanium to low carbon steel using a silver interlayer, *Mater. Charact.* (2008) 59, 10, 1481-1490.
- [3] N. Kahraman, B. Gülenç, F. Fındık: Corrosion and mechanical-microstructural aspects of dissimilar joints of Ti6Al4V and Al plates, *Int. J. Impact Eng.* 34, 8, 1423- 1432, 2007.
- [4] J. Oh, N.J. Kim, S. Lee, E.W. Lee: Correlation of fatigue properties and microstructure in investment cast Ti-6Al-4V welds, *Mat. Sci. Eng.* (2003) A. 340, 1-2, 232-242.
- [5] N. Kahraman: Titanyum levhaların patlamalı kaynak yöntemi ile farklı metallerle birleştirilmesi ve arayüzey özelliklerinin incelenmesi, Doktora Tezi, (2003) Gazi Üniversitesi Fen Bilimleri Enstitüsü, Ankara, Turkey.
- [6] W.A. Davis, J.R. Cross: C.E. ASM Handbook, Vol. 6, (1993) Metals Park, OH, USA.
- [7] W.A. Gerken, J.M. Cross, C. Hanson, J.Liu, P.S. Monson, J.C. Schley, J. Showalter: *Welding Handbook*, Vol. 4, American Welding Society, (1998) Miami, Florida, USA.
- [8] S. Lathabai, B.L. Jarvis, K.J. Barton: Comparison of keyhole and conventional gas tungsten arc welds in commercially pure titanium, *Mat. Sci. Eng. A.* (2001) 299, 1-2, 81-93.
- [9] Z. S. Annergren, I. Pan, D. Mai: Effect of Laser surface remelting on the corrosion behavior of commercially pure titanium sheet, *Mat. Sci. Eng. A.* (2003) 345, 1-2, 293-300.
- [10] S.H. Wang, M.D. Wei, L.W. Tsay: Tensile properties of LBW welds in Ti-6Al-4V alloy at evaluated temperatures below 450°C, *Mater. Lett.* (2003) 57, 12, 1815- 1823.
- [11] N. Suresh, G. Pillai, M. Mathew: Investigations into the effects of electron beam welding on thick Ti-6Al-4V titanium alloy, *J. Mater. Process. Tech.* (2007) 192-193, 83-88
- [12] S. Lathabai, B.L. Jarvis, K.J. Barton: Comparison of keyhole and conventional gas tungsten arc welds in commercially pure titanium, *Mat. Sci. Eng. A.* (2001) 299, 1-2, 81-93.
- [13] G.A. Kennedy: *Welding Technology*, A Division of Macmillan Publishing Company, 2. Edition, Mission Hills, California, (1982) 282-286.
- [14] C. S. Wu, M. Ushio, M. Tanaka: Analysis of the TIG welding arc behavior, *Computational Materials Science*, Cilt 7, No 3, (1997) 308-314.
- [15] R. J. Sacks: *Essentials of Welding*, Glencoe Publishing Company, (1984) 389-391.
- [16] G.K. Hicken: Gas-tungsten arc welding, Vol. 6. ASM Handbook, (1993) 190-193.
- [17] A. D. Althouse, C.H. Turnquist, W.A. Bowditch, K.E. Bowditch: Gas tungsten arc welding, *Modern Welding*, The Goodheart-Wilcox Company Inc, (1992) 327-328.
- [18] A. Durgutlu, Y. Kaya, N. Kahraman, B. Gülenç: Titanyum Levhaların TIG Kaynağı ile Birleştirilmesinde Akım Türünün Mikroyapı ve Mekanik Özellikler Üzerine Etkisi, 6 th International Advanced Technologies Symposium (IATS'11), (2011) Elazığ, Turkey.

- [19] Shi J., Song G., Chi J: Effect Of Active Gas On Weld Appearance And Performance İn Laser-TIG Hybrid Welded Titanium Alloy, *International Journal of Lightweight Materials and Manufacture* 1 (2018) 47-53.
- [20] Karpagaraj A., Sivashanmugam N., Sankaranarayanan K: Some Studies On Mechanical Properties And Microstructural Characterization Of Automated TIG Welding Of Thin Commercially Pure Titanium Sheets”, *Materials Science & Engineering A* 640 (2015) 180-189.
- [21] B. Wang, S. Xue, C. Ma, Y. Han, Z. Lin: Effect of combinative addition of Ti and Sr on modification of AA4043 welding wire and mechanical properties of AA6082 welded by TIG welding, *Trans. Nonferrous Met. Soc. China* 27(2017) 272-281.
- [22] S. Anık: Farklı metallerin Kaynağı, *Gedik Kaynak Dünyası*, (1988) İstanbul, Turkey 4-8.
- [23] D. R. Askeland: *The science and engineering of materials*, Vol. 1, Nobel Yayın Dağıtım, (1998) 194-288.
- [24] B. Oğuz: *Titanyum ve Alaşımlarının Kaynak Süreçleri*, Demir Dışı Metallerin Kaynağı, Oerlikon Yayını.
- [25] S. Y. Şirin, N. Y. Sarı, E. Kaluç: *Titanyum ve alaşımlarının kaynağı 1*, Makine Magazin, (1997) 19, 62-70.
- [26] A. Traidia, F. Roger, A. Guyot: Optimal parameters for pulsed gas tungsten arc welding in partially and fully penetrated weld pools, *International Journal of Thermal Sciences*, (2010) 49, 7, 1197-1208.
- [27] M. Balasubramanian, V. Jayabalan, V. Balasubramanian: Effect of microstructure on impact toughness of pulsed current GTA welded α - β titanium alloy, *Materials Letters*, (2008) 62, 6-7, 1102-1106.
- [28] M. Balasubramanian, V. Jayabalan, V. Balasubramanian: Developing mathematical models to predict tensile properties of pulsed current gas tungsten arc welded Ti-6Al-4V alloy, *Materials & Design*, (2008) 29, 1, 92-97.
- [29] M. Balasubramanian, V. Jayabalan, V. Balasubramanian: Effect of pulsed gas tungsten arc welding on corrosion behavior of Ti-6Al-4V titanium alloy, *Materials & Design*, (2008) 29, 7, 1359-1363.
- [30] V. Balasubramanian, V. Jayabalan, M. Balasubramanian: Effect of current pulsing on tensile properties of titanium alloy, *Materials & Design*, (2008) 29, 7, 1459-1466.
- [31] N. Kahraman: *Titanyum levhaların patlamalı kaynak yöntemi ile farklı metallerle birleştirilmesi ve arayüzey özelliklerinin incelenmesi*, Doktora Tezi, Gazi Üniversitesi Fen Bilimleri Enstitüsü, (2003) Ankara.
- [32] N. K. Babu, S. G. S. Raman, R. Mythili, S. Saroja: Correlation of microstructure with mechanical properties of TIG weldments of Ti-6Al-4V made with and without current pulsing, *Materials Characterization*, (2007) 58, 7, 581-587.
- [33] A. Durgutlu, N. Kahraman, B. Gülenç: Al-Si alaşımlarının TIG kaynağında darbeli akımın mikroyapı, sertlik, eğme ve çekme dayanımına etkisi, *G.Ü.T.E.F. Politeknik Dergisi*, (2008) 11, 4, 339-344.
- [34] A. Durgutlu, T. Fındık, U. Arabacı, B. Gülenç: Östenitik paslanmaz çeliğin TIG kaynağında akım türünün kaynak metali mikroyapısı ve sertlik değerine etkisi, *I. Uluslararası Kaynak Teknolojileri Konferansı*, Gazi Üniversitesi, (2009) Ankara, 591-597.
- [35] U. Doğan: *The Effect of TIG Welding On Microstructure And Mechanical Properties Of A Butt-Joined-Unalloyed Titanium*, (2005) *Metabh* 44 (2) 119-123.
- [36] B. Oğuz: *Titanyum Ve Alaşımlarının Kaynak Süreçleri* Demir Dışı Metallerin Kaynağı, Oerlikon Yayını.
- [37] <http://www.kobelco.co.jp/english/titan/files/details.pdf>

- [38] B.Wang, S. Xue, C. Ma, Y. Han, Z. Lin: Effect of combinative addition of Ti and Sr on modification of AA4043 welding wire and mechanical properties of AA6082 welded by TIG welding, Trans. Nonferrous Met. Soc. China 27(2017) 272–281.
- [39] G. Can: Titanyum Alaşımı Borular için Orbital Tungsten Asal Gaz (TIG) Kaynak Proses Parametrelerin Elde Edilmesi, Roketsan A.Ş. Özel Üretim Ve Test Teknolojileri Birimi, Elmadağ, Ankara.

SORUMLU YAZAR: Yahya Bozkurt, Marmara Üniversitesi, Teknoloji Fakültesi, Metalurji ve Malzeme Mühendisliği Bölümü, Göztepe Kampüsü, Kadıköy/İSTANBUL, +90 216 336 57 70, ybozkurt@marmara.edu.tr.

KISA ÖZGEÇMİŞLER

Sefa Enes Kılıç – 1997 yılında Aksaray’da doğdu. 2015 yılında Aksaray Teknik Lisesi’nden mezun oldu. Halen Marmara Üniversitesi Teknoloji Fakültesi Metalurji ve Malzeme Mühendisliği bölümünde 3.sınıf lisans eğitimine devam etmektedir.

Murathan Kalender – 1996 yılında İstanbul’da doğdu. 2014 yılında İsmet Aktar Anadolu Teknik Lisesi’nden mezun oldu. Halen Marmara Üniversitesi Teknoloji Fakültesi Metalurji ve Malzeme Mühendisliği bölümünde 3.sınıf lisans eğitimine devam etmektedir.

Yahya Bozkurt – 1975 Antakya doğumludur. Marmara Üniversitesi Teknik Eğitim Fakültesi Metal Eğitimi Bölümü’nden 2000 yılında mezun oldu. 2000 yılı Aralık ayında Marmara Üniversitesi Teknik Eğitim Fakültesi Metal Eğitimi Bölümünde Araştırma Görevlisi oldu. Prof. Dr. Serdar Salman ve Doç. Dr. Hüseyin Uzun danışmanlığında 2003 yılında başladığı doktora eğitimini Eylül 2008’de tamamladı. 2009 yılında Yardımcı Doçent, 2012 yılında Doçent, 2018 yılında da Profesör oldu. Halen aynı üniversitede görevine devam etmektedir.

Serdar Salman – 1962 İstanbul doğumludur. 1979-1980 yılında Ege Üniversitesi’nde okudu. İstanbul Teknik Üniversitesi Sakarya Mühendislik Fakültesi Metalurji Mühendisliği Bölümü’nden 1984 yılında mezun oldu. 1985 yılında Marmara Üniversitesi Teknik Eğitim Fakültesi Metal Eğitimi Bölümünde Araştırma Görevlisi oldu. 1991 yılında 9 ay süreyle YÖK– Dünya Bankası II. Endüstriyel Eğitim Projesi kapsamında İngiltere’de (Huddersfield Üniversitesi) eğitim ve araştırma amacıyla bulundu. 1992 yılında Marmara Üniversitesi Teknik Eğitim Fakültesi Metal Eğitimi Bölümünde Öğretim Görevlisi oldu. 1995 yılında MÜTEF Malzeme Eğitimi Anabilim Dalı’na Yardımcı Doçent olarak atandı. Aynı Anabilim dalında 1997 yılında Doçent, 2003 yılında ise Profesör oldu. 27/01/2003 ile 27/01/2006 tarihleri arasında Marmara Üniversitesi’nde Teknik Eğitim Fakültesi Dekan Yardımcılığı, 2007 yılında (3 ay) Dekan Vekili olarak görev yapmıştır. 2007-2008 yılları arasında 1 yıl GATECH-Atlanta Amerika’da misafir profesör olarak bulunmuştur. 2012-2015 Yılları arasında Mehmet Akif Ersoy Üniversitesi, Mühendislik-Mimarlık Fakültesi’nde Kurucu Dekanlık yapmıştır. Halen Milli Savunma Üniversitesi’nde rektör yardımcısı olarak görev yapmaktadır.

FARKLI MALZEMELERİN SÜRTÜNME KARIŞTIRMA KAYNAĞINDA TAKIM GEOMETRİSİNİN MEKANİK ÖZELLİKLERE ETKİSİ

Murathan Kalender^{1a}, Sefa Enes Kılıç^{1b}, Yahya Bozkurt^{1c}, Serdar Salman^{2d}

¹Marmara Üniversitesi, Teknoloji Fakültesi, Metalurji ve Malzeme Mühendisliği Bölümü, Göztepe Kampüsü,
Kadıköy-İstanbul, Turkey

²Milli Savunma Üniversitesi Rektörlüğü, Milli Savunma Üniversitesi, Maslak-İstanbul, Türkiye

^amurathankalender@hotmail.com, ^bsefaeneskilig@outlook.com, ^cybozkurt@marmara.edu.tr,

^dssalman@marmara.edu.tr

Özet

Sürtünme karıştırma kaynağı alüminyum, bakır, titanyum gibi malzemelerin birleştirilmesinde kullanılan bir katı hal birleştirme yöntemidir. Farklı yapılarıdaki malzemelerin geleneksel ergitme kaynak yöntemleri ile birleştirilmesinde gözenek, sıcak çatlak, yüksek ısı girdisi nedeniyle çarpılma ve kimyasal element kaybı gibi problemler meydana gelmektedir. Bu durumları elimine eden ve istenilen kalitede malzemelerin birleştirilmesini sağlayan sürtünme karıştırma kaynağı ön plana çıkmaktadır. Bu kaynak yöntemi, katı fazda ve ergime sıcaklığının altında yapıldığından diğer kaynak yöntemlerindeki kusurları en aza indirmektedir. Takım malzemesi ve geometrisi, bu yöntem için en önemli parametreler olup çekme ve akma mukavemeti, sertlik ve korozyon direnci gibi mekanik özellikleri geliştirmektedir.

Bu çalışmada, sürtünme karıştırma kaynağında kullanılan takımın geometrisi, aşınması, kaynak parametrelerinin farklı malzemeler üzerindeki mekanik özelliklere ve mikroyapıya olan etkisi literatür kapsamında incelenmiştir.

Anahtar Kelimeler: Sürtünme Karıştırma Kaynağı, Takım Geometrisi, Takım Aşınması

THE EFFECT OF MECHANICAL PROPERTIES OF TOOL GEOMETRY IN FRICTION STIR WELDING OF DIFFERENT MATERIALS

Abstract

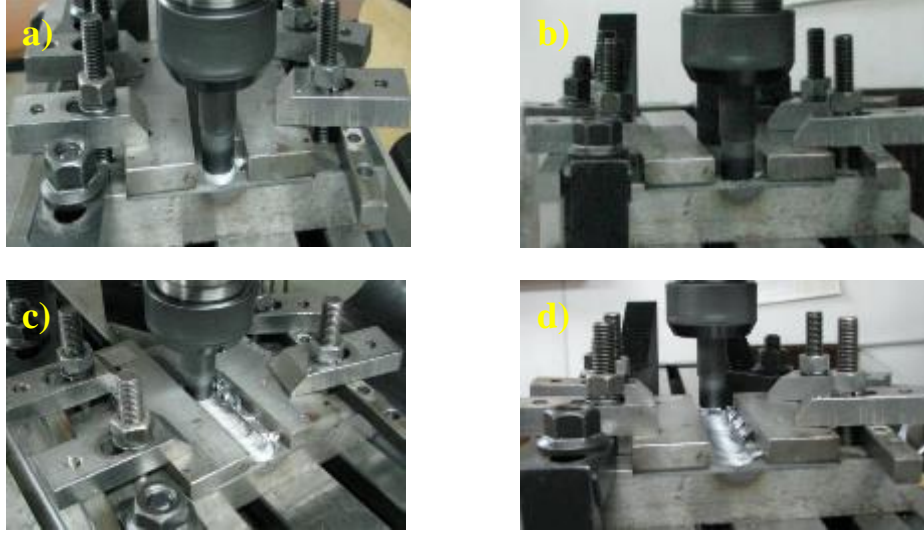
Friction stir welding is a solid state welding process which is used to join the soft materials like aluminium, copper, nickel, titanium etc. In joining of different structures materials with traditional fusion welding methods, problems occur such as pore, hot crack, high heat input, shock and chemical element loss. To eliminate this situation and join the desired quality of materials the friction stir welding is being used. This welding method minimizes defects in other welding methods due to being made at solid phase and below melting temperature. Tool material and its geometry are the most important parameters for this method and they develop mechanical properties such as tensile and yield strength, hardness and corrosion resistance.

In this study, the geometry and wear of welding tool and the effect of welding parameters on mechanical properties and microstructure for different materials used in friction stir welding were investigated with literature review.

Key Words: Friction Stir Welding, Tool Design, Tool Wear

1. Giriş

Son yıllarda, yeni ve gelişmiş yapılarıdaki malzemelerin kaynağı, endüstri için sorun teşkil etmektedir. Bu malzemelerin birleştirilmesinde kullanılan katı hal kaynak yöntemleri daha etkili olmuştur. Katı hal kaynak yöntemlerinden birisi de sürtünme karıştırma kaynağıdır [1]. Sürtünme Karıştırma Kaynağı (SKK), düşük maliyetli ve yüksek performans göstermesini isteyen bağlantılar için ideal bir yöntemdir. SKK prensibi, omuz ve uç dahil olmak üzere iki parçadan oluşan ergimeyen bir karıştırıcı yardımıyla takımın parça üzerinde ilerlemesidir. SKK, farklı hızlara sahip dönen omuz ve karıştırıcı uca sahip takımın iki levha arasına daldırılması ve birleştirme hattı boyunca hareket ettirilmesi ile gerçekleşir [2]. Şekil 1'de SKK işlem basamakları gösterilmektedir.



Şekil 1. SKK işlemi, a) SKK öncesi levha ile temas halindeki pim, b) Pimin temastan kaynaklanarak ısı oluşturması c) SKK işleminde plastik şekil değişimi d) SKK işleminin sona ermesi [2].

Takımın yüzeyi, yumuşayan metalden kaynaklı, ısı üretimi ve birleştirilen metalin ileri doğru mekanik hareketini sağlaması bakımından iki önemli etkiye sahiptir. Takım ile işlenecek parça arasındaki sürtünme hareketi yoluyla gelen ısı girişi, pim (karıştırıcı uç) etrafındaki bölgenin yumuşamasına sebep olur. Bu sırada, yumuşayan metal katı hal bağlantısı oluşturmak için ön bölgedeki ilerleyen taraftan arka bölgedeki geri çekilme tarafına şiddetli plastik deformasyona uğrayarak hareket ettirilir [3-6]. SKK'nın diğer geleneksel kaynak yöntemlerine göre avantajlarını metalurjik, çevresel ve enerji olmak üzere üç ana grupta inceleyebiliriz. SKK yöntemi katı fazla gerçekleştiğinden dolayı kaynak bölgesindeki malzemeye metalurjik olarak hasar vermez. İşlem sırasında sıcaklığın diğer kaynak yöntemlerine göre daha az olması, iş parçasındaki burulmaları en aza indirmektedir. Bu yöntem, iyi bir boyutsal kararlılık ve tekrar edilebilme özelliğine sahip olmasının yanı sıra alaşım elementleri üzerinde kayıplar oluşmaz. SKK sonrasında birleşim bölgesi küçük taneli mikroyapıya sahip olduğundan bu bölge mükemmel metalurjik özelliklere sahiptir. Isı girdisi nedeniyle iş parçasında çatlak oluşmaz. Çevresel ve enerji avantajlarına bakıldığında; gaz altı kaynaklarındaki gibi koruyucu gaza gerek yoktur. İşlem sonrasında yüzey temizliğine gerek kalmaz ve taşlama atıkları oluşmaz. SKK yöntemiyle gelişmiş malzemelerde birleştirme yapılırken bu malzemelerin hafif olmasında büyük rol alır. Hafif hava araçları, otomotiv ve gemi imalatında, yüksek hızlı ulaşım araçlarında bu yöntemden faydalanılır [7-9]. Metallerin SKK kaynağında işlem görürken hem parametrelerin hem de SKK için kullanılan takım ve bu takım alaşımının dikkatli tasarlanması gerekir. Bu parametrelerde önde gelen en önemli

problem yüksek sıcaklıklardır. SKK yöntemi bu sorunu ortadan kaldırarak homojen bir sıcaklık dağılımı sağlamaktadır. Takımın omuz ve karıştırıcı ucunun aşınması ve kırılması, takım malzemesinin seçimi için ciddi bir sınırlama getirmektedir. SKK sonucunda, takımlar işlem sırasında ulaşılan sıcaklıklarda yüksek mekanik dirence sahip olmalıdır. Bununla beraber aşınma ve oksitlenmeye karşı direnç sağlayabilmelidir. SKK işlemlerinde sıcaklığın tipik olarak işlenmiş malzeme için, erime sıcaklığının yaklaşık % 80' ine ulaştığı gözlemlenmiştir. Bununla birlikte, ana metalde oluşan sıcaklıkla birlikte takım içindeki sıcaklık önemli bir değişkendir [10].

Bu çalışmada, SKK' da kullanılan takımın geometrisi, aşınması, kaynak parametrelerinin farklı malzemeler üzerindeki mekanik özelliklere ve mikroyapıya olan etkisi literatür kapsamında incelenmiştir.

1. Sürtünme Karıştırma Kaynağı Tekniğinde Takım Geometrileri

2. Al Alaşımlarının SKK İşlemi

SKK yönteminde temel prensip, bir pimi ve omuz kısmı olan takımın birleştirilecek olan iki parçanın bitişik kenarlarına daldırılması ve hareket ettirilmesi ile gerçekleşen plastik deformasyon sonucu iki metalin katı halde birleştirilmesi işlemidir. SKK işleminde yüksek mukavemet elde etmek, esas olarak makine değişkenlerine ve takım tasarımına bağlıdır. Bunun yanında, SKK işleminde kullanılan levhaların bağlama biçimi ve kalıp tasarımı kaynak kalitesi için önemli parametrelerdir [11-14]. Takım geometrisi plastik şekil değişiminde gerçekleşen malzeme akışında ve dönme yönünde önemli bir rol oynamaktadır.

Elangovan ve Balasubramanian [15] AA-6061 ve AA-5086 alüminyum alaşımı üzerinde, düz silindirik, silindirik konik, dişli silindirik şekillerinde 18mm'lik omuz çaplarına sahip farklı takım pimi profili kullanarak 1100 dev/dak. takım dönmesi ve 22 mm/dak. takım ilerleme hızlarında SKK'lı birleştirme yapmışlardır. Kaynak bölgelerinin gerilme dayanımlarını, mikro sertliklerini ve mikroyapılarını incelemişlerdir. Bu araştırma, 1200 dev/dak'lık bir takım dönme hızı ile dişli silindirik pim profilli takım kullanılarak imal edilen kaynak bölgelerinin, diğer pimlere kıyasla üstün mekanik özellikler sergilediğini belirtmişlerdir. Dişli silindirik pim 169 MPa, düz silindirik pim ve konik silindirik pimlerin gerilmeleri sırasıyla 126 MPa ve 163 MPa olarak elde etmişlerdir. İncelemelerinde, dişli silindirik en az sayıda kusur ile üstün mekanik özellikler sağlamıştır.

Palanivel ve arkadaşları tarafından [16], takım pim profillerinin, benzer olmayan AA-6351 ve AA-5083-H111 alüminyum alaşımlı kaynakların mekanik ve metalurjik özellikleri üzerindeki etkisi incelenmiştir. Takım ilerleme hızı 36, 63 ve 90 mm/dak. ve takım dönme hızını 950 dev/dak. olarak ayarlamışlardır. Çalışmalarında düz kare profile sahip bir pim kullanmışlardır. Takımın omuz genişliği 18 mm, pim çapı 6 mm ve pim uzunluğu 5.7 mm'dir. Çalışma sonucunda 63 mm/dak. parametreye sahip denemede daha iyi mekanik özellikler bulunduğunu gözlemişlerdir.

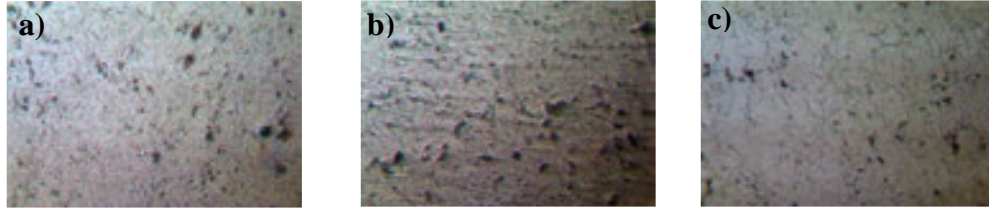
N.Srujana ve arkadaşları [17] yaptığı çalışmada ana malzeme olarak haddelenmiş 4 mm kalınlığında AA-6351 alüminyum levha kullanmışlardır. 150x75 mm boyutlarındaki parçalarıyla bir freze makinesi kullanılarak SKK işlemini yapmışlardır. SKK işlemi 900 dev/dak. dönme hızı ve 65 mm/dak. takım ilerleme hızında gerçekleştirilmiştir. Çekme mukavemeti ve sertlik gibi malzemenin mekanik özelliklerini, sırasıyla çekme testi ve Vickers mikrosertlik testi kullanarak değerlendirmişlerdir. SKK' ya başlamadan önce, birleştirilecek numuneler freze tablasına civatalanmış tutma kelepçelerini kullanarak sabitleme kalıbına sıkıca tutturmuşlardır. SKK işlemi için beş farklı takım pimi profili kullanmışlardır. Çalışma sonunda Tablo 1' de gösterilen 5 farklı takım ve pim profillerinin mekanik özellikler ve mikroyapılar üzerindeki etkisi değerlendirmişlerdir. Sonuç olarak, üçgen pim profili ile yapılan birleştirmelerin, işlem sırasında

daha fazla nüfuziyeti nedeniyle diğer takım profillerine göre Tablo 1' de gösterildiği gibi daha üstün mekanik özellikler sergilediğini göstermiştir.

Tablo 1. SKK ile Birleştirilen AA-6351 Alüminyum Alaşımının Takım Profili ve Mekanik Özellikleri [17].

Takım Profili	Çekme Dayanımı (MPa)	Akma Dayanımı (MPa)	Uzama (%)	Mikrosertlik (HV)
Düz Silindirik	168	100	9.3	40
Konik Silindirik	170	80	7.56	44
Dişli Silindirik	166	127	6.56	42
Kare	161	77	10.66	39
Üçgen	174	117	9.3	48

SKK ile birleştirilen AA-6351 alüminyum alaşımlarının karışım bölgesinden alınan mikroyapıları Şekil 2'de gösterilmiştir. AA-6351 alüminyum ana metal homojen olmayan kaba tane yapısından oluşur. Üçgen pimli takım ile birleştirilen numuneler dışındaki karışım bölgeleri, ana malzemeye kıyasla homojen olmayan ve ince taneli yapı sergilemiştir. Üçgen pimli takım (Şekil 2(f)) birleştirilen numune, diğer takımlara göre daha homojen bir mikroyapı sergilemiştir. Bu durum, üçgen takım ile SKK işleminde daha iyi mekanik özelliklerinin elde edildiğini göstermektedir. Kare pimli takım ile yapılan birleştirmede, işlem sırasında tanecik büyümesinin, zayıf mekanik özelliklere neden olduğu belirtilmiştir [17].



Şekil 2. Malzemenin mikro yapıları, (a) AA-6351 alüminyum ana metalin mikroyapısı, (b) kare pim, (c) üçgen pim [17].

2.1. Cu Alaşımlarının SKK İşlemi

Bakır ve alaşımları yaygın olarak kullanılan bir mühendislik malzemesi olup iyi süneklik, korozyon direnci ve iyi derecede elektriksel ve termal iletkenlik göstermektedir. Bakırın yüksek ısı yayılımı olduğundan, bakırın kaynağı geleneksel kaynak yöntemleri ile birleştirilmesi zordur. A.Kumar ve L. Suvarna Raju yaptıkları çalışmada [18] 3 mm kalınlığındaki bakır levhaları bir dikey freze makinesi ile birleştirmişlerdir. SKK ile birleştirilen bakırın takım profilleri ve mekanik özellikleri Tablo 2' de gösterilmiştir. SKK işleminde H13 takım çeliği kullanılmıştır. H13 takım çeliği düşük ve yüksek sıcaklıklarda aşınmaya karşı iyi direnç göstermektedir. Tokluk ve süneklik yüksek düzeyde olup işlenebilirlik derecesi yüksektir. Yüksek sıcaklıklara karşı iyi bir ısı direnci ve dayanıklılığı vardır. SKK işleminde takım olarak konik silindirik, dişli konik silindirik, üçgen, kare, beşgen ve altıgen geometrisine sahip olan pimler kullanılmıştır (Tablo 2). Optimum parametreleri 900 dev/dak. takım dönme hızı ve 40 mm/dak. takım ilerleme hızı olarak elde etmişlerdir. 6 farklı geometriye sahip karıştırıcı uçlu takımlar ile SKK yapılmış ve en iyi mekanik özellikleri kare geometriye sahip karıştırıcı uç ile elde edildiği belirtilmiştir. SKK esnasında, karışım bölgesinde kare ucun daha geniş yüzey alanına bağlı olarak daha geniş karıştırma hareketi

yaptığından dolayı sürtünme ısısı ve plastik deformasyon ile dinamik rekristalizasyona maruz kalmış ve mikroyapıda ince eş eksenli taneler görülmüştür.

Tablo 2. SKK ile Birleştirilen Bakırın Takım Profilleri ve Mekanik Özellikleri [18].

Takım Profili	Çekme Dayanımı (MPa)	Akma Dayanımı (MPa)	Uzama (%)	Mikrosertlik (HV)	Darbe Dayanımı (J)	Kaynak Verimliliği (%)
Konik Silindirik	168	109	13.5	85	65	1.09
Dişli Konik Silindirik	187	129	13.4	90	72	1.01
Üçgen	208	151	14	95	80	2.3
Kare	218	182	16	105	85	1.56
Beşgen	207	178	12	82	79	1.32
Altıgen	183	141	13	80	70	1.21

Dhananjayulu Avula ve arkadaşlarının yaptıkları çalışmada [19], 100 mm uzunluğunda, 40 mm genişliğinde ve 6 mm kalınlığında saf bakır levhaları SKK ile birleştirmişlerdir. Bakır plakanın kimyasal bileşimi Tablo 3' de gösterilmektedir. Isıl işlem için bakır plakaları 30 dakika boyunca 600 °C' de fırın içinde tutup ve ardından oda sıcaklığında soğumaya bırakmışlardır. Kullandıkları takım, vidalı konik pim profiline sahiptir. Takımın omuz çapı 15 mm, konik pimin geniş çapı 6 mm, konik pimin dar çapı 4 mm, pim uzunluğu 5.6 mm'dir. Isıl işlem görmüş bakır levhaları SKK ile başarılı bir şekilde birleştirmişlerdir. Birleştirme işlemi 635 dev/dak'lık takım dönme hızında ve 8 ile 19 mm/dak'lık takım ilerleme hızında gerçekleştirmişlerdir. Kullanılan ana metalin mekanik özellikleri ve yaptıkları çalışma sonucunda elde edilen mekanik özellikler aşağıdaki Tablo 3' de gösterilmiştir.

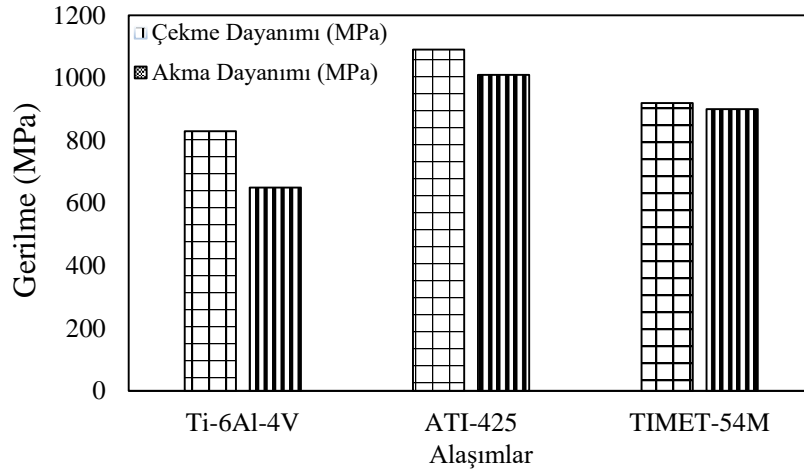
Tablo 3. SKK ile Birleştirilen Bakırın Mekanik Özellikleri [19].

Birleştirilen Malzeme		Çekme Dayanımı (MPa)	Akma Dayanımı (MPa)	Uzama (%)	Elastisite Modülü (MPa)
Ana Metal	Isıl İşlem Görmemiş	273.2	240.7	33.54	9318
	Isıl İşlem Görmüş	239.3	168.2	34.04	8020
SKK' lı Birleştirme	8 mm/dak. Takım ilerleme hızı	138.2	93.8	5.51	9342
	19 mm/dak. Takım ilerleme hızı	256.9	165.4	24.44	9704

2.2. Ti ve Alaşımlarının SKK İşlemi

Titanyum ve alaşımları -196 °C ile 593 °C aralığında özelliklerini kaybetmeden çalışma olanağı ve diğer emsal metallere göre daha hafif ve korozyona karşı mükemmel dayanım sağlar. Won-Bae Lee ve arkadaşları [22], 5.6 mm kalınlığındaki saf Ti levhaları su soğutma sistemi ile donatılmış ve sinterlenmiş bir TiC kaynak takımı kullanarak SKK işlemini gerçekleştirmişlerdir. Bu işlemi 1100 dev/dak. takım dönme hızı ve 500 mm/dak'lık takım ilerleme hızıyla yapmışlardır. Numunelere çekme testi uyguladıklarında birleşim yerinin enine gerilme mukavemeti, ortalama olarak 429 MPa değerini göstermiştir. Çünkü ısı tesiri altında kalan bölgede minimum sertlikle kırılma meydana gelmiştir. Önemli bir mikroyapısal farklılık olmadığını ve SKK işlemi sonucunda

Ti malzemesinin karışım bölgesinin ana metal ile karşılaştırıldığında herhangi bir kusur olmadan SKK'nın başarılı bir şekilde tamamlandığını belirtmişlerdir. M. Ramulu ve arkadaşları [20] yaptıkları çalışmada 3 mm kalınlık, 100 mm genişlik ve 600 mm uzunluktaki titanyum (Ti-6Al-4V), TIMET-54M ve ATI-425 levhaları birleştirmişlerdir. Yapılan çalışmada kullanılan takım malzemesi W-La (Tungsten Lantanyum) alaşımından yapılmıştır. Birleştirme işlemini 300 dev/dak'lık takım dönme hızında ve 100 mm/dak'lık takım ilerleme hızında gerçekleştirmişlerdir. Kullandıkları takımın omuz çapı yaklaşık 15,9 mm, pimin çapı 8,6 mm ve pim uzunluğu 1,4 mm'dir. Takıma 3°'lik açı vererek kaynak işlemini gerçekleştirmişlerdir. Üç titanyum alaşımını da (ATI-425, TIMET-54M ve Ti-6Al-4V) SKK yöntemi ile birleştirip mekanik özellikleri açısından kıyaslamışlardır. Bu alaşımlardan en iyi mekanik özellikleri ATI-425 titanyum alaşımı vermiştir (Şekil 3).

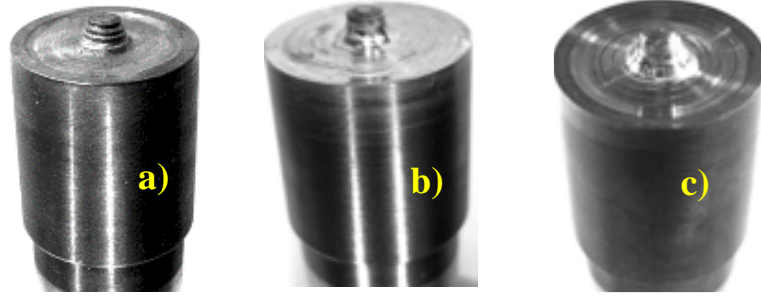


Şekil 3. SKK ile Birleştirilen Titanyum Alaşımlarının Mekanik Özellikleri [20].

2. Sürtünme Karıştırma Kaynağı Tekniğinde Takım Aşınması

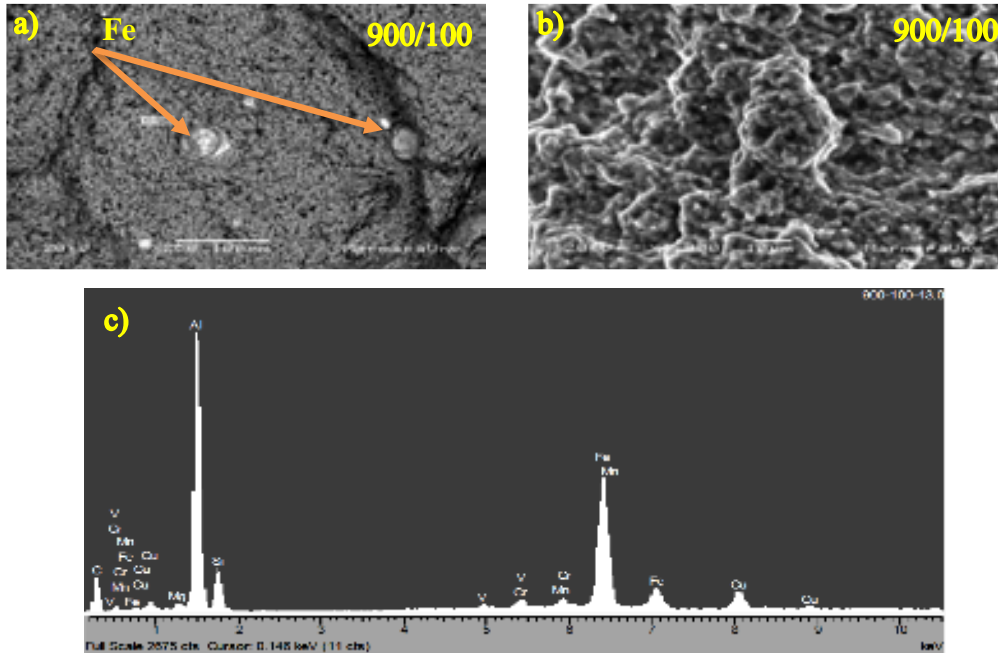
Aşırı takım aşınması takım şeklini değiştirir, böylece kusur oluşma olasılığını artırır ve muhtemelen kaynak kalitesini düşürür. Kesin aşınma mekanizması, iş parçası ve takım malzemeleri, seçilen takım geometrisi ve kaynak parametreleri arasındaki etkileşime bağlıdır [21].

Y.Bozkurt ve arkadaşları yaptıkları çalışmada [22], Al-2124 matris içerisine %25 SiC partikül takviyesi yapılmış (AA2124/SiCp/25) kompozit malzemeye SKK işlemi uygulamışlardır. Kullandıkları malzeme 400x260x50 mm ölçülerinde bir kütük şeklindedir. Kütük halindeki metal matrisli kompozit (MMK) malzemeyi, tel erozyon ile hassas bir şekilde 130x50x3 mm ölçülerinde keserek levha haline getirmişlerdir. Levha yüzeylerini, yüzey taşlama tezgâhında taşıyarak 3 mm kalınlığına getirmişlerdir. AA2124/SiCp/25-T4 MMK levha içerisinde sert ve keskin halde bulunan SiC partikülleri olduğundan, birleştirme esnasında kullanılan karıştırıcı takımın ucu aşınmıştır. SKK işlemini 900 dev/dak. takım dönme hızı ve 100 dev/dak. takım ilerleme hızındaki kaynak parametrelerinde yapılmıştır. SKK sonrası karıştırıcı uç çapının 4 mm'den 3,6 mm'ye düştüğünü belirterek aşınma oranının %10 olduğunu hesaplamışlardır. Karıştırıcı ucun kök kısmındaki çapının da 6 mm'den 5,7 mm'ye düşmesiyle bu bölgedeki aşınma oranının %5 olduğunu görmüşlerdir. Karıştırıcı ucun aşınmasından dolayı kopan Fe parçacıklarının durumunu XRD karakterizasyonu yaparak açıklığa kavuşturmuşlardır [22].



Şekil 4. SKK öncesi ve 900/100 kaynak parametrelerinde yapılan birleşme sonrası karıştırıcı uç görünüşleri; a) SKK öncesi takımın görünümü, b) SKK sonrası aşınmış haldeki takım (kök kısmında %5 aşınma kaybı) ve c) SKK sonrası aşınmış haldeki takım (uç kısmında %10 aşınma kaybı) [22].

Düşük süneklik ve yüksek aşınma direncine bağlı olarak alüminyum matrisli kompozitler SKK işleminde belirli sınırlamalara sahiptirler. Ekstrüde edilmiş veya haddelenmiş koşullar altında bulunan MMK'ların daha düşük sertlik ve daha yüksek plastisiteye sahip olduğu düşünüldüğünde, daha az takım aşınması olacaktır ve kaynak yükü ile yumuşak bir koşul altında kolayca elde edilmesi beklenmektedir [22]. Diğer araştırmacılar tarafından yapılan çalışmalarda [23,26] 6061/Al₂O₃p/10, A359/SiCp/20 ve AZ91/SiCp/10 kompozit levhaların birleştirilmesi esnasında SKK sırasında takım aşınması meydana geldiği belirtilmiştir. Karıştırıcı takım ucunun aşınması, aşınma direnci yüksek olan çok kristalli kübik boron nitritli (PCBN) takımlar kullanılarak en aza indirilebileceği ifade edilmektedir.



Şekil 5. 900/100 kaynak parametrelerinde SKK yapılan AA2124/SiCp/25-T4 MMK levhaların çekme deneyi sonrası karışım bölgesindeki kırık yüzey kesitleri; a,b) SEM görüntüleri, c) EDS analizi [22].

A.H. Feng ve arkadaşları yaptıkları çalışmada [25] toz metalurjisi ve ekstrüzyon ile üretilen AA-2009 /%15/SiCp kompozit malzemeleri birleştirmişlerdir. Ekstrüde edilmiş çubuklardan 8 mm kalınlığında levhalar kesmişlerdir. Parçaları ekstrüzyon doğrultusu boyunca 600 dev/dak'lık bir takım dönme hızında ve 50 mm/dak'lık bir takım ilerleme hızında birleştirmişlerdir. Omuz çapı 24 mm ve pim çapı 8 mm olan çelik malzemeli silindirik dişli bir pim kullanmışlardır. Çalışma sonunda AA2009/SiCp kompozit levhaları SKK yaparken takım çeliğinden imal edilmiş karıştırıcı uç çapının 6 mm'den 5,6 mm'ye düşmesi ile % 7'lik bir aşınma kaybı olduğunu açıklamışlardır. 6061/Al₂O₃p/10, A359/SiCp/20 ve AZ91/SiCp/10 MMK levhaların birleştirilmesi esnasında SKK sırasında takım aşınması meydana geldiği belirtilmiştir. Karıştırıcı takım ucunun aşınması, aşınma direnci yüksek olan çok kristalli kübik boron nitritli (PCBN) takımlar kullanılarak en aza indirilebileceği ifade edilmektedir [24,26].

3. Sonuçlar

Alüminyum levhaların birleştirilmesinde düz silindirik ve kare profilli takımlar ile üstün mekanik özellikler elde edilmektedir. Yüksek mekanik özellik, mikroyapıdaki ince ve homojen tanelerin oluşmasına bağlıdır. Bu durum ancak hızlı soğuma şartlarında sağlanmaktadır. Alüminyum için yüksek soğuma hızı optimum sıcaklığa bağlı olarak gerçekleşmektedir. Yüksek ısı girdisi yavaş soğumaya neden olacağından, sürtünmeye bağlı olarak yüksek devir/ilerleme hızı istenmez. 900-1200 dev/dak. dönme hızı 20-60 mm/dak. takım ilerleme hızları iyi sonuçlar vermiştir. Bakır ve alaşımlarının SKK işleminde, karışım bölgesinde kare ucun daha geniş yüzey alanına bağlı olarak daha geniş karıştırma hareketi yaptığından dolayı sürtünme ısı ve plastik deformasyon ile dinamik rekristalizasyona maruz kalmış ve mikroyapıda ince eş eksenli taneler görülmüştür. Bakırın yüksek ısı yayılımına sahip olduğundan 900 dev/dak. dönme hızı ve 40 mm/dak. takım ilerleme hızı optimum sonuçları vermiştir. Titanyum ve alaşımları için yapılan SKK işleminde Tungsten Lantanyum alaşımlı bir takım kullanılarak iyi mekanik özellikler elde edilebilmektedir. AA6061/Al₂O₃p/10, A359/SiCp/20 ve AZ91/SiCp/10 MMK levhaların birleştirilmesi esnasında SKK sırasında takım aşınması meydana geldiği belirtilmiştir. Takımların aşınmasında, aşınma direnci yüksek olan çok kristalli kübik boron nitritli (PCBN) takımlar kullanılarak en aza indirilebileceği ifade edilmiştir. Ayrıca, ekstrüde edilmiş veya haddelenmiş koşullar altında bulunan MMK'ların daha düşük sertlik ve daha yüksek plastisiteye sahip olduğu düşünüldüğünde, daha az takım aşınması olacaktır ve kaynak yükü altında kolayca elde edilmesi beklenmektedir.

4. Kaynaklar

- [1] M.K. Bilici, B. Bakır, Y. Bozkurt Y, İ Çalış: Taguchi Analysis of Dissimilar Aluminum Sheets Joined by Friction Stir Spot Welding, Pamukkale Üniversitesi Müh. Bilim Dergisi, 22(1), (2016), pp.17-23.
- [2] Y. Bozkurt, Z. Boumerzoug: Tool Material Effect on The Friction Stir Butt Welding of AA2124-T4 Alloy Matrix MMC, Journal of Materials Research and Technology Volume 7, (2018) pp. 29-38.
- [3] H. Uzun, C.D. Done, A. Argagnotto, T. Ghidini, C. Gambaro: Friction Stir Welding of Dissimilar Al 6013-T4 to X5CrNi18-10 Stainless Steel, Materials and Design, (2005) Vol. 26, pp. 41-46.
- [4] Y.N. Zhang, X. Cao, S. Larose, P. Wanjara: Review of Tools for Friction Stir Welding and Processing, Can. Metall. Q. 51 (3), (2012), pp. 250-261.

- [5] R.S. Mishra, Z.Y. Ma: Friction Stir Welding and Processing, Mater. Sci. Eng. R Rep. 50 (1–2), (2005) pp. 1–78.
- [6] P. Threadgill, A. Leonard, H. Shercliff, P. Withers: Friction Stir Welding of Aluminium Alloys, Int. Mater. Rev. 54 (2), (2009) pp. 49–93.
- [7] W. Höflich: EADS Technology Licensing Initiative Webinar(2010).
- [8] G. Tempus: New Aluminium Alloys and Fuselage Structures in Aircraft Design, Werkstoffe Für Transport und Verkehr, (2001) Zurich, Switzerland.
- [9] V. Richter-Trummer, E. Suzano, M. Beltrão, A. Roos, J.F. dos Santos, P.M.S.T. de Castro: Influence of The FSW Clamping Force on The Final Distortion and Residual Stress Field, Materials Science & Engineering A, Vol.538(0), (2012), pp. 81–88.
- [10] L. Fratini, F. Micari, G. Buffa, V.F Ruisi: A New Fixture for FSW Processes of Titanium Alloys, CIRP Annals- Manufacturing Technology 59(1), (2010), pp. 271-274.
- [11] P. Upadhyay, A. Reynolds: Effect of Backing Plate Thermal Property on Friction Stir Welding of 25-Mm-Thick AA6061, Metallurgical and Materials Transactions Vol. 45(4) (2014), pp. 2091–2100.
- [12] M. Imam , V. Racherla, K. Biswas: Effect of Backing Plate Material in Friction Stir Butt and Lap Welding of 6063-T4 Aluminium Alloy, The International Journal of Advanced Manufacturing Technology, Vol77 (9-12), (2014), pp.2181-2195
- [13] P. Upadhyay, A.P. Reynolds: Effects of Forge Axis Force and Backing Plate Thermal Diffusivity on FSW Of AA6056. Materials Science and Engineering: A, Vol. 558, (2012), pp. 394-402.
- [14]. S.A. Khodir, T. Shibayanagi, M. Naka: Control of Hardness Distribution in Friction Stir Welded AA2024-T3 Aluminum Alloy, Mater Trans, Vol.47(6), (2006), pp.1560–1567.
- [15] M. Ilangoan, S. Rajendra Boopathy, V.Balasubramanian: Effect of Tool Pin Profile on Microstructure and Tensile Properties of Friction Stir Welded Dissimilar AA 6061-AA 5086 Aluminium Alloy Joints, Defence Technology, Vol 11, (2015), pp. 174-184.
- [16] R. Palanivel, P. Koshy Mathews, N. Murugan: Influences of Tool Pin Profile on The Mechanical and Metallurgical Properties of Friction Stir Welding of Dissimilar Aluminum Alloy, International Journal of Engineering Science And Technology, Vol 2(6), 2010, pp. 2109-2115.
- [17] N. Srujana, O. Umadevi, G. Venkateswarlu: Influence of Tool Pin Profile on Microstructure and Mechanical Properties of Friction Stir Welded 6351 Aluminium Alloy, Research and Reviews: Journal of Engineering and Technology, 3 (2014), pp. 13-17.
- [18] A. Kumar, L. Suvarna Raju: Influence of Tool Pin Profiles on Friction Stir Welding of Copper, Department of Mechanical Engineering, NIT, Warangal, A.P, 27 (2012), pp. 1414-1418.
- [19] A. Dhananjayulu, K. Ratnesh, D.K. Dwivedi, N.K. Mehta: Effect of Friction Stir Welding on Microstructural and Mechanical Properties of Copper Alloy, World Academy of Science, Engineering and Technology International Journal of Mechanical and Mechatronics Engineering, 5(2) (2011), pp. 336-344.

- [20] M. Ramulua, K. Gangwara, A. Cantrella, P.Laxminarayanab: Study of Microstructural Characteristics and Mechanical Properties of Friction Stir Welded Three Titanium Alloys, 5 (2018), pp. 1082-1092.
- [21]Y. N. Zhang, X. Cao, S. Larose, P. Wanjara: Review of Tools For Friction Stir Welding and Processing, Canadian Metallurgical Quarterly, 51 (3) 2012, pp. 250-261.
- [22] Y. Bozkurt, H. Uzun, S. Salman: Sürtünme Karıştırma Kaynak Yöntemiyle Birleştirilen Aa2124/SiCp/25 Kompozit Levhaların Mekanik Özelliklerine Takım Aşınmasının Etkisi, J. Fac. Eng. Arch. Gazi Univ, 26(1) (2011), pp. 139-149.
- [23] W.B. Lee, C. Y. Lee, W. S. Chang, Y.M. Yeon, S.B. Jung: Microstructural Investigation of Friction Stir Welded Pure Titanium, Materials Letters, 59 (2005), pp. 3315 – 3318.
- [24] R.A. Prado, L.E. Murr, D.J. Shindo, K.F. Soto: Tool Wear in The Friction Stir Welding of Al Alloy 6061+20% Al₂O₃: A Preliminary Study, Scripta Materialia, 45 (2001), pp. 75-80.
- [25] A.H. Feng, Z.Y. Ma: Effect of Microstructural Evolution on Mechanical Properties of Friction Stir Welded AA2009/SiCp Composite, Composites Science and Technology, 68 (2008), pp. 2141-2148.

[26] W.B. Lee, C. Y. Lee, M.K. Kim, J.I. Yoon, Y.J. Kim, Y.M. Yoen, S.B. Jung: Microstructures and Wear Property of Friction Stir Welded AZ91Mg/SiC Particle Reinforced Composite, Composites Science and Technology, 66 (2006), pp. 1513–1520.

SORUMLU YAZAR: Yahya Bozkurt, Marmara Üniversitesi, Teknoloji Fakültesi, Metalurji ve Malzeme Mühendisliği Bölümü, Göztepe Kampüsü, Kadıköy/İSTANBUL, +90 505 616 84 73, ybozkurt@marmara.edu.tr.

KISA ÖZGEÇMİŞLER

Murathan Kalender – 1996 yılında İstanbul’da doğdu. 2014 yılında İsmet Aktar Anadolu Teknik Lisesi’nden mezun oldu. Halen Marmara Üniversitesi Teknoloji Fakültesi Metalurji ve Malzeme Mühendisliği bölümünde 3.sınıf lisans eğitimine devam etmektedir.

Sefa Enes Kılıç – 1997 yılında Aksaray’da doğdu. 2015 yılında Aksaray Teknik Lisesi’nden mezun oldu. Halen Marmara Üniversitesi Teknoloji Fakültesi Metalurji ve Malzeme Mühendisliği bölümünde 3.sınıf lisans eğitimine devam etmektedir.

Yahya Bozkurt – 1975 Antakya doğumludur. Marmara Üniversitesi Teknik Eğitim Fakültesi Metal Eğitimi Bölümü’nden 2000 yılında mezun oldu. 2000 yılı Aralık ayında Marmara Üniversitesi Teknik Eğitim Fakültesi Metal Eğitimi Bölümünde Araştırma Görevlisi oldu. Prof. Dr. Serdar Salman ve Doç. Dr. Hüseyin Uzun danışmanlığında 2003 yılında başladığı doktora eğitimini Eylül 2008’de tamamladı. Ocak 2009’da Yardımcı Doçent, 2012 yılında Doçent, 2018 yılında da Profesör oldu. Halen aynı üniversitede görevine devam etmektedir.

Serdar Salman – 1962 İstanbul doğumludur. 1979-1980 yılında Ege Üniversitesi’nde okudu. İstanbul Teknik Üniversitesi Sakarya Mühendislik Fakültesi Metalurji Mühendisliği Bölümü’nden 1984 yılında mezun oldu. 1985 yılında Marmara Üniversitesi Teknik Eğitim Fakültesi Metal Eğitimi Bölümünde Araştırma Görevlisi oldu. 1991 yılında 9 ay süreyle YÖK – Dünya Bankası II. Endüstriyel Eğitim Projesi kapsamında İngiltere’de (Huddersfield Üniversitesi) eğitim ve araştırma amacıyla bulundu. 1992 yılında Marmara Üniversitesi Teknik Eğitim Fakültesi Metal

Eđitimi Blmnde đretim Grevlisi oldu. 1995 yılında MTEF Malzeme Eđitimi Anabilim Dalı'na Yardımcı Doçent olarak atandı. Aynı Anabilim dalında 1997 yılında Doçent, 2003 yılında ise Profesr oldu. 27/01/2003 ile 27/01/2006 tarihleri arasında Marmara niversitesi'nde Teknik Eđitim Fakltesi Dekan Yardımcılıđı, 2007 yılında (3 ay) Dekan Vekili olarak grev yapmıřtır. 2007-2008 yılları arasında 1 yıl GATECH-Atlanta Amerika'da misafir profesr olarak bulunmuřtur. 2012-2015 Yılları arasında Mehmet Akif Ersoy niversitesi, Mhendislik-Mimarlık Fakltesi'nde Kurucu Dekanlık yapmıřtır. Halen Milli Savunma niversitesi'nde grev yapmaktadır.

A MIG WELDING AUTOMATION EQUIPPED DOUBLE TORCH FOR FILLET WELDING OF TRANSFORMER SIDEWALL STRENGTHENING PART'S FILLET WELDINGS WITH LINEARITY CORRECTION ABILITY.

Nihat ÇELİK^{1,a}, İlker EREN^{2,b}, Ersin AKYÜZ^{2,c}, Sercan SÜZEN^{3,d}

¹BALIKESIR ELEKTROMEKANİK SANAYİ TESİSLERİ A.Ş. (BEST TRANSFORMERS)

²TURKISH REPUBLICBALIKESIR UNIVERSITY

³2K WELDING MACHINERY & AUTOMOTION

^anihat.celik@besttransformer.com, ^bieren@balikesir.edu.tr, ^ceakyuz@balikesir.edu.tr,
^dsercan@2kwelding.com

Abstract

Power transformer tanks are usually made from mild steel as form in roughly rectangular prism with vertical aligned strengthening elements on lateral sidewalls. Those strengthening elements are welded to sidewalls by manually in conventional production methods. It is improved a welding automation which is containing a linearity correction and work sequence algorithm. The system is equipped 3 laser distance sensor; the first one of is dedicated for positioning in horizontal axis of first strengthening element on sidewall which is laid down upon a main chassis. The second one is dedicated for measuring vertical length of first strengthening element before starting welding auto mod. The second and third ones are dedicated for continuously checks and correlates un-linearity of settled -up torches in horizontal axis up to 100 mm via keeping distance between pre-saved values and actual values. A PLC program always drive the 10 servo motor for synchronized and safe running of automation

Key Words: Welding, automation, laser, sensor, linearity, correction.

Note: This proceeding paper is a part of TEYDEB 3150076: Design and prototype manufacturing of a novel multi-purposed CNC vertical machining center and welding automation for manufacturing of power transformer steel constructions” that supported by The Scientific and Technological Research Council of Turkey (TUBITAK).

1.Introduction

MIG/MAG welding process is generally well-known as a kind of work that based on skilled employees experience, carefulness and body strength. Except production organizations that substations are already designed as mass production lines, most of industrial facilities for production of machinery, steel constructions and shipyards still needfusion welding process driven via skilled employees and semi-automatic power sources and torches. If we accept that general fusion welding processes are “traditional”, then we can call all robotic welding implementations as a “technologic way of welding”. Robotic welding substations are spreading out very fast all around in the world, especially in manufacturing of automobile, household goods and partly mass production of machinery. [1]

Implementing of automatic welding system, apparent progress made in many years. There are different ways to make the automated welding system. One important way is welding robots in their welding system. Other is to build specially designed automated welding system.

Especially, tracking sensor in automation welding system is necessary and it is divided into touch type sensor and non-touch type sensor. In non-touch type sensor, there are several kinds of methods such as a method using vision system[2], a method using arc sensor [3], and a method using dual electromagnetic sensor[4]. In touch type seam tracking sensor, there is a method tracking welding seam mechanically [5].

In a fusion welding process, if parental materials are sensitively predictable by dimensionally and able to set up in a fixture before welding, manufacturer should have evaluate to use robotic welding technologies (RWT) on their process. RWT will make big differences on productivity, quality, efficiency, cycle time, welding workmanship and all over cost.

In the other hand, parental materials could have unique constructions and designs with their huge dimensions and gravities, also could not present to manufacturer to make steady and stable preassembled constructions (fit-up) before welding. If RWT processes evaluate for that kind of manufacturing process, it will found that huge investment costs and problematic risks for efficiency and productivity. Also present seriously risk for collapsing of investment. [6]

As an example, manufacturing of power transformer tanks (PTT) can be given with unique designs, bigger dimensions (Length=10 m, Width=5 m and Height=4,5 m) and gravities up to 40 tons. Each PTT's designed according to customer requirements supposing to give electrical and mechanical performances.

A power transformer tank contains mainly 5 segments:

- A bottom sheet or hull.
- Lateral side walls (long and short side walls)
- Frame for cover-plate connection
- Cable boxes
- Expansion tanks

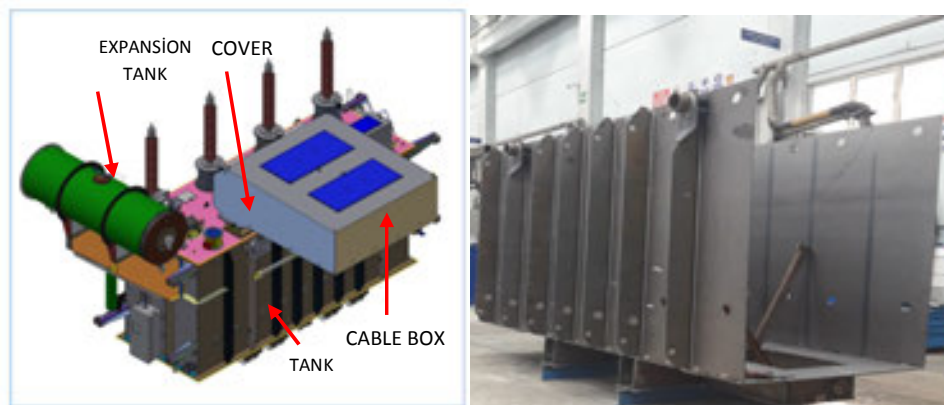


Figure 1: (a) Main construction of power transformer tank, (b) Pre-assembling of finished side walls on to the hull.

In this study, we focused on fusion welding of side walls. All parental components of side walls are manufactured from ISO EN S235JR/ ISO EN S355JR and being cut with CNC-OXY PLASMA machines in dimensional tolerance of ± 1 mm. Semi part parental materials are called on that stage as “ (horizontal) side sheets and (vertical) strengthening elements” as

given in Figure 2. Side sheets and strengthening elements are placed in a welding workstation to make preliminary assembling of finished lateral walls.

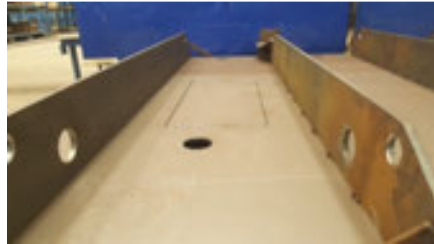


Figure 2: Pre-assembling of lateral walls before welding.

In the traditional method of manufacturing, it is to weld almost hundreds of meters single pass filled (SPFW) welding on the pre-assembled PTT by manually. Almost 95% of welding workloads of joints are SPFW. And about 50% of SPFW workloads are comes from lateral side walls of PTT.

Basically, side sheet's thickness can be change between 6 to 12 mm and strengthening element's thickness can be change between 15 to 30 mm according size of PTT. Also width of both can be change between 2000 to 3500 mm. Minimum 2 and maximum 15 pieces of strengthening element can located on to one side wall, so SPFW workload per tank can change 50 m to 250 m according to size of PTT. In traditional manufacturing way of welding that needs an experienced welder and semi-automatic MIG/MAG power source, rate of a work is observed almost 0,2-0.3 m/sec according to welder's care and responsibility. A simple torch carrier module can save little rate of work with such careful and responsible welder about 0.1 m/sec for SPWF workloads. Because of ratings of welding speed on traditional way of manufacturing of PTT, those sidewall workloads defined as a bottle-neck of all process. The ways of throwing out that bottle neck with traditional methods means that more work force, longer cycling time, more welder and working areas.

As a R&D team, we improved welding automation for SPWF workloads of side walls. The major technical problem, we solved, are presented below.

- Strengthening element are pre-assembled manually on to side sheets, because of that, it can be linearity problem longitudinal (2-5 mm) and vertically (1-3 mm) per each fit-up. It means that unstable welding route on the seam which is to be corrected by a **control method**. Otherwise throat thickness and penetration of welding can be failed thoroughly.
- The control method mentioned above is combined laser distance measuring sensor kit that collecting to data of distance at vertically from the lateral sheet and horizontally from strengthening elements. A PLC software running for keeping tips of torches on the almost at 45°(fillet welding) position to welding track to get necessary welding face, throat thickness and penetration.
- Both of torches should be started almost same time with a small lapsing that gives an opportunity to make fine tuning by operator.
- Because of design diversity, length of first strengthening have to be measured and for others, since ends of each strengthening elements can vary it should be described some distances those not to be welded.
- Automatically positioning for next strengthening element, scanning for next element and taking preposition than manually fine torches adjustment by camera.

- While torches running for welding, online monitoring of metal transfer, arc lengths and arc positions according to corner for both torches.
- Filtering of many deceptive parameters like changing of very sharp UV light emits, vibration, heat, welding spatters and smoke.
- Ability of fine and manually position arrangements for torches while running with welding because of nonfiltered deceptive conditions and perpendicularity differences on strengthening elements and vertically differences on lateral sheet.

2. The workflow:

2.1. Grounds of un-linearity problem and an offer for that:

Lateral side walls of transformer tank can be up to 12000 mm length and 4000 mm width according to design requirements. Dimensions stability at the end of hot roll-forming process is not being in narrow tolerances. Many linearity problems at sheet plates can be still remained by transversely or longitudinally. Sometime also deviation on the surface flatness can be observed from steel surface. Otherwise, oxy or plasma cutting processes are deceptive results on linearity of sliced strengthening elements and side walls because of locally excessive heat inputs and fast cooling.

Also in traditional fitting up process, employee has to make some straightening work for strengthening elements with C Formed Hydraulic Pressing Machinery by manually. Pre-assembling of strengthening elements onto side wall by tuck welds also needs to upper level care and concentration of employee. Those fitting up works almost fully bound to care of worker. So that on the, many un-linearity problems are loaded onto pre-assembled side walls before welding.

According to our measuring, size of un-linearity can be up to 10 mm thoroughly length of strengthening elements horizontally and 3 mm vertically. So any automation for this process could correct this un-linearity problem for both torches while metal transfer.

2.2. Implementation of laser distance sensors for the problem:

A researcher can face few correction methods on RWT industrial implementations. One of systems of listed below is generally used in RWT solutions [7]

- i. Laser beam tracking systems,
- ii. Touch tile tracking system,
- iii. Arc sensing tracking systems.

That technologic implementations are take placed many kind of industrial welding applications. In example, Colum-Boom systems for cylindrical constructions welding with arc sensing and laser beam tracking systems are very common industrialized in the mass production industrial applications. Also each RWT implementations are equipped with one of them at automotive manufacturing plants. All tracking systems have same working principle, such that a signal is produced and driven a DC motor that tip point of torches staying stable while moving on welding route. Laser displacements sensors (SICK OD2-P250W150I0) are used for these purposes.

2.3. Basic algorithm of automation:

Basic algorithm of our control system is presented below:

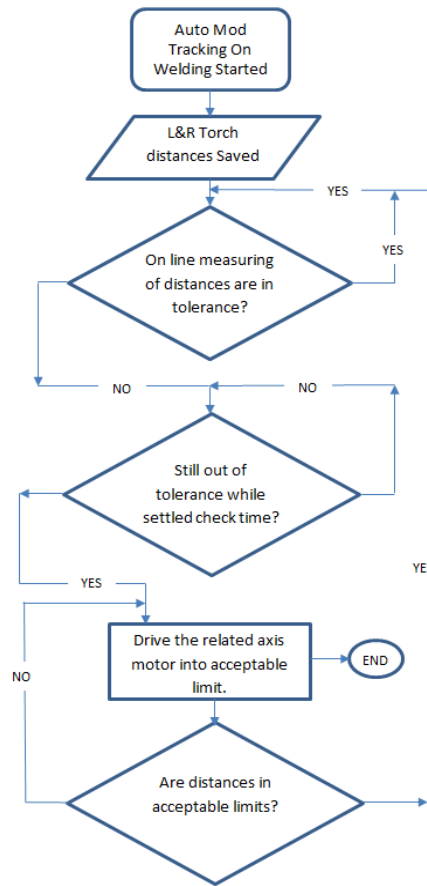


Figure 3: Basic algorithm of torch tracking program.

2.4. PLC program and control units:

Two PLC's are used in the system as one is Master and the other is Slave. While Master controls all servo drivers (4 axes, 8 drivers), slave transfers all I/O's to Master and controls X axes motors and drivers. CANopen protocol is used for communication between drivers. Second PLC, controls weaving motions of torches by step motors. Master generally controls all axes on work-center by manually and automatically. All I/O's taken from sensors according to program. Manual control of servo motors possible with program blocks for each servo motor. Another program block also makes possible torch tracking ability in auto mod. During auto mod, in case of failure in program, another program block makes it possible restarting of welding from where the failure is occurred.

2.5. Building up of welding center

Steel construction of welding center is designed in 3D CAD program. Length of base of machine is designed 10 m, width is 5 m, height of bridge from the top of base is designed 400 mm, and a steel construction is manufactured. Bridge is located onto linear guideways and equipped with helical rack and pinion with both sides to make easy motion on the axes X_1 and X_2 . Each leg of bridge is equipped AC servo motor for synchronized with each another.

Lateral sides of bridge are also equipped with linear guideways, helical racks, pinions and AC servo motors too. So each side of strengthening element possesses wire feeder carrier mechanism along by Y_1 and Y_2 axes.

Two special torch carrier mechanisms also designed and applied onto lateral Y_1 and Y_2 axes, so tips of torch have own motion freelance, weaving and adjustment ability in X_{t1} , X_{t2} , Z_{t1} and Z_{t2} axes. Welding sources are chosen like that a few welding I/O's (starts/ stops) can be shared with master PLC.



(a)

(b)

Figure 4: (a) General view from bridge of welding working center (b) positioning of torch carriers X_{t1} , X_{t2} , Z_{t1} and Z_{t2} axes at the starting point.



Figure 5: A finished & welded side walls with automation

3. Conclusions:

In this study, a welding automation is offered for side wall to strengthening element's double side instable linear fillet welding route of power transformer tank manufacturing process and explained basics of automation and major equipment. Problem of instability of welding linearity can be up to 10 mm for each side. Low cost laser distance measuring sensors are offered for solving of the linear instability problem of double side torches carrier axes running on a bridge same time instead of expensive and patent protected systems (laser tracking or arc length sensing modules.) Stability of throat thickness, form and penetration of finished welds are done in very acceptable performances where necessary quality limits.

With this automation, most of manual workmanship of power transformer tank manufacturing of side wall to strengthening elements fillet welding works are automatized and cycling time and working hours of process are decreased. So that, similarly on this study, or an improved types based on this studied working principles are could be offered for another manufacturing

industrial applications that contain instable linear welding routes like as shipyards, train wagons, steel constructing elements and containers for trucks.

In future, additional (X, Z and additionally radial axes) freedom of motion on torches can be designed for torch carrier axes, so instable circular or butt welding routes can be studied with based on mentioned algorithm. By this way, this study will be inspiring for researcher to design easy accessible and lowcost automations for huge containing instable welding routes.

4. References

- [1] Sá da Costa, JMG.; Pires, JN., Future welding robot developments, *Journal Robótica* **2001**, No 41, January]
- [2] K.W Um, S.H Rhee and D.C Kim "Modeling and Control of Welding Processes Using Vision Sensor", *Journal of Korean Welding Society*, Vol. 14, No. 4, pp. 7-15, August, 1996
- [3] C.H. Kim, S.J. Na, "A Study on Rotating Arc Using Hollow Shaft Motor", *Journal of Korean Welding Society*, Vol. 18, No. 5, pp. 589-594, October, 2000
- [4] J.H Shin, J.W. Kim "A study of a Dual-Electromagnetic Sensor for Automatic Weld Seam Tracking", *Journal of Korean Welding Society*, Vol. 18, No. 4, pp 330-339, August, 2000
- [5] B. Kam, Y. Jeon, S. Kim "Motion control of two-wheeled welding mobile robot with seam tracking sensor" *Industrial Electronics*, 2001. Proceedings ISIE 2001
- [6] Pires, J. N.; Sá da Costa, J., Object-oriented and distributed approach for programming robotic manufacturing cells. *Robotics and Computer-Integrated Manufacturing* **2000**, 16 (1), 29-42.
- [7] H. B. Cary "Arc Welding Automation", Taylor and Francis, 1995:

SHORT BIOGRAPHIES

Nihat Çelik –He received his bachelor's degree in Mechanical Engineering department from EskişehirOsmangazi University and his M.Sc. in Mechanical Engineering from Balıkesir University. He is currently studying Ph.D. in Mechanical Engineering at Balıkesir University. His doctoral research areas include electrical steels, electromagnetism and amorphous materials used in power and distribution transformers. He is also working as Mechanical Production Manager in BEST TRANSFORMERS TURKEY.

ErsinAkyüz –He received his bachelor's degree in Electrical Engineering department from Istanbul Technical University and his M.Sc. in Electrical and Electronics Engineering from Gazi University and he finished his Ph.D. in Mechanical Engineering from Balıkesir University. He is currently studying at Balıkesir University Vocational High School as a doctoral lecturer. Research areas include Renewable energy systems, Control and automation, and Internet of things, Cloud computing

İlker Eren – He received his Bachelor's Degree, M.Sc. and Ph.D. in Mechanical Engineering department from Balıkesir University. He is currently lecturing and researching at Balıkesir University Engineering Faculty. Researches lecturing areas are engineering math and Finite

Element Modelling methods and its software applications on design of machinery and load carrying constructions.

Sercan Süzen – He received his bachelor's degree in Electrical and Electronics Engineering from Sakarya University in 2010. He started his industrial automation carrier in 2013 in one of the automation company in Sakarya. Now he is one of cofounder and working ISP Group Company with his colleagues whose sharing same goal and ideal. He is currently studying M.Sc. in Electrical Engineering Department at Sakarya University.

MICROSTRUCTURAL PROPERTIES OF HIGH CHROMIUM WHITE CAST IRON / AISI 1030 STEEL WITH NICKEL INTERLAYER WELDED BY FRICTION WELDING

^aTanju TEKER, ^bEyyüp Murat KARAKURT

^{a, b}University of Adiyaman, Faculty of Engineering, Department of Materials Engineering, 02040, Adiyaman, Turkey.

tteker@adiyaman.edu.tr and ekarakurt@adiyaman.edu.tr

Abstract

In this study, high chromium white cast iron and AISI 1030 steel with nickel interlayer were combined depending on using different friction times by friction welding method. Welding morphologies were analyzed by Optical Microscopy (OM) and Microhardness analysis. Also, tensile test analysis was performed to determine the maximum tensile strength of the weld joints. As indicated in the literature, weld joints were divided into four zones as fully plastic deformed zone, deformed zone, partially deformed zone and base material. The highest microhardness values were obtained at weld joints exposed to 1600 rpm rotational speed and 12 sec friction time.

Key Words: Friction welding, High chromium white cast iron, AISI 1030, Microstructure, Microhardness.

1. Introduction

The friction energy can be used in the parts to be welded are joined as an available energy type. The first patent of the friction welding was taken in 1891 by J. H. Bevington [1-4]. Friction welding (FW) bases on the converting the mechanical energy into heat energy. It is necessary to consider this welding method as one of the hot pressure welding methods [5]. The working mechanism of the friction welding process is that while one of the parts to be welded is held constant, the other begins to turn at an angular velocity and then a pressure is applied in the axial direction. Thus, a heat transfer takes place from the fixed material to the other material, which has the axial rotational motion. This increase in temperature rises the contact zones to local melting temperature. As a result, permanent plastic deformations occur in these zones. Generally, the increase of temperature is lower than the melting temperature of the materials. Following the plastic deformations in the contact zones, the applied axial pressure can weld the materials without completely melting. This method is more like a forging process than a welding process, because the melting process does not occur completely during the joining of parts and no additional material is used. Since the welding melt pool does not form, the grain growth does not occur in large quantities. On the contrary, a fine-grained microstructure forms. As indicated in the Hall-Petch equation, this fine-grained microstructure does not cause intercrystalline embrittlement in the material [6-11]. High chromium white cast iron; as can be understood from its name, white cast irons contain a high proportion of chromium element. They can be used in various mineral drilling, processing mill, slurry pumps, brick molds and equipments for hard rock processing [12]. The most prominent feature of high chromium white cast iron is hardness since the carbon content is high.

In this study, effect of friction time on the characteristic microstructure and mechanical properties of the high chromium white cast iron and AISI 1030 materials welded with nickel interlayer by friction welding method was experimentally investigated.

2. Experimental

High chromim white cast iron (HCWCI) and AISI 1030 materials with a diameter of 12 mm and a length of 75 mm used in the experimental studies. The chemical compositions of these materials and nickel interlayer, which was used as interlayer during friction welding (FW), were given in Table 1. The welding process parameters made by using FW machine were showed in Table 2.

Table 1. The chemical components of materials used in experiments (wt.%).

Materials	Fe	Ni	C	Cr	Si	Mn	P	S	Mo	Nb	W
HCWCI	Bal.	0.5	3.2	27.4	1.16	2.3	0.01	0.02	2.3	0.03	0.4
AISI 1030	Bal.	-	0.36	-	0.25	0.8	0.02	0.04	-	-	-
Nickel	0.3	Bal.	0.06	0.02	0.6	-	0.006	-	0.68	0.2	0.4

Table 2. Friction welding process parameters.

Sample No	Rotational Speed (rpm)	Friction Time (sec)	Friction Pressure (MPa)	Forging Pressure (MPa)	Forging Time (sec)
S1	1600	8	80	150	8
S2	1600	10	80	150	8
S3	1600	12	80	150	8

For metallographic examinations; S1, S2 and S3 samples manually were cut into slices by cutter device. Interfaces of the weld zones of samples were grinded by 200-1200 mesh SiC grinding paper and then, polished by 1-3 μm diamond paste. While AISI 1020 sides were etched with a solution having %98 alcohol + %2HNO₃ at 3-5 sec, the HCWCI sides were etched with the Vilella solution (1 gr picric acid, 5 ml HCl and 100 ml Ethyl alcohol) at 5-10 sec. Microstructure photographs of the etched samples were analyzed by LEICA DM750 optical microscope device. Microhardness measurements were performed with HV scale of hardness under 100 g loads for 5 sec by QNESS Q10 test device. Also, Tensile tests were performed at a pulling speed of 1 mm/min by INSTRON tensile testing device having 50 000 N loading capacity in order to determine the bond strength of the weld samples.

3. Results and Discussion

3.1. Macro and Microstructure Results

The macro images and cross-sectional appearance of the all samples were given in Figs. 1a and 1b, respectively. When the macro surface photographs of S1, S2 and S3 samples were examined, it was obviously showed that S1, S2 and S3 samples did not have any cracks, gaps and unconnected zone on all weld zones.

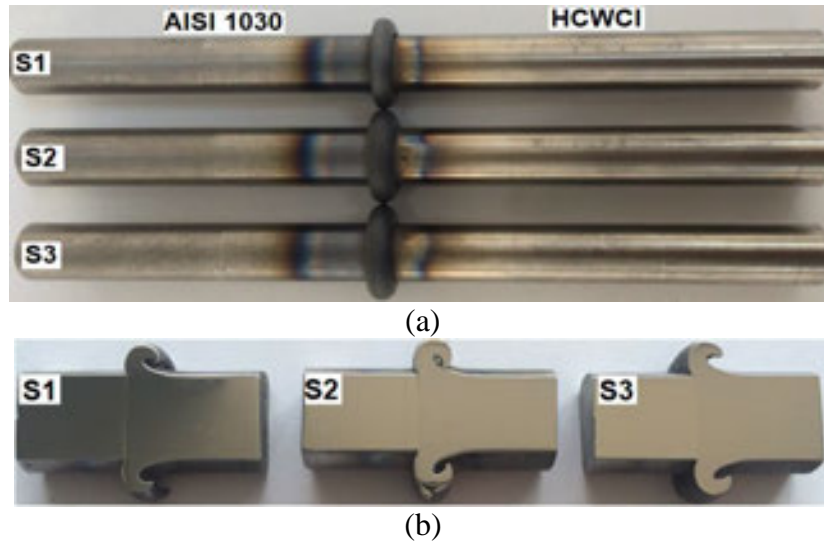


Figure 1. a) Macro images b) Cross-sectional views.

The weld joints were produced with 1600 rpm rotational speed, under 80 MP friction pressure and 150 MPa forging pressure for friction time of 8 sec and forging time of 8 sec by using nickel interlayer. Optical surface photograph taken from the weld zone of S1 sample was shown in Fig. 2. When the optical surface photograph of S1 sample was examined, it was determined that S1 sample was divided into three zones; the fully plastic deformed zone (FPDZ), the deformed zone (DZ), the partially deformed zone and base material (BM).

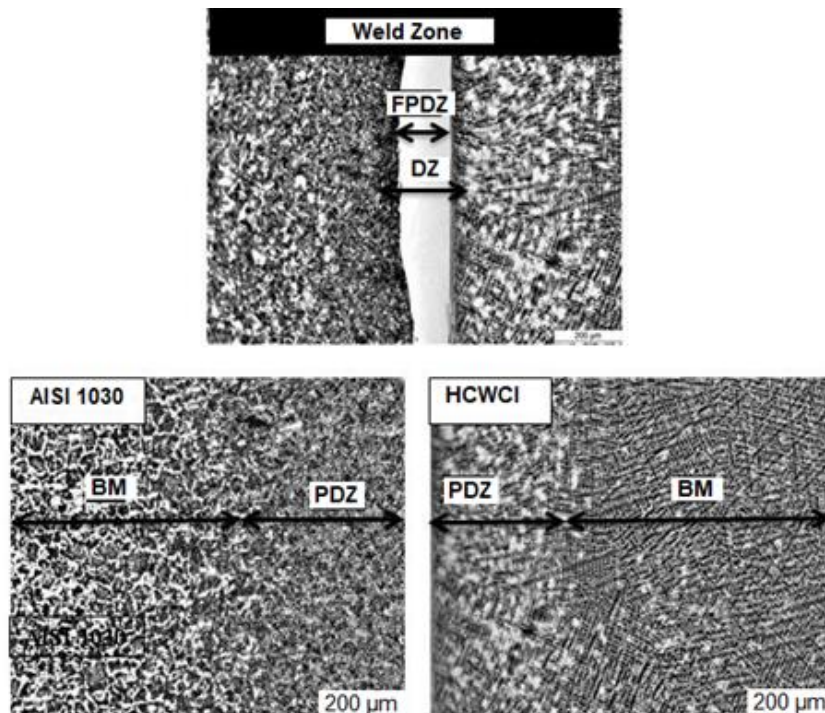


Figure 2. Optical photograph of S1 sample.

The weld joints were produced with 1600 rpm rotational speed, under 80 MP friction pressure and 150 MPa forging pressure for friction time of 10 sec and forging time of 8 sec by using nickel interlayer. The optical surface photograph taken from the weld zone of S2 sample was shown in Fig. 3. When the optical surface photograph of S2 sample was analysed, on the AISI

1030 side, a larger heat affected zone (HAZ) was formed while on the HCWCI side, there was a narrow HAZ near the weld zone.

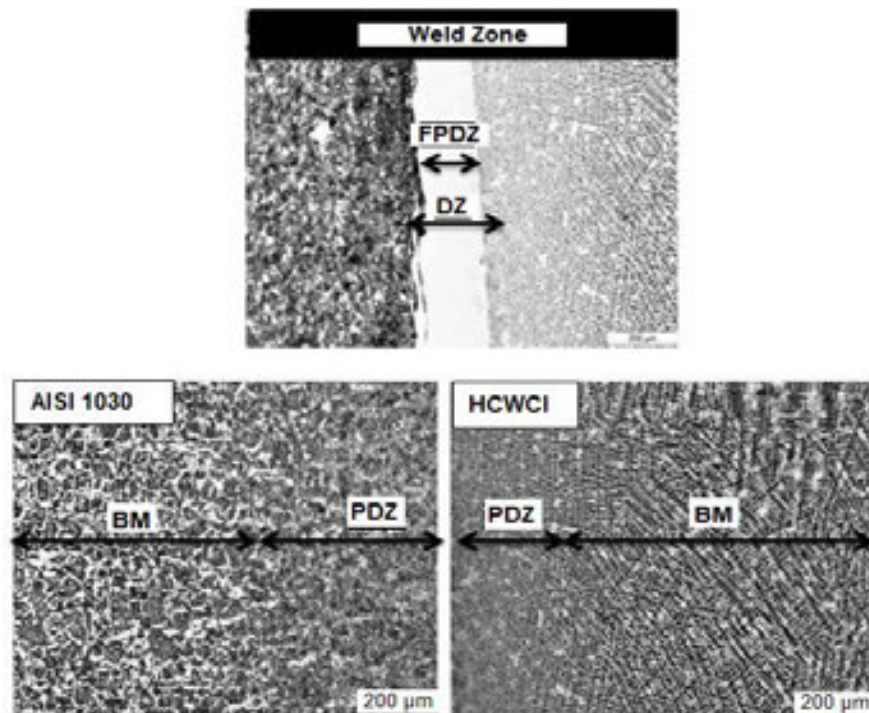


Figure 3. Optical photograph of S2 sample.

The weld joints were produced with 1600 rpm rotational speed, under 80 MP friction pressure and 150 MPa forging pressure for friction time of 12 sec and forging time of 8 sec by using nickel interlayer. Optical surface photograph taken from the weld zone of S3 sample was shown in Figure 4. When the optical surface photograph of S3 sample was observed, it was shown that the thickness of the nickel used as the interlayer became thinner due to the increased friction time.

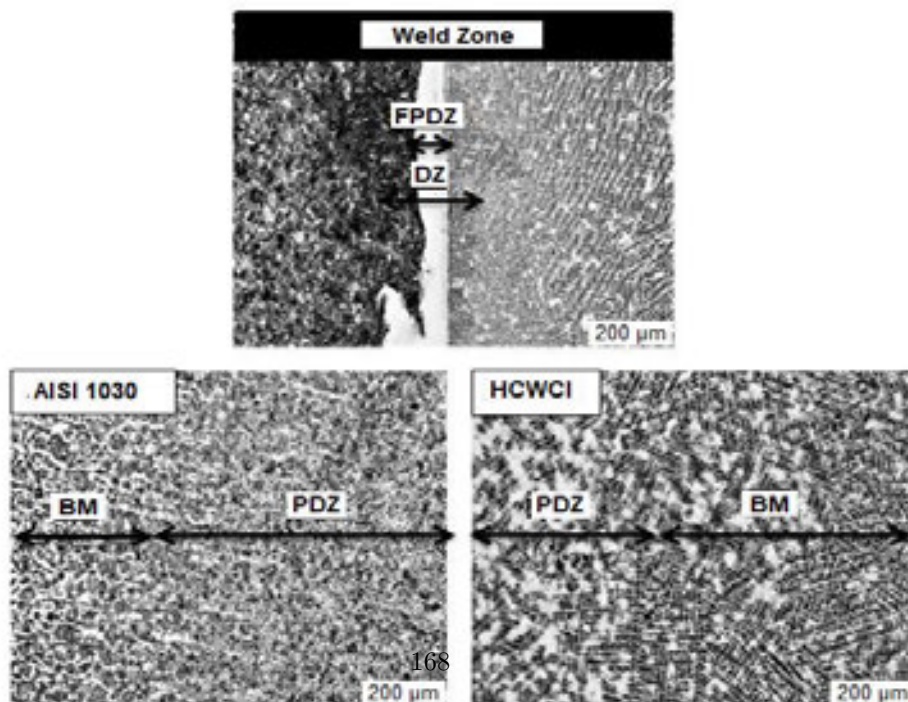


Figure 4. Optical photograph of S3 sample.

3.2. Microhardness Results

The microhardness test graph of S1, S2 and S3 samples was given in Fig. 5. When microhardness graph was examined, it was observed that the microhardness in the weld zone increased positively due to the increased friction time (8, 10 and 12 sec). Depending on the increased friction time, more heat input occurred and thus the weld zone reached higher temperatures. As a result, the rate of supercooling that occurred at higher temperatures had a significant effect on the microhardness.

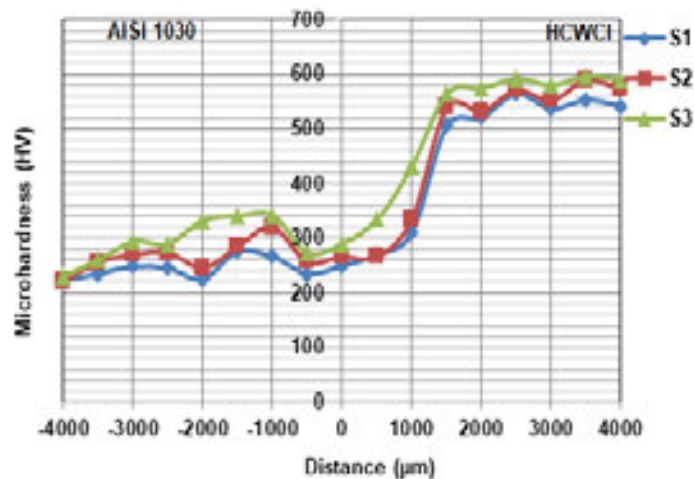


Figure 5. Microhardness - distance graphs of S1, S2 and S3 samples.

3.3. Tensile Test Results

The weld joints were produced with 1600 rpm rotational speed, under 80 MP friction pressure and 150 MPa forging pressure for a friction time of 8, 10 and 12 sec and forging time of 8 by using nickel interlayer. After tensile test, macro image of S1, S2 and S3 weld joints was given in Fig. 6. The maximum tensile values of S1, S2 and S3 weld joints were measured as 225, 236 and 264 MPa depending on the increasing friction time respectively. After the tensile test, the fracture of S1, S2 and S3 weld joints occurred in the weld zones without neck so fracture type can be described as brittle fracture.



Figure 6. Overview of S1, S2 and S3 samples after tensile test.

4. Conclusion

In this study, HCWCI and AISI 1030 steel were welded with 1600 rpm rotational speed, under 80 MP friction pressure and 150 MPa forging pressure for friction time of 8, 10 and 12 sec and forging time of 8 sec by using nickel interlayer. The following results were obtained.

1. There was no any cracks, gaps and unconnected zone on all weld joints.
2. The S1, S2 and S3 samples were divided into three zones; fully plastic deformed zone (PFDZ), the deformed zone (DZ), the partially deformed zone and base material (BM).
3. The hardness increments were found to be higher in the weld zones for S1, S2 and S3 samples. The rate of supercooling that occurred at higher temperatures had a significant effect on the microhardness.
4. The maximum tensile values of S1, S2 and S3 samples were measured as 225, 236 and 264 MPa depending on the increasing friction time respectively.

5. Acknowledgement

This study supported with the Project no. MÜFYL/2016-0002 by Adiyaman University, Scientific Researches Unit. The authors present endless thanks to Adiyaman University, Scientific Researches Unit provided financial support.

6. References

- [1] L.E. Doyle, J.L. Morris, J:L. Leach, G.F. Schrader: Manufacturing Processes and Metarials for Engineering, Prentice Hall Inc, USA, (1962).
- [2] A. Ertuğ: Sürtünme Kaynağı, Mühendis ve Makine Dergisi, 21 (1997), pp. 46-54.
- [3] H. Ateş, A. Kurt, M. Turker: Sürtünme Kaynağı, Kaynak Teknolojisi II. Ulusal Kongresi Bildiriler kitabı, TMMOB makine mühendisliği odası yayinevi, Ankara (1999).
- [4] K. Weman: Welding Processes Handbook, 2nd. Edition, Woodhead Publishing, USA, (2011).
- [5] H. Gurunauer, M.Y. Gürleyik: Döküm Parçaların Sürtünme Kaynağı, Mühendislik ve Makine Dergisi, 30 (2011), pp.357.
- [6] H. Kreye: Melting Phenomena in Solid State Welding Processes, Welding Journal, 56 (1977), pp. 154-158.
- [7] F.D. Duffin, A.S. Bahrani: Frictional Behavior of Mild Steel in Friction Welding, Wear, 26 (1973), pp. 53-74.
- [8] M. Rao, T.H. Hazlett: A Study of the Mechanisms Involved in Friction Welding of Aluminum Alloys, Welding Journal, 49 (1970), pp. 181-188.
- [9] G. Gürgenli, M. Onur, H. Aydın, H.E. Akata: Laboratuvar Tipi Basınçlı Hava Beslemeli Sürtünme Kaynak Tesisatı Geliştirilmesi Üzerine Bir Çalışma, İstanbul Aydın Üniversitesi Dergisi, 4 (2012), pp. 51-60.
- [10] J.J. Healy, D.J. McMullan, A.S. Bahrani: Analysis of Frictional Phenomena in Friction Welding of Mild Steel, Wear, 37 (1976), pp. 265-278.
- [11] A. Francis, R.E. Craine: A Model for Frictioning Stage in Friction Welding of Thin Tubes, International Journal of Heat and Mass Transfer, 28 (1985), pp. 1747-1755.

[12] T. Teker, S.O. Yılmaz and E.M. Karakurt: Effect of Different Rotational Speeds on Mechanical and Metallurgical Properties of Friction Welded Dissimilar Steels, *Materials Testing For Joining Applications*, 60 (2018), pp. 132-141.

SHORT BIOGRAPHIES

Assoc. Prof. Dr. Tanju Teker, born in 1971, is working in the Metallurgy and Materials Engineering Department, Engineering Faculty, Adiyaman University, Adiyaman Turkey. He graduated in Metallurgy Education from Gazi University, Ankara, Turkey, in 1997. He received his MSc and PhD degrees from Firat University, Elazig, Turkey in 2004 and 2010, respectively. His research interests include metal coating techniques, fusion welding method, solid state welding method and materials.

Res. As. Eyyüp Murat Karakurt, born in 1988, graduated from the Materials Science Engineering Department, Faculty of Engineering, Gebze High Technology University, Kocaeli, Turkey in 2011. He is working in the Metallurgy and Materials Engineering Department, Engineering Faculty, Adiyaman University Adiyaman, Turkey. His research interests are boronizing and welding.

THE INVESTIGATION OF MICROSTRUCTURE OF BINARY IRON NIOBIUM ALLOY COATING BY PACK BORONIZING METHOD

^aTanju TEKER, ^bEyyüp Murat KARAKURT

^{a, b} University of Adiyaman, Faculty of Engineering, Department of Materials Engineering, 02040, Adiyaman, Turkey.

teker@adiyaman.edu.tr and ekarakurt@adiyaman.edu.tr

Abstract

In this study, binary Fe-1Nb (at.%) alloy was boronized at 950, 1050 and 1150 °C different process temperatures for 3 hours by pack boronizing method. Effect of the increasing process temperature on the formation of boron layer was investigated experimentally. After boronizing treatment, microstructural changes occurring on the surfaces of the samples were examined by Scanning Electron Microscopy (SEM), Energy Dispersive Spectrometry (EDS), X-Ray Diffraction (XRD). It was observed that depending on the increased process temperatures, the pores in the boron layer increased and intensity of the Fe₂B phase decreased while the intensity of the FeB phase increased.

Key Words: Binary alloy, Pack boronizing, Boron layer, SEM, EDS, XRD.

1. Introduction

Boronizing which is surface treatment has a long history. Surface hardening process with boron diffusion in steels was first made by Moissan in 1895. Studies on boronizing surface treatment have accelerated since the 1970s. Today, boronizing is technologically advanced and is an alternative surface hardening method. In conventional surface hardening processes such as nitriding, carburization, etc., a surface hardness of 600-1100 HV is obtained while in the boron surface hardening (boronizing), very low friction coefficients are obtained besides 1500-2000 HV hardness. The boronizing is to get compounds such as Fe₂B and/or FeB by boron diffusion at the surface of the steel materials at high temperature. In industrial applications, single-phase boron layers consisting of Fe₂B are preferred because they are both less brittle and allow post-boron heat treatments. Industrial boronizing are successfully applied to steel, cast iron, nickel, cobalt, titanium, iron based and nonferrous metals by using any of the solid, liquid, gas or plasma media at 900-1150 °C for 2-12 hours. In the thermochemical surface hardening method, boron atoms thermochemically diffused to the metal surface in order to form a hard boron layer. The boron layer formed on the steel surface has got high hardness values and excellent resistant to abrasion and corrosion. The formation of the boron layer depends on the properties of the boronizing temperature, the processing time and the material. Boronizing treatment can be applied in different mediums as solid, liquid and plasma. Boronizing in the solid state is advantageous. Since this method is possible to get a smooth coating surface, the use of this method does not require surface cleaning processes. Therefore, boronizing in solid state is

preferred both in terms of application and smoothness; when the workpiece is removed from the powder, there is no adhesion of foreign matter to the surface of the workpiece.

In this study, binary Fe-1Nb (at.%) alloy was boronized at 950, 1050 and 1150 °C different process temperatures for 3 hours by pack boronizing method. Effect of the increasing process temperature on the formation of boron layer was investigated experimentally.

2. Experimental

Pure wt.% 99.97 iron and wt.% 99.98 niobium metal supplied commercially were prepared to be binary Fe-1Nb (at.%) alloy with dimensions of 80×10×10 mm. Binary Fe-Nb alloy manually were cut into 4 mm slices. The surfaces of samples were grinded by 80-1200 mesh SiC grinding paper and polished by 1-3 μm diamond paste to prepare for the boronizing treatment. As shown in Figure 1, samples placed in the pot were boronized at 950, 1050 and 1150 °C process temperature for 3 hours by Protherm furnace device. Elemental analyses of the samples were then performed by using a spectrometer device in order to determine the elementary content in the base metal was shown in the Table 1. The boronizing process parameters were showed in Table 2.

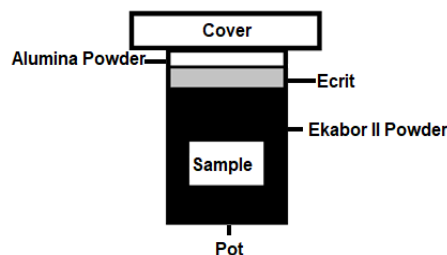


Figure 1. Arrangement of the samples in the pot.

Table 1. The chemical components of materials used in experiments (wt.%).

Base Metal (at.%)	Chemical Composition (wt.%)								
	Fe	Nb	C	Mn	Si	Ti	Cr	Ni	Others
Fe-1Nb	96.56	2.59	0.03	0.07	0.02	0.02	0.01	0.04	0.66

Table 2. Boronizing parameters.

Sample No	Base Metal (at.%)	Process Temperature (°C)	Process Time (hour)
S1	Fe-1Nb	950	3
S2	Fe-1Nb	1050	3
S3	Fe-1Nb	1150	3

After boronizing treatment, S1, S2 and S3 samples manually were cut into the middle. Interfaces of samples were grinded by 200-1200 mesh SiC grinding paper and then, polished by 1-3 μm diamond paste. Samples were chemically etched with a solution having 98% alcohol + 2% HNO₃ at 5-10 sec, Structural changes in the cross-sectional surfaces were analyzed by a using scanning electron microscope (SEM) (Zeiss EVO LS10) and energy dispersive spectrometry (EDS). The phase compositions of the boron layers were confirmed by X-Ray Diffraction (Rigaku RadB-DMAX II) at 40 kV, 30 mA, Cu Kα radiation source, and scanning at 2θ=30-80° on the surfaces.

3. Results and Discussion

3.1. Microstructural and Chemical Characterization Results

S1, S2 and S3 samples were boronized at the 950, 1050 and 1150 °C different process temperatures and for 3 hours process time. SEM micrograph taken from cross-sectional surfaces of S1 sample was shown in Fig. 2. When the SEM micrograph of S1 sample was examined, it was determined that the boron layer of S1 sample did not have a homogeneous penetration in the base metal.

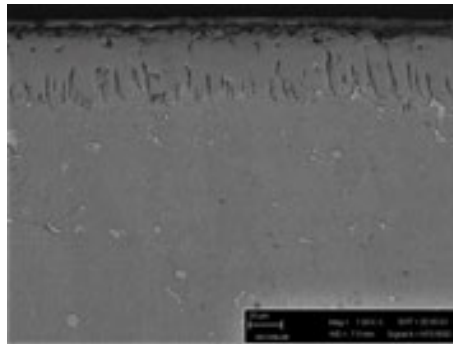


Figure 2. SEM micrograph of S1 sample.

SEM micrograph taken from cross-sectional surfaces of S2 sample was shown in Fig. 3. When the SEM micrograph of S2 sample was analyzed, it was shown that due to the increased process temperature, the amount of porosity increased at the surface of the boron layer and near the surface. In particular, the most prominent feature of this structure was seen in S2 sample having a boronizing temperature of 1050 °C.

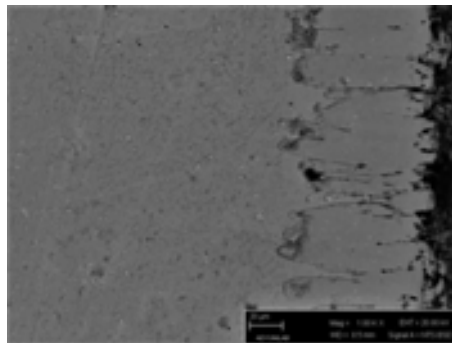


Figure 3. SEM micrograph of S2 sample.

SEM micrograph taken from cross-sectional surfaces of S3 sample was shown in Fig. 4. When the SEM micrograph of S3 sample was investigated, it was seen that a clear coating was not observed on the S3 sample because the boronizing temperature at the 1150 °C corrupted the chemical structure of boron powder and surface property of S3 sample.

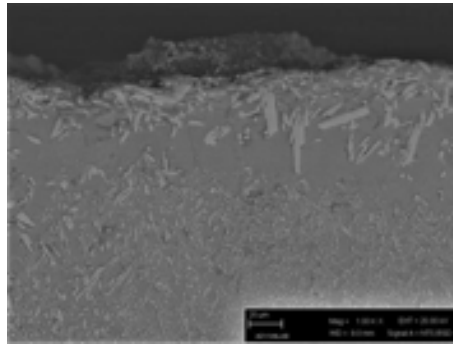


Figure 4. SEM micrograph of S3 sample.

The EDS analysis taken from cross-sectional surface of S1 sample was shown in Fig. 5. From the EDS analysis, it was understood that; boron atoms had a certain penetration on the surface of binary Fe-1Nb alloy. When moved further from the boron layer, the penetration of boron atoms decreased in base metal.

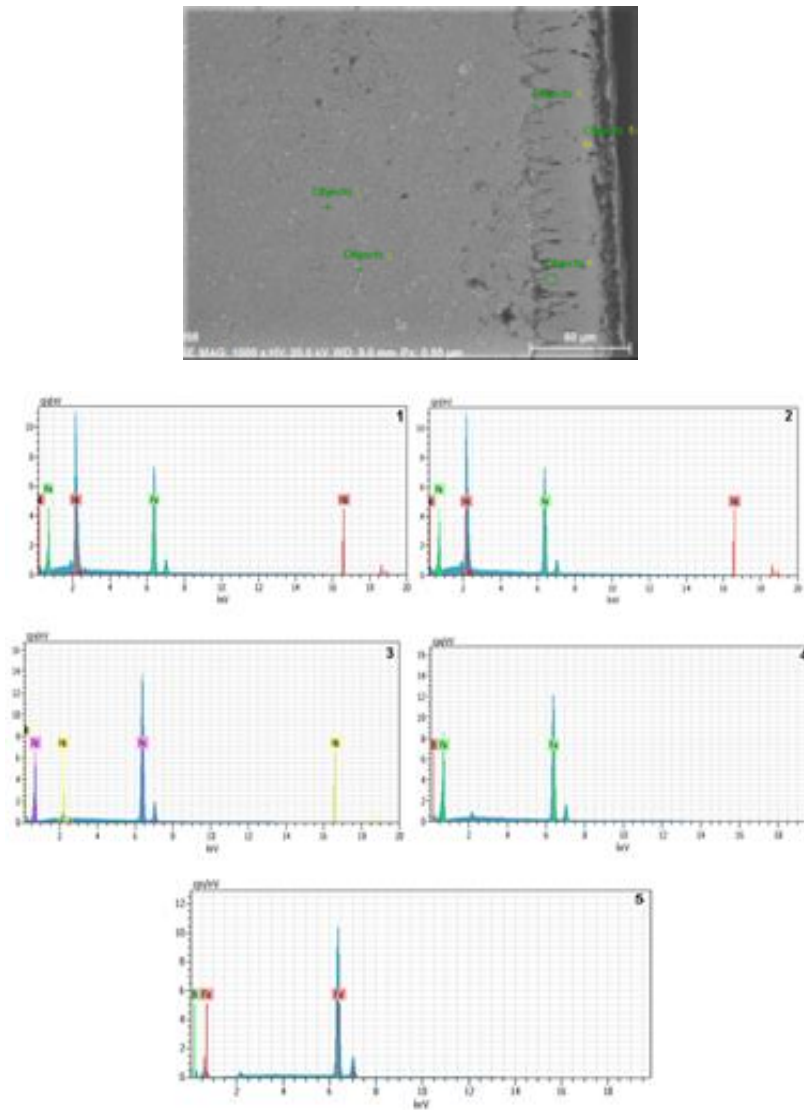


Figure 5. SEM micrographs of EDS analysis points of S1 sample.

3.2. X-Ray Analysis Results

X-ray diffraction analysis of S1, S2 and S3 samples was shown in the Fig. 6. The FeB with high boron concentration and Fe₂B with low boron concentration were determined as the main phases on the surfaces of S1, S2 and S3 samples. When XRD analysis results were evaluated, it was generally found that depending on the increased process temperatures, the intensity of the Fe₂B phase decreased while the intensity of the FeB phase increased.

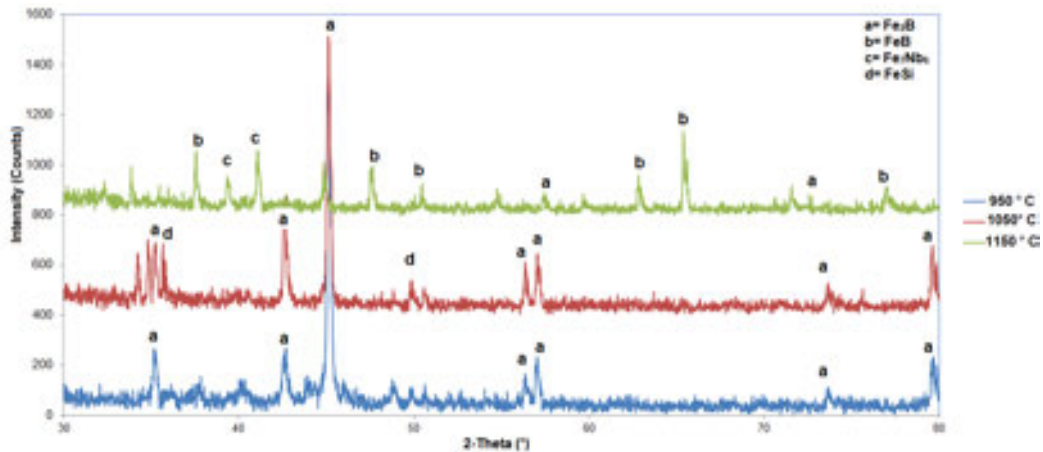


Figure 6. XRD patterns for S1, S2 and S3 samples.

4. Conclusion

In this study, binary Fe-1Nb (at.%) alloy was boronized at 950, 1050 and 1150 °C different process temperatures for 3 hours by pack boronizing method. Effect of the increased process temperatures on the formation of boron layer was investigated experimentally. The following results were obtained.

1. The boron layers of all samples did not have homogeneous penetration in the base metal.
2. Boron atoms had a certain penetration on the surface of binary Fe-1Nb (at. %) alloys. When moved further from the boron layer, the penetration of boron atoms decreased in base metal.
3. Depending on the increased process temperature, the intensity of the Fe₂B phase decreased while the intensity of the FeB phase increased.

5. Acknowledgement

This study supported with the Project no. MÜFMAP/2015-0007 by Adıyaman University, Scientific Researches Unit. The authors present endless thanks to Adıyaman University, Scientific Researches Unit provided financial support.

6. References

- [1] A.K. Sinha: Boriding (boronizing) ASM Handbook Of Heat Treating, ASM International, Materials Park, USA, (1991).
- [2] W. Fichtl: Boronizing And Its Practical Applications, Material Science and Engineering, 2 (1981), pp. 276-286.

- [3] T. Lampe, S. Eisenberg, E. Rodriguez Cabeo: Plasma Surface Engineering In The Automotive Industry-Trends And Future Prospectives, Surface Coating Technology, 174 (2003), pp. 1-7.
- [4] Y. Gencer: Influence Of Manganese On Pack Boriding Behaviour Of Pure Iron, Surface Coating Technology, 27 (2011), pp. 634-638.
- [5] K.H. Habig: Wear Protection Of Steels By Boriding, Vanadizing, Nitriding, Carburising, And Hardening, Material Science and Engineering, 2 (1980), pp. 83-92.
- [6] M. Tarakçı, Y. Gencer, Y. Azaklı and U. Şahintürk: Surface Modification Of Fe-8Si Alloy By Boronizing And Its Characterization, Journal Faculty Engineering Architect of Gazi University, 28 (2013), pp. 645-655.
- [7] S. O. Yilmaz, T. Teker, S. Karataş: Wear Behavior Of Iron Boride Coating On AISI 4140, Protection of Metals and Physical Chemistry of Surfaces, 52 (2016), pp. 119-127.
- [8] P. Geoeuriot, R. Fillet, F. Thevenot, J.H. Driver, H. Bruyas: The influence Of Alloying Element Additions On The Boriding Of Steels, Material Science and Engineering, 55 (1982), pp. 9-19.
- [9] M. Blazon, B. Stanojevic, V. Veljkovic: Effect Of Alloying Elements On The Formation Of Boride Layer On Steel, Scripta Materialia, 19 (1975), pp. 1153- 1156.

SHORT BIOGRAPHIES

Assoc. Prof. Dr. Tanju Teker, born in 1971, is working in the Metallurgy and Materials Engineering Department, Engineering Faculty, Adiyaman University, Adiyaman, Turkey. He graduated in Metallurgy Education from Gazi University, Ankara, Turkey, in 1997. He received his MSc and PhD degrees from Firat University, Elazig, Turkey in 2004 and 2010, respectively. His research interests include metal coating techniques, fusion and solid state welding methods and materials.

Res. As. Eyyüp Murat Karakurt, born in 1988, graduated from the Materials Science Engineering Department, Faculty of Engineering, Gebze High Technology University, Kocaeli, Turkey in 2011. He is working in the Metallurgy and Materials Engineering Department, Engineering Faculty, Adiyaman University, Adiyaman, Turkey. His research interests are boronizing and welding.

Surface properties of FeCrC alloy coating produced by powder feeding GTA cladding on AISI1040 steel

¹S. Osman YILMAZ, ²Tanju TEKER, ³Savaş DALMIŞ

^{1,3}University of Namık Kemal, Faculty of Engineering, Department of Machine Engineering, 59500, Çorlu-Tekirdağ, Turkey.

²University of Adiyaman, Faculty of Engineering, Department of Materials Engineering, 02040, Adiyaman, Turkey.

Abstract

In this study, FeCrC alloys were used for cladding on AISI 1040 steel substrate by using gas tungsten arc processing. Microstructural observations of the coated layers were examined by optic microscopy, X-ray diffraction and microhardness test. The obtained results indicated that there was a similar microstructure in the all clad layers. The adhesion of the clad layers to the base metal was very good and quite dense. The formation of FeCrC, Cr₇C₃, CrFe₄ was determined in the microstructure. High hardness up to 1550 HV was improved due to the volume fraction of carbides phases. Therefore, it is expected that these new classes of hardfacing alloys will be advantageous for applications requiring high wear resistance and high impact.

Key words: AISI 1040, GTA, FeCrC, Coating.

1. Introduction

Surface coatings are widely used to increase wear resistance of materials. Many studies have took up the features of the coating layers and benefited from them under appropriate conditions. Such research has taken into account the coating process, the base metal, the composition of the coating materials and the coating layer microstructure [1-7]. Various hard materials have been utilized to increase the abrasive resistance of the coating layers. Steels have an important role in many applications; However, surface coatings are an useful technic to enhance abrasive performance of steel. By providing a hard protective surface layer, the abrasion resistance of the surfaces on existing industrial parts, devices and machines forms the basis for hardfacing coating. This approach to the application of advanced protective metallurgical bonded thick cladds leads to the development of performance materials because a relatively low cost substrate can be utilized by the hardfacing cladding method. [8-12].

The large amount of carbide phase has excellent abrasion resistance. High chromium iron has good wear resistance and is widely utilized as a hard coating material in the mineral and mining industries. Due to the relatively low prices in conventional temperatures, Fe-Cr-C based hardfacing materials are used. Hardfacing¹⁷⁸ materials which commercially manufactured

have 3-5.5% carbon ratio in the alloys. M_7C_3 carbides with high Cr contents can only be found both second and next layers. The microstructures having M_7C_3 primary carbides at higher C concentrations have a good wear resistance [13-16].

This study aims a pure elemental powder mixtures FeCrC coating layer to examine the microstructure of the interface and crystallographic orientations.

2. Experimental Procedures

FeCrC alloy powder with the particle size of 75-150 μm was used in the present study. The powder composition was 64wt%Cr-6.2wt%C-0.02wt%S-0.03wt%P-1.5wt%Si with small contents in Fe balance (Table 1). AISI 1040 steel having a size of 100x30x10 mm was used as base metal in the GTA processing. The operating principle of GTA (Lincoln Invertec V205-T AC/DC) welding systems were schematically shown in Fig. 1. Welding device can make single axle, 300 mm constant advance motion in both directions. Speed control of the system motor is provided by an inverter located on the inverter. The process parameters used in experimental studies are listed in Table 2.

Table 1. Chemical composition of the powders (wt.%).

Alloy	Fe	Cr	Si	S	C	P
FeCrC	Bal.	64	1.5	0.02	6.2	0.03

Table 2. The process parameters used in experimental studies.

Powder and Dimensions (μm)	Current Intensity (A)	Welding Speed (mm/min.)	Gas Flow Rate (l/min.)
FeCrC	S1	100	14
	S2	110	14
	S3	120	14
	S4	130	14
	S5	140	14

The samples were prepared by grinding, polishing and etched with a solution having 2 wt.% NHO_3 + 98 wt.% Ethanol. The surface and cross-sectional morphologies of samples were observed by optical microscope device (LEICA DM750). The phase and compounds of the cladded surfaces were confirmed by X-Ray Diffraction (BRUKER D8 advance X-Ray diffractometer at 40 kV, 30 mA and Cu $K\alpha$ radiation source). The microhardness test analysis was used with HV hardness scale under 200 g loads at 0.5 μm intervals by QNESS Q10 test device.

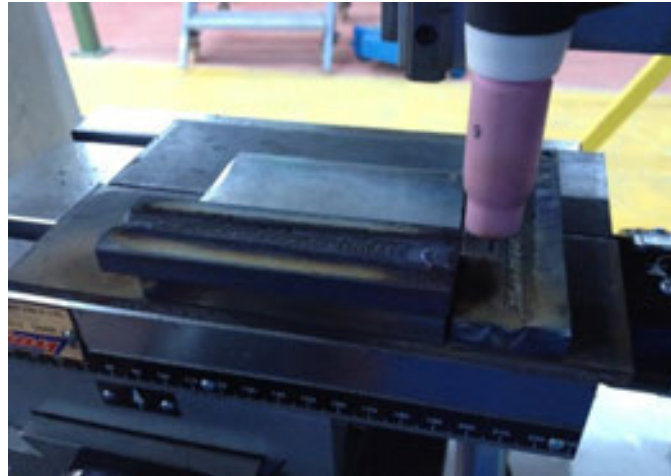


Figure 1. The operating principle of GTA welding systems.

3. Results and Discussion

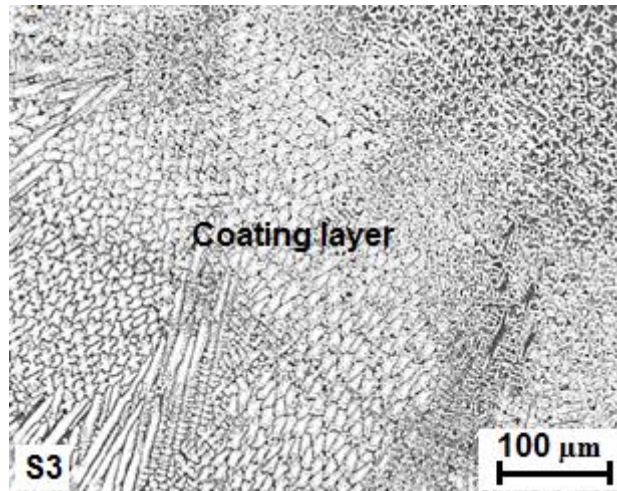
3.1. Metallurgical analysis

Surface and interface macrographs of S3 sample FeCrC based composite clad layer are given in Fig. 2. As can be shown in the figures, the widths of cladded surface of the S1-S5 samples are almost S1=5, S2=5.2, S3=5.4, S4= 5.7 and S5=6 mm. and the penetration depth of the samples are S1=1.7 S2= 1.9 S3= 2.4, S4= 2.6 and S5= 2.9 mm.

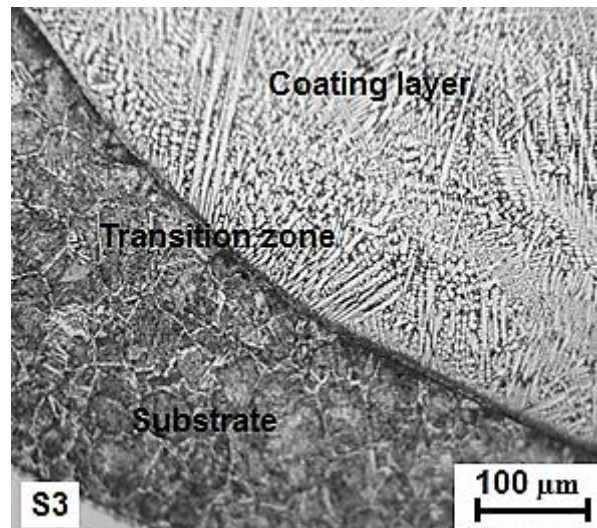


Figure 2. Macrographs of S3 sample FeCrC based composite coating.

Fig. 3 shows the optic micrographs of S3 sample FeCrC based composite clad layer. Three zones, being clad layer, HAZ and base metal, are identified on the cladded surfaces. As a result of the microstructural examinations, it has been determined that the main phase is face-centered cubic (fcc) austenite (γ) in case of minor phase's being M_7C_3 (M=Cr,Fe) carbide. The findings acquired are completely consistent with the typical concentrations of Fe, C and Cr in alloys generating austenite and M_7C_3 phases. The phases acquired in the GTA processed FeCrC clad layers are significant due to the similarity of the solidification mechanisms of the ternary Fe-Cr-C alloy system to the presented ones [11].



(a)



(b)

Figure 3. OM micrographs of FeCrC based S3 composite coating.
a) Coating layer, b) Transition zone.

In case of the combination of comparatively high power densities and particular energies with adequately low powder feed rates, melting of the base metal and the hypoeutectic formation are supported. Nevertheless, the decreased specific energy and power densities and the increased rate of powder feed determine the melting of the base metal and the emergence of hypereutectic microstructures. Lower specific energies and rapid solidification rates are caused by higher process rates, as a conclusion which microstructural grain refinement at the thickness of clad layer occurs. Chemical distribution is influenced by the volume of molten pool and base metal. Therefore, the presence of hypoeutectic or hyper-eutectic microstructures influencing crystal structures, in the microstructure of clad layers depends on the processing parameters, which have an effect on the relative amounts of the molten metal

from the base metal and the clad layers. Basically, the absorption of the heat input provided by the electrode takes place in the alloy powder mixture. Fig. 4 presents the findings of the XRD analyses of base metal and the clad layer of sample S3. It is clearly indicated that mainly FeCrC, Cr₇C₃, CrFe₄ constitute the coating layer.

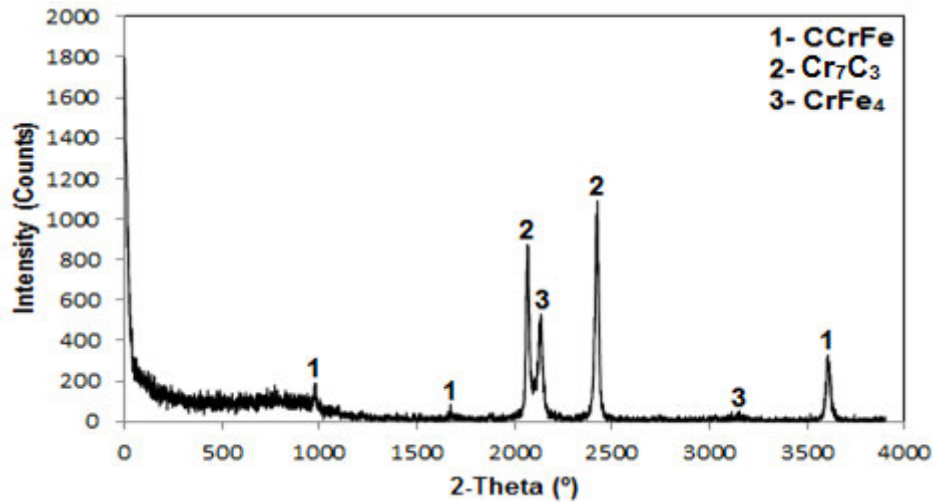


Figure 4. X-ray diffraction for S3 sample.

3.2. Hardness Analysis

Microhardness curves in the cross-section of the clad layers are given in Fig. 5. The hardness of clad layer changes values between 200 and 1550 HV, according to process parameters and the concentration of cladding powder. The hardness results are examined, the increasing in the heat input lead to melting of the AISI 1040 steel base metal and increases total thickness and width of clad layer but it reduces width of the clad layer thickness and average hardness values. The hardness values show that the significant surface hardening is performed by the GTA technic. Deep exchange of the clad layer hardness in the case of low process speed refers to coarsening of the microstructure produced, as shown in Fig. 5. Due to the fact that ferrite (α), austenite (γ), and M₃C carbides are much more softer M₇C₃ carbides cladding of GTA processing has higher hardness values than conventional methods [11-15].

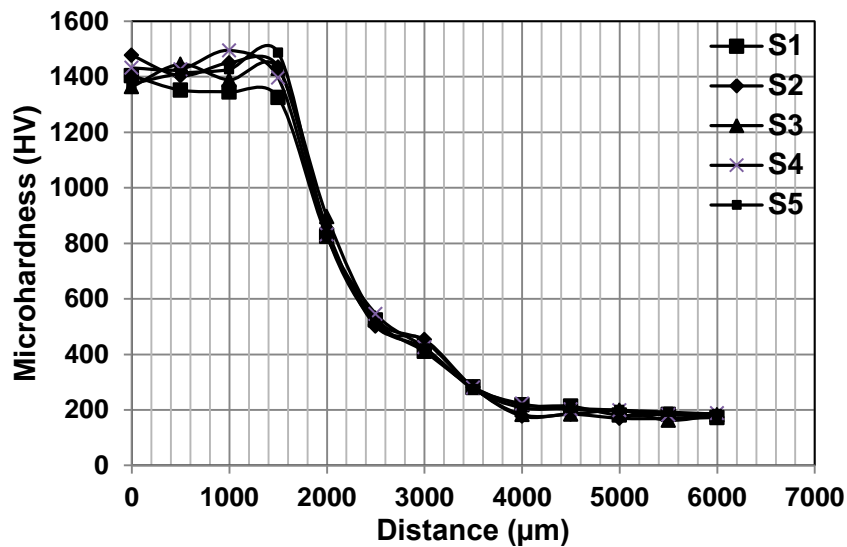


Figure 5. Microhardness curves of FeCrC based S1-S5 composite coatings.

4. Conclusion

In this study, FeCrC alloy were used to coating on AISI1040 steel base metal by GTA processing. The knowledge obtained can be summarized in the following points:

- 1) The higher heat input led to larger carbide sizes in the samples.
- 2) The microstructures of the coated surface have shown that the hypereutectic samples have the coarsest structure depending on the amount of heat input.
- 3) There are lower hardness values in hypoeutectic microstructures due to the fact that primary dendrites and the low concentration of Cr and C have the austenite phase.
- 4) The hardness of hyperreactive hardness improves by increasing rates of MC and M_7C_3 carbide phases.
- 5) The increase in hardness will take place if more M_7C_3 carbides are contained in the hypereutectic microstructures in the eutectic, as well as the primary phase.

References

- [1] D.J. Branagan, M.C. Marshall, B.E. Meacham: High toughness high hardness iron based PTAW weld materials, *Materials Science and Engineering A*, 428 (2006), pp. 116-123.
- [2] Y.C. Lin, S.W. Wang: Wear behavior of ceramic powder cladding on an S50C steel surface, *Tribology International*, 36 (2003), pp. 1-9.
- [3] J. Choi, S.K. Choudhuri, J. Mazumder: Role of preheating and specific energy input on the evolution of microstructure and wear properties of laser clad Fe-Cr-C-W alloys, *Journal of Materials Science*, 35 (2000), pp. 3213-3219. 183

- [4] N. Abe, J. Morimoto, M. Tomie, C. Doi: Formation of WC-Co layers by an electron beam cladding method and evaluation of the layer properties, *Vacuum*, 59 (2000), pp. 373-380.
- [5] W. Lu, D. Zhang, X. Zhang, R. Wu, T. Sakata, H. Mori: HREM study of TiB/Ti interfaces in a Ti-TiB-TiC in situ composite, *Scripta Materialia*, 44 (2001), pp. 1069-1075.
- [6] K.L. Wang, Q.B. Zhang, M.L. Sun, X.G. Wei, Y.M. Zhu: Rare earth elements modification of laser-clad nickel-based alloy coatings, *Applied Surface Science*, 174 (2001), pp. 191-200.
- [7] T. Teker, S. Karataş, S.O. Yılmaz: Microstructure and wear properties of FeCrC, FeW and FeTi modified iron based alloy coating deposited by PTA process on AISI 430 steel, *Archives and Metallurgy*, 59 (2014), pp. 925-933.
- [8] J. Nurminen, J. Näkki, P. Vuoristo: Microstructure and properties of hard and wear resistant MMC coatings deposited by laser cladding, *International Journal of Refractory Metals and Hard Materials*, 2 (2009), pp. 472-478.
- [9] J. Xie, N. Chen, J. Shen, L. Teng, S. Seetharaman: Atomistic study on the structure and thermodynamic properties of Cr₇C₃, Mn₇C₃, Fe₇C₃, *Acta Materialia*, 53 (2005), pp. 2727-2732.
- [10] A. Liu, M. Guo, H. Hu, Z. Li: Microstructure of Cr₃C₂-reinforced surface metal matrix composite produced by gas tungsten arc melt injection, *Scripta Materialia*, 59 (2008), pp. 231-234.
- [11] X. Liu, Y. Gu: Plasma jet clad-Cr₃C₂ composite coating on steel, *Materials Letters*, 60 (2006), pp. 577-580.
- [12] X. Liu, H. Wang: Microstructure and tribological properties of laser clad /Cr₇C₃/TiC composite coatings on -TiAl intermetallic alloy, *Wear*, 262 (2007), pp. 514-521.
- [13] J. Asensio, J.A. Pero-Sanz, J.I. Verdeja: Microstructure selection criteria for cast irons with more than 10 wt.% chromium for wear application, *Materials Characterization*, 49 (2003), pp. 83-93.
- [14] M.F. Buchely, J.C. L.M. Gutierrez León, A.Toro: The effect of microstructure on abrasive wear of hardfacing alloys, *Wear*, 259 (2005), pp. 52-61.
- [15] P.L. Shan, O. Kwon, T. Kim, K. Kim: Microstructure and wear property of Fe-MnCr-Mo-V alloy cladding by submerged arc welding. *Journal of Material Processing Technology*, 147 (2004), pp. 191-196.

[16] E.O. Correa, N.G. Alcântara, D.G. Tecco, R.V. Kumar: The relationship between the microstructure and abrasive resistance of a hardfacing alloy in the Fe-Cr-CNb-V system, Metallurgical and Materials Transaction A, 38 (2007), pp. 1671-1680.

CORRESPONDENCE ADDRESS:

Tanju TEKER

University of Adiyaman, Faculty of Engineering, Department of Materials Engineering,
02040, Adiyaman, Turkey.

E-mail address: tteker@adiyaman.edu.tr

Tel.: +90 416 2233800

SHORT BIOGRAPHIES

Tanju TEKER

Assoc. Prof. Dr. Tanju Teker, born in 1971, is working in the Metallurgy and Materials Engineering Department, Engineering Faculty, Adiyaman University, Adiyaman Turkey. He graduated in Metallurgy Education from Gazi University, Ankara, Turkey, in 1997. He received his MSc and PhD degrees from Firat University, Elazig, Turkey in 2004 and 2010, respectively. His research interests include metal coating techniques, fusion welding method, solid state welding method and materials.

S. Osman YILMAZ

Prof. Dr. S. Osman Yilmaz, born in 1966, is Professor at the University of Namık Kemal, Corlu, Tekirdağ in Turkey. He received his BSc from the Metallurgy and Materials Engineering Department, Faculty of Engineering, University of METU, Ankara, Turkey, in 1989, his MSc from the Metallurgy Department of the Institute of Science and Technology, University of Firat, Elazığ, Turkey in 1992 and his PhD from the Metallurgy Department, Institute of Science and Technology, University of Firat, Elazığ, Turkey in 1998. His research interests include metal coating techniques, surface modification, welding, metallurgy and materials.

I. Savaş DALMIŞ

I. Savaş DALMIS, born in 1975, is Assist. Prof. Dr. at the University of Namık Kemal, Corlu, Tekirdağ in Turkey. He received his BSc from the Teacher Training in Machine Department, Faculty of Technical Education, University of Marmara, Istanbul, Turkey, in 1997, his MSc from the Agricultural Machinery of the Institute of Science, University of Trakya, Edirne,

Turkey in 2000 and his PhD from the Agricultural Machinery Department, Institute of Science, University of Trakya, Edirne, Turkey in 2006. His research interests include Machine design, mechatronics system design, manufacturing technologies, Cad/Cam systems, tool designs and welding technologies.

INFLUENCE OF DYNAMIC STRAIN AGEING ON MICROSTRUCTURAL AND MECHANICAL PROPERTIES OF AISI 316L AUSTENITIC STAINLESS STEEL WELD METAL

Guma Alnaji Muhamed^{1,a}, Süleyman Gündüz^{2,b}

¹Higher Institute of Engineering Professions / Department of Mechanical Engineering / Libya

²Affiliation of author(s): Technology Faculty / Department of Manufacturing Engineering C / Karabük

^a gumamohamed1966@yahoo.com, ^b sgunduz@karabuk.edu.tr

Abstract

In this paper, dynamic strain ageing (DSA) behaviour in weld metal of 316L austenitic stainless steel (ASS) is presented. Welding process was conducted using the MIG welding technique. Tensile test was performed on weld metal at $1 \times 10^{-3} \text{ s}^{-1}$ strain rate for the temperatures of 25-800°C to determine the influence of DSA on the microstructure and strength of investigated material. The change in mechanical properties was more noticeable at ageing temperature of 500°C and 600°C in which the weld metal showed serrated behavior. Optic and scanning electron microscopes (SEM) were used to analyse the microstructure and fracture surfaces of tested samples. Weld metal of 316L ASS showed DSA behavior which are examined in terms of microstructure and mechanical properties. Analysis of the results indicated that locking of the mobile dislocations by substitutional and interstitial atoms is responsible for the occurrence of DSA in 316L ASS.

Key Words: Stainless steel, Dynamic strain ageing, Welding, Weld metal.

1. Introduction

Stainless steels consisted of five main groups; ferritic, austenitic, martensitic, duplex and precipitation hardening. ASS among them are widely used in many engineering applications from cryogenic temperatures to the high temperatures. They contain Cr and N both of which increase the corrosion resistance. These steels present excellent combination of corrosion resistance, ductility, toughness and weldability [1]. 316 ASS and its modified grades such as 316L(N) have been used as structural material in nuclear power plants, heat exchangers and pipelines. This alloy shows excellent high temperature mechanical properties with good toughness and machinability. Most of the service failures occurs either in the HAZ or in the weld metal. High temperature mechanical properties of 316 and 316L(N) ASS welds and weld joints has received considerable attention in recent years [2,3]. A serious drawback to using such steels and their weldments is the degradation of corrosion and mechanical properties within certain high temperature due to the microstructural changes [4].

All welding operations involve a heat source that causes primary melting. Subsequent solidification should lead to the formation of an integral joint. Much of the heat is spread from the fusion zone to the adjacent solid zones. However the combined effect of heating and residual stress can cause dynamic strain ageing to occur [5]. DSA is an atomic scale phenomenon that involves the mobility of solute atoms and mobile dislocations, or both. It is considered to contribute to embrittlement by effectively increasing the dislocation density for a given strain. A high

dislocation density, the fact that many dislocations will be pinned by interstitial atoms and that bowed dislocations need higher stresses for unpinning, mean that the local yield stress in the region will be higher, the phenomenon is commonly known as DSA [6]. DSA is associated with serrations on the stress-strain curve during a tensile test at the loaded strain rate. Each stress drop on the stress-strain curve corresponds to the formation of a band. The formation of these different types of bands depends on external parameters (temperature, strain rate and strain level) and internal parameters (alloy composition, type and content of solute atoms and density of mobile dislocations) [7].

While certain aspects of DSA [8, 9] of 316L ASS at temperature range of 200-800°C have been addressed, no information on DSA behaviour of weld metal at low and intermediate temperature is available in the open literature. For this reason, it is necessary to analyse the influence of DSA on mechanical properties of ASS weld metal at higher temperatures. The present work is concern with an investigation of the effect of DSA on the tensile behaviour of 316L ASS weld metal. An examination of microstructural changes depending on testing temperatures was conducted with a view to understanding the features which can affect the mechanical properties of 316L ASS aged at elevated temperatures.

2. Experimental

In the present experimental work, 316L ASS and a welding wire (AS MIG 316LSi) with a diameter of 1.2 mm were used. Table 1 shows the steel and welding wire compositions by wt. % which are used for joining. Steel was obtained as plates in the form of 350x150x8 mm. The steel plates were welded longitudinally under argon gas using Fanuc Robotic Lincoln Electric brand MIG welding machine with a single pass through an V-groove configuration at 30°. Welding parameters used in the present experimental work are given in Table 2.

Table 1. Chemical compositions of 316L austenitic stainless steel and welding wire (wt. %).

Materials	C	Si	Mn	Ni	Cr	Mo	N	S	P
316L	0.024	0.38	1.30	10.10	16.57	2.03	0.041	0.004	0.029
Welding wire	0.03	0.85	1.70	12.5	18.5	2.75	-	0.003	0.0025

Table 2. The welding parameters used in the gas metal arc welding (GMAW).

Current (A)	Voltage (V)	Welding Speed (cm/min)	Gas Flow Rate (lt/min)	Heat Input (kj/mm)
240	23	35	14	0.95

Tensile test specimens were cut from the weld metal and manufactured according to standart E8 (5 mm diameter and 30 mm gauge length). Figure 1 shows welded steel plates, weld metal cut tensile plane and machined tensile test specimen. Tensile tests were performed at 1×10^{-3} strain rate and temperatures of 25-800°C. After each test, stress and strain diagrams were obtained to derive yield strength (YS, 0.2%), ultimate tensile strength (UTS), elongation (%) and workhardening index (n).

Microstructure and fracture surface analyses of weld metal were done by using optic microscope, SEM and EDS analyzer. A mixture of 1 % nitric acid, 10 % oxalic acid and 89 % distilled water solution was used for electrolytic etching at a potential of 15-20 V to observe microstructure of samples.

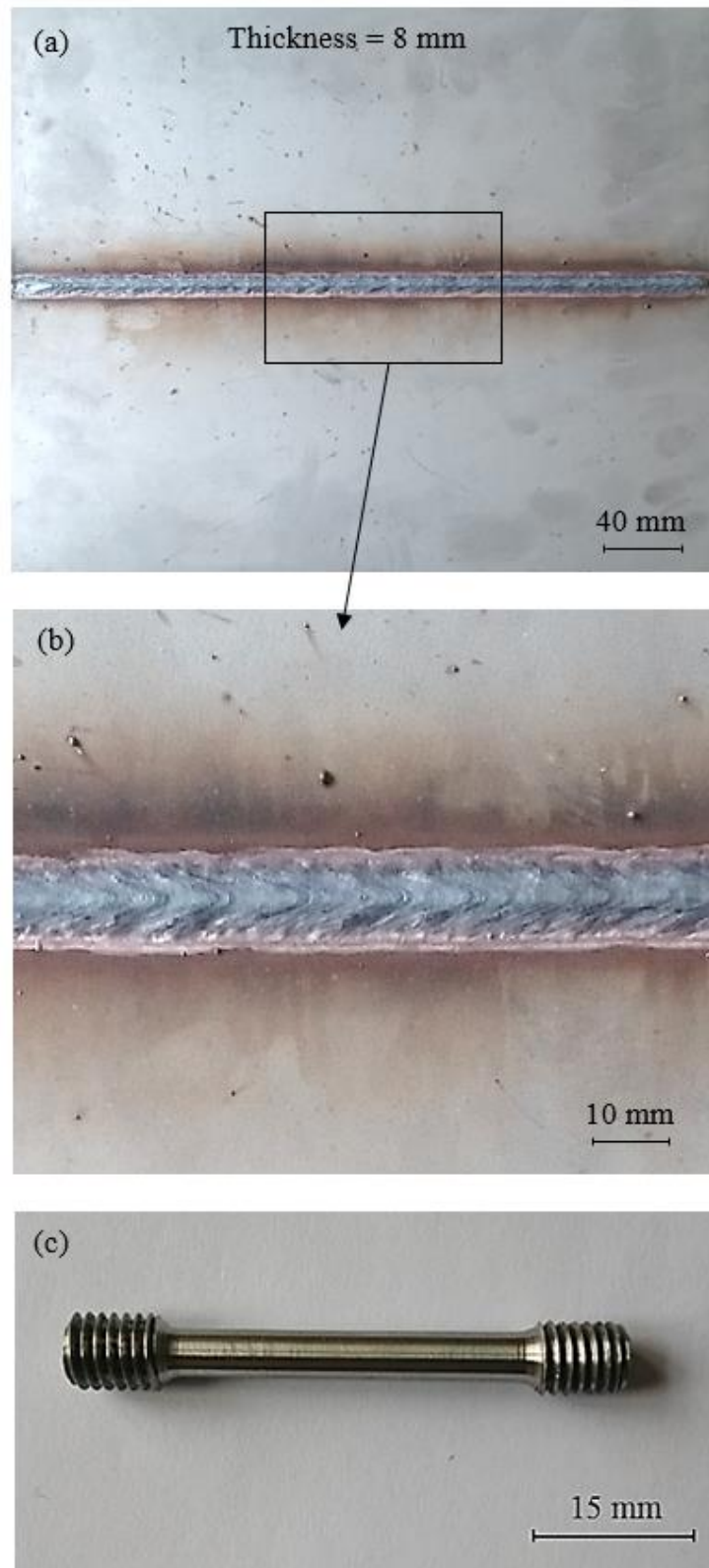


Figure 1. (a) Welded steel plates, (b) weld metal cut tensile plane and (c) tensile test specimen.

3. Results and Discussion

3.1. Microstructure

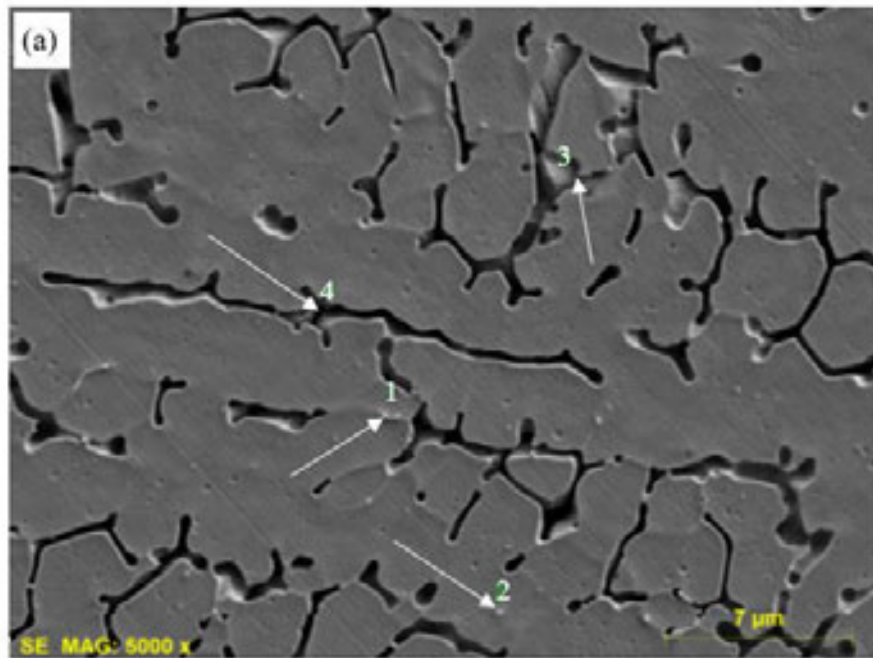
Figure 2a shows as-received metal microstructures of 316L ASS steel. As can be seen, the 316L ASS as-received metal is characterized by equiaxed austenite grains with a low delta ferrite which is more resistance to cracking compared to the a fully austenitic microstructure [10]. Weld metal microstructure obtained from 316L ASS steel tested at 25°C is also seen in Figure 2b. During the welding process, a solidification microstructure consisting of skeletal ferrite in large columnar austenite grains was observed in weld metal. The alignment of ferrite is along the heat flow direction due to incomplete primary $\delta \rightarrow \gamma$ transformation [11, 12]. The rapid cooling of the weld pool during welding process causes the formation of ferrite in the weld metal. Ferrite phase in weld metal increased due to rapid cooling after welding which prevented austenite phase transformation. This is consistent with earlier studies [13, 14]. Samples tested at 100-800°C showed similar weld metal microstructure consisted of austenite grains with skeletal ferrite.

In many applications, the ability to control the delta-ferrite content of stainless steel weld metal is important. For example, the ferrite number (FN) is often used as an indicator of the resistance to fissuring (hot tearing) that occurs in many of the 300-series stainless steels. Delta ferrite, rich in Cr and Mo, occurred during the welding of ASS is required up to a limit of about 4–5 ferrite number (FN) to prevent microfissuring or hot tearing of the weld metal [15].



Figure 2. Optical micrographs of (a) as-received ¹⁹⁰sample and (b) weld metal tested at 25°C.

Figure 3 shows detailed SEM micrograph and EDS analyses of 316L ASS weld metal tested at 400°C. As it is seen, the weld metal consisted of skeletal ferrite in austenitic matrix with some carbides which were distributed in the austenite matrix (Figure 3a). It was reported that the precipitation of carbides such as $M_{23}C_6$, MC , M_6C and M_7C_3 ($M = Cr, Mo$ and Fe) occurs in ASS during heat treatment and welding. The precipitation of carbides which depends the temperature and carbon content reduces corrosion resistance of stainless steel. The temperature in the range from 550 to 900°C allows chromium to diffuse away from the grain boundaries and to form carbides [12, 16-18]. Figure 3b also shows EDS analysis with the points 1-4 on the samples tested at 400°C. Points 1-3 contain Mo, Cr and C which indicated that $Cr_{23}C_6$ and Mo_6C precipitate particles occurred in the weld metal during cooling after welding. Point 4 taken from ferrite phase also contains higher Cr.



Mass percent (%)										(b)
Spectrum	C	N	Al	Si	Ti	V	Cr	Mn	Fe	Mo
1	5.00	1.09	0.00	0.77	0.00	0.00	17.76	2.24	71.40	1.73
2	4.89	1.27	0.00	0.87	0.00	0.81	17.28	2.38	70.66	1.84
3	3.31	0.09	0.00	0.94	0.40	0.00	19.90	2.21	71.47	1.68
4	0.72	0.00	0.26	0.39	0.24	1.31	20.36	5.38	69.91	1.42
Mean value:	3.48	0.61	0.07	0.74	0.16	0.53	18.83	3.05	70.86	1.67
Sigma:	1.99	0.66	0.13	0.24	0.19	0.65	1.53	1.55	0.73	0.18
Sigma mean:	1.00	0.33	0.07	0.12	0.10	0.32	0.77	0.78	0.37	0.09

Figure 3. (a) SEM micrograph of 316L ASS weld metal after testing at 400°C and (b) EDS analysis from indicated points.

The precipitation of the sigma phase, which is often observed in various series of stainless steels, is one of the main reasons for the deterioration of stainless steels' properties, for example, mechanical property, corrosion resistance, and weldability [19]. Sigma phase which is a tetragonal crystal structure forms in the Fe-Cr system at temperatures of 550-900°C. The presence of sigma phase in the matrix can increase the hardness and decrease the toughness, as well as the elongation of steel [20]. In the present work, the presence of sigma phase in the weld metal after testing in the temperature range of 100-800°C was not observed (Fig. 3). It is thought that tensile testing time at elevated temperatures was not enough for precipitation of sigma phase. The sigma phase was a second phase of a rich substitutional element. The diffusion of the substitutional element was very slow in austenite so that the nucleation of the sigma phase in austenite was difficult [16].

3.2. Mechanical Properties

DSA results of weld metal are seen in Table 3 which gives YS (0.2%), UTS and elongation (%) of samples tested at 25-800°C. As seen from Table 3 that weld metal showed small differences in YS and UTS up to 600°C, but it revealed drastic change when the test temperature was increased beyond 600°C. A decrease in elongation (%) values of weld metal was observed up to 600°C. A further increase in test temperature of 700°C or 800°C increased the elongation (%). This indicates that weld metal of 316L ASS is susceptible to DSA up to 600°C. This is due to the the presence of free C and N atoms in solution. The diffusion of solute atoms to dislocations will prevent the movement of the dislocations resulted in higher strength and lower ductility in steel [21].

Table 3. Mechanical properties of weld metal tested at temperatures of 200-800°C.

Test Temperatures (°C)	Yield Strength (0.2%, MPa)	Tensile Strength (MPa)	Elongation (%)
25	395	659	57
100	349	559	37
200	407	543	31
300	389	505	20
400	396	521	24
500	336	485	25
600	307	423	22
700	190	295	37
800	153	184	81

Heating and cooling rates in fusion welding are usually high and the heated metal subject to plastic strain during cooling. For this reason, fast cooling after welding does not allow full precipitation of carbides and nitrides. This resulted in an increase in the amount of uncombined C and N in solution in the weld metal which can cause DSA to occur. DSA is considered to contribute to higher strength in weld metal by effectively increasing the dislocation density for a given strain. A high dislocation density, the fact that many dislocations will be pinned by solute atoms and that bowed dislocations need higher stresses for unpinning, mean that strength in the weld metal will be higher [22, 23].

Workhardening index (n) which is used to determine the occurrence of DSA was evaluated according to the following Holloman equation [24] for weld metal.

$$\sigma = K\varepsilon^n \quad (1)$$

where σ is the true stress, ϵ is the true strain, n is the workhardening index, and K is the strength coefficient. The evaluated n values following equation 1 as a function of hot tensile test temperatures are seen in Figure 4. As can be seen, workhardening index increased in the temperature range of 400-600°C for weld metal. This shows the interaction between dislocations and interstitial solute atoms affecting the workhardening of 316L ASS weld metal. The increased workhardening index and increased tensile strength are believed to arise from greater than normal dislocation densities in steels that exhibit DSA. These high dislocation densities occur due to the pinning, which requires fresh dislocations to maintain the applied strain rate. Tensile testing at 400-600°C results in a stronger interaction between solute atoms and dislocation which increased the work hardening of a material, since the deformation at 400-600°C can produce greater number of dislocations due to interaction dislocations and interstitial solute atoms (C and N) contributed to stronger work hardening [25]. Kaçar and Gündüz [26] showed that the activation energy for strain ageing in AISI 430 ASS is bigger than plain carbon steel. For this reason, the weld metal of 316L ASS did not exhibit any yielding behaviour, because Cr decreases the C diffusion to dislocations at lower temperatures.

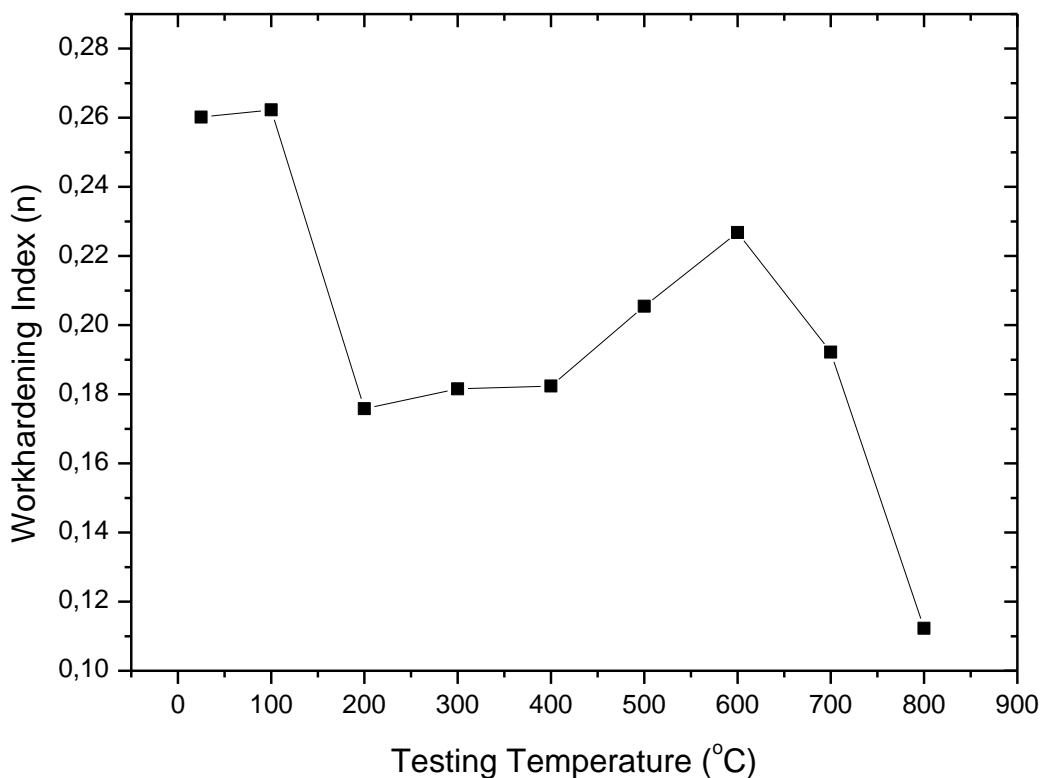


Figure 4. Workhardening index (n) values of the weld metal tested at different temperatures.

This is also confirmed in Figure 5 which shows YS values of weld metal at different testing temperatures. As can be seen, YS values of weld metal revealed a decrease when the testing temperature is increased to 100°C. YS then increased with rising temperature and reached a maximum at 400°C. This indicated the interaction between C and/or N with dislocation which prevented dislocation movement. YS values changed drastically above 600°C. This also shows that DSA is operative in weld metal at the test temperatures of 25-800°C. It is proposed that DSA occurs when the dislocations are temporarily held up at local obstacles in the glide plane [27].

When this work has been carried out, same authors were published a paper investigating DSA phenomena in 316L ASS under as-received and as-welded conditions. It was observed that as-

welded samples revealed lower values in elongation (%) but higher values in YS and UTS than the as-received samples at the temperatures of 25–800 °C. This showed that as-welded samples are more effected by DSA than the as-received samples. More detailed experimental results for the DSA behaviour of 316L ASS are available elsewhere [28]. However, the results obtained from the present study showed that weld metal is more susceptible to DSA than the as-received and as-welded samples with evidence more increase in strength but decrease in elongation (%) at the testing temperatures of 25-800 °C. This is due to the presence of higher Cr content in weld metal compared to that of as-received samples, because weld wire Cr content is about 18.5 wt. % which is higher than as-received samples. It is generally accepted that the elevated Cr content of the weld metal increases the strength of the steel [10, 29]. Higher strength of weld metal could also be due to heat input during welding, melting and solidification of the area as suggested by Lippold and Kotecki [30] who investigated welding metallurgy and weldability of stainless steel.

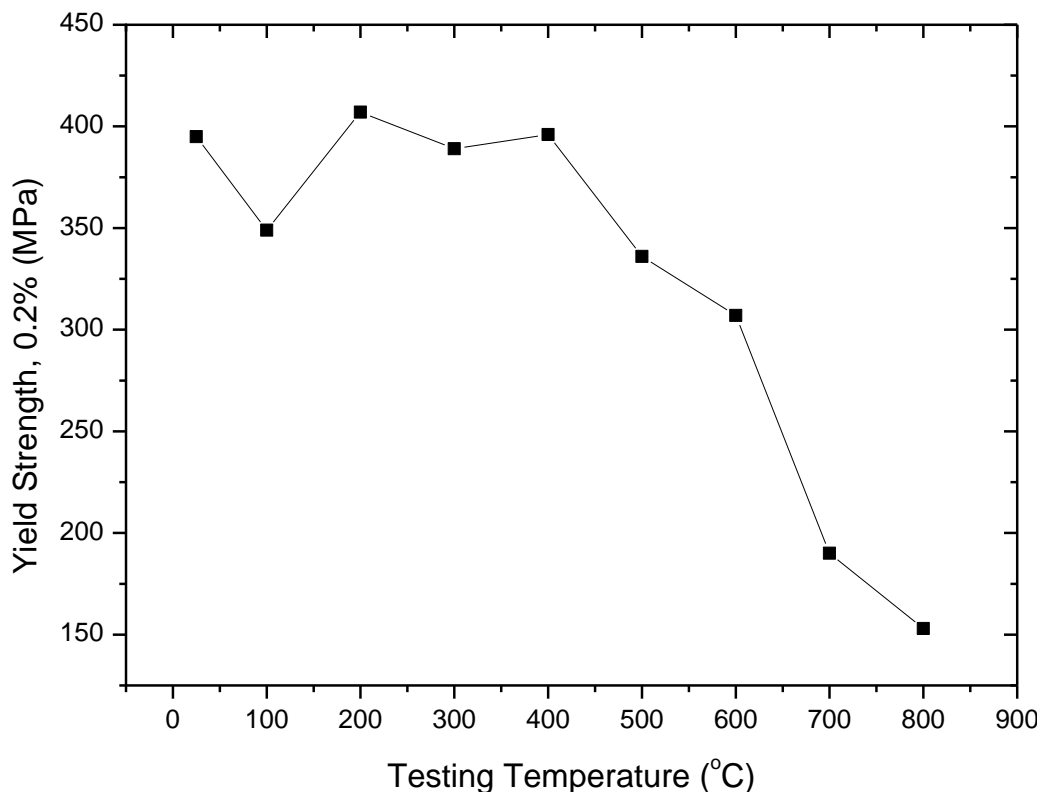


Figure 5. Yield strength values of the weld metal tested at different temperatures.

Stress and strain diagrams of weld metal tensile tested at temperatures of 25-800°C are seen in Figure 6. As is seen, stress and strain diagrams revealed serrated behaviour when the testing temperatures increased at a strain rate of $1 \times 10^{-3} \text{ s}^{-1}$. Serrated behavior which is the manifestation of DSA was observed during tensile testing at 500°C and 600°C. The serrations disappeared from the curves when the samples were tested at 700°C or 800°C. Such serrated behaviour occurs when the dislocations and solute atoms interact which may become an important controlling factor for strengthening. The interaction between dislocations and solute atoms causes the appearance of serrations on the curve, an increase in tensile strength and strain hardening, but a decrease in ductility. DSA will occur when the interstitial atoms diffuse and pin the dislocations. As a result of this, serrations occur because of rapid generation of new dislocations which are needed to sustain flow [31].

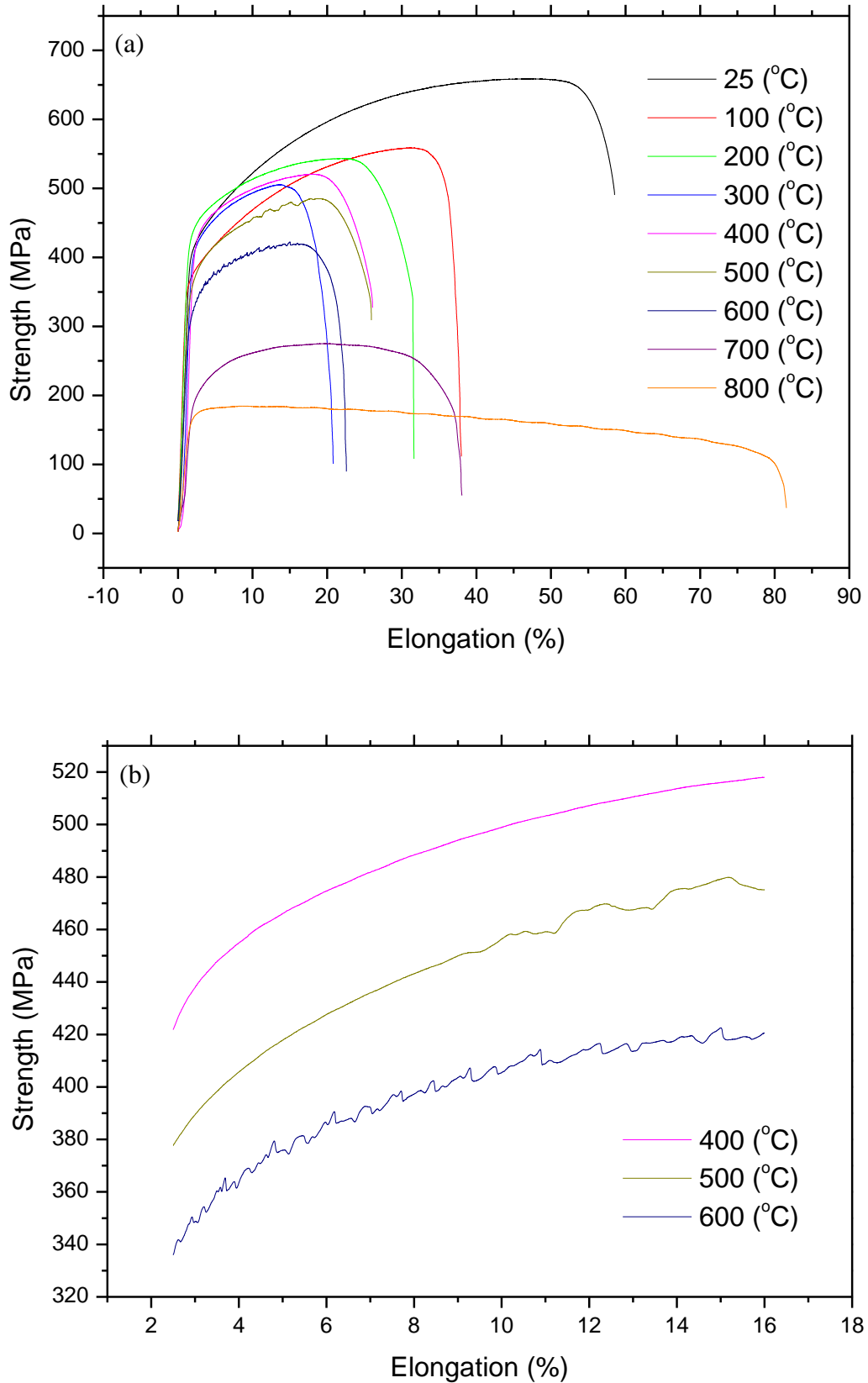


Figure 6. Stress and strain diagrams of weld metal: (a) full range profiles and (b) sections in large scale.

Deformation rate and temperature, which are very important for DSA, effect the diffusing solute atoms and the velocity of mobile dislocations. The presence or absence of serrations is governed by strain rate at a given temperature. Foreexample, dislocation diffusion is more higher than solute atoms for the occurence of DSA at low temperature and high deformation rate. However, DSA disappear at high temperature and low deformation rate, because dislocations can move with the solute atoms. Therefore, DSA can occur at the tempertures of intermediate strain rates [32]. It is clear from fregooing discussion that DSA takes place in weld metal of 316L ASS results from the interactions of dislocations and solute atoms at the temperatures of 200-600°C.

Serrated yielding also refers to the occurrence of repeated discontinuous yielding during plastic deformation. The discontinuous yielding is evidenced on a stress-strain curve by the appearance of serrations usually after reaching a critical level of plastic strain. On the basis of the appearance of serrations on the stress-strain diagrams, fives types of serrated yielding are often observed as shown in Figure 7. Type A serrations are related with the repeated initiation and continuous propagation of Luders bands along the gauge length of specimen in the strain direction. The initiation of each band resulted in the appearance of yield point on the stress-strain curve which is followed by a smooth curve during band propagation. They occur at the high strain rate and low temperature part of the DSA [33].

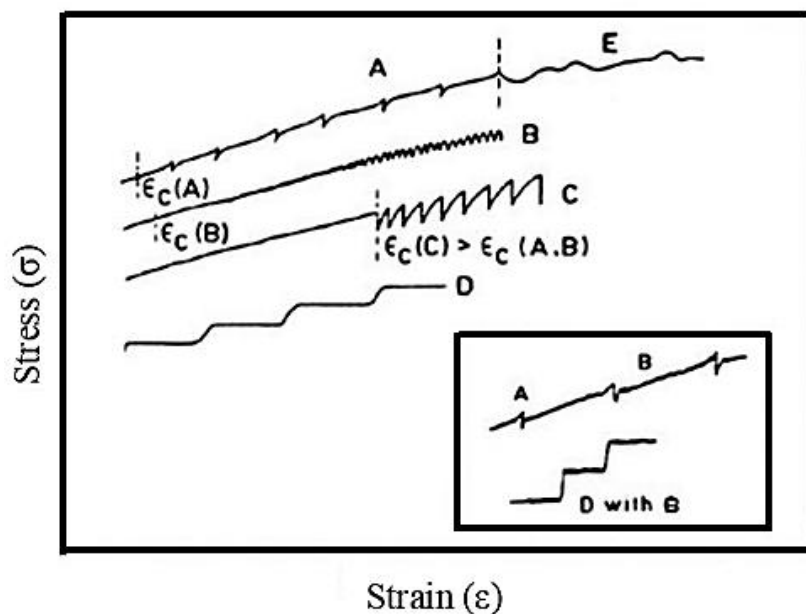


Figure 7. Various type serrations observed on stress and strain diagrams [34].

With type B serrations band propagation is discontinuous, with each hop or jump of the band resulting in a serration on the stress-strain diagram. Type B serrations often develop from type A at higher strain, or occur with plastic flow at lower strain rates and higher temperatures compared to the type A serrations. In practice serrations can be mixed in type A and B combinations. Type C serrations are similar to type B serrations in that deformation band propagation is discontinuous. Type C serrations are distinguished by stress drops which occur below the level of the stress-strain curve. Therefore, type C serrations considered to be caused by dislocation unlocking. It is normally observed at lower strain rates and high temperatures than type A and B serrations [34, 35].

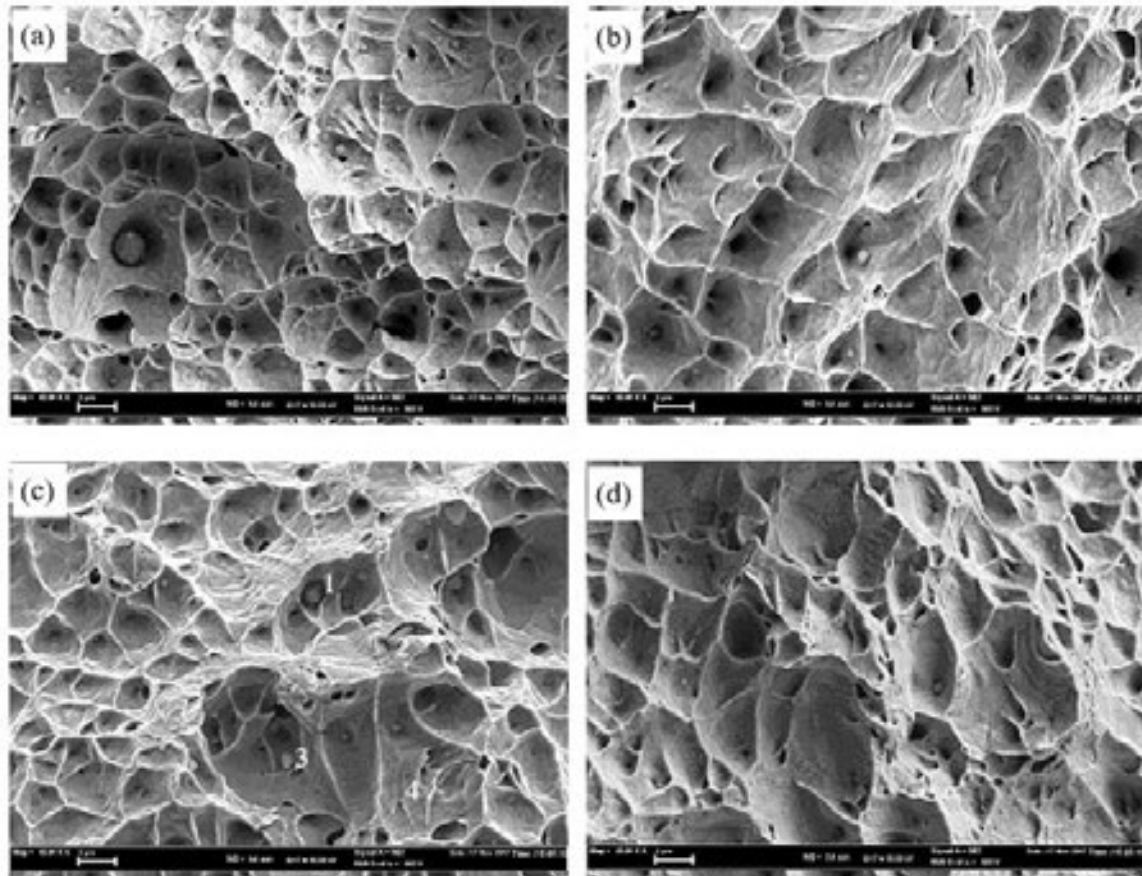
Type D serrations are plateaus in the stress-strain diagrams, which are observed because of shear band propagation with no workhardening in front of the moving band. Type D serrations may also

occur in a mixed mode with the type B. Type E serrations are similar to the type A, but do not show any workhardening during band propagation. Plastic flow instabilities of type E appear from the type A at high strain values [33]. Type D serrations are observed in the stress–strain diagrams of 316L ASS weld metal at high strain rate for the testing temperature of 500°C. In test conducted at 600°C, the amplitude of the serrations rised with strain and they cahged from types D to types A+E. Type A serrations occured at low strain and change over to type E serration at high strain. The tensile test results indicated that serrated behaviour was observed in 316L austenitic stainless steel at testing temperatures of 500 and 600°C. However serrated behaviour was not observed above 600°C. Different solute atoms and mechanisms can participate in the interactions of solute atom and mobile dislocation at different temperatures.

The DSA, observed at temperature of 500°C, shows itself as serrated flow of types D. Interaction of dislocations with C and N interstitial atoms during deformation is considered to be responsible for the DSA in ASS. At temperatures about 600°C, where the type A and E serrations are seen, the DSA can be attributed to the interaction of mobile dislocations with substitutional solute atoms such as Cr or Mo [36].

When the serrations behaviour results for weld metal obtained from this work are compared with the results obtained from other work [28] for the as-received and as-welded samples of 316L ASS. It was observed that weld metal revealed more pronounced serrations than as-received and as-welded samples owing to the presence of higher amount of solute atoms in solution [7]. Dissolution of carbides occurs in the weld metal results in larger amount of solute atoms in the solution. This cause more pronounced serrations in weld metal than as-received and as welded samples.

Figure 8 shows the SEM fractography of the weld metal tested at 25°C, 200°C, 400°C and 600°C. The fracture surface of weld metal tensile tested at 25°C and 200°C showed dimples with different sizes which is characteristic of ductile fracture. Dimple morphology dominated on the fracture surface. This indicated that ductile fracture mode which was represented by cup-like dimple rupture occurred in weld metal [28, 37]. Cleavage facets and dimples were observed in the weld metal after testing at 400°C or 600°C in which the samples also showed lower decrease in reduction of area. This suggests that DSA occurs in weld metal of 316L ASS. On the other hand, ductile dimples were observed in weld metal after testing at 800°C which increased elongation and reduction in area. Figure 8 also shows EDS analysis of weld metal which indicated the presence of complex Mn-Cr-Ti inclusions.



Mass percent (%) (e)

Spectrum	C	N	Al	Si	Ti	V	Cr	Mn	Fe	Ni	Mo
1	20.89	0.00	0.18	0.57	0.47	0.19	16.37	2.21	54.08	3.88	1.17
2	22.88	0.00	0.11	0.72	0.24	0.00	11.14	1.66	49.21	12.88	1.15
3	0.45	0.00	0.00	0.18	2.31	1.40	19.78	28.98	41.24	1.37	4.30
4	3.93	1.26	0.01	0.85	0.00	0.00	15.56	0.00	57.48	19.31	1.61
Mean value:	12.04	0.31	0.08	0.58	0.76	0.40	15.71	8.21	50.50	9.36	2.06
Sigma:	11.49	0.63	0.08	0.29	1.05	0.67	3.56	13.88	7.05	8.27	1.51
Sigma mean:	5.74	0.31	0.04	0.15	0.53	0.34	1.78	6.94	3.52	4.14	0.76

Figure 8. Fractography of weld metal tested at (a) 25°C, (b) 200°C, (c) 400°C and (d) 600°C and (e) correspondig EDS of the indicated particles in samples tested at 400°C.

4. Conclusion

In the present study, the DSA phenomena in AISI 316L ASS weld metal subjected to the hot tensile testing at temperature of 25-800°C was investigated. The main conclusions obtained from present study are summarized below:

1. Weld metal of 316L ASS which is susceptible to DSA showed small variation in YS and UTS values up to 600°C, but it revealed drastic change when the test temperature was increased beyond 600°C. A decrease in elongation (%) values of weld metal was observed with increasing temperature, reaching a minimum at 600°C. This is due to the the presence of free or uncombined C, N or Cr solute atoms in solution.

2. The workhardening index of weld metal increased in the temperature range of 400-600°C, but it decreased when the test temperature was raised to 700°C or 800°C. This shows the interaction between dislocations and solute atoms affected the workhardening of 316L ASS weld metal.
3. Stress and strain diagrams of weld metal revealed serrated behaviour when the testing temperatures increased at a strain rate of $1 \times 10^{-3} \text{ s}^{-1}$. Serrated behavior which is the characteristic of DSA was observed during tensile testing at 500°C and 600°C. The serrations were not observed on the stress and strain diagrams after testing at 700°C or 800°C
4. Fracture surface analysis indicated that weld metal showed ductile fracture mode after testing at 25°C and 200°C. Dimple morphology dominated on the fracture surface. However, cleavage facets and dimples were observed in the weld metal after testing at 400°C or 600°C in which the samples also showed lower decrease in reduction of area. This suggests that DSA occurs in weld metal of 316L ASS.

5. Acknowledgement

This work was supported by Scientific Research Projects Coordination Unit of Karabük University. Project Number: KBÜBAP-17-DR-169. The authors would like to thank Eren Sancar for his assistance in the welding of 316L austenitic stainless steel.

6. References

- [1] ASM International, *Stainless steel for design engineering*, 6 (2008), pp. 69-78.
- [2] S.G. Hong, S.B. Lee: Dynamic strain aging effect on the fatigue resistance of type 316L stainless steel, *Journal of Nuclear Materials*, 328 (2004), pp. 232-242.
- [3] M. Valsan, A. Nagesha, K. Bhanu Sankara Rao, R. Sandhya, S.L. Mannan, R. Baldev: A comparative evaluation of low cycle fatigue and creep-fatigue interaction behavior of 316 and 316(N) weld metals and weld joints, *Transaction of the Indian Institute of Metals*, 58 (2005), pp. 323–329.
- [4] O.H. Ibrahim, I.S. Ibrahim, T.A.F. Khalifa: Effect of aging on the toughness of austenitic and duplex stainless steel weldments, *Journal Material Science and Technology*, 26 (2010), pp. 810-816.
- [5] R.W.K. Honeycombe, H.K.D.H Bahadreshia: *Steels Microstructure and Properties*, 3th Edition, London: Butterworth-Heinemann (2006).
- [6] J.B. Seol, J.G. Kim, S.H. Na, C.G. Park, H.S. Kim: Deformation rate controls atomic-scale dynamic strain aging and phase transformation in high Mn TRIP steels, *Acta Materialia*, 131 (2017), pp.187-196.
- [7] Z. Huang, D. Wagner, C. Bathia: Some metallurgical aspects of dynamic strain aging effect on the Low Cycle Fatigue behavior of C–Mn steels, *International Journal of Fatigue*, 80 (2015), pp. 113–120.
- [8] K. Gopinath, A.K. Gogia, S.V. Kama, U. Ramamurty: Dynamic strain ageing in Ni-base superalloy 720Li, *Acta Materialia*, 57 (2009), pp. 1243-1253.
- [9] D. Yu, W. Yu, G. Chen, F. Jin, X. Chen: Role of dynamic strain aging in the tensile property, cyclic deformation and fatigue behavior of Z2CND18.12N stainless steel between 293 K and 723 K, *Material Science and Engineering A*, 558 (2012), pp. 730–736.
- [10] S. Kožuh, M. Gojić, L. Kosec: The effect of annealing on properties of AISI 316L base and weld metals, *Materials and Geoenvironment*, 54 (2007), pp. 331-344.
- [11] S. Kou: *Welding metallurgy*, 2nd Edition, Wiley Publishing, New Jersey (2003)
- [12] S. Kožuh, M. Goji, L. Kosec: Mechanical properties and microstructure of austenitic stainless steel after welding and post-weld heat treatment, *Kovove Materialy*, 47 (2009), pp. 253–262.

- [13] P. Sathiya, S. Aravindan, R. Soundararajan, A. Noorul Haq: Effect of shielding gases on mechanical and metallurgical properties of duplex stainless-steel welds, *Journal of Materials Science*, 44 (2009), pp. 114–121.
- [14] R. Yılmaz, M. Tümer: Microstructural studies and impact toughness of dissimilar weldments between AISI 316 L and AH36 steels by FCAW, *International Journal of Advanced Manufacturing Technology*, 67 (2013), pp. 1433–1447.
- [15] R. Sunil Goyal, M. Sandhya, K. Valsan, R. Bhanu Sankara: The effect of thermal ageing on low cycle fatigue behaviour of 316 stainless steel welds, *International Journal of Fatigue*, 31 (2009), pp. 447–454.
- [16] A.F. Padilha, P.R. Rios: Decomposition of austenite in austenitic stainless steels, *ISIJ International*, 42 (2002), pp. 325–337.
- [17] A.F. Padilha, R.L. Plaut, P.R. Rios: Annealing of cold-worked austenitic stainless steels, *ISIJ International (Japan)*, 43 (2003), pp. 135–143.
- [18] T. Sourmail: Precipitation in creep resistant austenitic stainless steel, *Materials Science and Technology*, 17 (2001), pp. 1–14.
- [19] C.C. Hsieh, W. Wu: Overview of intermetallic sigma (σ) phase precipitation in stainless steels, *International Scholarly Research Network*, 2012 (2012), pp. 1–17.
- [20] J. Lee, I. Kim, A. Kimura: Application of small punch test to evaluate sigma-phase embrittlement of pressure vessel cladding material, *Journal of Nuclear Science and Technology*, 40 (2003), pp. 664–671.
- [21] G. Ananthakrishna: Current theoretical approaches to collective behavior of dislocations, *Physics Reports*, 440 (2007), pp. 113–259.
- [22] B. Vargas-Arista, C. Angeles-Chavez, A. Albitar, J.M. Hallen: Metallurgical investigation of the aging process on tensile fracture welded joints in pipeline steel, *Materials Characterization*, 60 (2009), pp. 1561–1568.
- [23] B. Hutchinson, J. Komenda, G.S. Rohrer, H. Beladi, Heat affected zone microstructures and their influence on toughness in two microalloyed HSLA steels, *Acta Materialia*, 97 (2015), pp. 380–391.
- [24] J.H. Hollomon: Tensile deformation, *Transaction AIME, Iron Steel Division*, 162 (1945), pp. 268–289.
- [25] S. Gündüz: Dynamic strain aging effects in niobium microalloyed steel, *Ironmaking and Steelmaking*, 29 (2002), pp. 341–346.
- [26] R. Kaçar, S. Gündüz: Increasing the strength of AISI 430 ferritic stainless steel by static strain ageing, *Kovove Materialy*, 47 (2009), pp. 185–191.
- [27] A. Sarkar, A. Nagesha, P. Parameswaran, R. Sandhya, M.D. Mathew: Influence of dynamic strain aging on the deformation behavior during ratcheting of a 316LN stainless steel, *Materials Science and Engineering A*, 564 (2013), pp. 359–368.
- [28] G.A. Muhamed, S. Gündüz, M.A. Erden, D. Taştumur: Dynamic strain aging behaviour in AISI 316L austenitic stainless steel under as-received and as-welded conditions, *Metals* 362 (2017), pp. 2–15.
- [29] L. Hee-jin, L. Hae-woo: Effect of Cr content on microstructure and mechanical properties of low carbon steel welds, *International Journal of Electrochemical Science*, 10 (2015), pp. 8028–8040.
- [30] J.C. Lippold, D.J. Kotecki: *Welding metallurgy and weldability of stainless steels*, first Edition, John Wiley & Sons Inc, New Jersey (2005)
- [31] W.D. Callister, *Plastic deformation, material science and engineering—an introduction*, 7th Edition, Wiley, New York (2007)
- [32] S.G. Hong, S.B. Lee: The tensile and low-cycle fatigue behavior of cold worked 316L stainless steel: influence of dynamic strain aging, *International Journal of Fatigue*, 26 (2004), pp. 899–910.

- [33] P. Rodriguez: Serrated plastic flow, Bulletin of Materials Science, 6 (1984), pp. 653-663.
[34] P.G. McCormick, Dynamic strain ageing, Transaction of the Indian Institute of Metals, 39 (1986), pp. 98-106.
[35] L.H. Almeida, I. Le May, P.R.O. Emygdio: Mechanistic modelling of dynamic strain aging in austenitic stainless steels, Materials Characterization, 41 (1998), pp.137-150.
[36] M. Ivanchenko, Y. Yagodzinskyy, U. Ehrnstén, W. Karlsen, H. Hänninen: Manifestations of DSA in Austenitic Stainless Steels and Inconel Alloys, 20th International Conference on Structural Mechanics in Reactor Technology (SMiRT 20), August 9-14, Espoo/Finland, (2009), pp. 120-128.
[37] W.D. Callister, D.G. Rethwisch: Materials science and engineering, 8th Edition, John Wiley and Sons, New York (2011)

CORRESPONDENCE ADDRESS: Süleyman Gündüz, Karabük University, Technology Faculty, Manufacturing Engineering, Karabük-Turkey, 5055033620, sgunduz@karabuk.edu.tr.

SHORT BIOGRAPHIES

Guma Alnaji Muhamed – born in Libya and he is currently studying Ph. D in the Department of Manufacturing Engineering , Karabük University, Turkey.

Prof. Dr. Süleyman Gündüz– born in 1970, graduated from Gazi University, Ankara, Turkey in 1992, and received his M. Sc. degree in 1996 and his Ph. D degree in 2000 in the area of Metallurgy and Materials Engineering from Leeds University, UK. He is Professor in the Department of Manufacturing Engineering, Technology Faculty of Karabük University, Turkey.

3D SURFACE MORPHOLOGY AND ROUGHNESS ON TREATED SURFACE OF TI-6AL-4V ALLOY BY ND:YAG LASER: EFFECT OF SPOT SIZE

Ali GURSEL

Düzce University, Faculty of Engineering, Department of Mechanical Engineering,
Konuralp Yerleşkesi, B Blok 207, 81620 Düzce, Türkiye

aligursel@duzce.edu.tr, aligursel@yahoo.com Tel: +90 380 542 1036 Fax: +90 380 542 1037

Abstract

In this study, a 1.5 mm thick Ti-6Al-4V alloy plate surface was treated by SigmaLaser@300 Nd:YAG pulsed laser. The Nd:YAG laser parameters, such as spot size and shape, pulse energy and duration, travel speed, peak power and frequency of repetition, influence directly or synergistically the quality of pulsed seam welds and their morphology. Titanium and its alloys lead to successful application in various fields including the medical and aerospace industries due to the excellent corrosion resistance, high strength to weight ratio and high operating temperature. Among the reliable treatment techniques, laser surface treatment can provide significant advantages for the titanium alloys because of its precision, rapid processing capability and ability to control the parameters and their effects. Surface morphology and roughness are analyzed using Hirox 3D microscope, and the influence of the spot size was investigated. The seam and surface quality were characterized in terms of their morphology and microhardness.

Key Words: Ti-6Al-4V alloy – Nd:YAG laser – surface treatment – roughness

1. Introduction

Lasers have become one of the most multi-functional and powerful tool for materials processing. The laser system is also widely used in the repair of cutting and molding tools **Hata! Başvuru kaynağı bulunamadı..** Laser surface treatment has the greatest growth potential in the field of laser materials processing. Laser surface treatments offer a wide range of possibilities to achieve desired surface properties. The aim of surface treatment is to improve wear resistance, surface strength for load carrying (crush resistance), fatigue life and impact resistance, and to induce suitable residual and compressive stresses, etc. It's well known that the most of welding techniques are widely used for surface coating and treatments.

Titanium and titanium alloys are mostly used in the aerospace, biomedical, nuclear, defense and automotive industries due to their low density, good corrosion resistance and high operating temperature **Hata! Başvuru kaynağı bulunamadı..** Among the titanium alloys, Ti-6Al-4V is the best known, but with its features of strength, low thermal conductivity and high chemical reactivity, it is a difficult material to process using conventional machining and welding. Ti-6Al-4V alloy is widely used as material for load-bearing and non-load-bearing medical implants because of its excellent biocompatibility and corrosion resistance. Although its low hardness and poor wear resistance are still serious concerns, the majority of intended Ti-6Al-4V implant applications do not require very high wear resistance. Laser treatment can be used to solve these problems.

Joining Ti-6Al-4V alloys using pulsed Nd:YAG (neodymium-doped yttrium aluminum garnet) laser welding method was achieved by Akman et al. They showed that controlling of the laser

output parameters can change results precisely. Blackburn et al. **Hata! Başvuru kaynağı bulunamadı.** produced welds with high internal quality in Ti-6Al-4V alloy by using a laser as the source for the welding technique. They observed the common periodic behaviors in the vapor plume and keyhole under low-porosity welding conditions.

The special features and potential of laser welding technique provide many advantages, such as high scanning velocity, narrow heat-affected zone (HAZ), low distortion, excellent controllability and the ability to produce a high-intensity heat source, which is suitable for precision welding. The previous studies on Nd:YAG laser applications, show that it is possible to control the penetration depth and geometry of the laser weld bead by precisely controlling the laser output parameters. Although laser treatments have been widely reported to improve the mechanical and corrosion behavior of different steels and aluminum alloys, relatively few studies have investigated the properties of laser titanium and titanium alloy samples. Laser treatments have been performed with different types of laser sources such as CO₂ laser, Nd:YAG laser, excimer laser and high power diode laser, the latter presenting lower maintenance costs and higher efficiency than the others, representing a clear economical advantage. Thus, Sun et al. performed laser treatments on titanium (Grade 2) samples with a Nd:YAG laser. Ariyaratnam et al. **Hata! Başvuru kaynağı bulunamadı.** also focused on the etched dentin surfaces produced by the Nd:YAG laser, and bonding of resin composite to the laser-treated dentin was not significantly different from untreated dentin despite the fact that the surface roughness of laser-treated dentin was significantly higher than untreated dentin. In another study on wear treatment, a small molten pool is formed by each laser pulse, and within a few milliseconds it re-solidifies. When the pulse frequency is low, seam occurs in a conduction mode and a smooth, shallow molten pool is produced. However, when the pulse frequency is increased, a deeper, wider pool is obtained. The changed seam morphology affects the surface form and hardness as well.

The formation of laser seams and their subsequent quality are the result of a combination of various pulsed laser processing parameters, such as travel speed, average laser power, pulse energy, pulse duration, average peak power density and spot area. This abundance of parameters provides control of the thermal input with a precision not previously obtainable and also permits the application of a wide range of experimental conditions. On the other hand, controlling so many parameters increases the complexity of laser processing. However, effect of parameters on seam morphology and roughness does not take place in the literature.

In this study, surface of Ti-6Al-4V samples with 1.5 mm thickness is treated by SigmaLaser®300 Nd:YAG laser system, and effect of spot size on seam morphology and roughness is analyzed by 3D micrographs and microhardness plot.

2. Experimental

2.1. Materials and Methods

Ti-6Al-4V alloy sheet with chemical composition shown in Table 1 were prepared as 40×20×1.5 mm³ for treatment by the SigmaLaser®300 Nd:YAG laser system.

Table 1. The Chemical composition of Ti-6Al-4V (wt.%)

Components	C	Fe	N	O	Al	V	H	Ti
------------	---	----	---	---	----	---	---	----

Ti-6Al-4V	<0.08	<0.25	<0.05	<0.15	6	4	<0.03	Balance
-----------	-------	-------	-------	-------	---	---	-------	---------

The laser beam is focused on titanium plates and circle shape pulse has been applied to all samples. The spot sizes on the plates were adjusted from 0.2 mm to 1.2 mm. In order to evaluate the effects of spot size on the surface treatment of the Ti-6Al-4V samples, pulse duration, pulse repetition and peak power were determined as 4 ms, 28 Hz and 30% of 13 kW (3.9 kW), respectively. The focal depth parameter of laser applications as -0.2 mm is very common for surface treatment and for the repair of cutting and molding tools. The shallow seams are increasing the cooling rates and rapid cooling rates cause the occurrence of the martensite structure which is desired achievement of surface hardness. Pulse duration is another effective parameter for heat input. For welding applications, it is necessary to increase heat input for penetration depth. Longer pulse duration causes higher heat input. However, in this study, in order to obtain a harder surface for wear treatment, the heat input was limited, and the pulse duration was determined as 4 ms. All laser output parameters are also given in Table 2.

Table 2. Test parameters

Parameter	Values
Pulse Frequency	28 Hz
Peak Power	3.9 kW
Pulse Duration	4 ms
Spot Size	0.2, 0.4, 0.6, 0.8, 1.0, 1.2 mm
Welding speed	50 mm/min
Focal depth	-0.2 mm
Gas and pressure	(99.8%) Argon, 1.5 bar

At high temperatures, titanium is reactive with ambient gases. For this reason, and to protect against atmospheric effects, argon (99.8%) shielding gas was used at 1.5 bars to protect the melted pool from oxidation and porosities until solidification was sufficient. Therefore, it was crucial to use the shielding gas and to set up the nozzle in order to prevent the formation of turbulence on the sample surfaces during the application.

Microhardness measurements were performed according to the seam dimensions and values were obtained from the HAZ. Furthermore, 3D analysis was carried out to observe the morphology and surface roughness of the seams by Hirox 3D microscope KH-8700.

2.2. Surface Roughness Parameters

R_a is derived from the equation 1 in micrometer (μm) when the roughness curve is expressed as a function of y=f(x), considering x-axis to the mean line direction and y-axis to the vertical magnification of the roughness curve in the range of reference length l (see Figure 1a).

$$R_a = \frac{1}{l} \int_0^l |f(x)| dx = \frac{1}{n} \sum_{i=1}^n |y_i| \quad (1)$$

R_z is derived from the distance in micrometer (μm) between the highest peak and the lowest valley in the range of reference length l to the direction of mean line of the roughness curve (see Figure 1b).

$$R_z = R_p + R_v \quad (2)$$

RzJIS is also derived from the summation in micrometer (μm) of the mean value of each distance between the mean line and 5 peaks (Y_p) from the highest one, and the mean value of each distance between the mean line and the 5 valleys (Y_v) from the lowest one, reference length l (see Figure 1c).

$$R_{zJIS} = \frac{|Zp_1+Zp_2+Zp_3+Zp_4+Zp_5|+|Zv_1+Zv_2+Zv_3+Zv_4+Zv_5|}{5} \quad (3)$$

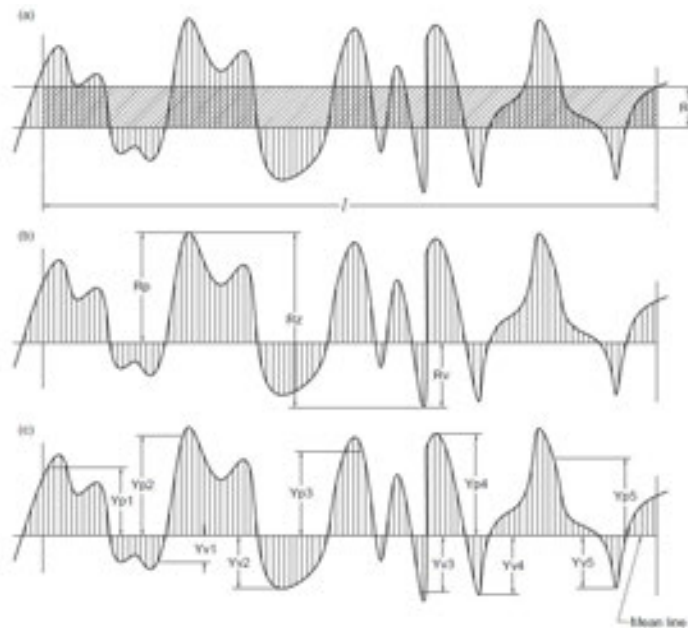


Figure 1: Definition of roughness parameters

3. Results and Discussions

It was previously proven that all parameters such as peak power, spot size, pulse frequency, pulse duration, welding speed and focal depth are affecting the seam morphology and properties; however investigation of seam morphology and roughness is novelty of this study. Spot size is one of the key parameters for the pulsed laser system. For seam geometry and surface hardness, it is crucial to control the pulse energy, in addition to the laser power, spot size, pulse length, and pulse repetition.

3.1. Micro-hardness measurements

Microhardness distributions have been analyzed using a SHIMADZU HMV microhardness tester by applying a load of 100 g. The microhardness test has been carried out at the surface of seams on the centerline of the weld pool, heat affected zones as border of the seam and work pieces, as HAZ of samples. As a result, at the transition zone of the weld seams, the hardness is in the maximum level and the melted and cooled material is compared to the base metal due to its rapid cooling rate (see Figure 2).

In previous studies. for wearing the surface by continuous wave Nd:YAG laser, the average hardness of melted region was higher by 15-22% than the average hardness of Ti-6Al-4V alloy

substrate. this study, it has been reached to 50-300% higher than base metal hardness in melted region by Nd:YAG pulsed laser. The difference in hardness between the transition zone and the base metal is over 700 HV in narrower spot size parameters. Different welding techniques such as electron beam and gas tungsten welding techniques, which were applied on Ti-6Al-4V alloys in previous studies, have shown that high power density of laser beam welding provides a lower heat input and a more rapid solidification when compared to the conventional techniques, so laser welding technique leads to higher hardness value. In heat-affected zone, the cooling rate is higher in transition zone than in weld pools. The difference between the transition zone and base metal is over 800 HV in 0.2 mm to 0.8 mm spot sizes.

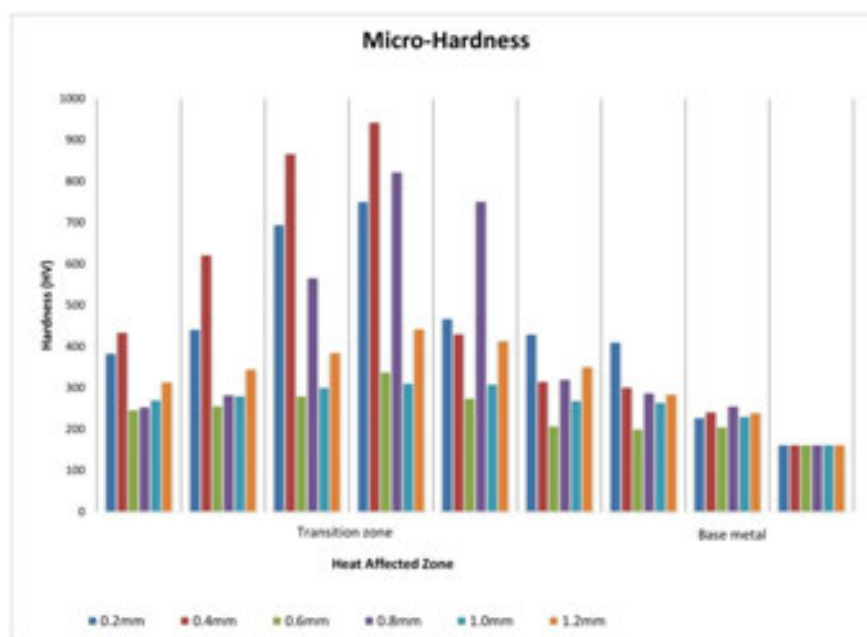


Figure 2: Microhardness distribution for different spot sizes

Higher beam concentration by smaller spot sizes, increased the target temperature producing steeper thermal gradients and severe thermal straining. It was expected that reducing the spot size causes the narrower seam and increases the cooling rate and hardness. High cooling rates cause the formation of martensite in the HAZ region. Therefore, it was obtained in this study while increasing the beam concentration, penetration depth and surface hardness also increased. It was reported by Sundaresan and Janaki that rapid cooling and subsequent martensitic transformation are effective strengthening methods for many titanium alloys. While having the microhardness values of Ti-6Al-4V alloy, the material behaves like a composite structure because of the martensite formation. As a result, overestimated values are occasionally seen during the measuring of microhardness, although average values were seen in this study (Figure 2).

3.2. Seam morphologies and widths

All parameters related to each other and welding or wearing properties. Any change of parameters for pulsed laser system, welding geometry, penetration depth, surface morphology and other properties are affected. If the melt pool is too large or too small, or if significant vaporization occurs during welding, unsuccessful results can be obtained. Therefore, the control

of laser power, pulse repetition, pulse length and spot size are very critical. Penetration depth is increased with increase of peak power, pulse repetition as heat input. However, narrower spot size is also increases the penetration depth because of the concentration of the energy.

In the previous studies, during the regular laser welding process, the spot size was determined as $\cong 0.1-0.7$ mm for Ti-6Al-4V alloy. A narrower fusion zone is an effective parameter, which allows the laser energy concentration to reach a deeper penetration for welding applications, in addition to causing less welding distortion. Owing to observation of the effect of fusion zone, different spot sizes were employed and the results in this study were investigated. It was also observed that while changing the spot sizes, the seam morphologies also changed in Figure 3. At the larger spot sizes, smaller grains sizes and the martensitic structures occurred on the seams, because of the rapid cooling.

Measured seams width is approximately constant (between 1.3 mm and 1.8 mm). This result can be explained with the beam concentration effected the seam depth more than their width. The penetration depth and HAZ are also related to laser peak power and beam concentration. The plasma absorption is very strong at the top of the weld (at the surface of the material), where the available laser energy is high; it leads to increasing of the weld pool and HAZ width larger than spot size (see Figure 3). The same effect has been reported by Weldingh and Kristensen.

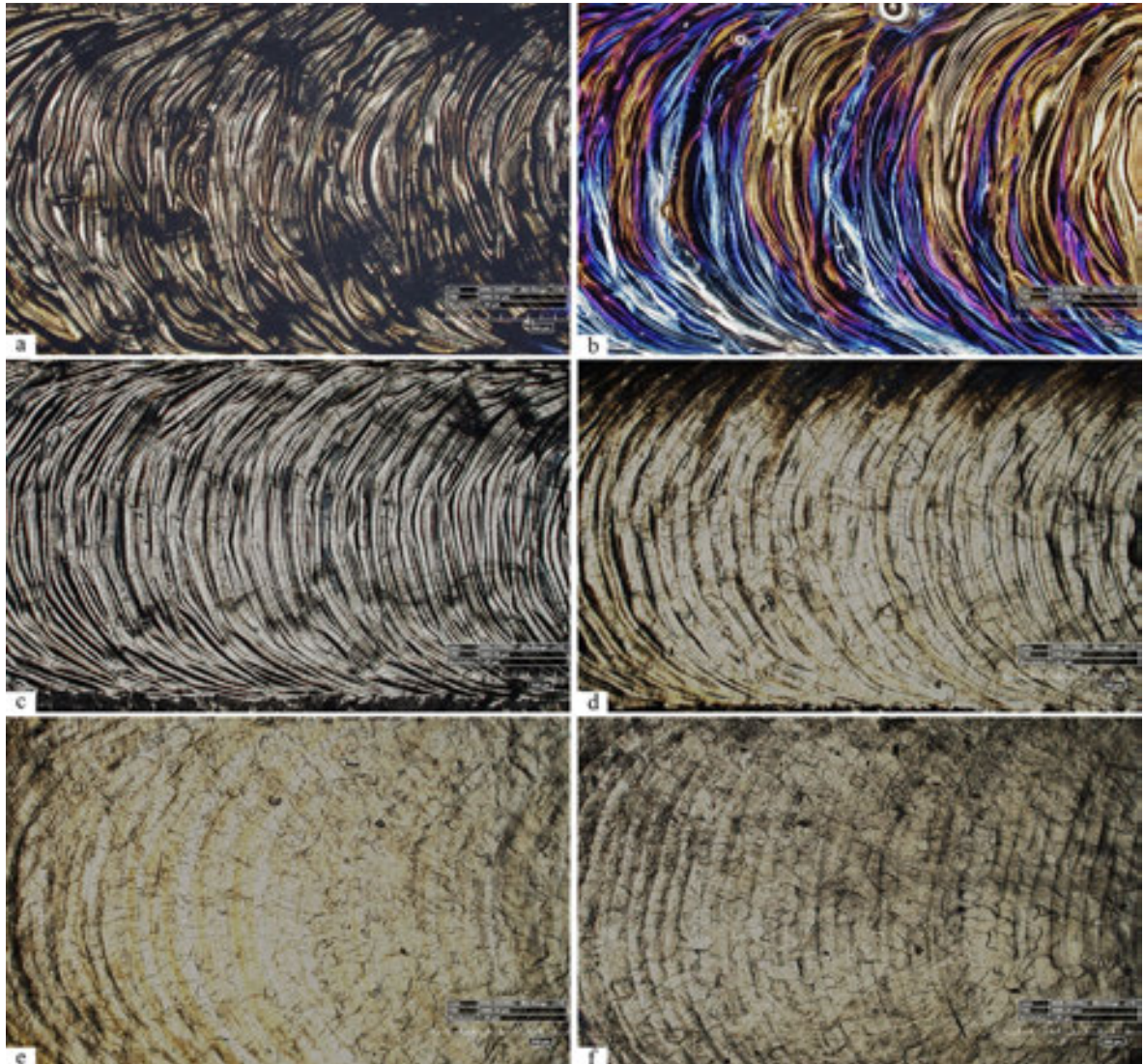


Figure 3: Weld seams of (a) 0.2 mm, (b) 0.4 mm, (c) 0.6 mm, (d) 0.8 mm, (e) 1.0 mm and (f) 1.2 mm spot sizes on Ti-6Al-4V alloy sheet

3.3. Surface roughness

The surface morphology and 3D plots of surface roughness of Ti-6Al-4V after surface treatment is shown in Figure 4. Arithmetical mean, maximum height and ten points mean roughness values were recorded for different spot sizes in Table 3. All roughness parameter values linearly decreased when spot size increased. Effect of the spot size on surface roughness of Ti-6Al-4V is shown in Figure 5. As seen from Figure 5, the values of Ra, Rz and RzJIM approximately decrease linearly with the increasing of the spot size. Narrower spot size is also increases the penetration depth because of the concentration of the energy. Literatures also reported that the surface roughness noticeably increased or decreased with an increase or decrease in different parameters, however effect of spot size on the surface roughness does not have its place in literatures. However, it is noteworthy that surface roughness will tend to reach a stable value with the increasing of spot size. The surfaces get smoother when spot size increases. According

to the above-mentioned results, when the results are correlated, and when optimum hardness and roughness values are considered, it can be concluded that the optimum parameter of spot size can be defined as 0.8 mm.

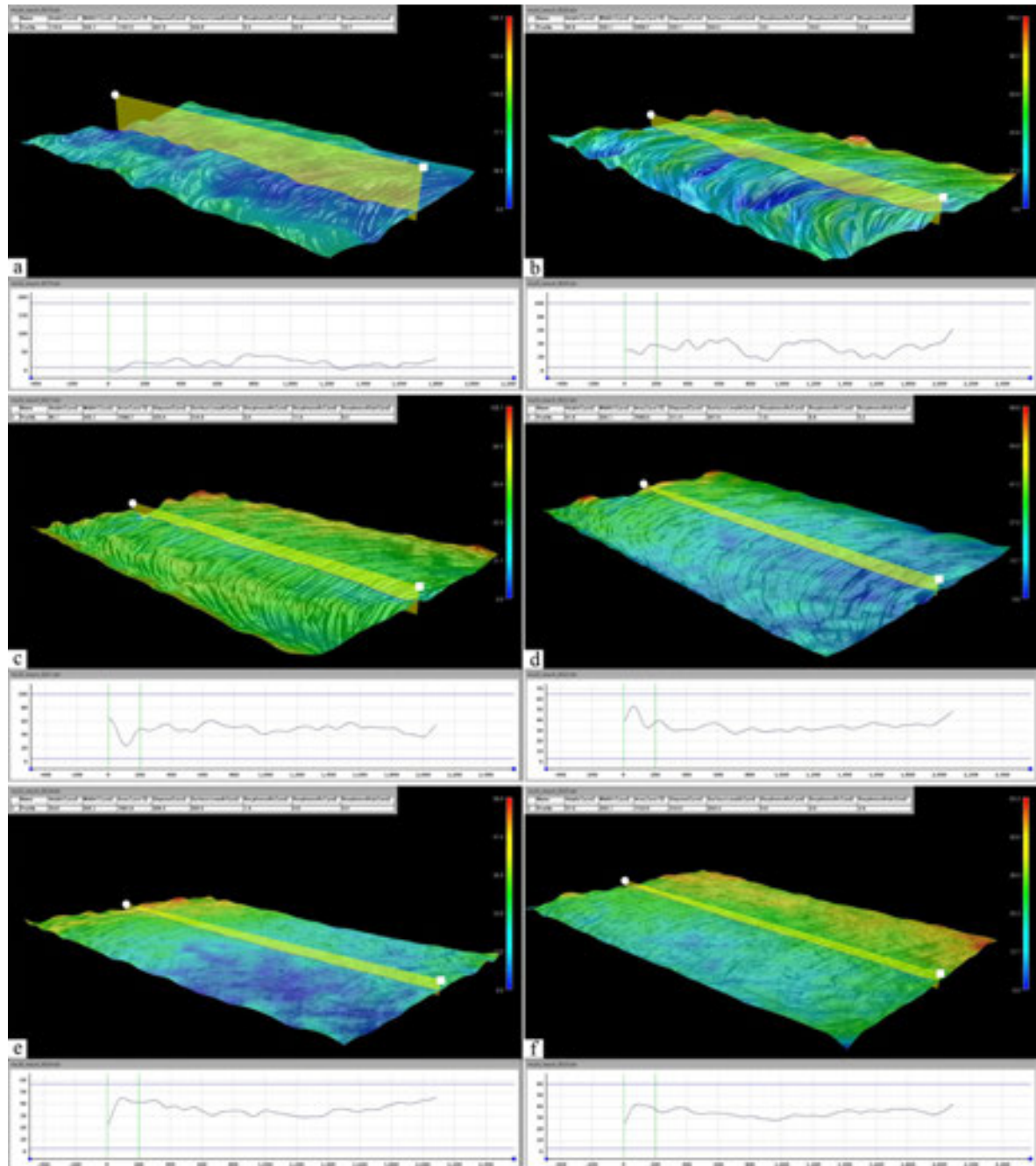


Figure 4: Surface roughness profiles of (a) 0.2 mm, (b) 0.4 mm, (c) 0.6 mm, (d) 0.8 mm, (e) 1.0 mm and (f) 1.2 mm spot sizes

Table 3: Surface roughness values

Arithmetical Mean Roughness Ra (μm)	Max. Height Roughness Rz (μm)	Ten Points Mean Roughness RzJIM (μm)	Spot Size (mm)
5.0	22.9	13.7	0.2
4.9	18.6	12.8	0.4
3.0	11.6	8.5	0.6
1.8	6.9	5.2	0.8
1.4	5.8	4.0	1.0
0.9	4.5	2.6	1.2

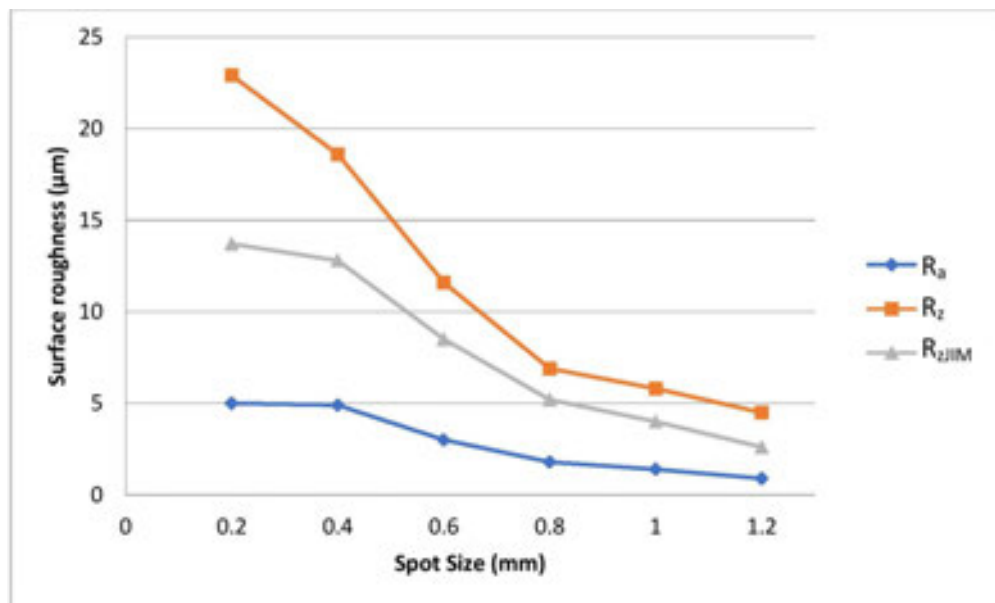


Figure 5: Effect of the spot size on surface roughness of Ti-6Al-4V

4. Conclusions

In this study, the effect of spot size was examined to compare other parameters. The results showed that, for Nd:YAG laser used for surface treatment, spot size is also an effective parameter on the seam morphology and cooling rate, which is related to harder and smoother surface.

The surface treatment on Ti-6Al-4V alloys was employed by Nd:YAG laser technique. The results yielded positive surface properties such as hardening and repairing of surface layer. In addition, the ability to control the seam morphology, surface roughness and geometry of the laser treatment by controlling the laser output parameters was noted. Controlling the penetration depth, seam geometry and size are essential in order to control morphology and to obtain higher hardness values and smooth surface.

Due to the rapid cooling rates of laser applications, the microhardness profile across the treatment indicated that, with all parameters, the hardness distribution in the fusion zone were higher than the parent metal. The applications were limited in focal depth, which was determined as -0.2 mm. The shallow focal depth caused to increase the seam widths and rapid cooling rates, which was enabled satisfactory effects and hardness to be obtained on the surface of workpiece.

The main goal of this study is to analyze the effects of the spot size on the surface roughness of laser weld seams, beside to previous studies [15]. Regarding to 3D analysis in this study, the surface roughness tends to reach a stable value with the increasing of spot size. The surfaces get smoother when spot size increases.

According to the test results, when the results are correlated, and when optimum hardness and roughness values are considered, it can be concluded that the optimum parameter of spot size can be defined as 0.8 mm. The seam morphology, surface roughness and wear properties were in excellent conditions as desired, at 8 mm spot size of the optimum level. At the over and lover of this optimum level, some surface cracks, and craters were seen.

5. References

- [1] A. Gursel: Effect of pulse repetition and peak power of Nd:YAG laser for surface treatment on Ti-6Al-4V alloy, *Düzce University Journal of Science & Technology*, 3 (2015), pp. 210-218.
- [2] A.K. Mondal, S. Kumar, C. Blawert, N.B. Dahotre: Effect of laser surface treatment on corrosion and wear resistance of ACM720 Mg alloy, *Surface & Coatings Technology*, 202 (2008), pp. 3187-3198.
- [3] S.H. Wang, M.D. Wei, L. W. Tsay: Tensile properties of LBW welds in Ti-6Al-4V alloy at evaluated temperatures below 450°C, *Materials Letters*, 57 (2003), pp. 1815-1823.
- [4] G. Casalino, F. Curcio, F. Memola, C. Minutolo: Investigation on Ti6Al4V laser welding using statistical and Taguchi approaches, *Journal of Materials Processing Technology*, 167 (2005), pp. 422-428.
- [5] J.C. Williams, E.A. Starke Jr.: Progress in structural materials for aerospace systems, *Acta Materialia*, 51 (2003), pp. 5775-5799.
- [6] M. Akbari, S. Saedodin, D. Toghraie, R. S. Razavi, F. Kowsari: Experimental and numerical investigation of temperature distribution and melt pool geometry during pulsed laser welding of Ti6Al4V alloy, *Optics & Laser Technology*, 59 (2014), pp. 52-59.
- [7] E. Akca, A. Gursel: The Effect of Diffusion Welding Parameters on the Mechanical Properties of Titanium Alloy and Aluminum Couples, *Metals*, 7 (2017), pp. 22.
- [8] E. Akca, A. Gursel: Influences of argon gas shielding on diffusion bonding of Ti-6Al-4V alloy to aluminum, *Revista de Metalurgia*, 53 (2017), pp. 088.
- [9] E. Akca, A. Gursel: Joining of dissimilar metals by diffusion bonding: Titanium alloy with aluminum, *Materials Testing*, 59 (2017), pp. 330-337.
- [10] V.K. Balla, J. Soderlind, S. Bose, A. Bandyopadhyay: Microstructure, mechanical and wear properties of laser surface melted Ti6Al4V alloy, *Journal of the Mechanical Behavior of Biomedical Materials*, 32 (2014), pp. 335-344.
- [11] E. Akman, A. Demir, T. Canel, T. Sınmazcelik: Laser welding of Ti6Al4V titanium alloys, *Journal of Materials Processing Technology*, 209 (2009), pp. 3705-3713.

- [12] J.E. Blackburn, C.M. Allen, P.A. Hilton, L. Li, M.I. Hoque, K.H. Khan: Modulated Nd:YAG laser welding of Ti-6Al-4V, *Science and Technology of Welding and Joining*, 15 (2010), pp. 433-440.
- [13] S. Zhao, G. Yu, H. Xiuli, H. Yaowu: Microstructural and mechanical characteristics of laser welding of Ti6Al4V and lead metal, *Journal of Materials Processing Technology*, 212 (2012), pp. 1520-1527.
- [14] A. Gursel: Effects of Nd:YAG laser pulse frequency on the surface treatment of Ti-6Al-4V alloys, *Materials Testing*, 58 (2016), pp. 395-400.
- [15] A. Gursel: The Wear Treatment by Nd:YAG Laser on Ti-6Al-4V Alloy: Effect of the Spot Size on Laser Beam and Seam Morphology, *Metallofizikai Noveishie Tekhnologii*, 37 (2015), pp. 1037-1048.
- [16] M.R. Amaya-Vazquez, J.M. Sanchez-Amaya, Z. Boukha, F.J. Botana: Microstructure, microhardness and corrosion resistance of remelted TiG2 and Ti6Al4V by a high power diode laser, *Corrosion Science*, 56 (2012), pp. 36-48.
- [17] Z. Sun, I. Annergren, D. Pan, T. A. Mai: Effect of laser surface remelting on the corrosion behavior of commercially pure titanium sheet, *Materials Science and Engineering A*, 345 (2003), pp. 293-300.
- [18] T.M. Yue, J.K. Yu, Z. Mei, H.C. Man: Excimer laser surface treatment of Ti-6Al-4V alloy for corrosion resistance enhancement, *Materials Letters*, 52 (2002), pp. 206-212.
- [19] N. Zaveri, M. Mahapatra, A. Deceuster, Y. Peng, L. Li, A. Zhou: Corrosion resistance of pulsed laser-treated Ti-6Al-4V implant in simulated biofluids, *Electrochimica Acta*, 53 (2008), pp. 5022-5032.
- [20] Poulon-Quintin, I. Watanabe, E. Watanabe, C. Bertrand: Microstructure and mechanical properties of surface treated cast titanium with Nd:YAG laser, *Dental Materials*, 28 (2012), pp. 945-951.
- [21] J. Arias, A. Benedetti, M. Cabeza, G. Castro, I. Feijoo, P. Merino, X.R. Novoa: Surface modification of 2017-T4 aluminum alloy by high power diode laser melting, *Surface and Interface Analysis*, 42 (2010), pp. 748-751.
- [22] L. Li: The advances and characteristics of high-power diode laser materials processing, *Optics and Lasers in Engineering*, 34 (2000), pp. 231-253.
- [23] M.T. Ariyaratnam, M.A. Wilson, A.S. Blinkhorn: An analysis of surface roughness, surface morphology and composite/dentin bond strength of human dentin following the application of the Nd: YAG laser, *Dental Materials*, 15 (1999), pp. 223-228.
- [24] Y.F. Tzeng: Process characterization of pulsed Nd:YAG laser seam welding, *The International Journal of Advanced Manufacturing Technology*, 16 (2000), pp. 10-18.
- [25] Y.F. Tzeng: Parametric analysis of the pulsed Nd:YAG laser seam-welding process, *Journal of Materials Processing Technology*, 102 (2000), pp. 40-47.
- [26] E.S. Gadelmawla, M.M. Koura, T.M.A. Maksoud, I.M. Elewa, H.H. Soliman: Roughness parameters, *Journal of Materials Processing Technology*, 123 (2002), pp. 133-145.
- [27] Q. Yunlian, D. Ju, H. Quan, Z. Liying: Electron beam welding, laser beam welding and gas tungsten arc welding of titanium sheets, *Materials Science and Engineering A*, 208 (2000), pp. 177-181.

- [28] P. Wanjara, M. Brochu, M. Jahazi: Thin gauge titanium manufacturing using multiple-pass-electron beam welding, *Materials and Manufacturing Processes*, 21 (2006), pp. 439-451.
- [29] V.C. Kumar: Process parameters influencing melt profile and hardness of pulsed laser treated Ti-6Al-4V, *Surface Coatings Technology*, 201 (2006), pp. 3174-3180.
- [30] S. Sundaresan, R.G.D. Janaki: Use of magnetic arc oscillation for grain refinement of gas tungsten arc welds in alpha-beta titanium alloys, *Science and Technology of Welding and Joining*, 4 (1999), pp. 151-160.
- [31] J. Weldingh, J.K. Kristensen: Very deep penetration laser welding—techniques and limitations, 8th NOLAMP Conference, Copenhagen, Denmark, 2001.
- [32] B. Chen, B.X. Huang, H. Liu, X.L. Li, M.T. Ni, C. Lu: Surface nano crystallization induced by shot peening and its effect on corrosion resistance of 6061 aluminum alloy, *Journal Materials Research*, 29 (2014), pp. 3002-3010.
- [33] Y.G. Liu, M.Q. Li, H.J. Liu: Nanostructure and surface roughness in the processed surface layer of Ti-6Al-4V via shot peening, *Materials Characterization*, 123 (2017), pp. 86-90.

INVESTIGATION OF MECHANICAL PROPERTIES OF FRICTION STIR SPOT WELDED LIGHT METAL ALLOYS

Ahmet ATAK^{1,a}, Aydın ŞIK^{2,b}

^{1,2}Gazi University, Dep. of Industrial Design, Eti Mah. Yükseliş Sok. 5, 06570 Maltepe Ankara–TURKEY
^aahmet.atak@gazi.edu.tr, ^baydins@gazi.edu.tr

Abstract

The use of light metals today is of great importance, for example in the automotive, aviation and aerospace industries, where energy consumption is minimized and thus the economy is being attempted. By using light metals, weight is reduced so that energy is saved. Aluminum and magnesium alloys are particularly used thanks to their lightweight. Vehicles in the automotive, aerospace and space industries are expected not only to have lightweight but also high static and dynamic strengths since they are exposed to static and dynamic cyclic loads.

However, the structural components can quickly become fatigued and fail under cyclic load due to the notch factor of the joining zones. Compared to the fusion welding method, joining of material is realized mechanically below the melting point of the material in the friction stir spot welding (FSSW) method. Thus, the fatigue strength of the assembly is much higher than that of the fusion welding.

In this study, Light metal alloy of magnesium AZ31B and aluminum EN AW 2024 were joined with FSSW method and mechanical properties of this joins were also carried out.

Key Words: Friction stir spot welding; Joining of Magnesium; Joining of Aluminum; Welding of Light Metals.

1. Introduction

In consequence of the limited energy resources in the world and the increasing awareness of energy saving in human beings, manufacturers in the automotive and aerospace industries are using lightweight metals to save fuel and thus saving energy in vehicles, they produce [1-5].

There are various technical problems in the resistance spot welding, which is one of the joining methods in fusion welding of light metals. The most important of these is the realization of the joining above melting point, which burns and cause brittleness of the material, the joining defects and the notch factor; causing fatigue damage to vehicles or machines exposed to cyclical dynamic loads [6-11].

In this study, aluminum alloys (EN AW 2024) and magnesium alloy (AZ31B) sheets were lab-joined by using FSSW method, and mechanical tests results are given.

2. Experimental

In order to verify the selected material a standard material tests were carried out. Tension-shear Test and three points banding tests were also carried after joining the materials.

2.1. Base Material Tension Tests

Mechanical properties of base material were verified by using INSTRON 3369 tension test machine according to ISO 6892-1. The dimensions and picture of tension test samples are given in Figure 1 and Figure 2.

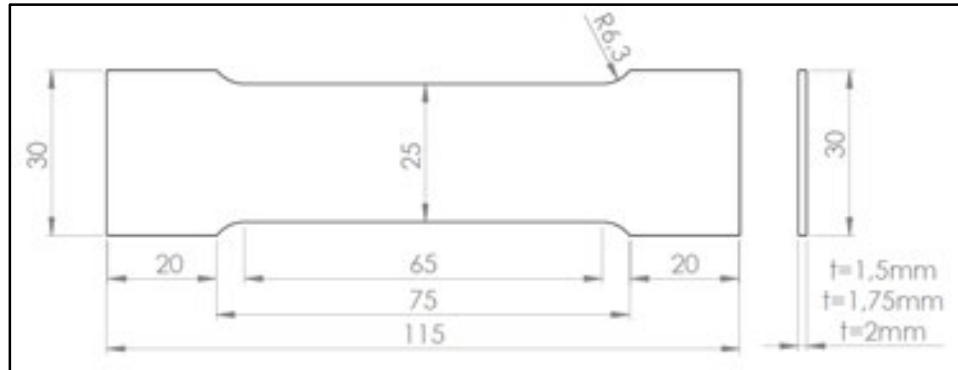


Figure 1. Tension Test sample dimension according to ISO 6892-1

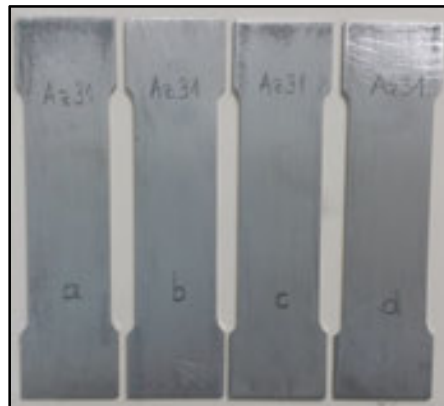


Figure 2. Tensile test samples of magnesium alloy AZ31B-O according to ISO 6892-1

Table 1. Chemical composition of magnesium alloy AZ31B[12]

Alloy	Al	Ca	Cu	Fe	Mn	Ni	Si	Zi	Mg
%	2,5-3,5	0,04	0,05	0,005	0,2-1,0	0,005	0,1	0,6-1,4	Kalan

Table 2. Mechanical properties of magnesium alloy AZ31B[12]

Temper	Tensile strength (MPa)	Yield stress (MPa)	Elongation (%)
T4	240	145	≥ 7

Table 1 and Table 2 show the chemical composition and mechanical properties of magnesium alloy sheet AZ31B accordingly with the standards [12].

Figure 3 shows the tensile test sample of aluminum alloy EN AW 2024-T4 accordingly with ISO 6892-1

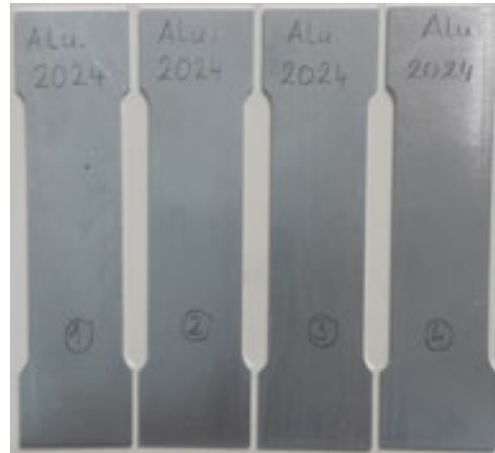


Figure 3. Tensile test samples of aluminum alloy EN AW 2024-T4 according to ISO 6892-1

Table 3. Chemical composition of aluminum alloy EN AW 2024-T4[13]

Element	Al	Cu	Mg	Mn	Fe	Cr	Zi+Ti	Zn	Si
%	90,7-94,7	3,8-4,9	1,2-1,8	0,3-0,9	0,5	0,1	0,15	0,25	0,5

Table 4. Mechanical properties of aluminum alloy EN AW 2024-T4 [13]

Temper	Tensile Strength (MPa)	Yield Strength (MPa)	Elongation (%)	Hardness (HB)
T4	≥ 425	≥ 275	≥ 12	120

Table 3 and Table 4 show the chemical composition and mechanical properties of aluminum alloy sheet EN AW 2024-T4 accordingly with the standards[13].

Since the materials which are having E Modulus lower than 150000 MPa are investigated, tension test speed were selected according to table 3 in ISO 6892-1 which is 1 mm/min respectively 18 MPa/s.

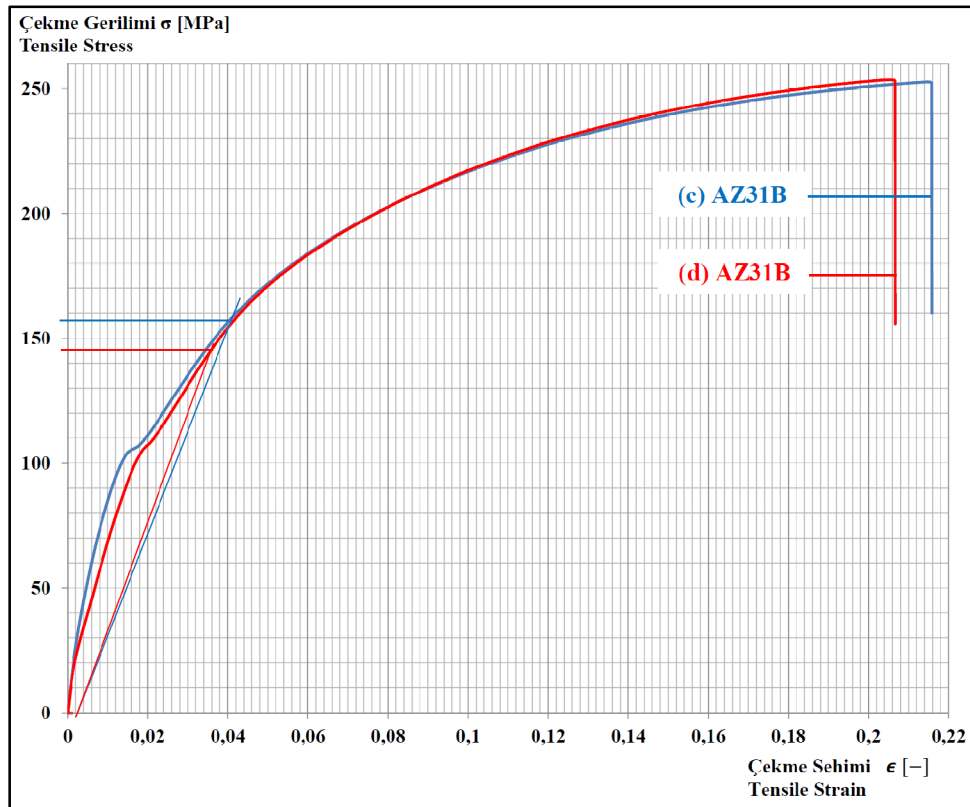


Figure 4. Tension test results of 1,5 mm thick magnesium alloy AZ31B with a tension speed of 1mm/min

Figure 4 shows the tension test results. Only two of the four prepared sample (a, b,c,d) gave a reliable results.

Table 5. Mechanical properties of 1,5 mm thick magnesium alloy AZ31B measured by the tension test with a tension speed of 1mm/min

Sample / Material	Tensile Strength σ_u [MPa]	Yield strength σ_y [MPa]	Yield rate A [%]
(c) AZ31B	252,6	156	21,8
(d) AZ31B	253,5	146	21,0
AZ31B (Avg.)	253	151	21,4

Table 5 shows the mechanical properties of 1,5 mm thick magnesium alloy AZ31B measured by the tension test with a tension speed of 1mm/min

Figure 5 shows the tension test results for aluminum sheets. All four tests samples (1,2,3,4) gave reliable test results.

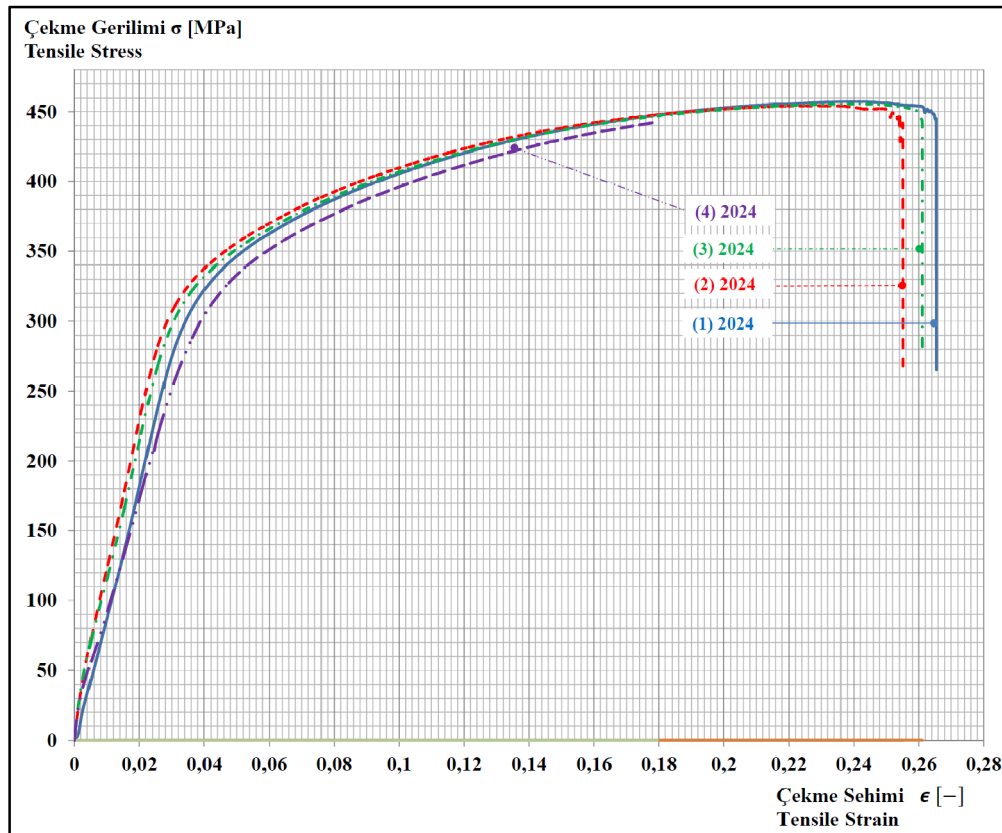


Figure 5. Tension test results of 1,2 mm thick aluminum alloy EN AW 2024-T4 with a tension speed of 1mm/min

Table 6. Mechanical properties of 1,2 mm thick magnesium alloy EN AW 2024-T4 accordingly to tension test with a tension speed of 1mm/min

Sample /Material	Tensile Strength σ_u [MPa]	Yield Strength σ_y [MPa]	Yield Rate A [%]
(1) EN-AW 2024	457,5	290	26,8
(2) EN-AW 2024	454,3	330	25,7
(3) EN-AW 2024	455,6	325	26,5
(4) EN-AW 2024	442,6	305	18,2
EN-AW 2024 (avg.)	452,5	312,5	24,3

Table 6 shows the mechanical properties of the aluminum alloy EN AW 2024-T4 material and the thickness of the 1.2 mm sheet measured by the tensile test at a speed of 1 mm / min.

Mechanical properties of magnesium alloy AZ31B and aluminum alloy EN AW 2024-T4 material were determined with the tensile tests. It was concluded that the provided values are in line with values in the standards corresponds the criteria of the standards and therefore the tests are considered as reliable.

2.2. Tensile-Shear Test

Standard test sample (AZ31B) welded with shoulder profile type A were exposed to tensile-shear tests. Figure6 show the force-elongation test results for test speed of 10mm/min. Average ultimate tensile strength of 4 EN AW 2024-T4 sample materials is 2820 N given in and figure 7.

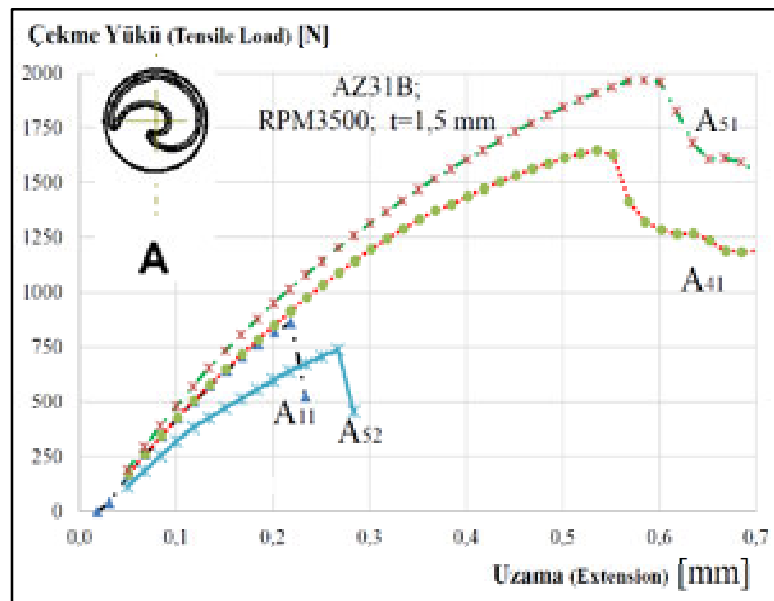


Figure 6.Force Elongation graphic of Tensile –shear tests results of 1,5 mm magnesium alloy AZ31B samples, A11,A41,A51

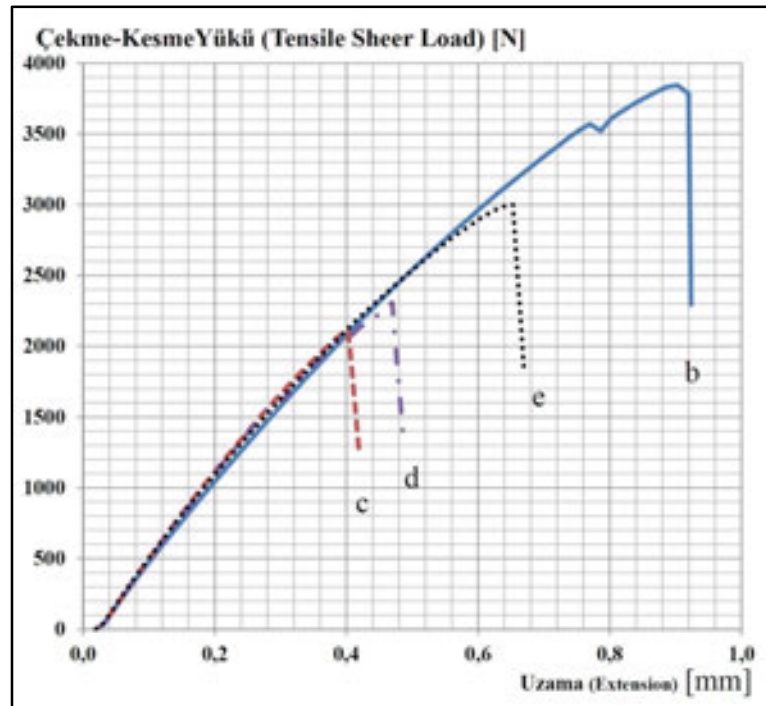


Figure 7.Force Elongation graphic of tensile –shear tests results of 1,2 mm aluminum alloy EN AW 2024-T4 samples, b,c,d and e

Table 7 show the tensile shear test results of different material such as AZ31B and EN AW 2024-T4 with joining of same shoulder profile (A)

Table 7.Comparison of tensile –shear test results of AZ31B and EN Aw 2024-T4 (Shoulder profile A)

Material	Ultimate shear force max.Fu [N]	Average shear force Fu [N]	Tensile strength fu [MPa]	Fu / fu [N/MPa]
AZ31B	1500	1290	240	5,4
EN AW 2024-T4	3850	2820	425	6,6

If we compare the average tensile forces obtained in tensile-shear tests to the tensile stress of the material,it can be said that this ratio of EN AW 2024-T4 material is bigger than that in AZ31B and therefore the joining of EN AW 2024-T4 are more robust.

2.2. Three points bending test

The set up and its dimensions used for the three point bending test according to ISO 7038 are shown in figure 8. According to this; $a = 2 * 1.5\text{mm} = 3\text{mm}$; $D = 6\text{ mm}$; $l = 15,5 + D + 3a * a / 2 = 25 * 1,5\text{ mm}$ and the cylinder diameters of the supports were selected as $d=50\text{ mm}$. An extra

15.5 mm has been added to the support pitch gauge 1 otherwise the lap area is touched by the support rollers during bending and thus causes incorrect measurement.

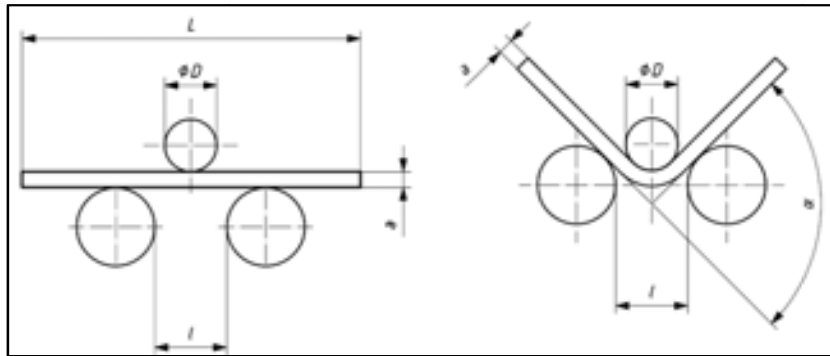


Figure 8.Set up dimensions for three point bending test according to ISO 7038

Figure 9 and figure 10 graphically shows the bending force vs bending deflection values of the three-point bending test after joining of 1,7 mm and 2,0 mm magnesium alloy AZ31B sheets with FSW. Joining conditions are 5-second plunge time and 15 seconds waiting

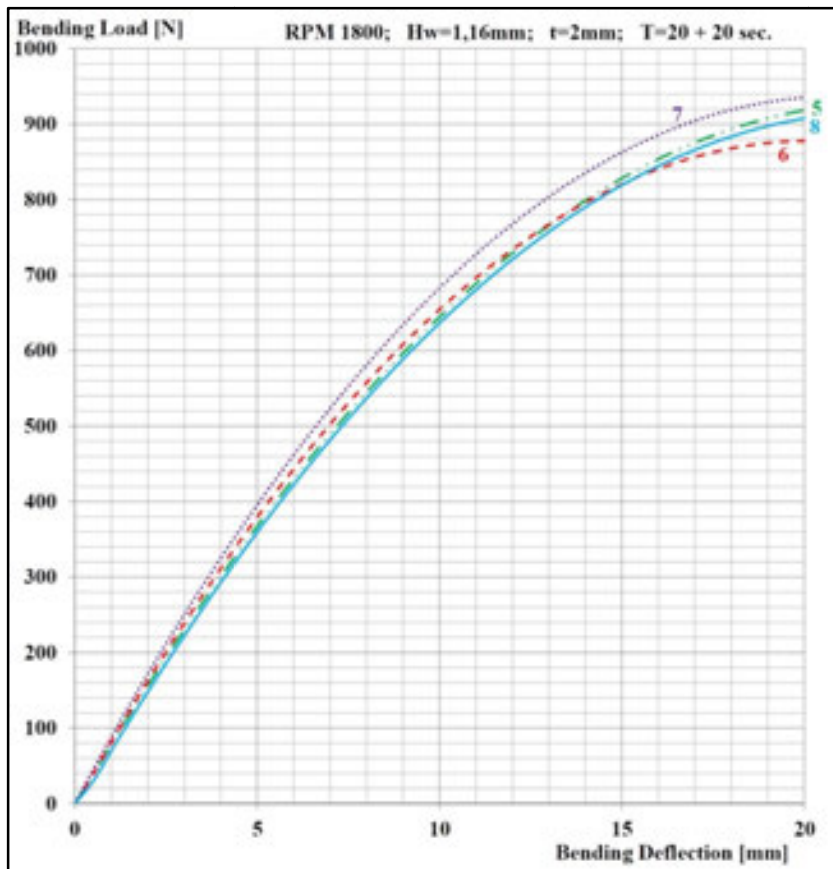


Figure 9.Graphical representation of Bending forces vs. Bending deflection according to three point bending test results of FSW welded 2,0 mm magnesium alloy AZ31B

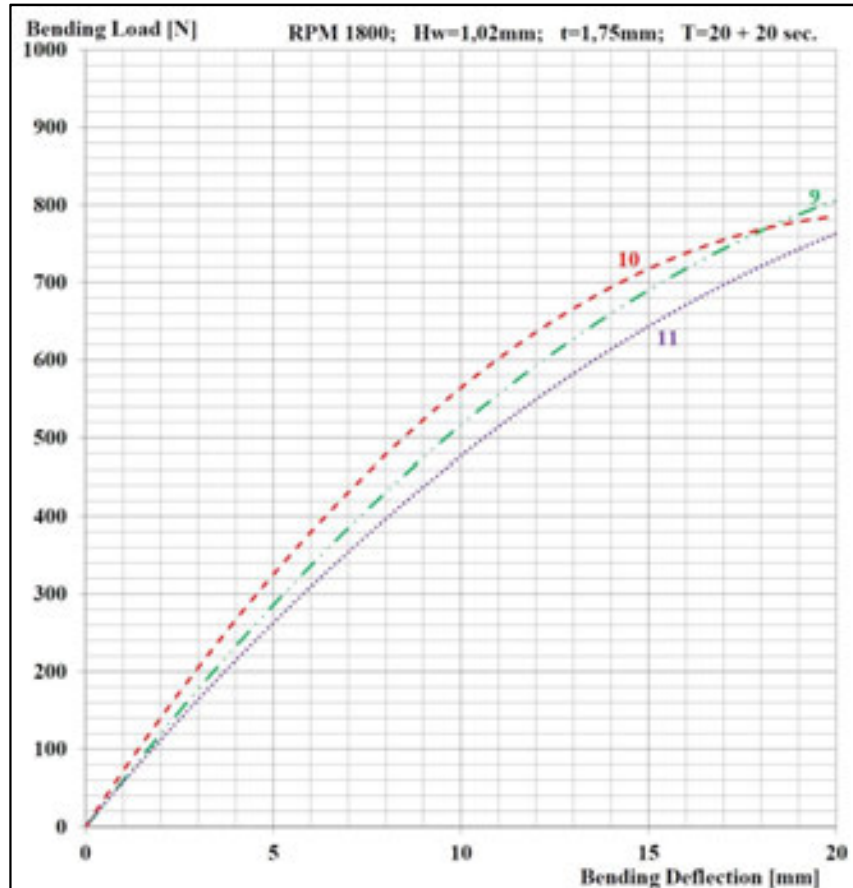


Figure 10. Graphical representation of Bending forces vs. Bending deflection according to three point bending test results of FSW welded 1,75 mm magnesium alloy AZ31B

3. Results and Conclusion

- It was found that magnesium alloy and aluminum alloy thin plates can be joined together with a friction stir spot welding
- Base material used in this study AZ31B and EN AW 2024 were tested for their and verified to be in accordance with the specifications given in the standard of mechanical properties.
- If the tensile forces of the base material are compared with the tensile force of the FSW materials, the tensile force in the joined material descends at least the half through the notch factor (about 2.5). This would not be the case if it were a continuous welding instead of a spot welding.
- A higher tensile-shear forces were obtained for aluminum alloy EN AW 2024 material joined with FSW compared to magnesium alloy AZ31B.
- If the three points bending test results of different thicknesses (1,75 and 2,0 mm) of magnesium alloy AZ31B sheets compared; almost similar results were obtained.

4. References

- [1] K. Kandemir, A. Ç. Can: Otomotiv Endüstrisi İçin Magnezyum Alaşımlarının Kullanım Potansiyeli, (2003), Pamukkale Üniversitesi Mühendislik Fakültesi Mühendislik Bilimleri Dergisi, 1, 37-45.
- [2] DTI., Magnesium Alloys And Processing Technologies For Light weight Transport Applications, (2004), Global watch mission report, U. K.
- [3] A. A. Kaya, E. F. Özdoğru, D. Abanoz, S. Yiğit, O. Yücel: Otomotivde Magnezyum Alaşım Uygulamaları, (2002), OTEKON02 Otomotiv Teknolojileri Kongresi , Bursa, s. 41-46.
- [4] A. ŞIK: Otomobil saclarının MIG/MAG kaynağında gaz karışımlarının bağlantının mekanik mekanik özelliklerine etkisi, Gazi Üniversitesi Endüstriyel Teknoloji Eğitimi, Doktora tezi, (2002).
- [5] A. ATAK, A. ŞIK, V. ÖZDEMİR: Sürtünme Karıştırma Nokta Kaynağı (SKNK) Yöntemi İle Otomotiv Sektöründe Kullanılan Magnezyum Alaşımlarının Birleştirilmesi, 9th International Automotive Technologies Congress, OTEKON 2018, Bursa-TURKEY.
- [6] A.ŞIK, Ö. AYABAŞ: Sürtünme karıştırma kaynağı ile yapılan Alüminyum kaynağında kaynak bölgesinin mekanik özelliklerinin incelenmesi, Gazi Üniversitesi Endüstriyel Sanatlar Eğitim Fakültesi Dergisi, (2003), Y.11, S.12, 30-43.
- [7] A. ŞIK: Sürtünme Karıştırma Kaynağı İle Birleştirilen Magnezyum Levhaların Mekanik Özelliklerinin İncelenmesi, (2010), SAÜ. Fen Bilimleri Dergisi, 14. Cilt 14, Sayı 2, 134-140.
- [8] M. K. KÜLEKÇİ M. K., A. ŞIK, E. Kaluç: Effects of Tool Rotation and Pin Diameter on Fatigue Properties of Friction Stir Welded Lap Joints, (2008), The International Journal of Advanced Manufacturing Technology, 36(9), 877-882.
- [9] A. Gerlich, M. Yamamoto, T. H. North: Local Melting and Cracking in Al 7075-T6 and Al 2024-T3 Friction Stir Spot Welds, Science and Technology of Welding and Joining, (2007), 12, 6, 474-475.
- [10] E. Kaluç, E. Taban: Otomotiv Endüstrisinde Direnç Nokta Kaynağına Alternatif Bir Yöntem: Sürtünen Elemanla Nokta Kaynağı (FSSW), (2007), Kaynak Teknolojisi VI.Ulusal Kongresi ve Sergisi, TMMOB Makine Mühendisleri Odası, 449.
- [11] E. Kaluç, E. Taban: Sürtünen Eleman İle Kaynak (FSW) Yöntemi, (2007), TMMOB Makine Mühendisleri Odası, TMMOB Makine Mühendisleri Odası, "Kaynak Teknolojisi VI. Kongre ve Sergisi Bildiriler Kitabı" 460, 60-77.
- [12] ASTM B 107/B 107M-07: Standard Specification for Magnesium-Alloy Extruded Bars, Rods, Profiles, Tubes, and Wire, Copyright © ASTM International, 100 Barr Harbor Drive, PO Box C700, West Conshohocken, PA 19428-2959, United States.
- [13] BS EN 485-2:2007: Aluminium and aluminium alloys-Sheet, strip and plate-Part 2: Mechanical properties, BRITISH STANDARD.

THE EFFECT OF THE OCCUPATIONAL HEALTH AND SAFETY EDUCATION ON STUDENT AWARENESS LEVEL IN VOCATIONAL AND TECHNICAL SECONDARY EDUCATION INSTITUTIONS

Arslan Kıvanç Yıldırım^{1,a}, Ömer Asal^{2,b},

¹ Gazi University

² Gazi University

^a arslan1000@gmail.com, ^b omerasal@gazi.edu.tr

Abstract

In this study, the effect of the occupational health and safety module on students' awareness level were investigated. This module is a part of the compulsory vocational development lessons in vocational and technical secondary education institutions. Whether or not there was a significant difference between the pretest which was conducted before the lesson and a posttest which was conducted after the lesson was explored. The test of forty questions which was implemented on a sample of one hundred students was conducted twice: before the lesson and after the lesson, and the results were interpreted on computer via the analysis performed with SPSS program.

Key Words: Occupational Health and Safety, Vocational and Technical Secondary Education.

1. Introduction

In 2012 there has been 62903 occupational accidents and illnesses 533 occupational illnesses in Turkey. 1.454 workers have lost their lives due to occupational accidents and occupational illnesses. Everyday 172 occupational accidents and 4 deaths caused by these occupational accidents have been occurring in our country.

When we look briefly on the law on Occupational Health and Safety, there are several important headings. In the new term they will be applied. These headings could be listed as follows:

- All the workers will work in safety.
- Preventive measures are more important than mere rules.



- Workplaces will be classified according their danger levels.
- There will be an occupational health and safety expert and on-site doctor in every workplace.
- There will be a common unit for occupational health and safety for workplaces.
- There will be government aid for small businesses.
- Risk assessment will become compulsory.
- Health checkup will be done before recruiting workers.
- Active record will be kept on occupational accidents and illnesses.
- Workplaces will be ready for emergencies.
- Workers will contribute to work health and safety.
- There will be education for workers on work health and safety.
- There will be boards for work health and safety.
- There will be worker right to abstain from working in dangerous situations.
- Coordination of work health and safety will be assured in workplaces.
- Work will be paused when life critical situations are detected.
- Precautions should be taken for big industrial accident risks.
- Administrative sanction will be more active.
- The law will be applied gradually.

This law has some enforcements on the part of employer. The employer must improve the conditions for work health and safety and must maintain them. The employer must take the suitability of the worker to the work health and safety into consideration. The employer must develop a general prevention policy by taking risk assessment reports into consideration. The employer must take every precaution including giving education to prevent occupational risks. The employer must also make the necessary control, measures and investigations which are necessary in the working environment, observe them and eliminate incompatibilities. The employer should take the necessary precautions so as not the workers go the places which includes life threatening risks. Lastly the employer should ensure coordination if the working environment is shared by more than one employer.

This law has some gains on the part of the worker. The workers can take advantage of the services of work health and safety without quota. They will be able to actively involve and propose related to the work health and safety endeavors. In the face of serious and close danger, they can abstain from work until the necessary precautions are taken. They will get education on work health and safety. They will be represented in work health and safety issues. On the other hand they mustn't endanger themselves and their colleagues in terms of work health and safety. They will use all the tools and accessories in a proper manner related to production and protection.

Occupational safety is the precautions taken to create a safe working environment by preventing workers from having occupational accidents.

Parallel to the industrialization and technological advances in our country and in the world, there was an increase in the problems related to the safety of the occupational safety of the workers in the workplace. It is necessary to take some precautions in advance and ensure the safety of workplaces.

The aims of the workplace safety can be listed as follows:

- To provide the workers with the best possible safe working environment
- To protect workers from the negative effects of working conditions
- To provide the best possible harmony with the work and the worker
- To eliminate the risks in workplace totally or reduce the hazards to the minimum
- To eliminate physical and moral damages that may occur.
- Increase the effectiveness in the workplace.

Occupational Health is a medical branch founded in order to preserve every workers' social, moral and physical health in the optimal level, to make the working conditions, and production tools suitable for health and by preventing workers from harmful effects to ensure the harmony of the work and the worker the in every occupation.

It is a known fact that the order of the workplace and its maintenance (cleaning); and the good organization of the workplace improves the spirits of the workers, improve the work effectiveness and prevents most of the occupational accidents.

In every workplace, there should be a plan and program which ensures the organization and the maintenance of the workplace and the preservation of these issues. In order for this to happen, the reasons and conditions causing disorganization should be eliminated, a routine should be set and the routine should be maintained via daily controls and tracking.

2. Experimental

In this part, an experimental study is described on whether Health and Safety at Work Education was useful on real data. 100 students were recruited for this study. A pre-test which was conducted before the education, and the post-test which was conducted after the education were evaluated and analyzed. The results of the mentioned pre-test and post-test were given in the Tab. 1.

Table 1. Pre-test and Post-test Results Before and After Health and Safety at Work Education

Pre-Test Results				Post-test Results			
43.0	39.0	42.0	35.0	68.0	68.0	62.0	51.0
33.0	33.0	32.0	36.0	71.0	82.0	73.0	59.0
45.0	43.0	40.0	48.0	68.0	74.0	74.0	75.0
39.0	53.0	35.0	53.0	72.0	76.0	78.0	77.0
43.0	42.0	34.0	26.0	69.0	79.0	83.0	79.0
45.0	30.0	45.0	35.0	68.0	74.0	82.0	65.0
52.0	48.0	48.0	41.0	72.0	78.0	87.0	68.0
31.0	57.0	46.0	41.0	76.0	64.0	63.0	75.0
32.0	46.0	51.0	45.0	77.0	72.0	66.0	81.0
48.0	49.0	40.0	41.0	76.0	71.0	74.0	79.0
45.0	35.0	34.0	33.0	67.0	70.0	61.0	60.0
36.0	35.0	40.0	42.0	73.0	79.0	63.0	72.0
38.0	33.0	35.0	30.0	64.0	71.0	79.0	65.0
45.0	36.0	36.0	36.0	70.0	63.0	69.0	74.0
39.0	35.0	42.0	49.0	60.0	73.0	74.0	74.0
53.0	47.0	38.0	36.0	80.0	76.0	70.0	70.0
45.0	39.0	54.0	48.0	71.0	74.0	63.0	68.0
26.0	49.0	33.0	46.0	83.0	70.0	63.0	67.0
38.0	43.0	44.0	42.0	77.0	67.0	77.0	76.0
38.0	40.0	37.0	46.0	68.0	72.0	82.0	78.0
49.0	27.0	35.0	41.0	73.0	64.0	65.0	65.0
41.0	32.0	37.0	45.0	73.0	79.0	68.0	87.0
29.0	47.0	43.0	45.0	75.0	68.0	75.0	72.0
39.0	42.0	26.0	29.0	76.0	72.0	68.0	78.0
52.0	40.0	41.0	44.0	72.0	76.0	71.0	83.0
Mean: 40,450				Mean: 71,990			
Variance: 47,705				Variance: 42,495			

The histogram and scatterplot graphs of these data were given in: Figure 1.

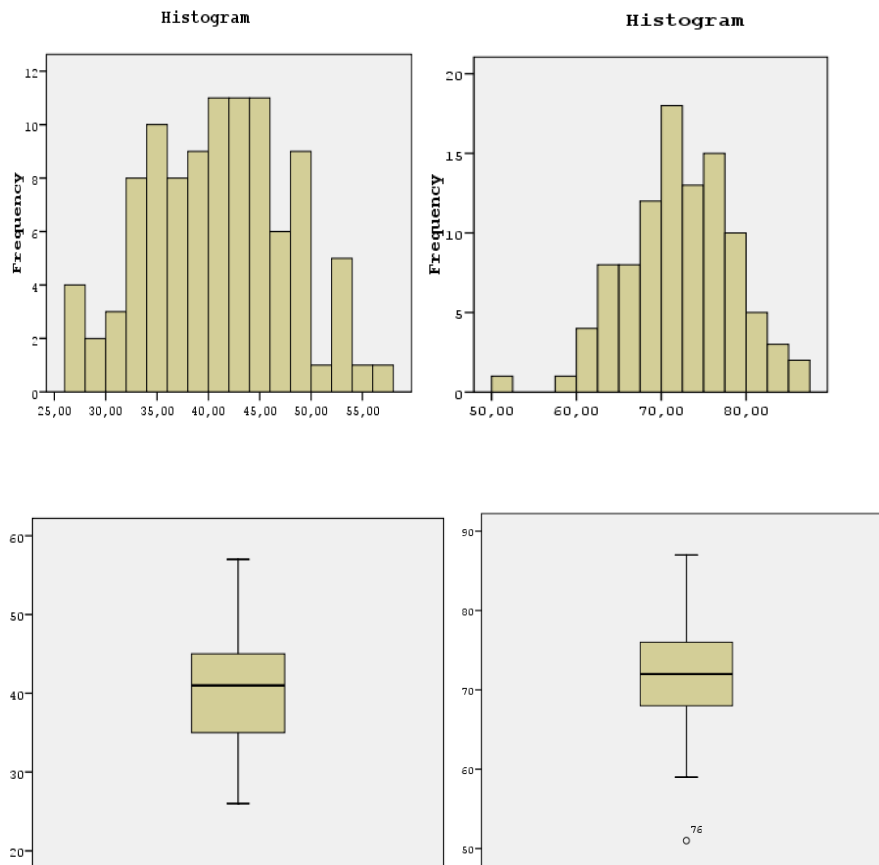


Figure1. Histogram and Scatterplot Graphs for the Pre-test (left) and Post-test (right) Before and After Health and Safety at Work Education

3.Results and Discussion

The null hypothesis for whether the education had an effect on the results would be as follows:

H₀: There is no effect of education on the test results.

The alternative hypothesis would be as follows:

H₁: there is an effect of education on the test results.

Since our study design is on pre and post-test design, a “Paired-t test” was made use of to test the null hypothesis. Before the T test the normality of the data was checked to confirm the hypothesis that the data was normal. In order to do this, we used Shapiro-Wilk test on the grounds that our sample consisted of 100 participants. The data were normal and the results were given in Tab. 2.

Table 2. Normality Test Results

Test of Normality			
	Stat.	df	Sig.
Pre-Test	0,989	100	0,566
Post-Test	0,990	100	0,652

According to the results in Tab. 2, it is stated that 95% of the observation of pre-test and post-test results will fall under normal distribution. The data were normally distributed

The Paired T test was conducted on the results in SPSS 16.0 statistical program and the results in the Tab. 3. Were obtained.

Paired Samples Test			
	Paired-T Testi statistiği	df	Sig. (2-tailed) (p)
Pre-test-Post-test	-33,866	99	0,000

Table 3. Paired Samples t test on Pre-test and Post-test Results Before and After Health and Safety at Work Education

4. Conclusion

When $\alpha = 0,05$ according to Tab. 3. $p < \alpha$. Therefore, the null hypothesis: "There is no effect of education on the test results" is rejected. Therefore, the Education which was conducted on students on After Health and Safety at Work is effective at 95% confidence level. In the light of this result, it is concluded that the Health and Safety at Work Education improves the students' knowledge on Work Safety.

7. References

Çalışma ve Sosyal Güvenlik Bakanlığı “6331 Sayılı İş Sağlığı ve Güvenliği Kanunu”
<https://www.csgb.gov.tr/media/2052/6331.pdf>

Milli Eğitim Bakanlığı “Mesleki Gelişim Dersi İş Sağlığı ve Güvenliği Ders Modülü”
http://www.megep.meb.gov.tr/mte_program_modul/moduller_pdf/%C4%B0%C5%9F%20G%C3%BCvenli%C4%9Fi%20ve%20%C4%B0%C5%9F%C3%A7i%20Sa%C4%9Fi%C4%B1%C4%9F%C4%B1.pdf

CORRESPONDENCE ADDRESS: Arslan Kıvanç Yıldırım, address: Hasandağ Street, No 14-15 Ankara, Turkey, Tel: +90 05512474988 E-mail: arslan1000@gmail.com.

SHORT BIOGRAPHIES

Arslan Kıvanç Yıldırım –He has his MS degree on Manufacturing Engineering at Gazi University. He is currently working as a teacher at Gazi Vocational High School in Ankara.

Asst. prof. Ömer Asal –He has his PhD degree from Physical Sciences Institute in Gazi University. He is currently working as an Asst. Prof. on Manufacturing Engineering at Gazi University

EFFECT OF PWHT TEMPERATURE AND TIME ON HARDNESS AND MICROSTRUCTURE OF 410NiMo WELD METAL

Uğur Özdemir^{1,a}, Selçuk Keskinilic^{1,b}, Filiz K. Acar^{1,c}, Fikret Kabakci^{2,d}
and Mustafa Acarer^{3,e}

¹ Gedik Welding Inc., Istanbul, Turkey

² Bulent Ecevit University, Alaplı Vocational School, Alaplı, Zonguldak, Turkey

³ Selçuk University, Faculty of Technology, Metallurgical and Materials Engineering, Konya, Turkey^a
uozdemir@gedik.com.tr, ^bskeskinkilic@gedik.com.tr, ^cfacar@gedik.com.tr, ^dfikretkabakci@yahoo.com^e
m_acarer@yahoo.com

Abstract

ASTM A743 CA6NM alloy is a martensitic stainless steel typically used in energy industry -runners and hydraulic turbine components- due to its superior toughness, yield and fatigue properties. In both the manufacturing, shielded metal arc welding is applied to join for this grade steels. However, weldability of the steels is limited due to formation of hard and brittle phases such as untempered martensite during welding and post weld heat treatment processes. The formation causes a reduction in toughness. In this study, influence of post-weld heat treatment procedure (single tempering and double tempering) and parameters on microstructure and hardness of AWS410NiMo all weld metal. Hardness tests were conducted from weld metal. Microstructures of the all weld metals subjected to different heat treatment process were characterized.

Key Words: 410 NiMo, all weld metal, heat treatment, hardness, microstructure

1. Introduction

Low carbon 13%Cr-4%Ni (CA6NM) martensitic stainless steels such as Alloy 410 (410NiMo) are used at elevated temperature and corrosive environments such as hydroelectric turbine runners, chemical and power industries due to having good mechanical and corrosion properties [1, 2]. These steels have high flow stress and toughness, high resistance to cavitation and reasonable weldability. Martensitic steels with low carbon content are always quenched and tempered to have good mechanical properties [3]. A post-weld heat treatment (PWHT) is then required to temper the brittle martensite. The use of 410NiMo steel and weld metal without PWHT is not recommended due to high level of residual stresses, cold cracking and poor fatigue resistance [3-5]. Another beneficial effect of this PWHT is to lower the residual stresses induced by welding [6]. Tempering temperature and time have a great influence on microstructure [7]. Two different tempering types were prescribed for 410NiMo martensitic stainless steel according to NACE MR0175 standard to acquire maximum 265 HB hardness [8]. The aim of this study is to evaluate the influence of the applied PWHT type on microstructure and hardness of 410NiMo weld metal deposited by the shielded metal arc welding (SMAW) process.

2. Experimental

In this study, effect of post weld heat treatment on the microstructure and hardness of 410NiMo weld metal was investigated. All weld metal was produced by shielded metal arc welding (SMAW) technique. A 25 mm thick weld metal was deposited on a 25 mm thick S355 JR substrate (250 mm × 350 mm) using GeKaElox B 410NiMo stick electrodes. The electrodes were fabricated by Gedik Welding Co. in Turkey. Welding parameters were given in Tab.1

Table 1. Welding parameters of produced 410NiMo All Weld Metal.

Weld Pass Number	Preheat and Inter Pass Heating (°C)	Current (A)	Voltage (V)	Weld speed (mm/min)	Heat Input (kJ/mm)
25	100-150	110	32	125	1.689

Preheat and interpass temperatures were held at 100 °C and 150 °C respectively. The weld metals were subjected to post weld heat treatment (PWHT) process (PWHT) as seen in Figure 1.

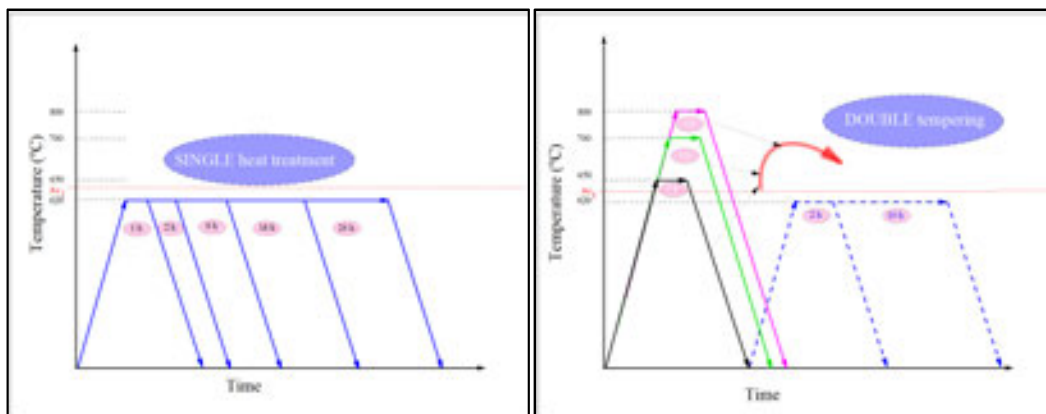


Figure 1. Systematic presentation of PWHT applied to weld metal.

Standart metallographic procedure was applied to PWHT'ed weld metal samples for microstructure characterization. Modified vilella's reagent (2.5 gr picric acid + 2.5ml HCl + 95ml Ethanol) [9] was prepared as etching solution. Nikon Eclipse MA100 inverted optical microscope was employed. RIGAKU ZSX Primus II X-Ray fluorescence device and LECO CS600 were used to determine chemical composition and carbon and sulfur content respectively. Chemical analysis of weld metal is shown in the Tab. 2. Hardness' of the weld metals were measured by Brinell hardness tester 187.5kgf-ϕ2.5mm ball diameter.

Table 2. Chemical analysis of weld metal.

	C	Mn	Si	Ni	Mo	Cr	Cu	V	Fe
ELOX B	0.03	0.58	0.21	5.29	0.52	11.23	0.04	0.037	Bal.
410 NiMo									

3. Results and Discussion

3.1. Microstructure

Figure 2 shows the microstructure of welded condition and single PWHT processes. Microstructure of the sample as welded condition has martensitic and thicker and harder than single or double PWHT'ed samples due to fresh martensite. Delta ferrite phase was not detected by optical microscopy investigation. Finer martensitic structure observed 620 °C 18h and 24 h PWHT. In the microstructure white area may be fresh martensite/retained austenite. Increasing tempering time, the lath and white area are finer.

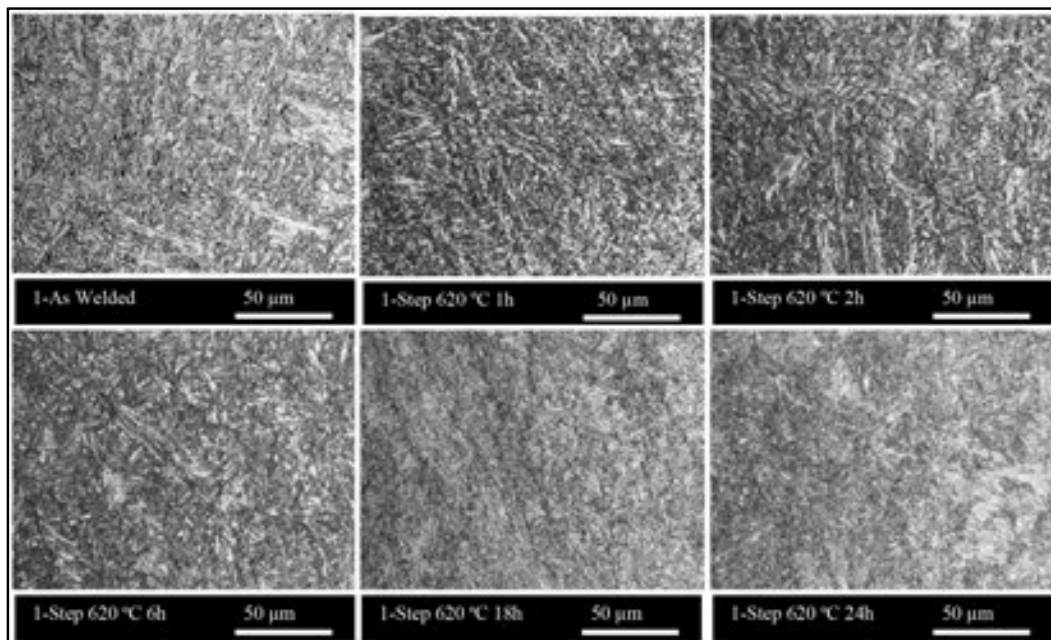


Figure 2. Microstructure of weld metal after single heat treatment processes.

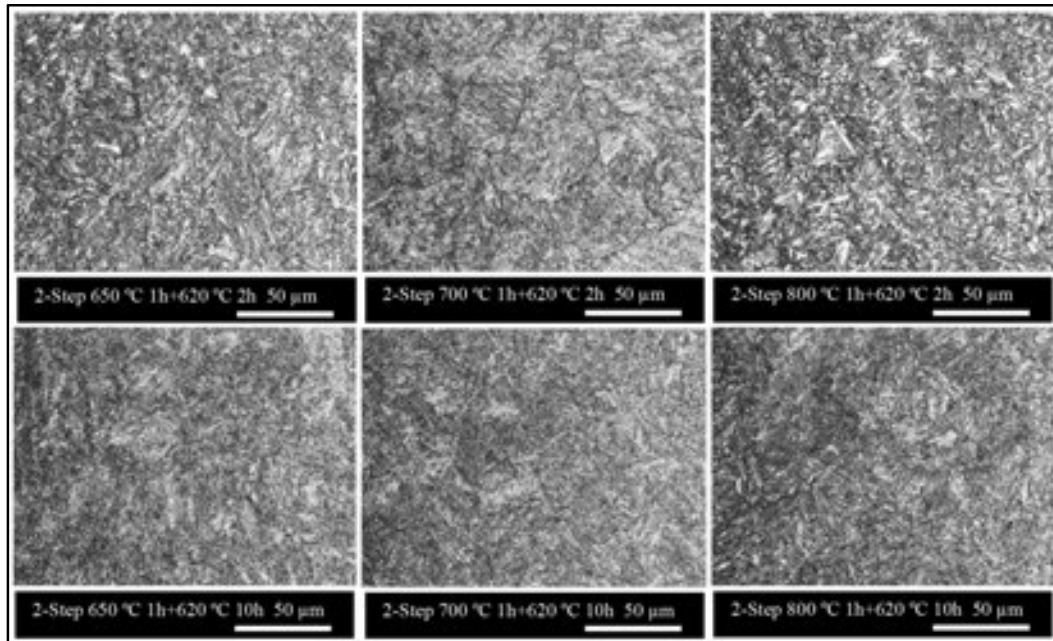
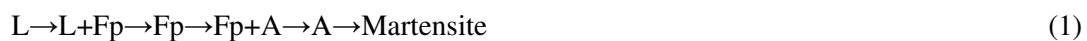


Figure 3. Microstructure of weld metal after double heat treatment processes.

Figure 3. shows double tempered 410NiMo weld metal microstructure. The samples were subjected to annealing at 650 °C, 700 °C, 800 °C which are above A_{C1} transformation temperature, for 1 h and cooling in air and then the samples were tempered at 620 °C for 2h and 10h. 620 °C is below the A_{C1} temperature inhibiting hard fresh martensite. Microstructure of the sample double tempered at 800 °C has more blocky white area. This is probably retained austenite, because hardness results (Figure 4) supports this result. Increasing tempering time from 2h to 10h finer microstructure was observed.

410NiMo martensitic stainless steel starts to solidification as δ ferrite. δ ferrite transforms to γ austenite above 1200 °C and fully transforms to γ austenite at 1200 °C. Austenite will transform to martensite. Then martensitic microstructure occurs after cooling room temperature [5, 10]. The sequence of the transformation was presented by [5] as below:



During solidification, alloying elements segregation can form between dendrites. Therefore δ ferrite can remain in the microstructure at room temperature. Retained austenite can also may remain between martensite laths [10].

3.2. Hardness

Hardness results are shown in Figure 4 while hardness is 350HB as welded condition, the hardness decreased with increasing tempering time at 620 °C in the single heat treatment process. In double tempering process, the samples tempered at 620 °C for 10h have the lowest hardness. The results agree with literature [11, 12]. Furthermore, the hardness limit for UNS S41425 steel is 265HB according to NACE 0175/ISO 15156. In this study, the limit was achieved in double tempering process. It can be concluded that double tempering causes considerable effect softening of martensite [12].

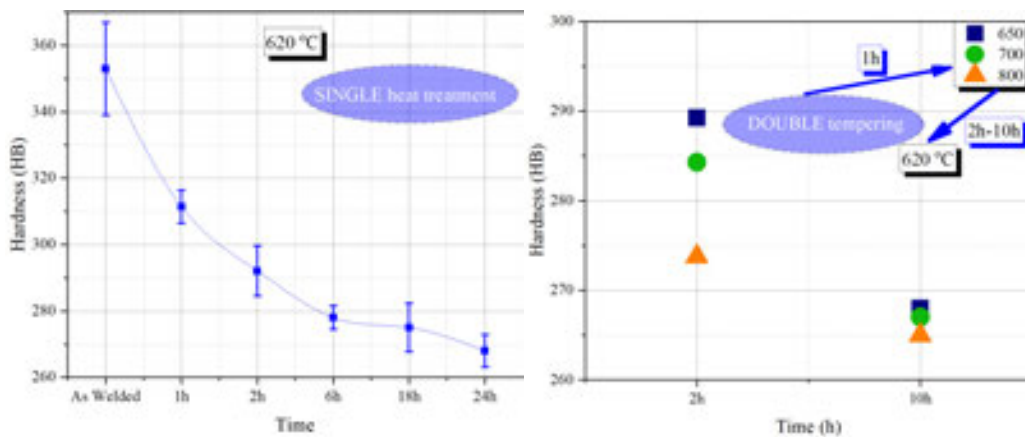


Figure 4. hardness results of 410NiMo weld metal after single and double heat treatment processes.

4. Conclusion

The effect of post-weld heat treatment temperatures on microstructure and hardness was investigated in the present study. Following conclusions could be drawn from this study;

1. Microstructure as welded condition has martensitic and delta ferrite phase was not observed by optical microscopy investigation.
2. Microstructures of the samples with single heat treatment 620 °C 1h, 2h and 6h have martensitic and may be some retained austenite/fresh martensite and thicker than 620 °C 18h and 24h.
3. Microstructures of the samples subjected to double tempering process finer structure was detected at 620 °C for 10h.
4. Increasing tempering time (620 °C) reduced hardness.
5. First heat treatment temperature in DOUBLE tempering hardness is affected by temperature, lower hardness was determined at higher first temperature.
6. Double tempering is vital for welded martensitic stainless steels due to hardness.

6. Acknowledgement

The authors would like to show their gratitude to Gedik Welding Inc. for providing welding consumables and facility use.

7. References

- [1] R.R. de Gouveia, A.G.M. Pukasiewicz, A.R. Capra, S.L. Henke, P.C. Okimoto: Effect of interpass temperature on microstructure, impact toughness and fatigue crack propagation in joints welded using the GTAW process on steel ASTM A743-CA6NM, *Welding International*, 29(6) (2015), pp. 433-440.
- [2] H.-J. HUTH: Fatigue design of hydraulic turbine runners, , 178p. Tese (Doutorado)-Department of Engineering Design and Materials, Norwegian University of Science and Technology, Trondheim, Norway (2005), pp.178.
- [3] P. Bilmes, , M. Solari, C. Llorente: Characteristics and effects of austenite resulting from tempering of 13Cr-NiMo martensitic steel weld metals, *Materials Characterization*, 46(4) (2001), pp. 285-296.

- [4]S.Godin, E.Boudreault, J.B.Lévesque, B.Hazel: On-site post-weld heat treatment of welds made of 410NiMo Steel, Proceedings of MS&T-COM, Montreal, Quebec, Canada(2013), pp.754-765.
- [5]D. Kotecki, J. Lippold: Welding metallurgy and weldability of stainless steels, Wiley,(2005), pp.64,188-206.
- [6]D.Thibault, P.Bocher, M.Thomas, M. Gharghouri, M. Côté: Residual stress characterization in low transformation temperature 13% Cr-4% Ni stainless steel weld by neutron diffraction and the contour method, Materials Science and Engineering:A, 527(23)(2010)pp. 6205-6210.
- [7]G.Krauss: Steels: Processing, Structure and Performance, ASM International, Materials Park, OH, (2005), pp. 251-262.
- [8]ISO15156: 2009 “Petroleum and natural gas industries-Materials for use in H₂S-containing Environments in oil and gas production”, NACE International, (2001) 1440.
- [9]J.Onoro: Martensite microstructure of 9–12% Cr steels weld metals, Journal of Materials Processing Technology, 180(1-3) (2006), pp.137-142.
- [10]M.M. Amrei, H.Monajati, D.Thibault, Y.Verreman, L. Germain, P. Bocher: Microstructure characterization and hardness distribution of 13Cr4Ni multipass weld metal. Materials Characterization, 111(2016), pp.128-136.
- [11]M.Divya, C.Das, V.Ramasubbu, S.Albert, A.Bhaduri: Improving 410NiMo weld metal toughness by PWHT. Journal of Materials Processing Technology, 211(12) (2011)p. 2032-2038.
- [12]S. Tavares, B.Almeida, D.Corrêa, J.Pardal: Failure of super 13Cr stainless steel due to excessive hardness in the welded joint. Engineering Failure Analysis, 91 (2018), pp. 92-98.

CORRESPONDENCE ADDRESS: Uğur Özdemir, Gedik Kaynak A.Ş. Ar-Ge Merkezi Şeyhli Mahallesi, Ankara Cd. No:306, 34906 Pendik/İstanbul, Mobile: +905557180952 and E-mail: uozdemir@gedik.com.tr

EFFECT OF COBALT ON THE MICROSTRUCTURE AND TOUGHNESS-HARDNESS PROPERTIES ON P91 WELD METAL

Fikret KABAKCI ^{1,a}, Mustafa ACARER ^{2,b}, Selçuk KESKINKILIC ^{3,c},
Filiz KUMDALI ACAR ^{3,d}, Uğur ÖZDEMİR ^{3,e}

¹Zonguldak Bülent Ecevit University

²Selçuk University

³Gedik Welding Company

^a fikret.kabakci@beun.edu.tr, ^b macarer@selcuk.edu.tr, ^c skeskinkilic@gedik.com.tr ^d facar@gedik.com.tr, ^e uozdemir@gedik.com.tr

Abstract (12 pt)

In this study, P91 weld metals with different Co contents were fabricated by shielded metal arc welding. To determine of effect of Co addition to P91 weld metal, microstructure and mechanical properties of the weld metals were characterized. While Co addition did not affect to the microstructure significantly, transformation temperatures changed. Also, when the post weld heat tempering time increased, hardness decreased but toughness increased. Co addition did not change the hardness and toughness.

Key Words: 9Cr steel weld metal, Effect of cobalt content, Weld metal microstructure.

1. Introduction

9-12% Cr ferritic-martensitic steels are widely used in fossil fuel and nuclear power plant construction materials such as main steam pipes. They are also used in petrochemistry industry. The steels are attractive material for the energy industry due to the high oxidation resistance, high creep strength, and low thermal expansion when compared with austenitic stainless steels [1-3]. P91 (P:pipe) is a member of high chromium steel family. The steel consists of 9% Cr, 1% Mo and 0.25% V. The steel is also known creep resistant steel. Superior creep properties are a reason of stable microstructure at elevated temperature for a long time due to carbides and carbonitrides in the microstructure. P91 steel is supplied in normalized and tempered condition. Fusion welding technics such as SMAW and GTAW are used to join of the steels. P91 steel has high hardenability properties, austenite to martensite transformation occur by cooling in air. Therefore, post welding heat treatment (PWHT) temperature must be under A_{c1} transformation temperature prevent the low toughness and high hardness due to fresh martensite. The Mn + Ni content is limited to 1.5% because they reduce the A_{c1} temperature [4]. However, Co, another austenite forming element, does not affect significantly on the A_{c1} transformation temperature [5]. There are limited studies the effect of cobalt on the P91 steel weld metal. Aim of this work is to investigate effect of the Co element on the microstructure and mechanical properties of the weld metal produced by the electrodes developed for the joining of P91 steels.

2. Experimental

In this work, effect of Co on microstructure and mechanical properties of P91 weld metal was investigated. All weld metals with different Co contents were produced by shielded metal arc welding (SMAW) technique. Stick electrodes were fabricated by Gedik Welding Co. in Turkey. Tab. 1 shows the chemical compositions of P91 weld metals. Tab. 2 summarizes the welding conditions used in this study. Preheat and interpass temperatures were held at 250-300 °C. The weld metals were subjected to post weld heat treatment process (PWHT) at 760 °C for 2h, 4h, 6h and 8h. Figure 1 illustrate the PWHT cycle applied to all weld metals.

Table 1. Chemical composition of modified P91 weld metals (wt%).

	C	Si	Mn	P	S	Cu	Ni	Cr	Mo	Co	Nb	V
WM91-M	0.09	0.20	0.74	0.01	0.01	0.03	0.47	9.42	1.06		0.03	0.23
WM91-M1	0.09	0.20	0.72	0.01	0.01	0.02	0.48	9.36	1.02	0.51	0.03	0.22
WM91-M2	0.10	0.20	0.71	0.01	0.01	0.03	0.49	9.43	1.11	1.05	0.02	0.22
WM91-M3	0.10	0.18	0.72	0.01	0.01	0.03	0.49	9.33	1.04	1.56	0.03	0.21

Table 2. The welding parameters used to produce weld metals.

Weld Pass Number	Preheat and Inter Pass Heating (°C)	Current (A)	Voltage (V)	Weld speed (mm/min)	Heat Input (kJ/mm)
25	230	130	33	125	2.05

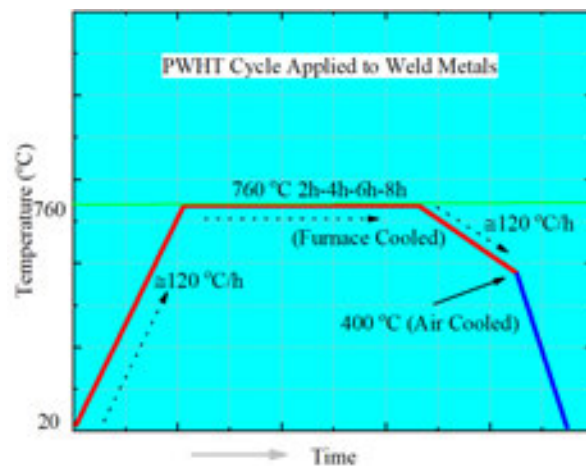


Figure.1 Schematic view of post weld heat treatment (PWHT) cycle.

For microstructure characterization, Nikon Eclipse MA100 inverted optical microscope was employed. Metallographic specimens were grinded up to 2000 grit SiC papers and then

polished diamond suspension 3 μ and 1 μ . Modified vilella's reagent (2.5 gr picric acid + 2.5ml HCl + 95ml Ethanol)[6] was prepared as etching solution. Transformation temperatures of the weld metals were determined by Mettler Toledo TGA/DSC 2 with Argon atmosphere up to 1000 °C temperature. Charpy impact test was also employed to determine toughness of the weld metals. Charpy impact test studied with 300 J capacity Losenhausen impact test machine. Hardness' of the weld metals were measured by Brinell hardness tester 187.5kgf- \varnothing 2.5mm ball diameter also used Q10 A+ QNESS model micro-hardness device under a load of 2000 gf.

3. Results and Discussion

Generally, microstructures have tempered martensitic microstructure. Figure 2 shows optical microstructure of all weld metals with different PWHT condition. Prior austenite grain boundary was not detected remarkably. Delta ferrite phase was not detected in all weld metal microstructure. Delta ferrite phase is important for high chromium steels due to causing deterioration effect to toughness, ductility and creep resistance. Cr_{EQ} includes delta ferrite forming elements such as Cr, Mo. Therefore, high Cr_{EQ} decreases toughness and creep resistance [7, 8]. Co can be added to weld metal to decrease Cr_{EQ} and to prevent delta ferrite phase in high Cr steels [6]. Finer microstructures were observed in all weld metals increasing PWHT time. In optical microscopy investigation, amount of Co did not affect the microstructure significantly. However finer martensitic microstructure was detected in the weld metal with 1.5% Co, PWHT'ed for 8 h.

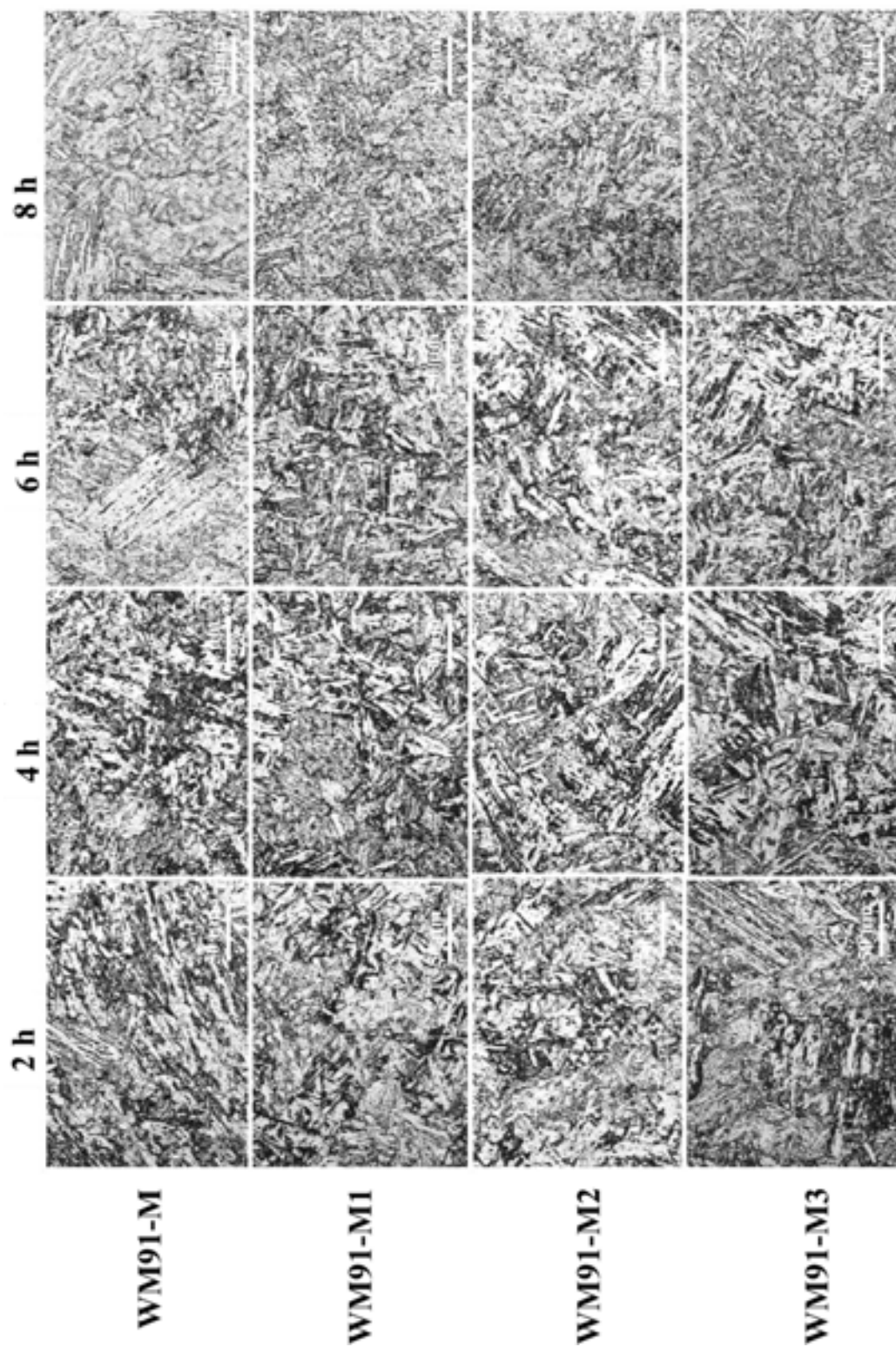


Figure 2. Microstructure of weld metals PWHT'ed at 760 °C 2, 4, 6, and 8 h.

To determine the transformation temperatures of the all weld metals with different Co contents, DSC analyses were carried out. Heating and cooling curves were given in Figure 3 and Figure 4 respectively. It was observed that $\alpha \rightarrow \gamma$ transformation temperatures of the all weld metals are above the PWHT, 760°C. It is important that PWHT should be selected below the A_{c1} transformation temperature due to not forming fresh martensite. Fresh (untempered) martensite increases hardness, yield and tensile strength but decrease toughness and ductility. In this study it was not observed fresh martensite in all of the weld metal microstructures. Hardness results support the microstructures. Curie temperatures, T_c , at which ferromagnetic materials lose their permanent magnetic field, were also determined by DSC heating. It can be seen that Curie temperatures were shifted with increasing Co addition (Figure 3 and Figure 4). Martensite start (M_s) temperatures were also determined with DSC cooling curves. While the all weld metals with 0.5% and 1% Co have higher M_s temperature than that of without Co, M_s of the weld metal with 1.5% Co is the lowest temperature. However, the difference of the M_s temperatures is not significantly and therefore it can be neglected.

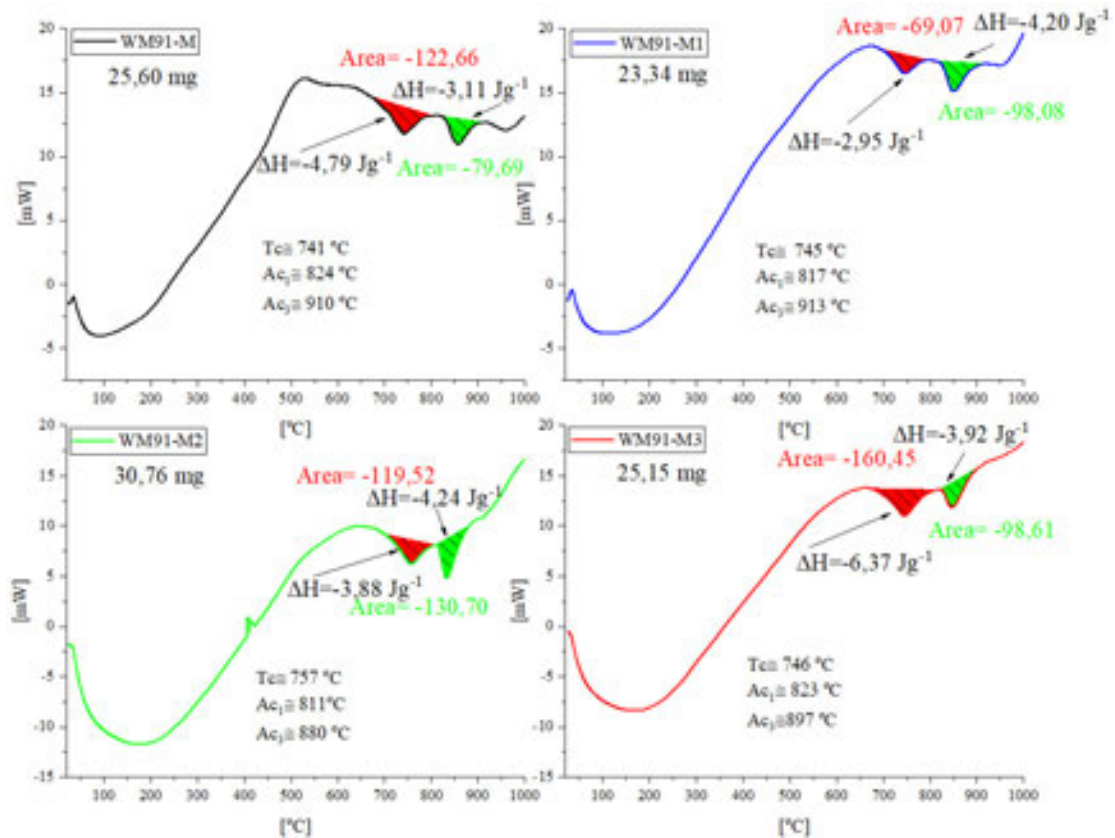


Figure 3. DSC plots of weld metals, heating rate 40 °Cmin⁻¹.

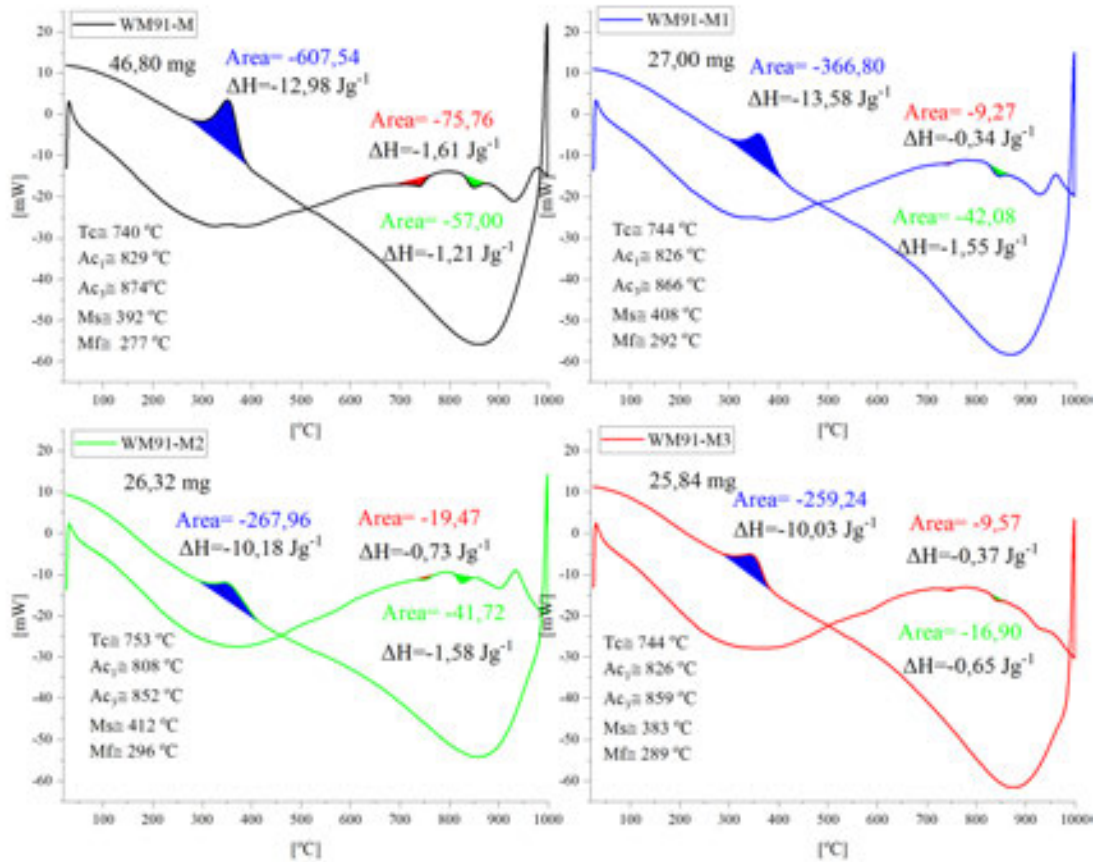


Figure 4. DSC plots of weld metals, heating and cooling rate 20 °Cmin⁻¹.

Hardness maps of the weld metal without Co can be seen in Figure 5. Before PWHT, hardness ranges from 460 to 400 HV. In multiple passes welding, the subsequent weld pass causes tempering effects former pass. After PWHT, hardness distributed as homogeny. Hardness and toughness of the all weld metals after PWHT were given in Figure 6. With increasing Co addition, neither hardness nor toughness changed. However, tempering time affected the hardness and toughness of the all weld metals. With increasing tempering time, while hardness decreased, toughness increased. Decreasing in hardness results from tempering martensite and decreasing carbon amounts due to carbide forming elements such as Cr and Mo dissolving from solid solution to carbide forming with carbon.

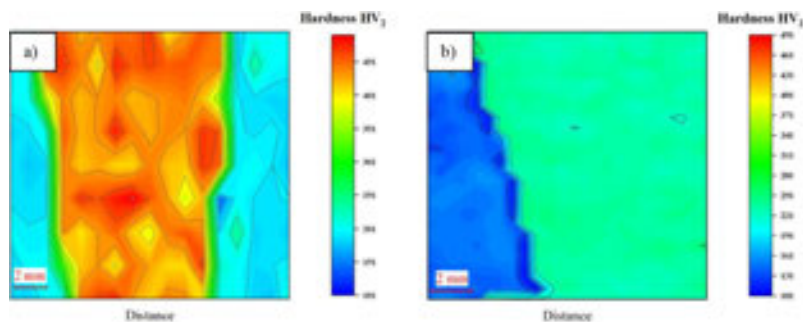


Figure 5. Hardness maps of weld metal (WM91-M) as welded a) and PWHT condition b).

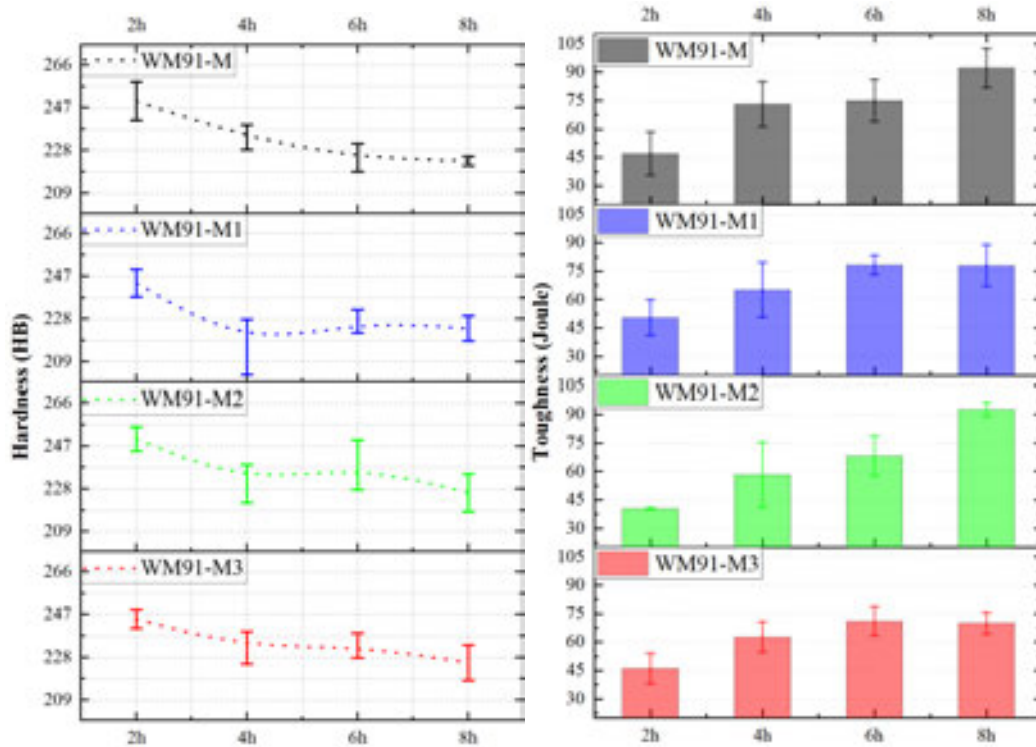


Figure 6. Hardness and Toughness plots of weld metals 760 °C 2h, 4h, 6h and 8h PWHT'ed.

4. Conclusion

In this study, it was aimed to investigate of the influence of Co addition to P91 steel weldmetal. From the results of this study the following conclusions can be drawn:

1. All of the weld metals showed same tempered martensitic microstructure.
2. With increasing PWHT time finer microstructures were observed.
3. While Curie temperatures were shifted by increasing Co amounts, Ms temperatures did not change significantly.
4. PWHT time improved hardness and toughness properties.

5. Acknowledgement

This work supported by Turkish Ministry of Science, Industry, Technology SAN-TEZ Projects under Grant Numbers 0374.STZ.2013-2

6. References

[1] A.Mandal, K. Guguloth, and T.K. Bandyopadhyay: Characterization of Microstructure and Mechanical Properties of 9.2Cr0.45V0.7C Heat-Resistant Steel, Metallography Microstructure and Analysis, (2016), pp. 95-107.

[2] A.Fedoseeva, N. Dudova, and R. Kaibyshev: Creep strength breakdown and microstructure evolution in a 3%Co modified P92 steel, *Materials Science and Engineering: A*, 654 (2016), pp. 1-12.

[3] M.Taneike, K. Sawada, and F. Abe: Effect of carbon concentration on precipitation behavior of $M_{23}C_6$ carbides and MX carbonitrides in martensitic 9Cr steel during heat treatment, *Metallurgical and Materials Transactions A*, 35 (2004), pp. 1255-1262.

[4] B.Arivazhagan, S. Sundaresan, and M. Kamaraj: Effect of TIG arc surface melting process on weld metal toughness of modified 9Cr-1Mo (P91) steel, *Materials Letters*, 62 (17-18)(2008), pp. 2817-2820.

[5] L.Helis, Y.Toda, T.Hara, H.Miyazaki, F.Abe: Effect of cobalt on the microstructure of tempered martensitic 9Cr steel for ultra-supercritical power plants, *Materials Science and Engineering: A*, 510-511 (2009), pp. 88-94.

[6] J.Oñoro: Weld metal microstructure analysis of 9-12% Cr steels, *International Journal of Pressure Vessels and Piping*, 83(2006), pp. 540-545.

[7] P.Wang, S. P.Lu, N. M.Xiao, D. Z.Li, Y. Y.Li, Effect of delta ferrite on impact properties of low carbon 13Cr-4Nimartensitic stainless steel, *Materials Science and Engineering: A*, 527(13-14) (2010), pp. 3210-3216.

[8] P. Mohyla, and Z. Kubon, Influence of delta ferrite on mechanical and creep properties of steel P92, 9th Liege Conference: Materials for Advanced Power Engineering, Julich-Germany(2010), pp.75-83.

CORRESPONDENCE ADDRESS: Fikret KABAKCI, Zonguldak Bulent Ecevit University Alaplı Vocational School ZonguldakAlaplı/Turkey , +90 (372) 378 20 05, fikret.kabakci@beun.edu.tr.

NUMERICAL MODELLING OF DYNAMICS OF CRASH BOX COLLISION GEOMETRY

OktayÇetinel^{1,a}, HakanAteş^{2,b}

¹Hacettepe University / Faculty of Engineering / Department of Mechanical Engineering

² Gazi University / Faculty of Technical Education / Department of Metallurgy

^aoktaycetinel@hacettepe.edu.tr, ^bhates@gazi.edu.tr

Abstract

An investigation was performed to identify the impact of cross-sectional geometry on the crashworthiness performance of vehicle crash boxes. A circular, square and rectangular cross sectional geometries of thin-walled crash box models are modeled using finite element method. The force-displacement behaviours, energy-displacement behaviours and crash force efficiencies were examined. The results showed that circular crash box had most favourable traits; displaying a desirable folding mode, stable force – displacement characteristics in combination with the highest specific energy absorption and crash force efficiencies rates, making this geometry the best geometry configuration overall. The results of the research will benefit the development of guidelines that will improve the impact performance of automotive crash boxes.

Keywords: Crash Boxes, Deflection analysis, finite element method

1. Introduction

In an impact collision, a car utilizes two separate elements; the first is a collapsible frontal crash zone, which is designed to dampen the impact effect and absorb the kinetic energy of the impact by deformation; the second element is the safety cage around the main compartment, which is designed to protect the occupants by resisting high crash forces whilst displaying little or no deformation [1].

The effective protection of passengers against fatal injury during a collision is achieved through the effective design and construction of the passenger compartment that should be as rigid as possible to ensure that the survival space is not crushed or catastrophically deformed. It is therefore obvious that the collapsible zones of the vehicle (i.e., crash boxes and bumper beams) must be designed to be physically weaker than the structure of the passenger compartment. The weaker collapsible structure ensures that, following a collision, the front zone of the vehicle crushes before any deformity of the passenger compartment occurs. The force of deformation also controls the deceleration of the vehicle. Therefore, the controlled manner in which the front of the vehicle collapses, controls the deceleration of the occupants [2]. This controlled deceleration determines the forces that are placed upon the occupants from passive safety features such as the airbag and seatbelts. These deceleration forces are often the cause of serious injury of the occupants of any vehicle involved in an impact collision.

It is, therefore, necessary to limit the maximum deformation force. This suggests that there are clearly defined maximum and upper limits of deformation force that can be applied to ensure the safety of the occupants [3]. It is also clear that the length of the collapsible zone, which controls the total deformation, is further in need of limitation. As such, strict limits are imposed on the dimensions of the vehicle as well as other design related boundary conditions.

It has been shown that the high stiffness coupled with the superior crash energy absorption potential of aluminium alloys makes these lightweight structures a cost-effective possibility for vehicle construction [4]. Both low and high speed impacts have been tested with appropriate aluminium protection systems, which have resulted in aluminium becoming the preferred material for vehicle safety as well as ensuring reasonable pedestrian protection, reduced repair costs and occupant safety. Included body structures have ranged from aluminium bumper beams, which include crash boxes, pedestrian protection systems and side impact beams.

Crash boxes display axial collapse due to the dissipation of kinetic energy from plastic strain energy causing plastic hinge formation and the catastrophic deformation of the walls of the tube. However, due to the material nonlinearity and large deformation process, it is often challenging to design the thin walled sections.

When designing these specific energy absorbing devices: They must be able to absorb high energy, be able to accept a crippling load, have a repeatable mode of collapse in order to maximize the crashworthiness performance of crash box [5]. The aim of this paper is to identify the crashworthiness performance of crash boxes with different cross sectional shapes in order to identify the most suitable design criteria for impact performance. A literature search and review for the geometries of crash boxes is given in the first section. The second section concentrates on the parametric study of the effect of cross sectional shape crashworthiness. The final section is focused on the study of the geometry configurations and the characteristics comparison of their force and energy absorption parameters.

2. Crashbox design

2.1 Rectangular and Square Crash Boxes

Energy is absorbed during axial compressive loading in rectangular and square crash boxes through a series of progressive folding deformations. A number of failure modes are exhibited with rectangular and square crash boxes. the desired failure mode of these geometries should display a regular folding formation throughout the axial crush loading, causing the stable collapse of the component [4]. These progressive folding patterns are able to absorb energy in a controlled and consistent manner [5].

A number of consistent secondary peaks and wavelength are exhibited within the load deflection curve for this mode are shown in figure 1:

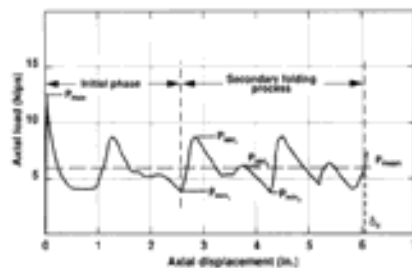


Figure 1. Typical load-deflection curve for a compact rectangular crash box [6]

By ensuring a proper geometrical design and the utilisation of suitable material properties, undesirable failure modes can be prevented. There are a number of undesirable failure modes which include:

Irregular folding; where there is no entire buckling of the cross-section but instead there is local plate buckling of the individual walls at different times and loads throughout the crush event. With this irregular folding, no regular folding patterns appear and there is no consistent exhibition of any secondary peaks and wavelengths within the load deflection curves [7]. A comparison of regular folding and irregular folding is shown in figure 2.

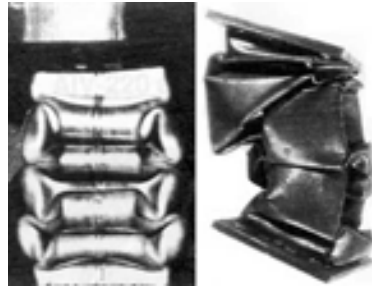


Figure 2. Regular folding (left) vs. irregular folding (right) [4]

Bending collapse due to aspect ratio folding mode occurs following the first fold formation. The folds within the opposite walls interfere and prevent further folding and induce bending of the member.

In rectangular and square crash boxes, the energy absorbing behaviour can be predicted by ensuring the following criteria are achieved:

The rectangular section needs to be compact, with each individual wall being supported by its connecting wall so that there buckling occurs across the entire cross section at the same load and time during the crash event [7].

The shorter wall of the rectangular cross section must be of adequate length to allow the half wavelength of the fold to fit [8].

2.2 Circular Crash Boxes

An acceptable energy of absorption capacity is displayed in two modes of failure for circular crash boxes that have been subjected to axial compressive loads [8]. These show consistent, repeating fold patterns within the load deflection curve. These patterns are the concertina axisymmetric folding mode and the diamond folding mode which are shown in figure 3 [9].

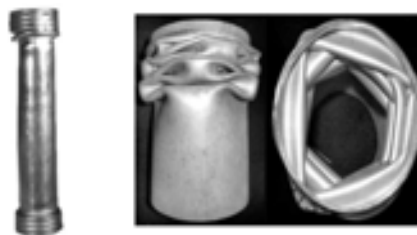


Figure 3. Axisymmetric (left) and diamond (right) folding pattern for circular crash boxes [4]

Concentric rows of outward facing folds are formed in the axisymmetric concertina mode. Mixed mode failures are often exhibited by circular sections, whereby the sections commence folding in an axisymmetric manner before changing to a diamond mode folding pattern.

2.3 Crashbox Design Analysis

The finite element method has been frequently utilised to research the collapse pattern of crash boxes. The numerical modelling of crash box crushing modelled by solid elements and shell elements were compared by Fyllingen et al. [8]. These authors identified that shell elements were a good choice for modelling thin walled tubes, particularly when identifying the notable reduction in computational time. The dynamic collapse of square aluminium columns was studied by Meguid et al. through the use of the LS Dyna explicit finite element solver [9]. These authors investigated the effect of different platforms used on the results and the influence of initial conditions and symmetric boundaries on the resulting mode of collapse. It was found that irregular collapse modes were linked to numerical errors in untriggered models. Due to its ability to capture global buckling modes of collapse, the half column model was suggested providing it was adequately constrained along one plane of symmetry. This allowed the elimination of spurious deformation modes that the untriggered full model configuration displayed.

The effect of triggering on the crashworthiness of circular aluminium tubes was studied by Marzbanrad et al. using explicit FEM. The authors utilised a number of trigger types including plastic folds, holes and notches [10]. It was discovered that the use of these triggers could reduce the initial crippling force. Nevertheless, no alternative optimal solutions were given.

3. Methodology

3.1 Numerical Test Setup

In order to identify the most efficient crash box design, with regards to cross sectional dimensions, a parametric study was performed. The crash boxes were modelled in Solidworks, meshed in HyperMesh and their axial impact were simulated using the LS-DYNA explicit finite element model.

Using the same impact test setup for numerical analysis as that of reference to Euroncap protocol [9]. The square, circular and rectangular crash boxes were collapsed at a 90 degrees angle into a rigid wall. 6063 T5 Aluminium was utilised as the material of choice as it is considered as the most preferred material for crash boxes [11].

Table 1. Material Properties of 6063 T5 Aluminium

Property	Value
Young's Modulus, E (MPa)	69200
Mass Density, ρ (kg/m ³)	2700
Poisson' Ratio, ν	0.33
Yield Strenght, (Mpa)	180
Specific Heat (J/kgC)	900

The dimensional properties of circular, rectangular and square crash boxes are given below. Their thicknesses and heights are fixed for effective cross sectional geometry comparison.

Table 2. Dimensional Properties of Crash boxes

	Circular	Rectangular	Square
Height	15 cm	15 cm	15 cm
Diameter	80 mm		
Width		100 mm	80 mm
Length		70 mm	80 mm
Thickness	2.75 mm	2.75 mm	2.75 mm

The force-displacement curve and energy-displacement curves are gathered from the simulation results for each of the crash box designs. The curves showed that there are a number of common crashworthiness criteria that can be used to evaluate the performance of the crash box.

Total Energy Absorption (TEA):

$$TEA(d) = \int_0^d F(d) dx \quad (1)$$

Specific Energy Absorption (SEA):

$$SEA(d) = \frac{1}{m_c} \int_0^d F(d) dx \quad (2)$$

Mean Crushing Force:

$$F_m(d) = \frac{1}{d} \int_0^d F(d) dx \quad (3)$$

Crash force efficiency (CFE):

$$CFE = \frac{F_m}{F_{max}} \quad (4)$$

The crash box models were meshed using the finite element software Hypermesh software and Standard Belytschko-Tsay finite elements allow the meshing of the geometry with five integration points across the stiffness-type. Rigid brick elements were used to model the impacting mass. The model is then attributed with gravity acceleration with the initial velocity of 50 kph being assigned to the mass. All degrees of freedom constrained the lower edge of the crash box. Only a vertical direction is allowed on the nodes of the tube constrained within the clamp for the duration of the physical test. A friction coefficient of 0.2 is used to define the nodes to surface algorithm describing the contact between the impacting mass and the crash box. The frictionless single surface contact models the self-contact of the crash box. There is an additional definition between the contact of the rigid wall and the impacting crash box in order to prevent the total bottoming out of the tube. There is a 300 mm distance from the rigid wall to the upper end of the crash box.

3.2 Crash Analysis

The explicit numerical method can be utilised due to the short period of time in which crash events occur. However, the more hardware demanding implicit approach can also be utilised, in which more variables can be added into the calculation [11].

The ability to simulate actual crash results is highly contact dependent and reliant on numerous factors, which can result in fatalities if not carried out correctly [8]. There are two main categories that define contact, which are segment based and nodal based contacts. The two main categories are subdivided into one-way and two-way contact types [12].

When different mesh constellations are used, the nodal based contact system requires more work. This is because there is a change in the node identification numbers that are dependent on the mesh constellation. Additionally, the contact search finds the nearest nodes on the different segments, which results in an unstable contact definition for the meshes consisting of elements with varying ratios.

During the contact, node segments are located using the segment based contact search, which is a preferred method for crash analysis [11]. The determination between one way or two way contact is determined by the checks for penetration on both the master and slave part or if these checks cover just the slave part.

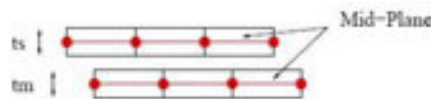


Figure 4. Offset for contacts

It is recommended that there is an offset of colliding parts to ensure there is no penetration prior to the intended contact as shown in Figure 4 [12].

3.3 Element Theory

The geometry of the crash boxes largely determines the choice of element type. Since the structure is thin walled, there are two possible element types in which to approach the problem. As such, the solid and shell elements are the two potential approaches [10]. According to the literature, a good reference point is the length over thickness ratio where the ratio presents a boundary between the solid and shell element choices [7].

There are many different element types to choose from with regards to working with solid and shell elements. The application and surface geometry determine the efficiency of an element type. The element type must be efficient and able to withstand key conditions when considering the folding and buckling of the elements that occur during crash analysis [10].

When simulating a crash, a shell element with a quadrilateral element type that has adequate amounts of integration points within the element and throughout its thickness is likely to be the most efficient. Solid brick elements often use the same formulation of integration points. One of the parts of the element formulation is the effective choice of the number of integration points within an element [12].

There are a number of well used formulations performed with quadrilateral shell elements within the LS-DYNA simulations. The Belytschko-Lin-Tsay formulation is one of the

recommended formulations and is denoted “ELFORM=2” that is able to give a single integration point on the surface of the element. An alternative element formulation is that of the fully integrated shell formulation which is denoted as “ELFORM=16” and provides four integration points on the surface of the element as shown in figure 5.

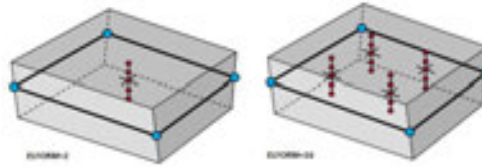


Figure 5. Element formulations for quadrilateral shell elements

Different results within the crash simulation are generated by varying the number of integration points on the element’s surface. A more accurate and safe buckling simulation is generated when four integration points are utilised on the elements surface in comparison to the single integration point formulation. Nevertheless, the more integration points there are on the surface of an element can induce element warping [11].

There is an agreement between the described element formulations for both solid and shell elements, which is largely a result of each element surface having the same integration point formulations.

Another important variable is the number of integration points (NIP) through the thickness of the element. It is recommended that a higher number of integration points are included, in order to provide an adequate approximation of the behaviour of the materials during nonlinear deformation [8]. Whilst it is recognised that the simulation time is longer for the elements with higher NIP numbers, the results are often theoretically more correct [7]. At least five integration points are commonly used during crash analysis [9].

The element construction often determines the element formulations as the recommended values often define the angular deviation, warping and skewing of the element. Inadequate simulation results can often occur due to the creation of a mesh with poor elements [8].

It is also necessary to define the element’s orientation during the element formulation. The global coordinate system is often used initially to define the element orientation and in so doing the element’s normal vector is defined. By defining the normal vector of the element allows the tracking of the NIP as well as which side of the element is top, bottom, left or right [12].

4. Results and Discussion

An investigation was performed to identify the folding mode, force vs. displacement and energy vs. displacement performance of circular, rectangular and square crashboxes and the results are represented below.

4.1 Circular Crash Box

4.1.1 Folding Mode Analysis

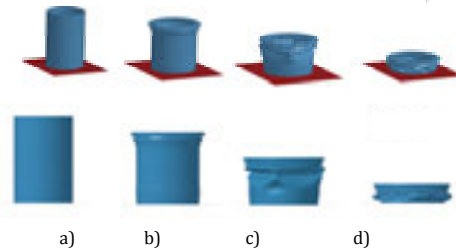


Figure 6. Circular Crash Box folding sequence at a) $x=0$ mm, b) $x=40$ mm, c) $x=80$ mm, d) $x=120$ mm respectively

Folding mode analysis was conducted to examine the effect of trigger type on the response of crash boxes. The crushing process of circular crash box is shown in Fig. 6. It can be seen that the crash box collapses following the concertina (axissymmetric) folding pattern on the surface in a progressive and stable manner. At the onset of the crushing process ($x=40$ mm), both hinges occur uniformly on the surface of the crash box. As the crash box is compressed further, two pairs of inclined plastic hinge lines are formed.

Comparing this collapse mode with the diamond mode of circular crash boxes reveals that the two modes are quite similar in shape. Therefore, the failure mode of the circular crash box is named the complete concertina (axissymmetric) mode in which all of the hinges develop well during the crushing process.

4.1.2 Force vs. Displacement Analysis

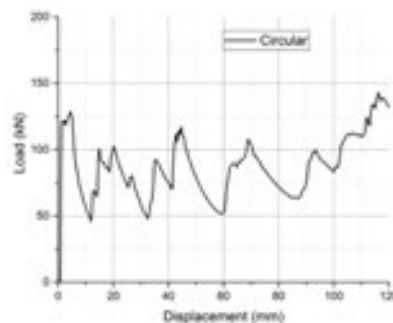


Figure 7. Force – displacement graph of Circular Crash Box

The force vs. displacement curve of circular crash box is plotted in Fig. 7. It can be seen that the high peak of force exists between the first interval of the circular crash box crush sequence ($x=0$ to $x=10$ mm). The force – displacement sequence between $x=20$ mm to $x=80$ mm shows a uniform fluctuation progression, which indicates a uniform folding pattern. On the other hand, force absorption substantially becomes larger after $x=100$ mm reaching a peak crash force of 142.74 kN. The mean crush force is calculated as 85.17 kN. The results of mean force value divided by peak crush force gave a crash force efficiency rate of 60%. This shows that the circular crash box is capable of absorbing high values of load even after on a %70 crushed pattern.

Therefore, it can be concluded that the circular crash box has successfully created a sequence with high force absorption and high load uniformity across the crushing interval.

4.1.3 Energy vs. Displacement Analysis

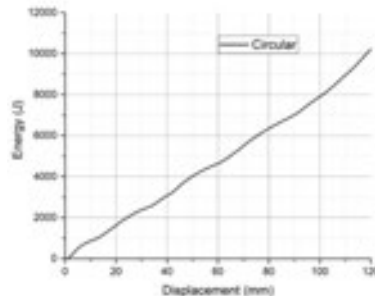


Figure 8. Energy – displacement graph of Circular Crash Box

The graph results of the circular crash box show that there is almost a linear increase pattern between energy – displacement values. This can be seen as the result of uniform folding pattern. The maximum absorbed energy value of circular crash box was 10220 Joules. By dividing this value to its mass, it resulted with a specific energy absorption rate of 37.46 kJ/kg.

A more non-linear behaviour for the energy of the circular geometry was observed until around the 60 millimetre of displacement mark. This can be seen as the result of the appearance of large hinges between that interval. Following this, the magnitude began to linearly increase. This magnitude increase further accelerated at a higher rate from around 120 millimetres of displacement.

4.2 Square Crash Box

4.2.1 Folding Mode Analysis

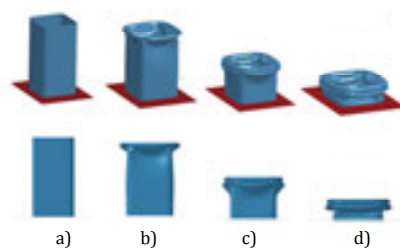


Figure 9. Square Crash Box folding sequence at a) $x=0$ mm, b) $x=40$ mm, c) $x=80$ mm, d) $x=120$ mm respectively

The crushing process of square crash box is shown in Fig. 9. From the analysis of the figure, the square crash box folds in regular folding manner in first two intervals of $x=40$ mm and $x=80$ mm. Then it progresses into an inconsistent and uncontrolled folding pattern as hinges become larger. This is an undesired form of folding pattern as it results in local plate buckling. At the onset of the crushing process ($x=40$ mm), a single hinge occurs on the surface of the crash box. As the crash box is compressed further, two pairs of non-uniform plastic hinge

lines are formed. In comparison to regular folding pattern of square crash boxes, it shows that the first two intervals behave in a similar manner whereas the last the time intervals of $x=80\text{mm}$ and $x=120\text{mm}$ results in an irregular folding fashion.

As a result, the failure mode of square crash box is a combination of both regular and irregular folding mode in which hinges seem to appear uniformly in first stages but then it progresses into an irregular folding pattern creating an undesired form.

4.2.1 Force vs. Displacement Analysis

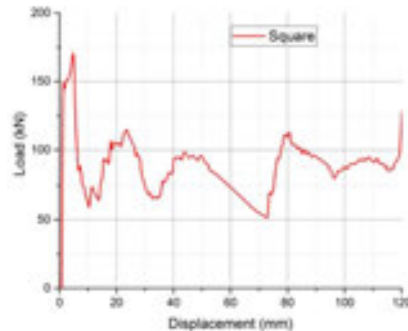


Figure 10. Force – displacement graph of Square Crash Box

Fig. 10 shows the force vs. displacement curve of square crash box. The force vs. displacement sequence between shows a uniform fluctuation between $x=20\text{mm}$ to $x=50\text{mm}$, then curve begins to fluctuate in an uncontrolled manner which can be seen as a result of irregular folding pattern.

Similarly to circular crash box, a high peak of force exists between the first interval of the square crash box crush sequence ($x=0$ to $x=10\text{mm}$).

However, force absorption rate declined sharply at $x=55\text{mm}$ to a value of 52 kN . This is a result of second non-uniform hinge appearing at $x=50\text{mm}$. The peak crush force is observed at $x=8\text{mm}$ with a value of 170.52 kN . The mean crush force is then calculated as 86.02 kN . This resulted in a slightly lesser crush force efficiency rate of 50% in comparison to circular crash box.

As a result, it can be concluded that the square crash box has created a sequence with high force absorption and poor load uniformity across the crushing interval.

4.2.2 Energy vs. Displacement Analysis

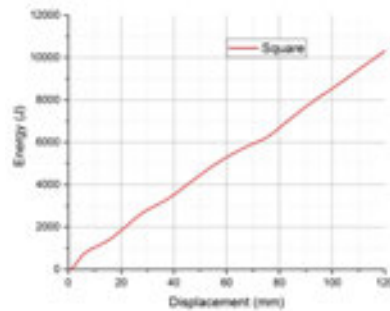


Figure 11. Energy – displacement graph of Square Crash Box

Energy – displacement graph of square crash box shows that there is a linearly increasing relationship between energy – displacement values. However, in comparison regular folding pattern, a more unstable curve was obtained due to unstable formation of hinges. The maximum absorbed energy value of square crash box was 10322 Joules. This resulted with a specific energy absorption rate of 30.63 kJ/kg. The behaviour of the curve was unstable until $x=80$ mm mark, after than interval the curve almost got into a linearly progressing pattern. This can be seen as the result of the bending collapse due to length.

4.3 Rectangular Crash Box

4.3.1 Folding Mode Analysis

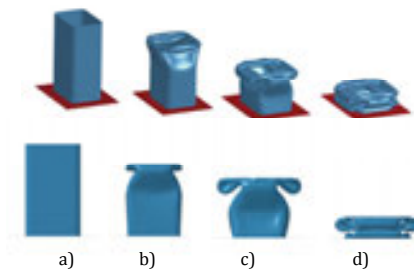


Figure 12. Rectangular Crash Box folding sequence at a) $x=0$ mm, b) $x=40$ mm, c) $x=80$ mm, d) $x=120$ mm respectively

Figure 12 represents the crushing process of rectangular crash box in 4 different time intervals. The figure shows that the crash box collapses following the bending collapse due to aspect ratio folding pattern. After the initiation of the first fold, the folds within the opposite walls interfere and prevent further folding and induce bending of the crash box. At $x=80$ mm distance interval the inclined plastic hinge lines travel away from the crash box corners, this results in partial crush buckling.

Comparing this collapse mode with the desired regular folding mode, this model shows a non-uniform buckling progression. As a result, the failure mode represents a model of bending collapse where only a single hinge forms and the formation restricts further folds to appear.

4.3.2 Force vs. Displacement Analysis

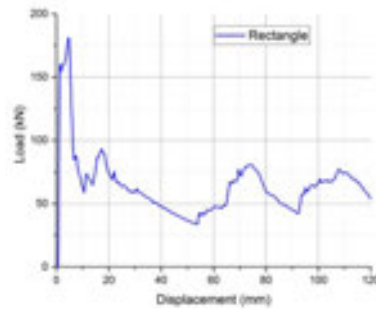


Figure 13. Force – displacement graph of Rectangular Crash Box

The force vs. displacement curve of rectangular crash box shows the highest peak of force between the first interval of the crash sequence ($x=0$ to $x=10$ mm) with a value of 181.22 kN. The analysis of the wavelengths of between second crash interval ($x=20$ mm to $x=60$ mm) shows a great decline in the force absorption values. This could be linked to the interference of the folds in the opposite walls causing the crash box to bend in an uncontrolled manner.

In contrast, force absorption behaviour partially becomes stable after $x=60$ mm. This shows that the first fold prevented the formation of further folds and eventually resulted the crash box to buckle as a whole body. From the graph, the mean crush force is calculated as 62.58 kN. After evaluation of results, crash force efficiency rate is obtained as 35%.

This shows that the rectangular crash box is not capable of absorbing high values of load due to its poor force absorption characteristics and unstable force displacement behaviour.

4.3.2 Energy vs. Displacement Analysis

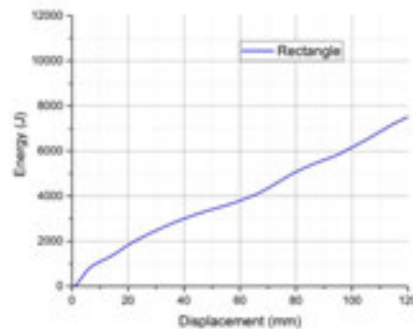


Figure 14. Energy – displacement graph of Rectangular Crash Box

By analysing the curve of energy vs. displacement graph of rectangular crash box, it can be seen that there is a much more unstable curve in comparison to other crash box geometries. This can be linked the non-uniform folding pattern of rectangular crash boxes. The maximum absorbed energy value of rectangular crash box was 7510 Joules. Specific energy absorption rate was evaluated as 20.90 kJ/kg. In the interval between $x=20$ mm to $x=60$ mm, the first fold appears causing a more non-linear curve in the energy - displacement graph of the rectangular crash box. After that displacement mark, the curve begins to reflect the same

curve behaviour observed in square crash box energy – displacement graph. Overall performance of energy absorption rates of rectangular crash box was recorded as the lowest performing geometry of all configurations.

5. Conclusions

In this study a finite element program was used to generate circular, square and rectangular cross sectional geometries of thin-walled crash box models.

The force-displacement behaviours of crash box configurations were investigated. There was a significant difference between the results of circular geometry displaying the highest force absorption and rectangular geometry showing the poorest performance overall. These results are attributed to the concertina (axisymmetric) and irregular folding and buckling collapse of these crash boxes.

The study also analysed energy-displacement behaviour of circular, square and rectangular crash boxes. It was discovered that the circular and square crash box configurations had close values of specific energy absorption rates. In contrast, the rectangular crash box resulted with the lowest values of specific energy absorption rates. This was linked to the interference of the opposite walls which resulted the whole body to collapse.

The crash force efficiencies were evaluated after finding peak and mean crash forces of each configuration and it was shown that altering crash box geometries had crucial effect on evaluating crashworthiness of a crash box. Circular geometry has performed the highest efficiency overall, showing that a round geometry did result better efficiency rates in comparison to rectangular and square crash boxes which had four sides which can be seen as an attribute of imperfection.

This was followed by a detailed examination of the key parameters. The results showed that circular crash box had most favourable traits; displaying a desirable folding mode, stable force – displacement characteristics in combination with the highest specific energy absorption and crash force efficiencies rates, have made this geometry the best geometry configuration overall.

6. References

Articles in Journals;

- [1] Blumhardt, R., FEM - crash simulation and optimization, *International Journal of Vehicle Design*, 26 (2001), pp. 331-347.
- [2] M. Langseth, O. Hopperstad, and A. Hanssen, "Crash behaviour of thin-walled aluminium members," *Thin-Walled Structures*, 32 (1998), pp. 127-150.
- [3] G. Cole and A. Sherman, "Lightweight materials for automotive applications," *Materials characterization*, 35 (1995), pp. 3-9.
- [4] T. Williams, A. De Pennington, D. Barton, and J. Coates, "The prediction of frontal impact crashworthiness of a spaceframe sports car," *International Journal of Crashworthiness*, 4 (1999), pp. 147-158.

- [5] S. Guillow, G. Lu, and R. Grzebieta, "Quasi-static axial compression of thin-walled circular aluminium tubes," *International Journal of Mechanical Sciences*, 43 (2001), pp. 2103-2123.
- [6] J. Reid, J. Rohde, D. Sicking, Box-beam bursting energy absorbing terminal, *Journal of Transportation Engineering*, 128 (2002), pp. 287-294.
- [7] A. Airoidi, G. Janszen, A design solution for a crashworthy landing gear with a new triggering mechanism for the plastic collapse of metallic tubes, *Aerospace Science and Technology*, (2005), pp. 445-455.
- [8] Ø. Fyllingen, O. Hopperstad, A. Hanssen, and M. Langseth, "Modelling of tubes subjected to axial crushing," *Thin-Walled Structures*, 48 (2010), pp. 134-142.
- [9] S. A. Meguid, M. Attia, J. Stranart, W. Wang, "Solution stability in the dynamic collapse of square aluminium columns," *International journal of impact engineering*, 34 (2007), pp. 348-359.
- [10] J. Marzbanrad, A. Abdollahpoor, B. Mashadi, "Effects of the triggering of circular aluminum tubes on crashworthiness," *International Journal of Crashworthiness*, 14 (2009), pp. 591-599.
- [11] L. Qing-fen, L. Yan-jie, W. Hai-dou, and Y. Sheng-yuan, "Finite Element Analysis and Shape Optimization of Automotive Crash-Box Subjected to Low Velocity Impact", *Measuring Technology and Mechatronics Automation*, (2009), pp. 791-794.

Book;

- [12] Hallquist J. O. "LS-DYNA theory manual", Livermore Software Technology Corporation, Livermore, (2006).

CORRESPONDENCE ADDRESS: OktayCetinel, 06440, 03124184129, oktaycetinel@hacettepe.edu.tr

SHORT BIOGRAPHIES

OktayCetinel-

MEng- University of Bath, Faculty of Engineering and Design, Dept. of Mechanical Engineering (2015).

PhD- Hacettepe University, Faculty of Engineering, Dept. of Mechanical Engineering (2016-continuing).

HakanAtes –

BSc- Gazi University, Technical Education Faculty(1992).

MSc-Gazi University, Institute of Science and Technology(1996).

PhD- Gazi University, Institute of Science and Technology(2003).

FARKLI İLAVE METALLER KULLANILARAK TIG KAYNAK YÖNTEMİ İLE BİRLEŞTİRİLEN 316 L PASLANMAZ ÇELİK VE L-605 KOBALT ESASLI SÜPERALAŞIM LEVHALARIN METALURJİK ÖZELLİKLERİNİN DEĞERLENDİRİLMESİ

Tolga Yılmaz^{1,a}, Ahmet Durgutlu^{1,b}

¹Metalurji ve Malzeme Mühendisliği / Teknoloji Fakültesi / Gazi Üniversitesi

^atolgayilmaz@gazi.edu.tr, ^bdurgutlu@gazi.edu.tr

ÖZET

Değişik endüstriyel uygulamalarda farklı özellikteki malzemeleri birleştirmek birçok araştırmacı için ilgi odağı olmuştur. Farklı metallerin kaynak işlemi, tasarım işlemlerinde esnekliği geliştirmek ve malzeme maliyetini azaltmak amacıyla tercih edilebilmektedir. Bu çalışmada, korozyon dayanımının istenildiği ortamlarda genelde tercih edilen 1,5 mm kalınlığındaki L-605 kobalt esaslı levhalar yine aynı kalınlıktaki 316 L paslanmaz çelik levhalar ile birleştirilmiştir. Birleştirme işlemleri, kobalt esaslı Turbaloy L-605 ve ER 316 L paslanmaz çelik olmak üzere iki farklı ilave metal kullanılarak argon koruyucu gazı atmosferinde TIG kaynak yöntemi ile gerçekleştirilmiştir. Elde edilen birleştirmelerden, kullanılan farklı özellikteki ilave metallerin kaynaklı malzemelerin kaynak bölgesine etkilerini görmek amacıyla numuneler hazırlanmış ve bu numunelere mikroyapı ve mikrosertlik testi uygulanmıştır. Deneysel çalışmalardan elde edilen veriler birbirleri ile kıyaslanarak tartışılmıştır.

Anahtar Kelimeler: TIG kaynağı, L-605 kobalt esaslı süperalaşım, 316 L paslanmaz çelik, Kaynaklanabilirlik.

EVALUATION OF METALLURGICAL PROPERTIES OF 316 L STAINLESS STEEL AND L-605 COBALT BASED SUPERALLOY SHEETS JOINED BY TIG WELDING METHOD USING DIFFERENT FILLER METALS

ABSTRACT

Combining different properties of materials in varied industrial applications has been a focus for many researchers. Welding of different metals can be preferred in order to improve flexibility in design process and reduce material cost. In this study, L-605 cobalt-based sheets with a thickness of 1.5 mm, which is generally preferred in environments where corrosion resistance is desired, are combined with 316 L stainless steel sheets of the same thickness. The joining processes were carried out by the TIG welding method in an argon protective gas atmosphere using two different additive metals, cobalt-based Turbaloy L-605 and ER 316 L stainless steel. Samples were prepared from the resulting assemblies in order to see the effects of the additional metals used in the different properties on the weld zone of the welded materials and microstructure and microhardness test were applied to these samples. The data obtained from experimental studies are discussed in comparison with each other.

Key Words: TIG welding, L-605 cobalt-based superalloy, 316 L stainless steel, Weldability

1. Giriş

Yüksek sıcaklıklarda, dayanımlarını koruyabilen ve yüksek sıcaklık direncine sahip olan süperalaşım, iyi korozyon ve oksidasyon direncine, üstün sürünme ve kopma dayanımına sahiptirler. Süperalaşım malzemelerin özellikle kullanıldığı yerler uçak, gemi, lokomotif ve enerji santrali, gaz türbinleri, roket tahrik sistemleri, kimya ve petrol tesisleri olarak sıralanabilir[1].

Genel olarak süperalaşım malzemeler demir esaslı, nikel esaslı ve kobalt esaslı olmak üzere üç ana başlıkta toplanırlar[2].

Kobalt esaslı süperalaşım, başlıca alaşım elementi kobalt olmak üzere önemli miktarda nikel, krom, tungsten daha az miktarda molibden, tantal, titanyum, niobiyum ve bazen de demir gibi elementler içermektedirler[3].

L-605 (Hayness-25) kobalt esaslı süperalaşım malzemeler çeşitli uygulamalarda yaygın olarak kullanılan bir türdür. Bu süperalaşım malzemeler, gaz türbinlerindeki yüksek sıcaklığa maruz kalan yerlerde, cerrahi implant işlemlerinde, nükleer reaktör parçalarında kullanılmaktadır[3].

Paslanmaz çeliklerin önemi içerdikleri krom oranının çok yüksek (%12) olmasından kaynaklanmaktadır. Bu malzemelerde krom miktarına bağlı olarak yüksek sıcaklıklarda oksidasyon direnci artmaktadır[4,5,6].

Östenitik paslanmaz çelik malzemelerde ise krom miktarının yanında nikel oranının da %8'in üzerinde olması östeniti oda sıcaklığında kararlı hale getirmektedir. Bu östenitik paslanmaz çelikler mükemmel mekanik özelliklere ve korozyon dayanımına sahiptirler[7].

Zor metallerin birleştirilmesinde yaygın olarak kullanılan TIG kaynağı, paslanmaz çelik, magnezyum, bakır, alüminyum ve diğer demirdışı metallerin kaynak işlemlerinde genellikle tercih edilmektedir. TIG kaynağı; bir tungsten elektrod ve iş parçası arasında oluşturulan ark sayesinde kaynak için gerekli ısı enerjisini sağlayan ve elektrodu saran bir nozuldan gönderilen asal gaz tarafından korunan kaynak yöntemidir. Kaynak torcundan çıkan koruyucu gaz, kaynak banyosu ile tungsten elektrodu hava ile temasından korumaktadır[8].

TIG kaynak yönteminin kullanıldığı bu çalışmada amaç, farklı özellikteki malzemeleri birleştirerek malzeme maliyetini azaltmak ve tasarım işlemlerinde esnekliği geliştirmektir. Malzemeler, aynı kalınlıktaki kobalt esaslı Turbaloy L-605 ve ER 316 L paslanmaz çelik olmak üzere iki farklı ilave metal kullanılarak argon koruyucu gazı atmosferinde TIG kaynak yöntemi ile birleştirilmişlerdir. Elde edilen birleştirmelerden, kullanılan farklı özellikteki ilave metallerin kaynaklı malzemelerin kaynak bölgesine etkilerini görmek amacıyla numuneler hazırlanmış ve bu numunelere mikroyapı ve mikrosertlik testi uygulanmıştır.

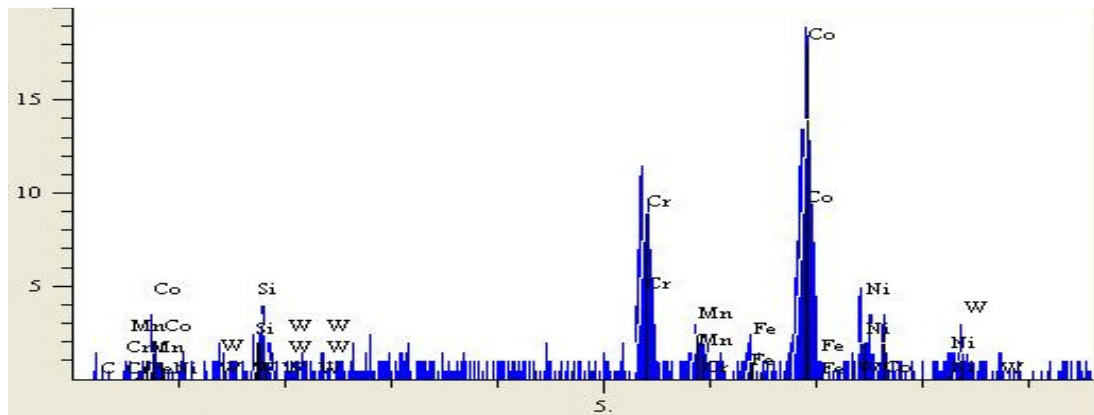
2. Deneysel Çalışma

Bu çalışmada, Tablo 1'de kimyasal kompozisyonları ve Şekil 1 ve 2'de EDS analiz sonuçları verilmiş olan 2 mm kalınlıkta L-605 (Hayness-25) kobalt esaslı süperalaşım ve 316L paslanmaz çelik malzemeler TIG kaynak yöntemi ile 26 cm/dk kaynak hızında ve 80 A. kaynak akımında argon koruyucu gazı atmosferinde birleştirilmiştir. Deneysel çalışmada bir grup numune kobalt esaslı süperalaşım L-605 ilave teli ile birleştirilirken, diğer bir grup numune ise paslanmaz çelik ilave tel kullanılarak birleştirilmiştir.

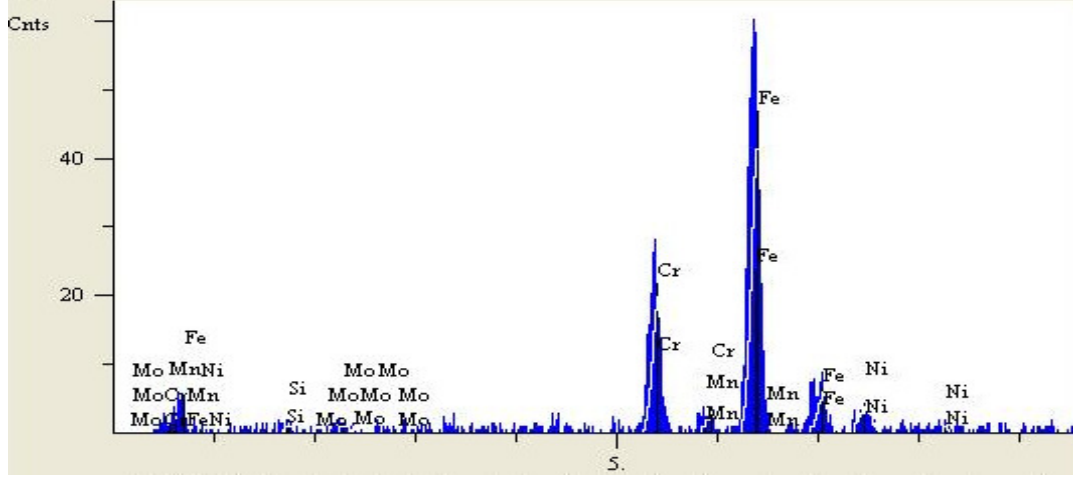
Tablo 1. L-605 süperalaşımın ve ER 316L paslanmaz çeliğin kimyasal kompozisyonları

ALAŞIM ELEMENTİ (% wt) – L-605				
C	Co	Cr	Fe	Mn
0.108	50.574	20.20	2.70	1.48
Ni	P	S	Si	W
10.40	0.006	0.002	0.23	14.30

ALAŞIM ELEMENTİ (% wt) – 316L			
C	Cr	Mo	Mn
0.008	18.50	2.70	1.75
Ni	Fe	Si	
12.00	Kalan	0.45	



Şekil 1. L-605 süperalaşımının EDS analizi



Şekil 2. 316L paslanmaz çeliğin EDS analizi

Kaynakla birleştirilmiş parçalardan, birleşme bölgesinin incelenebilmesi için numuneler hazırlanmıştır. Mikroyapı incelemesi için hazırlanan numunelere, bakalit ile sıcak gömme işlemi uygulanmıştır. Bakalite alma işleminden sonra numunelere 180, 240, 400, 600, 800 ve 1200 meshlik zımparalarla zımparalama işlemi uygulanmıştır. Zımpara işleminden sonra numuneler önce 6 µ daha sonra 3 µ'luk elmas pasta ile parlatılmıştır. Daha sonra parlatılan numuneler, kobalt esaslı süperalaşım için farklı paslanmaz çelik için farklı dağlayıcıyla dağlandıktan sonra farklı büyütmelerde olmak üzere optik mikroskopta görüntüler alınmış, en son olarak da sertlik ölçümleri gerçekleştirilmiştir. Gazi Üniversitesi Teknoloji Fakültesi Metalurji ve Malzeme Mühendisliği Bölümü Metalografi laboratuvarında bulunan Shimadzu HMV model mikro-sertlik ölçme cihazında 0,2 kgf yük uygulanarak sertlik ölçümleri yapılmıştır.

3. Sonuçlar ve Tartışma

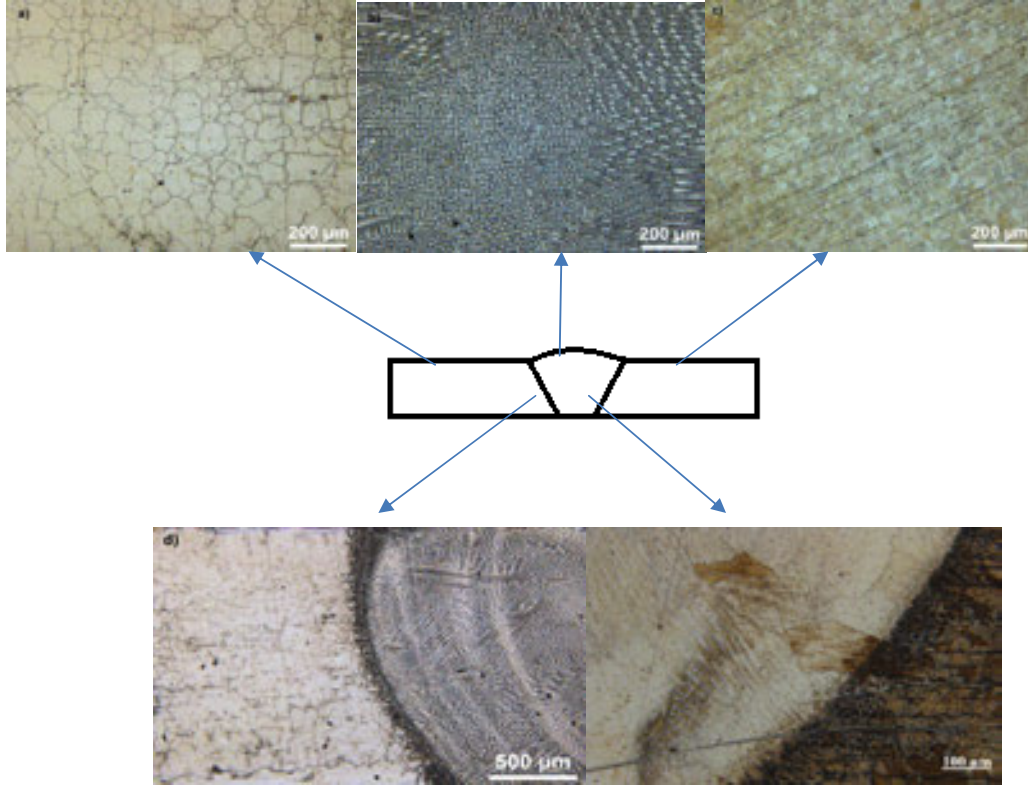
3.1. Mikroyapı Sonuçları

Kobalt malzemelerle paslanmaz çelik malzemelerin L-605 (Hayness-25) kobalt alaşımını ilave tel kullanılarak birleştirilmiş olduğu numunelerden elde edilen mikroyapı görüntüleri aşağıda Şekil-3'de verilmiştir.

a) L-605 ana malzeme

b) Kaynak Metali

c) ER 316L ana malzeme



d) L-605 ITAB

e) ER 316L ITAB

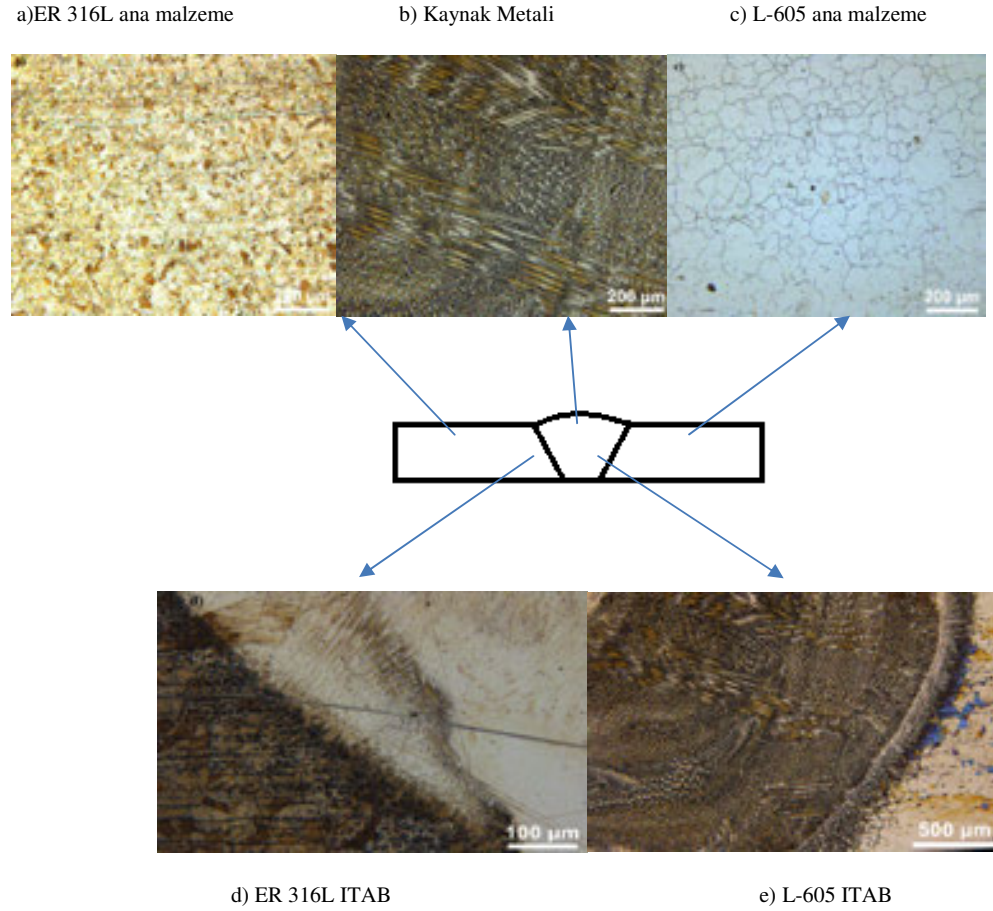
Şekil 3. TIG kaynağı ile L-605 ilave metal kullanılarak birleştirilen numunelerin mikroyapı görüntüleri

Yukarıda verilmiş olan mikroyapı görüntülerine bakıldığında her iki ana malzemenin de eş eksenli deformasyon izi olmayan tanelerden oluştuğu görülmektedir. Yine her iki malzemenin de geçiş bölgesi mikroyapıları incelendiğinde kaynak metalinde oluşan tanelerin ana malzemenin tanelerinin bir devamı şeklinde olduğu ve dendritler halinde ısı akış yönüne ters olacak şekilde kaynak metali merkezine doğru yönlendiği ve kaynak metali merkezinin daha çok eş eksenli tanelerden oluştuğu görülmektedir. Kaynak metali merkezindeki ısının karmaşıklığından dolayı yönelme gerçekleşmemiş olup oluşan taneler eş eksenli bir görünüm almıştır. Kaynak metali merkezinin sağında ve solunda oluşan taneler ise ısı akışının ters yönünde olacak şekilde meydana gelmiştir. Isı kaynak metali merkezinden ana malzemeye doğru akarken kaynak metalinin katılması ana malzemedan kaynak metali merkezine doğru olmaktadır. Tam merkezde yönelme görülmemektedir.

Yine yukardaki görüntülerden anlaşıldığı üzere L-605 kobalt esaslı ilave malzemenin kullanıldığı birleştirmelerde kobalt malzeme tarafında ve paslanmaz çelik malzeme tarafındaki

geçiş bölgelerinde herhangi bir çatlak veya gözenek oluşumuna rastlanmamış, geçiş bölgeleri tipik bir kaynak metaline geçiş bölgesi görünümündedir.

Kobalt malzemelerle paslanmaz çelik malzemelerin ER 316L paslanmaz çelik ilave tel kullanılarak birleştirilmiş olduğu numunelerden elde edilen mikroyapı görüntüleri aşağıda Şekil-4'de verilmiştir.



Şekil 4. TIG kaynağı ile ER 316L paslanmaz çelik ilave tel kullanılarak birleştirilen numunelerin mikroyapı görüntüleri

Yukarıda verilmiş olan ER 316L paslanmaz çelik ilave tel kullanılarak birleştirilen malzemelerin birleşme bölgesi mikroyapı görüntüleri incelendiğinde L-605 kobalt esaslı ilave metal kullanılarak elde edilen birleştirmelerin mikroyapı görüntüleri ile benzer bir şekilde olduğu görülmektedir. Bu görüntülerde de kaynak metaline geçiş bölgelerinde herhangi bir çatlak ve birleşme hatası görülmemektedir. Yine yukarıdaki görüntülerden tipik bir kaynak metaline geçiş bölgesi oluştuğu görülmektedir. Burada da kaynak metalinde oluşan taneler kaynak metaline merkezine doğru yönelmiş ve ana metalin tanelerinin bir devamı şeklinde oluşmuştur.

3.2. Sertlik Değerleri

Deneysel çalışmalarda kullanılan ana malzemelerden olan L-605 kobalt esaslı süperalaşım malzemenin sertlik değeri 335 HV_{0.2} ve 316L paslanmaz çelik malzemenin sertlik değeri ise 250 HV_{0.2} olarak belirlenmiştir. İlave metal olarak kobalt esaslı L-605 süperalaşım ilave metal kullanıldığında kaynak metalinin sertliği yaklaşık olarak 292 HV_{0.2} olarak tespit edilmiştir. Yine ilave metalin paslanmaz çelik ER 316L olduğu birleştirmelerde kaynak metalinin sertliğinin 283 HV_{0.2} olduğu görülmüştür. Kaynak metalinin kullanılan ilave metalin ve ana malzemenin karışımından meydana geldiği bilinmektedir. Her ne kadar soğuma şartlarının kaynak metallerinin sertlik değerleri üzerinde belirgin rol oynadığı bilinse de bu çalışmada elde edilen kaynak metali sertlik değerleri her iki ana malzemenin sertlik değerlerinin yaklaşık olarak ortalaması olacak şekilde karşımıza çıkmaktadır. Kaynak metallerinin sertlik değerleri paslanmaz çelik ana malzemenin sertlik değerinden daha yüksek bulunurken kobalt esaslı süperalaşım ana malzemenin sertlik değerinden daha düşük olduğu görülmüştür.

4. Sonuçlar

L-605 kobalt esaslı süperalaşım malzemeler ile 316L paslanmaz çelik malzemelerin farklı ilave metaller kullanılarak birleştirildiği ve elde edilen birleştirmelerin mikroyapı ve sertlik değerlerinin incelendiği bu çalışmadan aşağıdaki sonuçlar elde edilmiştir.

- Uygun parametreler dahilinde kobalt esaslı süperalaşım malzeme ile paslanmaz çelik malzemeler TIG kaynak yöntemiyle birleştirilebilmektedir.
- Kaynak metalinde oluşan taneler ısı akış yönüne ters olacak şekilde kaynak metali merkez çizgisine doğru yönelmektedir.
- Kaynak bölgesinde herhangi bir kaynak hatası ve çatlak oluşumuna rastlanmamıştır.
- Kaynak metalinde oluşan taneler ana malzeme tanelerinin bir devamı şeklinde meydana gelmiştir.
- Kaynak metali sertlik değerlerinin birleştirilen levhaların sertlik değerlerinin yaklaşık olarak ortalama değerinde olduğu görülmüştür.

5. Kaynaklar

[1]. A. Akdoğan Eker, Yıldız Teknik Üniversitesi, Kimya Metalurji Fakültesi, Metalurji ve Malzeme Mühendisliği Bölümü, Ders Notları, (2008), http://www.yildiz.edu.tr/~akdogan/lessons/malzeme2/Super_Alasimler.pdf

[2]. R. Yılmaz, Z. Barlas, Sakarya Üniversitesi, Teknoloji Fakültesi, Metalurji ve Malzeme Mühendisliği Bölümü, Ders Notları, http://content.lms.sabis.sakarya.edu.tr/Uploads/71353/48078/9_ni-co-super.alasimler.pdf

[3] V.V. Çay, S. Ozan: Süperalaşım ve Uygulama Alanları, Doğu Anadolu Bölgesi Araştırmaları, 2005, pp. 178-188

[4]. Weymueller, C., R., Welding the Austenitic Stainless Steels, Welding Design and Fabrication, 51, 6, 1978. 18. VanderVoort, G.F., Metallography, Principles and Practice, McGraw-Hill Book Company, New York, 1984.

[5]. Anık, S., Tülbentçi, K., Kaluç, E., Örtülü Elektrod ile Ark Kaynağı, Gedik Holding Yayını, İstanbul, 1991.

[6]. Kahraman N., Gülenç B., Akça H., Ark kaynak yöntemi ile birleştirilen östenitik paslanmaz çelik ile düşük karbonlu çeliğin mekanik özelliklerinin incelenmesi, G.Ü. Mühendislik-Mimarlık Fakültesi Dergisi, 17, 2, 75-85, 2002.

[7] Kahraman, N., Gülenç B., ve Akça H., "Ark Kaynak Yöntemi ile Birleştirilen Östenitik Paslanmaz Çelik ile Düşük Karbonlu Çeliğin Mekanik Özelliklerinin İncelenmesi", G.Ü. Mühendislik- Mimarlık Fakültesi Dergisi, Cilt 17, No 3, 75-85, 2002.

[8]. N. Kahraman, B. Gülenç: "Modern Kaynak Teknolojisi Kitabı", 3. Baskı, (2016), Ankara.

PATLAMALI KAYNAK YÖNTEMİ KULLANILARAK S235JR LEVHA YÜZEYLERİNİN ÖSTENİTİK PASLANMAZ ÇELİK (AISI 316L) VE FERRİTİK PASLANMAZ ÇELİK (AISI 430) LEVHALAR İLE KAPLANABİLİRLİĞİNİN ARAŞTIRILMASI

Özer Pamuk^{1a}, Ahmet Durgutlu^{2b}

¹Uşak Üniversitesi, Mühendislik Fakültesi

²Gazi Üniversitesi, Teknoloji Fakültesi

^aozerpamuk@hotmail.com, ^bdurgutlu@gazi.edu.tr

ÖZET

Bu çalışmada, S235JR levhalar AISI 316L ve AISI 430 paslanmaz çelik levhalar ile farklı patlayıcı oranları (R=1.5-2) kullanılarak katihal kaynak tekniklerinden olan patlamalı kaynak yöntemiyle kaplanmıştır. Birleşme arayüzeyinde meydana gelen değişimleri görmek amacıyla birleştirilen malzemeler mikroyapı ve sertlik incelemesine tabi tutulmuştur. Deneyler sonucunda AISI 316L-S235JR metal çiftinde patlayıcı oranının düşük (R=1.5) kullanıldığı numunelerde birleşme arayüzeyinde dalgalı bir yapının meydana geldiği ancak meydana gelen bu dalgalanmanın çok fazla olmadığı görülmüştür. Patlayıcı oranının yüksek (R=2) kullanıldığı numunelerde ise birleşme arayüzeyinde oluşan dalgaların boylarında ve genliklerinde artışların meydana geldiği belirlenmiştir. AISI 430-S235JR metal çiftinde ise, her iki patlayıcı oranında da (R=1.5-2) birleşme arayüzeylerinde çok az bir dalgalanmanın meydana geldiği görülmüş, ancak yüksek patlayıcı oranının (R=2) kullanıldığı numune arayüzeyinde oluşan dalgaların boylarında ve genliklerinde çok az bir artışın meydana geldiği tespit edilmiştir. Patlamalı kaynak işlemi sonrasında metal çiftlerinin birleşme arayüzeyi sertliklerinde levhaların orijinal sertliklerine göre bir miktar artış meydana geldiği belirlenmiştir. Bu artışın patlayıcı oranının artmasına paralel olarak arttığı tespit edilmiştir.

Anahtar Kelimeler: Patlamalı kaynak, Patlayıcı oranı, Mikroyapı, Sertlik.

INVESTIGATION OF THE POSSIBILITY COATING OF S235JR PLATE SURFACES USING EXPLOSIVE WELDING METHOD WITH AUSTENITIC STAINLESS STEEL (AISI 316L) AND FERRITIC STAINLESS STEEL (AISI 430) PLATES

ABSTRACT

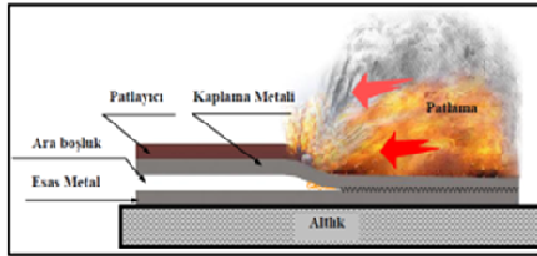
In this study, the S235JR plates were coated with AISI 316L and AISI 430 stainless steel plates with explosive welding method of solid state welding techniques using different explosive ratios (R=1.5-2). The joined materials were evaluated to microstructure and hardness analysis in order to see changes occurring in the joint interfaces. As a result of the experiments, it was observed that the AISI 316L-S235JR metal pair in which a low explosivity ratio (R=1.5) is used has a wavy structure, but this fluctuation did not too much. In the samples where the ratio of the explosive is high (R = 2), the increases in the length and amplitude of the waves appearing at the interface are determined. In the AISI 430-S235JR metal pair it was observed that there was very little ripple at the junction interfaces at both explosive ratios (R = 1.5-2) but at the sample interface where the high explosive ratio (R = 2) was used the wave lengths and amplitudes an increase has been detected. In the AISI 430-S235JR metal pair it was observed that there was very little ripple at the junction interfaces at both explosive ratios (R = 1.5-2) but at the sample interface where the high explosive ratio (R = 2) was used the waves lengths and amplitudes very little an increase has been detected. It has been determined that after the explosive welding process metal couples have a slight increase in their joint interface hardness compared to the original hardness of the plates. This increase was identified to increase parallel to the increase of the explosive ratio.

Key words: Explosive welding, Explosion ratio, Microstructure, Hardness

1. Giriş

Katı hal kaynak tekniklerinden biri olan patlamalı kaynakta patlama ile elde edilen yüksek basınç yardımı ile metal yüzeylerinde meydana gelen çarpışma neticesinde elde edilen çarpışma enerjisi vasıtasıyla yüzeyler, oluşan ilk temaslarını birbirleri üzerinde bir akış sergileyerek devam ettirmeleri sonucunda bir birleşme meydana gelmektedir. Kaynak sırasında meydana gelen temas basıncı oldukça yüksek olduğu için üst tabakanın kinetik enerjisi dalgalı bir arayüzeyin oluşmasına neden olmaktadır. Bu darbe neticesinde iki yüzey birbirlerine mekanik olarak kilitlenir. Bu kaynak yönteminde kaynak işlemini gerçekleştirmek için dışarıdan herhangi bir ısı verilmez. Patlayıcının infilak etmesinden dolayı bir ısı ortaya çıkmasına rağmen ısı transferi için yeterli zaman olmadığı için metaller arasında bir ısı akışı meydana gelmez ve çoğu zaman arayüzeyde difüzyon olayı gerçekleşmez [1-5]. Ancak araştırmacılar bazı durumlarda kaynak esnasında 0.1 µm kadar bir difüzyonun gerçekleştiğini belirtmişlerdir [6].

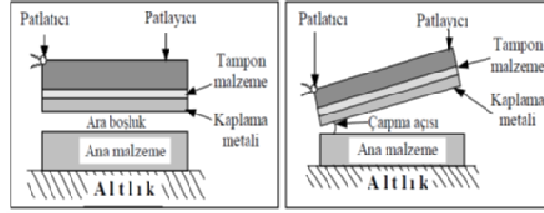
Patlamalı kaynak işleminde birleşmenin gerçekleşebilmesi için gerekli olan şartın fıskırma çarpışması biçiminde oluşan eğimli çarpışma olduğu ileri sürülmektedir. Fıskırma mekanizması, kaynaklanan levhaların yüksek hızda çarpışmaları neticesinde levhalar arasından dışarıya çıkmaya zorlanan ve çarpışmanın ucunda şekillenen metalin fıskırması için kontrol edilen levha hızı, basınç, çarpışma açısı ve çarpışma noktası hızının bulunduğu eğimli bir çarpışma olarak tanımlanmaktadır [7-9]. Patlama neticesinde oluşan yüksek basınç ile çarpışma noktasındaki temiz metal yüzeyleri yakın temasa zorlanmaktadır. Patlamalı kaynak işlemi iki aşamalı olarak düşünülebilir. Birincisi, fıskırma ile yüzey filmlerinin parçalanıp temizlenmesi, ikincisi, yüksek basınç ile atomlar arası kuvvetlerin birleşme arayüzeyi oluşturabileceği konum olan yakın temas için metal yüzeyleri zorlaması [10-12]. Patlamalı kaynak yönteminin şematik gösterimi Şekil 1'de gösterilmiştir.



Şekil 1. Patlamalı kaynak yönteminin şematik görünümü

Patlamalı kaynak yöntemi aynı ya da farklı türdeki metal ve alaşımlarının kaynağının yanında çok katlı ve tel ile güçlendirilmiş kompozit malzeme üretimi içinde kullanılabilir. Ayrıca bu kaynak yöntemi korozyon dayanımı istenen kaplamalı metallerin üretiminde de kullanılmaktadır [13-15].

Patlamalı kaynak yönteminde paralel düzlemde birleştirme ve açılı (eğik) düzlemde birleştirme olmak üzere iki geometrik şekil vardır. Bu yöntemde bir altık üzerine sırasıyla, ana malzeme, ara boşluk, ana malzemeye göre eğimli veya paralel yerleştirilmiş kaplama parçası, malzemelerin patlama sırasında hasara uğramalarını engellemek için tampon malzeme, patlayıcı malzeme ve füyne yerleştirilmektedir [16,17]. Patlamalı kaynak işleminin paralel ve açılı (eğik) düzlemde kaynak geometrileri Şekil 2'de gösterilmektedir.



Şekil 2. Patlamalı kaynak işleminin paralel ve eğik düzlemdeki şematik gösterimi

Patlamalı kaynak yönteminde de diğer kaynak yöntemlerinde olduğu gibi kabul edilebilir nitelikte kaliteli birleştirmelerin elde edilebilmesi için kaynak işlemini kontrol altında tutabilecek işlem parametrelerinin belirlenmesi gerekmektedir. Birleştirme işleminde arayüzeyi ve kaynak kalitesini etkileyen bazı önemli kaynak parametreleri; ara boşluk mesafesi (s), patlayıcı oranı (patlayıcı kütlesinin üst levha kütlesine oranı) (R), patlayıcının patlama hızı (V_d), üst levhanın çarpma hızı (V_p), çarpışma açısı (Q), kaynak hızı (V_c) ve altlık olarak sıralanabilir [15, 18, 19].

Bu çalışmada, gelişmiş ülkelerde yaygın bir şekilde kullanılan ancak ülkemiz endüstrisinde henüz istenilen yeri alamayan patlamalı kaynak yöntemi kullanılarak S235JR levha yüzeyleri AISI 430 ve AISI 316L paslanmaz çelik levhalar ile kaplanmıştır. Kaynak işlemleri sırasında patlamalı kaynak geometrilerinden olan paralel düzlemde kaynak geometrisi kullanılmıştır. Bu şekilde korozyon direnci geliştirilmiş, ısı transfer özellikleri artırılmış, elektriksel özellikleri iyileştirilmiş, kabul edilebilir dayanım değerleri ile iyi aşınma ve erozyon direncine sahip malzemelerin düşük maliyette üretilebilmesi amaçlanmıştır. Birleşme arayüzeyinde meydana gelen değişimleri görmek amacıyla birleştirilen malzemeler mikroyapı ve sertlik incelemesine tabi tutulmuştur.

2. Deneysel çalışmalar

Bu çalışmada, sabit ara boşluk mesafesi (s) ve farklı patlayıcı oranları ($R=1.5-2$) kullanılarak patlamalı kaynak yöntemi ile birleştirilen malzemelerin mikroyapı ve sertlik özellikleri belirlenmeye çalışılmıştır. Bu amaçla, 200x200x3,5 mm ebatlarında ve 160 HV_{0,3} sertlik değerine sahip S235JR levha yüzeyleri 200x200x1 mm ebatlarında 165 HV_{0,3} sertlik değerine sahip ferritik paslanmaz çelik (AISI 430) ve 195 HV_{0,3} sertlik değerine sahip östenitik paslanmaz çelik (AISI 316L) levhalar ile patlamalı kaynak geometrilerinden olan paralel düzlemde kaynak geometrisi yöntemi kullanılarak kaplanmıştır. Kaynak işlemi sırasında patlayıcı olarak M.K.E Barutsan A.Ş. tarafından üretilen % 92 Amonyum Nitrat, % 5 Motorin ve % 3 TNT içeren Elbar-5 kodlu toz patlayıcı kullanılmıştır. Kullanılan toz patlayıcı miktarı, üst levha olarak kullanılan ferritik paslanmaz çelik (AISI 430) ve östenitik paslanmaz çelik (AISI 316L) levhaların ağırlığı ile orantılı olarak belirlenmiştir. Tablo 1'de deneyler sırasında kullanılan patlayıcı oranı (R) ve miktarları verilmektedir.

Tablo1. Patlayıcı oranları ve miktarları

Numune No	Ana Malzeme	Kaplama Malzemesi	Patlayıcı	Üst levha ağırlığı (g) (m)	Patlayıcı Oranı (R)	Patlayıcı Miktarı (m x R) g
1	S235JR	AISI 430	Elbar-5	314	1,5	471
2				314	2	628
3		AISI 316L		314	1,5	471
4				314	2	628

Birleştirme işlemleri kum havuzu içerisine yerleştirilmiş olan ve yüzey düzgünlüğü ayarlanmış 1500x1500x150 mm ebatlarındaki çelik bir tabla üzerinde gerçekleştirilmiştir. Kaynak işlemi sırasında, patlamanın alt parçada oluşturabileceği zararları en aza indirebilmek için çelik tabla ile alt parça arasına 5 mm kalınlığında lastik bir tampon konulmuş ve böylece birleştirilen parçaların altlığın akustik özelliğinden etkilenecek ayrılmalarının ve geri fırlamalarının önüne geçilmesi amaçlanmıştır. Ara boşluk mesafesini (s) elde etmek için uygun kalınlıktaki rondelalar kullanılarak alt parçanın üzerinde dört köşesine gelecek şekilde yerleştirilmiş ve üst levha rondelaların üzerine yerleştirilerek uygun ara boşluk mesafesi ayarlanmıştır. Hazırlanan 210x210x50 mm boyutlarında patlayıcı kutuları üst levha üzerine yerleştirilerek kaynak düzeneği hazır hale getirilmiştir. Hazırlanan bu kaynak düzeneği elektrikli bir manyeto düzeneği tarafından patlatılarak kaynak işlemleri gerçekleştirilmiştir.

Kaynak işlemi sonrası arayüzeyde meydana gelen değişimleri görmek amacıyla birleştirilen malzemelerden patlama yönüne paralel olacak şekilde tel erozyon yöntemi ile mikroyapı numuneleri kesilerek hazırlanmıştır. Kesilen bu numuneler bakalite gömme, zımparalama ve parlatma işlemine takiben 2ml HNO₃ (Nitrik asit) ve 98 ml metanol bileşiminden oluşan dağlama solüsyonu ile dağlandıktan sonra optik mikroskop yardımı ile mikroyapı incelemesine tabi tutulmuştur. Mikroyapı incelemeleri LEICA marka DM 4000M model metal mikroskobu kullanılarak gerçekleştirilmiştir. Yine aynı numuneler, kaynak işlemi sırasında patlamanın neden olduğu yüksek hızdaki çarpışma neticesinde birleşme arayüzeyinde ve birleştirilen levhaların kesitleri boyunca oluşan sertlik değişimlerini görmek amacı ile sertlik ölçme işlemine tabi tutulmuştur. Mikrosertlik ölçümleri sırasında HVM marka Vickers mikrosertlik ölçme cihazı kullanılarak 300g yük 5 sn süre ile malzeme yüzeyine uygulanarak her iki malzemede birleşme arayüzeyinden başlayarak metal çiftlerinin yüzeylerine kadar belirli aralıklarla ölçümler yapılmıştır. Her bir noktadan üç adet sertlik değeri alınarak ve ortalama değer sertlik değeri olarak kabul edilmiştir.

3. Sonuçlar ve Tartışma

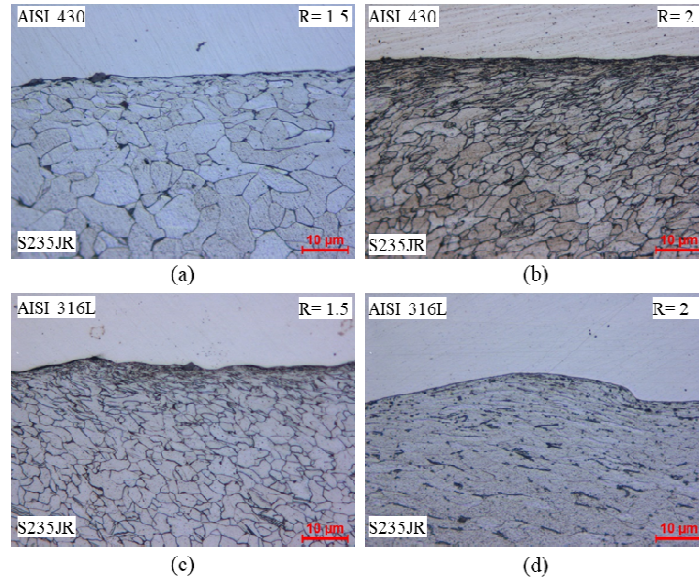
S235JR malzeme yüzeyi ferritik paslanmaz çelik (AISI 430) ve östenitik paslanmaz çelik (AISI 316L) levhalar ile patlamalı kaynak yöntemi kullanılarak başarılı bir şekilde kaplanmıştır. Birleştirilen malzemelerin kaynak işlemi sırasında kullanılan kaynak parametreleri ile olan ilişkileri belirlenmek amacıyla mikroyapı ve sertlik incelemesine tabi tutulmuştur.

3.1. Mikroyapı incelemesi

AISI 430-S235JR ve AISI 316L-S235JR metal çiftlerinden oluşan ve tek bir ara boşluk mesafesi (s) ile farklı patlayıcı oranları (R=1,5-2) kullanılarak patlamalı kaynak yöntemi ile birleştirilen malzemelerin birleşme ara yüzeylerine ait mikroyapı görüntüleri Şekil 3'de verilmiştir.

Şekil 3'de verilen ve AISI 430-S235JR metal çiftine ait olan mikroyapı görüntüleri incelendiğinde, patlayıcı oranının (R=1.5) kullanıldığı 1 numaralı numuneye ait (Şekil 3.a) birleşme arayüzeyinde oluşan dalgalanmanın çok az olup hemen hemen düz bir arayüzeye sahip olduğu görülmektedir. Bunun sebebinin patlayıcı oranının yeterli düzeyde olmadığından kaynaklandığı düşünülmektedir. Patlayıcı oranlarının (R= 2) kullanıldığı 2 numaralı numuneye ait (Şekil 3.b) birleşme arayüzeyinde oluşan dalgaların boylarında ve genliklerinde artışların meydana geldiği ancak bu artışın fazla olmadığı tespit edilmiştir. Yine Şekil 3'de verilen ve AISI 316L-S235JR metal çiftine ait olan mikroyapı görüntüleri incelendiğinde, patlayıcı oranının (R=1.5) kullanıldığı 3 numaralı numuneye ait (Şekil 3.c) birleşme arayüzeyinde dalgalı bir yapının meydana geldiği ancak arayüzeyde meydana gelen bu dalgalanmanın yeterli seviyede

olmadığı görülmüş ve bunun da sebebinin patlayıcı oranının yeterli düzeyde olmadığından kaynaklandığı düşünülmektedir. Patlayıcı oranının ($R=2$) kullanıldığı 4 numaralı numuneye ait (Şekil 3.d) birleşme arayüzeyinde oluşan dalgaların boylarında ve genliklerinde artışların meydana geldiği görülmektedir. Bu durum ise kullanılan patlayıcı oranının birleşme arayüzeyinde dalga oluşumunu sağlayacak seviyede olduğunu göstermektedir. Yine Şekil 3.d'de görüldüğü gibi birleşme arayüzeyinde üst levhadaki fişkırmmanın momentumundan kaynaklanan alt levhada oluşan deformasyon yanı sıra alt levhanın uç kısmında başlayan katlanma oluşumu görülmektedir. Aynı patlayıcı oranının kullanıldığı ($R=1.5, 2$) her iki metal çiftinde AISI 316L-S235JR metal çiftine ait birleşme arayüzeyinde oluşan dalgalanmanın AISI 430-S235JR metal çiftine ait birleşme arayüzeyinde oluşan dalgalanmaya oranla daha fazla olmasının sebebinin kaplama malzemesi olarak kullanılan AISI 316L levhanın sertliğinin AISI 430 levhanın sertliğinden daha yüksek olmasından kaynaklandığı düşünülmektedir. Birleştirme işlemi sonrası her iki metal çiftinde patlama neticesinde çarpışmanın neden olduğu deformasyondan dolayı birleşme arayüzeyine yakın bölgedeki tanelerin patlama yönüne paralel bir şekilde uzadığı görülmektedir. Ayrıca yüksek patlayıcı oranının kullanıldığı (Şekil 3.b-d) numunelerdeki tanelerin uzamasının düşük patlayıcı oranı ile elde edilen (Şekil 3.a-c) numunelere nazaran daha fazla olduğu görülmektedir. Bu durumun artan patlayıcı oranıyla beraber deformasyon oranının artmasından kaynaklandığı düşünülmektedir. Literatürde, patlama kaynak işlemlerinde patlayıcı oranının artmasıyla beraber birleşme arayüzeyinde meydana gelen deformasyon miktarının arttığı ve oluşan dalgalanmanın genliğinde ve boylarında artışların meydana geldiği belirtilmektedir [20].



Şekil 3. Birleştirilen metal çiftine ait birleşme arayüzeyi mikroyapı görüntüleri
a-) AISI 430/R=1.5, b-) AISI 430/R=2, c-) AISI 316L/R=1.5, d-) AISI 316L/R=2

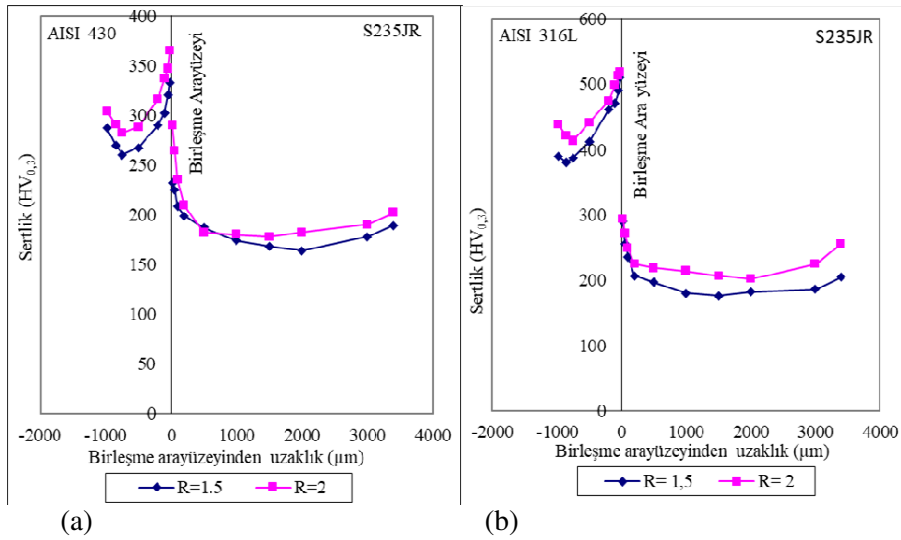
3.2. Sertlik sonuçları

Patlamalı kaynak yöntemi ile sabit ara boşluk mesafesi (s) ve farklı patlayıcı oranları ($R=1.5-2$) kullanılarak üretilen AISI 430-S235JR ve AISI 316L-S235JR metal çiftlerine ait sertlik ölçümleri yapılarak malzemelerin orijinal sertlik değerleri ile mukayese edilmiştir. Birleştirilen metal çiftlerine ait sertlik değerlerini belirlemek için 1 mm et kalınlığına sahip AISI 430 ve AISI 316L levhalarda, birleşme arayüzeyinden başlayarak malzemenin dış yüzeyine doğru 20, 50,

100, 200, 500, 750, 850, 980 μm mesafelerden ölçümler gerçekleştirilmiştir. Diğer yandan 3,5 mm et kalınlığına sahip S235JR levha için birleşme arayüzeyinden başlayarak malzemenin dış yüzeyine doğru 20, 50, 100, 200, 500, 1000, 1500, 2000, 3000, 3400 μm mesafelerden sertlik ölçümleri yapılmıştır. Birleştirmeyi meydana getiren metal çiftlerinden AISI 430 levhannın başlangıç sertlik değeri 165 $\text{HV}_{0,3}$, AISI 316L levhannın başlangıç sertlik değeri 195 $\text{HV}_{0,3}$, S235JR levhannın başlangıç sertlik değeri ise 160 $\text{HV}_{0,3}$ olarak tespit edilmiştir. Patlamalı kaynak işlemi ile üretilen malzemelere ait sertlik değerleri Tablo 2 de verilmiş ve grafiksel olarak Şekil 4'te gösterilmiştir.

Tablo 2. Metal çiftlerine ait sertlik değerleri ($\text{HV}_{0,3}$)

Numune No	1	2	3	4		
Malzemeler	AISI 430+ S235JR	AISI 430+ S235JR	AISI 316L+ S235JR	AISI 316L+ S235JR		
Patlayıcı Oranı	R= 1.5	R= 2	R= 1.5	R= 2		
Arayüzeyden uzaklık (μm)	AISI 430/AISI 316L	-980	287	304	345	358
		-850	270	291	331	349
		-750	260	282	329	342
		-500	267	288	372	396
		-200	290	316	445	464
		-100	302	337	471	498
		-50	320	347	490	513
		-20	333	365	510	518
		0			-	-
	S235JR	20	285	290	290	294
		50	245	264	256	272
		100	223	235	236	249
		200	199	209	216	232
		500	178	182	197	219
		1000	170	180	180	212
		1500	168	178	176	205
		2000	164	182	172	202
		3000	178	190	186	205
		3400	189	212	205	221



Şekil 5. Metal çiftlerine ait sertlik grafikleri

(a= AISI430-S235JR metal çifti, b= AISI 316L-S235JR metal çifti)

Tablo 2. incelendiğinde, AISI 430-S235JR metal çifti için patlayıcı oranının (R=1.5) olduğu 1 numaralı numunede, birleştirmeyi meydana getiren metal çiftlerinden başlangıç sertlik değeri 165 HV_{0,3} olan AISI 430 için birleşme arayüzeyine en yakın bölge olan 20 µm mesafedeki sertlik değeri 333 HV_{0,3} değerine ulaşmıştır. AISI 430'a ait sertlik değeri arayüzeyden levha merkezine doğru gidildikçe azalma göstererek 750 µm mesafede 260 HV_{0,3} olarak ölçülmüştür. Birleşme arayüzeyine en uzak mesafe olan ve yüzeye en yakın bölge olan 980 µm mesafede AISI 430'un sertliği tekrar 287 HV_{0,3} değerine yükseldiği belirlenmiştir. Birleştirmeyi meydana getiren metal çiftlerinden diğeri olan ve başlangıç sertliği 160 HV_{0,3} olan S235JR birleşme arayüzeyine en yakın mesafe olan 20 µm mesafedeki sertlik 285 HV_{0,3} değerine ulaşmıştır. S235JR malzemeye ait sertlik birleşme arayüzeyinden 2000 µm mesafeye gelinceye kadar sürekli azalma göstererek 164 HV_{0,3} olarak ölçülmüştür. Birleşme arayüzeyinden en uzak mesafe olan ve yüzeye en yakın bölge olan 3400 µm mesafede S235JR malzemenin sertliğinin tekrar 189 HV_{0,3}'ye yükseldiği belirlenmiştir. Patlayıcı oranının (R=2) kullanıldığı 2 numaralı numunede birleştirmeyi meydana getiren metal çiftlerindeki sertlik dağılımları artan patlayıcı oranına bağlı olarak 1 numaralı numune ile benzerlik göstermektedir. AISI 316L-S235JR metal çifti için patlayıcı oranının (R=1.5) olduğu 3 numaralı numunede, birleştirmeyi meydana getiren metal çiftlerinden başlangıç sertlik değeri 195 HV_{0,3} olan AISI 316L için birleşme arayüzeyine en yakın bölge olan 20 µm mesafedeki sertlik 510 HV_{0,3} değerine yükselmiştir. AISI 316L'ye ait sertlik birleşme arayüzeyinden levha merkezine doğru gidildikçe azalma göstererek 750 µm mesafede 329 HV_{0,3} olarak ölçülmüştür. Birleşme arayüzeyinden en uzak mesafe olan ve yüzeye en yakın bölge olan 980 µm mesafede AISI 316L'nin sertliği tekrar 345 HV_{0,3} değerine yükseldiği belirlenmiştir. Birleştirmeyi meydana getiren metal çiftlerinden diğeri olan ve başlangıç sertliği 160 HV_{0,3} olan S235JR için birleşme arayüzeyine en yakın mesafe olan 20 µm mesafedeki sertlik 290 HV_{0,3} değerine ulaşmıştır. S235JR malzemeye ait sertlik birleşme arayüzeyinden 2000 µm mesafeye gelinceye kadar sürekli azalma göstererek 172 HV_{0,3} olarak ölçülmüştür. Birleşme arayüzeyinden en uzak mesafe olan ve yüzeye en yakın bölge olan 3400 µm mesafede S235JR malzemenin sertliğinin tekrar 205 HV_{0,3}'ye yükseldiği belirlenmiştir. Patlayıcı oranının (R=2) kullanıldığı 4 numaralı numunede birleştirmeyi meydana getiren metal çiftlerindeki sertlik dağılımları artan patlayıcı oranına bağlı olarak 3 numaralı numune ile benzerlik göstermektedir.

Kaynak işlemi sırasında patlayıcının etkisiyle levhalarda meydana gelen çarpışma neticesinde birleşme arayüzeyinde oluşan soğuk deformasyon ile malzemelerde bir deformasyon sertleşmesi meydana gelmekte ve bu durum malzemelerin sertliklerinin artmasına neden olmaktadır. Meydana gelen deformasyonun şiddetinin arayüzeyden merkeze doğru ilerledikçe azaldığı için malzemelerin sertlikleri de azalarak orijinal sertlik değerlerine yaklaşmaktadır. Kaynak işlemi sonrası her iki malzemenin yüzey bölgelerinin sertlik değerlerinde de bir artış meydana geldiği görülmektedir. Bunun sebebi olarak, kaynak işlemi sırasında patlayıcının patlaması neticesinde meydana gelen şok dalgasının üst levhanın yüzeyinde meydana getirdiği deformasyon ve alt levhanın dış yüzeyinin altlık ile çarpışması neticesinde oluşan deformasyon olarak düşünülmektedir. Literatürde, patlamalı kaynak yöntemi ile üretilen kompozit malzemelerin sertlikleri üzerine yapılan çalışmalarda, en yüksek sertlik artışının arayüzeye yakın bölgelerde oluştuğunu, iç bölgelere gidildikçe sertlikte azalmaların meydana geldiği belirtilmektedir [21-24]. Yine literatürde, artan patlayıcı oranıyla beraber kompoziti meydana getiren malzemelerin sertlik değerlerinde bir artış meydana geldiğini, bunun nedeninin ise artan patlayıcı oranı ile meydana gelen deformasyon şiddetinin artmasından kaynaklandığı belirtilmektedir [1,2,21,25].

4. Sonular

Patlamalı kaynak yöntemi kullanılarak S235JR levha yüzeylerinin ferritik paslanmaz elik (AISI 430) ve östenitik paslanmaz elik (AISI 316L) levhalar ile kaplanabilirliğinin araştırıldığı bu çalışmada aşağıdaki sonuçlar elde edilmiştir.

1. S235JR levha yüzeyleri AISI 430 ve AISI 316L levhalar ile uygun kaynak parametreleri ile başarılı bir şekilde kaplanabilmektedir.
2. Birleşme arayüzeyinde oluşan dalgaların boylarında ve genliklerinde patlayıcı oranının artışına bağlı olarak azda olsa bir artış meydana geldiği görülmektedir.
3. Patlama neticesinde meydana gelen deformasyon nedeni ile patlayıcı oranının artışıyla beraber birleşme arayüzeyine yakın tanelerin patlama yönünde yönlendikleri görülmektedir.
4. Patlamalı kaynak işlemi sonrası birleştirmeyi meydana getiren levhaların sertliklerinde orijinal sertliklerine göre bir artış meydana geldiği ve en büyük sertlik artışının birleşme arayüzeyine yakın bölgelerde gerçekleştiği görülmektedir.
5. Genel olarak birleştirmeyi meydana getiren levhaların sertlik değerlerinde kullanılan patlayıcı oranının artışına bağlı olarak bir artış meydana gelmektedir.

5. Kaynaklar

[1] Kahraman N., Gülen B., Patlamalı Kaynak Yöntemi ile Birleştirilen Titanyum ve Bakır Levhaların Mikroyapı ve Korozyon Davranışlarının İncelenmesi, Politeknik Dergisi, 7(2) (2004) p.45-52.

[2] Durgutlu A., Gülen B., Patlama Kaynağıyla Paslanmaz elik – Bakır Levhaların Kaynaklanabilirliği ve Patlayıcı Oranının Birleşme Arayüzeyine Etkisi, Politeknik Dergisi, 5(3) (2002) p.243-247.

[3] Kearns W. H., Explosion Welding, Welding Handbook, 3th Edition, AWS, (1980)

[4] Patterson R.A., Fundamentals of Explosion Welding, 6th Edition, ASM Handbook, (1993)

[5] Gupta R. C., Kainth G. S., Swinging Wake Mechanism For Interface Wave Generation in Explosive Welding of Metals, Transactions of the ASME, 57 (1990) p.514-521.

[6] Yang Y., Xinming Z., Zhenghua L., Qingyun L., Adiabatic Shear Band on the Titanium Side in the Ti/Mild Steel Explosive Cladding Interface, Acta Mater, 44 (2) (1996) p.561- 565.

- [7] Cown G. R., Bergmann O. R., Holdzman A. H., Mechanism of Bond ZoneaveFormation in Explosive-CladMetals, MetallurgicalTransactions, 2 (1971) p.3145-3155.
- [8] Yang Y., Wang Z. M., Zhang S. R., SomeMetallurgicalBehaviours of AdiabaticShare on Ti Side in the Ti/Mild Steel ExplosiveCladdingInterface,. RareetalMaterialsandEngineering, 26 (1997) p.13-17.
- [9] Erza A.A., PrinciplesandPracticeof Explosive Metal Working, IndustrialNewspaper Ltd., (1973) p.276-289.
- [10] James F.K., Hay D.R., Amechanizm of ExplosiveBonding, MetallurgiaTransactions, 2 (1971) p.1953-1958.
- [11] Reid S.R., A Discussion of theMechanism of InterfaceWaveGeneration in ExplosiveWelding, Int. Journal of MechanicalScience, 6 (1974) p.399-413.
- [12] Yang Y., Li Z.H., Lu P.C., A TemperatureDistrubition Model of ExplosiveCladdingİnterfaceandItsAplication, Rare Metal MetarialsandEngineering, 29 (3) (2000) p.161-163.
- [13] Abe A., Numericalstudy of theMechanism of WavyInterfaceGeneration in ExplosiveWelding, JSME International Journal, 40 (3) (1997) p.395-401.
- [14] Abe A., NumericalSimulation of thePlasticLowFieldNeartheBondingSurface of ExplosiveWelding, Ournal of MaterialsProcessingTechnology, 85 (1999) p.62-165.
- [15] Acarer M., Patlamalı Kaynak İşlem Parametrelerinin Birleşmeye Etkisi, Doktora Tezi, Sakarya Üniversitesi Fen Bilimleri Enstitüsü, Sakarya/Türkiye, (2001)
- [16] James F. K., Hay D. R., A Mechanizm of ExplosiveBolding, MetallurgicalTransactions, 2 (1971) p.1953-1958.
- [17] Demirkol M., "Patlamalı Kaynak Yöntemi", II. Ulusak Kaynak Sempozyumu, İTÜ, İstanbul/Türkiye, (1989) pp.142-151.
- [18] Balasubramanian V., Rathinasabapathi M., Raghukandan K., Modelling of ProcessParameters in ExplosiveCladding of MildsteelandAluminium, Journal of MaterialsProcessingTechnology, 63 (1997) pp.83-88.
- [19] Livne Z., Munitz A., Characterization of ExplosivelyBondedIronandCopperPlates, Journal of MateralsScience, 22 (1987) pp.1495-1500.
- [20] Durgutlu, A., "Patlamalı Kaynak Yöntemi İle Bakır-Paslanmaz Çelik Malzemelerin Birleştirilmesi ve Arayüzeyin Mekanik-Mikroyapı Özelliklerinin incelenmesi", Doktora Tezi, Gazi Üniversitesi Fen Bilimleri Enstitüsü, Ankara/Türkiye, (2003).
- [21] Yan, Z., Cui L. S., and Zheng, Y. J., Microstructureandmartensitictransformationbehaviors of explosivelyweldedNiTi/NiTi laminates, ChineseJournal of Aeronautics, 20 (2007) pp.168-171.

[22] Gulbin, V.N., Kobelev, A.G., Borissov, D.E., Thermobimetals Mechanical Properties Produced by Explosive Welding With Rolling, Journal de Physique 4 (1997) pp.49-54.

[23] Truetnev, V.V., ve arkadaşları., Comparative Assessment of The Quality of The Explosive Joining of Aluminium to Titanium, Steel and Nickel, Svar. Roiz., 7 (1973) pp.19-21.

[24] Bina, M. H., Dehghani, F., and Salimi, M., Effect of heat treatment on bonding interface in explosively welded copper/stainless steel, Materials and Design, 45 (2013) pp.504-509.

[25] Kahraman, N., Titanyum levhaların patlamalı kaynak yöntemi ile farklı metallerle birleştirilmesi ve arayüzey özelliklerinin incelenmesi, Doktora Tezi, Gazi Üniversitesi Fen Bilimleri Enstitüsü, Ankara/Türkiye, (2003).

YAZIŞMA ADRESİ:

Özer PAMUK, Uşak Üniversitesi Mühendislik Fakültesi Malzeme Bilimi ve Nanoteknoloji Mühendisliği Bölümü Bir Eylül Kampüsü 64000 Merkez/UŞAK,
[Tel:02762212121/5052215620](tel:02762212121/5052215620)
e-mail: ozer.pamuk@usak.edu.tr

Dr. Öğrt. Üyesi Özer PAMUK: Uşak Üniversitesi Mühendislik Fakültesi Malzeme Bilimi ve Nanoteknoloji Mühendisliği Bölümü

Prof. Dr. Ahmet DURGULU: Gazi Üniversitesi Teknoloji Fakültesi Metalurji ve Malzeme Mühendisliği Bölümü

INVESTIGATION OF MICROSTRUCTURE AND CORROSION PROPERTIES OF THE INCONEL 625 WELD

Mustafa Tümer^{1,a}, Alptekin Kısasöz^{2,b}, Ahmet Karaaslan^{2,c}, Mithat Kerimak^{3,d}

¹Kocaeli University, Uzunçiftlik Nuh Çimento Vocational School, Kocaeli, Turkey

²Yıldız Technical University, Department of Metallurgical and Materials Engineering, Istanbul, Turkey

³Anadolu Casting Co., Kocaeli, Turkey

^a mustafa.tumer@kocaeli.edu.tr, ^b akisasoz@yildiz.edu.tr, ^c karaas@yildiz.edu.tr,

^d mzaimkerimak@anadoludokum.com.tr

Abstract

Inconel 625 is a nickel-based super alloy with high chromium and molybdenum content. Inconel 625 alloy is used in aggressive environments like petro-chemical applications, aeronautical and nuclear energy industries due to its higher mechanical properties and corrosion resistance. In this study, Inconel 625 specimens were joined with ERNiCrMo-3 filler metal by using MIG (metal inert gas) method. Also, relationship between microstructure and corrosion properties of the Inconel 625 weld was investigated. Microstructure properties of the weld metal were determined by light metal microscope (LOM). Moreover, corrosion properties of the weld metal and base material were examined by potentiodynamic polarization tests. Corrosion behavior and parameters of the electrochemical potentiodynamic polarization depending microstructure properties (comprised phases and grain types) were determined. Especially, various phases precipitated in the weld metal microstructure enhanced the corrosion rate of Inconel 625 weld.

Key Words: Superalloy, Inconel 625, Electrochemical corrosion.

1. Introduction

Nickel based Inconel 625 superalloy was widely used in aeronautical, energy, chemical, petrochemical and marine industries. Inconel 625 alloy exposes higher yield strength, fatigue strength, tensile strength, creep resistance in aggressive corrosive environments and also Inconel 625 has good weldability and hot strength [1, 2].

Inconel 625 alloy contains chromium in high proportions with molybdenum, iron and niobium. Microstructure of the Inconel 625 consists of solid-solute matrix structure and fine dispersed MC and M₆C types of carbides [3]. MC and M₆C carbides are hard and brittle phase comprised of niobium, molybdenum and nickel. Inconel 625 alloy has higher mechanical strength owing to nickel-chromium solid solution strengthen with molybdenum and niobium and this matrix structure eliminates the precipitation hardening process [4, 5]. Weld material has lower mechanical properties compared to base material in welding of Inconel 625 alloy. One of the main reasons of this phenomena is Laves phase. This phase is a typical intermetallic phase (A: Ni, Cr, Fe ve B: Nb, Mo, Ti) and occurs between dendritic structures during the solidification in welding process. Segregation of niobium in welding process causes the formation of Laves phase and precipitation of Laves phase in welding zone is inevitable. Also, initiation and propagation of cracks take place due to heterogenous microstructure in terms of alloying elements in welding zone [6, 7].

MortezaieeveveShamanian [8] studied dissimilar welding of Inconel 718 and AISI 310 alloys with various filler metals. It was determined that weld metal of the specimen joined with ERNiCrMo-3 type filler metal has lower corrosion rate compared to weld metal of the specimen joined with ERNiCr-3 type filler metal owing to higher chromium proportion. Also, Luer et al. [9] investigated the corrosion properties of coating produced with ErNiCrMo-3 filler metal in 15000 hours service condition. Luer et. al. showed that molybdenum and niobium segregated at interdendritic zones, solid solute matrix structure became poor in terms of alloying elements and intermetallic phases induced initiation and propagation of cracks. Experimental studies about nickel based superalloy was focus on welding of superalloy with appropriate filler metal, microstructural properties, physical and mechanical properties of the joints.

In this study, Inconel 625 alloy was joined with multi pass MIG method and also, relationship between microstructure and corrosion properties of Inconel 625 weld was investigated with potentiodynamic polarization tests.

2. Experimental

Inconel 625 superalloy were joined with ERNiCrMo3 filler metal by using multipass MIG welding method. Chemical composition of the base metal (Inconel 625) and the filler material (ERNiCrMo-3) were given in Table 1. Inconel 625 plates with a dimension of 200x100x15 mm³ were joined by V groove and Ar – 2%O₂ shielding gas with a 14 l/min flow rate. Heat input was calculated between 1.33 and 1.67 kJ/mm⁻¹.

Standard grinding and polishing procedures were applied and specimens were etched in 10% NaOH₃ solution with 10.4 V for 5 seconds. Microstructure examinations were carried out by light metal microscope and image analysis.

Table 1. Chemical composition of the base metal and the filler material.

	Cr	Mo	Nb	Fe	Ni
Inconel 625	21	9	3,4	4	Bal.
ERNiCrMo-3	22	9	3,5	1	Bal.

Potentiodynamic polarization tests were performed in 3.5% wt. NaCl solution at room temperature to determine the corrosion behavior of the specimens. Corrosion test were carried out by IviumCompactstatpotentiostat at a scanning rate 1 mV/s. Prior to each experiment Inconel 625 alloy was cut from welding zone and base material parts and each corrosion test was applied with 1 cm² surface area. Electrochemical cell was constituted by working electrode (Inconel 625 base material and Inconel 625 weld metal), reference electrode (Ag/AgCl electrode) and counter electrode (platinum plate). Counter electrode to working electrode surface ratio was equal to 4.

3. Results and Discussion

Microstructures of the Inconel 625 base material and the weld metal joined with ERNiCrMo-3 were given in Figure 1. Base metal consisted of fully austenitic structure. Also, weld metal had dendritic microstructure due to occurrence of rapid cooling at weld seam during the welding process. Moreover, inclusions were formed in dendritic microstructure as seen in Figure 1c.

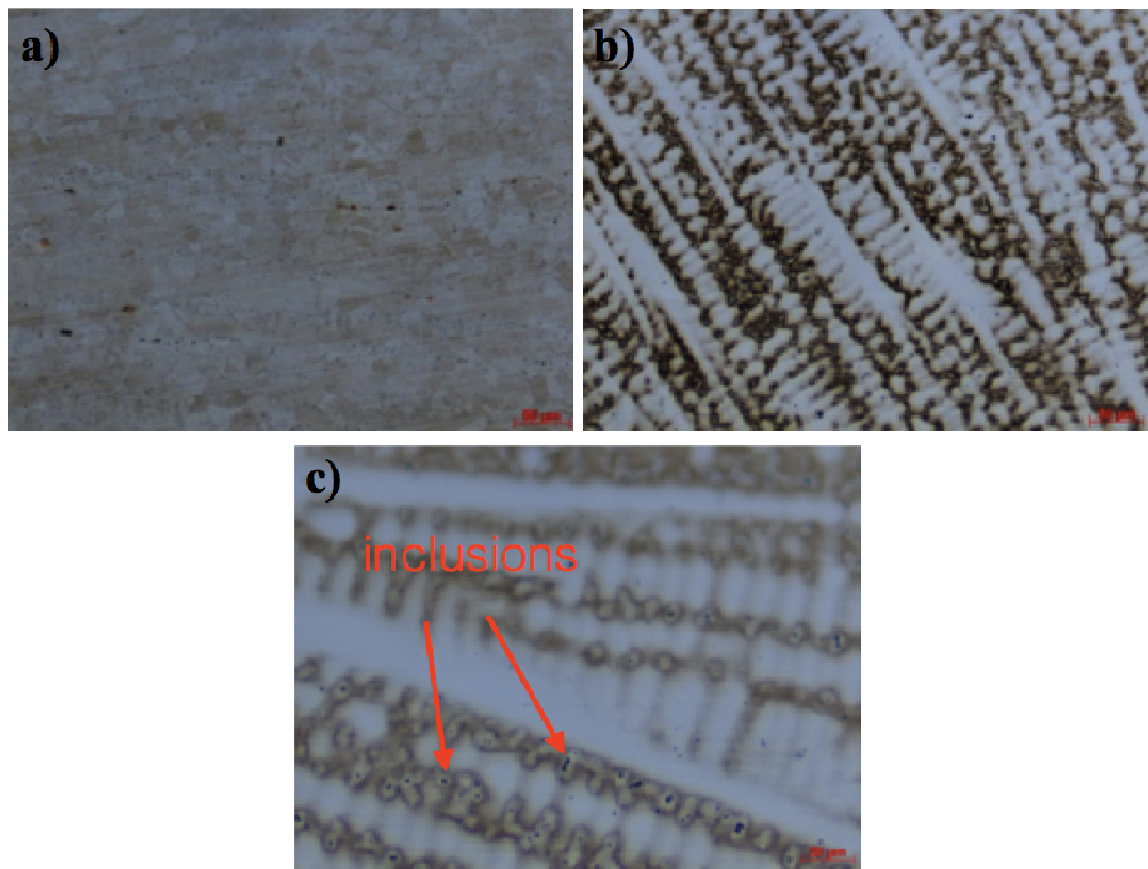


Figure 1. Microstructures of the Inconel 625 base material and the weld metal joined with ERNiCrMo-3; a) base material, b) and c) weld metal with various magnifications.

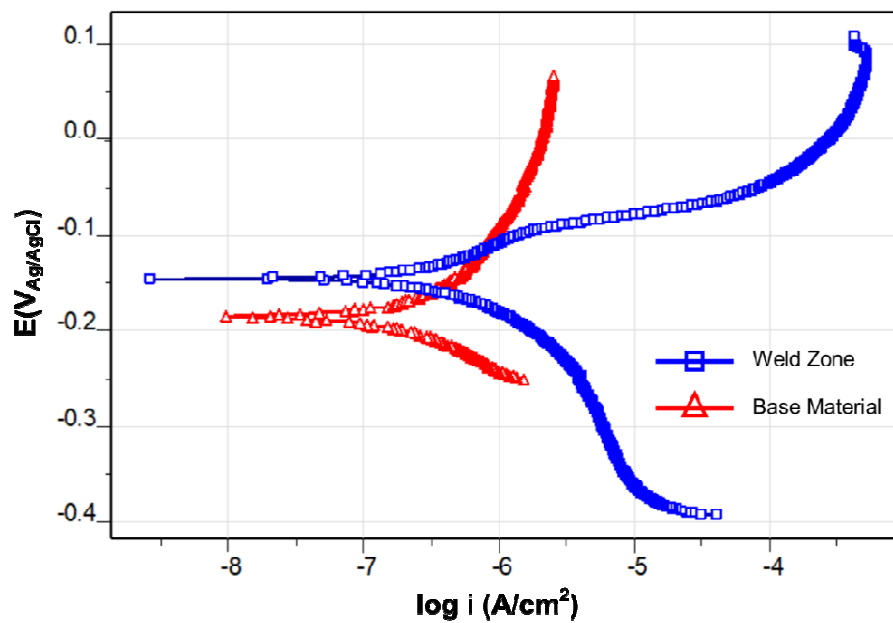


Figure 2. Potentiodynamic polarization curves of the base material and the weld metal.

Figure 2 shows the potentiodynamic polarization curves of the base material and the weld metal. Figure 2 demonstrates that both base materials and weld metal did not show the passivation behavior. The shape of the potentiodynamic polarization curves shows that the weld metal exhibits an active dissolution behavior, because the anodic current density steadily increases when the potential shifts in the noble direction. Moreover, current density of the base material showed rapid increase near the E_{corr} and this phenomenon indicates that pitting may occur instantly on the surface of the base material.

Table 2. Results of the potentiodynamic polarization tests.

	E_{corr} (V)	i_{corr} (10^{-8} x A/cm ²)	R_p (10^{-5} x ohm)	Corrosion rate (10^{-4} x mm/year)
Weld metal	-0.1445	35.330	0.51	36.10
Base metal	-0.1846	4.329	1.04	4.44

E_{corr} value of the weld metal was found higher than the E_{corr} value of the base material. Also, current density (i_{corr}) value of the base material was higher than the weld metal. Generally, E_{corr} indicates the corrosion resistance of the alloy. Moreover, i_{corr} represents kinetics and dynamic trends of the chemical reactions during the corrosion. Thus, weld metal had higher corrosion resistance compared to base material. But, higher corrosion kinetics occurred with the initiation of corrosion on the surface of weld metal. Especially, intermetallic phases occurred in the welding zone accelerated the corrosion kinetic for weld metal. Corrosion rate and polarization resistance parameters were given in Table 2 and these parameters were compatible with found E_{corr} and i_{corr} values.

4. Conclusion

In this study, corrosion behavior of Inconel 625 weld joined with multipass MIG method was investigated. Intermetallic phases were observed in the welding zone by microstructure analysis. Current density (i_{corr}) value of the base material was found higher than the weld metal. Higher corrosion kinetics occurred in the weld metal due to formation of intermetallic phases.

5. References

- [1] F. Xu, Y. Lv, Y. Liu, F. Shu, P. He, B. Xu: Microstructural evolution and mechanical properties of Inconel 625 alloy during pulsed plasma arc deposition process, *Journal of Materials Science and Technology*, 29 (2013), pp. 480-488.
- [2] J. F. Wang, Q. J. Sun, H. Wang, J. P. Liu, J. C. Feng: Effect of location on microstructure and mechanical properties of additive layer manufactured Inconel 625 using gas tungsten arc welding, *Materials Science and Engineering A*, 676 (2016), pp. 395-405.
- [3] G. Li, J. Huang, Y. Wu: An investigation on microstructure and properties of dissimilar welded Inconel 625 and SUS 304 using high-power CO₂ laser, *International Journal of Advanced Manufacturing Technology*, 76 (2014), pp. 1203-1214.
- [4] P. Ganesh, R. Kaul, C. P. Paul, P. Tiwari, S. K. Rai, R. C. Prasad, L. M. Kukreja: Fatigue and fracture toughness characteristics of laser rapid manufactured Inconel 625 structures, *Materials Science and Engineering A*, 527 (2010), pp. 7490-7497.

[5] F. J. Xu, Y. H. Lv, B. S. Xu, Y. X. Liu, F. Y. Shu, P. He: Effect of deposition strategy on the microstructure and mechanical properties of Inconel 625 superalloy fabricated by pulsed plasma arc deposition, *Materials and Design*, 45 (2013), pp. 446–455.

[6] G. D. Janaki Ram, A. V. Reddy, K. P. Rao, G. M. Reddy: Improvement in stress rupture properties of inconel 718 gas tungsten arc welds using current pulsing, *Journal of Materials Science*, 40 (2005), pp. 1497–1500.

[7] H. Naffakh, M. Shamanian, F. Ashrafizadeh: Microstructural evolutions in dissimilar welds between AISI 310 austenitic stainless steel and Inconel 657, *Journal of Materials Science*, 45 (2010), pp. 2564–2573.

[8] A. Mortezaie, M. Shamanian: An assessment of microstructure, mechanical properties and corrosion resistance of dissimilar welds between Inconel 718 and 310S austenitic stainless steel, *International Journal of Pressure Vessels and Piping*, 116 (2014), pp. 37-46.

[9] K. Luer, J. DuPont, A. Marder, C. Skelonis: Corrosion fatigue of alloy 625 weld claddings in combustion environments, *Materials at High Temperatures*, 18 (2001), pp. 11-19.

**CORRESPONDENCE ADDRESS: Mustafa Tümer, Kocaeli University,
UzunçiftlikNuhÇimento Vocational School, TR41180 Kartepe/Kocaeli, Turkey, +90 262
371 23 95 and mustafa.tumer@kocaeli.edu.tr**

SHORT BIOGRAPHIES

Mustafa Tümer –Dr. Tümer was born in 1978, Ankara. He is graduated as BS from ZonguldakKaraelmas University. He received his MSc and PhD from Kocaeli University. He studied at Ministry of National Education, Yardımcı Group, Türker Group, Gedik Co. He is currently working as a Lecturer at Kocaeli University, Vocational School of UzunçiftlikNuhÇimento, Programme of Welding Technology. He has also expertise on international welding engineering and non-destructive testing.

AlptekinKısaşöz –Dr. AlptekinKısaşöz, born in 1985, graduated with a PhD degree in Metallurgical and Materials Engineering from Yıldız Technical University, Istanbul, Turkey in 2015. He is a research assistant at the same university. His main research areas are heat treatment, physical metallurgy and welding metallurgy.

AhmetKaraaslan –Prof. Dr. mont. Dipl.-Ing. AhmetKaraaslan, born in 1968, studied Metallurgy and Materials Engineering from 1986 to 1990 at Yıldız Technical University, Istanbul, Turkey, and received his doctoral degree in 1999 from the Institute for Metals Science and Materials Testing at the Montan-University in Leoben, Austria. Since 1999, he is in the section Materials Engineering at Yıldız Technical University.

MithatKerimak –He was a student at Kocaeli University Metallurgical and Materials Engineering department in September 2002 as well as a part-time employee at AnadoluDöküm San A.Ş. He started his business life in quality department. After graduation, he has been working as a quality engineer and quality laboratory officer in the quality department of the firm.

TRIP ÇELİKLERİNİN PLAZMA ARK KAYNAK KABİLİYETİ

Büşra Karaoğlu^{1,a}, Ramazan KAÇAR^{2,b}, Hayriye Ertek EMRE^{3,c}, Batuhan BOZKURT^{4,d}

¹⁻⁴Karabük University, Technology Faculty, Manufacturing Engineering, Karabük, Türkiye^{1a}
^abusrakaraoglu2@gmail.com, ^brkacar@karabuk.edu.tr, ^chayriyeertek@karabuk.edu.tr,
^dbatuhnbozkrt@gmail.com

Özet

Yüksek performanslı modern otomotiv üretimi, yeni nesil çelik çeşitlerinin geliştirilmesine önyak olmuştur. Geleneksel yüksek dayanımlı düşük alaşımlı çeliklerin orta derecede şekil alma kabiliyetinden dolayı, dönüşümün neden olduğu plastiklik olarak adlandırılan (TRIP) çeliklerinin ve onların çinko kaplı türevleri geliştirilmiştir. Endüstride bilhassa otomobil darbe sönümleyici ve kiriş destekleyici parçalarının imalatında yüksek mukavemet ve şekil alabilirliklerinden dolayı geniş yelpazede kullanılmaktadır. TRIP çeliklerin mikroyapısı ferrit, beynit ve (%5-10) kalıntı östenit fazlarının matriste dağılımından ibarettir. TRIP çeliklerinin iyileştirilmiş mukavemet ve şekillendirilebilirliği genellikle yapıdaki kalıntı östenitten kaynaklanmaktadır. Deformasyon sırasında kalıntı östenit, martenzite dönüşerek yüksek mukavemet sağlamaktadır. Endüstride elektrik ark, tungsten ark kaynağı, gaz metal ark kaynağı, nokta direnç kaynağı, lazer, hibrit lazer gibi birçok kaynak yöntemi gibi birçok kaynak yöntemi ileri seviye yüksek mukavemetli çeliklerin kaynağında kullanılmaktadır. Bununla birlikte genişçe yürütülen literatür araştırmaları, TRIP çeliklerin plazma ark kaynak kabiliyeti ile ilgili bilgi eksikliğine işaret etmektedir. Bu sebeple bu çalışmada, plazma ark kaynağı ile birleştirilmiş TRIP çeliklerinin kaynak edilebilme kabiliyetleri ve kaynak sonrası birleştirmeme mekanik özellikleri ve içyapı değişimleri detaylı olarak incelenmiştir.

Anahtar kelimeler: TRIP çelikleri, Plazma ark kaynağı, Mekanik özellikler ve Mikroyapı.

PLAZMA ARC WELDABILITY OF TRIP STEELS

Abstract

The manufacturing of modern automotive vehicles with improved vehicle performance has driven the development of new steel grades. Since, the traditional HSLA steels has had modest formability, the transformation induced plasticity (TRIP) steels and their zinc coated products has been developed. They are widely used in the industry especially production of automobile parts, such as impact beams, bumper reinforcements, etc. due to higher combinations of strength and formability. A typical microstructure of TRIP steel consists of ferrite, bainite and retained austenite (usually about 5 to 10 %) distributed in the matrix.

The improved strength and ductility in TRIP steels is mainly due to the presence of retained austenite in the microstructure. During deformation, the retained austenite transforms to martensite for providing high strength. There are many methods such as electric arc welding, tungsten arc welding, gas metal arc welding, resistance spot welding, laser and hybrid laser welding methods for joining advanced high strength steel in industry. However, the extensive literature survey introduced that there is lack of information about plasma arc weldability about TRIP steels. For this reason, in this study, plasma arc weldability of TRIP steels is determined and mechanical properties and microstructure changes have been examined in detail after joining.

Keywords: TRIP steels, Plasma arc welding, Mechanical properties and Microstructure

1.Giriş

Çevreci, güvenli ve yüksek performanslı modern otomotiv üretimi için geliştirilen yeni nesil çelik çeşitlerinden birisi de dönüşümün sebep olduğu plastiklik anlamına gelen “Transformation Induced Plasticity” (TRIP) çelikleridir [1-4]. İleri yüksek mukavemetli (Advanced High Strength Steel, AHSS) çeliklerin en yeni türü olan bu çelikler yüksek mukavemet ve süneklik, mükemmel şekillendirilebilme ve ağırlıktan tasarrufun arandığı dikkatleri üzerlerinde toplamaktadırlar [5-6].

Otomotiv üreticileri araçlar üzerinde güvenlik, emülsiyon, yakıt tüketimi performanslarını iyileştirmek için birçok çalışmalar yürütmektedirler. Bu iyileştirmeler araç yapılarının birçok gereksinimini artırmaktadır. Bu gereksinimlerin statik, darbe ve değişken yüklemeli durumlarda dayanıklı ve güvenli olacak şekilde tasarlanıp üretilmesi de oldukça önem arz etmektedir [7-8].Endüstride bilhassa otomobil darbe sönümleyici ve kiriş destekleyici parçalarının imalatında yüksek mukavemet ve şekil alabilirliklerinden dolayı geniş yelpazede ileri seviye yüksek mukavemetli çelik grubunun üyelerinden olan TRIP çelikleri kullanılmaktadır [9-10].

Otomotiv imalatında olduğu gibi çok sayıda bileşenden oluşan ürünlerin imalatında yararlanılan birleştirme tekniklerinden en önemlilerinden biriside kaynaklı birleştirmelerdir. Endüstriyel uygulamalarda çelik başta olmak üzere birçok metalik malzemelerin birleştirmesinde ergitmeli kaynak yöntemlerinden elektrik ark kaynakları, gaz korumalı ark kaynak yöntemleri, elektrik direnç kaynak uygulamaları, yüksek enerjili ışın kaynak yöntemlerinden sıklıkla yararlanılmaktadır [11-15]. Ark kaynak yöntemlerinden birisi olan plazma ark kaynağı, uzay, nükleer, elektronik, gemi yapımı ve birçok endüstri dalında kullanılan bir kaynak yöntemidir. Özellikle, gelişmiş ülkelerde çok kullanılan plazma ark kaynağı ekonomikliği, yüksek verimliliği ve kaliteli dikişlerin oluşturulması gibi birçok üstünlüklere sahiptir [16].

Geniş ölçekte yürütülen literatür araştırmaları otomotiv imalat sanayinde yararlanılan TRIP çeliklerinin nokta direnç, lazer kaynak yöntemiyle birleştirilebilirlikleri ile ilgili çalışmalar yer almakla beraber bu çeliklerin plazma ark kaynak kabiliyetleri ile ilgili kapsamlı bir çalışmaya rastlanılmamıştır. Bu sebeple çalışmada TRIP çeliklerin plazma ark kaynak kabiliyetinin araştırılması amaçlanmıştır. Bu bağlamda TRIP800 çelik sac çifti plazma ark kaynak yöntemiyle birleştirilerek bağlantının mekaniksel özellikleri ve içyapısındaki dönüşümleri incelenmiştir.

2.Deneysel Malzeme ve Metot

2.1.Malzeme

Çalışmada kullanılmak üzere 1000 x1500 x1.5mm³ boyutlarında ticari olarak temin edilen TRIP800 kalite sac levhadan 100 x 750 x 1.5mm³ ebatlarında şeritler giyotin makasta kesilerek birleştirme için hazırlanmıştır. TRIP 800 kalite çelik sacın kimyasal bileşimi (% ağırlık) Tablo 1’de verilmiştir.

Tablo 1. TRIP800 kalite çelik sacın kimyasal bileşimi

Element (% ağırlık)	C	Si	Mn	P	S	Cr	Mo	Al	Fe
TRIP800	0,22	1,576	1,619	0,013	0,003	0,016	0,014	0,036	Kalan

2.2. Deney Numunelerin Birleştirilmesi

100 x 750 x 1.5mm³ ebatlarında TRIP800 çelik çifti plazma kaynağı ile alın altına birleştirme öncesi kaynak dikiş bölgesinin yüzeylerindeki çinko kaplama zımpara ile kaldırılmıştır. Daha sonra deney numuneleri Tablo 2'de özetlenen kaynak parametrelerinden yararlanılarak Şekil 1'de gösterilen "SeamerAirLiquide" marka plazma kaynak makinesi ile birleştirilmiştir. SP6 plazma kaynak torcunun yanı sıra kolay hareket kontrolü sağlayabilmek için "Megacycles" ile entegre "Nertamatic 450" donanımı kullanılmıştır. Deney numunelerini birleştirmek için TSENISO 14341-A standardına uygun Ø 1.2mm SG2 gaz altı kaynak ilave telinden yararlanılmıştır.

Tablo 2. Deney numunelerini birleştirmek için kullanılan kaynak parametreleri

Akım şiddeti (Amper)	Gerilim (Voltaj)	Kaynak ilerleme hızı (cm/dak)	Plazma gazı Varigon H5-8 (H +Ar) (lt/dak)	Koruma gazı (Argon)
69	26	40	3	%99.9



Şekil 1. Deney numunelerinin birleştirilmesinde kullanılan plazma ark kaynak makinesi

2.3. Kaynaklı Birleştirmelerden Deneysel Test Numunelerin Hazırlanması

Çalışmada kullanılan TRIP800 çelik ana malzemenin ve plazma kaynaklı deney numunelerin statik yük etkisi altındaki davranışlarını belirlemek için TS EN ISO 6892-1 ve TS EN ISO 4136 standardına uygun boyutlarda çekme deney numuneleri sırasıyla preste metal kesme kalıbıyla ve lazer kesme yöntemiyle keserek elde edilmiştir. Kaynaklı çekme numuneleri Şekil 2a ve b'de gösterilmiştir.



Şekil 2. a) Kaynaklı çekme numunesi b) Test edilen çekme numunesi

Hazırlanan çekme numunelerin deneyleri 50 kN kapasiteli SHIMAZDU marka çekme test cihazında 2mm/dak çekme hızında gerçekleştirilmiştir. Deneysel hataları minimize edebilmek amacıyla 3 adet deney numunesi test edilmiştir.

Sertlik ölçümü aynı hatta ve ana metalden kaynak metaline doğru belirli ölçüm sırası ile SHIMADZU marka Vickersmikrosertlik ölçüm cihazı kullanılarak gerçekleştirilmiştir. Batıcı uca 500g yük uygulanmıştır.

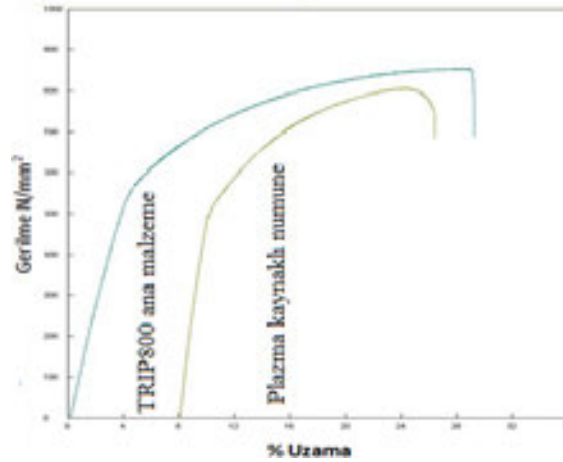
2.4. Metalografi Numunelerin Hazırlanması ve İncelenmesi

Metalografi numuneleri birleştirmelerin kaynak metali, ITAB ve ana metal bölgelerini kapsayacak genişlikte kaynak yönüne dik şekilde diskotom ile kesilmiş ve soğuk reçine ile kalıba alınmıştır. Numuneler klasik metalografi numune hazırlama yöntemleri uygulanarak hazırlanmıştır. Numuneler % 2 nitrik asit özeltisi içerisinde 1sn bekletilerek dağlanmış. İncelemeleri 4X-100X büyütme kapasitesine sahip optik mikroskopta gerçekleştirilmiştir.

3.Sonuçlar ve İrdelenmesi

3.1. Çekme Test Sonuçları

Çalışmada kullanılan TRIP800 çelik sacın ve plazma ark kaynaklı TRIP800 çelik birleştirmelerin ortalama gerilim-uzama eğrisi Şekil 2'de gösterilmiştir.



Şekil 2. TRIP800 ana malzeme ve plazma ark kaynaklı TRIP800 malzeme gerilme-uzama eğrisi

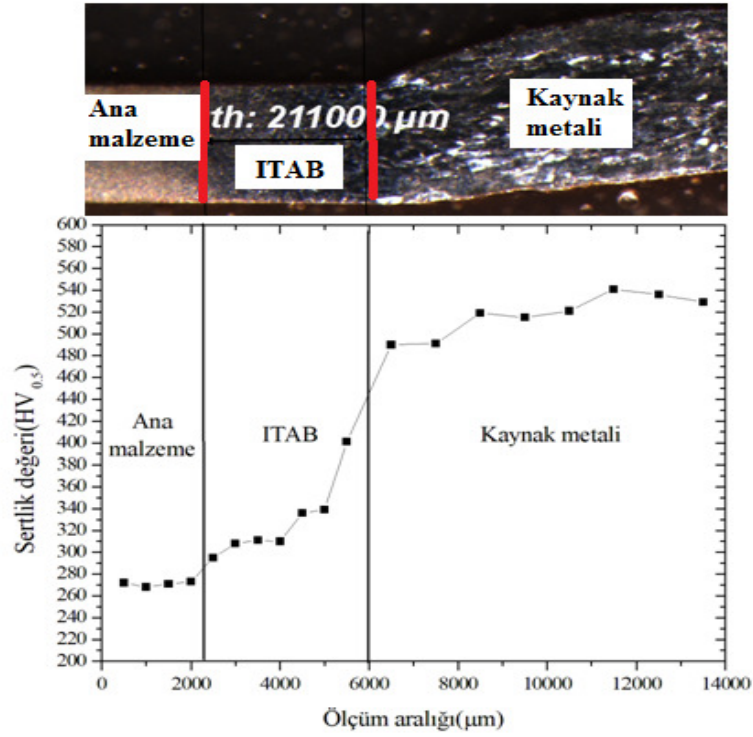
Şekil 2'den görüldüğü gibi çalışmada kullanılan TRIP800 çelik sac malzemenin akma dayanımı 540N/mm^2 ve maksimum çekme dayanımı 858 N/mm^2 tespit edilmiştir. TRIP800 ana malzemenin % uzama miktarı ise %24 olarak bulunmuştur.

Kaynaklı deney numunesinin statik yük etkisi altındaki davranışını tespit etmek için deney numuneleri çekme testine tabi tutulmuştur. Kaynaklı birleştirmelerin ortalama gerilme –uzama eğrisi de Şekil 2'de gösterilmiştir. Şekil 2'den görüldüğü gibi kaynaklı birleştirmenin ortalama akma ve çekme dayanımı sırasıyla 520 N/mm^2 ve 807 N/mm^2 bulunmuştur. Deney numunesinin ortalama uzaması %16 bulunmuştur. Test edilen kaynaklı deney numunelerinde kopmalar

birleştirmenin kaynak metalini ve ITAB'dan oluşmamış, TRIP800 ana malzemeden gerçekleşmiştir. (Şekil 2 b). Hasarın ana malzemeden meydana gelmesi TRIP 800 çelik sac malzemenin plazma ark kaynağı yöntemiyle SG2 ilave telinden yararlanılarak başarı ile birleştirilebileceğine işaret etmektedir. Birleştirmenin kaynak metalini ve ITAB'da kaynak termal çevrimin etkisiyle meydana gelen yapısal dönüşüm ve bunun sonucu olarak artan sertlik çekme testi sürecinde boyun vermenin bağlantısının en düşük akma dayanımına ve sertliğe sahip bölgesinden diğer bir ifadeyle ana malzemeden oluşması normal bir durumdur.

3.2. Sertlik Ölçümü Sonuçları

Çalışmada kullanılan plazma kaynaklı deney numunesinin kesitinde aynı hattan belirli aralıklarla ana malzeme, ITAB ve kaynak metalini de kapsayacak şekilde mikrosertlik ölçümü gerçekleştirilmiştir. Kaynaklı birleştirmenin sertlik dağılımı grafiksel olarak Şekil 3'de gösterilmiştir.



Şekil 3. Plazma ark kaynaklı numunenin sertlik dağılımı

Şekil 3'deki kaynaklı numunenin sertlik dağılımı grafiğine göre ferritmatriks içerisinde beynit ve kalıntı östenit fazlarından oluşan TRIP800 çelik sac ana malzemenin sertliği ortalama 270HV_{0,5} olarak bulunmuştur. Birleştirmenin ısı tesiri altındaki bölümünün sertliği ise ana malzemeden başlamak üzere ergime bandına doğru ilerledikçe (yaklaşık 2.1 mm boyunca) belirgin bir şekilde değişim göstermektedir. Kaynak termal çevrimin etkisiyle bu bölgede ulaşılan sıcaklık ve o sıcaklıkta bekleme zamanı ile meydana gelen tane boyutu sertlik değişiminin sebeplerinden birisidir. Bunun yanı sıra malzemenin kimyasal bileşimine bağlı olarak meydana gelen yapısal dönüşümle ortaya çıkan fazlar sertlik değişiminin diğer bir sebebi olarak düşünülmektedir [17].

Ergitme kaynaklı birleştirmeler için genellikle meydana gelen bölgeler kaynak metalini, ITAB ince taneli ve iri taneli bölgesi ve ana malzemedeki oluşmaktadır [18].

ITAB kısmi dönüşüme uğramış bölümünde sertlik $290HV_{0.5}$ ile $311HV_{0.5}$ arasında değişim göstermektedir. ITAB'nin ince taneli olarak adlandırılan bölümünde ise $336HV_{0.5}$ ile $401HV_{0.5}$ arasında dağılım sergilemektedir. ITAB'nin kaynak metaline en yakın bölümü olan kaba taneli bölümünde ise sertlik $401HV_{0.5}$ ile $491HV_{0.5}$ arasında değiştiği görülmektedir. Sonuç olarak ergime bandından başlamak kaydıyla ana malzemeye doğru gidildikçe ısı kaynağından uzaklaştıkça sertliğin belirgin şekilde yapısal oluşumlara bağlı olarak azaldığı görülmektedir. Birleştirmenin kaynak metalini olarak adlandırılan bölgesinde kaynak eksenine kadar (yaklaşık 5mm mesafe boyunca) gerçekleştirilen ölçümlerde sertliğin $499HV_{0.5}$ ile $551HV_{0.5}$ arasında dağılım sergilemektedir.

Kaynak metalindeki sertlikte meydana gelen bu dalgalanmanın kaynak metalinde meydana gelen fazlar ve onların morfolojilerinin yanı sıra kullanılan ilave metale bağlı olarak meydana gelen seyrelme ile ilgili olduğu düşünülmektedir.

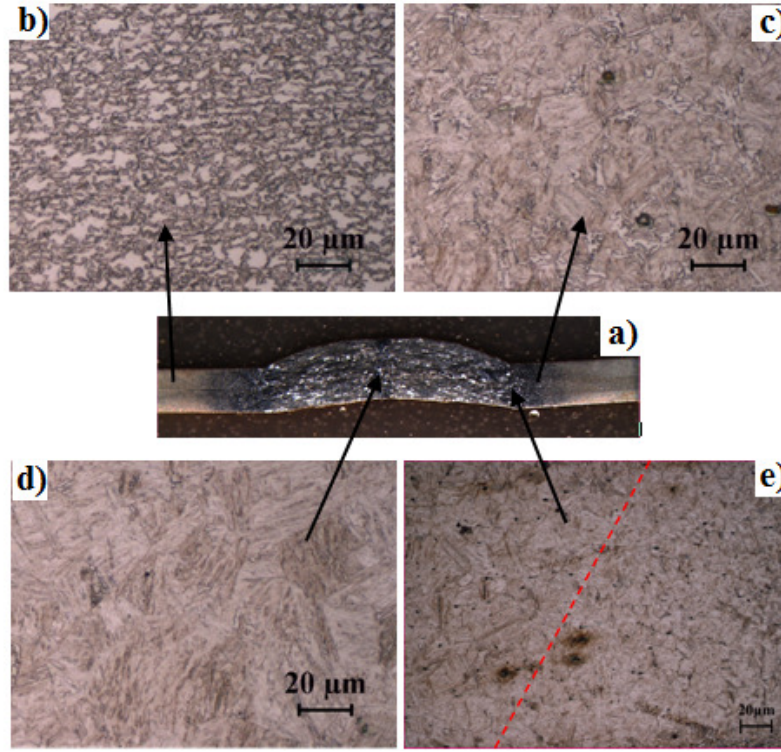
3.3. Mikroyapı İncelemeleri

Çalışmada kullanılan plazma kaynaklı deney numunesinin kesitinden ana malzeme, ITAB ve kaynak metalini de kapsayacak şekilde yapısal inceleme metalografik olarak gerçekleştirilmiştir. Kaynaklı birleştirmenin makro görüntüsü ve kaynaklı bağlantının bölümlerinin mikroyapı görüntüleri Şekil 4a-e'de gösterilmiştir.

Şekil 4a'dan görüldüğü üzere yüksek enerji yoğunluklu plazma ark kaynağı ile birleştirilen numunenin kaynak metalini dikiş genişliği yaklaşık 10mm ve ITAB genişliği ise her bir tarafta yaklaşık 2mm genişliğinde olduğu belirlenmiştir. Kaynak dikişinde herhangi bir kaynak hatası gözlenmemiştir.

Birleştirmenin TRIP800 çeliğinden oluşan ana malzemesinin mikroyapısı Şekil 4b'den görüldüğü gibi ferritmatrikste dağılım gösteren beynit ve kalıntı östenitten oluştuğu görülmektedir. Çalışmada mekanik özellikleri de belirlenen TRIP800 çeliğinin yüksek mukavemet ve şekillendirilebilirliğin sorumlusu olarak yapıdaki kalıntı östenitinmartenzite dönüşümüyle beraber ortaya çıkan martenzit ve şekillendirilebilirliğin sorumlusu ise ferrit ve vebeynit fazları olduğu düşünülmektedir.

Birleştirmenin ısı tesiri altındaki bölümünün mikroyapısı ana malzemedeki başlamak üzere ergime bandına doğru ilerledikçe kaynak termal çevrimin etkisiyle belirtilen bölgede ulaşılan sıcaklık ve o sıcaklıkta bekleme zamanı ile meydana gelen yapısal dönüşüm ürünleri farklılık göstermektedir. Aynı zamanda meydana gelen tanelerin boyutunda da farklılık gözlenmektedir. ITAB'ın kısmi dönüşümüne uğramış bölgesinden başlamak kaydıyla yapıda ferrit ve beynitinyanısıra kalıntı östenitin ve martenzit oluşumu göze çarparken (Şekil 4c), ITAB'ın ince taneli ve kaba taneli bölümünün büyük bir çoğunlukla martenzite dönüştüğü görülmektedir (Şekil 4e). Oluşan martenzitin morfolojisi ITAB kaba taneli bölümünde iğneselmartenzit iken ince taneli bölgede meydana gelen iğneselmartenzit levhaları daha kaba olduğu görülmektedir. ITAB'de bu yapısal oluşum farklılığının sertlik ölçüm sonuçlarıyla paralellik arz ettiği görülmektedir.



Şekil 4. a) Kaynaklı birleştirmenin makro görüntüsü ve b) TRIP800 ana malzeme c) ITAB d) Kaynak metalini e) Kaynak metalinden ITAB geçiş mikroyapı görüntüleri



Şekil 5. Kaynak metalinde ergime bandına yakın olan bölgede meydana gelen levhalı (Widmanstättenferrit) oluşumlar

Şekil 4.e'den görüldüğü gibi birleştirmenin kaynak metalini kolonsal taneleri büyük ölçüde martenzit fazının dekore ettiği görülmektedir. İlaveten kaynak metalinde kullanılan kaynak ilave metaline bağlı olarak ergime bandına yakın olan bölgelerde levhalı (Widmanstättenferrit) oluşumlar göze çarpmaktadır (Şekil 5). Benzer şekilde yapılan çalışmada GMAW (Gaz metal ark kaynaklı) TRIP800 birleştirmelerin kaynak metalini ve ITAB mikroyapılarında martenzit ve (allotromorfik, Widmanstätten ve poligonal tip) ferrit oluşumları belirlenmiştir[19].

4. Genel Sonuçlar

- TRIP800 çelik sac ana malzemenin akma dayanımı 540N/mm^2 ve maksimum çekme dayanımı 858N/mm^2 tespit edilmiştir. Malzemenin % uzama miktarı ise %24 olarak bulunmuştur.
- Kaynaklı birleştirmenin ortalama akma ve çekme dayanımı sırasıyla 520N/mm^2 ve 807N/mm^2 bulunmuştur. Deney numunesinin ortalama % uzama değeri %16 bulunmuştur. Test edilen kaynaklı deney numunelerinde kopma TRIP800 ana malzemeden gerçekleşmiştir.
- Ferritmatriks içerisinde beynit ve kalıntı östenit fazlarından oluşan TRIP800 çelik sac ana malzemenin sertliği ortalama $270\text{HV}_{0.5}$ olarak bulunmuştur. Birleştirmenin ısı tesiri altındaki bölümünün sertliği ise ana malzemeden başlamak üzere ergime bandına doğru ilerledikçe belirgin bir şekilde değişim göstermektedir. ITAB kısmi dönüşüme uğramış bölümünde sertlik $290\text{HV}_{0.5}$ ile $311\text{HV}_{0.5}$ arasında değişim gösterirken, ITAB'nin ince taneli olarak adlandırılan bölümünde ise $336\text{HV}_{0.5}$ ile $401\text{HV}_{0.5}$ arasında dağılım sergilemektedir. ITAB'nin kaynak metaline en yakın bölümü olan kaba taneli bölümünde ise sertlik $401\text{HV}_{0.5}$ ile $491\text{HV}_{0.5}$ arasında değiştiği görülmektedir. Birleştirmenin kaynak metali olarak adlandırılan bölgesinde sertlik $499\text{HV}_{0.5}$ ile $551\text{HV}_{0.5}$ arasında dağılım sergilemektedir.
- Yüksek enerji yoğunluklu plazma ark kaynağı ile birleştirilen numunenin kaynak metali dikiş genişliği yaklaşık 10 mm ve ITAB genişliği ise her bir tarafta yaklaşık 2 mm genişliğinde oluştuğu belirlenmiştir.
- TRIP800 çeliğinden oluşan ana malzemesinin mikroyapısı ferritmatrikste dağılım gösteren beynit ve kalıntı östenitten oluştuğu görülmektedir. ITAB mikroyapısı ana malzemeden başlamak üzere ergime bandına doğru ilerledikçe kaynak termal çevrimin etkisiyle belirtilen bölgede ulaşılan sıcaklık ve o sıcaklıkta bekleme zamanı ile meydana gelen yapısal dönüşüm ürünleri farklılık göstermektedir. ITAB'ın kısmi dönüşümüne uğramış bölgesinden başlamak kaydıyla yapıda ferrit ve beynitin yanı sıra kalıntı östenit ve martenzitten oluştuğu göze çarparken, ITAB'ın ince taneli ve kaba taneli bölümünün az miktarda ferrit içerirken büyük bir çoğunlukla martenzite dönüştüğü görülmektedir. Kaynak metalinin kolonsal tanelerini büyük ölçüde martenzit fazının dekore ettiği görülmektedir. Ayrıca kullanılan kaynak ilave metaline bağlı olarak ergime bandına yakın olan bölgelerde Widmanstätten ferrit tip levhali oluşumlar göze çarpmaktadır.

5. Kaynaklar

- [1] E. Biro, A. Lee: Welded Properties of Various DP600 Chemistries, Proc. Sheet Metal Welding Conference XI, Sterling Heights, Mich (2004).
- [2] N. Kapustka, C. Conrardy, S. Babu, C. Albright: Effect of GMAW Process and Material Conditions on DP 780 and TRIP 780 Welds, Welding Journal, 87 (2008) pp. 135-148.
- [3] Z. Yinghui, M. Yonli, K. Yonglin, Y. Hao: Mechanical properties and microstructure of TRIP steels produced using TSCR process, Journal of University of Science and Technology, Beijing, 13 (5) (2006) pp. 416-421.

- [4] D. Wu, L.Zhuang, L.Hui-sheng, Effect of Controlled Cooling After Hot Rolling on Mechanical Properties of Hot Rolled TRIP Steel, *Journal of Iron and Steel Research International*, 15 (2) (2008) pp. 65-70.
- [5] F.Hayat: TRIP Çeliklerinin otomotiv endüstrisinde kullanımının incelenmesi, *Gazi Üniv. Müh. Mim. Fak. Der.*, 25(4) (2010) pp.701-712.
- [6] L. Kučerová, M. Bystrianský: Comparison of Thermo-Mechanical Treatment of C-Mn-Si-Nb and C-Mn-Si-Al-Nb TRIP Steels, *Procedia Engineering* 207 (2017) pp. 1856–1861.
- [7] S.S.Nayaka,V.H. Baltazar Hernandeza,Y.Okita, Y.Zhou: Microstructure–hardness relationship in the fusion zone of TRIP steel welds, *Materials Science and Engineering A*, 551 (2012) pp. 73– 81.
- [8] H. Ding, D.Song, Z. Tang, P.Yang: Strain Hardening Behavior of aTRIP/TWIP Steel With 18.8% Mn, *Material Science and Engineering A*, 528(2011) pp. 868-873,
- [9] T.K. Pal, K.Chattopadhyay: Resistance Spot Weldability And High Cycle Fatigue Behaviour of Martensitic (M190) Steel Sheet, *Fatigue and Fracture of Engineering Materials and Structures*, 34 (2010) pp. 46-52.
- [10] International Iron & Steel Institute Committee on Automotive Applications, *Advanced High Strength Steel (AHSS) Application Guidelines*, March 2005.
- [11] N. Lun, D.C.Saha, A. Macwan, H. Pan, L. Wang, F. Goodwin, Y. Zhou: Microstructure and Mechanical Properties of Fibre Laser Welded Medium Manganese TRIP Steel, *Material and Design*, 131 (2017) pp. 450-459.
- [12] M.Mazar Atabaki, J.Ma, G.Yang, R.Kovacevic:Hybrid Laser/Arc Welding of Advanced High Strength Steel in Different Butt Joint Configurations,*Materials & Design*, 64 (2014) pp. 573-587.
- [13] K. B. Lee, S.T. Oh: Development of Durability Enhancement Technology for Arc Weldings in Advanced High Strength Steel (AHSS),*Journal of Welding and Joining*, 33(4) (2015) pp. 50-56.
- [14] C. Chovet, S. Guiheux:Possibilities Offered by MIG and TIG Brazing of Galvanized Ultra High Strength Steels for Automotive Applications *La Metallurgia Italiana*,(7-8) (2006) pp. 47-54.
- [15] K. Pal, S.K. Pal: Effect of Pulse Parameters on Weld Quality in Pulsed Gas Metal Arc Welding, *A Review Journal of Materials Engineering and Performance*, 20 (6)(2011) pp. 918–931.
- [16] E.Kaluç, E. Taban, Plazma Arkı ile Kaynak ve Endüstriyel Uygulamaları, *Makine Tek*, (2004)pp. 10-11.
- [17] J. Piccinia, H. Svoboda: Effect of the plasma arc welding procedure on mechanical properties of DP700 steel, *11th International Congress on Metallurgy & Materials SAM/CONAME*, *Procedia Materials Science* 1 (2012) pp. 50 – 57.
- [18] S. Kou: *Welding Metallurgy*, Jwilley&Sons, New Jersey, (2003) pp. 207-210.
- [19] G.Y. Perez-Medina, H.F. Lopez, F.A. Reyes-Valdés, A. Garza-Gomez, Luis M. López-Ochoa: Welding Effects on the Mechanical Integrity of a TRIP800 Steel: a Comparison of Laser CO₂ and GMAW Processes, *Archives of Metallurgy and Materials*, 59 (4) (2014) pp. 1427-1432.

CORRESPONDENCE ADDRESS: Ramazan KAÇAR, Karabük University, Technology Faculty, 78050, Turkey, Tel: +90 433 82 00/1091, e-mail: rkacar@karabuk.edu.tr

SHORT BIOGRAPHIES

Büşra Karaoğlu¹– 1991 Zonguldak doğumludur. Karadeniz Teknik Üniversitesi Metalurji ve Malzeme Mühendisliği lisans mezunudur. Karabük Üniversitesi İmalat Mühendisliğinde Yüksek Lisans öğrencisidir.

Hayriye Ertek Emre² – Karabük Üniversitesi, Teknoloji Fakültesi, İmalat Mühendisliği Bölümünde Dr. Öğretim Üyesi olarak görev yapmaktadır.

Ramazan Kaçar³ – Karabük Üniversitesi, Teknoloji Fakültesi, İmalat Mühendisliği Bölümünde Profesör Dr. Olarak görev yapmaktadır.

KAYNAK İLERLEME HIZININ LAZER KAYNAKLI TİTANYUM (GRADE 5) ALAŞIMININ MİKROYAPI VE MEKANİK ÖZELLİKLERİNE ETKİSİ

Şennur ARSLAN¹, Hayriye ERTEK EMRE², Ramazan KAÇAR³

¹⁻³Karabük Üniversitesi, Teknoloji Fakültesi, İmalat Mühendisliği Bölümü,
sennurarslan72@hotmail.com, hayriyeertek@karabuk.edu.tr, rkacar@karabuk.edu.tr

Özet

Yüksek yoğunluk–mukavemet ve iyi derecede korozyon dirençlerinden dolayı endüstride kimya sanayinden medikal sektöre kadar birçok alanda titanyum alaşımlarından yararlanılmaktadır. Bu çalışmada, bilhassa medikal alanda implant malzemesi olarak da kullanılan Ti6Al4V (Grade 5) titanyum alaşımının lazer kaynak yöntemiyle iki farklı kaynak ilerleme hızında (200, 250 cm/dak) birleştirilmesi gerçekleştirilmiştir. Kaynak ilerleme hızı değişiminin birleştirme mikroyapı ve mekanik özelliklerine etkisi incelenmiştir. Bu amaçla bağlantının dayanımı ve sertliği sırasıyla çekme ve mikrosertlik ölçümüyle belirlenmiştir. Çalışmadan elde edilen bulgulara göre artan kaynak ilerleme hızının birleştirmenin dayanımını ve sertliğini arttırdığı tespit edilmiştir.

Anahtar Kelimeler: Ti6Al4V (Grade 5) alaşımı, Lazer kaynağı, Kaynak ilerleme hızı, Mekanik özellik

Abstract

Effect of Welding Speed on the Microstructure and Mechanical Properties of Laser Welded Titanium (Grade 5) Alloys

Due to high strength-density rate and superior corrosion resistance, titanium alloys are used in industry especially chemistry and medical sectors. In this study Ti6Al4V (Grade 5) titanium alloys which are preferentially used in medical sector as an implant materials are joined by laser welding method with two welding speed (200, 250 cm/min). An effect of the welding speed on microstructure and mechanical properties of weldment is investigated. For this purpose, the strength and hardness of the weldment are evaluated by tensile test and hardness measurement respectively. According to findings, the strength and hardness of the weldment increases with increasing welding speed.

Keywords: Ti6Al4V (Grade 5) alloy, Laser welding, Welding speed, Mechanical properties

1. Giriş

Titanyum ve alaşımları, yüksek mukavemet, iyi korozyon dirençleri ve yüksek sıcaklık dayanımlarının yanı sıra düşük yoğunlukları nedeniyle, denizaltı, uçak ve uzay sanayi ve biyomedikal alanda dahil olmak üzere birçok endüstride yaygın olarak kullanılmaktadır [1]. Tribo-korozyona dirençli ve biyo-uyumlu titanyum ailesinden olan Ti6Al4V alaşımından ise havacılık, denizaltı, nükleer, sivil, kimyasal ve biyomedikal alanlarda yararlanılmaktadır [2,3]. Bilhassa yüksek korozyon direnci ve mükemmel yumuşak ve sert doku biyo-uyumluluğu gibi çekici özellikleri nedeniyle fizyolojik ortamda yük taşıyan ortopedik implantlar için yaygın bir şekilde uygulanmaktadır [4-7]. Bu uygulama alanlarının bazılarında mekanik aşınma ile korozyon vardır. Titanyum alaşımlarının tribo-korozyon ve korozyon özelliklerinin önemi denizaltı, deniz üstü platformları, biyomedikal implantlar ve diş hekimliğinde kullanımlarından kaynaklanır [8]. Bugün kullanılan tüm titanyum alaşımların %50 'sinden fazlası Ti6Al4V alaşımıdır [9]. Ti6Al4V iki fazlı bir $\alpha+\beta$ alaşımı olup içeriğindeki alüminyumun α dengeleyici, vanadyumun ise β dengeleyici element olarak görev yaptığı bilinir [10].

Titanyum ve alaşımlarının birleştirilebilirliği ile ilgili araştırma eksikliği vardır. Bu alaşımların yüksek sıcaklıkta oksijen ve azota karşı yüksek afiniteye sahip olması kaynaklı birleştirmelerinde oksit ve nitrür oluşumunu muhtemel kılmaktadır. Bu nedenle sıvı kaynak havuzunu korumak için özel dikkat ve önem gösterilmelidir [1]. Porozite oluşumu da titanyum alaşımlarının katılmış kaynak metalinde hapsolarak kalan gazların neden olduğu kaynak hatalarından bir diğeridir [11]. Ti6Al4V alaşımının birleştirilmesi sırasında malzeme kalınlığındaki artışla gözenekliliğin arttığı gözlenmiştir [12]. Bu nedenle, kaynak yapılacak malzemelerin kaynak sırasında kirlenmeye ve oksidasyona karşı uygun şekilde korunmaları önemlidir. Ti6Al4V alaşımlarının birleştirme korozyon direnci ve mekanik özelliklerini nasıl etkilediğini bilmek kullanım alanı açısından oldukça önemlidir [13].

Titanyum alaşımlarının kaynaklı birleştirmeleri ile ilgili farklı çalışmalar yürütüldüğü görülmektedir. Modern birleştirme teknolojilerinden biri olarak, lazer kaynağı ayırt edici özellikleri ve potansiyeli nedeniyle artan ilgi görmektedir. Bu kaynak yöntemini nitelikli kılan

dar bir alan üzerine odaklanmak suretiyle yüksek güç yoğunluğu elde edilerek kullanılabilmesi ve otomasyona uygunluğudur[14]. Lazer, tek renkli, düz, yoğun ve aynı fazlı paralel dalgalar halinde genliği yüksek, başka bir ifade ile suni radyasyon tetiklemesiyle oluşturulan bir ışık demetidir. Lazer kaynağının geleneksel termal birleştirme işlemlerine kıyasla birçok üstünlükleri vardır. Başlıca avantajları arasında yüksek tarama hızı, dar ısıdan etkilenen bölge (HAZ), düşük distorsiyon, mükemmel kontrol edilebilirlik ve hassas kaynak için uygun olan yüksek yoğunluklu bir ısı kaynağı üretme yeteneği sıralanabilir[15]. Lazer kaynak yöntemlerinden birisi olan CO₂ lazer kaynak yöntemi ise düşük ısı girdisi, yüksek yoğunlaşma enerjisi, yüksek kaynak ilerleme hızı, dar kaynak bölgesi, derin nüfuziyetli birleştirmeler elde edilebilmesi, yüksek mekanik dayanım, düşük distorsiyon ve ilave metal kullanmadan kaynak yapabilme imkânından dolayı geleneksel kaynak yöntemlerinden ayrılır [16].

Literatür araştırmaları, Ti6Al4V alaşımlarının lazer kaynağında oluşan yüksek yoğunluklu ısı girdisiyle ulaşılan maksimum sıcaklıktan hızlı soğumaya ve alaşımın kimyasal içeriğine bağlı olarak, kaynak sonrası kaynak metali ve ITAB mikroyapısının dönüşüme uğradığı dolayısıyla kaynak parametrelerinden etkilendiğini göstermektedir [17]. Atou vd. yaptıkları bir çalışmada [18] TIG ve lazer kaynaklı saf titanyumun, kaynaklı numune gruplarına göre mukayese edildiğinde daha düşük dayanım gösterdiği, fakat kaynak grubu arasında istatistiksel bir farkın olmadığını belirtmişlerdir. Başka bir çalışmada ise TIG ve lazer kaynaklı titanyum alaşımlarının birleştirmelerinin çekme dayanımlarını mukayese edildiğinde benzer sonuçlar elde edildiği rapor edilmiştir [19].

Bu çalışmada Ti6Al4V(Grade 5) alaşımının, CO₂ lazer kaynaklı birleştirmelerin özelliklerine kaynak parametrelerinden ısı girdisi üzerinde etkin rolü olan ilerleme hızının etkisi araştırılmıştır. Bu amaçla Ti6Al4V(Grade 5) alaşımının CO₂ lazer kaynak yöntemiyle 200 ve 250 cm/dak hızlarla birleştirilmesi gerçekleştirilerek bağlantıların mekanik özelliklerini belirlemek için çekme testleri ve sertlik ölçümleri gerçekleştirilmiştir. Ayrıca, birleştirmelerin mikroyapı incelemeleri de gerçekleştirilmiştir. Böylece birleştirmelerin mikroyapı ve mekanik özelliklerine kaynak ilerleme hızının etkisi tayin edilmiştir.

2. Deneysel Çalışmalar

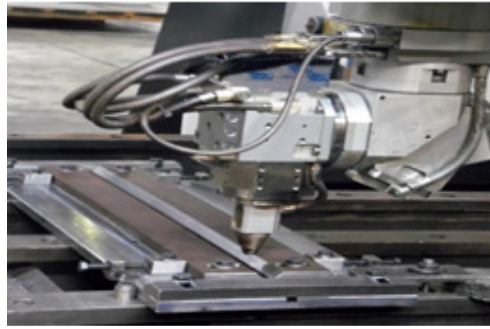
2.1. Deney numunelerinin kaynaklı birleřtirmesi

Bu alıřmada kullanılan Ti6Al4V (Grade 5) titanyum alařımının kimyasal kompozisyonu Tablo 1'de verilmiřtir. Birleřtirme iřlemi CO₂ lazer kaynak yntemi ile dolgu metali kullanılmadan hizmet alımı yoluyla gerekleřtirilmiřtir.

Tablo 1. Ana malzeme kimyasal bileřimi (% ağırlık)

Malzeme	Ti	AL	V	Fe	Si	Sn	C
Ti-6Al-4V	89.94	5.921	4.00	0.04	0.039	0.03	0.03

500x500x1.6mm ebatlarında Ti6Al4V (Grade 5) titanyum alařımı sac levhadan kaynaklı birleřtirme iin 70x500x1,6mm³ ebatlarında olacak řekilde řeritler řeklinde giyotinde kesilerek hazırlanmıřtır. Birleřtirilecek numune yzeyleri zımpara yardımıyla temizlenmiřtir. řekil 1'den grldę gibi TRUMPF LASERCELL 1005 marka CO₂ lazer kaynak makinesi ile numuneler nceden hazırlanmıř tutucu kalıba baęlanarak yatay pozisyonda alın altına ilave metal kullanılmadan Tablo 2'de belirtilen kaynak parametrelerinden yararlanılarak birleřtirilmiřtir.



řekil 1. CO₂ lazer kaynak yntemi ve numune baęlantı aparatı

Tablo 2. Kaynak parametreleri

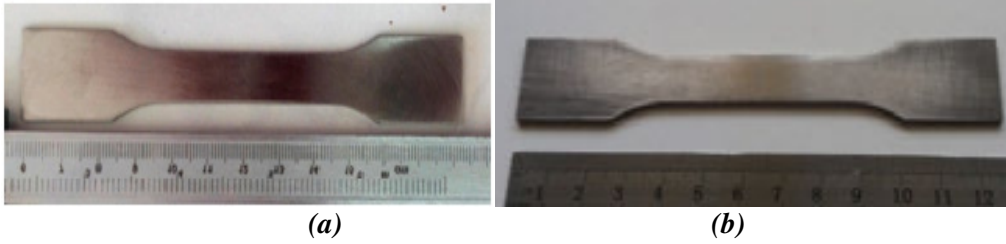
Lazer Gc (Watt)	Kaynak Hızı (cm/dak)	Koruyucu Gaz	Gaz Debisi (lt/dak)	Odak Mesafesi (mm)
3000	200 250	50% Ar+50% He	17.5	200

Birleřtirmede sreksizlik (gaz bořluę, atlak vb.) oluřup oluřmadıęını kontrol etmek amacıyla, deney numunesi zerinde radyografik muayene iřlemi ve sıvı penetrant muayene Gazi niversitesi laboratuvarında uygulanmıřtır. Radyografik muayenesi GemX-G200 model X-ray portablegenerator cihazıyla, 80kV enerji, 1200 A akım řiddeti, 10sn pozlama sresinde, X iřını cihaza olan uzaklıęı 40 cm olacak řekilde gerekleřtirilmiřtir.

alıřmada Ti6Al4V lazer kaynaklı birleřtirmenin ve ana malzemenin mekanik zelliklerini belirleyebilmek iin ekme testi uygulanmıř ve baęlantının sertlik incelemesi de gerekleřtirilmiřtir. ekme testi ve sertlik lm sonuları sırasıyla alt blmlerde verilmiř ve detaylıca tartıřılmıřtır. Ayrıca baęlantının mikroyapısı da incelenerek, mikroyapı deęiřimleri deęerlendirilmiřtir.

2.2. ekme test numunelerinin hazırlanması ve testi

Ana malzeme ve kaynaklı birleřtirmelerin mekanik özelliklerini belirlemek için çekme testi numuneleri TS EN ISO 4136 standardına uygun boyutlarda tel erozyon kesme işlemi ile çıkartılmıştır. Oluşabilecek hataları minimize edebilmek için 3 adet test numunesi Şekil 2'de gösterilen boyutlarda hazırlanmıştır. Test 50kN kapasiteli SHIMAZDU marka çekme test cihazında 2 mm/dak çekme hızında gerçekleştirilmiştir.



Şekil 2. Çekme test numuneleri a)200 cm/dk. hızla birleştirilmiş, b)250 cm/dk. hızla birleştirilmiş

2.3. Metalografi numunelerinin hazırlanması

Metalografi numuneleri birleřtirmelerin kaynak metali, ITAB ve ana metal bölgelerini kapsayacak şekilde kaynak yönüne dik disketon ile kesilmiş ve soğuk reçine ile kalıba alınmıştır. Numuneler klasik metalografi numune hazırlama yöntemleri uygulanarak hazırlanmış ve Kroll ayırıcı (100 ml H₂O + 6ml HNO₃ + 2ml HF) ile 15sn süreyle dağlanmıştır. Mikroyapı incelemeleri 5x-100x büyütme kapasitesine sahip optik mikroskopta gerçekleştirilmiştir.

Çalışmada ayrıca çekme test numunelerinin kırılma yüzeylerinin incelenmesinde Zeiss Ultra Pluss marka Taramalı elektron mikroskobu (SEM) ve EDS ünitesinden yararlanılmıştır.

İlave olarak kaynaklı birleřtirmenin sertlik ölçümü 500 g yük kullanılarak SHIMADZU marka mikrosertlik cihazında klasik metalografik yöntemlerle hazırlanan numune kesiti üzerinden kaynak metali ITAB ve ana malzemeyi kapsayacak şekilde aynı hat üzerinde gerçekleştirilmiştir.

3. Deneysel Sonuçlar

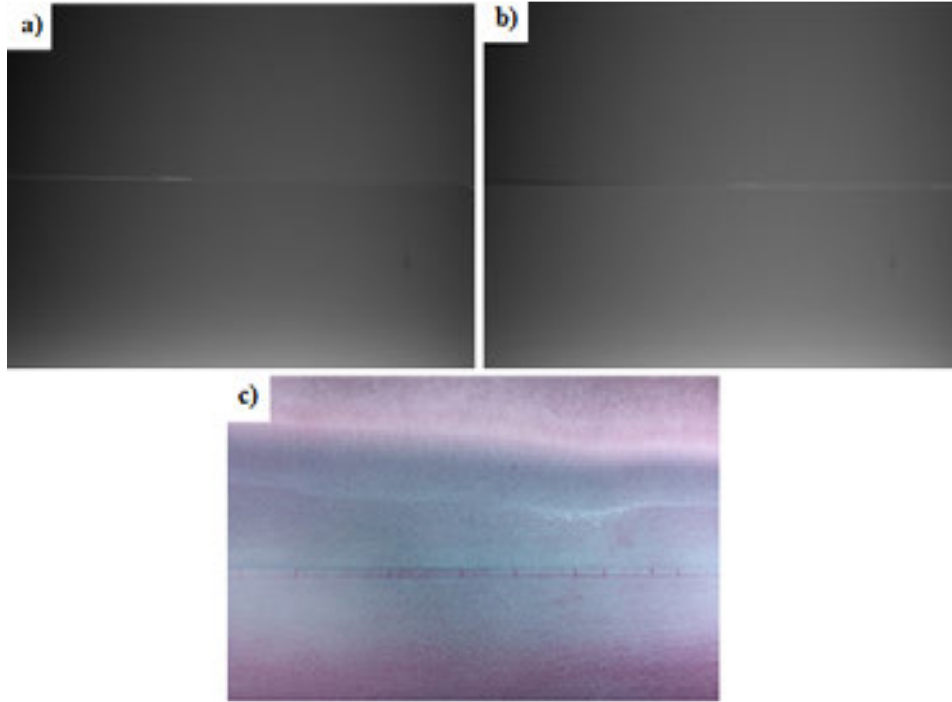
3.1. Kaynaklı birleřtirmelerin tahribatsız muayene yöntemleriyle muayenesi

Birleřtirmede süreksizlik (gaz boşluğu, çatlak vb.)oluşup oluşmadığını kontrol etmek amacıyla, deney numunesi üzerinde radyografik muayene işlemi ve sıvı penetrant muayene gerçekleştirilmiş elde edilen analiz filmi Şekil 3a-c'de gösterilmiştir.

Şekil 3a ve b'deki radyografik muayene filmleri üzerinden yararlanılarak yapılan değerlendirmeye göre iki farklı kaynak ilerleme hızıyla CO₂ lazer kaynak yöntemi ile birleştirilen deney numunelerinde bilhassa düşük ilerleme hızıyla birleştirilen numunede

underfill oluşumları ve her iki numunede dar bir kaynak dikişinin meydana geldiği görülmektedir. Ancak düşük kaynak ilerleme hızıyla birleştirilen numunenin daha yüksek ısı girdisine bağlı olarak kaynak dikişinin düşük ısı girdisiyle birleştirilen numuneye göre daha geniş oluştuğu görülmektedir.

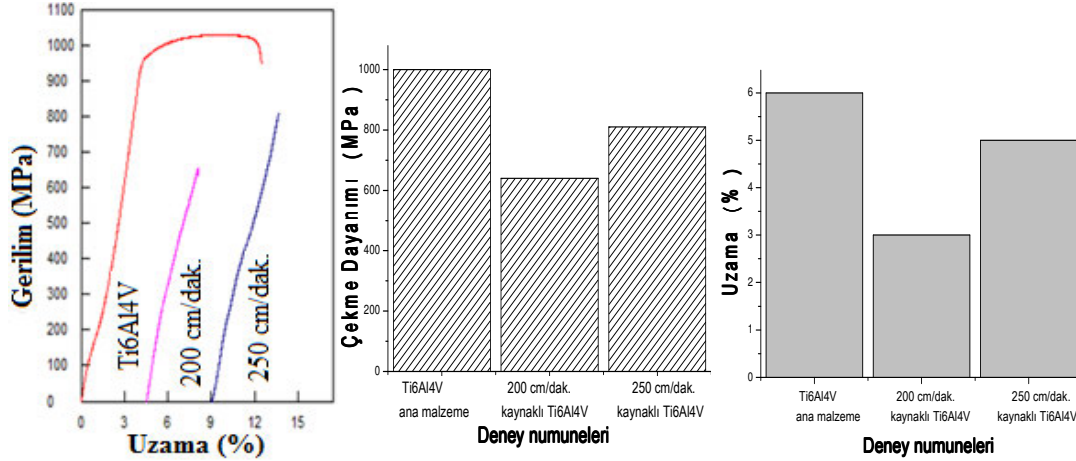
İlave olarak radyografik muayenede kaynak dikişinin kesitinde tam anlamıyla değerlendirilemeyen kesintilerin çatlak olup olmadığı sıvı penetrant yöntemiyle ortaya çıkarılması için muayene işlemi gerçekleştirilmiştir. Analiz sonucuna göre Şekil 3c'de görüldüğü gibi kaynak dikişi boyunca düzensiz aralıklarla kaynak dikişi kesiti boyunca çatlakların meydana geldiği görülmektedir. Ti6Al4V bir alpha-beta alaşımıdır. Bazı alfa-beta titanyum alaşımlarında bilhassa yüksek enerji kaynak uygulamalarında (GTA ve GMA kaynaklarında) hem ITAB hem de kaynak metalinde alt katılma çatlakları (subsolidus) oluştuğu rapor edilmektedir [20-21]. Bu kaynak çatlamaının temel sebebinin beta-alfa oluşum sıcaklığı hemen altındaki sıcaklıklarda genel bir süneklik kaybından kaynaklandığı belirtilmiştir [20]. Alpha-beta alaşımı Titanium malzemeye uygulanan farklı ısı girdisindeki kaynaklar mukayese edildiğinde, çatlama miktarı, daha düşük ısı girdisine sahip kaynaklarda daha az olmakla beraber her iki, düşük ve yüksek ısı girdisinde de çatlama meydana geldiği belirlenmiştir. Kaynak bölgesindeki çatlama miktarı ısı girdisi ile doğrusal olarak arttığı rapor edilmiştir. Ancak ısıdan etkilenen bölge boyutu nispeten sabit kalmıştır [21].



Şekil 3. Birleştirmenin radyografik muayene görüntüsü a) 200cm/dak, b) 250 cm/dak. c) sıvı penetrant muayene

3.1. Çekme deney sonuçları

Ti6Al4V ana malzeme ve farklı kaynak ilerleme hızlarında CO₂ lazer kaynaklı birleştirmelerin çekme testi gerilme-uzama eğrileri Şekil 4a ve deney numunelerin ortalama mukavemet ve %uzama değerleri grafiksel olarak Şekil 4b'de gösterilmiştir.



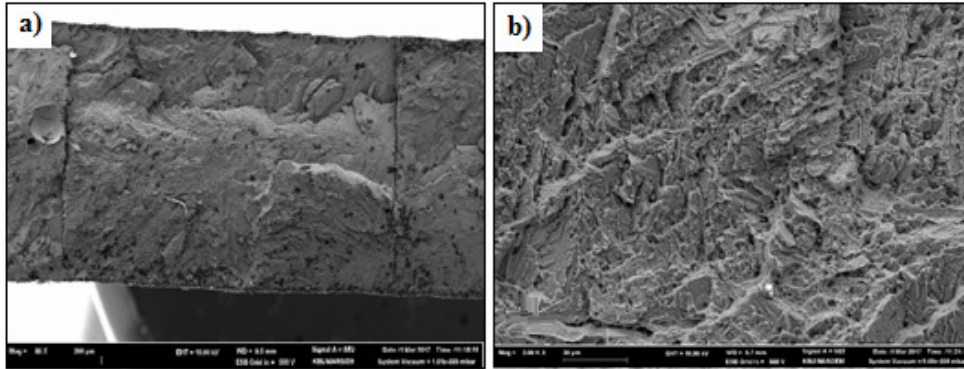
Şekil 4. Çekme deneyi gerilme-uzama eğrileri ve deney sonuçları

Şekil 4'den görüldüğü gibi, Ti6Al4V titanyum alaşımının çekme dayanımı yaklaşık 1000 MPa iken, lazer kaynaklı birleştirmelerden 200 cm/dk ve 250 cm/dk kaynak ilerleme hızlarında birleştirilen numunelerin ortalama sırasıyla çekme dayanımları 640 MPa ve 810 MPa olarak belirlenmiştir. Ti ana malzeme yüzde uzama miktarı %6 tespit edilirken sırasıyla 200 cm/dk ve 250 cm/dk kaynak ilerleme hızlarında birleştirilen numunelerin uzama miktarları ise %3 ve %5 olarak tespit edilmiştir. Yüksek kaynak ilerleme hızıyla diğer bir ifadeyle daha düşük ısı girdisiyle birleştirilen numunelerin yüksek ısı girdisiyle birleştirilenlere oranla çekme dayanımı 170MPa ve % uzama miktarı ise %2 daha fazla bulunmuştur. Düşük ısı girdisine bağlı olarak yapıda meydana gelen martenzit gibi sert fazların birleştirmenin ITAB daha dar ve daha ince taneli oluşu, yüksek kaynak ilerleme hızına bağlı kaynak bölgesinde underfill oluşumuna yeterince zaman olmaması birleştirmenin dayanımında artışın sorumluları olduğu düşünülmektedir. Lazer kaynaklı Titanyum alaşımlarında temel sorun underfill oluşumu ve kaynak bölgesinde porozite oluşumudur [22,23]. Yüksek ilerleme hızına bağlı dar bir ITAB oluşumu ve yapının daha ince taneli oluşu yüksek dayanımın yanı sıra daha yüksek %uzamanın sebebi olabilir.

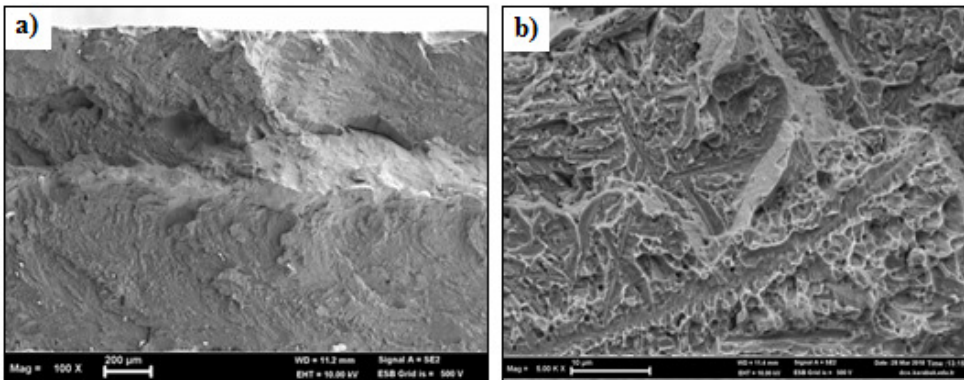
CO₂ lazer kaynaklı birleştirmelerden sırasıyla 200 cm/dk ve 250 cm/dk kaynak ilerleme hızlarında birleştirilen numunelerin çekme dayanımlarının ticari olarak temin edilen ana malzemeye oranla yaklaşık 360MPa, 190MPa, yüzde uzama miktarlarının ise yaklaşık %3 ve %1 daha düşük bulunmuştur. Titanyum alaşımlarının lazer kaynaklı birleştirmelerinin çekme dayanımının ana malzemeden daha düşük olduğu diğer çalışmalarda da rapor edilmiştir

[24].Kaynaklı birleştirmenin dayanımının daha düşük bulunmasının sebebi olarak kaynak termal çevrimine bağlı olarak birleştirme yapısının sert iğnesel martenzit fazının sorumlu olduğu düşünülmektedir. Aynı zamanda ana malzemeye göre daha düşük mukavemette ilave dolgu metali kullanılmamasından dolayı kaynak kesitindeki göçmenin (underfill) sorumlu olduğu düşünülmektedir.

Çekme testi sonrasında kırılma kaynak metalinden gerçekleşmiştir. 200cm/dak. ve 250 cm/dak. hızlarda birleştirilmiş test numunelerinin kırılma yüzeyleri SEM ile incelenmiş, kırık yüzey görüntüleri Şekil 5 ve 6'a ve b'de gösterilmiştir. Kırılma yüzey görüntüleri kesitte bir daralma oluşmaması ve yüzeydeki düzlemsel ayrılmalar kaynak metalinden kopan test numunesini genel olarak gevrek kırılma biçimiyle kırıldığına işaret etmektedir. Ayrıca kaynak ısı girdisine ve müteakip soğuma rejimine bağlı olarak martenzitik dönüşüm sergileyen ve gevrekleşen Ti6Al4V titanyumun kaynak metalinde Şekil 5a'da ve ayrıca birleştirme X-Ray radyografi filmi üzerinde gözlemlenen kaynak yönüne dik çatlaklar sonucu kopmanın kaynak metalinden olduğu düşünülmektedir.



Şekil 5: 200 cm/dak., ilerleme hızıyla birleştirilmiş lazer kaynaklı Ti6Al4V çekme numunesi kırılma yüzeyleri, a) düşük büyütme, b) yüksek büyütme

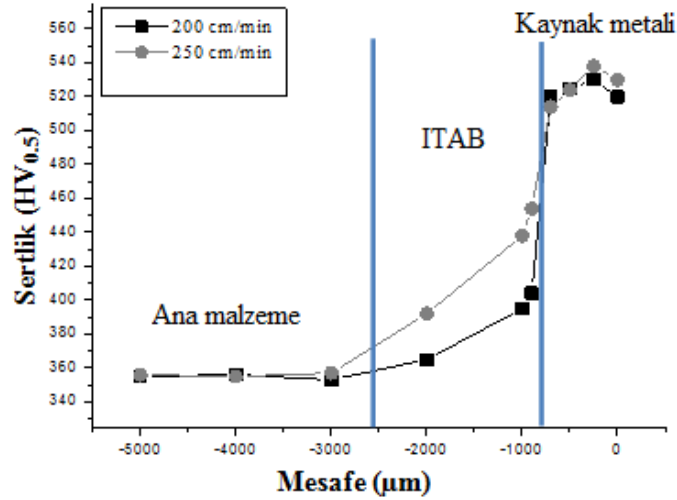


Şekil 6. 250 cm/dak., ilerleme hızıyla birleştirilmiş lazer kaynaklı Ti6Al4V çekme numunesi kırılma yüzeyleri, a) düşük büyütme, b) yüksek büyütme

Şekil 6 a ve b'den görüldüğü gibi artan kaynak ilerleme hızına bağlı hızlı soğuma rejiminden dolayı daha yüksek ilerleme hızıyla birleştirilen numunenin kırılma yüzeyinin daha düzlemsel oluşması ve kesit daralması meydana gelmemesi hasarın gevrek kırılma modeli ile oluştuğuna işaret etmektedir. Kaynak metalinin sertliğinin azda olsa daha yüksek bulunması bu sonucu desteklemektedir.

3.2. Mikrosertlik Ölçümü Sonuçları

Farklı kaynak ilerleme hızlarında birleştirilen lazer kaynaklı numunelerin aynı hat üzerinden ana malzeme, ITAB ve kaynak metalini sertlik ölçüm sonucu grafiksel olarak Şekil 7'de gösterilmiştir.



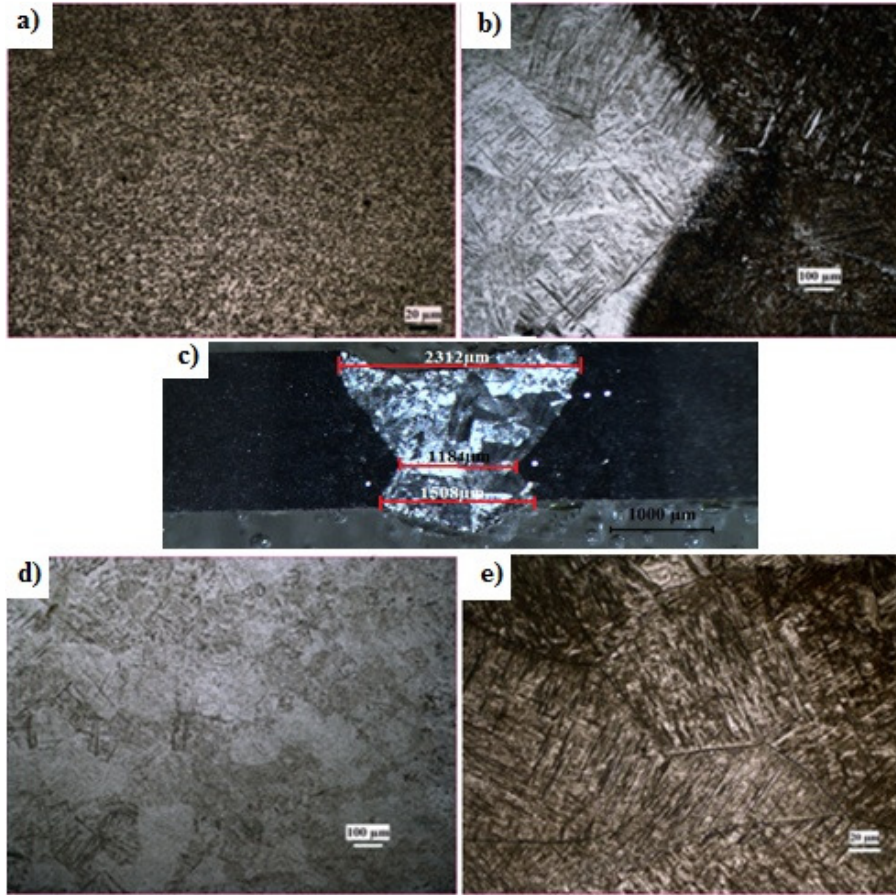
Şekil 7. Sertlik ölçüm sonucu

Şekil 7'de görüldüğü gibi, yüksek ısı girdisiyle diğer bir ifadeyle düşük kaynak ilerleme hızıyla elde edilen birleştirmenin kaynak metalini sertliği ortalama 522 HV_{0.5} düşük ısı girdisiyle birleştirilen numunenin de 525 HV_{0.5} olarak birbirine çok yakın bulunmuştur. Kaynak termal çevrimine bağlı olarak ilave metal kullanmadan gerçekleştirilen birleştirmelerde yapısal dönüşüm ürünü olan α' martenzit fazının sertliğinin birbirine yakın olması gayet doğal bir sonuçtur. Kaynak metalini kimyasal bileşime ve soğuma rejimine bağlı olarak asiküle α' martenzit yapısında oluştuğu için bağlantıda en yüksek sertliğin kaynak metalinde oluştuğu rapor edilmiştir [24-25]. Birleştirme sertliği ana malzemeden ITAB ve kaynak metaline doğru gidildikçe artış göstermektedir. Ancak daha yüksek ilerleme hızıyla birleştirilen numunenin ITAB sertliği yaklaşık 50 HV_{0.5} kadar belirgin bir şekilde yüksek bulunmuştur. Bu sertlik artışında ITAB'nin daha ince taneli olmasının etkili olduğuna inanılmaktadır. Ana malzeme sertliği ise ortalama 355 HV_{0.5} olarak belirlenmiştir. Martenzit hacim oranı kaynak metalinden ana malzemeye doğru gidildikçe azalmakta ve martenzit fazı ITAB ana malzeme ara yüzeyinde kaybolduğu için, ITAB sertliği kaynak metalinden ana

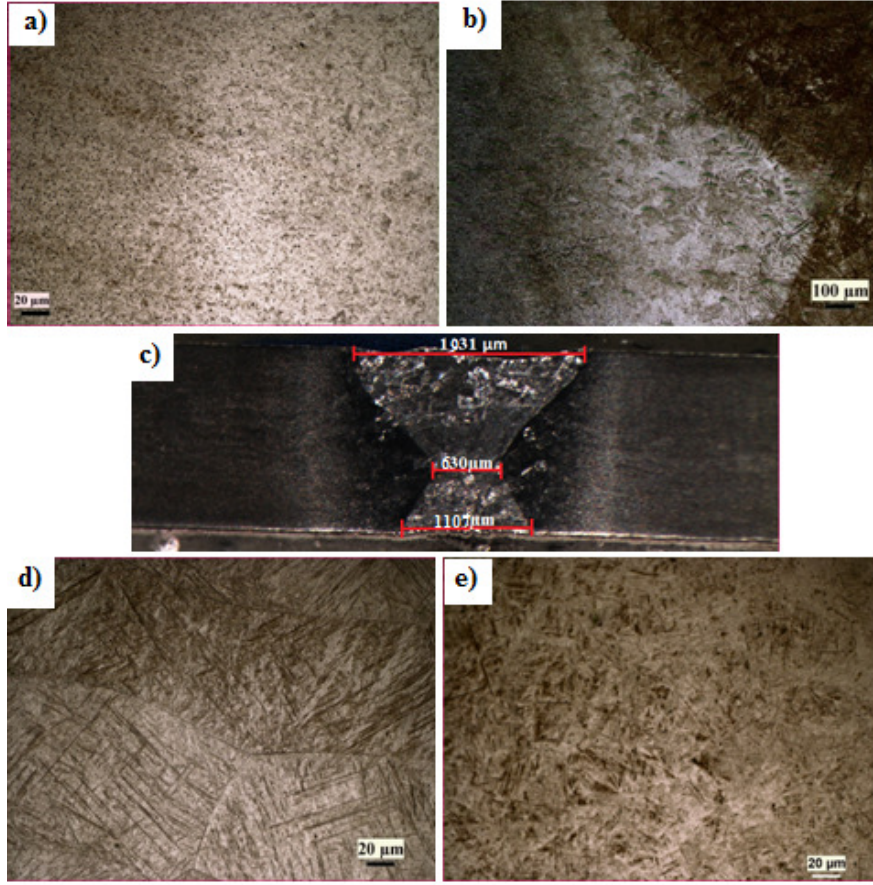
malzemeye gidildikçe azalma göstermektedir. Ayrıca ITAB'de tane irileşmesi sertliğin kaynak metaline göre daha düşük bulunmasının ana sorumlusu olduğu düşünülmektedir.

3.3. Mikroyapı incelemeleri

Kaynaklı birleştirmelerin mikroyapı görüntüleri Şekil 8-9 'da gösterilmiştir. Şekil 8 ve 9'dan görüldüğü gibi Ti6Al4V alaşımının CO₂ lazer kaynaklı birleştirmesi makro görüntüsü kaynak metalinin kase formunda oluştuğuna işaret etmektedir. Şekil 8 ve 9'dan görüldüğü gibi kaynak dikişi genişlikleri 200 cm/dak. kaynak ilerleme hızı ile birleştirilen malzeme kaynak metalini orta bölgesi için 1184 µm olarak ölçülürken, bu mesafe 250 cm/dak. kaynak ilerleme hızı ile birleştirilen numune için 630 µm olarak ölçülmüştür. Kaynak ilerleme hızının 200 cm/dak.'dan, 250 cm/dak.'ya artmasına bağlı olarak kaynak dikişinde bir daralma meydana gelmiştir.



Şekil 8. Lazer kaynaklı Ti6Al4V birleştirmesinin mikro yapısı (200 cm/dk)
a) Ana malzeme b) Ana malzeme/ITAB geçiş c) Birleştirme makro görüntü, d) ITAB
e) Kaynak metal



Şekil 9. Lazer kaynaklı Ti6Al4V birleştirmesinin mikro yapısı (250 cm/dk)
a) Ana malzeme b) Ana malzeme/ITAB geçiş c) Birleştirme makro görüntü, d) ITAB
e) Kaynak metali

Şekil 8 ve 9 a'dan görüldüğü gibi, Ti6Al4V ana malzeme koyu renkli β fazı ve açık renkli α matriksten oluşan tipik bir α - β yapısından meydana gelmiştir. Şekil 8 ve 9 b ve e'de gösterilen kaynak metalinin asiküler α' martenzit fazından oluştuğu görülmektedir. Kaynak metalinde oluşan martenzit yapının lazer kaynaklı birleştirmenin doğası gereği alaşımın kimyasal bileşimiyle ilişkili olarak yüksek soğuma hızı rejiminden dolayı meydana geldiği düşünülmektedir [26]. Benzer şekilde Ti6Al4V alaşımlarının lazer kaynağında kaynak metalinde oluşan yapının asiküler α' martenzit fazından meydana geldiği rapor edilmiştir [27]. Ti6V4Al alaşımlarının 410 °C/s'den daha hızlı soğuma hızlarında yapısının tamamen martenzitik olarak dönüşüm gösterdiği rapor edilmiştir [28].

Şekil 8 ve 9b ve d'den görüldüğü gibi, birleştirme ITAB'nin kaynak metaline yakın bölümünde ağırlıklı olarak α' martenzit fazından meydana gelirken ana malzemeye doğru gidildikçe az miktarda α' martenzit, taneler arası β ve ağırlıklı olarak birincil α fazından meydana gelmektedir. Ahn vd. Ti6Al4V titanyum alaşımını fiber lazer kaynağı ile farklı parametrelerde birleştirmişlerdir. Birleştirme mikroyapı incelemeleri sonucu benzer ITAB yapılarının oluştuğunu rapor etmişlerdir [29]. Başka bir çalışmada Wang vd., CO₂ lazer kaynağı ile 3.3 mm kalınlığındaki Ti6Al4V alaşımını 2.5kW lazer gücü ve 1.5 m/min. kaynak

ilerleme hızında birleştirmiş ve ITAB mikroyapısının beta dönüşüm sıcaklığının altında kalan bölümünün su verilerek sertleştirilmiş bir yapının oluştuğunu ifade etmişlerdir [24].

4. Genel Sonuçlar

Çalışmada Ti6Al4V alaşımın CO₂ lazer kaynak kabiliyeti araştırılmış elde edilen bulgular aşağıda özetlenmiştir.

- CO₂ lazer kaynaklı bağlantılardan sırasıyla 200 cm/dk ve 250 cm/dk kaynak ilerleme hızlarında birleştirilen numunelerin çekme dayanımlarının ana malzemeye oranla yaklaşık 360MPa, 190MPa, yüzde uzama miktarlarının ise yaklaşık %3 ve % 1 daha düşük bulunmuştur.
- Yüksek kaynak ilerleme hızıyla diğer bir ifadeyle daha düşük ısı girdisiyle birleştirilen numunelerin yüksek ısı girdisiyle birleştirilenlere oranla çekme dayanımı 170MPa ve % uzama miktarı ise % 2 daha fazla bulunmuştur.
- Çekme testi sonrasında kırılma kaynak metalinden gerçekleşmiştir. Test numunelerinin kesitinde bir daralma oluşmaması ve yüzeydeki düzlemsel ayrılmalar kaynak metalinden kopan test numunesini genel olarak gevrek kırılma biçimiyle kırıldığına işaret etmektedir. Kaynak ısı girdisine ve müteakip soğuma rejimine bağlı olarak mikroyapısal dönüşüm sergileyen ve gevrekleşen kaynaklı birleştirme X-Ray radyografi filmi üzerinde gözlemlenen kaynak yönüne dik çatlaklar sonucu kopmanın kaynak metalinden meydana gelmesinin sorumlusu olduğu düşünülmektedir.
- Yüksek ısı girdisiyle diğer bir ifadeyle düşük kaynak ilerleme hızıyla elde edilen birleştirmenin kaynak metali sertliği ortalama 522 HV_{0.5}, düşük ısı girdisiyle birleştirilen numunenin de 525 HV_{0.5} olarak birbirine çok yakın bulunmuştur. Birleştirme sertliği ana malzemeden ITAB ve kaynak metaline doğru gidildikçe artış göstermektedir. Ancak daha yüksek ilerleme hızıyla birleştirilen numunenin ITAB sertliği yaklaşık 50 HV_{0.5} kadar belirgin bir şekilde yüksek bulunmuştur. Bu sertlik artışında ITAB'ın daha ince taneli olmasının etkili olduğuna inanılmaktadır. Ana malzeme sertliği ise ortalama 355 HV_{0.5} olarak belirlenmiştir.
- Ticari olarak temin edilen Ti6Al4V alaşımı yapısı α - β fazlarından meydana gelmiştir. Lazer kaynaklı birleştirmenin kaynak metalinin asiküleri α' -martenzit fazından oluştuğu tespit edilmiştir. Birleştirme ITAB'ın kaynak metaline yakın bölümü ağırlıklı α' martenzit fazından meydana gelirken ana malzemeye doğru gidildikçe az miktarda α' martenzit, taneler arası β ve ağırlıklı olarak kabalaşmış birincil α fazından meydana gelmiştir.

5. Teşekkürler

Bu çalışma Karabük Üniversitesi Bilimsel Araştırma Projeleri Koordinasyon Birimi tarafından desteklenmiştir. Proje numarası. Proje numarası: KBÜBAP-18-DS-130. Adı geçen birime teşekkür edilir.

6. Kaynaklar

- [1] H. Huang, J. Wang, L. Liqun, M. Ninshu: Estimation of Laser Welded Deformation in Thin Layers by Efficient Numerical Modeling, *J. Mater. Process. Technol.*, 227(2016) pp.117 – 128.
- [2] M.J Donachie: Titanium, A. Technical Guide(second edition), ASM International, Metals Park, OH (2000).
- [3] S.H Wang, M.D Wei, L.W Tsay: The Tensile Properties of LBW Welds in Ti-6Al-4V Alloys at Temperatures below 450 ° C, *Mater Lett.*, 57(2003) pp. 1815 – 1823.
- [4] J.Fernandez, J.Damborene, J.Ruiz:Effect of Surface Hardening of High-Temperature Materials on Dimensional Stability, *Mater Des*, 23(2002) pp. 377-338.
- [5] L.S Bertol, W.K Júnior, F.P Silva, C. Direct: Metal Laser Sintering of Aumund-Kopp Ti-6Al -4V, *Mater Des*, 31(2010)pp. 3982-3398.
- [6] A. Bandyopadhyay, F. Espana, V.K Balla, S.Bose, Y.Ohgami: NM Effects of Porosity on Mechanical Properties and in Vivo Response of DaviesTi6Al4V Implants, *Acta Biomater*, 6(2010) pp. 1640 – 1648.
- [7] M.J Blackburn, D.R Malley: Plasma the Melting of Titanium Alloys, *Mater Des*, 14(1993), pp. 19-27.
- [8] <http://www.corrosionmaterials.com/alloys/titanium-grade-5/Corrosion> Materials, Titanium Class 5. (July 1, 2016)
- [9] <http://www.allvac.com>, Allvac: Titanium Technical Data sheet, Allvac Titanium 6Al-4V Alloy(2007).
- [10] C.Casavola, C.Pappalettere, G.Pluinage: Fatigue Resistance of Titanium Laser and Hybrid Welded Joints, *Materials and Design*, 32(5)(2011)pp.3127-3135.
- [11] S.Mueller, E. Stiles, R. Dienemann: Investigation of Porosity Formation During Welding of Ti-6Al-4V, *Laser Material Handling Conference Reports*, ICALÉOPaper(2006)304, p.133.
- [12] P. Hilton, J. Blackbur, P. Chong: The Source of Ti-6Al-4V by Laser Beams Emitted from Fiber, ICALÉO 2007, Orlando, FL. USA (2007).
- [13] A.M. El-Batahgy, T. DebRoy: Nd-YAG Laser Beam and GTA Welding of Ti-6Al-4V Alloy, *International Journal of Engineering and Technical Research (IJETR)*, 12 (2014) pp.43-50.
- [14] K.Y. Benyounis, A.G.Olabi, M.S.J. Hashmi: Multi-Response Optimization of CO₂Laser-Welding Process of Austenitic Stainless Steel, *Optics & Laser Technology*, 40(1)(2008)pp.76–87.
- [15] Shusen Zhao, Gang Yu, Xiuli He, Yaowu Hu: Microstructural and Mechanical Characteristics of Laser Welding of Ti6Al4V and Lead Metal, *Journal of Materials Processing Technology* 212(7), (2012)pp.1520-1527.
- [16] K.R. Balasubramanian, S. Siva Shanmugam, G. Buvanashekarana: Numerical and Experimental Investigation of Laser Beam Welding of AISI 304 Stainless Steel.", *Advances and Production Engineering & Management*, (2008)pp.93-105.
- [17] E.Akman, T.Canel, A. Demir, T.Sinmazcelik: Optimization of Pulsed Nd-YAG Laser Parameters for Titanium Seam-Welding, *AIP Conf. Proc.*, 899(2007), pp. 303-304.
- [18] J.A. Atoui, D.N.B.Felipucci, V.O. Pagnano, I.A.Orsi, M.A.D.ANóbito, O.L.Bezzon: Tensile and Flexural Strength of Commercially Pure Titanium Submitted to Laser and Tungsten Inert Gas Welds, *Brazilian Dental Journal*, (2013)pp.630-634.
- [19] H.W.Wiskott, M.T. Doumas, S.S. Scherrer, C.Susz, U.C. Belsler: Microstructures of Brazings and Welds Using Grade 2 Commercially Pure Titanium, *Int. J. Prosthodont*, 14(2001) pp. 40-47.

- [20] B. K. Damkroger, G. R. Edwards, B. B. Rath: Investigation of Subsolidus Weld Cracking in Alpha-Beta Titanium Alloys, *Welding Journal*, 7(1989) pp.290-302.
- [21] D. Hayduk, B. K. Damkroger, G. R. Edwards, D. L. Olson: Cracking Susceptibility of Ti-6Al-2Nb-1Ta-0.8Mo as Determined by the Varestraint Test, *Welding Journal*, 65(9)(1986) pp.251-260.
- [22] P. Hilton, J. Blackburn, P. Chong: Welding of Ti-6Al-4V with Fiber Delivered Laser Beams, *Proceedings of ICALEO 2007*, Orlando, Florida, 29 October-1 November 2007 (Laser Institute of America, Orlando, (2007), pp. 887-895.
- [23] S. Mueller, E. Stiles, R. Dienemann: Study of Porosity Formation During Laser Welding of Ti6Al4V, *Proceedings of ICALEO 2008*, Temecula, California, 20-23 October 2008 (Laser Institute of America, Orlando, (2008) pp. 133-138.
- [24] S.H.H.Wang, M.D.DWei, L.W.W.Tsay: Tensile Properties of LBW Welds in Ti-6Al-4V Alloy at Evaluated Temperatures below 450 °C, *Mater Lett*, (2003) pp.1815-1823.
- [25] F. Torsten, J.F. Dos Santos, M. Koca, M. Penasa: Mechanical and Microstructural Characterization of Laser Beam Welded Titanium Alloys, *ASM Proceedings of the International Conference: Welding Research*, (1998) pp.887-892.
- [26] S. Campanelli, G. Casalino, M. Mortello, A. Angelastro, A.D. Ludovico: Microstructural Characteristics and Mechanical Properties of Ti6Al4V Alloy Fiber Laser Welds, *Procedia CIRP*, 33(2015) pp.428-433.
- [27] X. Cao, M. Jahazi: Effect of Welding Speed on Butt Joint Quality of Ti-6Al-4V Alloy Welded Using a High-Power Nd:YAG Laser, *Optics and Lasers in Engineering*, 47(2009) pp.1231-1241.
- [28] T. Ahmed, H.J. Rack: Phase Transformation During Cooling in $\alpha+\beta$ Titanium Alloys, *Materials Science and Engineering*, 243 (1998) pp.206-211.
- [29] J. Ahn, L. Chen, C.M. Davies, J.P. Dear: Parametric Optimization and Microstructural Analysis on High Power Yb-Fiber Laser Welding of Ti-6Al-4V, *Optics and Lasers in Engineering*, (2016) pp.156-171.

CORRESPONDENCE ADDRESS: Hayriye ERTEK EMRE, Karabük Üniversitesi, Teknoloji Fakültesi, 78050, Türkiye, Tel: +90 433 82 00/1091, e-mail: hayriyeertek@karabuk.edu.tr

KISA BİYOGRAFİLER

Şennur Arslan¹ – Karabük Üniversitesi, Teknoloji Fakültesi, İmalat Mühendisliği Bölümünde yüksek lisans yapmaktadır.

Hayriye Ertek Emre² – Karabük Üniversitesi, Teknoloji Fakültesi, İmalat Mühendisliği Bölümünde Dr. Öğretim Üyesi olarak görev yapmaktadır.

Ramazan Kaçar³ – Karabük Üniversitesi, Teknoloji Fakültesi, İmalat Mühendisliği Bölümünde Profesör Dr. Olarak görev yapmaktadır.

A RESEARCH ON THE DIFFERENCE BETWEEN AUTOMATED AND HAND MADE ESD COATINGS PRODUCED ON STEEL PLATES

Ş. Talaş^{1,a}, B. Gökçe^{2,b}, Y. Kayalı^{1,c}

¹Afyon Kocatepe University, Faculty of Technology, Metallurgical and Materials Engineering,
Afyonkarahisar, Turkey

¹ Afyon Kocatepe University, Faculty of Technology, Mechatronics Engineering, Afyonkarahisar, Turkey

^astalas@aku.edu.tr, ^bbgokce@aku.edu.tr, ^cykayali@aku.edu.tr

Abstract

ESD coating is generally carried out by hand and an actuator is employed for this course of process in order to ease the formation of coating layer. However, a serious health hazard potentially exists and new automated systems are under investigation. Automated system ESD coatings have been compared to the manual ESD coatings and metallurgical and physical properties are investigated to reveal the difference between these two coating that are made on steel plates. This study also analyzes a macrostructures of both welds from the point of view of physical appearance.

Key Words: Low Energy Welding, surface coating, automated system,

1. Introduction

In the automotive industry where sheet metal materials are frequently used, spot welding or spot welding is used frequently for joining operations[1-3]. The most important features of this welding method are that one can easily make a large number of spot welds in a very short time at fixed pressure values. It is expected that the copper electrodes used will be resistant to the temperature effect caused by this repetitive spot welding and electrical conduction [4]. However, since copper has oxidation and easy deformation with increased service time, it needs to be cleaned, cooled or changed frequently for the continuity of the process[4, 5]. Coating the surface with a heat resistant material can be an option for the spot welding process as is shown by some reserachers [6-9]. ESD coating of surfaces of surfaces is expected to extend at least twice the amount of spot weld duration required for the service [7,8] and it is also economically advantageous. ESD processes are mostly carried out by hand it is exhausting and medically harmful process in long term for the joints and bone fractures and cracks can be observed due to vibration. The rays that are emitted during the coating process is also harmful for the eyes and skin in long term use.

The aim of this work is to demonstrate that the process can be automated and a similar result to which it is manually made, can be obtained eventually using M42 steel and W electrode. For this purpose, metallographic methods, optical and electron microscopy were used to determine the feasibility of both coatings.

2. Experimental Methods

SZ3000 coating machine was used for the coating process in which parameters such as frequency, voltage and rotation speed is kept constant for the purpose of comparison Figure 1a. Frequency of 600 kHz, voltage of 120V and 105 rpm applicator rotation speed were used to produce specimens. Same equipment was used to deposit a layer of coating using in house-built CNC machine and controller. Hand-made coatings were produced with 1 minute of holding time and applied on an area of 3 cm radius whereas automated coatings were deposited on approximately 2 cm x 2.5 cm rectangular area using a linear precision of 250 micron. Following the coating, all surfaces were cleaned and photographed at low magnification. A cross-sectional imaging was made on all specimens following the polishing and etching i.e. metallographic preparation. SEM microscopy was carried out on specimens coated by both methods using LEO VP210 SEM equipment. The electrode used for coating was W/W-Rh and the base plate was an M42 steel.

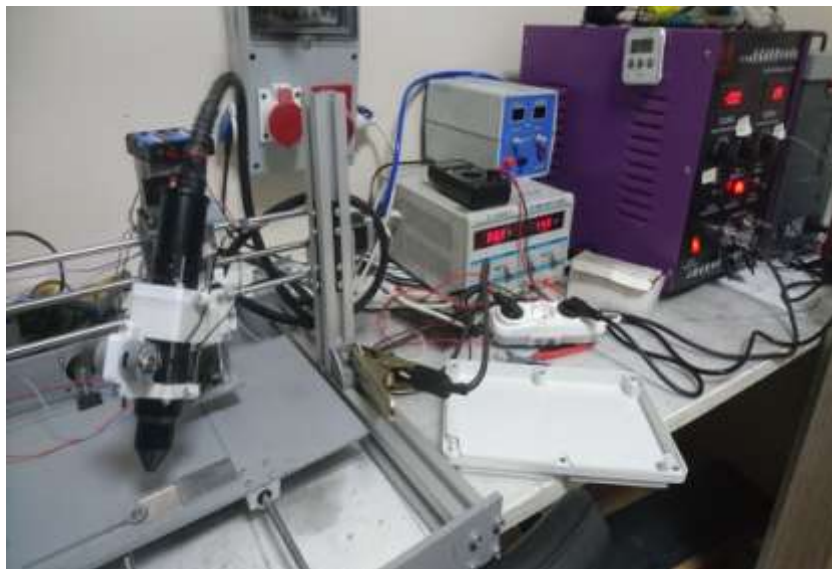


Figure 1. ESD setup and the automated system that is ready for the automation.



304
Figure 2. The coating plate for automated ESD coating equipment

3. Results and Discussion

ESD coating have been deposited manually and using automated system. The manual method includes a rotating system which gives non-continuous drops of arc pool which then forms a line of alloyed regions [2,4]. The surface of the specimen was cleaned prior to coating with a steel electrode. The coating is generally carried out using an applicator that is vibrated in order to prevent the electrode sticking to the surface [2,3] and also helps the movement of the hand which is easier compared to non vibrating handles; however, the vibration is also a source of roughness on the surface as seen in Fig 3. The image shown on the left is coated by hand and the image shown on the right is coated by automated ESD system. Manual coatings are finer in size and randomly distributed whereas automated coatings have a straight border and cleaner appearance with large drops of arc pools.

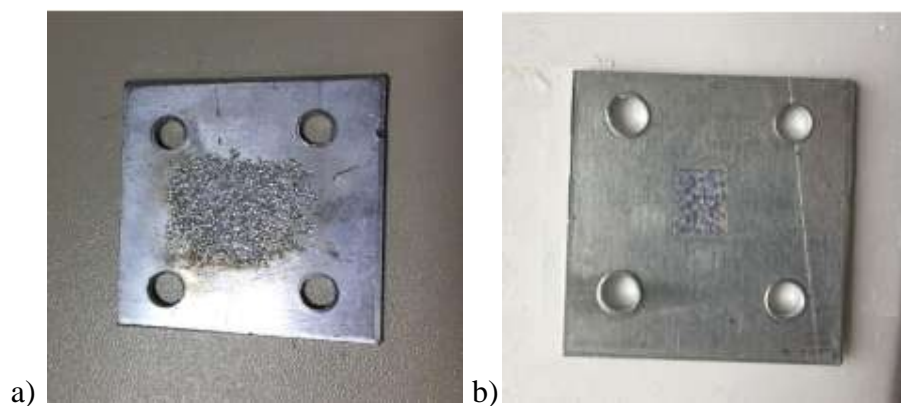


Figure 3. Coatings produced by hand a) and automated system b) automated system has a very regular border whereas hand-made coatings are relatively random-distributed.

Figure 4 shows images from the surface of manually made ESD coatings. The arc pools appear to be randomly distributed and the size of arc pools are also varying in size. The surface roughness is high and irregular arc pools are observed. SEM image, Fig 4a, supports this opinion and shows that surface profile is irregular and cracking leading to the failure of layer is obvious. Porosity is also another source of cracking which plays an important role in defect formation.



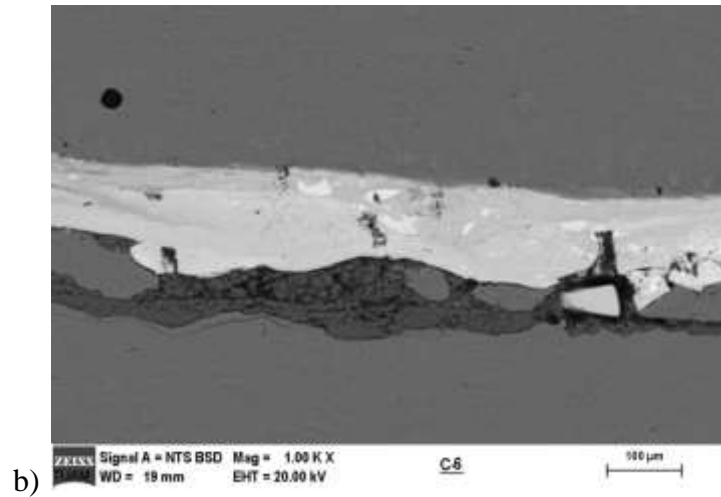
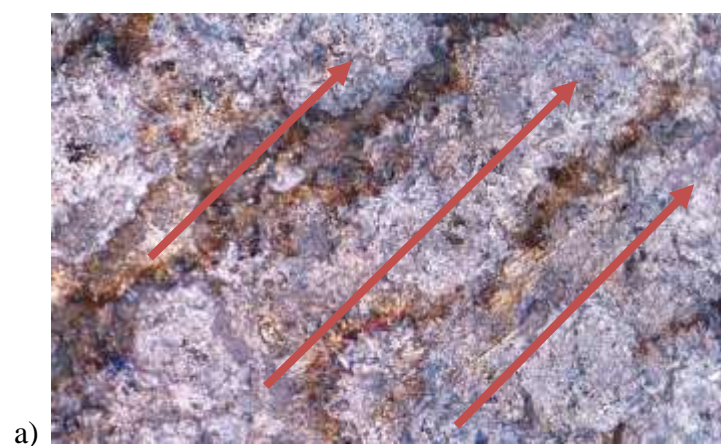


Figure 4. Images from coating layers taken from manually made ESD plate a) optical microscope image at 50x magnification, b) SEM-BSE image.

Compared to manually made ESD coating shown in Fig 4, Figure 5 shows automated ESD coating deposited on Al plate with steel electrode. The surface quality is shown to be relatively better than manual ESD coating and there is a banding as shown by arrows, which is a result of line rastering by the device. It can be seen that arc pools are regular and has a smoother appearance compared to manual coatings. SEM image shows, Fig. 5b, a saw teeth appearance of layers formed on the plate. The distance between seams of arc pools are the only drawback that is observed otherwise is classified as acceptable coating. The coating layer does not contain any porosity and cracking but there seems to be a separation line or delamination between the coating layer and base plate. Automated system is less sensitive to hand motions which may be the source of uneven surface coating deposition in manual coating process. This leads to eventually less cracking and less porosity, however, the delamination of coating layer is more prominent due to the force applied on the plate being irregular at times.



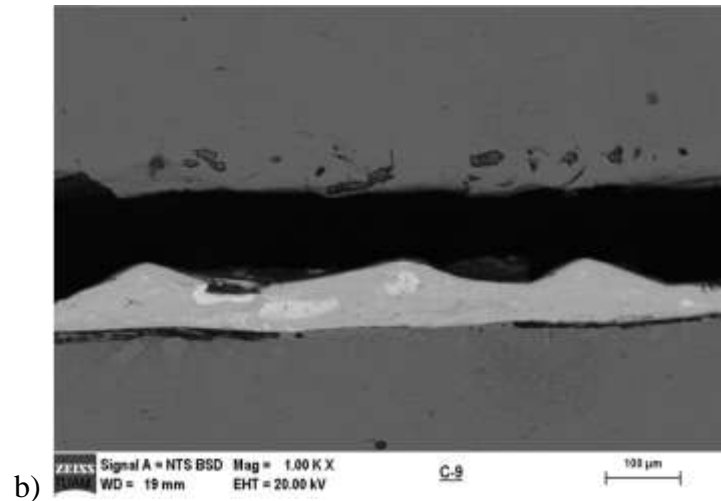


Figure 5. Automated ESD coating layer deposited on steel plate. Coating layer has a saw-teeth structure and less porosity, additionally, it possesses less cracking along the coating layer.

4. Conclusion

This study relates the two different coatings made by manually and automated system. Manual system has an advantage of overseeing the problem and rectifying it, accordingly. There are less porosity and but more cracking evolving during the coating process whereas automated system is less sensitive to hand moves which may be the source of uneven surface coating deposition. This leads to eventually less cracking and less porosity, however, the delamination of coating layer is more prominent due to the force applied on the plate being irregular at times.

6. Acknowledgement

This research is a part of study that is supported by BAP office of Afyon Kocatepe University with a project number of 17.KARİYER.197.

7. References

- [1] T. Dupuy: The Degradation of Electrodes by Spot Welding Zinc Coated Steels, *Welding in the World*, 42(6) (1999), pp.58-68,
- [2] E.A., Brown, G. L., Sheldon, A. E., Bayoumi: A Parametric Study of Improving Tool Life by Electrospark Deposition, *Wear*, 138 (1990), pp.137-151,
- [3] J. Gould: Application of Electro-Spark Deposition as a Joining Technology, *Welding Journal*, 90 (2003), pp.191s-197s,
- [4] R. Holliday, J.D. Parker and N.T. Williams: Electrode Deformation When Spot Welding Coated Steels, *Welding in the World*, 35(3) (1995), pp.160-164,
- [5] J.D. Parker, N.T. Williams and R.J. Holliday: Mechanisms of Electrode Degradation When Spot Welding Coated Steels, *Science and Technology of Welding and Joining*, 3(2) (1998), pp. 65-74,

- [6] A. Lesnjak and J. Tusek: Processes and Properties of Deposits in Electrospark Deposition, *Science and Technology of Welding and Joining*, 7 (2002), pp.391-396,
- [7] S. Talas, E. Mertgenç ve B. Gökçe: ESD coating of copper with TiC and TiB₂ based ceramic matrix composites, *Materials Science and Engineering*, 146 (2016), pp. 1-9.
- [8] C. Zheng, Y. Zhou: Surface Modification of Resistance Welding Electrode by Electro-spark Deposited Composite Coatings: Part I. Coating characterization, *Surface & Coatings Technology*, 201/3-4 (2006), pp.1503-1510.
- [9] Z. Chen, Y. Zhou: Surface modification of resistance welding electrode by electro-spark deposited composite coatings: Part 2. Metallurgical behaviour during welding, *Surface & Coatings Technology*, 201(6) (2006) pp.2419–2430.

CORRESPONDENCE ADDRESS: Şükrü Talaş, Afyon Kocatepe University, Faculty of Technology, ANS Campus, +902722281314, talas.sukru@gmail.com.

SHORT BIOGRAPHIES

Şükrü Talaş – Professor Dr. Şükrü Talaş was graduated from Marmara University, Technical Education Faculty, Department of Metallurgy Education, in 1993. He completed his MSc in 1997 in Brunel University, the UK and was finally granted a PhD degree in 2002 on C-Mn-Ti Steel Weld Metal Microstructures from Leeds University, the UK. He works as Associate Professor at the department of Metallurgical and Materials Engineering, Faculty of Technology, Afyon Kocatepe University.

Barış Gökçe – Assistant Professor Barış Gökçe was graduated from Afyon Kocatepe University, Faculty of Technical Education, Department of Metallurgy Education. He completed his MSc in Afyon Kocatepe University Institute of Natural Science and finally received his PhD degree from Afyon Kocatepe University Institute of Natural Science on the subject of statistical optimization of metallurgical processes. He mostly works on simulation of mechanical systems and their control.

Yusuf Kayalı – Assistant Professor Yusuf Kayalı was graduated from Afyon Kocatepe University, Faculty of Technical Education, Department of Metallurgy Education. He completed his MSc in Afyon Kocatepe University Institute of Natural Science and finally received his PhD degree from Afyon Kocatepe University Institute of Natural Science on the subject of wear of metals. He works on corrosion and wear of metals.

OTOMATİK ESD KAPLAMA İÇİN MEKATRONİK BİR SİSTEM TASARIMI

B. Gökçe^{1,a}, Ş. Talaş^{2,b}

¹Afyon Kocatepe Üniversitesi, Teknoloji Fakültesi, Mekatronik Mühendisliği Bölümü, Afyonkarahisar,
Türkiye

²Afyon Kocatepe Üniversitesi, Teknoloji Fakültesi, Metalurji ve Malzeme Mühendisliği Bölümü,
Afyonkarahisar, Türkiye

^abgokce@aku.edu.tr, ^btalas.sukru@gmail.com

Özet

ESD, tarihsel olarak insan eli ile operatörler tarafından yapılan bir kaplama yöntemidir. Uzman bir operatör tarafından sürekli olarak fiziksel işlem parametreleri kaplamının en iyi şekilde yapılması için uygulanır. Elektriksel parametrelerin kontrolü uygun elektrot ve kaplama malzemesinin eşleşmesi ile daha stabil hale gelmektedir. Her bir insan eliyle yapılan ESD kaplamaları arasında farklılıklar oluşmaktadır. Birikme açısı, hareket hızı, uygulama kuvveti gibi sürekli olarak değişen parametreler farklı operatörler tarafından yapılan kaplamalar veya farklı zamanlarda yapılan kaplamalar gibi hususlar, hem elektrik hem de fiziksel olarak parametrelerin etkilerini belirlemek için ESD kaplama sürecinin tam otomatikleştirme ihtiyacını ortaya çıkarmaktadır. Bu çalışmada ESD makinesinin fiziksel kontrol gereksinimlerini karşılamak için 3 eksenli bir CNC makinesi özel olarak üretilmiş ve uygulamalar yapılmıştır.

Anahtar kelimeler: ESD Kaplama, Otomasyon Sistemleri, 3D Sistemler

1. Giriş

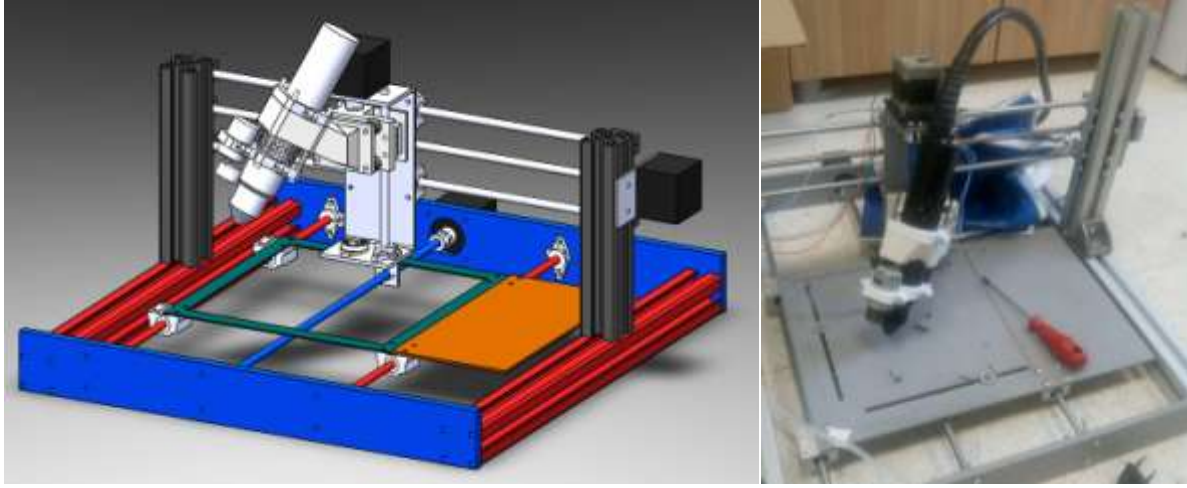
Elektro-kıvılcım birikme yöntemi (Electro Spark Deposition, ESD) bakır elektrotların, kalıpların, türbin kanatlarının, top namlularının ve diğer ekipmanların kullanım ömürlerinin uzatılmasında, tamirlerinde ve geliştirilmesinde aşınma ve paslanmaya karşı dayanıklı kaplamaların oluşturulmasını sağlayan bir mikro kaynak esaslı bir kaplama yöntemidir[1,2]. ESD yöntemi kullanılarak yapılan kaplama veya mikro kaynak yönteminde kapasitif bir boşalma ile eriyen bir elektrotun iş parçası üzerine alaşımın biriktirilmesi sağlanır. Eriyen elektrot malzemesinin taşınımı kıvılcım deşarjı ile plazma şeklinde oluşur. Diğer bir ifade ile tükenen bir elektrotun düşük zamanlı elektriksel palslar kullanarak kaplanacak malzeme yüzeyine aktarılması işlemidir. Pals süreleri bir kaç mikro saniyeden 4kHz gibi bir pals frekanslarında kaplama veya mikro kaynak yapmak mümkündür [3]. Bu yöntemin en önemli avantajlarından biriside, sağlığa zararlı atıklar, gazlar ve akışkanlar üretmemesidir [4,5]. Ayrıca vakum sistemine de ihtiyaç duymadığı için sistem basit bir şekilde kurularak kullanıma hazır hale getirilebilir ve hatta mobil olarak yapılabilmektedir. Kaplanacak metal ve alaşımlarının yüzey hazırlığının yapılmasına da gerek yoktur ve hemen hemen bütün metal ve alaşımlar, seramik ve seramik metal kompozitler bu yöntemle kaplanabilirler [4-7].

Otomotiv endüstrisinde kullanılan çelik saçların nokta kaynağı ile birleştirilmesinde kullanılan elektrotların kaplanması Zhen ve arkd tarafından çalışılmıştır. TiC kaplama elektrotu

kullanılarak yapılan deneylerde elde edilen sonuçlar oldukça başarılı olmuş ve daha sonra Ni ilavesi de yapılarak kaplama dayanımı artırılmak istenmiştir ve kaplama karakterizasyonu da yapılmıştır. ESD yöntemi ile bakır elektrotların titanyum karbür parçacıkları ve metal matrisli nikel kompozitler (TiCp/Ni MMC) ile kaplanması nokta kaynağında elektrot ömürlerini arttırdığı görülmüştür [6-8].

2. Deneysel metod

ESD kaplama işleminin insansız olarak yapılması için 3 eksenli CNC makinesi tasarımı ve üretimi gerçekleştirilmiştir. X, Y ve Z ekseninin hareketini kontrol etmek için ticari olarak temin edilen step motorları kullanmıştır. Universal ESD Machine ile entegre edilen döner aplikatör, Z-ekseni üzerindeki titreşim takozlarının bulunduğu platformuna monte edilmiştir. Şekil 1'de, CNC makinesi ile entegre ESD işleminin bir görüntüsünü göstermektedir. CNC tabanlı kontrol sistemleri ile aplikatörün ESD kaplaması yapılacak plaka üzerindeki hareket hızları ve Z eksenindeki ilerlemesi kademeli olarak kontrol edilmektedir.

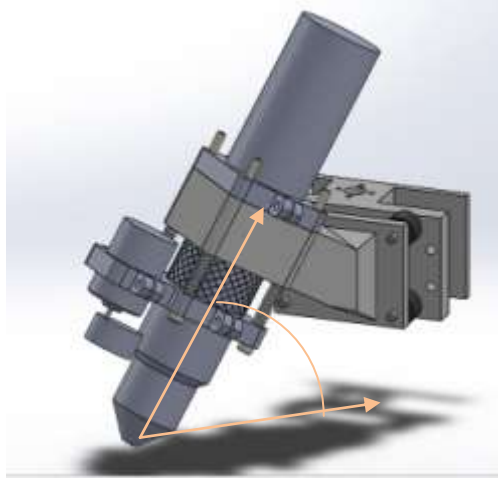


Şekil 1. Tasarımı gerçekleştirilen CNC tabanlı ESD uygulamasının görüntüsü

X, Y, Z kontrol sisteminin kullanılmasıyla dönen elektrot olmadan universal ESD makinesinden ark oluşumunu incelemek için diğer kütle transfer görüntüleri kaydedilmiştir. Elektrotlar sıfırlanmış yüzeyden 0.1 mm aşağı düşürülmüş ve daha sonra elektrotun daha yüksek uygulama kuvvetleri altında kıvılcım atlama oluşup oluşmadığı gözlemlenmiştir. ESD kaplama işleminde gelen ilk kıvılcım, elektrot üzerindeki temas noktalarının alt tabakaya temas ettiğinde gerçekleşmektedir. Potansiyel olarak çok küçük boşluklar kıvılcım oluşumuna ve ısınmaya neden olur ancak ilk temastan sonra, elektrot ileriye doğru hareket etmeye devam ettiğinde temas noktası varsa, ek kıvılcımlar ortaya çıkmaktadır.

Aplikatörün üzerinde bulunan titreşim motoru, elektrotun kaplama yüzeyine temasından itibaren, itici yayların uyguladığı normal kuvvet ile elektrot ve alt metal arasındaki sürtünme direncini azaltarak prosesin sürekliliğini sağlar ve aynı zamanda potansiyel ark boşluklarını kapatmaya yardımcı olmaktadır. Bu uygulamada elektrot, alt tabaka yüzeyine dik olmadığından, yani 60° derecelik bir açı ile durduğundan, yayların sağladığı karşı kuvvet, elektrotun temas yüzeyi

boyunca alt parça üzerinde kaymasını sağlamaktadır. Şekil 2'de gösterildiği gibi daha küçük düşük k katsayısına sahip olan yaylar hareketi kolaylaştırmaktadır.



Şekil 2. Aplikatörün ve Elektrodun alt parçaya temas açısı.

Uygulama, elektrotun tespit edilen ilk temastan itibaren 0.1 mm aşağıya doğru ilerlemesini sağlamış, daha sonra elektrot, 1 mm'lik güvenli bir pozisyona geri çekilmiştir. Elektrot ve alt kaplama metali arasındaki normal kuvvet azaldıkça ve sistemin döngüye devam ederek boşalması ile elektrot küçük yan hareketlere neden olduğundan, başka kıvılcımların üretilmesi de sağlanmaktadır. Elektrot geri çekilirken bir dizi ark oluşumları görülmüştür; elektrot ve yüzey arasında küçük mesafeler olduğunda kıvılcım oluşması ihtimali her zaman vardır. Ancak bu mesafe ESD gerilimi ile doğru orantılıdır. Kıvılcım ve ark yoğunluğu belirlemek için bir dizi parametre seti kullanılmıştır. Şekil 3'de, otomatik ESD işlemi görülmektedir. Elektronik devreler cihazın yan tarafında bulunmaktadır.



Şekil 3. ESD İlk temas görüntüleri ESD parametreleri: 450Hz, 100V.

3. Bulgular ve tartışma

Elektrotun kaplama metali yüzeyi boyunca yapmış olduğu hareket hızı ESD kaplama sürecini önemli ölçüde etkilemektedir. Özellikle, ESD aplikatörünün tasarımına bağlı olarak, elektrodun yan hareketi, elektrotun titreşimi ESD elektrotunun kaplama metali yüzeyine kalıcı olarak yapışmaması için çok önemlidir. Elektrotun döner ve titreşimli olması yapışmayı önlemek ve erimiş elektrot malzemesinin kaplama metali yüzeye atlamasını ve bağlanmasını sağlamak için

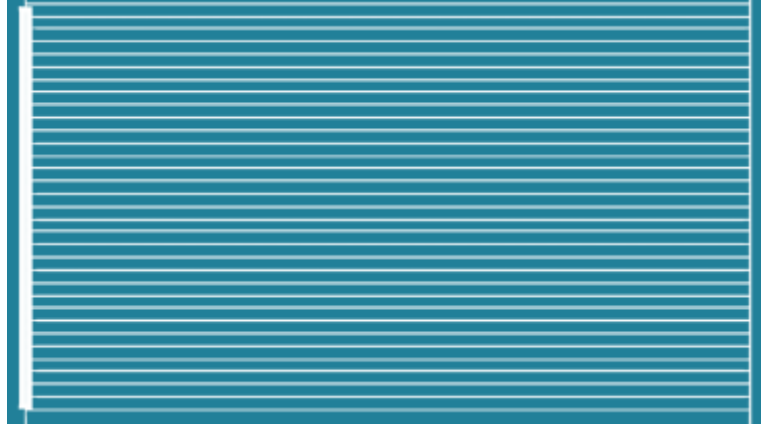
kullanılmaktadır. Bununla birlikte, herhangi bir ek hareket olmaksızın, elektrotun belirli bir yöndeki ilerleme hareketi ESD işlemi sırasında elektrotun yapışmasını engellemektedir.

Elektrotun belirli bir ilerleme hareketi kaplamadaki elektrottan saçılan damlacıkların kıvılcım ile transfer ve bağlanma kalitesini doğrudan etkilemektedir. Elektriksel parametrelere bağlı olarak, yüksek ilerleme hızları yetersiz kaplamalar ile boşlukların oluşmasını sağlamaktadır. Düşük ilerleme hızları ise belirli lokal alanlarda aşırı kaplamaya yol açmaktadır. Kaplamanın olmadığı çıplak alt tabaka alanlarında aşırı biriktirilme veya çok boşluklu kaplama, üst sıra kaplama tabakalarının alt sıra kaplama ile bağlanmasını engellemektedir. Bu durumda yeniden kaplama oluşacak şekilde alanın bozuk bir yapıya sahip olması ciddi bir kusurları oluşturabilir.

Kaplama sırasında ortaya çıkan ısı ve ısı transfer işlemi sırasında, ilerleme hareket hızından büyük ölçüde etkilenmektedir. Kaliteli ve etkili kaplama elde etmek için alt tabakanın ısı girdisinde bir azalma olması gerekir. Daha yüksek ilerleme hızları, aynı ESD parametrelerinde alt tabakaya ısı girdisini azaltır ve sonuç olarak kaplama sırasında çökme süresinin azaltılması, ESD elektrodunun aşırı ısınmasının olumsuz etkilerini azaltmak için önemli bir faktördür.

Bu çalışmada bilgisayarlı bir kontrol sistemi kullanıldığından elektrotun hareket örüntüsü oldukça önemlidir. Elektrotun alt kaplama malzemesi, elektrot çapı, diğer fiziksel ve elektriksel parametrelerin etkileşimi önemli olduğu kadar elektrotun ilerleme yönü ve hareket örüntüsü de kaplamanın kalitesini etkilemektedir. Geliştirilen 3 eksen CNC kaplama sisteminin sınır şartları elektrot hareket örüntüsü için dikkat edilmesi gereken hususlardan biridir.

Kullanılan farklı elektrot hareket desenleri ile çeşitli tarama yanal hareket modelleri geliştirilebilir. Tarama modellerinin geliştirilmesinde CNC'nin hızlanma oranı ve maksimum hareket sınırları dikkate alınmalıdır. Elektrot İlerleme ve hareket desenlerinde yön değişiklikleri sayısı, hızlanma ve yavaşlama olaylarını azaltmak için hareket deseni modellerinde yapılan değişiklikler, kaplamaların homojenliğini artıracaktır.



Şekil 4. Uygulamada kullanılan standart tarama deseni

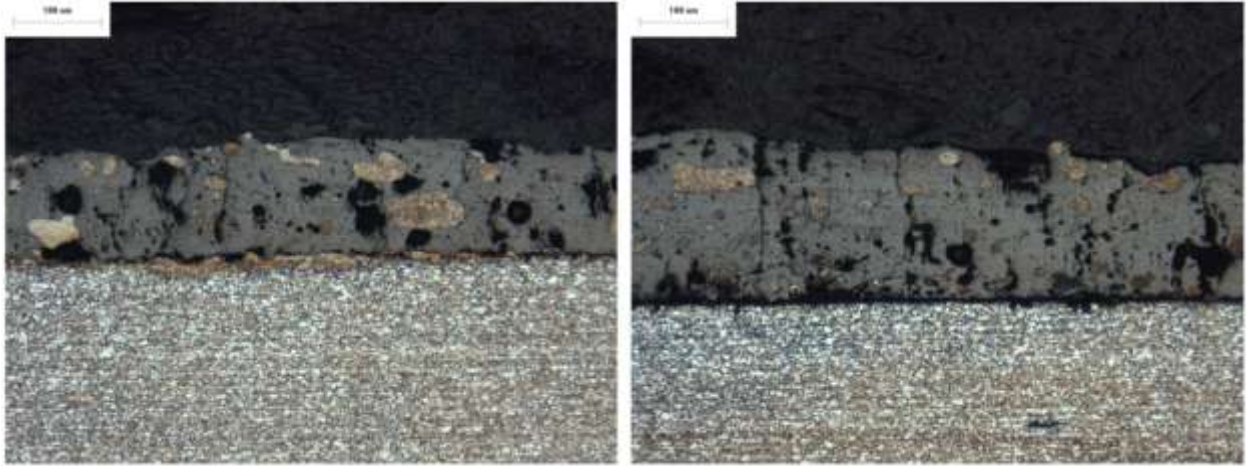
CNC tabanlı otomatik ESD kaplamanın test edilmesi için 0.2mm'lik standart kare model bir test uygulaması gerçekleştirildi. Uygulamada Şekil 4'te verilen standart tarama deseni kullanılmıştır. Kaplama işlemi için 5x5 mm'lik bir alanın üzerinde, 0.001mm'lik Z ekseninde sabit bir doğrusal adım ile kaplama metaline doğru ilerleme hareketi yapılmıştır. Toplam tarama için 0.25 mm'lik bir Z ekseninde aşağıya doğru ilerleme $\sqrt{2}$ toplam kaplama için 0.5mm'lik bir genişlik kullanılmıştır. Elektrotun ilk teması için başlangıçta 0.1mm'lik bir ilerleme aplikatörün Z

ekseninde aşağı doğru hareketi için eklenmiş ve daha sonra alt kaplama metalinde X- eksen yönünde bir tarama yapılarak, y yönünde de bir tarama gerçekleştirilmiştir. Tablo 1'de, CNC kontrolüyle gerçekleştirilen kaplama uygulaması için elektrik parametrelerinin etkisini belirlemek amacıyla kullanılan uygulama parametreleri verilmiştir.

Tablo 1. CNC Tabanlı ESD kaplama uygulaması

Test No	Gerilim (V)	kapasitans (UF)	Şarj hızı%	Frekans (Hz)
1	50	100	40	175
2	50	100	60	250
3	50	100	90	450
4	100	100	40	175
5	100	100	60	250
6	100	100	90	450

Şekil 5'deki CNC tabanlı otomatik kaplama ile yapılan kaplamanın kesit görüntüleri verilmektedir. Standart ilerleme modeli ile ESD kaplaması kullanırken kaplamaların kenarındaki yığılma etkisini gösterilmektedir. Kenardaki artan birikme süresi, yavaşlama ve hızlanma durumları ile yatay ilerleme geçişi arasındaki kademeli harekete bağlı olarak değişmektedir.



Şekil 5. CNC tabanlı otomatik kaplama ile yapılan kaplamanın kesit görüntüleri a) 50V, 540Hz ve b) 100V, 450Hz

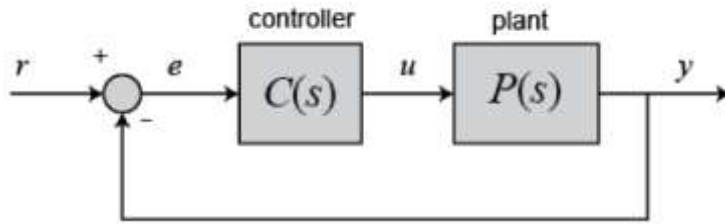
ESD kaplama sırasında operatörün uygulama gücü oldukça hassastır ancak insan hassasiyeti bile bir süre sonra sorun olabilmektedir. Bu durum hem otomatik hem de manuel işlemler sırasında büyük bir sorun olabilmektedir. ESD elektrotunun periyodik olarak aralıklı temasını korumak için bazı küçük uygulanan kuvvet gereklidir; aşırı kuvvet elektrotun kısa devre yapmasına ve ark'ın kesilmesine neden olmaktadır. Elektrotun ilk temasında, Z ekseninde aşağı doğru doğrusal bir artış ile başlanmıştır. Standart ilerleme modelinde ilk temaslarda kaplamalar meydana

gelmiştir ancak elektrot ısındığı zaman, birikme oranında değişiklikler gözlemlenmiş ve Z-ekseninde ilerleme oranında etkisiz hale getirmiştir.

Z eksenindeki ilerleme oranı, elektrot boyu, elektrot ve alt kaplama malzemeleri ile elektriksel parametreler ile doğrudan ilgilidir. Yani bu parametrelerden bağımsız değildir. Z-eksenindeki aşağı doğru ilerleme oranının, yatay eksenindeki ilerleme modelinin ark uzunluğuna göre her milimetresi için belirli bir elektrot aşağı ilerleme oranının olduğu belirlenmiştir.

Kuvvet geri beslemesi için bir kapasitif kuvvet sensörü, geliştirilen CNC sistemine entegre edilmiştir. Kapasitif kuvvet sensörden veri toplama işlemi 0.5V ile 1.5V arasındaki gerilimler ölçülerek sağlanmıştır. Veri toplama işlemi Windows tabanlı veri toplama yazılımları ve kullanıcı arayüzleri ile yapılmıştır. Kuvvet sensörü kaplama yapılacak plakanın alt yüzeyin altına konumlandırılmıştır. Kuvvet düz olarak uygulandığında iyi sonuç vermektedir. Ancak bu konum, kuvvet sensörünün, yay sisteminden gelen gürültü etkileri olmadan elektrot ile alt malzeme arasındaki normal kuvveti veya okumaları etkileyen Z eksenindeki sorunların tespit etmesini sağlamaktadır.

Kuvvet verisinden elde edilen bilgi ile aplikatörün z eksenindeki ileri hareketindeki değişim kontrol etmek için bir oransal-integral-türev veya PID kontrolörü tasarlanmıştır. PID sistemi, kontrol sürecinde bir sonraki süreci değiştirmek için son kaydedilen işlemde gelen hatayı geri besleyerek çalışmaktadır. CNC kuvvet geri besleme sistemi ile Şekil 6'da verilen sistem ESD sistemine bağlı olarak istenen kuvvet r girişi olarak ayarlanmıştır. Anlık kuvvet PID kontrolörüne y olarak verilir ve kontrol sinyali ise z eksenin mevcut konumudur. Kontrol sinyali G kollarına dönüştürülerek seri bağlantısı üzerinden GRBL kontrolörüne gönderilmiştir.



Şekil 6. Genel PID geri besleme sistemi

GRBL yazılımı USB seri bağlantısı üzerinden iletişim kurmak için kullanılmıştır. Bu dahili arabirim, kontrol modeli geliştirme yazılımı, programının G-Kodu gönderen yazılımına kuvvet sensörü ile arka plan işlemleri yürütmesini sağlamaktadır.

4. Sonuçlar

ESD kaplamalarının tamamının homojen ve kaliteli bir şekilde doğru yapılması için elektriksel parametreler oldukça önemlidir. Elektriksel parametreler dikkate alınarak kuvvet geri beslemeli ve otomatik kontrol sistemlerinin kullanılması ihtiyacını doğurmaktadır. Dahası, otomatik kaplama sistemlerinin kullanımı, endüstriyel ESD uygulamalarının kalitesini ve tekrarlanabilirliğini artıracaktır.

ESD güç kaynaklarında pils üretiminin temellerine dayanarak, voltajın artırılması ve frekans güç çıkışı üzerinde en önemli etkiye sahip olmaktadır. Kaplama sırasında elektrottan kaplama malzemesine malzeme transfer oranları, bozuk kaplamanın veya malzeme transferinin oluşması, kaplama oksidasyonu ile güç çıkışına bağlı olarak ısı üretimi ile ilişkilidir. Koruyucu gaz

kullanımı, yüksek güçlü parametrelerin kullanılmasına izin veren oksidatif etkileri kısmen veya tamamen ortadan kaldırılabılır veya hafifletebilir böylece kaplama oranı arttırılabilir.

Bu çalışma, mevcut bir ESD güç kaynağı kullanarak CNC tabanlı otomatik kaplama sisteminin geliştirilmesini sağlanmış ve evrensel bir kontrol sisteminin geliştirilmesinde etkili fonksiyonlar ve parametreler belirlenmiştir.

5. Teşekkür

Bu çalışma Afyon Kocatepe Üniversitesi Bilimsel Araştırma Projeleri Koordinasyon Birimi 17.KARİYER.230 nolu projesi ile desteklenmiştir.

6. Referanslar

- [1] J. L. Reynolds, R. L. Holdren, and L. E. Brown: "Electro-spark deposition", *Advanced Materials and Process*, 161(3) (2003), pp.35–37.
- [2] P. Z. Wang, G.S. Pan, Y. Zhou, J. X. Qu, and H.S. Shao: Accelerated electrospark deposition and the wear behavior of coatings, *Journal of Materials Engineering and Performance* 6(6) (1997), pp. 780–784.
- [3] A. Gangadhar, M.S. Shunmugam, P.K. Philip: Pulse Train Studies in EDM with Controlled Pulse Relaxation, *International Journal of Machine Tools & Manufacture*, 32/5 (1992) pp. 651-657.
- [4] J.L. Reynolds, R.L. Holdren, L.E. Brown: Electro-spark deposition, *Advanced Materials & Processes*, 161/3 (2003), pp. 35-37.
- [5] R. N. Johnson: Electro spark deposition: principles and applications, *Society of Vacuum Coaters, 45th Annual Technical Conference Proceedings, USA*, 87-92, (2002).
- [6] L. Naiming, L. Maolin, Z. Jiaojuan, ve arkd: Study on Fabrication and Corrosion Resistance of Ni-Based Alloy Coating on P110 Steel by Electro Spark Deposition, *Journal of Materials Engineering and Performance*, 22/5 (2013), pp.1365-1370.
- [7] C. Zheng, Y. Zhou: Surface modification of resistance welding electrode by electro-spark deposited composite coatings: Part I. Coating characterization, *Surface & Coatings Technology*, 201/3-4 (2006), pp.1503-1510.
- [8] Z. Chen, Y. Zhou: Surface modification of resistance welding electrode by electro-spark deposited composite coatings: Part 2. Metallurgical behaviour during welding, *Surf. Coat. Technol.* 201(6) (2006), pp.2419–2430.

SORUMLU YAZAR ADRESİ: Barış Gökçe, Afyon Kocatepe Üniversitesi, Teknoloji Fakültesi, Mekatronik Mühendisliği, +902722241418, bgokce@aku.edu.tr.

KISA BİYOGRAFİLER

Barış Gökçe – Yardımcı Doçent Dr. Barış Gökçe, Afyon Kocatepe Üniversitesi, Teknik Eğitim Fakültesi Metalurji Eğitimi Bölümü'nden mezun oldu. Yüksek lisansını Afyon Kocatepe Üniversitesi Fen Bilimleri Enstitüsü'nde tamamladıktan sonra, Afyon Kocatepe Üniversitesi Fen

Bilimleri Enstitüsü'nden doktora derecesini metalürjik süreçlerin istatistiksel optimizasyonu üzerine aldı. Çoğunlukla mekanik sistemlerin simülasyonu ve kontrolü üzerinde çalışmaktadır.

Şükrü Talaş – Prof. Dr. Şükrü Talaş, 1993 yılında Marmara Üniversitesi Teknik Eğitim Fakültesi Metalurji Eğitimi Bölümü'nden mezun oldu. Yüksek Lisansını 1997 yılında Brunel Üniversitesi'nde tamamladıktan sonra 2002 yılında İngiltere Leeds Üniversitesi'nden C-Mn-Ti içeren Kaynaklı Çelik Mikroyapıları konusunda doktora derecesini aldı. Afyon Kocatepe Üniversitesi Metalurji ve Malzeme Mühendisliği Bölümünde Profesör olarak görev yapmaktadır.

THE INFLUENCE OF THICKNESS OF INTERLAYER MATERIALS: BONDING TIME AND BONDING PRESSURE ON BONDING STRENGTH IN DIFFUSION WELDING

Ömer Faruk Özbilen^{1,a}, Ali Gürsel^{1,b}, Enes Akca^{2,c}

¹Department of Mechanical Engineering, Faculty of Engineering, Duzce University

²Department of Mechanical Engineering, Faculty of Engineering and Natural Sciences, International University of Sarajevo

^afarukozbilen@gmail.com, ^baligursel@yahoo.com, ^cenesakca@hotmail.com.tr

Abstract

In this study, some of the joining characteristics of diffusion bonding that thickness of interlayer materials, bonding time and bonding pressures and their influences were investigated in comparatively. There are some materials such as Copper, Zinc, Nickel and their alloys that generally were used on similar researches. The present work shows that when the thickness of interlayer is being increased as a consequence of that the strength of the bonding (shear strength in specific) with two materials is not changed. Nevertheless, diffusion layers are wider with an increase in temperature and wider diffusion zone can be obtained by increasing bonding time (until a specific level).

Key Words: Diffusion bonding, Cu interlayer, Zn Interlayer, Ni Interlayer, Bonding Shear Strength

1.Introduction

Diffusion bonding method is an alternate technique to join like and unlike materials with minimum dimensional tolerance. It is the solid state process in which two metallic surfaces are made to contact at the elevated temperature and pressure. Diffusion bonding process provides high eminence joints without post weld machining. The main process parameters of diffusion bonding embrace temperature, pressure and holding time. It is significant that the metallic surfaces should be spotless and free from oxides and nonmetallic films. In diffusion bonding technique microstructural changes were formed in the base metal which determines the mechanical properties of the bond at the interface. Diffusion bonding method can be used to weld the dissimilar materials with different chemical and mechanical properties. The present work reviews the influence of process parameters on diffusion bonded joints of dissimilar materials in the midst of and with no interlayer. Examination on the microhardness, laps hear and microstructures were made for various dissimilar diffusion bonded joints and finally some general conclusions are summarized [1].

Diffusion bonding is a solid state welding process employed joining the materials through the formation of bonds at atomic level at elevated temperatures and below the melting point of the metals in controlled or inert atmospheres. Diffusion bonding is relatively simple joining process, which is controlled by three important process parameters. They are bonding temperature, bonding pressure and holding time. In addition, these three parameters are interrelated and thus have an effect on each other [2].

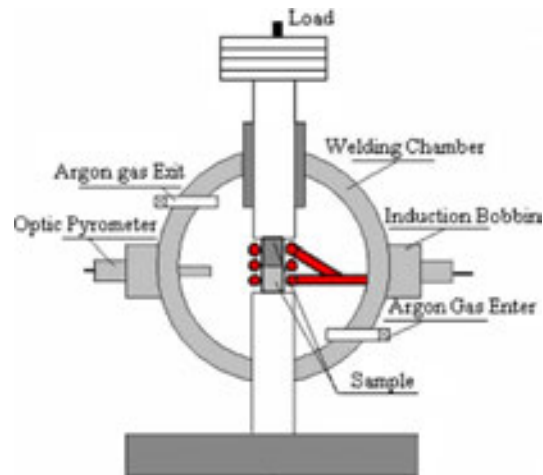


Figure 1. Schematic representation of the diffusion bonding apparatus. Adopted from[5]

2. Theoretical Procedure and Method

L.M. Zhao and Z.D. Zhang (2008) investigated that diffusion-bonding with a right interlayer is an effective solution to join dissimilar metals. Shear strength tests were carried out on samples with Mg-Al joints with only Zinc[3].

The maximum shear strength of Mg–Al joints using diffusion bonding directly is 41.3 MPa and it is not good. To increase the strength of Mg–Al joint, Zn alloy interlayer is adopted. The interlayer is prepared by alloying zinc with Al and Ce. They experimented that Zn alloy interlayer was prefabricated firstly on the surface of Al base sample by hot-dipping at 450 °C with a thickness of about 60 μm. Then all the bonding surfaces of samples were ground flat by 200 #, 400 #, 600 # grit SiC paper and cleaned in ethanol or acetone prior to diffusion-bonding. The thickness of Zn alloy interlayer after grinding is about 30 μm. They stated that by comparing interface structure and shear strength of diffusion-bonding of Mg–Al with and without Zn alloy interlayer, it can be concluded that the direct contact of Mg–Al cannot avoid a large number of Mg–Al intermetallic compounds which reduce mechanical performance of joints greatly. Shear strength tests were carried out on samples of the Mg–Al joints diffusion-bonded with Zn alloy interlayer at the same joining conditions. The lowest value is 75 MPa and the highest is 83 Mpa, which is twice that of the Mg–Al joints diffusion-bonded directly[3].

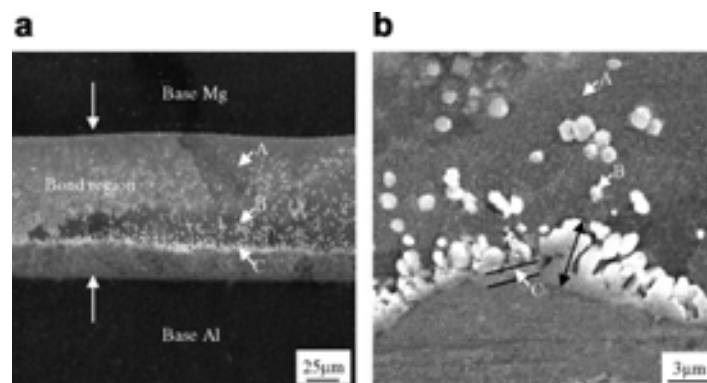


Figure 2. SEM images of Mg–Al diffusion-bonded with a Zn alloy interlayer at 360 °C for 3 s: (a) cross-section of the whole bond region; (b) high magnification of the bond region of the joint. Adopted from [3]

Peng He et al. (1999) bonded Titanium alloy and stainless steel 18Cr10Ni with Nickel interlayer of 30 μm thickness at a mixture of temperature ranging from 750 to 910 C with a holding time 5 to 30 min at 15MPa[4]. They saw that seen that a certain amount diffusion occurs between the interlayer and the parent metal and new-fangled phases formed at the interface. Also observed that the diffusion distance from the Ni to Ti alloy is long which indicates that a metallic compound film is formed by the diffusion layer. Diffusion layers are wider with an increase in temperature [4].

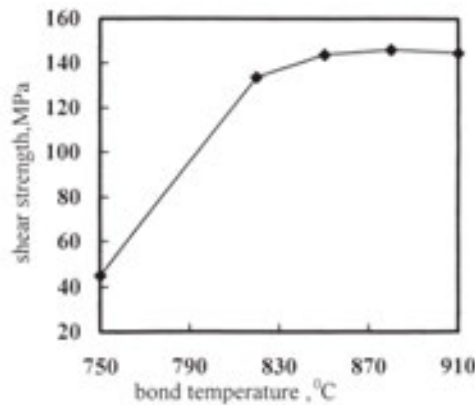


Figure 2. Effect of the bond temperature on the shear strength of the bond joint. Adopted from [4]

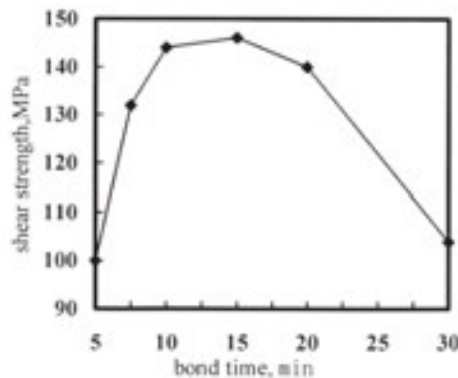


Figure 3. Effect of bond time on the shear strength of the bond joint. Adopted from [4]

It can be seen that when t is 5–10 min, the shear strength increases rapidly; when t is 10–15 min, the shear strength changes little, and with an increase of t , the shear strength is higher; when t is more than 15 min, the thickness of Ni–Ti metallic compounds increase remarkably, and the shear strength of the bond joint decreases[4].

Ti alloy and stainless steel were diffusion-bonded with copper as interlayer by Ozdemir(2009), and it is revealed that the shear strength increased with increase in the process temperature and holding time[5]. At low temperatures and holding times, bonding strength is lower due to imperfect diffusion of the mating surfaces. Maximum shear strength of 118 MPa was obtained in a sample bonded at 870 °C, bonding pressure of 1 MPa, and holding time of 90 min due to better diffusion of mating surfaces. The increase in the shear strength may be attributed to high diffusion rate of copper into Ti alloy under the conditions specified. The specimens of Ti-6Al-4V and AISI 304 were cut into specimens of 15×15×30 mm. Copper interlayer with dimensions of 15×15 mm were cut from a 60 μm thick plate [5].

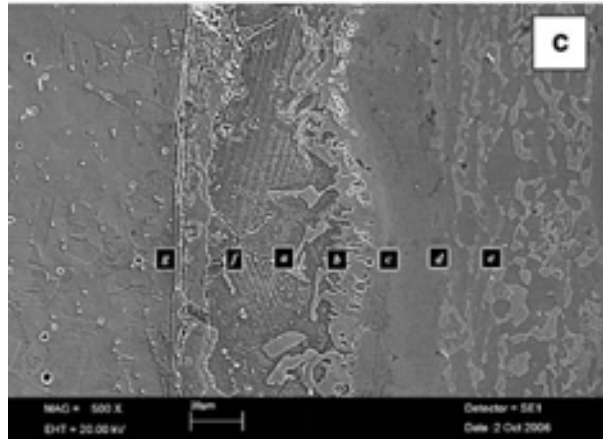


Figure 4. SEM micrographs of the interface zone of diffusion bonded Sample S9. Adopted from [5]

Table 1. EDS analysis results taken from on the point a, b, c, d, e and f of specimen S9. Adopted from [5]

	Alloy (% Atomic)					
	Al	Ti	Cr	Ni	Fe	Cu
A	5.11	26.43	-	-	-	68.46
B	0.72	41.83	-	-	-	57.45
C	4.23	64.68	-	-	-	31.08
D	9.55	84.13	-	-	-	6.32
E	9.42	90.58	-	-	-	-
F	6.82	28.15	-	-	-	65.03
G	-	-	19.48	7.28	73.24	-

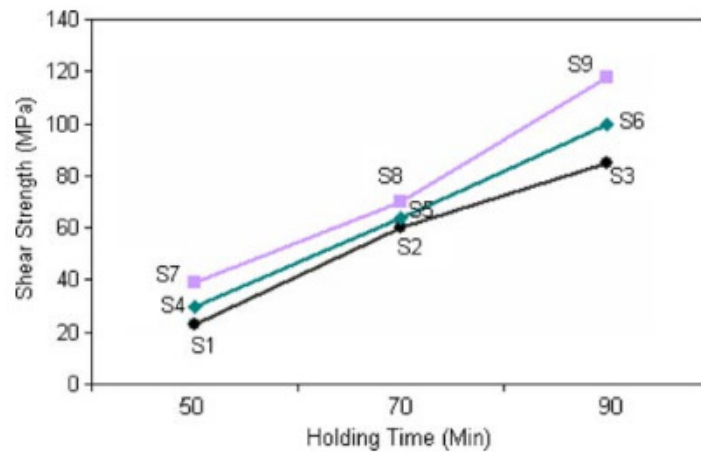


Figure 5. The shear stress- holding time relation of S9. Adopted from [5]

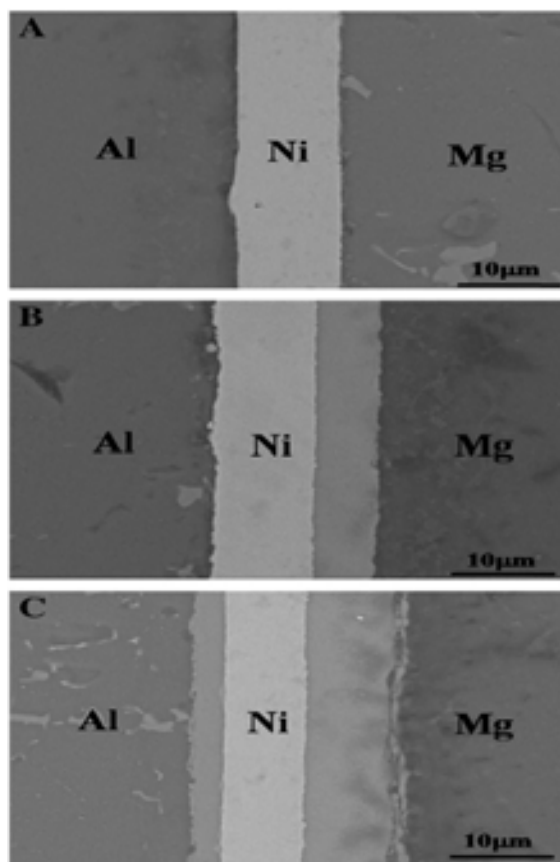


Figure 6. Microstructure evaluation at different holding time, (A) 30 min, (B) 60 min, and (C) 90 min. Adopted from [6]

J.Zhang, G. Luo, Y. Wang, Q. Shen, L. Zhang (2012) were investigated to bond aluminum and magnesium using a Ni interlayer for the first time[6]. The samples were cut into size of $\varnothing 25$ mm \times 5 mm. The interlayer metal used was N6, the major chemical composition was Ni (≥ 99.9 wt.%). The thickness of N6 was 10 μ m. The thickness of N6 was 10 μ m. Samples bonded at 440 $^{\circ}$ C under 1 MPa are studied in order to understand the microstructure changes in the diffusion zone[6]. It can be seen that at the holding time of 30 min (Fig. 6A), the reactions in the Mg–Ni and Al–Ni interface are not obvious. At the 60 min, it can be obviously seen in the Mg–Ni reaction layer and in the Al–Ni interface, a discontinuous reaction layer is also generated (Fig. 6B). In Figure 6C, both the thickness of the Mg–Ni and Al–Ni reaction layer increase, the joint is well-bonded and free from cracks and discontinuities can be seen.

3. Results and Conclusions

Based on the above discussions the following conclusions may be drawn.

Different experimental parameters were used such as pressure time, temperature, different interlayers and different alloys as interlayer. The samples in the experiments were done according to specimen standards. All of this parameters effect shear stress and the quality of bonding operation.

30 μm Zinc-alloy interlayer was used to join Magnesium and Aluminum by L.M. Zhao and Z.D. Zhang. By using Zinc-alloy instead of Zinc only, the shear stress increased considerably.

Same thickness of interlayer (30 μm) material as Nickel was used by Peng He (1999) to bond Titanium alloy and stainless steel 18Cr10Ni.

The shear strength increased with increasing process temperature and holding times in the experiment of Ozdemir (2009). The highest shear strength of 118 MPa was obtained in sample S9 (Figure 5) bonded at 870°C and holding time of 90 minutes due to better coalescence of mating surface.

All of experiments demonstrate us that shear strength is increased with increasing of temperature in the process by bonding with different interlayer materials. To evaluate for the bonding time aspect, it is obligated to keep the time at optimum level to make the best bonding with two different materials. When the time is being longer, the shear strength of bonding reduces remarkably. But the thickness of the interlayer does not affect the bonding strength.

4. References

- [1] G. Ramesh, V. C. Uvaraja, R. Santhosh Raj, A. Santhosh, K. R. Suraj: Persuade Of Development Parameters on Diffusion Coupled Joints of Dissimilar Materials – An Analysis, *International Journal of Advance Research, Ideas and Innovations in Technology*, 3 (2017), pp. 523-527.
- [2] N. Ravinder Reddy, V.V. Satyanarayana, M. Prashanti, N. Suguna: Application of TRIZ Methodology in Diffusion Welding System Optimization, *Management Systems in Production Engineering*, 25(2017), pp. 237-240.
- [3] L.M. Zhao, Z.D. Zhang: Effect of Zn alloy interlayer on interfacial microstructure and strength of diffusion-bonded Mg–Al joints, *Scripta Materialia*, 58 (2008), pp. 283-286.
- [4] Peng He, Jiuhai Zhang, Ronglin Zhou, Xiaoqiang Li: Diffusion Bonding Technology of a Titanium Alloy to a Stainless Steel Web With an Ni Interlayer, *Materials Characterization*, 43 (1999), pp. 287–292.
- [5] N. Ozdemir, B. Bilgin: Interfacial properties of diffusion bonded Ti-6Al-4V to AISI 304 stainless steel by inserting a Cu interlayer, *The International Journal of Advanced Manufacturing Technology*, 41 (2009), pp. 519–526.
- [6] J. Zhang, G. Luo, Y. Wang, Q. Shen, L. Zhang: An investigation on diffusion bonding of aluminum and magnesium using a Ni interlayer, *Materials Letters*, 83(2012), pp. 189-191.
- [7] E. Akca, A. Gursel: The Effect of Diffusion Welding Parameters on the Mechanical Properties of Titanium Alloy and Aluminum Couples, *Metals*, 7 (2017), pp. 22.
- [8] E. Akca, A. Gursel: Influences of argon gas shielding on diffusion bonding of Ti-6Al-4V alloy to aluminum, *Revista de Metalurgia*, 53 (2017), pp. 088.
- [9] E. Akca, A. Gursel: Joining of dissimilar metals by diffusion bonding: Titanium alloy with aluminum, *Materials Testing*, 59 (2017), pp. 330-337.
- [10] E. Akca, A. Gursel: The importance of interlayers in diffusion welding – A review, *Periodicals of Engineering and Natural Sciences*, 3 (2015), pp. 12-16.

CORRESPONDENCE ADDRESS: Ali

**Gürsel, Düzce Üniversitesi Konuralp Yerleşkesi Konuralp Merkez/Düzce, +90 506 206 31 61,
aligursel@duzce.edu.tr, aligursel@yahoo.com.**

SHORT BIOGRAPHIES

Ömer Faruk Özbilen – Omer Faruk Ozbilen was born in Bolu, Turkey in 1991. He received the bachelor degree in mechanical engineering from Uludag University in Bursa, Turkey in 2014. He started the master degree in mechanical engineering at Duzce University in 2017. He has been working in automotive sector for two and a half years, and he is currently working on diffusion welding applications for master's thesis.

Ali Gürsel – Dr. Ali Gursel was born in Gaziantep, Turkey in 1971. He acquired his bachelor and graduate degrees from Gazi University in Ankara, Turkey. He worked for the government and diplomatic missions, regarding educational issues and international projects. He managed to Duzce Technopark as General Director, between 2012 to 2013. He involved a project for defense materials as a research fellow at The City College of New York, USA (in 2013-2014). Dr Gursel followed his career on managerial and academic positions at the International University of Sarajevo, Bosnia and Herzegovina as Vice Rector and Director of Research Center besides his academic duties as Associate Professor in the Department of Mechanical Engineering. Dr Gursel is presently Associate Professor at Duzce University Department of Mechanical Engineering. His research areas are material science and material processes, composite materials, metallurgy, welding and joining technologies, weldability of dissimilar materials, solid state welding, adhesive bonding etc.

Enes Akca – Enes Akca, born in Istanbul in 1990, acquired his B.S. and M.S. degrees from the International University of Sarajevo, Bosnia and Herzegovina. He has been employed as academic staff at that university since the beginning of 2015 and is now Senior Assistant in the Department of Mechanical Engineering as well as a PhD candidate. He is also serving administrative duties as Mechanical Engineering Laboratory Assistant at the Research and Development Center of the International University of Sarajevo. His research areas include materials science, metallurgy, welding and joining technologies. Enes Akca is author of several journal-papers published in SCI journals.

3D SURFACE MORPHOLOGY AND ROUGHNESS ON TREATED SURFACE OF TI-6AL-4V ALLOY BY ND:YAG LASER: EFFECT OF SPOT SIZE

Ali GURSEL

Düzce University, Faculty of Engineering, Department of Mechanical Engineering,
Konuralp Yerleşkesi, B Blok 207, 81620 Düzce, Türkiye

aligursel@duzce.edu.tr, aligursel@yahoo.com Tel: +90 380 542 1036 Fax: +90 380 542 1037

Abstract

In this study, a 1.5 mm thick Ti-6Al-4V alloy plate surface was treated by SigmaLaser@300 Nd:YAG pulsed laser. The Nd:YAG laser parameters, such as spot size and shape, pulse energy and duration, travel speed, peak power and frequency of repetition, influence directly or synergistically the quality of pulsed seam welds and their morphology. Titanium and its alloys lead to successful application in various fields including the medical and aerospace industries due to the excellent corrosion resistance, high strength to weight ratio and high operating temperature. Among the reliable treatment techniques, laser surface treatment can provide significant advantages for the titanium alloys because of its precision, rapid processing capability and ability to control the parameters and their effects. Surface morphology and roughness are analyzed using Hirox 3D microscope, and the influence of the spot size was investigated. The seam and surface quality were characterized in terms of their morphology and microhardness.

Key Words: Ti-6Al-4V alloy – Nd:YAG laser – surface treatment – roughness

1. Introduction

Lasers have become one of the most multi-functional and powerful tool for materials processing. The laser system is also widely used in the repair of cutting and molding tools **Hata! Başvuru kaynağı bulunamadı..** Laser surface treatment has the greatest growth potential in the field of laser materials processing. Laser surface treatments offer a wide range of possibilities to achieve desired surface properties. The aim of surface treatment is to improve wear resistance, surface strength for load carrying (crush resistance), fatigue life and impact resistance, and to induce suitable residual and compressive stresses, etc. It's well known that the most of welding techniques are widely used for surface coating and treatments.

Titanium and titanium alloys are mostly used in the aerospace, biomedical, nuclear, defense and automotive industries due to their low density, good corrosion resistance and high operating temperature **Hata! Başvuru kaynağı bulunamadı..** Among the titanium alloys, Ti-6Al-4V is the best known, but with its features of strength, low thermal conductivity and high chemical reactivity, it is a difficult material to process using conventional machining and welding. Ti-6Al-4V alloy is widely used as material for load-bearing and non-load-bearing medical implants because of its excellent biocompatibility and corrosion resistance. Although its low hardness and poor wear resistance are still serious concerns, the majority of intended Ti-6Al-4V implant applications do not require very high wear resistance. Laser treatment can be used to solve these problems.

Joining Ti-6Al-4V alloys using pulsed Nd:YAG (neodymium-doped yttrium aluminum garnet) laser welding method was achieved by Akman et al. They showed that controlling of the laser

output parameters can change results precisely. Blackburn et al. **Hata! Başvuru kaynağı bulunamadı.** produced welds with high internal quality in Ti-6Al-4V alloy by using a laser as the source for the welding technique. They observed the common periodic behaviors in the vapor plume and keyhole under low-porosity welding conditions.

The special features and potential of laser welding technique provide many advantages, such as high scanning velocity, narrow heat-affected zone (HAZ), low distortion, excellent controllability and the ability to produce a high-intensity heat source, which is suitable for precision welding. The previous studies on Nd:YAG laser applications, show that it is possible to control the penetration depth and geometry of the laser weld bead by precisely controlling the laser output parameters. Although laser treatments have been widely reported to improve the mechanical and corrosion behavior of different steels and aluminum alloys, relatively few studies have investigated the properties of laser titanium and titanium alloy samples. Laser treatments have been performed with different types of laser sources such as CO₂ laser, Nd:YAG laser, excimer laser and high power diode laser, the latter presenting lower maintenance costs and higher efficiency than the others, representing a clear economical advantage. Thus, Sun et al. performed laser treatments on titanium (Grade 2) samples with a Nd:YAG laser. Ariyaratnam et al. **Hata! Başvuru kaynağı bulunamadı.** also focused on the etched dentin surfaces produced by the Nd:YAG laser, and bonding of resin composite to the laser-treated dentin was not significantly different from untreated dentin despite the fact that the surface roughness of laser-treated dentin was significantly higher than untreated dentin. In another study on wear treatment, a small molten pool is formed by each laser pulse, and within a few milliseconds it re-solidifies. When the pulse frequency is low, seam occurs in a conduction mode and a smooth, shallow molten pool is produced. However, when the pulse frequency is increased, a deeper, wider pool is obtained. The changed seam morphology affects the surface form and hardness as well.

The formation of laser seams and their subsequent quality are the result of a combination of various pulsed laser processing parameters, such as travel speed, average laser power, pulse energy, pulse duration, average peak power density and spot area. This abundance of parameters provides control of the thermal input with a precision not previously obtainable and also permits the application of a wide range of experimental conditions. On the other hand, controlling so many parameters increases the complexity of laser processing. However, effect of parameters on seam morphology and roughness does not take place in the literature.

In this study, surface of Ti-6Al-4V samples with 1.5 mm thickness is treated by SigmaLaser®300 Nd:YAG laser system, and effect of spot size on seam morphology and roughness is analyzed by 3D micrographs and microhardness plot.

2. Experimental

2.1. Materials and Methods

Ti-6Al-4V alloy sheet with chemical composition shown in Table 1 were prepared as 40×20×1.5 mm³ for treatment by the SigmaLaser®300 Nd:YAG laser system.

Table 1. The Chemical composition of Ti-6Al-4V (wt.%)

Components	C	Fe	N	O	Al	V	H	Ti
------------	---	----	---	---	----	---	---	----

Ti-6Al-4V	<0.08	<0.25	<0.05	<0.15	6	4	<0.03	Balance
-----------	-------	-------	-------	-------	---	---	-------	---------

The laser beam is focused on titanium plates and circle shape pulse has been applied to all samples. The spot sizes on the plates were adjusted from 0.2 mm to 1.2 mm. In order to evaluate the effects of spot size on the surface treatment of the Ti-6Al-4V samples, pulse duration, pulse repetition and peak power were determined as 4 ms, 28 Hz and 30% of 13 kW (3.9 kW), respectively. The focal depth parameter of laser applications as -0.2 mm is very common for surface treatment and for the repair of cutting and molding tools. The shallow seams are increasing the cooling rates and rapid cooling rates cause the occurrence of the martensite structure which is desired achievement of surface hardness. Pulse duration is another effective parameter for heat input. For welding applications, it is necessary to increase heat input for penetration depth. Longer pulse duration causes higher heat input. However, in this study, in order to obtain a harder surface for wear treatment, the heat input was limited, and the pulse duration was determined as 4 ms. All laser output parameters are also given in Table 2.

Table 2. Test parameters

Parameter	Values
Pulse Frequency	28 Hz
Peak Power	3.9 kW
Pulse Duration	4 ms
Spot Size	0.2, 0.4, 0.6, 0.8, 1.0, 1.2 mm
Welding speed	50 mm/min
Focal depth	-0.2 mm
Gas and pressure	(99.8%) Argon, 1.5 bar

At high temperatures, titanium is reactive with ambient gases. For this reason, and to protect against atmospheric effects, argon (99.8%) shielding gas was used at 1.5 bars to protect the melted pool from oxidation and porosities until solidification was sufficient. Therefore, it was crucial to use the shielding gas and to set up the nozzle in order to prevent the formation of turbulence on the sample surfaces during the application.

Microhardness measurements were performed according to the seam dimensions and values were obtained from the HAZ. Furthermore, 3D analysis was carried out to observe the morphology and surface roughness of the seams by Hirox 3D microscope KH-8700.

2.2. Surface Roughness Parameters

R_a is derived from the equation 1 in micrometer (μm) when the roughness curve is expressed as a function of y=f(x), considering x-axis to the mean line direction and y-axis to the vertical magnification of the roughness curve in the range of reference length l (see Figure 1a).

$$R_a = \frac{1}{l} \int_0^l |f(x)| dx = \frac{1}{n} \sum_{i=1}^n |y_i| \quad (1)$$

R_z is derived from the distance in micrometer (μm) between the highest peak and the lowest valley in the range of reference length l to the direction of mean line of the roughness curve (see Figure 1b).

$$R_z = R_p + R_v \quad (2)$$

RzJIS is also derived from the summation in micrometer (μm) of the mean value of each distance between the mean line and 5 peaks (Y_p) from the highest one, and the mean value of each distance between the mean line and the 5 valleys (Y_v) from the lowest one, reference length l (see Figure 1c).

$$R_{zJIS} = \frac{|Zp_1+Zp_2+Zp_3+Zp_4+Zp_5|+|Zv_1+Zv_2+Zv_3+Zv_4+Zv_5|}{5} \quad (3)$$

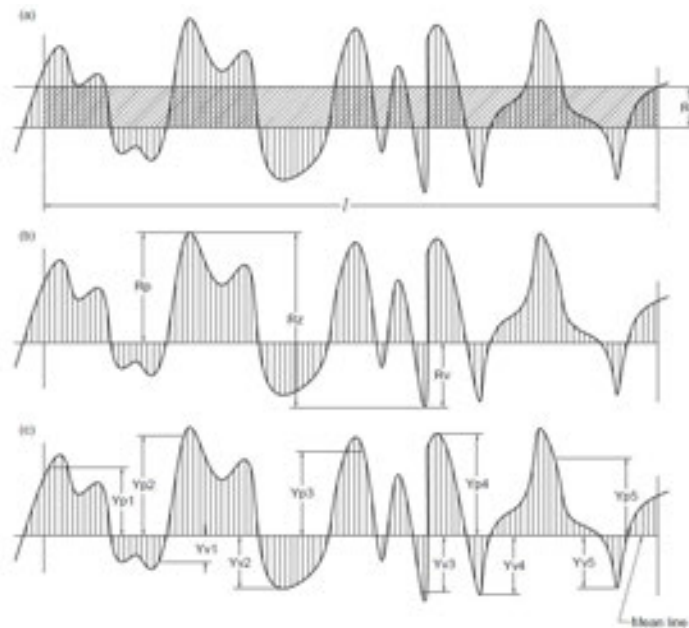


Figure 1: Definition of roughness parameters

3. Results and Discussions

It was previously proven that all parameters such as peak power, spot size, pulse frequency, pulse duration, welding speed and focal depth are affecting the seam morphology and properties; however investigation of seam morphology and roughness is novelty of this study. Spot size is one of the key parameters for the pulsed laser system. For seam geometry and surface hardness, it is crucial to control the pulse energy, in addition to the laser power, spot size, pulse length, and pulse repetition.

3.1. Micro-hardness measurements

Microhardness distributions have been analyzed using a SHIMADZU HMV microhardness tester by applying a load of 100 g. The microhardness test has been carried out at the surface of seams on the centerline of the weld pool, heat affected zones as border of the seam and work pieces, as HAZ of samples. As a result, at the transition zone of the weld seams, the hardness is in the maximum level and the melted and cooled material is compared to the base metal due to its rapid cooling rate (see Figure 2).

In previous studies. for wearing the surface by continuous wave Nd:YAG laser, the average hardness of melted region was higher by 15-22% than the average hardness of Ti-6Al-4V alloy

substrate. this study, it has been reached to 50-300% higher than base metal hardness in melted region by Nd:YAG pulsed laser. The difference in hardness between the transition zone and the base metal is over 700 HV in narrower spot size parameters. Different welding techniques such as electron beam and gas tungsten welding techniques, which were applied on Ti-6Al-4V alloys in previous studies, have shown that high power density of laser beam welding provides a lower heat input and a more rapid solidification when compared to the conventional techniques, so laser welding technique leads to higher hardness value. In heat-affected zone, the cooling rate is higher in transition zone than in weld pools. The difference between the transition zone and base metal is over 800 HV in 0.2 mm to 0.8 mm spot sizes.

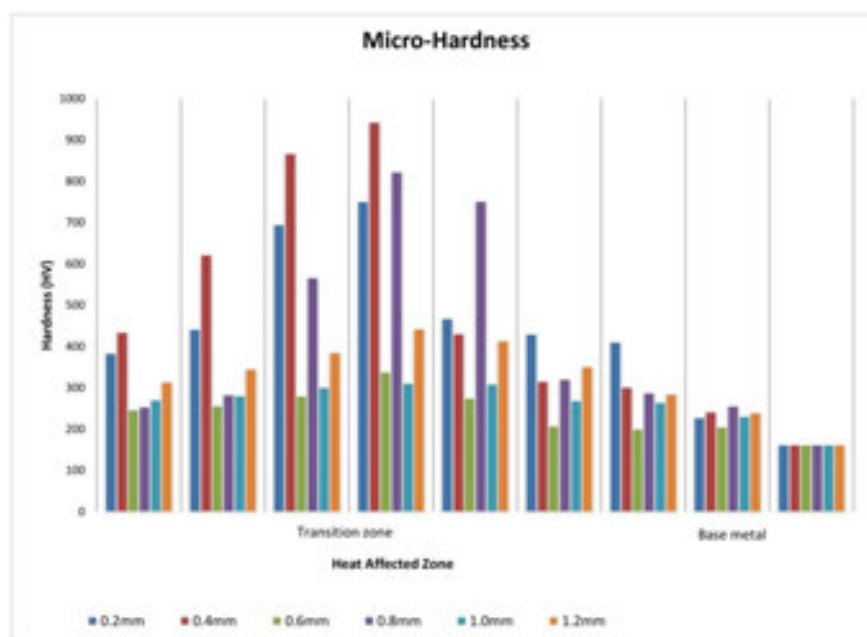


Figure 2: Microhardness distribution for different spot sizes

Higher beam concentration by smaller spot sizes, increased the target temperature producing steeper thermal gradients and severe thermal straining. It was expected that reducing the spot size causes the narrower seam and increases the cooling rate and hardness. High cooling rates cause the formation of martensite in the HAZ region. Therefore, it was obtained in this study while increasing the beam concentration, penetration depth and surface hardness also increased. It was reported by Sundaresan and Janaki that rapid cooling and subsequent martensitic transformation are effective strengthening methods for many titanium alloys. While having the microhardness values of Ti-6Al-4V alloy, the material behaves like a composite structure because of the martensite formation. As a result, overestimated values are occasionally seen during the measuring of microhardness, although average values were seen in this study (Figure 2).

3.2. Seam morphologies and widths

All parameters related to each other and welding or wearing properties. Any change of parameters for pulsed laser system, welding geometry, penetration depth, surface morphology and other properties are affected. If the melt pool is too large or too small, or if significant vaporization occurs during welding, unsuccessful results can be obtained. Therefore, the control

of laser power, pulse repetition, pulse length and spot size are very critical. Penetration depth is increased with increase of peak power, pulse repetition as heat input. However, narrower spot size is also increases the penetration depth because of the concentration of the energy.

In the previous studies, during the regular laser welding process, the spot size was determined as $\cong 0.1-0.7$ mm for Ti-6Al-4V alloy. A narrower fusion zone is an effective parameter, which allows the laser energy concentration to reach a deeper penetration for welding applications, in addition to causing less welding distortion. Owing to observation of the effect of fusion zone, different spot sizes were employed and the results in this study were investigated. It was also observed that while changing the spot sizes, the seam morphologies also changed in Figure 3. At the larger spot sizes, smaller grains sizes and the martensitic structures occurred on the seams, because of the rapid cooling.

Measured seams width is approximately constant (between 1.3 mm and 1.8 mm). This result can be explained with the beam concentration effected the seam depth more than their width. The penetration depth and HAZ are also related to laser peak power and beam concentration. The plasma absorption is very strong at the top of the weld (at the surface of the material), where the available laser energy is high; it leads to increasing of the weld pool and HAZ width larger than spot size (see Figure 3). The same effect has been reported by Weldingh and Kristensen.

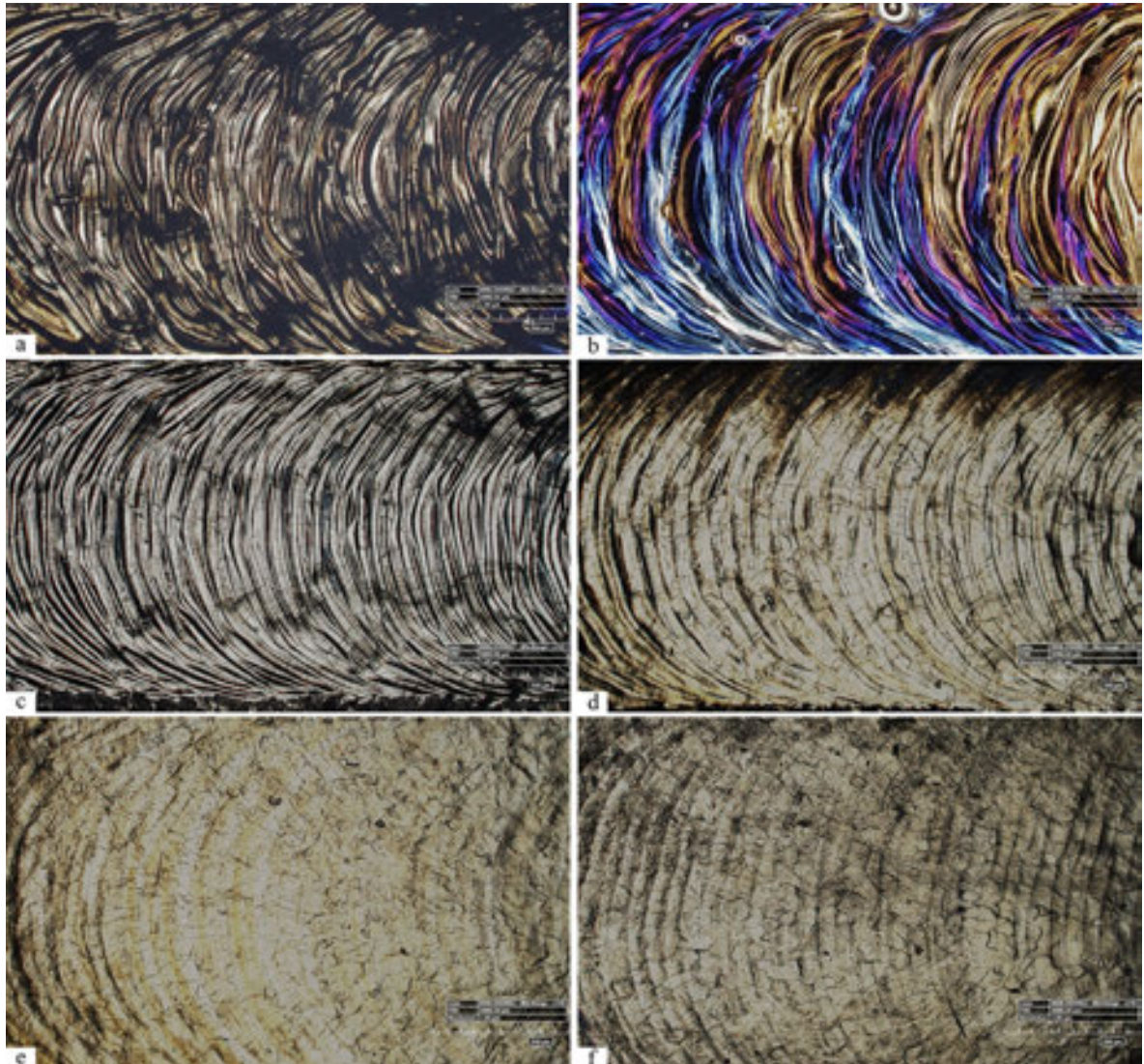


Figure 3: Weld seams of (a) 0.2 mm, (b) 0.4 mm, (c) 0.6 mm, (d) 0.8 mm, (e) 1.0 mm and (f) 1.2 mm spot sizes on Ti-6Al-4V alloy sheet

3.3. Surface roughness

The surface morphology and 3D plots of surface roughness of Ti-6Al-4V after surface treatment is shown in Figure 4. Arithmetical mean, maximum height and ten points mean roughness values were recorded for different spot sizes in Table 3. All roughness parameter values linearly decreased when spot size increased. Effect of the spot size on surface roughness of Ti-6Al-4V is shown in Figure 5. As seen from Figure 5, the values of Ra, Rz and RzJIM approximately decrease linearly with the increasing of the spot size. Narrower spot size is also increases the penetration depth because of the concentration of the energy. Literatures also reported that the surface roughness noticeably increased or decreased with an increase or decrease in different parameters, however effect of spot size on the surface roughness does not have its place in literatures. However, it is noteworthy that surface roughness will tend to reach a stable value with the increasing of spot size. The surfaces get smoother when spot size increases. According

to the above-mentioned results, when the results are correlated, and when optimum hardness and roughness values are considered, it can be concluded that the optimum parameter of spot size can be defined as 0.8 mm.

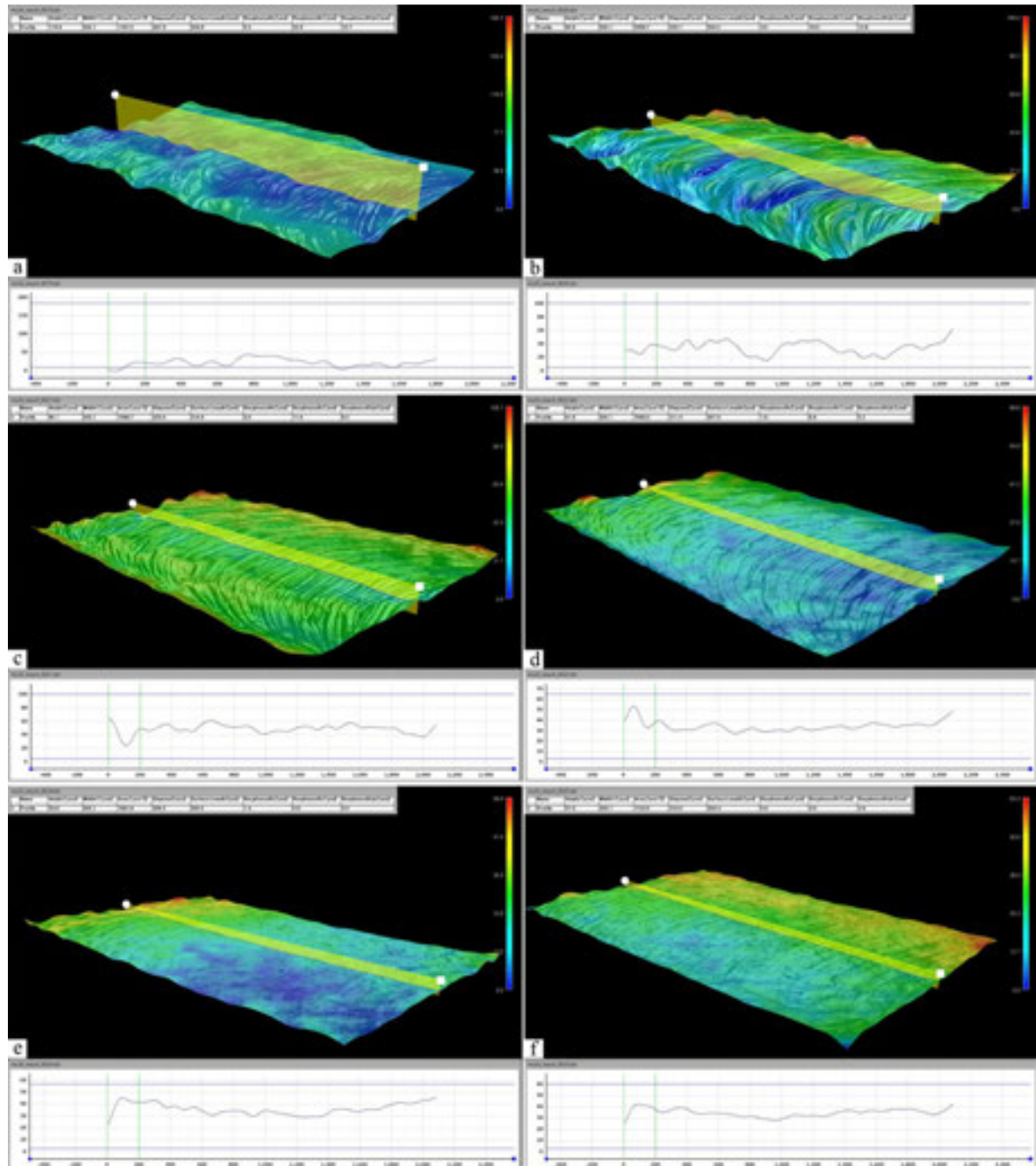


Figure 4: Surface roughness profiles of (a) 0.2 mm, (b) 0.4 mm, (c) 0.6 mm, (d) 0.8 mm, (e) 1.0 mm and (f) 1.2 mm spot sizes

Table 3: Surface roughness values

Arithmetical Mean Roughness Ra (μm)	Max. Height Roughness Rz (μm)	Ten Points Mean Roughness RzJIM (μm)	Spot Size (mm)
5.0	22.9	13.7	0.2
4.9	18.6	12.8	0.4
3.0	11.6	8.5	0.6
1.8	6.9	5.2	0.8
1.4	5.8	4.0	1.0
0.9	4.5	2.6	1.2

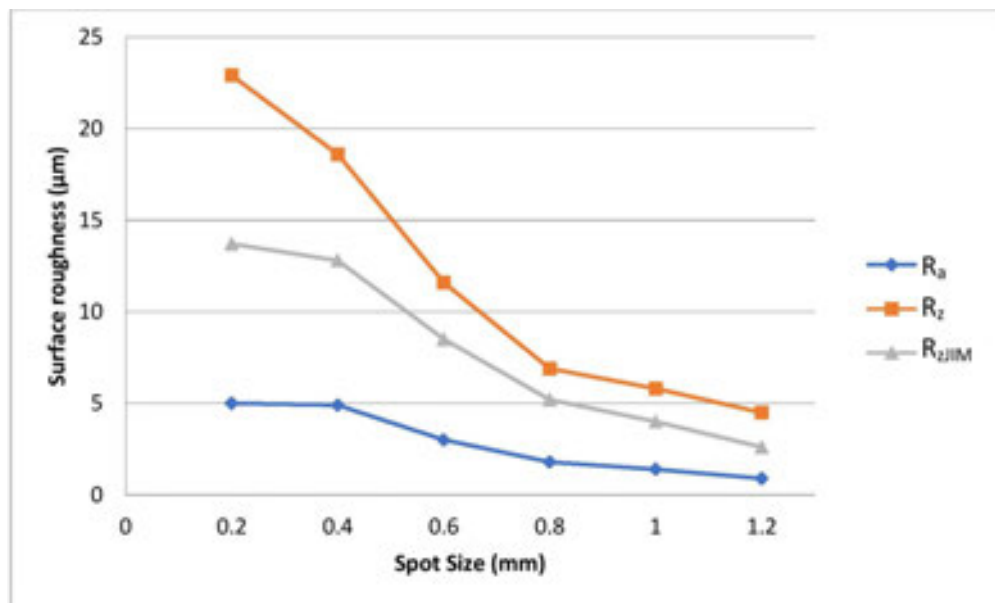


Figure 5: Effect of the spot size on surface roughness of Ti-6Al-4V

4. Conclusions

In this study, the effect of spot size was examined to compare other parameters. The results showed that, for Nd:YAG laser used for surface treatment, spot size is also an effective parameter on the seam morphology and cooling rate, which is related to harder and smoother surface.

The surface treatment on Ti-6Al-4V alloys was employed by Nd:YAG laser technique. The results yielded positive surface properties such as hardening and repairing of surface layer. In addition, the ability to control the seam morphology, surface roughness and geometry of the laser treatment by controlling the laser output parameters was noted. Controlling the penetration depth, seam geometry and size are essential in order to control morphology and to obtain higher hardness values and smooth surface.

Due to the rapid cooling rates of laser applications, the microhardness profile across the treatment indicated that, with all parameters, the hardness distribution in the fusion zone were higher than the parent metal. The applications were limited in focal depth, which was determined as -0.2 mm. The shallow focal depth caused to increase the seam widths and rapid cooling rates, which was enabled satisfactory effects and hardness to be obtained on the surface of workpiece.

The main goal of this study is to analyze the effects of the spot size on the surface roughness of laser weld seams, beside to previous studies [15]. Regarding to 3D analysis in this study, the surface roughness tends to reach a stable value with the increasing of spot size. The surfaces get smoother when spot size increases.

According to the test results, when the results are correlated, and when optimum hardness and roughness values are considered, it can be concluded that the optimum parameter of spot size can be defined as 0.8 mm. The seam morphology, surface roughness and wear properties were in excellent conditions as desired, at 8 mm spot size of the optimum level. At the over and lover of this optimum level, some surface cracks, and craters were seen.

5. References

- [1] A. Gursel: Effect of pulse repetition and peak power of Nd:YAG laser for surface treatment on Ti-6Al-4V alloy, *Düzce University Journal of Science & Technology*, 3 (2015), pp. 210-218.
- [2] A.K. Mondal, S. Kumar, C. Blawert, N.B. Dahotre: Effect of laser surface treatment on corrosion and wear resistance of ACM720 Mg alloy, *Surface & Coatings Technology*, 202 (2008), pp. 3187-3198.
- [3] S.H. Wang, M.D. Wei, L. W. Tsay: Tensile properties of LBW welds in Ti-6Al-4V alloy at evaluated temperatures below 450°C, *Materials Letters*, 57 (2003), pp. 1815-1823.
- [4] G. Casalino, F. Curcio, F. Memola, C. Minutolo: Investigation on Ti6Al4V laser welding using statistical and Taguchi approaches, *Journal of Materials Processing Technology*, 167 (2005), pp. 422-428.
- [5] J.C. Williams, E.A. Starke Jr.: Progress in structural materials for aerospace systems, *Acta Materialia*, 51 (2003), pp. 5775-5799.
- [6] M. Akbari, S. Saedodin, D. Toghraie, R. S. Razavi, F. Kowsari: Experimental and numerical investigation of temperature distribution and melt pool geometry during pulsed laser welding of Ti6Al4V alloy, *Optics & Laser Technology*, 59 (2014), pp. 52-59.
- [7] E. Akca, A. Gursel: The Effect of Diffusion Welding Parameters on the Mechanical Properties of Titanium Alloy and Aluminum Couples, *Metals*, 7 (2017), pp. 22.
- [8] E. Akca, A. Gursel: Influences of argon gas shielding on diffusion bonding of Ti-6Al-4V alloy to aluminum, *Revista de Metalurgia*, 53 (2017), pp. 088.
- [9] E. Akca, A. Gursel: Joining of dissimilar metals by diffusion bonding: Titanium alloy with aluminum, *Materials Testing*, 59 (2017), pp. 330-337.
- [10] V.K. Balla, J. Soderlind, S. Bose, A. Bandyopadhyay: Microstructure, mechanical and wear properties of laser surface melted Ti6Al4V alloy, *Journal of the Mechanical Behavior of Biomedical Materials*, 32 (2014), pp. 335-344.
- [11] E. Akman, A. Demir, T. Canel, T. Sınmazcelik: Laser welding of Ti6Al4V titanium alloys, *Journal of Materials Processing Technology*, 209 (2009), pp. 3705-3713.

- [12] J.E. Blackburn, C.M. Allen, P.A. Hilton, L. Li, M.I. Hoque, K.H. Khan: Modulated Nd:YAG laser welding of Ti-6Al-4V, *Science and Technology of Welding and Joining*, 15 (2010), pp. 433-440.
- [13] S. Zhao, G. Yu, H. Xiuli, H. Yaowu: Microstructural and mechanical characteristics of laser welding of Ti6Al4V and lead metal, *Journal of Materials Processing Technology*, 212 (2012), pp. 1520-1527.
- [14] A. Gursel: Effects of Nd:YAG laser pulse frequency on the surface treatment of Ti-6Al-4V alloys, *Materials Testing*, 58 (2016), pp. 395-400.
- [15] A. Gursel: The Wear Treatment by Nd:YAG Laser on Ti-6Al-4V Alloy: Effect of the Spot Size on Laser Beam and Seam Morphology, *Metallofizikai Noveishie Tekhnologii*, 37 (2015), pp. 1037-1048.
- [16] M.R. Amaya-Vazquez, J.M. Sanchez-Amaya, Z. Boukha, F.J. Botana: Microstructure, microhardness and corrosion resistance of remelted TiG2 and Ti6Al4V by a high power diode laser, *Corrosion Science*, 56 (2012), pp. 36-48.
- [17] Z. Sun, I. Annergren, D. Pan, T. A. Mai: Effect of laser surface remelting on the corrosion behavior of commercially pure titanium sheet, *Materials Science and Engineering A*, 345 (2003), pp. 293-300.
- [18] T.M. Yue, J.K. Yu, Z. Mei, H.C. Man: Excimer laser surface treatment of Ti-6Al-4V alloy for corrosion resistance enhancement, *Materials Letters*, 52 (2002), pp. 206-212.
- [19] N. Zaveri, M. Mahapatra, A. Deceuster, Y. Peng, L. Li, A. Zhou: Corrosion resistance of pulsed laser-treated Ti-6Al-4V implant in simulated biofluids, *Electrochimica Acta*, 53 (2008), pp. 5022-5032.
- [20] Poulon-Quintin, I. Watanabe, E. Watanabe, C. Bertrand: Microstructure and mechanical properties of surface treated cast titanium with Nd:YAG laser, *Dental Materials*, 28 (2012), pp. 945-951.
- [21] J. Arias, A. Benedetti, M. Cabeza, G. Castro, I. Feijoo, P. Merino, X.R. Novoa: Surface modification of 2017-T4 aluminum alloy by high power diode laser melting, *Surface and Interface Analysis*, 42 (2010), pp. 748-751.
- [22] L. Li: The advances and characteristics of high-power diode laser materials processing, *Optics and Lasers in Engineering*, 34 (2000), pp. 231-253.
- [23] M.T. Ariyaratnam, M.A. Wilson, A.S. Blinkhorn: An analysis of surface roughness, surface morphology and composite/dentin bond strength of human dentin following the application of the Nd: YAG laser, *Dental Materials*, 15 (1999), pp. 223-228.
- [24] Y.F. Tzeng: Process characterization of pulsed Nd:YAG laser seam welding, *The International Journal of Advanced Manufacturing Technology*, 16 (2000), pp. 10-18.
- [25] Y.F. Tzeng: Parametric analysis of the pulsed Nd:YAG laser seam-welding process, *Journal of Materials Processing Technology*, 102 (2000), pp. 40-47.
- [26] E.S. Gadelmawla, M.M. Koura, T.M.A. Maksoud, I.M. Elewa, H.H. Soliman: Roughness parameters, *Journal of Materials Processing Technology*, 123 (2002), pp. 133-145.
- [27] Q. Yunlian, D. Ju, H. Quan, Z. Liying: Electron beam welding, laser beam welding and gas tungsten arc welding of titanium sheets, *Materials Science and Engineering A*, 208 (2000), pp. 177-181.

- [28] P. Wanjara, M. Brochu, M. Jahazi: Thin gauge titanium manufacturing using multiple-pass-electron beam welding, *Materials and Manufacturing Processes*, 21 (2006), pp. 439-451.
- [29] V.C. Kumar: Process parameters influencing melt profile and hardness of pulsed laser treated Ti-6Al-4V, *Surface Coatings Technology*, 201 (2006), pp. 3174-3180.
- [30] S. Sundaresan, R.G.D. Janaki: Use of magnetic arc oscillation for grain refinement of gas tungsten arc welds in alpha-beta titanium alloys, *Science and Technology of Welding and Joining*, 4 (1999), pp. 151-160.
- [31] J. Weldingh, J.K. Kristensen: Very deep penetration laser welding—techniques and limitations, 8th NOLAMP Conference, Copenhagen, Denmark, 2001.
- [32] B. Chen, B.X. Huang, H. Liu, X.L. Li, M.T. Ni, C. Lu: Surface nano crystallization induced by shot peening and its effect on corrosion resistance of 6061 aluminum alloy, *Journal Materials Research*, 29 (2014), pp. 3002-3010.
- [33] Y.G. Liu, M.Q. Li, H.J. Liu: Nanostructure and surface roughness in the processed surface layer of Ti-6Al-4V via shot peening, *Materials Characterization*, 123 (2017), pp. 86-90.

THE EFFECT OF PULSE DURATION ON Nd:YAG LASER SURFACE TREATMENT FOR Ti-6Al-4V ALLOY

Ali GURSEL

Düzce University, Faculty of Engineering, Department of Mechanical Engineering,

Konuralp Yerleskesi, B Blok 207, 81620 Düzce, Türkiye

aligursel@duzce.edu.tr, aligursel@yahoo.com Tel: +90 380 542 1036 Fax: +90 380 542 1037

Abstract

The excellent corrosion resistance, high strength-to-weight ratio, and high operating temperature exhibited by titanium and its alloys have led to their successful application in various fields. However, they are difficult to process using conventional machining and welding methods. Furthermore, their low hardness and poor wear resistance features are still serious concerns in some applications. Laser techniques can provide significant advantages for titanium alloys because of their precision, rapid processing capability and ability to control the parameters and their effects. The morphology and the quality of pulsed seams are directly or synergistically influenced by Nd:YAG laser parameters such as pulse duration, shape, energy, spot size, travel speed, peak power and frequency of repetition. In this study, a 1.5 mm-thick Ti-6Al-4V alloy sheet surface was treated via Nd:YAG pulsed laser system. The influence of the pulse duration on the surface and seam morphology was investigated. The quality of the seam and surface was characterized in terms of the morphology and hardness.

Keywords: Ti-6Al-4V alloy, Nd:YAG laser, Surface treatment, Seam morphology, Pulse duration.

1. Introduction

Titanium and titanium alloys have been used extensively in the aerospace, biomedical, nuclear, defense and automotive industries due to their low density, good corrosion resistance and high operating temperature [1]. Among the titanium alloys, Ti-6Al-4V is the best known, but with its characteristic strength, low thermal conductivity and high chemical reactivity, it is a difficult material to process using conventional machining and welding methods [2]. The Ti-6Al-4V alloy is widely used as material for load-bearing and non-load-bearing medical implants because of its excellent biocompatibility and corrosion resistance. Although its low hardness and poor wear resistance are still serious concerns, the majority of intended Ti-6Al-4V implant applications do not require very high wear resistance [3]. Laser treatment can be used to solve these problems.

Surface treatments are applied in order to increase wear resistance and surface strength for load carrying (crush resistance), to induce suitable residual and compressive stresses, to improve tool life against fatigue and increase impact resistance, etc. It is recognized that most welding techniques are commonly used for surface coating/treatments [4]. Blackburn et al. (2010) produced welds with high internal quality in Ti-6Al-4V by using a laser as the source for the welding technique [5]. They observed common periodic behaviors in the vapor plume

and keyhole under low-porosity welding conditions. The special features and potential of this method offer many advantages such as high scanning velocity, a narrow heat-affected zone (HAZ), low distortion, excellent controllability and the ability to produce a high-intensity heat source suitable for precision welding[6]. Previous studies on Nd:YAG laser applications have shown that it is possible to control the penetration depth and geometry of the laser weld bead by precisely controlling the laser output parameters[7].

Although laser treatments have been widely reported to improve the mechanical and corrosion behavior of different steels and aluminum alloys[8], relatively few studies have investigated the properties of laser treated titanium and titanium alloy samples[9]. Laser treatments have been performed with different types of laser sources including the CO₂, Nd:YAG, excimer and high-power diode lasers. The latter offers lower maintenance costs and higher efficiency than the others, thus representing a clear economical advantage[10]. Consequently, Sun et al. (2003) performed laser treatments on titanium (Grade 2) samples with a Nd:YAG laser[11]. In another study on wear treatment, a small molten pool was formed by each laser pulse, and within a few milliseconds it re-solidified. When the pulse frequency was low, a seam was formed during the conduction mode and a smooth, shallow molten pool was produced. However, when the pulse frequency was increased, a deeper, wider pool was obtained. The changed seam morphology affected the surface form and hardness as well[4].

The formation of laser seams and their subsequent quality is the result of a combination of various pulsed laser processing parameters, including the travel speed, the average laser power, the pulse energy, the pulse duration, the average peak power density and the spot area[12]. This abundance of parameters provides control of the thermal input with a precision not previously obtainable and also permits the application of a wide range of experimental conditions[5]. On the other hand, controlling so many parameters increases the complexity of the laser processing[13]. The effect of pulse duration on the Nd:YAG laser surface treatment of Ti-6Al-4V titanium alloy was investigated in this study.

2. Experimental

In this study of wear treatment, the SigmaLaser@300 Nd:YAG laser system was employed on 40 × 20 × 1.5 mm specimens of Ti-6Al-4V titanium alloy sheet. The chemical composition in weight percentage of the titanium substrate is shown in Table 1.

Table 1. Chemical composition of Ti-6Al-4V

Materials	C	Fe	N ₂	O	Al	V	H	Ti
Content wt %	<0.08%	<0.25%	<0.05%	<0.15%	5.5%	3.5%	<0.03%	Balance

2.1. Test parameters

This study investigated the effect of pulse duration on laser seams produced using the SigmaLaser@300 Nd:YAG laser system on Ti-6Al-4V alloy workpieces. This system is commonly used in the repair of cutting and molding tools[4]. In order to evaluate the effects on the surface treatment of the Ti-6Al-4V workpieces, the suitable parameters were determined as a focal depth of -0.2 mm in order to obtain sufficient power density, a circular spot size of 0.8 mm and pulse durations of 2, 4, 6, 8, 10 and 12 ms. The parameters of pulse duration and frequency were correlated, and by increasing the pulse duration applied in this study, the frequencies decreased. For example, with pulse durations of 2, 4, 6, 8, 10 and 12 ms, the frequencies observed were 14, 14, 12, 9.2, 7.6 and 6.4 Hz, respectively. The various laser output parameters used in the experiments are given in Table 2.

Table 2. Test parameters

Parameter	Values
Pulse Frequency	14 – 14 – 12 – 9.2 – 7.6 – 6.4 Hz
Peak Power	3.9 kW
Pulse Duration	2 – 4 – 6 – 8 – 10 – 12 ms
Spot Size	0.8 mm
Welding speed	50 mm/min
Focal depth	-0.2 mm
Gas and pressure	(99.8%) Argon, 1.5 bar

Owing to the limitation of the fusion zone, the spot size was determined as 0.8 mm, which is a commonly used parameter for surface repair and property enhancement treatments. The parameter of focal depth was determined as -0.2 mm in this study. This parameter is also a very common one employed for surface treatment and for the repair of cutting and molding tools[4]. The shallow -0.2 mm seams increased the cooling rates. This rapid cooling was responsible for the martensite structure and the achievement of the desired surface hardness[14].

Pulse duration is another effective parameter which is needed to increase heat input for penetration depth in welding applications. A longer pulse duration causes higher heat input, depending on the material and geometry[15]. During the surface treatment applications in this study, the optimum level of hard surface for the Ti-6Al-4V alloy was obtained with a parameter of 10 ms pulse duration.

Based on previous research [4], the peak power was optimized as 3.9 kW, which is 30% of the 13 kW peak power of the SigmaLaser@300 Nd:YAG laser system. During the applications, the energy was transferred by means of a laser beam. When higher energy is used, much deeper penetration can be achieved, which is not desirable for surface treatment as the material can melt and vaporize.

At high temperatures, titanium is reactive with ambient gases. For this reason, and to protect

against atmospheric effects, argon (99.8%) shielding gas was used at 1.5 bar to protect the melted pool from oxidation and porosities until solidification was sufficient. Therefore, it was crucial to use the shielding gas and to set up the nozzle in order to prevent the formation of turbulence on the sample surfaces during the application.

2.2. Analysis

For analysis of the microstructures after the applications, the workpiece seams were prepared for optical microscopy using standard procedures of grinding, polishing and etching. Sandpaper (P200-, P400-, P800- and P1200-grit) was used for the grinding and solutions (3 μm and 6 μm) for the polishing.

Micro-hardness measurements were performed and the values were obtained from the HAZ according to the seam dimensions. Furthermore, a scanning electron microscopy (SEM) analysis was carried out to observe the morphology and surface of the seams.

3. Results and Discussion

Previous studies have shown that all parameters affect the seam geometry and morphology and their properties. Pulse duration is one of the key parameters for the pulsed laser system. For seam geometry and surface hardness, it is crucial to control the pulse energy in addition to the laser power, spot size, pulse length, and pulse repetition.

3.1. Seam morphology

During the applications of this study, seam width increased with the increase of pulse duration up to the optimum level of 10 ms. When this level was exceeded, at 12 ms, the seam width decreased due to the heat input unexpectedly. The figures below show the seam morphology of the specimens treated by 3.9 kW peak power. The peak power was optimized against the evaporation point of the Ti-6Al-4V alloy to prevent crater formation on the surface. The effect of pulse duration on the seams can be seen in Figures 1-6.

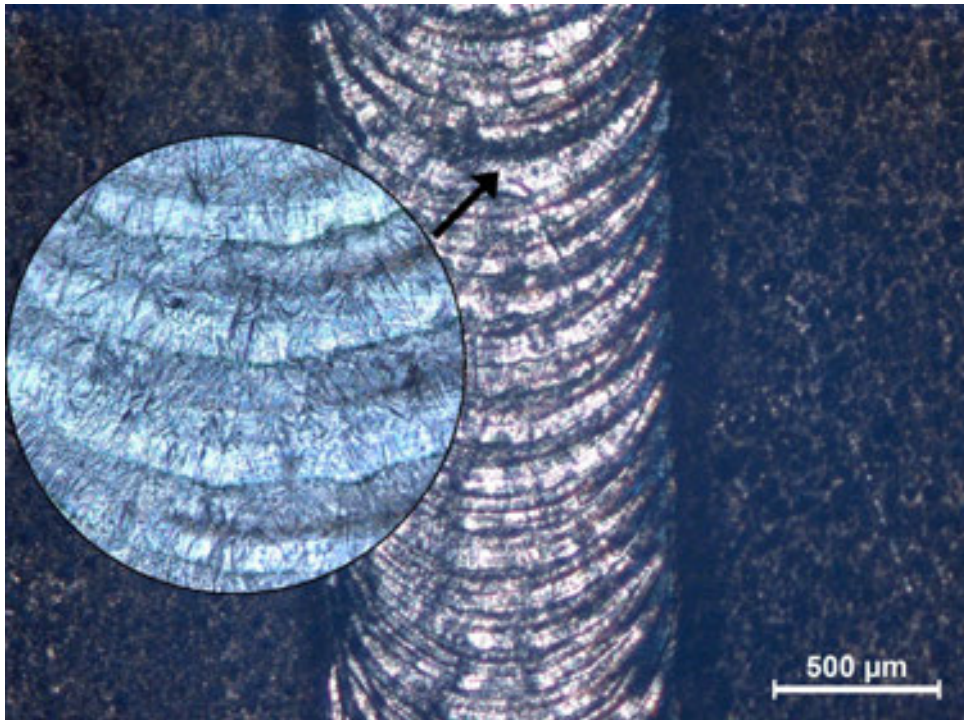


Fig. 1. Seam morphology: 2 ms pulse duration

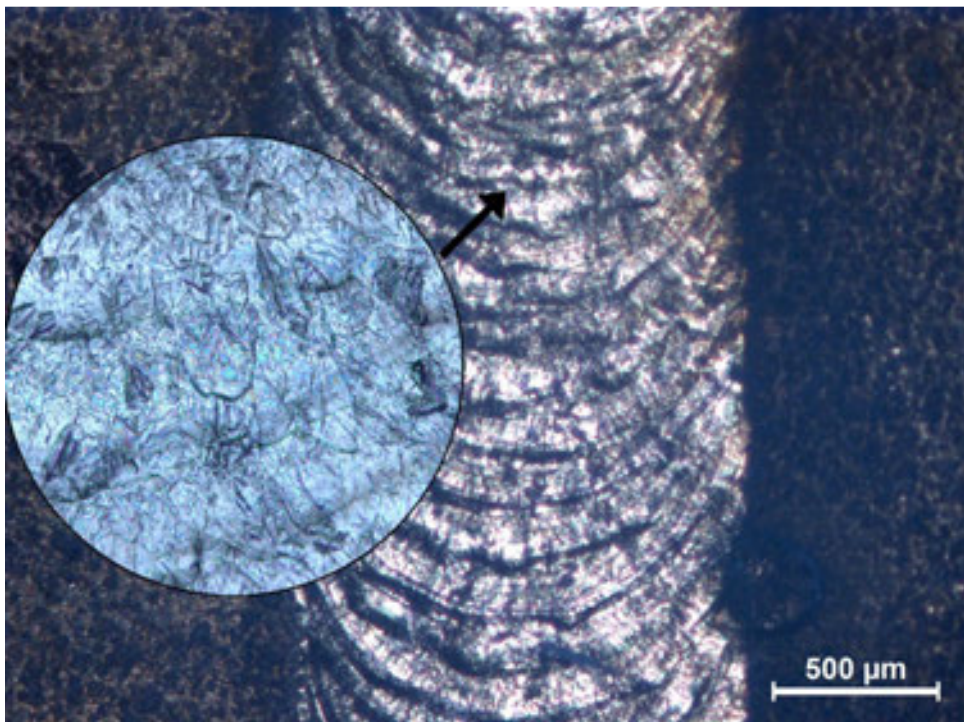


Fig. 2. Seam morphology: 4 ms pulse duration

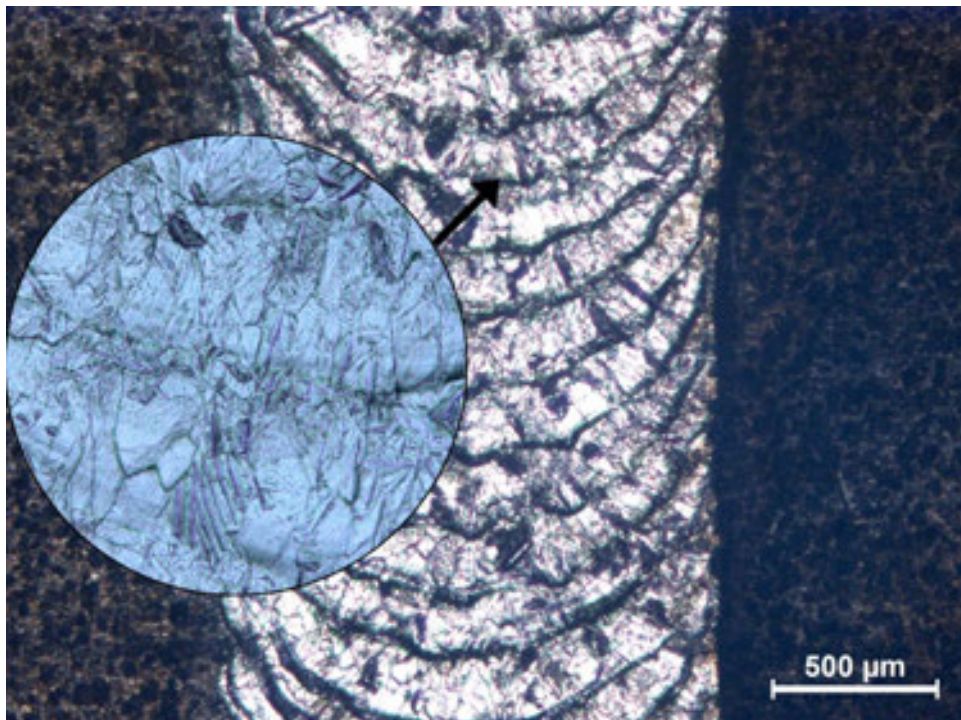


Fig. 3. Seam morphology: 6 ms pulse duration

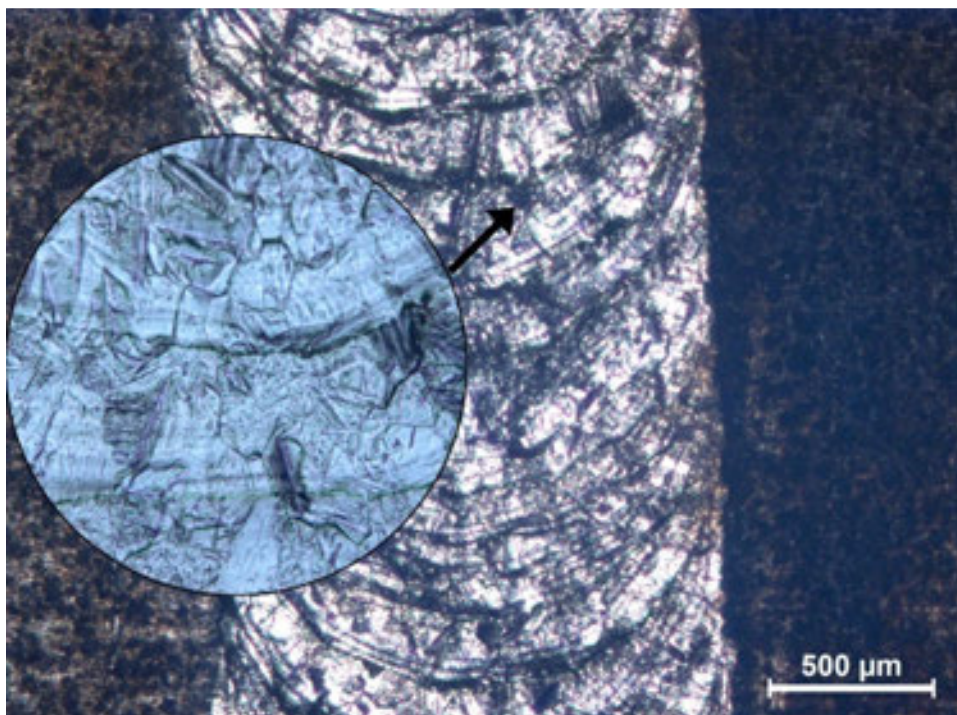


Fig. 4. Seam morphology: 8 ms pulse duration

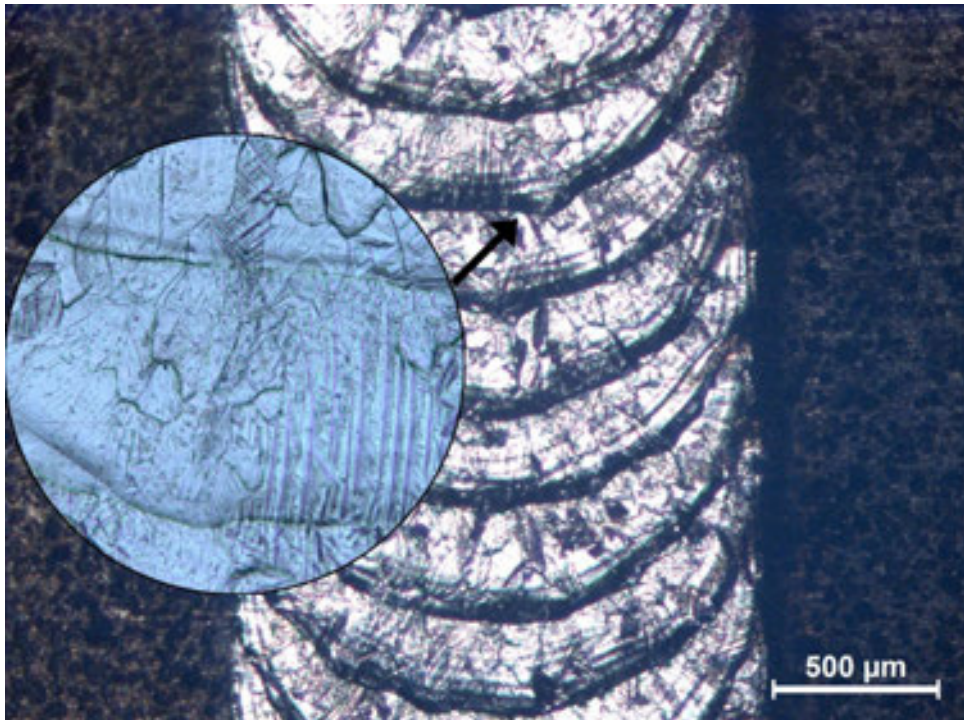


Fig. 5. Seam morphology: 10 ms pulse duration

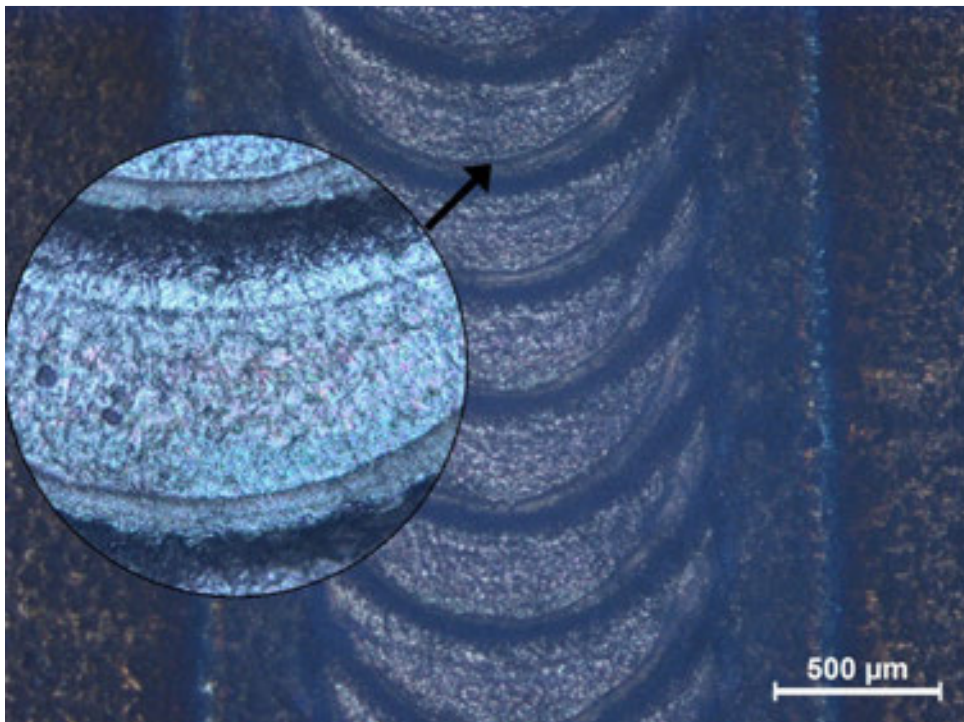


Fig. 6. Seam morphology: 12 ms pulse duration

3.2. Seam width

As illustrated in Figures 1-6, it was found that the seam width increased linearly with the pulse duration except for the pulse duration of 12 ms. At this longer duration level, the seam morphology was characterized by narrower but sharp, high layers. In addition, the HAZ increased more than with the other parameters (see Fig. 6). Pulse duration affected the seam morphologies in terms of heat input and cooling rates. Larger seams caused rapid cooling and created small grains and martensitic structures. A limiting of the increase of the seam width was observed, as seen in Figure 7.

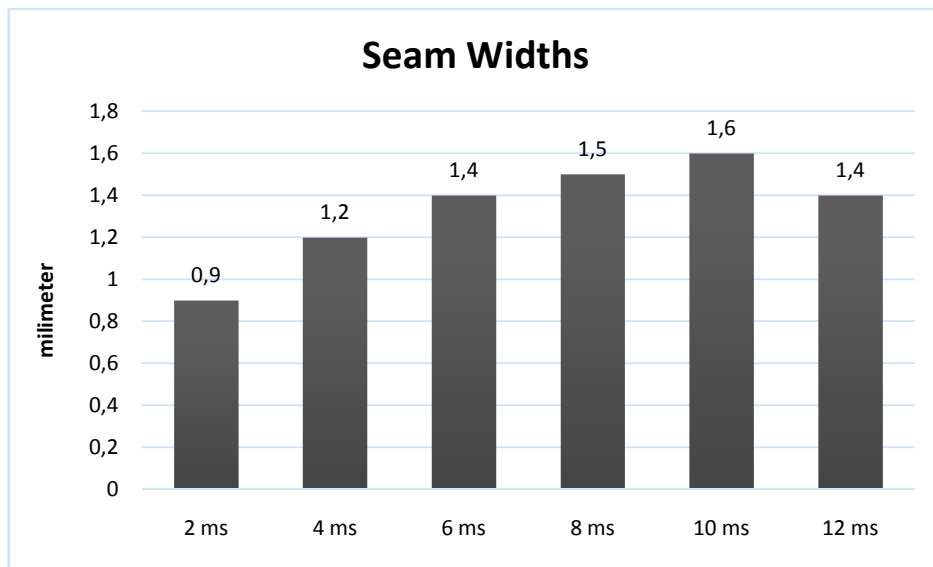


Fig. 7. Effect of pulse duration on seam width

The seams were measured as approximately 0.9 mm at 2 ms, 1.2 mm at 4 ms, 1.4 mm at 6 ms, 1.5 mm at 8 ms, 1.6 mm at 10 ms and 1.4 mm at 12 ms. These values can be explained by the heat input resulting from the pulse duration of the laser. The penetration depth, HAZ and seam width were also related to heat input which, in turn, was related to the laser pulse duration. Figure 7 shows that the laser energy enlarged the seam width, the same effect as was reported by Welding and Kristensen [16]. In this study, the largest seam was measured at 10 ms; furthermore, the large seam width caused the cooling rate and hardness to increase. In contrast to the linear increase of seam width based on pulse duration, a narrower seam width was obtained at the parameter of 12 ms. Owing to the limited focal depth of -0.2 mm, the seam size was observed to be larger than the spot size, as predicted.

3.3. Effect of pulse parameters on penetration and grains

The size and geometry of the seams were related to the laser parameters. The wear treatment layer on the surface, the grains, the penetration depth, and the HAZ are clearly seen in Figures 8-12. By increasing the pulse duration, deeper penetration was obtained without any loss on the surface.

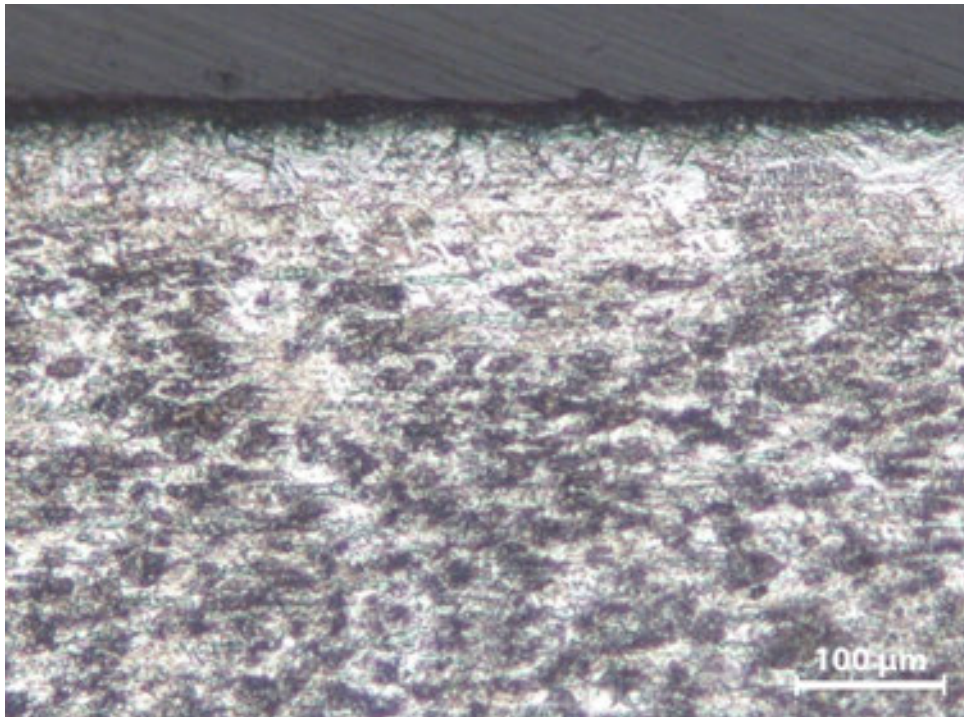


Fig. 8. Cross-section view at 2ms pulse duration

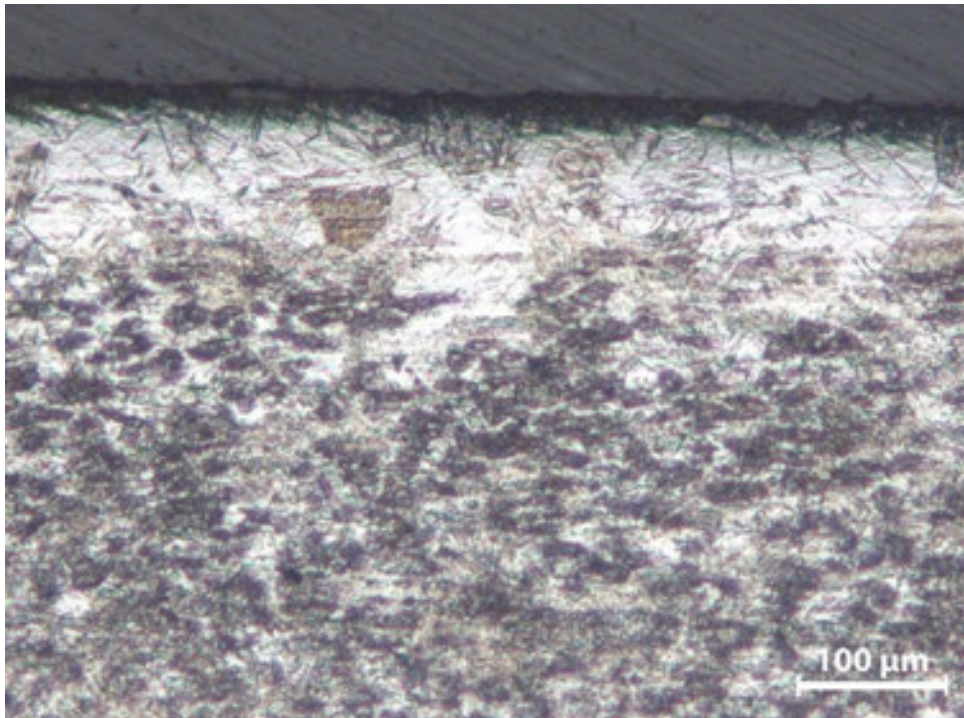


Fig. 9. Cross-section view at 4ms pulse duration

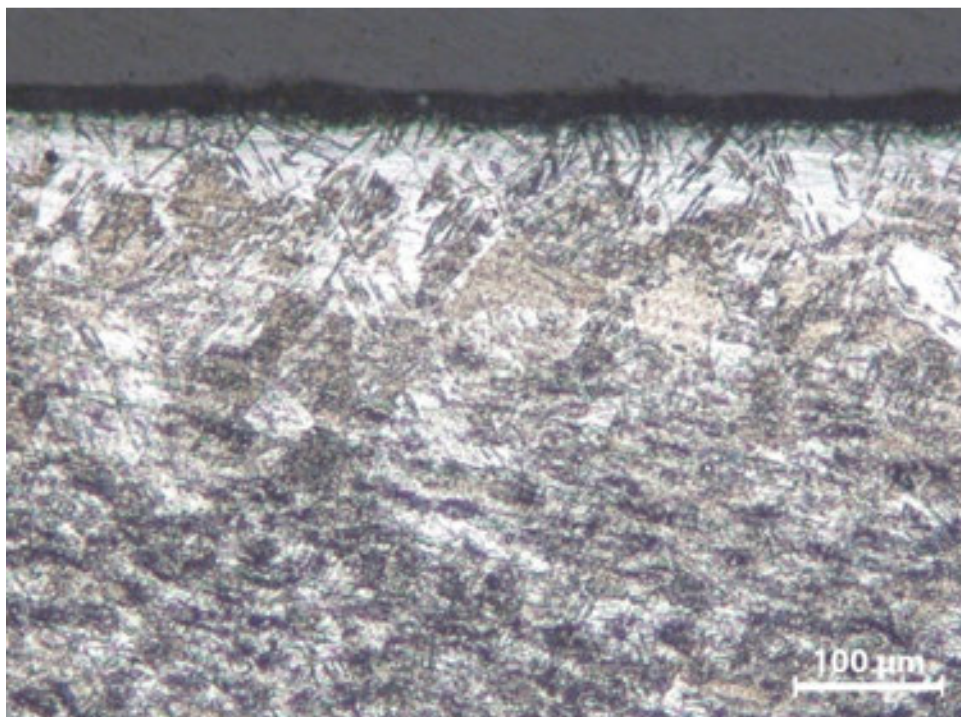


Fig. 10. Cross-section view at 6ms pulse duration

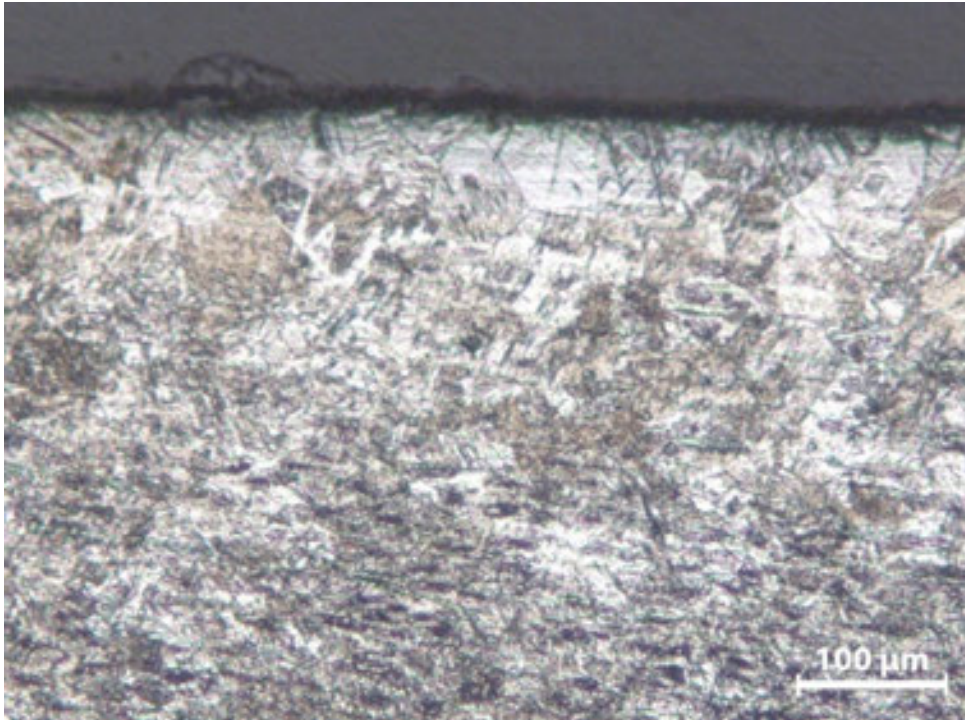


Fig. 11. Cross-section view at 8ms pulse duration

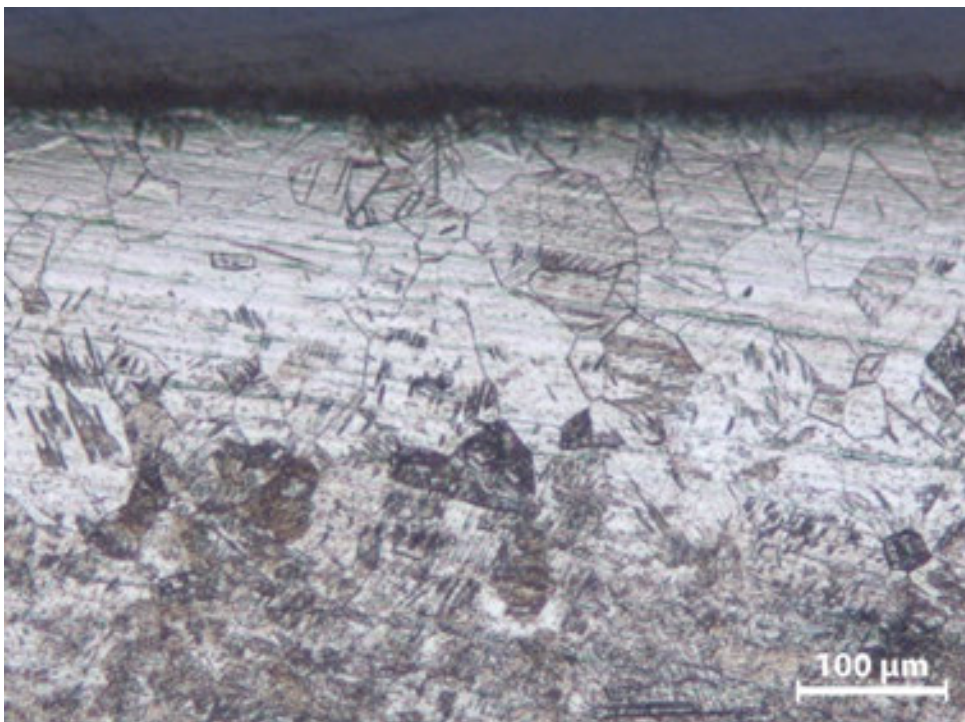


Fig. 12. Cross-section view at 10ms pulse duration

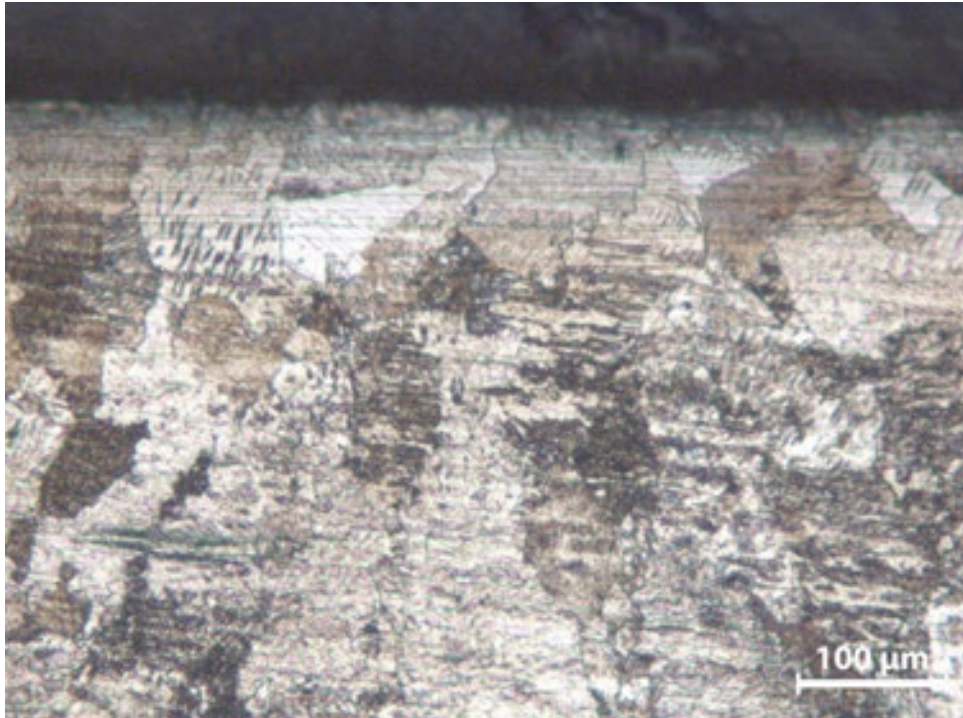


Fig. 13. Cross-section view at 12ms pulse duration

The figures show cutaway views (at 100 μm) of the blind seam. The penetration depth of the laser pulses are linearly increased based on duration (Figs. 8-12). When the optimum parameter of this study (10 ms) was exceeded, the grains, impurities and boundaries were burned and changed color due to the effect of the heat input related to laser pulse duration (Fig. 13). Moreover, the higher energy input caused the structure of the titanium alloy to be destroyed.

3.4. Micro-hardness

The hardness distributions of the seams were analyzed using a SHIMADZU HMV micro-hardness tester with a load of 100 g. The micro-hardness measurements were taken beginning from the center of the surface of the seam and straight along through the HAZ and base metal. As a result, at the transition zone of the seams, the hardness values were at the maximum levels and, due to the rapid cooling rate, the cooled material was superior compared to the base metal (Fig. 14).

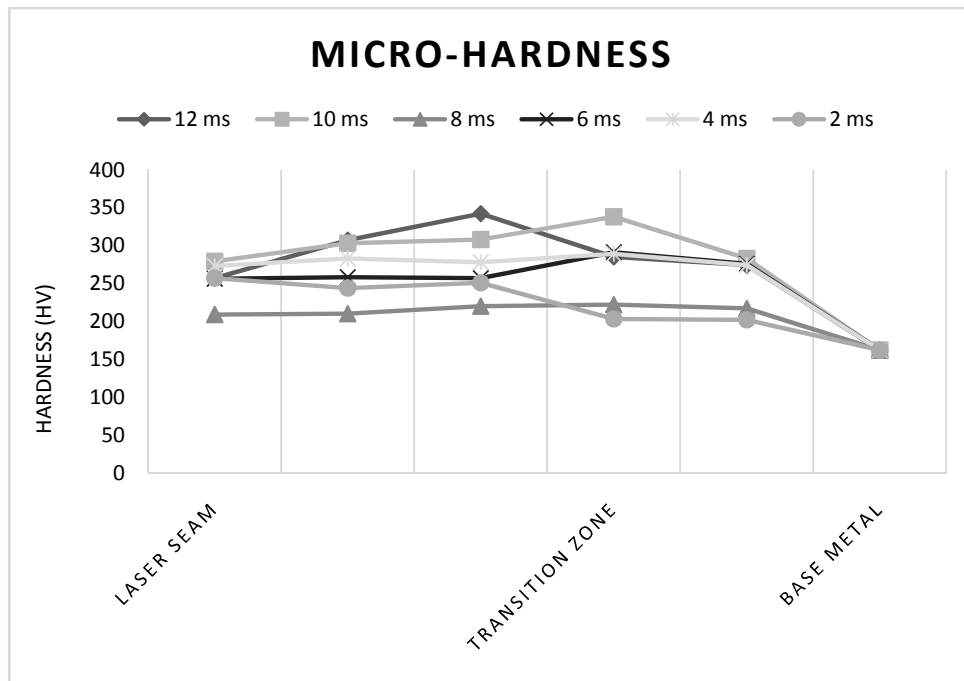


Fig. 14. Micro-hardness distribution of three regions at different pulse durations

At all parameters, higher hardness and better abrasion strength were obtained from the seam surfaces of the base metal. The base metal had a hardness of ~160 HV; however, after treatment, a surface hardness of over 210 HV was achieved. At the selected duration periods between 2 and 12 ms, the best hardness values were measured as 225 HV–345 HV.

In previous studies on surface wear using continuous wave Nd:YAG laser, the average hardness of the melted region was 15–22% higher than the average hardness of the Ti-6Al-4V alloy substrate [3]. In this study, using Nd:YAG pulsed laser, the base metal hardness attained in the melted region was 30–110% higher. The difference in hardness between the seam and the base metal were ~50–190 HV. Previous studies using different techniques such as electron beam and gas tungsten welding on Ti-6Al-4V alloys have shown that the high-power density of laser beam welding provides a lower heat input and a more rapid solidification when compared to conventional techniques [17]. Thus, in this study, the laser technique for surface treatment led to the higher hardness values.

Another noteworthy point is that, as predicted, the highest values were seen on the transition zones. After the transition zones, the hardness continued through to the base metal side of the HAZ. The cooling rate was higher in the transition zones than in the seam pools. Moreover, there was a difference of ~90 HV between the transition zone and the base metal at some parameters.

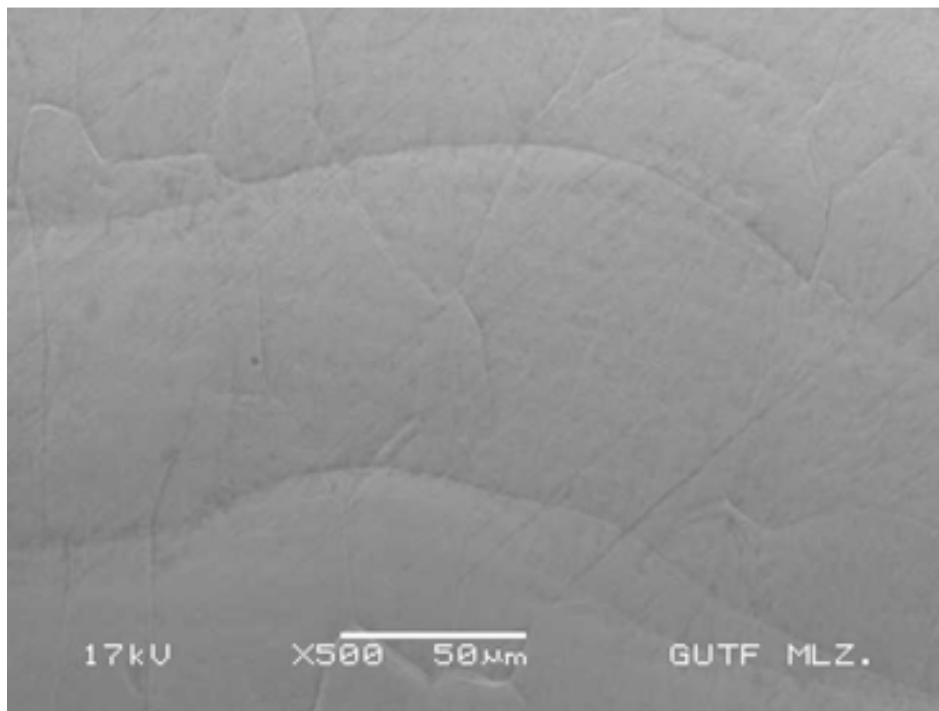
Higher heat input increases the target temperature, producing steeper thermal gradients and severe thermal straining. It was expected that by increasing total heat input to the target and reducing the cooling rate and the temperature gradient, the hardness would decrease with

the increasing heat input [18]. Nevertheless, in this study, at 2 ms duration, the heat input was at a minimum value and cooling rates were faster than with other parameters, and therefore the hardness values might be higher than with other parameters. However, at the longer durations of 10 and 12 ms, although there was still higher heat input, higher hardness values were obtained because of the larger seam width. The larger seam width affected the cooling and solidification rates [14].

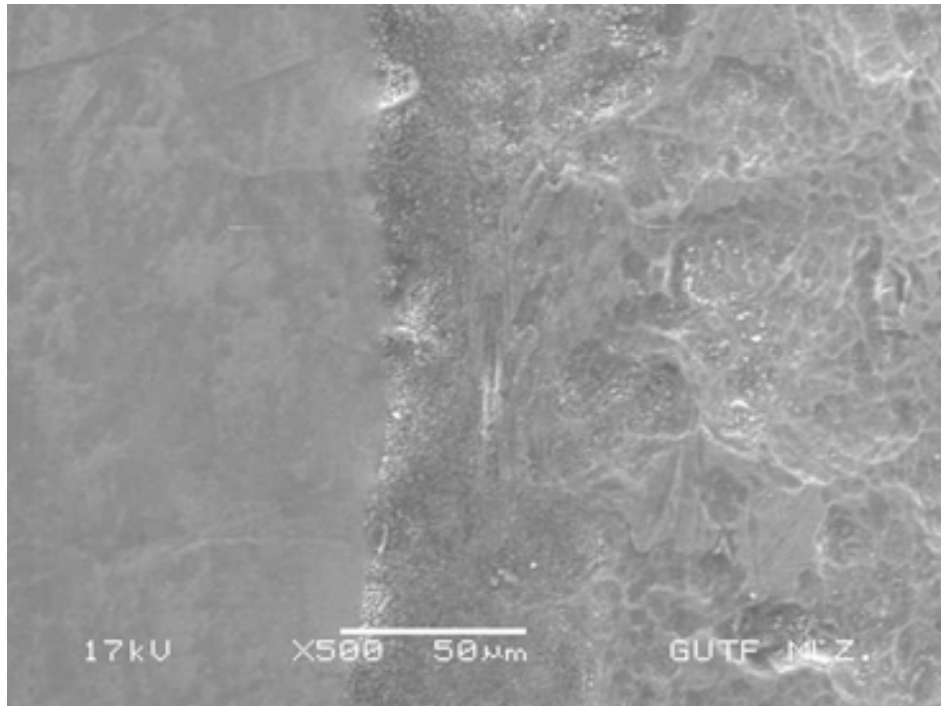
The large laser seam increase observed with the hardness of the Ti-6Al-4V was due to the rapid cooling rate. High cooling rates cause the formation of martensite in the HAZ. It was reported by Sundaresan and Janaki that rapid cooling and subsequent martensitic transformation were effective strengthening methods for many titanium alloys [15]. Although the material has the micro-hardness values of the Ti-6Al-4V alloy, it behaves like a composite structure because of the martensite formation. As a result, overestimated values are occasionally seen during the measuring of micro-hardness, although average values were seen in this study (Fig. 14).

3.5. SEM analysis

The effects of the laser treatment on specimen surfaces were detected by SEM. The seam morphology, base metal surface and transition zone of the workpiece are seen in Figure 15 a) and b).



a) Seam surface



b) Transition zone seam and base metal surface

Fig. 15. SEM analysis

In Figure 15 a) and b), the transition zone and base metal surfaces can be compared, and the surface morphology and oxide layer can be clearly observed on the base metal surface. The laser treatment on the Ti-4Al-6V alloy surface produced excellent results, such as the hardening and removing or repairing of surface cracks and cavities left over from the manufacturing of the base metal. In addition, the texture of the surfaces became smoother.

4. Conclusions

- 1) The Nd:YAG laser technique was employed for the surface treatment of Ti-6Al-4V titanium alloys. The results yielded positive surface properties such as the hardening and repairing of the surface layer. In addition, the ability to control the seam morphology and geometry of the laser treatment by controlling the laser output parameters was noted. Controlling the penetration depth, seam geometry and size are essential in order to control morphology and to obtain higher hardness values.
- 2) The heat input and cooling rates were likewise related to all parameters, including spot size, pulse energy, peak power, pulse frequency and pulse duration. This study investigated the effect of pulse duration on the Nd:YAG laser seams.
- 3) In the present study, increasing the pulse duration increased the heat input, causing a wider seam pool and higher, rapid cooling rates and resulted in a higher level of hardness,

especially in the transition zones. During the applications in this study, seam width increased with the increase of pulse duration up to the optimum level of 10 ms; however, seam width decreased unexpectedly at the 12 ms duration.

- 4) When the optimum level of pulse duration was exceeded, the titanium alloy was deformed by heat input. The deformation is clearly seen in Figure 13. The penetration depth increased at 12ms duration, causing a change in the alloy structure and burning the impurities in the base metal, and thus, the seam morphology and surface texture of the seam were not as apparent as with the other parameters.
- 5) Due to the rapid cooling rates of the laser applications, the micro-hardness profile across the treatment indicated that, with all parameters, the hardness distribution in the fusion zone was higher than that in the parent metal. The applications were limited in focal depth, which was determined as -0.2 mm. The shallow focal depth caused increased seam widths and rapid cooling rates, which enabled satisfactory effects and hardness to be achieved on the workpieces.
- 6) In this study, the effect of pulse duration was examined in comparison with other parameters. The results showed that for Nd:YAG laser used for surface treatment, pulse duration is also an effective parameter on the seam morphology and cooling rate, which are correlated with a harder and smoother surface.

5. References

- [1] G. Casalino, F. Curcio, F. Memola, C. Minutolo: Investigation on Ti6Al4V laser welding using statistical and Taguchi approaches. *Journal of Materials Processing Technology*, 167 (2005), pp. 422–428. DOI: 10.1016/j.jmatprotec.2005.05.031.
- [2] M. Akbari, S. Saedodin, D. Toghraie, R. S. Razavi, F. Kowsari: Experimental and numerical investigation of temperature distribution and melt pool geometry during pulsed laser welding of Ti6Al4V alloy. *Optics & Laser Technology*, 59 (2014), pp. 52–59. DOI: 10.1016/j.optlastec.2013.12.009.
- [3] V.K. Balla, J. Soderlind, S. Bose, A. Bandyopadhyay: Microstructure, mechanical and wear properties of laser surface melted Ti6Al4V alloy. *Journal of the Mechanical Behavior of Biomedical Materials*, 32 (2014), pp. 335–344. DOI: 10.1016/j.jmbbm.2013.12.001.
- [4] A. Gursel: Effects of Nd:YAG laser pulse frequency on surface treatment of Ti-6Al-4V alloys. *Materials Testing*, 58-5 (2016), pp. 395-400. DOI 10.3139/120.110867.
- [5] J.E. Blackburn, C.M. Allen, P.A. Hilton, L. Li, M.I. Hoque, K.H. Khan: Modulated Nd:YAG laser welding of Ti-6Al-4V. *Science Technology of Welding and Joining*, 15 (2010), pp. 433–440. DOI: 10.1179/136217110X12731414739718.

- [6]S. Zhao, G. Yu, H.Xiuli, H.Yaowu: Microstructural and mechanical characteristics of laser welding of Ti6Al4V and lead metal. *Journal of Materials Processing Technology*, 212 (2012), pp. 1520–1527. DOI: 10.1016/j.jmatprotec.2012.02.014.
- [7]E. Akman, A.Demir, T. Canel, T. Sinmazcelik: Laser welding of Ti6Al4V titanium alloys. *Journal of Materials Processing Technology*, 209 (2009), pp. 3705–3713. DOI:10.1016/j.jmatprotec.2008.08.026.
- [8]T.M. Yue, J.K. Yu, Z. Mei, H.C. Man: Excimer laser surface treatment of Ti–6Al–4V alloy for corrosion resistance enhancement. *Materials Letters*, 52-3 (2002), pp. 206–212. DOI: 10.1016/S0167-577X(01)00395-0.
- [9]A. Poulon-Quintin, I.Watanabe, E.Watanabe, C.Bertrand: Microstructure and mechanical properties of surface treated cast titanium with Nd:YAG laser. *Dental Materials*, 28-9 (2012), pp. 945–951. DOI: 10.1016/j.dental.2012.04.008.
- [10]J. Arias, A. Benedetti, M.Cabeza, G. Castro, I.Fejjoo, P. Merino, X.R.Novoa: Surface modification of 2017-T4 aluminum alloy by high power diode laser melting *Surface and Interface Analysis*, 42 (2010), pp. 748–751. DOI: 10.1002/sia.3301.
- [11]Z. Sun, I.Annergren, D. Pan, T.A. Mai: Effect of laser surface remelting on the corrosion behavior of commercially pure titanium sheet. *Materials Science and Engineering: A*, 345 (1–2) (2003), pp. 293–300. DOI: 10.1016/S0921-5093(02)00477-X.
- [12]Y.F. Tzeng: Process characterization of pulsed Nd:YAG laser seam welding. *The International Journal of Advanced Manufacturing Technology*, 16 (2000), pp. 10–18. DOI: 10.1007/PL00013126.
- [13]Y.F. Tzeng: Parametric analysis of the pulsed Nd:YAG laser seam-welding process. *Journal of Materials Processing Technology*, 102 (2000), pp. 40–47. DOI: 10.1016/S0924-0136(00)00447-7.
- [14]A. Gursel:Crack risk in Nd: YAG laser welding of Ti-6Al-4V alloy. *Materials Letters*, 197 (2017), pp. 233-235. DOI: 10.1016/j.matlet.2016.12.112.
- [15]S. Sundaresan,R.G.D. Janaki: Use of magnetic arc oscillation for grain refinement of gas tungsten arc welds in alpha–beta titanium alloys. *Science Technology of Welding and Joining*, 4 (1999), pp. 151–160.
- [16]J. Weldingh,J.K.Kristensen: Very deep penetration laser welding—techniques and limitations. In: *Proceedings of 8th NOLAMP Conference, Copenhagen – Denmark (2001)*.
- [17]. Q. Yunlian,D.Ju, H.Quan, Z.Liyong: Electron beam welding, laser beam welding and gas tungsten arc welding of titanium sheets. *Materials Science and Engineering: A*. 280 (2000), pp. 177–181. DOI:10.1016/S0921-5093(99)00662-0.
- [18]V.C. Kumar: Process parameters influencing melt profile and hardness of pulsed laser

treated Ti–6Al–4V. *Surface and Coatings Technology*, 201 (2006), pp. 3174–3180. DOI: 10.1016/j.surfcoat.2006.06.035.

CORRESPONDENCE ADDRESS: Ali GÜRSEL, Düzce University, Faculty of Engineering, Department of Mechanical Engineering, KonuralpYerleskesi, B Blok 207, 81620 Düzce, TR.Tel: +90380 542 1036 Fax: +90 380 542 1037 aligursel@duzce.edu.tr, aligursel@yahoo.com.

SHORT BIOGRAPHY

Dr. Ali Gursel was born in Gaziantep-Turkey in 1971. He acquired his bachelor and graduate degrees from Gazi University in Ankara, Turkey. He worked for the government and diplomatic missions, regarding educational issues and international projects. He managed to DuzceTechnopark as General Director, between 2012 to 2013. He involved a project for defense materials as a research fellow at The City College of New York, USA (in 2013-2014). DrGursel followed his career on managerial and academic positions at the International University of Sarajevo, Bosnia and Herzegovina as Vice Rector and Director of Research Center besides his academic duties as Associate Professor in the Department of Mechanical Engineering. DrGursel is presently Associate Professor at Duzce University Department of Mechanical Engineering. His research areas are material science and material processes, composite materials, metallurgy, welding and joining technologies, weldability of dissimilar materials, solid state welding, adhesive bonding etc.

JOINABILITY OF BRASS ALLOY BY FURNACE AND MICROWAVE BRAZING

Yasemin Aksu^{1,a}, İrem Burcu Algan^{1,b}, Ramazan Çıtak^{1,c}, Adem Kurt^{1,d}

¹Department of Metallurgical and Materials Engineering / Faculty of Technology /Gazi University

^a yasemindundar@gazi.edu.tr, ^b irembalgan@gazi.edu.tr, ^c citak@gazi.edu.tr, ^d ademkurt@gazi.edu.tr

Abstract

Comparing with conventional methods, microwave joining offers volumetric heating providing energy and time saving and environmentally friendly processes which reduces power consumption. Brazing studies in conventional and microwave furnaces were conducted for brass alloy, in this study. Ag-306 alloy was used for brazing processes at temperature of 850 °C. After holding 10 minutes in both of furnaces, air cooling was applied all of the specimens joining by overlapping technique. The characterizations of joints had been carried out through optical microscopy, scanning electron microscopy for microstructural analysis, tensile and microhardness tests for mechanical properties.

Key Words: Brazing, Microwave joining, Furnace joining, Overlapping

1. Introduction

Many similar and dissimilar materials are joint with brazing proces which use heat, filler metal, and a flux. Even if melting temperatures of filler metals are below the melting temperatures of the workpieces, the melting temperature of the filler metal is different for joining process. Brazing process takes place above 840° F / 450 ° C [1]. Brazing process is important for permanent joining, especially in electronic industry.

Conventional methods including blast furnace, induction furnace, electric arc furnace and crucible furnace for brazing waste a large amount of energy; therefore, microwave processing was introduced as a novel technique [2, 3]. Microwave furnace provides homogeneous heating where the energy is directly transferred to the material by electromagnetic field generated from electromagnetic waves with wavelengths range 10^3 to 1 mm and corresponding frequencies range 300 MHz to 300 GHz. Conversely, the material is heated nonhomogeneous where thermal energy is conducted from surface to the center which results in undesirable thermal gradients, in conventional furnace. Since microwaves provide volumetric heating there are several advantages of microwave furnaces such as high heating rate, shorter processing time, and low power consumption, manufacturing cost reduction and less environmental hazard [4, 5].

We have already carried out investigations on conventional and microwave joining methods of brass alloy. Both methods were applied for brazing in this study.

2. Experimental

Before joining, mechanical, chemical and ultrasonic cleaning were applied to the specimens. After grinding with emery paper of 120 grids, the specimens were immersed in nitric acid solution (65%) at room temperature for removing oxide layers then were rinsed in cold water and subsequently dried. Finally, ultrasonic cleaning were applied to the specimens in ethanol for 10 min.

Overlapping technique shown in Figure 1 was applied for brazed joints. The bulk plates of dimension $40 \times 20 \times 1$ mm with a gap of approximately 0.4 mm were used for joining. The gap was filled with filler metal, powdered flux (dekapan), before joining. Overlap length was chosen as 6 mm in order to obey the “3t to 6t rule”, where “t” is the thickness of thinnest of the two sheet metal pieces being brazed together [6].

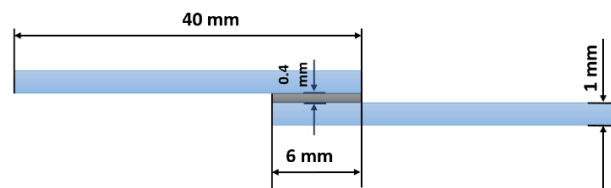


Figure 1. Schematic representation of overlap joining

Heraeus-KR 170 conventional and HAMILab-DS1500 microwave furnaces were used for joining applications. The filler metal was a Ag-306 alloy (30% Ag, 28% Cu, 21% Zn, 21% Cd) while the working temperature was 850 °C for brazing process. The furnace was heated to the desired temperature that takes 2 hours and then specimens were placed and held for 10 min, for conventional process. On the other hand, microwave furnace was heated with the specimens to the intended temperature simultaneously in 10 min and the specimens were held at this temperature for 10 min. Then the specimens were cooled to room temperature in the normal atmosphere.

Microstructure analyzes were done with Leica DM5000M optical microscope and Jeol JEM 6060 LV scanning electron microscopy (SEM). Elemental compositions were measured in IXRF (Integrated X-Ray Fluorescence) system. Shimadzu HVM-2 Vickers Hardness Tester with HV0.025 was used for microhardness test analyzes. Tensile strength of the joints was evaluated by an Instron 3369 Universal Test Machine as per ASTM standard (ASTM Designation: E8/E8 M – 09, 2009).

3. Results and Discussion

Optical and SEM images of both conventional and microwave brazing at 850°C with different magnifications are given in Figure 2. Optical microstructures clearly indicate the integration of base metal and braze alloy in both of brazing methods. However, the difference in between is the solidification rates. Since microwave furnace heat a material faster, rapid solidification occurs, and hence the obtained microstructure in microwave furnace has thinner network structure than that of in conventional furnace.

The points on which EDS analysis were carried out are given in Figure 2 and Table 1 shows the average elemental compositions for both of conventional and microwave brazing. Point 1 and 2 stand for the base metal and interface, respectively. According to the result of EDS analysis, Ag and Cd were diffused from brazing alloy into the base metal. Furthermore, point 3 and 4 represent

different regions of the brazing alloy. In the grain boundaries, point 3, Ag and Cd elements are rich while grains, point 4, consist of mostly Cu and Zn elements.

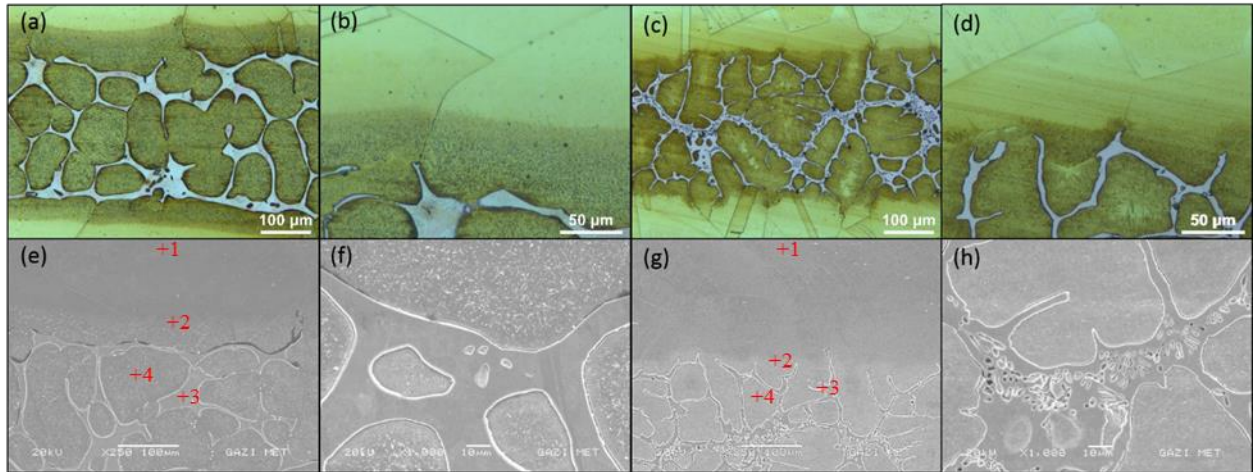


Figure 2. Optical micrographs of brazing in conventional furnace at (a) 200X, (b) 500X and in microwave furnace at (c) 200X and (d) 500X. SEM micrographs of brazing in conventional furnace at (e) 500X, (f) 1000X and in microwave furnace at (g) 500X and (h) 1000X.

Table 1. The results of EDS analysis for base metal, interface and brazing alloy.

Elements	1	2	3	4
Cu	71.7885	66.5845	2.0145	60.242
Zn	25.0595	25.7405	1.8675	26.3175
Ag	2.133	5.8425	64.709	11.5455
Cd	1.0415	1.8335	31.409	1.895

In the tensile tests, both specimens fractured in base metal and it shows that both brazings successfully joined the brass alloy (Figure 4). The results of tensile test is given in Figure 3. The plots showed that yield point for conventional and microwave brazing are 41 MPa and 78 MPa; tensile strengths are 226 MPa and 225 MPa; elongations are 119 % and 80 %, respectively. Both specimens showed similar tensile stresses but different elongations. Additionally, hardness results showed that microwave brazing was harder than furnace brazing resulted from solidification and microstructure differences.

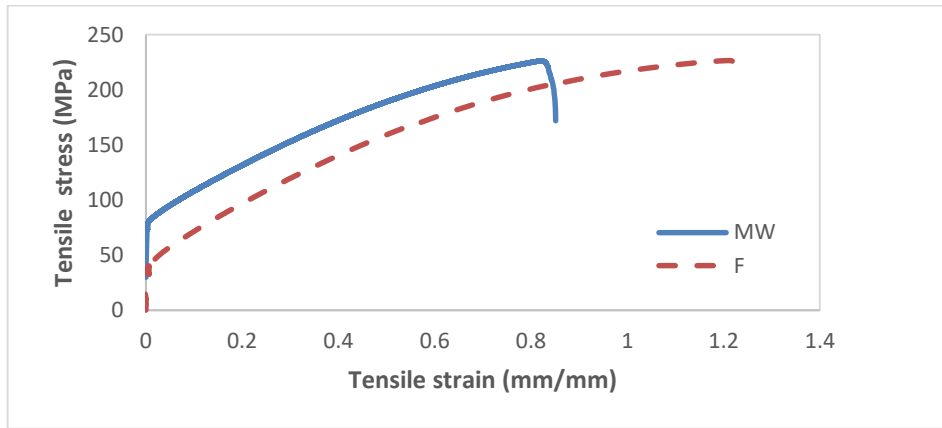


Figure 3. The tensile stress-tensile strain plot of brazed joints in conventional and microwave furnace.

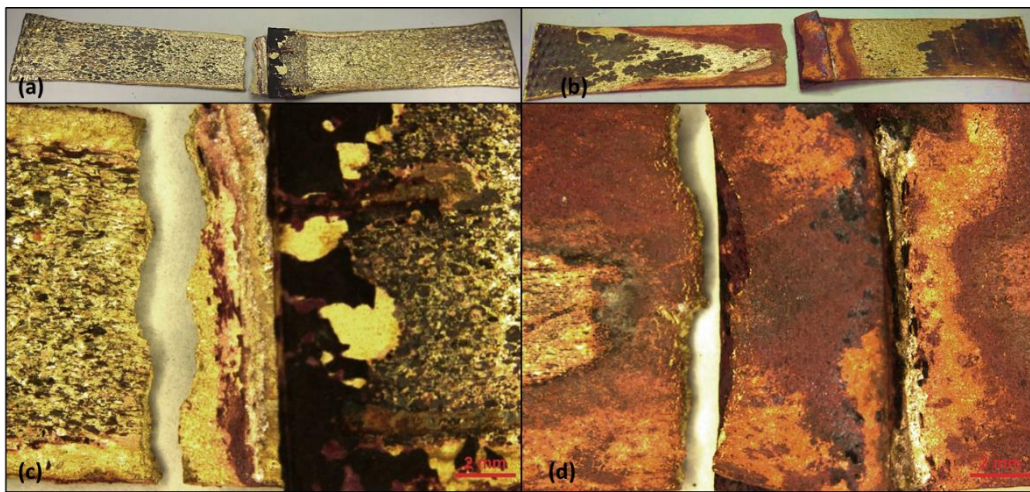


Figure 4. Macrographs of tensile fracture of brazing in conventional furnace at (a) and (c); in microwave furnace (b) and (d).

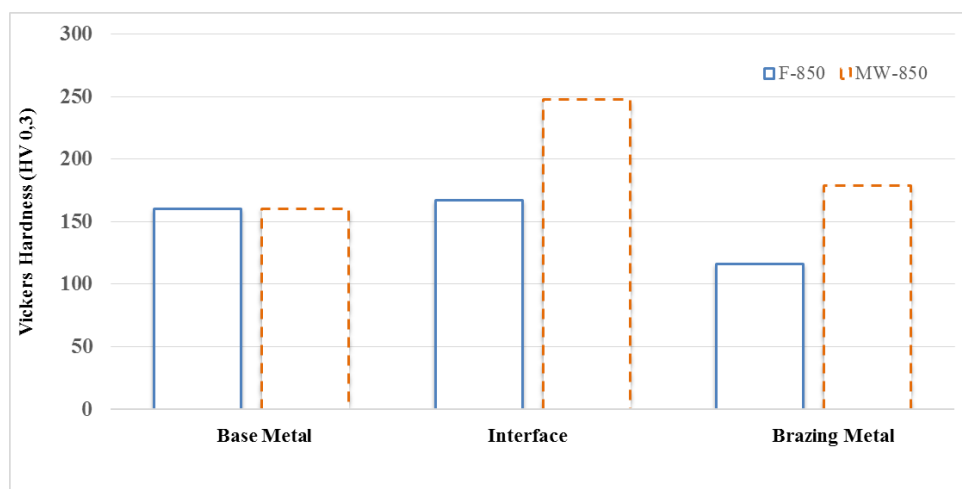


Figure 5. Microhardness values of base metal, braze and interface between them for conventional and microwave furnace.

Vickers microhardness values for conventional and microwave methods are 148 and 180 in base metal, 167 and 248 in the interface, 116 and 179 in brazing alloy, respectively. Since microwave brazing has dendritic like solidification, it has harder structure than conventional brazing. Similarly, as Figure 3 is seen, furnace brazing is more ductile than microwave brazing. On the other hand, due to diffusion of Ag and Cd elements from brazing metal into the base metal as seen in Figure 2, the hardness values of interface is higher than other two regions due to dispersion. Furthermore, the microhardness values of base metal and brazing metal are coherent with the literature [7, 8].

4. Conclusion

The joinability of brass alloy by conventional and microwave brazing have been studied, in this study. The results are:

- Brass alloy can be brazed successfully by conventional and microwave furnace.
- Brazing alloys showed different microstructure. Conventional brazing has regular grain structure while microwave is dendritic like grain structure.
- Ag and Cd diffuses from the brazing alloy into the base alloy.
- Both of the joinings fractured in base alloy during the tensile tests.
- Both brazing has similar tensile stress but microwave has lower elongation percentage.
- Hardness values of microwave brazing is higher than furnace brazing.
- Microwave brazing time is shorter than furnace brazing.

7. References

- [1] «SME,» Temmuz 2018. [Online]. Available: <http://www.sme.org/fmp/>.
- [2] J. I. Rasbudin, M. A. Adawiyah ve O. S. Azlina, «The effect of multiple reflow on intermetallic layer of Sn- 4.0AgCu/Cu by using microwave and reflow soldering,» *IOP Conf. Series: Materials Science and Engineering*, cilt 95, pp. 1-6, 2017.
- [3] M. Shukla, S. Ghosh, N. Dandapat, A. J. Mandal ve V. K. Balla, «Microwave-assisted brazing of alumina ceramics for electron tube,» *Bull. Mater. Sci.*, cilt 39, no. No:2, pp. 587-591, 2016.
- [4] A. Bansal, A. K. Sharma ve S. Das, «Metallurgical and mechanical characterization of mild steel-mild steel joint formed by microwave hybrid heating process,» *Sadhana*, no. Part 4, pp. 679-686, 2013.
- [5] D. Hoyr, Y. Adonyi ve S. Kim, «Microwave joining-part 1: closed-loop controlled microwave soldering of lead telluride to copper,» *Welding Journal*, cilt 95, pp. 141-145, 2016.

- [6] D. Kay, «Vac Aero International Inc.,» 10 7 2014. [Çevrimiçi]. Available: <https://vacaero.com/information-resources/vacuum-brazing-with-dan-kay/1398-braze-joint-design-how-much-overlap-is-enough.html>. [Erişildi: 07 2018].
- [7] [Online]. Available: <https://alloys.copper.org/alloy/C35350>.
- [8] S. Çınar, the effect of various wires using brazing of copper and alloys on microstructure and mechanical properties of, Ankara: Gazi University, 2010.

CORRESPONDENCE ADDRESS: Gazi University Faculty of Technology, Department of Metallurgy& Material Engineering, 06810, Teknikokullar-Ankara, +903122028750, irembalgan@gazi.edu.tr

SHORT BIOGRAPHIES

Yasemin AKSU – Yasemin AKSU was born in Ankara in 1989. She was graduated from Middle East Technical University (METU), Faculty of Engineering, Department of Metallurgical and Materials Engineering in 2012 then completed her master's degree in METU Graduate School of Natural Applied Science Metallurgy, Department of Metallurgical and Materials Engineering in 2015. She has been doing her PhD in Gazi University Graduate School of Natural Applied Science, Department of Metallurgical and Materials Engineering since September, 2016. She has been working as a research assistant in Gazi University Technology Faculty since February, 2013.

İrem Burcu ALGAN – İrem Burcu Algan was born in Ankara in 1989. She was graduated from Karadeniz Technical University, Faculty of Engineering, Department of Metallurgical and Materials Engineering in 2012 then completed her master's degree in Gazi University Graduate School of Natural Applied Science Metallurgy and Material Engineering Department in 2015. She works as a research assistant in Gazi University Technology Faculty since February, 2013 in addition continue her doctorate in Gazi University since September, 2015.

Ramazan ÇITAK – Ramazan Çıtak was born in Kırşehir in 1959. He graduated from Gazi University Technical Education Faculty in 1981. He got his master's degree from Gazi University in 1991 and PhD in 1999. He got World Bank and TÜBİTAK-NATO scholarship as visiting scholar in The Ohio-State University, USA in 1994 and 1997. He worked in Karaelmas University as an Assistant Professor between 1999 and 2002. He got Associate Professor Title in 2001 and full Professor Title in 2007. He has been working in Gazi University since 2002.

Adem KURT – Adem Kurt was born in Çorum in 1958. He graduated from Gazi University Technical Education Faculty in 1983 then he completed his master's degree in Gazi University in 1992, his doctorate in Fırat University Graduate School of Natural Applied Science Education of Metallurgy Department in 1996. He took his associate professor degree in 1999 Gazi University and he is professor since 2005 in there.

SANDWICH COMPOSITE PRODUCTION BY FORMING and JOINING SiC CERAMIC FOAMS BETWEEN AL FOAM PLATES

Ersin BAHÇECİ^{1,a}, Yusuf ÖZÇATALBAŞ^{2,b}, Volkan AYLIKCI^{1,c} Mehmet Hakan DEMİR^{3,d} Tolga DEPCI^{4,e}

¹Dept. of Metallurgical and Materials Engineering, Faculty of Engineering And Natural Sciences, Iskenderun Technical University (ISTE), , 31200, Iskederun, Hatay, TURKEY

²Dept. of Metallurgical and Materials Engineering, Faculty of Technology, Gazi University (GU), Ankara, TURKEY

³Dept. of Mechatronics Engineering, Faculty of Engineering And Natural Sciences, Iskenderun Technical University (ISTE), , 31200, Iskederun, Hatay, TURKEY

⁴Dept. of Engineering Science, Faculty of Engineering And Natural Sciences, Iskenderun Technical University (ISTE), , 31200, Iskederun, Hatay, TURKEY

^a ersin.bahceci@iste.edu.tr, ^b yusufoz@iste.edu.tr, ^c volkan.aylikci@iste.edu.tr,
^d mhakan.demir@iste.edu.tr ^e tolga.depci@iste.edu.tr

Abstract

In the present study, sandwich foams were produced by combining metallic foams which was aluminum alloy with new generation ceramicized foam parts. The ceramic foam forming process was performed by bringing two different materials together to form a SiC porous structure during foaming. The production is a composite of metal / ceramic sandwich composites which sandwiched together during the formation of a self-porous structure between two Al foam plates. Chemical structure and the morphology of the obtained ceramic foam part were characterized by microstructure images, DSC, TGand XPS. It can be said the bonding at atomic level in the metal ceramic foam interface. Strong bonding was observed as a resultsof the stripping tests. DSC, TGand XPS analysis showed that the ceramic foam part could be defined as silicon carbide.

Key Words: Al foam, SiC, ceramic foam, sandwich , composite

1. Introduction

Nowadays, the use of Al foams has increased considerably. Because of its low density, high strength, high thermal conductivity, very good absorbing ability and besides it can be shaped according to usage area, it is used in many engineering fields such as space and airplane applications, automotive industry, heat insulation applications and filter industry [1-6].

Sandwich panels are used in various applications where high hardness and strength are required and low weight is important[1, 2].Al foam-metal (bulk) sandwich composites are widely used in applications and it is seen that sandwich plates have superior performance in terms of properties such as durability and hardness compared to metal foam plates. Because of the high strength of sandwich plates to dynamic loads, researches continues to determine their

advantages relative to the monolithic design for potential applications to be made in impact-resistant structures [7].

In addition, ceramic foams are one of the materials that are becoming widespread today[8-10]. The ceramic foams, which are particularly interesting for applications requiring multifunctional materials, are used in applications such as ultra-lightweight panels, energy absorbing structures, heat dissipation environments, electrodes used in electric batteries, oil and water filters, ultrasonic deflectors, transport systems for catalysts and heat exchangers[11-14]. Ceramic foams are often preferred due to their high thermal resistance and resistance to corrosion, but they are also disadvantaged in some applications due to their fragile structure. The ceramic foams are used in applications as a single material, but also as composite materials by using adhesive, soldering and mechanical assembly methods of other kinds of materials [15-17]. But the greatest obstacle to the use of superior properties and lower costs of these materials, which cannot be used without bonding or additional processing, is the lack of proper bonding techniques for different materials such as metals and ceramics used in high temperature devices and protective armor. For this reason, the production of very low-cost and high-strength composite materials by joining ceramic-metal is very important in many important applications.

In this study, it is aimed to form ceramic foam by chemical reaction between two metal foam plates made of Al alloy material. The formation and joining of sandwich foams (metal foam / ceramic foam) using the properties of ceramic and metallic foams and without using any additional bonding material or joining process are investigated in detail.

2. Experimental

2.1. Material and Foaming Method

8%Si+0.8%Mg+0.8%TiH₂ (by weight) and the remaining Al powder % were mixed in Turbula and pressed in room temperature under 300 MPa pressure. After sintering block samples at 500 °C(15 minutes) they were extruded at 400 °C. Extruded sample was rolled gradually at 400 °C and plate shaped preform materials (that can be foamed) were produced [18, 19].

After being kept at the foaming temperature of 700 °C for about 15 minutes, the metallic foam which filled the mould cavity was taken with the mould out of the furnace and left for cooling in the circulating air. It was prepared by cutting as in Figure 1.

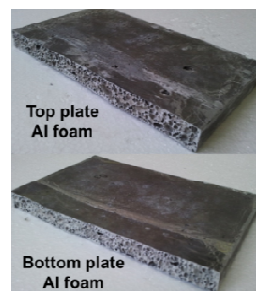


Figure 1. Al foam plates.

2.1. Method of Ceramic Foaming

In the ceramic foaming process, firstly the polymer (polyimide) and silicon carbide (SiC) powders are mixed homogeneously and the mixture powder is prepared. Then, a special mold design was made as shown in Figure 2 and the prepared mixture powder was filled between Al foam plates and allowed to stand for 5 hours at 580 ° C in an atmosphere protected oven to allow the polymer to leave the medium. SiC porous structure was obtained by leaving the polymer in the medium after these five hours.

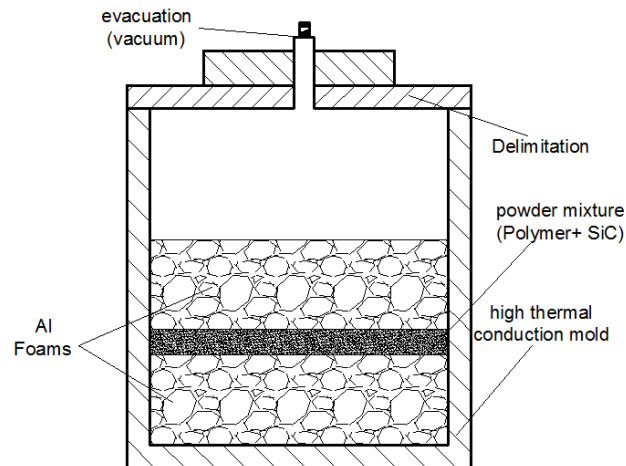


Figure 2. The schematic view of mold design and Al / Ceramic sandwich foaming process

3. Results and Discussion

In this study, the process containing mixed dust placed between Al foam plates was kept at 580 C for 5 hours in an atmosphere protected oven environment. At this time, water (H₂O) and polymer were removed from the medium and a porous structure with SiC and oxygen rich surface was formed. As the commercialization and patenting works for the product continue, detailed information about production cannot be given. It can be seen in Figure 3 that the rich oxygen on the surface of the ceramic foam brought about a bond between the metal ceramic by bonding with Al atoms on the aluminum foam surface.

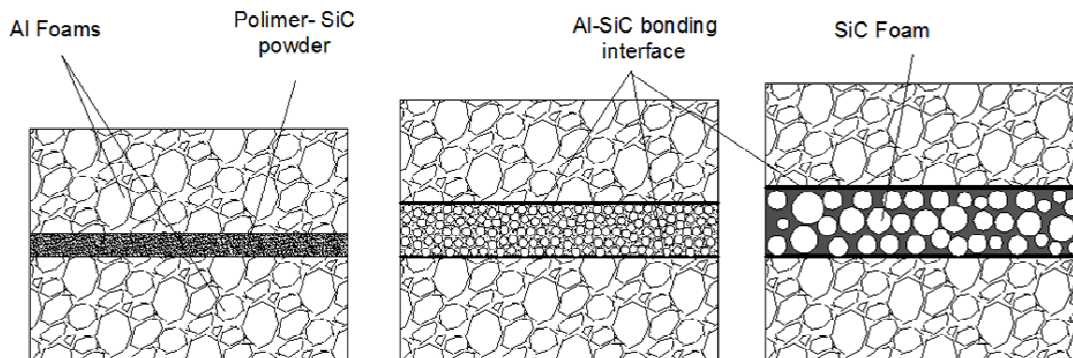


Figure 3. Stages of ceramic foam formation.

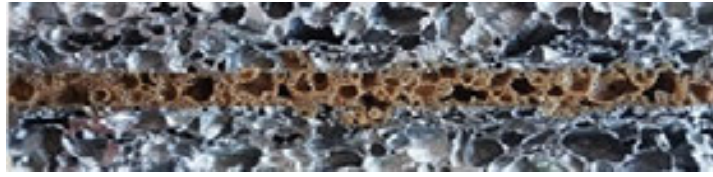


Figure 4. Al/SiC Sandwich foam

Figure 4 shows the produced foam and brown and black parts are showed SiC and carbon regions, respectively. It was observed that the cells in the Al foam were not coaxial but formed in different sizes. Moreover, the Al foam cell walls are distorted between neighboring cells during bubble formation and they lead to create large-sized cells in the foam. Although the ceramic foam cell size is smaller than that of aluminum, the cell wall is thicker. When examined in detail, the water and polymer that leave the environment form pores inside of the foam and it is seen that the shapes of the cells composed of these pores are irregular.

Figure 5 shows the DSC curve of the produced foam and it can be seen that the glass transition temperature of this foam is equal to -114.57°C . Accordingly, it can be said that the produced ceramic foam contains SiC material.

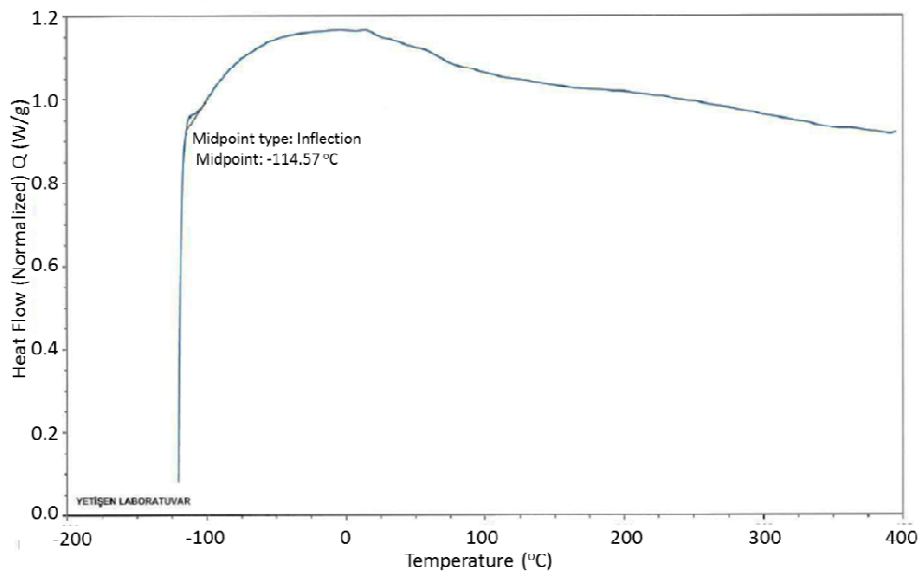


Figure 5. DSC analysis curve of ceramic foam

Figure 6 shows the TG analysis of the foam and the results show that mass loss is beginning at 50 °C. The mass loss from this temperature to 200 C⁰ occurs due to evaporation of the water in the ceramic material. It can be argued that the loss occurring at temperatures after 200C depends on the oxidation of carbon. It is clearly seen in the figure that the mass loss of the material increases after 300 C⁰ and there was a severe decrease in mass loss between 450 C⁰ and 700 C⁰. The reason of this severe decrease in weight of the material in this temperature range is the removal of thermoset polymer from the medium.

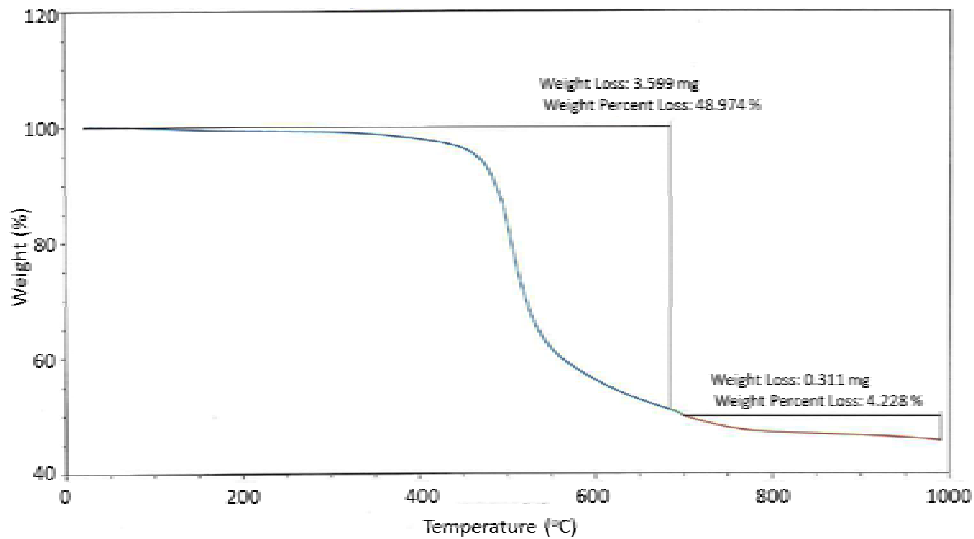


Figure 6. TG analysis curve of ceramic foam

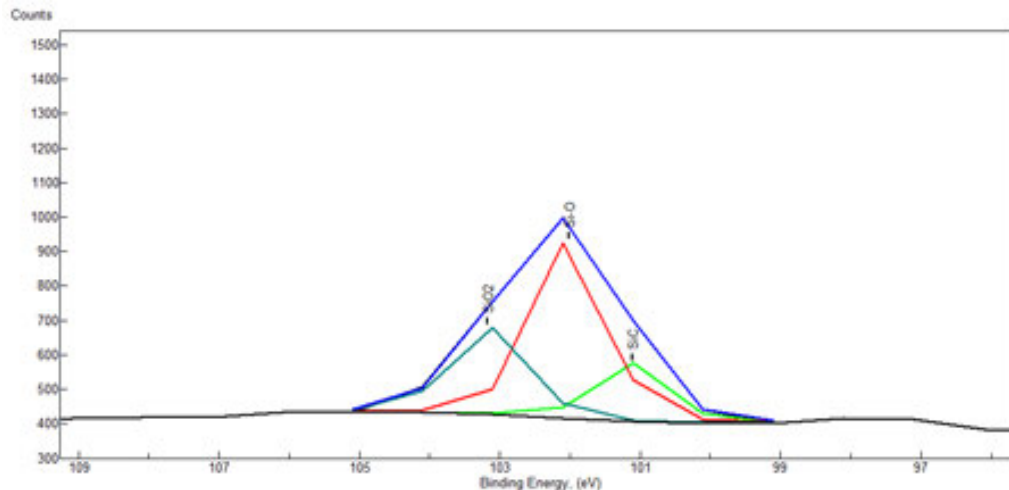


Figure 7. XPS analysis curve of Si element in the composition of SiC foam.

Figure 7 shows the XRD analysis of produced ceramic foam. It is attributed to SiO₂ and Si-O, respectively, probably according to the oxidation during the preparation of silicon carbide foam and the binding energy at 101.11 eV is ascribed to SiC [20].

4. Conclusions

This study involves the production and assembly of sandwich foams (metal foam / ceramic foam) with chemical reactions of ceramic foam between Al foam plates without the use of additional bonding material or joining process.

The results obtained in this study are as follows.

- The different sized cells form in the aluminum foam structure and the walls of these cell are thinner than the ceramic foam cell walls.
- The observed results in the characterization studies show that the porous structure formed between the Al plates is silicon carbide.
- After a series of reactions of the polyamide and SiC powders in the furnace, the large majority of the polymer leaves from the internal structure and SiC porous structure occurs. In the atmosphere protected environment, there is oxygen bonding of the Al surface with the rich oxygen of the glassy SiC surfaces. Sandwich composite production is carried out with this atomic bonding which occurs in the interfacial plane.

5. References

- [1] L.J Gibson, M.F Ashby, Cellular Solids Structure and Properties(2nd edition), Cambridge University Press, Cambridge, UK (1997)
- [2] M. F. Ashby, A. G. Evans, N. A. Fleck, L. J. Gibson, J. W. Hutchinson, H. N. G. Wadley, Metal Foams: A Design Guide, Butterworth Heinemann (2000)
- [3] H.P. Degischer, and B. Kriszt, Handbook of Cellular Metals: Production, Processing and Applications. Wiley-VCH. Weinheim. 1-363 (2002).
- [4] J.Banhart, Aluminium foams for lighter vehicles, International Journal of Vehicle Design (IJVD), Vol. 37, 2/3, (2005)
- [5] I. Jeon, K. Katou, T. Sonoda, T. Asahina, Ki-Ju Kang: Cell wall mechanical properties of closed-cell Al foam, Mechanics of Materials, 41, (2009), 60–73
- [6] A. Rabiei, L. J. Vendra: A comparison of composite metal foam's properties and other comparable metal foams, Materials Letters, 63-5, (2009) Pages 533-536
- [7] D. D. Radford, G. J. McShane, V. S. Deshpande, N. A. Fleck: The response of clamped sandwich plates with metallic foam cores to simulated blast loading, International Journal of Solids and Structures, Volume 43, Issues 7–8, (2006), Pages 2243-2259

- [8] P. Colombo, J.R. Hellmann, D.L. Shelleman: Mechanical properties of silicon oxycarbide ceramic foams, *J. Am. Ceram. Soc.*, 84 (10) (2001), pp. 2245-2251
- [9] J. H. Eom, Y. W. Kim, S. Raju: Processing and properties of macroporous silicon carbide ceramics: a review, *J. Am. Ceram. Soc.*, 1 (2013), pp. 220-242
- [10] M. K. Mishra, S. Kumar, A. Ranjan, N. E. Prasad: Processing, properties and microstructure of SiC foam derived from epoxy-modified polycarbosilane, *Ceramics International*, Volume 44, Issue 2, (2018), Pages 1859-1867
- [11] P. Ciambelli, G. Matarazzo, V. Palma, P. Russo, E. Merlone Borla, and M. F. Pidria. Reduction of soot pollution from automotive diesel engine by ceramic foam catalytic filter. *Topics in Ceramics*, 42-43. May 2007
- [12] Y. Zhang, J. Yu, S. Chen, S. Wan: Wastewater treatment using bioreactor with dual functional ceramic membrane, *Int. J. Environ. Pollut.*, 38 (3) (2009), pp. 318-327
- [13] R. Coquard, D. Rochais, D. Baillis: Experimental investigations of the coupled conductive and radiative heat transfer in metallic/ceramic foams, *International Journal of Heat and Mass Transfer*, Volume 52, Issues 21–22, (2009), Pages 4907-4918
- [14] W. Huo, Y. Chen, Z. Zhang, J. Liu, S. Yan, Jia-Min Wu, X. Zhang and J. Yang: Highly porous barium strontium titanate (BST) ceramic foams with low dielectric constant from particle-stabilized foams, *Journal of the American Ceramic Society*, 101, 4, (2017), pp.1737-1746
- [15] A. A. Shirzadi, Y. Zhu, H. K. D. H. Bhadeshia: Joining ceramics to metals using metallic foam, *Materials Science and Engineering: A*, Volume 496, Issues 1–2, (2008), Pages 501-506
- [16] A. K. Jadoon, B. Ralph, P. R. Hornsby: Metal to ceramic joining via a metallic interlayer bonding technique, *Journal of Materials Processing Technology*, Volume 152, Issue 3, (2004), Pages 257-265
- [17] M. Garcia-Avila, M. Portanova, A. Rabieia: Ballistic Performance of a Composite Metal Foam-ceramic Armor System, *Procedia Materials Science*, Volume 4, (2014), Pages 151-156
- [18] E. Bahceci: Effect of cell morphology on mechanical properties of closed cell metal foams and usability of photoelasticity method. University of Gazi Science Enstitute. Ankara. (2012)
- [19] E. Bahceci Y. Ozcatalbas: Microstructural Characterisation Of The AlSiMg Alloy Metallic Foams Produced With P/M Method. IN-TECH 2013. Budapest. Hungary. 459-463 (2013).
- [20] J.H. Deng, P. C. Sun, G. A.Cheng, R. T. Zheng: Improved field electron emission from SiC assisted carbon nanorod/nanotube hetero structured arrays by using energetic Si ion irradiation, *Surf.Coat.Technol.*228 (2013-37) S323–S327.

CORRESPONDENCE ADDRESS:

Assist. Prof. Dr. Ersin BAHCECI

Iskenderun Technical University, Faculty of Engineering and Natural Science, Dept. of Metallurgical and Materials Science, Iskenderun/Hatay TURKEY

+90 546 214 89 41 and E-mail: ersin.bahceci@iste.edu.tr

SHORT BIOGRAPHIES

First Author's Name – Assist. Prof. Dr. Ersin BAHCECI

Dr. Bahceci graduated from Gazi University, Technical Education Faculty, Department of Metallurgical Education in 2003. After completing his MSc at the Department of Metallurgical Education at Gazi University, he received his Ph.D. in Department of Metallurgical Education at Gazi University. He worked at Kastamonu University between 2010-2013 and then between 2013-2015 at Mustafa Kemal University. Since April 2015, he has been working as Assistant Prof. in Iskenderun Technical University, Department of Metallurgical and Materials Science Engineering.

Description of Research

Metal Matrix Composites, Powder Metallurgy, Machinability of Engineering Materials, Metal foams, Photoelasticity, Nanotechnology

Second Author's Name – Prof. Dr. Yusuf OZCATALBAS

He has been working as Prof. in Gazi University, Department of Metallurgical and Materials Science Engineering.

Description of Research

Machinability of Engineering Materials, Failure Methods and Plastic Forming Techniques Powder Metallurgy, Composite materials, Metal Foams, Resonant constructions, Steel and Heat Treatment.

Third Author's Name – Assist. Prof. Dr. Volkan AYLIKCI

He has been working as Assistant Prof. in Iskenderun Technical University, Department of Metallurgical and Materials Science Engineering.

Description of Research

Material characterization, Optics, Quantum

Fourth Author's Name – Assist. Prof. Dr. Mehmet Hakan DEMIR

Dr. Demir graduated from Kocaeli University, Engineering Faculty, Department of Mechatronics Engineering in 2009. After completing his MSc at the Department of Mechatronics Engineering at Istanbul Technical University, he received his Ph.D. in Department of Mechanical Engineering at Yıldız Technical University. Since April 2017, he

has been working as Assistant Prof. in İskenderun Technical University, Department of Mechatronics Engineering.

Description of Research

Thermoelastic stability analysis, Dynamics, Modeling and control, Artificial intelligence, Solidification thermodynamics.

Fifth Author's Name – Prof. Dr. Tolga DEPCI

He has been working as Assistant Prof. in İskenderun Technical University, Department of Engineering Science.

He is expert on mining and metallurgical area especially boron and boron compound and activated carbon.

EFFECT OF FILLER WIRE CHEMICAL COMPOSITION ON JOINT PROPERTIES OF 1050A ALUMINUM ALLOY

Oktay Cetinel^{1, a}, Volkan Kilicli^{2, b} and Hakan Ates^{2, c}

¹Department of Mechanical Engineering, Hacettepe University, Ankara, Turkey

²Department of Metallurgical and Materials Engineering, Faculty of Technology, Gazi University, 06560, Teknikokullar, Ankara, Turkey

^aoktaycetinel@gmail.com, ^bvkilicli@gazi.edu.tr, ^chates@gazi.edu.tr

Abstract

In the present study, the effect of filler wire chemical composition on joint properties of 1050A aluminum alloy has been investigated. In order to carry out experiments, AlSi5, AlSi12, and AlMg5 wires have been used as a welding filler material. The gas tungsten arc welding (GTAW) process has been preferred for joining of the 1050A aluminum alloy due to its comparatively easier applicability and better economy. The tensile properties, microhardness, and microstructures have been evaluated of the joints, and the results are compared. Experimental results showed that the joint welded with AlMg5 filler showed superior mechanical properties compared with other filler materials, and this is mainly due to the formation of very fine, the equiaxed microstructure in the weld zone.

Keywords: 1050A aluminum alloy, Filler Chemical Composition, Gas Tungsten Arc Welding (GTAW), Microstructure, and Tensile Properties.

1. Introduction

1050 A alloy is an aluminum alloy commercially pure and from wrought family. As a wrought alloy, instead of being used in casting, it is usually formed by extrusion or rolling. Due to high electrical conductivity, corrosion resistance and machinability, it is widely used in many areas such as electrical and chemical industries. The 1050A alloy is occasionally used for the production of heat sinks as it has a higher thermal conductivity than some other alloys' thermal conductivity. It has low mechanical strength compared to more alloyed metals. It can be strengthened by cold working treatment while it cannot be strengthened by heat treatment [1].

The 1050A aluminum alloy is a well-known class of aluminum for general sheet metal work where moderate strength is required. It is also known for its excellent corrosion resistance, high ductility, and highly reflective varnish. It is typically used for chemical process plant equipment, food industry containers, and lamp reflectors. Aluminum and its alloys have corrosion resistance in many different environments. This feature makes them important materials, along with offering them a wide range of industrial and marine applications. For this reason, in order to better understand the corrosion behavior of these materials, it is necessary to carry out further investigations under different conditions [2].

No attempt have been made so far on the effect of welding wire chemical composition on joint properties of 1050A aluminum alloy. In the present study, the effect of filler wire chemical composition on joint properties of 1050A aluminum alloy has been investigated.

2. Experimental Procedures

3 mm thick plate 1050A aluminum alloys specimens were obtained in cold rolled condition. The 100mmX130mm plates were cut from plates for welding. The chemical compositions of 1050A alloy and filler wires are given in Table 1 and Table 2, respectively. The gas tungsten arc welding (GTAW) process has been preferred for joining of the 1050A aluminum alloy and welding parameters are provided in Table 3.

Table 1. The chemical composition of 1050A alloy used in this study (wt.-%)

Si	Fe	Cu	Mn	Mg	Ni	Zn	Ti	Al
0.168	0.405	0.004	0.006	0.003	0.002	0.003	0.015	Remain

Table 2. The chemical composition of the welding wires (wt.-%)

Filler	Al	Si	Mg
AlSi5	95	5	-
AlSi12	88	12	-
AlMg5	95	-	5

Table 3. Welding Parameters

Welding methods	Gas Tungsten Arc Welding (GTAW)
Shielding Gas	Argon (Purity: 99.99%)
Electrode	Tungsten, 2mm diameter
Gas Flow	7.5 l/min
Current	AC 95A
Welding speed	0.07 m/min

Tensile specimens cut from welded plates by using electro-discharge machine (EDM) according to ASTM E8M-15 (Fig.1).

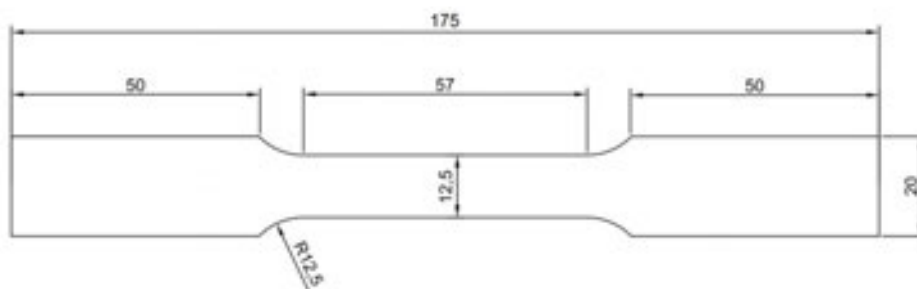


Figure 1. Tensile specimen dimensions prepared according to ASTM E8M-15.

Metallographic specimens were cut from welded plates and cold mounted for mechanical grinding, polishing with up to 1 μm diamond suspension and finally etched with Keller's

solution. Leica DMI5000M optical microscope was used for microstructural examinations. JEOL JSM 6060 LV scanning electron microscope was used for fractographic observations.

Tensile and hardness tests were performed to determine the mechanical properties of the welded specimens. Tensile tests were carried out at room temperature using an Instron 3369 universal testing machine with 50 kN loading capacity at a constant cross-head speed of 0.855 mm.min⁻¹ which corresponds to strain rate of 0.00025 s⁻¹. An extensometer set to a gauge length of 25 mm was used for strain measurement. The area of under the stress-strain curve was integrated to assess the work of fracture (absorbed energy). Three tensile specimens were tested for each condition and mean values were reported. Hardness tests were conducted in QnessQ30M hardness tester with Vickers (1kgf) hardness method.

3. Results and Discussions

3.1. Microstructures

The optical micrographs of welding zones and weld metals are shown in Fig. 2.a to Fig.2.c and Fig. 2.d to Fig.2.f, respectively. Uniformly distributed very fine precipitates have been observed in base metal (Fig. 3a). The coarser grain structure and grain growth has been observed in welding zones. Also, columnar grains have been observed near to weld metal. These results are parallel to previous investigations [3].

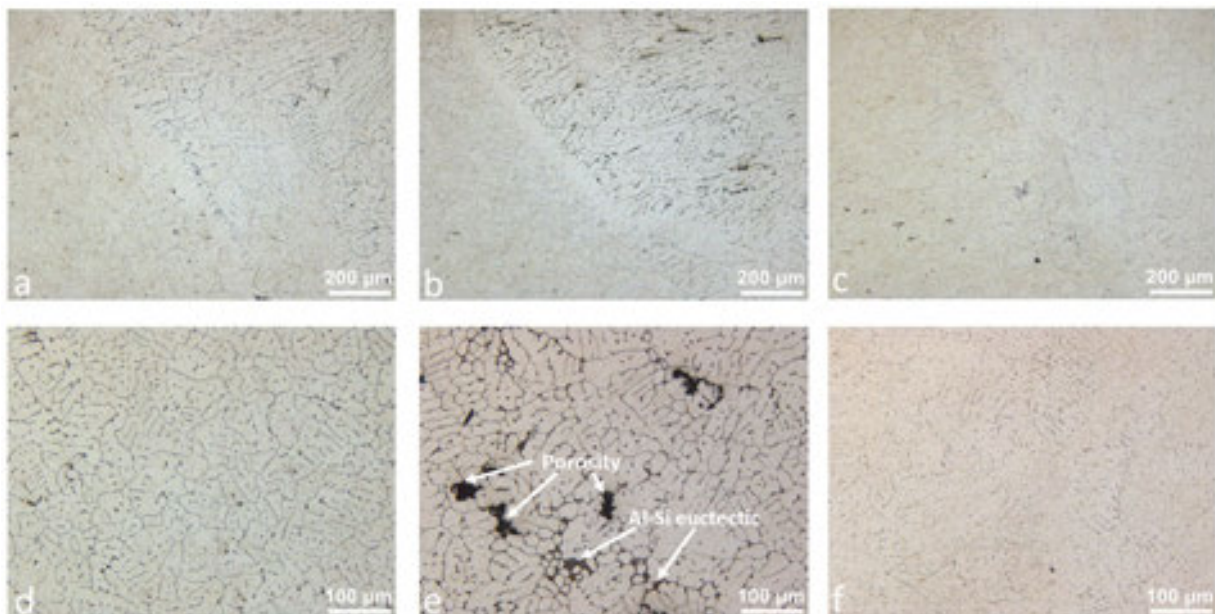


Figure 2. Optical micrographs of welding zones; a) AlSi5 transition zone, b) AlSi12 transition zone, c) AlMg5 transition zone, d) AlSi5 weld metal, e) AlSi512 weld metal and f) AlMg5 weld metal

3.2. Mechanical Properties

The mechanical properties are presented in Table 4. The yield stress and tensile stress of unwelded base metal are 107 MPa and 120 MPa, respectively. However, the yield stress and tensile stress of welded metals are lower than base metal. AlSi5 and AlMg5 have exhibited similar absorbed energy, yield stress and tensile stress. However, the elongations of AlSi5 filler material weld better than the AlMg5 filler material weld. Best mechanical properties obtained with the AlSi5 filler material. Low mechanical properties obtained in AlSi12 filler material due to the microporosity in weld metals (Fig.2.e).

Table 4. Tensile properties of welded specimens

Filler Materials	0.2% Yield Stress (MPa)	Ultimate Tensile Stress (MPa)	Total Elongation (%)	Absorbed Energy (Joule)	PSE (MPa.%)
Base Metal	107.03 ± 4.11	120.25 ± 3.81	6.57 ± 0.35	4.09 ± 0.99	790.04
AlSi5	29.85 ± 3.94	71.22 ± 1.02	18.9 ± 1.39	10.49 ± 0.93	1346.05
AlSi12	35.69 ± 2.44	68.06 ± 3.9	16.72 ± 5.07	8.56 ± 3.2	1137.96
AlMg5	32.6 ± 0.92	71.08 ± 1.77	11.12 ± 2.02	10.40 ± 1.68	790.40

PSE: Product of Strength and Elongation, it is calculating by multiplying UTS and Total Elongation values

The hardness values across the weld cross sections provided in Fig.3. All the filler materials exhibited similar hardness profiles. Nevertheless, AlMg5 weld metal hardness higher than AlSi5 and AlSi12 filler materials (Table 4). The hardness is greatly reduced in the heat-affected zone (3-11 mm from weld center) during welding processes. This is major the reason for the failure locations in the tensile test.

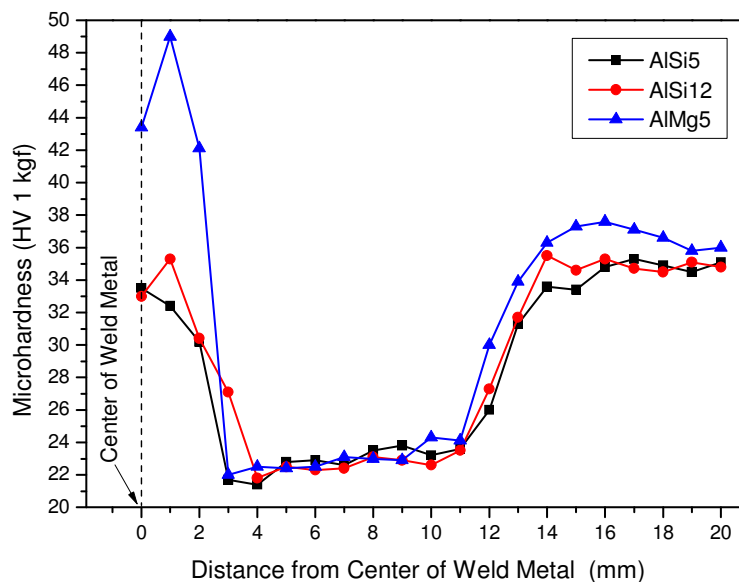


Figure 3. Hardness profiles of the welding zone

Table 4. Hardness values of weld metals

Filler Materials	Hardness (HV 1 kgf)
Base Metal	37.2 ± 0.7
AlSi5	34.6 ± 1.2
AlSi12	35.5 ± 0.6
AlMg5	48.4 ± 4.9

4. Conclusions

In the present investigations, the effect of filler wire material (AlSi5, AlSi12, and AlMg5) chemical composition on joint properties of 1050A alloy has been investigated. Following conclusions can be drawn from this study;

- 1- The highest weld metal hardness has been measured in the AlMg5 filler material.
- 2- AlSi5 filler material provided optimum mechanical properties.
- 3- Microporosities have been observed in weld metal using the AlSi12 filler material.

5. Acknowledgments

The authors wish to acknowledge the financial supports of Gazi University Scientific Research Fund (Project codes: GÜBAP 07/2013-01, 07/2013-02 and 07/2015-08), and Gazi University Welding and Joining Technologies Research and Application Center (KABTEM).

6. References

- 1- Hatch J.E. (Ed.): Aluminum: Properties and Physical Metallurgy, Aluminum Association, ASM International, USA, (1984).
- 2- R. Rosliza, W.B. Wan Nik: Improvement of corrosion resistance of AA6061 alloy by tapioca starch in seawater, *Current Applied Physics* 10 (2010) 221–229
- 3- A.K. Lakshminarayanan, V. Balasubramanian and K. Elangovan: Effect of welding processes on tensile properties of AA6061 aluminium alloy joints, *The International Journal of Advanced Manufacturing Technology*, 40(2009), pp.286-296.

CORRESPONDENCE ADDRESS: Dr. Volkan Kilicli, Gazi University, Faculty of Technology Department of Metallurgical and Materials Engineering, 06500 Teknikokullar/Ankara Turkey, Tel:+90 312 2028761 Fax:+90 312 2028947 e-mail: vkilicligazi.edu.tr

SHORT BIOGRAPHIES

Oktay Cetinel – MEng- University of Bath, Faculty of Engineering and Design, Dept. of Mechanical Engineering (2015). PhD- Hacettepe University, Faculty of Engineering, Dept. of Mechanical Engineering (2016- continuing). MEng- University of Bath, Faculty of Engineering and Design, Dept. of Mechanical Engineering (2015). PhD- Hacettepe University, Faculty of Engineering, Dept. of Mechanical Engineering (2016- continuing).

Volkan Kilicli – Dr. Volkan Kilicli is Assistant Professor at the Department of Metallurgical and Materials Engineering in Gazi University for six year. He received his B.Sc., M.Sc. and Ph.D. degree in same department in 2001, 2004 and 2010 respectively. His areas of interest are materials characterization by optical microscopy, SEM and X-RD, semi solid processing of aluminium alloys and heat treatments of irons and steels.

Hakan Ates – Dr. Hakan Ates is Professor at the Department of Metallurgical and Materials Engineering in Gazi University. He received his B.Sc., M.Sc. and Ph.D. degrees at the same University in 1992, 1996 and 2003 respectively. He completed post-doctoral study at University of Illinois at Urbana-Champaign. His areas of interest are welding, powder metallurgy, nanotechnology and materials characterization. He is member of the Welding Technologies Assosiation, Powder Metallurgy Assosiation. He has IWE, IWI-C diplomas and MT, PT, UT, RT L2 certificates.

RESIDUAL STRESS CHANGES AFTER HEAT TREATMENT ON SMAW WELDED PLATES

Galip BÜYÜKYILDIRIM^{1,a}, Georgy BATOV^{2,b}

¹Dr., Technical Manager: Ege Sonik-SQS

²Dr., General Manager: Kachestvo

^agalipbuyukyildirim@yahoo.com, ^bgbatov@mail.ru

Abstract

This paper presents an experimental work of analysis of strain state and residual stress of welds in unalloyed steel plates by using magnetic anisotropy indicator for mechanical stresses. The measurements are taken before and after the heat treatment based on comparison approach taking readings on a net at base metal, weld area and HAZ region. Test results were compared with X-ray testing on films and visual testing. The results showed compliance to the film evaluation reports and to the aim of the heat treatment process. Mechanical stresses in objects are not visible using conventional NDT methods, however they are usually the first and the main indicator of problems. This paper discusses a method to predict and avert potential failure; based on measuring the concentration and gradient of mechanical stresses in parts.

Key Words: Heat treatment, Residual Stresses, welding, SMAW

1. Introduction

The principle of magneto-elastic effect in materials (ferromagnetic materials change magnetic properties under the influence of mechanical stress) can be used to design inspection devices. This principle is used to build magneto-elastic and magneto-anisotropic indicators, including Indicator of Mechanical Stress, IMS.

Standard approaches to solving inspection challenges and ignoring certain physical phenomena have been long time obstacles for the widespread implementation of electromagnetic techniques in practice. It is known that the upper layer (0.2 mm) of metal has a typical stress conditions due to various stress influences like oxidation, mechanical micro-scratches, etc. Thus, some difficulties accrue in applications, for example, devices based on effect of Barkhausen. Another reason for low confidence of measurement of mechanical stresses using electromagnetic fields indicators is magneto-mechanical hysteresis and attempts to get the result by one of the parameters of hysteresis loops (for example, based only on coercive force σ_r or only on residual induction B).

Any relationship between B and σ has a point inverse relationship after which the connection between B and σ become reverse, i.e. the same level of output signal can be received for two different mechanical stresses. The phenomenon of mechanical hysteresis is observed for example, near and the zone of plastic flow (points 2-3, Fig 1). When constructions made from steel and which had suffered numerous mechanical changes including local plastic deformation in the process of preparing and mounting, conventional "strain gauges".

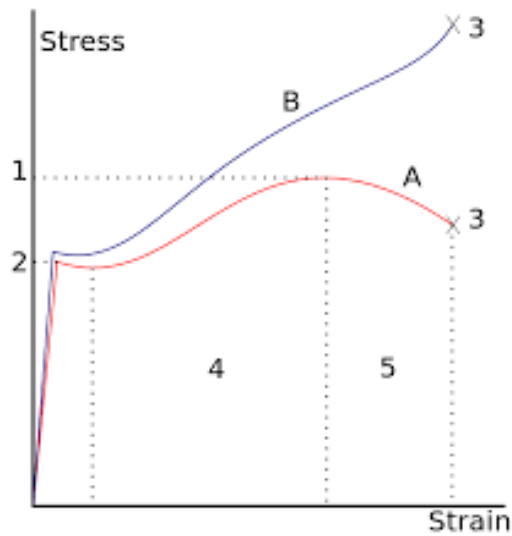


Figure 1. A stress–strain typical curve engineering stress (A) versus true stress (B):

1. Ultimate strength
2. Yield strength
3. Fracture
4. Strain hardening region
5. Necking region

This connection between mechanical stresses and magnetic properties called magnetoelastic sensitivity (Λ): where B is the magnetic induction and j is mechanical stress (load)

$$\Lambda = \partial B / \partial j \quad (1)$$

2. Principle of mechanical stress measurements

Principle of operation magneto-anisotropic converter based on effect of rotating magnetic induction vector B in the primary measurement coil. The voltage U at the output of the measuring coil ω is described by the Formula

$$U = K B_c S_0 f_{II} \sin \beta \omega \quad (2)$$

where B_c - average value of induction; S_0 - area covered by windings; K- coefficient proportionality; f_{II} - voltage frequency. β - angle between the vector measuring winding ω and magnetic induction B;

The formula obtained for similar direction vectors of σ and of B . By rotating vector B it is possible to characterize changes of its orthogonal components. A more detailed analysis shows that the output of "cross" magneto-anisotropic converter at once (i.e., before any processing) produces a signal proportional to the difference of Principal (Mechanical) Stresses (DPMS):

$$\tau = \frac{1}{2} (\sigma_1 - \sigma_2) \quad (3)$$

Achieved result is important, because according to the stress-strength criteria (Yield) deformation of material occurs when k tension strength

$$\tau_{\max} = \frac{1}{2} (\sigma_1 - \sigma_2) \geq \sigma_T(4)$$

Location of stress concentration appearance there is anomalous change of magnetic properties of metal. A detailed consideration of this physical nature and the fact that all useful information is contained in several parameters of hysteresis loop was resulted in development of the Indicator of Mechanical Stress (IMS) model and an algorithm to process information. Information processing algorithm used in Indicator of Mechanical Stresses make it possible to resolve the problem of magneto-mechanical hysteresis and provide accurate results.

Magneto-anisotropic ("cross") transducers used in IMS are two mutually-perpendicular U-shaped coils one is an activation coil and the other coil is a measuring coil. Transducers measure anisotropy of magnetic properties in ferromagnetic metals under external load using Magneto-elastic converters within the limitations of equipment. IMS measures Electromotive Force (EMF) by inducing a magnetic field which is generated by the excitation coil and picked up by the receiving coil, 2 perpendicular magnetic circuits in the probe (transducer). If material has isotropic magnetic properties, EMF induced in measuring coils mutually compensated and the output signal is Zero (well balanced magnetic field). If there is anisotropy of magnetic properties, unbalance of EMF occurs which results in appearance of output signal with values dependent on the value and orientation of main mechanical stresses upon the surface of metal being tested by detecting Mechanical Stress Concentration (MSC) and the difference of Principal Mechanical Stresses (DPMS). IMS results are dimensionless, i.e. qualitative comparison (less-than-equal). To assess the conditions and operational risk, it is not-so-important to find stresses but their concentration and rate of change of stress (gradients). Normally, in the centers (peaks) mechanical stress concentration (MSC) defects are formed. They are dislocation-generators. With sufficiently high gradients, these locations begin to move. Eventually, cracks develop. If (in the area under inspection) there are no stress concentrations or gradients, there will be no metal destruction.

IMS allows identification of MSC and gradients to show the exact coordinates and quantify their development without any additional measurements. This allows, on the one hand, to make conclusions about the current condition of the surveyed site and helps assessing the remaining life. On the other hand, to make conclusive decisions about location of the gradients and concentration in precisely location on the maps and how to deal with concentrators and gradients, i.e. to prevent these sources from occurrence and formation of defects.

The Magneto-Anisotropic("cross") transducers used in "IMS" are two mutually-perpendicular U-shaped coils. The transducers measure anisotropy of magnetic properties in ferromagnetic metals under external load using Magneto-elastic converters. "IMS" measures Electromotive Force (EMF) by inducing a magnetic field, which is generated by an excitation coil and picked up by a receiving coil. If the material has isotropic magnetic properties, EMF induced in measuring coils is mutually compensated and the output signal is Zero (well balanced magnetic field). If there is anisotropy of the magnetic properties, an unbalanced EMF (electromotive force) occurs. This results in an output signal with values dependent on the value and orientation of the main mechanical stresses. The equipment is suitable for testing all Fe steels and can be used on painted and/or coated surfaces with a maximum gap of 4 mm. Fig 2. Indicator of Mechanical Stresses (IMS) consist of data collector, probe (transducer) and Laptop for process and store results.



Figure 2. Indicator of Mechanical Stresses (IMS) consist of data collector, probe (transducer) and Laptop for process and store results

3. Experimental Results and Discussion

Selected cases provided below are to clarify applications and benefits using IMS as a tool to measure stresses (quality of welding, stress release etc. processes or safe of serviceability of as part of ISI or Preventive Maintenance, and early diagnostic for the aging construction. IMS could also be used for research and more in depth investigation of stress level inside the part.

Generally acceptable criteria for the stress gradient

(Used for 10 mm thickness, non-nuclear applications and strongly depends on metal conditions, without external/internal stresses). To be used with care.

These acceptance criteria are to be used with great consideration to the work conditions, is it under pressure or not, etc. Recommended surface temperature not to exceed 50-55°C (not to approach Curie Point of metals)

1- Stress gradient or Difference of Principal Mechanical Stresses (DPMS) up to 350 units (difference between top and bottom highest points) as acceptable working condition

2- DPMS from 350 to 400 as high working stress level can still be accepted, but it is recommended that the equipment be monitored for increase of stress gradient.

3- DPMS from 400 to 450 is considered as critical (defects could already have developed) and can be recommended for replacement as soon as possible (could be accepted, but with frequent monitoring)

4- Any DPMS 450 to 500 and above should be recommended for immediate care (even if there are no detectable defects)

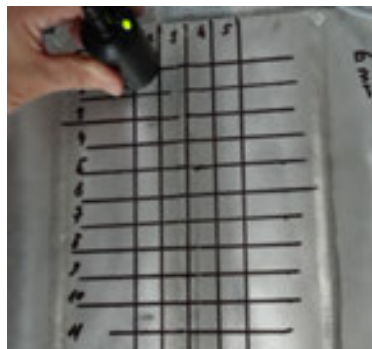


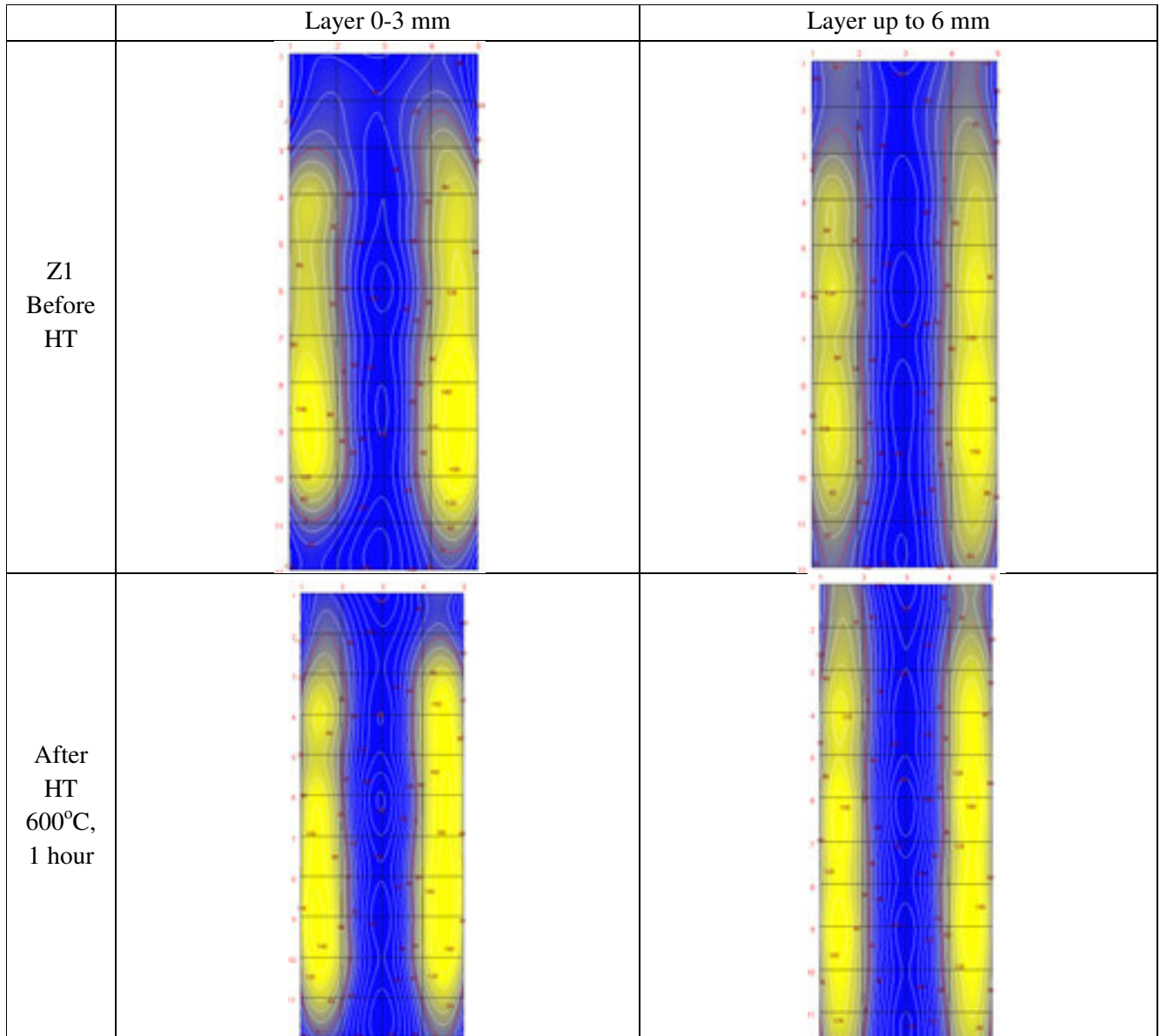
Fig. 3 Plate (general view) and the stress conditions (residual stress) measurement

Results were sliced by Layers 0-3 mm (sub-surface) and up to 6 mm wall depth from the inspected surface.

Plate 1, Welded plate, 8 mm wall thickness with embedded defect (confirmed by X-Ray)

Purpose: Evaluate stress relaxation (by layers) and the quality of Heat Treatment HT process (1 hour for 600°C over 1100°F)

The steps of the grid (X, Y) are 20mm, Line X3 located on weld's CL.



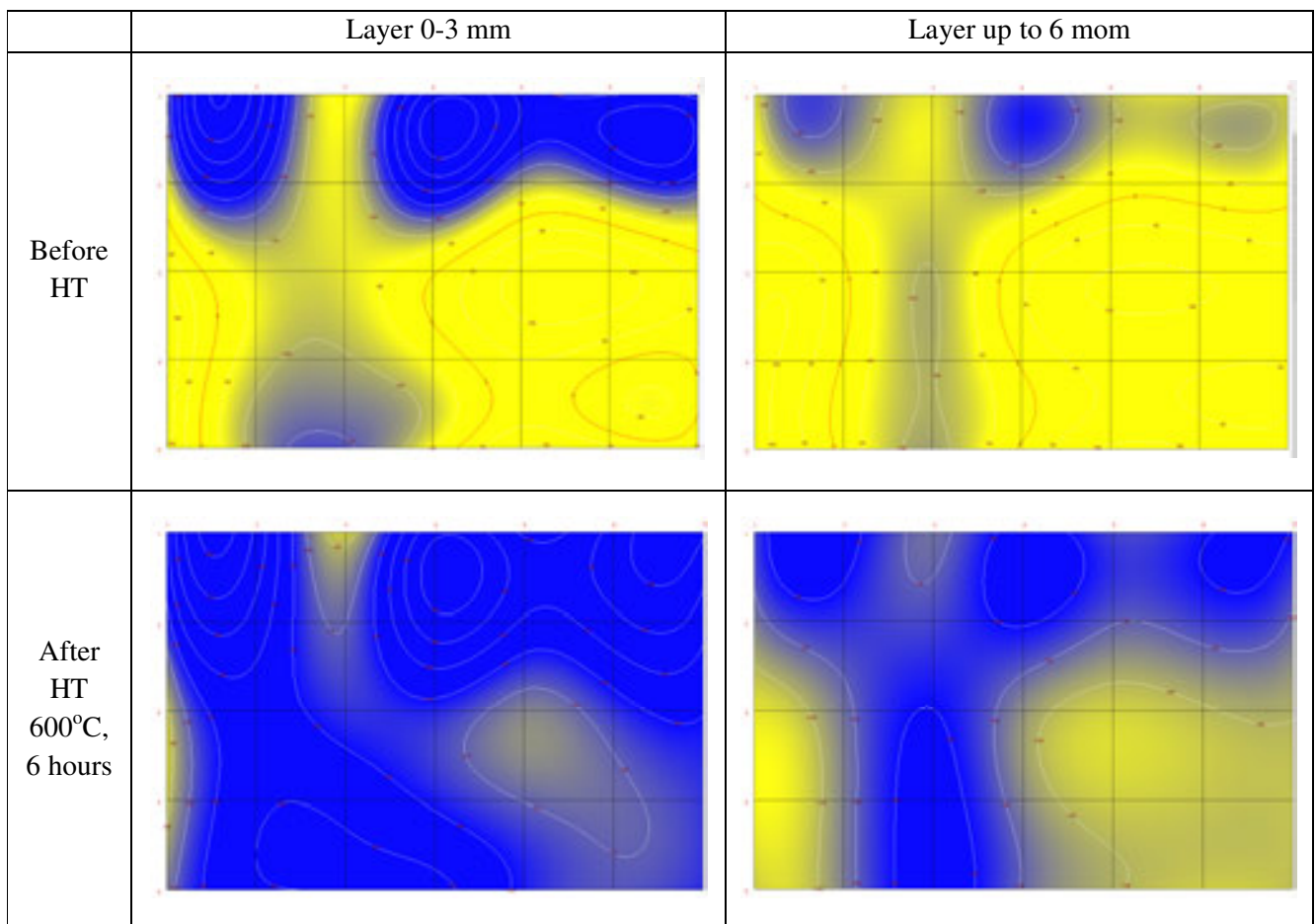
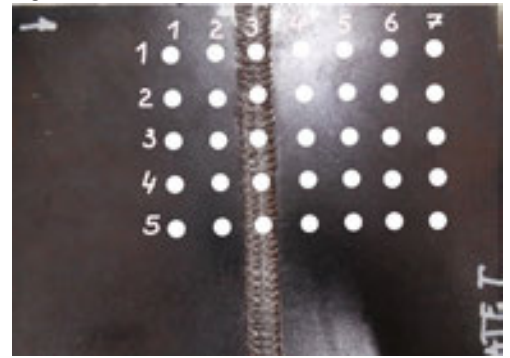
Notes:

1. Received DPMS cartograms of the weld residual stress do not contradict classical theory of distribution of welding stresses and deformations, where high stresses are concentrated along the weld joint with smooth transition through the zone thermal effect on stress of base metal.
2. On the cartogramme in blue area predominant compressive stresses, in yellow-tensile.

Plate 2, 10 mm wall thickness

Purpose: Evaluate stress distribution by layers and the quality of Heat Treatment HT at 6 hours and 600°C

The plate was measured by IMS for stress distribution before and after HT, results were sliced by Layers 0-3 mm (sub-surface) and up to 6 mm wall depth from the inspected surface.



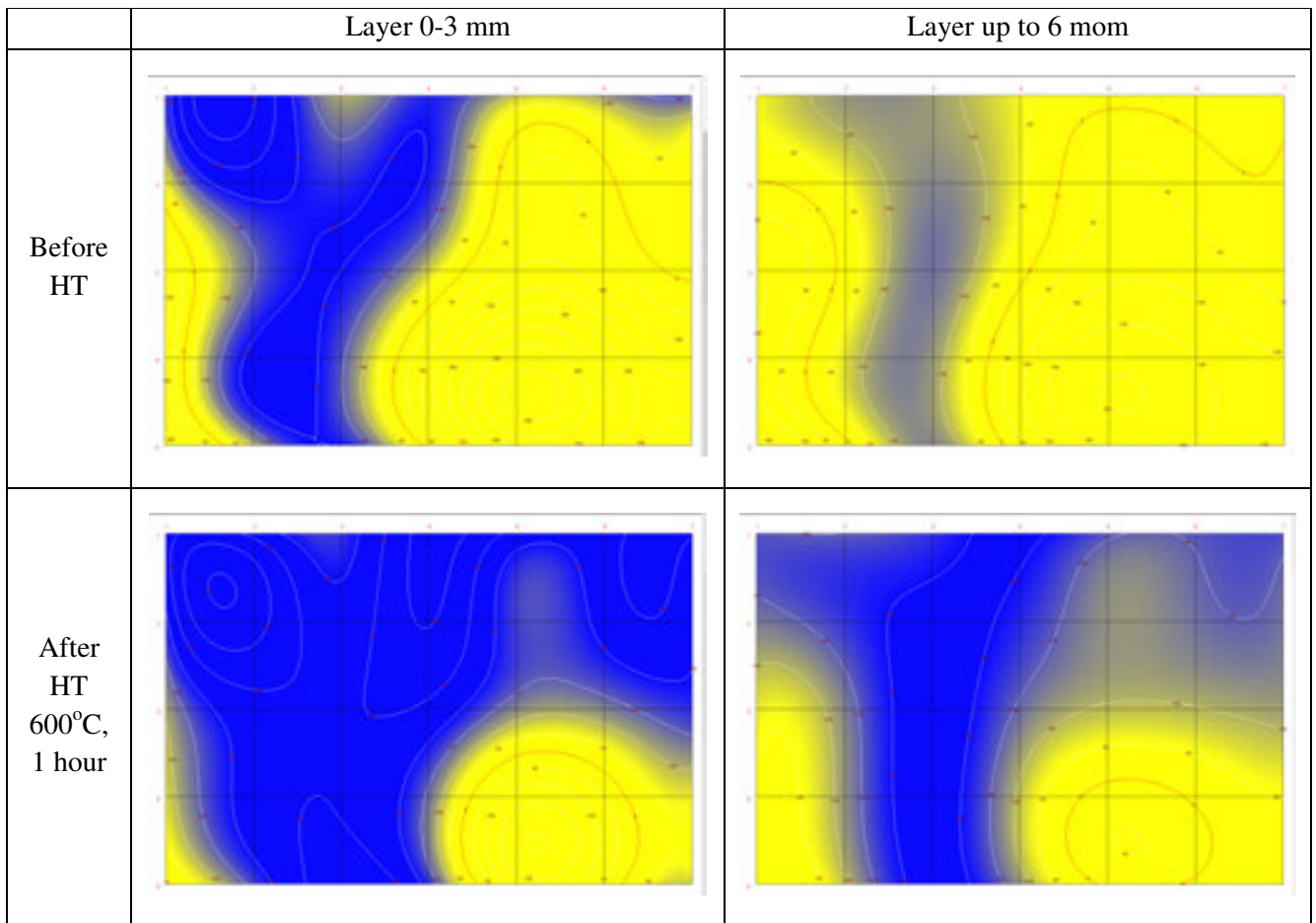
Notes:

1. Very unusual (not typical) stress distributions especially of the weld line X3), wild guess that the plates were heated or maybe the weld was done by low temp or low current.
2. Clearly visible the preference of stress relief at subsurface layer over the layer at the depth (wall's mid-section)
3. More precise results of stress differences and calculations are at the table of statistic maps (last page)

Plate 3, 10 mm wall thickness

Purpose: Evaluate stress distribution by layers and the quality of partial Heat Treatment HT at 1 hour and 600°C

The plate was measured by IMS for stress distribution before and after HT, with results sliced by Layer 0-3 mm (sub-surface) and Layer up to 6 mm wall depth.



Notes

1. Similar notes as the previous (results of the plate 1).
2. Visible noticeable that stress relief after partial HT is lesser quality compare to the full HT, more accurate results are calculations at the table.

Plate 4,
 The plate 10 mm wall thick with
 low quality weld (pores etc.)
 Purpose: Evaluate stress
 distribution and the quality of
 Heat Treatment (HT)

Step 1. The plate was measured by
 IMS for stress distribution before
 and after, HT for 600°C for 6
 hours.

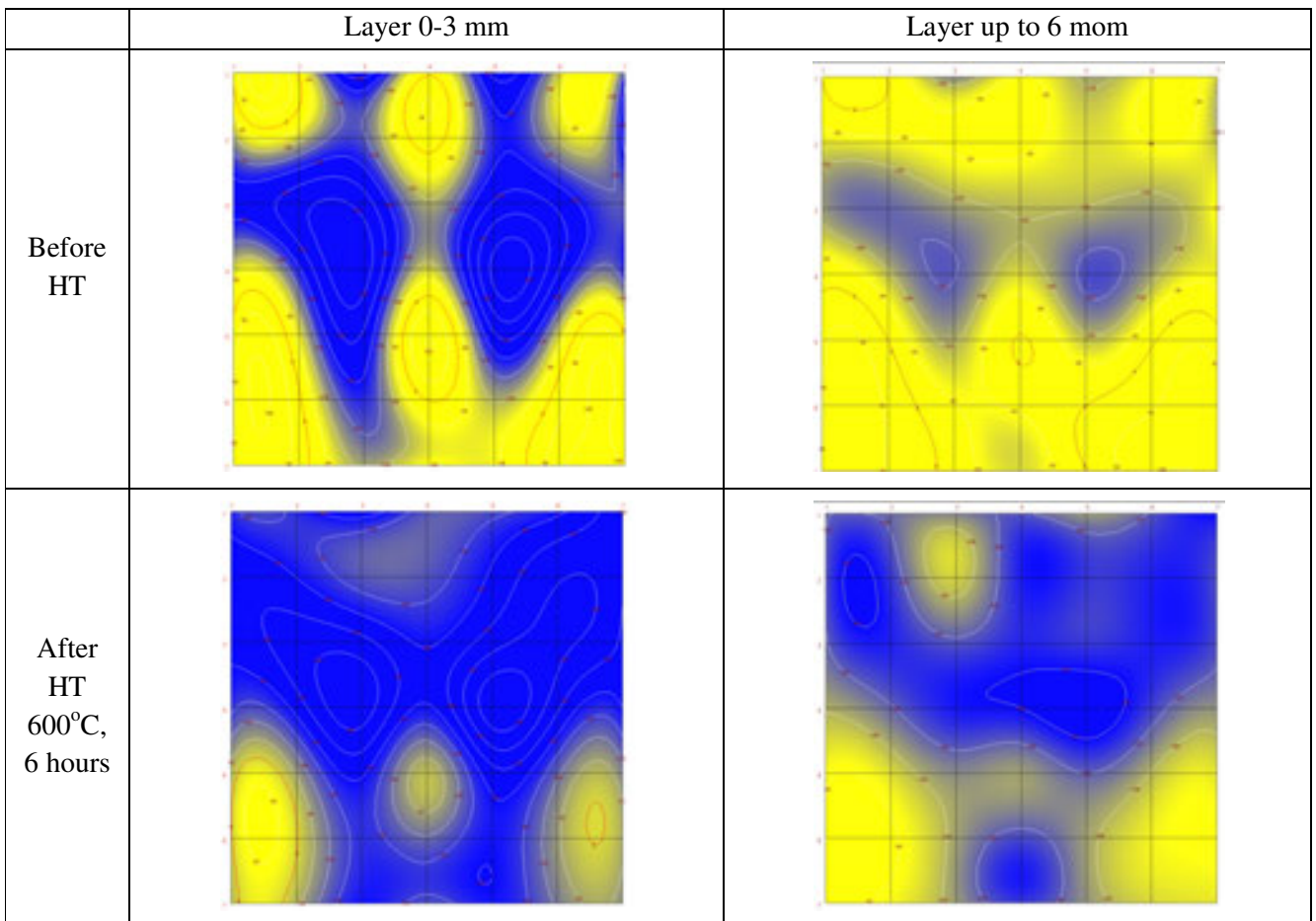
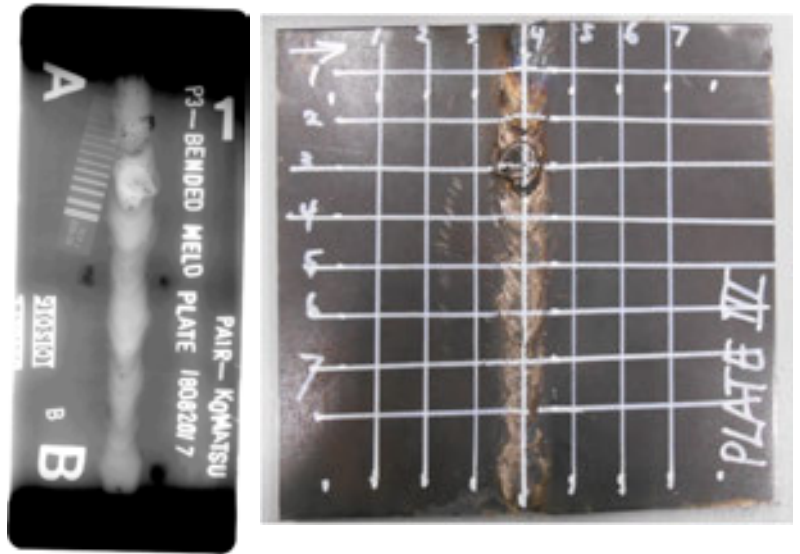


Fig. 4-5-6-7 Welded plates to confirm the quality of HT process

1. While in case of crack or lack of fusion we usually observe strongly oriented direction of stress distribution, in case of pores we observe randomly spread concentrations of mechanical stresses.
2. It is clearly noticeable that sub-surface layer (0-3 mm) is more stress affected than the second layer (up to 6 mm)
3. Strong indications at Y3-4 at X2-3 and at X5-6 (outside the weld, X4) were confirmed by X-ray as 2 holes located outside the weld (not weld related) but not visible.

4. Conclusion

4.1 The IMS method is a unique addition to the NDT and provides for a preemptive vision of potential equipment failure mechanisms by providing reliable information and accurate inspection results on the stress status of the item (object). Engineers can now proactively make decisions on “fitness for service” basis on the location and concentration of residual electromotive forces within the inspected equipment.

4.2 This technique can be used independently, or complimentary with conventional NDT to confirm critical findings, if required. 4.3 The IMS was originally designed for ferrite metals with thickness (depth) up to 12 mm and has been successfully proven. Using of “before and after” comparison approach for more reliable and more accurate findings. Any changes of metallurgical composition or thickness above 10-12 mm require additional investigation to determine acceptable stress levels. The stresses in the mid-section are most critical for future defect development. 4.4 Study on Stress Release by Heat Treatment or other methods, the quality and efficiency of the process, for the whole thickness of metal required special attention/investigation.

4.5 Care to be given when evaluating results for parts coming from site (due to residual stresses) versus those parts with artificial defects in lab. 4.6 Additional studies are recommended for each specific application (bigger thickness, Stainless Steel etc.) to assure more reliable results evaluation and to learn more about the applications or limitations of the Stress Indicator and to establish better credibility of expertise of evaluator (create data bank). Received cartograms of the weld residual stress do not contradict classical theory of distribution of welding stresses and deformations, where high tensile stresses are concentrated along the weld joint with smooth transition through the zone thermal effect into compressive stress of base metal. For consistency of results evaluation, the Statistic Map (provided by IMS software) for DPMS (Differential Principle Mechanical Stresses) was used Standard Deviation for integrity and homogeneously of comprising.

These study cases could be extend each plates by tensile test (destructive testing) and comparing data on strain results versus HT (full or partial) and to compare with the percentage of stress relief from maps (statistics) provided by Indicator of Mechanical Stresses (IMS).

Another topic for future investigations is the impact of various defects on stress build-up and stress relief.

5. References (some of references)

[1] Prof. Zhukov S.V., Mr. Zhukov V.S “Technical description of Indicator of Mechanical stresses”. Ferrologica LLC, Russia, 2008

[2] ASNT NDT Handbook, Volume 10, Section 7 and 8, USA, 2008

[3] Dr. BTHa, OtM. "NDT methods for testing Stress-Strain properties of oil pipes", Russian journal of NDT, Number 10, October 2002

CORRESPONDENCE ADDRESS:

Dr. Galip BÜYÜKYILDIRIM, EGE Sonik Kuzguncuk Mh. Icadiye Cd. No:51 Uskudar
Istanbul TR, +90 (532) 7486436, galipbuyukyildirim@yahoo.com

Dr. Georgy BATOV, Kachestvo Moscow, +7-916-227-75-27, gbatov@mail.ru

Dr. Galip BÜYÜKYILDIRIM – born in 1961, after completion of High School of Istanbul, he graduated as an Electronics and Communication Engineer from Electronics and Electrical Engineering Faculty at Technical University of Istanbul, where he got his MSc. Degree for Nuclear Energy Engineering. He worked as an expert researcher for Materials and Chemical Technologies Research Institute at MAM-TUBITAK between 1998-2002. In 2002, his work area shifted to the private sector as a technical consultant for different foreign companies. In 2013, his PhD. Degree were given by the Mechanical Engineering Faculty at Belgrade University.

Dr. Georgy BATOV –born in 1979, education Moscow State University Baumann, Machine Building Department, Ph.D. from the same university in 2013. Technical expert of Russian Accreditation Agency, expert in NDT, Level 3 certified in the methods MT,RT,PT,UT,VT,ET, TT. General director and head of the NDT personnel certification of Science Educational Center "Kachestvo".

ELECTROPLATING OF PASSIVE METAL HYDROXIDE COATING ON STEEL FOR CORROSION PREVENTION

Metin Bedir^{1,a}, Abdulcabbar Yavuz^{2,b}

¹Department of Engineering Physics, Gaziantep University, Sehitkamil, 27310, Gaziantep, Turkey

²Department of Metallurgical and Materials Engineering Gaziantep University, Sehitkamil, 27310, Gaziantep, Turkey

^a bedir@gantep.edu.tr, ^b ayavuz@gantep.edu.tr

Abstract

Zinc, cobalt and boron films were electrodeposited onto the low carbon steel by constant voltage from an aqueous pyrophosphate media. The first objective of this work is to determine if zinc, boron and cobalt based modified electrodes were stable on a steel substrate (AISI 4140). The second objective is to explore in what conditions metal modified electrodes could become stable metal hydroxide electrodes. The last objective is to determine the corrosion properties of the substrates (such as pitting and passivation) in 3 wt.% NaCl media. Firstly; Zn, B and Co films were electrodeposited onto steel substrate. Then, metal electrodes obtained potentiostatically were transferred in KOH solution and negative potential (typically -0.4 V) was applied (alkaline treatment). A different form of films covered the steel substrate due to the formation of hydroxide based metal composites. The film contains some unreacted metals after alkaline treatment.

The corrosion behavior of bare steel was compared with neat cobalt coating in terms of corrosion rate and corrosion potential by Tafel plot. A passive cobalt-based electrode (cobalt hydroxide) occurred after alkaline treatment. However, zinc hydroxide and boron hydroxide based electrodes were not stable on carbon steel and dissolved in polarization electrolyte. A significant change in corrosion current (i_{corr}) and corrosion potential (E_{corr}) for bare steel and modified electrodes in NaCl solution were reported. While uncoated steel has pitting corrosion in NaCl electrolyte, cobalt hydroxide surface is passivated because the formation of cobalt hydroxide surface is a barrier between steel and an aggressive media. In this work a new method for passivable metal hydroxide based coating is suggested.

Key Words: electrodeposition; passivation; corrosion resistance; cobalt, low carbon steel.

1. Introduction

Materials properties such as hardness, wear behavior and corrosion behavior are characterized to obtain desired applications. As bulk materials are limited, one method to meet the requirements of modern technology is to obtain modified electrodes with the defined properties [1–3]. There are numerous methods to cover the materials surface with a coating including chemical vapor deposition, electron beam evaporator, sputtering, dip coating, atomic layer deposition and cathodic arc deposition [4–6]. Among them electrodeposition is commonly used because materials properties such as composition, structure and morphology generally could be controlled by this technique [7,8] and it is simple and inexpensive to apply [9,10]. Electrodeposition techniques are used in this work for metal deposition and metal transformation to metal hydroxide to prevent steel from corrosion.

Metal and alloy corrosion are ubiquitous, and not only the global economy but also the environment are affected from it [11]. As several percent of GDP in developed countries is spent directly due to corrosion of materials, novel methods are studied to avoid or at least decrease the corrosion rate of metals/alloys [12,13]. The most desired method to cover metals/alloys by a passivable material to block the connection of the bulk materials with corrosive environments. Titanium and zinc are most widely used metals for corrosion protection as they both can spontaneously have their passive forms (such as titanium dioxide, zinc carbonate) on their surfaces [14–16]. Steel can form an unstable iron oxide on its surface and corrosion continues through bulk steel [17]. The aim of this study is to examine that carbon steel could be coated by a passive metal hydroxide film to increase corrosion resistivity. For this reason it was determined whether zinc, boron and cobalt based modified electrodes are stable on the steel substrate. Another objective is to determine corrosion behavior of substrates in 3wt.% NaCl media.

2. Experimental

Zinc, boron and cobalt coatings were electrodeposited potentiostatically from aqueous pyrophosphate bath. The set-up of cobalt deposition is presented in Figure 1. The plating solutions were prepared by dissolving 50 mM of metal chloride salt in deionized water including 0.7 M $K_4P_2O_7$ and 0.07 M KH_2PO_4 . All chemicals used in this research have analytical grade. The electrodeposition processes were performed in a three-electrode cell by means of a potentiostat (VersaSTAT 3, Princeton Applied Research, USA). Steel (AISI 4140) and Pt (0.2 cm²) were used as the working electrodes depending on test indicated in results and discussion part. The counter and reference electrodes were platinum flag and Ag/Ag (sat. KCl), respectively. Platinum working electrode used for metal deposition and corrosion studies was cleaned by immersing in saturated HNO_3 for few minutes.

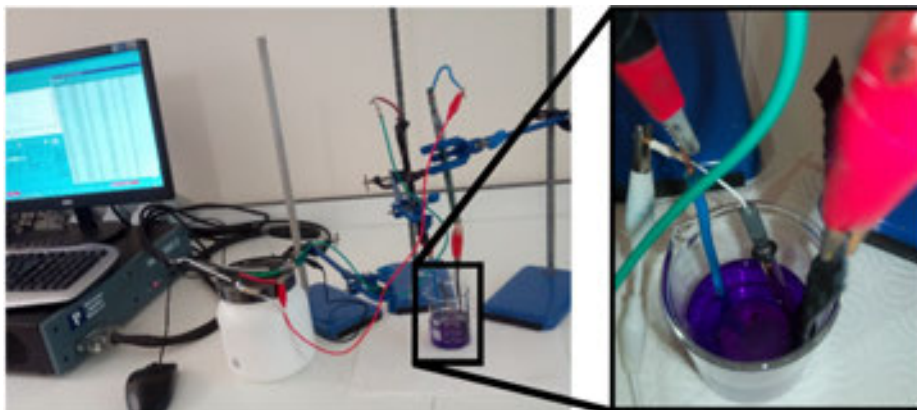


Figure 1: Photo of cobalt electrodeposition from pyrophosphate media. Deposition conditions are given in the text. The three-electrode cell connected to potentiostat for the deposition metals, transferring these metals to their hydroxide forms and measuring corrosion behavior of these films.

Carbon steel electrodes used as the substrate were insulated by epoxy and only one surface of steel was exposed to both electrolytes (deposition electrolyte and corrosion test electrolyte). AISI 4140 steel embedded in epoxy was sandpapered (SiC, P1000), polished (6 micron diamond suspension on a cloth) and washed using deionized water. All metal coatings were electrodeposited potentiostatically either on steel or on Pt working electrode, at $E < -1.1$ V vs.

Ag/AgCl(sat. KCl) reference electrode depending on metal reduction potential, from the electrolytes containing 50 mM metal chloride salts.

The films electrodeposited potentiostatically were transferred into a 3 wt.% NaCl electrolyte for corrosion analysis. A VersaSTAT 3 potentiostat was also used to perform the electrochemical corrosion study with a VersaStudio software program. Potentiodynamic polarization curves were obtained in the anodic direction in order to avoid direct oxidation of films. Metal films obtained on a substrate were rinsed with deionized water and transferred into 1 M KOH electrolyte to oxidize the metal films to their hydroxide forms by applying negative potential. All experiments presented in this work were conducted at a room conditions (20 ± 2 °C). Metal hydroxide films were transferred to a 3wt.% NaCl electrolyte for corrosion tests.

3. Results and Discussion

3.1. Deposition of Metals

Figure 2 illustrates the cyclic voltammogram of Pt in 50 mM CoCl_2 in pyrophosphate media between -1.0 and 1.5 V. The reason this experiment was conducted is to examine deposition potential of cobalt. The starting point of the scanning (at -1 V) there is a reduction and current density has directly around $610 \mu\text{A}$ because of hydrogen evolution and cobalt deposition. An oxidation peak around at -0.72 V could be associated to two oxidation either Co^0/Co^+ or $\text{Co}^0/\text{Co}^{2+}$. However, as there is no other oxidation peak up to -1.2 V which can be $\text{Co}^+/\text{Co}^{2+}$, the oxidation peak at -0.72 belongs to $\text{Co}^0/\text{Co}^{2+}$. The oxidation at around 1.2 V is well known oxygen gas evolution [18]. The reduction peak starting at around 0 V is associated to $\text{Co}^{2+}/\text{Co}^+$ because when -0.5 V was applied, cobalt deposition was not observed on platinum working electrode. As deposition and dissolution mechanism of zinc in pyrophosphate media was discussed in detail [19], they were not discussed here again. The presence of oxidation peak appeared just after hydrogen evolution for all metals indicates that metal films could be deposited at negative voltage (< -1 V) in pyrophosphate media [20]. Therefore, negative potentials (from -2.1 V to 1.1 V) were applied to carbon steel working electrode in pyrophosphate electrolyte to form cobalt film on steel presented in Figure 3.

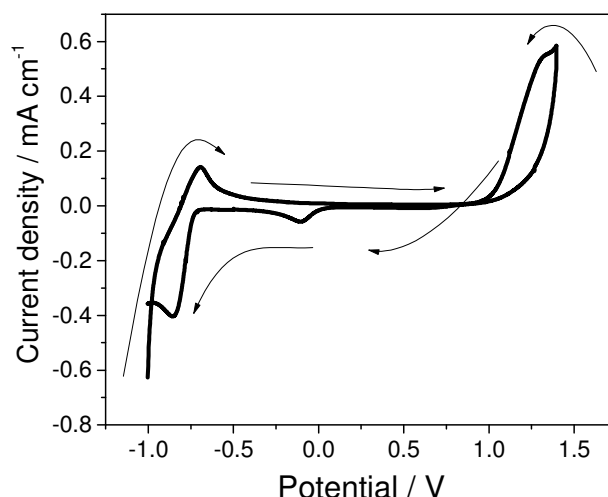


Figure 2: Cyclic voltammogram curve of Pt obtained from 50mM CoCl_2 with 0.7 M $\text{K}_4\text{P}_2\text{O}_7$ and 0.07 M KH_2PO_4 deposition bath between -1.0 V and +1.5 V at the scan rate of 20 mV s^{-1} . The arrows indicate the direction of current change.

Figure 3 illustrated that upon decreasing potential (to more negative side), negative current density increases. While current density is around -7 mA at -1.1 V and increases, the current density is around -192 mA and decreases at -2.1 V. The negativity of current density which is directly related to the amount of charge transfer is associated with metal deposition and hydrogen evolution. During deposition at more negative potential, more bubbles were observed around working electrode of carbon steel, which can indicate the formation of more hydrogen gas. At the same time, cobalt films were darker with lower deposition potential. Current densities are not constant with time (in Figure 3) because the surface of substrate was changed as cobalt was deposited on it and the new surface can cause different amount of hydrogen evolution. The expectation (from Figure 2) was to obtain a cobalt film by applying -1.1 V but the film was not clearly observed. Therefore, -1.5 V was applied to obtain Co film on steel. The same trend of elapsed time and current density by changing potential was observed for zinc and boron deposition on platinum as well and -1.5 V was applied for boron and zinc deposition as well. The metal films electrodeposited from aqueous pyrophosphate solution were transferred to 1 M KOH to form metal hydroxide films (see section 3.2). 3 wt.% NaCl solution then was used to examine their corrosion behavior. The corrosion behavior of metals and their hydroxide forms were compared and presented in subsequent sections.

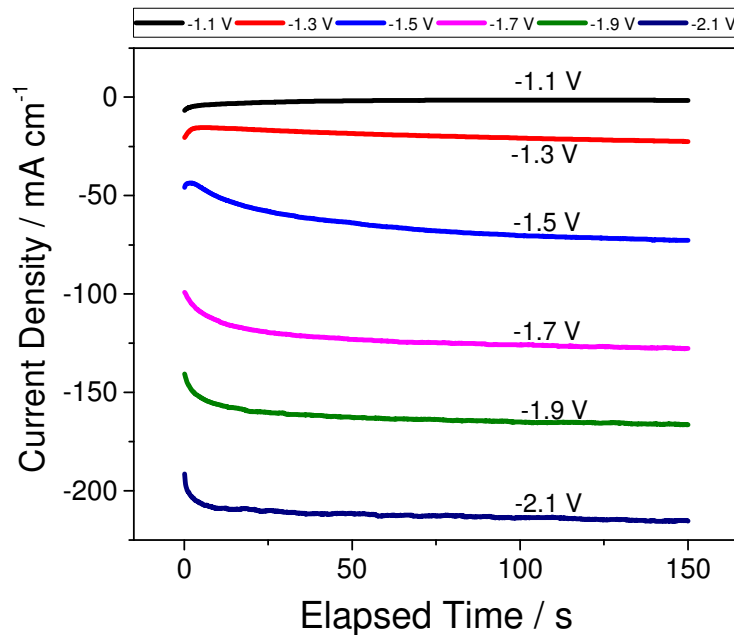


Figure 3 Chronoamperometric data for electrochemical deposition of cobalt from 50 mM CoCl₂ with 0.7 M K₄P₂O₇ and 0.07 M KH₂PO₄ deposition bath on AISI 4140 by applying different potential varying from -1.1 to -2.1 V.

3.2. Formation of Metal Hydroxides

Co, Zn and B films electrodeposited on steel were immersed in 1 M KOH and negative potentials were applied to obtain metal hydroxide films. Boron and zinc films were removed from steel by application of potential. However, cobalt film was changed to different color (see section 3.3) and remain stable on steel surface and not removed by tissue as well. Therefore, only

the data regarding transformation of cobalt to cobalt hydroxide are presented here. Figure 4 illustrate the change of cobalt to cobalt hydroxide form.

Figure 4 illustrated that most of cobalt becomes cobalt hydroxide at the beginning of potentiodynamic polarization (at around -0.7 V) meaning that oxidation of cobalt to cobalt hydroxide in KOH environment is at more negative potential. The aim to conduct the experiment illustrated in Figure 4 is to show that current approached to zero which is a case as can be seen at -0.4 V. The scan rate was selected as 1 mV s^{-1} to complete the transformation of cobalt film to its hydroxide form because lower scan rate means higher timescale. Indeed cobalt films become Co-Co(OH)₂ composite films after electrochemical treatment in KOH solution found by XRD[21]. After obtaining cobalt hydroxide films, they were transferred in 3 wt.% NaCl solution to examine the corrosion behaviors of the cobalt hydroxide modified electrodes and compare these results with that of cobalt films.

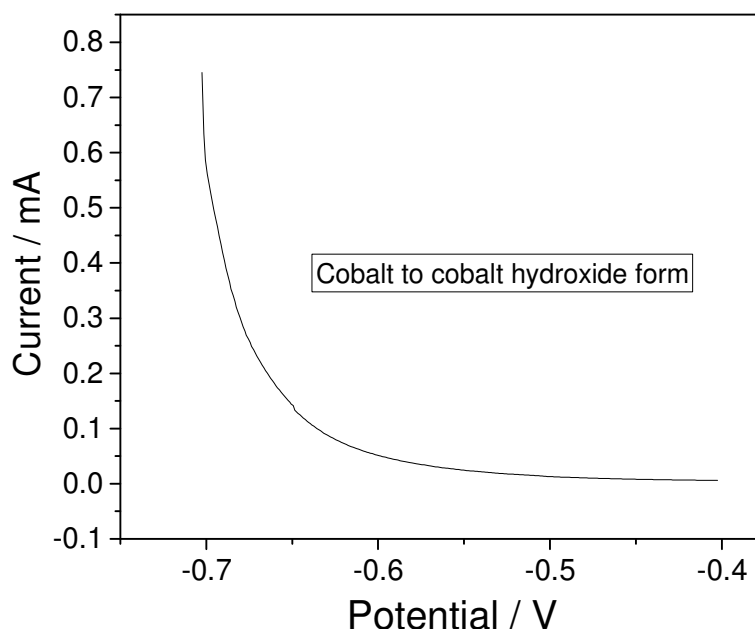


Figure 4: Linear sweep voltammetry data obtained from cobalt modified electrodes in 1 M KOH solution to have its hydroxide form. The scan rate of 1 mV s^{-1} . Potentials are against Ag/AgCl reference electrode.

3.3. Polarization of Cobalt Hydroxide

Cobalt film was deposited on carbon steel (Section 3.1.) and then this cobalt film was turned into cobalt hydroxide film in KOH media by applying -0.4 V (Section 3.2). The photos of bare steel, cobalt coated steel and cobalt hydroxide on steel are illustrated in Figure 5. Cobalt coated steel is brown presented in Figure 5b and this is turned to black (see Figure 5b) when it is treated with KOH. In this section corrosion behavior of cobalt and cobalt hydroxide films are elucidated by means of linear sweep voltammetry and these results are compared with bare (uncoated) steel. Corrosion resistivity of cobalt and cobalt hydroxide formed on steel is the same as that of bare steel because steel (iron) can dominate corrosion behavior. Therefore, cobalt and cobalt

hydroxide were obtained on platinum working electrode as platinum is not reacted with NaCl corrosion test solution in selected potential window.

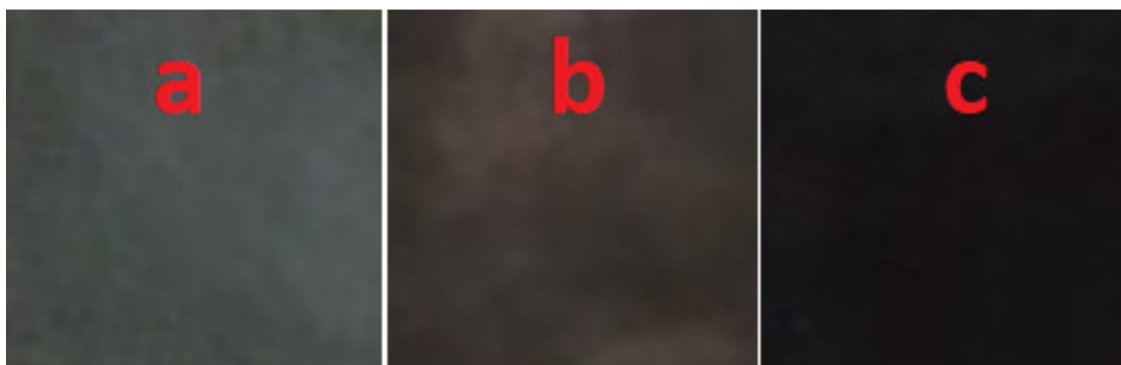


Figure 5: Images of (a) bare steel, (b) cobalt coated steel and (c) $\text{Co}(\text{OH})_2$ coated steel. Their growth details are given in the text. All images were obtained immediately after polarization.

Figure 6 illustrates linear sweep voltammetry response of bare steel, cobalt modified film and cobalt hydroxide modified film in 3 wt.% NaCl solution. Corrosion current density (i_{corr}) is an important parameter to compare corrosion resistivity of materials and i_{corr} of bare steel and modified films are tabulated in Table 1. As corrosion current density of cobalt modified electrode ($12.6 \text{ mA} \cdot \text{cm}^{-2}$) is four times smaller than that of bare steel ($50.2 \text{ mA} \cdot \text{cm}^{-2}$), corrosion resistivity of cobalt film is four times higher than that of bare steel.

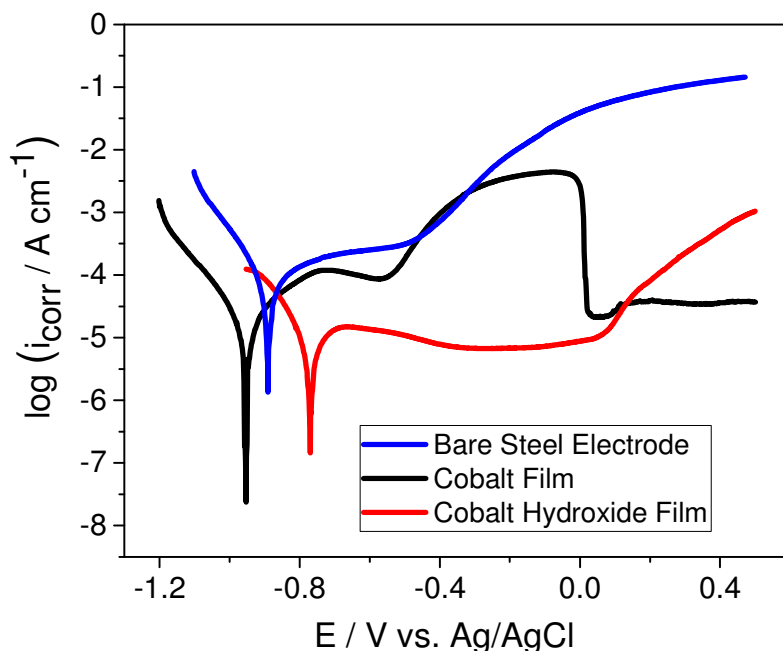


Figure 6: Potentiodynamic polarization curves of bare steel (blue line), cobalt coated (black line) and cobalt hydroxide coated (red line) electrodes in 3 wt.% NaCl electrolyte at a scan rate of 20 mV s^{-1} .

Corrosion resistivity of cobalt films was studied in detail[22,23]. In this work, corrosion behavior of cobalt hydroxide is focused on. Red line in Figure 6 illustrate corrosion current density of cobalt hydroxide is lower than that of cobalt film. i_{corr} value of cobalt hydroxide film is twelve and three times smaller than that of bare steel and cobalt film, respectively. Another advantage of cobalt hydroxide film is its stability at higher voltage. Normally bare steel and cobalt coated steel are oxidized at about -0.5 V after corrosion potential shown by blue and black lines of Figure 6. However, after polarization potential cobalt hydroxide film is stable until 0.1 V (indicated by red line of Figure 6).

Table 1: Corrosion potential(E_{corr}) and corrosion current density (i_{corr}) parameters of materials given in Figure 6.

Electrode	E_{corr} (V)	i_{corr} (mA · cm ⁻²)
Bare steel	-0.90	50.2
Cobalt film	-0.96	12.6
Cobalt hydroxide film	-0.78	3.98

Electrolyte solutions of electrodes after polarization were different and their photos are presented in Figure 7. The water in which bare steel was immersed (see Figure 7b) was yellow due to the pitting corrosion of steel but the color of the water (Figure 7d) in which the $Co(OH)_2$ film was immersed remained similar to deionized water (Figure 7a) due to passivation of $Co(OH)_2$ modified electrode. Polarization of cobalt film change the color of NaCl solution from transparent to greenish (Figure 7c) because of pitting corrosion of cobalt coated steel.

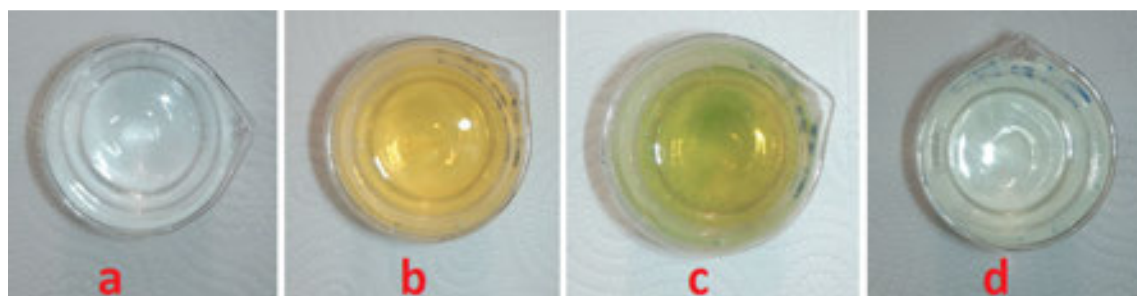


Figure 7:(a) 3 wt.% NaCl polarization solution. The electrolyte of (b) bare steel, (c) cobalt coated and (d) cobalt hydroxide coated electrodes after polarisation. Their linear sweep voltammeteries are presented in Figure 6.

4. Conclusion

Zinc, cobalt and boron films were electrodeposited potentiostatically on the low carbon steel (AISI4140) from pyrophosphate bath. Zinc, boron and cobalt based modified electrodes are stable on steel substrate. Co, Zn and B films were treated by 1 M KOH by applying negative potentials to transfer metals to their hydroxide forms. Metal modified electrode of cobalt can become stable metal hydroxide electrodes on steel by KOH treatment. During this process, color of cobalt film was changed to black. However, boron hydroxide and zinc hydroxide dissolve in the alkaline solution. Cobalt hydroxide electrode was transferred in 3 wt.% NaCl electrolyte to

characterize its corrosion behaviors by means of linear sweep voltammetry. Corrosion responses of modified electrodes are compared with uncoated steel.

Cobalt modified electrode is four times more corrosion resistive than bare steel and corrosion resistivity of cobalt hydroxide film is three times higher than that of cobalt coating. Additionally, cobalt hydroxide film is more stable than both (bare steel and cobalt film electrodes) at higher voltages. While bare steel and cobalt film are oxidized at about -0.5 V, cobalt hydroxide film is stable until 0.1 V. Electrolyte solutions of electrode polarization prove that bare steel has pitting corrosion but Co(OH)₂ film has passivation behavior in NaCl environment.

5. Acknowledgement

This study is supported by Gaziantep University, Scientific Research Projects Unit (BAPYB – MF.YLT.17.03).

6. References

- [1] H. Karimi-Maleh, F. Tahernejad-Javazmi, N. Atar, M.L. Yola, V.K. Gupta and A.A. Ensafi, A novel DNA biosensor based on a pencil graphite electrode modified with polypyrrole/functionalized multiwalled carbon nanotubes for determination of 6-mercaptopurine anticancer drug, *Ind. Eng. Chem. Res.* 54 (2015), pp. 3634–3639.
- [2] M. Ates and E. Topkaya, Nanocomposite film formations of polyaniline via TiO₂, Ag, and Zn, and their corrosion protection properties, *Prog. Org. Coatings* 82 (2015), pp. 33–40.
- [3] J. Shi, Y. Wang, Z. Gong, B. Zhang, C. Wang and J. Zhang, Nanocrystalline Graphite Formed at Fullerene-Like Carbon Film Frictional Interface, *Adv. Mater. Interfaces* 4 (2017), pp. 1601113.
- [4] P.-W. Chen, C.-T. Chang, M.M. Ali, J.-Y. Wu, Y.-C. Li, M.-H. Chen et al., Tantalum oxide film deposited by vacuum cathodic arc plasma with improved electrochromic performance, *Sol. Energy Mater. Sol. Cells* 182 (2018), pp. 188–195.
- [5] J. Hämäläinen, K. Mizohata, K. Meinander, M. Mattinen, M. Vehkamäki, J. Räisänen et al., Rhenium Metal and Rhenium Nitride Thin Films Grown by Atomic Layer Deposition, *Angew. Chemie Int. Ed.* (2018), .
- [6] I. Stassen, M. Styles, G. Greci, H. Van Gorp, W. Vanderlinden, S. De Feyter et al., Chemical vapour deposition of zeolitic imidazolate framework thin films, *Nat. Mater.* 15 (2016), pp. 304.
- [7] J. Ru, Y. Hua, C. Xu, J. Li, Y. Li, D. Wang et al., Morphology-controlled preparation of lead powders by electrodeposition from different PbO-containing choline chloride-urea deep eutectic solvent, *Appl. Surf. Sci.* 335 (2015), pp. 153–159.
- [8] K. Huang, J. Clausmeyer, L. Luo, K. Jarvis and R.M. Crooks, Shape-controlled electrodeposition of single Pt nanocrystals onto carbon nanoelectrodes, *Faraday Discuss.* (2018), .
- [9] N. Xu, D.K. Sarkar, X.-G. Chen and W.P. Tong, Corrosion performance of superhydrophobic nickel stearate/nickel hydroxide thin films on aluminum alloy by a simple one-step electrodeposition process, *Surf. Coatings Technol.* 302 (2016), pp. 173–

184.

- [10] A. Laszczyńska, W. Tylus, J. Winiarski and I. Szczygieł, Evolution of corrosion resistance and passive film properties of Ni-Mo alloy coatings during exposure to 0.5 M NaCl solution, *Surf. Coatings Technol.* 317 (2017), pp. 26–37.
- [11] E. Bastidas-Arteaga and M.G. Stewart, Economic assessment of climate adaptation strategies for existing reinforced concrete structures subjected to chloride-induced corrosion, *Struct. Infrastruct. Eng.* 12 (2016), pp. 432–449.
- [12] S. Roselli, C. Deyá, M. Revuelta, A.R. Di Sarli and R. Romagnoli, Zeolites as reservoirs for Ce (III) as passivating ions in anticorrosion paints, *Corros. Rev.* 36 (2018), pp. 305–322.
- [13] X. Luo, S. Yuan, X. Pan, C. Zhang, S. Du and Y. Liu, Synthesis and enhanced corrosion protection performance of reduced graphene oxide nanosheet/ZnAl layered double hydroxide composite films by hydrothermal continuous flow method, *ACS Appl. Mater. Interfaces* 9 (2017), pp. 18263–18275.
- [14] A. Balakrishnan, B.C. Lee, T.N. Kim and B.B. Panigrahi, Corrosion behaviour of ultra fine grained titanium in simulated body fluid for implant application, *Trends Biomater. Artif. Organs* 22 (2008), pp. 58–64.
- [15] J.A.C. Miramontes, P.C. Monsalve, F.E. López, C.G. Tiburcio, P.Z. Robledo and F.A. Calderón, Electrodeposition and Corrosion Resistance of Nanostructured Coatings Zinc-Carbon Black, *ECS Trans.* 76 (2017), pp. 1–7.
- [16] D. Zang, R. Zhu, W. Zhang, X. Yu, L. Lin, X. Guo et al., Corrosion-Resistant Superhydrophobic Coatings on Mg Alloy Surfaces Inspired by Lotus Seedpod, *Adv. Funct. Mater.* 27 (2017), pp. 1605446.
- [17] C.-Q. Cheng, L.-I. Klinkenberg, Y. Ise, J. Zhao, E. Tada and A. Nishikata, Pitting corrosion of sensitised type 304 stainless steel under wet-dry cycling condition, *Corros. Sci.* 118 (2017), pp. 217–226.
- [18] X. Lu and C. Zhao, Electrodeposition of hierarchically structured three-dimensional nickel-iron electrodes for efficient oxygen evolution at high current densities, *Nat. Commun.* 6 (2015), pp. 6616.
- [19] M.Y. Hacıbrahimoğlu and A. Yavuz, Deposition and Dissolution Mechanism of Cu-Zn Alloys in Pyrophosphate Medium, *Imp. J. Interdiscip. Res.* 2 (2016), .
- [20] D. Sylla, C. Savall, M. Gadouleau, C. Rebere, J. Creus and P. Refait, Electrodeposition of Zn-Mn alloys on steel using an alkaline pyrophosphate-based electrolytic bath, *Surf. Coatings Technol.* 200 (2005), pp. 2137–2145.
- [21] A. Yavuz, M.Y. Hacıbrahimoğlu and M. Bedir, Synthesis and characterisation of Co-Co(OH)₂ composite anode material on Cu current collector for energy storage devices, *Mater. Res. Express* 4 (2017), .
- [22] A. Kohn, M. Eizenberg, Y. Shacham-Diamand and Y. Sverdlov, Characterization of electroless deposited Co (W, P) thin films for encapsulation of copper metallization, *Mater. Sci. Eng. A* 302 (2001), pp. 18–25.

- [23] I.H. Karahan, O. Karabulut and U. Alver, A study on electrodeposited Zn–Co alloys, Phys. Scr. 79 (2009), pp. 55801.

CORRESPONDENCE ADDRESS:

MetinBedir : Department of Engineering Physics, Gaziantep University, Sehitkamil, 27310, Gaziantep, Turkey.

Tel: 00903601200/1070, email: bedir@gantep.edu.tr

AbdulcabbarYavuz :Department of Metallurgical and Materials Engineering Gaziantep University, Sehitkamil, 27310, Gaziantep, Turkey.

Tel: 00903601200/3907, email: ayavuz@gantep.edu.tr

SHORT BIOGRAPHIES

MetinBedir –He was born in 1965 and graduated from Department of Physics in Çukurova University. He received an MSc and PhD degrees from Department of Physics in Çukurova and from the Department of Engineering Physics in Gaziantep University, respectively. He started to work as a research assistant in the Department of Engineering Physics in Gaziantep University. He is a professor at Engineering Physics Department, Gaziantep University. His research area is Condense Matter Physics.

AbdulcabbarYavuz– He was born in 1985 and graduated from Department of Chemistry in Ankara University. He received PhD degree from Leicester University (England). He has been in the Department of Metallurgical and Materials Engineering in Gaziantep University since 2015. His research area is conducting polymer, corrosion and energy storage materials.

ARC STUD WELDING OF HOLLOW PARTS WITH DIFFERENT CROSS SECTIONS

Necip Fazıl YILMAZ^{1,a}, M. Veysel ÇAKIR^{2,b}, H. Ahmet EROL^{1,c}

¹University of Gaziantep, Department of Mechanical Engineering

²Kilis 7 Aralık University, Department of Mechanical Engineering

^anfyilmaz@gantep.edu.tr, ^bcakir@kilis.edu.tr, ^chuseyinahmeterol@gmail.com

Abstract

Arc Stud Welding is used extensively in the fields of automobile and industrial equipment manufacturing, boiler, building, bridge and railroad construction and shipbuilding. Due to its crucial importance, it is very significant to decide the influencing parameters for the mechanical and microstructural properties of the welded specimens. In this study, experimental studies were carried out to examine the arc stud welding of hollow parts with a constant outer diameter of 10 mm and different inner diameters of 6, 7 and 8 mm, respectively. Austenitic stainless steels were used for both stud and base metal. It is realized that hollow studs can be successfully welded by using arc stud welding. Welding joint quality is highly dependent on parameters such as welding current, welding time, plunge and lift. Mechanical properties of welded joints were investigated and microscopic views were taken to search the weld zone microstructure.

Key Words: Hollow Parts, Arc Stud Welding, Wall thickness, AISI 304

1.Introduction

Arc stud welding (ASW) is a process by which a metal stud is combined to a metal workpiece by heating both parts with an electric arc. Stud welding is a method of joining a bolt or specially formed nut to a workpiece generally in the form of a sheet or a plate.

In comparison with the other welding processes, the arc stud welding process has many advantages especially in increasing the productivity, due to a short time of welding cycle, the possibility of the process to automate, simplicity in the use of equipment, cost efficiency and the accuracy of stud location. In addition to that, stud welding shows high carrying capacities, while the process is robust and can easily be monitored by progress of current, voltage and stud movement [1]. In this method, welding elements are welded by an arc without additional material and no drilling, punching, thread cutting, bonding, riveting is required to fix the fastening element. In many areas stud welding is the cheapest joining techniques for parts. Especially in thin plates, stud welding is often the only technical solution.

ASW process has wide variety application area in industry owing to easy production and no need for qualifying member. Stud welding products are used for industrial and commercial constructions, bridges, military vehicles, boiler production, automobiles, trucks, railroads, shipbuilding, rolling stock, electrical parts, aircraft, metal furniture and other metal working industries [2].

Stud welding process includes the same electrical, thermal, metallurgical and mechanical principles as other welding process [3]. The stud welding quality process is affected from many factors such as stud design, materials, base metal thickness, stud cross section area, welding position, surface condition, environmental conditions and welding parameters (welding current, welding time, lift and plunge) [4].

In early times, this process had poor reliability of the weld zone and restrictions on the use of some materials. So, the method was used in joining of bolts and similar, parts for ships' fittings. In our day, due to the progression of welding equipment and stud materials, pins rectangular and several other shapes plates as well as bolts, can be welded very simply and rapidly. This process is now employed as a part of critical structures, and has become crucial welding process for automobile and bridge, building and railroad construction and shipbuilding [5]. As the sectorial importance of stud welding, the interest of researchers for this issue also increases.

Ramasamy [6] has focused on automotive industry applications with materials of corrosion-resistant aluminum-alloy sheet metals and aluminum stud welding process. In addition, based on the results, arc stud welding can be performed on 5754-O and 6062-T6 aluminum alloy sheets with consistency and minimal levels of porosity.

Ivan Samadric et al. [7] presented an on-line monitoring system with requires welding parameters when they are applying arc stud welding process at various electric arc stability changes. Moreover, they showed macro sections of welded joints with some different welding conditions to offering good quality or weld defects from welding joints.

Ivan Samardzic et al. [8] analyzed the influence of welding parameters and weld characteristic with the steel plate and pipe shape of base metal on the method of electric arc stud welding process. Due to parameter changes, welding joint characteristics analyzed with the measurement of hardness across the welding joints. They concluded that, higher welding time and current has largest depth of penetration with the base metal of pipe. They also showed that increasing of hardened zone is highly related with welding current.

Jeong-Soo Lee et al [9] revealed the importance of stud welding process with SUS304L stainless steel on ship building industry. They tried to find optimum stud welding parameters and they checked welding joints strength with applied mechanical tests. Experimental results showed that inappropriate parameters could affect the welding area significantly. The problems inside the welding areas are cracks, porosity and lack of fusion and inclusion of slugs inside welding joints.

Yılmaz and Hamza [10] carried out experimentally work by using 6,8,10 and 12 mm diameter stainless steel (AISI 304 Austenitic) stud bars to analyze tensile strength, bending strength and microstructure. They concluded that, the considered welding parameters must be selected properly in order to obtain good weld joint.

The aim of this work is to investigate an arc stud welding on hollow parts as a suitable method to combine AISI 304 stainless steel hollow studs with same stainless steel metal plates. In this research, an arc stud welding (ASW) parameters utilization has been studied on hollow parts. The previous studies are related with arc stud welding of solid studs and Taguchi methods with ANOVA. But it is realized that very little effort has been suffered for hollow parts and wall thicknesses or cross sectional area of studs were not found enough place in the studies. The place of this work in the literature, filling the gap of arc stud welding studies has been applied firstly with stainless steel hollow studs and parameters formation with various welding current, welding time, lift and plunge with different hollow stud thicknesses.

2. Experimental Study

2.1. Material Selection

The AISI 304 quality stainless steel is one of the most used materials in different application are such as; automotive, shipbuilding industry, medical applications, home appliances, food industry and pressure vessels. Stainless steels have a good compound of chemical and mechanical properties that are important for corrosion resistance and lifetime of steel structures [11]. Stainless steel is a material that contains a high chromium content that provides a chrome oxide layer on the surfaces when present in the air or other oxidizing areas. Furthermore, it is known that the austenitic stainless steel is suitable material for common fusion and resistance welding processes. The reason of the selection of AISI 304 stainless steel studs and plates for this study is that it has great mechanical properties, corrosion resistance, and easy availability in the store, low cost and appropriate material for stud welding process [12]. Mechanical and chemical properties of stainless steel used in this study are given in Tab. 1 and Tab. 2 respectively.

Table 1. Chemical properties of the AISI 304

GRADE		C	Mn	Si	P	Cr	Ni	N
AISI 304	min.	-	-	-	-	18.0	8.0	-
	max.	0.08	2.0	0.75	0.045	20.0	10.5	0.1

Table 2. Mechanical properties of the AISI 304

GRADE	Tensile Strength (MPa) min.	Yield Strength (MPa) min.	Elongation (% in 50mm) min.
AISI 304	515	205	40

2.2. Process Parameter Selection and Design of Experiments

There are many significant factors that affect the quality of the stud welding process. Choosing the stud welding process parameters to achieve a robust welding connection is a process that requires high attention and precision. These factors have different independent effects on welding joint performance.

Controlled parameters in this study are welding time, welding current, lift, plunge, and stud diameter and wall thickness. In the experimental studies, the hollow studs with a constant outer diameter of 10 mm and different inner diameters of 6, 7 and 8 mm, respectively are used. For all stud types the base metal thickness was chosen as 5 mm. The levels of each process parameter were derived through a series of preliminary experiments.

In our study, test groups have 4 factors and four levels. In order to see the effect of selected input parameters to welding performance design of experiments (Taguchi) method were used which gives logical parameter set combination in experiments. Design of experiments (DOE) is an approach used for decreasing the number of experiments to accomplish the optimum conditions [13]. It is a statistical technique that made it possible to investigate not only the effect of any factor but also their interactions. Using the Taguchi approach the experimental design and the results' analysis can be done with less effort and expenses. The experiments were designed by using L16 orthogonal arrays (OA) to examine effect of input parameters on tensile strength. The Taguchi method uses a special design of orthogonal array to study the entire parameter space with only a small number of experiments [14]. An orthogonal array also provides a balanced set of experimentation [15].

2.2. Experimental Setup

In this study, drawn arc stud welding method has been used with the shielding gas of argon. Arc stud welding can be done in different positions; vertical, downward and upside-down and etc. In this study, the downward position welding was designed. Figure 1 shows the experimental setup.

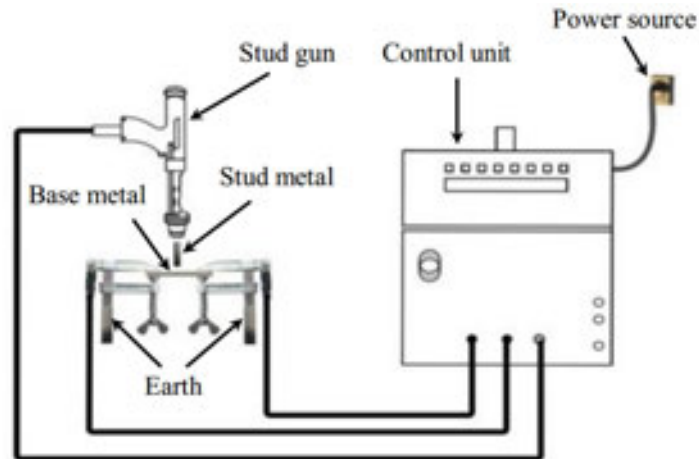


Figure 1. Schematic view of arc stud welding experimental setup [20]

Specimens were welded using the Soyer-BMK-16i type arc stud welding machine was used to join the stud and plate while argon gas was used as a shielding gas with constant flow rate of (15 l/min).

2.3 Tensile Test

To define the welding joint performance quality, prepared welding specimens were examined with the ISO 14555 standard procedure. Tensile test machine was used to determine the ultimate tensile strength of the welded joint. The standard tensile test specimens were made for each specimen was connected in a round shape, but for welded test specimens, one side is the stud and the other side is a flat plate. For this reason, a specially designed pulling device is used to perform the tensile test on the welded specimens (Figure 2.).

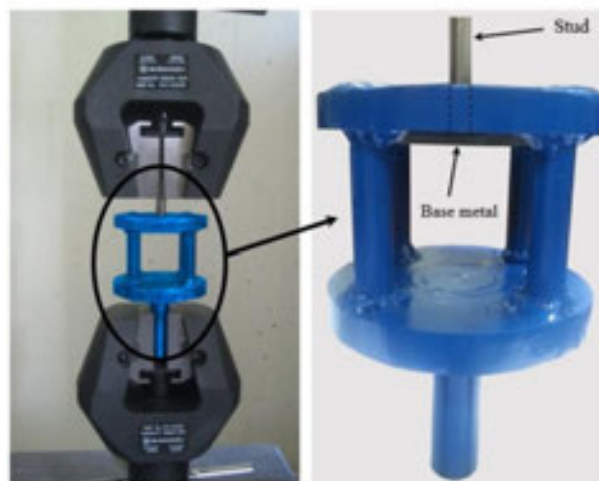


Figure 2. Specially designed fixture and tensile test application

Furthermore, small cylindrical bars which has 25 mm long and 6 mm diameter were put into the end of the hollow stud (non-welded end) to prevent jamming of the specimens during tensile testing (Figure 3). For each wall thickness, sixteen different parameter sets were achieved according to the design of experiment layout (Table 4). Three samples were realized for each parameter set.

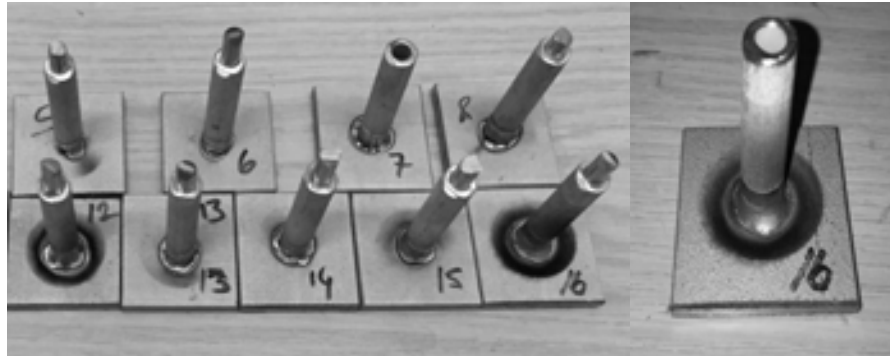


Figure 3. A view of welded specimens

2.3 Microstructural Analysis

Microstructural analysis helps to analyze welding zone. The mechanical properties of the weld joint strength are largely dependent on the changes in the microstructure properties [16]. Some welded specimens were cut from the middle of the stud by wire EDM (electrical discharge machining) for inspections of macro and microstructure of welded area. Chemical solution Glyceregia (10 ml nitric acid (HNO₃), 20 ml hydrochloric acid (HCl) and 30 ml glycerol) was used for etching samples according to the ASTM E 407-99 standard. The samples were swabbed about three minutes with a piece of cotton that has been immersed in the mentioned etchant. After etching operation samples were rinsed by a hot water followed by an alcohol and dried by hot air. Then, a 500x magnification Nikon microscope was used to show microstructural changes in the welding zones.

3. Results and Discussion

3.1 Tensile Test Results

When looking at the tensile test results, it is observed that some of the samples have a good joint performance (Figure 4-a); however, some samples have a poor or insufficient joint performance because of improper input parameters (Figure 4-b).

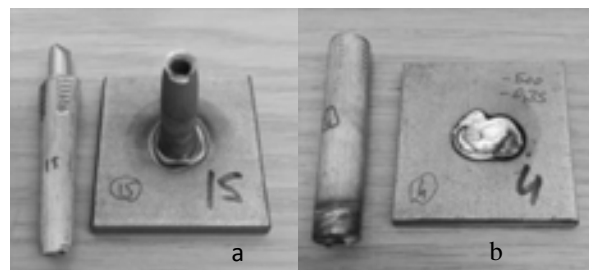


Figure 4. Specimen samples subjected to tensile test

If the weld joints have larger tensile strength, it is more preferable. Larger-to-better status were chosen as a performance characteristic in the analysis of the signal-to-noise (S/N) ratio. Obtained tensile strength values and corresponding S/N ratio for each test are shown in Tab. 3, Tab. 4 and Tab. 5. Maximum signal-to-noise ratio (S/N) shows the larger tensile strength value. Hence, optimum parameters levels of each inner diameter are; for 10-6 mm diameter are 800 ampere, 0.3 second, 2.5 mm plunge and 4 mm lift, for 10-7 mm diameter are 700 ampere, 0.25 second, 2 mm plunge and 3 mm lift, and for 10-8 diameter are 600 ampere, 0.25 second, 2.5 mm plunge and 4 mm lift. According to main effect plots (Figure 5), significant welding parameters are welding time and welding current. Increasing the welding current generally causes more tensile strength for most stud diameters. In order to obtain good strength, the welding time should be set between 0.25 and 0.30 for 10-6 mm and 0.20 and 0.25 seconds for other stud dimensions.

Table 3. For 10-6 mm stud diameter, tensile test results and S/N ratios

Exp. No	Welding Current(Amp)	Welding Time(Sec)	Plunge (mm)	Lift (mm)	Tensile Strength (MPa)	S/N ratio
1	500	0.20	2.0	2.5	212.3	46.54
2	500	0.25	2.5	3.0	324.1	50.21
3	500	0.30	3.0	3.5	491.3	53.83
4	500	0.35	3.5	4.0	432.3	52.72
5	600	0.20	2.5	3.5	312.2	49.89
6	600	0.25	2.0	4.0	338.7	50.60
7	600	0.30	3.5	2.5	507.5	54.11
8	600	0.35	3.0	3.0	438.3	52.84
9	700	0.20	3.0	4.0	377.7	51.54
10	700	0.25	3.5	3.5	509.3	54.14
11	700	0.30	2.0	3.0	678.4	56.63
12	700	0.35	2.5	2.5	569.5	55.11
13	800	0.20	3.5	3.0	623.9	55.90
14	800	0.25	3.0	2.5	652.5	56.29
15	800	0.30	2.5	4.0	711.7	57.05
16	800	0.35	2.0	3.5	687.4	56.74

Table 4. For 10-7 mm stud diameter, tensile test results and S/N ratios

Exp. No	Welding Current(Amp)	Welding Time(Sec)	Plunge (mm)	Lift (mm)	Tensile Strength (MPa)	S/N ratio
1	600	0.15	2.0	2.5	86.7	38.76
2	600	0.20	2.5	3.0	285.6	49.12
3	600	0.25	3.0	3.5	467.4	53.39
4	600	0.30	3.5	4.0	361.5	51.16
5	650	0.15	2.5	3.5	216.2	46.70
6	650	0.20	2.0	4.0	295.2	49.40
7	650	0.25	3.5	2.5	554.3	54.87
8	650	0.30	3.0	3.0	504.4	54.06
9	700	0.15	3.0	4.0	321.2	50.14
10	700	0.20	3.5	3.5	569.3	55.11
11	700	0.25	2.0	3.0	699.5	56.90
12	700	0.30	2.5	2.5	658.3	56.37
13	750	0.15	3.5	3.0	305.8	49.71
14	750	0.20	3.0	2.5	367.2	51.30
15	750	0.25	2.5	4.0	688.7	56.76
16	750	0.30	2.0	3.5	648.2	56.23

Table 5. For 10-8 mm stud diameter, tensile test results and S/N ratios

Exp. No	Welding Current(Amp)	Welding Time(Sec)	Plunge (mm)	Lift (mm)	Tensile Strength (MPa)	S/N ratio
1	450	0.15	2.0	2.5	1.60	4.08
2	450	0.20	2.5	3.0	25.3	28.06
3	450	0.25	3.0	3.5	190.1	45.58
4	450	0.30	3.5	4.0	109.6	40.80
5	500	0.15	2.5	3.5	92.50	39.32
6	500	0.20	2.0	4.0	245.6	47.80
7	500	0.25	3.5	2.5	353.7	50.97
8	500	0.30	3.0	3.0	279.6	48.93
9	550	0.15	3.0	4.0	189.1	45.53
10	550	0.20	3.5	3.5	323.2	50.19
11	550	0.25	2.0	3.0	468.3	53.41
12	550	0.30	2.5	2.5	430.8	52.69
13	600	0.15	3.5	3.0	387.0	51.75
14	600	0.20	3.0	2.5	476.7	53.56
15	600	0.25	2.5	4.0	584.2	55.33
16	600	0.30	2.0	3.5	568.2	55.09

The rank and delta values for different parameters levels for each diameter are shown in Table 6. Higher rank means the higher the influence of the parameter on the process/product performance. Rank has a proportional effect on the process - product performance. According to these results, it is found that welding current and welding time has a greater effect on the response characteristic. These parameters followed with plunge and lift afterwards.

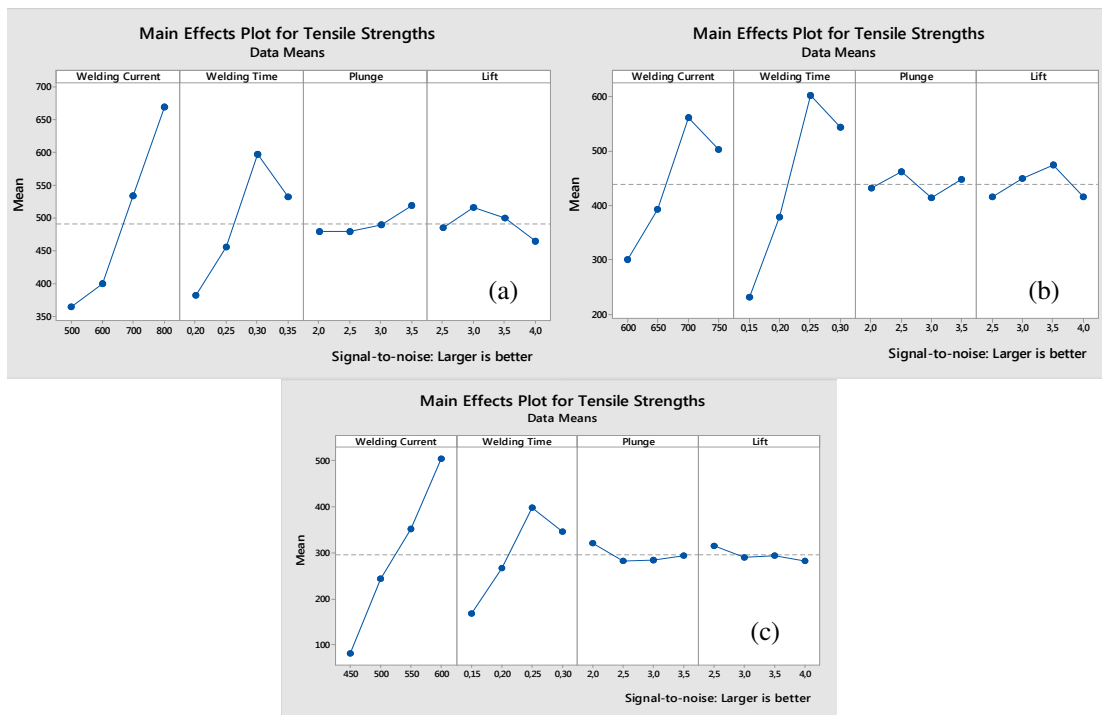


Figure 5. Main effect plots of (a) 10-6, (b) 10-7, (c) 10-8 mm diameters respectively.

Table 6. Response values of S/N ratio with Delta and Rank values

Stud diameter	Welding parameter	Signal to Noise ratio (dB)				Delta	Rank
		Level 1	Level 2	Level 3	Level 4		
10-6 mm	Welding current	50.82	51.86	54.36	56.5	5.67	1
	Welding time	50.97	52.81	55.40	54.35	4.43	2
	Plunge	52.63	53.06	53.62	54.22	1.59	3
	Lift	53.01	53.90	53.65	52.98	0.92	4
10-7 mm	Welding current	48.11	51.26	54.63	53.5	6.52	2
	Welding time	46.33	51.23	55.48	54.46	9.16	1
	Plunge	50.32	52.24	52.22	52.71	2.39	4
	Lift	50.33	52.44	52.86	51.87	2.53	3
10-8 mm	Welding current	29.63	46.76	50.45	53.94	24.3	1
	Welding time	35.17	44.91	51.32	49.38	16.15	2
	Plunge	40.1	43.85	48.4	48.43	8.33	3
	Lift	40.33	45.54	47.55	47.37	7.22	4

According to the results of tensile strength given in Tab. 3, 4 and 5, the ideal current and weld time values for stud inside diameters are plotted in Figure 6. According to this figures, it can be concluded that for 10-6 mm stud diameter, to obtain good welding quality welding current must be between 700 and 800 amperes and welding time must be between 0.3 and 0.35 seconds. Ideal parameter set for 10-7 mm stud diameter is 700-750 ampere welding current and 0.25-0.3 second welding time. For 10-8 mm stud diameter, these values are 550-600 ampere and 0.25-0.3 second.

3.2 Micro-Structural Analysis

Figure 6 represents the microstructural view of the different zones along the cross-sectional view of the welded parts that is the highest strength value of the 10-6 mm welding stud (Exp. No 15). Figure 6-A and E shows the morphology of the stud metal (hollow pipe) and base material which evidences the austenitic-grain microstructure of an AISI 304 stainless steel. Figure 6-B shows the morphology of the plate base material and fusion zone.

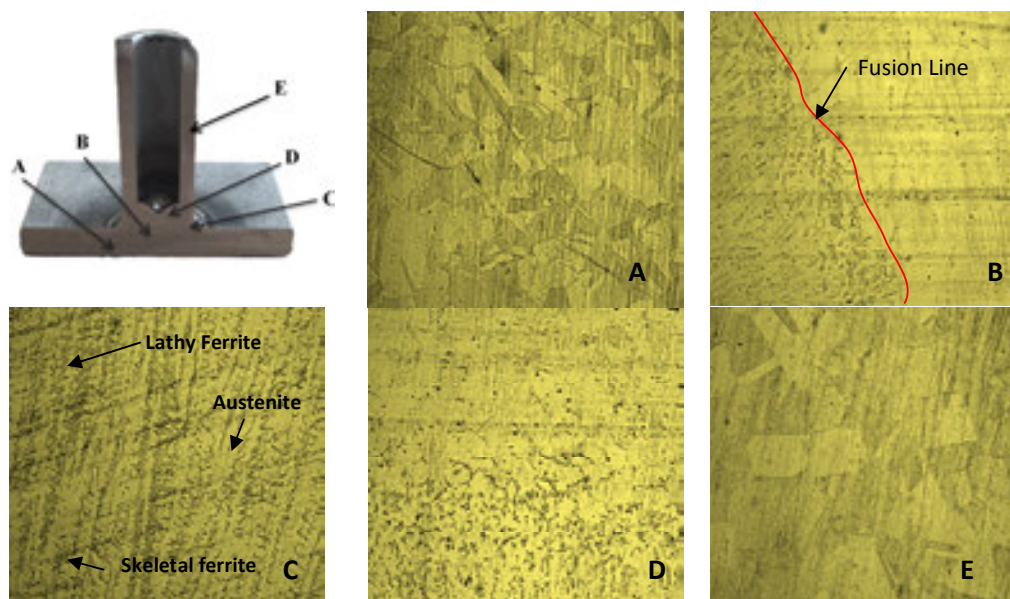


Figure5. Microstructural views of different zones

It has been observed that there is no change in the microstructure of the base and stud material since the heat generated during the welding process does not reach both the stud and the base metal which is showed in Figure 6-A and E. In the weld zone (Figure 6-C), formation of different ferrite morphologies appeared because of the non-equilibrium conditions associated with welding. Dendrites were formed along the fusion line to the weld center which mainly contains lathy and skeletal ferrite which occurred due high temperature during welding. The lathy ferrite microstructure can begin owing to higher ferrite contents and/or typical cooling rate after welding process. The cooling rate at the edges and at the fusion line is higher than in the middle of the weld zone and, consequently, the rate of austenite formation is less than in the middle of the weld metal, because the transformation of ferrite to austenite has less time for transformation.

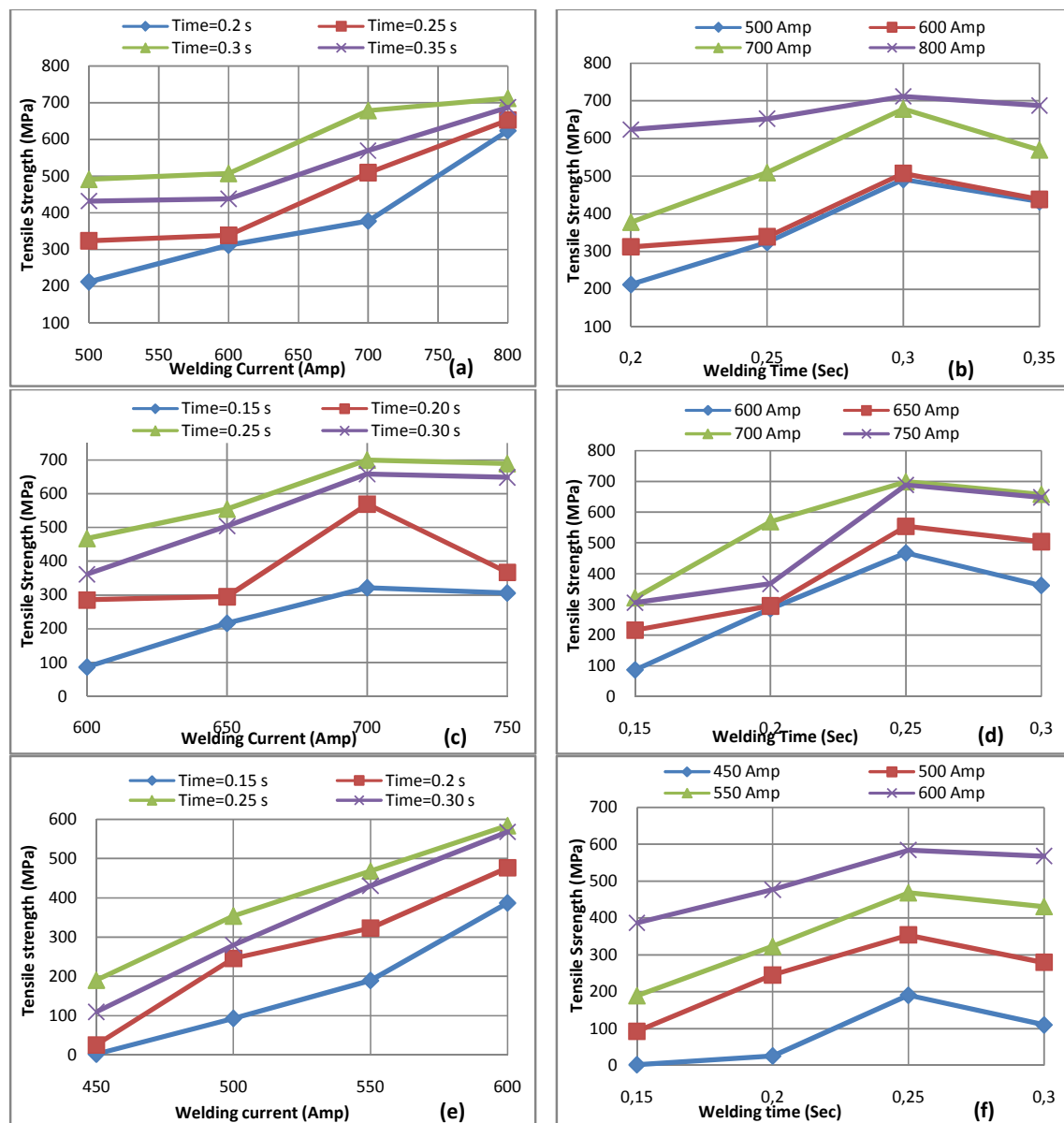


Figure 6. Welding current and welding time vs tensile strength diagrams for stud diameters of (a), (b) 10-6 mm (c),(d) 10-7 mm and (e),(f) 10-8 mm

4. Conclusion

In this study, experimental studies were carried out to examine the arc stud welding of hollow part. The specimens used in the experimental work are hollow parts with a constant outer diameter of 10 mm and different inner diameters of 6, 7 and 8 mm, respectively. Austenitic AISI 304 stainless steel as a stud and base metal was used. It is shown that hollow parts can be successfully welded by using arc stud welding technique. However, it is obviously understood that accurate welding parameters selection was important to obtain good quality welding joints. According to test results following consequences were revealed:

- When the average of the effect of the parameters on the welding quality of hollow parts is considered, it is seen that the most important parameters are welding current and welding time.
- Plunge has less effect on the tensile strength, increasing the plunge increases the tensile strength slowly. However, the effect of lift on the tensile strength is the least.
- Welding current and welding time might have been individually adjusted harmoniously; otherwise the welding quality will deteriorate due to the incomplete or excessive fusion.
- Short size plunge causes the formation of an incomplete weld fillet, however very long size plunge causes the formation of an uneven weld fillet and excessive splatter.
- If the lift is selected correctly, adequate heat will be generated for the welding process. In case of higher air gap, arc formation is terminated because of a formation of longer arc length. On the contrary, if there is inadequate air gap, short arc will occur directly with the base metal without any arc formation.
- To obtain good welding quality, welding current must be between 700 and 800 amperes and welding time must be between 0.3 and 0.35 seconds for 10-6 mm hollow stud. For 10-7 mm stud diameter, welding current and welding time should be between 700 to 750 amperes and 0.25 to 0.3 second. For 10-8 mm stud diameter, these values are 550-600 ampere and 0.25-0.3 second.
- In the weld zone, formation of different ferrite morphologies appeared because of the non-equilibrium conditions associated with welding. Dendrites mainly consisting of lathy and skeletal ferrites are formed due to the high temperature along the fusion line in the welding center. The lathy ferrite microstructure can begin owing to higher ferrite contents and/or typical cooling rate after welding process. The cooling rate at the edges and at the fusion line is higher than in the middle of the weld zone and, consequently, the rate of austenite formation is less than in the middle of the weld metal, because the transformation of ferrite to austenite has less time for transformation.

7. References

- [1]. B.A. Behrens, D. Größ and A. Jenicek: Stud welding within sheet metal working tools. *Prod. Eng. Res. Devel.*, 5, (2011), pp.283–292
- [2]. K.Weman: *Welding processes handbook*. Published by Woodhead Publishing Ltd, Abington Hall, Abington Cambridge CB 1 6AH, England, (2003).
- [3]. J. Hildebrand, H. Soltanzadeh: A Review on Assessment of Fatigue Strength in Welded Studs. *International Journal of Steel Structures*, 14 (2), (2014), pp.421-438
- [4]. Miller Electric Mfg. Co. *Arc Stud Welding Fundamentals*. United States of America. It is available on www.millerwelds.com, (2005).

- [5]. W Nishikawa: The principle and application field of stud welding. *Welding International*, 17 (9), (2003), pp. 699–705
- [6]. S. Ramasamy: Research and Development Department, Emhart Fastening Technologies, Drawn arc aluminum stud welding for automotive applications , 54(8), (2002), pp. 44-46
- [7] Ivan Samardzic, Stefanija Klaric and Marko Dunder. On line monitoring for defects in electric arc stud welding. 11th International Research/Expert Conference "Trends in the Development of Machinery and Associated Technology" TMT 2007, Hammamet, Tunisia, 5-9 September, (2007)
- [8]. I. Samardzic, I. Kladaric, S. Klaric: The Influence of Welding Parameters on Weld Characteristics in Electric Arc Stud Welding. *Metallurgy*, 48(3), (2009), pp. 181-185.
- [9]. J.S. Lee, Y.S. Ryu, N.I. Kim, B.J. Kim, Y.K. Kim, M.H. Kim: Stud welding for fixation of cryogenic insulation of membrane tanks in LNG ship building. *Trans. Nonferrous Met. China*, 19, (2009), pp. 271-S275.
- [10]. N.F. Yilmaz, A.A. Hamza: Effect of Process Parameters on Mechanical and Microstructural Properties of Arc Stud Welds. *Materials Testing*, 56(10), (2014), pp. 806-811
- [11]. T. Kumar, P. Jambulingam, M. Gopal and A. Rajadurai: Surface Hardening of AISI 304, 316, 304L and 316L SS Using Cyanide Free Salt Bath Nitriding Process. *International Symposium of Research Students on Materials Science and Engineering*, (2004).
- [12]. L.S. Kumar, S.M. Verma, P.P. Prasad, P.K. Kumar, T.S. Shanker: Experimental Investigation for Welding Aspects of AISI 304 & 316 by Taguchi Technique for the Process of TIG & MIG Welding. *International Journal of Engineering Trends and Technology*, 2(2), (2011), pp. 28-33.
- [13]. N.A. Armstrong: *Pharmaceutical experimental design and interpretation*. 2nd ed; Taylor & Francis group. New York, (2006), pp.5-50
- [14]. R.K. Roy: *Design of experiments using the Taguchi approach*. ISBN 978-0-471-36101-5. John Wiley & Sons. Inc. New York, (2001)
- [15]. G. Taguchi, S. Chowdhury, S. Taguchi: *Robust engineering*. McGraw Hill, New York (2000).
- [16]. M. I. Khan, M. L. Kuntz, E. Biro, Y. Zhou: Microstructure and Mechanical Properties of Resistance Spot Welded Advanced High Strength Steels. *Materials Transactions*, 49(7), (2008), pp. 1629 to 1637.

CORRESPONDENCE ADDRESS: M. Veysel ÇAKIR, Kilis 7 Aralık University, Faculty of Engineering Mechanical Engineering Department, Turkey, cakir@kilis.edu.tr

Necip Fazıl YILMAZ – He was born in Elbistan, Turkey in 1970. He received the BSc. degree in Mechanical Engineering Department from METU in 1991. He received his MSc, and PhD degrees in Mechanical Engineering from the Gaziantep University, Gaziantep, Turkey in 1996, 2002, respectively. He has been studying as Assoc. Prof. Dr. in Mechanical Eng. Dept. of Gaziantep University.

Mehmet Veysel Çakır – He was born in Besni, Turkey in 1974. He received his BSc, MSc, and PhD degrees in Mechanical Engineering from the Gaziantep University, in 1996, 2004 and 2014, respectively. From 2014 to 2017 he was Assis. Prof. Dr. in the Aircraft and Aerospace Engineering Dept. of Gaziantep University. He has been studying as Assist. Prof. Dr. in Mechanical Eng. Dept. of Kilis 7 Aralık University.

Hüseyin Ahmet Erol – he was born in Antalya, Turkey in 1991. He received his BSc, MSc, degrees in Mechanical Engineering from the Gaziantep University, in 2014 and 2018, respectively. He has been studying at Fimak Bakery Machines and Equipment Factory in Konya.

INVESTIGATION of CARBIDE PRECIPITATION of TIG WELDED AISI 304 PIPES

Necip Fazıl Yılmaz^{1,a}, Musa Yılmaz^{1,b}, Mahmut Furkan Kalkan^{1,c}

¹Mechanical Engineering Department, Faculty of Engineering, Gaziantep University
^anfyzilmaz@gantep.edu.tr, ^bmsyilmaz@gantep.edu.tr, ^cmfkalkan@gantep.edu.tr

Abstract

Austenitic stainless steel pipes (AISI 304) are highly used by the chemical, oil and gas industries. But welding of stainless steels have some limitations which causes weld decay problem during tungsten inert gas (TIG) welding process. This welding problem is caused by precipitation of chromium carbide ($Cr_{23}C_6$) at grain boundaries during the temperature changes from in the solidification stage. Currently, this problem has been eliminated by proposing the heat treatment or using low carbon content stainless steels. Current study proposes a new method to solve these problems and Austenitic stainless steel pipes are welded successfully. It is realized that if temperature transition from 800^oC to 500^oC is passed rapidly, carbon has not enough time to precipitate with chromium at the grain boundaries. Copper block is placed inside the pipe and refrigerant fluid was passed with a different temperature. Mechanical and microstructural properties of welded samples are investigated by carrying out hardness test, optical and scanning electron microscope analyses.

Key Words: TIG Welding, Carbide Precipitation, Weld Decay, Stainless Steel pipes

1. Introduction

Steels are the alloys of iron and other elements. Stainless steel mainly contains chromium (Cr) and nickel between 10.5 to 18 percent with iron and certain amount of carbon etc. Chromium and nickel especially in acidic environment provide a high corrosion resistance. Stainless steel in different chemical compositions are classified according to their physical, magnetic and corrosion properties [1]. Because of their facility of fabrication, production and welding, austenitic stainless steels (AISI 304) have widely usage areas and more popular than the other stainless steel types. AISI 304 are observed a single-phase, face centered cubic (FCC) structure over a wide temperature. [2]

Almost all welding methods used for other steels can also be used for stainless steels. Tungsten Arc Welding (TIG) is the popular joint type of austenitic stainless steels for maintenance works according to American welding society (AWS) specification [3-4]. Heat energy requirement for this welding method is provided by tungsten electrode and inert gas supplied by an arc between the workpiece and a nozzle. In this welding method, high quality, smooth surface and perfect welding can be obtained[5-7]. These steels are simply affected from attack by localized

corrosion, such as intergranular corrosion. Carbide precipitation (sensitization) is a form of anintergranular corrosion[8].

Carbide precipitation occurs in the heat affected zone during the welding especially on grain boundaries. For sensitization the critical range of temperature is about 500-800⁰C, depending on the steel chemical composition. If the temperature is held within the critical range for the longest time intervals, chromium carbide precipitation and chromium depletion occurs at grain boundaries. This defect is called carbide precipitation or weld decay (sensitization) [9,10].

Usage of stainless steel pipes and their TIG welding have widely usage areas in the industrial fields. Although stainless steels are providing good mechanical properties, carbide precipitation named as weld decay is a vital problem in application. In order to avoid from this problem, generally low carbon content of stainless steels (AISI 304L) are being used. But they are more expensive than AISI 304 steels. In this study, carbide precipitation in TIG welding of AISI 304 pipes is prevented with a new approach. Elemental, microstructure and hardness properties of the samples were investigated to prove the applicability of new proposed method used in this study.

2. Material and Method

In this study, the AISI 304 stainless steel sheet (3 mm thick and 100 mm length) was bended and tubularized to a diameter of 48 mm. The chemical composition of the AISI 304 stainless steel analyzed in the SEM/EDX device and itis presented in Table 1.

Table 1. Chemical composition of 304 quality austenitic stainless steel

C%	Si%	Cr%	Ni%	Mn%	S%	Mo%	P%	V%	Fe%
0.08	1	18-20	8-10	2	0,03	0,070	0,045	0,030	Bal.

A copper block having several holes was used to provide the cooling media during TIG welding process. Copper was used because it has superior properties both in terms of thermal conductivity and economy. Figure 1 shows the schematical view of copper block and AISI 304 stainless steel pipe. Stainless steel samples were TIG welded by INVERTEC V160-TP type welding machine.

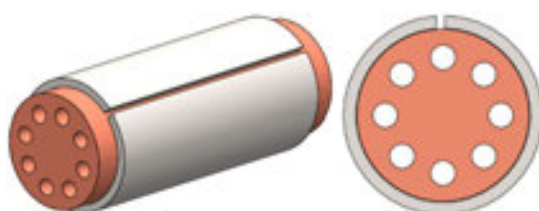


Figure 1. The copper block and the AISI 304 stainless steel pipe

3. Experimental Procedure and Set-Up

In this work, in Tungsten Arc Welding (TIG) process non-consumable tungsten electrode was used to deliver the current to welding arc. Welding procedure properties and phases of this work are listed sequentially.

Welding Procedure Specifications:

- Welding process : GTAW (Gas Tungsten Arc Welding)
- Filler Materials : No
- Shielded Gas : Argon
- Current : DC- 100A
- Electrode size-type : 2 mm-2% throated

Experimental set-up is shown in Figure 2. Previously manufactured copper block having several holes is placed inside the pipe. Diameter of each hole used to transmit water and provide continuous cooling is 7mm.

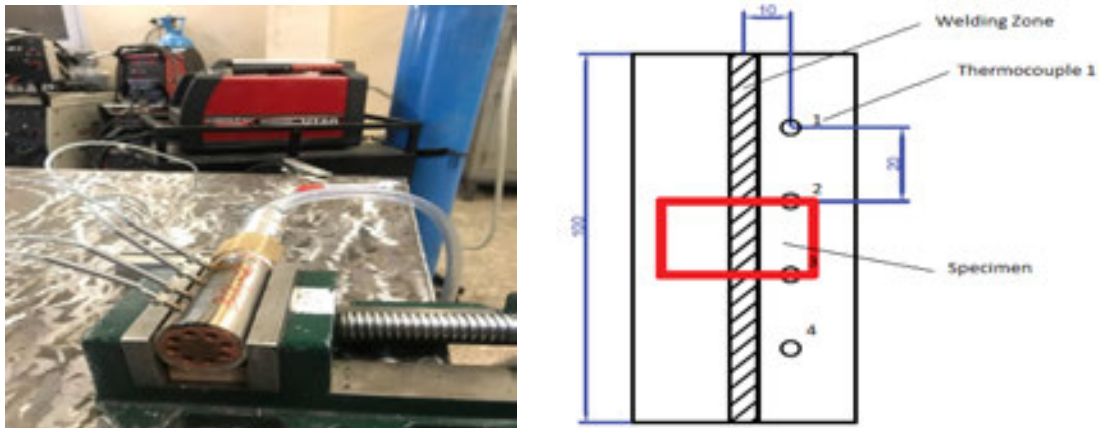


Figure 2. Experimental set-up

Temperature of the welding zone was measured instantly by thermocouple as shown in Figure 2. Temperature sensors (Type K thermocouple) were placed 10 mm away from the weld center and 20 mm intervals with each other to reveal the temperature distribution in the samples. Temperature distributions were recorded with the Verth CK104L data-logger device. Experiments were carried out with 4 different conditions as it is presented in Table 2.

Table 2. Experimental Conditions

Exp. Number	Sample			Temperature of Water		
	Name	Copper	Passing Fluid	Flowrate		
1	304-1	No	No	-	-	
2	304-2	Yes	No	-	-	
3	304-3	Yes	Water	30 l/min	24° C	
4	304-4	Yes	Water	30 l/min	8° C	

In order to examine the weld quality, samples were taken from the mid-section of weldment as shown in Figure 2. Specimens carefully grinded with 360, 600 and 1000 mesh SiC emery papers and specimens were polished by 0.3 μ m diamond solutions and polishing cloths with lubricant solutions to obtain reflective surface. Grinding and polishing operations were made with MetkonForcipol 2V device. All samples were chemically etched with Glyceregia, which is selected according to ASTM E 407-07 standard. The glyceregia consists of 30 ml of glycerol, 10 ml of nitric acid (HNO₃) and 30 ml of hydrochloric acid (HCL) [11]. The etchant was applied to sample about 4 minutes and after processing they were cleaned with alcohol.

Hardness values of the welded austenitic stainless steel specimens were measured with LHV-1 Micro vickers hardness measurement machine (Figure 3a). The indenter either the Vickers diamond pyramid or the knoop elongated was diamond pyramid. Hardness test values were determined by calculating the average of 3 successive measurements for each sample. Microstructural inspections and SEM-EDX analysis of weld area and heat affected zone is carried out with Nikon optical microscope and Zeiss Gemini SEM, respectively as shown in Figure 3b and 3c.

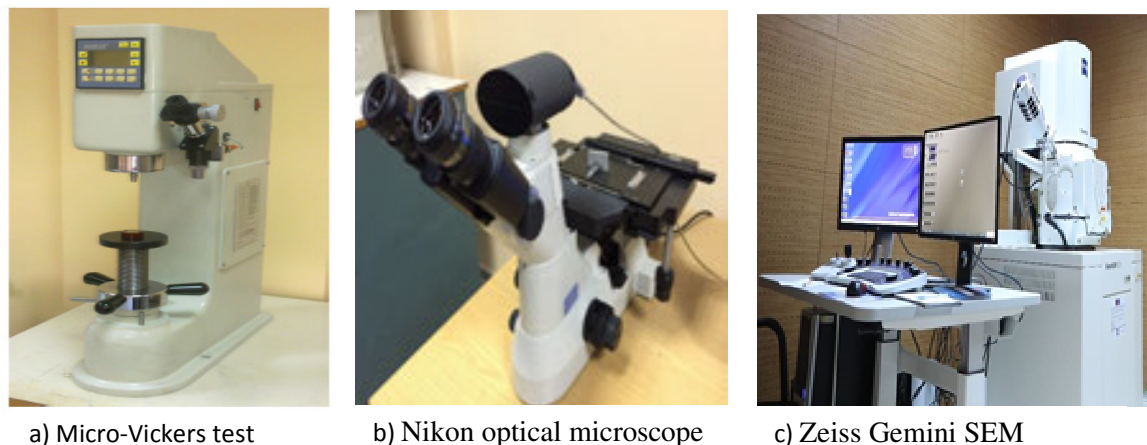


Figure 3. Hardness and Microstructural Analysis

4. Result and Discussion

4.1 Micro-Hardness Test

All prepared samples for micro-hardness test are tested according to the path shown in Figure 4 and hardness values were recorded.

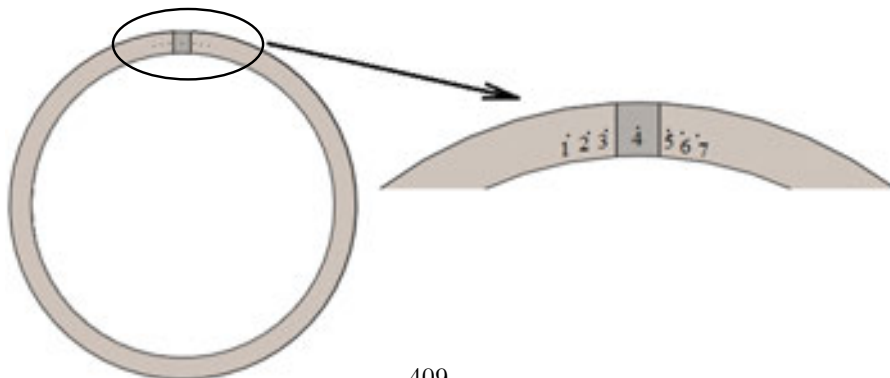


Figure 4. Illustration of Hardness Test Measurement

Table 3 shows the Vickers hardness value of the weldment. It is very clear from Table 3 and Figure 5 that highest hardness values are obtained from the fastest cooling condition. In this welding condition 8⁰C water passed through the holes previously made on copper block.

Table 3. Hardness Test Results

Experimental Runs	Tested Locations						
	1	2	3	4	5	6	7
1	160,2	162,4	169,5	179,6	167,7	159,7	159,9
2	165,0	164,3	180,1	195,9	181,5	164,6	163,4
3	163,2	166,0	189,6	202,3	185,7	163,4	163,4
4	164,1	165,5	196,6	213,1	197,3	165,2	163,7

Figure 5 shows that the micro-hardness at the center of the weld is higher than the HAZ and base metals and decreases as it approaches to base metal gradually.

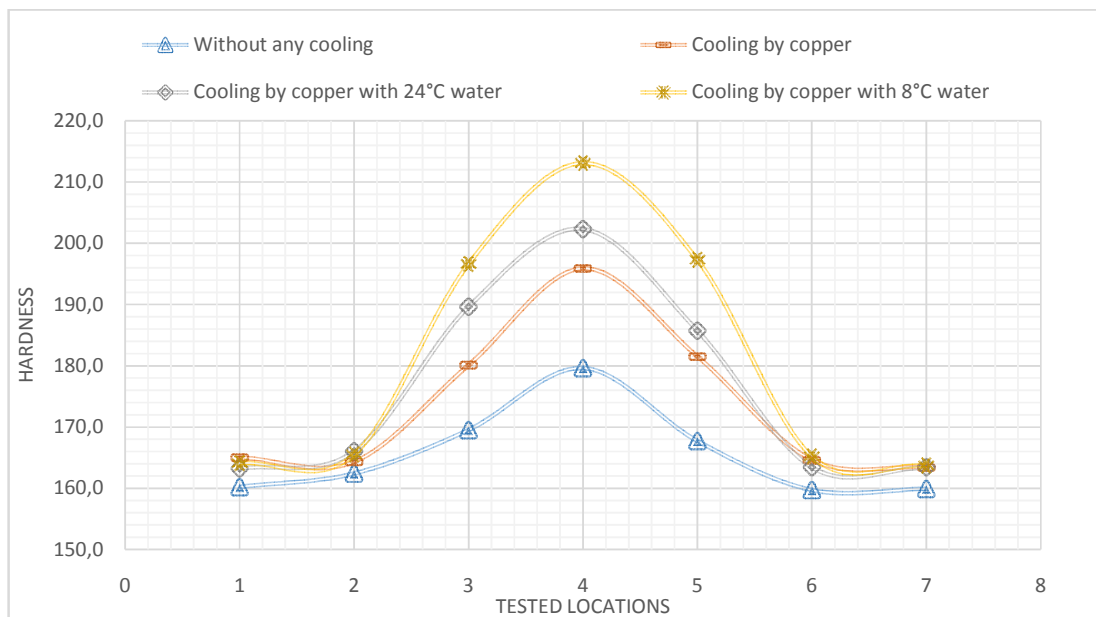
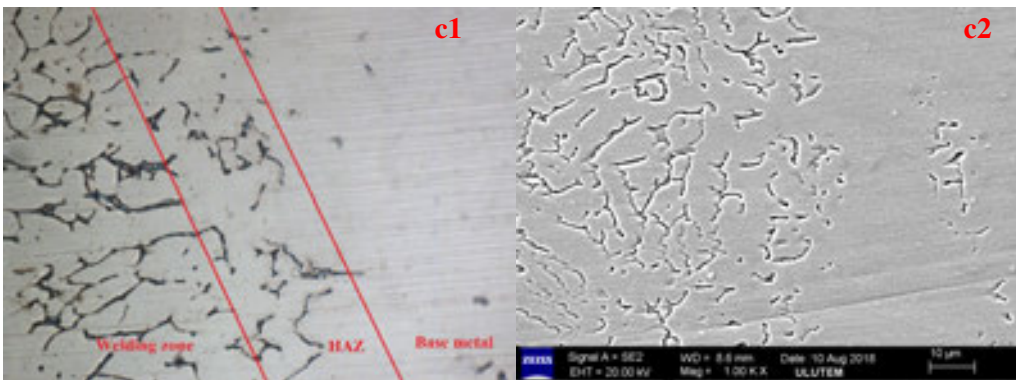
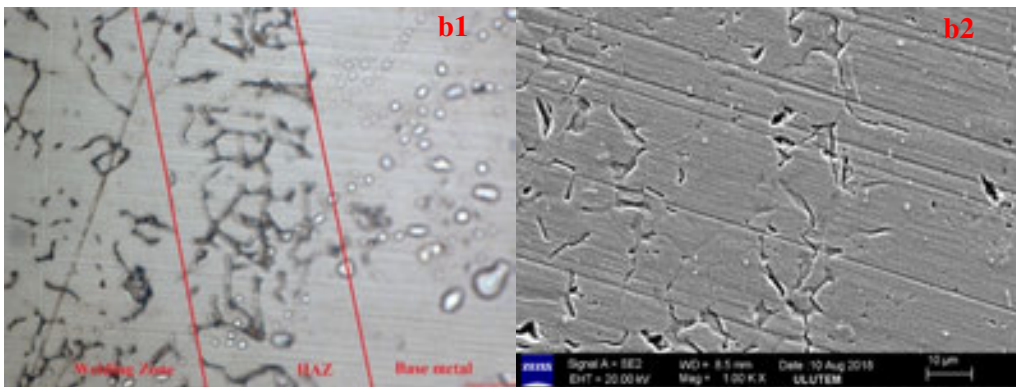
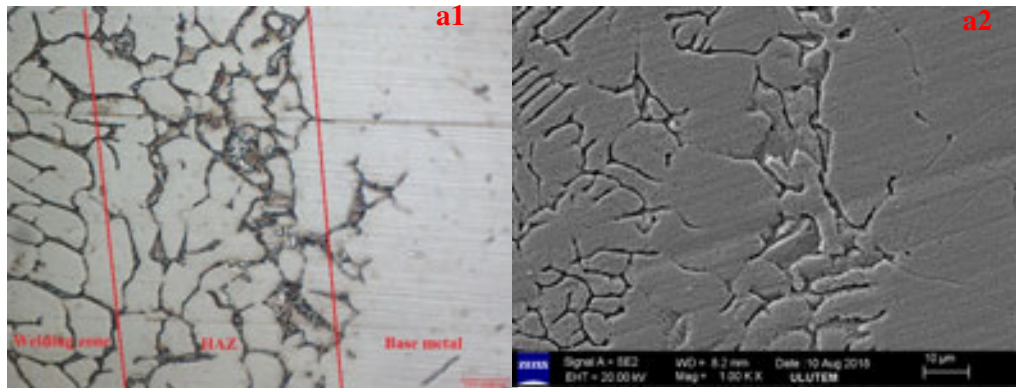


Figure 5. Micro-hardness Values Through Welding Zone

4.2 Metallographic Study

Different microscopic occurrences have emerged depending on the change in cooling rate. It is known that δ -ferrite formation occurs as a result of welded joints [12]. The formation of this dendritic build-up increases in the high-cooling time interval, but decreases in the low-cooling interval. As the weld metal is exposed to high temperatures, there is a more intense dendritic formation in this region [13]. Dendritic microstructure formations are increasing towards weld metal starting from the zone under heat.

Chromium carbide precipitations has high concentration of chromium. This chromium carbide particles locally reduce the content of chromium in the region adjacent to these chromium-rich precipitates. Since it spreads faster than carbon chromium, it is impossible for the chrome to be distributed homogeneously in the grains. This precipitation increases in the grain boundaries, while the chromium content decreases near the grain boundaries up to 13 percent [14].



d1

d2

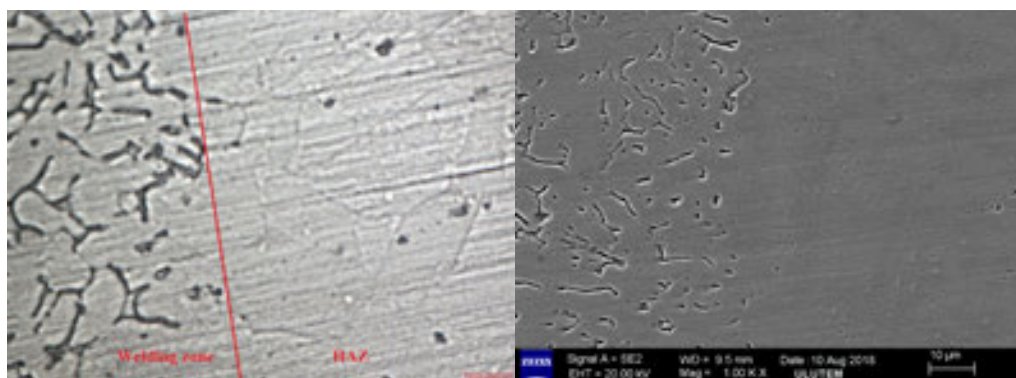


Figure 6. Optic (100x) and SEM (1000x) Images of welded samples a) Without any cooling b) Cooling by copper c) Cooling by copper with 24°C d) Cooling by copper with 8°C

Figure 6 (from a1 to d1) shows the microstructural view of welded sample while (a2 to d2) show SEM images. Along with observations on random grain boundaries, Figure 6a shows typical carbide precipitation behavior which was obtained at no cooling condition. Figure 6b also displays carbides nucleated at grain boundaries but relatively fewer amounts than Figure 6a. Lower tendency of nucleation and grain growth was observed when the copper block is placed inside the pipe as shown in Figure 6c. No carbide precipitation behavior was observed on the grain boundaries as the cooling rate increased by copper with 8°C water (Figure 6d).

5. Conclusion

In this study, a series of experiments were done and the samples in different cases were examined in terms of mechanical and microstructure properties. Under the light of current studies, it is observed that fast cooling did not allow the opportunity to start to sensitization and interaction of carbon with chromium. It means that there is no intergranular corrosion in grain boundaries and it can be said that the weld decay problem has been solved. Within this study a new method is proposed to reduction of carbide precipitation problem in stainless steel pipes. In this method there is no necessary to expensive equipment and this method is too easy for any welding or maintenance. Hardness values were recorded that hardness was increased with cooling rate.

6. Acknowledgement

This study is supported by Gaziantep University Scientific Research Projects Unit. Authors would like to thank to Uluğbey High Technology Application and Research Center (ULUTEM) in Gaziantep University for their support on this study.

References

- [1] Cobb HM, International A. The History of Stainless Steel: ASM International; 2010.
- [2] Mutlah Shafi Fuhaid: Reduction of Weld Decay Effect of Stainless Steels Used in Medical and Food Sector That Weld by TIG Process, M.Sc. Thesis in Mechanical Engineering, Gaziantep University, Türkiye (2013)

- [3]E. Gözütok: The influence of argon-hydrogen gas mixture on mechanical and microstructural properties of the joints in TIG welding of stainless steels, M.SC. Thesis in Medical Engineering, University of Karabük, Türkiye (2009)
- [4] R. Winston Revie and Herbert H. Uhlig. (2008). Corrosion and Corrosion Control, 4th edition. John Wiley & Sons, Inc, Canada.
- [5] E. Gözütok, N. Kahraman, A. Durgutlu, B. Gülenç, “The Influence of Hydrogen Addition to the Shielding Argon Gas in TIG Welding of AISI 304 Materials” 1st International Conference On Welding Technologies, ICWET'09, 11-13 June Ankara/Turkey, (2009), pp. 778-786.
- [6] C. Odabaş, “PaslanmazÇeliklerinKaynağı, AskaynakKaynakTekniğiSanayiveTicaret A.Ş, 2007.
- [7] A. Durgutlu, “ Experimental Investigation of the Effect of Hydrogen in Argon As a Shielding Gas on TIG Welding of Austenitic Stainless Steel, Materials and Design, 25 (2004), pp. 19-23
- [8]Jiao Jingpin, Sun Jungun, Li Guanghai, Wu Bin, He Cunfu, “ Evaluation of the intergranular corrosion in austenitic stainless steel using collinear wave mixing method” NDT & E International, 69 (2015), pp. 1-8
- [9] Yılmaz N.F., Fuhaid M.S., “Reduction of Weld Decay Effect of Stainless Steels Used in Medical and Food Sector that Weld by TIG Process”,Innovative Materials And Structures'13, (2013), pp. 167-174
- [10] Tomoyuki Fujii, Keiichiro Togho, Yota Mori, YoshinobuShimamura, “ Crystallography of intergranular corrosion in sensitized austenitic stainless steel” Materials Characterization, 144 (2018), pp. 219-226
- [11] ASTM International. (2007). E 407-07 Standard Practice for Microetching Metals and Alloys. United States: ASTM International
- [12]Chopra O, Gruber E, Alexandreanu B, Chen Y, Shack W. Crack Growth Rates of Irradiated Austenitic Stainless Steels in BWR Environments at 289 °C. ASME 2007 Pressure Vessels and Piping Conference: American Society of Mechanical Engineers; 2007. pp. 253-68.
- [13] Yılmaz N.F., Kurt, H.İ., Oduncuoğlu, M., Çakır, M.V., “Investigation of the Effect of Substrate Type on Chromium Carbide Storage in Welding Processes”El- Cezerî Journal of Science and Engineering, 2017, 4(3); 341-348.
- [14] G. H. Aydoğdu, M. K. Aydınol, 2006, Determination of susceptibility to intergranular corrosion and electrochemical reactivation behavior of AISI 316L type stainless steel, Corrosion Science 48, pp. 3565-3583.

**CORRESPONDENCE ADDRESS: NecipFazıl Yılmaz, Mechanical Engineering
Department, Faculty of Engineering, Gaziantep University, 27310, Gaziantep/Turkey, +09
(342) 317 15 94 – nfyilmaz@gantep.edu.tr**

SHORT BIOGRAPHIES

NecipFazıl Yılmaz – Dr. NecipFazıl Yılmaz was born in Elbistan in 1970. He completed his primary, secondary and high school in Gaziantep. He received his BSc Degree in Mechanical Engineering Department from METU, MSc and PhD Degree in Mechanical Engineering Department from Gaziantep University. He is Assoc Professor in Mechanical Engineering Department, Gaziantep University.

Musa Yılmaz – Musa Yılmaz was born in Elbistan in 1991. He completed his primary, secondary and high school in Elbistan. He received his BSc and MSc Degree in Mechanical Engineering Department from Gaziantep University. He is lecturervocational school of higher education in NaciTopçuoğlu, Gaziantep University.

MahmutFurkanKalkan – MahmutFurkanKalkanwas born in Ankara in 1994. He completed his primary, secondary and high school in Gaziantep. He received his BSc Degree in Mechanical Engineering Department from Gaziantep University. He is researcher assistant in Mechanical Engineering Department, Gaziantep University.

JOINABILITY OF DIFFERENT POWDER METAL MATERIALS WITH MICROWAVE AND INDUCTION HEATING

İrem Burcu Algan^{1,a}, Yasemin Aksu^{1,b}, Yusuf Çiftçi^{1,c}, Nurcan Ünlü^{1,d},
Ramazan Çıtak^{1,e}, Yusuf Özçatalbaş^{1,f}, Adem Kurt^{1,g}

¹Department of Metallurgical and Materials Engineering / Faculty of Technology / Gazi University

^airembalgan@gazi.edu.tr, ^byasemindundar@gazi.edu.tr,
^cyusuf.cift95@gmail.com ^dnlunurcan92@gmail.com, ^ecitak@gazi.edu.tr, ^fyusufoz@gazi.edu.tr, ^g
ademkurt@gazi.edu.tr,

Özet

Sinter lehimlemede indüksiyon ve mikrodalga uygulamaları işlem süresini önemli oranda azaltır ve böylelikle enerji açısından verimli bir süreç elde edilebilir. Bu çalışmada, tek yönlü soğuk pres ile üretilen farklı toz metal malzemelerin sinterlehim ile birleştirilebilme özellikleri incelenmiştir. Sırasıyla ortalama parçacık boyutu 20 µm ve 40 µm olan bakır ve paslanmaz çelik tozları 700, 800 ve 900 MPa basınçla preslenerek 12 mm çapında ve 3 mm yüksekliğinde numuneler üretilmiştir. İndüksiyon ile ısıtma 450°C sıcaklık ve 2900 Hz frekansta Argon atmosferinde gerçekleştirilirken, mikrodalga ısıtma 450°C sıcaklık ve 900 W güç kullanılarak atmosfer ortamında gerçekleştirilmiştir. Mikroyapı analizleri optik mikroskop ile yapılırken, mekanik analizler mikrosertlik testi (HV 0,3) ile yapılmıştır.

Anahtar Kelimeler: Mikrodalga, indüksiyon, toz metalürjisi, bakır, paslanmaz çelik

1. Giriş

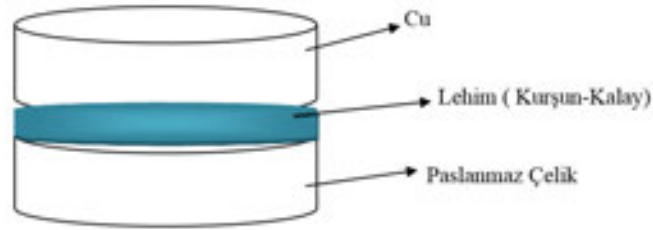
Toz metalürjisi, 20. yy'da ortaya çıkmış ve günümüzde hızla gelişmektedir. Toz metalürjisi ile üretilen parçalar pek çok değişik alanda kullanılmaktadır. Dişliler, kendinden yağlamalı burçlar, elektrik kontakları, sert kesici takım uçları vb. birçok parça toz metalürjisi yöntemi ile üretilmektedir [1,2].

Toz metalürjisinde üretilecek uygun bileşime sahip olan tozlar, ilk işlem olarak uygun bir kalıp içinde preslenmektedir. Presleme sonrasında en önemli işlem olan sinterleme işlemi, ergime sıcaklığı altında ve genellikle koruyucu atmosferde gerçekleştirilir. Bu işlemde; parça, fırın içine konur ve korozyondan korunması için fırın içerisine koruyucu gaz gönderilir. Fırındaki parçanın içindeki yağlayıcıların temizlenmesi için numuneler ön ısıtmaya tabi tutulur. Oksit indirgenmesinin ardından fırının sıcak bölgesinde sinterleme işlemi gerçekleşir ve fırından çıkan parça soğumaya bırakılır [3]. Hızlı sinterleme teknikleri, sinterleme süreleri kısaltılarak enerji ve zaman tasarrufu sağlanabilmektedir. Örneğin indüksiyon sinterlemede, işlem görece malzeme değişken akım taşıyan iletken bobin ile bir seferde ısıtılır. Isı transferi, diğer ısıtma sistemlerinden 3000 kez daha iyidir [4]. Diğer yandan mikrodalga sinterlemede ısı, verilen elektromanyetik enerjinin doğrudan malzemeyle etkileşimi sonucunda açığa çıkması sebebiyle

hızlı ve verimli şekilde numunenin ısıtılması sağlanır[5]. Sinterleme ve lehimleme işlemi eş zamanlı gerçekleştirildiğinde işlem süresi kısaltılarak zamandan ve enerjiden tasarruf edilebilir. Ayrıca bu eş zamanlı işleme hızlı ısıtma tekniklerinin uygulandığında, homojen bir ısı transferinin gerçekleştirilmesi ile ürün kalitesinin artırılabilir.

2. Deneysel Çalışmalar

Bu çalışmada, 20 ve 80 µm toz tane boyut aralığında olan Cu ve SS (paslanmaz çelik) tozları hassas terazide her birinden 3 gr olacak şekilde tartıldıktan sonra 12 mm çapında ve 3 mm uzunluğundaki kalıpta, 700, 800 ve 900 MPa basınçlarda soğuk olarak preslenmiştir. Üretilen numunelerin ham yoğunlukları hesaplandıktan sonra, yüzeyleri ince zımpara yardımıyla temizlenmiş ve arayüze Pb-Sn (%40 Pb) (lehim) tozu homojen bir şekilde yerleştirilmiştir (Şekil 1).



Şekil 1. Cu-paslanmaz çelik numunelerin mikrodalga lehim işleminin şematik görünüşü

Üretilen iki set numuneden 1. grup numunelere HAMILab-DS1500 marka cihazda mikrodalga sinter lehim; 2. grup numunelere ise Reterm marka cihazda indüksiyon sinter lehim işlemi uygulanmıştır. Mikrodalga sinter lehimleme işlemi, 900 watt güç ve 450 °C sıcaklıkta 5, 10 ve 15 dakika sürelerde; indüksiyon sinter lehim işlemi ise Ar atmosferinde, 450 °C sıcaklık ve 2900 Hz frekansta 5 dakikada gerçekleştirilmiştir. Sinterleme ve eş zamanlı lehimleme işlemi için kullanılan mikrodalga fırın ve indüksiyon ısıtma düzeneği Şekil 2' de verilmiştir.

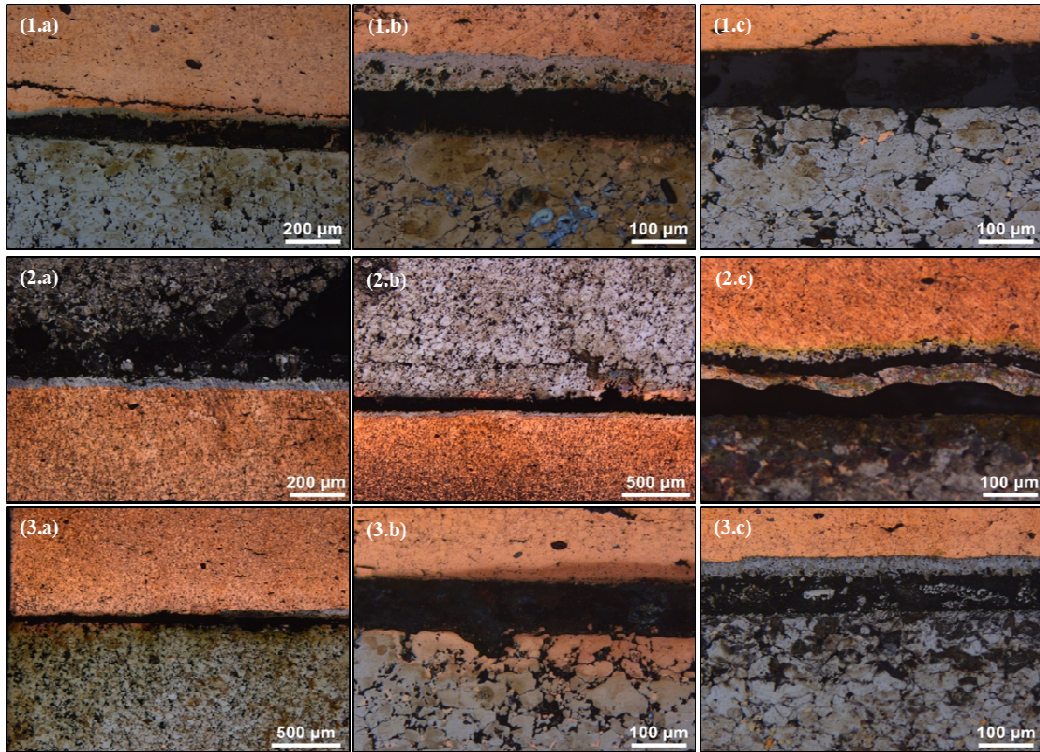


Şekil 2. (a) Mikrodalga fırın ve (b) indüksiyon ısıtma düzeneği

Sinterlehimlenen numunelerin Leica DM5000M model optik mikroskopta mikroyapı analizi ve Shimadzu HMV-2 model mikrosertlik cihazında sertlik testleri yapılmıştır.

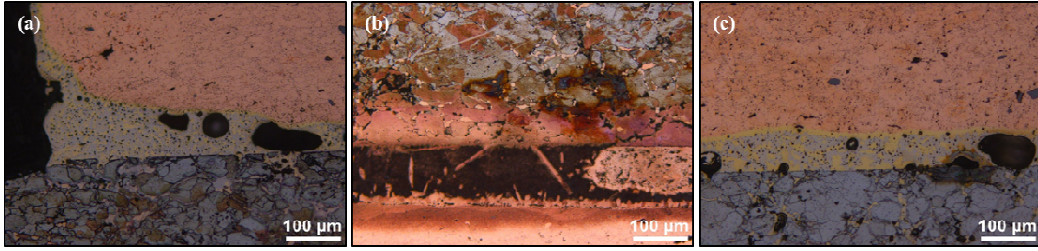
3. Sonuçlar ve Tartışma

Şekil 3'te Cu ve SS parçaların değişik basınç ve sürelerde birleşme mikroyapıları verilmiştir. Birleşme ara yüzeyinde lehim tabakasının artan sinterleme süresine bağlı olarak difüzyon ve buharlaşma yoluyla ara yüzeyden genellikle Cu tarafına ince bir film halinde geçiş bölgesi oluşturduğu gözlenmektedir. Birleşme esnasında oluşan bağ kuvvetinin etkisiyle en düşük basınçta preslenen numunenin birleşme ara yüzeyine paralel katmanlı çatlak oluştuğu görülmektedir. Bunun bakırın genişmesi ve ara yüzey lehim bölgesinin Cu tabakayı SS tarafına çekme gerilmeleri sonucu oluştuğu düşünülmektedir. Artan sinterleme süresiyle özellikle Cu tarafında birleşme ara yüzeyine paralel mikro çatlakların meydana geldiği gözlenmiştir. Bununla beraber 796 ve 884 MPa basınçta preslenmiş SS numunelerde, artan sinterleme süresinin tane irileşmesine yol açtığı ve taneler arasında gözeneklerin irileşmesine neden olmuştur. 884 MPa'da 10 dakikasinterlenmiş numunenin ara yüzeyinde lehim tabakası katmanlı şekilde Cu tarafında bir geçiş bölgesi; SS tarafında ise Cu+lehim malzemesinden oluşan dalgalı bir birleşme tabakası oluşturmuştur. Sinterleme süresinin artmasıyla 15 dakika sinterleme süresinde Cu ve SS ara yüzeyinde homojen denebilecek bir lehim birleşme bölgesi meydana gelmiştir.



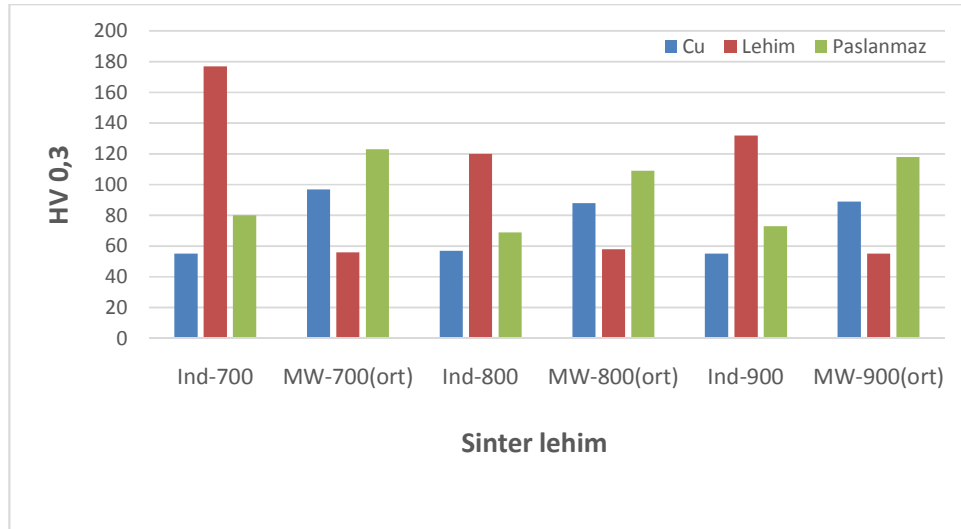
Şekil 3. (1) 700 MPa, (2) 800 MPa ve (3) 900 MPa basınçta preslenen Cu ve SS parçaların (a) 5, (b) 10 ve (c) 15 dakikada mikrodalga ile lehimlenen bölgelerinin mikroyapıları.

Şekil 4' te indüksiyon ısıtma ile lehimlenen malzemelerin mikroyapısı verilmiştir. Buna göre, 700 ve 900 MPa basınçla preslenen numunelerin birleşme arayüzeyinde başarılı şekilde bağlanma görülmüş, ancak her üç numunenin de arayüzey bölgesinde gaz boşlukları ve oksit tabakaları tespit edilmiştir.



Şekil 4. (a) 700 MPa, (b) 800 MPa ve (c) 900 MPa basınçta preslenen Cu ve SS parçaların indüksiyon ısıtma ile elde edilmiş lehim bölgelerinin mikroyapıları.

Şekil 5'te, hem indüksiyon hem de mikrodalga ısıtma ile lehimlemede, toz malzemelerin presleme basıncı arttıkça sertliğin azaldığı görülmektedir. Bu duruma, pres basıncının artması ile birlikte artan sinterleme süresinin sebep olduğu düşünülmektedir. İndüksiyonla ısıtılarak lehimlenen malzemelerde lehim bölgesi en yüksek sertliğe sahipken, mikrodalga ile lehimlenen numunelerin lehim bölgesi düşük sertliktedir.



Şekil 5. İndüksiyon ve mikrodalga ısıtma ile lehimlenen Cu-SS malzemelerin sertlik değerleri

4. Sonuç ve Öneriler

Mikrodalga ve indüksiyon ısıtma ile sert lehimleme yapılan bu çalışmada:

- Farklı basınçlarda preslenen toz metal malzemelerin, mikrodalga ve indüksiyon gibi hızlı ısıtma yapabilen sistemlerle sert lehimlenebildiği görülmüştür.
- Yüksek presleme basıncı ve hızlı ısıtma etkisi, lehim arayüzeylerinde presleme yönüne dik çatlaklar oluşturmuştur.
- Lehimleme işleminin atmosfer korumalı ortamda yapılması, gaz boşluklarının ve kesintili arayüzey bağlantılarının önlenebileceği düşünülmektedir.

5. Kaynaklar

1. F. Nutku: Toz Metalurjisi ile Üretilen Parçaların Tahribatsız Muayenesi, Yüksek Lisans Tezi, Yıldız Teknik Üniversitesi Fen Bilimleri Enstitüsü, İstanbul, (2003).
2. Sarıtas, S., "Powder I. Ulusal Toz Metalurjisi konferansı Bildiri kitabı", Gazi Üniversitesi İletişim Fak. Matbaası, Ankara. (1996).
3. Ersümer, A: Toz Metalurjisi Sert Metal Sinterleme, İstanbul Üniversitesi Matbaası, İstanbul, (1970).
4. Randal M. German, "Sintering theory and practice" The Pennsylvania State University Park, Pennsylvania, A Wiley – Interscience Publication, John Wiley & Sons, INC., USA, pp. 313-362, 373-400, 403-420, 1996.
5. Yıldız, K. and Alp, A., "Using of Microwave in Metallurgical Processes", Metalurji TMMOB, 24(125): 1300-4824, (1999).

CORRESPONDENCE ADDRESS: İrem Burcu Algan, Gazi University Faculty of Technology, Department of Metallurgy & Material Engineering, 06810, Teknikokullar-Ankara, +903122028799, irembalgan@gazi.edu.tr

SHORT BIOGRAPHIES

İrem Burcu ALGAN – İrem Burcu Algan was born in Ankara in 1989. She was graduated from Karadeniz Technical University, Faculty of Engineering, Department of Metallurgical and Materials Engineering in 2012 then completed her master's degree in Gazi University Graduate School of Natural Applied Science Metallurgy and Material Engineering Department in 2015. She works as a research assistant in Gazi University Technology Faculty since February, 2013 in addition continue her doctorate in Gazi University since September, 2015.

Yasemin AKSU – Yasemin AKSU was born in Ankara in 1989. She was graduated from Middle East Technical University (METU), Faculty of Engineering, Department of Metallurgical and Materials Engineering in 2012 then completed her master's degree in METU Graduate School of Natural Applied Science Metallurgy, Department of Metallurgical and Materials Engineering in 2015. She works as a research assistant in Gazi University Technology Faculty

since February, 2013 in addition continue her doctorate in Gazi University Graduate School of Natural Applied Sciene,Department of Metallurgical and Materials Engineering since September, 2016.

Yusuf Çiftçi –Yusuf Çiftçi was born in Ankara in 1992. He was graduated from Gazi University, Faculty of Technology, Department of Metallurgical and Materials Engineering in 2018.

NurcanÜnlü–NurcanÜnlüwas born in Konya in 1992.She was graduated from Gazi University, Faculty of Technology, Department of Metallurgical and Materials Engineering in 2018.

AUTOMATED ULTRASONIC TESTING FOR SPIRALLY SAW WELDED PIPES

Hakan ATEŞ^{1,a}, Galip BÜYÜKYILDIRIM^{2,b}

¹Prof. Dr.: Metallurgical and Materials Engineering / Faculty of Technology / Gazi University

²Dr., Technical Manager: Ege Sonik-SQS

^a hates@gazi.edu.tr, ^b galipbuyukyildirim@yahoo.com

Abstract

Spirally SAW welded pipes are used for many applications in huge projects. Like pipelines for natural gas transport and the weld quality of the production should be monitored precisely for fitness of purpose. Automated ultrasonic testing is widely used for SAW applications on pipe mills. It is the same method described in ISO 9712 standard as UT, but with an addition of automation in many key points (laser tracking, body lamination check etc.). The main standard for pipe testing is ISO 10893.

Key Words: Submerged Arc Welding, Weld Quality Control, Ultrasonic Testing, Production Monitoring

1. Introduction

In this paper, the application of “Ultrasonic Testing-UT” , one of the volumetric techniques on NDT will be discussed for pipe production, specially on HSAW (helical SAW) welded pipes. Other applications of UT are known for ERW, LSAW and seamless pipes, where the ultrasonic weld inspection is carried out in an automated manner. For being a process flow, the pipe production is consisting on many steps and QA/QC (quality assurance and quality control) is an important part of it, which uses radiography and ultrasonic testing as main parameters to check the weld quality. In pipe mills, both testing systems are part of the production line. As the goal they should not limit the capacity of the production on the mill. The UT systems could be on-line, off-line, body lamination or strip lamination type. A very robust mechanics for the automated or semi-automated inspection system is combined with sophisticated multi-channel ultrasonic electronics which allow trouble-free operation in an industrial environment with many electromagnetic and acoustical noise sources (motors, transformers, welding equipment).



Figure 1. Picture of an AUT testing system.

2 Coupling Techniques for Ultrasonics

Since air has poor conducting capabilities for sound and ultrasound, water is commonly used for the coupling, which is allowing the mechanical energy of sound to penetrate into the steel. There are different types of coupling, e.g. immersion, water gap, direct coupling and the most common use is water as a coupling agent. For larger pipe diameters the oval steel surface suggests a probe guidance on the pipe and special concepts for coupling. Two of the coupling methods are mostly encountered in industrial applications. One technique is water gap coupling. When the probe is mounted on a probe carrier and the distance of the probe active surface to the pipe surface is in the order of 0.5 mm. The probe shoe or carrier is guided along the pipe surface by rollers or by hard metal parts. For bigger curvatures of the pipe surface, like small pipe diameters, the shoes are machined curved and different sets of shoes have to be used for different diameter intervals and the gap shall be adjusted carefully within the probe carrier. There are some advantages on this technique: Dual-element probes can be applied offering small untested zones at the front and back surface of the pipe. Secondly, large face probes can be used in order to achieve a wider test area per probe. The test area is not limited in size, but 25 mm is an acceptable size for one probe crystal in length to ensure stable coupling conditions and to find the required defect size. Other dimensions could be 37,5 mm and 50 mm in length for 5 mm width of the crystals for normal probes, 8X9 mm rectangular or Ø10 mm circular shape for angular probes. The amount of water for gap coupling is rather small which reduces the capacity on the water circulation system requirements.

In case the production parameter changes or weld geometry (weld width, pipe wall thickness) requires different incidence angles or higher number of probes, probes with those incidence angles have to be mounted (resulting in increase of change-over times for the testing system and a large number of probes). After having the disadvantage of high probe and shoe wear (especially for rough or black pipe surface), resulted in the need of many curved shoes and the limited test speed (typical 0.5 m/sec) led to the introduction of water jet coupling (also called squirter technique) by KARL DEUTSCH in the 1970's. Water jet coupling offered a higher near-field resolution and longer lifetime of the probes. In this method water is guided as a jet flow through a plastic nozzle to the component surface. The diameter of the water jet has to be large enough to carry the entire ultrasonic beam energy and to be free of air bubbles and turbulences for a good signal-to-noise ratio. Straight-beam or normal immersion probes are used for this application. A long water column (30 – 50 mm) between probe and pipe surface guides the ultrasound. To produce a requested angle incidence, the entire probe holder is mechanically tilted to the component surface. This technique is basically with no wear. Only the rollers which guide

the probe carrier along the pipe surface have to be changed from time to time. Testing speeds up to 2 m/sec are possible.

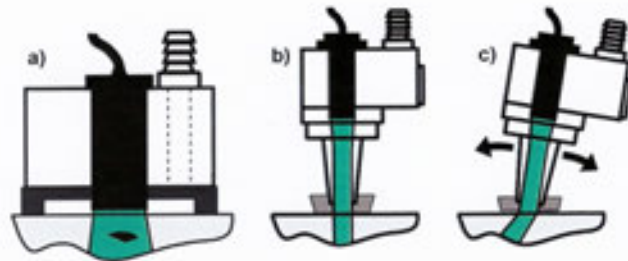


Fig. 2: Gap and Jet Coupling, a) gap coupling, used for lamination and strip testing with single or dual- element probes, b) wear-free jet coupling with straight-beam incidence, c) jet coupling with angular incidence for high-speed weld inspection and convenient angle adjustment.

3 Test Configurations for the Ultrasonic Inspection of Welded Pipes

For weld inspection in pipes, the cross-section to be tested is reduced to the weld itself and to the heat-affected zones on both sides of the weld. The welding process is automated, which makes an automated configuration of testing system possible. The common detection and measurement tasks are:

- Longitudinal volumetric defects (internal, external, mid-seam)
- Longitudinal laminar defects with perpendicular orientation with respect to pipe surface (tandem setup)
- Transverse defects (internal, external)
- Lamination testing of the Heat-affected Zone (HAZ)
- Wall thickness measurement (over the weld for ERW-pipes, in HAZ for SAW-pipes)
- Weld profile monitoring

Each test task requires the respective incidence angle resulting in a testing system with a multitude of electronic channels and probes. The use of probe pairs centered with respect to the weld allows for the detection of typical oblique defects within the weld and also for using the through-transmission signal for constant coupling check between the two probes. If the V-transmission signal is missing or weakened, either the coupling, the probe or the entire system is not working correctly. Thus, the transmission signal is constantly supervised and ensures the stable operation of the system. If the typical ultrasonic sound beam diameters can not cover the entire wall thickness, more than one probe pair has to be used.

3.1 Detection of Longitudinal Defects

Longitudinal defects require approximately one probe pair for every 7-10 mm of pipe wall thickness. Many testing systems make use of two probe pairs, using one probe pair for the internal pipe wall and the second pair for the external pipe wall. Many common international test specifications can be satisfied with this setup. The test defects are external and internal notches of longitudinal orientation. As an alternative, through-drilled holes in diameter of 1,5 mm or 3 mm centered to the weld seam are used.

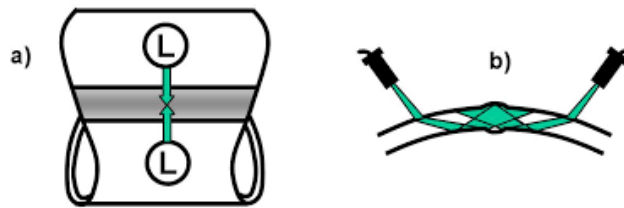


Fig. 3: Longitudinal Defect Detection. a) top view of probe pair with angular incidence with respect to the weld, b) cross-sectional view of probe pair and pipe, here shown for the detection of external defects.

Thick-walled pipes might require additional probes for the detection of longitudinal mid-seam defects. For SAW-pipes with walls up to 50 mm, up to five probes pairs are used. One or more tandem setups with four probes (two on each side of the weld) are then required. In case of SAW-pipes, the weld seam material is completely molten during the welding process therefore, an incomplete bond between the weld bevel surfaces hardly occur. The use of tandem testing systems is required in some testing specifications but its usage remains questionable.

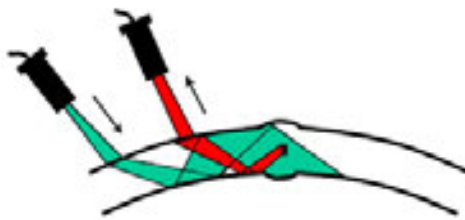


Fig. 4: Tandem Testing. Defects in mid-seam are detected with a two-probe setup, one probe acting as a transmitter and one probe as a receiver.

3.2 Detection of Transverse Defects

In case of SAW-pipes, only inclusions or pores within the weld might show transverse reflectivity. Since the weld bead of SAW-pipes is not machined, the coupling and guidance of the probes is more difficult and requires a sophisticated testing mechanism.

Conventional testing systems for SAW-pipes use the K or X-configuration where two/four probes are mounted next to the weld. Two probes work as transmitter – receiver arrangement and their V-reflection signal is used to detect transverse defects. This setup requires perfect positioning of two probes with respect to the weld and also a rather complicated mechanism for probe adjustment with respect to the pipe geometry (wall thickness, pipe diameter).

Therefore, modern testing systems for SAW-pipes make use of water jet coupling for an on-bead transverse flaw detection. Although the weld surface of SAW-pipes is not perfectly smooth, the desired ultrasonic coupling can be achieved with proper design of the probe holders. The incidence angle is typically 45 degrees and only the distance of the two probes might need adjustment for coupling check purposes (V-transmission).

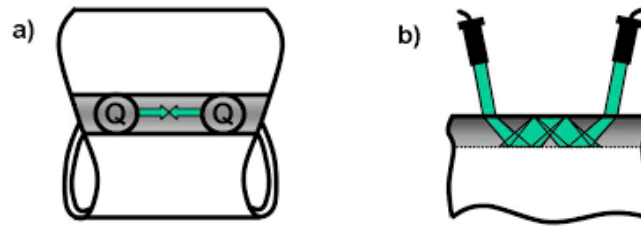


Fig. 5: On-Bead Transverse Defect Detection. a) Top view of on-bead probe pair with respect to weld, b) cross-sectional view of probe pair and pipe.

3.3 Detection of Laminations

Besides the weld itself, the heat-affected zone (HAZ) deserves special attention. In many cases, pre-inspected strips or plates are used for the pipe production. In that case, the inspection for laminations within the HAZ might be omitted. Most international specifications allow for either inspection of the strip edges before pipe forming OR the lamination inspection on the welded pipe. Dependent on the type of pipe and the used test specification, a test trace of 15 – 25 mm on both sides of the weld is inspected. For strong pipe curvatures, two probes should be used on both sides of the weld to ensure straight-beam incidence. Dual-element probes are used in order to ensure small dead zones on internal and external pipe surfaces. If high testing speeds are required, jet coupling with straight-beam probes is employed.

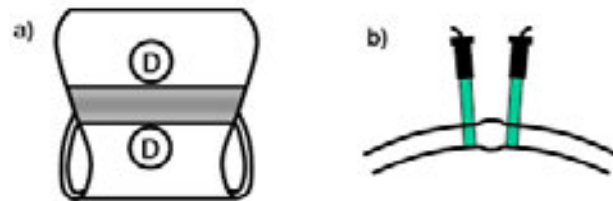


Fig. 6: Lamination Testing within heat-affected zone. a) Top view of probe pair position with respect to the weld, b) cross-sectional view of probe pair and pipe.

Spirally submerge-arc-welded pipes (SAW-pipes) use steel sheet coils as input material. The coils are usually not pre-inspected. Therefore a full-body inspection is often carried out after the welding process in an oscillating manner. A strip inspection before pipe forming is rarely used. The problem of strip testing directly before welding is the coupling water. The water has to be entirely removed before welding for not disturbing the welding process. Limited space typically designated to the uncoiling machine makes this a difficult task.

3.4 Pipe End Testing

The pipe ends deserve extra attention. If the pipes are used for pipelines for the transportation of fluids (water, oil or gas), they are circumferentially welded in the field. For SAW-pipes, the pipe end zone to be inspected for laminations is typically 25 – 50 mm thick. Also, the part of the weld which was not covered by the automated weld testing system (in the normal case the last 100 mm of the weld seam) should be further inspected – either manually with a portable flaw detector and angle-beam contact-probes or in an automated manner. For SAW-pipe ends, the ultrasonic test should cover at least 50 mm. Again, the untested portion of the weld should be

inspected with angle-beam probes for longitudinal defects. Many test specifications require an additional magnetic particle test of the end bevel and the weld close to the pipe end (typically 300 mm).

The ultrasonic pipe end test can be integrated into the ultrasonic weld testing system using separate probe carriers for that purpose. The probes are usually placed onto the external pipe wall in the 12 o'clock position while the pipe is rotating.

If separate pipe end systems are used, the pipe end can either be inspected from the internal or external pipe wall. Using the internal pipe wall allows for a probe movement closer to the pipe end (no bevel on internal pipe wall) and therefore producing narrower untested edge zones (<10 mm).

Dependent on the required throughput and the test specification, the same or a separate testing system is used for the pipe end and/or full-body inspection. If the same testing system is used for both test procedures, a testing portal with moveable carriage is common. The testing portal shows the advantage that the weld is inspected without pipe movement, thus avoiding vibrations which could degrade the test results. In a second step, the carriage is moved backwards while the pipe is rotating. Either the pipe ends are tested or the entire pipe body is tested in helical test traces. The typical throughput for such a combined testing system is 60 pipes/hour.

4 Ultrasonic Inspection of HSAW-Pipes

Helically welded pipes are typically produced with diameters of 350 to 2500 mm. They are used for water pipelines, but also for the transportation of other fluids (e.g. oil and gas). More or less extensive NDT is carried out in accordance to the later pipe usage. In comparison to LSAW pipes, spiral pipes are fairly easy to produce, because a range of pipe diameters can be achieved without changing the width of the input material -by changing the weld angle-. On the other hand, the control of the welding head and the weld test require careful position control and the output of a spiral pipe mill is rather limited. The pipe wall thickness is limited to about 25 mm.

The first ultrasonic weld inspection is carried out directly after welding. The probes are mounted to a stationary machine stand which is height-adjustable in accordance to the pipe diameter. The test position is in 12 o'clock. The motor for the seam tracking is mounted to the cantilever beam to center the probe pairs with respect to the weld. It longitudinal defects are always checked for with one or two probe pairs. Transverse defect detection (K- arrangement) and lamination detection are often incorporated into the process.

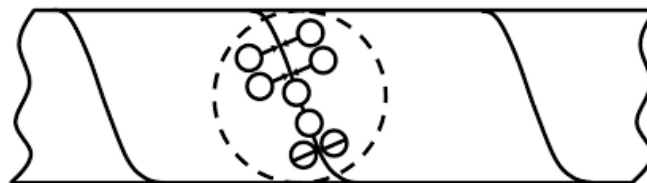


Fig. 7: Online-Ultrasonic Weld Test directly after welding with six probes (2 longitudinal, 2 transverse, 2 laminations).

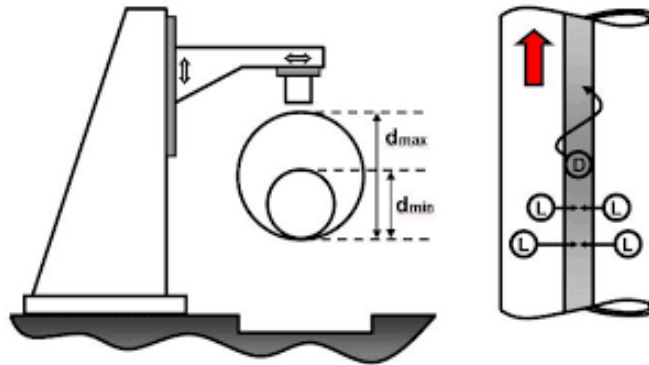


Fig. 8: Testing setup for spiral pipe inspection. a) Machine frame (stand), b) cantilever beam (boom) with vertical adjustment, c) probe carriers with horizontal position adjustment, d) spiral SAW-pipe, and e) foundation with water drainage (closed water circuit).

After pipe cutting, a second ultrasonic test is performed offline. The number of probes is equal or higher than the first inspection, **because this inspection is important for the final customer**. Since the testing mechanics have to be adjustable in accordance to the weld angle, space is rather limited, therefore for more than four probe pairs, a second weld testing mechanism and a second machine stand is needed. Longitudinal probe pairs, sometimes tandem probes, transverse and lamination probes are supplied. Since water is critical to the welding process, the strip inspection is often carried out after the hydrostatic test. To increase the coverage of each probe, oscillating probe movements are typically used. The weld and strip inspection requires a smooth helical pipe movement with respect to the probes, making the seam tracking a difficult and important task.

The pipe end inspection can be done in the same setup and requires one pipe rotation for each pipe end. The probe carriers are typically guided by rollers on the pipe end for shorter untested ends.

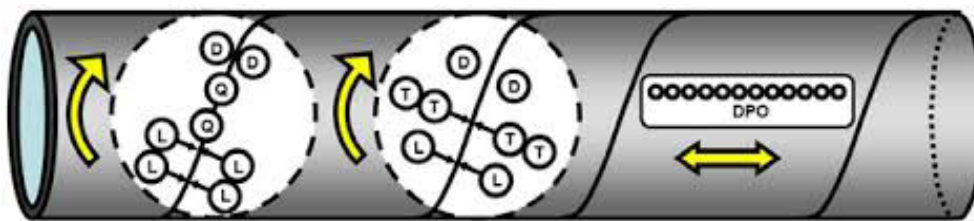


Fig. 9: Ultrasonic offline test after hydrostatic test with 32 probes. a) front pipe end testing, b) longitudinal defect detection – internal, external and mid-seam tandem, c) transverse defect (X-configuration) and lamination detection, d) oscillating strip inspection between the welds, and e) second pipe end testing.

5 Summary

This article contains a brief overview on automated ultrasonic inspection of welds of various pipe types. Some inspection steps might be carried out with portable test equipment (e.g. pipe end test), but the weld inspection in accordance with all internationally relevant standards must be automated. The pipe geometry, the production process, and the pipe usage determine the

number of required probes and setup. Recent updates for some test specifications enforce a large number of ultrasonic probes, e.g. the SHELL standard.

6 References

Proceeding :

- [1] W. A. K. Deutsch, P. Schulte, M. Joswig, R. Kattwinkel: Automated ultrasonic pipe weld inspection, 17th WCNDT, 25-28 October Shanghai-China (2008)
- [2] ISO 9712: Non-destructive testing -- Qualification and certification of NDT personnel
- [3] ISO 9756: Submerged arc-welded steel tubes for pressure purposes – Ultrasonic testing of the weld seam for the detection of longitudinal and/or transverse imperfections.
- [4] ISO 12094: Welded steel tubes for pressure purposes – Ultrasonic testing for the detection of laminar imperfections in strips/plates used in the manufacture of welded tubes.
- [5] ISO 3183-3: Petroleum and natural gas industries – Steel pipe for pipelines – technical delivery conditions, Part 3.
- [6] API Specification 5L: Specification for Line Pipe.

Book ;

- [7] V. Deutsch, M. Platte, M. Vogt: Ultraschallprüfung – Grundlagen und industrielle Anwendungen (Ultrasonic Testing – Principles and Industrial Applications), 372 pages, Springer Publishing House, 1997.
- [8] E. Ginzel: Automated Ultrasonic Testing of Pipeline Girth Welds - 2nd Edition, 322 pages, Eclipse Scientific Publishers, 2005

CORRESPONDENCE ADDRESS:

Prof. Dr. Hakan ATEŞ, Gazi Üniversitesi, Teknoloji Fakültesi, Metallurji ve Malzeme Mühendisliği Bl. 06500 Besevler Ankara TR, +90 (312) 2028782, hates@gazi.edu.tr

Dr. Galip BÜYÜKYILDIRIM, EGE Sonik Kuzguncuk Mh. Icadiye Cd. No:51 Uskudar Istanbul TR, +90 (532) 7486436, galipbuyukyildirim@yahoo.com

Prof. Dr. Hakan ATEŞ – born in 1971, in Haymana near Ankara. In 1988, he completed Haymana Industrial Vocational High School and started Department of Metallurgy Education, Faculty of Technical Education at Gazi University. He graduated from Department of Metallurgy Education in 1992. He served as a technical teacher for one year Gemerek Industrial Vocational High School in Sivas and his academic carrier as a research assistant started in 1993 at Gazi University, then received his MSc. Degree in 1996 and PhD degree in 2003 from IS&T at Gazi University, where he was acting as Faculty coordinator for Leonardo da Vinci Program. He has

currently a Prof. Dr. title in the Department of Metallurgy and Materials, Faculty of Technology at Gazi University.

Dr. Galip BÜYÜKYILDIRIM – born in 1961, after completion of High School of Istanbul, he graduated as an Electronics and Communication Engineer from Electronics and Electrical Engineering Faculty at Technical University of Istanbul, where he got his MSc. Degree for Nuclear Energy Engineering. He worked as an expert researcher for Materials and Chemical Technologies Research Institute at MAM-TUBITAK between 1998-2002. In 2002, his work area shifted to the private sector as a technical consultant for different foreign companies. In 2013, his PhD. Degree were given by the Mechanical Engineering Faculty at Belgrade University.

NOKTA DİRENÇ KAYNAKLI İLERİ YÜKSEK MUKAVEMETLİ ÇELİK SAÇLARIN TAGUCHİ METODU İLE DAYANIM OPTİMİZASYONU

Ramazan KAÇAR^{1,a}, Khaled Omer Marwan^{2,b}, Hayriye ERTEK EMRE^{3,c}

¹⁻³İmalat Mühendisliği Bölümü, Teknoloji Fakültesi, Karabük Üniversitesi, Karabük, Türkiye
^arkacar@karabuk.edu.tr, ^bk_gewa@yahoo.com, ^chayriyeertek@karabuk.edu.tr

Özet

Bu çalışmada, ileri yüksek mukavemetli çeliksınıfından farklı kalınlıktaki TRIP800-DP600 çelik çifti nokta direnç kaynağı ile farklı kaynak parametrelerinde birleştirilmiştir. Kaynaklı birleştirmelerin dayanımlarının Taguchi yöntemi ile optimizasyonu araştırılmıştır. Taguchi L₉ ortogonal dizini esas alınarak yapılan deney tasarımına göre belirlenen kaynak parametrelerinde birleştirilen numunelerin dayanım ve enerji absorpsiyon belirlenmesi için çekme makaslama testi gerçekleştirilmiştir. Deney sonuçlarının optimizasyonu "en yüksek en iyi" yaklaşımı esas alınarak gerçekleştirilmiştir. Deneysel yöntemle elde edilen verilerin ortalaması alınarak değerlendirmeler yapılmıştır. Analiz sonuçlarına göre farklı kalınlıktaki TRIP800-DP600 farklı cins çelik sac birleştirmesi dayanım ve enerji absorpsiyon optimizasyonunda en önemli kaynak parametresinin kaynak zamanı olduğu belirlenmiştir. Taguchi ile belirlenen en yüksek dayanımı veren kaynak parametresi ile deneysel çalışmayla elde edilen dayanımın örtüştüğü tespit edilmiştir.

Anahtar kelimeler: TRIP800 çeliği, Taguchi metodu, Çekme makaslama dayanımı, Kaynak akım şiddeti, Kaynak zamanı

STRENGTH OPTIMIZATION OF RESISTANCE SPOT WELDED ADVANCED HIGH STRENGTH STEELS BY TAGUCHI METHOD

Abstract

In this study, the dissimilar thickness TRIP800-DP600 steels couple which is members of advanced high strength steel (AHSS) steel group are joined with the resistance spot weld in various welding parameters. Optimization of the strength of the weldment has been investigated by the Taguchi method. Tensile shear tests were carried out to determine the strength and energy absorption of the weldment for selected welding parameters that was determined according to the experimental design based on the Taguchi L₉ orthogonal array. The optimization of the test results was carried out based on the "the better-is the best" approach. The evaluations were made by taking the average of the experimental data. According to the results of analysis, the welding time is most important welding parameters in the optimization of weldment strength and energy absorption for the TRIP800-DP600 sheet steels having unequal sheet thickness. The welding parameter giving the highest strength determined by Taguchi method coincides with the actual strength value that was evaluated by the experimental study.

Keywords: TRIP800 steel, Taguchi method, Tensile shear strength, Welding current, Welding time

1. Giriş

Otomotiv endüstrisinde yakıt tasarrufunu azaltmak için kullanılan yeni nesil çelikler ileri yüksek mukavemetli çelikler (AHSS) olarak adlandırılmaktadır [1-3]. Bu çeliklerin kullanımıyla araçlarda herhangi bir mukavemet kaybı olmaksızın, parça kesitinin inceltmesiyle ağırlık yönünden tasarruf sağlanmaktadır [4]. Yüksek mukavemetli yeni nesil çelik gruplarından otomotiv endüstrisinde kullanılan önemli bir bölümü çift fazlı (DP) ve TRIP çeliklerinden meydana gelmektedir. Bu çelikler emniyetin önemli olduğu otomotiv sektöründe, araç gövdesinde, kazalar neticesinde oluşabilecek hasarları en iyi şekilde karşılayabilme özelliğine sahiptirler [5-10].

Çift fazlı çelikler; yumuşak ferrit ve sert martenzit fazından oluşan düşük karbonlu çeliklerdir. TRIP çelikleri DP'lerden farklı olarak yapılarında kalıntı östenit fazı içerirler. Kalıntı östenit deformasyona bağlı olarak martenzit fazına dönüşerek gerinim birikmesini engeller ve sertlik artışına neden olur [11-16].

Nokta direnç kaynağı otomotiv endüstrisinde yaygın olarak kullanılan kaynak yöntemleri içerisinde ön sırada yer almaktadır. Literatür araştırmalarında, farklı kalitede DP ve TRIP çeliklerinin nokta direnç kaynağında akım şiddeti, kaynak zamanı, elektrot baskı kuvveti, tutma zamanı ve elektrot geometrisi gibi kaynak parametrelerin değişiminin kaynak kabiliyetine etkileri çalışılmıştır [17-20].

Son zamanlarda, nokta direnç kaynaklı birleştirmelerin mekanik özelliklerinin optimizasyonuna dayalı araştırmaların arttığı görülmektedir [21-26]. Optimizasyon, işleme çıktıları için optimal kaynak parametrelerinin bulunması ve performansın iyileştirilmesi için önemli bir adım olarak nitelendirilmektedir. Optimizasyon yöntemlerinden biri olan Taguchi metodu, düşük maliyetli gelişim döngüsüne sahip olup sistem ve süreç tasarımında ürün performansını iyileştirebilen bir problem çözme aracıdır [27]. Bu metod, toplam performans üzerindeki önemli iyileştirmeler için sonuçlar üzerindeki en etkili parametreleri belirleyen deneysel ve analitik kavramları birleştirir. Bunun için Taguchi metodu az sayıda deney ile bütün süreci kapsayacak bir çalışma için ortogonal dizilerin özel bir tasarımını kullanır [28].

Bu çalışmada, farklı kalınlıktaki TRIP800-DP600 çelik çiftinin nokta direnç kaynaklı birleştirmelerinin çekme makaslama dayanımı ve enerji absorpsiyonlarının optimizasyonu için farklı kaynak parametrelerinde (kaynak elektrod kuvveti, kaynak zamanı ve kaynak akım şiddeti) Taguchi analizi uygulanmıştır.

2. Malzeme Ve Yöntem

2.1. Malzeme

Çalışmada, sırasıyla 1,5 mm ve 1 mm olmak üzere farklı kalınlıktaki TRIP800-DP600 çeliği nokta direnç kaynağı ile birleştirilmiştir. Kullanılan çeliklerin kimyasal bileşim analiz

sonuçları Tablo 1’de verilmiştir. Farklı kalınlıkta nokta direnç kaynağı ile birleştirilecek olan TRIP800-DP600 numune çifti 100x30x1.5mm ve 100x30x1mm ölçülerinde kesilerek hazırlanmıştır. Çelik sac şeritler 30x30 mm kısmı üst üste gelecek şekilde tutucu kalıp kullanılarak birleştirme işlemi gerçekleştirilmiştir.

Tablo 1. Deneysel çalışmada kullanılan çeliklerin kimyasal kompozisyonu (% ağırlık)

	C	Si	Mn	Cr	Mo	Al	Fe
DP600	0,13	0,35	1,426	0,637	0,013	0,053	Rest
TRIP800	0,2	1,66	1,69	0,006	0,011	0,43	Rest

2.2.Nokta direnç kaynağı

Birleştirme işlemi 60kVA gücünde, BAYKAL SP60 marka elektronik akım ve zaman kontrollü, pnömatik basma donanımlı AC nokta direnç kaynak makinesinde gerçekleştirilmiştir. Taguchi analizi için kullanılan kaynak parametrelerinden kaynak akım şiddeti, kaynak zamanı ve elektrot kuvveti parametreleri, ön deneysel çalışmalar sonucundan optimum değerler arasından seçilerek belirlenmiştir. Kaynak parametreleri Tablo 2’de verilmiştir. Tutma zamanı ve elektrot baskı kuvveti tüm birleştirmeler için 15 çevrim (1 çevrim 0,02sn) ve 6 kN olarak seçilmiştir. Deneysel küresel başlı F16 tip elektrot (Cu-Cr-Zr) kullanılmıştır.

2.3.Çekme Makaslama Testi

Birleştirmelerin dayanım ve enerji absorpsiyonuna kaynak parametrelerinin etkilerinin optimizasyonu için seçilen her bir deney parametresi için deneysel değerlendirme yapabilmek için daha önceki çalışmalar için birleştirilmiş 5 adet çekme makaslama test numunesine, çalışmanın güvenilirliğini arttırmak amacıyla ilave olarak 3 çift çekme makaslama test numunesi daha eklenmiştir. Toplamda çalışmada her bir deney parametresi için 8 adet çekme makaslama testi gerçekleştirilerek, cihazın mevcut programı kullanılarak ortalama çekme-makaslama dayanımları ve enerji absorpsiyonları hesaplanmıştır. Kaynaklı malzeme çiftleri, SHIMADZU marka çekme test cihazında 5 mm/dak çekme hızında koparıncaya kadar çekme makaslama deneyine tabi tutulmuştur.

2.4.Deneysel Tasarım

Bu çalışmada, Taguchi yöntemiyle en uygun parametreler seçilerek en uygun çekme makaslama dayanımı ve enerji absorpsiyonunun belirlenmesi amaçlanmıştır. Belirlenen kaynak parametreleri (faktörler) ve bunların seviyeleri Tablo 2’de verilmiştir.

Tablo 2. Farklı kalınlıktaki çelik çifti için deney parametreleri ve her bir seviyedeki değerleri

Metal sac kalınlıkları	Sembol	NDK parametreleri	Birim	Seviye	Seviye	Seviye
				1	2	3
1mm-1.5 mm	A	Elektrod kuvveti	kN	4	5	6
	B	Kaynak akımı	kA	5	7	9
	C	Kaynak zamanı	çevrim	15	20	25
1 çevrim=0.02 sn						

Tablo 2'deki kaynak parametreleri dikkate alınarak, çalışma için en uygun tasarım olarak 9 deneyli Taguchi L₉ dizini seçilmiştir. Taguchi yöntemiyle yapılan optimizasyon işlemleri için Minitab 15 yazılımı kullanılmıştır.

2.5. Taguchi Metodu ile Analiz

Bu çalışmanın amacı, nokta direnç kaynaklı bağlantılarda en yüksek çekme makaslama dayanımı ve enerji absorpsiyonunu elde etmektir. Bu nedenle, çalışmada “en büyük en iyi” yaklaşımı kullanılmış olup, S/N oranlarının hesaplanmasında Eş.1'den yararlanılmıştır [12]. Burada, y_i her deney sonucunda elde edilen veriyi, n ise deney sayısını göstermektedir. L₉ dizine göre ölçülen çekme makaslama dayanımı (kN) ve enerji absorpsiyon (J) değerleri ve Sinyal/Gürültü (Signal/Noise) S/N oranına dönüştürülmekte ve decibel (dB) olarak ifade edilerek Tablo 3'te verilmiştir.

$$S/N = -10 \log \left(\frac{1}{n} \sum_{i=1}^n \frac{1}{y_i^2} \right), i=1,2 \dots k \quad (1)$$

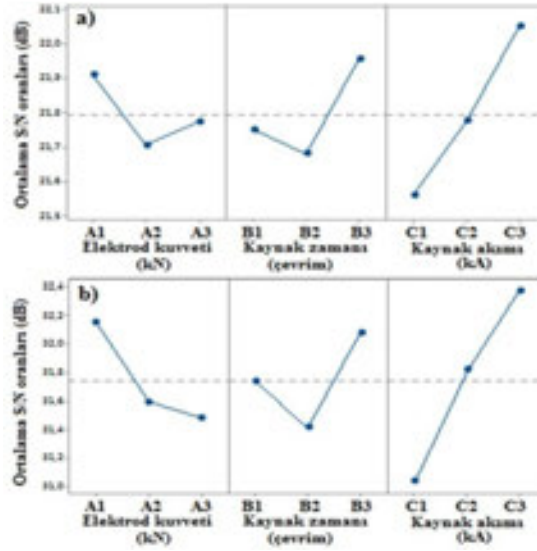
Tablo 3. Taguchi L₉ deney tasarımı

Deney no.	Kaynak parametreleri			Çekme makaslama dayanımı (kN)	S/N oranı (dB)	Enerji Absorpsiyonu (J)	S/N oranı (dB)
	Elektrot kuvveti (kN)	Akım şiddeti	Kaynak zamanı				
1	4	5	15	12,0	21,5836	37	31,3640
2	4	7	20	12,2	21,7272	40	32,0412
3	4	9	25	13,2	22,4115	45	33,0643
4	5	5	20	12,2	21,7272	38	31,5957
5	5	7	25	12,3	21,7981	39	31,8213
6	5	9	15	12,0	21,5836	37	31,3640
7	6	5	25	12,5	21,9382	41	32,2557
8	6	7	15	11,9	21,5109	33	30,3703
9	6	9	20	12,4	21,8684	39	31,8213

3. Deney Sonuçları ve Optimizasyon

3.1. Deney Sonuçlarının Analizi

Her bir kaynak parametresi için çekme makaslama dayanımı ve enerji absorpsiyonuna ait S/N oranları ortalama grafikleri sırasıyla Şekil 1a ve b'de gösterilmiştir. Taguchi optimizasyon yöntemine göre, maksimum S/N oranı performans karakteristiği için en iyi faktör seviyesini göstermektedir [11,12]. Ayrıca, Tablo 4'te her bir parametre için S/N oranları ortalaması, toplam ortalama S/N oranı, maksimum ve minimum değerleri arasındaki fark değerleri (Delta) görülmektedir.



Şekil 1. a) Çekme makaslama dayanımı, b) Enerji absorpsiyon değerleri için, kaynak parametrelerinin S/N oranları

Tablo 4. Ortalama S/N oranları tablosu

Testler	Sembol	NDK parametreleri	Birim	S/N oranı			Toplam Ort.S/N (dB)	Delta
				Seviye 1	Seviye 2	Seviye 3		
Çekme Makaslama Dayanımı(kN)	A	Elektrod kuvveti	kN	21,91*	21,70	21,77	21,79	0,20
	B	Kaynak akımı	kA	21,75	21,68	21,95*		
	C	Kaynak zamanı	çevrim	21,56	21,77	22,05*		
Enerji Absorpsiyonu (J)	A	Elektrod kuvveti	kN	32,16*	31,59	31,48	31,63	0,67
	B	Kaynak akımı	kA	31,74	31,41	31,82*		
	C	Kaynak zamanı	çevrim	31,03	31,82	32,38*		

Not: *Optimum seviye

Çekme makaslama dayanımları ve enerji absorpsiyonları için Şekil 1a ve b'deki grafikler ve Tablo 4'te verilen S/N oranlarının optimum seviyeleri incelendiğinde en yüksek değerlere, elektrotbaskı kuvveti için seviye 1, kaynak akımı için seviye 3 ve kaynak zamanı için seviye 3 de ulaşıldığı görülmektedir. Optimal çekme makaslama dayanımı ve enerji absorpsiyon değerine ulaşmak için kullanılacak kaynak parametreleri A1B3C3 şeklinde belirlenmiştir.

3.2. Varyans Analizi (ANOVA)

Çekme makaslama dayanımı ve enerji absorpsiyonları için ANOVA analizi sonuçları Tablo 5 ve Tablo 6'da verilmiştir. Burada, her bir değişkenin sonuçlar üzerindeki serbestlik derecesini gösteren SD değerleriyle, kareler toplamı (KT), kareler ortalaması (KO), F değerleri ve yüzde katkı oranları görülmektedir.

Tablo 5. Çekme makaslama dayanımı S/N oranları için varyans analizi

Sembol	NDK parametreleri	SD	KT	KO	F	Katkı Yüzdesi
A	Elektrod kuvveti	2	0,14000	0,07000	1,75	11,47
B	Kaynak akımı	2	0,26000	0,13000	3,25	21,32
C	Kaynak zamanı	2	0,74000	0,37000	9,25	60,65
	Hata	2	0,08000	0,04000		6,56
	Toplam	8	1,22000			

Tablo 6. Enerji absorpsiyonu S/N oranları için varyans analizi

Sembol	NDK parametreleri	SD	KT	KO	F	Katkı Yüzdesi
A	Elektrod kuvveti	2	16,222	8,1111	10,43	18,96
B	Kaynak akımı	2	13,556	6,7778	8,71	15,84
C	Kaynak zamanı	2	54,222	27,1111	34,86	63,40
	Hata	2	1,556	0,7778		1,80
	Toplam	8	85,556			

Tablolar incelendiğinde çekme makaslama dayanımı için en etkili kaynak parametresinin %60,65 ile kaynak zamanı iken, bir sonraki etkili parametrenin ise %21,32 ile kaynak akımı olduğu görülmektedir. Birleştirmelerin çekme makaslama dayanımı üzerinde elektrot baskı kuvveti etkisinin %11,47 olarak daha az olduğu tespit edilmiştir.

Deney numunelerinin enerji sönmleme kapasitelerine bakıldığında, en yüksek etkinin kaynak parametrelerinden %63,40 ile kaynak zamanı, ardından %18,96 ile elektrot baskı kuvveti ve daha sonra %15,84 ile kaynak akımı olduğu belirlenmiştir. Buna göre farklı kalınlıktaki çelik çifti nokta kaynak birleştirmesinin çekme makaslama dayanımı ve enerji absorpsiyon değerleri için belirlenen kaynak parametrelerinin en etkili olanı kaynak zamanı iken, diğer faktörlerin etki oranları değişim göstermiştir. Çekme makaslama dayanımını etkileyen en etkili ikinci parametre kaynak zamanı iken, enerji absorpsiyon değerleri için en etkili ikinci parametre elektrot baskı kuvveti olduğu görülmektedir.

3.3. Doğrulama Deneyleri

Taguchi yöntemine göre, optimal sonuçları verecek parametrelerin tahmininden sonra, optimizasyonda son aşama olarak doğrulama deneyleri yapılarak optimizasyonun doğruluğu test edilmektedir. Ancak, tahmin edilen seviyeler; optimizasyon öncesi yapılan deneysel çalışmaların arasından biri olduğu taktirde doğrulama deneylerine gereksinim olmaksızın,

optimizasyonun performansı test edilebilmektedir [29]. Bu çalışmada, çekme makaslama dayanımı ve enerji absorpsiyonu için tahmin edilen optimal seviyeler yapılan deneyler içerisinde mevcuttur.

Tablo 7’de tahmini ve deneysel sonuçların karşılaştırılması verilmiştir. Çekme makaslama dayanımı ve enerji absorpsiyonunun tahmini için yapılan analiz sonuçları ile doğrulama deneyleri sonuçlarının S/N oranları ve farklar dikkate alınır, fark oranının oldukça az (<0,2) olduğu görülmektedir. Taguchi optimizasyonunun kaynak çıktılarının performans karakteristiklerinin belirlenmesinde uygulanan basit ve güvenilir bir yöntem olduğu bir kez daha kanıtlanmıştır.

Tablo 7. Doğrulama deney sonuçları

	Optimum parametreler Farklar		
	Tahmin edilen	Deneysel	
Seviye	A1B3C3	A1B3C3	
Çekme makaslama dayanımı(kN)	13,0667	13,2	0,1333
S/N oranı (dB)	22,3226	22,4115	0,0889
Seviye	A1B3C3	A1B3C3	
Enerji absorpsiyonu (J)	45,1111	45	0,1111
S/N oranı (dB)	33,1317	33,0643	0,06749

4. Genel Sonuçlar

Bu analiz çalışmasında elde edilen bulgular aşağıdaki şekilde özetlenebilir:

- Deneysel çalışmalarda, daha az deney ile daha verimli sonuçlara ulaşılması için uygulanan Taguchi L9 deney tasarımı ve optimizasyonu farklı kalınlıktaki TRIP800-DP600 çelik nokta direnç kaynaklı birleştirme işlemi için başarılı bir şekilde uygulanmıştır.
- Taguchi optimizasyonu sonucunda, farklı kalınlıktaki TRIP800-DP600 farklı cins çelik birleştirmelerinin çekme makaslama dayanımının optimizasyonunda, en etkili kaynak parametresinin %60,65 ile kaynak zamanı olduğu, bir sonraki etkili parametrenin ise %21,32 ile kaynak akımı olduğu bulunmuştur. Kaynak parametrelerinden elektrot baskı kuvveti etkisinin %11,47 olarak diğer ikisine göre daha az etkili olduğu tespit edilmiştir.
- Birleştirmelerin enerji absorpsiyon kapasitelerinin optimizasyonunda ise kaynak parametrelerinden sırasıyla %63,40 ile kaynak zamanı, %18,96 ile elektrot baskı kuvveti ve %15,84 ile kaynak akımının etkili olduğu belirlenmiştir.
- Çekme makaslama dayanımı ve enerji absorpsiyonlarının S/N oranları ortalamaları grafikleri incelendiğinde optimum seviyelerinin her ikisi içinde aynı olup A1B3C3 olarak belirlenmiştir.

- Elde edilen optimizasyon verileriyle deneysel çalışma verilerinin örtüştüğü görülmektedir.

5. Teşekkürler

Bu çalışma Karabük Üniversitesi Bilimsel Araştırma Projeleri Koordinasyon Birimi tarafından desteklenmiştir. Proje numarası: KBÜ-BAP-17-DR-200. Adı geçen birime teşekkür edilir.

6. Kaynaklar

- [1] F. Öztürk, S. Toros, E. Esener, E. Uysal: Otomotiv Endüstrisinde Yüksek Mukavemetli Çeliklerin Kullanımının İncelenmesi, Mühendis ve Makina, 50 (586) (2009) pp. 44-45.
- [2] Word Auto steel, Advanced High Strength Steel (AHSS) Application Guide Lines, 4th ed., <http://www.wordautosteel.org>, (2009).
- [3] S. Brawser, L.A.Pepke, G.Weber, M.Rethmeier: Deformation Behavior Of Spot Welded High Strength Steels for Automotive Applications, MaterSci Eng. A, 527 (2010) pp.7099-7108.
- [4] D.W.Zhao, Y.X.Wang, S.Shang, Z.Lin: Multi-Objective Optimal Design of Small Scale Resistance Spot Welding Process with Principal Component Analysis And Response Surface Methodology, J. Intell Manuf. 26 (2013) pp.1-14.
- [5] G.Song, T.Vystavel, N.Vander Pers, J.T.M.de Hassan, W.Sloof:Relation Between Microstructure and Adhesion of Hot Dip Galvanized Zinc Coatings on Dual-Phase Steel, Acta Mater, 60 (2012) pp. 2973-2981.
- [6] R. Lagneborg: New Steels and Steel Applications for Vehicles, Materials and Design, 12 (1991) pp. 3-14.
- [7] H.Hayashi, T.Nokagawa: Recent Trends in Sheet Metals and Their Formability In Manufacturing Automotive Panels, J. Materials Processing Technology, (1994) pp. 455-487.
- [8] K.Mari, S. Maki, Y. Tanoka:Warm and Hot Stamping of Ultra High Tensile Strength Steel Sheets Using Resistance Heating CIRP Analyst, Manufacturing Technology, 54 (2005) pp. 209-212.
- [9] International Iron and Steel Institute, Project Reports on UltraLight Steel Auto Body, (2006).
- [10] C.W.Zhang, D.Raabge: Interaction Between Recrystallization and Phase Transformation During Intercritical Annealing Cold-Rolled Dual-Phase Steel: A Cellular Automation Model, Acta Mater, 60 (2012) pp. 5504-5517.
- [11] Z.Yinghui, M.Yonli, K.Yonglin, Y. Hao: Mechanical Properties And Microstructure of TRIP Steels Produced Using TSCR Process, Journal of University of Science and Technology, Beijing, 13 (5) (2006)pp. 416-421.
- [12] D. Wu, L. Zhuang, L. Hui-sheng:Effect of Controlled Cooling After Hot Rolling On Mechanical Properties of Hot Rolled TRIP Steel, Journal of Iron and Steel Research International, 15 (2) (2008) pp.65-70.
- [13] S. Koh-Ichi, M. Toshiki, H. Shun-Ichi, M. Yoichi:Formability of NbBearing Ultra High Strength TRIP-Aided Sheet Steels, Journal of Materials Processing Technology, 177 (1) (2006)pp.390–395.
- [14] L.Skoalova, R. Divišová, D.Jandová: Thermo-Mechanical Processing of Low-Alloy TRIP Steel, Journal of Materials Processing Technology, 175 (1)(2006) pp.387–392.

- [15] S.Wen, L.Lin, B.C.D.Cooman, P.Wollants, C.Yang: Thermal Stability of Retained Austenite in TRIP Steel After Different Treatments, *Journal of Iron and Steel Research, International*, 15 (1)(2008) pp. 61-64.
- [16] L.Zhuang, W.Di, H.Rong: Austempering of Hot Rolled Si-Mn TRIP Steels, *Journal of Iron and Steel Research International*, 13(5) (2006) pp. 41-46.
- [17] M.I. Khan, M.L. Kuntz, Y. Zhou: Effects of Weld Microstructure on Static and Impact Performance of Resistance Spot Welded Joints in Advanced High Strength Steels, *Sci Technol. Weld Join.* 13 (2008) pp. 294-304.
- [18] X. Sun, E.V. Stephens, M.A. Khaleel: Effects of Fusion Zone Size and Failure Mode on Peak Load and Energy Absorption of Advanced High Strength Steel Spot Welds Under Lap Shear Loading Conditions, *Eng. Fail Anal.* 15 (2008) pp.356-67.
- [19] J.D. Radakovic, M.D. Tumuluru: Proceeding of the International Sheet Metal Welding Conference XIII, (2008).
- [20] O. Kwon, S.C.Baik: Manufacture and application of advanced high strength steel sheets for auto parts manufacture, Pohang: POSCO (2005) pp. 785-90.
- [21] M.Pouranvari, S.P.H.Marashi, D.S. Safanama: Failure Mode Transition in AHSS Resistance Spot Welds. Part II: Experimental investigation and model validation, *Materials Science and Engineering: A*, 528 (29-30) (2011) pp. 8344-8352.
- [22] G. Thakur, T.E. Rao, M.S. Mukhedkar, V.M. Nandedkar: Application of Taguchi Method for Resistance Spot Welding of Galvanized Steel, *ARNP Journal of Engineering and Applied Sciences* 5(1) (2010) pp. 22-26.
- [23] H.L. Lin, T. Chou, C.P. Chou: Optimization of Resistance Spot Welding Process Using Taguchi Method and A Neural Network Experimental Techniques, *Society for Experimental Mechanics*, (2007) pp. 30-36.
- [24] S. Chaudhary, V.K. Sharma, K. Rana: *International Journal of Enhanced Research in Science Technology & Engineering*, 3(10) (2014) pp.217-221.
- [25] N. Muhammad, Y.H.P Manurung, M.Hafidzi, S.K. Abas, Ghalib Tham, E.Haruman: Optimization and Modeling of Spot Welding Parameters with Simultaneous Multiple Response Consideration Using Multi-Objective Taguchi Method and RSM, *Journal of Mechanical Science and Technology* 26 (8) (2012) pp. 2365-2370.
- [26] A.G. Thakur, T.E. Rao, M.S. Mukhedkar, V.M.Nandedkar: Application of Taguchi Method For Resistance Spot Welding Of Galvanized Steel, *ARNP Journal of Engineering and Applied Sciences* 5(11) (2010) pp. 22-26.

CORRESPONDENCE ADDRESS: Ramazan KAÇAR, Karabük University, Technology Faculty, 78050, Turkey, Tel: +90 433 82 00/1091, e-mail: rkacar@karabuk.edu.tr

SHORT BIOGRAPHIES

Ramazan Kaçar¹ – Karabük Üniversitesi, Teknoloji Fakültesi, İmalat Mühendisliği Bölümünde Profesör Dr. Olarak görev yapmaktadır.

Khaled Omer Marwan² – Karabük Üniversitesi, Teknoloji Fakültesi, İmalat Mühendisliği Bölümünde doktora yapmaktadır.

Hayriye Ertek Emre³ – Karabük Üniversitesi, Teknoloji Fakültesi, İmalat Mühendisliği Bölümünde Dr. Öğretim Üyesi olarak görev yapmaktadır.

GAS METAL ARC WELDABILITY OF AA5083-A GRADE COUPLE BY USING TRANSITION PLATE

Alparslan Parlak^{1,a}, Ramazan Kaçar^{2,b}

^{1,2}Karabük University, Technology Faculty, Manufacturing Engineering, Karabük, Turkey
^{1a}alparslanparlak@hotmail.com, ^brkacar@karabuk.edu.tr

Abstract

Ships, boats and especially yachts are made of steel and aluminum alloys. However, they cannot be joined to aluminum alloys of steels by fused welding methods. For this reason, the transition plates are used to join the steels to the aluminum alloys. In this study, AA5083 aluminum alloy was joined by robotic GMAW method using the transition plate to A-grade steel material. Tensile, three-point bending test and hardness measurements were performed to determine the mechanical properties of the welded joint. Microstructure examination was also carried out. The relationship between the mechanical properties of the joint and the microstructure has been studied extensively. As a result, A-grade steel and AA5083 aluminum alloy can be successfully joined using the robotic gas metal arc welding method utilizing the aluminum-steel transition plate.

Keywords: AA5083 aluminum alloy, A-grade steel, Transition plate, Gas metal arc weldability

1. Introduction

According to the Turkish Trade Court, the ship is a marine vessel capable of swinging, maneuvering, and moving on the water by taking advantage of the lifting force of the water. The yacht is a sailboat or motorboat used for racing or private sightseeing [1]. The shipbuilding industry has a high export rate in the maritime transportation sector which is the most preferred means of transportation in international trade [2-5]. It has a very high added value and requires technological advances such as research in welding techniques and appropriate materials [6]. The yacht and boat industry is different from the shipbuilding industry in terms of content, scope and technology. Long time for large investments in the shipbuilding industry, large seaside locations are needed. However, yacht and boat manufacturing industry can operate in a short time and smaller places with smaller investment. Our country has shown a steady rise especially in the super yacht (24 m and above). In the delivery of super yacht, the number and length of yachts increased to the third place in the world. According to the data of January 2017, it is still in 3rd place with a total length of 3508 meters [7].

When referring to the technical specifications of the materials used in ship and yacht construction, it is necessary to understand the properties such as strength, brittleness, resistance to fatigue and resistance to burning, ability to meet tensile, compressive and shear stresses on ships or yachts and hardness [7]. Various materials are used in yacht and yacht manufacturing. These materials; wood, steel, aluminum, fiber reinforced plastics or composites etc. can be varied as. Undoubtedly, in the selection of materials, it can be decided on the most appropriate material yachts or yachts to be built, or yachts and navigation boats should be decided firstly for the purpose of using the yachts. In shipbuilding the main alternative materials to commonly used

steels are extra high strength steels, aluminum alloys, plastics and fiber reinforced composites [8].

In order for a steel material to be used in a ship, yacht or boat, it must first be inspected, stamped and stamped by a rating agency that will certify the maritime transport vehicle [9]. Class organizations have given the letters symbols ranging from A to E by subjecting the used steels to a specific grouping. It clearly indicates the conditions under which steel materials are to be used and what mechanical properties should be used.

Along with steels, aluminum alloys are used in the construction of small vessels such as research vessels, yachts, sailboats, and ferryboats[9]. Aluminum alloys, which are preferred because they are light in passenger ships and on the platforms, offer an advantage in large military vessels thanks to their low magnetic permeability[9]. The first aluminum alloys developed to resist the corrosive effect of seawater contained less than 2.5% - 6 Mg of Mn, Cr, Be and Ti. Nowadays 5xxx and 6xxx series aluminum alloys use this area because their tensile strengths are high, ductility and machinability are good [10].

It is not a matter of joining aluminum alloys to steel materials by utilizing the fusion welding methods. Nowadays, when an aluminum material is joined to a steel material by a fusion welding method, an intermediate material called transition or transition plate is used[11]. In other words, the upper half of this intermediate is from aluminum and the lower half is from steel. The steel part of this transition piece is welded to the steel structure and the aluminum part is welded to the aluminum structure. Thus, the assembly of the aluminum structure to the steel structure is completed.

There are different welding methods that are used in the manufacturing process in shipbuilding. The arc welding with shielded electrode is the first welding method used in this field because it has simple welding equipment. Over time, due to the disadvantages of this welding method, a semi-automatic method of using an undergas arc welding has begun. In recent years, the rapid development of microelectronic technologies, the discovery of laser sensors, the application of numerically controlled computer identification systems and the development of mechanization systems have enabled robots to weld[12]. Today, parallel to the development of technology, robot technology, laser welding and various hybrid welding methods have been successfully used in ship manufacturing sector. Advantageous aspects of these welding methods have begun to be evaluated in the joining of similar or dissimilar materials[13].

Some considerations need to be taken in order to increase the quality of marine craft such as ships, yachts and boats and to provide the required service characteristics. These include: the determination of the structure and mechanical properties of shipbuilding steels, the selection of the appropriate welding method and welding consumable, the causes of distortion due to thermal expansion and shrinkage during welding, and the choice of welding remedies, welding plans and welding parameters[14].

For this purpose; A grade steel-AA5083 aluminum alloy with transition plate "triclاد" was used to investigate the possibility of joining by a robotic gas metal arc welding (GMAW) method. The tensile, three-point bending test and hardness measurements were performed taking into consideration the loads to which the welded joints would be subjected under service conditions. Microstructure examination was also carried out.

2. Experimental Method and Material

The chemical composition of commercially available A-grade steel in sizes of 10 x 100 x 325 mm³ and 10 x 100 x 325 mm³ commercially available AA5083 aluminum alloy materials used in the study was analyzed and the results are given in Table 1.

Table 1. Chemical composition (weight%) of A-Grade steel, AA5083 aluminum alloy, aluminum and steel side of the transfer piece.

A-Grade Steel	C	Si	Mn	P	S	Cr	Ni	Mo	Cu	Ti
	0.143	0.176	1.02	0.019	0.003	0.026	0.017	0.019	0.011	0.016
	Al	V	Co	W	Nb	Fe				
	0.047	0.002	0.002	0.043	0.034	Rest				
AA5083 Aluminum alloy	Mg	Al	Si	S	Cr	Mn	Fe	Ni	Cu	Zn
	2.486	96.48	0.27	0.004	0.013	0.350	0.283	0.007	0.033	0.046
	As	Zr	Ga							
	0.002	0.001	0.008							
Transition plate (steel)	C	Mn	Si	Cr	Ni	Cu	Mo	Fe		
	0.061	0.299	0.028	0.028	0.001	0.070	0.001	Rest		
Transition plate (AA1050)	Mn	Si	Mg	Zn	Cu	Ti	Fe	Al		
	0.01	0.163	0.036	0.024	0.146	0.027	0.516	Rest		
Transition plate (AA5086)	Mn	Si	Mg	Zn	Cu	Ti	Fe	Cr	Al	
	0.421	0.210	4.33	0.146	0.034	0.011	0.271	0.144	94.41	

In addition, the aluminum-steel transition plate was utilized to join the AA5083 alloy plate used in the study with the A-grade steel plate by the robotic GMAW method. The steel side of the explosive welded aluminum-steel transition plate is commercially obtained in dimensions of 12 x 25 x 700 mm³ and the aluminum side is 13 x 25 x 700 mm³. The aluminum side of the transition plate is made up of two types of aluminum plates. The intermediate of the transition plate consists of AA1050 aluminum with a thickness of 8 mm and the other part consists of AA5086 aluminum with a thickness of 5 mm. The thickness of the transition plate is equal to the thickness of AA5083 aluminum alloy as well as A grade steel. For this reason, the transition plate was cut with water jet and then machined from both surface of the plate to 6 x 24 x 325 mm³ dimensions. The chemical composition analysis of the transition plate was also carried out by aluminum and steel side. The results are shown in Table 1. Similarly, the AA5083 aluminum and A-grade steel plates used in this work are milled on the surface to have a thickness of 6 mm.

A macro-image of the A-grade steel, AA5083 aluminum alloy sheet and aluminum-steel transition plate to be used in the experimental work is shown in Fig. 1 a.

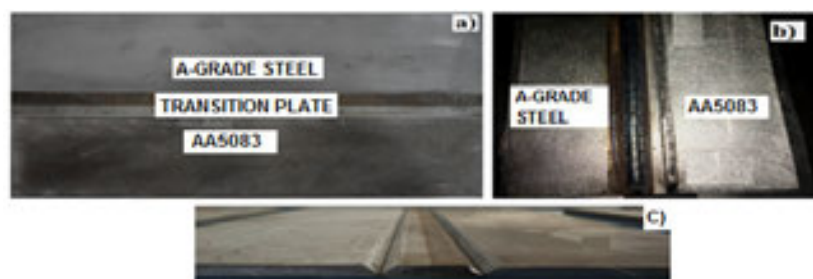


Figure 1. Macro view of a) A-grade steel, AA5083 aluminum alloy and aluminum-steel transition plate used in the study b) Weld groove prepared before welding and c) Grade-AA5083 couple joint by utilizing the transition plate by robotic GMAW method.

2.1. Preparation of Test Samples Prior to Welding

It is aimed to combine the A-grade steel and AA5083 aluminum alloy used in the work with the robotic GMAW method. For this reason, the welding groove (60° V shape) is machined on both sides of the aluminum-steel transition plate by using milling machine. On one surface of the A-grade steel and the AA5083 aluminum plates, a weld groove (60° V shape) was also opened (Figure 1b). The aluminum sheets to be joined are placed on the aluminum side of the transition plate and the steel plates are placed on the steel side of the transition plate and then ready to be joined by the robotic gas metal arc welding machine. FD-B4 Type GEKA ROBOT welding robot and WELBEE Inverter P400 gas metal arc welding machine are shown in Figure 2.

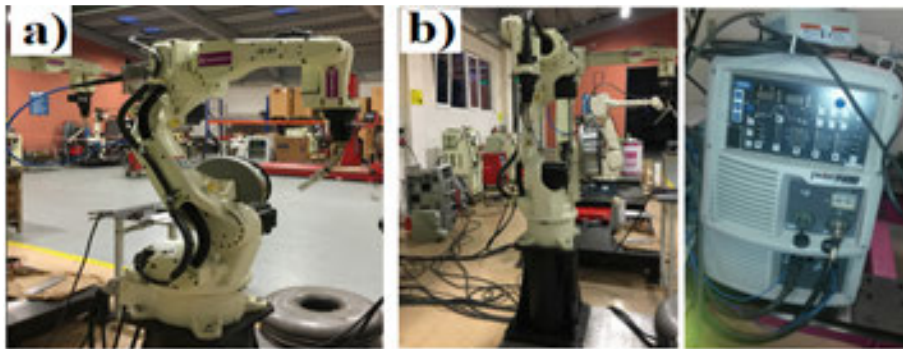


Figure 2. a) The welding robot and b) GMAW machine used in the study

R71 flux cored wire with a diameter of 1.2 mm is commercially available to join the steel side of the assemblies to the steel side of the transition plate. The chemical composition and properties of R71 flux-cored wire are given in Table 2. The AlSi5 additional wire of 1.2 mm in diameter was used to join the aluminum side of the assembly. The chemical composition and properties of the weld filler metal are also shown in Table 2.

Table 2. Properties of welding consumable used in the study

R 71 Flux core filler metal	Chemical composition (%)		C	Si	Mn	P	S	Fe
			0,06	0,05	1,3	0,015	0,015	Rest
	Mechanical properties	Heat treatment	Yield strength (N/mm ²)	Tensile strength (N/mm ²)	V Notch toughness		Elongation (Lo=5d0) (%)	
None heat treated		min. 420	500-600	- 40°C	-20°C	min. 22		
AlSi5 filler metal	Chemical composition (%)			Si	Mn	Fe	Al	
				5.0	<0,05	<0,8	Rest	
	Mechanical properties			Yield strength (N/mm ²)	Tensile strength (N/mm ²)	Elongation (Lo=5d0)(%)	Melting temperature (C°)	
			110	150	15	575-633		

The carbon dioxide and argon are used as protection gas on the steel side and the aluminum side of the assembly respectively.

2.2. Welding of Experimental Samples

The steel side of the assembly was joined at a current intensity of 194 A at a wire feed rate of 885 cm/min using R71 flux cored wire with a diameter of 1.2 mm under 23 V of voltage. The connection was welded with a gas metal arc welding machine with a direct current in the welding robot under a carbon dioxide shielding gas, with a flowing rate of 16 liters /min at a welding speed of 60 cm/min. The aluminum side of the connection was welded with a 14 liters/min argon gas flowing rate at the 300 cm/min feeding rate using an AlSi5 filler metal of 1.2 mm in diameter at a welding current of 100 A and a voltage of 17 V. The welding speed rate was 35 cm/min with a direct current was used for robotic gas metal arc welding machine. Grade A-AA5083 couples, which are assembled using the transition plate by the GMAW method, are shown in Figure 1c. After welding, milling is performed from the joining surfaces to reduce the thickness from 6 mm to 5 mm.

2.3. Preparation of Test Samples and Testing

The tensile test and the three-point bend test were utilized with a laser cutting machine when the test specimens were cut. Figure 3 a and b show the CAD drawing of the test specimens and macro image of test samples.

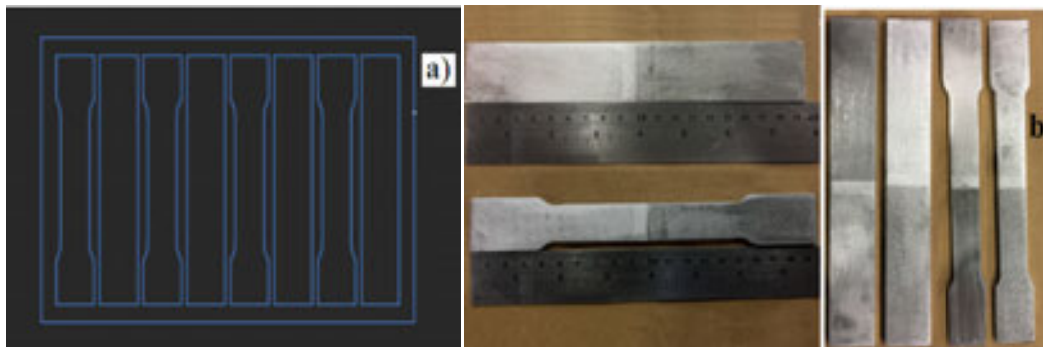


Figure 3. a) CAD drawing of the test specimens b) Macro image of test samples

In order to minimize experimental errors, a set of three tensile test specimens conforming to EN895 and three-point bending test specimens was prepared conforming to EN ISO 5173 standard. The test was carried out at a strain rate of 1 mm/min with a 50 kN SHIMAZDU tensile tester. The three-point bending test was carried out on with a 10-ton capacity ALSA brand universal hydraulic tensile testing machine. A holding mold was developed in order to apply a three point touch test in the direction of thickness in the work piece. Figures 4 a and b show the tensile, three-point bending test processes and developed holding mold.

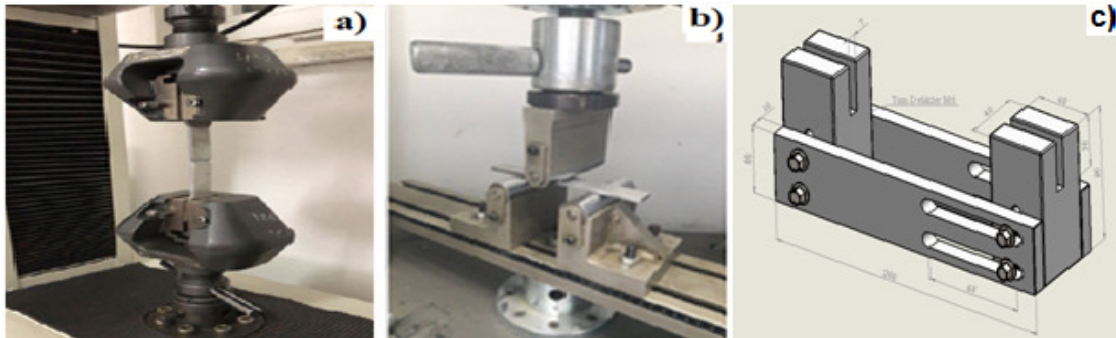


Figure 4. a) Tensile test, b) three-point bend test c) holding mold

The hardness measurement of the welded joint was carried out by using the FV-700 SHIMADZU brand Vickers microhardness tester including the weld metal, HAZ and base metal. A 500g load was applied to the indenter.

2.4. Preparation of Metallographic Sample and Etching

The metallographic specimens were cut at the upright position in the welding direction, including weld metal, HAZ and base metal areas. The specimens were polished with 6, 3 and 1 micron diamond paste, respectively, after grinding using 240, 320, 600, 800, 1000, 1200, 2500 mesh sandpaper sheets respectively. After polishing, the steel side of the joint is etched with a 2% nitric acid solution and the aluminum side is etched with a Keller etchant. Microstructure studies were carried out on an optical microscope with a magnification of 5x-100x.

3. Results and Discussion

3.1 Tensile test results

The mechanical properties of the welded joint have been determined. For this purpose, the behavior of the AA5083-A grade steel pair under the static load effect was investigated. The prepared test specimens were subjected to tensile test. The tensile test results are shown in Fig.5. The mean stress-strain curve is shown in red color.

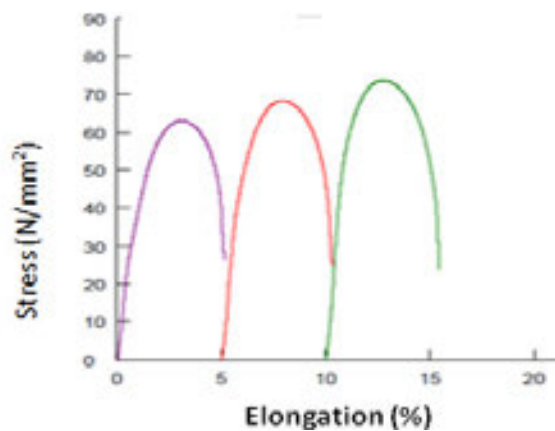


Figure 5. The stress-strain curves of tensile test samples

As can be seen from Fig. 5, the mean tensile strength of the test specimens is 68.39 MPa and the elongation % is 2.96. As a result of the test, the sample is interrupted by the aluminum side of the transition plate (Figure 6). This indicates that there is no problem in welded assemblies of the AA5083 aluminum plate to the aluminum side of the transition plate, on the steel side of the A-grade steel transition plate, as well as the explosion welding of the transition plate. The break in connection is presented on the AA1050 aluminum of the transition plate with the lowest yield strength of materials used in the assembly. This is an expected and desired situation.

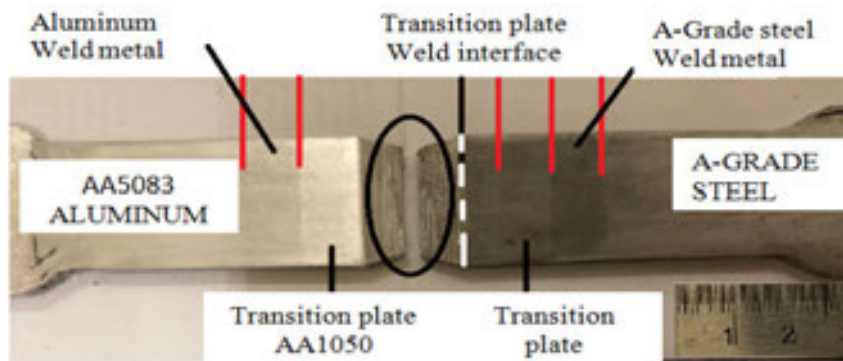


Figure 6. The fracture region of tensile test sample.

Also, the fracture surface of the tensile test specimens was investigated. For this purpose, fracture surface images were taken, and the results are shown in Fig. 7.

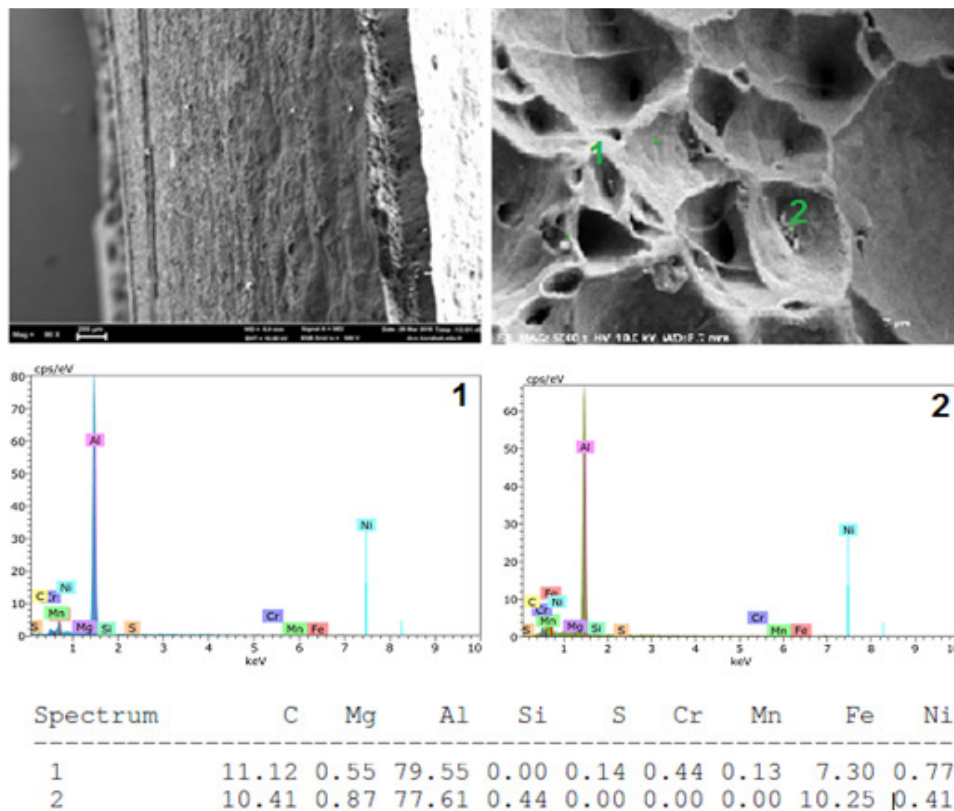


Figure 7. Fracture surface of tensile test specimen and EDS analysis from points numbered 1 and 2.

The reduction on the cross section in the macro image of Fig. 6 and the dimples in the surface in Fig. 7 also point to the failure of the test sample with the ductile fracture behavior.

It is evident that the strength of the welded joints is acceptable when the breakage is formed by AA1050 aluminum, starting from the zone with the lowest yield strength of the joint and starting with a ductile fracture behavior. As can be seen from the EDS analysis, Fe-containing formations on the AA1050 aluminum transition plate are thought to form the forefoot for the onset of fracture.

3.2 Three-point bending test results

The test specimens prepared to determine the ductility of AA5083-A-grade steel couples joined by robotic gas metal arc welding method using aluminum-steel transition plate were subjected to three-point bending test. The average stress elongation curve of the test result and tested samples are shown in Fig. 8.



Figure 8. Three-point bending load-displacement curve and tested samples

As can be seen from Fig. 8, the maximum bending strength of the test specimens is 325 N/mm². The test specimens cracked after being shaped to about 80° from the aluminum steel interface of the transition plate. This suggests that the formability is limited. There are no cracks in the transition plate A-grade steel and AA5083 aluminum alloy robotic gas metal arc welded joints.

In addition, the three-point bending specimen obtained from the assembly was subjected to three-point bending test in the direction of thickness with the developed holding mold. As shown in Fig. 8, the crack was formed at the AA1050-steel interface of the transition plate after being shaped at 80° in the tested test sample. As expected, more loads were needed to shape the sample in the thickness direction.

3.3. Hardness measurement results

The hardness distribution of the AA5083 aluminum-A grade steel couples joined with the robotic GMAW method using the transition plate was determined by microhardness measurement. The hardness profile of the welded assembly was made in the same line from the cross section of welded assembly A-grade steel and AA5083 aluminum base material, aluminum-steel transition plate, weld metals and HAZ. The measurement results are graphically shown in Fig. 9.

As can be seen from Fig. 9, the average hardness of A-grade steel was determined as 140HV_{0.5}. Because A-grade steel is a low carbon steel, its structure is generally consistent with pearlite and ferrite grains [15]. The hardness of AA5083 aluminum is measured as 90HV_{0.5}.

The average hardness of the AA1050 alloy of the transition plate was found to be 30HV_{0.5} and the steel side was 170HV_{0.5}. It is expected that the hardness in areas near the interface of the transition plate will increase due to the deformation associated with the impact of the detonation. The hardness with 30HV_{0.5} on the AA1050 side of the transition plate was measured to be 70HV_{0.5} on the AA5086 side.

The HAZ hardness of the A-grade steel-transition plate steel side is also measured. Hardness measurement results were found to range between 170-240 HV_{0.5}. Depending on the temperature reached in HAZ and the holding time at this temperature, rapid cooling after welding occurs due to the nature of the fusion welding. For this reason, it is expected that the hardness associated with structural transformation in HAZ will vary. Microstructure results also support this. All of the hardness values in welded assembly were not exceed critical hardness level which is the maximum acceptable hardness that vary depending on the material group according to the hardness test standards of TS EN ISO 9015 [16].

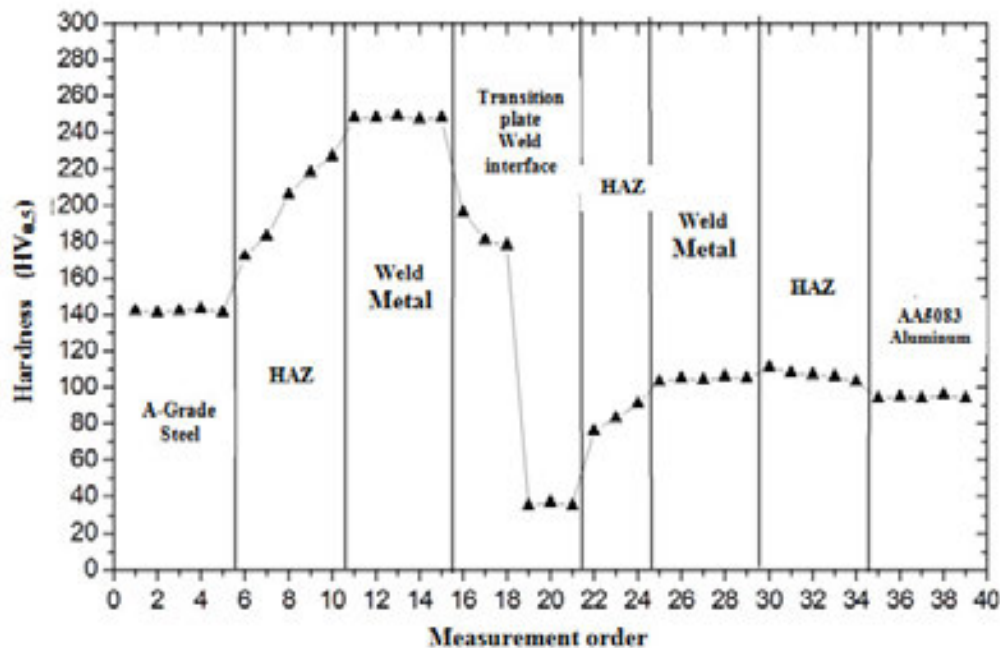


Figure 9. Hardness distribution of AA5083 aluminum-A grade steel couple joined with robotic GMAW method using transition plate

The HAZ hardness of the AA5083 aluminum alloy-transition plate AA5086 aluminum side is also measured. Hardness measurement results were found to range between 80-100 HV_{0.5} for both side of the HAZ. Depending on the temperature reached at the HAZ and the duration at that temperature, the precipitation may be responsible for the slight increase in hardness. Microstructure studies support this. The weld metal hardness of the A-grade steel-transition sheet welded with R71 flux cored wire was found to be 250 HV_{0.5} on average, which is

related to the phases formed in the structure. However, the weld metal hardness of the AA5083 aluminum alloy-transition plate welded with AlSi5 filler metal was found to be 100 HV_{0.5} on average.

3.4. Microstructure Evaluation

The microstructure of the AA5083 aluminum-A grade steel couple joined with the robotic GMAW method using the transition plate was investigated. For this purpose, A-grade steel and AA5083 aluminum base metal, aluminum-steel transition plate, weld metals and HAZ microstructure images were taken. The results are shown in Figure 10 a-i.

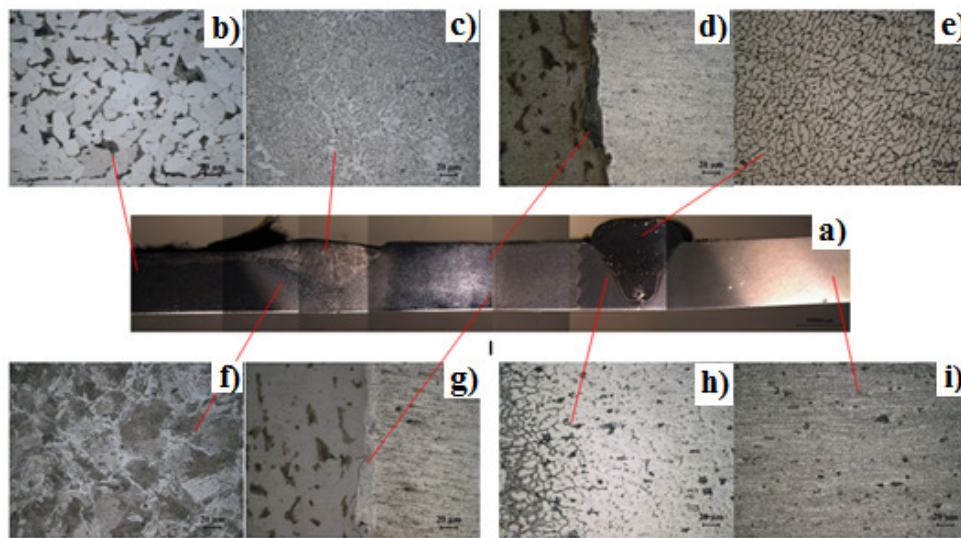


Figure 10. a) Macrostructure image of AA5083 aluminum-A grade steel couple joined by robotic GMAW method using transition plate. Microstructure of b) A-grade steel, c) Weld metal of A-grade steel-steel side of the transition plate d) Interface of the transition plate e) Weld metal of AA5083-AA5086 aluminum side of the transition plate f) HAZ of A-grade steel-steel side of the transition plate g) Interface AA1050-AA5086 of the transition plate h) HAZ of AA5083-AA5086 aluminum side of the transition plate i) AA5083 aluminum

As seen from Fig. 10 a, the commercially available transition plate consists of three parts. The first part is low carbon steel (ASTM A516-55). The aluminum part appears to be composed of two parts. The first part of aluminum is made of AA1050 quality aluminum, the second part of aluminum is usually made of AA5086 aluminum alloy. The AA1050-AA5083 alloy sheets were joined to each other by explosive welding. The wavy interface image of the explosion welding in Fig. 10 confirms this. It is stated by the manufacturer that the AA1050 aluminum plate is welded on the steel side of the transition plate with explosion welding. The interface image shown in Figure 10 d and g confirms this. However, in the AA1050 aluminum-steel explosive weld interface, the wave frequency became wider (Fig. 10 d and g). The frequency of the wave structure is related to the density of the materials to be welded. The greater difference in density between the two materials causes the greater the difference in the sinus wave of the wavy structure of the weld interface. The wavelength amplitude ratio obtained when joining dissimilar

materials with explosive welding is less than that of the similar type of material [17]. As the transition plate is produced by the explosive welding method, the grains are deformed in near the joint interface due to high collision speed. As seen in Fig. 10 g, the steel side of the aluminum-steel transition plate is made up of equiaxial fine grains. The structure is generally composed of more ferrite and fewer pearlite grains. It is expected that a small amount of pearlite phase will form between the ferrite grains due to the low amount of carbon in the steel chemical composition.

Because the aluminum side of the transition plate is made of AA1050 aluminum alloy, it is seen that the structure is formed from coaxial grains. There are particles thought to be connected to the Fe-Al intermetallic alloys like FeAl_2 , Fe_2Al_5 and FeAl_3 in the chemical composition [18]. 1xxx alloys cannot be aged because they are single-phase alloys with the exception of small inclusions or intermetallic compounds.

Depending on the chemical composition elements it contains, the A-grade steel structure of the joint are composed of co-axial ferrite grains as well as a pearlite phase (Fig. 10 b). Depending on the amount of carbon contained in the steel, it is expected to contain more pearlite phases than the transition plate. The chemical composition and mechanical properties of the A-grade steel sheet used in the manufacture of marine craft are similar to those of the general structural steel S235 []. It is a steel grade with high formability and very good weldability because of its very limited alloy elements which affect the hardenability of the steel.

A-grade steel-transition plate HAZ microstructure joined with R71 flux-cored filler metal was also investigated. It is clear from the microstructure of HAZ that, adjacent to the melting band, A-grade steel HAZ consists of large grains of Widmanstätten ferrite, grain boundary ferrite and pearlite (Fig. 10 f). As welding proceeds, γ -Fe grains in the HAZ grow and the amount of grain growth increases rapidly near the weld fusion zone, leading to the development of the coarse-grained region at the HAZ [19]. This region of the HAZ is closer to the fusion zone and contains larger grains than those in the base metal due to the high temperature and low cooling rate [20]. The structure of the weld metal of the combination is composed of the columnar grains extending towards the welding axis. In general, the microstructure of the weld metal was composed of predominantly acicular ferrite with various proportions of grain boundary ferrite and Widmanstätten ferrite (Fig. 10 c).

Depending on the chemical composition elements it contains, the AA5083 aluminum structure appears to coalesce from equiaxial grains (Fig. 10 i). Due to its corrosion resistance, AA5083 alloy, which is used in the production of marine vessels, is an aluminum type with high formability and very good weldability. Rolling tracks and fine grained homogeneous precipitates (Mg_2Si) are projected in the structure of the main material. 5xxx alloys do not have Mg_2Al_3 stable structure and cannot be heat treated. Properties of these alloys can be improved by strain hardening, solid solution hardening and grain size control [21].

As mentioned earlier, the AA5083 aluminum-aluminum side of the transition plate is joined with AlSi_5 filler metal by the robotic gas metal arc welding method. Next to the weld metal is the HAZ, which starts with the fusion line. Depending on the temperature reached and the time it takes to stand at this temperature, coarse grained structure appears in this region of the HAZ adjacent to the fusion line (Fig. 10 h). It has been reported that grain coarsening affects mechanical properties, reduces hardness and strength. The coarse precipitates formed in HAZ attract attention.

[22].

The typical dendritic structure appears to form the aluminum weld metal, since the weld metal of the joint is welded using the AlSi5 additive wire (Fig.10 e). Due to the effect of rapid cooling, the precipitates formed in the weld metal structure are scattered in wider intervals. Apparently, the grain has grown in the HAZ of the AA5083 aluminum alloy and AA5086 aluminum side of the transition plate.

4. General Results and Recommendations

Findings obtained in the study can be summarized as follows.

- The average tensile strength of the test specimens is 68.39MPa and elongation is 2.96%. As a result of the test, the sample is broken by the AA1050 aluminum side of the transition plate. The dimples in the surface and cross section reduction in the fracture surface image indicate the failure of the test sample with the ductile fracture behavior.
- The maximum bending strength of the test specimens was found to be 325 N/mm² on average. The three-point bending test samples were cracked after the specimens were shaped to about 80° from the aluminum-steel interface of the transition plate. This suggests limited formability.
- The average hardness of A-grade steel is 140HV_{0.5} and the hardness of AA5083 aluminum is 90HV_{0.5}. The average hardness of AA1050 aluminum of the transition plate is found to be 30HV_{0.5} and the steel side is 170HV_{0.5}. HAZ hardness of AA5086 -AA5086 aluminum alloys of the transition plate were found in the range of 90-110 HV_{0.5}. The hardness of the weld metal of the A-grade steel and the steel part of the transition plate of the sample joined with R71 flux cored wire was measured. Based on the phases formed in the structure, it was found to be 250 HV_{0.5} on average. However, the weld metal hardness of the AA5083 aluminum alloy-transition plate welded with AlSi₅ filler metal was found to be 100 HV_{0.5} on average.
- HAZ hardness of A-grade steel-steel side of the transition plate were found in the range of 170-240 HV_{0.5}. Depending on the temperature reached in HAZ and the waiting time at this temperature, rapid cooling after welding occurs due to the nature of the fusion welding method. For this reason, it is expected that the hardness of the HAZ will vary depending on the structural transformation. Microstructure results also support this.
- The commercially available transition plate consists of three parts. The first part is low carbon steel (ASTM A516-55). The aluminum part appears to be composed of two parts. The first part of aluminum is made of AA1050 quality aluminum, the second part of aluminum is usually made of AA5086 aluminum alloy. The AA1050-AA5083 alloy sheets were joined to each other by explosive welding. However, the wave frequency is larger in the AA1050 aluminum-steel joining interface obtained from the explosive weld. Deformation of the grains occurred in the region near the interface of the transition plate associated with the collision.
- The steel-side structure of the aluminum-steel transition plate consists of equiaxed grains. The structure is made up of more ferrite and less perlite grains,

volumetrically. Coexistence of AA1050 and AA5086 aluminum alloys with explosive weld is observed in the structure of the transition plate.

- Depending on the chemical composition elements contained, the A-grade steel structure of the assembly is composed of fine equiaxed ferrite grains as well as perlite phase. It appears that HAZ is composed of large grains of Widmanstätten ferrite, grain boundary ferrite and pearlite. In welding metal; predominantly acicular ferrite with grain boundary ferrite and Widmanstätten ferrite. HAZ of the A-grade steel and steel side of the transition plate is decorated with ferrite and bainite phases.
- The AA5083 aluminum alloy structure of the weldment is composed of coarse grains. Fine homogeneous precipitates are observed in the grain. The precipitates formed in addition to coarse grains in HAZ have been found to be rough. The weld metal consists of dendritic structure. The precipitates formed in the weld metal are scattered over a wider range. Apparently, the grain has grown in the HAZ of the AA5083 aluminum alloy and AA5086 aluminum side of the transition plate.

As a result; A-grade steel and AA5083 aluminum alloy can be successfully welded with robotic GMAW method using the Al-steel transition plate.

5. Acknowledgement

This work was supported by Scientific Research Projects Coordination Unit of Karabük University. Project Number: KBÜ-BAP-18-YL-049.

6. References

- [1] Türk Uluslararası Gemi Sicili Yönetmeliği, Resmi Gazete Tarihi: 23.06.2000, Resmi Gazete Sayısı: 24088.
- [2] M. Stopford: Maritime Economics, Chapter 7, New York, (1997).
- [3] I. Chrzanowski, M. Krzyanowski, K. Luks: Shipping Economics and Policy, Fairplay Publications, London (1979).
- [4] P. Fuentes, W. Couvillion, A. Allen: Potential Effects of Technological Advances in Transportation on the Trade of Food Products between the U.S. and Latin America, J. Food Distr. Res. 35 (2004) pp. 9-106.
- [5] D.J. Eyres: Ship Construction, Butterworth-Heinemann Ltd., Sixth Ed. (2006) 359.
- [6] A. Clayton, N. Ribeiro, H. Henein, Douglas G. Ivey, S. Duarte Brandi: Evaluation of AH36 microalloyed steel welded joint by submerged arc welding process with one and two wires Materials Research. 19 (2016) pp. 143-152
- [7] M. Yavuz Yılmaz: İMEAK Deniz Ticaret Odası Deniz Ticareti Dergisi, Mart (2017).
- [8] B. Hayman, M. Dogliani, I. Kvale, A.M. Fet: Technologies for reduced environmental impact from ships – ship building, maintenance and dismantling aspects, ENSUS 2000 Marine Science and Technology for Environmental Sustainability. United Kingdom, Norwegian University of Science and Technology (2000).
- [9] TÜRK LOYDU, Kısım 1, Bölüm 3-2, Tekne Yapım Kuralları (2015).
- [10] Woodhead Publishing, Non Ferrous Metals, Welding Metallurgy of Non-Ferrous Metals and Cast Iron, Revised edition, ISBN:85573 174 6, (1994).
- [11] A. Eker Akdoğan: Alüminyum ve Alaşımlarının Otomotiv Endüstrisinde Kullanımı, Yıldız Teknik Üniversitesi Makine Mühendisliği Bölümü, İstanbul (2008).

- [12] M. Aydın, Ülkemizde Yat ve Gezinti Teknesi Dizaynı, Üretimi ve Kullanımı, Gemi ve Deniz Teknoloji Dergisi, 197 (2003).
- [13] M. Asarkaya, Tersanelerde Uygulanan ve Uygulanabilecek Kaynak Yöntemleri, Gemi Mühendisliği ve Sanayimiz Sempozyumu (2004) pp. 252–267.
- [14] Ö.F. Sukas, Ö.K. Kınacı, Ş. Bal: A Review on Prediction of Ship Manoeuvring Performance, Part 1, Gemive Deniz Teknolojisi, 23, (2017), pp. 37-75.
- [15] F. Hayat, H. Uzun: Microstructural and mechanical properties of dual-phase steels welded using GMAW with solid and flux-cored welding wires, Int. J. Mat. Res. (formerly Z. Metallkd.) 103 (2012) pp. 828-837.
- [16] TS EN ISO 9015-2: Destructive tests on welds in metallic materials - Hardness testing - Part 2: Microhardness testing of welded joints (2011).
- [17] R.C. Gupta, G.S. Kainth: Swinging wake mechanism for interface wave generation in explosive welding of metals, Journal of Applied Mechanics, 57 (1990) pp. 514-521.
- [18] P. Matysik, S. Józwiak, T. Czujko: Characterization of Low-Symmetry Structures from Phase Equilibrium of Fe-Al System-Microstructures and Mechanical Properties Materials, 8 (2015) pp. 914-931.
- [19] P. Varghese, M. Siva Prasad, F. Joseph, M. John Varkey, K. Antony, A. Sreekanth: The Effect of Repeated Repair Welding on the Corrosion Behaviour of Austenitic Stainless Steel and Mild Steel Dissimilar Weldment, Proceedings of International Conference on Advances in Materials, Manufacturing and Applications (AMMA), April 9-11, (2015) pp. 864-869.
- [20] W. E. John, W. Joe, R. Thorsten, A. P. Todd: Mapping Phase Transformations in the Heat-Affected-Zone of Carbon Manganese Steel Welds using Spatially Resolved X-Ray Diffraction, International Conference on Trends in Welding Research 6 (2002) pp. 1-6.
- [21] Ç. Batuk: AA7075 Alüminyum Alaşımlarının Konik Şekillendirilebilirliğine İşlem Parametrelerinin Etkisi, Yüksek Lisans Tezi, Fen Bilimleri Enstitüsü, Karabük Üniversitesi, (2018).
- [22] H. Cetinel, M. Ayvaz: Microstructure and Mechanical Properties of AA 5083 and AA 6061 Welds Joined with AlSi5 and AlSi12 Wires, Materials Testing, 56 (2014) pp. 884-890.

CORRESPONDENCE ADDRESS: Ramazan KAÇAR, Karabük University, Technology Faculty, 78050, Turkey, Tel: +90 433 82 00/1091, e-mail: rkacar@karabuk.edu.tr

SHORT BIOGRAPHIES

Alparslan Parlak¹ – is a post graduate student in Manufacturing Engineering Department of Institute of Science and Technology in Karabük University.

Ramazan Kaçar² – is a Doctor in Manufacturing Engineering Department of Technology Faculty in Karabük University.

NOKTA DİRENÇ KAYNAĞI İLE ÇELİK HASIR ÖRGÜ İMALATINDA KAYNAK AKIMININ BİRLEŞMEYE ETKİSİ

Adem KURT, Aytaç TALAŞ, Emre ALPKAYA, Yusuf ÖZÇATALBAŞ

ÖZET

Bu çalışmada inşaat sektöründe kullanımı yaygınlaşan çelik hasır örgü tellerin üretiminde kullanılan nokta direnç kaynağında kaynak akımının birleşme arayüzeyinin metalürjik özellikleri ve sertlik özelliklerine etkisi araştırılmıştır. Bu amaçla 6 mm çapında nervürlü düşük karbonlu çelik teller 600, 800 ve 900 Amperde 5 bar basınçta nokta direnç kaynağı ile birleştirilmişlerdir. + şekilde birleştirilen numuneler birleşme noktasına 45 derece açıyla kesilerek birleşme arayüzeyi parlatılıp dağlanarak metalografik olarak incelenmiş ve kaynak akımının oluşturduğu ısı girdisine bağlı olarak kaynak metali ve ITAB daki değişimler incelenmiştir. Artan ısı girdisiyle ITAB da tane irileşmesi artarken sertliğin azaldığı gözlenmiştir.

THE EFFECT OF CURRENT TO JOINED ON THE STEEL WICKER KNITTING PRODUCTION

Adem KURT, Aytaç TALAŞ, Emre ALPKAYA, Yusuf ÖZÇATALBAŞ

ademkurt@gazi.edu.tr

ABSTRACT

In this study, the effect of welding current on the metallurgical properties and hardness properties of the weld interface was investigated in the spot welding used in the production of steel wire mesh used in the construction sector. For this purpose, 6 mm diameter ribbed low carbon steel wires are joined with 600, 800 and 900 Amperes 5 bar pressure spot welding. + bonded samples were cut at a 45 degree angle to the junction and polished and metallographic at the interface. The weld metal and ITAB changes were investigated depending on the heat input generated by the welding current. With increasing heat input, it was observed that ITAB also increased in graininess and decreased in hardness.

1. GİRİŞ

1877'de ABD'de bir rastlantı sonucu bulunan nokta direnç kaynağı seri imalata uygun oldukça yaygın bir kaynak yöntemidir. Kaynak işlemi, bir düğmeye ya da pedala basarak makinayı devreye sokan ve devreden çıkaran operatörler tarafından hızla gerçekleştirilir. Bu nedenle, özellikle ark kaynağı, gaz kaynağı, sert ve yumuşak lehimleme gibi diğer termik birleştirme yöntemleriyle karşılaştırıldığında, kaynak başına düşen işçilik masrafı bu yöntemde oldukça düşüktür. Bu kaynak yöntemi, ilave malzeme kullanılmadığından, sağladığı hafiflik, yüksek mukavemeti, özel beceri gerektirmemesi ve kaynak hızının yüksek oluşundan dolayı günümüzde otomotiv, uçak endüstrisi ve metal eşya imalatında büyük ölçüde kullanılmaktadır.

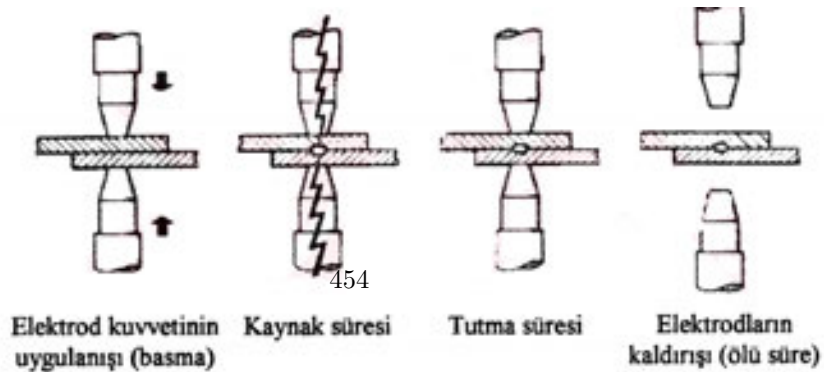
Nokta direnç kaynağı, elektrotlar tarafından uygulanan kuvvet altında bir arada tutulan iş parçalarında, geçen elektrik akımına karşı iş parçalarının gösterdikleri dirençten elde edilen ısı ile parçaların tek ya da çok noktada bölgesel olarak eritilip basınç altında birleştirilmesine dayanan bir yöntemdir. Bu kaynak yönteminde, birleştirilecek parçalar bakır elektrotlar arasına sabitlenir. Kapanan elektrotlar öncelikle parçaların birleşik kalabilmesi için gereken kuvveti uygularlar. Daha sonra parçaların yüzeyleri üzerinden yüksek akım geçirilir. Bu sayede parça ısınır. Yeterli ısıya ulaşıldığında akım kesilir ve birleşme yüzeyi basınç altında soğutulur. Bu sırada elektrotların da yüksek sıcaklığa ulaşmasını engellemek için elektrotlar su ile soğutulur. Parça soğuduktan sonra elektrotlar yukarı kaldırılır ve parça çıkarılır.

Bu kaynak yöntemi sayesinde genellikle 1,5 ila 13 mm çapında nokta kaynakları elde edilir. Aynı kalınlıkta iki parçanın birleştirileceği durumda parça kalınlığı maksimum 3 mm'dir. Elde edilen kaynak parçaların birleşme ara yüzeyleri arasında bir çekirdek şeklindedir ve elde edilen kaynak profili elektrotun şekliyle aynıdır. Oluşan çekirdeğin kesiti oval olmakla birlikte, üstten görünüşü elektrotun şekliyle aynıdır.

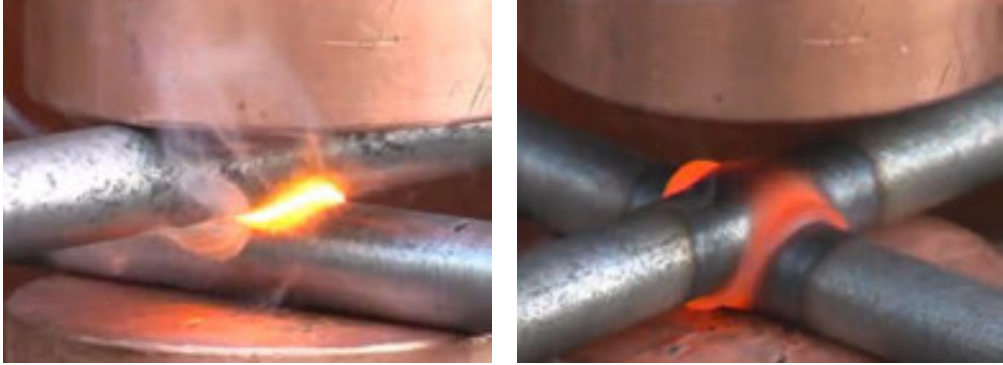
Ayrıca yüksek mukavemetli bir nokta kaynağı elde edebilmek için, iki punta arasında 25 ila 50 mm mesafe olmalıdır. Bunun yanında atılan puntalar kenarlardan da aynı miktarda uzak olmalıdır.

Bütün direnç kaynağı metotları, uygun bir akım şiddeti-kaynak zamanı düzenlemesi gerekir. Kaynak bölgesinin ısınma ve soğuma hızları, zaman ekonomisi bakımından mümkün olduğunca yüksek olmalıdır.

Genel olarak nokta direnç kaynağı, dört periyottan meydana gelir: basma, kaynak, tutma ve ölü süre.



- a) **Basma Süresi:** Elektrot kuvvetinin il uygulandığı an ile kaynak akımının verildiği ilk an arasında geçen süredir. Bu aralık, solenoid hareketli silindirik valfinin çalışması ve üst elektrot tutucunun üst elektrotu iş parçasıyla temas haline getirilmesi ve elektrot kuvvetinin tamamını uygulaması için zaman sağlar. Bu zaman, parçaların yakın temasını sağlamaya yetecek kadar olmalıdır.
- b) **Kaynak Süresi:** Kaynak akımının devreden geçtiği zaman aralığıdır. İnce taneli yapı çeliklerin birçoğunda, basit karbonlu çeliklere normal olarak uygulanandan biraz daha uzun kaynak süresinin kaynak kabiliyeti eğrisini genişlettiği ve böylece kabul edilebilir kaynak akım sınırlarının arttığı görülmüştür.
- c) **Tutma Süresi:** Kaynak akımının kesilmesinden sonra, nokta kaynağının metali katılaşıncaya kadar elektrot kuvvetinin etkisinin devam ettiği zaman aralığıdır. Bazı ince taneli yapı malzemeleri tutma süresine hassastır. 25 ila 50 arasındaki periyot sayılarında (1/2 ila 1 sn.), bu malzemeler soyma deneylerinde ara yüzeyde yırtılma eğilimi gösterir.
- d) **Ölü Süre:** Tutma zamanının sonundan bir sonraki çevrimdeki basma zamanının başlangıcına kadar geçen, elektrotların iş parçasıyla temasta olmadığı zaman aralığıdır. Otomatik çevrimde, ölü zaman, elektrotların geri çekildiği ve iş parçasının kılavuzlandığı, kaldırıldığı veya pozisyonunun değiştirildiği süredir.



Şekil 1.1 Hasır örgülerin T birleştirilmesi

Artan akım, kaynak akımının tamamının bir anda uygulanması yerine düşük bir değerden istenilen değere birkaç periyotta yükseltilmesinin izin verir. Düşük ilk akım ya da kaynak akımı, akım ilk uygulandığında metal fişkırmasını azaltır ya da önler.

Azalan akım, kaynak akımının aniden kesilmesi yerine, düşük bir değere kademeli olarak düşürülmesine izin verir ve soğutma süresi gradyanını uzatarak ısı işleme uygun metallerin bazı tiplerinde iyi kaynak elde edilebilmesine yardımcı olur. Özellikle karbon miktarı %0,15'i aşmadığı düşük karbonlu çeliklerin kaynağında nadiren ihtiyaç duyulmakla birlikte, sertleşebilir çeliklerin kaynağında olduğu gibi soğutma hızının sınırlı olduğu durumlarda kullanılmaktadır.

Isı, iş parçalarına oranla elektrotlardan daha hızlı uzaklaşmaktadır. Bu yüzden soğutma zamanı sırasında, kaynak akımı kesikken, iş parçaları ısının çok azını kaybederken elektrotlar ısılarının çoğunu uzaklaştırır.

Nokta direnç kaynağında kaynak çekirdek formu ve kaynak mukavemeti direnç ve kaynak süresine bağlıdır. Kaynak sırasında direnç yoluyla oluşan ısı Joule kanununa göre aşağıdaki eşitlikle hesaplanabilir.

$$Q = 0.23 \cdot I^2 \cdot R \cdot t$$

Burada,

Q = Isı miktarı

I= Akım

R = Elektrik direnci

t = time

Toplam direnç, elektrodların temas dirençleri ve malzeme dirençlerinden oluşur. Levhaların malzeme dirençleri ve levhalar ile levha ve elektrot arasındaki temas dirençleri, alüminyum ve çelik için çok farklı büyüklük derecelerine sahiptir. Kaynak parametreleri (akım, zaman, kuvvet) malzemenin ısı iletkenlik özelliklerine göre değişir. Alüminyum yüksek iletkenlik, düşük elektrik direncine sahip olduğundan yüksek kaynak akımı, düşük kaynak zamanı ve özel elektrod kuvveti seçmek gerekir.

2.Deneysel Çalışmalar

Bu çalışmada, inşaat sektöründe kullanılan düşük karbonlu \varnothing 6 mm kesitli çelik teller farklı amperlerde 5 Bar basınçta nokta direnç kaynağı ile birleştirilerek kaynak akımlarının birleşme ara yüzeyine ve metalürjik özelliklere etkisi araştırılmıştır. Bu çubuklar birbirlerine dik şekilde 90° açı ile nokta direnç kaynağı ile kaynak edilmişlerdir (Şekil 1.1). Kaynaklı numuneler Şekil 2.1'deki gösterilen yerlerden 45° açı ile kesilerek metalografik inceleme için bakalite alınarak hazırlanmışlardır.



Şekil 2.1: 45° açı ile kesilmiş kaynak numunesi

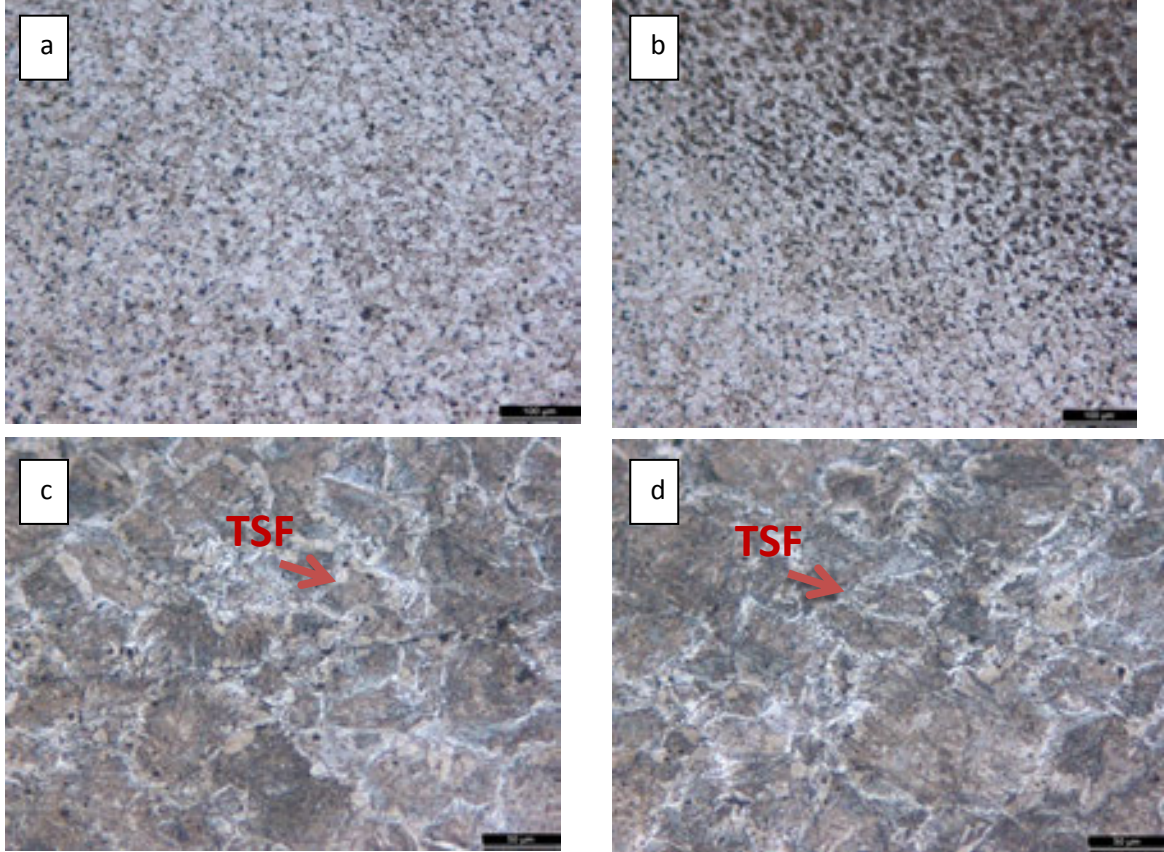
Bakalite alınan farklı amperlerde kaynak yapılmış numuneler mikro yapı incelemeleri için 120, 400, 800 ve 1200'lük zımparalar ile zımparalanarak dağlama için hazırlandılar. Parlatılmış numuneler iç yapıda bulunan fazların ve tane sınırlarının görülebilmesi için %3 Nital kullanılarak dağlanmıştır.

Metalografik işlemler ile hazırlanan numuneler optik mikroskopta incelenerek akım değerlerine bağlı olarak farklı ısı girdilerinin oluşturduğu mikro yapı fotoğrafları çekilerek değerlendirilmiştir.

3.Sonuçlar ve Tartışma

3.1.Mikroyapı sonuçları

Farklı akım yoğunluklarında birleştirilen numunelerin kaynak ara yüzeyi ve kaynak bölgesindeki görüntüleri Şekil 3.1’de verilmiştir.



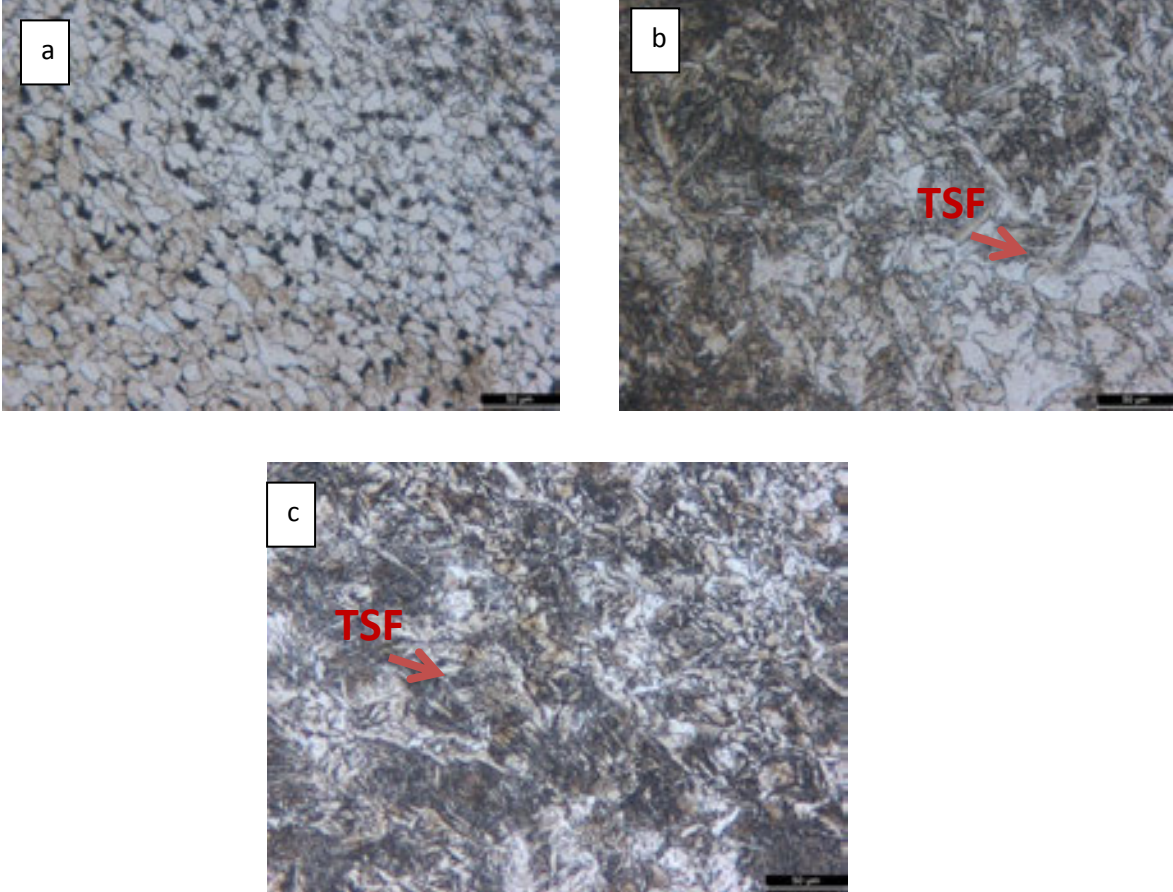
Şekil 3.1 600 A de birleştirilen numunelerin mikroyapısı

Şekil 3.1 (a)’da 600 amperde birleştirilen numunenin esas metal yapısı görülmektedir. Mikro yapı tipik düşük karbonlu çelik mikro yapısını gösterip ferritik yapıda ortalama 40 mikron boyutlarında tane yapısından oluşmaktadır.

Şekil 3.1 (b)’de kaynak bölgesine doğru yaklaştıkça ısının etkisi ile yeniden kristalleşme sonucu tanelerin östenite dönüşümünün başladığı ancak hızlı ısınma ve soğuma sonucu dönüşümün tamamlanamadığı kısmen dönüşmüş bölge gözükmemektedir.

Şekil 3.1 (c)'de ise, birleşme bölgesinde ısının etkisi ile tane irileşen bölge açık olarak görülmektedir. Birleşme ara yüzeyi bir çizgi şeklinde net olarak görülürken tane boyutunun ara yüzeyinin her iki tarafında yaklaşık aynı boyutta olduğu, ısının her iki parçaya da homojen dağıldığını göstermektedir.

Şekil 3.1 (d)'de tane irileşen bölgede tane sınırları tane sınırı ferrit ağları ile örülmüş tane içlerine doğru widmanstatten ferrit plakalarının oluştuğu görülmektedir.

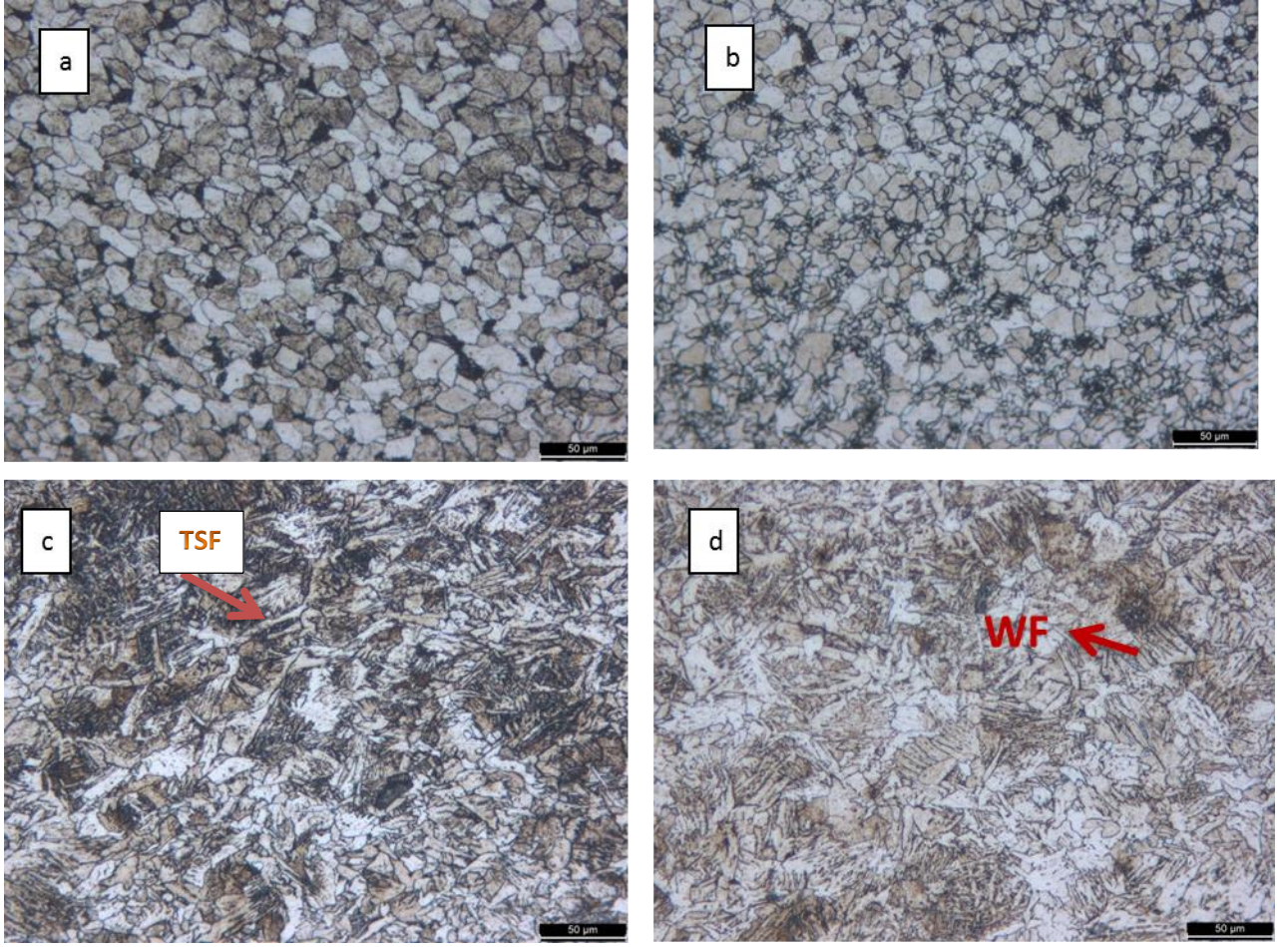


Şekil 3.2 800 A'de birleştirilen numunelerin mikroyapısı

Şekil 3.2'de 800 amperde birleştirilen numunelerin mikro yapıları verilmiştir. Burada da esas metal ve kısmen dönüşmüş bölge açık olarak Şekil 3.2 (a)'da görülmektedir. Mikro yapıda tane yapısının yaklaşık 40 mikron civarında olduğu, tane sınırlarında kısmen östenite dönüşümlerin başladığı kaynak merkezine yaklaştıkça dönüşüm miktarının arttığı görülmektedir. Kısmen bölgeyi takiben iri tanelerin oluştuğu (Şekil 3.2 (b)) ve tane boyutunun yaklaşık 70 mikronlara büyüdüğü tane sınırları ve tane içlerinde ferrit tabakalarının kalınlaştığı gözlenmektedir.

Kaynak ara yüzeyinin mikro yapısı Şekil 3.2 (c)'de verilmektedir. Akımın artması ile ısı girdisi arttığından ara yüzey kaybolarak tek bir metal ara yüzeyi şeklinde birleşme olduğu mikro yapıdan anlaşılmaktadır. Tane sınırlarında oluşan tane sınırı ferrit tabakalarından tane

içlerine doğru widmanstatten ferritlerin büyüdüğü, östenit tanelerin içerisinde iğnemi yapıda asiküler ferrit oluştuğu görülmektedir.



Şekil 3.3 900 A'de birleştirilen numunelerin mikroyapıları

Şekil 3.3 (a)'da ise 900 amperde birleştirilen numunelerin esas metal mikro yapıları verilmiştir. Yine birleşme bölgesine doğru yaklaştıkça esas metalin yüksek ısı sebebiyle mikro yapısında östenit dönüşümün başladığı kısmen dönüşmüş bölge Şekil 4.3 (b)'de görülmektedir. Hızlı ısıtma sonucu sıcaklık denge diyagramında dönüşüm sıcaklığının üstüne çıkmasına rağmen hızlı ısıtma sebebiyle dönüşümün tamamlanamadığı bu nedenle tane sınırında yeni fazların kısmen oluştuğu görülmektedir.

Şekil 3.3 (c)'de kaynak merkezinden kaynak ara yüzeyinin fark edilmeyecek şekilde kaybolduğu ve kaynak metali mikro yapısının ergitmeli kaynak yöntemlerindeki oluşan mikro yapıya benzemesi yüksek ısı girdisinin etkisi ile oluştuğu düşünülmektedir.

Şekil 3.3 (d)'de kaynak metali içerisinde beyaz renkli ferrit tabakaları tane sınırlarını kaplarken tane sınırları ferritlerde tane içlerine doğru widmanstatten ferrit plakalarının parmak şeklinde uzadıkları görülmektedir. Widmanstatten ferrit plakalarının boyutlarının uzun olması artan akım sebebi ile ısı girdisinin artıp soğuma hızının yavaşlaması ile açıklanabilir.

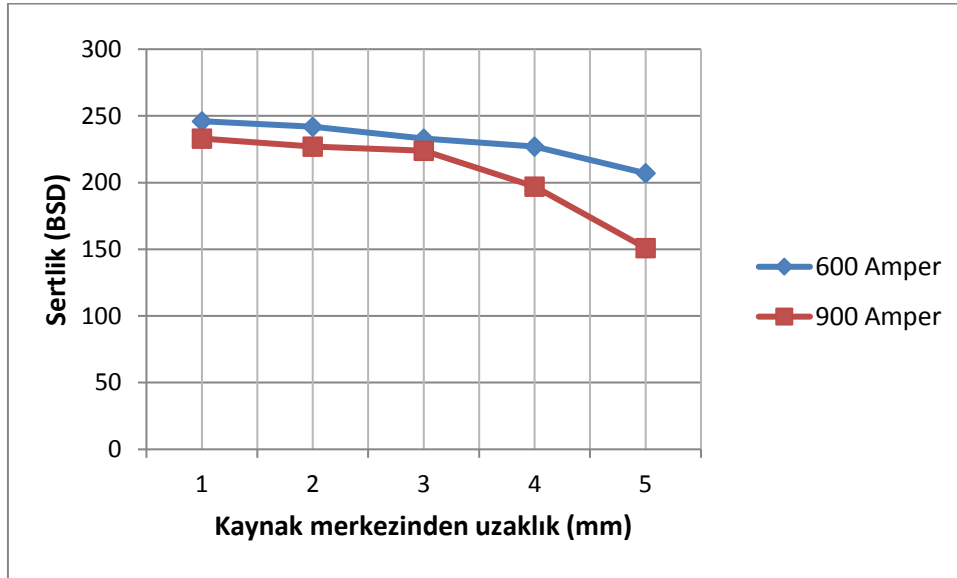
3.2. Sertlik İncelemeleri

Kaynaklı birleştirmelerde ısı girdisi hem metalografik yapıya hem de sertlik gibi özellikleri önemli derecede etkileyen bir faktördür. Bu nedenle bu çalışmada ısı girdisinin kaynak bölgesinin sertliğine olan etkisini belirlemek amacıyla en düşük ve en yüksek akımlarda (600 ve 900 Amper) direnç kaynağıyla birleştirilen numunelerin sertlikleri ölçülerek Tablo 3.1’de verilmiştir.

Tablo 3.1. En düşük ve en yüksek akımlarda (600 ve 900 Amper) direnç kaynağıyla birleştirilen numunelerin sertlikleri ölçüleri

Kaynak Akımı	Kısmen dönüşmüş bölgeden kaynak merkezine doğru BSD				
600	207	227	233	242	246
900	151	197	224	227	233

Buradan görüleceği gibi 600 amperde birleştirilen numunelerin kısmen dönüşmüş bölgesinin sertliği 207 BSD iken kaynak metaline doğru sırasıyla 227, 233, 242, 246 olarak artmaktadır. Buna karşılık 900 amperde birleştirilen numunelerin kısmen dönüşmüş bölgesinin sertliği 151 BSD’den başlayıp sırasıyla 197, 224, 227 ve kaynak metali merkezinde 233 BSD olarak 600 amperde kaynak yapılandan daha düşük sertlik değeri oluşmuştur. Bunun sebebi 900 amperde ısı girdisi daha yüksek olduğundan soğuma hızının yavaş olması sertliğin 600 ampere göre daha düşük çıkmasına sebep olmuştur.



Şekil 3.4. Nokta direnç kaynağında kaynak akımı ve sertlik ilişkisi

4. Sonuçlar

inşaat sektöründe kullanımı gün geçtikçe yaygınlaşan çelik hasır örgü tellerin üretiminde kullanılan nokta direnç kaynağında kaynak akımının birleşme arayüzeyinin metalürjik yapıları

ve sertlik özelliklerine etkisinin belirlenmesi amacıyla yapılan bu çalışmada aşağıdaki sonuçlar elde edilmiştir.

- Kaynak akımı şiddeti arttıkça sertliğin düştüğü görülmüştür.
- 600 A'da kaynak bölgesine doğru yaklaştıkça ısının etkisi ile yeniden kristalleşme sonucu tanelerin östenite dönüşümünün başladığı ancak hızlı ısınma ve soğuma sonucu dönüşümün tamamlanamadığı kısmen dönüşmüş bölge gözükmemektedir.
- 800 A'da akımın artması ile ısı girdisi arttığından ara yüzey kaybolarak tek bir metal ara yüzeyi şeklinde birleşme olduğu anlaşılmaktadır.
- 900 A'da kaynak merkezinden kaynak ara yüzeyinin fark edilmeyecek şekilde kaybolduğu ve kaynak metali mikro yapısının ergitmeli kaynak yöntemlerindeki oluşan mikro yapıya benzemesi yüksek ısı girdisinin etkisi ile oluştuğu düşünülmektedir.
- Bu çalışmada 600 A akımının üzerindeki akım değerlerinde birleşme arayüzeyinde ergime katılaşma gerçekleştiği 600 A de katıfazda (sıcak basınç kaynağı mekanizması) birleşme gerçekleştiği söylenebilir.

Kaynaklar

INVESTIGATION OF DIFFUSION AREA OF WC-Co PART PRODUCED BY INSERTED POWDER INJECTION MOLDING METHOD

Harun KOÇAK^{1,a}, Mehmet SUBAŞI^{2,b}, Çetin KARATAŞ^{3,c}

¹ Selcuk University / Cihanbeyli Vocational School

² Gazi University / Technical Sciences Vocational School

³ Gazi University / Faculty of Technology / Department of Manufacturing Engineering

^aharunkocak@selcuk.edu.tr, ^bmsubasi@gazi.edu.tr, ^ccetink@gazi.edu.tr

Abstract

The Inserted Powder Injection Molding (IPIM) method has been developed to overcome the dimensional limitation (<10 mm) in part production by powder injection molding. This developed method consists of three basic steps: injection of feedstock, debinding and sintering. In this study, firstly inserts were prepared from HSS material. Then a nickel (Ni) interlayer was formed on the inserts with a thickness of 100 µm (± 3 µm). Inserts with Ni intermediate layer were placed into the mold and WC-Co (9%) feedstock was injected onto them. After the injection, the samples were subjected to debinding processing and then sintered in an atmosphere controlled furnace at a temperature of 1200 °C for 240 minutes. Elemental transition between HSS/Ni/WC-Co was investigated by EDS analysis and hardness profile was created by measuring at certain intervals in the diffusion zone. It has been determined that the average hardness of the HSS zone 671 HV, the hardness of the intermediate layer is 247 HV, and the average hardness of the injected zone near the intermediate area is 1152 HV. Nickel intermediate layer was diffused an average 2.02 % in HSS and 1.08% in WC-Co .

Key Words: Inserted Powder Injection Molding, WC-Co, Nicel, Diffusion, HSS

1. Introduction

In general small parts are produced by the Powder Injection Method (PIM) . As the part size increases bond removal gets harder and the cost increases. For this reason, IPIM method was found out for the production of bigger parts by PIM method [1,4]. A prepared part under the name insert is placed in to the mould and feeding stock is injected on it. Production of bigger parts can be accomplished by the IPIM method by decreasing the wall thickness of the injected section owing to the insert. When the same metallic materials are used both in the insert and the injected section , a solid joining can be obtained. However, in the production made by using different materials such as metal insert and ceramic stock , the physical and chemical characteristics of the materials affect the obtaining of desired strength value at the interlayer significantly. Therefore, in order to get benefit from different characteristics of ceramic and metallic materials at the same time and to be able to produce eligible parts with these materials new methods have to be investigated to make the joining of these materials possible.

Tungsten carbide – Cobalt (WC-Co) is widely used in several sectors due to its outstanding characteristics. WC-Co is widely used in the production of cutting tools employed in different sectors such as machinery and mining due to its higher hardness and strength level, outstanding wear resistance, higher melting point and better thermal conductivity [5]. However carbides are brittle by themselves and are sintered at high temperature. Cobalt and liquid phase are sintered to decrease the sintering temperature and brittleness. For this reason their mechanical properties are changing depending on the amount of cobalt and particle size [6,7]. Toughness of WC-Co material depending on the amount of cobalt can be improved but the obtained toughness doesn't become sufficient for some applications. Cementite carbides are being used by joining metal materials especially with steels.

In most of the methods while parts are produced by joining two different materials it is stated that physical and chemical properties of materials must be close to each other [8,9]. However, the physical and chemical properties of WC-Co and metal materials are different from each other. This difference affects the common sintering behaviors and cause the show up of defects between the material pair [10,11]. For this reason it is getting harder joining of materials having different characteristics or producing parts from these materials. In some studies on this subject, when an interlayer was applied between WC-Co and the metal materials it is specified that problems arising from material specifications decreased [12,13]. Cementite carbide materials are usually tried to be joined with steels and generally nickel is used as the interlayer because its thermal characteristics are close to steel [12,14].

In this study, part production was made thru IPIM method by using HSS insert and WC-Co feeding stock. Ni interlayer was used to increase the diffusion bond between HSS inserts and WC-Co feeding stock. In the study first of all HSS inserts were prepared and 100 µm (± 3 µm) thick Ni interlayer was placed on it by electrolytic coating. After coating of Ni interlayer onto HSS insert, WC-Co feed stock was injected. Following the debinding, the sample was sintered at 1200 °C for 240 min. After the sintering treatment diffusion zone was examined by the aid of EDS analysis and micro hardness was measured in the intermediate zones. As a result of the tests and analyses, hardness profile and element transition ratios were determined.

2. Material and Method

Inserts of the samples used in the tests were prepared from M2 type HSS (1.3343) material. WC-Co(9%) feed stock was injected onto the inserts. 100 µm Ni interlayer was used to provide joining in the intermediate zone. Feeding stock was taken ready from Ryer company. Chemical composition of the HSS material and that of WC feed stock are given in Tables 1 and 2 respectively. The important characteristics of the elements (for diffusion) of the materials used in the tests are given in Table 3.

Table 1. Chemical composition of M2 HSS material (%)

C	Si	Mn	Cr	Mo	Ni	V	W	Co
0,9	0,25	0,3	4,10	5,0	0	1,8	6,40	0

Table 2. Chemical composition of WC-Co (9%) feeding stock (%)

Elements	C	Cr	Fe	Mo	Ni	W	Co	O
W. (%)	5,54	0,01	0,01	0,01	0,01	Kalan	8,94	0,05

Table 3. Properties of some elements in materials

Properties Elements	Melting Temp. (°C)	Boiling Temp. (°C)	Density (g/cm ³)	Atomic radius (nm)	Activation energy (kJ/mol)	Thermal expansion (10 ⁻⁶ /°C)	Lattice system
Ni	1455	2730	8.9	0,125	298	13.4	FCC
Co	1495	2900	8.9	0,125	292	13	HCP
Fe	1539	2740	7.87	0,124	239	11.8	BCC
W	3422	5930	19,3	0,193		4.5	BCC

2.1. Preparation of inserts and application of interlayer

On the study first of all, inserts of 6,3 diameter were prepared from M2 HSS material and were coated (with $\pm 3 \mu\text{m}$ tolerance) by $100 \mu\text{m}$ Ni . In the coating , Nickel coating bath supplied by Teknik Döküm company was used. Electrolytic coating conditions used in coating of interlayer onto insert are given in Table.4. The interlayer thickness was verified by measuring from the diameter surface thru an X-Ray measuring device.

Table.4. Electrolytic Ni coating conditions

Anode	Bath temperature	Voltage	Current density	Waiting time
Electrolytic Nickel	50-60 °C	2.5-3 V	4A/dm ²	1 μm for 2 min.

2.2. Inserted powder injection moulding

Injection process was made in the ARBURG Allrounder 220S injection moulding board. The inserts were prepared from M2 HSS steel and then coated by Ni interlayer and placed in a mould then WC-Co feed stock was injected to the outer part (Fig 1). Optimum injection parameters were determined by considering values advised by the feed stock produced company. Parameters used in the injection process are given in Table.5.

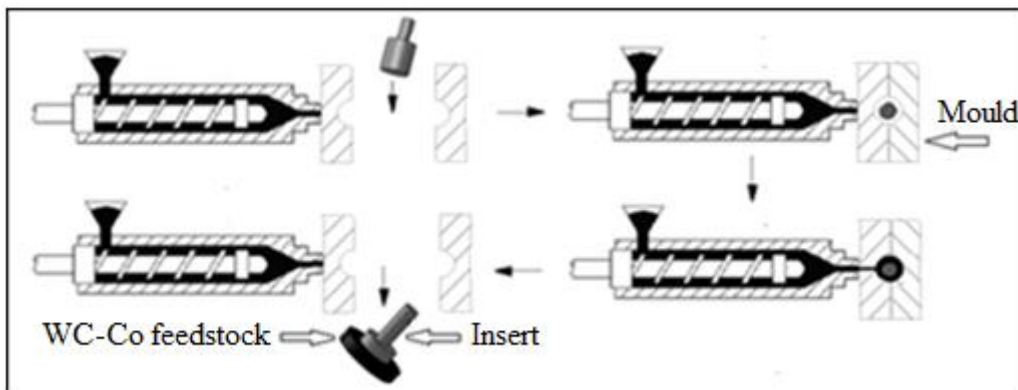


Figure 1. Inserted powder injection moulding process

Table 5. Injection parameters

Injection temperature	Injection pressure	Holding pressure	Injection speed	Mold temperature
200 °C	280 bar	80 bar	10 cm ³ s ⁻¹	60 °C

2.3. Debinding and sintering processes

Following the injection process test samples are taken into ethanol at 60 °C for 48 hrs and subjected to chemical debinding treatment. After debinding treatment , test samples were sintered in atmosphere controlled furnace (95% N₂ and 5% H₂) at 1200 °C for 240 min by taking into consideration the thermal characteristics of WC-Co (9%) and HSS materials.

2.4. Hardness measurement and EDS analysis

Hardness of the Nickel coating before sintering was measured under suitable conditions for coating at 3 different zones according to TS 6503 EN ISO 4516 standard. After sintering the micro hardness in the intermediate zone was measured as (HV 0.2) under 200 gf with 0.2 intervals. Scanning examinations were made by using LEICA light microscope and EDS analyses in JEOL JSM-6060LV scanning electron microscope (SEM).

3. Results and Discussion

In this study the part in Fig.2 was successfully produced by the inserted powder injection method. Joining was obtained in the intermediate zone by using 100 µm Ni interlayer between the M2 HSS Insert and WC-Co feed stock.

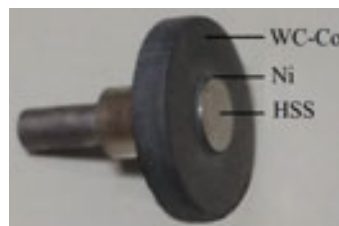


Figure 2. The part produced by the IPIM method

3.1. Examination of Ni interlayer before sintering

In this study for the inserted part production, Ni interlayer was used to increase the element diffusion created at the stage of sintering between the HSS and WC-Co feed stock. For this reason, Ni interlayer and insert inter surface was examined and controls were made whether porosities and separations (that may affect the diffusion adversely) exist or not. After creating of the Ni interlayer on the insert before sintering, top section of the samples were polished and insert/interlayer (Ni) zone was examined with an optical microscope. As a result of the examinations no defects such as porosity and separation were observed between the insert and interlayer (Fig. 3).

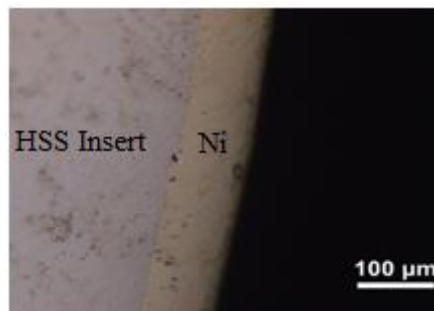


Figure 3. Ni interface on insert (HSS)

During sintering between the HSS insert and WC-Co, because of the element transitions, hardness of the Ni interlayer changes too [12,15]. For this reason, hardness of the interlayer was measured before sintering by coating the HSS insert with 100 µm Ni to make comparison before and after sintering. Hardness of the Ni interlayer obtained by Electrolytic coating method came out to be in the interval of 568,8-594,5 HV0.2 (Fig. 4).



Figure 4. Micro hardness of nickel coating before sintering

3.2. Element transitions in HSS/Ni/WC-Co intermediate zone

It is stated that in the spectral analysis made by the producing company (M2 HSS) consisted of 81.83% Fe and 6.19% W [16]. According to the analysis there are no Co and Ni in the HSS material (Table 1). In the intermediate zone of the HSS/Ni/WC-Co sample prepared for the study, EDS analysis was made at 20 points (Fig 5). The graph obtained from the EDS analysis is given in Fig.6. In the EDS analysis after sintering it was seen that the amount of Fe near the intermediate zone decreased to 60.07% average. Besides, while an average of 14.5% W diffusion occurred from WC-Co to the insert, Diffusion was an average of 4.27% in the case of Co. It was also observed from the EDS analysis that Ni amount diffused to HSS insert from the interlayer was an average of 2.02% whereas Ni amount diffused to WC-Co side was an average of 1.08 %.



Figure 5. Region where EDS analysis is made on the part

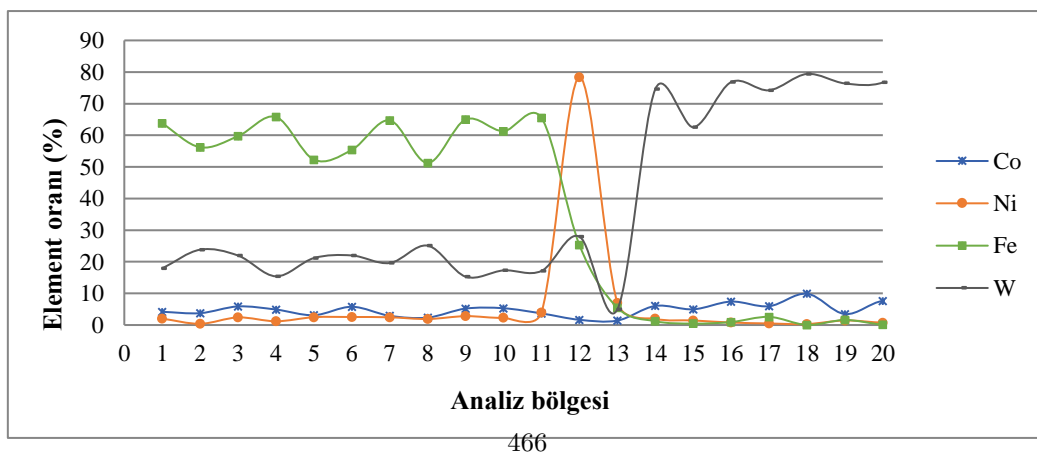


Figure 6. Profile of element concentration in intermediate zone (HSS/Ni/WC-Co, 1200 °C, 240 min.)

Ni is an interlayer material having a corrosion resistance and an excellent plasticity at high temperatures [17] and has a good solid dissociation in Fe and Co [18-19]. For this reason Ni interlayer could sufficiently diffuse to the steel side for joining. However existence of 9% Co in the WC feed stock makes the diffusion of Ni interlayer towards the WC-Co side easier. Even if Tungsten has a bigger atomic diameter and higher melting point than the other elements (Table.3) it was subjected to diffusion in a greater extent. In the diffusion mechanism, when the difference in the element amount between two materials increases concentration gradient becomes higher and element transition ratio increases too [20]. For this reason W diffused to HSS insert more than other elements.

3.3. Hardness profile of the intermediate zone

Following the sintering process at 1200 °C for 240 min, micro hardness measurement was made in the intermediate zone of WC-Co/Ni/HSS sample in 0.2 intervals to constitute the hardness profile (Fig. 7). In the catalogue of M2 HSS, material hardness is specified as 295 HV0.2 [16]. According to hardness measurements after sintering an average hardness value of HSS insert near the injected area was measured as 671 HV0.2. In the measurements made on the diameter center of HSS insert, hardness was 507 HV0.2. In spite of the fact that sintering was carried out at 95% N₂ and 5% H₂ control atmosphere and at 5°C/min cooling speed, hardness of M2 HSS insert increased approximately two times. It was determined that in the areas near the injected zone (close to outer section) hardness of HSS insert was even higher. In the EDS analysis an average diffusion of 14.5% W, 4.27% Co and 2.02% Ni was determined from WC-Co to HSS insert. Higher hardness of outer part of HSS insert was attributed to the diffusion of these elements to the insert during sintering. In some studies in which diffusion welding method was investigated it is stated that W, Ni and Co diffuse to the steel side and create an intermetallic compound and this way a solid solution is formed in the diffusion zone and for this reason in places near the intermediate zone hardness change [12-15].

In the WC-Co side it was seen that hardness value changed in between 737-1160 HV0.2 towards the outer part from the intermediate zone (Fig 7). In the outer part 0.8 mm away from the intermediate zone, hardness of WC-Co didnot change much and was around 1160 HV0.2. In literature it was stated that hardness of sintered WC-Co changed in the interval 1100-2000HV0.2 depending on Co ratio, powder size and sintering conditions [21-22]. In this study, sintering was made at 1200 °C. by taking into consideration the thermal properties of HSS insert. At this sintering temperature the hardness value obtained on WC-Co side was consistent with literature.

As for the hardness of Ni interlayer, it was measured as 247 HV0.2. It was observed that hardness of Ni interlayer decreased compared to the value beforehand.

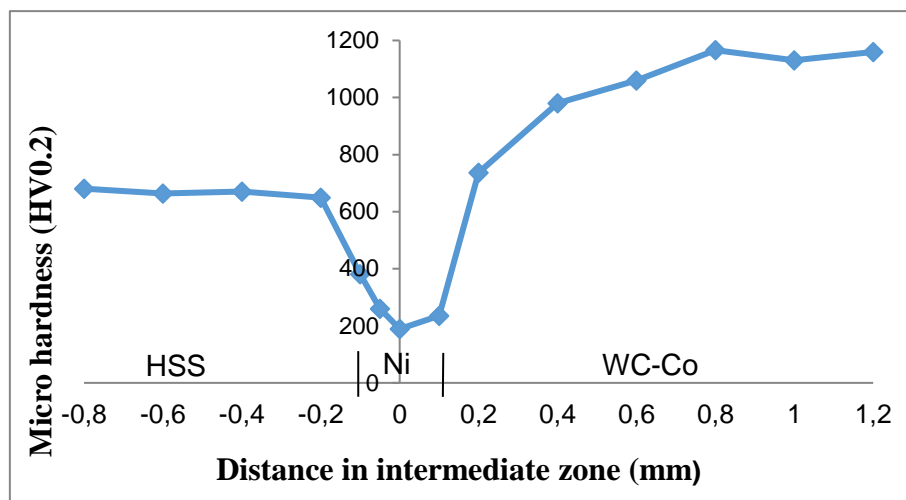


Figure 7. Hardness profile in intermediate zone (1200 °C, 240 min, 100 µm Ni)

4. Conclusion

The results obtained in this study are as follows:

- As a result of sintering process (by employing IPIM Method) made in the atmosphere controlled furnace at 1200 C for 240 min by using 100 µm Ni interlayer, parts of M2 HSS (outside) and WC-Co (inside) could be produced.
- When the intermediate surface which was created by 100 µm thick Ni interlayer (made by electrolytic coating) and insert was examined before sintering, no defects such as porosity and separation were observed.
- While before sintering, hardness of Ni interlayer was 581.65 HV0.2 average whereas after sintering was an average of 247 HV0.2.
- While the Ni amount diffused into HSS insert was 2.02%, the amount of Ni amount diffused into WC-Co side was an average of 1.08%.
- It was specified that there was a diffusion of 14.5% W, 4.27% Co and 2.02% Ni from the WC-Co side to HSS insert.
- Diffusion of elements such as W, Ni, Co into HSS insert increased the hardness in areas of insert close to intermediate zone.
- Diffusion of Ni element to the WC-Co side caused a drop of hardness in the sections of WC-Co near intermediate zone.

5. Acknowledgments

This research was sponsored by the Scientific and Technological Research Council of Turkey (TÜBİTAK), Project No: 115M437. The authors would like to express their sincere appreciation to TÜBİTAK organization and Selçuk University for their financial supports.

6. References

- [1] A. Safarian, M. Subaşı, Ç. Karataş: Reducing debinding time in thick components fabricated by powder injection molding, *International Journal of Materials Research*, 106, (2015), pp.527-531.

- [2] Ç. Karataş, S. Sarıtaş: Rheological Properties Of Mixed Gas Water Atomized Stainless Steel Powder MIM Feedstock, *The International Journal of Powder Metallurgy*, 37, (2001) pp. 39-44.
- [3] Ç. Karataş, S. Sarıtaş: Toz Enjeksiyon Kalıplama: Bir Yüksek Teknoloji imalat Metodu, *Gazi Ün. Mühendislik Mimarlık Fakültesi Dergisi*, 13, (1998), pp. 193.
- [4] A. Safarian, M. Subaşı, Ç. Karataş: The effect of sintering parameters on diffusion bonding of 316L stainless steel in inserted metal injection molding, *Int J Adv Manuf Technol*, 89, (2017), pp. 2165–2173.
- [5] A. Fayyaz, N. Muhamad, A.B. Sulong: Microstructure and physical and mechanical properties of micro cemented carbide injection moulded components, *Powder Technology*, 326, (2018), pp. 151-158.
- [6] A. Parasiris, K.T. Hartwig, M.N. Srinivasan: *Scripta Mater.*, 42, (2000), pp. 875–80.
- [7] X. Wang, Z.Z. Fang, H.Y. Sohn: Grain growth during the early stage of sintering of nanosized WC-Co powder, *Int. J. Refract. Met. Hard Mater.*, 26, (2008), pp. 232–241.
- [8] A. Passerone, M.L. Muolo: Metal-Ceramic Interfaces: Wetting and Joining Processes, *Int. J. Mater. Prod. Technol.*, 20, (2004), pp 420–439.
- [9] M. M. Atabaki: Recent Progress In Joining Of Ceramic Powder Metallurgy Products To Metals, *Association of Metall. Engineers of Serbia*, 16, (2010), pp. 255-268.
- [10] P.Z. Cai, D. J.Green, G. L. Messing: Constrained Densification of Alumina/Zirconia Hybrid Laminates, I: Experimental Observations of Preprocessing Defects, *J. Amer. Ceram. Soc.*, 80, (1997), 1929-1939.
- [11] D. F. Heaney, P. Suri, R. M. German: Defect-free sintering of two material powder injection molded components, *Journal of Materials Science*, 38, (2003), pp. 4869 – 4874.
- [12] Z. Zhonga, T. Hinokib, A. Kohyamab: Effect of holding time on the microstructure and strength of tungsten/ferritic steel joints diffusion bonded with a nickel interlayer, *Materials Science and Engineering A*, 518, (2009), pp. 167–173.
- [13] J.X. Zhang, R.S. Chandel, Y.Z. Chen, H.P. Seow: Effect of residual stress on the strength of an alumina–steel joint by partial transient liquid phase (PTLP) brazing, *Journal of Materials Processing Technology*, 122, (2002), pp. 220–225.
- [14] H. Chen, K. Feng, J. Xiong, Z. Guo: Characterization and stress relaxation of the functionally graded WC–Co/Ni component/stainless steel joint, *Journal of Alloys and Compounds*, 557, (2013), pp.18–22.
- [15] M.I. Barrena, J.M. Gomez, L. Matesanz: Interfacial microstructure and mechanical strength of WC–Co/90MnCrV8 cold work tool steel diffusion bonded joint with Cu/Ni electroplated interlayer, *Materials and Design*, 31, (2010), pp.3389–3394.
- [16] <http://www.osmanli-bohler.com/upload/pdf/S600DE.pdf>
- [17] J. Zhang, Y. Xiao, G.Q. Luo, Q. Shen, LM. Zhang: Effect of Ni interlayer on strength and microstructure of diffusion-bonded Mo/Cu joints, *Mater Letters*, 66, (2012), pp.113–116.
- [18] A. Prince, H. Okamoto: Handbook of ternary alloy phase diagrams, *Materials Park: ASM International*, (1995).

- [19] C.M. Fernandes, A.M.R. Seno: Cemented carbide phase diagrams: a review, *Int J Refract. Met. Hard. Mater.*, 29, (2011), pp.405–418.
- [20] A. Kurt: Toz Metalden Üretilen Bronz Yatağın Düşük Karbonlu Çeliğe Difüzyon Kaynağı ile Birleştirilmesi, Doktora Tezi, Fırat Üni. Fen Bilimleri Enst. Elazığ, pp. 25-48 (1996).
- [21] M.A. Xueming, J.I. Gang: Nanostructured WC±Co alloy prepared by mechanical alloying, *J Alloys and Compounds*, 245, (1996), pp.30-32.
- [22] A. Parasiris, K.T. Hartwig: Consolidation of advanced WC-Co powders, *International Journal of Refractory Metals & Hard Materials*, 18, (2000), pp.23-31.

Correspondence address

Dr. Harun KOÇAK
Cihanbeyli Vocational School Selcuk University Konya TURKEY
Tel: +90 3326734089
E-mail: harunkocak@selcuk.edu.tr

Dr. Harun KOÇAK, was born in 1985. He completed his undergraduate studies in 2007, his master's degree in 2011 and his doctorate in 2018 at Gazi University. He is still working as a lecturer at Selçuk University Cihanbeyli Vocational School. Academic studies are focused on machining techniques, powder injection molding and coating techniques.

Dr. Mehmet SUBAŞI, was born in 1979. He completed his undergraduate studies in 2001, his master's degree in 2006 and his doctorate in Gazi University in 2015. He is still working as a lecturer at Gazi University Technical Sciences Vocational School. Academic studies have focused on plastic injection molding, powder injection molding and sheet metal molding techniques.

Assoc. Prof. Dr. Çetin KARATAŞ was born in 1958. He completed his master's degree in 1992 and his doctorate in Gazi University in 1998. Despite the fact that manufacturing engineering works in different areas, concentrates on powder injection molding. He is a board member of Turkish Powder Metallurgy Association.

FARKLI TOZ METAL MALZEMELERİN MİKRODALGA VE İNDÜKSİYON ISITMA İLE BİRLEŞTİRİLEBİLİRLİĞİ

İrem Burcu Algan^{1,a}, Yasemin Aksu^{1,b}, Yusuf Çiftçi^{1,c}, Nurcan Ünlü^{1,d},
Ramazan Çıtak^{1,e}, Yusuf Özçatalbaş^{1,f}, Adem Kurt^{1,g}

¹Department of Metallurgical and Materials Engineering / Faculty of Technology / Gazi University

^airembalgan@gazi.edu.tr, ^byasemindundar@gazi.edu.tr,

^cyusuf.cift95@gmail.com ^dnlunurcan92@gmail.com, ^ecitak@gazi.edu.tr, ^fyusufoz@gazi.edu.tr, ^gademkurt@gazi.edu.tr,

Özet

Sinter lehimlemede indüksiyon ve mikrodalga uygulamaları işlem süresini önemli oranda azaltır ve böylelikle enerji açısından verimli bir süreç elde edilebilir. Bu çalışmada, tek yönlü soğuk pres ile üretilen farklı toz metal malzemelerin sinterlehim ile birleştirilebilme özellikleri incelenmiştir. Sırasıyla ortalama parçacık boyutu 20 µm ve 40 µm olan bakır ve paslanmaz çelik tozları 700, 800 ve 900 MPa basınçla preslenerek 12 mm çapında ve 3 mm yüksekliğinde numuneler üretilmiştir. İndüksiyon ile ısıtma 450°C sıcaklık ve 2900 Hz frekansta Argon atmosferinde gerçekleştirilirken, mikrodalga ısıtma 450°C sıcaklık ve 900 W güç kullanılarak atmosfer ortamında gerçekleştirilmiştir. Mikroyapı analizleri optik mikroskop ile yapılırken, mekanik analizler mikrosertlik testi (HV 0,3) ile yapılmıştır.

Anahtar Kelimeler: Mikrodalga, indüksiyon, toz metalürjisi, bakır, paslanmaz çelik

1. Giriş

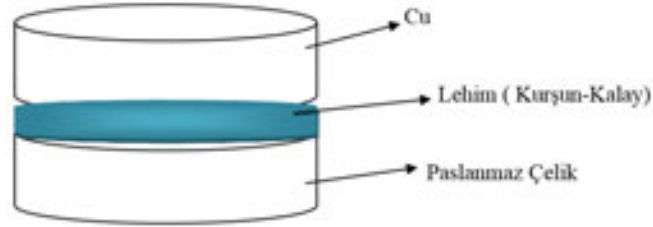
Toz metalürjisi, 20. yy'da ortaya çıkmış ve günümüzde hızla gelişmektedir. Toz metalürjisi ile üretilen parçalar pek çok değişik alanda kullanılmaktadır. Dişliler, kendinden yağlamalı burçlar, elektrik kontakları, sert kesici takım uçları vb. birçok parça toz metalürjisi yöntemi ile üretilmektedir [1,2].

Toz metalürjisinde üretilecek uygun bileşime sahip olan tozlar, ilk işlem olarak uygun bir kalıp içinde preslenmektedir. Presleme sonrasında en önemli işlem olan sinterleme işlemi, ergime sıcaklığı altında ve genellikle koruyucu atmosferde gerçekleştirilir. Bu işlemde; parça, fırın içine konur ve korozyondan korunması için fırın içerisine koruyucu gaz gönderilir. Fırındaki parçanın içindeki yağlayıcıların temizlenmesi için numuneler ön ısıtmaya tabi tutulur. Oksit indirgenmesinin ardından fırının sıcak bölgesinde sinterleme işlemi gerçekleşir ve fırından çıkan parça soğumaya bırakılır [3]. Hızlı sinterleme teknikleri, sinterleme süreleri kısaltılarak enerji ve zaman tasarrufu sağlanabilmektedir. Örneğin indüksiyon sinterlemede, işlem görece malzeme değişken akım taşıyan iletken bobin ile bir seferde ısıtılır. Isı transferi, diğer ısıtma sistemlerinden 3000 kez daha iyidir [4]. Diğer yandan mikrodalga sinterlemede ısı, verilen elektromanyetik enerjinin doğrudan malzemeyle etkileşimi sonucunda açığa çıkması sebebiyle hızlı ve verimli şekilde numunenin ısıtılması sağlanır [5]. Sinterleme ve lehimle işlemi eş zamanlı gerçekleştirildiğinde işlem süresi kısaltılarak zamandan ve enerjiden tasarruf edilebilir. Ayrıca

bueş zamanlı işleme hızlı ısıtma tekniklerinin uygulandığında, homojen bir ısı transferinin gerçekleştirilmesi ile ürün kalitesinin artırılabilir.

2. Deneysel Çalışmalar

Bu çalışmada, 20 ve 80 µm toz tane boyut aralığında olan Cu ve SS (paslanmaz çelik) tozları hassas terazide her birinden 3gr olacak şekilde tartıldıktan sonra 12 mm çapında ve 3 mm uzunluğundaki kalıpta, 700, 800 ve 900 MPa basınçlarda soğuk olarak preslenmiştir. Üretilen numunelerin ham yoğunlukları hesaplandıktan sonra, yüzeyleri ince zımpara yardımıyla temizlenmiş ve arayüze Pb-Sn (%40 Pb) (lehim) tozu homojen bir şekilde yerleştirilmiştir (Şekil 1).



Şekil 1. Cu-paslanmaz çelik numunelerin mikrodalga lehim işleminin şematik görünüşü

Üretilen iki set numuneden 1. grup numunelere HAMILab-DS1500 markacihazda mikrodalga sinter lehim; 2. grup numunelere ise Reterm marka cihazda indüksiyon sinter lehim işlemi uygulanmıştır. Mikrodalga sinter lehimleme işlemi, 900 watt güç ve 450 °C sıcaklıkta 5, 10 ve 15 dakika sürelerde; indüksiyon sinter lehim işlemi ise Ar atmosferinde, 450 °C sıcaklık ve 2900 Hz frekansta 5 dakikada gerçekleştirilmiştir. Sinterleme ve eş zamanlı lehimleme işlemi için kullanılan mikrodalga fırın ve indüksiyon ısıtma düzeneği Şekil 2' de verilmiştir.

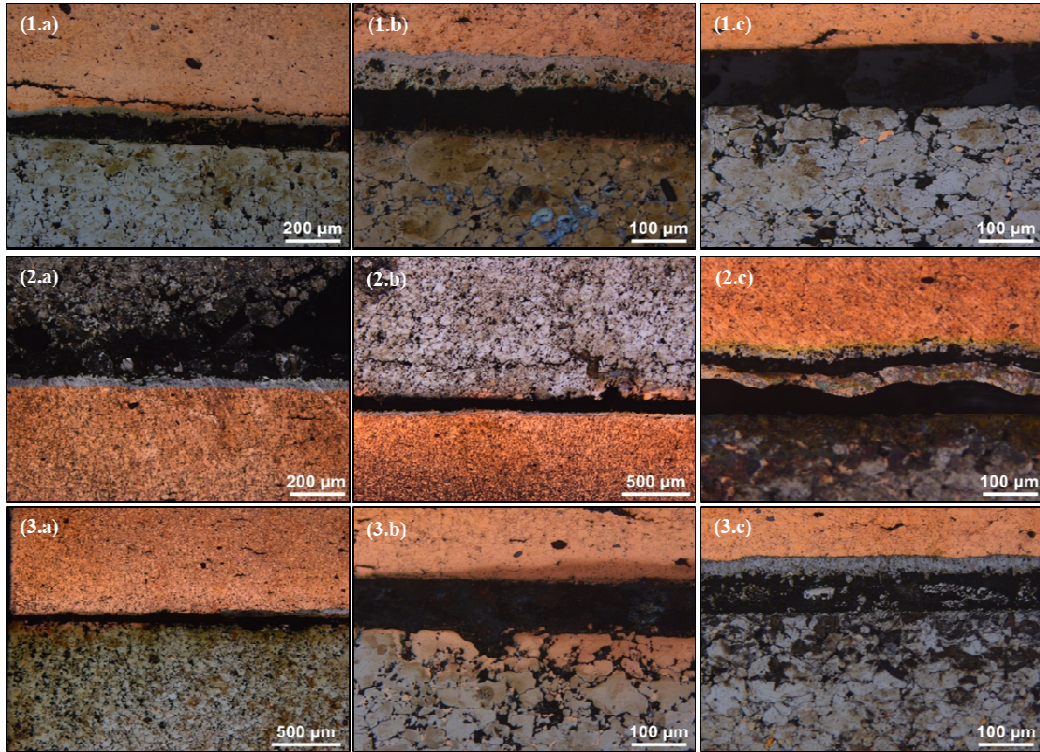


Şekil 2.(a) Mikrodalga fırın ve (b) indüksiyon ısıtma düzeneği

Sinterlehimlenen numunelerin Leica DM5000M model optik mikroskopta mikroyapı analizi ve Shimadzu HMV-2 model mikrosertlik cihazında sertlik testleri yapılmıştır.

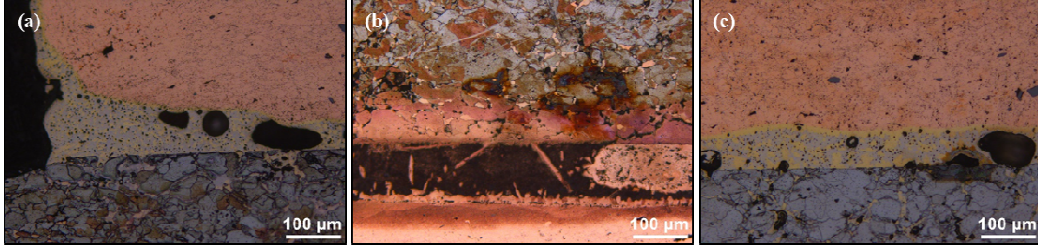
3. Sonuçlar ve Tartışma

Şekil 3'te Cu ve SS parçaların değişik basınç ve sürelerde birleşme mikroyapıları verilmiştir. Birleşme ara yüzeyinde lehim tabakasının artan sinterleme süresine bağlı olarak difüzyon ve buharlaşma yoluyla ara yüzeyden genellikle Cu tarafına ince bir film halinde geçiş bölgesi oluşturduğu gözlenmektedir. Birleşme esnasında oluşan bağ kuvvetinin etkisiyle en düşük basınçta preslenen numunenin birleşme ara yüzeyine paralel katmanlı çatlak oluştuğu görülmektedir. Bunun bakırın genişlemesi ve ara yüzey lehim bölgesinin Cu tabakayı SS tarafına çekme gerilmeleri sonucu oluştuğu düşünülmektedir. Artan sinterleme süresiyle özellikle Cu tarafında birleşme ara yüzeyine paralel mikro çatlakların meydana geldiği gözlenmiştir. Bununla beraber 796 ve 884 MPa basınçta preslenmiş SS numunelerde, artan sinterleme süresinin tane irileşmesine yol açtığı ve taneler arasında gözeneklerin irileşmesine neden olmuştur. 884 MPa'da 10 dakikasinterlenmiş numunenin ara yüzeyinde lehim tabakası katmanlı şekilde Cu tarafında bir geçiş bölgesi; SS tarafında ise Cu+lehim malzemesinden oluşan dalgalı bir birleşme tabakası oluşturmuştur. Sinterleme süresinin artmasıyla 15 dakika sinterleme süresinde Cu ve SS ara yüzeyinde homojen denebilecek bir lehim birleşme bölgesi meydana gelmiştir.



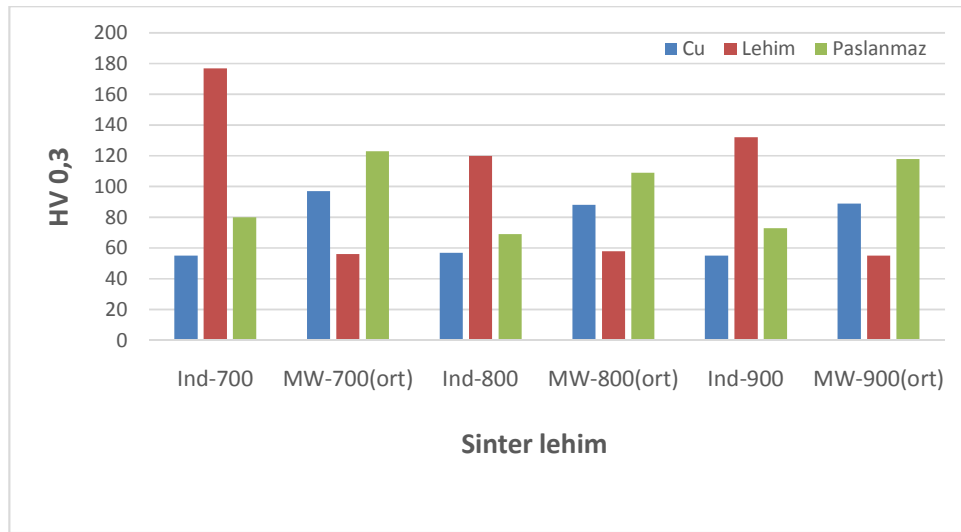
Şekil 3. (1) 700 MPa, (2) 800 MPa ve (3) 900 MPa basınçta preslenen Cu ve SS parçaların (a) 5, (b) 10 ve (c) 15 dakikada mikrodalga ile lehimlenen bölgelerinin mikroyapıları.

Şekil 4' te indüksiyon ısıtma ile lehimlenen malzemelerin mikroyapısı verilmiştir. Buna göre, 700 ve 900 MPa basınçla preslenen numunelerin birleşme arayüzeyinde başarılı şekilde bağlanma görülmüş, ancak her üç numunenin de arayüzey bölgesinde gaz boşlukları ve oksit tabakaları tespit edilmiştir.



Şekil 4. (a) 700 MPa, (b) 800 MPa ve (c) 900 MPa basınçta preslenen Cu ve SS parçaların indüksiyon ısıtma ile elde edilmiş lehim bölgelerinin mikroyapıları.

Şekil 5'te, hem indüksiyon hem de mikrodalga ısıtma ile lehimlemede, toz malzemelerin presleme basıncı arttıkça sertliğin azaldığı görülmektedir. Bu duruma, pres basıncının artması ile birlikte artan sinterleme süresinin sebep olduğu düşünülmektedir. İndüksiyonla ısıtılarak lehimlenen malzemelerde lehim bölgesi en yüksek sertliğe sahipken, mikrodalga ile lehimlenen numunelerin lehim bölgesi düşük sertliktedir.



Şekil 5. İndüksiyon ve mikrodalga ısıtma ile lehimlenen Cu-SS malzemelerin sertlik değerleri

4. Sonuç ve Öneriler

Mikrodalga ve indüksiyon ısıtma ile sert lehimleme yapılan bu çalışmada:

- Farklı basınçlarda preslenen toz metal malzemelerin, mikrodalga ve indüksiyon gibi hızlı ısıtma yapabilen sistemlerle sert lehimlenebildiği görülmüştür.

- Yüksek presleme basıncı ve hızlı ısıtma etkisi, lehim arayüzeylerinde presleme yönüne dik çatlaklar oluşturmuştur.
- Lehimleme işleminin atmosfer korumalı ortamda yapılması, gaz boşluklarının ve kesintili arayüzey bağlantılarının önlenebileceği düşünülmektedir.

5. Kaynaklar

1. F. Nutku: Toz Metalurjisi ile Üretilen Parçaların Tahribatsız Muayenesi, Yüksek Lisans Tezi, Yıldız Teknik Üniversitesi Fen Bilimleri Enstitüsü, İstanbul, (2003).
2. Sarıtas, S., "Powder I. Ulusal Toz Metalurjisi konferansı Bildiri kitabı", Gazi Üniversitesi İletişim Fak. Matbaası, Ankara. (1996).
3. Ersümer, A: Toz Metalurjisi Sert Metal Sinterleme, İstanbul Üniversitesi Matbaası, İstanbul, (1970).
4. Randal M. German, "Sintering theory and practice" The Pennsylvania State University Park, Pennsylvania, A Wiley – Interscience publication, John Wiley & Sons, INC., USA, pp. 313-362, 373-400, 403-420, 1996.
5. Yıldız, K. and Alp, A., "Using of Microwave in Metallurgical Processes", Metalurji TMMOB, 24(125): 1300-4824, (1999).

CORRESPONDENCE ADDRESS: İrem Burcu Algan, Gazi University Faculty of Technology, Department of Metallurgy & Material Engineering, 06810, Teknikokullar-Ankara, +903122028799, irembalgan@gazi.edu.tr

SHORT BIOGRAPHIES

İrem Burcu ALGAN – İrem Burcu Algan was born in Ankara in 1989. She was graduated from Karadeniz Technical University, Faculty of Engineering, Department of Metallurgical and Materials Engineering in 2012 then completed her master's degree in Gazi University Graduate School of Natural Applied Science Metallurgy and Material Engineering Department in 2015. She works as a research assistant in Gazi University Technology Faculty since February, 2013 in addition continue her doctorate in Gazi University since September, 2015.

Yasemin AKSU – Yasemin AKSU was born in Ankara in 1989. She was graduated from Middle East Technical University (METU), Faculty of Engineering, Department of Metallurgical and Materials Engineering in 2012 then completed her master's degree in METU Graduate School of Natural Applied Science Metallurgy, Department of Metallurgical and Materials Engineering in 2015. She works as a research assistant in Gazi University Technology Faculty since February, 2013 in addition continue her doctorate in Gazi University Graduate School of Natural Applied Science, Department of Metallurgical and Materials Engineering since September, 2016.

Yusuf Çiftçi –Yusuf Çiftçi was born in Ankara in 1992. He was graduated from Gazi University, Faculty of Technology, Department of Metallurgical and Materials Engineering in 2018.

NurcanÜnlü–NurcanÜnlüwas born in Konya in 1992.She was graduated from Gazi University, Faculty of Technology, Department of Metallurgical and Materials Engineering in 2018.

INVAR36 ÇELİĞİNİN MIG KAYNAK YÖNTEMİ İLE KAYNAKLANABİLİRLİĞİNİN ARAŞTIRILMASI

Selçuk Tombul^{1,a}, Mehmet AKKAŞ^{2,b}, Mustafa BOZ^{1,c}

¹İmalat Mühendisliği Bölümü / Teknoloji Fakültesi / Karabük Üniversitesi

²Cide Rifat Ilgaz Meslek Yüksekokulu / Kastamonu Üniversitesi

^aselcuk_tombull024@hotmail.com, ^bmehmetakkas@kastamonu.edu.tr, ^cmboz@karabuk.edu.tr

Özet

Bu çalışmada, gaz metal ark (MIG) kaynak yöntemi ile Invar36 (ASTM A36) çelik malzemesinin kaynaklanabilirliği araştırılmıştır. Bu amaçla, Invar36 çelik malzemesine talaşlı imalat yöntemi ile x ve v kaynak ağızı açılmış ve seramik altlık kullanılarak fikstür üzerine yerleştirilerek ilave metal (AWS 5.14 ERNi-1) ile birleştirme işlemi yapılmıştır. X kaynak ağızı geometrisine sahip numuneler için farklı parametreler uygulanarak toplamda 19 paso, v kaynak ağızı geometrisine sahip numuneler için ise 18 paso uygulanmıştır. Kaynaklı numunelerin kaynaklanabilirliğini tespit etmek amacıyla numunelere tahribatlı ve tahribatsız muayene yöntemlerinden eğme testi, sertlik analizi, görsel muayene ve sıvı penetrant muayenesi yapılmıştır. Deneysel sonuçlara göre; TS EN ISO 15614-1:2004/A2:2012 test değerlendirme standardına göre kaynaklı numunelerin 180° eğme testlerinde kaynaklı bağlantı bölgelerinde herhangi bir tahribat görülmemiştir. Aynı değerlendirme standardına göre X ve V kaynak ağız geometrisine sahip numunelerin ana malzeme, ITAB ve kaynak bölgelerinden alınan sertlik sonuçlarına göre kaynak ağızı geometrisinin sertliğe önemli bir etkisinin olmadığı tespit edilmiştir. Görsel muayene sonuçlarına göre, bütün kaynaklı numunelerin birleşme bölgeleri TS EN ISO 5817 standardına göre değerlendirilmiş ve yapısal bir bozukluk olmadığı tespit edilmiştir. TS EN ISO 23277 değerlendirme standardına göre yapılan sıvı penetrant muayenesi sonucu numunelerde herhangi bir çatlağa, yanma oluşu ve gözeneğe rastlanmamıştır.

Anahtar kelimeler: MIG kaynağı, Invar36, Kaynak ağızı

1. Giriş

Gaz metal ark kaynağı (GMAK), endüstride demir ve demir dışı malzemelerin kaynağında en çok kullanılan kaynak yöntemidir [1]. Ergitmeli bir kaynak yöntemi olan bu kaynak yöntemi hem bir üretim hem de bir tamir yöntemi olarak endüstride yerini almıştır [2-4]. Yüksek kaynak hızı, otomatik olarak uygulanabilmesi [5], yüksek metal biriktirme oranı, curuf olmayışı ve bütün pozisyonlarda kolaylıkla yapılabilmesi yöntemin önemli avantajlarından [6].

Invar 36 malzeme ya da yaygın olarak kullanılan diğer adıyla Nilo Alloy 36 malzeme bir nikel demir alaşımı malzemesidir. Invar, aynı zamanda FeNi36 olarak bilinen bir nikel-demir alaşımı olan çok düşük termal genleşme katsayısına sahip önemli bir metaldir. Bu malzeme temel olarak % 36 nikel ve % 64 demir elementi içermektedir. Bu alaşımın en temel özelliği az genleşmesidir ve bu sebeple birçok ölçüm cihazında ve kontrol cihazlarında kullanılmaktadır. Çok az genleşmesi sebebiyle havacılık gibi alanlarda sıkça kullanılmaktadır. Ayrıca çeşitli kompozit malzemelerde, referans uzunluklarında, mezüre ve metre ölçüm cihazlarında, yüksek hassasiyet gerektiren parçalarda, termostat millerinde oldukça sık kullanılmaktadır. Çelik malzemeler içerisinde malzeme numarası 1.3912 olarak yer alan bu malzeme aynı zamanda UNS K93600 ve UNS K93601 olarak da literatürde gösterilmektedir [7].

Invar 36 telekomünikasyon, havacılık ve uzay mühendisliği alanlarında, dolayısıyla ısı değişimine bağlı ölçüsel değişikliklerin en aza indirilmesi gereken yerlerde kullanılır [8]. Invar 36 Boeing

D33028 ve ASTM F1684 gereksinimlerine uygun olarak üretilmektedir. Bundan dolayı daha iyi kaynak kabiliyeti için kimyasal bileşimindeki sülfür ve fosfor sınırlandırılmıştır. Invar 36 özellikle kompozit kalıp üretimi için önemli bir malzemedir, bu amaçla da yüksek mukavemet ve boyutsal kararlılık özelliklerini bir arada taşımaktadır. Bu nitelikler, kalıp tasarımcılarına hafiflik ve etkili hava akışı için en iyi şekilde getirilebilecek alt yapı tasarımlarında Invar 36 malzemesini tercih etmelerine olanak sağlamaktadır. Invar 36, aynı zamanda karbon fiberin yataklanıp, reçine kalıbın içine enjekte edildiği, reçine enjeksiyonlu kalıplama tekniği ile üretilen kalıplarda da kullanılmaktadır [9-12].

Invar malzemenin işlenmesi nispeten zordur. Düşük kesme hızlarında talaş kaldırılarak şekillendirme yapılması tavsiye edilir. Bu durum şekillendirme zamanının uzamasına ve maliyetin artmasına neden olur.

Invar 36 malzemesi birçok alanda kullanılan pahalı bir malzemedir. Bu malzemenin ergitmeli kaynak yöntemleri ile kaynaklanabilirliği literatürde oldukça sınırlıdır. Bu amaçla, bu çalışmada gaz metal ark kaynak yöntemi ile Invar36 çelik malzemesinin kaynaklanabilirliği araştırılmıştır.

2. Deneysel Çalışmalar

Bu çalışmada, 500x300x28 mm ebatlarında ve Tablo 1'de kimyasal bileşimleri verilen Invar 36 çelik levhalar gazaltı ark kaynak yöntemi ile birleştirilmişlerdir. Birleştirme işlemlerinde literatürde verilen bilgiler doğrultusunda, farklı metallerin kaynaklı bağlantılarında tavsiye edilen ve kimyasal bileşimi Tablo 2'de verilen 1,2 mm AWS 5.14 ERNi-1 ilave metal (tel) ve koruyucu gaz olarak da saf argon gazı (EN ISO 14175 % Ar) kullanılmıştır. Kaynak işlemleri FRONIUS WPuls Synergic AV-4000 tip yeni nesil kaynak makinesinde operatör yardımıyla yapılmıştır. Kaynak esnasında kullanılan kaynak parametreleri X ve V kaynak ağız geometrileri için PA kaynak pozisyonunda Tablo 3'de verilmiştir.

Tablo 1. Invar36 alaşım malzemesinin kimyasal bileşimi.

Element	Fe	Ni	Mn	Si	Sn	Cu	Al	W
İçerik (%)	60,77	38,654	0,350	0,137	0,038	0,024	0,016	0,012

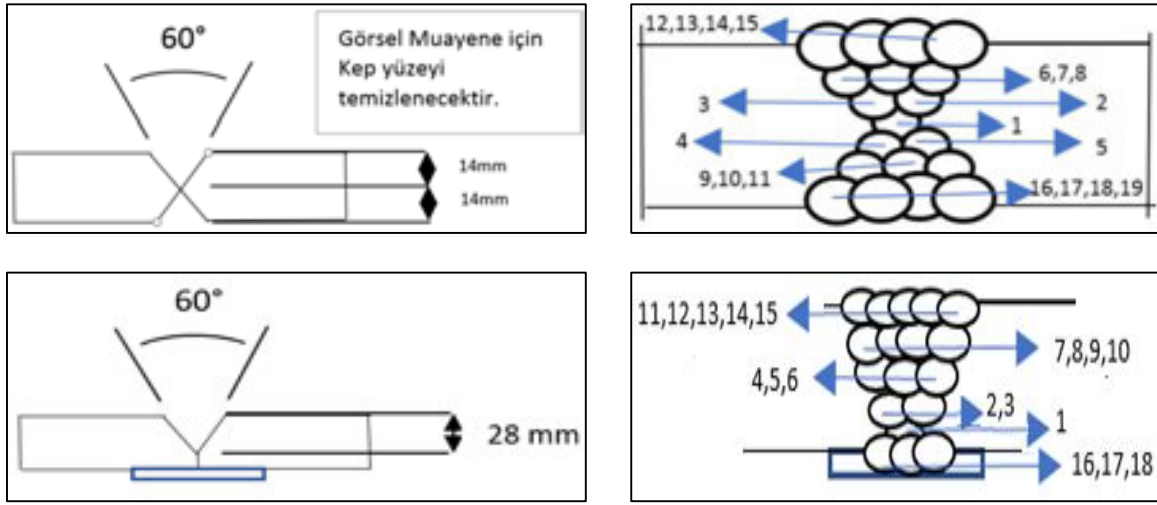
Tablo 2. AWS 5.14 ERNi-1 ilave metalin kimyasal bileşimi.

Element	Ni	Co	Cr	Fe	Mn	Mo	Ti	Cu	W	Al	Diğer
İçerik (%)	Kalan	27-32	26-29	3.5 max	1 max	0.70 max	0.2-0.6	0.5 max	0.5 max	0.4 max	0.51

Tablo 3. Kaynak Parametreleri.

Paso	Dolgu Malzemesi (mm)	Akım (A)	Voltaj (V)	Akım Tipi ve Kutuplama	Tel Besleme Hızı (m/dk)	Kaynak Hızı (mm/s)
1	Ø 1,2	200-220	23-25	DC (+)	15-17	10-12
2,3	Ø 1,2	220-230	23-24	DC (+)	13-15	8-12
4-6	Ø 1,2	220-230	23-24	DC (+)	13-15	8-12
7-10	Ø 1,2	180-200	20-21	DC (+)	11-13	8-12
11-15	Ø 1,2	170-190	19-20	DC (+)	10-12	8-12
16-19	Ø 1,2	180-200	20-21	DC (+)	11-13	8-12

X ve V kaynak geometrileri için bağlantı dizaynı ve paso sıralaması Şekil 1'de gösterilmiştir. Çalışmalarda kullanılan kaynak parametre değerlerine, yapılan ön çalışmalar sonucu karar verilmiştir. Kaynak işlemi biten numuneler açık havada soğumaya bırakılmıştır. Kaynak sonrası kaynaklı numunelerden elde edilen makro görüntüler Şekil 1'de verilmiştir.



Şekil 1. Numunelerin bağlantı dizaynı ve paso sıralamaları.

Şekil 2'de X ve V kaynak ağzı açılarak birleştirilmiş kaynaklı numune görselleri verilmiştir.



Şekil 2. X ve V kaynak ağzı geometrisine sahip numunelerin görüntüsü.

Kaynak işlemi tamamlanan numunelere eğme testi uygulamak amacıyla TS EN ISO 5173:2010 standardına göre numune kalınlığı 10 mm ve kaynak yönüne 90° olacak şekilde 4 adet numune

hazırlanmıştır. Hazırlanan numuneler WEW 1000D Model, 1000 kN kapasiteli Universal Test cihazında ve oda sıcaklığında test edilmişlerdir. Hazırlanan iki numune kep yönüne, diğer iki numune ise kök paso yönüne 180° eğme yapılmıştır. Eğme testi için mesnetler arası mesafe 65 mm ve mandrel çapı ise 40 mm olarak seçilmiştir.

Kaynaklı numunelerin sertlikleri SHBRV-187.5 Digital Display Universal Hardness Tester marka cihaz ile TS EN ISO 9015-1:2011 standardına göre HV cinsinden ölçülmüştür. Sertlik ölçümlerinde 1000 g yük kullanılmış ve ana malzeme bölgesinden 9 adet, ITAB'dan 15 adet ve kaynak metalinden ise 9 adet ölçüm alınarak ortalamaları alınmıştır.

Şekil 2'de verilen X ve V kaynak ağız geometrisine sahip numunelerin görsel muayenesi TS EN ISO 5817 standardına göre 2500 Lux ışık şiddetinde Min 30°-Max 600 mm bakış doğrultusunda el feneri, çelik cetvel, kaynak kumpası, bridge cam kumpas ve büyüteç yardımıyla yapılmıştır.

Öncelikle Penetrant testi yapılacak numune yüzeyi asetonla ve yumuşak bir bez ile ön temizliğe tabi tutulmuştur. Muayeneyi gerçekleştirebilmek amacıyla gerekli aydınlatma şiddeti Lux Meter cihazında 2500 görünür ışık şiddetine ulaştıktan sonra numune yüzeyi göz ile kontrol edilmiştir. Kontrolü yapılan yüzeye renkli kontrast penetrant sıvısı (CR 50) uygulanarak 15 dakika beklemeye bırakılmıştır. Bekleme süresinin dolmasının ardından fazla penetrant çözücü sprey (CR 60) yardımıyla temizlendikten sonra geliştirici (CR 70) adımı verdiğimiz sprey yüzeye uygulanarak, kusurların olup olmadığı muayene edilmiştir.

3. Deneysel Sonuçlar ve Tartışma

3.1. Eğme Testi

Kaynaklı numunelerin kaynaktan sonra şekillendirilerek kullanılabileceğini belirlemek için eğme testleri yapılmış ve eğme numune görüntüleri Şekil 3'de verilmiştir.

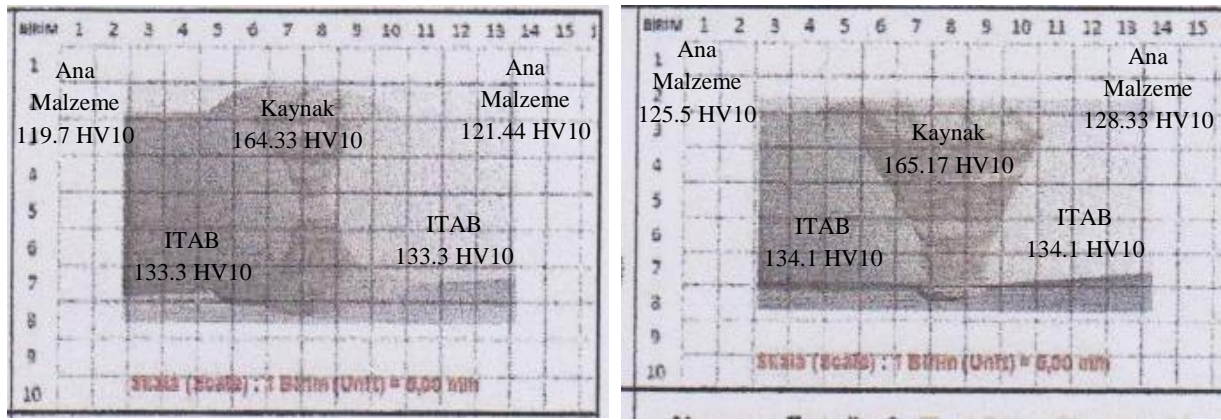


Şekil 3. Eğme testine tabi tutulan numuneler

Şekil 2’de verilen eğme test numuneleri incelendiğinde gerek X kaynak ağzı açılarak birleştirilmiş numune gerekse V kaynak ağzı açılarak birleştirilmiş numune eğme yüzeylerinde herhangi bir kaynak hatasına (çatlak, yırtılma vb) rastlanılmamıştır. Özellikle V kaynak ağzı açılmış kaynaklı numunenin kök eğmesi diğer eğmelere göre daha riskli olduğu düşünülerek bu numuneler daha hassas incelenmiş ve eğmelerin hatasız olduğu sonucuna varılmıştır.

3.2. Sertlik Testi

Kaynaklı numunelerin kaynak bölgesinde meydana gelen değişimleri incelemek için sertlik testi uygulanmıştır. Uygulanan test sonucu elde edilen makro ölçüm görüntüleri Şekil 4’de verilmiştir.



Şekil 4. X ve V kaynak ağzı geometrisine sahip numunelerden alınan sertlik ölçüm sonuçları.

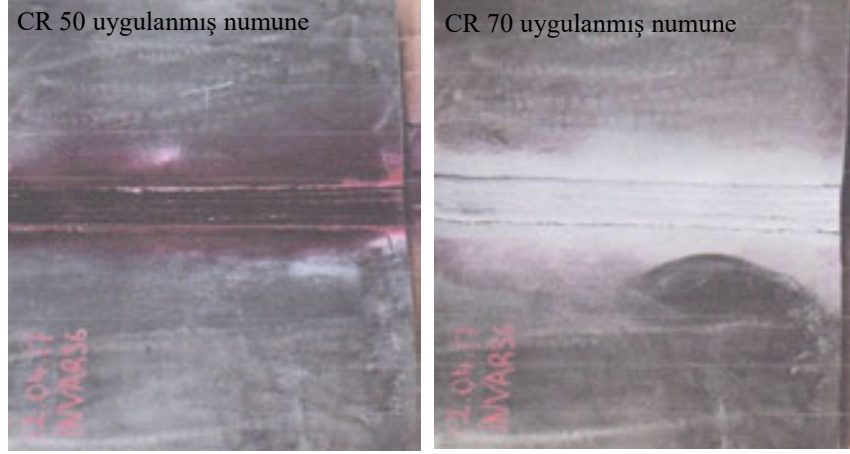
Şekil 3 incelendiğinde hem X kaynak ağzı açılarak birleştirilmiş numunenin hem de V kaynak ağzı açılarak birleştirilmiş numuneden en yüksek sertlik değerleri kaynak metalinden ölçülürken onu sırasıyla ITAB ve ana malzeme takip etmektedir. X ve V kaynak ağzıları açısından değerlendirildiğinde her üç ölçüm bölgesinde de (ana malzeme, ITAB ve kaynak metali) sonuçların birbirlerine son derece yakın olduğu tespit edilmiştir.

3.3. Görsel Muayene

Kaynaklı numunelerin görsel muayeneler (gözle muayene) gerekli teçhizatlar ve gerekli şartlar altında gerçekleştirilmiş ve kaynak yüzeylerinde herhangi bir yüzey hatasına (eksik veya fazla kaynak kepi, kökte sarkma, yüzey pasolar arası bindirme hatası vb) rastlanılmamıştır.

3.4. Penetrant Testi

Kaynaklı numunelerin yüzey kusurlarını hassas belirleyebilmek için numunelere sıvı penetrant testi uygulanmıştır. Kaynaklı numunelere uygulanan Penetrant testi sonrasında numunelerin görüntüleri Şekil 5’de görülmektedir.



Şekil 5. Renkli kontrast ve geliştirici uygulanan numunelerin görüntüleri.

Şekil 5’deki numuneler floraşal ışık altında incelenmiş ve herhangi bir yüzey kaynak hatasına (gözenek, gaz boşluğu, yenme olukları, makro ve mikro çatlak, yetersiz ergime vb) rastlanılmamıştır.

4. Sonuçlar

- ✓ Kaynaklı numunelere, her iki yöne uygulanan eğme testlerinde (kök ve kep eğme), kaynaklı numuneler 180°’ye kadar sorunsuz bir şekilde eğilebilmiştir.
- ✓ Tüm numunelerde en yüksek sertlik değerleri kaynak metalinden, en düşük sertlik değerleri ise ana malzemelerden ölçülmüştür.
- ✓ Kaynaklı numunelere gözle yapılan muayene sonucunda, kaynak yüzey hatalarına (eksik veya fazla kaynak kepi, kökte sarkma vb) rastlanılmamıştır.
- ✓ Kaynaklı numunelere yapılan sıvı penetrant testi sonucunda, kaynak bölgesinde, çatlak, gözenek, gaz boşluğu vb kaynak hatalarının bulunmadığı tespit edilmiştir.

5. Kaynaklar

[1] Praveen P., Yarlagadda P.K.D.V. ve Kang M.J., "Advancements in pulse gas metal arcwelding", Journal of Materials Processing Technology, Cilt 164-165, 1113-1119, 2005.

- [2] Suban M., ve Tusek J., "Dependence of Melting Rate in MIG/MAG Welding on the Type of Shielding Gas Used", Journal of Materials Processing Technology, Cilt 119, No 1-3, 185-192, 2001.
- [3] Gülenç B, Candan İ. ve Kahraman N, "Mig-Mag Kaynağı ile Birleştirilen Boruların Tahribatlı ve Tahribatsız Muayenesi", Gazi Üniversitesi Mühendislik Mimarlık Fakültesi Dergisi, Cilt 21, No 4, 631-637, 2006.
- [4] Absi Alfaro S.C., Carvalho G.C. ve Melo Junior S.A., "Stand offs indirect estimation in GMAW", Journal of Materials Processing Technology, Cilt 157-158, 3-7, 2004.
- [5] Kaçar R., ve Kökemli K., "Effect of Controlled Atmosphere on the MIG-MAG Arc Weldment Properties", Materials & Design, Cilt 26, No 6, 508-516, 2005.
- [6] Raymond J. S., Essentials of Welding, Glencoe Publishing Company, California, 327-334, 1984.
- [7] <http://www.muhandisalemi.com/invar-metalifeni36-ve-kullanim-alanlari/>
- [8] Lement , B. S., Averbach, B. L. and Cohen, M., "The Dimension Stability of Invar, Trans. ASM, 43, 1071, 1950.
- [9] Jacobs, S.F., "Dimensional Instability of Invars, Applied Optics, 1984
- [10] Yoder , Jr. P. R., Opto-Mechanical Systems Design, Third Edition, CRC Press, 2006.
- [11] Montgomery, D.C., Design and Analysis of Experiments, John Wiley & Sons, Toronto Singapore, 1991.
- [12] Bağcı, E., Kurt, M., Bakır, B., Basmacı, G., Aslan, E., Invar36 Demir-Nikel Alaşımının CNC Freze Tezgahında İşlenmesinde Kesme Parametrelerinin Yüzey Pürüzlülüğü Üzerindeki Etkilerinin İncelenmesi, 14. uluslararası Denizli Malzeme Sempozyumu, 2012.

CORRESPONDENCE ADDRESS: Mehmet AKKAŞ, Kastamonu Üniversitesi Mühendislik ve Mimarlık Fakültesi Makine Mühendisliği Bölümü, 0 543 217 33 69 and mehmetakkas@kastamonu.edu.tr

SOLID STATE DIFFUSION WELDING OF COPPER WITH ALUMINUM ALLOY

Walid Bedjaoui, Zakaria Boumerzoug, Lamia Baghdadi*

Department of Mechanical Engineering, LMSM, Faculty of Science and Technology, University of
Biskra, B.P. 145, Biskra, 07000, Algeria.

*email: zboumerzoug@yahoo.fr Tel : 00 213 775759694

Abstract

The aim of this work is to study the effect of the time during the bonding process of copper with an industrial aluminum alloy by solid-state welding technique at 600 °C. Optical microscopy, scanning electron microscopy, and microhardness measurements were used as techniques of characterization. We have found that the prolonging time had an effect on the microstructure of the interface and its mechanical properties. The optimum welding time has been determined.

Key words: solid-state, welding, interface, mechanical properties

1. Introduction

Welding is a process of joining materials into one piece. Diffusion bonding or diffusion welding is a solid-state welding (SSW) technique used in metalworking, capable of joining similar and dissimilar metals [1]. During this process, atoms interdiffusion across the interface represents the main process mechanism. This technology has an essential importance when others competitive procedure cannot be used to characteristics reasons or material characteristics [2]. The process is dependent of a series of variables: time, applied pressure, bonding temperature, atmosphere, material characteristics, and roughness and contamination degree of mating surfaces [2].

Diffusion welding is a very attractive technology for the advanced materials, especially, when the conventional fusion welding processes degrades the melt properties. Aluminum and Copper has more significance in electrical and electronic application such as solar energy collectors or light weight electric motors and actuators [3]. Joining and welding of aluminum with copper is described in limited publications [4-9]. According to these published works, the main joining techniques of copper to aluminum were friction welding, ultrasonic welding, laser beam welding, roll welding, diffusion welding, and explosion welding. Joining of aluminum to copper through a melting leads to brittle intermetallic compounds like Al_2Cu , $AlCu$, and Al_4Cu_9 which cause failure of the joint already during cool down [4]. Consequently, solid-state welding below the melting temperature is the appropriate solution.

The objective of our work is to provide more microstructural details of the joint copper /aluminum alloy welded by SSW at 600 °C.

2. Experimental procedures

The chemical composition of the two materials are given in tables 1 and 2.

Table 1: Chemical composition of copper

Element	Cu	Zn	Pb	Sn	P	Fe	Ni
Wt %	99.7	0.0017	0.0164	0.0015	0.0006	0.0740	0.0122

Table2: Chemical composition of aluminum alloy

Element	Al	Si	Fe	Cu	Mn	Mg	Zn	Cr
Wt %	91.8	0.609	0.307	5.49	0.591	0.649	0.112	0.0765

Before bonding process, surfaces samples were polished and cleaned. The welded samples were firstly cut perpendicular to the joining surface. The microstructure and quantitative chemical analyses of the joints were performed by an optical microscope and scanning electron microscope with Energy-dispersive X-ray spectroscopy EDS capability. Specimens used for optical and scanning electron microscopic observations were polished and etched with a HNO₃ reagent. The hardness on the weld joint was measured by Vickers tester (SHIMADZV) using 100gf.

Results and discussion

a. Optical observations and microhardness distribution

Figure 1 presents the microstructures of the weld joint Cu/Al alloy realized at 600 °C for different time of bonding. This heat treatment regenerates an interface between the base metals. The thickness of this interface changes by changing the time during a bonding process and the main developed phenomenon inside the interface was the recrystallization reaction. In addition, there is a formation of a thin intermetallic layers at the bonding interface (Copper side) of welded dissimilar Cu/Al alloy joints (Fig.1.c). This intermetallic layer has been observed in Al/Cu joint performed by friction stir welding process and thin IMC layers provide high joint strengths [5].

The hardness distribution was determined on two sides of the bonded joints. In our case, the hardness values of the aluminum sides were higher than copper side. However, the hardness of the welding zone is less high than in aluminum side. The hardness values indicate that the prolonging time has an effect on interface hardness. The hardness variation has a relationship with the phase transformation inside the interface. The main transformations were the occurrence of new grains in the interface which affect the mechanical properties of the joint.

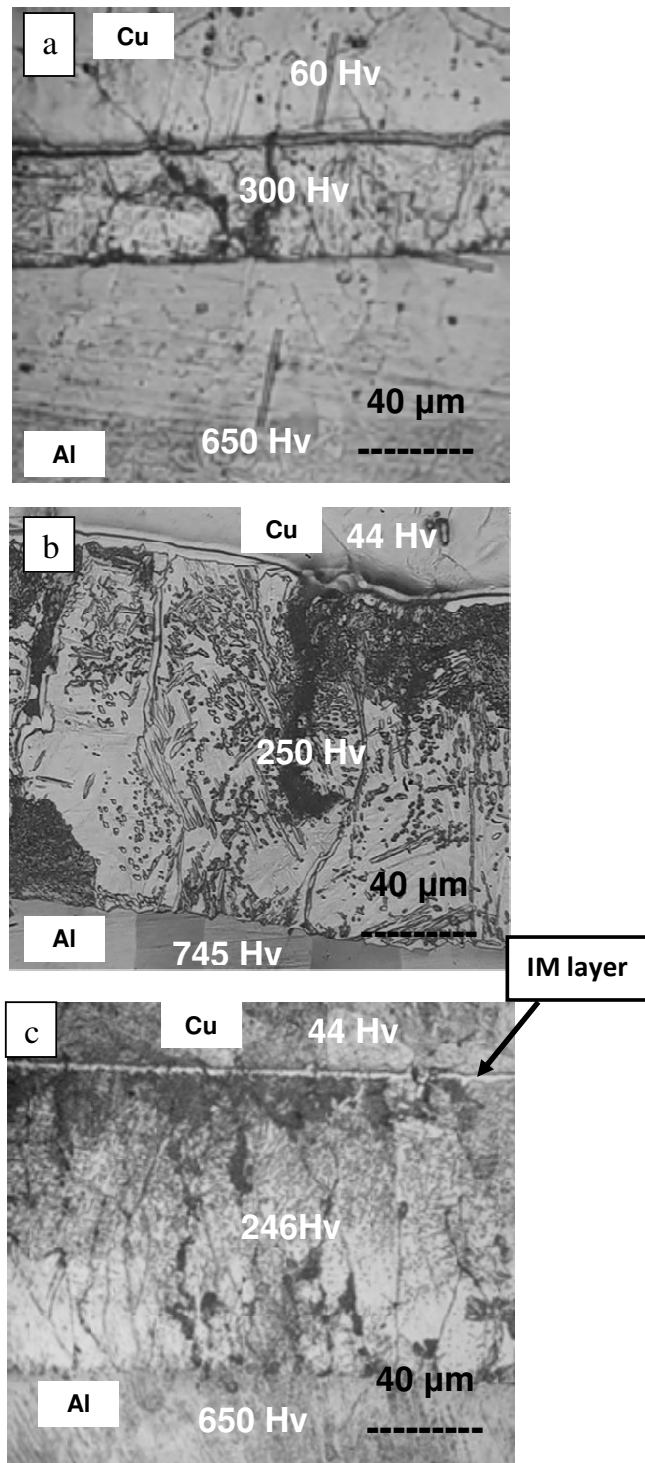


Figure 1. Microstructures of the weld joint Cu/Al alloy realized at 600 °C for different time of bonding : (a) 24 h , (b) 78 h and (c) 92 h.

b . SEM observations

Figure 2 shows SEM observations of the joint cross-section of the Cu/Al alloy after welding for different time. The interface structure of the joint showed that the

intermetallic (IM) uniform layer was formed along the interface and near the copper side which is probably rich on atomic copper. This IM layer is more visible after 92 h of welding time (Fig.2c).However, some defects like micropores were observed in the welded joint. In addition to this IM layer, by increasing welding time, a large interdiffusion zone is formed between the two base metals, which contains new grains and phases(Fig.2b and c).The main new observed phases werelamellar precipitatesformed at grain boundaries (Fig.2b and c). These precipitateswere formed by a discontinuous precipitation as observed in many binary alloys [10].

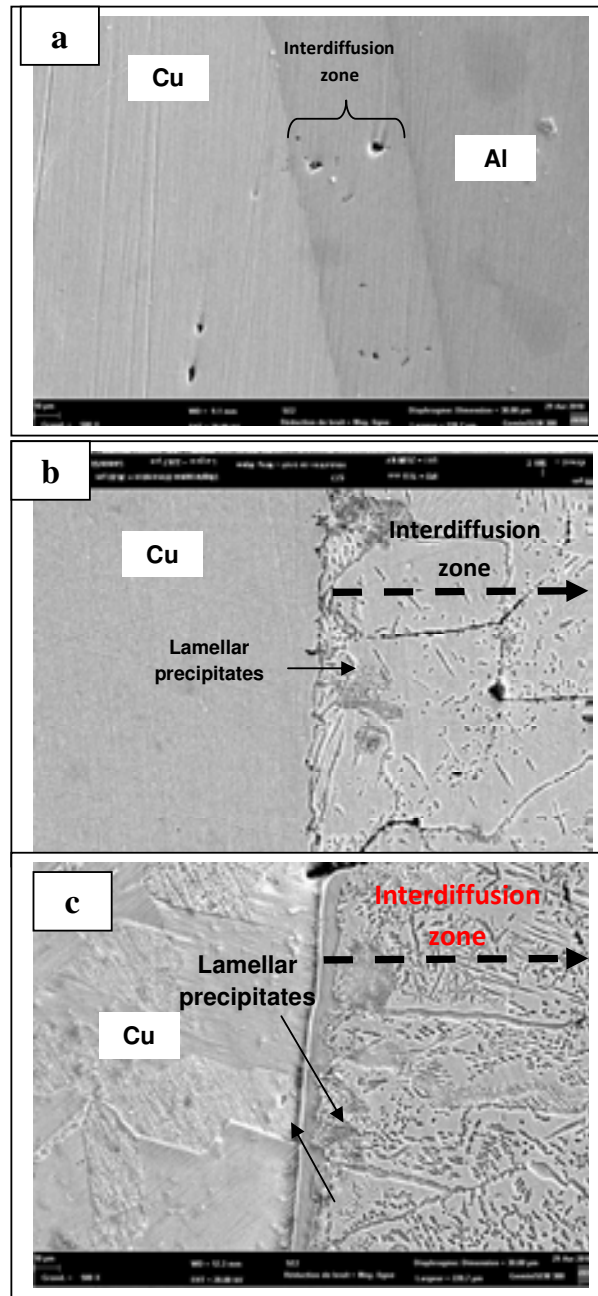


Figure 2. SEM observations of the weld joint Cu/Al alloy realized at 600 °C for different time of bonding : (a) 24 h , (b) 78 h and (c) 92 h.

Figure 3 presents the EDS analysis along welded Cu/Al alloy. It has been reported that the literature data for diffusion of copper and aluminium confirm a higher diffusion of copper and aluminium[4]. The diffusion of atomic copper from the base metal to the aluminium side is confirmed (Yellow curve) and vice-versa, the atomic aluminium diffuses from the base metal to the copper side is also confirmed (Red curve), which form an interdiffusion zone between the two base metals, as indicated in figure 3. This width of the interdiffusion zone increases by increasing the welding time at 600 °C.

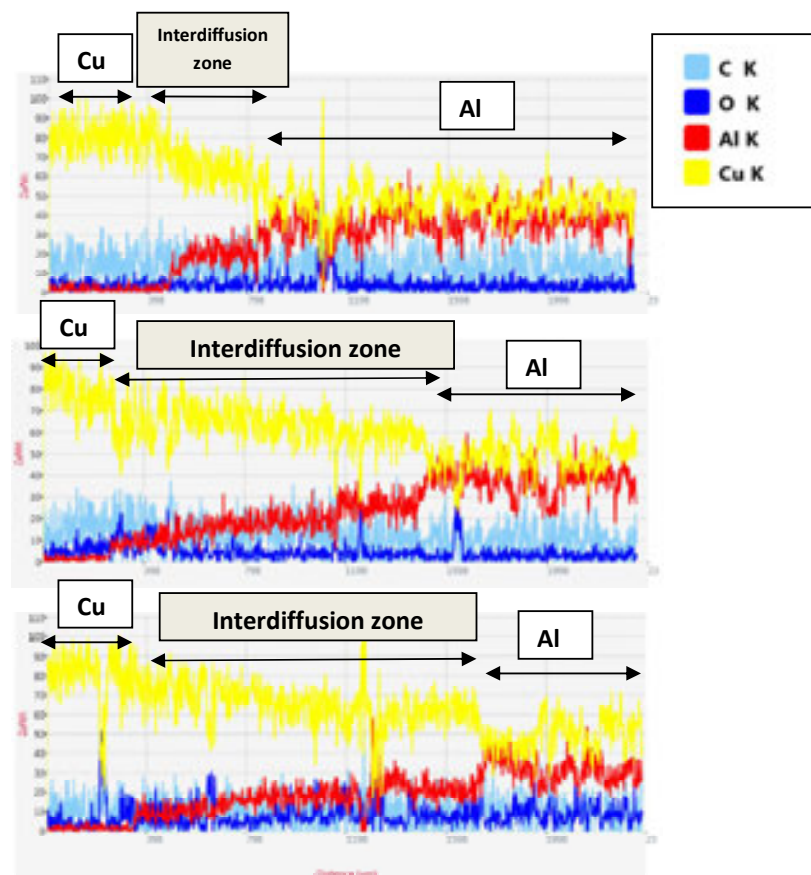


Figure 3. **Elements profile plot**(EDS) along the weld joint Cu/Al alloy realized at 600 °C for different welding time : (a) 24 h , (b) 78 h and (c) 92 h.

Conclusion

Our investigation represents a contribution to the study of the welded Cu/Al alloy. The applied joining process was solid-state welding at 600 °C. The results can be summarized as follows :

- Solid –state welding technique was successfully applied to joining copper to aluminum.
- Interface in welded joint has been formed between copper and aluminium with a thin intermetallic layer.
- The interdiffusion process has been confirmed by EDS analysis and the largest interdiffusion zone was obtained after prolonging the welding time.
- The prolonging welding time leads to the discontinuous precipitation inside Cu/Al interface.

References

- [1] K. VanDyke, G. Streeter, J. Driher, L. Leyer, Diffusion bonding 4 -September 2012 (Retrieved 2016-02-17)
- [2] T. Violeta, L. Mariana, L. Lucia, A. Georgeta, International Conference Innovative Technologies for Joining Advanced Materials, ISIM Timisora, 7-8 June 2007.
- [3] R.S. Chope, S.P. Gadewar, M.P. Khond, M.J. Rathod, Study on laser beam welding of copper and aluminum joint, Journal of Mechanical and Civil Engineering, pp.65-75, 2017.
- [4] J.P. Bergmann, Franziska Petzoldt, Rene Schurer and Stefan Schneider, Welding in the World, July 2013, volume 57, issue 4, pp 541-550.
- [5]. R. Marstatt, M. Krutzlinger, J. Luderschmid, M.F. Zaeh and F. Haider, IOP Conf. Series. Materials Science and Engineering 181 (2017) 012002
- [6] I.Bhamji, R.J. Moat, M. Preus, P.L. Threadgill, A.C. Addison and M.J. Peel, Linear friction welding of aluminum to copper , Science and Technology of Welding and Joining, 2012, Vol.17, No. 4, 314-320.
- [7] C.Y. Chen and W.S. Hwang, Effect of Annealing on the interfacial structure of aluminum-copper joints, Materials Transactions, Vol.48, No.7 , pp.1938-1947,2007.
- [8] M. Maeda, Y. Takahashi, Ultrasonic bonding of aluminum and copper wires in power electronics, Proceeding of the 1st international Joint Symposium on Joining and Welding, Osaka, Japan, 6-8 , Novembre 2013.
- [9] B. Gunlenc, Investigation of interface properties and weldability of aluminum and copper plates by explosive welding method, Materials&Design Vol. 29, Issue 1, 2008 pp.275-278.
- [10] P. Zieba, Recent developments on discontinuous precipitation, Arch. Metall. Mater. 62 , 2, 955-968, 2017.

API BORULARININ KAYNAKLI BİRLEŞTİRMELERİNDE AKMA MUKAVEMETİ DEĞERLERİNİN TAGUCHI METODU İLE OPTİMİZASYONU

Hakan ADA^{1,a}, Cemil ÇETİNKAYA^{2,b},
Tayfun FINDIK^{2,c}, Ahmet DURGUTLU^{2,d}

¹Kastamonu University, Faculty of Engineering and Architecture, Department of Mechanical Engineering

²Gazi University, Faculty of Technology, Department of Metallurgy and Material Science Engineering

^ahakanada@kastamonu.edu.tr, ^bcetin@gazi.edu.tr, ^ctayfunfindik@gazi.edu.tr, ^ddurgutlu@gazi.edu.tr

Özet

Bu çalışmada, API 5L X65 malzemedan üretilmiş çelik borular, elektrik ark kaynağı yöntemiyle birleştirilmiştir. Birleştirme işlemlerinde deney düzeneği Taguchi metodu kullanılarak oluşturulmuştur. Taguchi metodunda giriş parametreleri akım şiddeti, kaynak yönü ve elektrod türü olarak belirlenmiştir. Kaynakla birleştirilmiş numunelerin sergilediği akma mukavemeti değeri ise çıkış parametresi olarak belirlenmiştir. Üç aşamalı olarak gerçekleştirilen çalışmanın birinci aşamasında Taguchi L16 ortogonal dizini esas alınarak deneylerde kullanılacak faktör ve seviyelere göre parametreler belirlenmiştir. İkinci aşamada ise Taguchi deney düzeneğine uygun olarak kaynaklı birleştirme işlemleri gerçekleştirilmiş ve birleştirmelerden alınan numunelerin akma mukavemeti değerleri belirlenmiştir. Son aşamada ise deneylerden elde edilen veriler kullanılarak Taguchi metodu ile en uygun kaynak parametreleri tespit edilmeye çalışılmıştır. Taguchi metoduyla optimum sonucun tahmin ve tespit edilmesinden sonra, doğrulama deneyleri yapılmış ve optimizasyon kontrol edilmiştir. Sonuçta, deneyler ve doğrulama testlerinden elde edilen akma mukavemeti değerleri ile tahmin edilen değerler arasındaki farkın birbirine yakın olduğu görülmüştür. Sonuç olarak; Taguchi optimizasyonunun akma mukavemeti sonuçlarının tahmininde başarı ile uygulanabileceği görülmüştür.

Anahtar Kelimeler: API 5L X65, Örtülü elektrodla ark kaynağı (SMAW), Optimizasyon, Taguchi metodu, Akma mukavemeti

OPTIMIZATION OF YIELD STRENGTH OF WELDED JOINTS OF API 5L X65 PIPES BY TAGUCHI METHOD

Abstract

In this study, the joint performance of API 5L X65 steel pipes welded using shielded metal arc welding method was examined by Taguchi method. As performance indicators, strength of current, welding direction and electrode type were considered as input parameters, and the yield strength exhibited by the welded samples was determined as the output parameter. The study was carried out in four stages, and in the first stage, the experiment was designed based on Taguchi L16 orthogonal array. In the second stage, welding of joints was carried out according to a Taguchi experiment setup. In the third stage, yield strengths of these welded samples were determined. In the last stage, the most suitable input parameters were determined by Taguchi method using the data obtained from the experiments. After estimation of the parameters, verification tests were performed and accuracy of optimization was checked as a final step of optimization. Consequently, it was concluded that Taguchi optimization can be successfully applied in the estimation of yield strength results.

Key Words: API X65, Shielded metal arc welding (SMAW), Optimization, Taguchi method, Yield Strength

1.Giriş

Petrol ve doğalgaz en önemli enerji kaynakları olarak insan hayatında ve uluslararası ilişkilerde önemli bir yere sahiptir. Yakın tarih, petrol ve doğalgazın sadece enerji kaynakları olmadığını, aynı zamanda siyasi, ekonomik, kültürel ve askeri boyutlara da sahip olduğunu ve bu nedenle stratejik önemini ortaya koymaktadır [1]. Böylesine hem ekonomik, hem de stratejik önemi bulunan petrol ve doğalgazın buldukları kaynaklardan çıkarılarak ayırma istasyonlarına, ayırma işleminden çıkan ürünlerinse kullanım yerlerine taşınmaları gereklidir. Yüksek basınçlarla gerçekleştirilen bu taşıma işlemi ise büyük çaplı çelik borular ile yapılmaktadır [2]. Uzak mesafelere petrol ve gaz ürünlerini taşımak için faydalanabilecek en kolay ve en ucuz yolun boru hatlarını kullanmak olduğu herkes tarafından bilinmektedir. Gelişmiş boru hattı sistemleri dünyanın her yerinde üretim alanlarından tüketicilere, petrol, petrol ürünleri ve doğalgaz taşımaktadır. Dünyada enerjiye olan ihtiyacın artması da yüksek taşıma kapasitesine sahip yüksek basınçlı boru hatlarının inşa edilmesini gerektirmektedir [3].

Günümüzde hat borularının imalatında kullanılan çelikler API (American Petroleum Institute) 5L standardına göre üretilmektedir. API 5L X65 çelikleri, boru hatlarının yapım işlerinde kullanılan yüksek mukavemetli ve düşük alaşımlı çelik türlerinden biridir [4]. API standardında, "X" sınıfında değerlendirilen malzemelerin ana özelliği, ince taneli ferrit ve perlit yapılarının termomekanik işlemler sonucunda elde edilmesidir. Özellikle yüksek basınçlı boru hatlarında tercih edilen bu malzemeler, mikroyapısında ince taneli asiküler ferritin hâkim olduğu, kontrollü termomekanik haddeleme yöntemi ile üretilen çeliklerdir [5-7]. API çeliklerinde ana mikroalaşım elementi, titanyum ve vanadyum ile kombinasyonu olan niyobyumdur (Nb/V, Nb/Ti, Nb/V/Ti). Bu yapılar çeliklerin akma gerilimini ve tokluğunu olumlu yönde etkilemektedir [8-10]. Bu çelikler düşük maliyet, kolay elde edilebilirlik ve yüksek mekanik özelliklere sahip olması nedeniyle günümüzde boru hattı taşımacılığında yaygın olarak kullanılmaktadır [11,12].

Kaynak parametrelerinin daha verimli bir şekilde seçilmesini sağlamak, harcanan zamanı ve malzemeyi azaltmak için Taguchi metodu alternatif bir yaklaşım olarak devreye girmektedir. Temel olarak Taguchi metodu, yüksek kalite sistemleri için güçlü bir yöntemdir. Maliyet, kalite ve performans tasarımlarını optimize etmek için basit, verimli ve sistematik bir yaklaşım sunmaktadır. Taguchi metodu son yıllarda çok geniş bir kullanım alanı bulmaktadır. Bu metod, bir ürün ya da prosesin mühendislik optimizasyonunu; sistem tasarımı, parametre tasarımı ve tolerans tasarımı gibi üç adımlık bir yaklaşım içerisinde çözebilmeyi amaçlamaktadır [13,14]. Klasik deney tasarım yöntemlerinin kullanımı endüstriyel şartlar altında verimli olamamaktadır. Sistemi etkileyen faktörlerin sayısı arttıkça gerekli olan deney sayısı da hızlı bir şekilde artmakta, maliyetler yükselmekte, uygulamalar zorlaşmaktadır. Böyle durumlarda kesirli faktöriyel tasarım olan Taguchi metodu uygulaması daha verimli ve kolay olmaktadır. Karar vermeyi gerektiren birçok durumda da Taguchi metodu başarı ile uygulanabilmektedir [15].

Yüksek işletme basınçları altında, petrol ve doğalgaz hat borularının performansına yönelik kalite ihtiyaçları ise her geçen gün daha da artmaktadır. Kullanılan çelik malzemenin türü, malzeme kalınlığı, uygulanacak kaynak yöntemi, bu kaynak yöntemine uygun ekipmanlar, kaynak metalinin kimyasal bileşimi ve mekanik özellikleri, ilave kaynak metali miktarı, kaynak hızı ve diğer kaynak parametreleri petrol ve doğalgaz hat borularının performansını etkileyen önemli faktörlerdir. Belirtilen bu faktörlerin tümü kaynak tasarımı çalışmalarının önemini vurgulamaktadır. Farklı yöntemler ve parametreler dâhilinde gerçekleşen kaynak işlemleri farklı performanslar ortaya koymaktadır. Yüksek basınç uygulamalarına güvenle cevap verilebilecek

boruların üretilmesi ve boru hatlarının inşa edilmesinde gerekli kalite seviyesinin yakalanabilmesi için kaynak tekniğinin ve buna bağlı olarak kaynak parametreleri seçiminin doğru bir şekilde yapılması gerekmektedir. Boruların birleştirildiği yapım işlerinde genel olarak, kaynak parametreleri ile malzemenin mekanik-kimyasal özellikleri ve kaynak dikişinde istenilen performans özellikleri (mukavemet ve tokluk gibi) arasında bir ilişkinin kurulamadığı, kaynak parametrelerinin çoğu zaman deneme yanılma yöntemi ile belirlendiği görülmektedir. Kaynak tekniğinin doğru seçilememesi kalite kontrol işlemlerinde alışılmışın dışına çıkılmasını engelleyerek, ya gereksiz yönde fire verilmesine, ya da belirli hataların farkına varılamamasına yol açmaktadır. Benzeri nedenlerden dolayı, kaynak güvenilirliği kaynak hızının düşük tutulması ile sağlanmaya çalışılmakta, bu ise hem verimliliğin düşmesine hem de maliyetlerin artmasına neden olmaktadır. Buradaki temel eksiklik, kaynak parametrelerinin seçimine yönelik sistematik bir yöntemin oluşturulamamasıdır.

Bu çalışmada; yukarıda belirtilen eksikliklerin giderilmesine yönelik olarak petrol ve doğalgaz boru hatları için üretilen API (American Petroleum Institute) 5L standardında ve X65 kalitesindeki çelik boruların kaynaklı birleştirme işleminin Taguchi metoduyla optimizasyonu yapılarak, birleştirmelerden optimum akma mukavemeti değerlerinin elde edilmesi planlanmıştır. Birleştirme işlemlerinde, servis şartlarında yaygın olarak kullanılan örtülü elektrodla ark kaynak yöntemi tercih edilmiştir. Performans göstergesi olarak her bir kontrol yöntemine uygun girdi parametreleri (akım, kaynak yönü ve elektrod türü) tespit edilmiştir. Belirlenen parametreler ile gerçekleşen kaynak işlemlerinden elde edilen akma mukavemeti değerleri çıkış parametresi olarak analiz edilmiştir. Elde edilen test sonuçlarına göre de kaynaklı birleştirmeler için gerekli optimizasyon sağlanmıştır. Taguchi metoduyla elde edilen tahminsel sonuçlar, doğrulanmış gerçek deney sonuçları ile karşılaştırılıp, en uygun parametreler tespit edilmeye ve Taguchi metodunun parametre belirleme çalışmalarındaki verimliliği ortaya konulmaya çalışılmıştır.

2. Deneysel Çalışmalar

Bu çalışmanın amacı, endüstriyel uygulamalara katkı sağlayarak, gerçek ve akılcı çözümler üretebilmektir. Bu amaç dikkate alınarak, faktör seçiminde günümüz boru hattı yapım işlerinde kullanılan süreç parametreleri, işletme şartları ve kaynak yöntemleri tercih edilmeye çalışılmıştır. Bu kapsamda; doğalgaz ve petrol taşımacılığında kullanılan boru malzemesi toprak kayması, göçük gibi dış kuvvetlerin sebep olduğu plastik deformasyona maruz kalabileceği için, dışarıdan gelebilecek olumsuz etkilere karşı koyabilecek mekanik özelliklere sahip olan X65 malzemesi tercih edilmiştir. Kaynak işlemlerinde ise akım şiddeti değeri, elektrod türü (Selülozik ve Bazik) ve kaynak yönü (aşağıdan yukarı ve yukarıdan aşağı) gibi parametreler dikkate alınmıştır. En uygun parametreler seçilerek, kaynaklı birleştirmeler için ideal akma mukavemeti değerlerinin belirlenmesi amaçlanmıştır. Deneylerde 110-140, 120-150, 130-160, 140-170, 150-180, 160-190, 170-200 ve 180-210 A aralığında akım şiddeti değerleri kullanılmış, borular iki farklı yönde (aşağıdan yukarı ve yukarıdan aşağı yönde) ve iki farklı elektrod türü (selülozik ve bazik) ile birleştirilmiştir. Belirlenen şartlar neticesinde Taguchi L16 deney düzeneği (8*2*2) ile deneyler gerçekleştirilmiştir. Taguchi metodu ile belirlenen şartlar Çizelge 1'de, Taguchi L16 deney düzeneği ise Çizelge 2'de verilmiştir.

Çizelge 1. Deney faktörleri ve seviyeleri

Sembol	Faktörler (Kaynak Parametreleri)	Seviyeler							
		1	2	3	4	5	6	7	8
A	Akım Şiddeti (A)	110-140	120-150	130-160	140-170	150-180	160-190	170-200	180-210
B	Kaynak Yönü	Aşağıdan Yukarıya↑	Yukarıdan Aşağıya↓						

C	Elektrod Tipi	Selülozik	Bazik	
---	---------------	-----------	-------	--

Çizelge 2. Taguchi L16 deney düzeneği

Deney numarası	-A- (Akım Şiddeti) (Amper)	-B- (Kaynak Yönü)	-C- (Elektrod Tipi)
1	1 (110 – 140)	1 (Aşağıdan yukarıya ↑) ↑	1 (Selülozik)
2	1 (110 – 140)	2 (Yukarıdan aşağıya ↓)	2 (Bazik)
3	2 (120 – 150)	1 (Aşağıdan yukarıya ↑) ↑	1 (Selülozik)
4	2 (120 – 150)	2 (Yukarıdan aşağıya ↓)	2 (Bazik)
5	3 (130 – 160)	1 (Aşağıdan yukarıya ↑) ↑	1 (Selülozik)
6	3 (130 – 160)	2 (Yukarıdan aşağıya ↓)	2 (Bazik)
7	4 (140 – 170)	1 (Aşağıdan yukarıya ↑) ↑	1 (Selülozik)
8	4 (140 – 170)	2 (Yukarıdan aşağıya ↓)	2 (Bazik)
9	5 (150 – 180)	1 (Aşağıdan yukarıya ↑) ↑	2 (Bazik)
10	5 (150 – 180)	2 (Yukarıdan aşağıya ↓)	1 (Selülozik)
11	6 (160 – 190)	1 (Aşağıdan yukarıya ↑) ↑	2 (Bazik)
12	6 (160 – 190)	2 (Yukarıdan aşağıya ↓)	1 (Selülozik)
13	7 (170 – 200)	1 (Aşağıdan yukarıya ↑) ↑	2 (Bazik)
14	7 (170 – 200)	2 (Yukarıdan aşağıya ↓)	1 (Selülozik)
15	8 (180 – 210)	1 (Aşağıdan yukarıya ↑) ↑	2 (Bazik)
16	8 (180 – 210)	2 (Yukarıdan aşağıya ↓)	1 (Selülozik)

DeneySEL çalışmaların, yukarıda belirtilen Taguchi deney düzeneğine uygun olarak gerçekleştirilebilmesi için çelik boru, elektrod ve gerekli ekipmanlar sağlanmış ve birleştirme işlemleri gerçekleştirilmiştir.

2.1. Materyal ve Metod

Deneylerde Çizelge 3'te kimyasal kompozisyonu ve mekanik özellikleri verilen API 5L X65 kalitesinde, 12,7 mm kesit kalınlığında ince taneli yapı çeliği kullanılmıştır. İlave tel (elektrod) olarak ise selülozik ve bazik elektrodlar kullanılmıştır. Selülozik elektrod ile yapılan birleştirmelerde kök pasoda 3,25 mm çapında AWS E6010 kodlu elektrod kullanılmış olup, sıcak paso, ara paso ve kapak pasolarda ise 4,00 mm çapında AWS E8010 kodlu elektrod kullanılmıştır. E6010 ve E8010 kodlu selülozik elektrodların kimyasal kompozisyonu ve mekanik özellikleri Çizelge 4 ve 5'te verilmektedir. Bazik elektrod ile yapılan birleştirmelerde ise AWS E9018-D1-H4 kodlu elektrod kullanılmış olup, kök pasoda 3,25 mm, diğer pasolarda ise 4,00 mm çapında elektrodlar tercih edilmiştir. AWS E9018-D1-H4 kodlu elektrodun kimyasal kompozisyonu ve mekanik özellikleri Çizelge 6'da verilmiştir.

Çizelge 3. Deneylerde kullanılan X65 malzeme kimyasal kompozisyonu ve mekanik özellikleri.

Element (%)	C	Si	Mn	P	S	Cr	Ni	Mo
	0,064	0,29	1,61	0,008	0,0018	0,021	0,001	0,001
	Cu	Al	Ti	V	Nb	N	Fe	C _{E_s}
	0,008	0,035	0,023	0,051	0,052	0,0028	97,83	0,348
Mekanik Özellikler	Akma Muk. (MPa)		Çekme Muk. (MPa)		Uzama (min) (%)		Darbe Enerjisi (0°C) (Joule)	
	566		650		34		209	

Çizelge 4. AWS/ASME FA.5.1. E6010 kodlu selülozik elektrod kimyasal analiz ve mekanik özellikleri.

Kaynak Metalinin Tipik Kimyasal Analizi			Kaynak Metalinin Tipik Mekanik Özellikleri (%)			
C	Si	Mn	Akma Muk. (min) (N/mm ²)	Çekme Muk. (min) (N/mm ²)	Uzama (%)	Çentik Darbe Enerjisi (0 °C) (min) (Joule)
0,10	0,20	0,50	470	530	26	60

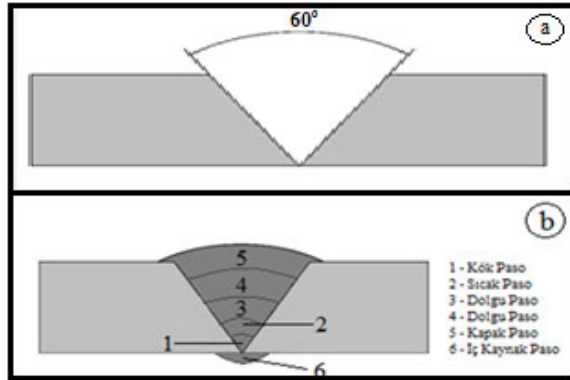
Çizelge 5. AWS/ASME FA.5.1. E8010 kodlu selülozik elektrod kimyasal analiz ve mekanik özellikleri.

Kaynak Metalinin Tipik Kimyasal Analizi				Kaynak Metalinin Tipik Mekanik Özellikleri (%)			
C	Si	C	Si	Akma Muk. (min) (N/mm ²)	Çekme Muk. (min) (N/mm ²)	Uzama (%)	Çentik Darbe Enerjisi (-20 °C) (min) (Joule)
0,10	0,20	0,80	0,90	500	570	24	60

Çizelge 6. AWS A5.5. E9018-D1-H4 kodlu bazik elektrod kimyasal analiz ve mekanik özellikleri.

Kaynak Metalinin Tipik Kimyasal Analizi				Kaynak Metalinin Tipik Mekanik Özellikleri (%)		
C	Si	C	Si	Akma Muk. (min) (N/mm ²)	Çekme Muk. (min) (N/mm ²)	Çentik Darbe Enerjisi (-50 °C) (min) (Joule)
0,075	0,40	1,60	0,45	550	610-780	47

Saha birleştirmelerinde yoğunlukla kullanılan, örtülü elektrodla elektrik ark kaynak yöntemi birleştirme metodu olarak tercih edilmiş, kaynak işlemleri redresör tipi kaynak makinesinde gerçekleştirilmiştir. Birleştirme işlemlerinde kaynak ağzı geometrisi ve paso sıralaması Şekil 1'de verilmektedir. Kaynaklı birleştirme işlemlerinde; parçalar öncelikle kaynak işlemine hazırlanmıştır. Tozaltı kaynak yöntemiyle spiral olarak üretilmiş olan 1.066,8 mm (42" çapında), 12,7 mm et kalınlığındaki API 5L X65 kalitesindeki çelik borular otomatik plazma kesme makinesi ile 300 mm genişliğinde kesilmiştir. Kesilen borulara 30° kaynak ağzı açılarak, kaynak işlemine hazırlanmıştır. Her bir deney yarım boru birleştirmesi olacak şekilde, yani tam bir boru çevresi ikiye bölünerek, bir çevreden iki deney elde edilecek şekilde kaynak işlemleri gerçekleştirilmiştir (Şekil 2). Toplam 16 boru parçası bir araya getirilerek 8 tam boruda 16 deney gerçekleştirilmiştir. Deneyler, yeterli miktarda numune hazırlayabilmek için her boru birleştirmesinden 2 adet olacak şekilde tekrar edilmiştir. Kaynak işlemi için hazırlanmış boru malzemeler Şekil 2'de görülmektedir.



Şekil 1. a) Kaynak ağzı geometrisi,
b) Paso sıralaması.

Şekil 2. Kaynak işlemi için hazırlanan borular.

Taguchi metodu yardımıyla maliyet ve zaman kriterleri dikkate alınarak, en uygun kaynak parametreleri Çizelge 2'de verildiği gibi L16 (8*2*2) düzeninde belirlenmiş ve kaynak işlemleri bu düzenlemeye uygun olarak Çizelge 7'de belirtildiği gibi seçilerek gerçekleştirilmiştir. Deneylerde kök pasoları sabit bir akım şiddeti değerinde (100 Amper) birleştirilmiş olup, elektrodun ergime gücü ve metal yığılma kapasitesi düşünülerek, sıcak paso ile birlikte akım şiddeti değeri her pasoda 10 Amper artırılmıştır. Kaynak işleminin sonunda borular kapak pasoda (5. paso) kullanılan akım şiddeti değerinde, içeriden de ayrıca iç kaynak (6. paso) işlemine tabi tutulmuştur. Bu kapsamda belirlenen deney düzeneğinin son hali, paso geçişlerinde akım şiddeti değerlerinin yükseltilmesi ihtiyacı sonucu ve Çizelge 2'de belirtilen akım şiddeti değerlerinin sabit oranda (10 A) artırılması neticesinde Çizelge 7'de görüldüğü gibi oluşturulmuştur. Kaynaklı birleştirme işlemlerinde kaynak hızı sabit tutulmuş olup, birleştirmeler kök pasoda 120 mm/dak, diğer pasolarda ise 150 mm/dak kaynak hızında gerçekleştirilmiştir. Farklı parametrelerde gerçekleştirilen deneylerde, sabit değerde bir kaynak hızına ulaşabilmek için; elektrotların yanma süresi ve dikiş boyları hesaplanarak birleştirme işlemleri gerçekleştirilmiş ve böylece kaynak hızları kontrol altında tutulmuştur. Deneylerde kullanılan bazik elektrotlar 250 – 300 °C'de 1 saat süre ile kurutularak hiç bekletmeden, selülozik elektrotlar ise özelliği gereği kurutulmadan kaynak işlemine tabi tutulmuştur.

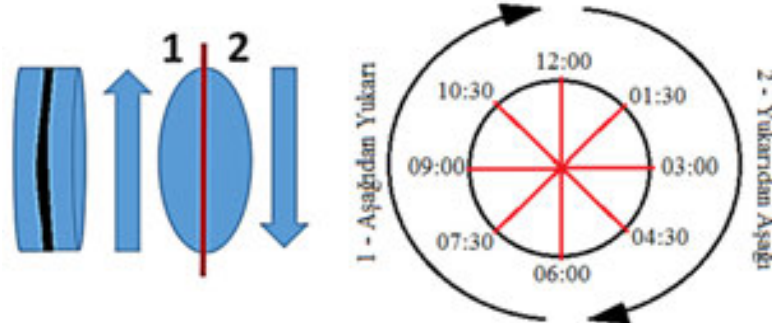
Çizelge 7. Taguchi L16 deney düzeneği ile oluşturulan ve deneylerde kullanılan parametreler.

Deney No	Kaynak Yönü	Elektrod Türü	Akım Şiddeti (Amper)					
			Kök Paso	Sıcak Paso	Dolgu Pasoları		Kapak Paso	İç Kay. Pas.
			Ø 3,25 mm	Ø 4,0 mm				
			-Paso 1-	-Paso 2-	-Paso 3-	-Paso 4-	-Paso 5-	-Paso 6-
1	Aşağıdan yukarı ↑	Selülozik	100	110	120	130	140	140
2	Yukarıdan aşağı ↓	Bazik	100	120	130	140	150	150
3	Aşağıdan yukarı ↑	Selülozik	100	130	140	150	160	160
4	Yukarıdan aşağı ↓	Bazik	100	140	150	160	170	170
5	Aşağıdan yukarı ↑	Selülozik	100	150	160	170	180	180
6	Yukarıdan aşağı ↓	Bazik	100	160	170	180	190	190
7	Aşağıdan yukarı ↑	Selülozik	100	170	180	190	200	200
8	Yukarıdan aşağı ↓	Bazik	100	180	190	200	210	210
9	Aşağıdan yukarı ↑	Selülozik	100	180	190	200	210	210
10	Yukarıdan aşağı ↓	Bazik	100	180	190	200	210	210
11	Aşağıdan yukarı ↑	Selülozik	100	180	190	200	210	210
12	Yukarıdan aşağı ↓	Bazik	100	180	190	200	210	210
13	Aşağıdan yukarı ↑	Selülozik	100	180	190	200	210	210
14	Yukarıdan aşağı ↓	Bazik	100	180	190	200	210	210
15	Aşağıdan yukarı ↑	Selülozik	100	180	190	200	210	210
16	Yukarıdan aşağı ↓	Bazik	100	180	190	200	210	210

Çekme Numunelerinin Hazırlanması ve Çekme Testi

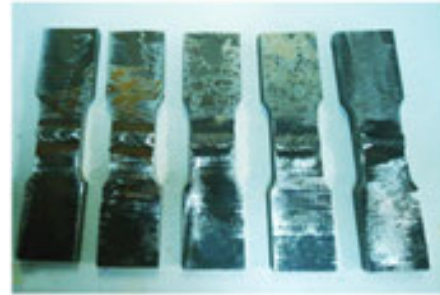
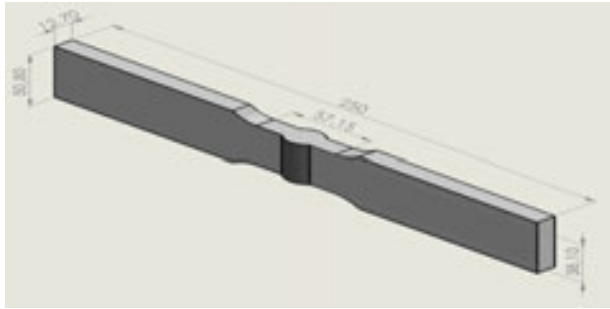
Test numunelerinin hazırlanması safhasında; kaynak işlemlerinde elektrod açısına bağlı olarak kaynak pozisyonunun etkileri düşünülerek, her bir deneye ait boru parçası, Şekil 3'te şematik

olarak görüldüğü gibi dört bölgeye ayrılmıştır. İncelemeler; kaynak yönüne göre (aşağıdan yukarı ve yukarıdan aşağı) değerlendirilmiştir. Yukarıdan aşağı yönde saat 12:00 – 01:30, 01:30 – 03:00, 03:00 – 04:30 ve 04:30 – 06:00 pozisyonu ve aşağıdan yukarı yönde saat 06:00 – 07:30, 07:30 – 09:00, 09:00 – 10:30 ve 10:30 – 12:00 pozisyonlarından alınan numuneler çekme testine tabi tutularak sonuçlar elde edilmiştir.



Şekil 3. Numunelerin alındığı bölgelerin şematik gösterimi.

Çekme testleri kapsamında her bir deney için test numuneleri ASTM E8 standardına uygun olarak, ana malzeme ve Şekil 3'te belirtilen 4 ayrı bölgeden 5'er adet alınarak hazırlanmıştır. 16 deney için 64 bölge ve ana malzemeden alınan toplam 325 adet çekme numunesi hazırlanmıştır. Çekme testi için standarda uygun olarak hazırlanan numunelerin şematik gösterimi Şekil 4'te, bu gösterimdeki ölçülere uygun olarak hazırlanan numunelerin görüntüsü ise Şekil 5'te verilmiştir.



Şekil 4. Çekme testi numunesinin şematik gösterimi Şekil 5. Çekme test numuneleri

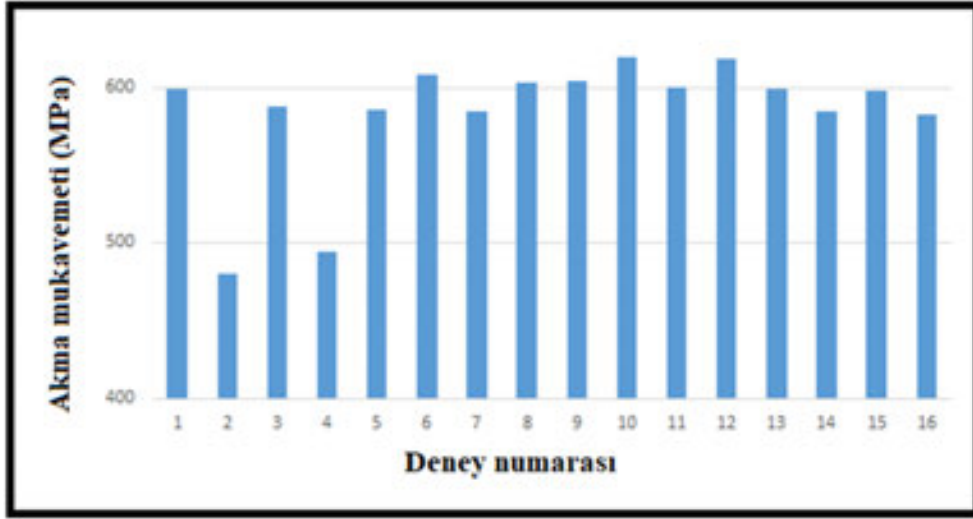
Boru birleřtirmeleri haricindeki kaynaklı birleřtirmelerin test numunelerinin hazırlama işlemlerinde çekme testi aşamasında numunelerin yüzey pürüzlülüğü hassasiyeti için kaynaklı yüzeylerin (kep ve kök) tıraşlanması gerektiği bir gerçektir. Ancak boru malzemelerdeki ovalik nedeniyle kaynak kepi ve kökü tıraşlandığında, kaynak bölgesi metalurjik özelliklerini kaybedeceğinden, çekme numuneleri Şekil 5'te görüldüğü üzere tıraşlanmamıştır.

3. Deney– Optimizasyon Sonuçları ve Tartışma

Deney Sonuçlarının Değerlendirilmesi

Ana malzemeden ve Şekil 3'te şematik olarak gösterilen bölgelerden her bir deney için standarda (ASTM E8) uygun olarak 5'er adet numune alınmış ve numunelerin akma mukavemeti değerlerine bakılmıştır. Ana malzemeden alınan numunelerin akma mukavemeti ortalaması 566 MPa olarak tespit edilmiştir.

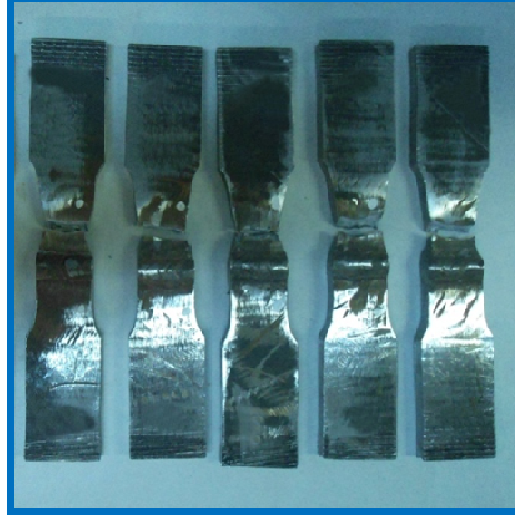
Kaynaklı birleştirmelerin standarda uygun olarak gerçekleştirilen çekme testleri sonucunda elde edilen akma mukavemeti değerlerinin grafik görüntüsü ise Şekil 6'da verilmiştir..



Şekil 6. Akma mukavemeti sonuçları

Şekil 6'da verilen akma mukavemeti sonuçları irdelendiğinde; Deney 2 ve 4 haricindeki tüm deneylerde birleştirmelerin akma mukavemetlerinde ana malzeme değerlerinin üzerinde sonuçlar görülmüştür. Test sonuçlarına bakıldığında en düşük akma mukavemeti değerleri sırasıyla 479 ve 490 MPa ile 2 ve 4 numaralı deneylerde elde edilmiştir. En yüksek akma mukavemeti değeri ise 610 MPa ile 10 numaralı deneyde ölçülmüştür. Kaynak işlemlerinde ısı girdisinin ne denli önemli olduğu bilinmekte olup, düşük akım değerlerinde hatalar oluşması muhtemeldir [16-18]. Bu nedenle, 2 ve 4 numaralı deneylerde kopmalar kaynak metalinden gerçekleşmiş, bu deneylerin haricindeki tüm deneylerde kopmaların tamamı ergime sınırının yaklaşık 20 mm ilerisinde ana malzemelerde tespit edilmiştir. Bu durum; pratikte kaynak işleminin başarılı bir performans sergilediğini göstermekte olup, uygulanan kaynak işleminin statik yüklemelerdeki dayanımının kaynak metalinde, ana malzemeye göre daha iyi sonuçlar sergilediğini göstermektedir. Buna sebep olarak ise kaynaklı bölgede yüksek ısı girdileri ve hızlı soğumadan kaynaklanan ince taneli ve iğnemsiz yapıların oluşması gösterilebilmektedir. Oluşan ince taneli yapıların mekanik özellikleri olumlu yönde etkilediği daha önceki çalışmalarda da bildirilmiştir [19]. İnce taneli yapılar deformasyona karşı mukavemet gösterdiği için kopmalar kaynak metali dışında, deformasyonun nispeten daha kolay olduğu ve daha iri tane yapısına sahip olan ana malzemelerde meydana gelmiştir. Ayrıca kaynak kepi ve kökünün standart gereği tıraşlanmaması, dolayısıyla kaynak metalinde kesit kalınlığının artması, kopmaların buradan olmasına mani olmuştur. Yine kaynaklı bölgenin çekme testi işlemlerinde numunelerin % uzama değerleri, ana malzemeye oranla daha düşük çıkmıştır. Buna paralel olarak kaynaklı numunenin, akma ve çekme mukavemetinin artmasının yine kaynaklı bölgenin deformasyona karşı gösterdiği direnç nedeniyle olduğu söylenilebilir [20-22]. 2 ve 4 numaralı deneylerde ise; çekme testi esnasında kopmanın kaynak metalinden gerçekleşmesine; söz konusu deneylerde bazik elektrod ile yukarıdan aşağı pozisyonda yeterli akım şiddeti değerlerinin sağlanamamasının neden olduğu düşünülmektedir. Söz konusu deneylerde bazik elektrod için akım şiddeti değerlerinin düşük olması nedeniyle yeterli nüfuziyet sağlanamadığı ve birleşme eksikliği görüldüğü söylenilebilir. Söz konusu deneylerin çekme testi uygulamalarında kaynak bölgesi kendisinden beklenen özellikleri sergileyememiş, birleşme eksikliğinden kaynaklanan yetersiz ergime ve nüfuziyet nedeniyle kopmalar kaynak metalinden gerçekleşmiştir. Diğer deneylerde ise kaynaklı

birleştirmeler kendisinden beklenen görevleri yerine getirmiş ve daha mukavemetli bir özellik sergilemiştir. Bu nedenle kopmaların tümü ana malzemelerden olmuştur. Ana malzemelerden kopan bir deney grubuna ait görüntüler Şekil 7'de verilmiştir.



Şekil 7. Çekme testi sonrası numunelerin görüntüsü.

Sonuçların Taguchi Metodu ile Analizi

Taguchi L16 ortogonal düzeni çerçevesinde her bir deneyden elde edilen akma mukavemeti değerlerinin ortalaması alınarak o deney için söz konusu analiz değerleri belirlenmiştir. Deneyler sonucunda ölçülen akma mukavemeti değerleri ve sinyal/gürültü oranları Çizelge 8'de verilmiştir.

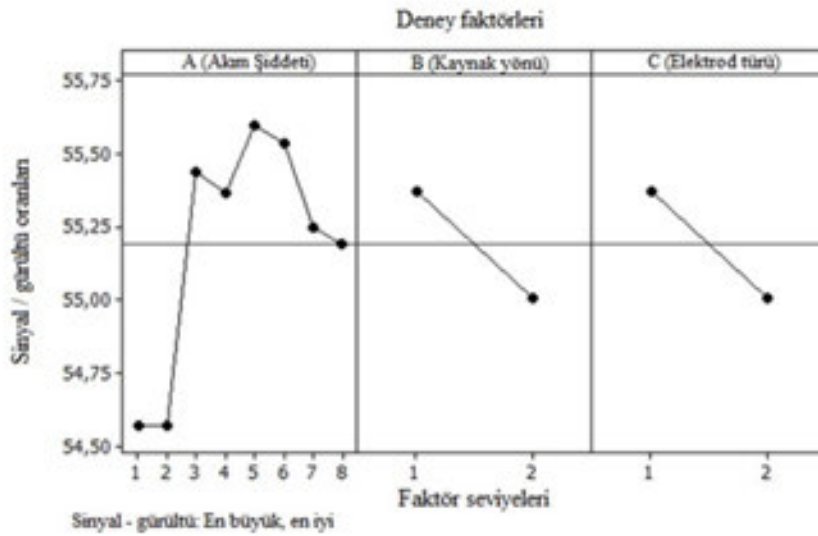
Çizelge 8. Deneysel çalışmalardaki girdilere bağlı olarak akma mukavemeti için elde edilen çıktılar ve sinyal/gürültü (S/N) oranları.

Deney No	-A- Akım Şiddeti Aralığı (A)	-B- Kaynak Yönü	-C- Elektrod Türü	Akma Mukavemeti	
				Deney Sonucu (MPa)	S/N Oranları
1	110-140	Aşa. Yuk. ↑	Selülozik	598	55,5340
2	110-140	Yuk. Aşa. ↓	Bazik	479	53,606
3	120-150	Aşa. Yuk. ↑	Selülozik	585	55,3431
4	120-150	Yuk. Aşa. ↓	Bazik	490	53,8039
5	130-160	Aşa. Yuk. ↑	Selülozik	581	55,2835
6	130-160	Yuk. Aşa. ↓	Bazik	602	55,5919
7	140-170	Aşa. Yuk. ↑	Selülozik	578	55,2386
8	140-170	Yuk. Aşa. ↓	Bazik	595	55,4903
9	150-180	Aşa. Yuk. ↑	Bazik	595	55,4903
10	150-180	Yuk. Aşa. ↓	Selülozik	610	55,7066
11	160-190	Aşa. Yuk. ↑	Bazik	589	55,4023
12	160-190	Yuk. Aşa. ↓	Selülozik	607	55,6638
13	170-200	Aşa. Yuk. ↑	Bazik	586	55,3580
14	170-200	Yuk. Aşa. ↓	Selülozik	571	55,1327
15	180-210	Aşa. Yuk. ↑	Bazik	583	55,3134
16	180-210	Yuk. Aşa. ↓	Selülozik	567	55,0717

Çizelge 8’de verilen akma mukavemeti sonuçlarının Taguchi metodu yardımıyla optimizasyonu yapılmıştır. Bu optimizasyon işlemi, Taguchi kayıp fonksiyonu olarak bilinen ve aynı zamanda sinyal/gürültü oranı fonksiyonu olarak kullanılan eşitliklerden “en büyük en iyi” (Eşitlik 1) kullanılarak S/N oranları hesaplanmıştır.

$$\frac{S}{N} = -10 \log \left(\frac{1}{n} \sum_{i=1}^n \frac{1}{y_i^2} \right) \quad (\text{Eşitlik 1})$$

Eşitliklerde y_i , performans yanıtını, i gözlem değerini, n bir denemede test sayısını ifade etmekte olup, deneysel sonuçlar neticesinde S/N oranlarına bağlı olarak optimum parametreler tahmin edilmiştir. Akma mukavemeti değerleri için kontrol faktörlerinin S/N oranlarının grafiksel gösterimi Şekil 8’de verilmiştir.



Şekil 8. Akma mukavemeti için S/N oranları ana etki grafiği.

Akma mukavemeti için yapılan optimizasyonda uygun kaynak parametreleri Şekil 8’de verilen sinyal/gürültü oranlarından yararlanılarak ve “en büyük, en iyi” fonksiyonuna uygun olarak “A5B1C1” olarak bulunmuştur. Burada; A5, 150 – 180 Amper akım şiddeti aralığını, B1, aşağıdan yukarı kaynak yönünü, C1 ise, selülozik elektrodu ifade etmektedir.

Doğrulama Deneyleri ve Sonuçları

Taguchi metoduna göre, optimum sonuçları verecek parametrelerin tahmininden sonra, optimizasyonda son aşama olarak doğrulama deneyleri yapılmış ve optimizasyonun doğruluğu kontrol edilmiştir. Tespit ettiğimiz “A5B1C1” parametrelerinde üç adet kontrol deneyleri sonucunda elde edilen deney sonuçlarının ortalaması alınarak sonuçların güvenilirliği irdelenmiştir. Buna göre ideal çekme değerlerinin elde edilmesinde, optimize edilmiş kaynak parametreleri sırasıyla, Çizelge 9’da verilmiştir.

Çizelge 9. Maksimum çekme mukavemeti için doğrulama test sonuçları.

	Başlangıç Kaynak Parametresi	Optimum Kaynak Parametreleri	
		Tahminsel	Deneysel
Seviye	A8B2C2	A5B1C1	A5B1C1

Akma mukavemeti (MPa)	585	624,5	575
S/N ratio (dB)	55.3431	55.9618	55.1934
İyileştirme oranı: 0.1497 dB			
Tahminsel hata: 0.7684 dB			

Deneysel çalışmalarda elde edilen değerler ile tahmin edilen değerler arasındaki fark göz ardı edilebilecek seviyededir. Bu durumda Taguchi optimizasyonunun mekanik test değerleri tahmininde başarı ile uygulanabildiği görülmüş, Taguchi metodu ile kaynak işleminde parametre optimizasyonunun uygun bir şekilde yapılabileceği yapılan bu çalışma ile ispatlanmıştır.

Çizelge 9'da başlangıç değerleri, tahminsel değerler ve doğrulama değerleri birbiriyle mukayese edildiğinde; optimizasyon işlemlerinde akma mukavemeti için % 8,6 iyileşme görüldüğü tespit edilmiştir.

4. Sonuç

Gerçekleştirilmiş olan çalışmadan elde edilen sonuçlar aşağıda özetlenmiştir:

- ✓ Deney 2 ve 4'te yetersiz ergime ve birleşme eksikliği hatası görüldüğünden, söz konusu deneylerin yeterli mukavemet değerlerini sağlayamadığı ve hatta ana malzemeden daha düşük mukavemet değerleri sergilediği görülmüştür.
- ✓ Birleşme eksikliği olan 2 ve 4 numaralı deneylerin haricindeki birleştirmeler, kaynak metaline yaklaşık 20 mm mesafeden, ana malzemeden kopmuştur. Çekme testlerinde kaynak bölgesi şekil değişimine karşı daha yüksek direnç gösterirken, kopmalar plastik deformasyonun daha kolay olduğu bölge olan ana malzeme tarafında gerçekleşmiştir.
- ✓ Çekme testlerinin tümü incelendiğinde; deneyler içerisinde en yüksek akma mukavemeti değeri kaynak yönü ve uygulanan akım şiddeti değerlerinin etkisine bağlı olarak Deney 10'da (yukarıdan aşağı yönde, selülozik elektrod, 150 - 180 680 MPa parametrelerde) ölçülmüştür.
- ✓ Akma mukavemeti sonuçları kapsamında yapılan Taguchi optimizasyonunda; optimum kaynak parametreleri "A5B1C1" olarak bulunmuştur. Burada; A5, 150 – 180 Amper akım şiddeti aralığını, B1, aşağıdan yukarı kaynak yönünü, C1 ise, selülozik elektrodu ifade etmektedir.
- ✓ Tespit edilen akma mukavemeti için "A5B1C1" parametrelerinde üç adet doğrulama deneyi gerçekleştirilmiş ve bu deneylerin akma mukavemeti sonuçlarının ortalaması alınarak Taguchi metodu ile tahminsel sonuçların güvenilirliği belirlenmiştir.
- ✓ Başlangıç parametre değerleri, tahminsel değerler ve doğrulama değerleri birbiriyle mukayese edildiğinde; Taguchi metoduyla optimizasyon işlemlerinde, maksimum çekme mukavemeti için % 8,6 oranında iyileşme tespit edilmiştir.
- ✓ Doğrulama testleri ve deneysel çalışmalardan elde edilen maksimum çekme mukavemeti sonuçları ile tahmin edilen değerler arasındaki farkın göz ardı edilebilecek seviyede olduğu görülmüş, Taguchi optimizasyonunun maksimum çekme mukavemeti sonuçlarının tahmininde başarı ile uygulanabildiği görülmüştür.

5. Teşekkür

Yazarlar, boru malzemesinin temin edildiği NOKSEL Çelik Boru San. A.Ş., çekme testlerinin gerçekleştirildiği Emek Boru Makine San. ve Tic. A.Ş. ile 07/2016-05 numara ile kayıtlı proje kapsamında sağlanan destekler için, Gazi Üniversitesi Rektörlüğü Bilimsel Araştırma Projeleri Koordinasyon Birimine teşekkürlerini sunar.

6. Kaynaklar

- [1] F. Umbach: Global Energy Security and The Implications for The EU, Energy Policy, 38 (2010), 1229 – 1240.
- [2] H. Ada, S. Aksöz, T. Fındık, C. Çetinkaya, M. Gülsün: Examination of Microstructure and Mechanic Properties of Oil and Gas Pipelines Joined with Submerged Arc Welding Method. Journal of Polytechnic, 19(3)(2016), 275-282.
- [3] Y. D. Han, H. Y. Jing, L. Y. Xu: Welding Heat Input Effect on The Hydrogen Permeation in The X80 Steel Welded Joints, Materials Chemistry and Physics 132 (2012), 216–222.
- [4] API Specifications 5L: Specifications for Line Pipe, 45th Edition (2012), American Petroleum Institute, USA.
- [5] S. H. Hashemi: Strength - Hardness Statistical Correlation in API X65 Steel, Mater. Sci. Eng. A, 528 (2011), 1648–1655.
- [6] M. Rakhshkhorshid, S. H. Hashemi: Experimental Study of Hot Deformation Behavior in API X65 Steel, Materials Science & Engineering A, 573 (2013), 37–44.
- [7] S.H. Hashemi, D. Mohammadyani: Characterization of Weldment Hardness, Impact Energy and Microstructure in API X65 Steel”, Int. J. Pressure Vessels Piping, 98 (2012): 8–15.
- [8] A. Radovic, N. Bajic, V. Grabulov: Specific Quality of The Weld Metal of Welded Joints of Finegrained Microalloyed Steels, Zavarivanje 96 (1996), 61–72.
- [9] N. Bajic, V. Šijacki-Zeravcic, M. Rakin, K. Kovacevic: Structure Optimization of Weld Metal and HAZ in Microalloyed High Strength Steel Welded Joints, YUCOMAT 2005, Herceg Novi, ISBN: 86- 80321-08-7(2005), 193–200.
- [10] N. Bajic, V. Šijacki-Žeravi: The Analysis of Change of Structural and Mechanical Properties of Welded Joints of Microalloyed Nb/V Steel Grade by Changing The Composition of Filler Material, Internat. Conf. On Welding (2003), Belgrade.
- [11] M. Sangeetha, S. Rajendran, T. S. Muthumegala, A. Krishnaveni: Green Corrosion Inhibitors - An Overview, Zaštita Materijala, 52(2011), 3-19.
- [12] S. Aksöz, H. Ada, T. Fındık, C. Çetinkaya, B. Bostan, İ. Candan: “Examination of The Effect of Welding Operation on Microstructure And Mechanic Properties in Joint of API 5L X65 Steels Welded with Electric Arc Welding Method, El-Cezeri Journal of Science and Engineering, 4:1 (2017), 72-81.
- [13] R. Çakıroğlu, A. Acır: Optimization of Cutting Parameters on Drill Bit Temperature in Drilling by Taguchi Method, Measurement, 46:9 (2013), 3525-3531.
- [14] J. P. Davim: A Note The Determination of Optimal Cutting Conditions for Surface Finish Obtained in Turning Using Design of Experiments, Journal of Materials Processing Technology, 116(2003), 305-308.
- [15] H. Oktem, T. Erzurumlu, I. Uzman: Application of Taguchi Optimization Technique in Determining Plastic Injection Molding Process Parameters for A Thin-Shell Part”, Materials and Design 28 (2007), 1271–1278.
- [16] V. Onar, S. Aslanlar: Welding Time Effect of Welding Joints in Micro Alloyed and TRIP 800 Steels in Resistance Spot Welding, Acta Physica Polonica A, 131 (2017), 389-391.

- [17] V. Onar, S. Aslanlar, N. Akkaş: Effect of Welding Current on Tensile–Peel Loading of Welding Joints in TRIP 800 and Micro-Alloyed Steels in Resistance Spot Welding, *Acta Physica Polonica A*, 132 (2017), 822-824.
- [18] B. Çevik: Examination of Mechanic and Microstructure Properties of S275 Structural Steel, Joined with Different Cored Wire”, *Journal of Polytechnic*, 20(3)(2017), 675-680.
- [19] P. Lehto, H. Remes, T. Saukkonen, H. Hänninen, J. Romanoff: Influence of Grain Size Distribution on the Hall–Petch Relationship of Welded Structural Steel”, *Materials Science and Engineering*, 592 (2014), 28–39.
- [20] S. Aksöz, H. Ada, A. Özer: Microstructure and Mechanic Properties of API 5L X70 Steel Pipes Manufactured with Submerged Arc Welding Method, *GU J Sci, Part C*, 5(1) (2017), 55-64.
- [21] H. Ada, S. Aksöz, T. Findık, C. Çetinkaya, B. Bostan, İ. Candan: Examination of the Effect of Welding Operation on Microstructure and Mechanic Properties in Joint of API 5L X65 Steels Welded with MAG Welding Method, *Çukurova University Journal of The Faculty of Engineering and Architecture*, 31:(ÖS 1)(2016), 1- 9.
- [22] N. Kahraman, B. Gülenç, A. Durgutlu: Examination of The Effect of Free Wire Length in Low Carbon Steels Welded with Submerged Arc Welding Method on Microstructure and Mechanic Properties, *Gazi University Journal of Sciences*, 18 (3)(2005), 473-480.

SORUMLU YAZARADRES: Tayfun FINDIK, Gazi Üniversitesi, Teknoloji Fakültesi, Metalurji ve Malzeme Mühendisliği Bölümü – Teknikokullar ANKARA/Türkiye, +903122028783, +905333673957, tayfunfindik@gazi.edu.tr

KISA BİYOGRAFİLER

Hakan ADA –Ankara’da doğdu – 1980. Gazi Üniversitesi Teknik Eğitim Fakültesi Metal Öğretmenliği Bölümü’nden mezun oldu. 2017 yılından beri Kastamonu Üniversitesi Mühendislik ve Mimarlık Fakültesi’nde Dr. Öğr. Üyesi olarak görev yapmaktadır. Çalışmaları kaynak ve malzeme bilimi üzerinedir.

Cemil ÇETİNKAYA –Aksaray’da doğdu – 1959. Gazi Üniversitesi Teknoloji Fakültesi’nde Prof. Dr. unvanıyla görev yapmaktadır. Çalışmaları kaynak ve malzeme bilimi üzerinedir.

Tayfun FINDIK –Sinop’ta doğdu – 1976. Gazi Üniversitesi Teknoloji Fakültesi’nde Dr. Öğr. Üyesi unvanıyla görev yapmaktadır. Çalışmaları kaynak ve malzeme bilimi üzerinedir.

Ahmet DURGUTLU –Bilecik’te doğdu – 1971. Gazi Üniversitesi Teknoloji Fakültesi’nde Prof. Dr. unvanıyla görev yapmaktadır. Çalışmaları kaynak ve malzeme bilimi üzerinedir.

RAY BİRLEŞTİRMEDE ALÜMİNOTERMİT VE YAKMA ALIN KAYNAK YÖNTEMLERİ; TEKNİK VE MALİYET YÖNÜNDEN KARŞILAŞTIRILMA

M. Emin AKAY*; Fikri DEMİR**

* KBÜ Mühendislik Fakültesi, Raylı Sistemler Mühendisliği Programı, Karabük, Türkiye.

** Türkiye Demiryolu Makineleri Sanayi ve Ticaret AŞ - TÜDEMSAŞ, Sivas, Türkiye.

ÖZET

Günümüzde rayların kaynakla birleştirilmesi yaygınlaşan bir uygulamadır. Sürekli hale getirilen ray yüzeyleri sayesinde daha kaliteli bir tren seyri sağlanırken, daha az bakıma ihtiyaç duyulmaktadır. Bu bildiride; yaygın olarak kullanılan alüminotermite ve yakma alın kaynak yöntemlerinin maliyet ve teknik açıdan karşılaştırılarak en avantajlı yöntemi tespit etmek amaçlanmıştır. Çalışma sonucunda, kaynak teknik özelliklerine bakıldığında, Alüminotermite kaynağında kaynak bölgesinde sertleşen kısmın daha uzun olduğu, dokunun daha kaba taneli olduğu görülmüştür. Yapılan kaynağın; yorulma, eğilme ve gerilme dayanımlarına bakıldığında da, yakma alın kaynağının mukavemetinin daha yüksek olduğu görülmüştür. Kaynak maliyeti açısından karşılaştırma sonucunda da, birim zamanda yapılan yakma alın kaynağı sayısının diğerinin 8 katı kadar çıktığı, kaynağın servis ömrünün uzunluğu görülmüştür. yakma alın kaynağı yönteminin tek zayıf yanı ilk yatırım maliyetinin yüksekliği olmaktadır.

Anahtar Kelimeler: Uzun kaynaklı ray (UKR), alüminotermite ve yakma alın kaynağı, teknik özellikler, maliyet

RAIL JOINING METHODS ALUMINOTERMITE AND FLASH BUTT WELDINGS; COMPARISON IN TERMS OF TECHNICAL AND COST ASPECTS

ABSTRACT

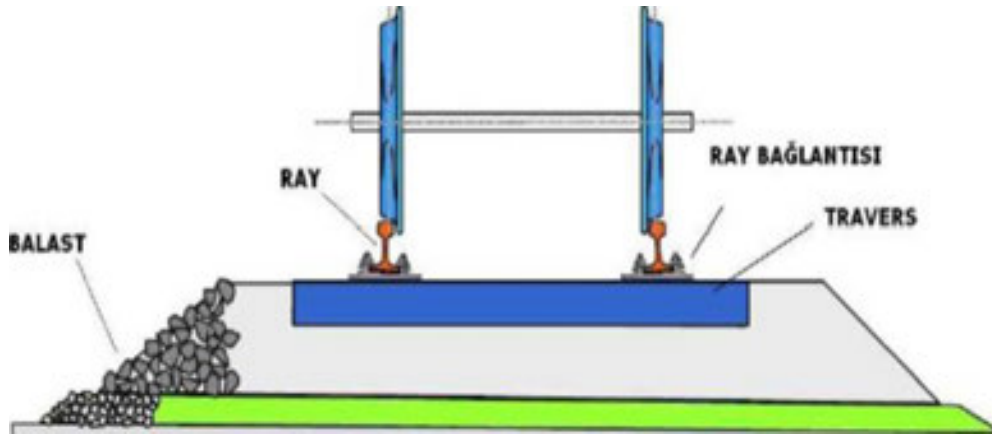
Nowadays, the railway tracks are usually welded continuously. Due to continuous welded rail joints provide better rolling surface and require less maintenance than the joinings with fishplate. In this paper, it is aimed to compare two different rail welding methods as aluminothermic and flash butt weldings in terms of technical properties and cost. Related with results as technical properties of welding methods, aluminothermic welding creates longer hardened area due to welding heat, and coarser crystal structure. Other evaluation of welding process as mechanical strengths in terms of fatigue, bending and stress, here flash butt welding method gives better results. There is another comparison of welding process as welding cost. According to the results, number of welds done in unit time of flash butt welding method is 8 times bigger and longer service life. The only negative side of flash butt welding method is higher investment cost.

Key Words: Continuous welded rails (CWR), aluminothermic and flash butt welding methods, technical properties, cost

1. RAYLI SİSTEMLER ÜST YAPISI VE RAYLAR

1.1. Raylı Sistem Üstyapısı

Raylı sistemler; demiryolu ve kentçi taşıma sistemleri olarak iki türde çeşitlenmektedir. Taşıtlarının güvenli, konforlu ve ekonomik olarak seyrini sağlayan ve altyapı üzerine döşenmiş bulunan malzeme ve elamanlarının tümüne Üstyapı denir. Şekil 1.1'de balastlı bir zemin üzerine oturan hat en kesiti gösterilmiştir. Raylı sistem taşıtları, boden denilen flanşlı kısma sahip tekerlekleriyle, rayın kılavuzlaması sayesinde, yuvarlanarak yol alırlar. Raylar; selet, bağlantı elemanları ve traversler ile bir bütün olarak montajlanır ve balastlı tabaka üzerine yerleştirilir. Taşıtların statik ve dinamik yükleri, tekerleklerden balast tabakasına transfer edilerek, emilir ve taşıtlar emniyetle seyir yaparlar.



Şekil 1.1. Balastlı hat üstyapısı

Bir demiryolu üstyapısının genel olarak görevleri şunlardır [Arlı ve Öztürk, 2009];

- Taşıtlara düzgün ve pürüzsüz bir yuvarlanma yüzeyi sağlamak,
- Demiryolu taşıtlarından gelen statik ve dinamik yükleri güvenle ve kalıcı şekil değişikliğine uğramadan karşılamak ve azaltarak altyapıya iletmek,
- Elastiklik, uzun servis ömrü ve ekonomiklik,
- Yüzey sularını bünyesinden kolayca uzaklaştırabilmek,

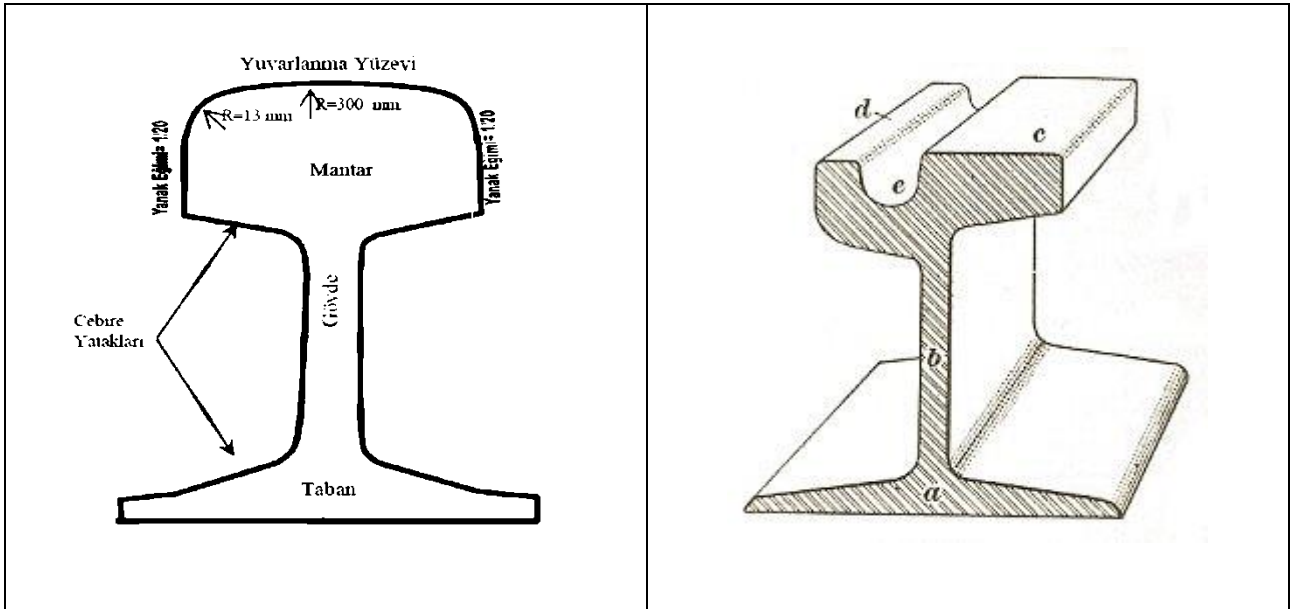
1.2. Raylar

Tren tekerlekleri ile direkt temasta bulunan, aşınmaya karşı dayanıklı ve esneklik kabiliyeti yüksek çelikten imal edilirler. Raylar raylı sistemdeki görevleri nedeniyle; ağır dingil kuvveti, yüksek hız, yanıl zorlamalar, korozyon, vb. etkenlerle, farklı statik ve dinamik yüklere maruz kalmaktadır. Bu

sebepten ötürü raylar bu etkileri karşılayabilecek özelliklerde olmalıdır. Raylar patenli ve oluklu olmak üzere iki biçimde üretilirler. Patenli raylar demiryollarında ve metro sistemlerinde kullanılırken, oluklu raylar da tramvay hatlarına uygulanmaktadır. Ray türleri Şekil 1.2’de gösterilmiştir.

Rayların özellikleri kullanma alanına göre aşağıdaki gibi sıralanabilir [Arlı ve Öztürk, 2009]:

- Hareket yüzeyi yeterince geniş ve tekerlek - ray temasından doğan yüzey basıncını minimize edecek şekilde imal edilmelidir.
- Mantar yüksekliği uzun bir hizmet süresi için aşınmaya yetecek yükseklikte olmalıdır.
- Ray gövdesi taşıma kapasitesi ve esneme mukavemeti açısından yeterli kalınlığa ve kesite sahip olmalıdır.
- Statik sebeplerden dolayı ağırlık merkezi, yaklaşık ray yüksekliğinin yarısı kadar olmalıdır.
- Mantar yüksekliği ve taban genişliği yeterli bir devrilme emniyeti sağlayacak şekilde seçilmelidir.



Şekil 1.2. Mantar tipi ve oluklu Raylar

Raylar; mantar, gövde, taban olarak üç kısma ayrılır. Raylar düşük karbonlu ve perlitik yapıli çeliklerden 6 - 8 kademeli “profil haddeleme” yöntemiyle üretilirler.

1.2.1. Rayın Görevleri

Raylar raylı sistem taşıtları çalışırken, aşağıdaki görevleri yaparlar [MEGEP, 2013]:

- Tekerleklerle düzgün ve pürüzsüz bir yuvarlanma yüzeyi sağlamak ve tekerlekleri kılavuzlamak,
- Araçların tekerleklerireh gelen dingil yüklerini uygun bir yük dağılımı ile traverslere iletmek,
- Aşınmaya karşı dayanıklı olmak,
- Sinyal akımlarını iletmek.

Rayların beklenen görevleri yerine getirebilmesi için, belirli kimyasal ve mekanik özelliklere sahip olması gereklidir.

1.2.2. Rayın Kimyasal Yapısı

Raylar tekerlek bodeniyle sürekli temas halinde bulduklarından dolayı birbirlerini aşındırırlar. Asıl amaç, ray ve bodenin beraberce aşınmasının en düşük düzeyde olmasını sağlamaktır. Bu amacı gerçekleştirmek için, ray çeliğinin kimyasal bileşimi önem arzeder. Ray çeliği içinde demir dışında, karbon, silis ve manganez'in belirli miktarda bulunması icap eder. Gerekli metallerin ray içindeki oranları aşağıda belirtilmiştir [Kumbasar, 1972 ve Özaraç, 2005]:

- Karbon, ray çeliği bünyesinde % 0,4 – 0,6 oranında bulunur, C oranı artarsa, çelik gevrekleşir.
- Silisyum, çeliğin oksitlenmesini zorlaştırır, ayrıca malzemenin daha akıcı ve ince tanecikli ve homojen olmasını sağlar. Rayın cinsine göre silisyum miktarı% 0,3 – 0,5 arasında değişir.
- Manganez, çeliği sert ve darbeye mukavemetli yapar. Ray çeliği içindeki Mn oranı karbonun 2 - 3 katı kadardır.
- Fosfor, Hidrojen ve Kükürt ise rayda bulunması istenmeyen zararlı elementlerdir.

1.2.3. Rayın Mekanik Özellikleri

Rayların maruz kaldıkları statik ve dinamik yüklere karşı, belirli mekanik dayanımları olmalıdır. Dayanımının yükselmesi çeliğin kimyasal tertibini değiştirmekle, karbon miktarını çoğaltıp, manganez karıştırmakla temin edilir. Bu ise rayda zamanın azalmasına yani kırılma dayanımının artmasına neden olur. Tablo 2.1' de rayların mekanik özellikleri gösterilmiştir.

Tablo 1.1. Rayların mekanik özellikleri (Esveld, 2001).

Çekme Dayanımı (N/mm ²)	Kopma Uzaması (%)	Sertlik (BHN)	Çekme Dayanımı (N/mm ²)	Kopma Uzaması (%)	Sertlik (BHN)
680-830	14	-	>770	12	220-260
880-1030	10	-	>880	10	260-300
880-1030	10	-	>880	10	260-300
>1080	9	-	>1080	9	320-360
>680	14	200-240	>1175	9	350-390

Rayda aşınma dayanımının yüksek olması istendiği gibi, kopma uzamasının da % 10'dan az olması istenmez. Perlitik çeliklerde mekanik özellikler büyük ölçüde sementit (Fe₃C) tabakalarının

kalınlıklarına ve tane boyutlarına bağlıdır. Ray dayanımı, tane boyutları ve sementit tabakalar arasındaki kalınlığa bağlıdır.

Rayların cebireli bağlantılar yerine birbirine kaynatılması, son yıllarda yaygın bir şekilde uygulanmaktadır. Diğer demir - çelik ürünlerinde olduğu gibi, raylarda da kaynak kabiliyeti, karbon oranı ile ters orantılıdır. Karbon çelikleri özelliğindeki raylar kolay kaynak yapılabilmektedir. Çeliğe katılan Mn, Cr, Si, Mo gibi alaşım metaller ise kaynak kabiliyetine olumsuz etkilemektedir. Alaşım elementleri, kaynak esnasında martenzit oluşumuna, dolayısıyla sertlik ve gevrekliğin artmasına sebep olurlar [Aytekin, 1989].

2. RAY BİRLEŞTİRME VE KAYNAK YÖNTEMLERİ

Demiryolu inşaatları büyük teknik bilgi ve beceri gerektiren operasyonlar olup, işlerin önemli aşamalardan birisi, rayların uygun yöntemlerle, doğru şekilde birleştirilerek hattın oluşturulmasıdır. Günümüzde, rayların cebireli olarak birleştirilmesi daha az tercih edilmekte olup, yerini sürekli kaynaklı birleştirmelere bırakmaktadır. Kaynaklı ray birleşim bölgeleri, cebireli birleşimlere göre; daha az bakım gerektirmekte, kaliteli tren seyri ve daha uzun servis ömrü sağlamaktadır. Ancak, zamana bağlı yorgunluk, daha yüksek tren hızları, yüksek aks yükü ve artan trafik yoğunluğu nedeni ile kaynakların hasar görmesi kaçınılmazdır.

Raylar, cebireyle veya kaynaklı olarak birbirlerine birleştirilirler. Cebireli birleştirmede raylar, gövdelerine açılmış deliklere takılan Cebire (fishplate) adlı ek parça birleştirilmektedir. Ray uçlarına da **conta** denir. Şekil 2.1’de Cebire ile ray birleştirme gösterilmiştir.



Şekil 2.1. Rayların cebire (fishplate) yardımıyla birleştirilmesi

Dünya genelinde, demiryolu hatları inşasında Elektrik ark kaynağı, Gaz basınç kaynağı, Alüminotermite kaynağı ve Yakma alın kaynağı olarak 4 farklı yöntem bulunmaktadır. Alüminotermite ve yakma alın kaynakları en yaygın yöntemlerdir.

2.1. Uzun Kaynaklı Ray (UKR) Uygulaması

Çeşitli boylardaki rayların birleştirilerek uzun boyda ray elde edilmesine, uzun kaynaklı ray (UKR) denmektedir. Demiryolu ray kaynak metotlarındaki genel uygulama, ray uçlarının karşılıklı hale getirilerek, düşey ve yatay olarak ray başlarının birbirine kaynakla birleştirilmesidir. TCDD işletmesi demiryolu atelyelerde alın kaynağı, sahada alın kaynağı ve alüminotermite kaynağı metotlarını uygulamaktadır.

Alüminotermite kaynağı günümüzde genellikle tamir amaçlı olarak sahada kullanılmakta olup, yöntemin, yakma alın kaynağı yöntemine göre en önemli dezavantajı birleştirme için kullanılan malzemenin ana malzemedenden farklılık göstermesidir. Bu farklılıktan dolayı zamanla gerek atmosferik şartlar, gerekse ray üzerinden geçen tekerleğin sürtünme kuvveti ile kaynak bölgesi aşınmaktadır. Aşınan bu bölgeler gürültü yaparak yolcu konforunu, vuruşu yaparak da alt yapıyı ve yuvarlanma yüzeyini bozmaktadır. Bu nedenle günümüzde yeni hatlarda yakma alın kaynağı tercih edilmektedir.

Sıcaklık değişimleri raylarda ilave gerilmeler meydana getirir. Kısa raylarda (12 – 24 - 36 metre) bu gerilmeler, ray uçlarında bırakılan boşluklarla elimine edilmektedir. Rayların uzaması suretiyle meydana gelen bu kuvvetlerin uzun kaynaklı raylarda mutlaka yol üst yapısı içerisinde giderilmesi gerekir. Bu sebeple de üst yapıda, ray ile traversler arasında kuvvetli bir gerilme direnci, boyuna ve çaprazına sürtünme direnci ile, iyi bir balast yatağı veren sağlam yapı gereklidir [Günoral, 2018].

2.1.1. Uzun Kaynaklı Ray (UKR) Uygulamasının Üstünlükleri

Cebireli bağlantı yerine UKR uygulanması aşağıdaki faydaları sağlanmaktadır [Rangwala, 2007]:

- Ray uçlarındaki aşınmaların ve raylarda sünmenin azalmasından dolayı ray ömrü artar.
- Ray birleşimlerinin azalmasıyla, yol yapım masrafları azalırken, bakım masrafları da % 25 düşer.
- UKR kullanıldığında, yüzeyin düzgün çalışmasından ötürü yolcu konforu olumlu etkilenir.
- Ray birleşim bölgelerinin azalmasıyla, kazalarının ve sabotajların önüne önemli ölçüde geçilir.
- Uzun kaynaklı ray kullanılmasıyla, rayların enine, boyuna ve uzunlamasına stabil olması sağlanır.

2.2. Alüminotermite Kaynağı

Bu tür kaynak, birleştirici malzemenin veya ısıya dayanıklı potalar içinde, termokimyasal reaksiyon sonucu eritilerek, kaynak boşluğu bırakılan ve ⁵⁰⁸iki ray ucuna yerleştirilen tuğla kalıplar içerisine akıtılmasıyla yapılan bir ray birleştirme kaynağıdır. Termit malzemesi demir oksit (Fe₂O₃) ve

alüminyum (Al) karışımından oluşmaktadır. Bu karışım özel tutuşturma çubukları (maytap. vs.) vasıtasıyla tutuşturularak reaksiyon gerçekleştirilir. Meydana gelen reaksiyon formül 3.1. ile ifade edilir [Esveld, 2001].



Bu yöntem bir döküm işlemi olup, demir oksit ve ince taneli alüminyumdan oluşan karışım, noktasal olarak ateşlendiğinde 1.200 °C sıcaklığa ulaşmaktadır. Bu sıcaklıkta karışım içerisinde ekzotermik (ısıveren) bir tepkime başlar ve sıcaklık 3.000 °C ye kadar yükselir. Tepkime sonucunda ergimiş demir elde edilir. Kullanılan teçhizat ve malzeme portatiftir ve harici güç kaynağı gerekmemektedir. Kaynak sonucunda, kaynak yerine uzak ray bölgesinde sertlik 275 HB iken, kaynak bölgesinde 285 HB'ye yükselmektedir [Onay, 2011].

Alüminotermite kaynak, dünyada en sık kullanılan ray birleştirme yöntemlerinden olup, özellikle ray bakım ve tamirat işlerinde çok tercih edilir. Alüminotermite kaynağı uygulaması Şekil 2.2'de gösterilmiştir.



Şekil 2.2. Alüminotermite kaynağının uygulanması

2.3. Yakma Alın Kaynağı

Şekil 2.3'de yakma alın kaynak makinesi gösterilmiştir. Demiryolu uygulamalarında kullanılan bu yöntemde raylar hem sahada, hem de fabrika ortamında kaynatılabilmektedir. Sabit kaynak tesisinde bu yöntemde 24 V düşük gerilim, 80.000 A yüksek akım kullanılmaktadır.

Yakma alın kaynağı işleminde temel olarak; akım, basınç ve süre olarak, üç parametre kontrol edilmektedir. Bu parametreler kaynak edilecek malzemenin yapısına ve boyutuna göre değişmektedir. Farklı malzemelerin kaynağı, geniş kesite sahip olan ray, şaft gibi yapıların kaynağı



Şekil 2. 3. Yakma alın kaynak makinesi

bu parametrelerin ayarlanması ile gerçekleştirilir. Bu yöntemde bakır alaşımlı elektrotların kaynak yapılacak malzemelere teması ile, yüksek akım altında ark oluşumu ve ortaya çıkan ısı ile malzemelerin kaynak sıcaklığına erişmesi amaçlanır.

3. UKR UYGULAMASININ TEKNİK VE MALİYET YÖNÜNDEN KARŞILAŞTIRILMASI

Demiryolu hatlarında optimum kaynak yönteminin belirlenmesinde, hem kaynak kalitesi, hem de kaynak yöntemi maliyeti dikkate alınmalıdır. Yöntemlerin teknik özellikleri kaynak kalitesini belirlemektedir.

3.1. Mekanik Özellikler Karşılaştırması

Bu başlık altında; kaynak sertlikleri ve kaynak mukavemeti açısından mukayese yapılacaktır.

3.1.1. Kaynak sertlikleri

Alüminotermite kaynağı sertlik grafiğine göre, kaynaklarda kaynak ve HAZ (ısıdan etkilenen bölge) bölgesinin toplam uzunluğu 120-160 mm arasındadır. Kaynaktaki sertlik değişimi kaynak performansını belirlemektedir. Bu yüzden HAZ bölgesinin dar olması arzu edilir [Onay, 2011].

Yakma Alın kaynağı sertlik sonuçlarına göre, yapılan kaynaklarda kaynak ve HAZ bölgesinin toplam uzunluğu 40-60 mm'dir. Isıdan etkilenmemiş ray çeliğine göre, ısıdan etkilenmiş bölgenin sınırındaki sertliğin azaldığı, ısıdan etkilenmiş bölgenin, kontrollü soğutulmuş tane yapısına göre farklılık arz

ettiği görülmüştür. Isıdan etkilenmiş bölgenin iri tane yapısının, erime sıcaklığına çok yakın sıcaklıklarda malzemenin ısıtılmasının bir sonucu olarak birleşme yüzeylerinin yanında oluştuğu, bitişindeki normalize olmuş bölgelerin ise ince taneli olduğu tespit edilmiştir [Onay, 2011].

3.1.2. Kaynak mukavemeti

Tablo 3.1’de iki yöntemin mukavemetleri karşılaştırılmıştır. Kaynak dayanımları; yorulma, eğilme ve çekme dayanımları açısından incelendiğinde, yakma alın kaynak yönteminin, alüminotermite kaynak yöntemine göre çok daha yüksek bir performans gösterdiği görülmektedir. Yüksek dingil yükleri altındaki demiryolu hatlarında alüminotermite kaynaklarda meydana gelen kusurların büyüklüğü, azımsanmayacak ölçüde fazladır [Mutton ve Alvarez, 2004].

Tablo 3.1. Yöntemlerin kaynak mukavemetleri karşılaştırması

Karşılaştırma parametresi	Yakma alın kaynağı	Alüminotermite kaynağı	R260 S49 Ray (minimum)
Yorulma mukavemeti (kg/mm ²)	35	22	19
Eğilme mukavemeti (ton)	125	103	125
Gerilme mukavemeti (kg/mm ²)	80	76	88

2004 yılında Fransız Ulusal Demiryolu Şirketi (SNCF) şebekesinde tespit edilmiş ray kırıklarından % 34’ü alüminotermite kaynak, % 3’ü ise yakma alın kaynağı bölgelerindedir. Amerika’da ağır dingil yükleri altında alüminotermite ve yakma alın kaynakları, 33 ton dingil yükü olan araçların ray üzerinde 65 milyon gros ton yük geçtikten sonra, kırılma yüzdeleri karşılaştırılmıştır. İnceleme sonucunda kırıkların % 29’unun alüminotermite kaynak, % 3’ünün ise yakma alın kaynaklarda meydana geldiği tespit edilmiştir [Lichtberger, 2005]. Almanya’da demiryollarında her 100 km’de 1 ray kırığı meydana gelmektedir. Bir yıl içinde toplam 650 adet ray kırığı tespit edilmiş, bunların 220 adedinin alüminotermite kaynak bölgelerinde olduğu görülmüştür [Lichtberger, 2005].

Bir başka karşılaştırma da muhtelif teknik özellikler açısından yapılarak, Tablo 3.2’de verilmiştir. Sonuçlar incelendiğinde, Yakma alın kaynağının Alüminotermite kaynağından pek çok yönden üstün olduğu görülmektedir.

3.2. Maliyet Açısından Karşılaştırılması

Kaynak Yöntemlerinin mukayesesinde; amortisman, malzeme ve işçilik maliyetleri esas alınacaktır. Amortisman maliyetleri; Alüminotermite yönteminde; makine bedeli ve makine servis ömrünü

kapsamakta iken, Yakma alın kaynak makinesinin amortisman maliyeti 15 yıl/3600 gün olan servis ömrüdür.

Tablo 3.2. Teknik özellikler açısından kaynak tekniklerinin karşılaştırılması

Teknik özellikler	Yakma alın kaynağı	Alüminotermite kaynağı
Kaynak süresi (dk)	7	58
Mikro yapı	Tam perlitik dövme	Kısmi perlitik döküm
HAZ uzunluğu (mm)	40 - 60	125 - 185
Çevre kirliliği etkisi	Düşük	Yüksek
Kişisel tehlike	Düşük	Yüksek
Hatalı kaynak oranı	% 0,1	% 3
Kaynak yöntemi	Yarı otomatik	Manuel
Kaynak kalitesi	Yüksek	Düşük
Yorulma dayanımı (kg/mm ²)	35	22
Eğilme dayanımı (ton)	125	103
Gerilme dayanımı (kg/mm ²)	80	76
Taşınabilirlik	Düşük	Yüksek
Farklı kesitlerin kaynağı	Düşük	Yüksek

3.2.1. Kaynak Süresi ve Üretim Performansı

Alüminotermite Kaynak ekibi bir ayda ortalama olarak 22 iş günü çalışmakta olup, bir kaynağın ortalama yapım süresi 58 dakikadır. Bir alüminotermite kaynak ekibi, 5 kişiden oluşmakta olup, ekip şefi, ön hazırlık ve kaynak işlemini yapan 2 usta, bir taşlama ustası ve bir ara elemandan meydana gelmektedir.

Yakma Alın kaynak işlemi 5 kişiden oluşur, ekipte; ekip şefi, kaynak öncesi ray başlarını taşıyan 2 işçi, bir adet kaynak sonrası kaba ve ince taşlama ustası ve yakma alın kaynağı makinesi operatörü bulunur. Bir ayın ortalama olarak 22 iş gününden oluştuğu kabul edilmiştir.

Tablo 3.3’de iki kaynak tekniğinin uygulanması için gerekli süreler ve performanslar karşılaştırılmıştır.

Tablo 3.3. Kaynak tekniklerinin işlem süresi iş verimi açısından karşılaştırma tablosu

Alüminotermite Kaynağı		Yakma Alın Kaynağı	
İşlemler	İşlemlerin Süresi (dk)	İşlemler	İşlemlerin Süresi (dk)
Rayların ayarlanması	12	Rayların ayarlanması	2
Kalıp bağlanması	12	Kaynak operasyon	3
Ön ısıtma	6	Kaynak ara mesafesi zaman kayışı	2
Döküm	3		
Soğuma ve sıyırma	10		

Taşlama ve kurulum	15		
TOPLAM	58	TOPLAM	7
8 saat/gün çalışmayla yapılan kaynak sayısı	8	8 saat/gün çalışmayla yapılan kaynak sayısı	68

Tablo 3.3’de görüldüğü gibi Yakma Alın Kaynağının verimi, Alüminotermite Kaynağının 8 katından fazladır.

Malzeme maliyetleri içine Alüminotermite kaynağında; kaynak porsiyonu, pota, tuğla kalıp, sıvama macunu, maytap, ray taşlama taşı, ön tavlama malzemeleri ve kaynak makinelerini çalıştıran yakıt, yağ vb. maddeler girmektedir. Yakma Alın kaynağında malzeme maliyeti kapsamına; yakıt, yağ ve ray taşlama taşı bedelleri girmektedir.

İşçilik gideri her iki kaynak tekniğinde de 5 kişilik ekip gideridir. Tablo 3.4’de her iki kaynak yönteminde “bir kaynak operasyonunun maliyeti” gösterilmiştir

Tablo 3.4. Birim kaynak maliyetleri tablosu

Kaynak yöntemi	Amortisman (€)	Malzeme (€)	İşçilik (€)	Diğer (€)	Toplam (€)
Alüminotermite	2,04	69,25	46,58	11,79	129,66
Yakma alın	8,35	12,16	4,79	47,06	72,36
Maliyet farkı					57,30

Tablo 3.4 sonuçlarına göre, alüminotermite kaynağında; malzeme ve işçilik giderleri yüksek iken, yakma alın kaynağında ise, diğer giderler (yedek parça, işçilik, nakliye ve sigorta) yüksektir.

4. GENEL DEĞERLENDİRME

Her iki kaynak yöntemi değerlendirildiğinde yakma alın kaynağının üstünlükleri açısından aşağıdaki sonuçlara varılmıştır:

- Kaynak süresi çok kısadır (58 dk. yerine 7 dk). Kaynak otomatize edilebilir.
- Yapılar her iki kaynakta da perlitik’dir. Isıdan etkilenen bölge küçüktür.
- Kaynak kalitesi yüksek, kaynak anında kişisel tehlike ve çevre kirliliği etkisine düşüktür.
- Hatalı kaynak oranı çok düşüktür (% 3 e karşılık, % 0,1).
- Mekanik dayanımlar yüksektir.

Yakma alın kaynağının zayıf yanları ise; ilk yatırım maliyetinin yüksekliği ve farklı kesitlerin kaynak kabiliyetinin zayıflığıdır.

KAYNAKLAR

Arlı, V., "Demiryolu Mühendisliği", Birsen Yayınevi, İstanbul, 2015.

Arlı, V. ve Öztürk Z., " Demiryolu Mühendisliği", İstanbul Ulaşım AŞ Yayınları, İstanbul, 2009.

Aytekin V., "Ray Malzemelerinde Gelişmeler ve Türkiye'de Ray Üretimi", Ulaşımında Raylı Taşıt Sempozyumu, s. 327, Adapazarı, 1989.

Esveld C., "Modern Railway Track", Second Edition, MRT - Productions, 2001, Delft University of Technology, The Netherlands.

Günoral Ş., "Balastlı Üst Yapılarda Yol Bakım ve Tamirâtı", 2nci baskı, Karabük Üniversitesi yayını, 2018.

Kumbasar F., "Üstyapı ve Demiryolu Mekaniği", Güven Yayınevi, Ankara, 1972.

Lichtberger, B. "Track compendium" First edition, Eurail Press, 2005.

Mutton, P. J. ve Alvarez, E. F., "Failure Modes in Aluminothermic Rail Welds Under High Axle Load Conditions, Engineering Failure Analysis", Volume 11, Issue 2, 2004.

Onay M., "Demiryollarında Alüminotermite Kaynak ile Yakma Alın Kaynak Yöntemlerinin Teknik ve Ekonomik Yönden Karşılaştırılması", Yüksek lisans tezi, Bahçeşehir Üniversitesi, 2011.

Özkul F., "Demiryollarında Ray Birleştirme Yöntemlerinin İncelenmesi, Alüminotermite ve Yakma Alın Kaynak Yöntemlerinin Karşılaştırılması", Yüksek Lisans Tezi, İTÜ Fen Bilimleri Enstitüsü, 2014.

Özsaraç U., "Raylı Taşıtlarda Teker Bandajı - Ray Sisteminde Dolgu Kaynağı ve Sabo Parçalarının Aşınma ve Yorulma Davranışlarının İncelenmesi", Yüksek lisans tezi, Sakarya Üniversitesi, Fen Bilimleri Fakültesi, 2005.

Rangwala C., "Railway Engineering", Charotar Publishing House, India, 2007.

METAL-METAL KOMPOZİT ÜRETİMİNDE DÖKÜM BİRLEŞTİRME TEKNİĞİ VE NORMALİZASYONUN ETKİLERİNİN İNCELENMESİ

Hasan HASIRCI

Gazi Üniversitesi, Teknoloji Fakültesi, Metalurji ve Malzeme Mühendisliği, Teknikokullar, Ankara, TÜRKİYE.
hasirci@gazi.edu.tr

Özet

Kompozit ürünler gün geçtikçe önemi artan malzemelerdendir. Metal-metal kompozitler ise son yıllarda önemi hızla artan kompozitlerdendir. Kompozit malzemeler çok çeşitli amaçlarla ve farklı teknikler kullanılarak üretilmektedir. Bu çalışmada metal-metal kompozit üretiminde döküm birleştirme tekniğinin kullanımı, ısıtma işlemi uygulanması ve kompozitin özelliklerine etkileri değerlendirilmiştir. Bu amaçla katı haldeki Beyaz Dökme Demir ile sıvı haldeki 4140 Çeliğinin birleştirilmesi işlemi gerçekleştirilmiştir. Birleştirilen malzemeler daha sonra ara yüzey bağının artırılması ve özelliklerinin geliştirilmesi amacıyla 1, 2, 3 ve 4 saat normalizasyon işlemine tabi tutulmuştur. Bu çalışma sonunda; döküm birleştirme tekniği kullanılarak metal-metal kompozit üretiminin başarıyla yapılabildiği ve normalizasyon ısıtma işlemi ile ara yüzeyin geliştirilebildiği tespit edilmiştir.

Anahtar Kelimeler: Metal-metal kompozit, Döküm birleştirme tekniği, Normalizasyon

INVESTIGATION OF THE EFFECTS OF CAST JOINING TECHNIQUE AND NORMALIZATION IN METAL-METAL COMPOSITE PRODUCTION

Abstract

Composite products are increasingly important materials. Metal-metal composites are composites that have increased rapidly in recent years. Composite materials are produced for a variety of purposes and using different techniques. In this study, the use of casting joining technique in metal-metal composite production, the application of heat treatment and the effects on composite properties were evaluated. For this purpose, the joining of solid White Iron and liquid 4140 Steel has been carried out. The combined materials were then subjected to 1, 2, 3 and 4 hours of normalization in order to increase the interfacial bonding and improve its properties. At the end of this study; it has been found that metal-metal composite production can be successfully performed using a casting joining technique and that the interface can be improved by normalization heat treatment.

Keywords: Metal-metal composite, Casting joining technique, Normalization

1. Giriş

Kompozit malzemeler, farklı amaçlarla çok farklı kullanım alanlarına sahip malzemelerin başında gelmektedir. Bu nedenlerle farklı beklentilere sahip kompozitlerin üretimi gerekmektedir. Bu malzemeler sıvı karıştırma ve toz metalurjisi gibi bazı yöntemler ile üretilmekte ve gerektiğinde ısıtma işlemiyle daha üst beklentileri karşılayabilecek hale getirilebilmektedirler [1-4]. Günümüzün modern teknolojisi; uzay, uçak ve otomotiv endüstrisi gibi ileri teknoloji alanında kullanılmak üzere hafif, üstün ve kendine has özelliklere sahip yeni malzemelere ihtiyaç duymaktadır. Uzay, havacılık ve otomotiv sektörlerinde, mukavemet/ağırlık, mukavemet/yoğunluk oranları gibi malzeme özelliklerinin önemli olduğu ağırlığa duyarlı alanlarda kullanılan malzemelerin mukavemet

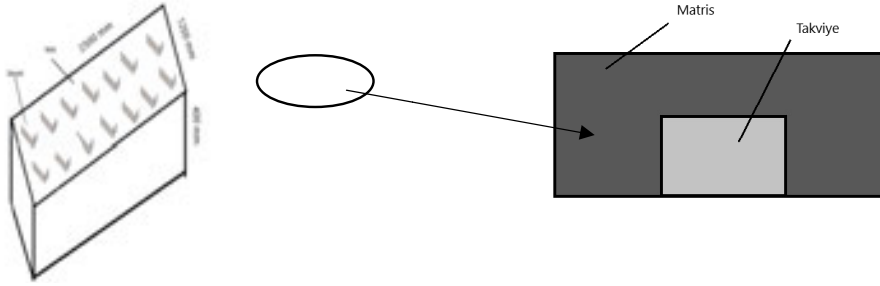
limitlerinin zorlanması, belirli kurallar içinde farklı malzemelerin karıştırılarak özelliklerinin geliştirilmesini önemli kılmış ve bu alanda da önemli gelişmelere yol açmıştır. Sahip oldukları özelliklere rağmen, kompozit malzemelerin üretim maliyetlerinin alaşımlara kıyasla daha yüksek olmasından dolayı kullanımları endüstriyel olarak istenen seviyelere ulaşamamıştır. Ancak son yıllardaki gelişmelere bakarak bu malzemelerin kullanımlarının yaygınlaştığı ve bu yaygınlaşmanın giderek artacağını söylemek mümkündür [1]. Kompozit malzemeler, ana malzeme alaşımlarına göre; metal esaslı, polimer esaslı ve seramik esaslı kompozitler olarak gruplandırılmaktadır. Polimer esaslı kompozitler; Kısmen düşük sıcaklıkta (5-50 °C) kullanılabilir. Üretim maliyetleri düşüktür. Seramik esaslı kompozitler; yüksek sıcaklıktaki üretimleri ve gevrek bir yapı teşkil etmeleri sebebiyle metal esaslı kompozitler daha ön plana çıkmaktadır. Metal esaslı kompozitlerin üretimleri son yıllarda önemli bir artış göstermektedir. Metal esaslı kompozitlerin gelişmesindeki önemli neden; teknolojinin sürekli yenilik istemesi ve hayati ihtiyaçların ön plana çıkmasıdır [2,3]. Kompozit malzemeler içerisinde önemli bir yere sahip olan MMK'ler(Metal MatrisliKompozit) üzerine son yıllarda yoğun bir şekilde çalışılmaktadır. Metal esaslı kompozitlerin yerlerine kullanıldıkları diğer malzemelere göre yüksek mekanik özelliklere sahip olduğundan bu kompozitlere duyulan ilgiyi artırmıştır [2]. Yüksek mekanik özelliklere sahip sürekli fiberlerle takviye edilmiş alüminyum esaslı kompozitler üzerinde çok sayıda araştırma yapılmaya devam edilmektedir. Elde edilen kompozitler dikkat çeken özellikler göstermelerine rağmen üretimlerinin zor, takviye elemanlarının pahalı ve çok masraflı olmasından dolayı ticari uygulamalarda kendine yer bulamamaktadır. Bu sınırlamalardan dolayı MMK'ların kullanımları özel alanlarla sınırlandırılmıştır [3].Parçacık takviyeli MMK'ların özelliklerini pek çok faktör etkilemektedir. Bunlar; ana malzemenin bileşimi, takviye malzemesi, takviye boyutu, şekli ve hacimsel oranı, takviye dağılımı gibi faktörlerdir. Kompozit malzeme üretimi sırasında bunlar çok iyi kontrol edilmelidir [4]. Parçacık takviyeli MMK'ların üretimi elyaf takviyeli kompozitlere göre daha kolay ve ucuzdur. Parçacık takviyeli MMK'ların en ucuz ve kolay üretim yolu da döküm tekniğidir, yaygın olarak sıvı karıştırma metodu kullanılmaktadır [5,6,7].Sıvı hal üretim yönteminde karşılaşılan ısıtma probleminden dolayı takviye elemanlarının arzu edilen şekilde karıştırılma güçlüğünden dolayı alternatif üretim yöntemi olarak katı hal üretim yöntemi tercih edilmektedir. Yaygın olarak kullanılan toz metalurjisi yönteminde ise farklı karekterlerdeki toz ve takviye elemanlarının birbirine sinter olmamalarındaki yetersizliktir [5,8,9].Metal MatriksKompozit (MMK) üzerine yapılan araştırmalar son 20 yıldır çok fazla ve etkileyici boyuttadır. MMK'lar üzerinde yapılan çalışmalar, özellikle yüksek sıcaklıklarda kullanılabilen dayanımı yüksek, rijit malzemelerin geliştirilmesi yönünde yoğunlaşmaktadır. Kompozit malzemelerde takviye elemanı olarak partikül, tabaka ve fiberler yaygın olarak kullanılmaktadır. Yüksek performansı sayesinde fiberle takviye edilmiş malzemeler, oda sıcaklığında ve daha yüksek sıcaklıklarda takviye edilmemiş yapılara göre çok iyi yüksek performans sergilemektedirler [10]. Ne var ki polimer matrikskompozitlerin araştırma sonuçları kolaylıkla ticari uygulamalara taşınırken; metal matrikskompozitler, bu konuda biraz yavaş kalmıştır. Bunun nedeni, metal matrikskompozitlerin üretim zorluğu ve özellikle ara faz mukavemetinin zayıflığıdır [11]. Bununla birlikte, MMK'ler üretim güçlüğü, işleme güçlüğü, yüksek maliyet ve diğer malzemeler gibi geriye dönüşümünün (recycle) istenilen düzeyde olamaması gibi bir takım dezavantajlara da sahiptir [10,11]. Dökmedemirler, dünya da ve ülkemizde en yaygın üretilen ve kullanılan malzeme grubundandır. Özellikle, Beyaz Dökme Demir (BDD) diğer döküm türlerine göre özellikle sert ve aşınmaya dirençli olması sebebiyle, çok tercih edilen ve en yaygın malzemedir. Özellikle yüksek Cr'lu BDD malzemeler; çimento ve maden sektörü için aşınmaya dirençli silindir, hadde, öğütme topu, darbeli kırıcı ve taşıyıcı parçaların üretiminde kullanılmaktadır [2].Isıl işlem; bir malzemenin özelliklerini ve/veya iç yapısını değiştirmek amacıyla, o malzemeye belli bir sıcaklık-zamanprogramı dahilinde uygulanan bir ısıtma ve soğutma işlemleri dizisidir. Isıl işlem, üç ana safhadan oluşur. Bunlar ısıtma, ısıtılan sıcaklıkta bekletme ve soğutma safhalarıdır. Bütün ısıl işlem yöntemlerinde bu üç ana safha geçerlidir. Fakat uygulanan ısıl işlem türüne göre, ısıl işlem sıcaklığı, bekletme süresi, ısıtma ve tutma hızı gibi parametreler değiştirilir. Normalizasyon ısıl işlemi de genellikle 800-950 °C

sıcaklıkta 30-120 dakika bekletmenin ardından durgun havada oda sıcaklığına kadar soğutma işlemidir. Bu işlem sonunda malzemelerin mekanik özellikleri iyileştirilmektedir [12-14].

Bu çalışmanın amacı; MMK malzemelerin bir türü olan Metal-Metal Kompozit (hem matris hem de takviye metalden) malzemenin döküm yöntemiyle üretimi, laboratuvarında mekanik ve yapısal olarak incelenmesi gerçekleştirilecektir. Daha sonra ise piyasada kullanılan aşınmaya dirençli parçalara uygulanarak ömürlerinin uzatılması ve gerçek performanslarının belirlenmesi hedeflenmektedir. Bu araştırmada üreteceğimiz malzemenin matrisi 4140 kalite çelik olup içerisinde parçalar halinde Beyaz Dökme Demir (BDD) takviyeler bulunacaktır. Çelik matris darbe dayanımı ve süneklik sağlarken, aşınmaya karşı ise BDD direnç sağlayacaktır. Çalışmanın en önemli tarafı kalıp boşluğuna yerleştirilen katı takviye üzerine sıvı matris malzemesi dökülerek en uygun kompozit malzeme üretim parametrelerinin belirlenmesidir. Aynı zamanda bu parçalara uygulanan ısıl işlemler bu çalışmada kullanılarak ısıl işlemin döküme göre avantaj ve dezavantajları da test edilecektir.

3. Deneysel Çalışmalar

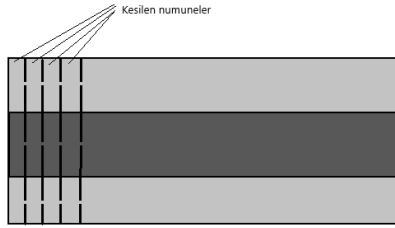
Bu çalışmada Metal-Metal Kompozit malzemenin döküm yöntemiyle üretimi gerçekleştirilmiştir. Bu kompozit; matris olarak 4140 çeliği (4140), takviye ise beyaz dökme demir (BDD) malzemenin üretilmiştir. Malzeme seçiminde 4140 çelik matrisin darbe dayanımı ve süneklik sağlarken, aşınmaya karşı ise BDD direnç sağlayacaktır. Üretimde takviye katı, matris ise sıvı halde malzeme kullanılmıştır. MMK malzemesinden üretilmesi hedeflenen aşınma plakası şematik gösterimi Şekil 1.a'da verilmiştir. Bu çalışmada numune olarak kullanılmak üzere Şekil 1.b'de şematik gösterimi verilen 165x40x250 mm boyutlarındaki plaka şeklindeki kompozit parça üretilmiştir. Takviye malzemenin ölçüleri 35x35x250 mm'dir. Döküm işlemleri reçineli kum kalıp kullanılarak, 300 °C'ye ön ısıtma yapılmış katı haldeki BDD takviyelerin üzerine 1580 °C sıcaklıktaki sıvı haldeki 4140 çelik malzemenin doldurulması ile gerçekleştirilmiştir (Şekil 2). Hazırlanan kalıpların yüzeyleri dökümden önce temiz yüzey ve düşük kalıp reaksiyonu için Zr esaslı alkol içerikli boya ile kaplanmış ve kurutulmuştur. Döküm işleminden sonra CNC freze tezgahında MMK numunesinin tüm yüzeyleri temizlenmiştir. Daha sonra ATAS marka su soğutmalı abrasif diskli kesme cihazı kullanılarak döküm numune plakasından enine olacak şekilde 5 mm kalınlığında parçalar şeklinde numuneler alınmıştır (Şekil 3). Alınan numuneler kullanılarak yapısal ve mekanik incelemeler gerçekleştirilmiştir. Piyasada kullanılan aşınma plakaları kullanılmadan önce gerilim giderme bir miktar sertleştirme amacıyla piyasadaki uygulamalara benzetilerek atmosfer kontrolsüz kamara tip fırında normalizasyon işlemine tabi tutulmaktadır. Bu nedenle numuneler test edilmeden önce bazılarında 900 °C'de 1, 2, 3 ve 4 saat süreyle normalizasyon işlemi uygulanmıştır. Her bir şart için 3 adet numune üretilmiştir. Yapısal incelemeler için matris ve takviyeyi birlikte kapsayan numuneler hazırlanmıştır. Numuneler standart metalografik hazırlık işlemlerinden (zımparalama ve parlatma) geçirildikten sonra % 2 nital ile yüzeyler dağlanmış. Bu yüzeyler üzerinde mikro yapısal ve matris/takviye ara yüzey analizleri Leica marka mikroskop kullanılarak gerçekleştirilmiştir. Üretilen numuneler sertlik testlerine tabi tutulmuştur (Şekil 4). Sertlik testleri EmcoTEST cihazında HV30 cinsinden her bir durum ve bölge için en az 5 adet olacak şekilde yapılmıştır. Sonuçlar kısmında ortalama sonuçlar verilmiştir. İstatistiksel olarak ± 5 değer aralığı uygun kabul edilmiştir. Bu numuneler ayrıca XRD faz ve SEM-EDS element analizine de tabi tutulmuştur.



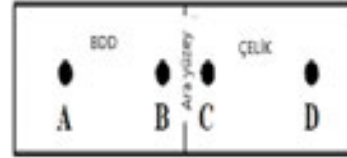
Şekil 1. Hedef aşındırma plakası ve deneysel çalışmalar için üretilen kompozit numunenin şematik gösterimi



Şekil 2. Döküm işlemi için kullanılan kalıpların boyanması, kurutulması ve döküm sonrası üretilen kompozit numunenin çıkarılması



Şekil 3. Döküm plakadan numune alımının şematik gösterimi

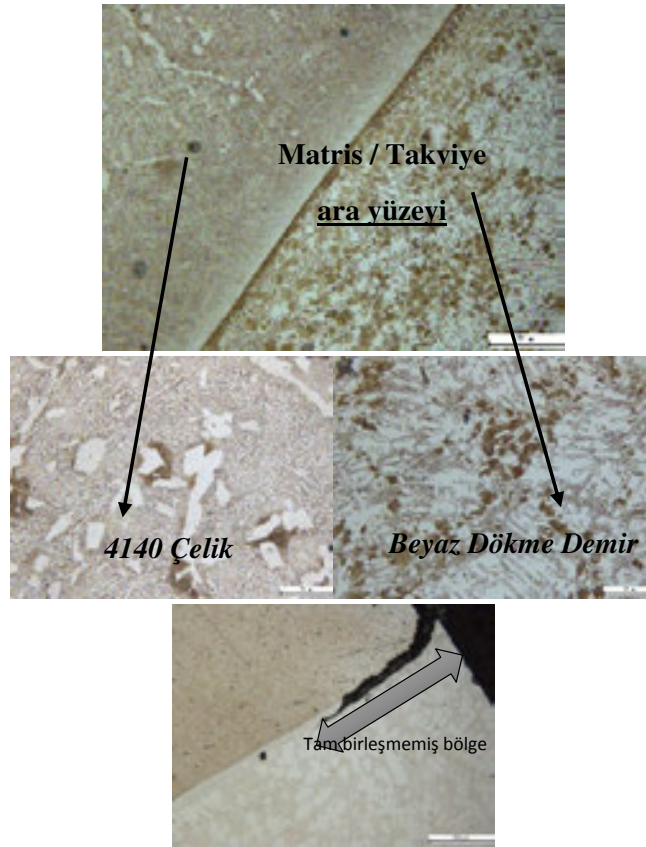


Şekil 4. Sertlik testlerinin uygulanması

4. Deneysel Sonuçların Değerlendirilmesi

Üretilen numunelerden elde edilen matris/takviye yapısal optik mikroskop görüntüleri Şekil 5 ve 6'da verilmiştir. Görüntüler incelendiğinde döküm durumu (Şekil 5) ve gerilim giderme sonrasında (Şekil 6.a) BDD takviye ve 4140 çelik matris yapıları açıkça görülmektedir. Her iki malzemenin yapısının döküm şartlarına uygun şekilde oluştuğu görülmektedir. Buna göre BDD'de metal karbürler, sementitler, ferritik yapılar ve çelikte ise küreselimsi sementitler ve perlitik yapılar bulunmaktadır. Matris/takviye ara yüzeyi incelendiğinde çizgi halinde çoğunlukla aralıksız, bütünleşmiş, ancak özellikle numunenin tabanına yakın kısımlarda yüzeyden içeriye doğru 1-2 mm derinlikte tam olarak birleşmemiş (kaynaşmamış) kısımların olduğu görülmektedir. Ancak, bu tür parçalar dökümden sonra talaşlı imalata (torna, freze vb.) tabi tutulmaktadır. Bu işlem sırasında döküm şartları ve yüzey kalitesine bağlı olarak yüzeyden 1-5 mm talaş kaldırılmaktadır. Bu nedenle bu birleşmemiş kısımların talaşlı imalat sırasında yüzeyden kaldırılıp yok edilmesi ve tam bir birleşme sağlanmış matris/takviye yüzeyinin elde edilmektedir. Özetle bu durum bir sorun oluşturmayacaktır. Numunelerimiz de talaşlı imalata tabi tutulduğundan bu görüntü kalmamıştır. Isıl işlem malzeme yapısında difüzyon meydana getiren bir işlemdir. Normalizasyon işleminde de çözündürme sırasında sıcaklık ve süreye bağlı olarak difüzyon meydana gelmektedir. Bu çalışmada

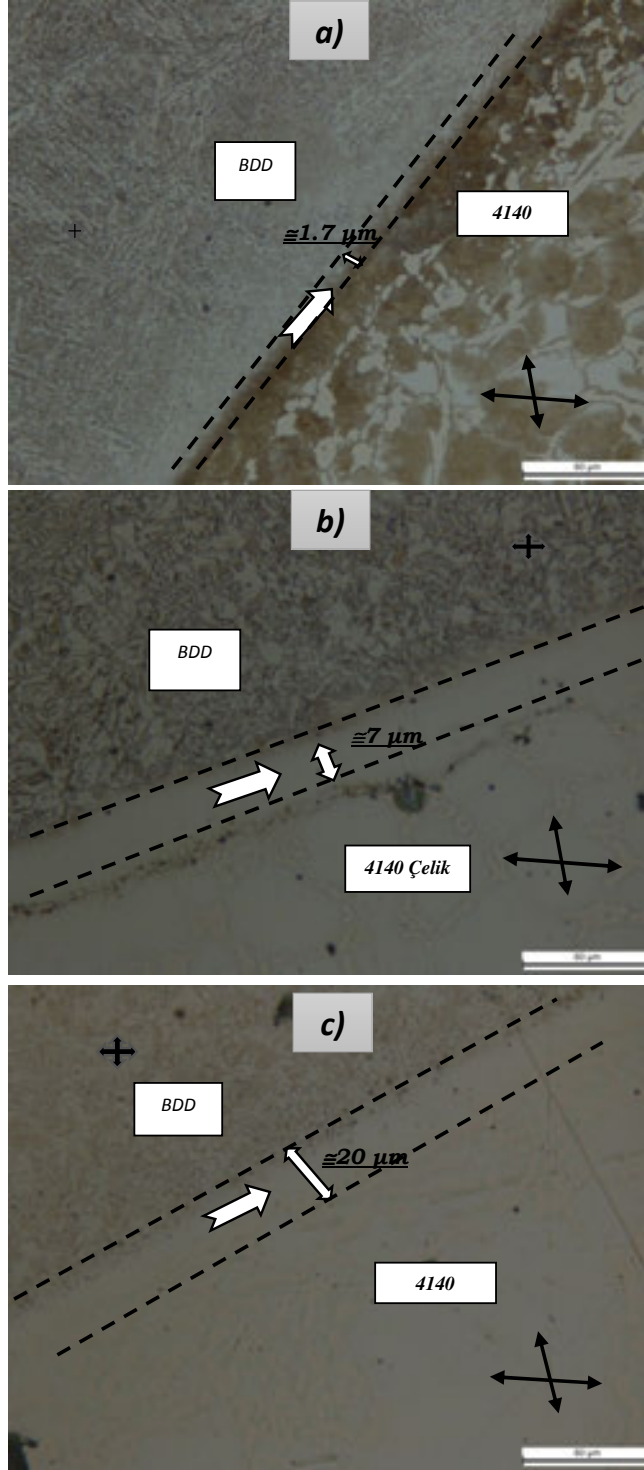
sıcaklık sabit olup, süre artırılarak difüzyona dolayısıyla ara yüzeye etkileri gözlenmiştir. Şekil 6'da verilen ısıtım işlemi uygulanmış numunelerin yapıları incelendiğinde; gerilim giderme uygulamasının (Şekil 6.a) her iki malzemenin yapısında da bir değişim ve dönüşüm meydana getirmediği tespit edilmiştir. Aynı zamanda arayüzeyde de bir değişim söz konusu değildir. Çünkü bu numuneye gerilim giderme uygulanmıştır. Bu ısıtım işleminin sıcaklığı düşük olduğundan (450-550 °C) ara yüzeyde değişim meydana getirebilecek düzeyde difüzyon için yeterli termodinamik şartlar oluşmamış ve dolayısıyla yapısal değişim meydana gelmemiştir. Matris/takviye ara yüzeyi çok dar olup, tespit edilebilen ara yüzey genişliği ortalama 1,7 µm kadardır. Şekil 7'de uygulanan işlemlere bağlı olarak matris/takviye ara yüzey boyutunun değişimi verilmiştir. Sonuçlar incelendiğinde; hem normalizasyon uygulanması hem de normalizasyon süresinin artması ara yüzey katman kalınlığının artmasına yol açtığı görülmektedir.

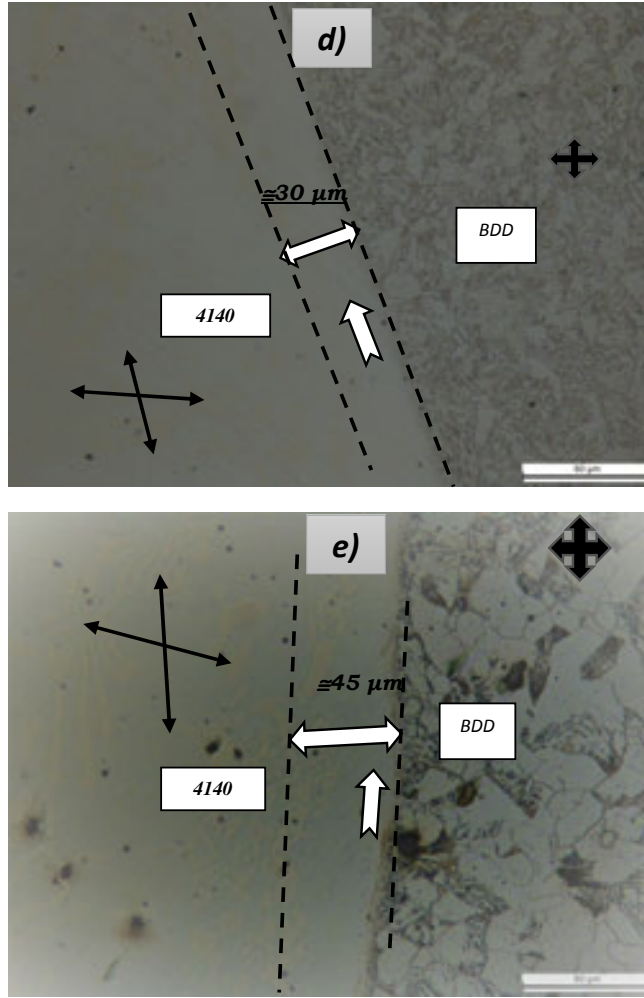


Şekil 5. Döküm durumunda matris/takviye arayüzey optik mikroskop görüntüleri

Şekil 6.b-e'deki numuneler incelendiğinde ise normalizasyon süresinin artmasıyla matris/takviye ara yüzeyinin difüzyona bağlı olarak genişlediği, 1 saat ısıtım işlemi uygulandığında ortalama 7 µm olan ara yüzey genişliğinin 4 saat süresinin sonunda ortalama 45 µm'ye kadar genişlediği tespit edilmiştir. Başlangıçta düz bir hat şeklinde olan ara yüzey yapısının, normalizasyon süresindeki artışa bağlı olarak her iki malzemenin ortak bileşim ve yapılarını içeren geçiş bölgesi haline dönüştüğü görülmüştür. Bu genişleme, bileşim ve yapılar bakımından homojenleşmeyi beraberinde getirdiğinden daha sağlam ve olabildiğince homojen özelliklerde ara yüzey oluşmasına neden olmaktadır. Bu geniş ve olabildiğince homojen ara yüzey ise üretilen kompozit malzemenin mekanik etkenlere karşı daha iyi bir performans sergilemesine yol açmaktadır. Bu ara yüzey oluşumu sonucunda çalışma ortamında kompozit malzemeye uygulanan mekanik etkiler nedeniyle; ara yüzeyden kolayca çatlak oluşturup, hızlı ve kolay bir şekilde deforme olması, dolayısıyla kopması

önlenmiş yada zorlaştırılmış olmaktadır. Bunun sonucunda çok daha dayanıklı ve uzun ömürlü kompozit parça üretilebilmektedir. Diğer yandan; normalizasyon ısıl işlemi sonucunda, hem matris hem de takviye malzemesinin mikro yapısında da değişimler meydana gelmektedir. Döküm ve gerilim giderme işlemi sonucunda BDD ve 4140 çelik malzemelerinin olağan mikro yapılarında değişimler ve dönüşümler meydana gelmektedir.



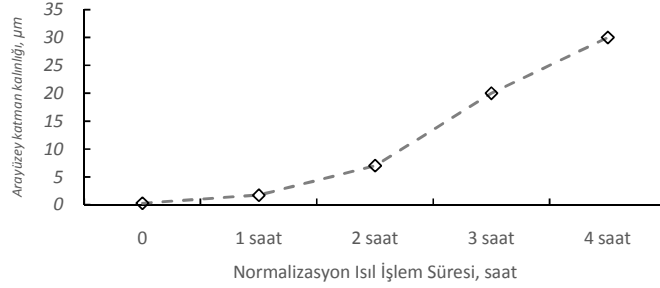


Şekil 6. Isıl işlem görmüş numunelerin mikro yapısal görüntüleri; a) gerilim giderilmiş, b) 1 saat normalizasyon, c) 2 saat normalizasyon, d) 3 saat normalizasyon ve e) 4 saat normalizasyon işlemi uygulanmış

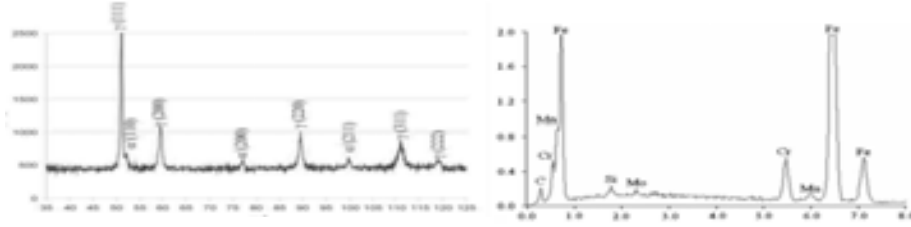
Normalizasyon süresinin artması ara yüzey katman kalınlığını artırırken, uzun süre ısıl işlem uygulanması yapısal kabalaşmalara yol açmaktadır. Normalizasyon işlemi malzemeye bağlı olarak 850-1050 °C gibi yüksek sıcaklıkta çözündürme uygulaması yapılan bir ısıl işlem türüdür. Uzun ısıl işlem süresi uygulandığında bu yüksek sıcaklıklarda malzeme (metal matris ve takviye) yapısında difüzyonun kolay olmasına bağlı olarak ara yüzey katman kalınlığı kolayca artarken (Şekil 6 ve 7), aynı zamanda mikro ve makro yapıda kabalaşmalara yol açmaktadır (Şekil 6.b-e). Bu kabalaşmaların mekanik ve özellikle bu çalışmadaki hedef parça için aşınma özelliklerine etkileri de değerlendirilmek zorundadır.

Yapısal incelemeler yapılırken kabalaşmanın yanında mekanik ve aşınma özelliklerini belirleyen en önemli faktörlerden birisi olan faz tür ve dağılımlarının da incelenmesi gerekmektedir. Bu amaçla yapılan XRD ve SEM-EDS analiz sonuçları Şekil 8'de verilmiştir. Bu analiz sonuçları; 4140 çelik matris malzeme yapısında ferrit, kalıntı östenit, sementit ve alaşım karbür fazlarının bulunduğunu, BDD takviye yapısının ise ferrit, dönüşmüş ledeburit ve alaşım karbür fazlarından meydana geldiğini göstermektedir. Fakat sürenin artmasına bağlı olarak hem matriste hem de takviye malzemede perlit oluşumlarının da meydana geldiği görülmektedir. Bu yapısal değişimler neticesinde özelliklerde de

değişim olması beklenmektedir. Ara yüzeye bakıldığında ise matris ve takviye bileşiminin her ikisinin de yansıdığı, benzer yapıların meydana geldiği görülmektedir. Bu nedenle çelik matris tarafında bir miktar sert faz olan sementit ve çok küçük boyutlu alaşım karbürlerin miktarında artış meydana gelmiştir.



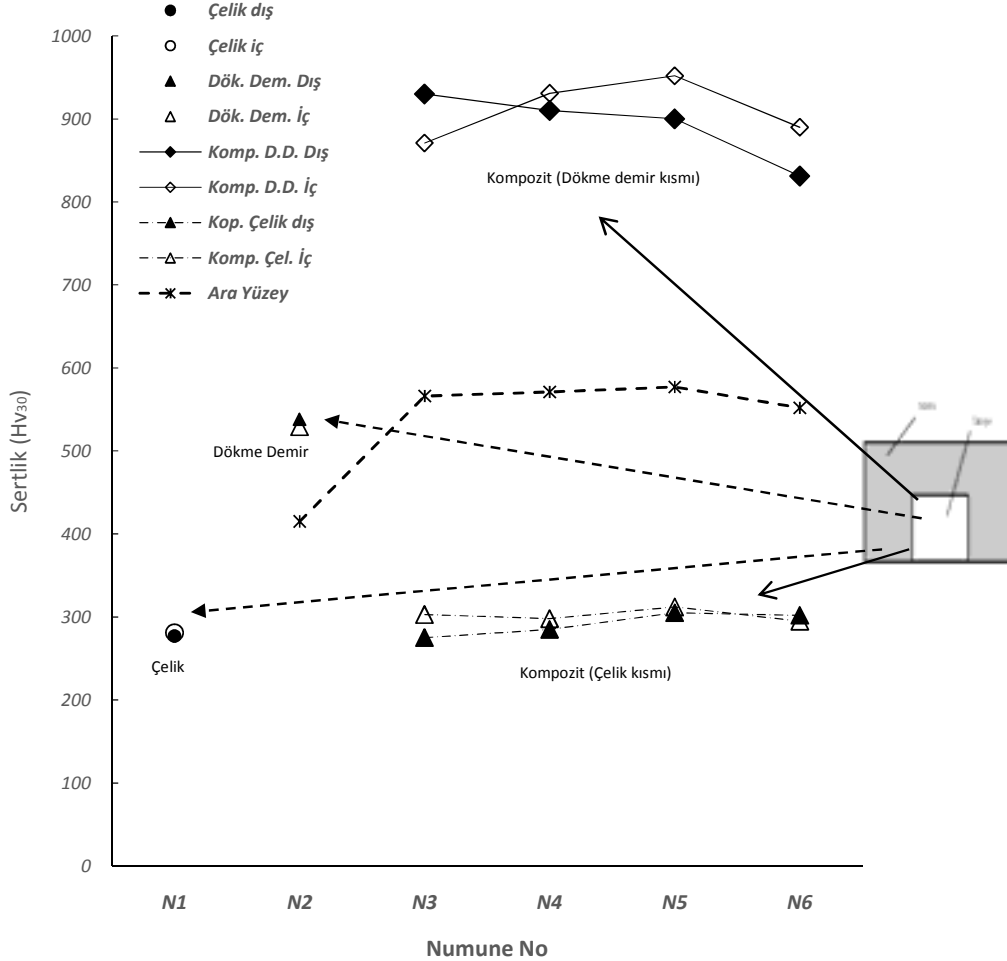
Şekil 7. Normalizasyon ısıl işlem süresine bağlı olarak matris/takviye ara yüzey katmanının değişimi



Şekil 8. Üretim şartlarına bağlı olarak numune yapılarında meydana gelen fazlar ve element dağılımları

Bu çalışmada uygulanan işlemlerin etkilerinin değerlendirilebilmesi için sertlikteki değişimler incelenmiş ve elde edilen sonuçlar Şekil 9'da verilmiştir. Sonuçlar incelendiğinde, genel olarak normalizasyon uygulanması neticesinde sertliğin arttığı görülmektedir. Ancak, matris, takviye ve ara yüzey için ayrı ayrı değerlendirme yapmak gerektiği görülmektedir. Matrise bakıldığında normalizasyon uygulaması sertliği genel olarak (\cong % 15) artırmıştır. Çelik matrisin takviyeye uzak olan (Komp. Çelik İç) kısımlarında sertlik değişimi sınırlı kalırken, bu değişimin takviyeye yakın kısımlarda (Komp. Çelik Dış) daha fazla olduğu görülmektedir. Bu artışın iki nedeni bulunmaktadır. Birincisi normalizasyon ısıl işlemi malzemelerin sertliğinin bir miktar artırması, ikincisi ise BDD kısmından çelik kısmına doğru difüze olan elementlerin etkisiyle sertliği artıran karbür içerikli fazların meydana gelmesidir. Her iki oluşum da malzeme davranışına tam uyum göstermektedir. Ancak sürenin artması (4 saat) ile yapısal kabalaşma meydana gelmiş ve buna bağlı olarak da sertliğin bir miktar azalmasına neden olduğu tespit edilmiştir. BDD takviyeden elde edilen sonuçlar değerlendirildiğinde, BDD malzemenin sertleştirilebilirliğinin çok daha yüksek olması nedeniyle sertlikte % 85-90 aralığında bir artışın meydana geldiği tespit edilmiştir. BDD takviyenin iç ve dışı ayrı ayrı değerlendirildiğinde ise; iç kısımda (Komp. D.D. iç) difüzyona bağlı olarak yeni ve küçük boyutlu sert karbür fazı oluşumlarına bağlı olarak daha fazla artış meydana gelirken, dış kısımda (Komp. D.D. Dış) yapısal kabalaşmaya ve bir miktar perlit oluşumu nedeniyle sertliğin daha az arttığı görülmektedir. Yapısal dönüşümler sertliği doğrudan etkileyen faktörlerdendir. Burada olduğu gibi BDD gibi yüksek sertliğe sahip malzemelerde uzun süre yapılan işlemler yapısal kabalaşmaya ve nispeten yavaş soğutma (normalizasyon işleminde havada soğutma) nedeniyle perlitik dönüşüme bağlı olarak ferrit oluşumu neticesinde sertlikte bir miktar azalma görülebilmektedir. Isıl işlem süresinin uzaması benzer şekilde takviye malzemesinin de sertliğinde bir miktar azalmaya neden olmuştur. Son olarak ara yüzey incelendiğinde; normalizasyon uygulanması neticesinde sertlikte % 37-43 aralığında bir artış meydana gelmiştir. Yukarıda matris ve takviye için yapılan değerlendirmelerin burada da geçerli olduğu, ısıl işlem uygulaması neticesinde difüzyona bağlı

olarak sertliđi yüksek olan nispeten küçük boyutlu karbür fazların etkisiyle ara yüzey sertliđi artmış, fakat sürenin uzamasına bađlı olarak yapısal kabalaşma etkisiyle bir miktar (\cong % 2.5) azalma meydana geldiđi görülmüştür. Bu sertlik sonuçları; hedef parçalara ticari uygulanmakta olan normalizasyon işleminin 4140 çelik/BDD kompozit malzemesine de ara yüzey bađının geliştirilmesi amacıyla uygulanması gerektiđini, ancak bu işlemin süresinin belirli bir sınırdaki tutulması gerektiđini açıkça göstermektedir.



Şekil 8. Uygulanan işlemlere bađlı olarak metal-metal kompozit malzemelerde sertliđin deđişimi

5. SONUÇLAR

Bu çalışmada; ticari olarak kullanılacak üzere üretilmesi hedeflenen aşındırma plakası prototipi için 4140 çelik matris ve BDD takviye malzemelerinin birleştirmesi için döküm ve ardından normalizasyon işlemleri uygulanmıştır. Bu birleştirme için kullanılan üretim şartlarına bađlı olarak yapısal ve sertlik özelliklerindeki deđişimleri incelenmiştir. Elde edilen sonuçlar aşağıda verilmiştir. Bu sonuçlara göre;

- ✓ 4140 çelik ile BDD malzemelerin uygun şartların oluşturulması neticesinde döküm ile başarılı bir şekilde birleştirilebildiđi,

- ✓ Dökümün ardından uygulanan normalizasyonun matris/takviye birleşme ara yüzeyinin yapı ve mekanik özelliklerini çok daha fazla geliştirebildiği,
- ✓ Bu gelişme nedeniyle ısıtma işlem uygulamasının mutlaka yapılması gerektiği,
- ✓ Isıtma işlem süresinin artmasıyla matris/takviye ara yüzey katman kalınlığının arttığı,
- ✓ Katman kalınlığının artmasıyla mekanik özelliklerin geliştirilebileceği,
- ✓ Normalizasyon işlem süresinin çok uzamasıyla meydana gelen yapısal değişim ve kabalaşmalardan dolayı mekanik özelliklerin bir miktar kötüleştiği, bu nedenle ısıtma işlem süresinin sınırlandırılması gerektiği tespit edilmiştir.

KAYNAKLAR

- [1] M.Simsir, L.C. Kumruoğlu and A. Öze, “An investigation into stainless-steel/structural alloy-steel bimetal produced by shell mould casting”, *Mater Des*, 30 (2009) pp.264–70.
- [2] O. Yılmaz and H. Çelik, “Electrical and thermal properties of the interface at diffusion bonded and soldered 304 stainless steel and copper bimetal”, *J Mater Process Technol* 141 (2003) pp.67–76.
- [3] B.Kurt, N. Orhan and A. Hascalik, “Effect of heating and cooling rate on interface of diffusion bonded gray cast iron to medium carbon steel”, *Mater Des*; 28:22 (2007) pp.29–33.
- [4] H.DManesh and A.K. Taheri, “An investigation of deformation behavior and bonding strength of bimetal strip during Rolling”, *Mech Mater*; 37:5 (2005) pp.31–42.
- [5] P. Kazanowski, M.E. Epler and W.Z. Misiolok, “Bi-metal rod extrusion – process and product optimization”, *Mater Sci Eng A*; 369:1 (2004) pp.70–80.
- [6] R. Kacar and M.Acarer, “An investigation on the explosive cladding of 316L stainless steel-din-P355GH steel”, *J Mater Process Technol* 152:9 (2004) pp.1–6.
- [7] S. Berski, H. Dyja, A. Maranda and J.Nowaczewski, “Analysis of quality of bimetallic rod after extrusion process”, *J Mater Process Technol*; 177:58(2006) pp.2–6.
- [8] B.V. Krishna, P. Venugopal and K.P.Rao, “Applicability of the groove pressing technique for grain refinement in commercial purity copper”, *Mater Sci Eng A* ; 407 (2005) pp.77–83.
- [9] Y.H.Liu, H.F.Liu and S.R.Yu, “Study on interface of high speed/structural steel bimetal composites”, *Special Casting & Nonferrous Alloy*; 2:1(2001) pp.7–9.
- [10] B.J.Yang, A.Hattiangadi, W.Z.Li and G.F.Zhou, “Simulation of steel microstructure evolution during induction heating”, *Mater Sci Eng A*; 527: 29(2010) pp.78–84.
- [11] G.L.Xie, H.Sheng, J.T.Han and J.Liu “Fabrication of high chromium cast iron/low carbon steel composite material by cast and hot rolling process”, *Mater Des*; 30:306(2010) pp.2–6.
- [12] H.Hasırcı, “AISI D6 Çeliğinin Adhesif Aşınma Direncine Isıtma İşlem Şartları Ve Kayma Hızlarının Etkileri” *Journal of the Faculty of Engineering and Architecture of Gazi University*, 25 (3), (2010) pp.587-592.
- [13] H.Hasırcı, M.Tabur, F.Gül ve M.İzci, “Borlama Ve Normalizasyon İşlemlerinin AISI 4140 Çeliğinin Adhesif Aşınma Direncine Etkileri ”, 14.Uluslararası Metalurji ve Malzeme Kongresi, 15-18 Ekim İstanbul – TÜRKİYE, (2008) pp.35-42.

- [14] Hasirci, H., Gül, F., " Borlanmış A1sı 4140 Çeliğinde Bor Katman Kalınlığının Abrasif Aşınma Davranışına Etkisi", V. *Demir-Çelik Kongresi Bildiriler kitabı*, , 1-3 Nisan, Karabük – TÜRKİYE, (2011) pp. 170-182.

EN 10346:2015 Çeliği Nokta Direnç Kaynağının Sonlu Elemanlar İle Analizi

Ahmet Çetkin^{1,a}, Mehmet Çakmakkaya^{2,b}, Halil AYTEKİN^{3,c}

¹Teknoloji Fakültesi, Makine Mühendisliği, Afyon Kocatepe Üniversitesi

²Teknoloji Fakültesi, Otomotiv Mühendisliği, Afyon Kocatepe Üniversitesi

³Teknoloji Fakültesi, Metalurji ve Malzeme Mühendisliği, Afyon Kocatepe Üniversitesi

^aacetkin@aku.edu, ^bcakmakkaya@aku.edu.tr, ^chaytekin@aku.edu.tr

Özet

Bu çalışmada nokta direnç kaynağının kaynak parametrelerinin kaynak kalitesi üzerindeki etkileri çalışılmıştır. Otomasyona yatkınlığı göz önüne alındığında, nokta direnç kaynağı otomotiv, uzay, elektronik vb. endüstrilerde kullanılan sac plakaların birleştirilmelerinde en çok kullanılan metotlardan biridir. Malzemelerin elektriksel, termal, mekanik ve metalürjik değişimleri gibi birçok fiziksel olay kaynak parametrelerinin etkisi altındadır. Kaynak bağlantısı, oldukça fazla sayıda parametreye bağlı olarak bağlantının dayanım kalitesini değiştirdiği bir yapıya sahiptir. Özellikle ısıl girdiyi oluşturan kaynak akım değeri, kaynak basıncı ve uygulama sürelerindeki değişimler ve bununla birlikte sac parçasının ve nokta direnç kaynağı yüzey özellikleri, farklı kalınlıklardaki sac bağlantının kalitesini oldukça etkiler. Bu çalışmada DIN EN 10327-04 çinko kaplı sacların kaynak parametrelerine bağlı olarak nokta kaynak bağlantı kalitesi simüle edilmiş ve böylece çekirdek oluşumu temel alınarak kaynak kalitesinin değişimi belirlenmiştir.

Anahtar Kelimeler: Nokta direnç kaynağı, kaynak çekirdeği formu, kaynak parametreleri, sonlu elemanlar.

1.Giriş

Nokta kaynağı, otomotiv endüstrisinde en yaygın sac birleştirme yöntemlerinden biridir. Tipik bir araç imalatında yaklaşık 2000–5000 adet (RSW) nokta kaynağı kullanılmaktadır [1,2,3]. Günümüz otomobil üreticisi firmalar, yakıt tüketiminde cimri otomobilleri üretmeyi hedefliyor. Bununla birlikte çevreyi koruma amaçlı farklı enerji kaynaklarından yararlanmayı da sürdürmektedirler. Malzeme bilimindeki gelişmelere paralel olarak hafif malzemelerin geliştirilmesi ve bu malzemelerin daha yüksek mukavemete ve daha az kütle oranına sahip olmaları bunların cazibesini arttırmıştır. Bu hafif malzemeler araçların ağırlığında önemli oranda azalmayı sağlamış ve başarıyla uygulanmaktadır. Bunlar, yüksek mukavemetli alaşımlı çelikler, alüminyum alaşımları, magnezyum alaşımları, plastik ve kompozit malzemelerdir [4]. Otomobil üretiminde Ağırlık azaltma yöntemi, aynı zamanda, her iki metalin avantajlarını gösterebilen ve

benzersiz bir mekanik özellik kazandırabilen, benzer malzemelerin birleştirilmesini de teşvik etmektedir [5].

Birçok makalede, metallerin sahip olduğu mekanik ve fiziksel özelliklerinin farklı olması bunların füzyon kaynağı ile birleştirilmesinin zor olduğu, birleştirme ara yüzeyinde gerilme konsantrasyonu ve stres süreksizliği bağlı olarak gerilme üretme eğilimi olduğu bildirilmiştir [6]. Sac metallerin birleştirilmesinde birincil kaynak prosesi; Direnç Nokta Kaynağı (RSW) dır. Bu kaynak yönteminin ağırlıklı olarak otomotiv endüstrisinde kullanılmasının nedeni, diğer kaynak yöntemlerine göre daha efektif, verimliliği yüksek, düşük maliyetli ve güvenilir alternatif bir kaynak tekniği olarak hizmet verebilir olmasıdır [7]. Elektrik direnç kaynağı (RSW), birbiri üzerine bindirilen metal levhalar üzerinden elektrotlar yardımı ile geçirilen elektrik akımına karşı, bu metal levhaların gösterdiği dirençten oluşan ısı yardımıyla gerçekleşir. Parçalar kısmi olarak eritilerek kaynak için gerekli kaynak banyosu oluşturulur. Kaynak banyosunun oluşumundan itibaren elektrik akımı kesilerek iş parçalarına elektrotlar ile uygulanan basınç devam eder ve bu basınç altında tabakalar arasında katılma gerçekleşir sökülemeyen türden bir birleşme sağlanmış olur [8].

Son zamanlarda RSW ile yapılan kaynakların kalitesini iyileştirmek için hem deneysel hem de sayısal olarak çalışmalar yapılmıştır. Yapılan deneysel çalışmalarda kaynak çekirdek formasyonu üzerine, farklı parametrelerin kaynak özellikleri üzerindeki etkisi hakkında değerli bilgiler sağlanmıştır [9, 10, 11].

Gelişmiş yüksek mukavemetli çeliklerin (AHSS) ve çift-fazlı (DP) çeliklerin kullanım alanlarındaki artışa paralel olarak bu tür çelik levhaların RSW'si üzerinde çeşitli deneysel çalışmalar yapılmıştır [12, 13, 14, 15, 16, 17, 18].

2. Analiz

Bu çalışmada Tablo 1'de kimyasal ve Tablo 2' de mekanik özellikleri verilen DIN EN 10327-04 çinko kaplı malzeme kullanılmıştır. Malzeme soğuk şekillendirmeye uygun düşük karbonlu ve çinko ile kaplanmış galvanize çelik olup kalitesi DX52D+Z olarak belirlenen Ereğli 1312 sac plakalardır.

Tablo 1. Deneysel çalışmada kullanılan malzemenin spektral analizi

Kimyasal Bileşim	C	Si	Mn	P	S	Ti	Fe
%	0,12	0,50	0,60	0,10	0,045	0,30	Kal.

Tablo 2. Deneysel çalışmada kullanılan sac malzemenin mekanik özellikleri

Akma Mukavemeti (MPa)	Çekme Mukavemeti (MPa)	Uzama (%)
117	207	21

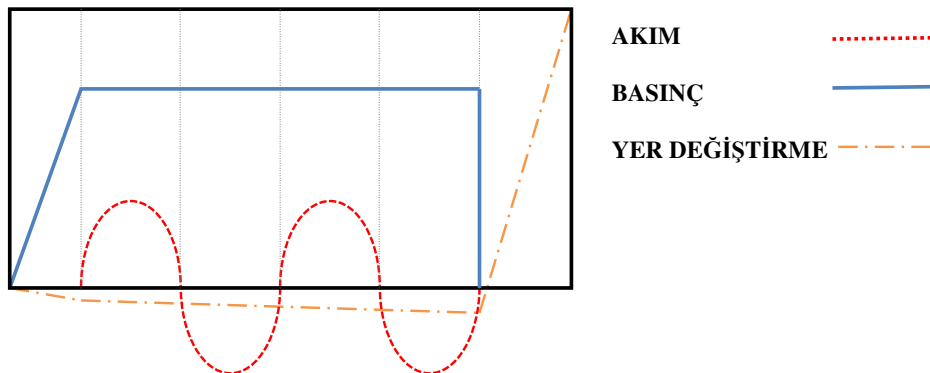
Tablo 3. Analizde kullanılan malzemelerin bazı özellikleri

	Saclar	Kapsül
Elastite Modülü (N/mm ²)...(x10 ³)	205	110
Poisson Oranı (mm/mm)	0.29	0.33
Yoğunluk (tonne/mm ³)...(x10 ⁻⁹)	7.858	8.9
Termal Genleşme Katsayısı (1/°C)...(x10 ⁻⁶)	11.7	17.2
Özgül Isı (mJ/Tonne•°C)...(x10 ⁶)	472	420
Termal İletkenlik Katsayısı (mW/mm•°C)	49.8	360
Elektriksel İletkenlik (mΩ•mm) ⁻¹	6.25	58.8
Ortam sıcaklığı (°C)	25	
Elektrotların İçindeki Suyun Sıcaklığı (°C)	25	
Hava Konveksiyon Katsayısı (W/m ² . °C)	21	
Su Konveksiyon Katsayısı (W/m ² . °C)	300	

Tablo 3'te analizde kullanılan bazı değerler yer almaktadır [19,20,21]. Çekirdek bölgesinde oluşan yapıyı tam olarak simüle edebilmek için, malzemenin plastiklik bölgesinde dayanım davranışının ve elektriksel iletim ve ısı geçirenlik (tablo 3) gibi özelliklere ait değerlerin, kaynak anında değişen basınçlar ve sıcaklık (oda sıcaklığından ergime noktası ve üzerine) altında nasıl değişikliğe uğradığının verilmesi gerekir. Buna rağmen kullandığımız malzemelerin özelliklerinin değişimleri üzerinde daha önceden çalışmalar yapılmamıştır. Bu çalışmaların oldukça zor ve pahalı olacağı da aşikârdır. Buradaki tablolarda kullandığımız değerler oda sıcaklıklarındaki özellikleridir. Bu nedenle, gerçekçi olmak gerekirse, yapılan analizin tam ve net bir sonuç verebilmesi ve uygulamalardaki sonuçlarla karşılaştırılabilmesi oldukça zordur. Burada elde edeceğimiz veriler daha çok, kullanılan parametrelerdeki değişimlerin çekirdek formasyonundaki değişimleri nasıl etkilediğini görmek ve uygulamalarda bu verileri temel alarak parametre seçimlerini yapmak olmalıdır.

Burada en önemli parametreler olan kaynak kapsülünün basınç değeri, akım işlem süresi ve akım şiddeti parametreleri kullanılarak kaynak bölgesi analiz edilmiştir. Analizde baskı, kaynak akımı ve süresi için alt ve üst sınırlar belirlenmiştir. Zira baskının çok yüksek olması elektriksel direncin düşmesine ve sonucunda ısıl yoğunluğun azalmasına, tam tersi bu baskının azaltılması çok yüksek bir direnç nedeni ile kaynağın yapılamamasına neden olur. Akım yoğunluğunun erime bölgesinde etkili olduğu bilinmektedir. Aynı akım yoğunluğunda kaynak basıncının etkisi, yoğunluğuna göre erime bölgesinde daha az bir etki göstermektedir. Nokta direnç kaynaklarında elektrotu çevreleyen havada ve elektrotlar arasında iletim boyunca kaybolan ısıyı karşılamak üzere yeterli ısı üretilmelidir. Bundan dolayı kaynak akımında alt ve üst sınırlar mevcuttur. Kaynak akımı çok yüksekse, elektrotlar arasındaki metalin tamamı, kaynak bölgesinin erime sıcaklığına ulaşmasıyla akışkan hale gelir, bunun sonucunda kapsülün metale doğru deplasman olur. Kaynak akımı için seçilen üst sınırın aşılması durumunda kaynak bölgesindeki erimiş metal, serbest bulunduğu kanaldan bölge dışına doğru fıskırır. Bunun sonucunda yeterli kaynak kalitesi elde edilemez. Kaynak akımının yetersiz olduğu durumda, ısı birikmeden önce kaybolacak, yeterli füzyon gerçekleşmeyecektir. Düşük akım seviyeleri, minimum çekirdek çapından çok küçük değerlerin meydana gelmesine ve bazen hiç oluşmamasına neden olur. Yapılan çalışmalarda çekirdek genişliğinin, çekirdek yüksekliğinin ve bunların birbirlerine göre oranının kaynak kalitesini oldukça değiştirdiği görülmüştür. Daha küçük genişlikler ve daha büyük çekirdek yüksekliği değerleri, bağlantıların dayanımlarının düşmesine neden olmaktadır [22].

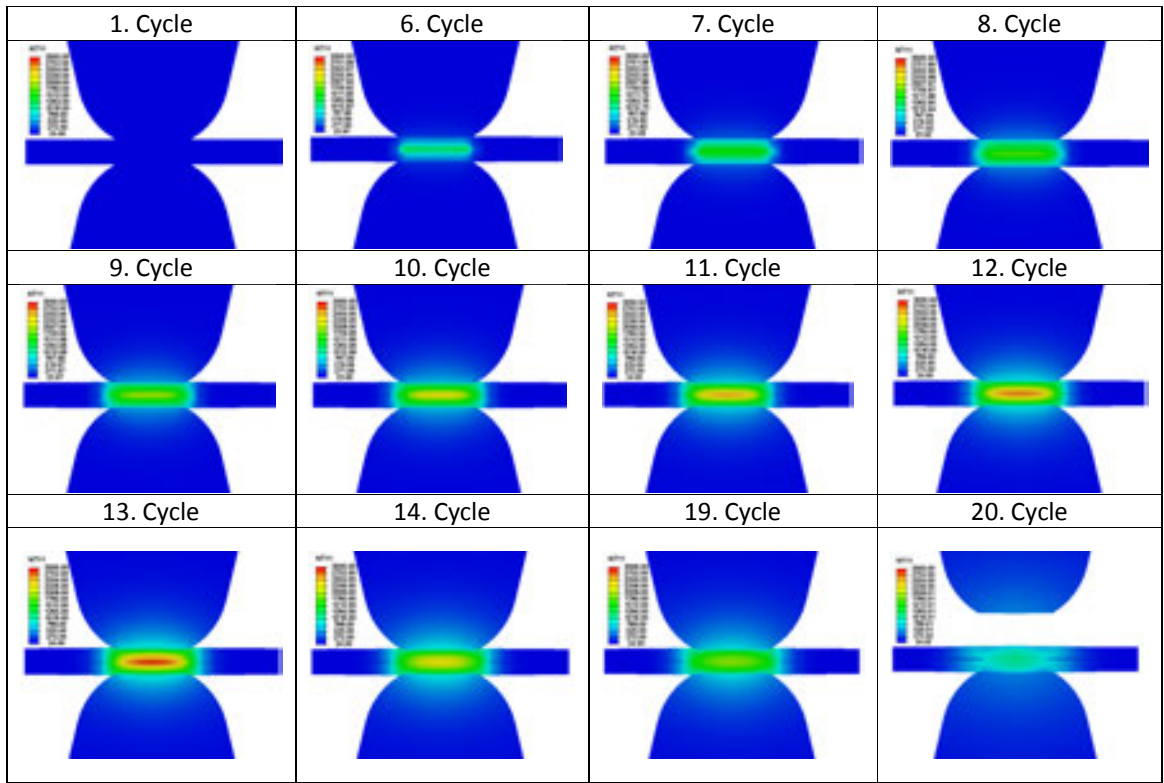
Şekil 1.'de analiz için kullanılan akım şiddeti, uygulanan basınç ve elektrot kapsülünün deplasmanının tüm çevrim boyunca değişimi görülmektedir.



Şekil. 1 Uygulama parametrelerinin zamanla değişimi

Analiz “Coupled Thermal-Electrical-Structural” (Bileşik Isıl-Elektriksel-Yapısal) ısı geçiş analizi olarak uygulamadaki yapıya uygun olarak dört ayrı basamak halinde gerçekleştirilmiş olup bu basamaklar temas ve basınç zamanı, kaynaklama zamanı, tutma zamanı ve ayrılma ve soğuma zamanıdır. Basınç zamanı için 5 cycle, tutma zamanı için 1 cycle ve soğuma zamanı içinde pratik uygulamalarda olduğu gibi 5 cycle seçilmiştir. Her bir kapsül yaklaşık 4000 ve her bir saç ise yaklaşık 6750 elemana bölünmüş, yapıya istenen çözüm hızı için çeyrek modelleme tekniği uygulanmıştır.

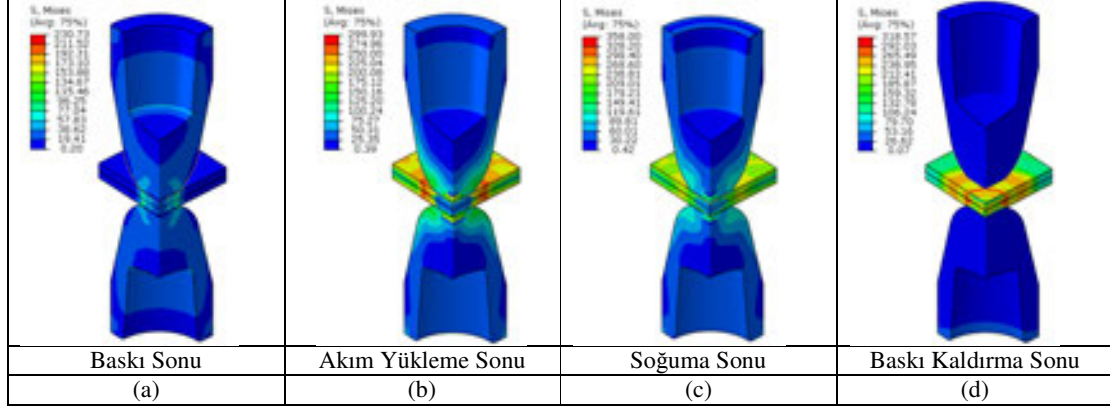
Tam bir çevrim boyunca sıcaklığın model üzerindeki dağılımı Şekil 2.’de verilmiştir.



Şekil 2. Çözüm ağı bazında ısı dağılımının zamanla değişimi

Şekil 2’den görüldüğü üzere, temas oluşması ve saçlara basınç uygulama, alternatif gerilim altında kaynaklama ve çekirdeğin oluşması, akımın kesilip baskının kaldırılmadan önce bir süre tutma ve ayrılma, son olarak soğuma zamanıdır. Burada verilen sıcaklık değeri çözüm ağı bazında ağ noktaları üzerindeki ısı yayılım değerleridir. Analiz bir elemanın üzerindeki ağ noktalarının ortalama değeri de verebilmektedir.

Nokta kaynağı çevrimi boyunca uygulanan kuvvetlerin etkisi ile oluşan VonMises gerilmeleri Şekil 3.'te verilmiştir.

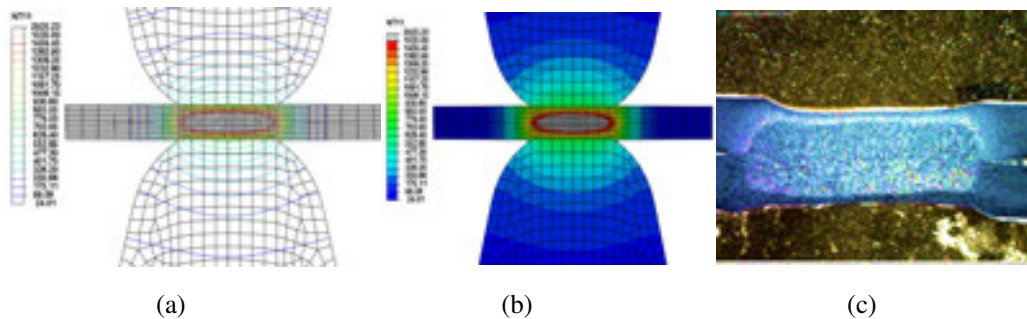


Şekil 3.Çevrim basamaklarının sonunda Mises gerilmeleri

Özellikle çevrim sonunda (Şekil 3d) termomekaniksel olarak oluşan intermetalikbağlanmanın sonucunda kaynak bölgesi üzerinde artık gerilmeler açıkça görülmektedir.

Kaynakta ısı geçişinin zamanın fonksiyonu olmasından dolayı, uygun çekirdek çapının gelişmesi için gereken süre, akım ne kadar yükseltirse yükseltisin, sınırlı ölçüde kaldığı görülmektedir. Kısa kaynak süresi ve yüksek akım şiddeti veya uzun kaynak süresi düşük akım şiddeti kullanarak aynı nokta çapını elde etmek mümkündür. Kaynak zamanı azaldıkça, ısı kayıpları da azaldığı için işlemin ısı verimi artar. İşlem hızlı olduğu için, sadece kaynak bölgesinde erime sıcaklığına ulaşır ve levhaların dış yüzeyinde aşırı ısınma olmadan kaynak işlemi sona erer.

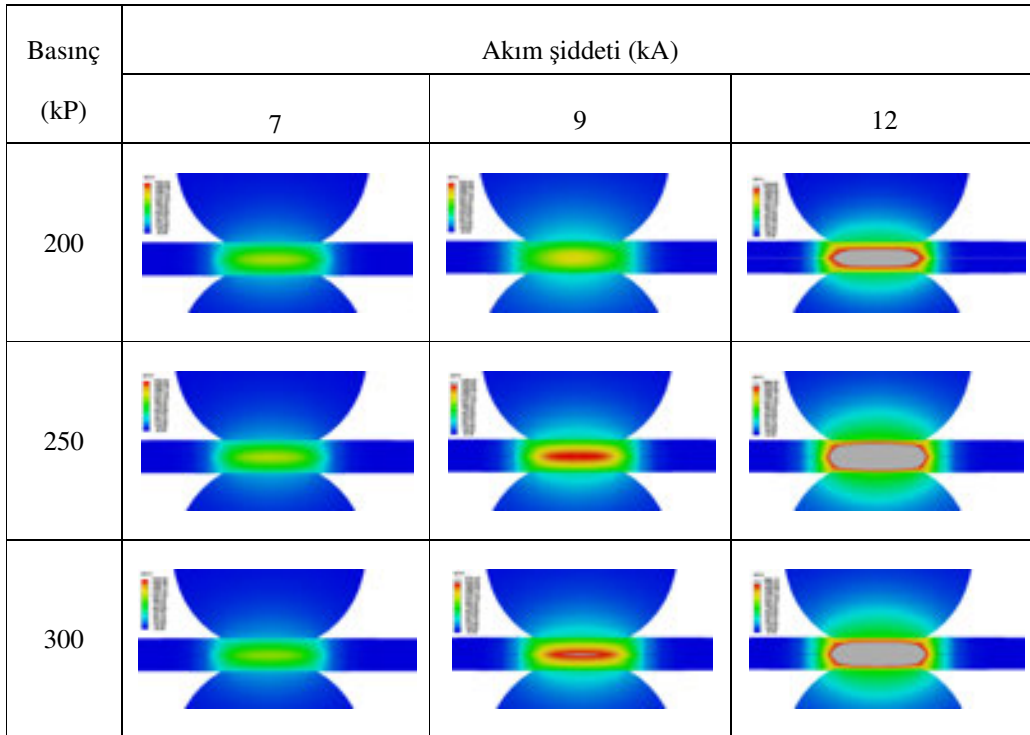
Şekil 4.'te Çekirdek etrafında ısı yayılımı görülmektedir.



Şekil 4. Çekirdek etrafında ısı yayılımı

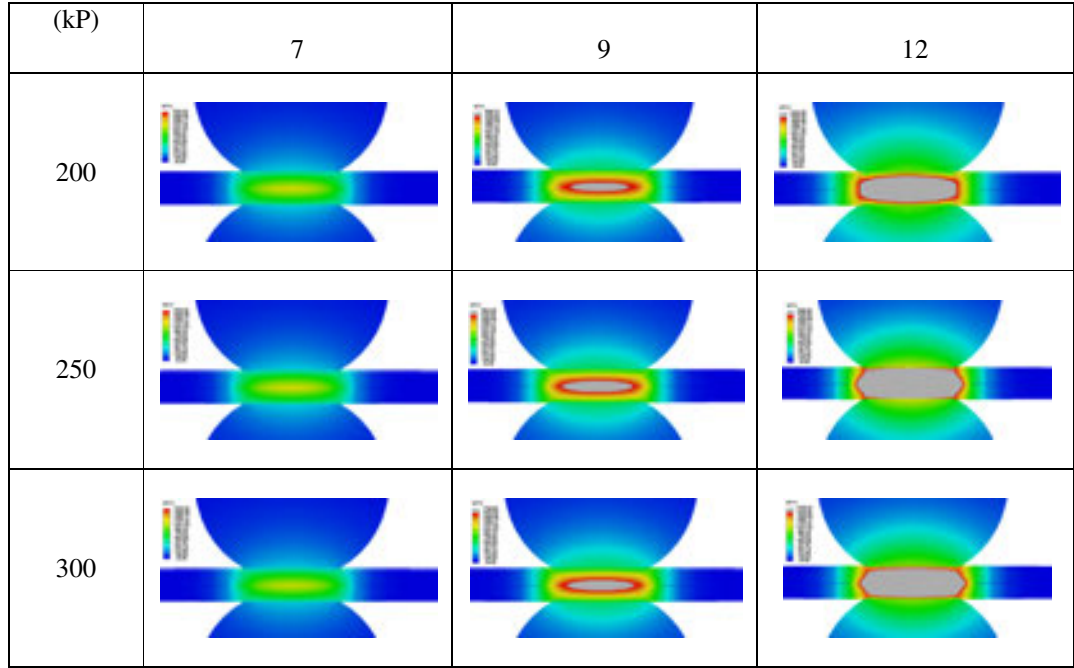
Burada her bölgede farklı ısı girişi ve sonucunda oluşan farklı metalografik yapı elde edilmektedir (Şekil 4c). Elektrot uçlarında yüksek sıcaklık değerlerine ulaşılması sonucunda elektrot uçlarının kısa sürede bozulma problemi oluşacaktır. Bununla birlikte uzun süreli kaynakta, sacın dış yüzeyi de ısındığı için elektrot içine gömülür ve derin izler bırakır. Bu da dayanım kalitesinin düşmesi dışında maliyetin artmasına ve sacın dış yüzeyinde istenmeyen bir görüntü oluşmasına neden olur. Galvanizli çeliklerde, daha yüksek kaynak akımları kullanıldığından, elektrotların temas yüzeylerindeki sıcaklık aşırı yükselir elektrot kapsülünün sertliği azalır. Bu durum, çok hızlı bir şekilde boyutları kabul edilemez derecedeki küçük kaynak çekirdeklerinin oluşmasına, elektrotların yüzeylere yapışmasına, temas yüzeylerinin deforme olmasına ve genişlemesine sebep olur [23]

Seçilen 200, 250, 300 kP (kilopound) basınç altında 7, 9 ve 12 kA (kiloamper) akım şiddetinde 4, 6 ve 8 cycle akım uygulama süreleri sonucunda analizden elde edilen veriler Şekil 5-6-7' de verilmiştir. Burada seçilen değerler üretimle ilgili uygulamalarda kullanılan değerler ile kaynak makinalarının üreticilerinin tavsiye ettikleri değerler baz alınarak seçilmiştir [24,25].

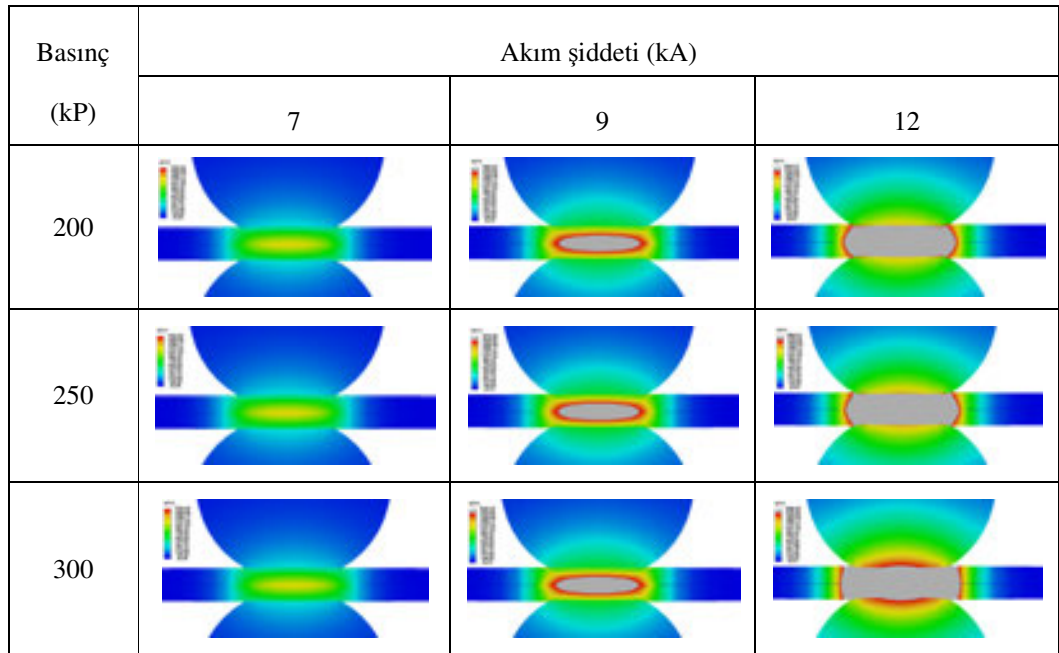


Şekil 5. 4 cycle süre ile yapılan nokta kaynağı

Basınç	Akım şiddeti (kA)
--------	-------------------



Şekil 6. 6 cycle süre ile yapılan nokta kaynağı



Şekil 7. 8 cycle süre ile yapılan nokta kaynağı

Genel olarak şekil 5, 6 ve 7'ye bakıldığında, söz konusu çeliğin kaynak bölgesi geometrisinin (boyutu ve şekli), değişen basınç, akım ve süre ile birlikte değiştiği gözlenmektedir. Bu durum sonlu elemanlar ile yapılan modellemenin ve özellikle de malzeme özelliklerinin nispeten doğru

tanımlandığının bir işaretidir. Artan basınç, akım ve süre ile kaynak bölgesinin boyutunun arttığı da görülmektedir. Ayrıca, kaynak parametrelerinin optimum değerleri olarak; kaynak akımı 12kA, kaynak süresi 6 cycle ve elektrot baskı kuvveti 250kP olarak belirlenmiştir,

3.Sonuç ve Tartışma

Bu çalışmada, elektrik direnç punta kaynağı ile kaynak edilmiş EN 10346:2015 çeliklerinde kaynak parametreleri sonlu elemanlar yöntemi ile analiz edilerek optimize edilmiştir. Yapılan çalışmalar sonucunda elde edilen sonuçlar aşağıdaki şekilde özetlenebilir:

- Kaynak parametrelerinin optimum değerleri kaynak akımı 12kA, kaynak zamanı 6 cycle ve elektrot baskı kuvveti 250kP olarak belirlenmiştir,
- Kaynak parametrelerinin çekirdek çapına etkisinin derecelendirilmesi ise kaynak akımı, kaynak zamanı ve elektrot baskı kuvveti şeklindedir. Kaynak akımı oransal anlamda en etkin parametredir. Bununla birlikte, kaynak süresi ve elektrotların baskı kuvveti etkisi oranları birbirine yakındır,
- Kaynaklı bağlantıların mukavemeti kaynak akımı ve elektrot baskı kuvvetinin artması sonucunda istenilen değerlerde alabilecektir. Fakat, kaynak süresi arttıkça parçada daha yüksek ısı girdisi oluşmakta ve bunun sonucunda bağlantı dayanımı azalacaktır.
- Daha yüksek kaynak mukavemet değerlerine ısı tesiri altında kalan bölgenin daha dar alan oluşturan akım değerlerinde ve kısa süreli kaynak parametrelerinin etkili olduğu belirlenmiştir. Kaynak parametrelerinin bu değerler arasında seçilmesi sonucunda genel itibarıyla nispeten daha sünek kırılma karakteristiği sergileyeceği düşünülmektedir.

4.Sonuç

Bu makale nokta direnç kaynağı sonuçlarının sonlu elemanlar yöntemi kaynaklanacak malzemenin özelliklerinin bilinmesi durumunda kaynak parametrelerinin seçilmesinde belirleyici olacaktır. Direnç kaynağı işleminin kalitesinde iyileşmesinde katkı sağlayacaktır.

Yapılan araştırma, nokta kaynağının sonlu elemanlar ile analizinde kaynak parametrelerinin önemli olduğunu göstermiştir. Kaynak akımı, kaynak süresi ve kaynak için gerekli kuvvet kaynak bölgesinde oluşabilecek çekirdek formunun büyüklüğü hakkında bilgi alabilme olasılığını sağlamıştır.

Ek olarak çekirdek formunun belirlenmesinde yeterli füzyonun oluşup oluşmadığının kontrolünde sonlu elemanlar analizi yönteminin ön bilgi verebileceği görüldü.

Kaynak bölgesi geometrisi ile bağlantının mekanik özellikleri olan ilişkisi bir sonraki çalışmanın konusudur.

7. References

- [1] G. Wu, et al., Experiment and modeling on fatigue of the DP780GI spot welded joint Int. J. Fatig., 103 (2017), pp. 73-85
- [2] S. Wu, et al. Thermo-mechanically affected zone in AA6111 resistance spot welds J. Mater. Proc. Tech., 249 (2017), pp. 463-470
- [3] Z.L. Ni, F.X. Ye Ultrasonic spot welding of Al sheets by enhancing the temperature of weld interface Mater. Lett., 208 (2017), pp. 69-72
- [4] [Sakchai Chantasri, Pramote Poonayom, Jesada Kaewwichit, Waraporn Roybang, Kittipong Kimapong, Effect of Resistance Spot Welding Parameters on AA1100 Aluminum Alloy and SGACD Zincoated Lap Joint Properties, International Journal of Advanced Culture Technology Vol.3 No.1 153-160 (2015)
- [5] Zhang, H., Liu J., Microstructure characteristics and mechanical property of aluminum alloy/stainless steel lap joint fabricated by MIG welding-brazing process, Materials Science and Engineering A., Vol. 528, pp. 6179-6185, (2011)
- [6] Dehmolaei, R., Shamanian, M., Kermanpur A., "Microstructural characterization of dissimilar welds between alloy 800 and HP heat-resistant steel," Materials Characterization, Vol. 59, pp. 1447-1454, (2008)
- [7] Mohsen Eshraghi, Mark A. Tschopp, Mohsen Asle Zaeem, Sergio D. Felicelli Effect of resistance spot welding parameters on weld pool properties in a DP600 dual-phase steel: A parametric study using thermomechanically-coupled finite element analysis, Materials and Design 56 (2014) 387-397
- [8] Wei P, Wu T. Electrical contact resistance effect on resistance spot welding. Int J Heat Mass Transfer 2012;55:3316-24
- [9] S. Florea, K.N. Solanki, D.J. Bammann, J.C. Baird, J.B. Jordon, M.P. Castanier Resistance spot welding of 6061-T6 aluminum: failure loads and deformation Mater Des, 34 (2012), pp. 624-630,
- [10] R.S. Florea, C.R. Hubbard, K.N. Solanki, D.J. Bammann, W.R. Whittington, E.B. Marin Quantifying residual stresses in resistance spot welding of 6061-T6 aluminum alloys sheets via neutron diffraction measurements J Mater Process Technol, 212 (11) (2012), pp. 2358-2370

- [11] R.S. Florea, D.J. Bammann, A. Yeldell, K.N. Solanki, Y. Hammi Welding parameters influence on fatigue life and microstructure in resistance spot welding of 6061-T6 aluminum alloy Mater Des, 45 (2013), pp. 456-465
- [12] V.H. Baltazar Hernandez, M.L. Kuntz, M.I. Khan, Y. Zhou Influence of microstructure and weld size on the mechanical behaviour of dissimilar AHSS resistance spot welds Sci Technol Weld Joining, 13 (8) (2008), pp. 769-776
- [13] M.I. Khan, M.L. Kuntz, P. Su, A. Gerlich, T. North, Y. Zhou, Resistance and friction stir spot welding of DP600: a comparative study, Sci Technol Weld Joining, 12 (2007), pp. 175-182
- [14] M. Pouranvari, E. Ranjbar Noodeh Resistance spot welding characteristic of ferrite–martensite DP600 dual phase advanced high strength steel-Part II: Failure mode World Appl Sci J, 15 (11) (2011), pp. 1527-1531
- [15] M. Marya, X. Gayden Development of requirements for resistance spot welding dual-phase (DP600) steels Part 1 – The causes of interfacial fracture Weld Res (2005), pp. 172s-182s
- [16] M. Marya, X. Gayden Development of requirements for resistance spot welding dual-phase (DP600) steels Part 2: Statistical analyses and process maps Weld Res (2005), pp. 197s-204s
- [17] S. Aslanlar, A. Ogur, U. Ozsarac, E. İlhan Welding time effect on mechanical properties of automotive sheets in electrical resistance spot welding Mater Des, 29 (2008), pp. 1427-1431
- [18] P. Rogeon, P. Carre, J. Costa, G. Sibilía, G. Saindrenan Characterization of electrical contact conditions in spot welding assemblies, J Mater Process Technol, 195 (2008), pp. 117-124
- [19] https://www.erdemir.com.tr/Sites/1/upload/files/Urun_Katalogu-2017-1269.pdf (2019)
- [20] High-Temperature Characteristics Of Stainless Steels, A Designers Handbook Series N- 9004
- [21] Property Tables And Charts (SI Units), ResearchGate
- [22] N. Akkaş, E. Ferik, E. İlhan, S. Aslanlar, The Effect of Nugget Sizes on Mechanical Properties in Resistance Spot Welding of S235JR(Cu) Steel Sheets Used in Railway Vehicles, Special issue of the 2nd International Conference on Computational and Experimental Science and Engineering (ICCESEN 2015), (2016), 130, pp. 60-63
- [23] M Vural, A. Akkuş, E. On the Resistance Spot Weldability of Galvanized Interstitial Free Steel Sheets With Austenitic Stainless Steel Sheets, Journal of Material Processing Technology, (2004), Volume 153-154, pp 1-6.
- [24] <http://www.tuffaloy.com/standard-electrodes/straight-electrodes.html> (2018)
- [25] <http://www.teknikmalzeme.com.tr/> (2018)

THE EFFECTS OF WELDING PARAMETERS ON PENETRATION IN DUPLEX STAINLESS STEELS WELDMENTS

Ramazan Yılmaz^{1,a} and Merve Koruç^{1,b}

¹Sakarya University, Technology Faculty, Department of Metallurgical and Materials Engineering, Esentepe,
Sakarya, Turkey

^aryilmaz@sakarya.edu.tr; ^bg140908034@sakarya.edu.tr

Abstract

In this study, AISI 2205 duplex stainless steel were welded by GTAW (Gas Tungsten Arc Welding) using ER 2209 consumable. Automatic GTAW welding machine was used to obtain exact values of each parameter. The effects of welding parameters such as welding current and welding speeds used in welding process on the penetration were investigated. Weld bead size and shape such as bead width and depth were important considerations for penetration. Welding current and welding speeds were chosen as welding parameters, therefore, duplex stainless steels were welded using various current and travel speeds. The study was shown that welding parameters has influence on the penetration, microhardness and microstructures of the weldments. Depth of penetration increased depending on increasing of welding current.

Key Words: GTAW, AISI 2205, welding parameters, penetration, duplex stainless steel.

1. Introduction

Duplex stainless steels (DSS) are based on Fe-Cr-Ni alloy system and consist of nearly equal amounts of ferrite and austenite phases at room temperature. Those type of steels offer an excellent combination of mechanical properties, various types of corrosion resistances, which are superior to that of austenitic stainless steels. Due to the significant improvements both in material design and weldability of duplex stainless steels, those materials are involved in many applications in which especially stress corrosion cracking and pitting corrosion are required since 1980. Duplex stainless steels have been widely used in offshore oil and gas, chemical petrochemical and pulp and paper industries, high velocity injection in geothermal wells and gas transmission lines, power generation etc. [1, 2].

GTAW (Gas Tungsten Arc Welding) is a modern welding method that is suitable for joining stainless steel and providing great appearance and high quality welding. In this welding technique, electrical arc is formed between the joined metal and the tungsten electrode. The arc region should be protected by the inert gas or mixture gases from the harmful effect of the environment. The tungsten electrode is elevated to high temperatures to provide the electron emission required for continuation of the arc during the welding process. GTAW technique has many advantages compared to other joining methods, but it has some disadvantages too. Particularly, it is considered that there is not a suitable method for materials having thicker section. On the other hand, it is rather slower therefore generally reduction is seen in the welding performance [3]. As with every welding technique, welding parameters appropriate to the material must be carefully determined and applied in order to ensure the best welding quality in GMAW processes. The parameters applied during the welding significantly affect the welding

geometry and the mechanical properties of the weldment. It is known that the welding parameters used in TIG welding such as welding current, welding voltage, welding speed, shielding gas type, and its flow quantity, arc length, welding pole and welding design significantly affect welding bath geometry. Among these parameters, the welding current is one of the most important variables and the change in the welding current affects the depth of penetration, welding width, heat input, metal deposition ratio and welding quality [4]. Penetration is one of the important parameters for the quality weldment of the materials. Thus, precisely understanding of controlling effects of penetration factors such as shielding gas compositions and current values play critical role for generation satisfactory weld joint with proper weld geometry and deeper penetration [5]. Thus, weldments with optimum properties are realized in thin-sectioned parts. So far, many researchers have investigated on the influence of welding parameters on penetration in various welding methods [4-10]. It is considered that the effects of welding parameters such as welding current and speed are very complicated when compared with other variables in welding process. The variation of the welding current directly affects the amount of heat input to the welding pool. Therefore, the weld geometry and the P / W ratio vary depending on the heat input and heat dissipation [11]. It is emphasized that the influence of the difference in the composition of the gas composition during welding is important [4, 9, 11]. Deep penetration values were obtained in active GTAW performed by applying various oxides to the surface of the material to be welded [3]. The amount of hydrogen in the shielding gas also increases the amount of penetration in the stainless steels [12]. The mechanical properties of welded joints by the addition of hydrogen to argon gas are positively affected [12].

The joints should be safe and strength; therefore, welding parameters such as speed and heat input must be controlled. In this study, duplex stainless steel materials were welded on plate using automatic welding machines with various welding parameters such as current and speed. The effect of welding parameters on the welding geometry, penetration, microstructure and hardness distribution have been investigated.

2. Experimental Procedure

AISI 2205 grades duplex stainless steels were used in this study. ER 2209 a filler material with diameter of 0.8 mm was used. The chemical composition of base materials and filler materials were given in Table 1. GMAW technique with automatic welding machines is used. Bead-on-plate weld were made on stainless steels plates by dimension of 50x50x4 mm³ under gas composition with argon + H₂ 5%. Tungsten 2% GMAW electrode with a diameter of 2.4 mm and 9 mm diameter nozzle were used in the studies. Two different welding speeds (4.2 and 5.2 ms⁻¹) and three different welding currents were applied at 110, 140 and 170 amperes.

Table 1. Chemical composition of base and filler materials used in the study

Base and filler material	Chemical composition (wt %)								
	C	N	Mn	Si	Cr	Ni	P	S	Mo
AISI 2205	0,03	-	2	1	21-23	4,5-6,5	0,035	0,015	2,5-3,5
ER 2209	0,01	0.17	1,5	0,5	22,7	8,5	-	-	3,2

Microstructural examination was carried out on cross section of the weldments. The specimens were mounted later flatted and then grounded using SiC abrasive paper with grit ranges from 180 to 1200. Then the sample were then lightly polished using 1 μm alumina slurry. Samples were then washed, cleaned by alcohol and then dried, followed by electrolytic etching in 10 % oxalic

acid at 10.4v for 30 s. Macrostructural examinations were carried out using a NIKON SMZ800 stereo microscope and optical examination were performed using a NIKON ELIPSE L 150 model optical microscopy. The Vickers microhardness measurements of the welded parts were carried out with the MH3 METKON device with a load of 300 g for 15 seconds. Microhardness measurements were taken at certain intervals along a line from the top to the bottom of the weld in the welded section.

3. Results and Discussion

3.1. Penetration

In order to determine the influence of weld parameters, basic welding beams were performed using different welding currents and speeds on the duplex stainless steel sheets using with and without consumable. The depth (P), width (W) and seam height (H) values related to penetration were measured from the macro structural images obtained with the Stereo microscope given in Figure 1. When the images of the samples obtained with various welding parameters are examined, both the penetration depth and width of the weld increase in parallel with the increase of the welding current. The parameters such as the welding currents, the welding voltage and the welding speed are given in Table 2. It shows that the penetration depth and welding beam heights increases with increasing of welding amperage values.

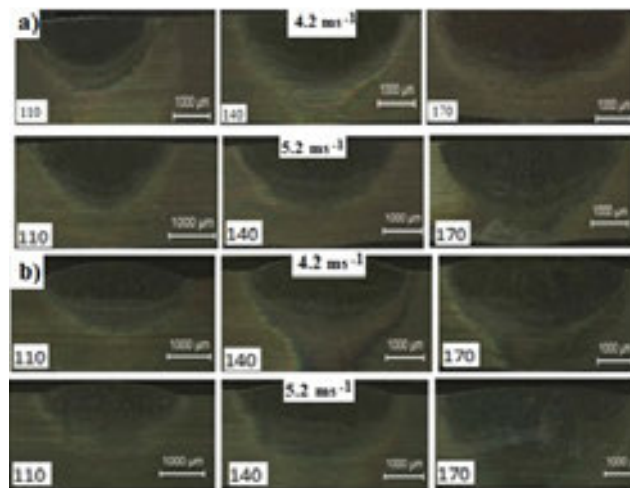


Figure 1. Stereo microscope images taken from cross sections of welding beams using a) without b) consumable in different welding currents

Figure 2 shows the variation of the penetration values obtained from the weld performed at different travel speeds and with and without additional metal. As clearly shown in the figure, the penetration values increase due to the increase of the welding current. The penetration values obtained from welds performed with additional metal are higher than those without additional wire. However, the difference between these penetration values decreases and become almost equal when 170 Amper welding current is used. The reason for this is thought that some of the energy is spent in melting additional wire, thus lowering penetration values is obtained. Depending on the increase of welding current, the effect of this decreases and the penetration values increase. This is felt and more important when the welding speed increases and at low welding current values. Higher penetration values are obtained in welds performed with additional wire at high welding currents. On the other hand at higher welding currents and speeds, the welding width decreases and the penetration increases.

Table 2. The measurements values of penetration obtained from different welding parameters

Welding current (Amp.)	Welding voltage (volt.)	Welding speed (mms ⁻¹)		Type of welding	
				Without welding wire	With welding wire
				Penetration (µm)	
110	15.5	4.2	P	828	594
			H	46.9	365
			W	3448	3469
140			P	1016	979
			H	47	318
			W	4443	4406
170			P	1162	1136
			H	58	271
			W	5427	5339
110	16.5	5.2	P	990	537
			H	83	255
			W	2912	3203
140			P	1063	818
			H	47	255
			W	4037	4042
170			P	1271	1349
			H	37	172
			W	5083	5094

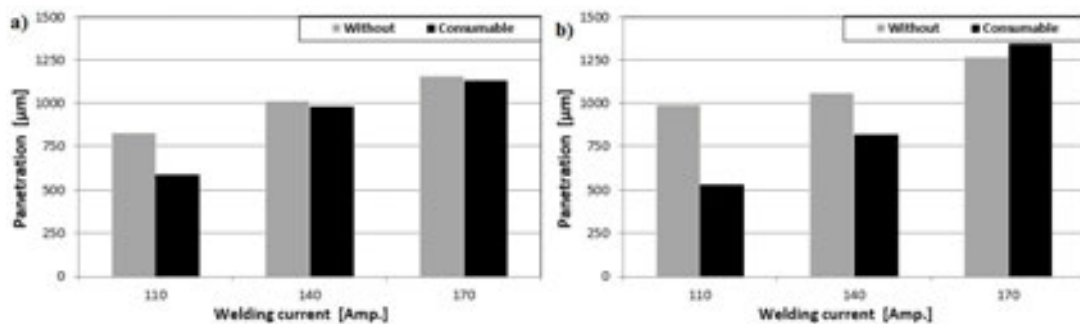
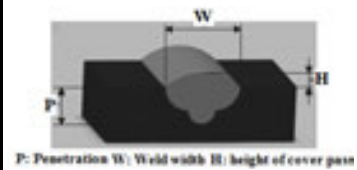


Figure 2. Variations in penetration values for various welding parameters

In Figure 3, variation of weld penetration depth to weld width ratio according to welding current values in duplex stainless steels welded using different welding parameters is given. As can be seen, the P/W ratio varies depending on the increase of welding current values in duplex stainless steels. The highest P/W ratio in samples welded with low welding current was obtained in samples welded at 5.2 ms⁻¹ welding speed without using additional wire while the lowest value was obtained in the specimens welded with the speed of 5.2 ms⁻¹ and welding wire. As explained earlier, the reason of that is consuming of some of the energy for melting of wire. Lower P/W values were obtained in samples welded without using wire, which indicates lowering in performance. Increasing of the current values during the weld process resulted in spreading weld width rather than penetration depth and thus, affects penetration depth and weld performance negatively. In welded samples performed with consumable wire, P/W ratio increase

with increasing of the welding current values. Higher P/W ratios were obtained by increasing the welding speed in the samples welded using the welding current of 170 amp. With the increase of the welding speed, penetration increases and the weld width decreases. Thus, it improves welding performance.

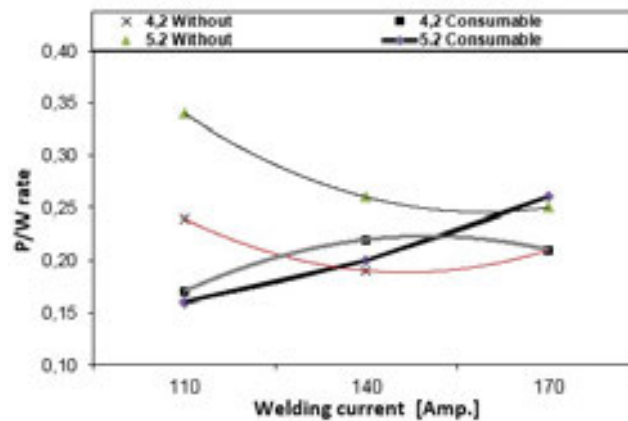


Figure 3. Variation of welding penetration depth /weld width (P/W) ratio according to welding current values

In the previous work [3, 6, 13], the Marangoni heat transfer mode in the GTAW process varies depending on the welding pool surface tension and heat transfer behavior in the system. If the surface tension of the weld metal decreases with the temperature, the heat spreads sideways of the materials thus, lower penetration value is obtained. On the other hand, when the surface tension of the weld metal decreases due to temperature increase, the heat flows into depth and penetration increase. Elements such as Cr, Si, Ni and Mn available in the composition of the stainless steels react with oxygen. Then forms the boundary layer on the weld pool surface, allows the Marangoni thermal conduction to be made centrally and increase penetration depth [13]. In the present work, argon+H₂5% is used as the shielding gas and there is no oxygen in its composition. However, since hydrogen is an active gas, pore-free and clean weld beams can be obtained due to the ability to remove any oxygen present in the weld metal [8, 10]. Due to having high heat transfer coefficient of the hydrogen gas, it provides deeper penetration [10, 12].

3.2. Microhardnes measurements

In Figure 4 (a and b), the effects of the welding parameters on the hardness values are given. The hardness values obtained from the samples welded at a welding speed of 4.2 ms⁻¹ ranged from 320 to 242 Hv, while those welded at a welding speed of 5.2 ms⁻¹ ranged from 325 to 244 Hv and those values are very close to each other. It appears that the hardness values decreases toward to the depth and then is raised in the HAZ (heat affected zone). It is attributed to residual tensions and dislocations occurred because of differences between cooling rates in the weld metal [14]. The highest hardness value was obtained in samples welded using 110 amperes welding current and consumable metal. In addition, the reasons of the differences of hardness values are due to the formation of different phases in the weld metal depending on welding conditions. When argon + hydrogen mixture is used as the shielding gas, it has high thermal conductivity and ionization energy and provides more heat input increase in the weld metal [12]. As the welding current values increase, the heat input increases and but the cooling rate decreases. Thus, causes expansion of the austenite field and lower hardness values in the weld metal.

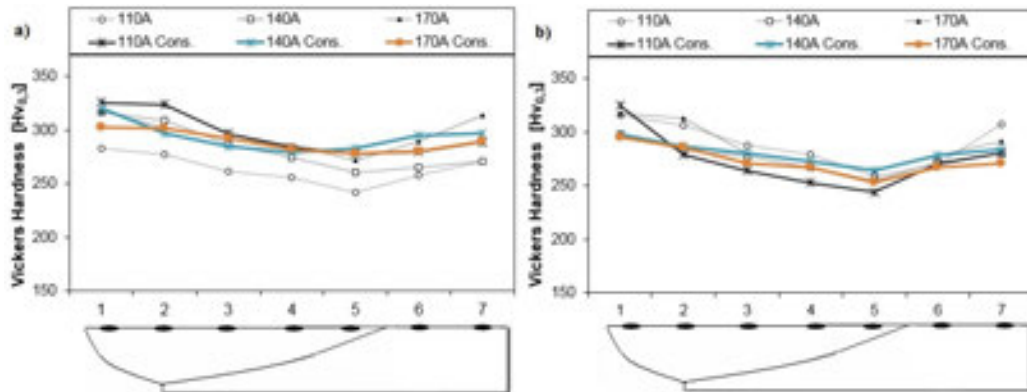


Figure 4. Microhardness values obtained from sections of duplex stainless steels welded at different welding currents and a) 4.2 b) 5.2 ms⁻¹ welding speeds

3.2. Microstructures examinations

Optical microscope images taken from the weld metal of the duplex stainless steels weldments using with and without additional metal at different welding current values are given in Figure 5. As can be seen, there are some differences in the microstructures due to the change in welding current values and the use of additive metal. In duplex stainless steels, both the temperature values reached and the amount of heat inputs are varies depending on the welding currents during welding process. As a result, the cooling rate is changing and different microstructures and phases are formed. As can be seen from the images, the welding current value increases the austenite area and decreases the hardness values.

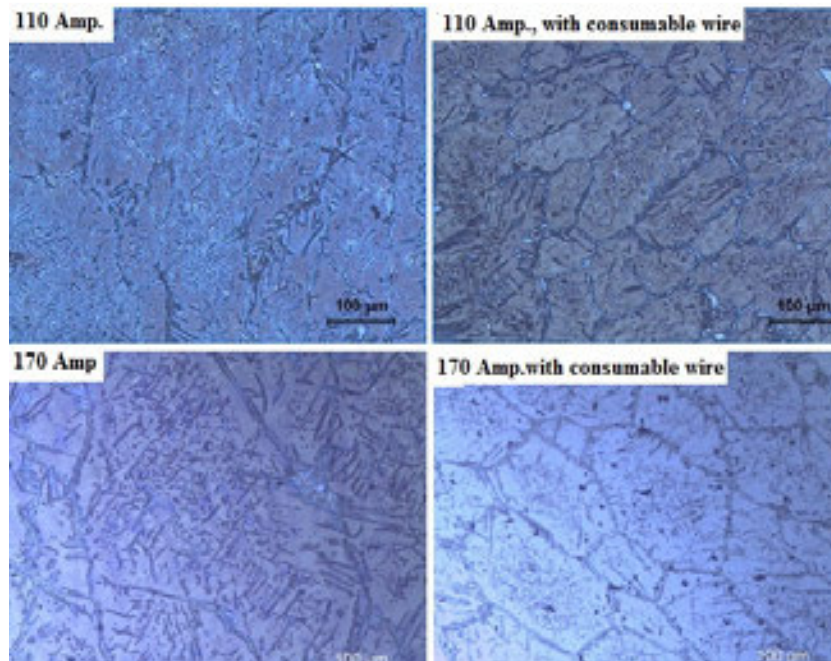


Figure 5. Optical microscope images of duplex stainless steels weld metal performed at different welding parameters

4. Conclusion

The following conclusions were drawn from the experimental work:

1. Welding parameters such as welding current increase and the use of additional metals effect on penetration. Penetration increases with increment of welding current values. In low welding current values, the use of additional metal negatively affects the penetration, while the increase in welding current values reduces the contradiction related with penetration.
2. The P/W ratio is higher in the weld performed without additional metal at low welding current values, On the other hand, the P/W ratio in the weld performed using consumable is increased parallel to the increment of the welding current values.
3. The effects of different welding parameters on the hardness values are not great and they show similar hardness values and the hardness values decreases into towards depth.
4. Welding parameters effect on the microstructure of the weld metal and there are some differences in the microstructure. The increase in the welding current values affects the phase ratio in the microstructure. Therefore, lower hardness values are obtained in the weld metal carried out at higher welding currents

5. Acknowledgement

This study was carried out within the scope of the 2209A Undergraduate Student Project of the Scientific and Technological Research Council of Turkey (TÜBİTAK) with the number of 1919B011700502. The authors would like thank to the TÜBİTAK for financial support. It was also supported by the SAU Scientific Research Projects Commission (SAÜ-BAPK) with the project number of 2018-3-15-299 for its support for the presentation of this article in the conference. and KROMEL Company authorities, especially to the Mechanical Engineer Ayhan ŞEKER for facility of automatic GTAW welding machine.

6. References

- [1] N. R. Gunn: Duplex stainless steels, Abington Publishing, England, (1997)
- [2] J.C. Lippold, D.J. Kotecki: Welding Metallurgy and Weldability of Stainless Steels, John Wiley & Sons, USA, (2005)
- [3] P.J. Modenesi, E.R. Apolinaário, I.M. Pereira: TIG Welding With Single-Component Fluxes, Journal of Materials Processing Technology, 99 (2000), pp. 260-265.
- [4] I.S. Kim, J.S. Son, I.G. Kim, J.Y. Kim, O.S. Kim: A study on Relationship between Process Variables and Bead Penetration for Robotic CO₂ Arc Welding, Journal of Materials Processing Technology, 136 (2003) pp.139–145.
- [5] L. Shanping, F. Hidetoshi, N. Kiyoshi: Marangoni Convection and Weld Shape Variations in Ar–O₂ and Ar–CO₂ Shielded GTA Welding, Materials Science and Engineering 380 (2004) pp.290–297.
- [6] N. Murugan, V.Gunaraj: Prediction and control of weld bead geometry and shape relationships in submerged arc welding of pipes”, Journal of Materials Processing Technology, 168 (2005) 478–487.
- [7] I.S. Kim, Y.J. Jeong, I.J. Son, I.J. Kim, J.Y. Kim, I.K. Kim, P.K.D.V. Yaragada: Sensitivity analysis for process parameters influencing weld quality in robotic GMA welding process, Journal of Materials Processing Technology, 140 (2003) pp. 676–681.

- [8] R. Yılmaz, T. Tehçi: The Effects of Welding Parameters and Composition of Stainless Steel on the Penetration, 11th International Conference on Welding Technologies and Exhibition ICWET, 09, Ankara, 11-13 Haziran (2009) s. 972-982.
- [9] M. Tümer, R. Yılmaz: The Effects of Welding Parameters and Gases Composition on Microstructure and Penetration of Stainless Steels”, International Congress on Advances in Welding Science and Technology for Construction, Energy and Transportation Systems (AWST-2011), 24-25 October Antalya, (2011) pp.483-488.
- [10] R. Yılmaz, T. Tehçi: Ostenitik Paslanmaz Çeliklerin TIG Kaynağında Kaynak Akımı ve Kompozisyonun Nüfuziyete Etkisi, SAÜ. Fen Bilimleri Dergisi, 16 1 (2012) s.53-61.
- [11] L. Shanping, F. Hidetoshi, N. Kiyoshi: Influence of Welding Parameters and Shielding Gas Composition on GTA Weld Shape, ISIJ International, 45 (2005). Pp. 66-70.
- [12] Yılmaz, R., Barlas Z., “Paslanmaz Çeliklerin Gazaltı Kaynak Yöntemi ile Birleştirilmesinde Koruyucu Gaz Kompozisyonunun Mikroyapı ve Mekanik Özelliklere Etkisi”, Pamukkale Üniversitesi Mühendislik Bilimleri Dergisi, 11 3 (2005) s.391-400.
- [13] S.Lu, H. Fujii, K. Nogi: Marangoni Convection and Weld Shape Variations in Ar-O₂ and Ar-CO₂ Shielded GTA Welding, Materials Science and Engineering A, 380 (2004) pp. 290-297.
- [14] M.T. Liao, P.Y. Chen: The Effect of Shielding Gas Compositions on the Microstructure and Mechanical Properties of Stainless Steel Weldments, Materials Chemistry and Physics, 55 (1998) pp.145-151.

CORRESPONDENCE ADDRESS: Ramazan YILMAZ, Sakarya University, Technology Faculty, Department of Metallurgical and Materials Engineering, Esentepe Campus 54187, SAKARYA, TURKEY, 0264 295 6494 and ryilmaz@sakarya.edu.tr

SHORT BIOGRAPHIES

Ramazan Yılmaz – He received his PhD degree from the Manchester Materials Center in 1998. Since then he has been working as a lecturer at Sakarya University. He is now a professor at the Department of Metallurgy and Materials Engineering at Faculty of Technology. The working areas include welding technology, powder metallurgy, coating technology and composite materials..

Merve Koroç – She was born in 1996 in Gebze, Kocaeli. She graduated from the Department of Metallurgy and Materials Engineering at Sakarya University, Faculty of Technology In 2018. She is interested in the topics related to material joining, microstructure and mechanical properties characterizations. She carried out 2209 A student project supported by TUBITAK.

DISSIMILAR WELDING OF AISI 316L AND AISI 2205 STAINLESS STEELS BY GTAW

Ramazan Yılmaz^{1, a}, Büşra Nur Yıldırım^{1, b} and Esra Tokmak^{1, b}

¹Sakarya University, Technology Faculty, Department of Metallurgical and Materials Engineering, Esentepe,
Sakarya, Turkey

^aryilmaz@sakarya.edu.tr; ^byiildirimbusra@gmail.com; ^cesraa.tkmkk@gmail.com

Abstract

In this study, AISI 316L austenitic stainless steel and AISI 2205 duplex stainless steel pair were joined with automatic GTAW (Gas Tungsten arc welding) machine by using ER309L, ER316L and ER 2209 stainless steel filler metals. The effects of chemical composition of consumables on microstructure, microhardness distribution and tensile strength of welded materials were investigated. Microstructure examinations were performed using optical microscope, scanning electron microscope (SEM) and SEM/EDS (energy dispersive spectroscopy). It is observed that lower tensile strength values of the weldment used all consumables than that of base materials. On the other hand, similar elongation and microhardness values of the weldments were obtained. Highest tensile values were obtained at weldments used ER 2209 filler metal among weldments.

Key Words: GTAW, AISI 316L, AISI 2205, Dissimilar, Tensile, Microhardness

1. Introduction

Some construction systems used in various industrial applications are composed by different appropriate materials together in order to be operated efficiently and effectively. In this way, many new systems have been developed to meet the industrial needs. Hence, it is necessary to join different metals each other without any damage. However, their welding joint of dissimilar metals is quite harder than joining the similar metals and therefore, more attention should be necessary due to having different physical, mechanical and metallurgical properties of the materials. Differences in dilution and microstructure can be occurred depends on types of materials and consumable used in joint of dissimilar metals, chemical compositions and welding conditions [1-4]. Weld metal composition consist of two different materials and consumables this results in some problems such as difference in thermal expansion coefficients of the joined materials, residual stresses generating in weld metal. Therefore, those problems should be taken into consideration before joining of dissimilar materials [4-6]. Different types of steels are used together in various engineering applications, these materials need to be joined with a welding methods. Constructions generated by different types of stainless steels are used widely in high temperature application, petrochemical and chemical facilities, energy plants in recent years. [3-6]. Efficiency of features of each material in the same structure and their and economic use are based on position that this material is used in the application.

Stainless steels are widely used engineering materials in a variety of industrial sectors due to their better mechanical properties and corrosion resistance. First material used in this study is austenitic stainless steel that is produced at a high rate due to excellent properties such as corrosion resistance, ductility, toughness, and weldability [6-8]. The other material used in this study is duplex stainless steel that is compositionally formulated and thermo-mechanically

processed to provide a two-phase microstructure having equal proportions of ferrite and austenite phases [9]. The trend of duplex stainless steels usage is steadily increasing day by day in many industrial areas due to their higher strength, toughness, corrosion resistance and providing affordable price than austenitic stainless steels, therefore, inevitable materials that is required for environments such as oil, chemical and petrochemical [6, 10–11].

Nowadays, dissimilar metal welding is widely used to join stainless steels together in various applications such as, gas pipeline and petrochemical industry. Reasons for these combinations may be economic or various property considerations [6,9,12]. Stainless steels are involved in joints of varying degrees of dissimilarity. It is very important to make a suitable selection of filler metal to produce a proper joint that will provide adequate service performance. For joining of those materials without any problems, proper welding method should be chosen [6, 9, 11-13]. GTAW (Gas Tungsten Arc Welding) is a modern welding method that is suitable for joining stainless steel and providing great appearance and high quality welding. A good control of welding parameters is possible in gas tungsten arc welding (GTAW) that is makes it more practical for welding dissimilar weld joints [9, 11-13].

In this study, two different stainless steels, AISI 2205 (duplex stainless steel) and AISI 316L (austenitic stainless steel), were welded together by gas tungsten arc welding process, using different types of filler metals with codes ER 309L, ER 316L and ER 2209. The effects of filler metals on the mechanical properties and microstructure of the dissimilar weldments has been investigated. For this, the mechanical properties such as tensile strength, elongation and micro hardness variation in cross section of the weldment were determined. Parallel work was also carried out on microstructure of the weldments.

2. Experimental Procedure

AISI AISI 2205 grades duplex stainless steels and AISI 316L austenitic stainless steel plates by dimension of 110mm, 600mm, 3 mm were used in the research. In order to determine the effects of the filler materials compositions on the mechanical properties of the weldments, two-sided welding technique were performed with an automatic GTAW welding machine in flat position and butt joint using ER316LSi, ER 2209 and ER 309L filler metals with 0.8 mm, 08 mm and 1,6 mm diameters respectively. Welding currents were 150 ampere for the both of upper side and underside and welding voltage of 15.9 volt at a welding speed of 7.1 mms⁻¹ under gas composition of argon + H₂ 5% with flow rate of 6 lt/min were applied. 2.4 mm diameter tungsten with 2% thorium electrode and 9 mm diameter of the nozzle were used during welding processes. After lowering first upper side welding pass temperature to less than 150 °C, second underside welding pass was conducted. The chemical composition of base materials and filler materials were represented in Table 1. Welding parameters used in the study is given in Table 2.

Table 1. Chemical compositions of base materials and filler metals used and Creq, Nieq values.

Base materials and filler metals	Elements (wt %)											
	C	Mn	Si	Cr	Ni	P	S	Mo	Cu	N	Creq	Nieq
AISI 316L	0,03	2	0,75	17,5	10,5	0,045	0,03	2,50	-	0,10	21,13	12,4
AISI 2205	0,02	1,44	0,32	23,41	4,81	0,02	0,01	3,15	0,23	0,23	27,04	6,13
ER 309L	0,02	1,8	0,4	23,2	13,4	0,02	0,015	0,10	0,08	0,05	24	14,9
ER 316LSi	0,01	1,8	0,9	18,4	12,2	0,03	0,025	2,60	0,12	-	22,35	13,4
ER 2209	0,01	1,5	0,5	22,7	8,5	0,023	0,01	3,2	-	0,17	26,65	9,55

Table 2. The parameters used in the welding process

Filler metals	Diameter of Filler metals (mm)	Welding currents (Ampere)	Welding voltage (Volt)	Number of passes	Shielding gas and polarity	Welding speed (mms ⁻¹)	Flow rate (ltmin ⁻¹)	Heat input (kJmm ⁻¹)
ER 309L	0,8	150	15,9	2	Ar+%5 H ₂ DCEN	7	6	1.pass 0,24 2.pass 0,24
ER 316LSi	0,8							
ER 2209	1,6							

Samples were taken from the weldments by cutting laser jet. for tensile strength, microhardness measurements and microstructure examinations. The samples for microstructure examination and microhardness measurements were taken into bakelite. Grinding were carried out under water using SiC emery papers with grit numbers from 220 to 1200 respectively. Later polished using 1 µm diamond paste and then washed with water and dried. Those samples later were electrolytically etched by being kept in 10 % oxalic acid solution for 15 s at 10.4 V. After the etching procedure the weldment parts, the surfaces were cleaned with alcohol and then the microstructures of specimens were examined with NIKON ECLIPSE L 150 optical and JEOL JSM-6060LV scanning electron microscope. SEM and SEM/EDS techniques were also used to examine microstructure of the weldments.

Vickers micro-hardness measurements were taken cross sections across the entire width of the weldments prepared for metallographic examination. Micro-hardness measurements were conducted through cross-section of polished weldment profile covering each base material, transition zone, and weld metal with brand of LEICA VMHT MOT applying 300 g of load and 15 s dwell times at an interval of ~1 mm. Tensile tests were carried out on the weldments using with the model of INSTRON tensile equipment with the speed of 5 mm.min⁻¹. Three specimens were used for each parameter and then tensile and impact toughness values of the weldments were determined by calculating their arithmetic mean.

3. Results and Discussion

3.1. Microstructures examinations

The Optical microstructure images taken from the as-received base materials used in this study were given in Figure 1 (a and b). The average grain size of AISI 316L austenitic stainless steels is between 25-30 µm and some of twinning lines on the grains were seen. The grains distributions are homogenous. AISI 2205 duplex stainless steels composed of ferrite and austenite phases. Dark colored phases are ferrite while light colored phases are austenite. It is seen that the grain size of the ferrite phase is about 5x50 µm dimension and is directed towards the pressing direction. Distribution of those phases in the microstructure is heterogeneous. In the microstructure, the proportions of these two phases are equal and approximately 50%.

During the visual inspection of the weldments made, according to the AWS D1 visual evaluations. no weld defects were encountered. Figure 2 shows the microstructure images taken from the weld metal of AISI 316L austenitic and AISI 2205 duplex stainless steels dissimilar weldments using various filler metals. As seen from the microstructure, the weld metal obtained by using different filler metal is varied. This is resulted in simply effects on the mechanical properties of the weldments. When using ER 309L metal, as a filler metals vermicular d ferrite, latty ferrite and widmanstätten austenite (WA) sideplates and grain boundary austenite (GBA) allotriomorphs. partially transformed austenite (PTA) and intragranular austenite (IGA) phases are available in the microstructure. The lower part of the weld metal covers a larger area of the

austenite phase the upper part. This is attributed to the higher heat input of the weld metal. When the weld metal is exposed to critical temperatures for a while, formation of the austenite phase in the microstructure increases and the expansion of the austenite grains formed previously are occurred. When ER 316LSi metal is used, shorter lathy ferrites are seen. There are also dendritic delta ferrites and wide austenitic areas. The weld metal microstructure obtained by using the ER 2209 filler metals contains some ferrites phases oriented in different directions and large austenite areas.

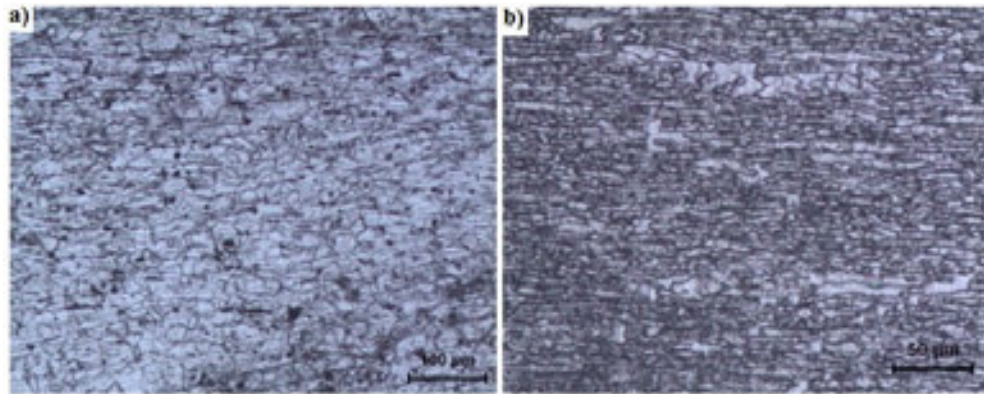


Figure 1. Optical microstructural images of a) AISI 316 L austenitic stainless steel and b) AISI 2205 duplex stainless steel base materials.

Figure 2 shows the microstructure images taken from the weld metal of AISI 316L austenitic and AISI 2205 duplex stainless steels dissimilar weldments using various filler metals. As seen from the microstructure, the weld metal obtained by using different filler metal is varied. This is resulted in simply effects on the mechanical properties of the weldments. When using ER 309L metal, as a filler metals vermicular δ -ferrite, lathy ferrite and Widmanstätten austenite sideplates and grain boundary austenite allotriomorphs, partially transformed austenite, intragranular austenite phases are available in the microstructure. Similar results have been obtained in previous studies [11-13]. The lower part of the weld metal covers a larger area of the austenite phase the upper part. This is attributed to the higher heat input of the weld metal. When the weld metal is exposed to critical temperatures for a while, formation of the austenite phase in the microstructure increases and the expansion of the austenite grains formed previously are occurred. When ER 316LSi metal is used, shorter lathy ferrites are seen. There are also dendritic delta ferrites and wide austenitic areas. The weld metal microstructure obtained by using the ER 2209 filler metals contains some ferrites phases oriented in different directions and large austenite areas.

Figure 3 shows the microstructures taken from the interfaces between the weld metal and the base metals according to the filler metals used in the welding of dissimilar metals. There were differences in microstructure in each side interfaces of the weldments used even the same filler metal. The weldment with ER309L filler metal consists of austenite and duplex metals mixture on the inner side of the weld metal at the AISI 316L austenitic stainless steels side. Grain boundary austenite occurred around the ferrite grains and intragranular austenite and partially transformed austenite phases are happened in the inner parts of those ferrite grains. It is observed that there are intense vermicular δ -ferrite in the interface very closed to AISI 316L base material. The width of this section is around 60-80 μm . In addition, grain growth in AISI316L austenitic stainless steels have been identified in the transition zones. On the AISI 2209 duplex stainless steel side, the inner regions consist of ferrite and austenite grains. Austenite grains are in the

Figure 2. Microstructural variations of the weld metals according to the filler metals used.

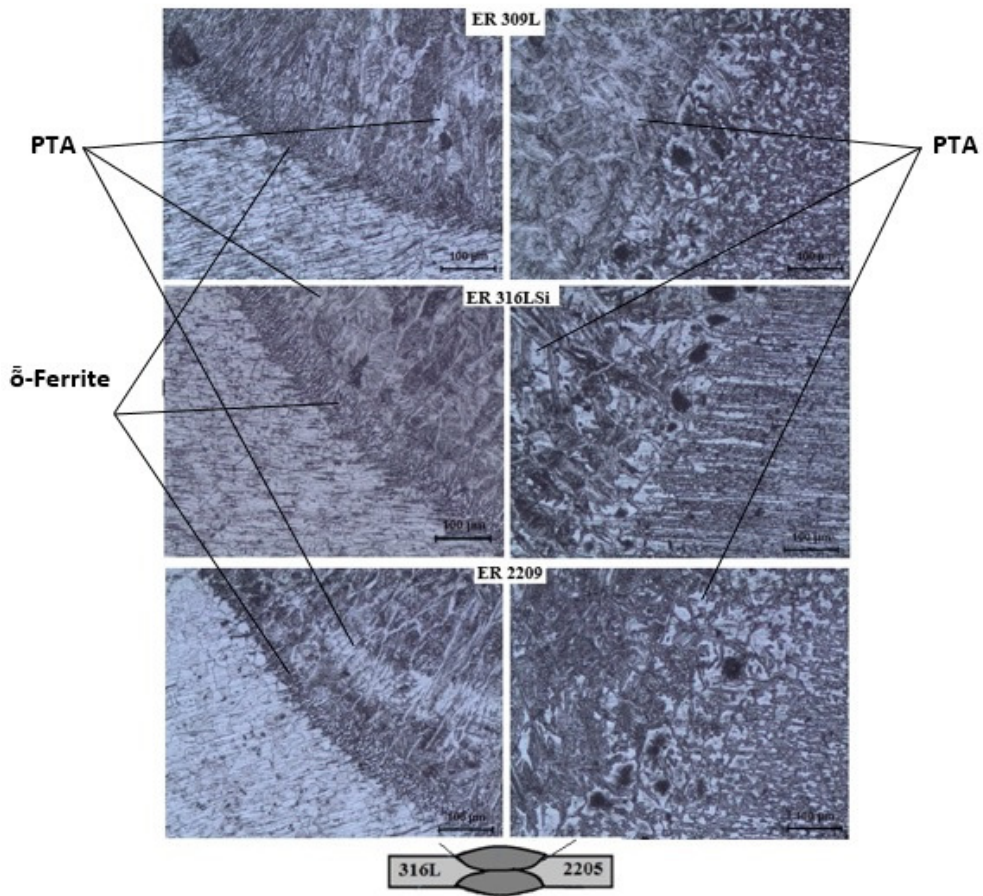


Figure 3. Optical microstructural images of transition zones in the weld performed with different types of filler metals

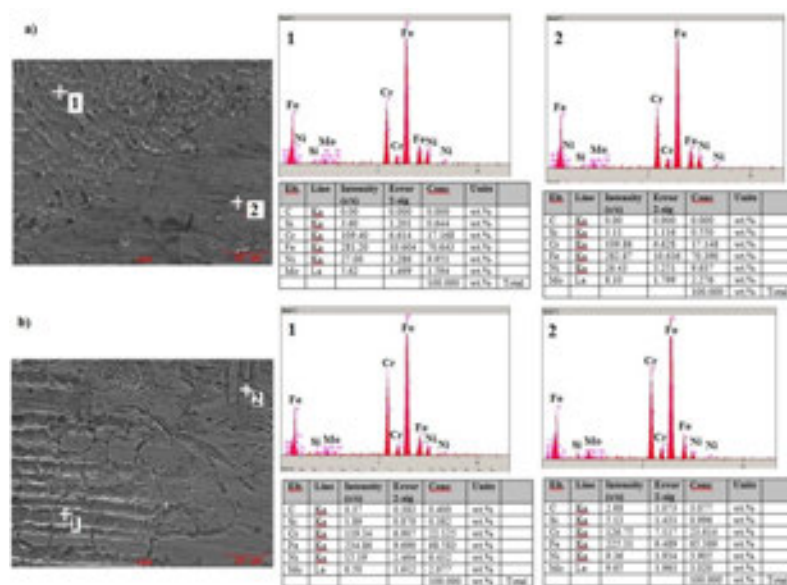


Figure 4. SEM EDS analysis taken from transition area a) AISI 316L austenitic stainless steel side b) AISI 2205 duplex stainless steel side of the weldment used ER 316LSi filler metals

SEM micrograph and SEM / EDS analyzes from the interface of both side of metals welded using ER 316LSi filler metal are given in Figure 4 (a and b). On the weld metal of the AISI 316LSi side in the point 1, the amount of Ni, Si and Mn elements were found to be higher than that of heat effected zone in the point 2. The amount of Cr and Fe elements are similar to each other. SEM / EDS does not have a carbon element at both points of the microstructure. On the AISI 2205 side, it was observed that the amount of C was spread to the heat affected zone in EDS analyzes taken from the heat effected zone close to base metal. At this point the amount of Si, Cr, Mn increases while the amount of Ni decreases. The amount of nickel is decreasing. Nickel in the filler metal is thought to diffused towards to the base metal of AISI 2209. Similar results have been obtained in previous studies [11, 12].

3.2. Tensile Tests and Microhardness Measurements

The results of tensile strength and elongation values obtained from the tensile testing were presented in Figure. 5 (a and b). As can be seen from the figure, all the dissimilar weldments performed various filler metals show lower and similar tensile strength and elongation values due to discontinuous in the microstructure of the base materials caused by welding, therefore, resulted in a decrease in the tensile properties. AISI 2205 duplex stainless steels have the highest yield and strength values in comparison with the values of the all weldments and AISI 316 austenitic stainless steel. The difference between the maximum and the lowest values of tests is higher than that of the others. This can be attributed that the microstructure of AISI 2205 duplex stainless steels is not homogeneous. Similar tensile strength values were obtained in the tests of the weldments. The samples welded with ER 316LSi filler metal have lower yield and tensile strength values. This is because AISI 316 austenitic stainless steels are soft and have lower yield and tensile strength values than others. The highest yield and tensile strength were obtained in the samples welded with ER 2209 filler metal. This is because weld microstructure consist of dense ferrite phase is and this phase is also resistant to be shaped. However, it is lower than the values of the AISI 2205 base metal and the ER 2209 filler metal. This is due to the fact that the weld metal has more heterogeneous structure and crack starts and its progress in the weld metals much easier under the load. Failure after the tests for the samples welded with ER 309L and ER 316LSi filler metals were occurred at the transition zone while first crack started in the weld metal of the samples welded with ER 2209 and progressed towards to AISI 316L austenitic stainless steels side. Micrographs and the results of tensile properties after the tests are given in Figure 6 (a and b). The obtained results indicate that filler metal composition affects the strength and elongation values of the weldments.

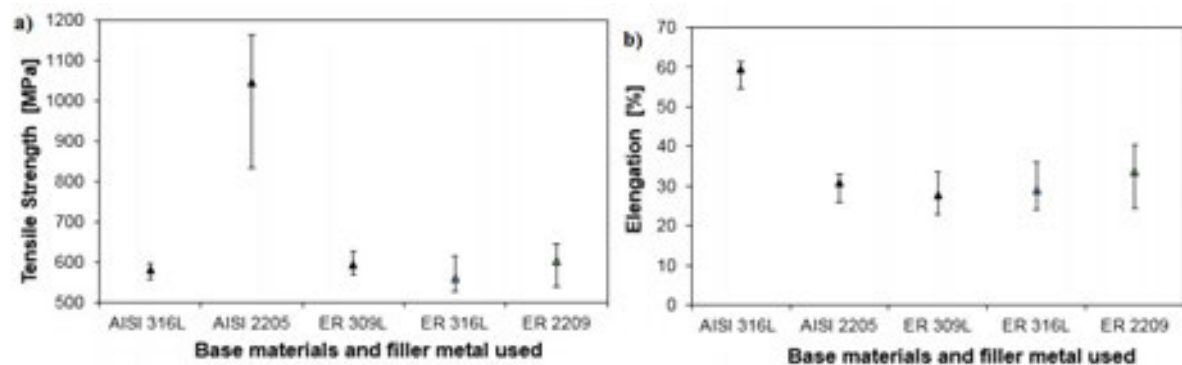


Figure 5. (a) Effect of the filler metals on the tensile strength and (b) the elongation of the weldments

The microhardness profile taken across the weldment is depicted in Figure 7. Higher hardness values were obtained in weld metal of the weldment with ER 2209 filler metal. This is due to the formation of hard phases, microstructure depending on filler metal composition and internal stresses occurred during welding. ER 2209 filler metal has a higher hardness values due to existence of hard phases in the microstructure compared to the others. The results obtained are consistent with previous studies [12].

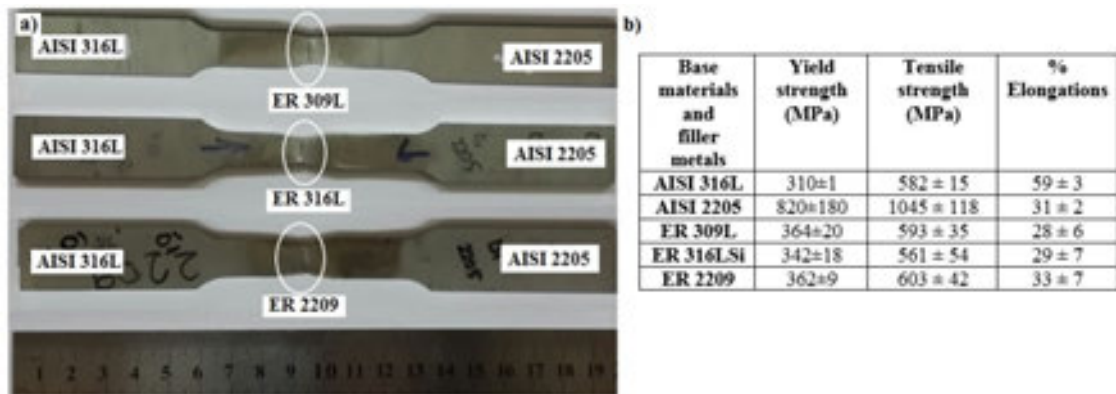


Figure 6. (a) The photographs of the samples exposed the tensile test. (b) The yield, tensile and % elongation values of the weldments

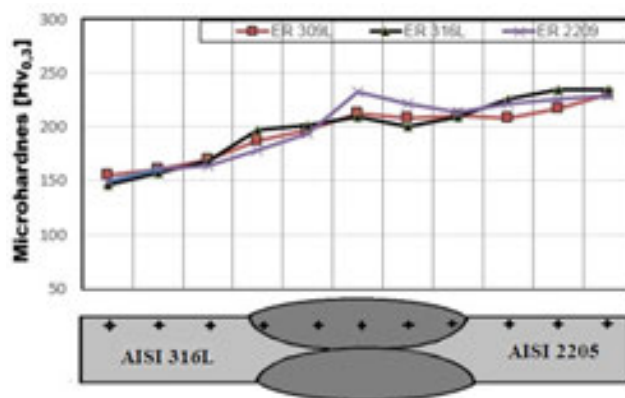


Figure 7. Microhardness variations across the weldments of dissimilar materials depending on filler metals

4. Conclusions

The following conclusions were drawn from the experimental work:

1. The filler metal composition used in AISI 316L-AISI 2205 stainless steels dissimilar weldments affects the microstructure and phase ratio of the weld metal. The most affected is among them is the weldment with ER 2209 filler metal and its AISI 2205 duplex stainless steel side.

2. In SEM/EDS analysis, element percentage values are different in interfaces of the both side. This shows the diffusion mechanism are occurred at the transition zone.
3. Similar values were obtained in tensile tests of weldments. The tensile strength values obtained are very close to the AISI 316 austenitic stainless steel while those values much lesser than that of AISI 2205 duplex stainless steel. Similar results also were obtained in % elongation values. These values are much lowered than that of AISI 316L austenitic stainless steel while very similar to that of AISI 2205 duplex stainless steel. Breaks of the weldments after the tests were mostly occurred transition zone of the AISI 316 austenitic stainless steel side.
4. The filler metal composition affected the distribution of micro hardness values of weldments and the highest hardness values were obtained in weld metals and the weldments with ER 2209 filler metal.

5. Acknowledgement

This study was carried out within the scope of the 2209A Undergraduate Student Project of the Scientific and Technological Research Council of Turkey (TÜBİTAK) with the number of 1919B011701041 The authors would like thank to the TÜBİTAK for financial support. It was also supported by the SAU Scientific Research Projects Commission (SAÜ-BAPK) with the project number of 2018-3-15-299 for its support for the presentation of this article in the conference and KROMEL Company authorities for facility of automatic GTAW welding machine.

6. References

- [1] J. Yashar, A. Masoud: Sub-Surface Stress Measurement of Cross Welds in a Dissimilar Welded Pressure Vessel. *Materials & Design*, 85 (2015), pp. 82–90.
- [2] P. Kaha, M. Shrestha, J. Martikainen: Trends in Joining Dissimilar Metals by Welding *Applied Mechanics and Materials*, 440 (2014), pp 269-276
- [3] T. Maruyama Arc Welding Technology for Dissimilar Joints *Welding International*, 17 (2003), 4, pp 276–281
- [4] M, Sireesha V, Shankar, S.K, Albert, S. Sundaresan: Microstructural Features of Dissimilar Welds between 316LN Austenitic Stainless Steel and Alloy 800, *Materials Science and Engineering A* 292 (2000), pp.74–82.
- [5] P, Bala Srinivasan, M.P. Satish, Kumar: Microstructural and Electrochemical Characterization of a Thin-Section Dissimilar Stainless Steel Weld Joint, *Materials Chemistry and Physics*, 115 (2009) pp. 179–184.
- [6] J.C. Lippold, D.J. Kotecki: Dissimilar welding of stainless steels, in: *Welding Metallurgy and Weldability of Stainless Steels*, John Wiley & Sons, Inc., Hoboken, New Jersey, (2005). pp.287–308.
- [7] K.G. Budinski and M.K. Budinski: *Stainless Steels*, Engineering Material, 6th Edition, (1999).
- [8] C. Odabas: *PaslanmazÇelikler*, As KaynakYayınları, 1. Baskı, İstanbul, (2002)
- [9] A. Moteshakker, I. Danaee: Microstructure and Corrosion Resistance of Dissimilar Weld-Joints between Duplex Stainless Steel 2205 and Austenitic Stainless Steel 316L *Journal of Materials Science & Technology*, 32 (2016) pp. 282–290.

- [10] A.A. Iris: Duplex Stainless Steels: Brief History and Some Recent Alloys, Recent Patents on Mechanical Engineering 1 (2008), pp. 51-57
- [11] H. Tasalloti, P. Kah, J. Martikainen: Effect of Heat Input on Dissimilar Welds of Ultra-High Strength Steel and Duplex Stainless Steel: Microstructural and compositional analysis, Materials Characterization, 123 (2017), pp. 29–41.
- [12] K. D. Ramkumar, A. Singh, S. Raghuvanshi, A. Bajpai, T. Solanki, M. Arivarasu, N. Arivazhagan, S. Narayanan: Metallurgical and Mechanical Characterization of Dissimilar Welds of Austenitic Stainless Steel and Super-Duplex Stainless Steel – A Comparative Study, Journal of Manufacturing Processes, 19 (2015), pp. 212–232.
- [13] A. Eghlimi, M. Shamanian, M. Eskandarian, A. Zabolian, J.A. Szpunar: Characterization of Microstructure and Texture Across Dissimilar Super Duplex/Austenitic Stainless Steel Weldment Joint by Super Duplex Filler Metal, Materials Characterization. 106 (2015), pp. 27–35.

CORRESPONDENCE ADDRESS: Ramazan YILMAZ, Sakarya University, Technology Faculty, Department of Metallurgical and Materials Engineering, Esentepe Campus 54187, SAKARYA, TURKEY, 0264 295 6494 and ryilmaz@sakarya.edu.tr

SHORT BIOGRAPHIES

Ramazan Yılmaz– He received his PhD degree from the Manchester Materials Center in 1998. Since then he has been working as a lecturer at Sakarya University. He is now a professor at the Department of Metallurgy and Materials Engineering at Faculty of Technology. The working areas include welding technology, powder metallurgy, coating technology and composite materials..

BüşraNur YILDIRIM–She was born in 1996 in Eminönü, İstanbul. She graduated from the Department of Metallurgy and Materials Engineering at Sakarya University, Faculty of Technology in 2018. She is interested in the topics related to material joining, polymers and quality control. She knows Solidworks and Autocad programs medium level. She carried out a 2209 A student project supported by TUBITAK.

EsraTokmak–She was born in 1995 in Osmangazi, Bursa. She graduated from the Department of Metallurgy and Materials Engineering at Sakarya University, Faculty of Technology in 2018. She is interested in the topics related to material joining, plastics and heat treatment. She is good on using Solidworks and Catia programs. She was a researcher in 2209 A student project supported by TUBITAK.

SOĞUK BASINÇ KAYNAĞINDA BASINÇ PERİYOTUNUN BİRLEŞEBİLİRLİĞE VE ELEKTRİKSEL İLETKENLİĞİNE ETKİSİ

Hüseyin KÜÇÜKÖNER^{1,a}, Adem KURT^{2,b}

¹ Gazi Üniversitesi Kaynak ve Birleştirme Teknolojileri Araştırma ve Uygulama Merkez Müdürlüğü

² Gazi Üniversitesi Teknoloji Fakültesi Metalürji Malzeme Mühendisliği Bölümü

^ahuseyin.kucukoner@gazi.edu.tr, ^bademkurt@gazi.edu.tr

Özet

Bu çalışmada alüminyum, bakır ve pirinç malzemeler soğuk basınç kaynak yöntemi ile farklı periyotlarda (3,4,5) mekanik basınç uygulanarak birleştirildiler. Birleştirilen Al- Al, Al-Cu ve Al- pirinç malzeme çiftlerinin elektriksel iletkenlikleri ölçülerek birleştirme periyotunun iletkenliğe ve mekanik yapıya etkileri incelendi. Ayrıca birleştirilen malzeme çiftlerinin birleşme ara yüzlerinden esas metal tarafına doğru sertlik ölçümü yapıldı. Artan kaynak basınç ve periyotunun sertliği arttırdığı ve elektrik direncini artırarak iletkenliği azalttığı gözlemlenmiştir.

Anahtar Kelimeler: soğuk basınç kaynağı

1. Giriş

Soğuk basınç kaynağı demir dışı ve sünek malzemelerin kaynağında kullanılan malzemeleri yalnızca basıncın etkisiyle birleştiren bir kaynak yöntemidir. Birleştirme işlemi oda sıcaklığında gerçekleştiği için metalürjik dönüşümler ve sıcaklığın etkisiyle ortaya çıkan problemler bu kaynak yönteminde ortaya çıkmazlar[1].

Soğuk basınç kaynak işlemi bilimsel olarak ilk defa 1724 yılında J.I. Desaguliers tarafından çalışılmıştır. Desaguliers çapları 25mm olan kurşun topları presleyip döndürdüğünde malzemelerin kuvvetli bir şekilde birleştiğini görmüş ve bu çalışmasını zamanın bilimsel dergilerinde yayınlamıştır. İlk zamanlarda kaynağın yeniden kristalleşme ya da enerji hipotezi nedeniyle gerçekleştiği düşünülmüşse de bu iddialar zamanla çürütülmüştür[2-3].

Soğuk basınç kaynağı kısaca atomik seviyede temiz ve düzgün iki metal yüzeyinin bir araya getirilmesiyle temas yüzeyleri arasında metalik bağ oluşumu olarak açıklanabilir[1].

Çoğu soğuk basınç kaynak makinelerinde çoklu yandan basınç yöntemi kullanılır. Bu yöntemde malzeme kalıba sokulduğunda ve makine her çalıştırıldığında malzeme kalıp tarafından kavranır ve ileri doğru beslenir. Böylece temas yüzeyleri birbirlerine itildiklerinde tüm yüzey boyunca gerinir ve genişler. Ara yüzeydeki oksit ve tüm katışıklar merkezden dışarıya doğru itilir ve bağ oluşumu gerçekleşir[1].

Demir dışı metallerin çoğu soğuk basınç kaynağına elverişlidir, en çok işlem yapılanlar ise bakır ve alüminyum olmakla birlikte pirinç, çinko, gümüş, nikel, altın gibi metallerde kaynağa elverişlidir.

2. Deneysel Çalışmalar

2.1 Malzeme

Bu çalışmada 4mm çapındaki alüminyum, bakır ve pirinç teller kullanılmıştır. Soğuk basınç kaynak yöntemiyle Al-Al, Al-Cu ve Al-Pirinç malzeme çiftleri birleştirilip kaynaklı malzemelerin elektrik dirençleri ölçülmüş ve ana malzemelerin elektrik dirençleriyle karşılaştırılmıştır. Ayrıca kaynaklı malzemelerin sertlik ölçümleri ve mikro yapı incelemeleri yapılarak mekanik özellikleri belirlenmiştir.

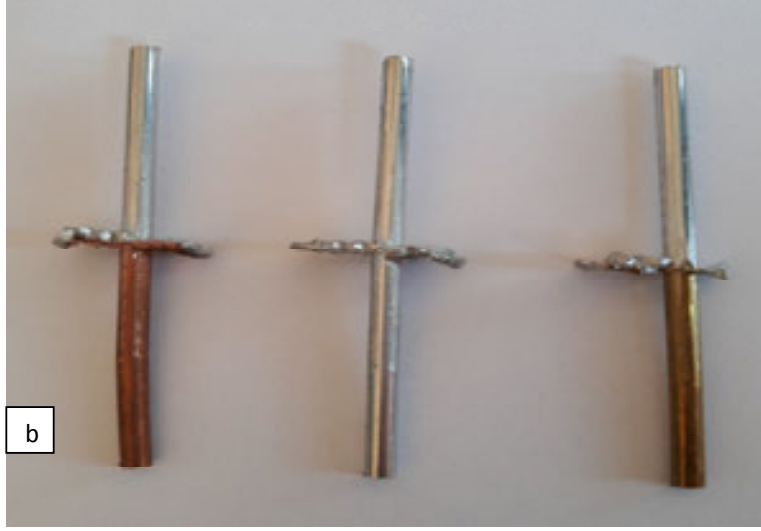
2.2 Kaynak İşlemi

Kaynak işlemi şekil 1 de görüntüsü verilen Gazi Üniversitesi Kaynak ve Birleştirme Teknolojileri Uygulama ve Araştırma Merkezinde bulunan Silver Gain DA100model soğuk basınç kaynak makinasında yapılmıştır. 50mm boyunda kesilen malzemeler yüzey hazırlık işlemlerinden sonra 3, 4ve 5 periyotlarda birleştirilmiştir.Al- Al ve Al-Cu birleştirmeleri soğuk kaynak makinasının standart kolu kullanılarak yapılmış fakat Al – Pirinç kaynağı makinanın standart kuvvet kolu uzatılarak gerçekleştirile birmiştir.Al-Al ve Al-Cu malzeme çiftlerinde ilk periyotta kısmi bir birleşme gözlemlenirken Al-Pirinç malzemede bu birleşme ikinci periyotta görülmüştür.Birleştirilen numunelerin görüntüsü şekil 2. de verilmiştir.



Şekil1. Soğuk basınç kaynak makinesi

a



Şekil 2. a) birleştirilen tellerin önden görünüşü b) birleştirmelerin üstten görünüşü

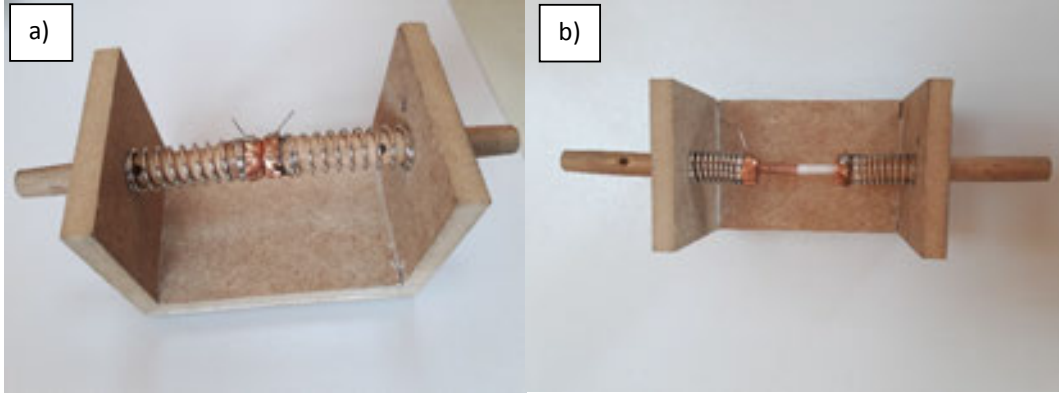
2.3 Elektrik iletkenliği

Elektrik direnç ölçüm işleri Gazi Üniversitesi Fen Fakültesi Fizik bölümünde bulunan KEITLEY 2400 Source Meter model akım voltaj ölçüm cihazında yapılmıştır(şekil 4). Sağlıklı bir ölçüm yapabilmek için malzemelerin çapakları alınmış, boyları 30mm olacak şekilde kesilmiş ve şekil 3. de görülen aparat kullanılmıştır. Tüm ölçüm işlemi boyunca voltaj 0.5 volt ta sabit tutularak malzemelerin akım değerleri tespit edilmiştir. Akım değerleri bulunan ve gerilimi bilinen malzemelerin dirençleri aşağıdaki formüldeki gibi hesaplanmıştır.

$$V=IxR$$

Burada;

V: VoltajI: Akım R: Direnç



Şekil 3. Akım voltaj ölçümlerinde kullanılan numune tutma aparatı



Şekil 4. Elektrik iletkenlik test cihazı

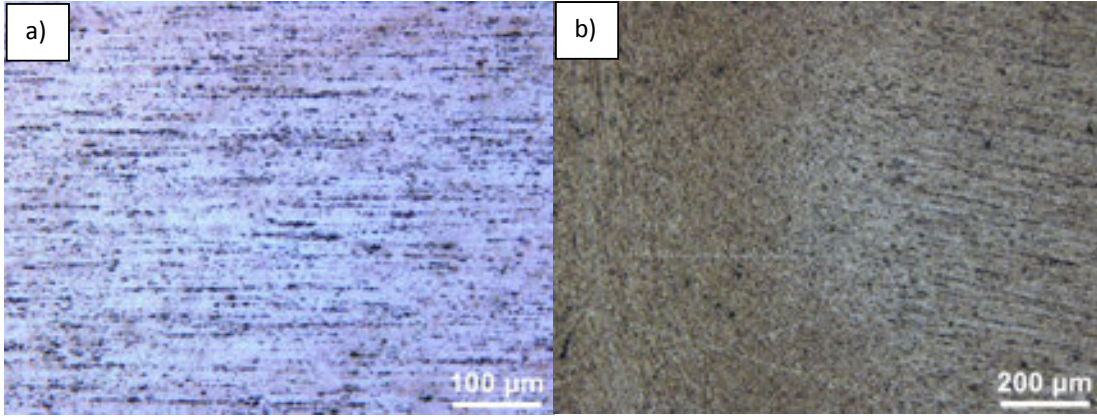
3. Sonuçlar ve Tartışma

Kaynak sırasındaki uygulanan deformasyon basıncın etkisiyle ara yüzeydeki malzeme ve yabancı maddeler merkezden yan yüzeylere doğru yönlendirilerek kaynak bölgesi dışına itilmiş bu sayede birleşmeyi olumsuz yönde etkileyecek olan kirliliğin önüne geçilmiştir. Aynı zamanda yan yüzeylerde bulunan çapak boşluklarından dışarı çıkan fazla malzeme kaynak etrafında halkalar halinde çapaklar oluşturmuştur. Bu sayede temiz bir temas yüzeyi elde edilmiştir. Temiz ve düz yüzeylerin atomik düzeyde bir araya getirilmesiyle de ana malzeme kadar güçlü bir birleştirme elde edilmiştir.

3.1 Mikro Yapı Sonuçları

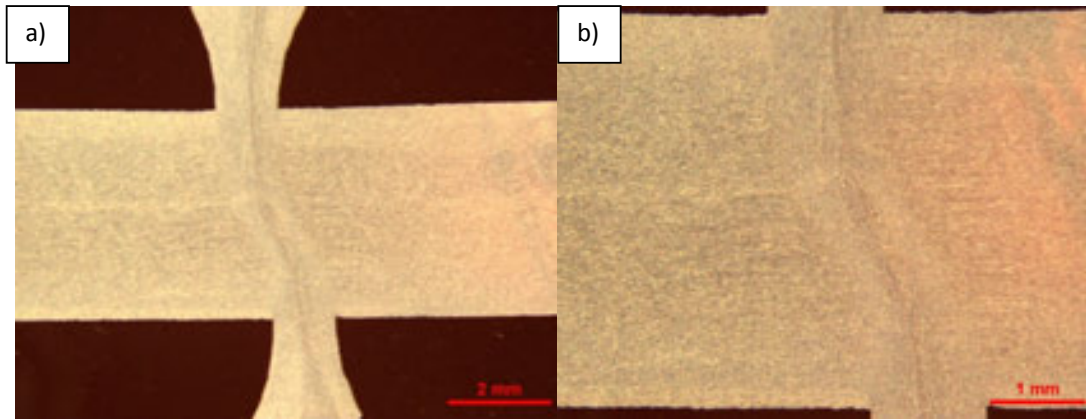
Al-Al

Alüminyum – alüminyum birleştirme çiftinde birleşme yüzeyleri düzgün bir hat boyunca uzanmış şekilde ve yaklaşık 25µm genişliğinde oluşmuştur. Tane yapısındaki değişimlerin pirinç ve bakır malzemeye göre dana net ve keskin sınırlara sahip olduğu gözlemlenmiştir. Şekil 5 a ve b de görüldüğü üzere ana malzemede boyuna lineer uzanan taneler kaynak bölgesinde basıncın etkisiyle kuvvet yönüne dik ve daha kısa formda oluşmuştur. Soğuk deformasyonun etkisiyle tanelerde ana malzemeden kaynak bölgesine doğru küçülmenin olduğu ve bu küçülmenin periyot sayısı ile kısmi oranda arttığı gözlemlenmiştir. Tane yapısı değişime uğramış bölge genişliği yaklaşık 1.3mm olarak ölçülmüştür. Alüminyum ana malzeme tane boyutu 150- 250µm tane yapısı değişime uğrayan bölgede ise 20-50µm tane boyut aralığı ölçülmüştür. Periyot sayısının tane yapısına etkisi çok sınırlı olduğu gözlemlenmiştir.



Şekil 5. Al-Al Malzeme çiftinde a) ana malzeme, b) Deformasyonla tane yönelmesi bölgesi

Şekil 6 da birleşme arayüzeyinden çapak oluşumu ve birleşme bölgesinde tane yapısının değiştiği bölge gösterilmektedir. Şekil 6 a ve b de görüldüğü üzere birleştirilen alüminyum numunelerin merkezinden itibaren tanelerin dış çapa doğru yönelerek çapak oluşturdukları ve tane yapısında çapak yönüne doğru yönelmiş tanelerden oluştuğu görülmektedir.

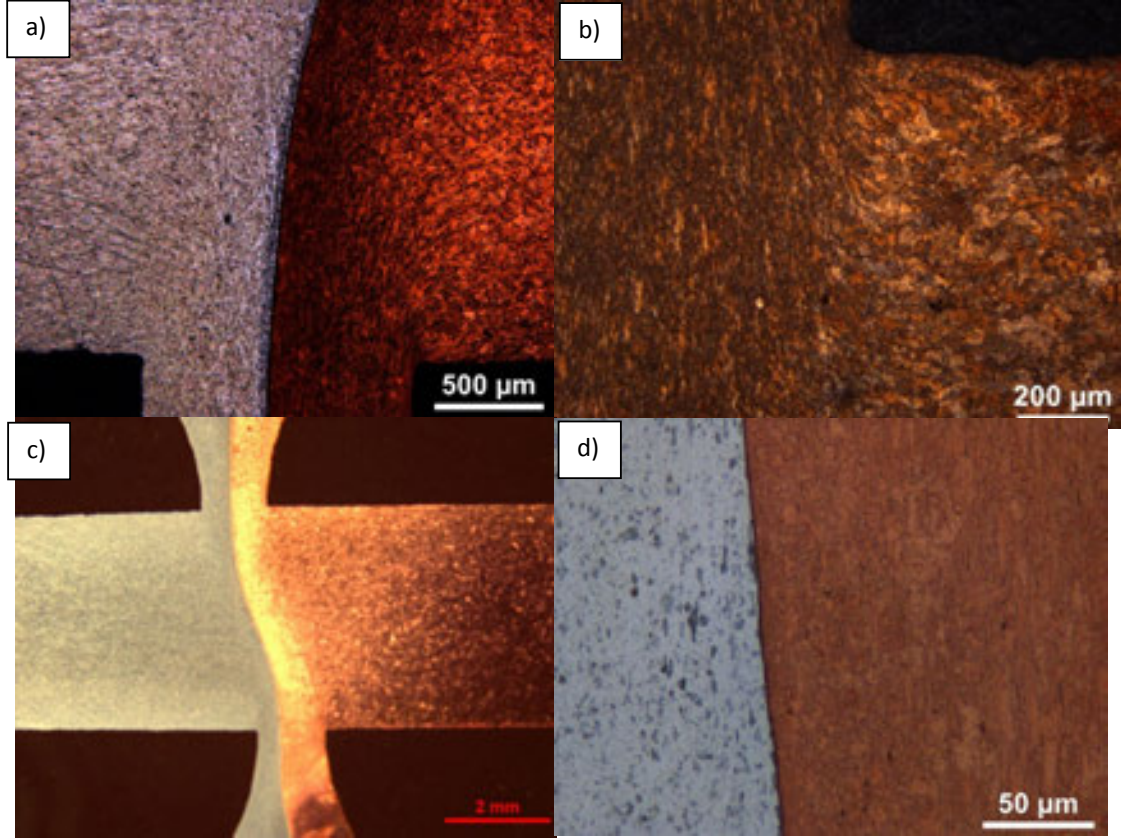


Şekil 6. Birleşme arayüzeyinde tane yapısının değiştiği bölgenin makro görüntüsü

Al-Cu

Alüminyum-bakır malzeme çiftinin soğuk basınç kaynağının mikro yapısına bakıldığında bakır tanelerinin dağlama sonucu daha net tane yapısı görüntüsü verdiği görülmektedir. Bu malzeme çiftinin de alüminyum tanelerinin bir önceki Al-Al birleştirmesindeki özellikleri sergilediği görülmüş kaynak bölgesindeki tane yapısında Al-Al kaynağına göre bir farklılık gözlenmemiştir.

Bakırın mikro yapısı incelendiğinde ana malzemenin çok köşeli düzensiz geometrik tanelerden teşkil olduğu, tane boyutlarının ise 20-80 μ m aralığında olduğu görülmektedir. Temas yüzeyindeki taneler basıncın etkisiyle deformasyon yönüne dik bir şekilde boyları uzayarak enine daralmış ve kalıp boşluklarının bulunduğu yan yüzeylere doğru plastik akış göstererek yönlenmiştir (şekil 7. a, b, c). Ayrıca birleşme çizgisinden ana malzemeye doğru yaklaşık 40 μ m genişliğindeki bölgede deformasyon sonucu tanelerin 5 μ m seviyelerine küçülerek daha küresel bir form aldığı görülmüştür (şekil 7. d). Birleşme ara yüzeyinden ana malzemenin yaklaşık 750 μ m içlerine kadar tane yapısındaki değişimlerin devam ettiği görülmüştür. Periyot sayısı arttıkça tane boyutunda kısmi oranda küçülmenin yanı sıra deformasyon bölgesinin çapak oluşumuna bağlı olarak azaldığı gözlemlenmiştir.



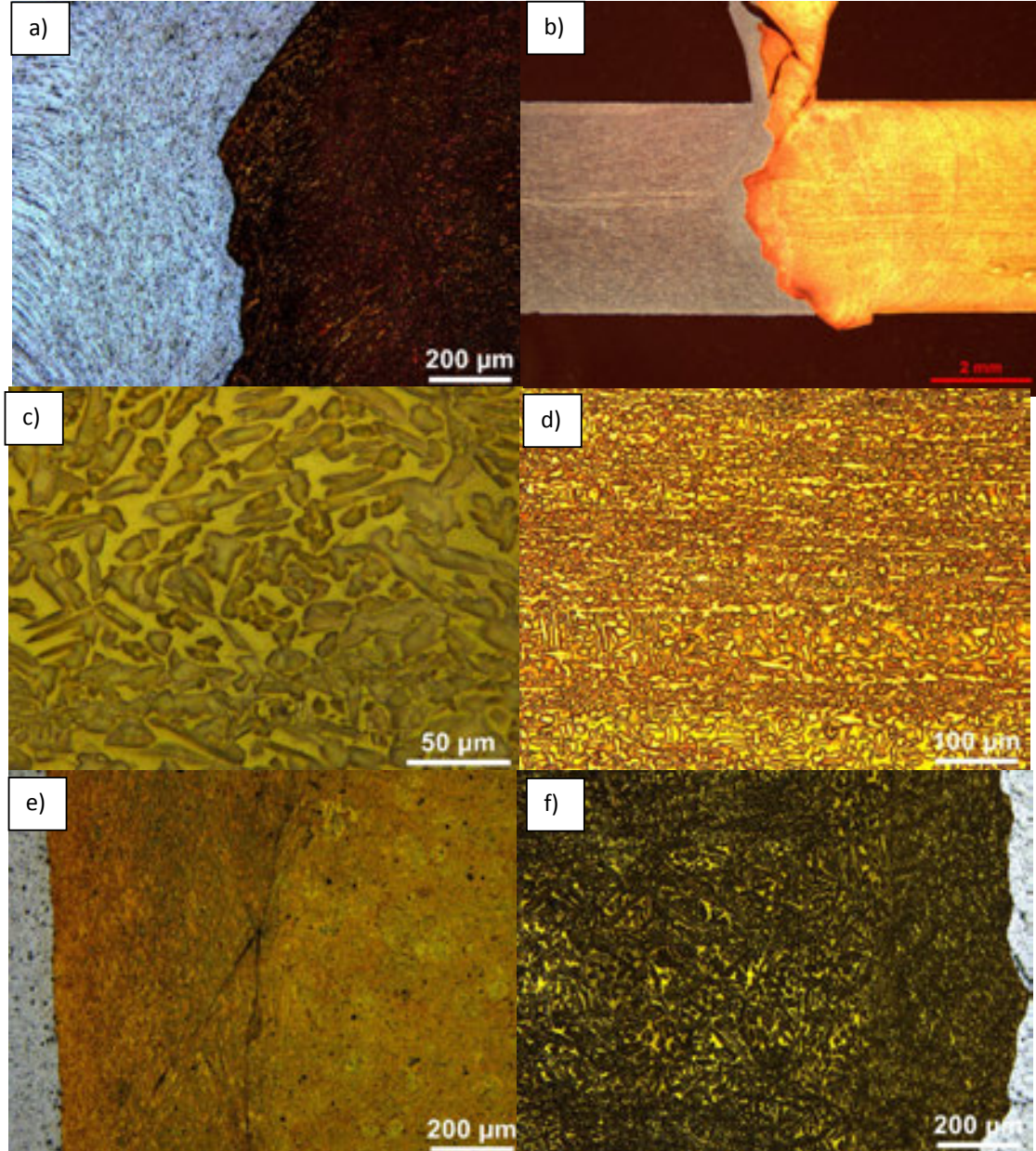
Şekil 7. Al-Cu malzeme çiftinin birleşme arayüzeyi

Al- Piriñç

Piriñç malzemenin daha sert ve gevrek olması sebebiyle kaynak birleşme yüzeyi Al-Al ve Al-Cu kaynağındaki malzeme çiftleri gibi düzgün bir hat şeklinde oluşmamış, birleşme arayüzeyi alüminyum tarafına doğru girinti çıkıntılar şeklinde meydana gelmiştir (Şekil 8. a ve b).

Pirinç ana malzemede Cu-Zn yapısı bantlı tane yapısı şeklinde boyuna üst üste şeritler olduğu gözlenmiştir(şekil 8. c ve d). Yaklaşık 140µm genişliğinde oluşan şeritler zincir şeklinde birbirini takip eder şekildedir.

Birleşme ara yüzeyine yakın tanelerin diğer birleştirmelerde olduğu gibi basıncın etkisiyle ana malzeme tanelerine göre küçülerek enine uzadığı ve yan yüzeylere doğru yönlendiği görülmektedir. Bununla beraber pirincin sert olması sebebiyle plastik akış süreksizlik göstererek kaynak kırılması şeklinde davranmıştır (Şekil 8. a, e, f).

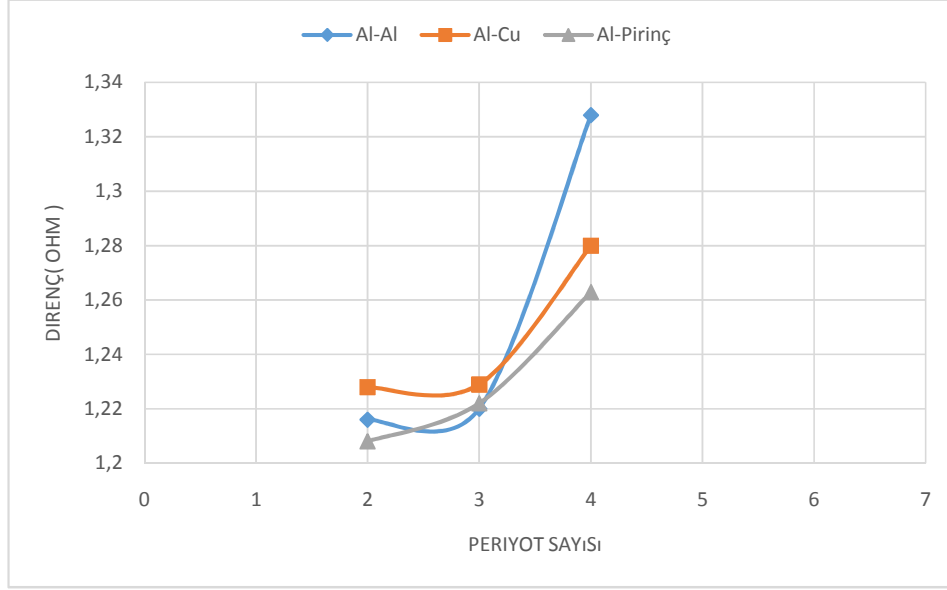


Şekil 8.A1- pirinç malzeme çifti

3.2 Elektrik İletkenliği Sonuçları

Basınç kaynağı ile birleştirilmiş numunelerde birleştirme periyodunun tane yapısını değiştireceğinden elektrik iletkenliğine etkisini belirlemek amacıyla her birleştirme çifti için elektrik iletkenlikleri ölçülerek baskı periyodunun elektrik iletkenliğine etkisi belirlenmiştir.

Al-Al malzeme çiftinin elektrik iletkenliğine karşı gösterdiği direnç Şekil 9 ve Tablo 1 de verilmiştir. Buradan görüleceği gibi



Şekil 9. Birleştirme çiftlerinin elektriksel dirençleri

Tablo 1. Soğuk basınç kaynaklı malzemelerin elektriksel dirençleri

Malzeme	Elektriksel direnç(ohm)			
	Esas metal	3 periyot	4 periyot	5 periyot
Alüminyum	1,185			
Bakır	1,205			
Pirinç	1,150			
Al-Al		1,216	1,220	1,328
Al-Cu		1,228	1,229	1,280
Al-Pirinç		1,208	1,222	1,263

Birleşme üçüncü periyottan itibaren başladığından Al-Al malzeme çiftinde üçüncü periyotta 1,216ohm olan direnç dördüncü periyotta 1,220ohm'a beşinci periyotta 1,328ohm'a çıkmıştır. Buradan artan periyot sayısı ile deformasyon miktarının artması ve tane boyutunun küçülmesiyle elektrik akımına karşı direncin arttığı söylenebilir.

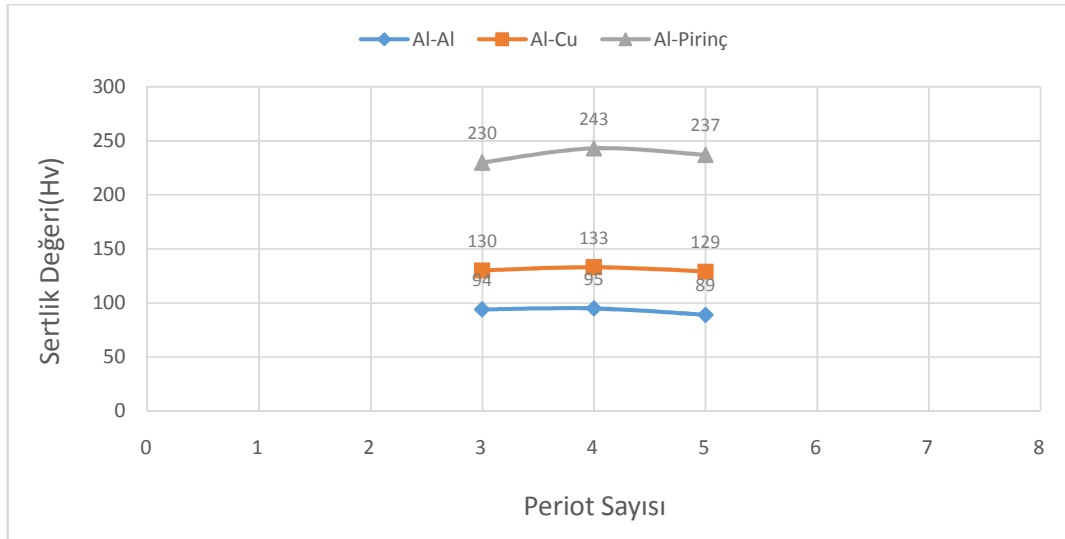
Cu-Al çiftinde üçüncü periyotta 1,228ohm, dördüncü periyotta 1,229ohm ve beşinci periyotta 1,280ohm direnç ölçülmüştür. Üç ve dördüncü periyotlarda çok az da olsa direnç artışı olduğu gözlenmektedir bununda hem farklı malzeme çifti olmasından hem de artan periyotla deformasyon sertleşmesinin sonucu olduğu düşünülmektedir.

Al-Pirinç malzeme çiftinde alüminyumun direnci 1,185ohm, pirinç malzemenin direnci 1,150ohm olarak ölçülmüş olup üçüncü periyotta direnç 1,208ohm, dördüncü periyotta 1,222ohm, beşinci periyotta 1,263ohm olarak ölçülmüştür. Burada periyot sayısı arttıkça birleşme ara yüzey direncinin arttığı görülmektedir. Benzer şekilde deformasyon sertleşmesinin elektrik direncini arttırdığı görülmektedir.

3.3 Mikro Sertlik Sonuçları

Yapılan mikro sertlik ölçme çalışmasında tüm malzemeler Hv1kg ve 10X büyütme kullanarak gerçekleştirilmiştir. Sertlik ölçme işlemi ana malzemeden birleşme ara yüzeyine doğru 0.3mmlik adımlarla üç hat oluşturularak yapılmıştır.

Artan baskı periyotu ile mikro sertlik değerleri her üç birleştirme türünde de artan basınç periyotu ile dördüncü Periyota kadar artış göstermiş beşinci Periyotta her üç birleştirme türünde de sertlik azalması görülmüştür. Artan baskı periyotu ile deformasyon miktarı artarak sertlik artışına sebep olurken dördüncüperiyottan sonra açığa çıkan ısı ile deformasyonun kolaylaşması sonucu deformasyon sertleşmesi mekanizması yerine ısıl işlem etkisi ile sertlikte azalma meydana gelmiştir. Birleştirilen malzemelerin mikro sertlik değerleri şekil 10 da verilmiştir.



Şekil 10. Birleştirme çiftlerinin mikro sertlik değerleri

Alüminyum ana malzeme sertlik değeri 70Hv iken 3periyot uygulanarak yapılan birleştirmenin kaynak bölgesi 94Hv, 4 periyot uygulanan kaynak bölgesi 95Hv ve 5 periyot uygulanan kaynak bölgesi değeri de 89Hv ölçülmüştür. Burada kaynak bölgesinin ana malzemeden %30 civarlarında daha sert olduğu görünmektedir. Bunun sebebi ise kaynak bölgesinin soğuk deformasyonla ince taneli bir yapıya dönüşmesi ve buna bağlı bir deformasyon sertleşmesidir.

Bakır esas metalin sertlik değeri 75Hv ölçülürken periyot sayısına göre Al-Cu kaynak bölgesinin sertlik değerleri ortalama %42 artış göstererek 3 periyot 130hv, 4 periyot 133hv ve 5 periyot 129Hv değerlerine yükselmişlerdir. Burada soğuk deformasyon sebebiyle oluşan deformasyon sertleşmesi oranı Al-Al kaynağından daha büyük olduğu görülmektedir.

Bu çalışmada kullanılan en sert malzeme olan pirincin sertlik değeri 178Hv olarak ölçülmüştür. Al –Pirinç kaynağında kaynak bölgesi sertlik değerleri üçüncü periyotta 230 Hv, dördüncü periyotta 243 Hv, beşinci periyotta 237 Hv olarak ölçülmüştür.

4. Sonuçlar

Soğuk basınç kaynağı ile birleştirme sırasında baskı periyotunun birleştirme ve elektriksel iletkenliğe etkisinin belirlenmesi amacıyla yapılan bu çalışmada aşağıdaki sonuçlar elde edilmiştir.

1. Bu çalışmada her üç birleştirme çiftinde de 3. Periyota kadar birleşme elde edilememiştir.
2. Üçüncü periyottan sonra 4. ve 5. Periyotlarda birleştirme yapılarak bu periyotla birleştirilen numunelerdemekanik ve metalürjik özellikler ölçülmüştür.
3. Artan basınç periyodu ile kritik bir periyota kadar(4. periyot) mikro sertlik artarken bu periyottan sonra artan basınca bağlı sertlik düşmektedir.
4. Birleştirilen numunelerde basınçla sertliğin artması sonucu elektrik iletkenliğinin azaldığı , direncin arttığı gözlemlenmiştir.
5. Pirinç gibi sert malzemelerde malzemenin plastik akış göstermemesi birleşmeyi olumsuz yönde etkilemektedir.
6. Tüm birleştirme türlerinde elektriksel iletkenlik, iletkenliği yüksek malzemeden daha düşük, iletkenliği düşük malzemeden daha yüksek çıkmıştır.

5. Kaynaklar

[1] <http://www.coldpressurewelding.com>

[2] Y. Abe, F.Sato, I. Ideno: Development Of A ContactWireColdPressure Welding Device, JR EAST Technical Review-No. 6, pp. 23-30

[3]A. EfeColdPressureandResistanceWelding of CopperWires, Msc. Thesis, İstanbul Technical UniversityInstitute of ScienceandTechnology, İstanbul/Turkey, (2000),pp. 3-4.

İletişim Bilgileri: Hüseyin KÜÇÜKÖNER, Gazi Üniversitesi Kaynak ve Birleştirme Teknolojileri Araştırma ve Uygulama Merkez Müdürlüğü Teknikokullar/Ankara, 0(544)5508054

Kısa Özgeçmiş

Hüseyin KÜÇÜKÖNER – 1985 yılında Tarsus'ta doğmuştur.2009 yılında Dumlupınar Üniversitesi'nde teknisyen olarak çalışmaya başlamıştır. Gazi Üniversitesi Teknik Eğitim Fakültesi Metal Öğretmenliği Bölümü'nden 2014 yılında mezun olmuştur. 2015 yılından itibarenGazi Üniversitesi Kaynak ve Birleştirme Teknolojileri Araştırma ve Uygulama Merkez Müdürlüğünde teknisyen olarak çalışmaya devam etmektedir.

Adem KURT – 1958'de Çorum Alaca'da doğdu. Lisans eğitimini 1983' de Gazi Üniversitesi Teknik eğitim Fakültesinde, Yüksek lisans eğitimini 1992'de Gazi Üniversitesi Fen Bilimleri Enstitüsü'nde doktora eğitimini ise 1999 yılında Fırat Üniversitesi Fen Bilimleri Enstitüsü'nde tamamlamıştır. 1999 yılında Gazi Üniversitesinde “doçenç” ünvanı almıştır ve 2005 yılından itibaren Gazi Üniversitesi Teknoloji Fakültesi Metalürji ve Malzeme Mühendisliği Bölümü'nde profesör olarak görev yapmaktadır.

ÇELİK YAPILARDA KULLANILAN T PROFİLİN KAYNAKLI İMALATINDA OLUŞAN AÇISAL DISTORSİYONLARIN OPTİMİZASYONU

İlhan YİĞİT^{1,a}, Serkan APAY^{2,b}

¹Yiğitler Yapı Tic. ve San. Ltd. Şti. Doğanlı Mevkii Düzce / TURKEY

²Düzce Üniversitesi Teknoloji Fakültesi Makine ve İmalat Müh. Böl. Düzce / TURKEY

^a ilhanyigit@yigitleryapi.com.tr, ^b serkanapay@duzce.edu.tr

Özet

Deprem kuşağı üzerinde yer alan ülkemizde, çelik yapıların kullanım alanları ve sıklığı giderek artmakta ve önem kazanmaktadır. Çelik yapı; taşıyıcı sistemlerin çelikten üretildiği, çoğunlukla fabrika binaları, spor tesisleri, depo ve atölyelerin imalatında kullanılan, geniş açıklıklara ve yüksekliğe sahip sistemlerdir. Çelik yapılar diğer taşıyıcı sistemlere göre üstün mekanik özelliklere, statik yeteneklere ve uygulama kolaylığına sahiptir. Çelik yapılar hızlı, güvenli ve ekonomik olması nedeniyle tercih edilmektedir. Çelik yapıların imalatında genellikle kaynaklı imalat yöntemleri tercih edilmektedir.

Kaynaklı imalat işlemleri kullanılarak birleştirilen parçalar işlem esnasında ısınma ve soğuma çevrimlerine maruz kalırlar. Isı etkisinin şiddetine, malzemelerin mekanik özelliklerine ve çelik yapının biçimine bağlı olarak ısınan parçaların genleşmesi çevresindeki soğuk bölge tarafından engellenir. Bu engelleme sonucunda malzemelerde artık gerilmeler ve kalıcı şekil değişimleri, distorsiyonlar oluşur. Kaynaklı imalat esnasında oluşan distorsiyon ve artık gerilmeler, son ürünün boyutsal toleransların dışına çıkmasına neden olacağı gibi, yapısal elemanlarda ikinci mertebe etkilerinin artmasına, dinamik yükler altında çalışan elemanlarda da yorulma dayanımında düşmelere neden olur.

Bu çalışma kapsamında kaynaklı çelik yapılardan T profili imalatı esnasında kullanılan farklı kaynak yöntemlerinin, yapıda oluşacak distorsiyon (çarpılma) üzerine etkileri incelenmiş ve Taguchi Optimizasyon metodu uygulanarak optimum çarpılma değerlerini belirlemiştir.

Anahtar Kelimeler: Açısal Distorsiyon, Gazaltı Kaynağı, Taguchi Optimizasyonu, Tozaltı Kaynağı.

1. Giriş

Yapı çelikleri 1980 ve 1990'lı yıllarda çelik yapılar kompozit kiriş ve döşemelerinin imalatında etkili bir şekilde kullanımı ile birlikte Batı Avrupa ülkelerinde ve özellikle İngiltere'de daha çok kullanılan bir malzeme haline gelmiştir. Ülkemizde henüz yeterli derecede kullanılmayan yapı çelikleri özellikle 1999 Marmara depremi sonrasında inşaat sektöründe adından sıkça söz edilen bir yapı malzemesi olmuştur [1].

Kaynaklı birleştirmelerin bir parçası olduğu tüm imalat süreçlerinde, kaynak prosesi sonrası oluşan artık gerilme ve distorsiyonlar, gerek işleme maruz yapısal elemanın boyutsal hassasiyetleri açısından gerekse de ürünün uzun dönem performans sınırlarını belirlemesi açısından oldukça önemlidir. Bu nedenle kaynaklı imalat sonrası oluşan bu artık gerilme ve distorsiyonların kontrolü, özellikle karmaşık geometrilere sahip ve dinamik etkiler altında zorlanan yapısal elemanlar için önemlidir [2, 3].

Bu önem nedeni ile literatürde kaynaklı imalat sonrası oluşan distorsiyon ve artık gerilmelerin miktarını belirleyebilmek için yapılmış birçok çalışma bulunmaktadır. Bu çalışmalar deneysel veriler üzerine kurulu olanlar ile sayısal modellerden oluşmaktadır. Kaynaklı imalat prosesi kullanılarak birleştirilen parçalar, işlem esnasında ısınma ve soğuma çevrimlerine maruz kalırlar. Isı etkisinin şiddetine, malzemelerin mekanik özelliklerine ve konstrüksiyonun biçimine bağlı olarak ısınan parçaların genişmesi çevresindeki soğuk bölge tarafından engellenir. Bu engelleme neticesinde malzemelerde artık gerilmeler ve kalıcı şekil değişimleri yani distorsiyonlar oluşur [4].

Artık gerilmeler, kaynaklı konstrüksiyonlarda distorsiyon hasarlarına, yorulma ömründeki azalmalara, gerilmeli korozyon çatlağına ve malzemenin mekanik özelliklerinin azalmasına neden olmaktadır. Bu nedenle artık gerilmelerin malzemenin giderilmesi ciddi kaynaklı konstrüksiyonlar için çok büyük önem arz etmektedir. Bununla birlikte artık gerilmelerin miktarının ölçülmesi ve bunun etkili bir şekilde giderildiğinin ispat edilmesi de önem kazanmaktadır [2]. Açısal distorsiyonlar; ısıtma gerilmeleri, konstrüksiyonun rijitliği ve malzemenin metalürjik özellikleri olmak üzere üç ana değişkenden etkilenmektedir. Kaynak akımı değeri artışı ise kaynaklı birleştirme işlemi bölgesel ısı girdisi değerlerini arttırmaktadır. Bu nedenle yapısal çeliklerden profil, kiriş ve kolon gibi ürünlerin kaynaklı birleştirmesinde en uygun kaynak akımı değerinin tayini minimum açısal distorsiyonu ve bunun sonucu minimum fabrikasyon maliyetinin tayini için incelenmesi gereken önemli bir değişken olmaktadır [5, 6].

2. Deneysel Çalışmalar

Bu çalışmada, S355J2+N yapısal çelik malzemelerden üretilen T profilinde, kaynak yöntemi ve parametrelerinin açısal distorsiyon değerlerini Taguchi yöntemi ile optimize etmeye ve optimum değerleri belirlemeye çalışılmıştır.

2.1. Deney Numunesi ve Deneylerin Yapılışı

Deneyde kullanılan S355J2+N yapı çeliğine ait kimyasal bileşim Tablo 1'de, mekanik özelliklerine ait veriler ise Tablo 2'de verilmiştir. Numuneler, T profili şeklinde kaynatılmadan önce üzerindeki şekil bozuklukları giderilmiştir. Kaynak öncesinde numuneler birbirlerine puntalanmış ve T profil geometrisi oluşturulmuştur. Kaynak öncesi oluşturulan T profilleri Şekil 1'de verilmiştir.

Tablo 1. S355J2+N Yapısal çelik kimyasal bileşim (Ağırlıkça %).

C%	Mn%	P%	Ni%	Al%	S%	Si%	Fe%
0,17	1,34	0,011	0,05	0,028	0.009	0.02	Kalan

Tablo 2. S355J2+N Yapısal çelik mekanik özellikleri.

Akma Dayanımı (N/mm ²)	Çekme Dayanımı (N/mm ²)	Uzama (N/mm ²)	Darbe Direnci (Joule)	Sertlik
430	555	26	20 °C 29J	189 HB



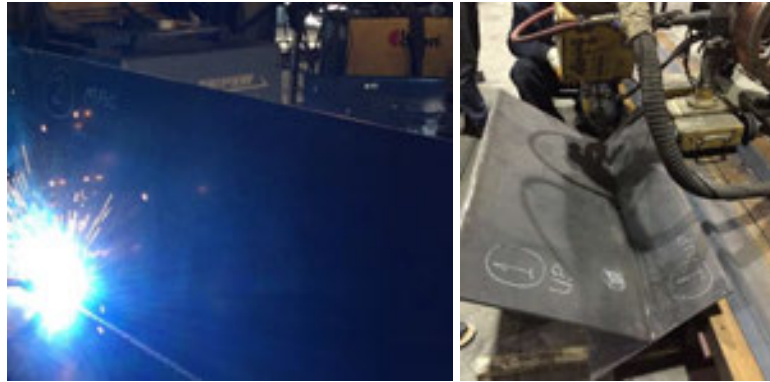
Şekil 1. T profillerin kaynak öncesi hazırlanması.

Puntalama işlemi sonrası, T profillerin kaynak işlemine geçilmiştir. Kaynatma işlemi Gazaltı ve Tozaltı kaynak yöntemleri kullanarak yapılmıştır. Açısal çarpılma, distorsiyon oluşumunu görebilmek adına profiller farklı akımlarda, farklı voltajda ve farklı kaynak hızlarında kaynatılmışlardır. Deneylerde kullanılan kaynak parametreleri Tablo 3’de verilmiştir.

Tablo 3. Deneylerde kullanılan kaynak parametreleri.

Kaynak Yöntemi	Akım Değeri (Amper)	Voltaj Değeri (V)	Kaynak Hızı (mm/sn)
Gazaltı Kaynak	205 - 225	28 - 30	6 - 8
Tozaltı Kaynak	450 - 500	30 - 34	6 - 8

Şekil 2’de, Tablo 3’de verilen parametreler ile yapılan kaynaklar görülmektedir. Kaynak işlemi sonrasında biten numuneler ve yapılan ölçümlere ait görüntüler ise Şekil 3’de verilmiştir.

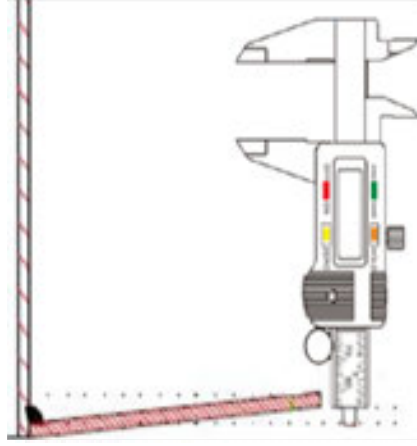


Şekil 2. T profillerin kaynatılması işlemi.



Şekil 3. T profillerin kaynatılması işlemi sonrası çarpılma ölçümleri.

Ölçümün nasıl yapıldığını gösteren resim Şekil 4'de şematik olarak verilmiştir. Buna göre dijital kumpas T profilin dışından merkeze doğru olan noktaya ayarlanmıştır. Buna göre profil alt plakasının kaynak sonrası ne kadar şekil değiştirdiği tespit edilmiştir.



Şekil 4. T profillerin çarpılma ölçümleri şematik gösterimi.

2.2. Taguchi Deney Tasarımı

Deneyisel çalışmalarda doğru sonuca ulaşabilmek için doğru deney tasarımının yapılması gerekmektedir. Yapılan çalışmada, deney tasarım ve analiz yöntemi olarak Taguchi metodu kullanılmıştır. Dr. Genichi Taguchi tarafından geliştirilen bu yaklaşımda, sonuçları analiz edebilmek için S/N oranı olarak bilinen bir istatistiksel performans ölçüsü kullanılır. Deneylerden elde edilen sonuçlar sinyal/gürültü oranına (S/N) çevrilerek değerlendirme yapılır. S/N oranındaki S sinyal faktörünü, N ise gürültü faktörünü ifade etmektedir. Sinyal faktörü sistemden alınan gerçek değeri, gürültü faktörü ise deney tasarımına katılmayan fakat deney sonucuna etki eden faktörleri ifade etmektedir. Gürültü kaynakları, elde edilmek istenen performans karakteristiklerinin hedef değerden sapmasına sebep olan tüm değişkenlerdir [7]. S/N oranlarının hesaplanmasında; karakteristik tipine bağlı nominal en iyi, en büyük en iyi ve en küçük en iyi metotları kullanılır [8]. Bu çalışmadaki S/N değerlerinin belirlenmesinde, işleme verimliliği bakımından distorsiyon değerinin en küçük olması istenildiği için eşitlik 1'de verilen **“en küçük en iyi”** prensibine karşılık gelen formül kullanılmıştır. Burada; yi ölçülen çarpılma değerini, n ise yapılan deney sayısını ifade etmektedir.

$$S/N = -10 \log \left(\frac{1}{n} \sum_{i=1}^n y_i^2 \right) \quad (1)$$

S355J2+N yapısal çelikten gazaltı ve tozaltı kaynak yöntemleri ile T profili üretiminde kullanılan kontrol faktörleri ve seviyeleri Tablo 4'de verilmiştir.

Tablo 4. Kontrol faktörleri ve seviyeleri.

Sembol	Kontrol Faktörleri	Seviye 1	Seviye 2
A	Kaynak Yöntemi	Gazaltı Kaynak	Tozaltı Kaynak
B	Akım Değeri (Amper)	205	450
C	Kaynak Hızı (mm/sn) ₆₉	6	8

3. Bulgular ve Tartışma

3.1. Açısal Distorsiyon Optimizasyonu

S355J2+N yapısal çelikten gazaltı ve tozaltı kaynak yöntemleri ile T profili üretiminde, Taguchi L8 deney tasarımına göre gerçekleştirilen açısal distorsiyon deneyleri sonucunda elde edilen çarpılma değerleri ile hesaplanan S/N oranları, Tablo 5'te verilmiştir.

Tablo 5. Deney tasarımı, Çarpılma ve S/N oranları.

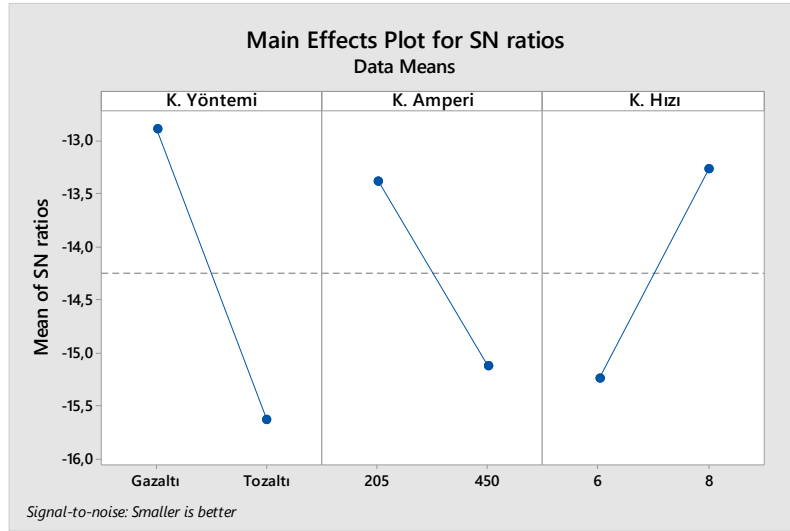
Deney No	(A) Kaynak Yöntemi	(B) Akım (Amper)	(C) K. Hızı (mm/sn)	Çarpılma (mm)	S/N oranı (dB)	Tahmin Edilen Çarpılma (mm)
1	Gazaltı	205	6	4,89	-13,7862	4,5675
2	Gazaltı	205	8	3,04	-9,6575	3,4875
3	Gazaltı	450	6	5,67	-15,0717	5,5475
4	Gazaltı	450	8	4,47	-13,0062	4,4675
5	Tozaltı	205	6	5,77	-15,2235	6,1225
6	Tozaltı	205	8	5,52	-14,8388	5,0425
7	Tozaltı	450	6	7,01	-16,9144	7,1025
8	Tozaltı	450	8	5,99	-15,5485	6,0225

Kontrol faktörlerinin optimum seviyeleri ve performans karakteristiği (açısal distorsiyon) üzerinde bu faktörler arasından en etkili olanının belirlenmesinde Taguchi metoduyla oluşturulan S/N yanıt tablosu kullanılmaktadır. Bu tablodaki en küçük S/N değerleri, o kontrol faktörüne ait optimum seviyeyi göstermektedir. Açısal distorsiyon üzerinde her bir kontrol faktörünün etkisini gösteren S/N yanıt tablosu Tablo 6'da verilmiştir.

Tablo 6. Deney tasarımı, Çarpılma ve S/N oranları.

Seviye	Kaynak Yöntemi	Kaynak Amperi	Kaynak Hızı
1	-12,88	-13,38	-15,25
2	-15,63	-15,14	-13,26
Delta	2,75	1,76	1,99
Sıralama	1	3	2

Tablo 6 incelendiğinde, açısal distorsiyon üzerinde en etkili faktörlerin sırasıyla kaynak yöntemi, kaynak amperi ve kaynak hızı olduğu görülmektedir. S355J2+N yapısal çeliğinden T profili imalatında optimum açısal distorsiyon değeri; kaynak yönteminin birinci seviyesinde, kaynak amperinin birinci seviyesinde ve kaynak hızının ikinci seviyesinde elde edilmiştir. Kontrol faktörlerinin yani kaynak parametrelerinin optimum değerlerini gösteren ana etki grafiği Şekil 5'de verilmiştir. S/N yanıt tablosunda olduğu gibi ana etki grafiğinde de en büyük S/N değerleri, o parametreye ait optimum seviyeyi göstermektedir. Buna göre kaynak yöntemi, kaynak amperi ve kaynak hızı için sırasıyla optimum değerler Gazaltı kaynak yöntemi ile, 205 amper değerinde ve 8 mm/sn kaynak hızı olarak belirlenmiştir.



Şekil 5. S/N oranları için ana etki grafiği.

3.2. Varyans Analizi (ANOVA)

Deney tasarımında kullanılan tüm kontrol faktörlerinin birbiriyle olan etkileşimleri, performans karakteristiği üzerinde nasıl bir etki meydana getirdiği ve parametrelerin farklı seviyelerinin performans karakteristiğinde ne gibi değişimlere sebep olduğunun belirlenebilmesi için varyans analizi yapılmaktadır [9]. Çarpılma üzerinde, kontrol faktörlerinin etki seviyelerini belirlemek amacıyla yapılan varyans analizi sonuçları Tablo 7’de verilmiştir. Burada, her bir değişkenin önem seviyesini gösteren F değerleri ve yüzde katkı oranları (PCR) görülmektedir. Bu analiz %95 güvenilirlik ve %5 önem seviyeleriyle gerçekleştirilmiştir. Kontrol faktörlerinin etkisi F değerlerinin karşılaştırılmasıyla belirlenir. F değeri en büyük olan faktör, sonuca en fazla etki eden faktördür. ANOVA sonuçlarına göre açısız çarpılmayı etkileyen en önemli parametrenin %49,49’luk oranla kaynak yöntemi olduğu görülmüştür. Kaynak hızı ise %23,88’lik oranla kaynak yönteminden sonra en etkili olan parametredir. Çarpılma üzerinde en az etkiye sahip parametrenin %19,66’lık oranla kaynak amperi olduğu görülmüştür.

Tablo 7. ANOVA tablosu.

Kontrol Faktörü	Serbestlik Derecesi (DF)	Kareler Top. (SS)	Kareler Ort. (MS)	F-Değeri	P-Değeri	Katkı Oranı (PCR)
K. Yöntemi	1	4,8360	4,8360	28,40	0,006	49,49%
K. Amperi	1	1,9208	1,9208	11,28	0,028	19,66%
K. Hızı	1	2,3328	2,3328	13,70	0,021	23,88%
Hata	4	0,6811	0,1703			6,97%
Toplam	7	9,7708				100,00%

3.2. Doğrulama Testi

Taguchi tekniği ile optimizasyonda son aşama, optimum kaynak parametre seviyelerini kullanarak kaynak karakteristiklerinin (kaynak yöntemi, amper ve kaynak hızı) gelişimini tahmin etme ve sonuçların karşılaştırılmasıdır. Taguchi methodu ile hesaplanan optimum değerler yapılan deney tasarımında yer aldığı için doğrulama deneyleri yapılmamıştır. Doğrulama deneyi yerine hesaplanan ve doğrulanan kaynak seviyelerinin deneysel sonuçları karşılaştırılması Tablo 7'de verilmiştir. Bu çalışma ile S355J2+N yapısal çelikten T profilinin imalatında, açısız distorsiyon miktarının kaynak parametrelerinin değişimi ile etkilendiği Taguchi deneysel tasarım ve optimizasyon metodu kullanılarak bir kez daha ispat edilmiştir.

Tablo 7. Doğrulama testi sonuçları.

Hesaplanan Değerler	Doğrulama Deneyi	Fark
A1B1C2	A1B1C2	-
Çarpılma 3,48 mm	Çarpılma 3,04 mm	0,44 mm
S/N -11,0079 (dB)	S/N -9,65747 (dB)	-1,35043 (dB)

4. Sonuç

Yapılan deneysel çalışma sonucu elde edilen veriler aşağıda sıralanmıştır;

- S355J2+N yapısal çelikten imal edilen T profilin açısız distorsiyon miktarına kaynak yönteminin, amper değerinin ve kaynak hızının önemli etkileri olduğu görülmüştür.
- T profili imalatında optimum açısız distorsiyon değeri; gazaltı kaynak yöntemi ile 205 amper değeri ve 8 mm/sn kaynak hızı ile elde edilmiştir.
- ANOVA sonuçlarına göre, açısız çarpılma üzerindeki en etkili parametrenin %49,49'lük oranla kaynak yöntemi, %23,88'lik oranla kaynak hızı ve %19,66'lık oranla kaynak amperi olduğu görülmüştür.
- Optimum kaynaklı imalat şartlarındaki çarpılma miktarı sırasıyla hesaplamalar ve doğrulama deneyleri sonucu 3,48 mm ve 3,04 mm olarak bulunmuştur.
- Doğrulama deneyleri sonucunda Taguchi optimizasyonunun başarıyla uygulandığı görülmüştür.

Bu sonuçlara göre, S355J2+N yapısal çeliğinin T profili imalatı işlemindeki, minimum açısız çarpılma miktarının belirlenmesinde, Taguchi deneysel tasarım metodunun başarılı bir şekilde uygulanabileceği görülmüştür.

5. Kaynaklar

- [1] Şık. A.: MIG/MAG kaynak yöntemi ile birleştirilen çelik malzemelerde ilave tel türleri ve koruyucu gaz karışımlarının eğmeli yorulma ömürlerine etkilerinin araştırılması," *Gazi Üniversitesi Mühendislik Mimarlık Fakültesi Dergisi*, cilt 4, no. 22, pp. 769-777, 2007.
- [2] E. TOPARLAK: "Kaynaklı Konstrüksiyonlarda Titreşimle Gerilme Giderme ve Uygulamaları", İstanbul: İstanbul Teknik Üniversitesi Fen Bilimleri Enstitüsü Yüksek Lisans Tezi, 2011.
- [3] A. O. Cynthia L. Jenney: "Welding Handbook", USA: American Welding Society, 2015.
- [4] U. VURAL: "Kaynaklı İmalat Sonrası Oluşan Distorsiyonların Sonlu Elemanlar Yöntemi İle Analizi", İstanbul: İstanbul Teknik Üniversitesi Fen Bilimleri Enstitüsü Yüksek Lisans Tezi, 2009.
- [5] LONG, H., GERY, D., CARLIER, A., MAROPOULOS, P. G.: Prediction of Welding Distortion in Butt Joint of Thin Plates, *Materials and Design* 30 (2009) pp. 4126-4135.
- [6] TSENG, K. H., CHOU, C. P., The Study of Nitrogen in Argon Gas on the Angular Distortion of Austenitic Stainless Steel Weldments, *Journal of Materials Processing Technology* 142 (2003) pp. 139-144.
- [7] Turgut E. and Dikici A.: Optimization of design parameters of Co-axial heat exchanger with Taguchi method, 6th International Advanced Technologies Symposium (IATS'11), Elazığ, Turkey, pp. 278-281, (2011).
- [8] Masmıati N. and Sarhan Ahmed A. D.: Optimizing cutting parameters in inclined end milling for minimum surface residual stress –Taguchi approach, *Measurement*, 60 (2015), pp. 267–275.
- [9] KARABATAK, M., KARA, F.: AISI D2 Soğuk İş Takım Çeliğinin Sert Tornalanmasında Yüzey Pürüzlülüğünün Deneysel Optimizasyonu, *Politeknik Dergisi*, 19 (2016) pp. 349-355.

CORRESPONDENCE ADDRESS: Serkan APAY, Düzce Üniversitesi Teknoloji Fakültesi Makine ve İmalat Müh. Böl. D Blok Kat 3 Düzce/TÜRKİYE, +90 380 542 11 33 - 2252 ve serkanapay@duzce.edu.tr

KISA BİYOGRAFİLER

İlhan YİĞİT – 1982 Düzce doğumlu. Lisans eğitimi Zonguldak Karaelmas Üniversitesi Mühendislik Fakültesi Makine Mühendisliği Bölümü 2008 yılı mezunudur. Uluslararası Kaynak Mühendisliği diplomasını ODTÜ'den 2008 yılında almıştır. Evli ve 1 kız çocuk babasıdır. Yiğitler Çelik Yapı Ltd. Şti. Genel Müdür olarak görev yapmaktadır.

Serkan APAY – 1980 İzmir doğumlu. Lisans ve lisansüstü eğitimlerini Ankara Gazi Üniversitesi Metal Eğitimi bölümünde tamamlamıştır. Evli ve 1 kız çocuk babasıdır. Düzce Üniversitesi'nde öğretim üyesi olarak görev yapmaktadır.

ELECTRICAL AND OPTICAL PROPERTIES OF CADMIUM OXIDE CARBON NANOTUBE NANOCOMPOSITE

Ömer Güler^{1,a}, Öyküm Başgöz^{1,b}, M. Gökhan Albayrak^{2,c}, Seval Hale
Güler¹, Mehmet Takgün², Kazım Buğra Gürbüz¹, Mustafa Taşkın¹

¹ Mersin University, Engineering Faculty, Metallurgical and Materials Eng. Dept., 33100, Mersin, Turkey

² Fırat University, Engineering Faculty, Metallurgical and Materials Eng. Dept., 23119, Elazığ, Turkey

^aoguler@mersin.edu.tr, ^boykumbasgoz@mersin.edu.tr, ^cmgalbayrak@firat.edu.tr

Abstract

In this study, cadmium oxide based carbon nanotube reinforced material was produced and the optical and electrical properties of the obtained composite were investigated. After the carbon nanotubes used as reinforcement material were synthesized using the chemical vapor deposition method, they were supplemented at different ratios to the commercially available cadmium oxide powders. As another group of samples; cadmium oxide powders were synthesized by the sol-gel method and the carbon nanotubes were again supplemented at different ratios. Synthesized carbon nanotubes were subjected to TEM examination. Composite materials obtained were examined by SEM. Then, the changes in the electrical conductivity of the composites obtained by temperature were measured. The optical properties of the composites were determined by taking UV-vis spectrometers.

Key Words: Carbon Nanotube, Cadmium Oxide, Sol-Gel, Composite.

1. Introduction

In recent years, the application areas of metal oxides have grown to a large extent due to their new electrical, catalytic and optical properties, so researchers primarily work with these materials because of their optical and structural properties of metal oxides [1-4]. Transparent oxide conductors such as copper oxide (CuO), zinc oxide (ZnO), tin oxide (SnO) and cadmium oxide (CdO) are of interest due to their semiconductor optoelectronic properties [5].

CdO is an n-type semiconductor. It has 2.2 - 2.8 eV direct and 0.55 eV indirect band gap and is used in many applications such as photodiode, solar cells in the result of low electrical resistance, high optical transparency [6-8]. CdO is n-type semiconductors in the rock salt crystal structure of NaCl (surface-centered cubic structure) [9]. Since CdO-structured semiconductors have an extraordinarily large carrier mobility in the visible region and good optical transparency, their use is increasing [10-12]. CdO is used in making photodiodes, solar cells, flat panel displays, optical communication, thin film resistors, phototransistors, photovoltaic, transparent conductive electrodes, liquid crystal displays and IR detectors due to their high conductivity, high permeability and low band gap properties [13-15]. The physico - chemical properties of CdO depend not only on chemical composition but also on size, shape, surface morphology and production technique [16]. There are many different methods for producing CdO in the literature.

As a result of these methods, CdO acquisition at nano size is made possible. Physical, chemical and thermal hydrothermal methods [17-18], template assisted method [19], solvothermal method [20], mechanochemical method [21-22], thermal disruption method [23], photosynthetic method [24] sonochemical method [25] are production methods. Sol-gel technique for preparing pure and doped CdO films is a cost-effective method of controlling size and morphology [26], and nanoparticles are one of the most promising methods for synthesizing nanoparticles.

The idea of doping carbon nanotubes has attracted the attention of researchers because it allows them to control their electronic properties (intercalation reaction with electron donors or recipients) [27]. In addition, the absence of certain band voids in MWCNT provides added value to photovoltaic efficiency by absorbing light over a broad wavelength range [28]. Isolated CNTs have an electrical conductivity of $2 \times 10^7 \text{ s/m}$, a capacitance of 10^{13} A/m^2 and a thermal conductivity of 3500 W/mK [29].

The purpose of this work is to reinforce the above mentioned CNTs with very good electrical properties by using two different cadmium oxide matrices and to examine the change in electrical and optical properties that will occur in the structure compared to pure CdO.

2. Experimental

In this study, CdO synthesized by sol-gel method was used as matrix. CNTs synthesized by Chemical Vapor Deposition (CVD) method were used as reinforcement material and nanocomposites with CdO matrix were synthesized by powder metallurgy method. Carbon nanotube synthesis was performed using a single crystal silicon (100) substrate. This substrate was first washed with acetone followed by ethanol in an ultrasonic bath. Then, the substrate was placed in the middle of a tube furnace on a boat, the inside of the tube furnace was vacuumed with a pump and purged. The furnace was then heated to $650 \text{ }^\circ\text{C}$ in an argon (Ar) atmosphere at a flow rate of 1 liter per minute through the system. After the tube furnace reached $650 \text{ }^\circ\text{C}$, the flow of Ar gas was interrupted and acetylene (C_2H_2) gas was introduced for 40 minutes. At the end of 40 minutes, the acetylene gas was cut off and the Ar gas was again supplied to the system until the furnace cooled to room temperature. Characterization of the obtained nanotubes was performed by X-ray diffraction (XRD) and transmission electron microscopy (TEM). Jeol Jem 2100 F brand TEM device was used.

Carbon nanotubes were added to the CdO synthesized by the sol-gel method at 0.1, 0.2, 0.5 and 1% by weight. For a homogenous mixture, the alcohol carbon nanotube mixture was mixed in an ultrasonic mixer and then the appropriate amount of CdO was added. The alcohol was mixed with a magnetic stirrer until evaporation. The resulting powder mixture was pelletized by pressing at a pressure of 600 MPa and then sintered at $450 \text{ }^\circ\text{C}$. In order to compare the properties of the sol-gel produced CdO, the Acros Organic brand (Code: 223792500, 99% purity) CdO was readily available. The production of the H1-encoded nanocomposite with the ready CdO matrix was similarly performed and compared with the CdO-matrix nanocomposite synthesized by the sol-gel method.

Table 1. Codes and other characteristics of samples.

Samples Codes	The type of CdO	The amount of CNT (% w)
H₁	Commercial	-
S₁	Sol-Gel	-
S₂	Sol-Gel	0.1
S₃	Sol-Gel	0.2
S₄	Sol-Gel	1

2.1. Production of Carbon Nanotubes

Figure 1 shows the XRD analysis of carbon nanotubes produced by the chemical vapor deposition method. As can be seen, the powders gave both a violent and broad peak at about 26°, which overlaps with the peaks of the carbon nanotubes in the database of the XRD (Pixel analysis Diffrac Evaluation Software ICDD tag No. 00-058-1638). The fact that the pikes are wide indicates that the powders are nano-sized according to Debye-Scherrer equality. Debye-Scherrer equality;

$$D=0.9 \lambda / \beta_{hkl} \cos\theta$$

D is the crystal size, B is the maximum peak intensity half-peak width in radians, θ is the Bragg angle, λ is the wavelength of the light used in the diffraction [29].

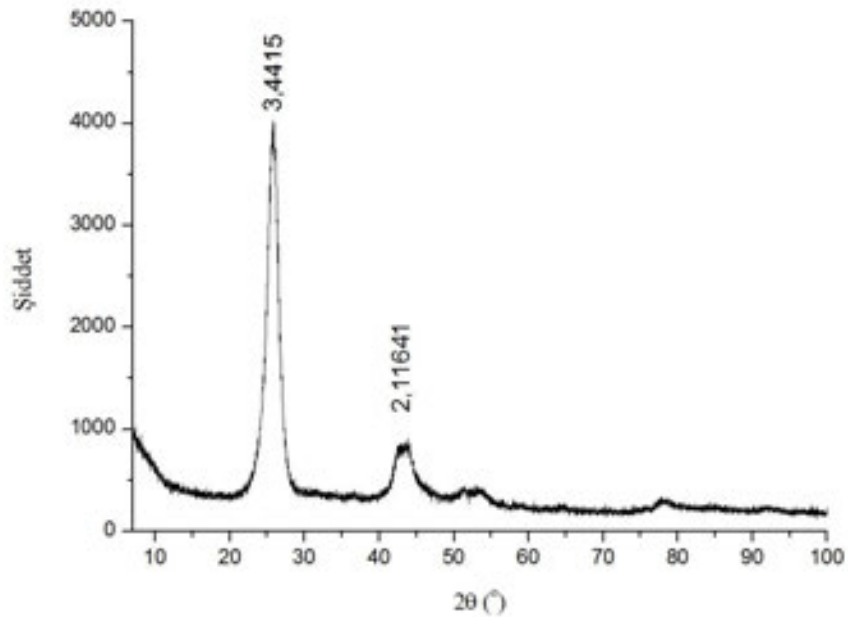


Figure 1. XRD analysis results of carbon nanotubes produced.

TEM images of the carbon nanotubes produced in Figure 2 are given. As can be seen, the structures obtained are carbon nanotubes. There is a gap in the middle of the structures obtained, and on both sides there are walls with certain thicknesses. The produced carbon nanotubes vary in diameter from 15 to 20 nm and vary in size from 1-5 μm .

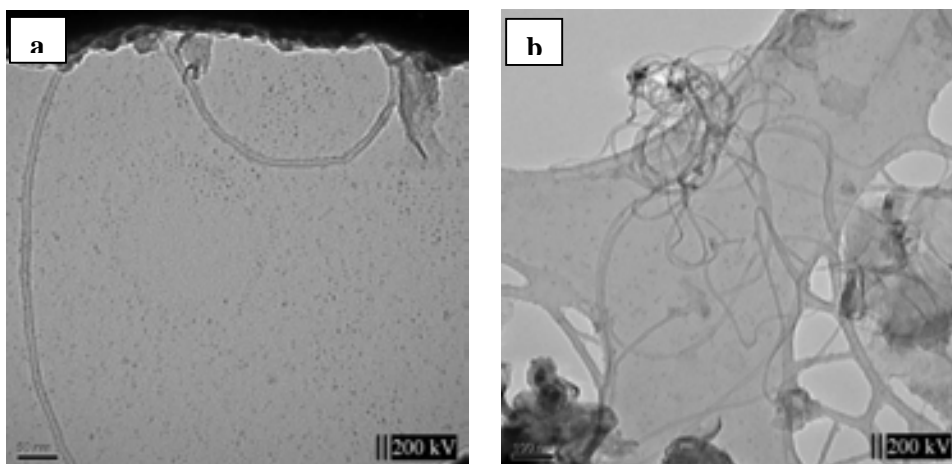


Figure 2. TEM images of the produced carbon nanotubes.

Some particles have black particles in the joint or tip (Fig. 2.b). These particles are nano-sized iron particles that have been used as catalysts during the synthesis of carbon nanotubes. Carbon nanotubes grow on these particles.

2.2. Production of CdO Via Sol-Gel Method

For synthesis, 1 mole of cadmium acetate dihydrate was used, 46 moles of methanol, 0.2 moles of glycerol and 0.5 moles of triethylamine. Firstly, cadmium acetate was dissolved in 23 moles of methanol using a magnetic stirrer. Stirring is carried out until the mixture has a transparent color. Glycerol was added and then triethylamine and the remaining methanol mixture added. The whole mixture was stirred at 60 ° C for 2 hours in a magnetic stirrer. The mixture was stirred at room temperature for 12 hours in a magnetic stirrer to obtain a homogeneous mixture. Calcination heat treatment was applied in order to remove the solvent in the thoroughly homogenized solutions by mixing. The resulting powder mixture was calcined at 600 ° C for 1 hour and a brown powder was obtained at the end of the treatment. The flow chart of the method mentioned in Fig. 3 is given.

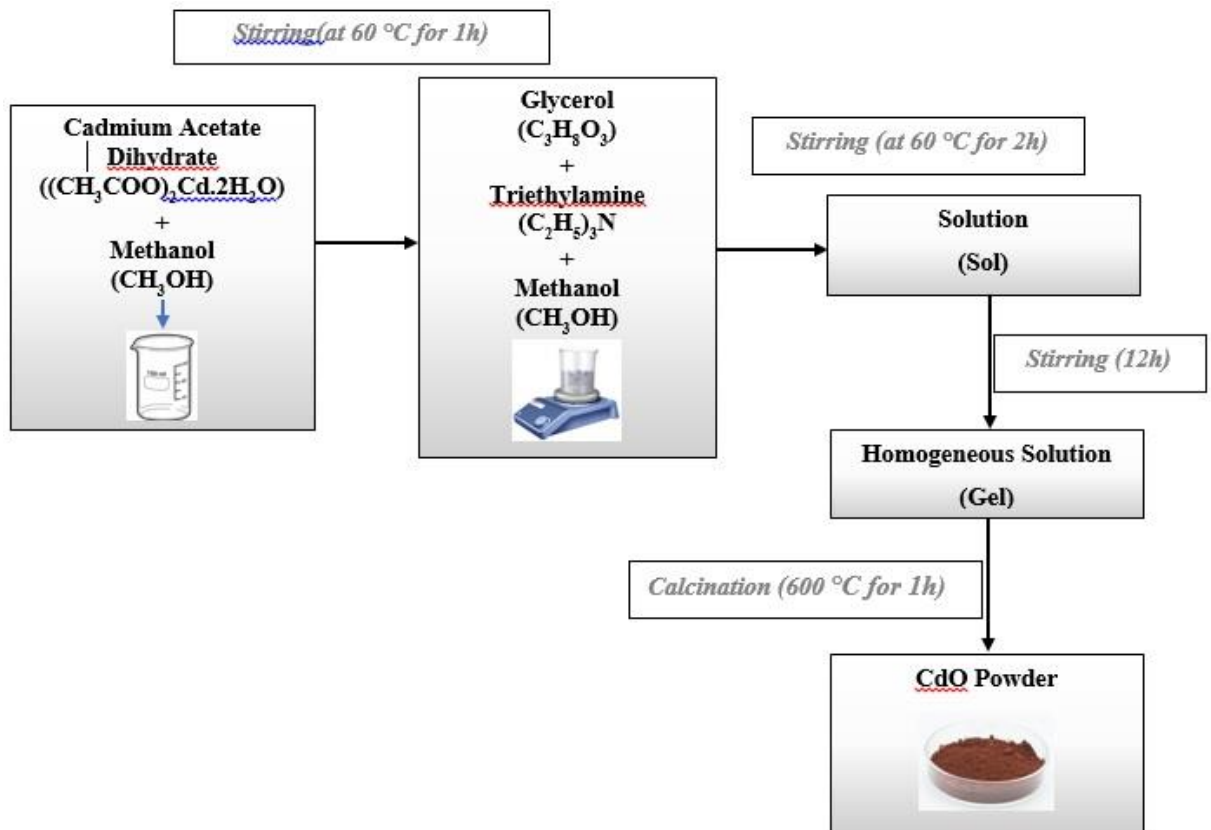


Figure 3. CdO synthesis flow diagram by sol-gel method.

3. Results and Discussion

3.1. Microstructure Examination Results of CdO-KNT Composite

Microstructures of the resulting composites were determined by scanning electron microscopy. Jeol Jsm 7001 F electron microscope used in this study was used. In Figure 4, microstructure images of H_1 sample and S_x series are given.

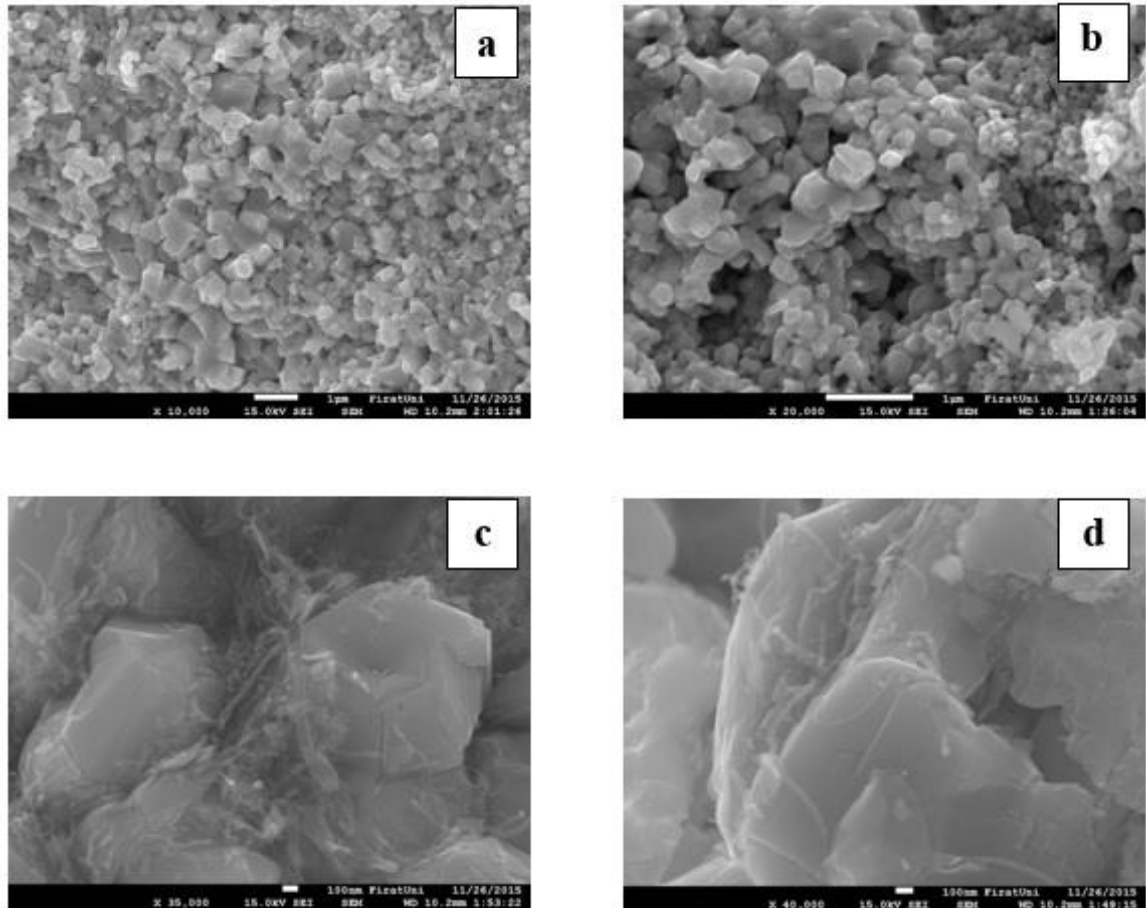


Figure 4. Microstructure images of H_1 sample and S_x series. a) H_1 , b) S_1 , c) S_2 , d) S_4 samples.

Figure 4.a gives a SEM image of sample H_1 . The H_1 sample is commercially available pure CdO. When the microstructure images are examined, a structure consisting of many particles in homogeneous and close to each other is seen.

In Figure 4.b, SEM image of S_1 sample is given. Sample S_1 is pure CdO produced by the sol-gel method. The structures formed as shown are homogeneous spherical shaped particles, the size of the particles being around 100 nm.

Figure 4.c shows a SEM image of sample S_2 . The sample S_2 is a CdO matrix 0.1% CNT reinforced composite sample produced by the sol-gel method. It can be said that the CNTs are distributed homogeneously within the structure. In addition, there were not CNT pellets found in the structure.

In Figure 4.d, a SEM image of sample S_4 is given. S_4 sample is a composite sample of CdO matrix 1% CNT reinforced by the sol-gel method. Although there are homogeneously distributed regions of CNTs in the structure, it is not uncommon to find the regions where the CNTs are scattered and clustered as in the H_5 sample.

3.1.1. Investigation of Electrical Properties of CdO-KNT Composite Samples Produced

The conductivity of the produced semiconducting samples was changed according to the temperature by applying the temperature values in the range of 300-433 K by applying 0,5-5 V current in a dark environment. KEITHLEY 6517A electrometer was used to measure the current values of the samples according to the temperature. Figure 4 shows the electrical conductivity measurements of samples S_1 , S_2 , S_3 and S_4 , respectively.

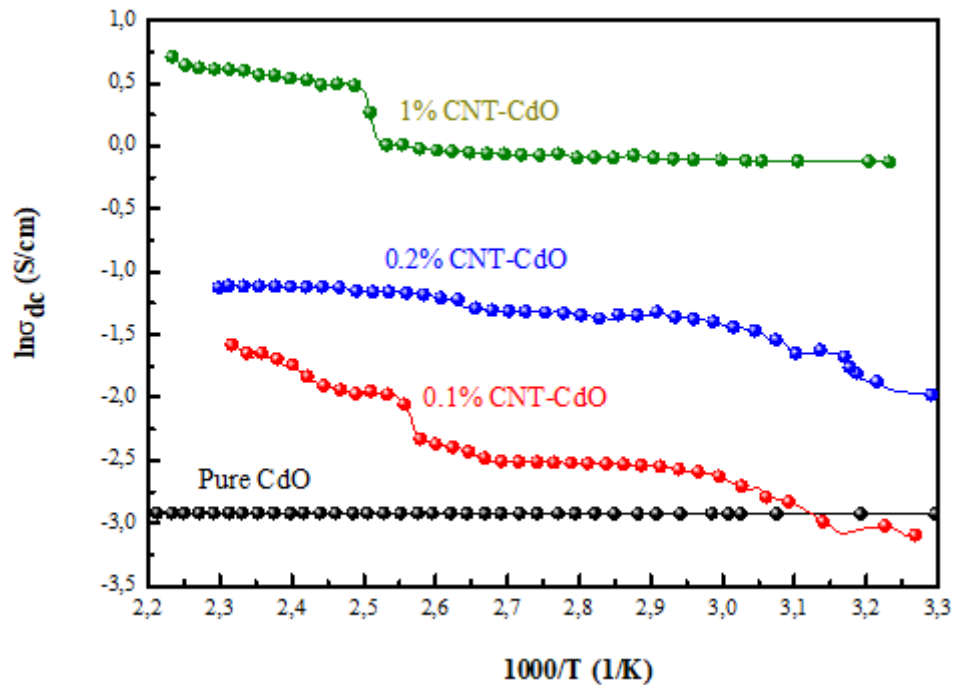


Figure 5. Electrical properties of composites of S_x samples.

Conductivity values of pure CdO, 0.1%, 0.2 and 1 CNT doped CNT-CdO composites at room temperature were found to be 5.37×10^{-2} , 4.9×10^{-2} , 1.44×10^{-1} and 8.8×10^{-1} S/cm, respectively. These values show that the conductivity at room temperature of the composite increases with increasing KNT ratio compared to pure CdO.

3.1.2 Investigation of Optical Properties of CdO-CNT Composite Samples

Produced

In Fig. 6, reflection-wavelength spectrum graphs of CdO and S_1, S_2, S_3 and S_4 samples with 0.1, 0.2 and 1 CNT added by sol-gel method are given.

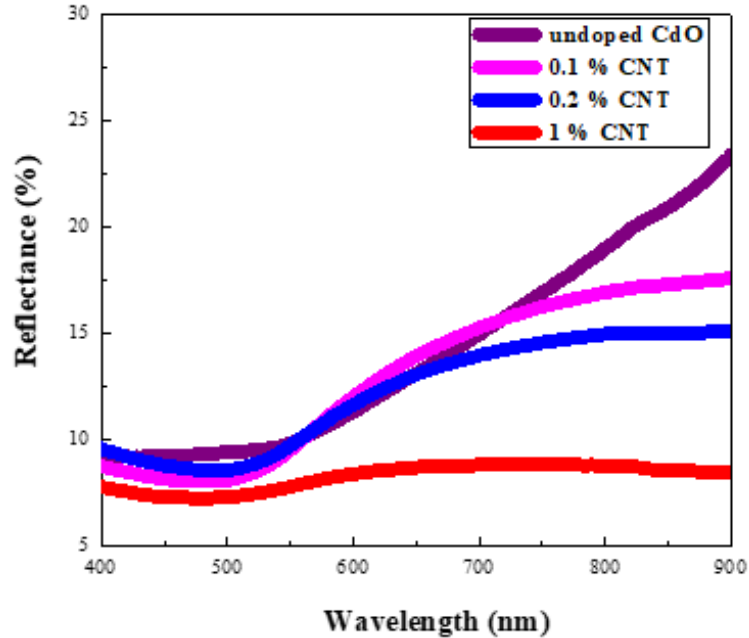


Figure 6. Reflection-wavelength spectrum of S_x series samples.

In Figure 6, reflectance values were measured (%) for all samples between 400-900 nm wavelengths. Reflectance values of CNT-doped samples decreased in the reflection-wavelength spectrum graph shown in Figure 5. An increase in reflectance values is observed after 500 nm wavelength range when the S_x series exhibits similar reflectance characteristics at a wavelength range of 400-500 nm. However, a lesser increase is observed in the sample of 1% CNT added compared to the others. It might be that the reason for this is due to the increase in the rate of CNT in the structure and the difficulty in homogeneous distribution. The S_1 has the highest reflectance value and the S_4 has the lowest reflectance value.

In Fig. 7, a graph of the change of the S_x series $(ahv)^2$ according to $h\nu$ (photon energy) is given.

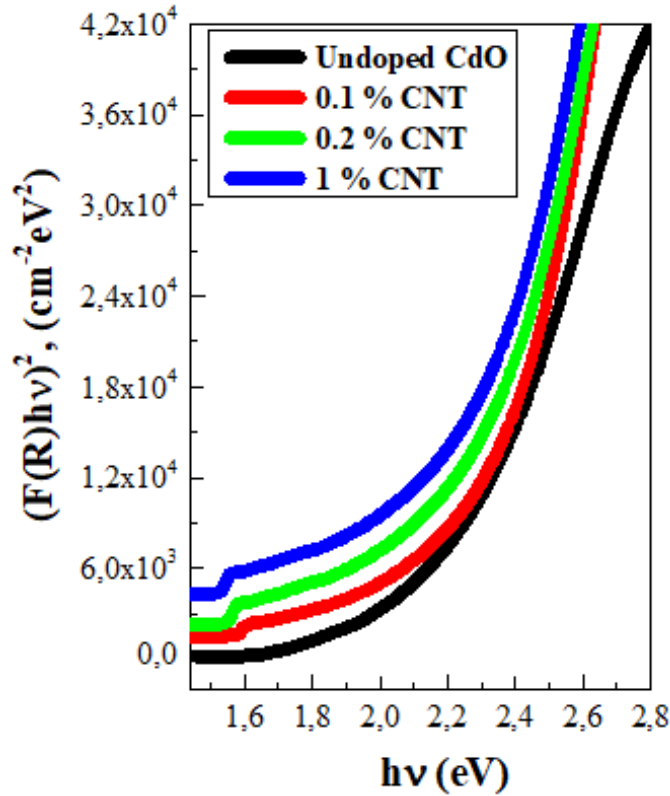


Figure 7. A graph of the change of the S_x series $(ahv)^2$ according to $h\nu$ (photon energy)

To determine the bandgap values of CNT doped and undoped CdO nanowires, optical absorption method was used on diffuse reflectance. The Kubelka-Munk function transforms the reflectance values into absorbance. The Kubelka-Munk theory is usually used to analyze the diffuse reflectance spectra obtained from samples with low absorbance. The Kubelka-Munk formula can be expressed by the following relation:

$$F(R) = (1-R)^2 / 2R \quad (1)$$

Where R represents the diffuse reflectance. F (R) is the Kubelka-Munk function corresponding to the absorbance. F (R) values were converted to linear absorption coefficient with the following relation.

$$\alpha = \frac{F(R)}{t} = \frac{\text{Absorbance}}{t} \quad (2)$$

Here t is the thickness of the sample. It is estimated that CdO has a direct optical band gap (bandgap). Thus, the optical band gaps of the CdO samples can be determined using the following relationship.

$$\alpha h\nu = C(h\nu - E_g)^{1/2} \quad (3)$$

$$D = 0.9 \lambda / \beta_{hkl} \cos\theta \quad (4)$$

C is a constant, α absorbance coefficient, and $h\nu$ is the photon energy. $h\nu$ (photon energy) versus $(ahv)^2$ graph, optical absorption method and equation 5. Equation 3 is used when the

crystal size of the samples is determined using the Debye-Scherrer relationship. Where D is the crystal size, β_{hkl} is the peak width of half maximum density, θ is the diffraction angle and λ is the wavelength of the X-ray [30, 31]. The bandgap values calculated in this way are given in Table 2.

Table 2. Sample contents and E_g values.

Sample Code	The type of CdO	Amount of CNT (% w)	E_g (eV)
H ₁	Commercial	-	1,75
S ₁	Sol - Gel	-	1,88
S ₂	Sol - Gel	0,1	2,02
S ₃	Sol - Gel	0,2	1,93
S ₄	Sol - Gel	1	1,84

The bandgap values calculated in Table 2 do not show a decrease or increase parallel to the contribution of CNT. CdO produced by the sol-gel method seems to have a wider E_g value when compared to CdO produced by the ready-made CdO and the left-handed CdO.

3.1. Comparison of Electrical and Optical Properties of Commercial and Sol-Gel Produced CdO Matrix Composites

Comparative graphs were drawn to investigate how the properties of the CdO-matrix composite synthesized by the sol-gel method are changed from electrical and optical point of view compared to commercially available CdO. In Figure 8, comparative electrical conductivity plots of samples S₁ and H₁ are given.

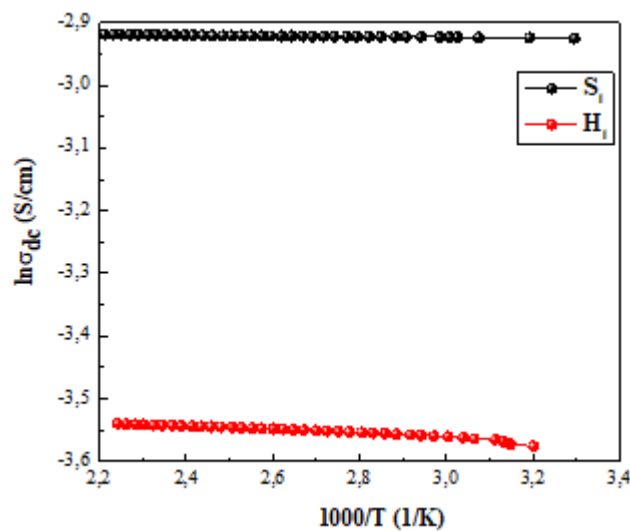


Figure 8. Electrical properties of the composites of samples S₁ -H₁.

The graph of Figure 8 clearly shows that the CdO (S_1) synthesized by the sol-gel method has better electrical properties than the ready-supplied CdO (H_1). Figure 9 shows the reflection-wavelength spectrum graph of samples S_1 and H_2 .

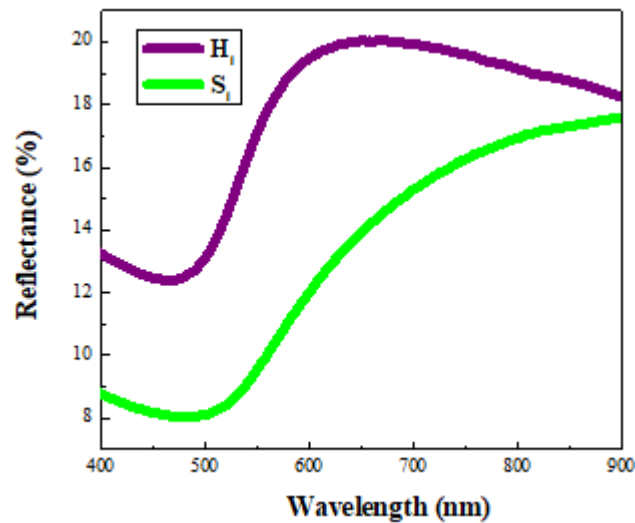


Figure 9. Reflection-wavelength spectrum of S_1 - H_1 samples.

The H_1 sample provided at 400-500 nm wavelengths has a higher reflectance value than the S_1 sample synthesized by the sol-gel method. A sharp increase in the reflectance value is observed after 500 nm for sample S_1 . The CdO synthesized by the sol-gel method exhibits low reflectance at low wave lengths and almost the same reflectance value at 900 nm wavelength as supplied.

Figure 10 shows a graph of the change of H_1 (photon energy) of samples (S_1H_1) of samples S_1 - H_1 .

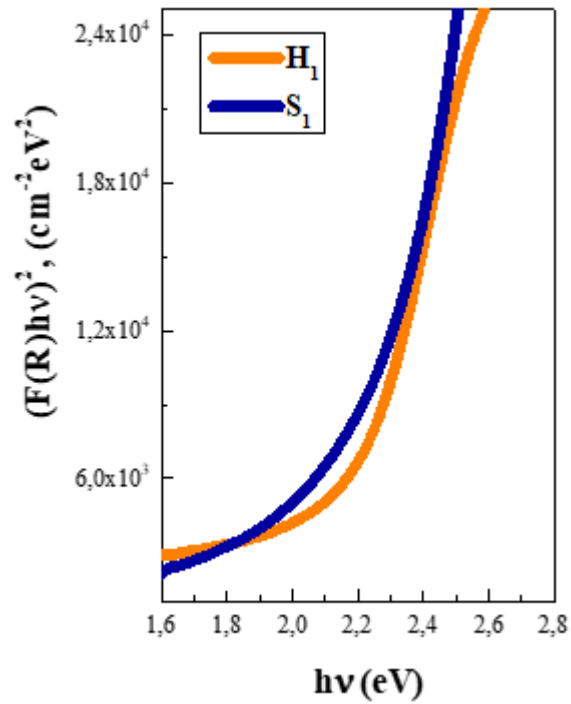


Figure 10. $S_1 \sim H_1$ samples $(ah\nu)^2 \sim h\nu$ (photon energy) change graph.

The E_g value of the H_1 sample was 1.75 eV while the E_g value of the S_1 sample was 1.88 eV. It has been found that CdO synthesized by the sol-gel method broadens the bandgap value.

4. CONCLUSION

Using the CVD method, carbon nanotubes with diameters ranging from 15 to 25 nm and varying from 2 to 5 μm in diameter were synthesized. The resulting carbon nanotubes were reinforced in commercially available CdO at 0.1, 0.2 and 1% to produce composite samples called H groups. The carbon nanotubes produced by the sol-gel method were reinforced with 0.1, 0.2 and 1% carbon nodules to produce composite samples called S groups.

SEM studies of the produced composites showed that the production of a homogeneous composite structure was difficult with the increase of the amount of carbon nanotubes. In samples containing 1% CNT, it was found that some regions contained carbon nanotubes in bulk without disintegration.

As a result of the electrical examinations of the produced composites depending on the temperature; it was found that the electrical conductivity increased with the carbon nanotube increase in both sample groups. In addition, it has been observed that the CdO-containing composites produced with Sol-Gel have higher electrical conductivities than the CdO-containing composites already provided.

As a result of optical examinations, the forbidden energy ranges of all samples have been determined. In the H group samples, the forbidden energy range of the pure CdO sample was found to be 1.75 eV and increased to the maximum level with 0.1% CNT content with the increase of KNT and then decreased with the increase of CNT. Composite containing 1% CNT was found to have a forbidden energy range of pure CdO. For the S group samples, the forbidden energy range of the pure CdO sample was found to be 1.88 eV and it was found that it increased to the maximum level with the content of 0.1% CNT with the increase of CNT and then decreased with the increase of CNT. Composite containing 1% CNT was found to have a forbidden energy range of pure CdO.

Consequently, it was determined that the composites using CdO produced by Sol-Gel showed better performance in terms of electrical and optical properties than the H group samples.

5. REFERENCES

- [1] Dong, Wenting;Zhu, Congshan. Optical properties of surface-modified CdO nanoparticles. *Optical Materials*, 2003, 22.3: 227-233.
- [2] LI, Feng; ZHANG, Changwen; ZHAO, Mingwen. Magnetic and optical properties of Cu-doped ZnO nanosheet: First-principles calculations. *Physica E: Low-dimensional Systems and Nanostructures*, 2013, 53: 101-105.
- [3] GULINO, Antonino; COMPAGNINI, Giuseppe; SCALISI, Alessandro A. Large third-order nonlinear optical properties of cadmium oxide thin films. *Chemistry of materials*, 2003, 15.17: 3332-3336.
- [4] Farmanzadeh, Davood; Valipour, Azadeh. Adsorption of benzene and toluene molecules on surface of pure and doped cadmium oxide nanosheets: A computational investigation. *Applied Surface Science*, 2018.

- [5] C. Aydin, H.M. El-Nasser, F. Yakuphanoglu, I.S. Yahiaa, M. Aksoy, 2011, “Nanopowder Synthesis of Aluminum Doped Cadmium Oxide via Sol–Gel Calcination Processing”, *Journal of Alloys and Compounds* 509, 854–858.
- [6] Azizar M., M.K.R. Rahman Khan, 2014, “Effect of Annealing Temperature on Structural, Electrical and Optical Properties of Spray Pyrolytic Nanocrystalline CdO Thin Films”, *Mater. Sci. Semicond. Process.* 24 26–33.
- [7] Yakuphanoglu F., 2011, “Synthesis and Electro-Optic Properties of Nanosized-Boron Doped Cadmium Oxide Thin Films for Solar Cell Applications”, *Sol. Energy* 85, 2704–2709.
- [8] Balmuri, S. R., Selvaraj, U., Kumar, V. V., Anthony, S. P., Tsatsakis, A. M., Golokhvast, K. S., & Raman, T. (2017). Effect of Surfactant in Mitigating Cadmium Oxide Nanoparticle Toxicity: Implications for Mitigating Cadmium Toxicity In Environment. *Environmental research*, 152, 141-149.
- [9] Zheng, B.J., Lian, J.S., Zhao, L., Jiang, Q., 2010. “Optical and Electrical Properties of In-Doped CdO Thin Films Fabricated by Pulse Laser Deposition”, *Applied Surface Science* 256, 2910–2914.
- [10] Coutts, T.J., Young, D.L., Li, X., Mulligan, W.P., Wu, X., Vac, J., 2000. “Search for Improved Transparent Conducting Oxides: A fundamental investigation of CdO, Cd₂SnO₄, and Zn₂SnO₄”. *Sci. Technol. A* 18, 2646.
- [11] Metz A.W., Ireland J.R., Zheng J.G., Lobo R.P., Yang Y., Ni J., Stern C.L., Dravid V.P., Bontemps N., Kannewurf C.R., Poepelmeier K.R., Marks T.J., 2004. “Transparent conducting oxides: texture and microstructure effects on charge carrier mobility in MOCVD-derived CdO thin films grown with a thermally stable, low-melting precursor”, *J. Am. Chem. Soc.* 126, 8477.
- [12] Kumaravela, R., Menakaa, S., Regina, S., Snegaa, M., Ramamurthia, K., Jeganathan, K., 2010. “Electrical optical and structural properties of aluminum doped CdO thin films prepared by spray pyrolysis technique”, *Materials Chemistry and Physics* 122, 444.

- [13] Bhosale, C.H., Kambale, A.V., Kokate, A.V., Rajpure, K.Y., 2005. Structural, optical and electrical properties of chemically sprayed CdO thin films, *Materials Science and Engineering B*, 122, 67–71.
- [14] Uplane, M.D., Kshirsagar, P.N., B Lokhande, B.J., Bhosale, C.H., 1999. “Stability and Electronic Properties of Zn_xCd_{1-x}O Alloys”, *Mater. Chem. Phys.* 1, 8630.
- [15] Peter, L.M., 1979. “The photoelectrochemical properties of anodic Bi₂S₃ films, *Journal of Electroanalytical Chemistry and Interfacial Electrochemistry*”, Volume 98, Issue 1, Pages 49-58.
- [16] Divine Mbom Y. , Josepha Foba T. , Agwara Moise O., Joseph Ketcha M., 2014, “CdO Nanoparticles by Thermal Decomposition of a CadmiumHexamethylenetetramine Complex”, *Journal of Materials Science Research*; Vol. 3, No. 3.
- [17] Ye, M., Zhong, H., Zheng, W., Li, R., Li, Y., 2007, “Ultralong Cadmium Hydroxide Nanowires: Synthesis, Characterization, and Transformation into CdO Nanostrands. *Langmuir*, 23(17), 9064-9068.
- [18] Zhang, J., Wang, Y., Lin, Z., Huang, F. 2010, “Formation and Self-Assembly of Cadmium Hydroxide Nanoplates in Molten Composite-Hydroxide Solution”, *Crystal Growth & Design*, 10(10), 4285-4291.
- [19] Prakash, T., Arunkumar, T., Sathiyasa Raj, D., Jayaprakash, R. (2013). “Surfactant-aided Variation in CdO Nanocomposites Morphology”, *Physics Procedia*, 49, 36-43.
- [20] Ghoshal, T., Biswas, S., Nambissan, P. M. G., Majumdar, G., De, S. K. (2009). “Cadmium Oxide Octahedrons and Nanowires on the Micro-Octahedrons: A Simple Solvothermal Synthesis”, *Crystal Growth & Design*, 9(3),
- [21] Tadjarodi, A., Imani, M. (2011). “A novel nanostructure of cadmium oxide synthesized by mechanochemical method”. *Materials Research Bulletin*, 46(11), 1949-1954.

- [22] Tadjarodi, A., Imani, M. (2011b). "Synthesis and characterization of CdO nanocrystalline structure by mechanochemical method". *Materials Letters*, 65(6), 1025-1027.
- [23] Shi, W., Wang, C., Wang, H., Zhang, H. (2006). "Hexagonal Nanodisks of Cadmium Hydroxide and Oxide", *Journal of Materials Science Research* Vol. 3, No. 3; 2014 11 with Nanoporous Structure. *Crystal Growth & Design*, 6(4), 915-918.
- [24] Andeani, J. K., Mohsenzadeh, S. (2013). "Phytosynthesis of Cadmium Oxide Nanoparticles from *Achillea wilhelmsii* Flowers". *Journal of Chemistry*, 2013, 1-4.
- [25] Ramazani, M., Morsali, A. (2011). "Sonochemical syntheses of a new nano-plate cadmium (II) coordination polymer as a precursor for the synthesis of cadmium (II) oxide nanoparticles", *Ultrasonics Sonochemistry*, 18(5), 1160-1164
- [26] Aydın, C., El-Nasser, H.M., Yakuphanoglu, F., Yahia, I.S., Aksoy, M., 2011. "Nanopowder synthesis of aluminum doped cadmium oxide via sol-gel calcination processing", *Journal of Alloys and Compounds* 509, 854.
- [27] Duclaux, L. (2002). Review of the doping of carbon nanotubes (multiwalled and single-walled). *Carbon*, 40(10), 1751-1764.
- [28] Kumar, S. S., Vairam, S., Neelakandeswari, N., & Aruna, S. (2018). Effect of metal oxide charge transfer layers on the photovoltaic performance of carbon nanotube heterojunction solar cells. *Materials Letters*, 220, 249-252.
- [29] S.P. Yakala, S.S. Yawale, G.T. Lamdhade, Tin oxide and zinc oxide based doped humidity sensors, *Sensors and Actuators A: Physical*, 135 (2007), pp. 388-393.
- [30] Ates, T.; Tatar, C.; Yakuphanoglu, F. Preparation of semiconductor ZnO powders by sol-gel method: Humidity sensors. *Sensors and Actuators A: Physical*, 2013, 190: 153-160.
- [31] S.P. Yawale, S.S. Yawale, G.T. Lamdhade, Tin oxide and zinc oxide based doped humidity sensors, *Sensors and Actuators A: Physical*, 135 (2007), pp. 388-393.

**CORRESPONDENCE ADDRESS: Ömer Güler, Mersin University, Engineering Faculty,
Metallurgical and Materials Eng. Dept., 33100, Mersin, Turkey, oguler@mersin.edu.tr**

THE EFFECT ON TENSILE-SHEAR STRENGTH OF ELECTRODE PLUNGE DEPTH DEPENDING ON WELDING TIME IN RESISTANCE SPOT WELDING OF TRIP 800 AND MICRO ALLOYED STEEL SHEETS

Volkan Onar^{1,a}, Fatih Özen^{2,b}, Uğur Özaraç^{2,c}, Melih Kekik^{2,d}, Yusuf Sadi
Aslanlar^{3,e}, Salim Aslanlar^{2,f}

¹ Department of Mechanical and Manufacturing Engineering, Faculty of Technology, Pamukkale
University, Denizli, Turkey.

² Department of Manufacturing Engineering, Faculty of Technology, Sakarya University, Sakarya, Turkey
³ YıldızKalıpSanayi ve Ticaret A.Ş., ARGE Merkezi, Arnavutköy/İstanbul, Turkey

^avonar@pau.edu.tr., ^bozsarac@sakarya.edu.tr, ^cfatihozen@sakarya.edu.tr, ^dmelihkekik@gmail.com,
^eyusuf.aslanlar@yildizkalip.com, ^faslanlar@sakarya.edu.tr.

Abstract

The aim of study, the effect of the depth of electrode plunge on the tensile-shear strength depending on the welding time in resistance spot welding of TRIP 800 and micro alloyed steel sheets has been analyzed. There are too many welding methods in the automotive industry. But, the most widely used method of welding is the electric resistance spot welding (RSW). In this paper presentation, used of TRIP 800 steel sheet having 1.5 mm and micro alloyed steel sheets having 1 mm. Electrical resistance spot welding was used in the lap joint welding position of joining these steels. The electrode force was kept constant at 6 kN. The welding times was selected increasing the period from 10 to 30 periods by 5 periods (1 period = 0.02 s) and different weld currents, ranging from 10500 A to 16500 A in 500 A steps. Electrode plunge depths of specimens were determined of the welded specimens by the metal microscope. The effect of electrode plunge depth on tensile-shear strength was analyzed. The highest tensile-shear strength of 6200 N in 0,9 mm electrode plunge depth was obtained at a period of 20 cycles

Key Words: TRIP Steels, Electrode Plunge Depth, Tensile – Shear Strength, Welding Time

1. Introduction

Today, in automobile sector, TRIP 800 steel sheets and micro-alloyed steel sheets are using respectively in automobile chassis and body parts. Use of these steel sheets provides increase of on crash performance of automobiles, comfort and safety of automobiles, at the same time, decrease in the chassis and body parts weight of automobiles [1-5]. Therefore the fuel economy can be obtained and pollution of the environment is reduced. Welding is the most important joining and mounting technique in automobile sector. Resistance spot welding (RSW) technique is the most used joining method in new generation vehicles in automotive sector. In addition, RSW is appropriate for robotic applications and mass production in automobile manufacturing [6-10].

The aim of study, the relationship between tensile– shear strength and electrode plunge depth of welded micro-alloyed and TRIP 800 steel sheets using resistance spot welding technique was investigated.

2. Experimental

The TRIP 800 and micro alloyed (DX56D – Z) galvanized steel sheets used in this study were obtained from respectively EMARC Automotive and Sarigözoğlu, Their chemical compositions are shown in Tab.1 and Tab.2. Their mechanical properties are shown in Tab. 3. TRIP steel sheets having 1.5 mm thicknesses and micro alloyed (DX56D – Z) steel sheets having 1mm thicknesses.

Table 1.Chemical composition of TRIP steel sheets [wt%]

% C	% P	% Mo	% Ti	% Sn	% Si	% S	% Ni	% Cu	% V
0,179	0,011	0,025	0,014	0,01	1,719	0,007	0,074	0,1	0,013
% Mg	% Mn	% Cr	% Al	% Nb	% W	% Fe			
0,001	1,691	0,065	0,027	0,053	0,04	95,902			

Table 2.Chemical composition of DX56D – Z steel sheets [wt%]

% C	% Si	% Mn	% P	% S	% Si	% Fe
0,12	0,50	0,60	0,10	0,045	0,30	98,33

Table 3.Mechanical properties of couple of steel sheets.

	Yield strength [MPa]	Tensile strength [MPa]	Total elongation [%]
TRIP 800	523	881(min780)	36
DX56D+ Z	171,4	337,5	39

The samples were overlapped with 30 mm spacing and welded is shown in Figure 1. For welding specimens, the welding current was increased from 8000 A to 16500 A by 500 A increments. 6 kN electrode pressure was chosen and clamping time and hold time of electrode (25 periods) were kept constant while other welding parameters such as 10, 15, 20, 25 and 30 periods weld times were preferred. These welding parameters are shown in Figure 2.

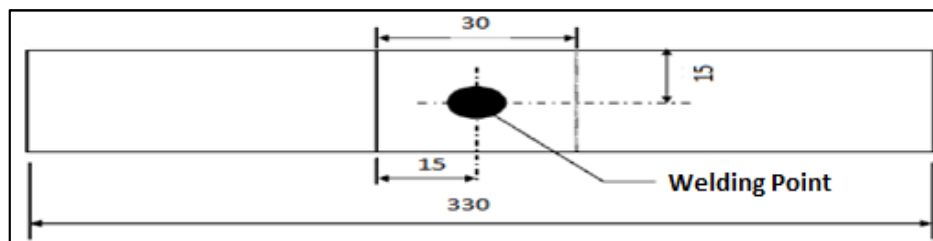


Figure 1.The dimensions of the materials of specimens

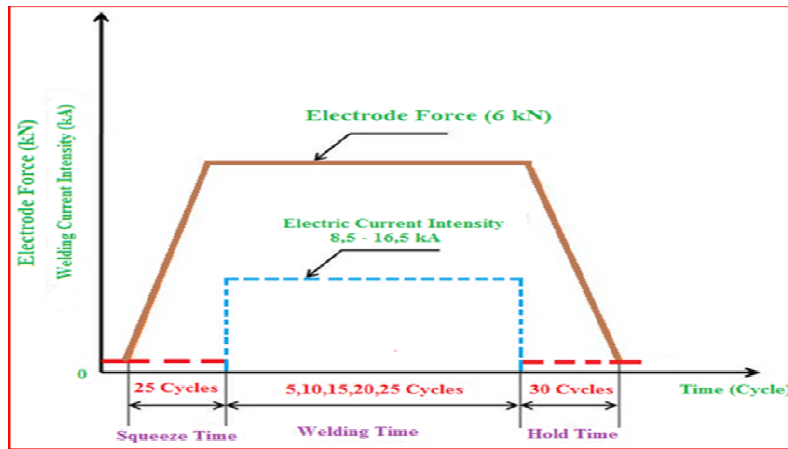


Figure 2. Welding parameters

3. Results and Discussion

In low welding current application, small electrode plunge depths consists, due to low heat in the welding zone. And then in high current density, big electrode plunge depths obtains. Along with the increase in electrode plunge depth, the tensile shear strength of the welded joint also increases. Electrode plunge depths are increases with increasing weld current. However, this increase up to a certain point and then falls rapidly. In high welding currents due to the eruption of molten metal, in the steel sheets thickness are decreased, therefore the tensile shear strength is decreasing. These situations are shown in Fig.3 and in Fig.4.

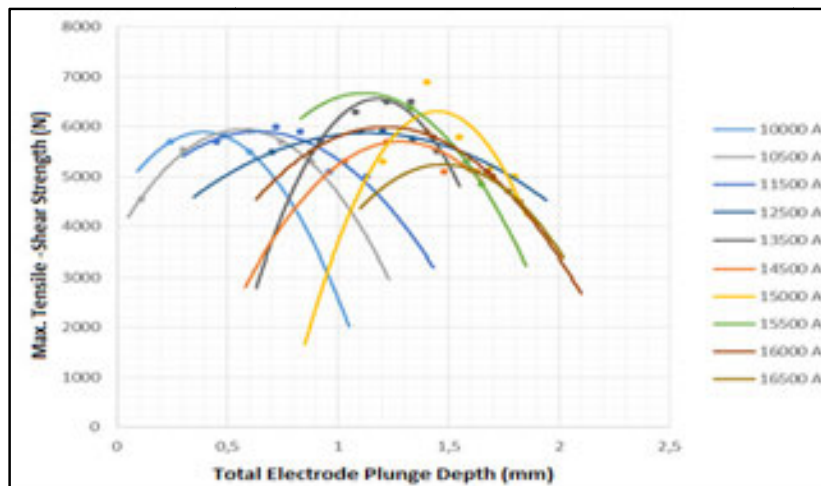


Figure 3. The relationship between total electrode plunge depth and tensile - shear strength depending on welding current

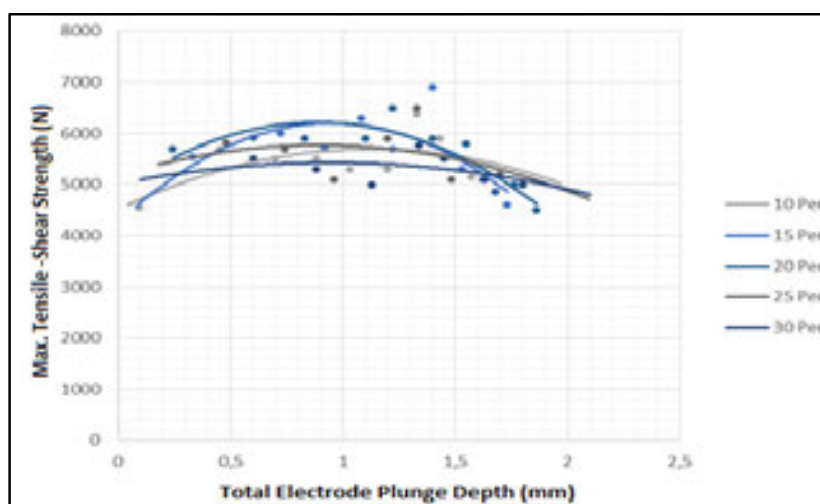


Figure 4. The relationship between total electrode plunge depth and tensile - shear strength depending on welding time

4. Conclusion

The experimental results obtained using 6 kN electrode force are given below;

1. The maximum tensile shear strength was obtained as 6600 N at the electrode plunge depth of 1,2 mm at the welding current of 15500 A current value.
2. The maximum tensile shear strength was obtained as 5600 N at the electrode plunge depth of 1,2 mm at the welding time of 10 period value, as 6200 N at the electrode plunge depth of 0,9 mm at the welding times of 15 and 20 periods, as 5900 N at the electrode plunge depth of 1 mm at the welding time 25 period and as 5400 N at the electrode plunge depth of 1 mm at the welding time 30 period.
3. The tensile - shear strength increased when the electrode plunge depths were increased but the tensile - shear strength decreased after certain of electrode plunge depth.
4. It is observed that tensile - shear strength decreases with the increase of the welding time and welding current intensity.
5. It has been observed that tensile - shear strength decreases at higher electrode plunge depth due to heat input. This is consistent with the results obtained in literature studies and the results of experimental studies

5. References

- [1] M. Mimer, L.E. Svensson, R. Johansson, *Weld. World* 48, 14 (2004).
- [2] O.J. Kwon, K. Lee, G. Kim, K.-G. Chin, *Mater. Sci. Forum* 638-642, 136 (2010).
- [3] F. Varol, M. Ekici, E. Ferik, U. Ozsarac, S. Aslanlar, *Acta. Phys. Pol. A* 127, 965 (2014), doi: 10.12693/APhysPolA.127.965
- [4] F. Varol, U. Ozsarac, S. Aslanlar, A. Onat, M. Ekici, E. Ferik, *Acta. Phys. Pol. A* 127, 968 (2015), doi: 10.12693/APhysPolA.127.968
- [5] M. Ekici, U. Ozsarac, *ActaPhys. Pol. A* 125, 529 (2014).
- [6] V. Onar, S. Aslanlar, N. Akkaş, *ActaPhysicaPolonica A* 132, 822 (2017) doi: 10.12693/APhysPolA.132.822
- [7] Özyürek, D., "An effect of weldcurrentandweldatmosphere on theresistance spot weldability of 304L austeniticstainlesssteel", *Materialsand Design* 29:597–603, 2008.
- [8] P. Marashi, M. Pouranvari, S. Amirabdollahian, A. Abedi, M. Goodarzi, *Mater. Sci. Eng. A* 480, 175 (2008), doi: 10.1007/s11665-011-0078-y
- [9] N. Akkaş, E. İlhan, *Acta. Phys. Pol. A* 125, 497 (2014), doi: 10.12693/APhysPolA.125.497
- [10] Onar V., "Tırp Çelikler İle Mikroalaşımli Çeliklerin Elektrik Direnç Nokta Kaynağında Birleştirilebilirliğinin İncelenmesi", *Sakarya Üniversitesi, Fen Bilimleri Enstitüsü, Doktora tezi, Sakarya, Türkiye, 2017.*

CORRESPONDENCE ADDRESS: Volkan ONAR, Department of Mechanical and Manufacturing Engineering, Faculty of Technology, Pamukkale University, Denizli, Turkey, +905076992532, vonar@pau.edu.tr.

SHORT BIOGRAPHIES

Volkan ONAR – He was born in İstanbul in 1984. He completed his primary and secondary education in Kocaeli. He got B.Sc. degree from Gazi University, Department of Technical Education in 2007. Besides, He graduated M. Sc. Degrees from Gazi University, Department of Metal Education in 2010. He graduated Ph. D. at Sakarya University, Department of Material and Metallurgy Engineering in 2017. He worked as a Research Assistant in the Department of Manufacturing Engineering at Pamukkale University 2012 to 2017. He has been working as an Assistant Professor in the Department of Mechanical and Manufacturing Engineering at Pamukkale University since 2017.

Fatih ÖZEN – He was born in Trabzon, Turkey in 1989. He graduated from Sakarya University, Faculty of Engineering, Mechanical Engineering department. He is PhD student in Manufacturing engineering. He is research assistant since 2014 in Sakarya University. His main interest area are welding and manufacturing processes.

Uğur ÖZSARAC – He was born in Çorum, Turkey in 1971. He graduated from METU, Department of Metallurgical Engineering as an engineer in 1995. He started to Sakarya University as Research Assistant. He has been working in same University as an Associate Professor since 1995. His research areas are Welding metallurgy, Brazing and cold metal transfer (CMT)., +90 (264) 295 65 02, ozsarac@sakarya.edu.tr.

Melih KEKİK – He was born in Bursa in 1993. He completed his primary and secondary education in Bursa. He got B.Sc. degree from Sakarya University, Department of Metallurgical and Materials Engineering in 2016. Besides, He graduated M. Sc. Degrees from Sakarya University, Department of Metallurgical and Materials Engineering in 2018.

Yusuf Sadi ASLANLAR – He was born in Sakarya in 1993. He completed his primary, secondary and high school education in Sakarya. He got B.Sc. degree from Sakarya University, Department of Industry Engineering in 2016. He has been continuing M. Sc. Degrees at Sakarya University, Department of Material and Metallurgy Engineering since 2016. He has been working as a Project Engineer at Yıldız Kalıp Industry & Trade Inc. since 2017.

Salim ASLANLAR – He was born in Adapazarı in 1965. He completed his primary and secondary and high school education in Adapazarı. He got B.Sc. degree from Fachhochschule Niederrhein University in Krefeld, Germany, Department of Mechanical and Manufacturing Engineering in 1987. He has been working as a Professor in the Department of Mechanical and Manufacturing Engineering at Sakarya University. His research areas are welding metallurgy, Brazing and cold metal transfer.

EFFECT OF NUGGET SIZES ON TENSILE-SHEAR STRENGTH IN RESISTANCE SPOT WELDING OF TRIP 800 AND MICRO ALLOYED STEEL SHEETS USED IN AUTOMOTIVE INDUSTRY

Volkan Onar^{1,a}, Uğur Özsarac^{2,b}, Fatih Özen^{2,c}, Melih Kekik^{2,d}, Yusuf Sadi
Aslanlar^{3,e}, Salim Aslanlar^{2,f}

¹Department of Mechanical and Manufacturing Engineering, Faculty of Technology, Pamukkale
University, Denizli, Turkey.

²Department of Manufacturing Engineering, Faculty of Technology, Sakarya University, Sakarya, Turkey

³YıldızKalıpSanayi ve Ticaret A.Ş., ARGE Merkezi, Arnavutköy/İstanbul, Turkey

^avonar@pau.edu.tr., ^bozsarac@sakarya.edu.tr, ^cfatihozen@sakarya.edu.tr, ^dmelihkekik@gmail.com,
^eyusuf.aslanlar@yildizkalip.com, ^faslanlar@sakarya.edu.tr.

Abstract

In this paper, effect of nugget size on tensile-shear in resistance spot welding of TRIP 800 and micro alloyed steel in used of automotive industry has been analyzed. In automotive industry, resistance spot welding (RSW) is a extensively used joining technique. Fundamentally, when we look a automobile is composed of dissimilar steels. For this reason, joining of dissimilar steels was gained importance. The use of RSW method is increasing day by day in automotive industry. In this paper, used of micro alloyed steel sheets having 1 mm. and TRIP 800 steel sheet having 1.5 mm. Resistance spot welding method was used for joining of dissimilar steels as in lap joint position. Electrode force was kept constant at 6 kN. The welding times was selected increasing the period from 10 to 30 periods by 5 periods (1period = 0.02s) and different weld currents, ranging from 10500 A to 16500 A in 500 A steps. The effect of nugget size on tensile-shear strength was analyzed. The highest tensile-shear strength of 6285 N in 1.25 mm nugget size was obtained at welding current of 15500 A and period of 15 cycles.

Key Words: TRIP Steels, Electrode Plunge Depth, Tensile – Shear Strength, Welding Time

1. Introduction

Today, the development of new generation steel in the automotive sector has gained importance for weldability of dissimilar steels and non-ferrous materials. It is seen that welding methods are the most commonly used joining method when the automotive sector is taken into consideration. It is seen that TIG (Tungsten Inert Gas) and MIG (Metal Inert Gas) - MAG (Metal Active Gas) welding methods, which are called as gas metal arc welding methods, are used as basic joining methods as they are in other sectors. However, resistance spot welding method is the most commonly used welded joining method in the automotive industry. In fact, the resistance point welding method is the oldest known welding method. When the historical process is examined, the resistance spot welding process is seen in the production of jewelry and

weapons in the oldest cultures [1-5].It has been the most preferred method in the present and will be the most preferred method in future periods due to its suitability for automation with development in the industry.The disadvantage is that it is only used in overlay type connections.In this context, researchers have found welded parts that about 80% of resistance spot welding method is used when considering the welded parts of a modern vehicle [6-12].

Recently, TRIP (Transformation-Induced Plasticity) steels are one of the high strength steels that have recently started to be used in automotive chassis.TRIP steels provide high strength due to have different phases (ferrite, bainite, martensite and residual austenite precipitated between grain boundaries) in its micro structures. TRIP steels are chosen for several reasons. They are increased safety thanks to high strength and with it the weight reduction in the vehicles thus reducing fuel consumption and reducing damage to the environment. The situation is different in the automobile body. Micro-alloyed (DX56D – Z) galvanized steels are used in automobile bodies. The properties of these steel are easily formed and are resistance to corrosion [13].

However, sufficient strength able to be obtained as a result of the welding process the resistance spot welding can be achieved by controlling welding parameters.At this point, the most important parameters draw attention as electrode pressure force, welding time and welding current [14].

In this study, effect of nugget size on tensile-shear in resistance spot welding of TRIP 800 and micro alloyed (DX56D – Z) steels in use of automotive industry has been analyzed.

2. Experimental

The materials studied are TRIP steel sheets having 1.5 mm thicknesses and micro alloyed steel sheets having 1mm thicknesses, which are used respectively in automobile chassis and automobile body parts. The mechanical property of TRIP steel and micro alloyed (DX56D – Z) steels sheets and the chemical composition of these sheets are, respectively, shown in Tabs. 1, 2 and 3.

Table 1. Mechanical properties of couple of steel sheets.

	Yield strength [MPa]	Tensile strength [MPa]	Total elongation [%]
TRIP 800	523	881(min780)	36
DX56D+ Z	171,4	337,5	39

A current and timer controlled resistance spot welding machine having 120 kVA capacity and pneumatic application mechanism. Welding was carried out by using water cooled conical Cu–Cr electrodes having a contact surface of the same diameter (6 mm).

Table 2. Chemical composition of TRIP steel sheets [wt%]

%C	%P	%Mo	%Ti	%Sn	%Si	%S	%Ni	%Cu	%V
0,179	0,011	0,025	0,014	0,01	1,719	0,007	0,074	0,1	0,013
%Mg	%Mn	%Cr	%Al	%Nb	%W	%Fe			
0,001	1,691	0,065	0,027	0,053	0,04	95,902			

Table 3. Chemical composition of micro alloyed steel sheets [wt%]

%C	%Si	%Mn	%P	%S	%Si	%Fe
0,12	0,50	0,60	0,10	0,045	0,30	98,33

The samples were overlapped with 30 mm spacing and welded. For welding samples, 10, 15, 20, 25 and 30 periods weld times were chosen while other welding parameters such as chosen electrode pressure (6 kN) and hold time and clamping time of electrode (25 periods) were kept constant. The welding current was increased from 8000 A to 16500 A by 500 A increments. Welding parameters are shown in Figure 1.

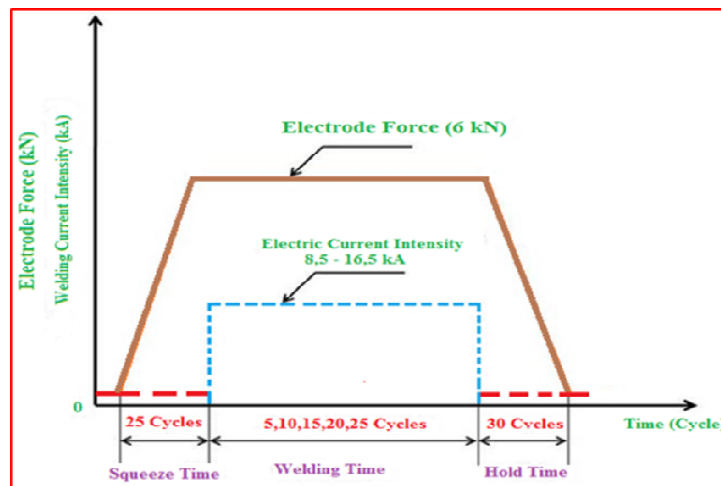


Figure 1. Welding parameters

Nugget widths (d_1), nugget heights (d_2) were measured and also nugget size ratios (d_2/d_1) were calculated with an optical microscope. Weld nugget geometry is shown in Figure 2. The effect of nugget size on tensile shear strength was investigated by taking into consideration the obtained results from the measured nugget sizes.

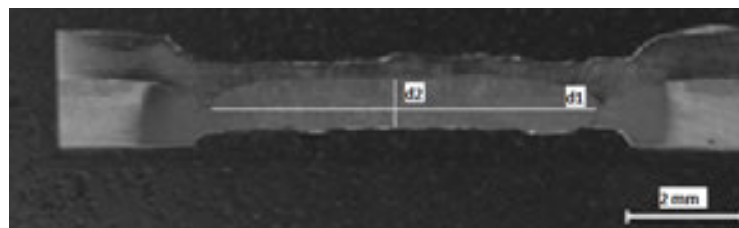


Figure 2. Weld nugget geometry.

3. Results and Discussion

In low welding current application, small weld nugget diameters were obtained due to low heat application to welding zone. But in high welding current applications, big weld nugget diameters were obtained. Nugget diameters are increases with increasing weld current. Because of with decrease in the steel sheets thickness, the tensile shear strength is decreasing as shown in Figure 3 and 4. Total weld nugget height decreases while the welding current increases however, the tensile shear strength is increased. This event is shown in Figure 5 and 6. With increasing welding current and welding time molten metal quantity is increases and then molten metal is expulsion in welding nugget. For this reason the nugget size ratio increases. Therefore falls tensile shear strength of the welded samples as shown in Figure 7 and 8.

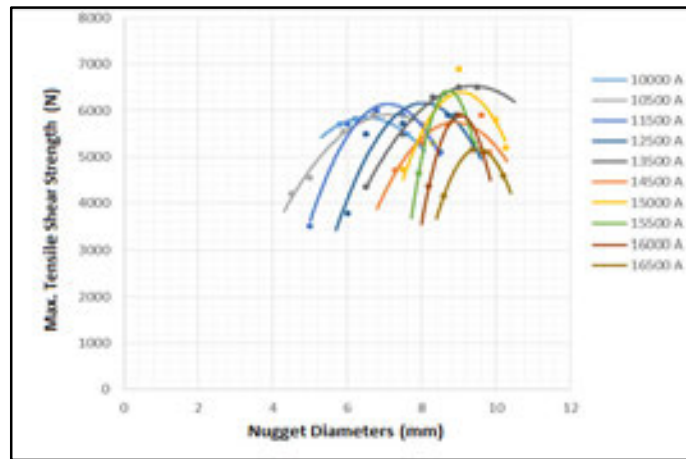


Figure 3. The relationship between nugget diameters and tensile - shear strength depending on welding time

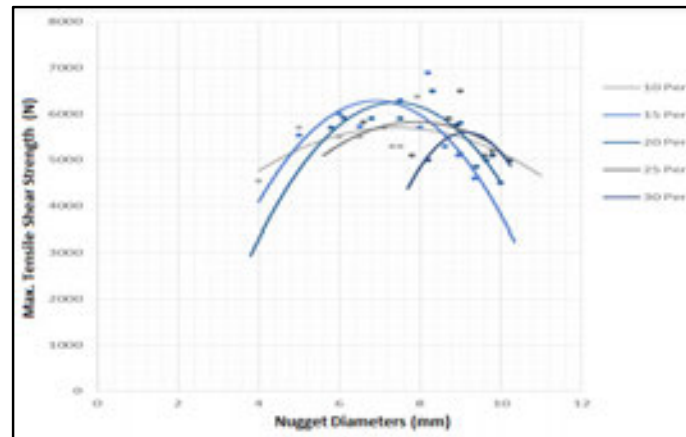


Figure 4. The relationship between nugget diameters and tensile - shear strength depending on welding current intensity

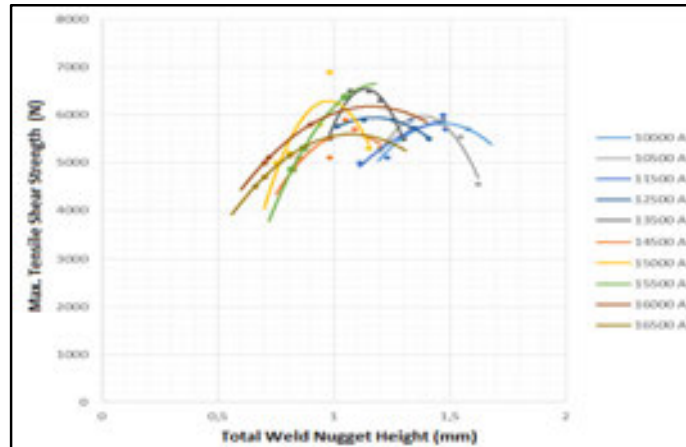


Figure 5. The relationship between total weld nugget height and tensile - shear strength depending on welding time

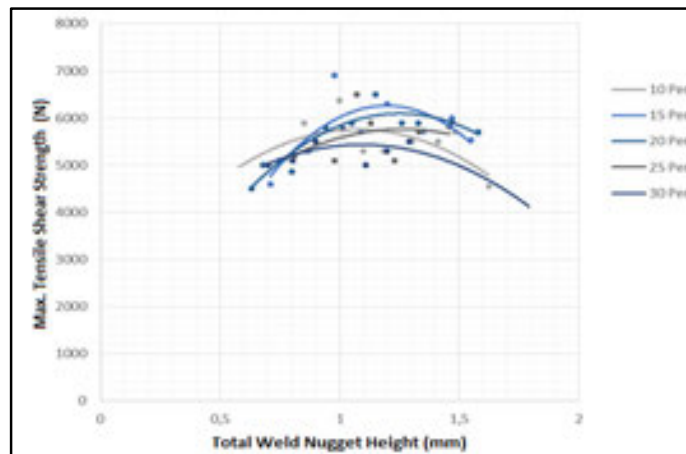


Figure 6. The relationship between total weld nugget height and tensile - shear strength depending on welding current intensity

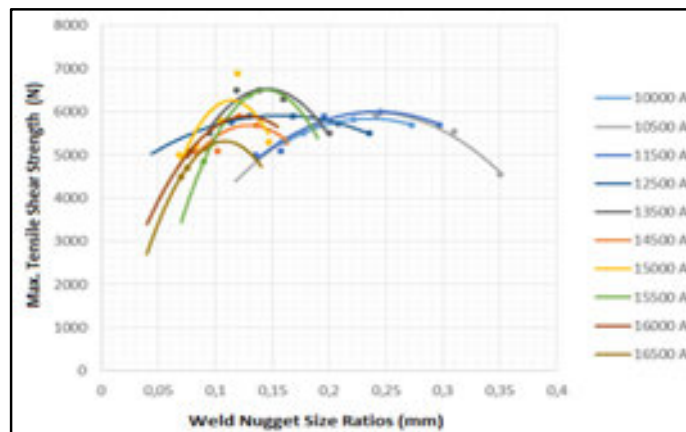


Figure 7. The relationship between weld nugget size ratio and tensile - shear strength depending on welding time

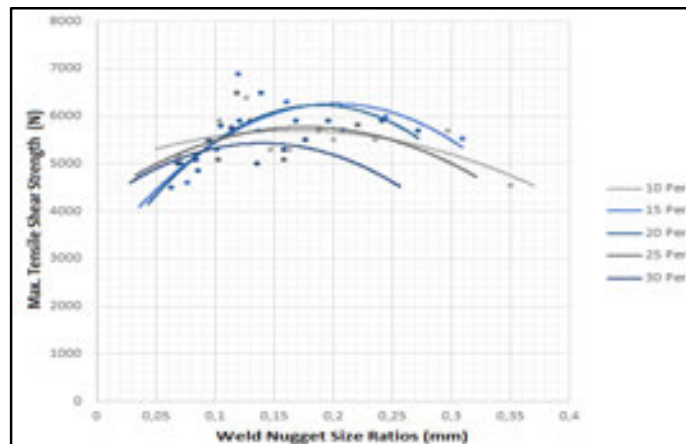


Figure 8.The relationship between weld nugget size ratio and tensile - shear strength depending on welding current intensity

4. Conclusion

The experimental results obtained using 6 kN electrode force are given below;

- Tensile shear strength increased up to 7.5 mm nugget diameter at 10500 A current value while tensile - shear strength decreased due to the increase of heat input and welding time at welded joints having a nugget diameter above this value.
- At 13500 A and 16500 A, it was observed that the tensile -shear strength increased until the welding nugget diameter was 9.5 mm. And then tensile-shear strength decreased when the nugget diameters were increased shown as in the graphical results.
- The tensile - shear strength increased when the nugget diameters were increased but the tensile - shear strength decreased after certain of nugget diameter.
- It is observed that tensile - shear strength decreases with the increase of the welding time.
- The highest tensile-shear strength was obtained as 6600 N at the welding nugget height of 1,1 mm at the welding current of 16500 A depending on the welding current intensity.
- The highest tensile-shear strength was obtained as 6580 N at the welding nugget size ratio of 0,15 mm at the welding current of 13500 A depending on the welding current intensity.
- The highest tensile-shear strength was obtained as 6580 N at the welding nugget diameter of 9,5mm at the welding current of 13500 A depending on the welding current intensity.
- It has been observed that tensile - shear strength decreases at higher nugget diameters due to heat input. This is consistent with the results obtained in literature studies and the results of experimental studies

5. References

- [1] ASM, MetalsHandbook: Welding, BrazingandSoldering, Volume 6, 1993.
- [2] M. Mimer, L.E. Svensson, R. Johansson, Weld. World 48, 14 (2004), doi: 10.1007/BF03266421
- [3] O.J. Kwon, K. Lee, G. Kim, K.-G. Chin, Mater. Sci. Forum 638-642, 136 (2010), doi: 10.4028/www.scientific.net/MSF.638-642.136
- [4] F. Varol, M. Ekici, E. Ferik, U. Ozsarac, S. Aslanlar, Acta. Phys. Pol. A 127, 965 (2014), doi: 10.12693/APhysPolA.127.965
- [5] F. Varol, U. Ozsarac, S. Aslanlar, A. Onat, M. Ekici, E. Ferik, Acta. Phys. Pol. A 127, 968 (2015), doi: 10.12693/APhysPolA.127.968
- [6] V. Onar, S. Aslanlar, N. Akkaş, ActaPhysicaPolonica A 132, 822 (2017) doi: 10.12693/APhysPolA.132.822
- [7] AWS, Safetyandhealthfactsheetno: 21, 1999.
- [8] Groover, M.P., Fundamentals of modern manufacturing: materials, processesandsystems, Third Edition, John Wiley&SonsInc. 2007.
- [9] Özyürek, D., "An effect of weldcurrentandweldatmosphere on theresistance spot weldability of 304L austeniticstainlesssteel", Materialsand Design 29:597–603, 2008.
- [10] P. Marashi, M. Pouranvari, S. Amirabdollahian, A. Abedi, M. Goodarzi, Mater. Sci. Eng. A 480, 175 (2008), doi: 10.1007/s11665-011-0078-y
- [11] N. Akkaş, E. İlhan, Acta. Phys. Pol. A 125, 497 (2014), doi: 10.12693/APhysPolA.125.497
- [12] Ö. Savaş, Acta. Phys. Pol. A 127, 921 (2015), doi: 10.12693/APhysPolA.127.921
- [13] ONAR V., "Trıp Çelikler İle Mikroalaşımli Çeliklerin Elektrik Direnç Nokta Kaynağında Birleştirilebilirliğinin İncelenmesi", Sakarya Üniversitesi, Fen Bilimleri Enstitüsü, Doktora tezi, Sakarya, Türkiye, 2017.
- [14] Akkaş N., "Raylı sistem araçlarında kullanılan atmosferik korozyona dayanıklı çelik saçların birleştirilme kabiliyetinin incelenmesi", Sakarya Üniversitesi, Fen Bilimleri Enstitüsü, Doktora tezi, Sakarya, Türkiye, 2015.

CORRESPONDENCE ADDRESS: Volkan ONAR, Department of Mechanical and Manufacturing Engineering, Faculty of Technology, Pamukkale University, Denizli, Turkey, +905076992532, vonar@pau.edu.tr.

SHORT BIOGRAPHIES

Volkan ONAR –He was born in İstanbul in 1984. He completed his primary and secondary education in Kocaeli. He got B.Sc. degree from Gazi University, Department of Technical Education in 2007. Besides, He graduated M. Sc. Degrees from Gazi University, Department of Metal Education in 2010. He graduated Ph. D. at Sakarya University, Department of Material and Metallurgy Engineering in 2017. He worked as a Research Assistant in the Department of Manufacturing Engineering at Pamukkale University 2012 to 2017. He has been working as an Assistant Professor in the Department of Mechanical and Manufacturing Engineering at Pamukkale University since 2017.

Uğur ÖZSARAC –He was born in Çorum, Turkey in 1971. He graduated from METU, Department of Metallurgical Engineering as an engineer in 1995. He started to Sakarya University as Research Assistant. He has been working in same University as an Associate Professor since 1995. His research areas are Welding metallurgy, Brazing and cold metal transfer (CMT)., +90 (264) 295 65 02, ozsarac@sakarya.edu.tr.

Fatih ÖZEN – He was born in Trabzon, Turkey in 1989. He graduated from Sakarya University, Faculty of Engineering, Mechanical Engineering department. He is PhD student in Manufacturing engineering. He is research assistant since 2014 in Sakarya University. His main interest areas are welding and manufacturing processes.

Melih KEKİK – He was born in Bursa in 1993. He completed his primary and secondary education in Bursa. He got B.Sc. degree from Sakarya University, Department of Metallurgical and Materials Engineering in 2016. Besides, He graduated M. Sc. Degrees from Sakarya University, Department of Metallurgical and Materials Engineering in 2018.

Yusuf Sadi ASLANLAR – He was born in Sakarya in 1993. He completed his primary, secondary and high school education in Sakarya. He got B.Sc. degree from Sakarya University, Department of Industry Engineering in 2016. He has been continuing M. Sc. Degrees at Sakarya

University, Department of Material and Metallurgy Engineering since 2016. He has been working as a Project Engineer at Yıldız Kalıp Industry & Trade Inc. since 2017.

Salim ASLANLAR –He was born in Adapazarı in 1965. He completed his primary and secondary and high school education in Adapazarı. He got B.Sc. degree from Fachhochschule Niederrhein University in Krefeld, Germany, Department of Mechanical and Manufacturing Engineering in 1987. He has been working as a Professor in the Department of Mechanical and Manufacturing Engineering at Sakarya University. His research areas are welding metallurgy, Brazing and cold metal transfer.

İSTİHDAM ODAKLI YENİ BİR MESLEKİ VE TEKNİK EĞİTİM MODELİ TASARIMI

Mehmet YAZAR^{1,a}, Mustafa KÖROĞLU^{2,b}

¹Ankara Keçiören Şehit Mehmet Karakaşoğlu Mesleki ve Teknik Anadolu Lisesi

²Ankara Yeni mahalle Gezi Mesleki ve Teknik Anadolu Lisesi

^amehmet_yazar@hotmail.com, ^bmkoroglu69@hotmail.com

Özet

Bu çalışmada Türkiye'deki mesleki ve teknik eğitim sisteminin sorunları, nitelikli insan gücü yetiştirme ihtiyacı ve mesleki ve teknik eğitimin her kademesine iş piyasasının aktif katılımının sağlandığı, istihdam odaklı yeni bir mesleki ve teknik eğitim modeli üzerinde durulmuştur.

Mesleki ve teknik eğitimin, iş piyasasına insan kaynağı yetiştirme, insan kaynaklarının becerilerini iş piyasasının talepleri doğrultusunda geliştirme, iş piyasasının mesleki ve teknik eğitime katılımını sağlama ve istihdamı artırma gibi birçok işlevi sayılabilir.

Ülkemizde birçok işveren, mesleki ve teknik eğitim almış nitelikli işgücü ihtiyacı bulunduğunu ancak aradığı özellikte elemanı bulamadığını ifade ederken, birçok insanımız da çalışabileceği bir iş bulamamaktan şikâyetçidir.

Ülkemizin nitelikli işgücü ihtiyacının karşılanması için sektörün taleplerine kulak veren bir Milli Eğitim Bakanlığı, sektörle etkili işbirliğini öngören yeni mesleki ve teknik eğitim modelinin hayata geçirmesi oldukça önem arz etmektedir.

Günümüz teknolojisindeki hızlı gelişmeler mesleki ve teknik eğitim modelimizin yeniden gözden geçirilmesini gerekli kılmaktadır. Türkiye'deki mesleki eğitim sistemi kalıplaşmış eğitim sistemi anlayışıyla devam ettiği için bu liselere giden ve mezun olan öğrencilerin günümüz ihtiyaçlarını ve iş piyasasının taleplerini karşılayamamaktadır. Mesleki eğitim sistemi içindeki okullar teknolojik gelişmelere ve iş piyasası taleplerine ayak uyduramadığından bu okullardaki öğrencilerin başarı seviyesi düşük olmasına neden olmaktadır.

Bu çalışmada Türkiye'deki mesleki ve teknik eğitim faaliyetlerinin her aşamasına iş piyasasının aktif katılımı ile günümüzdeki ve gelecekteki ihtiyaçları karşılayacak istihdam odaklı yeni bir mesleki ve teknik eğitim modeli tasarlanmıştır.

Anahtar Sözcükler: İstihdam, Mesleki Eğitim Modeli

Abstract

In this study the problems of vocational and technical education system in Turkey, qualified manpower training needs and vocational and technical education that ensure the participation of the labor market at all levels, employment-oriented focused on a new vocational and technical education model.

Vocational and technical education, labor market, human resource development, human resources skills in line with the demands of the labor market development, labor market participation in vocational and technical training and employment can be considered as many functions.

While many employers in our country say that there is a need for qualified workforce who have received vocational and technical education but cannot find the element they are looking for, many of our people complain that they cannot find a job to work with.

In order to meet the needs of our country's qualified labor force, a Ministry of National Education, which has listened to the demands of the sector, is very important to implement a new vocational and technical education model which foresees effective cooperation with the sector.

Rapid developments in today's technology necessitate a review of our vocational and technical training model. To continue with vocational training system stereotypical understanding of the education system in Turkey is going to meet these high school students and graduates today's needs and the demands of the job market. As the schools in the vocational education system cannot keep up with the technological developments and labor market demands, the success level of the students in these schools is low.

In this study, active participation and employment-oriented to meet current and future needs of the job market every stage of vocational and technical education activities in Turkey designed a new model of vocational and technical education.

Key Words: Employment, Vocational Training Model

1. Giriş

Türkiye, ekonomik kalkınma sürecinde yapısal ve demografik dönüşümler yaşamış, büyük oranda kentleşmiş, orta gelirli bir ülkedir. Türkiye ekonomisinin en önemli büyüme kaynağı bugüne kadar kırdan kente göç ile gerçekleşen verimlilik artışı olmuştur. Bu verimlilik artışının devamının sağlanması ve istenilen seviyeye getirilmesi mesleki ve teknik eğitim planlamasının iyi yapılmasına bağlıdır. Ülkemiz insan kaynağının en verimli şekilde değerlendirilmesi için mesleki ve teknik eğitim modeli oluştururken sektörün nitelikli işgücü ihtiyacının belirlenmesi, insan kaynağının analiz edilmesi ve planlamanın her aşamasında eğitim sektör işbirliğinin gerçek manada uygulanması ile istihdam odaklı yeni bir mesleki ve teknik eğitim modeli tasarımı ile gerçekleşecektir.

İş gücü kaynağı olan insan bilim, teknoloji ve sektördeki değişime uygun olarak değişen işgücü ihtiyacının karşılanabilmesi öğretim programlarının sürekli güncellenmesi ve geliştirilmesine günümüzde ihtiyaç duyulduğu gözlenmektedir[6].

Mesleki öğretim programları birey, toplum ve iş hayatının ihtiyaçlarına duyarlı olmalı ve gelişen teknolojiye uygun olarak sürekli bir şekilde sistemli olarak yenilenmelidir. Teknoloji ve iş hayatı değişirken programlar aynı kalırsa ihtiyaçlar karşılanamaz. Çünkü yapılan işin ve eğitim ihtiyacının değişmesi, eğitim programlarında değişmesine neden olmaktadır [6].

İstihdam odaklı yeni bir mesleki ve teknik eğitim modeli tasarımı ile sektördeki gelişmelere ve bu gelişmelere dayalı nitelikli işgücü ihtiyacına cevap veren, esnek yapıda bir model ile mümkündür

Günümüzde insan kaynağı teknolojik gelişme ve sektör taleplerine göre şekillenmektedir. Son yıllarda el becerisi/beden gücüne sahip insan yerine, bilgiye ulaşabilen, bilgiyi sorgulayan, teknolojinin kullanılması ve beyin gücüyle yorum yaparak ortaya çıkan problemlere çözüm üretebilen, bir teknik eleman modeline ihtiyaç vardır [5].

Ülkelerin ekonomin gelişmişliğinde sektörün ihtiyacı olan nitelikte insan gücü yetiştirmeye bağlıdır. Ülkemiz bu konuda sektörün ihtiyaçlarına cevap verememektedir. Sektörün nitelikli işgücü ihtiyacı ile mesleki ve teknik eğitim almış işgücünün yeterliliklerinin uyumaması istihdam odaklı yeni bir mesleki ve teknik eğitim modeli tasarlamayı bir zorunluluk haline getirmiştir.

Mesleki ve teknik Anadolu liselerinde, birçok alan/dal kapanma tehlikesi ile karşı karşıya kalmıştır. İlköğretimde, öğrencilerin bilimsel olarak mesleğe yönlendirilmesi yapılmadığı gibi, meslek lisesi mezunlarına yükseköğretime geçişte getirilen kısıtlamalar bu sonucu doğurmuştur. Mesleki ve teknik eğitim yükseköğretim kurumlarının öğrenci kaynağı Mesleki

ve Teknik Anadolu liseleri olması nedeniyle yüksek öğretime giden öğrenciler de istenilen seviyenin çok altında kalmıştır [3]. Sektörün nitelikli işgücü ihtiyacının karşılanması için istihdam odaklı yeni bir mesleki ve teknik eğitim modeli tasarımına ihtiyaç vardır. İstihdam odaklı yeni bir mesleki ve teknik eğitim modeli ile sektörün eğitim planama ve uygulama faaliyetlerine aktif katılımı ile sektörün istemiş olduğu nitelikli işgü yetiştirilmiş olacaktır.

2. Mesleki ve Teknik Eğitimle İlgili Tespit Edilen Olumsuzluklar

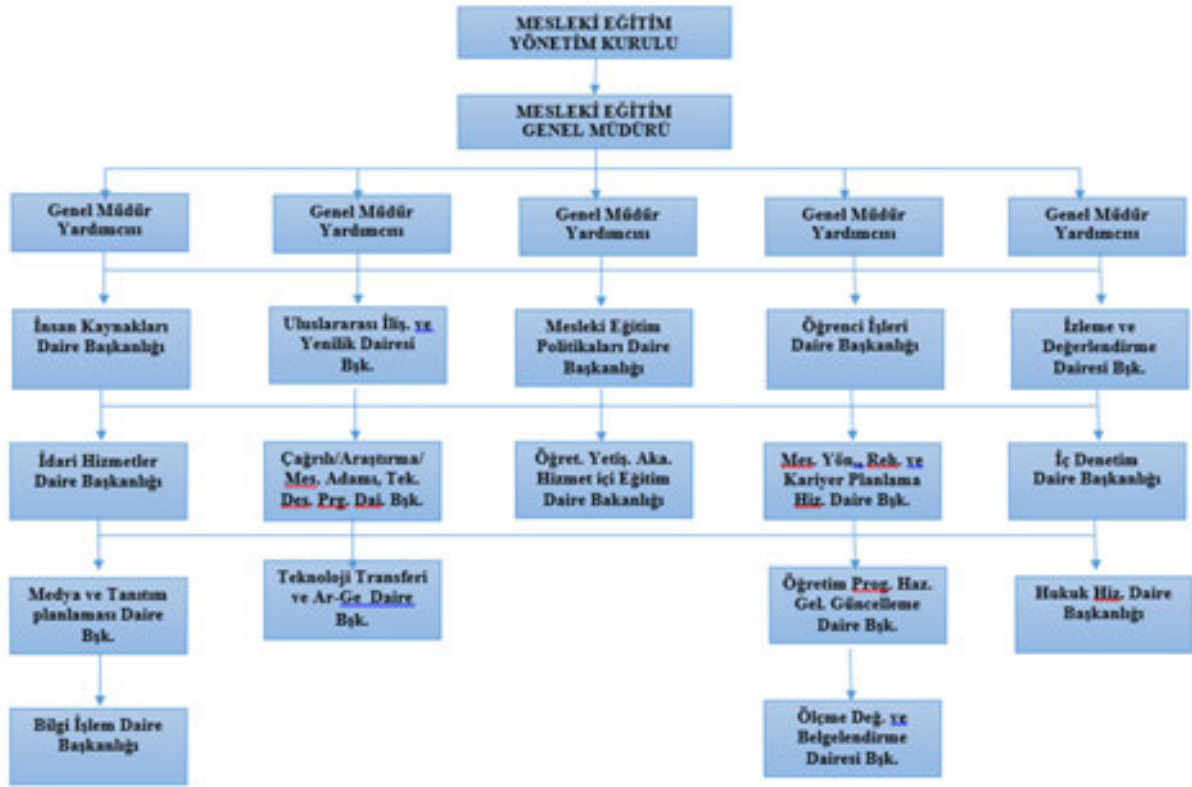
Ülkemiz mevcut mesleki ve teknik modelinde birçok olumsuzluğun tespit edilmiş ve bu çalışmayla aşağıdaki sorunlar çözüm üretilmeye çalışılmıştır. Tespit edilen

- Eğitim-sektör işbirliğinin yeterli olmaması,
- Eğitim kalitesinin düşük olması,
- Meslek dersleri yetiştiren fakültelerin sektörden taleplerini dikkate almaması,
- Mesleki ve teknik eğitimde istihdam edilen öğretmenlerin sektör ile uygun bilgi ve beceriye sahip olmaması,
- Milli Eğitim Bakanlığı öğretmen atama kriterlerinin mesleki liyakate bağlı olmaması,
- Milli Eğitim Bakanlığı öğretmen yetiştirme ve hizmetiçi politikasının yeterli olmaması,
- Mesleki ve teknik eğitimdeki öğretim programlarının sektör ihtiyaçlarına cevap vermemesi,
- Mesleki ve teknik eğitim yapısının gelişen teknolojiyle kendini yenileyecek esnekliğe sahip olmaması,
- Mesleki eğitimin sahip olduğu olumsuz algının öğrenci tercihlerini etkiliyor olması,
- Mesleki eğitimin çağın ve sektörün ihtiyaçlarını karşılamıyor olması,
- Türkiye’de eğitimle ilgili gelecek perspektifinin net olmaması,
- Öğrencilerin mesleki ve kariyer yönlendirmesinde planlamasının olmaması,
- Rekabetçiliğin yıkıcı etkisinin artacak olması

olumsuzluklardan bazılarıdır.

3. İstihdam Odaklı Yeni Nesil Bir Mesleki Eğitim Yönetim Modeli Tasarımı

İstihdam odaklı yeni bir mesleki ve teknik eğitim tasarımı yapılırken eğitim sektör işbirliği temel kriter alınarak aşağıdaki gibi tasarlanmıştır.



Şekil 1. İstihdam Odaklı Yeni Nesil Bir Mesleki Eğitim Yönetim Modeli Tasarımı

3.1 Yönetim

3.1.1. Mesleki Eğitim Yönetim Kurulu

- Milli Eğitim Bakanlığı
- Çalışma ve Sosyal Güvenlik Bakanlığı
- Bilim Sanayi ve Teknoloji Bakanlığı
- Kalkınma Bakanlığı
- Türkiye Odalar ve Borsalar Birliği
- Eğitim Sendikaları
- İşçi Sendikaları
- İşveren Sendikaları
- KOSGEB
- MYK

temsilcilerinden oluşturulmaktadır.

3.1.1.2 Mesleki Yönetim Kurulu Görevleri

- Mesleki Eğitim Üst Politikalarının Belirlenmesi
- Objektif Kriterlere Göre Mesleki Genel Müdürünün Seçilmesi
- Objektif Kriterlere Göre Mesleki Eğitim Genel Müdürlüğü Yönetimini Seçilmesi
- Performans İzlenmesi ve Değerlendirilmesi

- ✓ Hizmet içi eğitim (Yönetici ve öğretmenlere)
- ✓ Sertifikasyon ve kariyer basamakları
- ✓ Prim sistemi

oluşmaktadır.

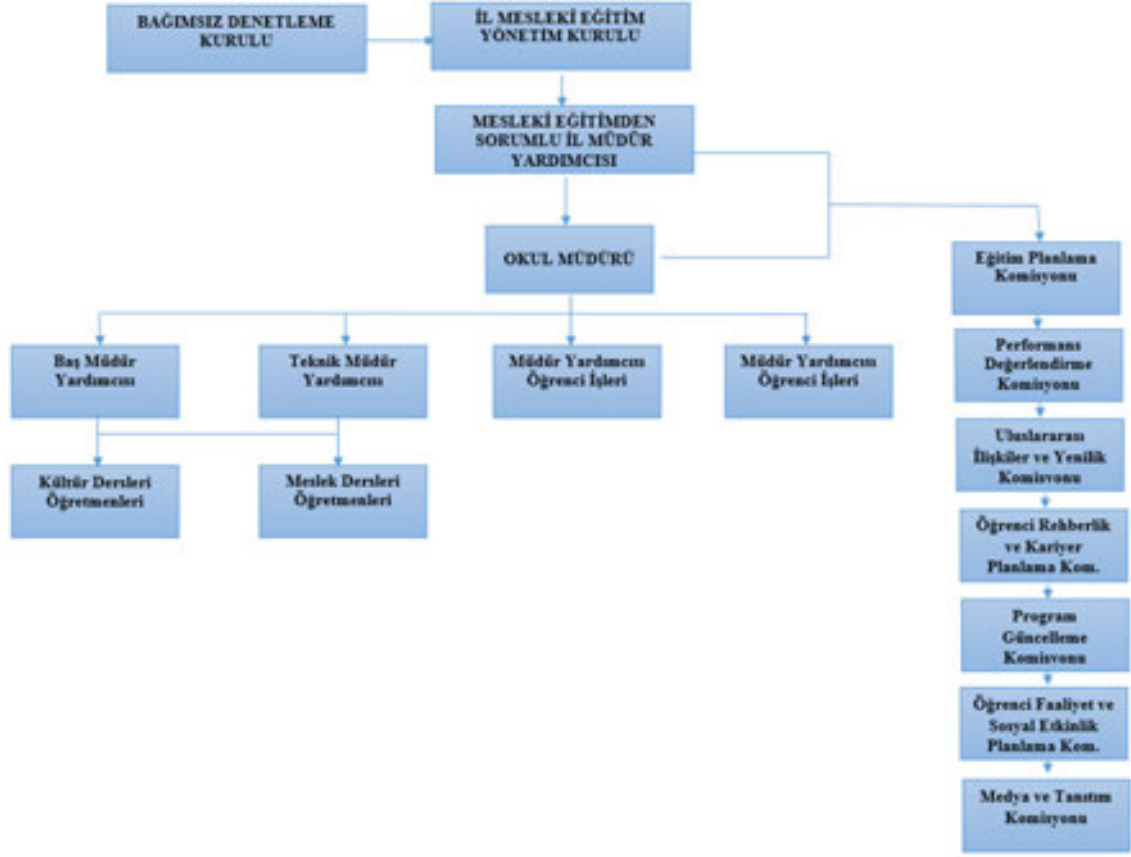
3.1.1.2.1 Mesleki Yönetim Kuruluna Bağlı Birimler:

- Mesleki Eğitim Genel Müdürlüğü
 - ✓ Genel Müdür
 - Genel Müdür Yardımcısı
 - ❖ İnsan Kaynakları Daire Başkanlığı
 - ❖ İdari Hizmetler Daire Başkanlığı
 - ❖ Medya ve Tanıtım planlaması Daire Başkanlığı
 - ❖ Bilgi İşlem Daire Başkanlığı
 - Genel Müdür Yardımcısı
 - ❖ Uluslararası İlişkiler ve Yenilik Dairesi Başkanlığı
 - ❖ Çağrılı Destek, Araştırma Destek, Teknoloji destek ve Meslek Adamı Destek Programları Daire Başkanlığı
 - Genel Müdür Yardımcısı
 - ❖ Mesleki Eğitim Politikaları Daire Başkanlığı
 - ❖ Öğretmen Yetiştirme Akademisi ve Hizmetiçi Eğitim Merkezleri Daire Başkanlığı
 - Genel Müdür Yardımcısı
 - ❖ Öğrenci İşleri Daire Başkanlığı
 - ❖ Mesleki Yönlendirme Rehberlik ve Kariye Planlama Hizmetleri Daire Başkanlığı
 - ❖ Öğretim Programları Hazırlama Geliştirme ve Güncelleme Daire Başkanlığı
 - ❖ Ölçme Değerlendirme ve Belgelendirme Dairesi Başkanlığı
 - Genel Müdür Yardımcısı
 - ❖ İzleme ve Değerlendirme Dairesi Başkanlığı
 - ❖ İç Denetim Daire Başkanlığı
 - ❖ Hukuk Hizmetleri Daire Başkanlığı

birimlerden oluşturulmuştur.

4. İstihdam Odaklı Yeni Nesil Bir Meslek ve Teknik Lisesi Okul Yönetim Modeli

İstihdam odaklı yeni bir mesleki ve teknik lisesi tasarımı yapılırken eğitim sektör işbirliği temel kriter alınarak aşağıdaki gibi tasarlanmıştır.



Şekil 2. İstihdam Odaklı Yeni Nesil Bir Meslek ve Teknik Lisesi Okul Yönetim Modeli

4.1 Yönetim

4.1.1. İl Mesleki Yönetim Kurulu Üyeleri

- Sektör temsilcileri,
- İŞKUR il müdürlüğü temsilcisi
- Yerel yönetimler (Belediyeler, İl Özel İdare)
- Sendika Temsilcileri
- İl/ilçe müdürlüğü temsilcisi
- Meslek odaları temsilcileri,
- KOSGEP İl müdürlüğü Temsilcisi
- Veli/öğrenci/öğretmen

temsilcilerinden oluşturulmaktadır.

4.1.1.1. İl Mesleki Yönetim Kurulu Görevleri:

- Objektif kriterlere göre okul müdürlerinin seçilmesi
- Performans değerlendirmesi (360 derece)
- Hizmet içi eğitim
 - ✓ öğretmenlere

- ✓ Sertifikasyon ve kariyer basamakları
- Prim sistemi
- Performans Düşüklüğünde
 - ✓ Birinci Yılda Birim Okul Değiştirme
 - ✓ İkinci Yılda Hizmetiçi Eğitime Geri Döndürme

4.1.1.2.1 İl Mesleki Yönetim Kurulu'na Bağlı Birimler:

- Bağımsız Denetleme Kurulu
- Mesleki Eğitim Sorum İl Milli Eğitim Müdür Yardımcısı
- Mesleki eğitim Planlama Komisyonu
- Performans Değerlendirme Komisyonu
- Uluslararası İlişkiler Teknoloji Transferi Komisyonu
- Öğrenci Rehberlik ve Kariyer Planlama Komisyonu
- Program İnceleme ve Yenileme Komisyonu
- Öğrenci Faaliyetleri ve Sosyal Etkinlik Planlama Komisyonu
- Medya ve Tanıtım Komisyonu
- Okul Müdürü
- Baş Müdür Yardımcısı,
- Teknik müdür Yardımcısı,
- Müdür Yardımcısı,
- Müdür Yardımcısı,
- Kültür Dersleri Öğretmenleri,
- Meslek Dersleri Öğretmenleri

birimlerin oluşturulmuştur.

4.2. Öğretmen

Öğretmen seçim kriterleri;

- Meslek dersi öğretmenlerinin 3 gün sektörde mesleki gelişmelerinin sağlanması. Sektörde kazandığı deneyime göre öğretmenlerin ücret politikası belirlemek. Ayrıca öğretmenlerin sektör deneyimlerine göre sınıf seviyesinde ders vermesi sağlanması
- Öğretmen seçimi
- Kuruma ilk atanan öğretmenlerin adaylık sürecinde 6 ay zorunlu sektör stajı uygulanması
- Okula atandıktan sonra 1 yıl sektörde çalışması
- Görev süresince sektördeki yenilikleri takip etmek için yılda en az 1 aylık sektörde eğitim alması – çalışması
- Eğitim ve öğretimin gelişim/değişimi ile ilgili hizmetçi eğitimler alması (sanal eğitimler, bakanlık tarafından verilecek e-egitimler)
- Eğitimci kalitesinin yükseltilmesi için sektör tecrübesinin artırılması

olarak belirlenmiştir.

4.3. Öğrenci

Öğrenci seçim kriterleri;

- Öğrencilerin seçimine ilişkin iş ve işlemler
- Mülakat ve beden yeterliliği
- İlköğretim başarı puanı
- Dokuzuncu sınıfta direkt alana yerleştirme (sözleşme sigorta girişleri yapılır)
- Öğrenci danışmanı (okul ve işletmede)

- Mezuniyet sonrası planlama
- Öğrenci kariyer ofisi
 - ✓ Kariyer günleri
 - ✓ Profesyonel sunumları
 - ✓ Bilgi yetenek testleri
- İşe yerleştirme
- Sürekli mesleki gelişimi işletme tarafından sağlanması olarak belirlenmiştir.

4.4. Eğitim – Öğretim Süreci

4.4.1. Öğretim Programları

Öğretim programlarının yapısı;

- Esnek programlar
 - ✓ Eğitim 3 dönemden oluşur (mesleğin özelliğine göre toplam süre 1 ile 3 yıl arasında değişir)
- Genel bilgi derslerin mesleğin gerektirdiği asgari yeterliliklere cevap vermels
- Girişimcilik dersleri son seneye doğru verilmesi
- Zorunlu seçmeliler
 - ✓ Sosyal etkinlikler
 - Sosyal gelişim merkezlerinin müfredata entegre edilmesi, çıktılar doğrultusunda öğrencinin başarı değerlendirilmesinde kullanılması (satranç, sportif faaliyet, müzik aleti) ve projelerde kullanılması
 - ✓ Sanat dalı
 - ✓ Yabancı dil
- Sektör uyumlu atölyelerin düzenlenmesi
 - ✓ 9.sınıfta işletmeye uyum eğitimlerinin başlaması
 - ✓ Okul içinde özel işletmeler ve atölyeler kurulması,
- Çeşitlendirilmiş öğretim yöntemleri
 - ✓ Sanal gerçeklik (VR)
 - ✓ E-öğrenme
 - ✓ Online eğitim modülleri
- Eğitim ortamı
 - ✓ Merkezi ileri teknoloji laboratuvarları kurulması
 - ✓ High-tech simülasyon tırları oluşturulması,
 - ✓ Bilgisayar laboratuvarları kurulması(her okulda)
 - ✓ İleri teknoloji şehir müzeler kurulması(teknolojinin tarihi gelişimini izleyebilecekleri)
 - ✓ Oyun laboratuvarları kurulması(müfredatın oyunlaştırılması)
- Öğrencilerin sanat ve artistik alanlarda yan dal eğitimi: Disiplinler arası beslenme (Sanat – teknoloji – bilim)
 - ✓ Kurumsal, görsel, kurgusal zekayı geliştiren: 12. Sınıfta 2. Dönem çoklu zekayı geliştiren dersler: 3 boyutlu zekâ Uzamsal zekâ. Görsel zekâ derslerinin verilmesi
 - ✓ Gelişim – bilişim – iletişim
 - ✓ Tasarım felsefesi
 - ✓ Sanat kuramları
 - ✓ Çevre bilinci

- Ölçme değerlendirme
 - ✓ Yıllık bağımsız değerlendirme
 - ❖ %60 pratik
 - ❖ %40 teorik
 - Network
 - ✓ E-platform (öğrenci&sektör)
 - ✓ Okul tabanlı kapsamlı dinamik izleme veri tabanının oluşturulması
 - ✓ Nüfus, Emek arz-talep, İş piyasası ihtiyaç analizi (bölgesel), iş gücü haritası, Gelecek mesleklerin eğilim analizi, Sektör envanterinin çıkartılması, Sektör üretimlerindeki projeksiyonun belirlenmesi, Değişim parametrelerinin takip edilebildiği database
 - ✓ İş ilanları haritası
- olarak planlanmıştır.

5. Sonuç ve Değerlendirme

Yapılan bu çalışma ile Yönetim yapısının

- Kurum idarecileri liyakat, mesleki tecrübe ve mesleki çalışmaları göz önünde bulundurularak seçilmelidir.
- İdareciler (müdür ve müdür yardımcıları) öğretmenlerine çalışmaları ve yaptıkları yönlendirmeler ile her açıdan örnek olmalıdır.
- Mesleki eğitim verebilecek kurumların idari yapıları buna uygun olmalı (Örneğin; mesleki eğitim verecek bir kurumun başında sınıf öğretmeni müdür olmamalı)

Öğretmen yapısının

- Öğretmenlerin ilk atamaları mesleki yeterliliğe dayalı sınavlarla seçim yapılmalı,
- Öğretmenlerin sektörle işbirliği ve akademik çalışmaları teşvik edilerek imkan sağlanmalı,
- Milli Eğitim Bakanlığı öğretmenler için belirli bölgelerinde kuracağı mükemmeliyet merkezleri eğitim ortamları vasıtasıyla yeniliğe açık günümüz eğitim ve sanayi işbirliğine uygun donanım ve programlarca desteklenen öğretmen yetiştirme akademileri oluşturmalı,
- Öğretmenlere gereken değer verilmelidir sistemin merkezinde lokomotifinin öğretmen olduğu hissettirilmelidir.
- Öğretmenler haftanın her günü okulda olmalı veya okul işletme işbirliği çerçevesinde işletmede bulunmalı çalıştığı ortamdan sorumlu olmalı sistemin dışına çıkmak isteyen heyecanını kayıp etmiş öğretmenlerin 3600 ek gösterge verilerek emekliliğinin önü açılmalıdır.

Öğrenci yapısının

- Mesleki eğitim merkezlerine gelecek öğrenci ve kursiyerlere beceri testlere tabi tutularak mesleğe yönlendirilmelidir.
- Mesleki eğitimde yaş sınırı kaldırılmalı öğrenciler/kursiyerler ihtiyaçları olan program yeterlilikleri kazandıklarında sistemin dışına çıkmalarına müsaade edilmelidir.
- Öğrencilerin eğitim sistemine girişte veya üst öğrenime devamlarında yetenekleri becerileri değerlendirilmeli objektif kriterler oluşturulmalıdır.

- Öğrencilerin/kursiyerlerin programlara devamında veya üst eğitim ve öğretime devamlarında alan öğretmenlerin yönlendirmeleri öne çıkarılmalı kurulacak bir komisyon marifetiyle oluşturulmalıdır.

Okul Yapısının

- Meslek eğitim merkezleri şeklinde belirli alanları ve dalları kapsayan bir yapıda kampüsler şeklinde oluşturulmalıdır. Eğitim bölgesi ve sektör istihdam ihtiyaçlarına göre eğitimler verilmelidir.
- Yapılacak merkezlerde alana ait sektörün ihtiyaçlarına cevap verecek yeterlilikleri kazandıracak standart makine teçhizat ve donanımlar sektörle birlikte sağlanmalıdır.
- Bazı programlar için işletmelerin eğitim merkezleri kullanılmalı boya, kimya, asansör, raylı sistemler vb. gibi durumlarda işletmelerle iş birliğinde önü açılmalıdır. Yapılacak ortak program sonucu eğitim alanlar direk işyerine devam etmelidir.
- Merkezlerimizdeki atölye ve laboratuvarlar 7 gün 24 saat eğitim öğretim ve kurs programları için açık olacak şekilde yeniden yapılandırılmalıdır

Program Yapısının

- İş piyasasının ihtiyaçlarını dikkate alan meslek standartlarına ve yeterliliğe dayalı uzmanlar tarafından hazırlanan modüler yapıda geliştirilen programlar oluşturulmalıdır.
- Mesleki eğitimde sınıf geçme sisteminden vazgeçilerek modül geçmeyi esas alan sertifikaya bağlı kazanımları ölçen ve değerlendiren bir yapıda yeniden oluşturulmalıdır.
- Programlar modüler yapıda sisteme giriş ve çıkışlara müsaade eden yapıda oluşturulmalıdır.

Genel şartların ise

- Mesleki eğitim için okul-sanayi iş birliğinin artırılmalıdır.
- Teknik öğretmenlerin işletmeler ile diyalog kurmaları sağlanmalı, işletmede mesleki eğitim verilmelidir (Eğitim bölgesi içerisinde bu eğitimler mahalli yapılmalıdır).
- Mesleki teknik gezilere öncelik verilmeli 10-11 sınıflar sektör hakkında bilgilendirilmeli. Nasıl bir nitelikli elemana ihtiyaç var? Sektör bizlerden ne istiyor sorusu sık sık sorularak gelişmeler takip edilmelidir.
- Alan ve dal yeterliliklerinden ortak olanların üzerine esnek modüller alınarak yeterlilikler zenginleştirilmelidir.
- Rehberlik servisinden mesleki eğitimde okul-aile-sektör iş birliği sağlanmalı okul uygun eğitim vermeli aile çocuğunun okulu bitirince nerede hangi ortamda çalışacağını bilmeli buna yönelik rehberlik çalışmaları yapılabilir.
- İdari yapı yüzünden alanlar birbirinden kopmamalı alanlar arasında iş birliğine gidilerek ortak çalışmalar yapılmalıdır.
- Uygulanabilir projelere destek verilerek ortak alan çalışmaları sağlanmalıdır.
- Eğitim kurum yönetici, öğretmen ve diğer personelin teknolojik gelişmeleri takibi sağlanmalıdır.
- Haftalık ders programları öğrencilerimizin çok yoğun okul içerisinde sosyal faaliyet alanları oluşturulmalı ve kullanıma açık olmalı. Öğrencilerimiz bu alanları günün her saatinde kullanmalıdır.

Tasarlanan Bu Modelle Beklenen Sonuçlar

- Öğretmen ve öğrencilerin eleştirel ve problem çözme becerisine sahip bireyler olarak yetiştirilmesi,
- Hayatın farklı katmaları arasında işbirliği kurma becerisine sahip bireyler yetiştirilmesi,
- Bireylere zihinsel çeviklik ve esneklik kazandırılması,
- Bireylere inisiyatif alma ve girişimcilik becerilerinin kazandırılması,
- Sözlü ve yazılı iletişim becerilerinin kazandırılması,
- Bilgiye ulaşma ve ulaşılan bilginin işleme becerisinin bireylere kazandırılması,
- Meraklanma ve hayal kurma becerilerinin bireyler kazandırılması,
- Okul-sektör işbirliği bilen ve uygulayan bireyler yetiştirilmesi,
- Disiplinler arası ve alanlar arası programlara olan taleplerin artması,
- Mesleki yeterlilik ve standartların bir zorunluluk haline getirilmesi,
- Nitelikli iş gücü yetiştirilmesi ile sektörde rekabetin artacak olması,
- Türkiye'nin katma değeri yüksek ihracatı destekleyen gelecek vizyonununa uygun bireyler yetiştirilmesi,
- Eğitimde çağın gerekleri ve dünyayla uyumlu yeni bir modelin tasarımı amaçlanmıştır.

Kaynakça

- [1] ANONYMOUS. Türkiye'de Mesleki Teknik Eğitimde Gelişmeler, MEB Yayınları, (1991)
- [2] R. Kılıç, Mesleki ve teknik eğitimin yeniden yapılandırılmasında modüler yaklaşım, Teknik Eğitim Dergisi, s. 17, (1998)
- [3] A. Mahiroğlu Teknik Eğitim Fakültesi Mezunlarını İzleme Araştırması, METARGEM Yayınları, (1996).
- [4] Yeni öğretmen yetiştirme düzeni, 1. Mesleki Teknik Eğitim Sempozyumu, Karabük Teknik Eğitim Fakültesi, s. 461,(1998).
- [5] L. Mcfarland, ve M. Vickers, The Context and Rationale for the Reform of Vocational and Technical Education, In Vocational and Training for Youth Towards Coherent Policy and Practice, pp 7-18, OECD, (1997)
- [6] T. Tayan Meslek Liseleri Ö.S.Y.S. Kılavuzu, Ankara (1996)
- [7] A. Karabulut, M. Marul, Mesleki ve Teknik eğitim Modeli Tasarımı, milli eğitim Dergisi sayı 194 (2011)

AN INVESTIGATION ON THE DIFFUSION BONDING ABILITY OF B₄C-Fe-Ni CERAMIC-METAL COMPOSITES

A. YONETKEN*, A. EROL

* Afyon Kocatepe University, Faculty of Engineering, Afyonkarahisar/Turkey,
yonetken@aku.edu.tr

Afyon Kocatepe University, Faculty of Technology, Afyonkarahisar/Turkey,
aerol@aku.edu.tr,

Abstract

In this study, composites produced from Ni coated B₄C-Fe powders, (B₄C-Fe)Ni, were used to form (B₄C-Fe)Ni/Cu and (B₄C-Fe)Ni/AISI 316 Stainless steel diffusion couples using preloaded compression system under Ar atmosphere. Diffusion bonding was carried out by varying bonding 2.5MPa pressure and 735°C temperature. 30 min. while kept under Ar. atmosphere. Shimadzu 100kN universal tensile machine was employed to test diffusion couples and compression test results showed that (B₄C-Fe)Ni/Cu diffusion couples yielded the best results of 14,3MPa compared to other diffusion couples. Hardness values ranging from 200 to 300HV were also obtained from surface measurements. Standard metallographic techniques and SEM were used to characterize the particles along the bondline as well as microstructural features.

Keywords: Diffusion Bonding, Mechanical Specification, Powder Metallurgy, Electroless Nickel Plating, Different Materials.

1. Introduction

Particles produced by using powder metallurgy method are usually brought into use without any additional processing. Yet, machine operation and bonding should be applied if necessary. Therefore, studies have focused on the machine ability and bonding capability of P/M particles under different processing conditions in recent years.

Diffusion bonding is solid state bonding formed by controlled diffusion by applying heat and pressure for a certain period of time with the minimum of macroscopic deformation between mating surfaces under relevant atmosphere protection [1,2,3]. Due to the above mentioned characteristics of diffusion bonding method, it is more widely used in material couples where bonding of different material couples through traditional methods is problematical. This method was developed for airplane and space industry and nuclear technology. It is possible to reach the strength of values of the actual material approximately in the diffusion bonding of the same

material couples [4]. Materials that form a phase between brittle metals, materials that have various melting temperatures and elastic limits, metal and non-metal materials can be bonded via this method [5-7].

Diffusion event, which is defined as displacement among solid, liquid and gaseous phases due to heat effect, stems from the stabilization of kinetic energies arising from thermal movements and the reduction in the regional density of the differences. In diffusion event, it is possible to displace such elements as atoms, molecules, atom groups or electrons at various amounts. However, different displacement rates may lead to volume changes in certain areas around the reaction centre [12].

The factors that affect the bonding capability of P/M particles are closely related to the own characteristics of the production method. The most significant characteristic that affects the bonding capability of P/M particles is the existence of pores [9-10].

In this study, electroless nickel plated B_4C -Fe powders, were bonded after sintering to material couples of composite $(B_4C-Fe)Ni/Cu$ and $(B_4C-Fe)Ni/AISI 316$ Stainless steel produced under the same conditions at optimum bonding parameters and their microstructure and mechanical specifications, were examined.

2. EXPERIMENTAL PROCEDURE

2.1. Materials Used in the Experiments

In this study, B_4C -Fe powder at 99% purity with a size of 20 micron was used. Ceramic metal composite was produced by electroless nickel plating of B_4C -Fe powders and sintering them at $1100^\circ C$. Two different material groups were used in the experiments. 1st Group was $(B_4C-Fe)Ni/Cu$ ceramic metal composite, 2nd Group material was $(B_4C-Fe)Ni/AISI 316$

These composites, which were sintered after being coated with Ni, were compressed with 2.5MPa pressure and $735^\circ C$ temperature. 30 min. during diffusion bonding process at a temperature below melting temperature and their bonding was performed in a tube oven under argon atmosphere.

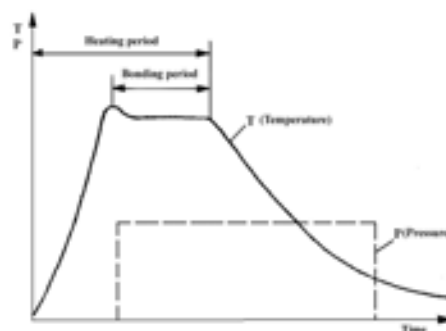


Figure 1. Diagram of Temperature, Pressure and Time in Diffusion Bonding

The samples bonded with diffusion bonding unit are shown in Figure 2. The samples were bonded by means of the mechanism by controlling the deformation rate of the pressure on the material.

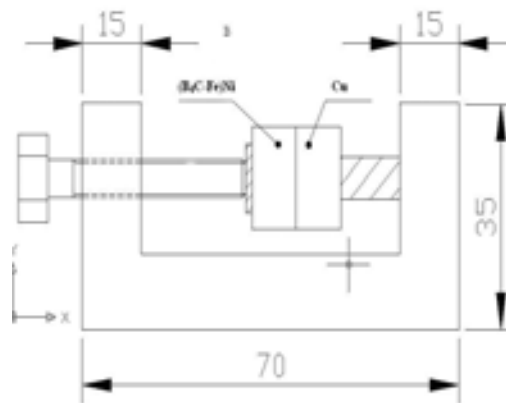


Figure 2. Diffusion bonding unit where the samples were combined with screw system

The test samples prepared in accordance with the cross-sectional areas given in Table 1 were placed within the compression device in vertical position. The plastic deformation amounts of the test samples under gradually increased compression loads were determined. Compression load reached the maximum load value that the samples could withstand and then fell down, and there occurred a crack on the material from which P/M. was produced due to a visible deformation along the height of the sample. Stress-Form change graphics were presented. So, it was determined that visible cracks without fracture on the bonding spots of the various diffusion bonded material couples were to occur unavoidably on the sample produced with P/M. method.

Table 1. Sample sizes of Compression Experiment

Samples	Thickn ess (mm)	Width (mm)	Heigh t (mm)
(B ₄ C- Fe)Ni/Cu	10	10	15
(B ₄ C- Fe)Ni/AISI 316	10	10	15

As can be seen in Table 2, (B₄C-Fe)Ni/Cu and (B₄C-Fe)Ni/AISI 316 composite materials that we prepared in compliance with (B₄C-Fe)Ni samples of 10mm square prism were compressed under appropriate load in the clamp designed in accordance with the values given in table below. Diffusion bonding was conducted according to the experimental conditions in the tube oven under argon atmosphere. The samples were left to natural cool down in the oven after bonding process.

Table 2. Parameters applied to samples in the diffusion bonding experiment

Sample name	Temperatur e °C	Pressure(MPa)	Time(min)
(B ₄ C-Fe)Ni/Cu	735	2.5	30
(B ₄ C-Fe)Ni/AISI 316	735	2.5	30

The shear tests were carried out with shear testing apparatus shown in Figure 3 which was prepared specially in order to establish the shear strength of the samples after bonding. The surfaces of the samples were sanded with abrasives of 1000 meshes to determine the metallographic structures of the samples, the diffusion bondings of which were performed. At the end of the tests, the microstructures of the samples were examined by optical microscopy, SEM and EDX.

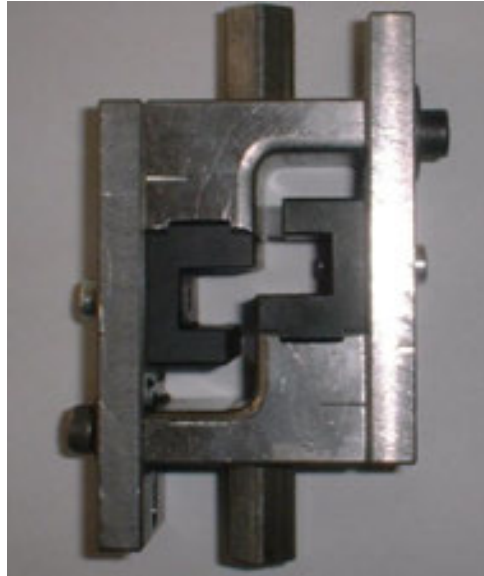


Figure 3. Shear test sample apparatus

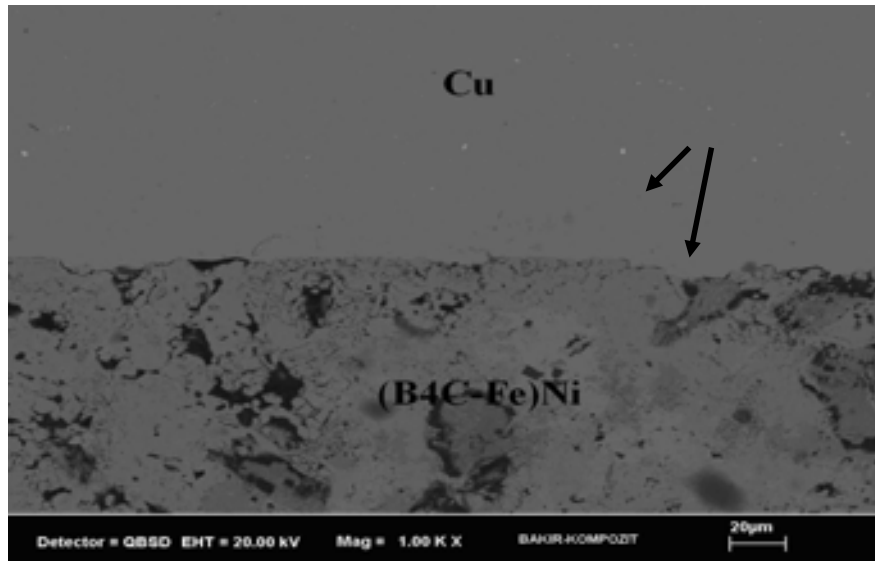
2. Results and Discussion

The shear stress values of the samples were given in Table 3. The highest shear stress was observed in (B₄C-Fe)Ni/Cu couple as 14.3Mpa.

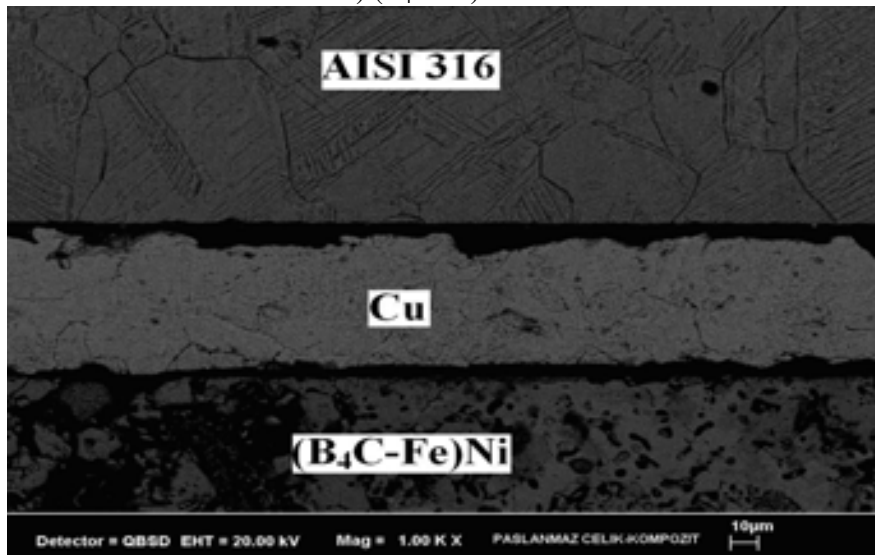
Table 3 Shear-Stress values

Material Couple	Temperature °C	Time(min)	Shear Strength (Mpa)
(B ₄ C-Fe)Ni/Cu	735	30	14,3
(B ₄ C-Fe)Ni/AISI 316	735	30	10,4

SEM photographs taken from the bonding spots of the diffusion bonded samples were examined. The bonding line can be clearly observed in the photographs (See Figure 5).



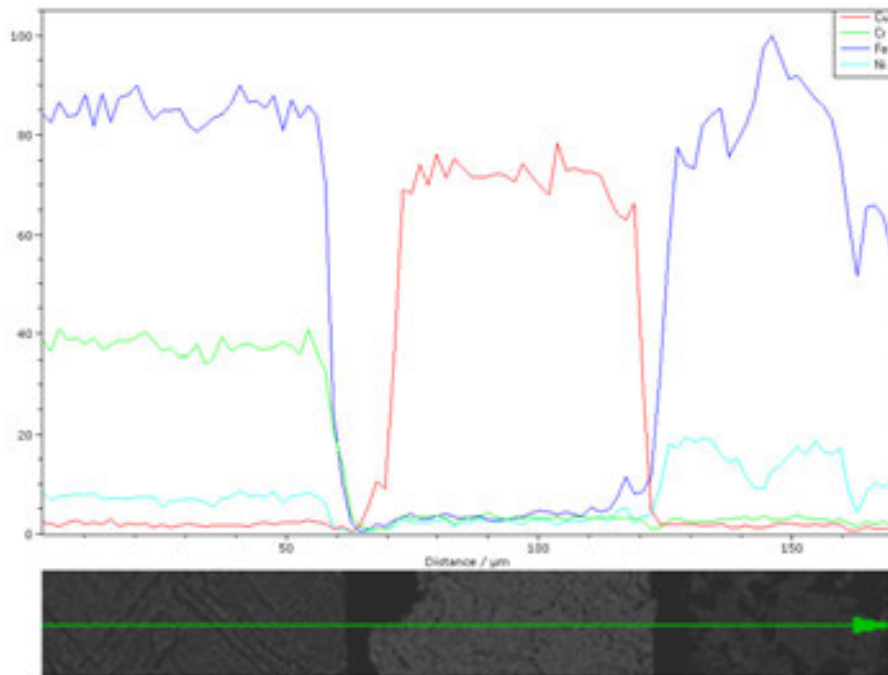
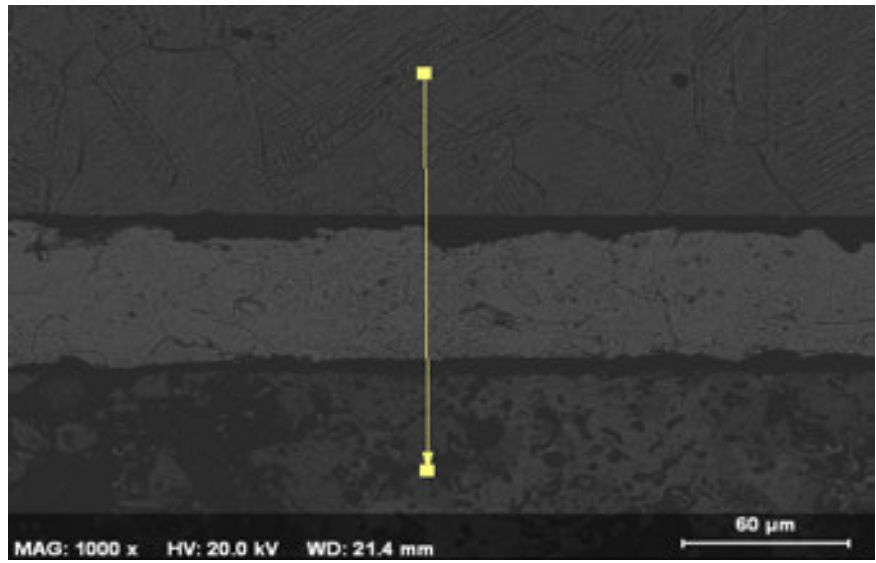
a) (B₄C-Fe)Ni/Cu



b) (B₄C-Fe)Ni/AISI 316

Figure 4 The SEM 1kX photographs showing the bonding spots of the composite produced by (B₄C-Fe)Ni/Cu and (B₄C-Fe)Ni/AISI 316.

The EDX line analysis 1kX photographs showing the bonding spots of the composite produced by (B₄C-Fe)Ni/Cu/AISI 316. Linear EDX analysis was applied to the diffusion source region. While the steel peak in the steel-copper transition zone decreased, the copper peak increased. The copper-composite transition region increased copper while the composite peak increased. It is understood that the different types of materials in which the diffusion event takes place combine with the diffusion source.



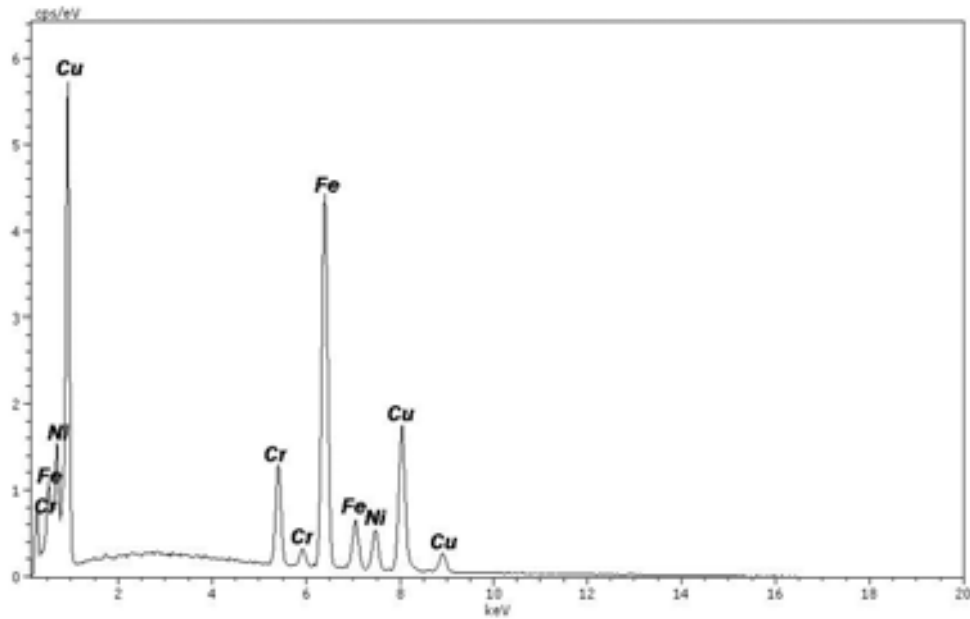
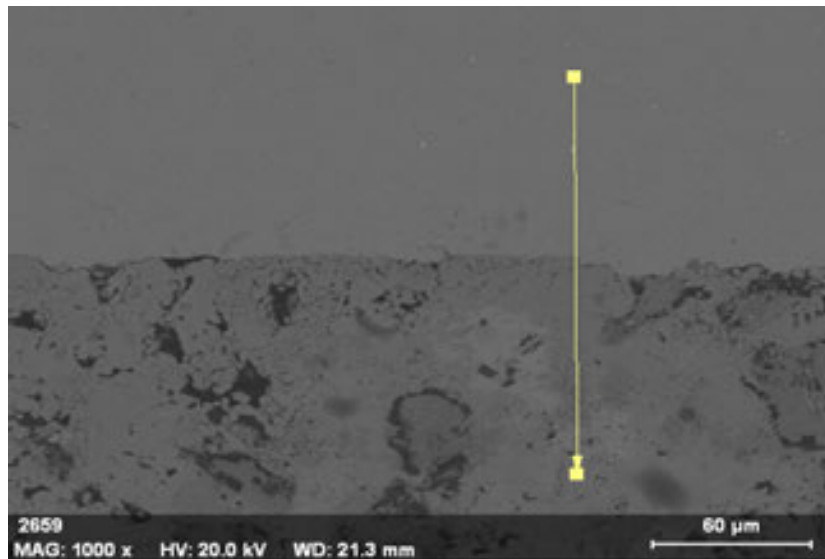


Figure 5 The EDX line analysis 1kX photographs showing the bonding spots of the composite produced by (B₄C-Fe)Ni/Cu/AISI 316.

Linear EDX analysis was applied to the diffusion source region. While the composite peak in the composite-copper transition zone decreased, the copper peak increased. It is understood that the different types of materials in which the diffusion event takes place combine with the diffusion source(Fig.6). The elemental analysis showed that Cu, Fe and Ni peaks were determined.



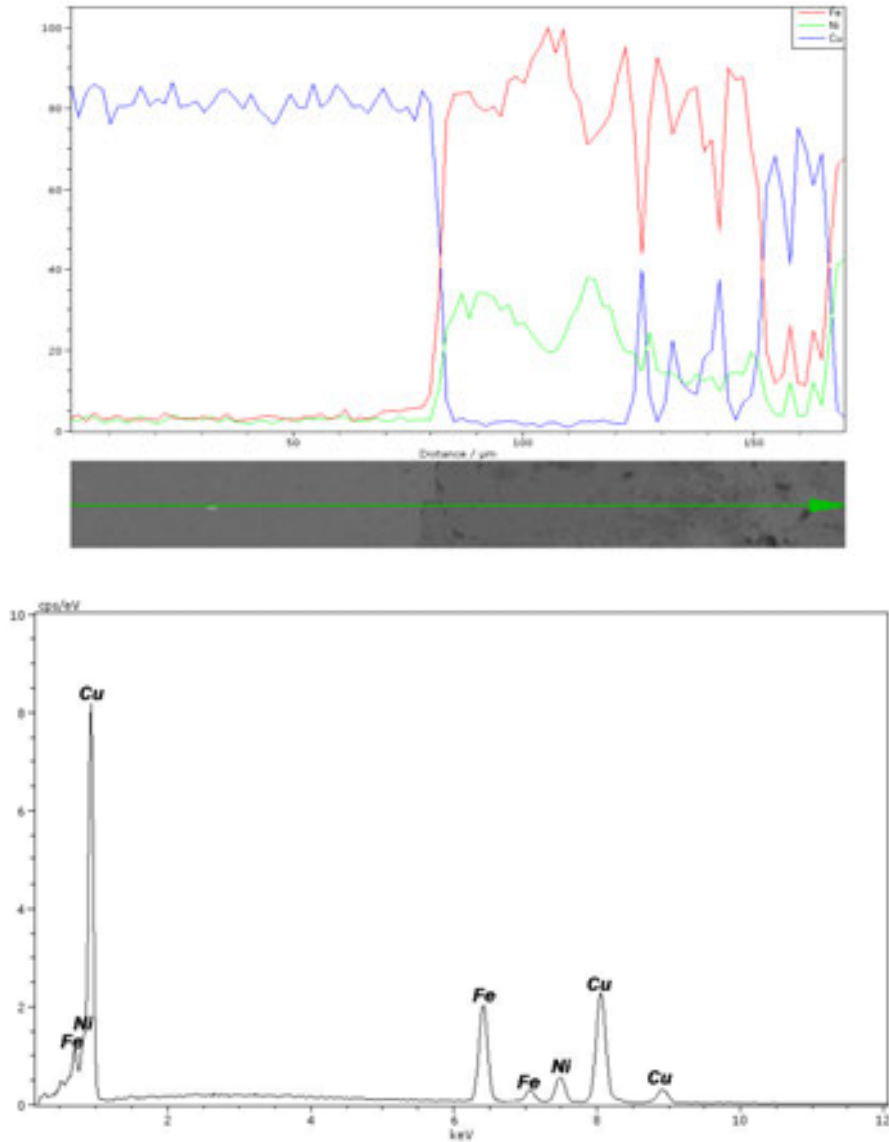


Figure 6 The EDX line analysis 1kX photographs showing the bonding spots of the composite produced by $(B_4C-Fe)Ni/Cu$.

As can be seen in Table 4, $(B_4C-Fe)Ni/Cu$ and $(B_4C-Fe)Ni/AISI\ 316$ composite materials Maximum strength of the samples in accordance with the values given in table below.

Table 4. Maximum strength of the samples

Sample name	B_{max} MPa	Max stretching	%
$(B_4C-Fe)Ni/Cu$	16,34	32,145	
$(B_4C-Fe)Ni/AISI\ 316$	9,64	23,654	

4. Conclusions

Our production composite sample containing B₄C-Fe 30% Ni by weight was bonded to the sample itself by using diffusion bonding method. When analysed the microstructures of bonding, neither grain growth nor change in microhardness was observed in the interface.

While the microhardness in the interface had a higher value when again the same composite sample containing 70% WC and 30% Ni by weight was bonded WC(Ni) using diffusion bonding method, the hardness values in the heat influence area were observed to decline towards the main material.

When examined the structure in the interface, the hardness values were observed to increase due to the reduction of the voids among the grains (See Figure 4). The microstructure in the interface was thought to occur due to the pressure applied during diffusion bonding.

.

5. REFERENCES

- [1]Anık, Selahattin., Technics of Welding, (Birsen Publication, 1996)
- [2]Technology of Welding. (Gedik Education Publication) sf. 320-336
- [3] Kaynak Teknolojisi 2. Symposium (M.M.O.1999), sf.21-226
- [4]Mühendis “Machine magazine” (M.M.O.1994), Kaynak Özel Sayısı
- [5]Çelik,S., Ay, İ., 1996, ‘Koruyucu gaz altında difüzyon kaynağı ve uygulaması’ J. Of engineering and environmental Science, 163-70
- [6]Ay, İ., Çelik, S., Çelik, İ., 2000, ‘Bars of Aluminium and Cu abrassive difussion welding properties of compare’ 8. Denizli Malzeme sempozyumu, 264-273
- [7]Varol, R., Tunay, R. Fatih., Tüfekçi, K., ‘Toz Metal (T/M) Parçaların Elektron Işın Kaynağı İle Birleştirilmesi
- [8]Kurt, A., v.d., (1996), Powders of Pure ferrit pressed P/M particle Low Carbon of Stainless MIG Welding with investigation of welding 1. National Powder Metallurgy Conference, Bildiri Kitabı s. 595-602, G.Ü., Ankara.
- [9]Ratzi, R., et al., (1997), Joining of PM Stell and Conventional Steel by Laser Welding, Euro PM 97, Proce. Of Advance Structural PM Component Production, pp. 158-164, October 15-17, Munich, Germany.
- [10]Kurt, A., et al., (1997), Investigation of Diffusion Welding Parameters for Welding of PM Bronze to a Mild Steel, PM 97, Proce. Of Advance Structural PM Component Production, pp. 219-227, October 15-17, Munich, Germany.
- [11]Gültekin, N., (1991), Welding Technics., Ergin Ofset, İstanbul.
- [12]Ozcan, Ç., 2001 ‘Investigation of Welding Methods Used in Ship Construction’ Marmara Üniv., Makine Müh. İstanbul.

INFLUENCE OF DYNAMIC STRAIN AGEING ON MICROSTRUCTURAL AND MECHANICAL PROPERTIES OF AISI 316L AUSTENITIC STAINLESS STEEL WELD METAL

Abstract

In this paper, dynamic strain ageing (DSA) behaviour in weld metal of 316L austenitic stainless steel (ASS) is presented. Welding process was conducted using the MIG welding technique. Tensile test was performed on weld metal at $1 \times 10^{-3} \text{ s}^{-1}$ strain rate for the temperatures of 25-800°C to determine the influence of DSA on the microstructure and strength of investigated material. The change in mechanical properties was more noticeable at ageing temperature of 500°C and 600°C in which the weld metal showed serrated behavior. Optic and scanning electron microscopes (SEM) were used to analyse the microstructure and fracture surfaces of tested samples. Weld metal of 316L ASS showed DSA behavior which are examined in terms of microstructure and mechanical properties. Analysis of the results indicated that locking of the mobile dislocations by substitutional and interstitial atoms is responsible for the occurrence of DSA in 316L ASS.

Key Words: Stainless steel, Dynamic strain ageing, Welding, Weld metal.

1. Introduction

Stainless steels consisted of five main groups; ferritic, austenitic, martensitic, duplex and precipitation hardening. ASS among them are widely used in many engineering applications from cryogenic temperatures to the high temperatures. They contain Cr and N both of which increase the corrosion resistance. These steels present excellent combination of corrosion resistance, ductility, toughness and weldability [1]. 316 ASS and its modified grades such as 316L(N) have been used as structural material in nuclear power plants, heat exchangers and pipelines. This alloy shows excellent high temperature mechanical properties with good toughness and machinability. Most of the service failures occurs either in the HAZ or in the weld metal. High temperature mechanical properties of 316 and 316L(N) ASS welds and weld joints has received considerable attention in recent years [2,3]. A serious drawback to using such steels and their weldments is the degradation of corrosion and mechanical properties within certain high temperature due to the microstructural changes [4].

All welding operations involve a heat source that causes primary melting. Subsequent solidification should lead to the formation of an integral joint. Much of the heat is spread from the fusion zone to the adjacent solid zones. However the combined effect of heating and residual stress can cause dynamic strain ageing to occur [5]. DSA is an atomic scale phenomenon that involves the mobility of solute atoms and mobile dislocations, or both. It is considered to contribute to embrittlement by effectively increasing the dislocation density for a given strain. A high dislocation density, the fact that many dislocations will be pinned by interstitial atoms and that bowed dislocations need higher stresses for unpinning, mean that the local yield stress in the region will be higher, the phenomenon is commonly known as DSA [6]. DSA is associated with serrations on the stress-strain curve during a tensile test at the loaded strain rate. Each stress drop on the stress-strain curve corresponds to the formation of a band. The formation of these

different types of bands depends on external parameters (temperature, strain rate and strain level) and internal parameters (alloy composition, type and content of solute atoms and density of mobile dislocations) [7].

While certain aspects of DSA [8,9] of 316L ASS at temperature range of 200-800°C have been addressed, no information on DSA behaviour of weld metal at low and intermediate temperature is available in the open literature. For this reason, it is necessary to analyse the influence of DSA on mechanical properties of ASS weld metal at higher temperatures. The present work is concern with an investigation of the effect of DSA on the tensile behaviour of 316L ASS weld metal. An examination of microstructural changes depending on testing temperatures was conducted with a view to understanding the features which can affect the mechanical properties of 316L ASS aged at elevated temperatures.

2. Experimental

In the present experimental work, 316L ASS and a welding wire (AS MIG 316LSi) with a diameter of 1.2 mm were used. Table 1 shows the steel and welding wire compositions by wt. % which are used for joining. Steel was obtained as plates in the form of 350x150x8 mm. The steel plates were welded longitudinally under argon gas using Fanuc Robotic Lincoln Electric brand MIG welding machine with a single pass through an V-groove configuration at 30°. Welding parameters used in the present experimental work are given in Table 2.

Table 1. Chemical compositions of 316L austenitic stainless steel and welding wire (wt. %).

Materials	C	Si	Mn	Ni	Cr	Mo	N	S	P
316L	0.024	0.38	1.30	10.10	16.57	2.03	0.041	0.004	0.029
Welding wire	0.03	0.85	1.70	12.5	18.5	2.75	-	0.003	0.0025

Table 2. The welding parameters used in the gas metal arc welding (GMAW).

Current (A)	Voltage (V)	Welding Speed (cm/min)	Gas Flow Rate (lt/min)	Heat Input (kj/mm)
240	23	35	14	0.95

Tensile test specimens were cut from the weld metal and manufactured according to standart E8 (5 mm diameter and 30 mm gauge length). Figure 1 shows welded steel plates, weld metal cut tensile plane and machined tensile test specimen. Tensile tests were performed at 1×10^{-3} strain rate and temperatures of 25-800°C. After each test, stress and strain diagrams were obtained to derive yield strength (YS, 0.2%), ultimate tensile strength (UTS), elongation (%) and workhardening index (n).

Microstructure and fracture surface analyses of weld metal were done by using optic microscope, SEM and EDS analyzer. A mixture of 1 % nitric acid, 10 % oxalic acid and 89 % distilled water solution was used for elctrolytic etching at a potential of 15-20 V to observe microstructure of samples.

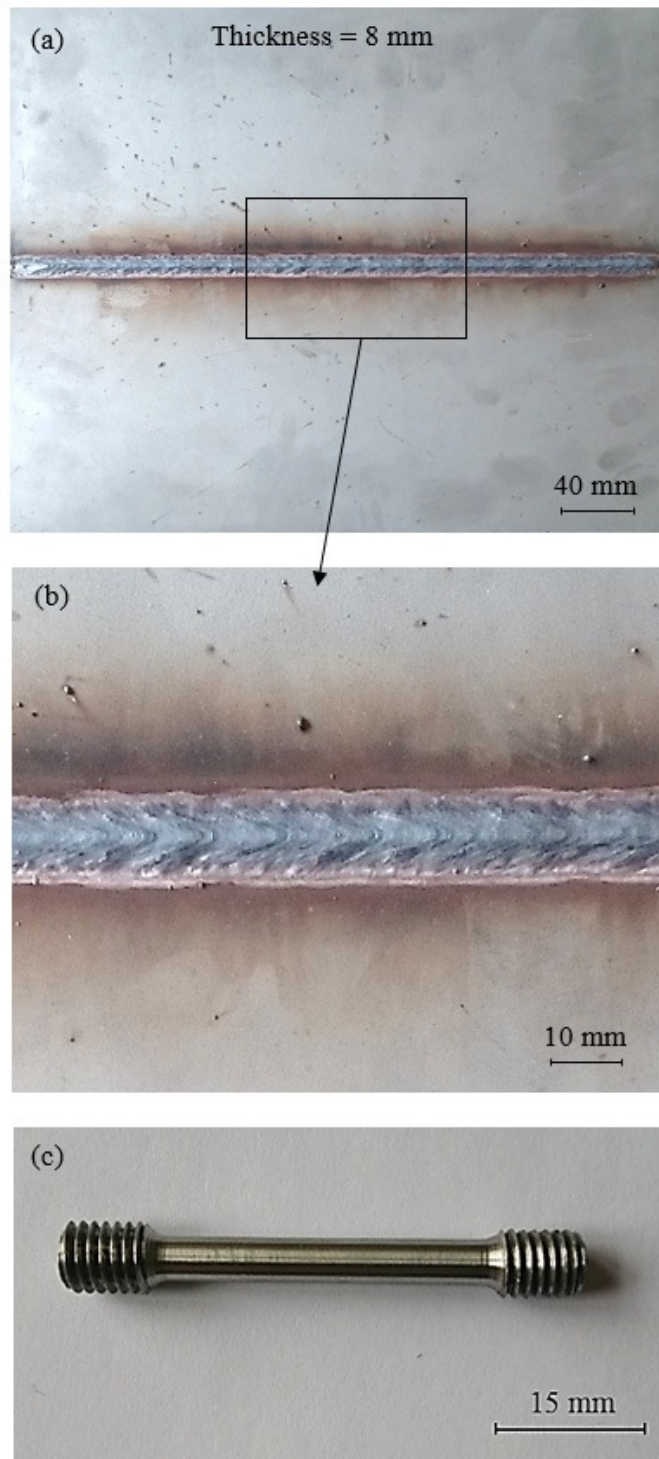


Figure 1. (a) Welded steel plates, (b) weld metal cut tensile plane and (c) tensile test specimen.

3. Results and Discussion

3.1. Microstructure

Figure 2a shows as-received metal microstructures of 316L ASS steel. As can be seen, the 316L ASS as-received metal is characterized by equiaxed austenite grains with a low delta ferrite which is more resistance to cracking compared to the a fully austenitic microstructure [10]. Weld metal microstructure obtained from 316L ASS steel tested at 25°C is also seen in Figure 2b. During the welding process, a solidification microstructure consisting of skeletal ferrite in large columnar austenite grains was observed in weld metal. The alignment of ferrite is along the heat flow direction due to incomplete primary $\delta \rightarrow \gamma$ transformation [11, 12]. The rapid cooling of the weld pool during welding process causes the formation of ferrite in the weld metal. Ferrite phase in weld metal increased due to rapid cooling after welding which prevented austenite phase transformation. This is consistent with earlier studies [13, 14]. Samples tested at 100-800°C showed similar weld metal microstructure consisted of austenite grains with skeletal ferrite.

In many applications, the ability to control the delta-ferrite content of stainless steel weld metal is important. For example, the ferrite number (FN) is often used as an indicator of the resistance to fissuring (hot tearing) that occurs in many of the 300-series stainless steels. Delta ferrite, rich in Cr and Mo, occurred during the welding of ASS is required up to a limit of about 4–5 ferrite number (FN) to prevent microfissuring or hot tearing of the weld metal [15].

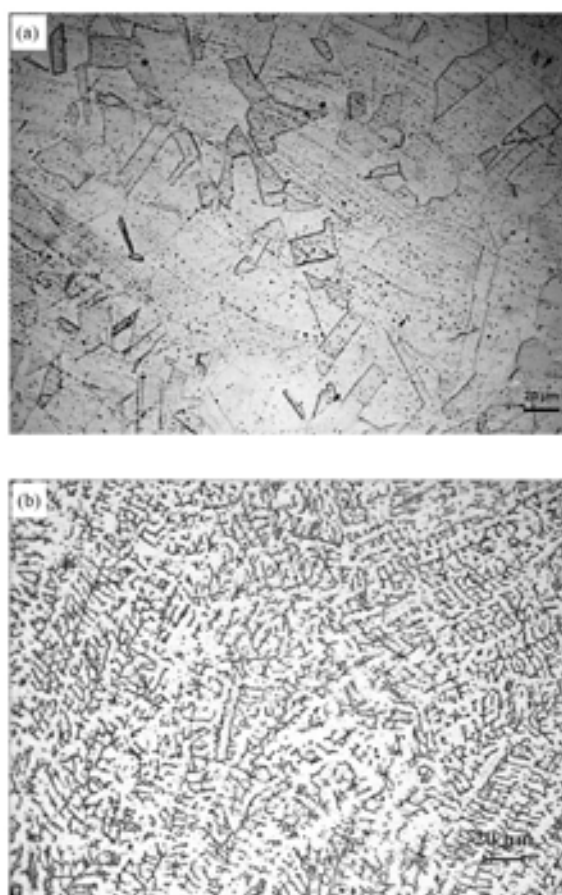
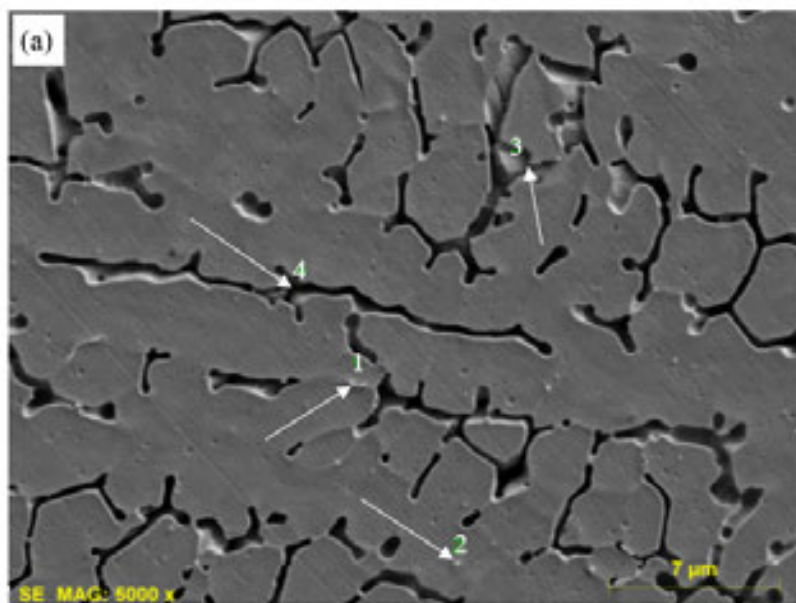


Figure 2. Optical micrographs of (a) as-received sample and (b) weld metal tested at 25°C.

Figure 3 shows detailed SEM micrograph and EDS analyses of 316L ASS weld metal tested at 400°C. As it is seen, the weld metal consisted of skeletal ferrite in austenitic matrix with some carbides which were distributed in the austenite matrix (Figure 3a). It was reported that the precipitation of carbides such as $M_{23}C_6$, MC , M_6C and M_7C_3 ($M = Cr, Mo$ and Fe) occurs in ASS during heat treatment and welding. The precipitation of carbides which depends the temperature and carbon content reduces corrosion resistance of stainless steel. The temperature in the range from 550 to 900°C allows chromium to diffuse away from the grain boundaries and to form carbides [12, 16-18]. Figure 3b also shows EDS analysis with the points 1-4 on the samples tested at 400°C. Points 1-3 contain Mo, Cr and C which indicated that $Cr_{23}C_6$ and Mo_6C precipitate particles occurred in the weld metal during cooling after welding. Point 4 taken from ferrite phase also contains higher Cr.



Mass percent (%)										(b)
Spectrum	C	N	Al	Si	Ti	V	Cr	Mn	Fe	Mo
1	5.00	1.09	0.00	0.77	0.00	0.00	17.76	2.24	71.40	1.73
2	4.89	1.27	0.00	0.87	0.00	0.81	17.28	2.38	70.66	1.84
3	3.31	0.09	0.00	0.94	0.40	0.00	19.90	2.21	71.47	1.68
4	0.72	0.00	0.26	0.39	0.24	1.31	20.36	5.38	69.91	1.42
Mean value:	3.48	0.61	0.07	0.74	0.16	0.53	18.83	3.05	70.86	1.67
Sigma:	1.99	0.66	0.13	0.24	0.19	0.65	1.53	1.55	0.73	0.18
Sigma mean:	1.00	0.33	0.07	0.12	0.10	0.32	0.77	0.78	0.37	0.09

Figure 3. (a) SEM micrograph of 316L ASS weld metal after testing at 400°C and (b)EDS analysis from indicated points.

The precipitation of the sigma phase, which is often observed in various series of stainless steels, is one of the main reasons for the deterioration of stainless steels' properties, for example, mechanical property, corrosion resistance, and weldability [19]. Sigma phase which is a tetragonal crystal structure forms in the Fe-Cr system at temperatures of 550-900°C. The presence of sigma phase in the matrix can increase the hardness and decrease the toughness, as well as the elongation of steel [20]. In the present work, the presence of sigma phase in the weld metal after testing in the temperature range of 100-800°C was not observed (Fig. 3). It is thought that tensile testing time at elevated temperatures was not enough for precipitation of sigma phase. The sigma phase was a second phase of a rich substitutional element. The diffusion of the substitutional element was very slow in austenite so that the nucleation of the sigma phase in austenite was difficult [16].

3.2. Mechanical Properties

DSA results of weld metal are seen in Table 3 which gives YS (0.2%), UTS and elongation (%) of samples tested at 25-800°C. As seen from Table 3 that weld metal showed small differences in YS and UTS up to 600°C, but it revealed drastic change when the test temperature was increased beyond 600°C. A decrease in elongation (%) values of weld metal was observed up to 600°C. A further increase in test temperature of 700°C or 800°C increased the elongation (%). This indicates that weld metal of 316L ASS is susceptible to DSA up to 600°C. This is due to the presence of free C and N atoms in solution. The diffusion of solute atoms to dislocations will prevent the movement of the dislocations resulted in higher strength and lower ductility in steel [21].

Table 3. Mechanical properties of weld metal tested at temperatures of 200-800°C.

Test Temperatures (°C)	Yield Strength (0.2%, MPa)	Tensile Strength (MPa)	Elongation (%)
25	395	659	57
100	349	559	37
200	407	543	31
300	389	505	20
400	396	521	24
500	336	485	25
600	307	423	22
700	190	295	37
800	153	184	81

Heating and cooling rates in fusion welding are usually high and the heated metal subject to plastic strain during cooling. For this reason, fast cooling after welding does not allow full precipitation of carbides and nitrides. This resulted in an increase in the amount of uncombined C and N in solution in the weld metal which can cause DSA to occur. DSA is considered to contribute to higher strength in weld metal by effectively increasing the dislocation density for a given strain. A high dislocation density, the fact that many dislocations will be pinned by solute atoms and that bowed dislocations need higher stresses for unpinning, mean that strength in the weld metal will be higher [22, 23].

Workhardening index (n) which is used to determine the occurrence of DSA was evaluated according to the following Holloman equation [24] for weld metal.

$$\sigma = K\varepsilon^n \quad (1)$$

where σ is the true stress, ϵ is the true strain, n is the workhardening index, and K is the strength coefficient. The evaluated n values following equation 1 as a function of hot tensile test temperatures are seen in Figure 4. As can be seen, workhardening index increased in the temperature range of 400-600°C for weld metal. This shows the interaction between dislocations and interstitial solute atoms affecting the workhardening of 316L ASS weld metal. The increased workhardening index and increased tensile strength are believed to arise from greater than normal dislocation densities in steels that exhibit DSA. These high dislocation densities occur due to the pinning, which requires fresh dislocations to maintain the applied strain rate. Tensile testing at 400-600°C results in a stronger interaction between solute atoms and dislocation which increased the work hardening of a material, since the deformation at 400-600°C can produce greater number of dislocations due to interaction dislocations and interstitial solute atoms (C and N) contributed to stronger work hardening [25]. Kaçar and Gündüz [26] showed that the activation energy for strain ageing in AISI 430 ASS is bigger than plain carbon steel. For this reason, the weld metal of 316L ASS did not exhibit any yielding behaviour, because Cr decreases the C diffusion to dislocations at lower temperatures.

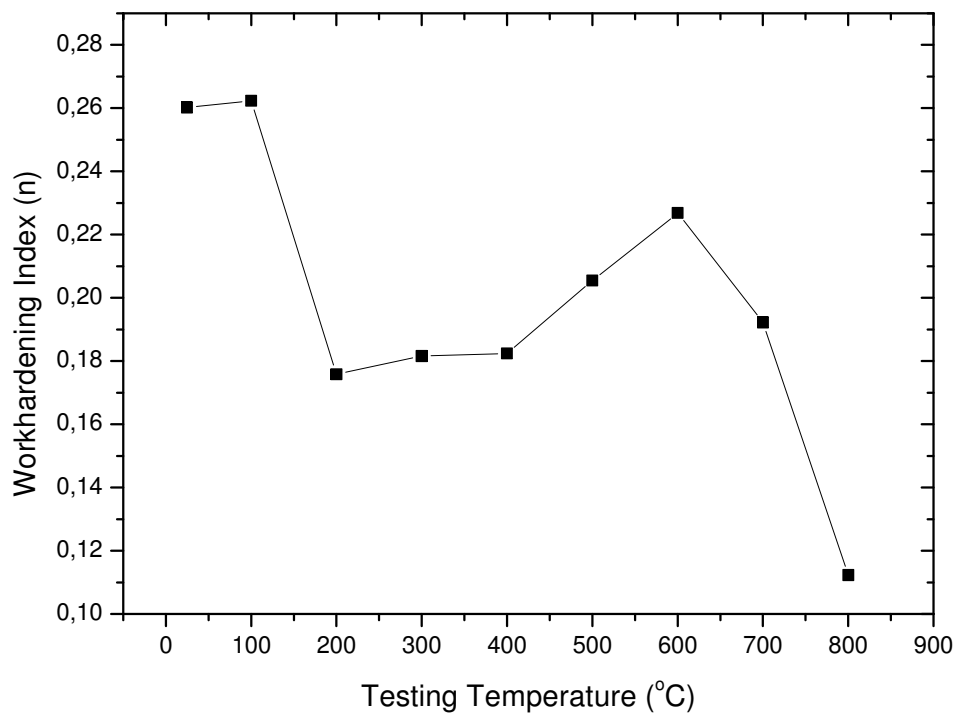


Figure 4. Workhardening index (n) values of the weld metal tested at different temperatures.

This is also confirmed in Figure 5 which shows YS values of weld metal at different testing temperatures. As can be seen, YS values of weld metal revealed a decrease when the testing temperature is increased to 100°C. YS then increased with rising temperature and reached a maximum at 400°C. This indicated the interaction between C and/or N with dislocation which prevented dislocation movement. YS values changed drastically above 600°C. This also shows that DSA is operative in weld metal at the test temperatures of 25-800°C. It is proposed that DSA occurs when the dislocations are temporarily held up at local obstacles in the glide plane [27].

When this work has been carried out, same authors were published a paper investigating DSA phenomena in 316L ASS under as-received and as-welded conditions. It was observed that as-

welded samples revealed lower values in elongation (%) but higher values in YS and UTS than the as-received samples at the temperatures of 25–800 °C. This showed that as-welded samples are more effected by DSA than the as-received samples. More detailed experimental results for the DSA behaviour of 316L ASS are available elsewhere [28]. However, the results obtained from the present study showed that weld metal is more susceptible to DSA than the as-received and as-welded samples with evidence more increase in strength but decrease in elongation (%) at the testing temperatures of 25-800 °C. This is due to the presence of higher Cr content in weld metal compared to that of as-received samples, because weld wire Cr content is about 18.5 wt. % which is higher than as-received samples. It is generally accepted that the elevated Cr content of the weld metal increases the strength of the steel [10, 29]. Higher strength of weld metal could also be due to heat input during welding, melting and solidification of the area as suggested by Lippold and Kotecki [30] who investigated welding metallurgy and weldability of stainless steel.

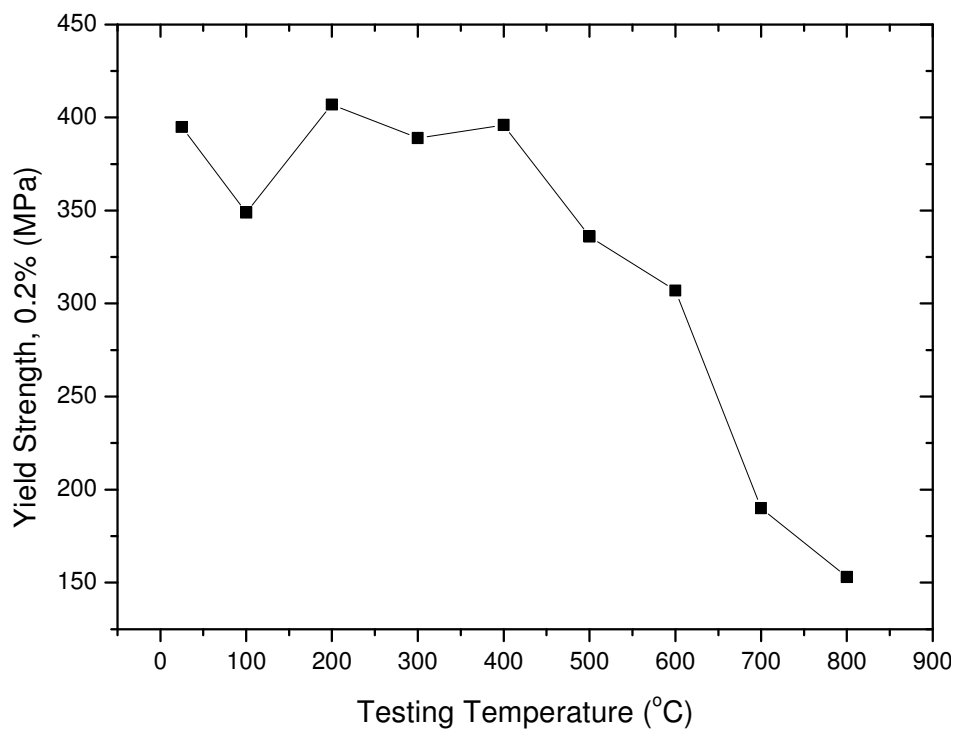


Figure 5. Yield strength values of the weld metal tested at different temperatures.

Stress and strain diagrams of weld metal tensile tested at temperatures of 25-800°C are seen in Figure 6. As is seen, stress and strain diagrams revealed serrated behaviour when the testing temperatures increased at a strain rate of $1 \times 10^{-3} \text{ s}^{-1}$. Serrated behavior which is the manifestation of DSA was observed during tensile testing at 500°C and 600°C. The serrations disappeared from the curves when the samples were tested at 700°C or 800°C. Such serrated behaviour occurs when the dislocations and solute atoms interact which may become an important controlling factor for strengthening. The interaction between dislocations and solute atoms causes the appearance of serrations on the curve, an increase in tensile strength and strain hardening, but a decrease in ductility. DSA will occur when the interstitial atoms diffuse and pin the dislocations. As a result of this, serrations occur because of rapid generation of new dislocations which are needed to sustain flow [31].

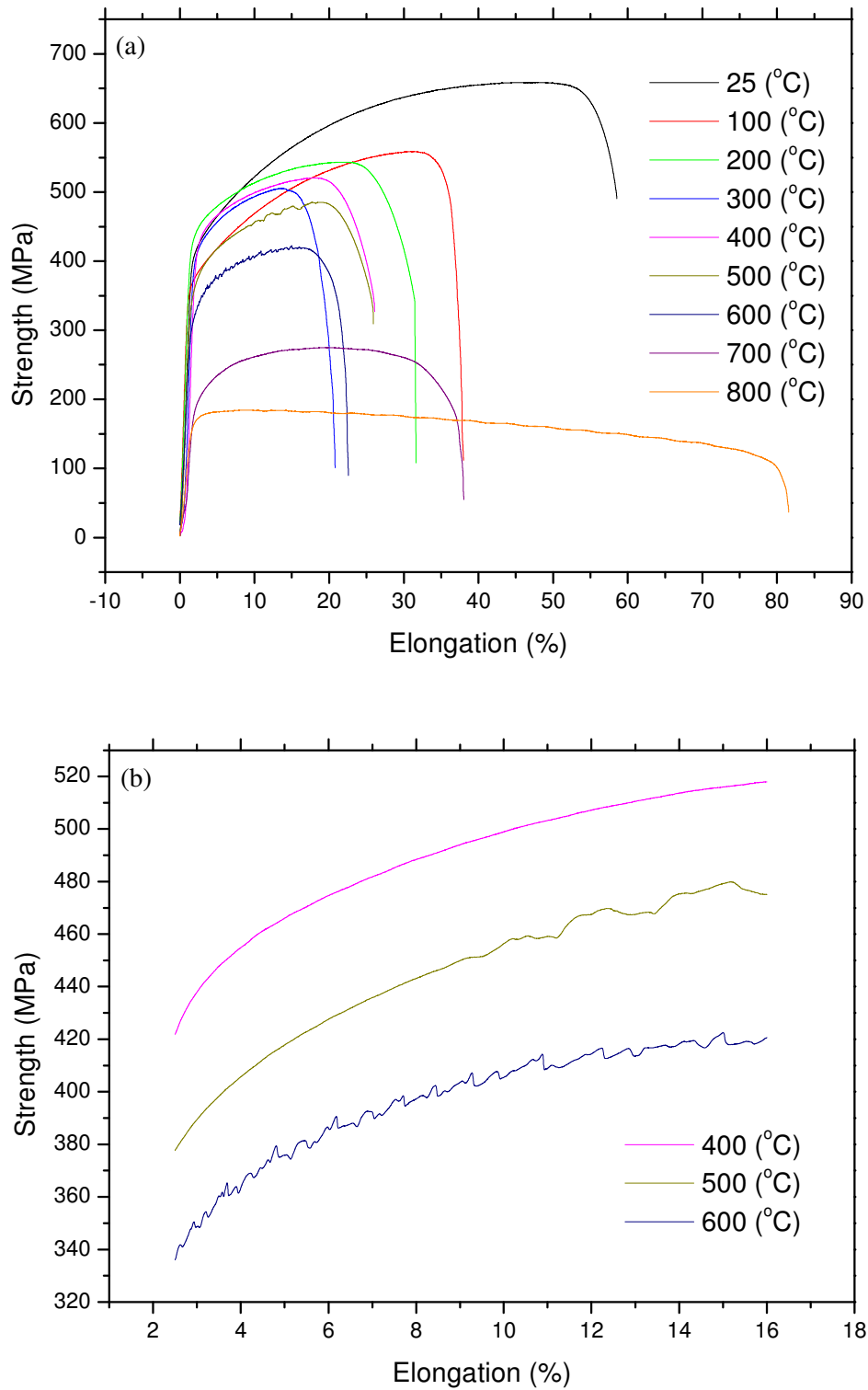


Figure 6. Stress and strain diagrams of weld metal: (a) full range profiles and (b) sections in large scale.

Deformation rate and temperature, which are very important for DSA, effect the diffusing solute atoms and the velocity of mobile dislocations. The presence or absence of serrations is governed by strain rate at a given temperature. Foreexample, dislocation diffusion is more higher than solute atoms for the occurrence of DSA at low temperature and high deformation rate. However, DSA disappear at high temperature and low deformation rate, because dislocations can move with the solute atoms. Therefore, DSA can occur at the temperatures of intermediate strain rates [32]. It is clear from fregoing discussion that DSA takes place in weld metal of 316L ASS results from the interactions of dislocations and solute atoms at the temperatures of 200-600°C.

Serrated yielding also refers to the occurrence of repeated discontinuous yielding during plastic deformation. The discontinuous yielding is evidenced on a stress-strain curve by the appearance of serrations usually after reaching a critical level of plastic strain. On the basis of the appearance of serrations on the stress-strain diagrams, fives types of serrated yielding are often observed as shown in Figure 7. Type A serrations are related with the repeated initiation and continuous propagation of Luders bands along the gauge length of specimen in the strain direction. The initiation of each band resulted in the appearance of yield point on the stress-strain curve which is followed by a smooth curve during band propagation. They occur at the high strain rate and low temperature part of the DSA [33].

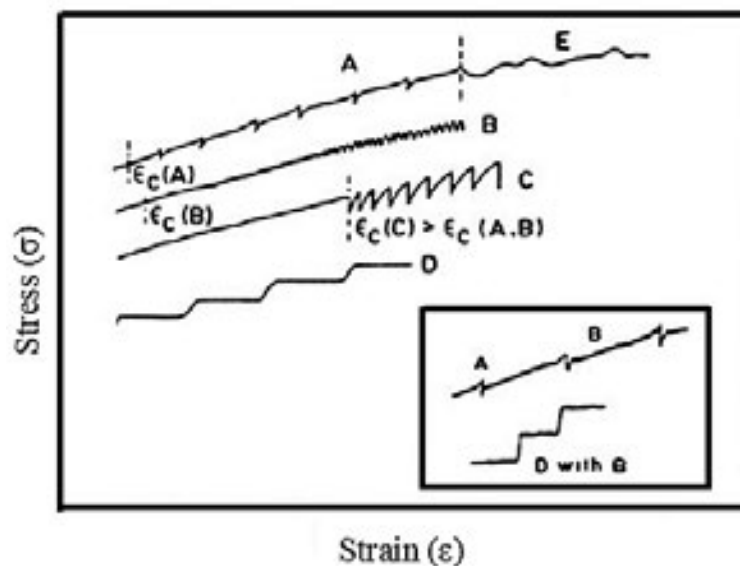


Figure 7. Various type serrations observed on stress and strain diagrams [34].

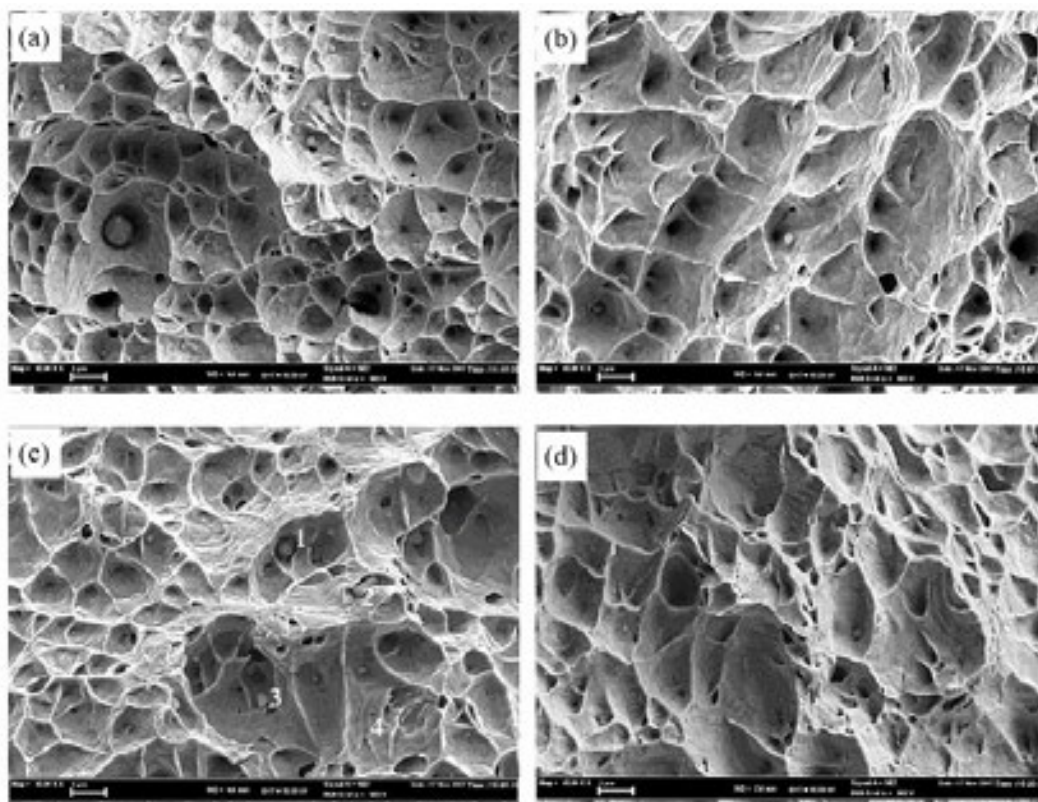
With type B serrations band propagation is discontinuous, with each hop or jump of the band resulting in a serration on the stress-strain diagram. Type B serrations often develop from type A at higher strain, or occur with plastic flow at lower strain rates and higher temperatures compared to the type A serrations. In practice serrations can be mixed in type A and B combinations. Type C serrations are similar to type B serrations in that deformation band propagation is discontinuous. Type C serrations are distinguished by stress drops which occur below the level of the stress-strain curve. Therefore, type C serrations considered to be caused by dislocation unlocking. It is normally observed at lower strain rates and high temperatures than type A and B serrations [34, 35].

Type D serrations are plateaus in the stress-strain diagrams, which are observed because of shear band propagation with no workhardening in front of the moving band. Type D serrations may also occur in a mixed mode with the type B. Type E serrations are similar to the type A, but do not show any workhardening during band propagation. Plastic flow instabilities of type E appear from the type A at high strain values [33]. Type D serrations are observed in the stress-strain diagrams of 316L ASS weld metal at high strain rate for the testing temperature of 500°C. In test conducted at 600°C, the amplitude of the serrations rised with strain and they cahged from types D to types A+E. Type A serrations occured at low strain and change over to type E serration at high strain. The tensile test results indicated that serrated behaviour was observed in 316L austenitic stainless steel at testing temperatures of 500 and 600°C. However serrated behaviour was not observed above 600°C. Different solute atoms and mechanisms can participate in the interactions of solute atom and mobile dislocation at different temperatures.

The DSA, observed at temperature of 500°C, shows itself as serrated flow of types D. Interaction of dislocations with C and N interstitial atoms during deformation is considered to be responsible for the DSA in ASS. At temperatures about 600°C, where the type A and E serrations are seen, the DSA can be attributed to the interaction of mobile dislocations with substitutional solute atoms such as Cr or Mo [36].

When the serrations behaviour results for weld metal obtained from this work are compared with the results otained from other work [28] for the as-received and as-welded samples of 316L ASS. It was observed that weld metal revealed more pronounced serrations than as-received and as-welded samples owing to the presence of higher amount of solute atoms in solution [7]. Dissolution of carbides occurs in the weld metal results in larger amount of solute atoms in the solution. This cause more pronounced serrations in weld metal than as-received and as welded samples.

Figure 8 shows the SEM fractography of the weld metal tested at 25°C, 200°C, 400°C and 600°C. The fracture surface of weld metal tensile tested at 25°C and 200°C showed dimples with different sizes which is characteristic of ductile fracture. Dimple morphology dominated on the fracture surface. This indicated that ductile fracture mode which was represented by cup-like dimple rupture occured in weld metal [28, 37]. Cleavage facets and dimples were observed in the weld metal after testing at 400°C or 600°C in which the samples also showed lower decrease in reduction of area. This suggests that DSA occurs in weld metal of 316L ASS. On the other hand, ductile dimples were observed in weld metal after testing at 800°C which increased elongation and reduction in area. Figure 8 also shows EDS analysis of weld metal which indicated the presence of complex Mn-Cr-Ti inclusions.



Mass percent (%) (e)

Spectrum	C	N	Al	Si	Ti	V	Cr	Mn	Fe	Ni	Mo
1	20.89	0.00	0.18	0.57	0.47	0.19	16.37	2.21	54.08	3.88	1.17
2	22.88	0.00	0.11	0.72	0.24	0.00	11.14	1.66	49.21	12.88	1.15
3	0.45	0.00	0.00	0.18	2.31	1.40	19.78	28.98	41.24	1.37	4.30
4	3.93	1.26	0.01	0.85	0.00	0.00	15.56	0.00	57.48	19.31	1.61
Mean value:	12.04	0.31	0.08	0.58	0.76	0.40	15.71	8.21	50.50	9.36	2.06
Sigma:	11.49	0.63	0.08	0.29	1.05	0.67	3.56	13.88	7.05	8.27	1.51
Sigma mean:	5.74	0.31	0.04	0.15	0.53	0.34	1.78	6.94	3.52	4.14	0.76

Figure 8. Fractography of weld metal tested at (a) 25°C, (b) 200°C, (c) 400°C and (d) 600°C and (e) corresponding EDS of the indicated particles in samples tested at 400°C.

4. Conclusion

In the present study, the DSA phenomena in AISI 316L ASS weld metal subjected to the hot tensile testing at temperature of 25-800°C was investigated. The main conclusions obtained from present study are summarized below:

1. Weld metal of 316L ASS which is susceptible to DSA showed small variation in YS and UTS values up to 600°C, but it revealed drastic change when the test temperature was increased beyond 600°C. A decrease in elongation (%) values of weld metal was observed with increasing temperature, reaching a minimum at 600°C. This is due to the presence of free or uncombined C, N or Cr solute atoms in solution.

2. The workhardening index of weld metal increased in the temperature range of 400-600°C, but it decreased when the test temperature was raised to 700°C or 800°C. This shows the interaction between dislocations and solute atoms affected the workhardening of 316L ASS weld metal.
3. Stress and strain diagrams of weld metal revealed serrated behaviour when the testing temperatures increased at a strain rate of $1 \times 10^{-3} \text{ s}^{-1}$. Serrated behavior which is the characteristic of DSA was observed during tensile testing at 500°C and 600°C. The serrations were not observed on the stress and strain diagrams after testing at 700°C or 800°C
4. Fracture surface analysis indicated that weld metal showed ductile fracture mode after testing at 25°C and 200°C. Dimple morphology dominated on the fracture surface. However, cleavage facets and dimples were observed in the weld metal after testing at 400°C or 600°C in which the samples also showed lower decrease in reduction of area. This suggests that DSA occurs in weld metal of 316L ASS.

5. Acknowledgement

This work was supported by Scientific Research Projects Coordination Unit of Karabük University. Project Number: KBÜBAP-17-DR-169.

6. References

- [1] ASM International, *Stainless steel for design engineering*, 6 (2008), pp. 69-78.
- [2] S.G. Hong, S.B. Lee: Dynamic strain aging effect on the fatigue resistance of type 316L stainless steel, *Journal of Nuclear Materials*, 328 (2004), pp. 232-242.
- [3] M. Valsan, A. Nagesha, K. Bhanu Sankara Rao, R. Sandhya, S.L. Mannan, R. Baldev: A comparative evaluation of low cycle fatigue and creep-fatigue interaction behavior of 316 and 316(N) weld metals and weld joints, *Transaction of the Indian Institute of Metals*, 58 (2005), pp. 323-329.
- [4] O.H. Ibrahim, I.S. Ibrahim, T.A.F. Khalifa: Effect of aging on the toughness of austenitic and duplex stainless steel weldments, *Journal Material Science and Technology*, 26 (2010), pp. 810-816.
- [5] R.W.K. Honeycombe, H.K.D.H Bahadeshia: *Steels Microstructure and Properties*, 3th Edition, London: Butterworth-Heinemann (2006).
- [6] J.B. Seol, J.G. Kim, S.H. Na, C.G. Park, H.S. Kim: Deformation rate controls atomic-scale dynamic strain aging and phase transformation in high Mn TRIP steels, *Acta Materialia*, 131 (2017), pp. 187-196.
- [7] Z. Huang, D. Wagner, C. Bathia: Some metallurgical aspects of dynamic strain aging effect on the Low Cycle Fatigue behavior of C-Mn steels, *International Journal of Fatigue*, 80 (2015), pp. 113-120.
- [8] K. Gopinath, A.K. Gogia, S.V. Kama, U. Ramamurty: Dynamic strain ageing in Ni-base superalloy 720Li, *Acta Materialia*, 57 (2009), pp. 1243-1253.
- [9] D. Yu, W. Yu, G. Chen, F. Jin, X. Chen: Role of dynamic strain aging in the tensile property, cyclic deformation and fatigue behavior of Z2CND18.12N stainless steel between 293 K and 723 K, *Material Science and Engineering A*, 558 (2012), pp. 730-736.
- [10] S. Kožuh, M. Gojić, L. Kosec: The effect of annealing on properties of AISI 316L base and weld metals, *Materials and Geoenvironment*, 54 (2007), pp. 331-344.
- [11] S. Kou: *Welding metallurgy*, 2nd Edition, Wiley Publishing, New Jersey (2003)
- [12] S. Kožuh, M. Goji, L. Kosec: Mechanical properties and microstructure of austenitic stainless steel after welding and post-weld heat treatment, *Kovove Materialy*, 47 (2009), pp. 253-262.

- [13] P. Sathiya, S. Aravindan, R. Soundararajan, A. Noorul Haq: Effect of shielding gases on mechanical and metallurgical properties of duplex stainless-steel welds, *Journal of Materials Science*,44 (2009), pp. 114–121.
- [14] R. Yılmaz, M. Tümer: Microstructural studies and impact toughness of dissimilar weldments between AISI 316 L and AH36 steels by FCAW, *International Journal of Advanced Manufacturing Technology*,67 (2013), pp. 1433–1447.
- [15] R. Sunil Goyal, M. Sandhya, K. Valsan, R. Bhanu Sankara: The effect of thermal ageing on low cycle fatigue behaviour of 316 stainless steel welds, *International Journal of Fatigue*,31 (2009), pp. 447–454.
- [16] A.F. Padilha, P.R. Rios: Decomposition of austenite in austenitic stainless steels, *ISIJ International*,42 (2002), pp. 325-337.
- [17] A.F. Padilha, R.L. Plaut, P.R. Rios: Annealing of cold-worked austenitic stainless steels, *ISIJ International (Japan)*,43 (2003), pp. 135-143.
- [18] T. Sourmail: Precipitation in creep resistant austenitic stainless steel, *Materials Science and Technology*,17 (2001), pp. 1-14.
- [19] C.C. Hsieh, W. Wu: Overview of intermetallic sigma (σ) phase precipitation in stainless steels, *International Scholarly Research Network*, 2012 (2012), pp.1-17.
- [20] J. Lee, I. Kim, A. Kimura: Application of small punchtest to evaluate sigma-phase embrittlement of pressure vessel cladding material, *Journal of Nuclear Science and Technology*, 40 (2003), pp. 664–671.
- [21] G. Ananthkrishna: Current theoretical approaches to collective behavior of dislocations, *Physics Reports*,440 (2007), pp. 113–259.
- [22] B. Vargas-Arista, C. Angeles-Chavez, A. Albitar, J.M. Hallen: Metallurgical investigation of the aging process on tensile fracture welded joints in pipeline steel, *Materials Characterization*. 60 (2009), pp. 1561-1568.
- [23] B. Hutchinson, J. Komenda, G.S. Rohrer, H. Beladi, Heat affected zone microstructures and their influence on toughness in two microalloyed HSLA steels, *Acta Materialia*,97 (2015), pp. 380–391.
- [24] J.H. Hollomon: Tensile deformation, *Transaction AIME, Iron Steel Division*,162 (1945), pp. 268–289.
- [25] S. Gündüz: Dynamic strain aging effects in niobium microalloyed steel, *Ironmaking and Steelmaking*,29 (2002), pp. 341-346.
- [26] R. Kaçar, S. Gündüz: Increasing the strength of AISI 430 ferritic stainless steel by static strain ageing, *Kovove Materialy*,47 (2009), pp. 185–191.
- [27] A. Sarkar, A. Nagesha, P. Parameswaran, R. Sandhya, M.D. Mathew: Influence of dynamic strain aging on the deformation behavior during ratcheting of a 316LN stainless steel, *Materials Science and Engineering A*,564 (2013), pp. 359–368.
- [28] G.A. Muhamed, S. Gündüz, M.A. Erden, D. Taştemur: Dynamic strain aging behaviour in AISI 316L austenitic stainless steel under as-received and as-welded conditions, *Metals* 362 (2017), pp. 2-15.
- [29] L. Hee-jin, L. Hae-woo: Effect of Cr content on microstructure and mechanical properties of low carbon steel welds, *International Journal of Electrochemical Science*,10 (2015), pp. 8028-8040.
- [30] J.C. Lippold, D.J. Kotecki: *Welding metallurgy and weldability of stainless steels*, first Edition, John Wiley & Sons Inc, New Jersey (2005)
- [31] W.D. Callister, *Plastic deformation, material science and engineering—an introduction*, 7th Edition, Wiley, New York (2007)
- [32] S.G. Hong, S.B. Lee: The tensile and low-cycle fatigue behavior of cold worked 316L stainless steel: influence of dynamic strain aging, *International Journal of Fatigue*,26 (2004), pp. 899–910.

- [33] P. Rodriguez: Serrated plastic flow, *Bulletion of Materials Science*,6 (1984), pp. 653-663.
- [34] P.G. McCormick,Dynamic strain ageing,*Transaction of the Indian Institute of Metals*,39 (1986), pp. 98-106.
- [35] L.H. Almeida, I. Le May, P.R.O. Emygdio: Mechanistic modelling of dynamic strain aging in austenitic stainless steels, *Materials Characterization*,41 (1998), pp.137-150.
- [36] M. Ivanchenko, Y. Yagodzinsky, U. Ehrnstén, W. Karlsen, H. Hänninen: Manifestations of DSA in Austenitic Stainless Steels and Inconel Alloys, 20th International Conference on Structural Mechanics in Reactor Technology (SMiRT 20),August 9-14, Espoo/Finland,(2009), pp. 120-128.
- [37] W.D. Callister, D.G. Rethwisch: *Materials science and engineering*, 8th Edition, John Wiley and Sons, New York (2011)

CORRESPONDENCE ADDRESS: Süleyman Gündüz, Karabük University, Technology Faculty, Manufacturing Engineering, Karabük-Turkey, 5055033620,sgunduz@karabuk.edu.tr.

SHORT BIOGRAPHIES

Guma Alnaji Muhamed – born in Libya and he is currently studying Ph. D in the Department of Manufacturing Engineering , Karabük University, Turkey.

Prof. Dr. Süleyman Gündüz–born in 1970, graduated from Gazi University, Ankara, Turkey in 1992, and received his M. Sc. degree in 1996 and his Ph. D degree in 2000 in the area of Metallurgy and Materials Engineering from Leeds University, UK. He is Professor in the Department of Manufacturing Engineering, Technology Faculty of Karabük University, Turkey.

Overview of Recent Progress in Soldering Materials

Muhamad Zamri Yahaya, Ahmad Azmin Mohamad*

¹School of Materials and Mineral Resources Engineering, Universiti Sains Malaysia, 14300, Nibong Tebal,
Pulau Pinang, Malaysia

^a muhamadzamriyahaya@usm.my, ^b aam@usm.my

Abstract

This work provide an overview on current development in lead-free solders. Recent progress based on new composition of the lead-free solders, important characteristic of solder joints, mechanical performance and corrosion resistance were discussed accordingly with selected literatures. Insight on the future of lead-free solders development were presented at the end of the topic.

Key Words: Lead-free solders; nanoindentation; corrosion.

1. Introduction

Merits such as low cost and low melting temperature of the Sn-Pb solders were most preferred in electronic industries before the official banning in 2006 [1]. The Sn-Ag-Cu (SAC) families were intensively studied and show great potential in replacing the Sn-Pb due to their good mechanical and reflow properties[2].

Concern on reliability of electronic devices rose rapidly as the devices were getting smaller. The demand in increased features with capability to operate in extreme condition had great impact in lead-free (Pb-free) solder development. The mechanical and corrosion factor were indeed significant in influencing the Pb-free solder performance in such condition.

This work focuses on the Pb-free solder composition, the physical properties and applications. The corrosion influences were included in discussing the overall reliability of the Pb-free solder.

2. Composition

Various alloying elements (eg. Ag, Bi, Al, Cu, In, Sb, Zn) had been studied in improving the Sn-based solder. Such improvement were aim in controlling intermetallic compound (IMC) formation, ensuring near eutectic melting point, to enhance corrosion resistance and mechanical properties [3, 4].

Binary system is an example of basic composition for the Pb-free solder alloy such as the Au-Sn, Bi-Sn, Sn-Ag, Sn-Cu, Sn-In and Sn-Zn. However, properties of these binary alloy system are insufficient for any real-time applications [5]. Thus, ternary and even quaternary solders have been proposed, such as Sn-Ag-Cu, Sn-Ag-Bi, and Sn-Ag-Zn-Al solders[6, 7]. Still, formation of brittle IMC layer during soldering remain a major issues. Now, the trend of incorporating nanoparticles (producing composite solders) were reported to suppress the growth of these IMC layer [2].

3. Joints

Providing joints or interconnections of components are the main purpose of solder alloy materials. The rise on the concern in term of the reliability and structural integrity of the joints had made the particular subject achieved significant interest among researchers.

The IMC within the joint plays an important role toward such reliability and thus must receive proper attention. A relatively thick IMC negatively affects the long-term reliability of the solder interconnection which is due to their brittle behavior [8, 9]. With the miniaturization of solder joints, volume fraction of these brittle IMC were greater thus theoretically reduced the performance of the overall interconnection.

In inhibiting the growth of the IMC, few types of substrate finishes have been employed. Such include the electroless nickel electroless palladium immersion gold (ENEPIG). ENEPIG is a tri-layered structure of electroless Ni, electroless Pd, and immersion Au layer and mostly uses in advance electronic application. The Ni layer serves as diffusion barriers between the solder and the Cu pad; inhibiting the growth of interfacial IMC [10].

The incorporation of non-interacting reinforcements (TiO_2 , Al_2O_3 , CeO_2 , Fe_2NiO_4 , graphene, TiC , ZnO , ZrO_2 and CNT) can also suppressed the growth of the IMC. The interaction of these inert reinforcement (mostly nano in size) with the molted solder allow size refinement on the IMC [11]. This subsequently improved the overall properties of the solder joints.

4. Nanoindentation

In mechanically evaluate the solder joints, most technique involves tensile, shear and hardness characterization. However, in dealing with miniaturized joint and samples, high resolution equipment such as the nanoindentation excels. The utilization of nano-sized Berkovich tip allow precise measurement on the deformation behavior of the solder alloy including the elastic modulus, creep properties and the fracture toughness [12]. The standard nanoindentation analysis includes the area and depth displacement evaluation correspondingly to the applied load (Figure 1) [13].

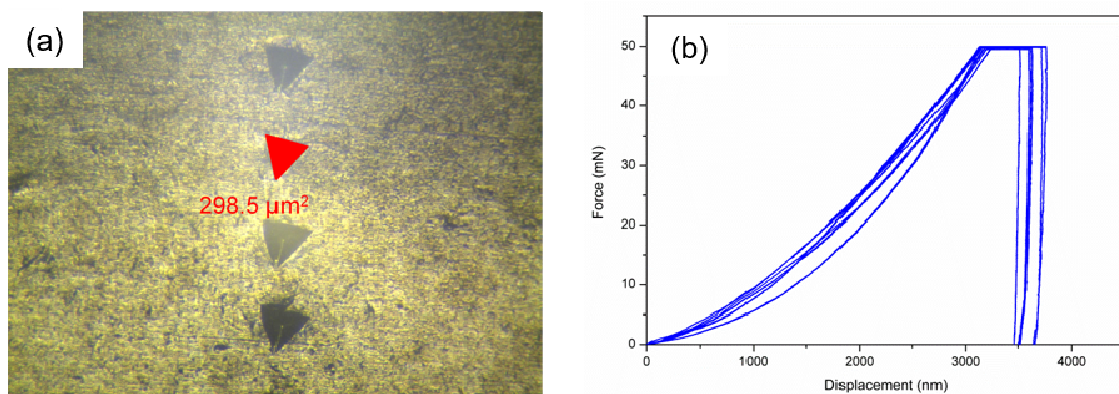


Figure 1: Hardness analysis from the nanoindentation (a) area of indentation mark of the SAC305-0.5T and (b) hysteresis plot of the applied load for SAC305-0.5T, adapted from ref. [13]

5. Corrosions

Extreme operation condition of electronic devices today indeed required proper material selection for solder alloy concerning on corrosion. In the presence of corrosion attack, the mechanical and electrical failure could lead to the malfunction of the product. Currently, not much had been reported on the corrosion property of lead-free alloy in corrosive environments. In overall, the corrosion of lead-free solder mainly originated either within the circuit (flux corrosion) or environment corrosion[14].

5.1 Flux corrosion

Flux residue produced during soldering remained on the joint which in the end contribute to the flux corrosion. Presence of a aggressive ions such as Cl⁻ or Br⁻ in flux can further increase the corrosion tendencies. Worsen, flux residues resin also accumulate dust and debris during operation which later serves as hydrophilic surface; acting as a medium for reaction between the lead-free solder and the ions [15].

Failure analysis of flux corrosion can be utilized by drop of solution (DI water or flux solution). Another view of the flux influence on the corrosion can also be observed on the center matrix and solder/substrate interfaces of the Cu/Sn-Zn/Cu butt joint configuration (**Figure 2**) [16].

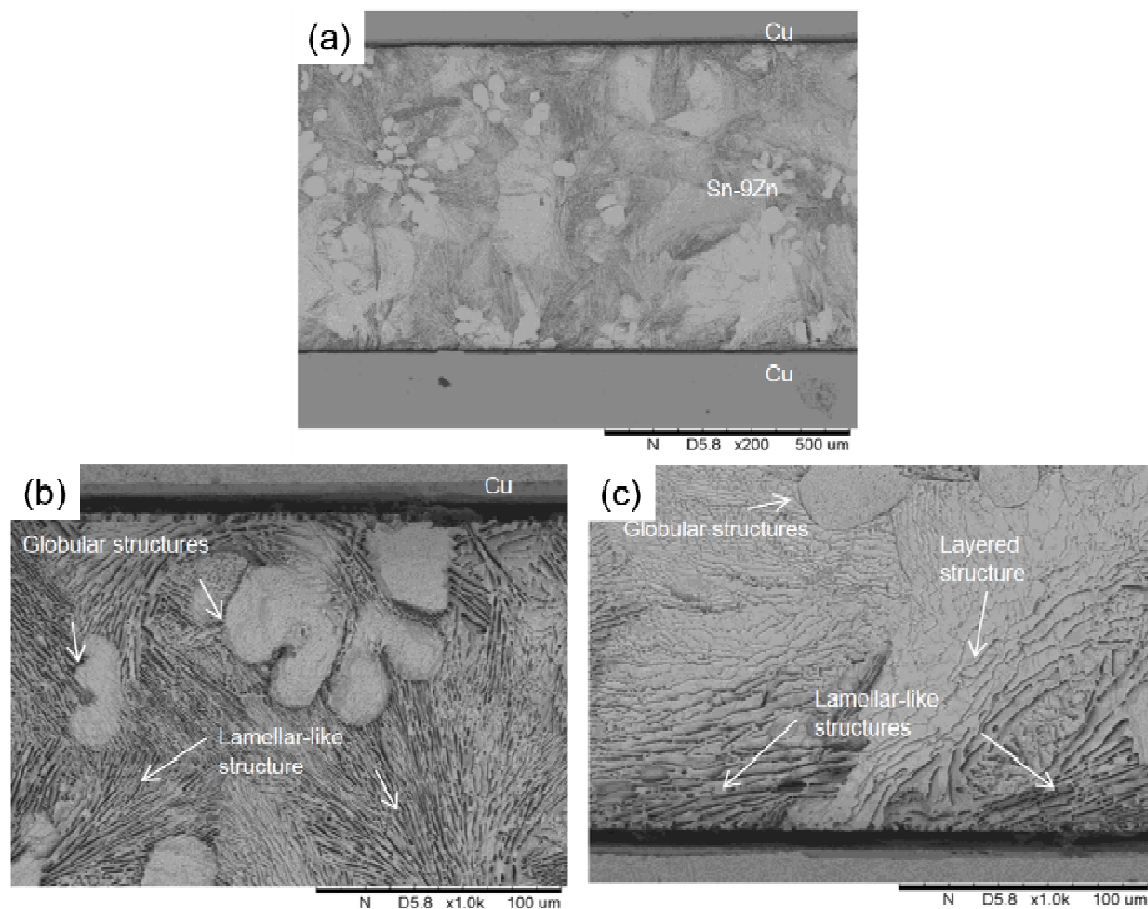


Figure 2: SEM micrograph the Cu/Sn-Zn/Cu butt joint after immersion in 6 M KOH (a) the overall view of the joint (b) the top end of the Cu/solder interface and (c) the bottom end of the Cu/solder interface, adapted from ref. [16]

5.2 Environment

Moisture and aggressive medium (eg. Cl⁻ and OH⁻ ions) contain in the atmosphere are another source for corrosion attack on solder joint. In improving the corrosion properties, various solder alloy composition with new elements are introduced however retaining other properties was indeed challenging.

Studies on corrosion of solder alloys can be accomplished in varying aspects. Example of the analysis that can be apply include the open circuit potential, galvanic cell, polarization, electrochemical impedance spectroscopy etc.

A significant way of studying corrosion is through the combination on the effect of corrosion and the mechanical properties [17]. The corrosion-mechanical studies may varies, for example, effect of immersion time of Cu/Sn-9Zn/Cu (**Figure 3**) [16]. The focus is more on preferential dissolution of Zn and Sn. The formation of corrosion product and grooves proved the cause of joint failure. Later, formation of cracks are the final stage cause the mechanical properties of solders.

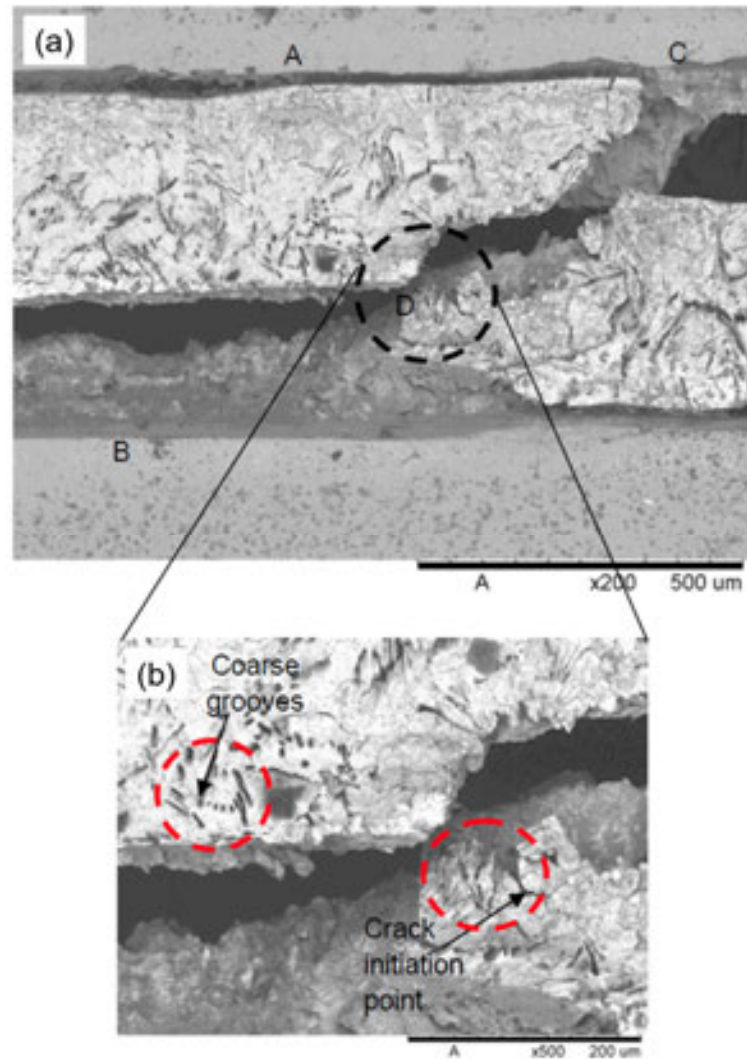


Figure 3: SEM images of the (a) corroded Cu/Sn-9Zn/Cu butt joint after tensile test and (b) magnified images at D, adapted from ref. [16].

5. Conclusions

The wide lead-free solder characterization, properties, mechanism and applications clearly revolutionized the development of current lead-free solders. Additional factor such as corrosion were observed to be a crucial factor in the reliability of solder joints. Studies and researches on lead-free solder will indeed continue as promising yet challenging field in the future.

6. Acknowledgement

The authors appreciate the financial support provided by the FRGS grant (203/PBahan/60713377).

7. References

- [1] F. Gao, T. Takemoto, H. Nishikawa, A. Komatsu, Microstructure And Mechanical Properties Evolution Of Intermetallics Between Cu And Sn-3.5Ag Solder Doped By Ni-Co Additives, *J. Electron. Mater.*, 35 (2006) 905-911.
- [2] M.Z. Yahaya, F.C. Ani, Z. Samsudin, S. Sahin, M.Z. Abdullah, A.A. Mohamad, Hardness Profiles of Sn-3.0Ag-0.5Cu-TiO₂ Composite Solder by Nanoindentation, *Mat. Sci. Eng. A-Struct.*, 669 (2016) 178-186.
- [3] H.R. Kotadia, P.D. Howes, S.H. Mannan, A Review: On The Development of Low Melting Temperature Pb-Free Solders, *Microelectron. Reliab.*, 54 (2014) 1253-1273.
- [4] M.G. Affendy, M.Z. Yahaya, A.A. Mohamad, Corrosion of Sn-9Zn solder joints: a review, *Int. J. Electroactive Mater*, 2 (2014) 8-16.
- [5] L. Tsao, Corrosion Resistance of Pb-Free And Novel Nano-Composite Solders in Electronic Packaging, Corrosion Resistance, InTech2012.
- [6] P. Vianco, J. Rejent, Properties of Ternary Sn-Ag-Bi Solder Alloys: Part ii—Wettability And Mechanical Properties Analyses, *J. Electron. Mater.*, 28 (1999) 1138-1143.
- [7] S.C. Cheng, K.L. Lin, The Thermal Property of Lead-Free Sn-8.55Zn-1Ag-xAl Solder Alloys and Their Wetting Interaction With Cu, *J. Electron. Mater.*, 31 (2002) 940-945.
- [8] L.M. Lee, A.A. Mohamad, Interfacial Reaction of Sn-Ag-Cu Lead-Free Solder Alloy on Cu: A Review, *Adv. Mater. Sci. Eng.*, 2013 (2013).
- [9] M. Yang, Y.-H. Ko, J. Bang, T.-S. Kim, C.-W. Lee, S. Zhang, M. Li, Growth Inhibition of Interfacial Intermetallic Compounds by Pre-Coating Oriented Cu₆Sn₅ Grains on Cu Substrates, *J. Alloys Compd.*, 701 (2017) 533-541.
- [10] M. Ratzker, A. Pearl, M. Osterman, M. Pecht, G. Milad, Review Of Capabilities Of The ENIG Surface Finish, *J. Electron. Mater.*, 43 (2014) 3885-3897.
- [11] J. Shen, Y.C. Chan, Research Advances In Nano-Composite Solders, *Microelectron. Reliab.*, 49 (2009) 223-234.
- [12] M.Z. Yahaya, A.A. Mohamad, Hardness Testing of Lead-Free Solders: A Review, *Solder. Surf. Mt. Tech.*, 29 (2017) 203-224.
- [13] M.Z. Yahaya, Synthesis of TiO₂ Nanoparticles and Characterization of Sn-3.0Ag-0.5Cu/TiO₂ via Nanoindentation and Selective Electrochemical Etching Universiti Sains Malaysia2018.
- [14] A. Guédon-Gracia, H. Frémont, B. Plano, J.-Y. Delétage, K. Weide-Zaage, Effects of Salt Spray Test On Lead-Free Solder Alloy, *Microelectron. Reliab.*, 64 (2016) 242-247.
- [15] M.S. Jellesen, D. Minzari, U. Rathinavelu, P. Møller, R. Ambat, Corrosion Failure Due to Flux Residues in An Electronic Add-On Device, *Eng. Fail. Anal.*, 17 (2010) 1263-1272.
- [16] M.F.M. Nazeri, Corrosion Study of Sn-Zn-xIn LeadFree Solders in 6 M KOH Solution, Universiti Sains Malaysia2014.
- [17] M.F.M. Nazeri, A.A. Mohamad, Effect of Exposure To Alkaline Solution On Sn-9Zn Solder Joints, *Journal of Materials Processing Technology*, 219 (2015) 164-172.

CORRESPONDENCE ADDRESS: Assoc. Prof. Dr Ahmad Azmin Mohamad, School of Materials and Mineral Resources Engineering, Universiti Sains Malaysia, 14300, NibongTebal, Pulau Pinang, Malaysia.+60 4599 6118. aam@usm.my

SHORT BIOGRAPHIES

Muhamad Zamri Yahaya– Dr. Muhamad Zamri Yahaya is an active research fellow at the School of Materials and Mineral Resources Engineering, Universiti Sains Malaysia. He obtained his PhD in 2018 focusing on lead-free solder researches. His current work involves the formulation of nanoparticles bearing lead-free solder alloys, hardness evaluation of solders and the selective electrochemical etching on solder alloys.

Ahmad Azmin Mohamad –Assoc. Prof. Dr. Ahmad Azmin Mohamad is an active researcher at School of Materials and Mineral Resources Engineering, Universiti Sains Malaysia. During his 12 years' experience in field of solder, corrosion and batteries, Dr Ahmad Azmin had authored almost 50 publication titles. He also had complete various researches grants of more than RM 3 million. His current work on solder alloys involves the investigation on composite solder alloys, electrochemical analysis of solder, corrosion properties of solder and the mechanical performance of solder alloys.

INVESTIGATION ON WEAR BEHAVIORS OF WC AND Ti6Al4V COATED AISI 316L STAINLESS STEEL BY ESD COATING METHOD

Yusuf KAYALI^{1,a}, Şükrü TALAŞ^{1,b}

¹Afyon Kocatepe University, Faculty of Technology, Metallurgical and Materials Engineering, ANS Campus, 03200, Afyonkarahisar, Turkey

^aykayali@aku.edu.tr, ^btalas.sukru@gmail.com

Abstract

AISI 316 L austenitic stainless steel has a wide range of applications in various sectors of industry (chemistry, petrochemical industry, paper industry, nuclear engineering, dairy equipment) due to high corrosion resistance at high temperatures. In addition to these superior properties, they are limited in their use due to their low hardness and poor abrasion performance. Therefore, surface modification of materials used in recent years has been on the rise due to the development of technology and the expectation of superior properties over materials. Electrospark deposition (ESD) is a special microbonding process used to coat a base material, known as a substrate, with an electrode, which is a stronger, more durable and more durable topsheet, and is a suitable name for surface modification of stainless steels. In this study, WC and Ti6Al4V coatings were applied to the surface of AISI 316 L stainless steel with ESD Method. As a result of abrasion tests, AISI 316 L stainless steel has been improved with low surface hardness and abrasion resistant coatings. AISI 316 L stainless steel wear resistance is 3-10 times less than the resistance of the coating.

Key Words: ESD, Wear Behaviour, WC, Ti6Al4V

1. Introduction

AISI 316 L stainless steels have a wide variety of uses in various industry sectors including chemistry, petrochemistry, paper industries, and nuclear engineering due to its high corrosion resistance at high temperatures. Furthermore, due to its biocompatibility and high corrosion resistance, it has been used in medicine as an implant material [1]–[5]. Despite such superior properties, its uses have been limited because it has a low hardness and weak wear performance [1], [3], [5]. In order to remove these limitations, many studies have been conducted with the aim of improving the surface hardness of AISI 316L stainless steel as well as its corrosion and wear behaviors. These studies include Ti coating via the physical vapor deposition (PVD) method [3], [6], diamond-like carbon (DLC) coating [7], Cr₂B spray-coating[8], hard Cr coating [9], sol-gel [6], plasma nitriding [2], [5], boriding [1], and thin, hard coatings using several plasma-based surface technologies[10].

Coatings are normally used to improve the corrosion and wear properties of metals. There are numerous coating methods, e.g. galvanizing, electrode position, electroless plating, metal spraying, physical vapor deposition (PVD), chemical vapor deposition (CVD), etc., that provide coatings that protect metals in aggressive mediums [1], [3], [11]. Electrospark deposition is a

micro welding process that uses short duration electrical pulses to deposit electrode materials onto conductive substrates. ESD is increasingly used to repair damaged high value precision products or modify their surfaces for specific properties [12]. ESD has broad range of application in aerospace, defense, automotive, and medical industries [13].

In this study, the effect of WC and Ti6Al4V coatings deposited by ESD techniques on surgical AISI316 L stainless steel is investigated and evaluated for wear behavior in dry medium. The wear properties of coated and non-coated AISI 316 L stainless steels were also studied for comparison.

2. EXPERIMENTAL PROCEDURE

2.1 Materials

The chemical analysis of AISI 316 L austenitic stainless steel specimens with a dimension of 15 mm x 15 mm used in experimental study is given in Table 1 and a microstructural image in as received condition is given in Figure 1.

Table 1. Chemical composition of AISI 316 L austenitic stainless steel used in experimental work.

Type	Chemical composition (% wt)										
	C	Cr	Ni	Si	Mn	Mo	S	P	Cu	N	Ti
AISI 316L	0,02	16,89	10,62	0,39	01,50	2,11	0,03	0,033	0,34	0,054	0,008



Figure 1. Optical Microstructure (x100) of AISI 316 L austenitic stainless steel in as received condition.

2.2. ESD coating

The images of the ESD coating setup prepared for the rotation of the substrate material and the coating machine, the passage of the current for the coating process is eased by using are given in Fig.2. This process was carried out for 230 rpm, 6 x 170 Hz with 90-volts parameter range. Here,

argon gas is purged onto the metal surface to improve the surface smoothness and the ESD coating is carried out for 2 minutes.



Figure 2. Coating machine and coating experiment setup.

During the coating process, the copper base was rotated at a certain speed, and the vibrating electrode was contacted with the applicator on the electrode to provide a spark jump. Figure 3 shows a schematic representation of the coatings to be formed on the surface of AISI 316 L stainless steel.

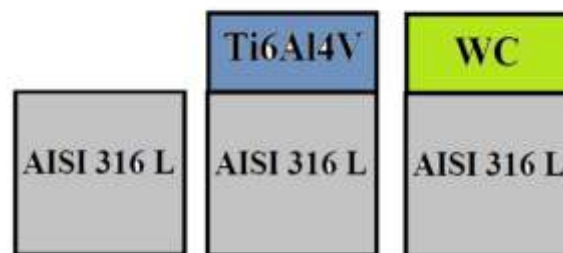


Figure 3. Schematic presentation of coatings.

2.3 Metallographic study

The pieces prepared for the metallographic investigations were cut through and then passed through 120, 240, 320, 400, 600, 800, 1000 and 1200 abrasives respectively and polished with 3 micrometer diamond paste. The polished surfaces were polished with a stainless steel grinder (1 part HNO₃, 1 part HCl, 1 part pure water) to reveal microstructures. Microstructures were examined and photographed with an Olympus BX-60 optical microscope and LEO 1430 VP SEM microscope. The layer thicknesses were again measured with the aid of an optical micrometer attached to the same optical microscope. The layer thickness was determined by taking averages of at least fifteen measurements made from the surface of the metallographic sample.

X-ray diffraction analysis was performed for the characterization of the coating layer formed on the surface by the ESD coating method. X-ray diffraction analyzes of the samples were carried out with Shimadzu XRD-6000 X-ray diffractometer using CuK α ($\lambda = 1.5406 \text{ \AA}$) radiation between 20-100 degrees.

Hardness measurements of the coatings formed on the surfaces of the samples were made using a Vickers tip under a load of 50 gr from the surface with SHIMADZU HMV-2 model hardness device. Averages were calculated by taking 10 measurements from the surface of the coated samples.

2.4 Wear tests

The abrasion tests were carried out using the ball-on-disk method in the abrasion device according to ASTM G-77 standard. WC-Co based 8 mm diameter balls were used in the experiments. Wear tests were carried out at dry medium and a room temperature for total distance of 250 m at a slip rate of 0.2 m / s at 330 rpm using a 8 mm track radius under 5 N load. Using separate WC-Co balls for each test, faults that could be caused by surface damage were removed. Prior to the abrasion test, each specimen and WC-Co ball was cleaned with a alcohol. The coefficient of friction is obtained from the friction force, which is recorded in relation to the slip distance. Wear patterns, wear areas and depths obtained as a result of wear tests were determined with Rugosimeter brand roughness device (Figure 4). As a result of the wear tests, the friction coefficient, wear rate graphs are plotted depending on the coating conditions.

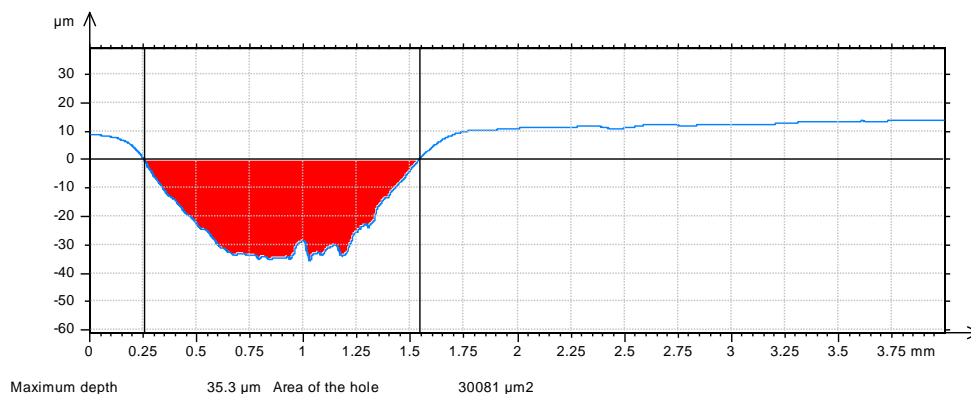


Figure 4. Wear profile of uncoated AISI 316 L austenitic stainless steel in dry environment.

3. RESULTS AND DISCUSSION

3.1 Microstructural analysis

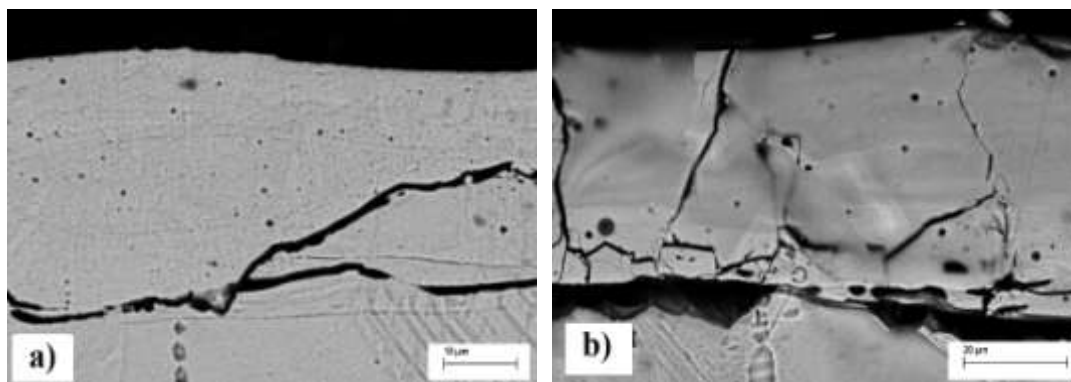


Figure 5. SEM images of a) WC and b) Ti6Al4V coated AISI 316 L austenitic stainless steel by ESD method.

SEM images of the AISI 316L alloy coated with ESD method are shown in Fig.5. In the case of WC, Ti6Al4V coatings, cracks and delamination occurred with high hardness, resulting in horizontal discontinuity, and cracks were found in Fig.5a, indicating vertical thermal expansion difference. Particularly, in the SEM image shown in Fig. 5b, it is considered that cracks occur during cutting, as well as stress cracks due to the fact that Ti6Al4V coating material is generally suitable for intermetallic formation.

3.2 X-Ray analysis

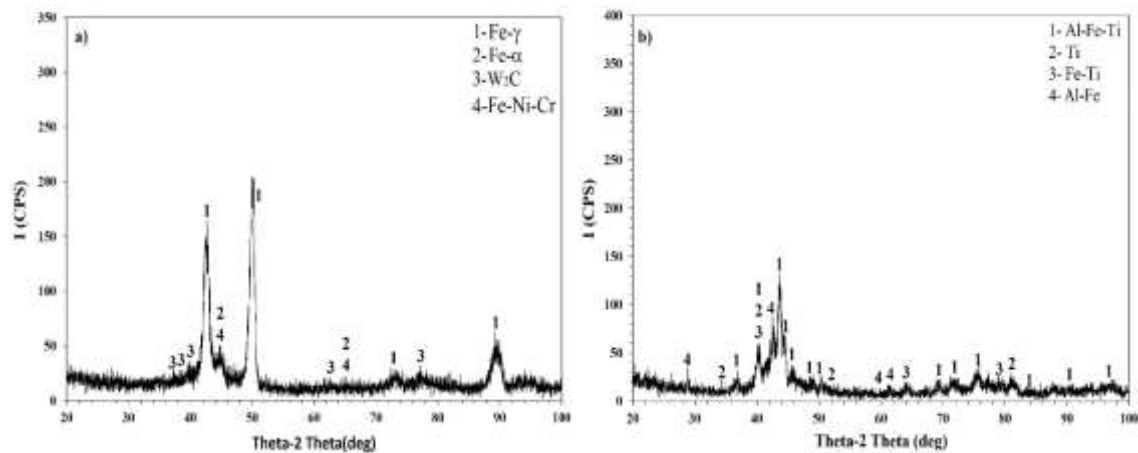


Figure 6. ESD method a) WC b) X-ray analysis of Ti6Al4V coated AISI 316 L austenitic stainless steel.

In the XRD results given in Figure 6a, it is considered that only WC on AISI 316L coatings resulted in a larger number of additional phases than WC on Ti6Al4V coatings, and that the intermetallic phases appeared with an increase in the amount of W from WC together with Ni (Fe- γ) in the stainless steel. Figure 6b shows the XRD results of the Ti6Al4V coating. Due to the large number of components, the number of alloy systems has increased. It is observed that the most dominant phases belong to the Fe-Al-Ti alloy system which is followed by FeAl and NiAl systems that are intermetallic in nature, after Fe-Al-Ti phase system.

3.3. Coating layer thickness and microhardness

In the optical microscope examinations after the coating process by the ESD coating method, it is seen that almost all the samples of the coating layer have a homogeneous thickness. AISI 316 L stainless steel surface was coated with different materials by ESD coating method and the layer thickness obtained was 31.79-47.53 μm , so microhardness measurements were made under 50 gr load. The surface hardness values of the AISI 316 L stainless steel covering layer and the uncoated steel are given in Table 2. The hardness of the coating layer was found between 422 HV0.05 and 978 HV0.05. However, the hardness of the main material is 232 HV0.05. It has been found that the surface hardness of the materials is increased by plating process (except Nickel coating).

Table 2. Layer Thickness and Microhardness Values.

Coating Conditions	Coating thickness (µm)	Microhardness values (HV _{0.05})
AISI 316 L	-	232
WC coated	31.79	978
Ti6Al4V coated	47.53	422

4.4. Wear tests

Depending on the coating conditions of the AISI 316 L austenitic stainless steel coated in Fig. 7 and Table 3, the friction coefficient and wear rate change of the abraded samples are shown in the dry environment. The lowest coefficient of friction is found in WC coated specimens and the highest coefficient of friction is determined in uncoated AISI 316 L austenitic stainless steel specimen. It was determined that the coefficient of friction of the coated specimen varied from 0.59 to 0.68 while the coefficient of friction of the uncoated specimen was 0.76. When the wear rates obtained from the wear tests were examined, the wear rates varied from 68,186x10⁻⁶ mm³ / Nm to 604,508x10⁻⁶ mm³ / Nm. With coating processes, a reduction in wear rate was detected. Wear resistance of coated specimens was very high compared to uncoated specimens.

Table 3. Results from wear tests

Substrate	AISI 316 L	
Coating conds.	Friction coefficient (µ)	Wear rate 10 ⁻⁶ (Nm/mm ²)
No costing	0,76	604,508
WC coated	0,59	68,186
Ti6Al4V coated	0,68	268

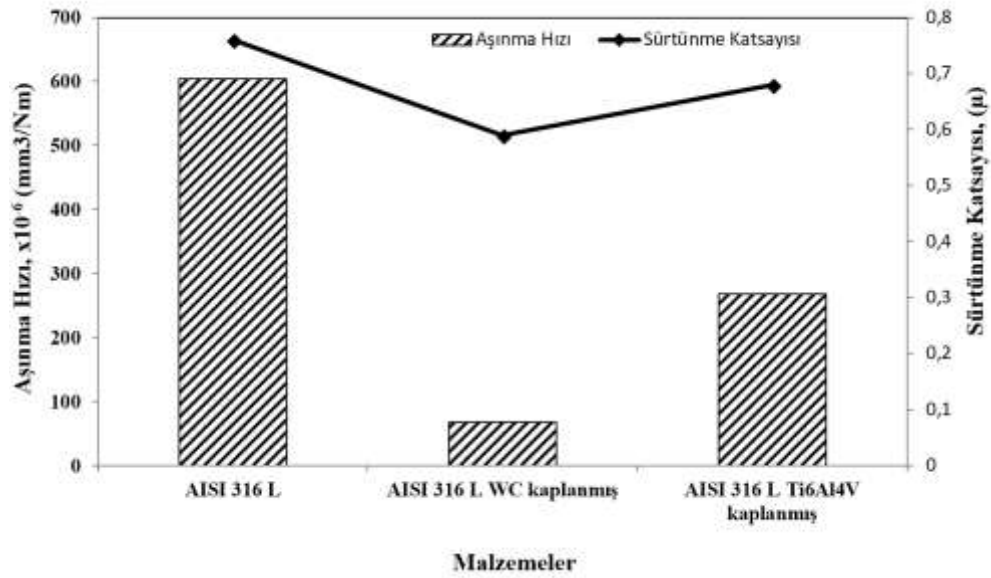


Figure 7. Wear speed and friction coefficient diagram of AISI 316 L stainless steel with different coatings by ESD method.

Table 4. Wear depth and profile results.

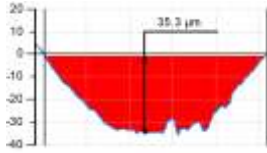
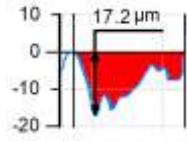
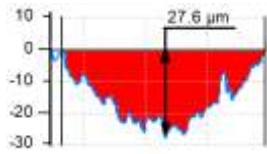
Coating Conds.	Coating thickness (μm)	Wear depth (μm)	Wear area (μm ²)
AISI 316 L	-		30081
WC coated AISI 316 L	31,59		3393
Ti6Al4V coated AISI 316 L	47,53		13336

Table 4 gives the wear depth, wear area and layer thickness values of AISI 316 L austenitic stainless steel, which has been untreated and coated with different materials. According to the hardness of the coating layer, decreases in wear depths and field values were found. The highest wear trace depth was found on the uncoated sample, the lowest wear trace depth was found on the WC coated specimens. As a result of the abrasion tests of the coated samples, it was found that the wear of the coated layer was maintained in the coating layer according to the coating layer thicknesses. As a result of the wear tests of the untreated samples, the wear depth reached 35.3 μm .

4. CONCLUSION

The results obtained on the AISI 316 L stainless steel surface as a result of coating of different materials by ESD method are given below.

- 1- WC, Ti6Al4V successfully formed on the surface of AISI 316 L stainless steel with ESD method. Phases such as Fe- γ , Fe- α , W₂C, Fe-Cr-Ni, Fe-Ti, Al-Ti and Fe-Al-Ti were obtained in the obtained coating layers.
- 2- The surface hardness of the AISI 316 L stainless steel is increased by the coating process. The highest surface hardness was found to be 978 HV_{0.05}. The surface hardness of AISI 316 L stainless steel without process is 232 HV_{0.05}. Thus, the surface hardness was increased about 4 times by the coating process.
- 3- With the coating processes made, the corrosion resistance of AISI 316 L stainless steel has increased in both coatings. The lowest wear resistance was obtained as 68,186 Nm / mm² in WC coated specimens. The wear resistance of AISI 316 L stainless steel has increased approximately 10 times.
- 4- Friction coefficient decreased with coating process.

5. References

- [1] Y. Kayali, A. Büyüksaçış, and Y. Yalçın, "Corrosion and wear behaviors of boronized AISI 316L stainless steel," *Met. Mater. Int.*, vol. 19, no. 5, pp. 1053–1061, 2013.
- [2] L. Gil, S. Brühl, L. Jiménez, O. Leon, R. Guevara, and M. H. Staia, "Corrosion performance of the plasma nitrided 316L stainless steel," *Surf. Coatings Technol.*, vol. 201, no. 7 SPEC. ISS., pp. 4424–4429, 2006.
- [3] E. De Las Heras *et al.*, "Duplex surface treatment of an AISI 316L stainless steel; microstructure and tribological behaviour," *Surf. Coatings Technol.*, vol. 202, no. 13, pp. 2945–2954, 2008.
- [4] L. Nosei, S. Farina, M. Ávalos, L. Náchez, B. J. Gómez, and J. Feugeas, "Corrosion behavior of ion nitrided AISI 316L stainless steel," *Thin Solid Films*, vol. 516, no. 6, pp. 1044–1050, 2008.
- [5] A. Çelik, Y. Arslan, A. F. Yetim, and I. Efeoglu, "Fatigue behaviour of duplex treated AISI 316L stainless steel," *Kov. Mater.*, vol. 45, no. 1, pp. 35–40, 2007.
- [6] L. Chenglong, Y. Dazhi, L. Guoqiang, and Q. Min, "Corrosion resistance and hemocompatibility of multilayered Ti-58

Mater. Lett., vol. 59, no. 29–30, pp. 3813–3819, 2005.

- [7] M. Azzi, M. Paquette, J. A. Szpunar, J. E. Klemberg-Sapieha, and L. Martinu, “Tribocorrosion behaviour of DLC-coated 316L stainless steel,” *Wear*, vol. 267, no. 5–8, pp. 860–866, 2009.
- [8] L. R. Jordan, A. J. Betts, K. L. Dahm, P. A. Dearnley, and G. A. Wright, “Corrosion and passivation mechanism of chromium diboride coatings on stainless steel,” *Corros. Sci.*, vol. 47, no. 5, pp. 1085–1096, 2005.
- [9] L. Fedrizzi, S. Rossi, F. Bellei, and F. Deflorian, “Wear-corrosion mechanism of hard chromium coatings,” *Wear*, vol. 253, no. 11–12, pp. 1173–1181, 2002.
- [10] P. A. Dearnley and G. Aldrich-Smith, “Corrosion-wear mechanisms of hard coated austenitic 316L stainless steels,” *Wear*, vol. 256, no. 5, pp. 491–499, 2004.
- [11] G. K. Kariofillis, G. E. Kiourtsidis, and D. N. Tsipas, “Corrosion behavior of borided AISI H13 hot work steel,” *Surf. Coatings Technol.*, vol. 201, no. 1–2, pp. 19–24, 2006.
- [12] K. Korkmaz, “Investigation and characterization of electrospark deposited chromium carbide-based coating on the steel,” *Surf. Coatings Technol.*, vol. 272, pp. 1–7, 2015.
- [13] Z. Jiao, “Surface Modification of Stainless Steel by Electro-Spark Deposition,” 2016.

CORRESPONDENCE ADDRESS: Yusuf Kayalı, Afyon Kocatepe University, Faculty of Technology, ANS Campus, +902722281314, ykayalı@aku.edu.tr.

SHORT BIOGRAPHIES

Yusuf Kayalı – Assistant Professor Yusuf Kayalı was graduated from Afyon Kocatepe University, Faculty of Technical Education, Department of Metallurgy Education. He completed his MSc in Afyon Kocatepe University Institute of Natural Science and finally received his PhD degree from Afyon Kocatepe University Institute of Natural Science on the subject of wear of metals. He works on corrosion and wear of metals.

Şükrü Talaş – Professor Dr. Şükrü Talaş was graduated from Marmara University, Technical Education Faculty, Department of Metallurgy Education, in 1993. He completed his MSc in 1997 in Brunel University, the UK and was finally granted a PhD degree in 2002 on C-Mn-Ti Steel Weld Metal Microstructures from Leeds University, the UK. He works as Associate Professor at the department of Metallurgical and Materials Engineering, Faculty of Technology, Afyon Kocatepe University.

TOZ METALURJİSİ İLE ÜRETİLEN MALZEMELERİN LAZER KESME ÜZERİNE BİR ARAŞTIRMA

Ş. Talaş^{1,a}, Y. Kayalı^{1,b}, A. Çetkin^{2c}

¹Afyon Kocatepe University, Faculty of Technology, Metallurgical and Materials Engineering,
Afyonkarahisar, Turkey

²Afyon Kocatepe University, Faculty of Technology, Mechanical Engineering, Afyonkarahisar, Turkey

^a stalas@aku.edu.tr, ^b kayali@aku.edu.tr, ^c acetkin@aku.edu.tr

Özet

Toz metalurjisi ile üretilen parçalar genel olarak otomotiv endüstrisinde yaygın olarak kullanılmaktadır. Bu parçaların kullanılmasının nedenleri arasında, üretim kolaylığı ve karmaşık şeklin kaybı nedeniyle en önemlisi işleme operasyonunun zamanının geri kazanılmasıdır. Ek olarak, daha ucuza mal olabilir. Ancak, son derece yüksek kaliteli çelikler üretebilen son ürünler üzerinde bazı araştırmalar yapılmış ve bu çelikler daha sonra çeşitli yerlerde kullanılabilir. Lazer otomasyon sistemine adapte edilebildiği veya otomasyona dayalı seri üretim için kullanılabilirliği için karmaşık şekillerin kesileceği veya işlemenin gerçekleşeceği tahmin edilmektedir. Farklı sinter sıcaklıklarında hazırlanan çelik ve bakır bazlı toz malzemelerin lazerle kesilmesinden ve kesilmesinden sonra arayüzey ve kesme kalitesinin araştırılması gerçekleştirilmiştir. Sinterleme sıcaklığı arttıkça, kesme kalitesi artar ve oluşan bileşiklerin bileşimi kısmen değişir.

Anahtar kelimeler: Lazer kesim, toz metalurjisi, sinterleme

1. Giriş

Lazer kelimesi, 'Light Amplification by Stimulated Emission of Radiation' sözcüklerinin baş harflerinin bir araya gelmesi ile oluşur ve uyarılma yayını ile monokromatik olarak ışığın kuvvetlendirilmesi anlamına gelmektedir. 1970'lerde kullanılmaya başlanan lazer, kesme, kaynak, delme ve markalama işlerinde, ölçme ve daha birçok alanda ciddi pazar oluşturmuştur. Lazer hücresi, gaz veya sıvı maddeler ile doldurulmuş ince bir boru olabildiği gibi çeşitli kristal veya cam gibi katı maddelerden de oluşmuş olabilir (Çelen, Çaligülü 2009). Mühendislik malzemelerinin çeşitlenmesi, zorlu karmaşık tasarımlar ve boyutsal hassasiyet gibi sorunlar Lazer'i daha değerli kılmıştır. Modern işleme metotları arasında, lazer ışınıyla kesme yöntemi bu teknolojinin en geniş uygulama sahalarından biridir. Genellikle metaller için olsa da, diğer türden malzemelerin (kauçuk, kağıt, kumaş vb.) kesilmesi veya işlenmesinde kullanılan lazer kesim teknolojisi hızla hayatımıza giren metotlardandır [1-8].

Lazer ışınımı ile malzeme kesme bölgesinde ani olarak eritilir ve eriyen malzeme inert bir gaz vasıtasıyla dışarı atılır. Genellikle azot ve argon inert gaz olarak kullanılır. Kesme hızı, malzeme kalınlığı ve malzemenin erime sıcaklığıyla ters orantılı olup, lazerin gücü ile doğru orantılıdır (Mungan 2006). Yüksek alaşımlı çeliklerin oksitlerinin erime sıcaklıkları, çeliğin erime sıcaklığından daha yüksek olduğundan oksit eriyikleri kesme yarığında daha zor akar. Bununla birlikte alaşımlı çelikler, ısıl iletkenlikleri düşük olduğundan fazla ısı biriktirmeye meyillidir. Kaliteli bir kesim sonucu elde etmek istiyorsak lazer gücünün darbeleri çalıştırılması

gerekmektedir. Darbeler arasında süre bulunduğundan dolayı malzeme biraz sıcaklığını yitirmektedir. Bu sayede yanma sonrasında oluşan ısısının etkisi kontrol altında alınmış olmaktadır. Lazer ışınıyla yakarak kesme işleminde diğer bir sınır, çelik kimyasal yapısında bulunan karbon miktarıdır [2,4,6,7].

Toz metalürjisi ile üretilen parçalar genel olarak otomotiv endüstrisinde sıklıkla kullanılmaktadır. Bu parçaların kullanılma nedenleri arasında en önemli yeri tutan neden üretim kolaylığı ve karmaşık şekil nedeni ile kaybedilecek olan talaşlı imalat işleme zamanının geri kazanılmasıdır. Ayrıca, hata ayıklama da daha kolay olmakta ve çok daha ucuza mal edilme mümkün olmaktadır. T / M yönteminin genel olarak avantajları ise: yüksek malzeme kullanım oranı, düşük malzeme kaybı, yüksek üretim hızları, düşük maliyet, düzgün yüzey, yakın tolerans değerlerinin elde edilmesi, karmaşık şekilli parçaların imalatı, yüksek ergime sıcaklığına sahip metallerin imalatı, yüksek yoğunluğa sahip parça üretimi, metal matriks kompozit ve metal alaşımları üretimi, üstün mikro yapısal özelliklere sahip parça üretimi, belirli derecede gözeneklilik ve geçirgenlik şeklinde sıralanabilir[1-5].

Bu çalışmada, toz metalürjisi ile üretilmiş olan değişik malzemelerin lazer enerjisi kullanarak kesilmesi araştırılmıştır.

2. Deneysel metod

Mikro yapılarının incelenmesi için hazırlanmış olan numuneler metalografik olarak zımparalama işlemine tabii tutulmuştur. Zımparalama ve parlatma işlemleri Metkon marka, Gripon 2V model zımpara cihazı ile ortalama 250 devir/dakika hızında gerçekleştirilmiştir. Lazer kesim deneyleri Afyon Kocatepe Üniversite, Merkezi Laboratuvar, Mekanik İşlemler bölümünde yapılmıştır. Deneyler, TLS firmasının ürettiği 400W gücünde olan 3T LASER markalı fiber lazer tezgâhında gerçekleştirilmiştir. Tezgâh görseli Şekil 1'de gösterilmektedir.

Üretilen ilk sinterlenmiş toz karışımı karbon içeren çelik tozu (Alfa Aesar sinterlenmesi ile elde edilecek olan demir esaslı sinterler ve diğeri ise içerisinde değişik aşındırıcı veya seramik ikinci faz bulunan demir tozu karışımları olacaktır. Karışımlar önce karıştırılacak ve daha sonra 900C de sinterlenecek ve iç yapı analizi yapılacaktır. Analiz aşamasından sonra, malzemeler ince bir şekilde kesilecek ve lazer cihazı ile ergitilecektir. Kesim aşamasında, değişik parametreler kullanılacak özellikle kesme gazının etkisi de incelenecektir. Kesimden sonra kesilen yüzeyler incelenecektir. Kesme parametreleri şunları içerebilir: ışın çapı, kafa yüksekliği vb.. SEM ve optik mikroskoplar yardımıyla karakterize işlemi yapılacaktır.

Paslanmaz çelik olarak Alfa Aesar firmasından temin edilen -100 mesh boyutunda SAE 316-L türü ve 67.5:17:13:2.5 ağırlık oranlarında Fe:Cr:Ni:Mo içeren toz kullanılmıştır. Demir tozu ise -325 mesh ve 98% saflıkta olup ve Demir tozu ile sinterleme ile elde edilen (Cr,Mo)₃C tozu içeren sinterlenmiş karışım kullanılmıştır.

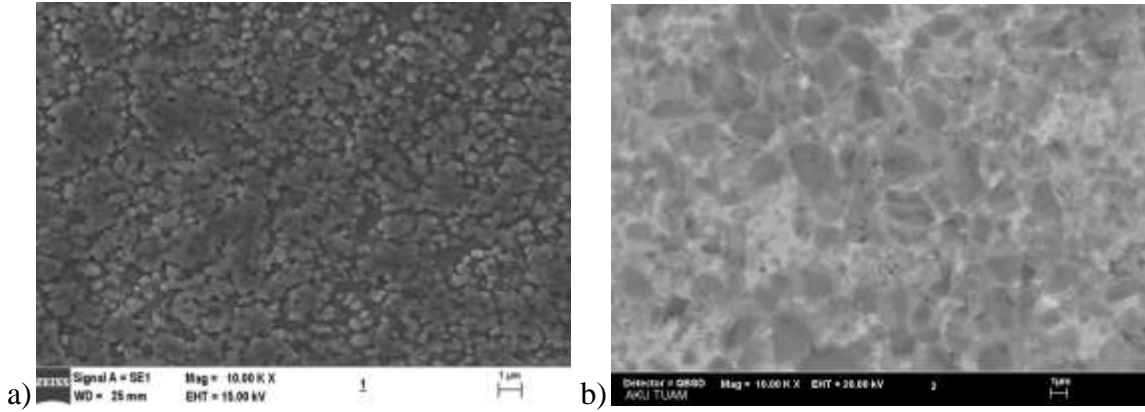
Hazırlanan toz karışımlarından 316L paslanmaz çelik tozu 990°C'de 1.5 h sinterlenmiştir. Sinterleme için Protherm PTF serisi maksimum kullanım sıcaklığı 1200°C olan tüp fırın kullanılmıştır. Demir tozu ve Cr₃C₂ toz karışımının sinterlenmesi ise yine aynı tür fırında 2h süre 990°C'de yapılmıştır. Sinterlemenin ardından herhangi bir yüzey işlemi yapılmamıştır. Metalografik olarak dağlama yapılmadan sadece ince zımpara ile temizlenerek lazer kesme yapılmıştır.



Şekil 1. 3T LASER Markalı Fiber Lazer.

Parametrelerin karşılaştırma amacıyla sabit tutulduğu kesme işlemi için TLS3000 lazer kesim makinesi kullanıldı. Aynı ekipman, azot gazı kullanılarak sinterlenmiş metal tozlarından yapılan numuneleri kesmek için kullanıldı. Kesimin ardından tüm yüzeyler temizlendi ve daha sonra düşük büyütme ile fotoğraflandı. Parlatma ve aşındırma, yani metalografik preparasyonu takiben tüm örneklerde kesitsel bir görüntüleme yapıldı. SEM mikroskopi, LEO VP serisi SEM ekipmanı kullanılarak Lazer ile kesilen numuneler üzerinde gerçekleştirildi.

3. Sonuçlar ve tartışma

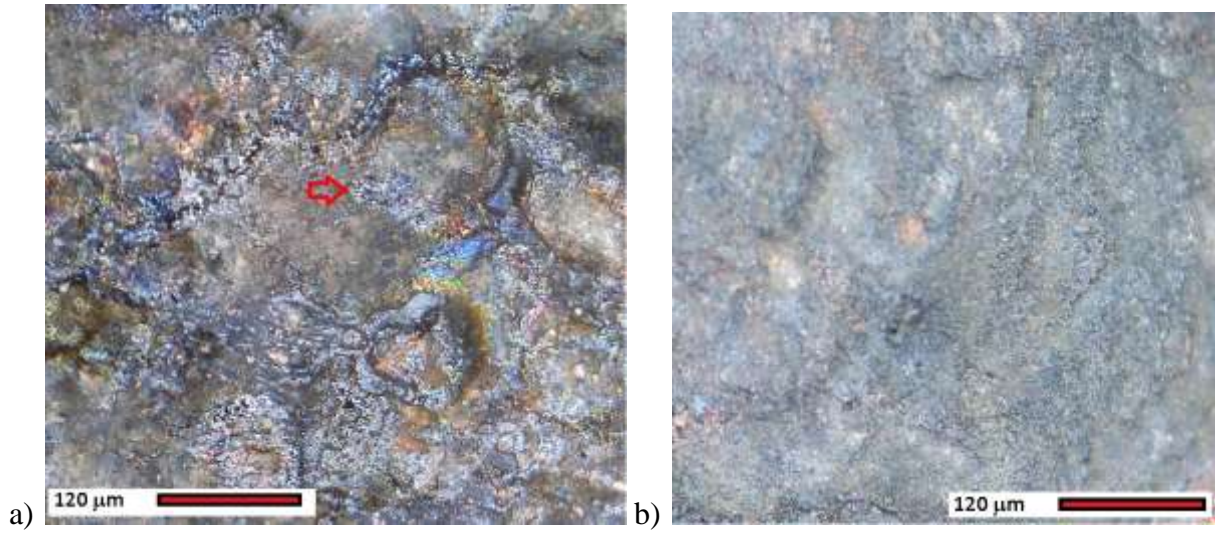


Şekil 2. a) Alaşım T/M ürünü çelik sinterin kesilmiş ara yüzeyi b) Demir tozu ve Cr_3C_2 karışımının SEM görüntüsü

Şekil 2, sinterlenmiş peletlerin yüzeyinden alınan içyapı görüntülerini göstermektedir. Paslanmaz çelik tozlarının sinter sonrası değişik büyüklüklere sahip olduğu görülmektedir ve rastgele dağıtılmış gibi görünmektedir. Yüzey pürüzlülüğü yüksektir ve düzensiz ark havuzları gözlemlenmiştir. Şekil 2 b de ise karbürlü demir tozunun sinteri EBSD ile görüntülenmiştir. karbürler daha siyah olarak görülmektedir. Yüzey profilinin düzensiz ancak çatlama yol açmayacak nitelikte küçük boşluklar veya porozite içerdiği ve bunun aynı zamanda kusur oluşumunda önemli bir rol oynayan başka bir gerilim artırıcı etki yarattığı bilinmektedir.

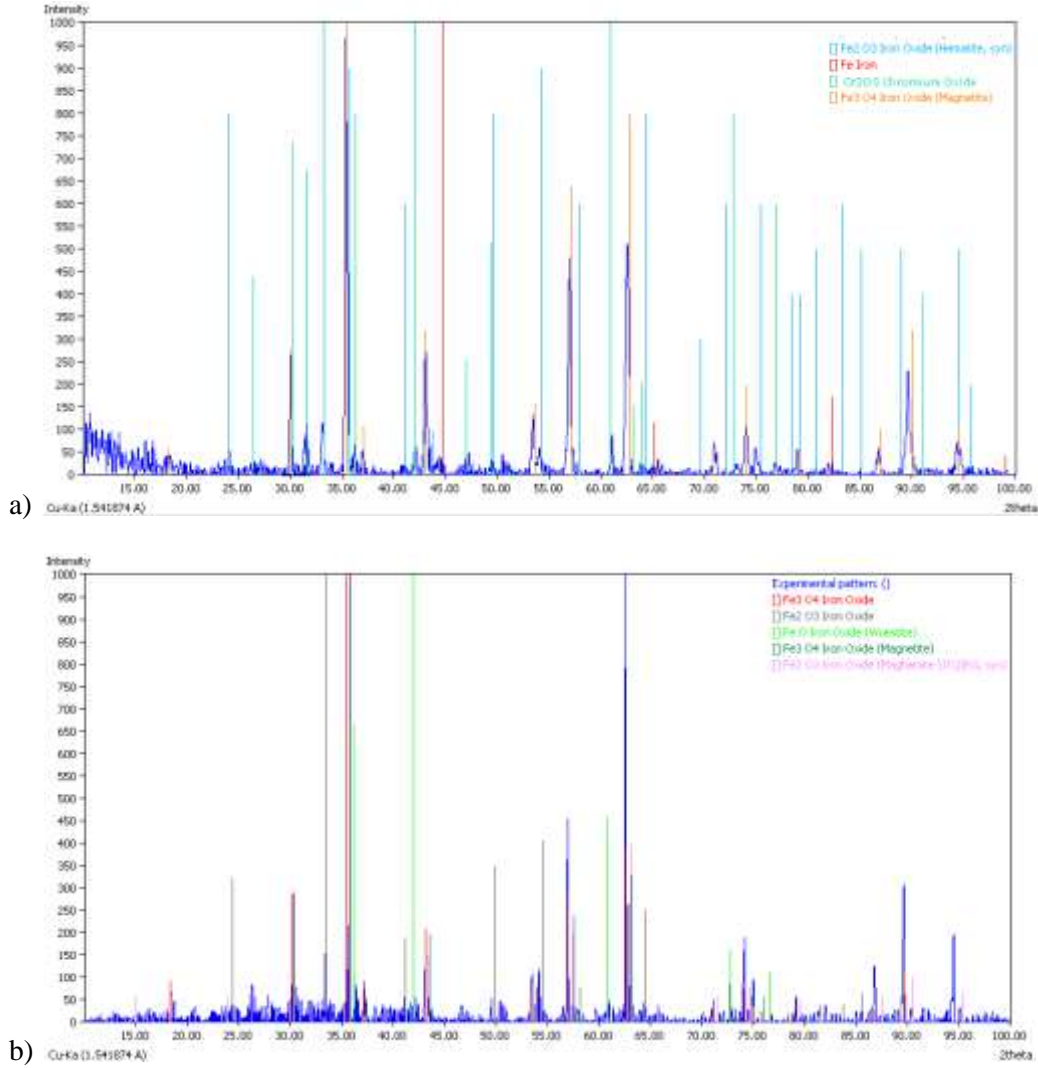
Birçok metalik malzemelerin kesiminde en sık karşılaşılan problem, kalınlığı 2 mm'nin fazla olan metallerde kılcal bantlaşma şeklinde çapak oluşumu gözlenmektedir. Bunun nedeni ise oksit eriyiğinin metalik eriyiğine göre daha düşük yüzey enerjisine sahip olmasıdır. Ancak, arayüzey destekli oksit oluşumu sırasında oksijenin etkisi, kesme sırasında daha çok yüksek sıcaklığın

etkisi ile damlacık haline gelen metalik yapının dış kısmının oksitlenmesi ile oksit tabaka ilerlemesi gerçekleşir ve bu çapaklar bu mekanizmadan dolayı merkezlerinde metal bulunduklarından uzaklaştırılmaları zor olmaktadır. Lazer ile kesimde, düşük alaşımli çeliklerde metalin kendi eriyiği, metalin oksidine göre daha katı hale getirilir. Bunun sebebi ise temiz bir kesme imkânı sağlamaktadır. Lakin bu durumunun geçerli olmadığı durumlar bulunmaktadır. Öneğin yüksek alaşımli CrNi çeliklerinde, oksitlerinin erime sıcaklıkları, alaşımli çeliğin erime sıcaklığından daha yüksektir ancak ısı kapasiteleri daha yüksek olması ve ısı iletkenliklerinin düşük olması nedeniyle fazla ısı biriktirmeye ve oksitlenmeye daha meyillidir [3, 5-8].



Şekil 3. a) Paslanmaz çelik kesme yüzeyi b) Demir+karbür kesme yüzeyi

Şekil 3'te gösterilen paslanmaz çelik ve demir+karbür sinterlerinin lazer ile yapılan kesimler ile karşılaştırıldığında, yüzey kalitesinin, paslanmaz çelikte, demir+karbür sintere göre göreceli olarak daha iyi olduğu ve oklarla gösterildiği gibi, sinter sırasında tam bir tane sınırı iyileşmesi beklenmediğinden dolayı tane sınırlarının oksitlenmesi meydana gelmiştir. Demir+karbür sinterlerin kesilmesi sırasında ise, oksidasyonun daha homojen bir şekilde ortaya çıktığı yanmanın düzenli daha pürüzsüz bir görünümü sağladığı görülebilir. Yüzey oksit tabakası herhangi bir gözeneklilik ve çatlama içermemektedir, ancak kaplama tabakası ve taban plakası arasında bir ayırma çizgisi veya delaminasyon olmadığı görülmektedir. Daha az çatlama ve daha az gözenekliliğe yol açan yanma işleminin paslanmaz çelikte daha belirgin olduğu bununda mekanik ve ısı özellikleri birbirinden farklı olan çok sayıda oksit olmasında kaynaklandığı düşünülmektedir, bununla birlikte, kesme yüzeyi üzerinde uygulanan kuvvet nedeniyle kaplama tabakasının delaminasyonu daha belirgindir [7,8].



Şekil 4. a) Paslanmaz çelik kesim yüzeyinin XRD sonucu b) Demir tozu + (Cr, Mo)3C nin kesim yüzeyinden alınan XRD sonucu

Kesim yüzeylerinden alınan XRD sonuçlarına bakılırsa, Şekil 4, paslanmaz çeliklerin kesim yüzeylerinde klasik Fe_xO_y bileşikler oluşurken, çoğunluklu olarak Fe_3O_4 türü kolay oluşan zayıf oksitlerin yanında, oluşumu daha zor olan ve daha fazla demirin bağlanmasıyla ortaya çıkan FeO türü oksitlerde bulunmaktadır. Paslanmaz çelik sinterlerin lazer kesimi sonucunda ise, Cr_2O_3 türü oksitlerin yanında demir (Fe veya Cr) serbest olarak ortaya çıkmıştır. Fe_3O_4 türü basit oksitlerin ise diğer oksit türlerine göre daha fazla olduğu gözlemlenmiştir. Bu aşamada, paslanmaz çeliğin yanma ürünleri, diğer elementlerin oksitlerinin miktarı ile orantılıdır. Demir den daha aktif olarak ortaya çıkan Cr_2O_3 oksidi, demir oksitlere göre daha düşük bir çözünüm sıcaklığına sahip olması ile beraber soğuma sırasında kesme sırasında kullanılan basınçlı havanın etkisi ile oksit yaptığı düşünülmektedir. Serbest oksijen veya serbest Cr bulunması ise yüzey oksit tabakasının mekanik etki sonucu dökülmesi sonucu alt kısımlardaki reaksiyona girmemiş bölgedeki metalik kısım olduğu düşünülmektedir. Ellingham oksit oluşum diyagramlarını dikkate alacak olursak (9), oksit oluşum sırası elementlere göre sıralanacak olursa Cr, Fe ve Ni olmaktadır. Bu koşullarda, Ni'in yapmış olduğu NiO en oluşumu diğerlerine göre daha erken başlar ve diğerlerinden daha düşük serbest enerji değerinde olup ve ergime noktası $1200^{\circ}C$ civarında iken Cr ve Fe'nin oksitleri ($2/3 Cr_2O_3$ ve Fe_3O_4) kısmen daha yüksek ergime noktasına sahip oldukları için ve en önemlisi negative olarak daha düşük serbest enerjisine değerine sahip

olmalarından dolayı soğuma sırasında daha önce oluşmaktadır. Kullanılan sıcaklık aralığında, metal ve metalin oksidi yoğun bir durumda yani sıvı veya katı olarak bulunur ve oksijen ise gaz durumundadır. Gazın sahip olduğu molar enerji, entropi değerini azaltıcı bir yapıya yani bileşik yaparak karışım serbest molar enerjisini düşürerek entropi değişimini başarı ile tamamlar. Her bir metalin oksidasyonu için, ½ mol O₂ bağlanması aşağı yukarı bütün metaallerin için benzer olsa da afinite katsayıları ve aktivite sabitleri bu dengeyi değiştirmektedir. Paslanmaz çeliğin kesilmesi sırasında ortaya çıkan Fe/Cr piklerinin, yeterince yüksek sıcaklıklarda, ΔG'nin işaretinin pozitif olması (genellikle ΔG/dT negatiftir) nedeniyle oksite çözünerek serbest metal + oksijene ayrışacaktır. Fe/Cr pikleri benzer bir serbest enerji değişiminin yani negatif değerlikli entropi değerinin artması yani A-A bağlarının oluşumu ile sonlaması yol açmaktadır. Cr'un C varlığında çözünmesi teorik olarak mümkün değildir ancak bu çelik L serisi olduğu için CrxCy serisi karbür oluşumuna burada rastlanmamıştır.

4. Sonuçlar

Lazer kesim paslanmaz çelik tozu ve demir tozu+(Cr, Mo)₃C içeren aşındırıcı toz karışımının sinterlenmiş durumdaki peletlere uygulanmıştır. Paslanmaz çeliklerin kesilmesi sırasında herhangi bir yanma problemi veya kısmi ergime problemi yaşanmazken, karbürü demir tozunun lazer kesimi sırasında reaktif bir reaksiyonun meydana geldiği görülmektedir. Daha fazla kıvılcım oluşumunun meydana geldiği karbür demir tozu karışımının kesimi sonucunda daha çok demir oksitler (FeO, Fe₂O₃) görülürken, paslanmaz çelikte ise Cr₂O₃ ve FeO oluşumu görülmektedir.

6. Teşekkür

Bu çalışma Afyon Kocatepe Üniversitesi BAP birimi tarafından desteklenen 17.TEKNOLOJİ.06 numaralı proje ile gerçekleştirilmiştir.

7. References

- [1] Welding Handbook, Vol. 3 9th Ed., ,(2007), American Welding Society, Miami, FL, Pp. 598 - 602
- [2] Tunç, M. (2015), CO₂ Lazer Kesim Tezgâhlarında Kesme Parametrelerinin Yüzey Pürüzlülüğüne Etkilerinin İncelenmesi. Yüksek Lisans Tezi, Karabük Üniversitesi, Fen Bilimleri Enstitüsü, Karabük
- [3] Triantafyllidis, D., Schmidt, M. J. J. and Li, L., (2003), Comparison Of High Power Diode Laser And Nd:YAG Laser Microwelding Of K-Type Thermocouples, *Journal Of Materials Processing And Technology*, **138**: 102-108.
- [4] Ürgüplü, M. ve Köksal S. (2015), Lazer İle Kesme İşlemlerinde Kesim Kalitesine Etki Eden Parametreler. *Isites Valencia –Spain Syf:865- 875*
- [5] Özden, H., (2010) “Lazer ile İmalat Yöntemleri”, *Makinatek Dergisi*, Sayı:**151**, S. 106-112
- [6] ANIK S., OĞUR A. ve VURAL M. (1996), Termik Kesme Teknolojisi. *Gedik Eğitim Vakfı Yayını*, **2**: 112- 121

[7] Özcan, M. (2003), Değişik Malzemelerin İşlenmesinde Kullanılan Nd:YAG Lazerleri İçin Etkin Bir Güç Kaynağının Tasarımı Ve Uygulanması, Doktora Tezi, Selçuk Üniversitesi, Fen Bilimleri Enstitüsü, Konya.

[8] Mungan, M.C. (2006) Lazer İle Kesme Ve Endüstriyel Uygulamalar. Yüksek Lisans Tezi, Mustafa Kemal Üniversitesi, Fen Bilimleri Enstitüsü, Antakya

[9] Ellingham, H. J. T. (1944), "Transactions and Communications", J. Soc. Chem. Ind. (London), 63 (5): 125

BAŞLICA YAZAR ADRESİ: Şükrü Talaş, Afyon Kocatepe Üniversitesi, Teknoloji Fakültesi, ANS Kampüsü, +902722281314, talas.sukru@gmail.com.

KISA BİYOGRAFİLER

Şükrü Talaş, 1993 yılında Marmara Üniversitesi, Teknik Eğitim Fakültesi, Metalurji Eğitimi Bölümü'nden mezun oldu. Yüksek Lisansını 1997 yılında Brunel Üniversitesi'nde tamamladıktan sonra 2002 yılında Çelik Kaynaklı Metal Mikroyapılar da C-Mn-Ti etkisi konusunda Leeds Üniversitesi, İngiltere'den doktora derecesini aldı. Afyon Kocatepe Üniversitesi, Teknoloji Fakültesi Metalurji ve Malzeme Mühendisliği Bölümü'nde Profesör olarak görev yapmaktadır.

Barış Gökçe – Yardımcı Doçent Barış Gökçe, Afyon Kocatepe Üniversitesi, Teknik Eğitim Fakültesi Metalurji Eğitimi Bölümü'nden mezun oldu. Yüksek lisansını Afyon Kocatepe Üniversitesi Fen Bilimleri Enstitüsü'nde tamamladıktan sonra, Afyon Kocatepe Üniversitesi Fen Bilimleri Enstitüsü'nden doktora derecesini metalürjik süreçlerin istatistiksel optimizasyonu üzerine aldı. Çoğunlukla mekanik sistemlerin simülasyonu ve kontrolü üzerinde çalışır.

Yusuf Kayalı – Yardımcı Doçent Yusuf Kayalı, Afyon Kocatepe Üniversitesi, Teknik Eğitim Fakültesi, Metalurji Eğitimi Bölümü'nden mezun oldu. Yüksek lisansını Afyon Kocatepe Üniversitesi Fen Bilimleri Enstitüsü'nde tamamladıktan sonra Afyon Kocatepe Üniversitesi Fen Bilimleri Enstitüsü'nden metal aşınma konusunda doktora derecesini aldı. Korozyon ve metal aşınması üzerine çalışır.



ICWET '18
26-28 September / Sarajevo

